SHALE ENERGY ENGINEERING 2014

TECHNICAL CHALLENGES, ENVIRONMENTAL ISSUES, AND PUBLIC POLICY

EDITED BY Christopher L. Meehan, Ph.D., P.E.;
Jeanne M. VanBriesen, Ph.D., P.E.;
Farshid Vahedifard, Ph.D., P.E.;
Xiong Yu, Ph.D., P.E.; and Cesar Quiroga, Ph.D., P.E.

ASCE

SHALE ENERGY ENGINEERING 2014

TECHNICAL CHALLENGES, ENVIRONMENTAL ISSUES, AND PUBLIC POLICY

PROCEEDINGS OF THE 2014 SHALE ENERGY ENGINEERING CONFERENCE

July 21–23, 2014
Pittsburgh, Pennsylvania

SPONSORED BY
The Energy Division of the American Society of Civil Engineers

EDITED BY
Christopher L. Meehan, Ph.D., P.E.
Jeanne M. VanBriesen, Ph.D., P.E.
Farshid Vahedifard, Ph.D., P.E.
Xiong Yu, Ph.D., P.E.
Cesar Quiroga, Ph.D., P.E.

Published by the American Society of Civil Engineers

Published by American Society of Civil Engineers
1801 Alexander Bell Drive
Reston, Virginia, 20191-4382
www.asce.org/bookstore | ascelibrary.org

Any statements expressed in these materials are those of the individual authors and do not necessarily represent the views of ASCE, which takes no responsibility for any statement made herein. No reference made in this publication to any specific method, product, process, or service constitutes or implies an endorsement, recommendation, or warranty thereof by ASCE. The materials are for general information only and do not represent a standard of ASCE, nor are they intended as a reference in purchase specifications, contracts, regulations, statutes, or any other legal document. ASCE makes no representation or warranty of any kind, whether express or implied, concerning the accuracy, completeness, suitability, or utility of any information, apparatus, product, or process discussed in this publication, and assumes no liability therefor. The information contained in these materials should not be used without first securing competent advice with respect to its suitability for any general or specific application. Anyone utilizing such information assumes all liability arising from such use, including but not limited to infringement of any patent or patents.

ASCE and American Society of Civil Engineers—Registered in U.S. Patent and Trademark Office.

Photocopies and permissions. Permission to photocopy or reproduce material from ASCE publications can be requested by sending an e-mail to permissions@asce.org or by locating a title in ASCE's Civil Engineering Database (http://cedb.asce.org) or ASCE Library (http://ascelibrary.org) and using the "Permissions" link.

Errata: Errata, if any, can be found at http://dx.doi.org/10.1061/9780784413654.

Copyright © 2014 by the American Society of Civil Engineers.
All Rights Reserved.
ISBN 978-0-7844-1365-4 (CD-ROM)
ISBN 978-0-7844-7860-8 (PDF)
Manufactured in the United States of America.

Preface

In recent years, new technologies that utilize horizontal drilling and hydraulic fracturing techniques have led to a rapid expansion of the shale oil and gas industry, offering access to new sources of hydrocarbon fuels that hold the promise of energy independence for the United States. At the same time, there has been public concern about the potential environmental effects of these new technologies, with varying environmental regulations being implemented at the state and federal level in response to their rapid deployment. Consequently, some areas of the country are witnessing a rapid growth in the number of wells for exploration, while other areas have delayed this development pending further environmental studies. Additionally, the rapid growth of the shale energy industry in some areas has imposed new demands on the people and infrastructure in local communities. Moving forwards, the challenge for our society is to develop a holistic approach to shale oil and gas exploitation that enables economic growth and prosperity, while minimizing negative environmental impacts and socio-economic disturbances in our communities.

Civil and Environmental Engineers have as their core mission the protection of the public health, safety, and welfare. With this in mind, the Energy Division of the American Society of Civil Engineers (ASCE) has organized a new, broadly-themed conference, entitled "Shale Energy Engineering 2014: Technical Challenges, Environmental Issues, and Public Policy." This conference was held July 21-23, 2014 in Pittsburgh, Pennsylvania, and its goals were to provide a forum for: discussing the technical challenges associated with shale oil and gas development from a civil engineering perspective, exploring the critical environmental and infrastructure issues that exist in this industry, and presenting public policy solutions that enable safe development of shale oil and gas resources. The conference was organized into the following four tracks: (1) Water Resources Management in Shale Oil & Gas Development; (2) Geological and Geotechnical Aspects of Shale Oil & Gas Well Development; (3) Environmental, Regulatory, and Public Policy Issues; and (4) Supporting Infrastructure Development for Shale Oil & Gas Production.

The following volume contains the Proceedings from ASCE's 2014 Shale Energy Engineering Conference. In this volume, seventy-three papers are included from authors presenting at the conference in the four track areas noted above. Three types of paper submissions were allowed for the conference: research letters, technical papers, and case study papers. Research letters are 5-6 pages long, and highlight cutting-edge research projects or particularly innovative practice-oriented projects. Technical papers are 7-10 pages long, and detail the findings from research- or practice-oriented projects that are of broad interest to the shale energy engineering community. Case study papers are 10-15 pages long, and provide more extensive details, photographs, and descriptions about an individual field project.

Paper sessions at the conference were organized by 34 session chairs. In this volume, the reader will find them listed as Members of the Review Board. They were assisted by 80 professional colleagues to perform a minimum of two anonymous reviews for each paper by experts in the corresponding subject area.

On behalf of the conference organizers and the ASCE Energy Division, we wish to express our gratitude to all of the session chairs and reviewers for their diligent and tireless efforts to make these Proceedings a reality. We also wish to extend our thanks to Elaine Watson, Barbara Whitten, Donna Dickert, Drew Caracciolo, and Naida Caton, our core conference planning support team within ASCE. Finally, we would like to thank the authors for their contributions to the Proceedings. The papers that have been submitted by our colleagues do a great service to the shale energy engineering profession.

The Editors

Christopher L. Meehan
Jeanne M. VanBriesen
Farshid Vahedifard
Xiong Yu
Cesar Quiroga

SHALE ENERGY ENGINEERING 2014: CONFERENCE ORGANIZING COMMITTEE

Conference Chair

Kemal Niksic, P.E., M.ASCE., Hatch Mott MacDonald

Conference Co-Chairs

Jonathan L. Tan, M.ASCE, Black & Veatch
Christopher L. Meehan, Ph.D., P.E., M.ASCE, University of Delaware

Technical Program Chair

J. Daniel Arthur, P.E., SPEC, M.ASCE, ALL Consulting

Technical Publication Committee Chair and Chief Editor

Christopher L. Meehan, Ph.D., P.E., M.ASCE, University of Delaware

Track Chairs

Water Resources Management
Paul A. Bizier, P.E., BCEE, F.ASCE, Barge, Waggoner, Sumner, and Cannon, Inc.
Jeanne M. VanBriesen, Ph.D., P.E., M.ASCE, Carnegie Mellon University

Geological/Geotechnical
Khalid Farrag, Ph.D., P.E., PMP, M.ASCE, Gas Technology Institute
Farshid Vahedifard, Ph.D., P.E., M.ASCE, Mississippi State University

Environmental/Regulatory/Public Policy
Gregory F. Scott, P.E., M.ASCE, Buchart Horn, Inc.
Xiong Yu, Ph.D., P.E., M.ASCE, Case Western Reserve University

Supportive Infrastructure/Technology
James H. Anspach, P.G., M.ASCE, Cardno
Cesar Quiroga, Ph.D., P.E., M.ASCE, Texas A&M Transportation Institute

Technical Publication Co-Editors

Water Resources Management
Jeanne M. VanBriesen, Ph.D., P.E., M.ASCE, Carnegie Mellon University

Geological/Geotechnical
Farshid Vahedifard, Ph.D., P.E., M.ASCE, Mississippi State University

Environmental/Regulatory/Public Policy
Xiong Yu, Ph.D., P.E., M.ASCE, Case Western Reserve University

Supportive Infrastructure/Technology
Cesar Quiroga, Ph.D., P.E., M.ASCE, Texas A&M Transportation Institute

Local Committee Chair

Nathaniel S. Hayes, P.E., M.ASCE, The Gateway Engineers

Sponsorship/Exhibits Committee

Kenneth E. Hill, P.E., M.ASCE, ALL Consulting
Ryan L. Hayes, Gateway Engineers

Student Activities Committee

Kyle Bibby, Ph.D., University of Pittsburgh
Xiong Yu, Ph.D., P.E., M.ASCE, Case Western Reserve University

REVIEW BOARD

James Anspach
Kenneth Bell
Kyle Bibby
Steven Bloser
Timothy Brett
Lindsey Bryson
Andrew Bunger
Lucy Mar Camacho
Rick Chalaturnyk
Lee Clapp
Brian Ellis
Khalid Farrag
Victor Kaliakin
Olya Keen
Lawrence (Larry) Lennon
Hua Li
Paul Mathisen
Melody Matter
Christopher Meehan
Mais Nijim
Cesar Quiroga
James Sassin
Jeff Schubert
Gregory Scott
John Sheehan
Less Shephard
Jonathan Shimko
Kristin Smith
Farshid Vahedifard
Luis Vallejo
Julie Vandenbossche
Megan Walsh
Rich Williams
Xiong Yu

REVIEWERS

Jorge Abad
James Anspach
Dan Arthur
Kenneth Bell
Kyle Bibby
Paul Bizier
Steven Bloser
Mehmet Boz
Michael Borden
Susan Brantley
Andrew Bunger
Elizabeth Casman
Eric Cavazza
Matthew Cavazza
Rick Chalaturnyk
Amy Childress
Jordan Ciezobka
Lee Clapp
Aimee Curtright
Melih Demirkan
Elizabeth Eide
Brian Ellis
Mostafa Elshahed
Khalid Farrag
Ali Fatehi
Quan Gao
Daniel Giammar
Kelvin Gregory
Yuan Guo
Chanjuan Han
Jianying Hu
Jim Huebler
Tom Iseley
Victor Kaliakin
Bill Kappel
Jeffrey Keaton
Olya Keen
Carl Kirby
Eric Koglin
Hillary Kronebusch
Hua Li
Yang Li
Karl Linden
Debotyam Maity
Paul Mathisen
Meagan Mauter
Christopher Meehan
Philip Meis
Douglas Melton
Austin Mitchell
Kimia Mortezaei
Jean-Philippe Nicot
Mais Nijim
Kent Perry
Peter Phillips
Chris Proulx
Brian Rahm
Joris Remmers
Elizabeth Rowan
Michael Sadowsky
Iraj Salehi
Jeff Schubert
Gregory Scott
John Sheehan
Les Shephard
Jonathan Shimko
Stanley States
Ray Sterling
Heiner Strathmann
Farshid Vahedifard
Jeanne VanBriesen
Avner Vengosh
Radisav Vidic
Megan Walsh
Yuxin Wang
Rich Williams
Jessica Wilson
Dave Yoxtheimer
Xiong Yu
Mark Zoback

Contents

Water Resources Management in Shale Oil and Gas Development

Water Resources and Groundwater Issues in Shale Development

Modeling of Land Movement due to Groundwater Pumping from an Aquifer System with Stress-Dependent Storage **1**
D. H. Kang, H. J. Lee, and J. Li

Baseline Water Quality Monitoring Prior to Hydraulic Fracturing to Promote Scientifically-Based Transparency **11**
George Mathes, Carly Sowecke, Cherrie Nelson, Marjorie Bedessem, and Dan Hruska

Feasibility of Using Brackish Groundwater Desalination Concentrate as Hydraulic Fracturing Fluid in the Eagle Ford Shale **23**
Nima Ghahremani and Lee Clapp

Produced Water Management and Treatment Technologies

Evolution of Best Management Practices and Water Treatment in High-Volume Hydraulic Fracturing Operations **33**
J. Daniel Arthur, Brian Bohm, and Damian Zampogna

Recycling of Produced and Flowback Water in Oil and Gas Drilling Operations through Hydraulic Fracturing in Texas **45**
Mehmet A. Boz

Review of Flowback and Produced Water Management, Treatment, and Beneficial Use for Major Shale Gas Development Basins **53**
Guanyu Ma, Mengistu Geza, and Pei Xu

Characterization of Waste Waters from Hydraulic Fracturing **63**
Paul F. Ziemkiewicz, Yongtian He, and John D. Quaranta

Electrodialysis Treatment of Flow-Back Water for Environmental Protection in Shale Gas Development **74**
Maria Peraki and Ehsan Ghazanfari

Conversion of Marcellus Production Wastewater into Salable Products **85**
Timothy Keister

Environmental Issues in Produced Water Disposal

Regulation of TDS and Chloride from Oil and Gas Wastewater in Pennsylvania **95**
Eric H. Chase

Management of Produced Water in Pennsylvania: 2010–2012 ..... **107**
Jeanne M. Van Briesen, Jessica M. Wilson, and Yuxin Wang

Evaluating Leachability of Residual Solids from Hydraulic Fracturing in the Marcellus Shale 114
Stephanie Countess, Gregory Boardman, Richard Hammack, Alexandra Hakala, Shekar Sharma, and Jeffrey Parks

Geological and Geotechnical Aspects of Shale Oil and Gas Well Development

Geotechnical Aspects of Shale Oil and Gas

The Role of Shallow Surface Investigations in Appalachian Shale Energy Development 121
John T. Henning and Steven Ladavat

Geomechanical Characterization of Shale Formations for Sustainable Production..... 133
Rafael Villamor Lora and Ehsan Ghazanfari

Comminution of Solids Due to Kinetic Energy of High Shear Strain Rate: Implications for Shock and Shale Fracturing..... 144
Zdeněk P. Bažant and Ferhun C. Caner

Guided Ultrasonic Waves for the Nondestructive Evaluation Imaging of Pipes..... 151
Piervincenzo Rizzo, Abdollah Bagheri, and Kaiyuan Li

Mechanical Behaviors of an Anisotropic Shale Rock..... 159
Q. Gao, J. L. Tao, J. Y. Hu, and X. Yu

Shale Fracturing for Energy Recovery: Current Issues and Review of Available Analytical and Computational Models..... 168
Giuseppe Buscarnera, Gianluca Cusatis, Aleksander Zubelewicz, and Zdeněk P. Bažant

Particle Stacking Model to Simulate Sedimentary Rock Microcracks 180
Sangho Lee

Geomechanics and Numerical Simulation of Hydraulic Fracturing

Fracture Mechanics Evaluation of Parameters Associated with Horizontal Hydrofracturing 191
Luis E. Vallejo and Jason Shamrock

Numerical Simulation of Simultaneous Growth of Multiple Interacting Hydraulic Fractures from Horizontal Wells 201
Andrew P. Bunger and Anthony P. Peirce

Subcritical Crack Propagation Enhanced by Chemical Injection.....211
M. M. Hu and T. Hueckel

Numerical Analysis on Deformation Behavior of Expandable Casing and Contact Evaluation of Its Threaded Connection 219
Xinpu Shen and Guoyang Shen

Hydro-Mechanical Coupled Model of Hydraulic Fractures Using the eXtended Finite Element Method 230
D. J. Youn and D. V. Griffiths

Modeling Flow Regime in Shale Using Isogeometric Analysis 239
Shahriar Shahrokhabadi, Farshid Vahedifard, and Ehsan Ghazanfari

Characterizing and Validating Seismic Impact

Towards a Real-Time Forecast of Induced Seismicity for Enhanced Geothermal Systems 246
Dimitrios C. Karvounis, Valentin S. Gischig, and Stefan Wiemer

Predicting the Seismic Hazard Due to Deep Injection Well-Induced Seismicity 256
Ali Fatehi, Richard Quittmeyer, Melih Demirkan, Jose Blanco, and Jeffrey Kimball

Numerical Simulation of Induced Seismicity Due to Hydraulic Fracturing of Shale Gas Reservoirs 265
Kimia Mortezaei and Farshid Vahedifard

Geological Aspects of Shale Oil and Gas

Rock Excavation Index Approach for Estimating Blast Rock for Shallow Pipeline Construction 273
Jeffrey R. Keaton and Luther H. Boudra

Rock Behavior under High Pressure and High Temperature (HPHT) 280
Mudasar Zahoor

Influence of Mineralogy on the Index Properties and Durability of Crushed Shales ... 288
L. Sebastian Bryson and Isabel Cristina Gomez-Gutierrez

Hydraulic Fracturing Characterization and Field Monitoring

Interpretation Challenges for In Situ Stress from Mini-Frac Tests in Soft Rocks/Hard Soils 298
Nadia ShafieZadeh and Rick Chalaturnyk

Field Borehole Testing of Anisotropic Shale Rock 310
X. Yu

Numerical Estimation of Casing Integrity under Injection Pressure for Fracturing of Shale Gas Formation 318
Xinpu Shen

Environmental, Regulatory, and Public Policy Issues

Environmental Effects of Hydraulic Fracturing and Mitigation

Analysis of Hydraulic Fracturing Chemical Disclosure Data from FracFocus 326
J. Daniel Arthur, H. William Hochheiser, and Roy Arthur

Erosion and Sediment Controls 337
Lauren R. Parker

Stormwater Runoff and the Oil and Gas Industry: A State-by-State Review of Regulations and Surface Water Quality Impacts 347
Megan Walsh, Christine Pomeroy, and Kirsten Eliassen

Subpart W—Past, Present, and Future **356**
David J. Larson and Kristian A. Macoskey

Effective Use of Cementitious Materials, Ground Granulated Blast Furnace Slag, and Bentonite in Treating Contaminants on Polluted Land **364**
Mary Allagoa

VOC Emission Monitoring at Eagle Ford Shale Drill Sites Using Wireless Sensor Network for Understanding Emission Generation and Dispersion **374**
Nikhil Mantrawadi, Mais Nijim, David Ressegiue, Gerald Ogumerem, Lee Clapp, and Alvaro Martinez

Life Cycle Assessment of Air Toxins for Natural Gas Production, Transport, and Power Generation in the Marcellus Shale Region **384**
David D. Good, Jorge Abad, and Vikas Khanna

Effect of Fractures on Methane Migration in Shallow Groundwater Aquifer **395**
Liwei Zhang, Nicole Anderson, and Daniel J. Soeder

Best Environmental Practices

Strategies for Sustainable Management of Oilfield Wastes and Wastewaters in Shale Resource Plays **404**
J. Daniel Arthur and B. Greg Casey

The Impact of Shale Gas/Oil Waste on MSW Landfill Composition and Operations **412**
Eric D. Chiado

Restoration of Streams and Wetlands Following Pipeline Construction Projects **421**
Paul A. Kanouff

Ensuring Sustainable Development of Shale Gas Transmission Infrastructure by Applying State-of-the-Art Methods in Geomorphology **430**
M. Logan Cline, K. Michael Cline, Daniel J. Barton, and Paul C. Rizzo

Best Management Practices for Access Roads for Shale Energy Development with Consideration to Surface Waterbodies **446**
Elizabeth Myers Toman and Gordon R. Keller

Environmental Regulations and Risk Management in Shale Oil and Gas Production

Shale Gas Well Pad Air Quality Permitting in Ohio and West Virginia **457**
Kristian A. Macoskey, Gerard G. Alberts, Donald Gray, and Robert A. Bosiljevac

The Grey Science of Wetland Avoidance **467**
William T. Acton

Improving Impact Analysis of the Eagle Ford Shale Oil and Natural Gas Production on Regional Rural Communities **474**
Gerardo J. Pinzon, Jianhong-Jennifer Ren, and Kim D. Jones

SPCC Planning for Oil Drilling, Workover, and Production Facilities **484**
Martin J. Hamper

A Review of NORM/TENORM in Wastes and Waters Associated with Marcellus Shale Gas Development and Production 492
Jeffrey P. Schubert, Michael F. Rosenmeier, and Mark P. Zatezalo

An Integrated Emergency Evacuation System for Real-Time Operations—A Case Study of Eagle Ford Shale Gas Area, South Texas 502
Young Lee, Joon-Yeoul Oh, Nuri Yilmazer, Aritra Ghosh, and Md Naim Hossain

Public Policy Issues Related to Shale Oil and Gas Production

Waters of the United States: Understanding Definitions and Jurisdictional Determinations Specific to Shale Resource Development 512
J. Daniel Arthur, Jon Seekins, David Winter, and David Alleman

How API's Shale Gas Standards and Best Practices Support Sustainable Shale Gas Development 520
David Lee Miller

The Influence of Hydraulic Fracturing on the Water Market in Texas 530
Margaret A. Cook and Michael E. Webber

Investigation and Analysis of Social Impacts of Eagle Ford Shale on Local Communities 543
Hua Li, Jieming Chen, Jennifer E. Pearce-Morris, Brenda Hannon, Kai Jin, Lian Yang, Emilio Alaniz, Jaime Herrera, and Ruth Zabelin

Supporting Infrastructure Development for Shale Oil and Gas Production

Roadway Assessment, Monitoring, Repair, and Reconstruction Technologies

Issues and Options for Oversize/Overweight Permitting of Petroleum-Related Trucks in a Performance-Based Regulatory Context: The Manitoba Experience 552
Mark J. Reimer, Jonathan D. Regehr, and Jan McKee

Geosynthetic Solutions for Paved and Unpaved Applications 565
D. Lipomi and M. H. Wayne

The Positive Environmental and Cost Impact of Geosynthetics in Well Pad and Access Road Construction 576
Bruce A. Lacina, John D. Herrmann, and Monte Madsen

Use of Geosynthetics for Reinforcing/Stabilizing Unpaved Roads under Full-Scale Truck Axle Loads 591
Xiaochao Tang, Murad Abu-Farsakh, Shadi Hanandeh, and Qiming Chen

Non-Destructive Evaluation and Reinforced Design of Gravel Heavy Haul Road Structures in Northern Alberta 603
Fadi M. Jadoun, Khaled Galal, Edward Wilson, Amr Ayed, and Khaled Helali

Confined-Aggregate-Concrete MEPCO Loading Dock Road, Morgantown, WV—A Case Study 619
Samuel G. Bonasso

Best Practices for Stakeholder Coordination

Road Impacts from Shale Energy Development 633
Paul W. Wilke

Assessing the Impacts of Shale Oil and Gas Developments on Rural Texas Highway Infrastructure 643
Timothy Miller and James M. Sassin

Heavy Roadway User Permit Release Coordination 654
Scott K. Nale

Protecting PennDOT's Infrastructure 664
Melody Matter and John Voda

Pipeline Detection, Mapping, and Monitoring

Blockage Detection in Pipeline Networks for Gas and Oil 676
Paolo Bocchini, Alessandro Marzani, and Aman Karamlou

CSA S250-11 and CI/ASCE 38-02—How to Effectively Utilize These Utility Standards for Shale Energy Projects 684
Lawrence Arcand

Underground (Well) Mapping Re-Visited 693
Earl F. Burkholder

Best Practices for Site Development

Design of Bulk Railway Terminals for the Shale Oil and Gas Industry 704
C. Tyler Dick and Lynn E. Brown

Management of Impoundments for Unconventional Resource Development: Application, Planning, Design, Best Practices, and Regulatory Considerations 715
J. Daniel Arthur, Brian Bohm, and Kevin Shepard

Storage Tank Secondary Containment 724
D. S. Soemantri

Modeling of Land Movement due to Groundwater Pumping from an Aquifer System with Stress-Dependent Storage

D. H. Kang[1], Ph.D., P.E., H. J. Lee[2], and J. Li[3], Ph.D., P.E., HG., D.WRE, F.ASCE

[1]Research Associate, Morgan State University, Baltimore, MD 21251, U.S.A.,
E-mail: donghee.kang@morgan.edu
[2]Research Assistant, Morgan State University, Baltimore, MD 21251, U.S.A.,
E-mail: hylee1@morgan.edu
[3]S.P. Massie Chair Professor, Morgan State University, Baltimore, MD 21251, U.S.A.,
E-mail: jiang.li@morgan.edu

ABSTRACT: Discharge of subsurface fluids (water, oil and gas) causes land subsidence and earth fissures. Numerical simulation of land movement due to groundwater withdrawal from an aquifer system has been conducted in this paper. A hyperbolic stress-strain relation has been introduced, which leads to a stress-dependent specific storage coefficient and further to a nonlinear flow equation. Three secondary physical laws and a bulk flow relation have been invoked to develop a new module that is incorporated into the parent code MODFLOW. A conceptual model for an aquifer system with a well has been established. Three-dimensional land movement due to discharge has been simulated using both linear and nonlinear models. The results indicate that land movement using a linear model can be likely overestimated when compared to that using a nonlinear model. This conclusion is consistent with the stress-dependent specific storage coefficient derived in this paper. The numerical simulation demonstrates that a hyperbolic model may provide better prediction than an exponential model, another nonlinear model previously applied. Sensitivity analysis of parameters indicates that the hydraulic diffusivity plays a significant role in response to land movement while pumping.

INTRODUCTION

Hydraulic fracturing, a technique used in horizontal wells, injects millions gallons of water along with sand and chemicals at high pressure into a wellbore to create small fractures so that the natural gas can be released from the shale formation. The application of hydraulic fracturing at least results in two related issues. First, hydraulic fracturing needs significant amount of water. Pumping water from adjacent aquifer systems causes land subsidence and earth fissures that may impose threads to environment and society (Poland, 1984). This is also true for extracting gas from the shale formation that underlies the aquifer systems. Second, the cracks caused by groundwater discharge and hydraulic fracturing may occur initially at depth, then

grow and develop upward. The cracks in an aquifer system may migrate upward and eventually become earth fissures on the land surface (Sheng et al., 2003). The geologic discontinuity caused by such discharge activity may open a door for pollutant intrusion to aquifer systems for water supply. Contamination can be caused by leakage of the fluid with various chemicals for hydraulic fracturing. The investigation in this paper addresses the first issue. Namely, discharge groundwater from an aquifer system causes land subsidence and earth fissures.

Over the past decades, many experts have attempted to develop modules to evaluate transient land subsidence accurately and efficiently by making use of the MODFLOW, a program developed by USGS for simulation of groundwater flow. Different modules established by previous investigators were only able to deal with the vertical displacement (subsidence). However, occurrence of significant horizontal movement caused by ground water withdrawal indicates that land movement is more than one-dimensional vertical movement (Helm, 1994). In the present paper, a new package is developed not only for three-dimensional (3-D) movement in response to groundwater withdrawal from an aquifer system but also for a specific storage coefficient that is stress or hydraulic head dependent. Zhang (2009) developed a module (DIS) and embedded it to a preexisting version MODFLOW-96 to simulate the 3-D transient land movement. Zhang's module is inherently a linear elastic model due to the MODFLOW assumes that the specific storage coefficient is a constant. In reality, however, the specific storage normally is not a constant and related to stress history instead. Using a constant storage coefficient may result in inaccurate prediction of aquifer movement. Therefore, the stress-dependent or hydraulic head-dependent specific storage coefficient was applied to a new module which is based on a mechanics model simulating nonlinear stress-strain relationship of soils. The module for material nonlinearity (NDIS) using an exponential model was first developed and incorporated into the MODFLOW-96 by Li and Ding (2013). However, the volume compression simulated by the exponential model can be kept going forever as long as loading increases. In reality, this is not true as the volume of soil mass cannot be compressed to zero due to conservation of mass. Therefore, a new hyperbolic relation between bulk stress and stain is introduced in this investigation. For purpose of comparison, three modules (i.e., a linear and two nonlinear ones) are incorporated in the same version of MODFLOW developed by McDonald and Harbaugh (1988).

The purpose of this research is to investigate impacts of the new nonlinear hyperbolic model on the land subsidence in response to groundwater discharge. To do so, first to establish a conceptual model of an aquifer system with a single fully penetrating pumping well, then to develop a numerical model for simulating aquifer movement impelled by hydraulic force, and finally to evaluate linear and nonlinear stress-strain models and to present the results according to geological properties chosen in this paper.

BASIC EQUATIONS

Groundwater flow equation

A governing equation for three-dimensional transient groundwater flow through a

saturated anisotropic porous material in a Cartesian coordinate system is expressed by (Todd and Mays, 2005):

$$\frac{\partial}{\partial x}\left(K_x\frac{\partial h}{\partial x}\right)+\frac{\partial}{\partial y}\left(K_y\frac{\partial h}{\partial y}\right)+\frac{\partial}{\partial z}\left(K_z\frac{\partial h}{\partial z}\right)-W=S_s\frac{\partial h}{\partial t} \quad (1)$$

where h is the transient hydraulic head for an unsteady flow; the terms K_x, K_y and K_z are three components of hydraulic conductivity in the principal directions x, y and z; S_s is the specific storage coefficient that can be either a constant for linear poroelasticity or a stress-dependent variable for nonlinear poroelasticity; the term W denotes a volumetric flux per unit volume and represents sources and/or sinks of water mass within an aquifer system.

Aquifer movement in terms of the Darcy-Gersevanov Law

In an aquifer system, bulk flux through permeable, deformable and saturated porous material based on volume fraction can be (Helm, 1984):

$$\mathbf{q}_b=(1-n)\mathbf{v}_s+n\mathbf{v}_w=\boldsymbol{q}+\mathbf{v}_s \quad (2)$$

where $\mathbf{q}_b$ is the bulk flux; n is the porosity; $\mathbf{v}_s$ is the velocity of solid; $\mathbf{v}_w$ is the velocity of the interstitial fluid, $\mathbf{q}$ [= $n(\mathbf{v}_s-\mathbf{v}_w)$] is the specific discharge. The bolded variables stand for vectors throughout the paper. Moreover, Gersevanov's generalization of the Darcy's law (Gersevanov, 1934) can be given by:

$$\mathbf{q}=n(\mathbf{v}_s-\mathbf{v}_w)=-\mathbf{K}\boldsymbol{\nabla}h \quad (3)$$

where $\boldsymbol{\nabla}$ is a vector and denotes the differential operator for gradient. The expression (3) suggests that for given bulk flux and relative water flow, aquifer velocity can be found. For the commonly assumed non-rotating averaged laminar water flow past grains and for non-rotating averaged granular motion within a saturated representative elemental volume, bulk flux can be assumed to be (Helm, 1979)

$$\mathbf{q}_b=-\mathbf{K}\boldsymbol{\nabla}\theta \quad (4)$$

where θ is the flux potential of $\mathbf{q}_b$ and needs to be determined such that the aquifer velocity can be found from (5) below. If the flux potential is assumed to be the constant hydraulic head h_s for a steady flow, i.e., $\theta = h_s$ (Helm, 1979), inserting (4) into (3) results in the aquifer velocity in terms of the Darcy-Gersevanov law by:

$$\mathbf{v}_s=\mathbf{q}_b-\mathbf{q}=-\mathbf{K}\boldsymbol{\nabla}(h_s-h) \quad (5)$$

For given boundary and initial conditions, h can be found from the transient flow equation (1). Similarly, h_s can be solved from the steady flow equation which is called Laplace's equation that reduces by dropping the term on the right-hand side of (1). It should be noted that the bulk flow $\mathbf{q}_b$ does not change with time for unchanging boundary conditions during a given stress period whereas transient flow $\mathbf{q}$ is a

function of time. The velocity field of solids $\mathbf{v}_s$ is then computed as a resulting function of time and coordinates. As time progresses, the transient relative flow $\mathbf{q}$ approaches the bulk flow $\mathbf{q}_b$ and as a consequence the velocity of the solids tends with time towards zero (Helm, 1979). The displacement field of solids can be computed through integrating the velocity field of solids over the time as follows:

$$\mathbf{u}_s = \int_{t_0}^{t} \mathbf{v}_s \, dt + \mathbf{u}_{s0} \tag{6}$$

where subscript 0 stands for the initial value of aquifer's displacement or velocity. The velocity and displacement fields of the solid frame vary with time.

Nonlinear poroelastic sedimentary materials

A hyperbolic model is introduced in the paper. For purpose of comparison, the nonlinear exponential model is also discussed. The two nonlinear stress-strain relations are applied to model incremental changes in volume of sedimentary materials.

Volume stress and strain relation as an exponential function

From a conventional consolidation test of soils in a laboratory, the relation between the void ratio e and the effective volume stress σ'_v can be written as: $\delta e = C_c \delta \log(\sigma'_v)$ where $\delta e = e_0 - e$ and $\delta \log(\sigma'_v) = \log(\sigma'_v/\sigma'_{v0})$; e and e_0 are current and initial void ratios, respectively; σ'_v and σ'_{v0} are the current and initial effective volume stresses, respectively; δ denotes the increment of a variable; C_c (>0) denotes the slope of the virgin curve $e - \log(\sigma'_v)$. The semi-log relation after divided by the term $1 + e_0$ can be further expressed by an exponential function in terms of incremental volume stress and strain:

$$\delta\sigma'_v = \sigma'_{v0}\left[e^{2.3\frac{(1+e_0)\delta\varepsilon_v}{C_c}} - 1\right] \tag{7}$$

where the volume strain $\delta\varepsilon_v = \delta e/(1+e_0)$. Thus, the specific storage coefficient becomes a parameter related to effective volume stress (Li and Ding 2013):

$$S_s(\sigma'_v) = \frac{\partial \varepsilon_v}{\partial \sigma'_v}\gamma_w = S_{s0}\frac{\sigma'_{v0}}{\sigma'_v} \tag{8}$$

where S_{s0} ($=\gamma_w\alpha_0$) is the initial specific storage coefficient, the term α_0 ($= C_c/[2.3(1+e_0)\sigma'_{v0}$) denotes an initial volume compressibility of aquifer's skeleton and γ_w is the unit weight of pore water. Equation (8) indicates that when a pump is turned on (at $t = t_0^+$), S_s equals S_{s0} because of $\sigma'_v = \sigma'_{v0}$, and then reduces as time progresses. Changes in S_s is inversely proportional to the current effective stress, which means that S_s decreases with increasing effective volume stress or suggests that an aquifer system hardens through compaction in response to pumping activity. The fact of $S_s \leq S_{s0}$ after the pumping starts implies that the aquifer system with

nonlinear poroelastic sediments may deform less than that with linear poroelastic sediments.

The effective stress can be normally presented by the hydraulic head, which can be done by applying Terzaghi's principle of effective stress: $\sigma_v = \sigma'_v + p$ (Terzaghi, 1925) and Hubbert's potential (Hubbert, 1940): $h = z + p/\gamma_w$ in which p is excess water pressure and z is elevation above a chosen datum. Accordingly, the specific storage coefficient in (8) becomes:

$$S_s(h) = S_{s0}\frac{\sigma'_{v0}}{\sigma_{v0} - \gamma_w(h-z)} \tag{9}$$

where σ_{v0} is the total volume stress and is assumed to be constant. Expression (9) is particularly helpful for numerical simulation using a program with a flow equation written in terms of hydraulic head such as the MODFLOW.

Volume stress and strain relation as a hyperbolic function

One of disadvantages of the volume stress-strain relation described by the exponential function (7) is that the volume compression can be kept going forever with increased loading. Apparently this is not true in reality. Mass of soils cannot be compressed to zero due to conservation of mass if one observes a one-dimensional consolidation test in laboratory. Therefore, a hyperbolic model for the stress-stain relationship is introduced below:

$$\delta\varepsilon_v = \frac{\delta\sigma'_v}{(a + b\delta\sigma'_v)} \tag{10}$$

where the terms a and b are constitutive parameters and have clear physical meanings. The term 1/a stands for the initial compressibility of an aquifer system at a small stress level, and 1/b represents the ultimate volume strain when the effective stress becomes significantly large. It is not difficult for one to draw such a conclusion from (10) by letting σ'_v approach to zero or infinity, respectively. Accordingly, the stress-dependent S_s can be found as:

$$S_s(\sigma'_v) = \frac{\partial\varepsilon_v}{\partial\sigma'_v}\gamma_w = S_{s0}\frac{1}{(1+\delta\sigma'_v b/a)^2} \tag{11}$$

where the term $S_{s0} = \gamma_w/a$ is the initial specific storage coefficient, and 1/a, as discussed in (10), equals the initial compressibility α_0. Similarly, after applying the principal of effective stress and the potential function to (11), S_s in terms of hydraulic head can be found in the following form:

$$S_s(h) = S_{s0}\frac{1}{[1+(\sigma_{v0} - \gamma_w(h-z)b/a]^2} \tag{12}$$

The specific storage coefficient in (12) is based on the hyperbolic stress-strain relation (10) and is incorporated with (1) for numerical computation. Similar to that

in the exponential model in (8) and (9), the specific storage coefficient of the hyperbolic model decreases with either increase of effective stress in (11) or decrease of the hydraulic head in (12), which suggests the aquifer system will be hardening due to losing its storage of water.

NUMERICAL MODELING

The property of the aquifer system

The numerical simulation is based on a conceptual model that consists of an aquitard and two aquifers with a fully penetrating pumping well (see Figure 1). The top layer (Layer 1) is an unconfined aquifer and the bottom layer (Layer 3) is a confined aquifer instead. The aquitard (Layer 2) serves as a hydraulic separator between two aquifers.

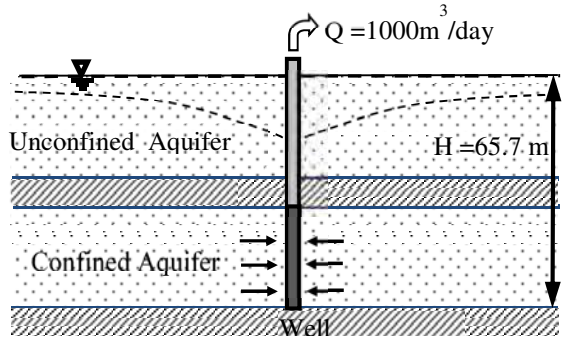

FIG. 1. A conceptual model of an aquifer system

The boundaries of the numerical model in the horizontal directions are specified as a constant-head condition. The initial drawdown is set to equal zero. The brief information of properties of the conceptual model is given in Table 1.

Table 1. Parameters of the model

	Geologic Layers		
Properties	**1**	**2**	**3**
K_h (m/d)*	**6.00E+0**	**6.00E-3**	**5.00E+0**
K_v (m/d)*	**3.00E+0**	**4.00E-3**	**2.50E+0**
S_{skv} **	**1.00E-3**	**4.00E-3**	**1.00E-3**
S_{ske} **	**1.00E-5**	**1.00E-4**	**1.00E-5**
Thickness (m)	**3.02E+1**	**5.30E+0**	**3.02E+1**

*K_h, K_v - horizontal and vertical conductivities
**S_{skv}, S_{ske} - storage coefficients on the virgin and swelling curves.

Table 2. Parameters for S_s

Layer	σ_v	σ'_{v0}	z(m)*
1	**317.10**	**166.10**	**-15.10**
2	**683.23**	**354.73**	**-32.85**
3	**1049.35**	**543.35**	**-50.60**

* z is a middle point of each layer for elevation

To simulate 3-D subsidence at a basin-wide scale in an efficient and accurate way, the three-layer aquifer system is discretized horizontally, and each layer is represented by a grid of 37 rows by 37 columns. The total number of elements equals 4107 (= 37 x 37 x 3). Variable grid spacing is considered in the grid design to

improve the accuracy of the numerical simulation nearby the pumping well where sharp changes in drawdown occur. The parameters for S_s (see Table 2) are evaluated using the unit weight of soil and water and the coefficient of earth pressure at rest. The soil unit weight is 21.0 kN/m^3 for two aquifers and 15.5 kN/m^3 for the aquitard. The well is pumped at a constant rate of 1,000 m^3/d for a 100-day stress period.

A discharging well is installed through the column located at row 19 and column 19 into the confined aquifer in Layer 3. As indicated in (9) and (12), S_s requires three coefficients (σ_v, σ'_{v0} and z). The three parameters in each layer are calculated and listed in Table 2. The computation starts with running the program for steady flow first, then run it again for transient flow. Three values of the applied hydraulic diffusivity (= K_v/S_s) are 3,125, 6,250, and 12,500 m^2/day. Three pumping rates (500, 1,000, and 2,000 m^3/day) and aquifer depth (15.2, 30.2, and 60.2 m) are adopted to evaluate the displacement sensitivity by various parameters.

Four criteria factors are used in the Strongly Implicit Procedure (SIP) package in the MODFLOW for solution, and they are: 1. the error criterion is set at 0.001; 2. the acceleration parameter is 1.0; 3. the maximum number of iterations equals 50; 4. a seed of 0.001 is specified for use in calculating the iteration parameter.

RESULTS AND ANALYSIS

For purpose of comparison of the linear, exponential, hyperbolic models, subsidence in Layers 1 and 2 are displayed in Figures 2-A, and the cumulative subsidence of the three layers is presented in Figure 2-B. It shows that Layer 2 (5.3 m) near the confined aquifer is the largest contributor to the cumulative settlement per unit layer thickness at the land surface than Layer 1(30.2 m). This is because Layer 2 is located on the top of the confined aquifer from which groundwater is pumped out so Layer 2 experiences significant depressurization that results in larger increase in the effective stress and in turns causes large settlement.

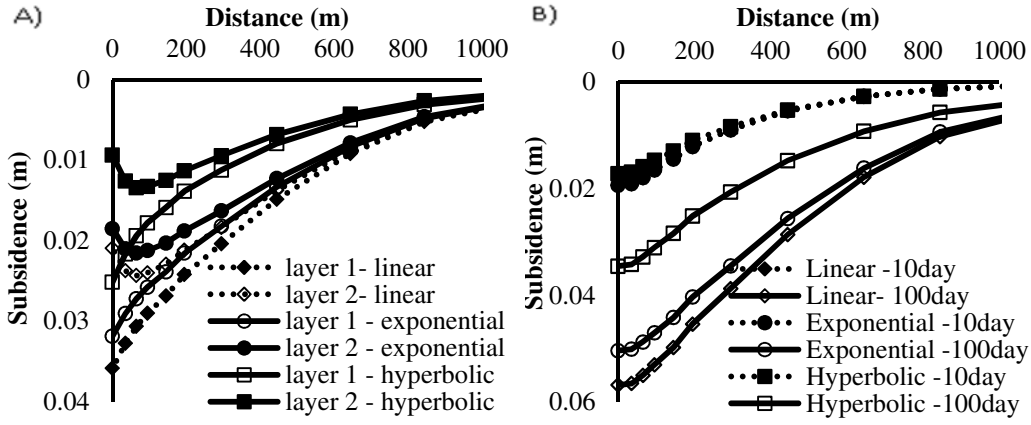

FIG. 2. A) Settlement at each layer, B) Cumulative subsidence

Figure 2-A also indicates in both Layers 1 and 2, the largest settlement takes place near the well and decreases quickly along radial distance. The peak displacements occurs at around 65m from the center of groundwater pumping well. In the vicinity of the pumping well, the displacement of solid matrix approaches zero because the well

screen is assumed to be permeable only to water, not to the solid grains. The well screen is designed to stop the grains from moving horizontally relative to the movement of the well bore. The inward moving grains will tend to accumulate in the surrounding area of the well and will form a compression zone around the well.

One may note that the results in Figures 2-A and 2-B show that both the individual and cumulative subsidence from a linear model is larger than that from nonlinear models, hyperbola subsidence is the smallest among the three models, and cumulative subsidence differences for each model are increasing by pumping time. The difference of results between the linear and nonlinear models can be explained by the specific storage coefficient in equations (9) and (12) that suggest that $S_s \leq S_0$ after the pump turns on (only when $t = t_0^+$, $S_s = S_0$). Therefore, subsidence in response to groundwater discharge using a linear model can be overestimated, particularly for a long term discharge with large pumpage. In contrast, the nonlinear models with consideration of material hardening may give more accurate results when compared to the linear model with a constant S_s. The exponential model reflects a lager displacement than the hyperbolic model does because of the latter has the stress-strain relation with an ultimate limit 1/b of volume compression. Figure 2-B also compares the result between pumping period of 10 day and 100 day for a pumping rate 1000 m^3/day. The aquifer vertical displacement after 10 day pumping reaches its value about 2 cm near the pumping well for all three models. In contrast, after 100 day pumping, the displacement at the same location is indicated as 5.7 cm, 5.0 cm and 3.5 cm for a linear, an exponential and a hyperbolic model, respectively. If the maximum subsidence predicted by a linear model using a given value of hydraulic diffusivity at a lower boundary is set as a reference, one can see how sensitive displacement is to the ratio K_v/S_s (hydraulic diffusivity).

Figure 3 shows that when $K_v/S_s > 6{,}000$ m^2/day, the slopes or the difference of sensitivity to subsidence between the linear and exponential models is insignificant. In contrast, when $K_v/S_s < 6{,}000$ m^2/day, the slope of the curve from the exponential model starts deviated from the linear model and both nonlinear models show slightly less sensitive to K_v/S_s than the linear model does. In general, the subsidence is significantly sensitive to hydraulic diffusivity for $K_v/S_s < 6{,}000$ m^2/day when compared to $K_v/S_s > 6{,}000$ m^2/day for all three models. The subsidence from the linear model seems more sensitive than that from the two nonlinear models according to Figure 3.

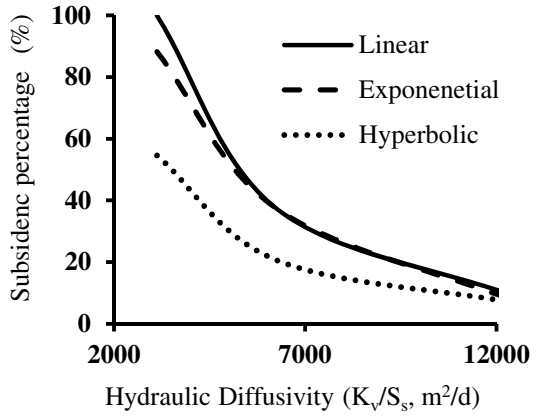

FIG. 3. Subsidence vs. hydraulic diffusivity

Additional analysis is carried out for different pumping rate (500, 1,000, and 2,000 m^3/day) and aquifer depth (at 15.2, 30.2, and 60.2 m) so that the model sensitivity to various parameters can be estimated. It is interesting to note that Figure 4-A displays

that the nonlinear models are less sensitive to changes in pumping rates than the linear model is. Moreover, Figure 4-B shows that the straight line has a larger slope for a linear model than a nonlinear model (the exponential or hyperbolic model), which means the linear model is more sensitive to changes in aquifer thickness than the nonlinear one. Figure 4 also exhibits that increasing pumping rate induces larger settlement. In contrast, increasing aquifer thickness (Layer 3) reduces the settlement at the given location.

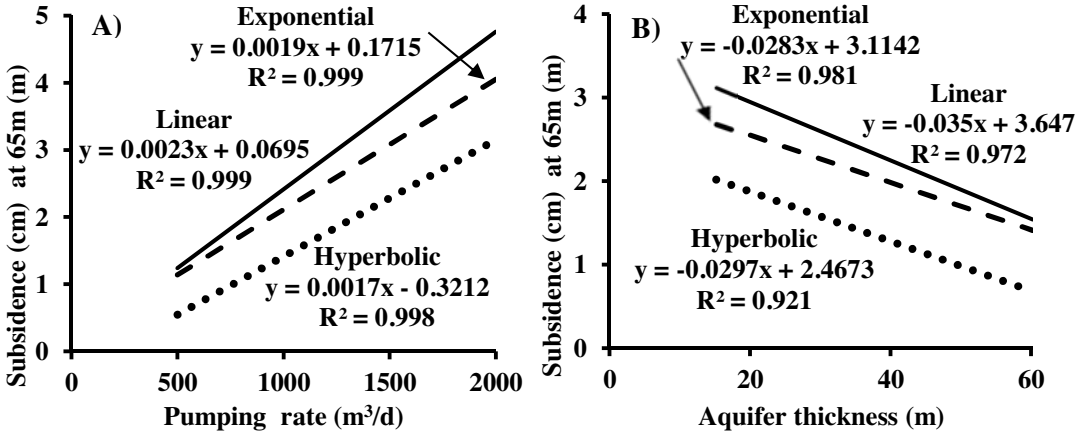

FIG. 4. A) Deformation vs. pumpage, B) Displacement vs. aquifer thickness (in Layer 3) at 65 m from the centre of the well

SUMMARY AND CONCLUSION

Summary and conclusions of this paper are given below:

1. A new hyperbolic model for volume stress-strain relationship has been introduced, which is essential for soils with a strong strain-hardening behavior that cannot be appropriately described by an exponential model. The stress or head dependent specific storage coefficient has been developed
2. A new module for the hyperbolic model has been developed. In fact, both the linear and two nonlinear models were embedded in MODFLOW-96 that was modified to simulate the 3-D land movements.
3. A conceptual model established comprises a pumping well, an aquitard and two aquifers in a basin-wide scale for the numerical simulation with 4,107 elements.
4. Comparison of a linear model to two nonlinear models (i.e., exponential and hyperbolic models) has been carried out. The results from simulation indicate that a linear model may produce a higher velocity and larger displacement than that of the two nonlinear models do. This suggests that the magnitude of land subsidence predicted by a linear model is likely overestimated when compared to that done by a nonlinear model, particularly for a long pumping period. Furthermore, the exponential mode results in a larger aquifer deformation than the hyperbolic model does.

5. Sensitivity analysis for hydraulic diffusivity shows that displacement decreases with an increasing hydraulic conductivity (K_v/S_s). A higher hydraulic conductivity imposes a quicker hydraulic response to any external load. Sensitivity analysis for pumping rates and aquifer thickness indicates that a linear model is more sensitive to both the changes in pumping rates and aquifer thickness than the two nonlinear models are.

ACKNOWLEDGMENTS

The research and writing this paper were supported by US Department of Energy under the contract DE-NA0000720 through the program of S.P. Massie Chair of Excellence in Environmental Disciplines.

REFERENCES

Gersevanov, N.M. (1934). "The foundation of dynamics of soils (in Russian)." Leningrad: Stroiizdat.

Helm, D.C. (1979). “A postulated relation between granular movement and Darcy’s law for transient flow." *Evaluation and Prediction of Subsidence*, S.K. Saxena, ed., ASCE, NY, 417-440.

Helm, D.C. (1984). “Analysis of sedimentary skeletal deformation in a confined aquifer and the resulting drawdown.” Rosenshein, J.S. and Bennett, G.D., ed., *Groundwater Hydraulic*.

Helm, D.C. (1994). “Horizontal aquifer movement in a Theis-Thiem confined aquifer system.” *Water Resources Research*, 30, 953-964.

Hubbert, M.K. (1940). "The theory of ground-water motion." *J. Geol*., 48(8), 785-944.

Li, J. and Ding, D. (2013) “Modeling 3D land movement due to groundwater pumping with a variable parameter.” *Global View of Engineering Geology and the Environment,* Beijing, China, 457-462.

McDonald, M.G. and A.W. Harbaugh, (1988). “A modular three-dimensional finite-difference ground-water flow model.” *Techniques of Water-Resources Investigations of the USGS*: Chapter A1, Book 6, USGS.

Poland, J.F. (1984). “Guidebook to studies of land subsidence due to ground-water withdrawal.” UNESCO Studies and Reports in Hydrology no. 40. New York: Unipublications.

Sheng, Z., D.C. Helm, and J. Li, 2003, Mechanisms of earth fissuring caused by groundwater withdrawal, Environmental and Engineering Geoscience, 9(4) 351-362.

Terzaghi, K. (1925). “Settlement and consolidation of clay.” *Eng*. *News, Rec*. 95, 874-878.

Todd, D.K. and Mays, L.W. (2005). "Groundwater Hydrology.” Third edition, John Wiley & Sons, Inc.

Zhang, L. (2009). “A model for transient three-dimensional underground deformation response to groundwater pumpage.” Doctoral Dissertation of Morgan State University.

Baseline Water Quality Monitoring Prior to Hydraulic Fracturing to Promote Scientifically-Based Transparency

George Mathes[1], P.E, Carly Sowecke[2], P.G., Cherrie Nelson[3], REM/CSEM, Marjorie Bedessem[4], Ph.D., P.E., Dan Hruska, P.E.[5]

[1]Vice President, Trihydro Corporation, 1252 Commerce Dr., Laramie, WY 82072 U.S.A, E-mail: gmathes@trihydro.com
[2]Geologist, Trihydro Corporation, 1252 Commerce Dr., Laramie, WY 82072 U.S.A, E-mail: csowecke@trihydro.com
[3]Environmental Scientist, Trihydro Corporation, 1252 Commerce Dr., Laramie, WY 82072 U.S.A, E-mail: cnelson@trihydro.com
[4]SeniorEngineer, Trihydro Corporation, 1252 Commerce Dr., Laramie, WY 82072 U.S.A, E-mail: mbedessem@trihydro.com
[5]Engineer, Trihydro Corporation, 1252 Commerce Dr., Laramie, WY 82072 U.S.A,, E-mail: dhruska@trihydro.com

ABSTRACT: Oil and gas industry leaders, stakeholders, and regulatory agencies understand the importance of protecting groundwater resources. Many oil and gas companies proactively engage in voluntary groundwater sampling both prior to and after hydraulic fracturing (fracing) events to document groundwater conditions, promote scientifically-based transparency, and ensure that public health is not impacted as a result of development operations. These baseline water quality (BWQ) programs have tremendous potential for promoting mutual understanding, collaboration, and "win-win" development of oil and gas resources. A BWQ program often involves sampling water sources before drilling commences and after the drilling and fracing process is complete. Water samples are analyzed for chemical constituents that occur naturally within aquifers, as well as constituents related to oil and gas activities. Techniques for analyzing total petroleum hydrocarbons (TPH) can determine if low level TPH detections are related to oil and gas activity or if the detections are due to naturally occurring carbon sources. If methane is present in the water samples, methane isotopic analysis may be performed to determine the provenance of the gas. Statistical analyses can be utilized to further interpret the results of the BWQ and draw conclusions with regard to overall significance.

INTRODUCTION

Advances in drilling technology, including the use of horizontal drilling and hydraulic fracturing (fracing), have led to a resurgence in domestic petroleum production. The combined use of these technologies enables oil and gas companies to drill and produce hydrocarbons from low-permeability shale and tight sand

formations which previously were not economically viable. The expansion of oil and gas production activities into new areas has raised concerns about the potential for environmental and health impacts. One of the primary concerns is the potential effect that horizontal drilling and fracing could have on groundwater resources, including public and private water supply wells.

In response to these concerns, states such as Colorado, Montana, New York, Ohio, Pennsylvania, and Wyoming, have promulgated regulations, recommendations, or programs for baseline water quality (BWQ) monitoring of existing water wells. Water wells are sampled in the vicinity of the proposed oil and gas wells, prior to drilling, in order to characterize the general water quality. Colorado and Ohio recently increased the required number of water wells to sample, expanded the radius of the water well search, and increased the laboratory parameter list and/or the quantity or frequency of sampling. Several states including Colorado, New York, and Wyoming now require or recommend ongoing groundwater monitoring activities after the drilling and fracing activities are complete (Colorado State 2013, Ohio State 2013, New York State 2013, Wyoming State 2013).

A properly designed BWQ monitoring program will provide data that can be analyzed to identify spatial and temporal trends in groundwater quality within a region; including naturally occurring changes and/or variability of groundwater quality within an aquifer. BWQ data can provide a statistical basis to calculate predictive levels which are used to identify potential changes to water quality associated with anthropogenic activities such as oil and gas production, agriculture, urbanization, and industry. This BWQ data can also be used in conjunction with a timeline of events to validate complaints from stakeholders, evaluate root cause, and determine if additional assessment is necessary to characterize a situation. For example, it is fairly common to detect methane in groundwater samples collected from wells. However, methane originates from both biogenic sources (bacterial activity) and thermogenic sources (hydrocarbons subjected to high temperature and pressure). Further laboratory analysis must be completed to determine the origin of the methane.

GROUNDWATER VARIABILITY AND SAMPLING CONSIDERATIONS

Not all changes in water quality are caused by anthropogenic activities. Natural changes or variations in water quality are caused by a number of environmental factors including groundwater depth, (e.g. residence time), type of aquifer (e.g., sandstone, limestone, basalt, etc.), origin of groundwater (surface water, rainwater, stream loss, etc.), the flow regime, climate, and seasonal changes.

The type and concentration of dissolved constituents present in groundwater may vary dramatically from well to well as a result of the respective groundwater being in contact with different geologic materials (chemical composition or solubility), having been in contact with the aquifer minerals for significantly different periods of time (residence time), or localized fracture interconnectedness. Comparing groundwater from different regions indicates that climate influences groundwater characteristics. In addition, seasonal variations in water quality from a single well have been observed in association with changes to the chemical state of the groundwater, (i.e.,

temperature, pH, and oxidizing-reducing potential). These parameters influence the amount and character of the dissolved constituents which can then produce changes in the types of bacteria present as well as the taste, odor, and appearance of the water.

Changes in the chemical state of the water within an aquifer can also be caused by different water levels and annual recharge events (Fetter 1980). Table 1 illustrates typical natural water compositions for various types of water including rainwater, seawater, groundwater in different types of aquifers, and groundwater that has been in contact with the aquifer for different periods of time (Hem 1989).

Table 1. Natural Water Compositions for Different Water Types

Location	Milwaukee County, Wisconsin	Grand Canyon, Arizona	Umatilla County, Oregon	Richland County, Montana
Water Source	Water Well	Spring	Water Well	Water Well
Water Bearing Formation	Niagara Dolomite	Limestone in Supai Formation	Basalt in Columbia River Group	Fort Union Fm. (sandstone/shale)
Feet Below Ground Surface	500	Not Applicable	761	500
Calcium (mg/L)	33	6.5	32	3
Magnesium (mg/L)	28	1.1	12	7.4
Bicarbonate (mg/L)	241	77	220	2080
Sulfate (mg/L)	88	15	11	1.6
Chloride (mg/L)	1	17	7.9	71
Nitrate (mg/L)	1.2	0.4	2.9	0.2
Hardness as CaCO3 (mg/L)	224	20	129	38
Specific Conductance (MilliSiemens)	511	167	358	2960
Total Dissolved Solids	326	222	225	2060
pH (unit)	8.2	6.7	7.4	8.3

Mg/L = milligrams/Liter
USGS, 1989

Not only is it important to understand natural variations in water quality within the aquifer, it is also important to consider the designated well use or type. Most state BWQ monitoring regulations require monitoring of wells permitted for specific designated water uses (e.g., domestic, stock, irrigation). It is optimal to sample the same well for ongoing monitoring even though a property owner may have several wells on their land. In addition, domestic wells are generally preferred for BWQ monitoring over stock or irrigation wells since the goal of the BWQ is protecting

human health. Stock and irrigation wells are often completed in shallow aquifers which may contain higher concentrations of specific ions and total dissolved solids than is allowed for human consumption because livestock and agriculture can tolerate higher levels of these constituents (Hem 1989).

Additional factors to consider during the well selection process may include other potential sources of contaminants, the groundwater flow direction, well design, condition, and history (e.g., date and quality of construction, maintenance, power requirements etc.), and accessibility. Gathering as much information about the well as possible including construction techniques and construction materials, total depth, screened depth, piping, storage systems, treatment systems, etc., can help with evaluating possible man-made sources of variability and impacts associated with a particular well.

Typical BWQ programs include a variety of analytes, including but not limited to cations, anions, general parameters, bacteria, organic constituents, glycols, and alcohols. Many states are now requiring BWQ analysis prior to drilling as previously mentioned. While the states' required analyte list varies, a characteristic list may include the following analytes: pH, specific conductance, temperature, oxidation-reduction potential, turbidity, dissolved oxygen, total dissolved solids, dissolved gases (methane, ethane, propane), alkalinity, bromide, chloride, fluoride, sulfate, nitrate and nitrite as N, phosphorus, calcium, iron, magnesium, manganese, potassium, sodium, barium, boron, selenium and strontium, presence of bacteria (iron related, sulfate reducing, and slime forming), diesel range organics (DRO), gasoline range organics (GRO), oil range organics (ORO), benzene, toluene, ethylbenzene, xylenes, and naphthalene. Field observations such as odor, water color, sediment, bubbles, and effervescence may also be required.

In some BWQ sampling programs, operators choose to include constituents contained in their drilling fluids or hydraulic fracturing fluids and are specific to their drilling program. Such examples of these additions may include: glycols, alcohols, aldehydes, and/or semi-volatile organic compounds.

While designing and implementing a BWQ monitoring program, it is important to consider natural variation of the groundwater, type and history of the water well, and regional groundwater characteristics. Furthermore, it is essential to be consistent with sample collection methods, sample analysis methods, and process for selecting water wells for BWQ monitoring programs.

TECHNICAL METHODS

If the laboratory results indicate the presence of any anomalous, higher-than-background, or operator-sensitive constituents in a groundwater sample, a variety of technical methods are available characterize the constituents reported in the sample. For example, DRO and GRO are organic constituents not normally detected in groundwater. Methane, due to heightened media coverage of oil and gas drilling activities, has become a public awareness issue and may be an operator-sensitive constituent. Methods that may further characterize these constituents if detected in a groundwater include the following:

- Massachusetts Department of Environmental Protection (MDHE) method for the determination of mass extractable petroleum hydrocarbons with presumptive certainty by GC/FID (MAEPH)
- MDHE method for the determination of mass volatile petroleum hydrocarbons with presumptive certainty by GC/FID-PID (MAVPH) (MDEP, 2004)
- Silica gel clean up
- Methane isotopic analysis

A brief summary of each analytical method is provided in the following sections.

MAEPH/MAVPH and Silica Gel Cleanup for GRO/DRO Analysis

Although GRO and DRO are constituents which are not typically present in groundwater, operators often include these analytes in the BWQ analytical suite as a safeguard against future complaints, as well as a marker or indicator of changes to the water quality. Generally, GRO is defined as having a carbon range of C4 to C12 and the carbon range for DRO is from C8 to C26. The higher carbon chains (typically above C26) can be defined as ORO or residual range organics (RRO) ranging from C20 to C45. When GRO, DRO, ORO/RRO are combined, they are referred to as "total petroleum hydrocarbons" (TPH).

Laboratory analytical method 8015B is commonly used for analyzing GRO/DRO in water, though this method does not specifically differentiate between hydrocarbons and non-hydrocarbons; the method analyzes all naturally occurring organic matter that falls within the same carbon range. To determine if a sample contains hydrocarbons possibly related to oil and gas production activities, it is necessary to use an analytical method that can separate non-hydrocarbon molecules from hydrocarbon molecules.

There are two types of hydrocarbon molecules: aliphatic (chain structure) and aromatic (ring structure). Analytical method MAEPH/VPH uses both flame ionization and photoionization detection to differentiate between aliphatic and aromatic structures by specifically fractioning out and reporting concentrations of C5-C8 aliphatics, C9-C12 aliphatics, and C9-C10 aromatics. The MAEPH/EPH method is used to separate out C9-C18 aliphatics, C19-C36 aliphatics, and C11-C22 aromatics. The relative concentrations of these different carbon ranges and aliphatic/aromatic structures are evaluated to identify and separate the hydrocarbon species.

The silica gel clean-up method utilizes the properties of the petroleum hydrocarbon structure to separate the polar, or naturally occurring organics, from non-polar, or petroleum-related constituents (ADEC, 2006; BCME, 2004). The silica gel clean-up method only works for extracted TPH fractions, the heavier end of the carbon ranges such as DRO. The silica gel is applied to the sample and the polar components are removed. Typically, these naturally occurring organic components can include leaves, pine needles, roots, animal fats, lignins, tannins, etc. If the sample consists of the lighter end organics (GRO fraction), then the sample can be prepared using the purge and trap method.

Methane Isotopic Analysis

Methane can be divided into two categories: gas with a thermogenic origin or gas with a biogenic origin. Thermogenic gas is derived from deeply buried organic matter that has been subjected to high temperatures and pressures occurring over a geologic time scale. Biogenic gas is derived from shallow microbial processes, typically associated with decomposition of organic matter (Pierce and LaFountain, 2000). Methane isotopic analysis is commonly used to fingerprint the dissolved gas concentration in water using the relative ratios of carbon isotopes and hydrogen isotopes—e.g. determining if the gas is thermogenic or biogenic in origin. Often, the thermogenic gas is associated with oil and gas development and the biogenic gas is associated with shallow microbial activity not attributed to oil and gas development.

Although methane can be divided into two isotopic categories, methane molecules are comprised of one carbon atom and four hydrogen atoms (Pierce and LaFounain, 2000). Carbon has two naturally occurring stable isotopes: ^{12}C and ^{13}C. Bacteria prefer to use ^{12}C, the lighter isotope with 6 protons and 6 neutrons (Chanton et al., 2005). Similarly, hydrogen has two naturally occurring stable isotopes, protium and deuterium, with deuterium as the heavier isotope. Therefore, methane produced by bacteria through anaerobic respiration is depleted in the heavier ^{13}C and deuterium isotopes and has a different fingerprint, or signature, compared to more thermally mature methane (Coleman et al., 1981). Using these chemical properties, scientists can plot and compare the ratios of these two elements' isotopes to determine the methane provenance as biogenic or thermogenic.

Figure 1 plots these data points in typical δ-notation (delta notation):

$$\delta = \left[\frac{R\ sample}{R\ standard} - 1\right] x\ 1000 \qquad (1)$$

R_{sample} refers to the ratio of $^{13}C/^{12}C$ or $^{2}H/^{1}H$ in the sample. $R_{standard}$ refers to the ratio of $^{13}C/^{12}C$ or $^{2}H/^{1}H$ in the standard. Delta notation is used because the rarer isotope (usually the heavier isotope) is difficult to measure with high precision. Therefore, instead of using the concentration of the isotope, laboratories compare the difference in concentration of the sample isotopes to a standard, thus delta notation. More positive values indicate that the sample has more of the rare isotope than the standard, and more negative values indicate that the sample has less of the rare isotope than the standard. Typically, laboratories use standard mean ocean water as the standard for the hydrogen isotope (Craig, 1961). For the carbon isotope, the Pee Dee Belemnite (PDB) is commonly used as a laboratory standard (Craig, 1957). The PDB is based on a Cretaceous marine fossil and has a high $^{13}C/^{12}C$ ratio, thus giving most naturally occurring material a more negative $\delta^{13}C$ value.

While plotting isotopes is useful, other studies report that these plots do not always reveal the true gas provenance and additional lines of evidence must be employed (Martini et al., 1998; Pierce and LaFountain, 2000). Information about the reservoir, geologic structures, history of oil and gas development, and isotopic composition of the target gas should be examined as well. The gas compositional analysis from the

water sample should be examined to determine if concentrations of heavier gases are present, such as ethane, propane, butane, or pentane. Researchers and scientists have used the ratio of methane/ethane or methane/(ethane+propane) as an additional tool to corroborate the presence or absence of thermogenic methane (Martini et al., 1998).

As an example, Figure 1 shows a plot of water samples collected within the Green River Basin and Big Horn Basin in Wyoming. Samples A, B, D, E, F, H, I, J, L, and M exhibit a carbon to deuterium ratio that falls in the "near-surface" microbial (i.e., biogenic) gas range. Samples C, G, K, and O exhibited a carbon to deuterium ratio that falls on the edge of the thermogenic gas range and exhibits a mixed isotopic signature. Sample N exhibits a mixed gas isotopic signature as it falls on the edge of the thermogenic and near-surface microbial ranges. Research has shown that coal seams may produce methane gas that has both a biogenic and thermogenic isotopic signature (Alleman, et al., 2005).

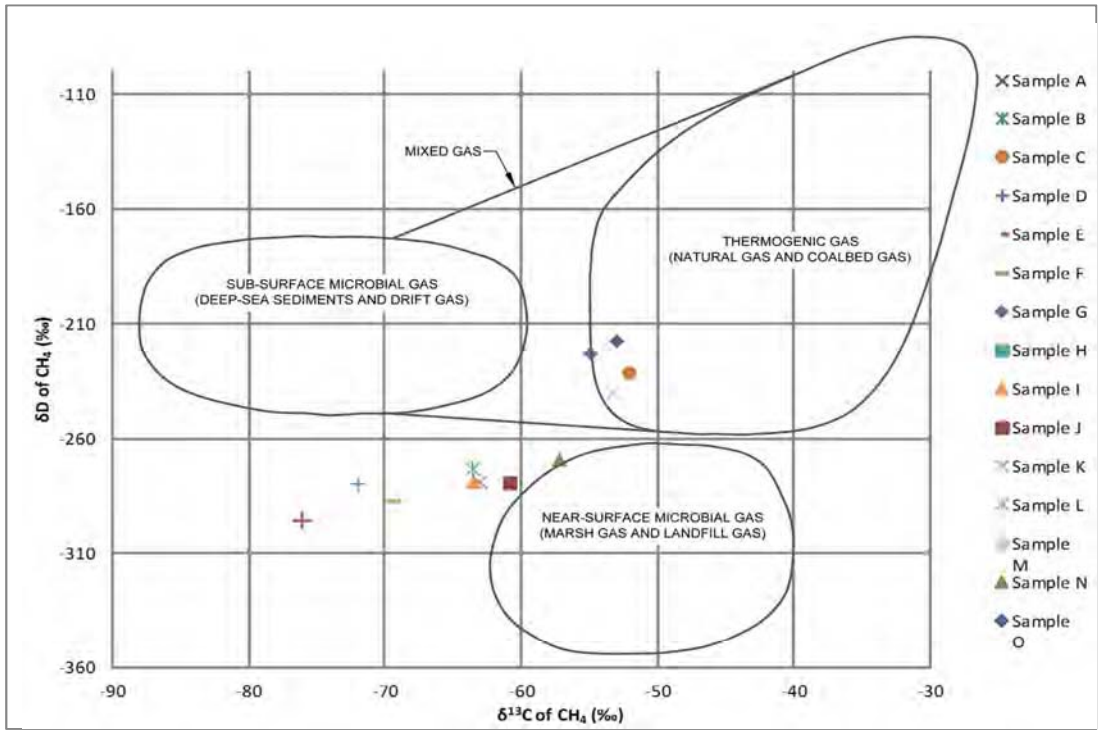

FIG 1. Methane Isotopic Data. Chemical analysis based on standards accurate to within 2%. Analysis is of gas extracted from water by headspace equilibration. Analysis has been corrected for helium added to create headspace. Gas groupings based on Coleman, 1995.

DATA ANALYSIS

Data analysis is an integral part of a BWQ sampling program. Thorough data analysis can help identify risks early in the process, track and monitor data, and

statistics can identify statistically significant data trends. Three common data evaluation and analysis tools are discussed below.

Comparison to Background and Seasonal Variations

Comparing data to previously published background levels is an important part of the data evaluation process. While BWQ is typically collected prior to oil and gas development, there may also be existing data from past studies that can serve as a background for ambient constituent concentrations.

Background levels for aquifers may be established by researching previously published literature from federal or state agencies, university data, or other background sample results from a nearby study area. Additionally, examining these data can illustrate a seasonal variation in sample results, proving useful when conducting sampling and/or monitoring over a period of years or months.

With many states now requiring BWQ sampling prior to oil and gas development, the need for technically sound BWQ data is becoming increasingly important. The Wyoming Oil and Gas Conservation Commission (WOGCC) recently promulgated a rule that requires operators to notify the WOGCC if any methane sample varies by more than 5.0 mg/L from any two consecutive sampling events. However, using available background data, a change in methane concentration may prove to be a natural variation in that aquifer. Additionally, seasonal changes and barometric pressure changes can vary widely over any given day, consequently affecting methane concentrations in groundwater (NDEQ, 2011).

Although several seasonally variable parameters may influence methane partitioning to groundwater, in the context of BWQ evaluation, barometric pressure is likely the most significant factor. The relationship between methane flux and barometric pressure is well-documented in a variety of settings (e.g. landfills, swamps, etc.; Xu et al., 2012). Methane flux to the atmosphere has been observed to have a strong inverse relationship with barometric pressure, the equilibrium kinetics of which dictate partitioned soluble methane concentrations proportionally decrease. Empirical observations of surface water have demonstrated an 18% increase in flux of methane per each millibar (mb) decrease in barometric pressure (Mattson and Likens, 1990). Methane flux has also been shown to vary significantly over very brief temporal scales coinciding with significant barometric pressure drops; variations of up to two orders of magnitude on a scale of minutes have been observed (Tokida et al., 2007).

Local barometric pressure varies both on a seasonal and daily basis. Casper, Wyoming, for example, has a July mean daily high barometric pressure of approximately 835 mb circa 8 am, and a mean daily low barometric pressure of approximately 831 mb circa 5 pm. By comparison, March has a mean daily high barometric pressure of approximately 830 mb circa 10 am, and a mean daily low circa 4 pm (WRDS 2008). Local barometric pressures can also acutely dip to below normal lows, often accompanying inclement weather. The dynamic relationship between methane and barometric pressure, under the correct site conditions, could contribute to enough soluble methane concentration variability to trigger further investigation thresholds, such as described with the aforementioned WOGCC rule.

Statistical Analysis

The purpose of collecting BWQ data is to establish a measure of the ambient constituent concentrations for a given area or aquifer, so that any effects of subsequent anthropogenic activities (e.g. oil and gas production) can be detected and quantified. These baseline concentrations are often referred to as "background" in that they are used as standards against which new sample data are compared, using a variety of statistical methods. Although some "published background" data are available, those values are typically generalized for a region and it is usually advisable to develop site-specific BWQ values that can account for specific localized geochemical influences, as well as seasonal effects.

In order to use statistics to compare data to background, it is necessary to ensure that the data meet certain requirements. There must be at least 6 to 8 samples in any data set that will be statistically evaluated, and those samples, if from the same well, must be temporally independent; that is, they must be sufficiently separated in time so as to reflect changes in groundwater that occur over time. In addition, it is necessary to confirm that the data meet specific quality requirements, i.e. that the laboratory used appropriate analysis methods and adhered to quality assurance and quality control procedures.

The first critical consideration in assembling a BWQ data set is to ensure that there are no trends in the data; i.e. that there is no statistically significant, ongoing increase or decrease in constituent concentration(s). One popular tool that is used to evaluate data for the presence of trends is the Mann-Kendall test; this test is not affected by extreme values and is independent of any data distribution requirements. On the other hand, linear regression is generally discouraged as a trend analysis tool, as it is very susceptible to influence by extreme values, and distribution of the data must be taken into account when developing the analysis algorithm. Data from each well are evaluated for trends independent of the other wells, and if a statistically significant trend is identified prior to commencement of fracing or other activities, the data (and that well) should be considered for exclusion from the baseline data set. Likewise, the concentrations from a given well, collected prior to commencement of activities requiring groundwater monitoring, should be absent of any discernible level shift.

The presence of seasonal effects in groundwater constituent concentrations is often best-identified graphically, by plotting data values against sampling date and evaluating the result for cyclical patterns; it should be noted that at least three full cycles-worth of data should be used to evaluate for seasonality. Seasonal effects can also be evaluated using the Kendall Seasonality test, but with either method, if seasonal effects are present, the data may need to be adjusted to account for them. Adjustment methods include reducing sample frequency and some numerical methods as described in the Unified Guidance (EPA 2009).

Once the baseline data set of at least 6 to 8 samples have been assembled and verified to be absent trends, level shifts, and seasonal effects, the data can be used to establish background "limits", against which subsequent sample concentrations are compared. Although several statistical limits exist, the prediction limit has emerged as a preferred method for detection monitoring in groundwater. The prediction limit

is designed to capture future values with a specified confidence, based on the preceding, or baseline, measured values, and incorporates a predetermined retesting strategy in the case of an exceedance. In other words, the baseline values are used to calculate a prediction limit, and when a sample value exceeds that limit, retests of one to three samples are used to verify that a change in groundwater quality has occurred. Similar to prediction limits are control charts which use the baseline data to create a limit against which new sample values are plotted. In both cases, if the new sample data do not exceed the limit, they are added to the baseline data - if their addition does not contribute to creating a trend in the baseline data set.

To summarize, baseline data sets, generally collected individually from each well, are used to statistically determine whether a change to groundwater quality has occurred. The data are used to determine whether constituent concentrations are increasing or decreasing and to calculate limits above which sample values are not expected to fall, except in the case of a change to groundwater quality. It is important to note that a single exceedance or multiple exceedances in a single well do not constitute proof that the activities of interest (e.g. oil and gas production) have impacted groundwater quality; these statistical tests require retesting to ensure their validity, and thorough exploration of potential contributing factors is prudent. The statistical tests discussed here and other methods related to statistical evaluation of groundwater data, not discussed in this document are presented in detail in the EPA Unified Guidance (EPA 2009) and in the forthcoming ITRC Groundwater Statistics and Monitoring Compliance guidance (ITRC 2014).

CONCLUSIONS

Domestic oil and gas exploration and production has increased over the last decade as a result of advanced drilling technologies and a desire for domestic energy autonomy. Accompanying the increase in domestic energy production, the United States has seen additional regulations and scrutiny of oil and gas extraction processes. These regulations have spurred the development of state BWQ and/or programs as a means for documenting water quality prior to oil and gas development. Many factors contribute to water quality in an aquifer including residence time, aquifer rock type, origin of groundwater, the flow regime, climate, and seasonal changes. Advanced analytical techniques may be utilized to determine if a detected constituent could be related to oil and gas activity. These techniques are useful in pre-drill sampling as well as post-drill sampling events and are intended to protect both the operator and the landowner. Statistical analysis should be utilized to establish statistically significant trends in data. Rules and regulations requiring BWQ are in the early stages of development, though they are already proving to be a useful tool in the oil and gas exploration and production process for both the producer and the stakeholder.

REFERENCES

Alaska Department of Environmental Conservation (ADEC), Division of Spill Prevention and Response, Contaminated Sites Remediation Program, 2006. Biogenic Interference and Silica Gel Cleanup. Technical Memorandum, 06-001. 5 p.

Alleman, D., Duda, J., Lagiovane, P. 2005. Coalbed Natural Gas. Strategic Center for Natural Gas and Oil, Policy Facts U.S. Department of Energy. www.netl.doe.gov/scngo

British Columbia Ministry of Environment, Lands and Parks (BCME), 2004. Analytical Method 10 for Contaminated Sites, Silica Gel Cleanup of Extractable Petroleum Hydrocarbons. Prepared pursuant to Section 53 of the Contaminated Sites Regulation under the Waste Management Act. 15 p.

Chanton, J., Chaser, L., Glasser, P., Siegel D. 2005. Carbon and Hydrogen Isotopic Effects in Microbial Methane from Terrestrial Environments. Chapter 6 in Stable Isotopes and Bioshphere-Atmosphere Interactions, Processes and Biological Controls Eds. Flanagan, L., Ehleringer, J., and Pataki, D. Elsevier Academic Press, Great Britian. p. 86-101.

Coleman, D., Risatte J., Schoell, M., 1981. Fractionation of carbon and hydrogen isotopes by methane-oxidizing bacteria. Geochim Cosmochim Acta 45: 1033-1037.

Coleman, D., 1995. Advanced in the Use of Geochemical Fingerprinting for Gas Identification. Presented at the American Gas Association Conference in San Francisco, California and at the Society of Petroleum Engineers Continuing Education Seminar "Engineering Applications for Michigan" Mt. Pleasant, Michigan. 9 p.

Colorado State. 2013. Colorado Oil and Gas Conservation Commission Rules and Regulations, Sections 318 and 609.

Craig, H., 1957. Isotopic standards for carbon and oxygen and correction factors for mass spectrometric analysis of carbon dioxide. *Geochim. Cosmochim. Acta 12,* 133-149.

Craig, H., 1961. Standard for reporting concentrations of deuterium and oxygen-18 in natural waters. Science 133, 1833-1834.

Fetter, C.W. 1980. Applied Hydrogeology. Columbus (OH): Charles E. Merrill Publishing Company. 488 p.

Hem, John D. 1989. Study and Interpretation of the Chemical Characteristics of Natural Water. Washington: United State Geological Survey. 236 p.

ITRC 2014, Groundwater Statistics and Monitoring Compliance, to be released 2014

Water Resources Data System (WRDS) <http://www.wrds.uwyo.edu/sco/climateatlas/pressure.html> Accessed 11/13/2013

Mattson, M. and Likens, G., 1990, Air Pressure and Methane Fluxes, Nature, v. 347, p. 718-719

Martini, A., Walter, L., Budai, J., Ku, T., Kaiser, C., SChoell, M., 1998. Genetic and temporal relations between formation waters and biogenic methane: Upper Devonian Antrim Shale, Michigan Basin, USA. Geochimica et Cosmochimica Acta, v. 62, Issue 10, p. 1699-1720.

New York State. 2011 Revised Draft Supplemental Generic Environmental Impact Statement SGEIS on the Oil, Gas and Solution Mining Regulatory Program

Ohio State. 2013. 129th General Assembly Amended Substitute Senate Bill Number 315; Sec. 1509.06.

Ohio State. 2013. 129th General Assembly Amended Substitute Senate Bill Number 315; Sec. 1509.06.

Pierce, J., and LaFountain, L., 2000. Application of Advanced Characterization Techniques for Identification of Thermogenic and Biogenic Gases. SCS Engineers Presentation. <http://www.scsengineers.com/Papers/Application_of_Advanced_Characterization_Technicques_Pierce_LaFountain.pdf>

Xu, L., Amen, J., Lin, X., Welding, K., 2012, Impact of Changes in Barometric Pressure on Landfill Methane Emission, 2012 Global Waste Symposium, Phoenix Arizona, 6 p. <http://www.wastesymposium.com/gws2012/CUSTOM/Uploads/XuLiukangFinalAb12.pdf>

Wyoming State. Wyoming Oil and Gas Conservation Commission Rules and Regulations Chapter 3, Section 46

Feasibility of Using Brackish Groundwater Desalination Concentrate as Hydraulic Fracturing Fluid in the Eagle Ford Shale

Nima Ghahremani[1] and Lee Clapp[2], Ph.D., P.E.

[1]Doctoral Candidate, Texas A&M University-Kingsville, Department of Environmental Engineering, 917 W. Avenue B, Kingsville, TX, 78363, U.S.A., nima.ghahremani@tamuk.students.edu.
[2]Associate Professor, Texas A&M University-Kingsville, Department of Environmental Engineering, 917 W. Avenue B, Kingsville, TX, 78363, U.S.A., lee.clapp@tamuk.edu.

ABSTRACT: Recent estimates predict over 20,000 wells will be drilled for hydraulic fracturing in the Eagle Ford Shale over the next 15 years, accounting for approximately 5-7% of the total water use within the main 16-county area, and as high as 89% in one rural county. Since each well requires about 10000-25000 m^3 of water, there is significant concern about fresh water consumption in drought-stricken South Texas. Hence, development of the Eagle Ford Shale will require water management strategies that maximize use of non-potable water. The main objective of this study is to evaluate the feasibility of using reject concentrate streams from groundwater RO desalination plants located within the Eagle Ford Shale region as hydraulic fracturing fluid. This could have two synergistic advantages: (1) elimination of brackish desalination concentrate discharges to surface waters, and (2) provision of a source of water for the oil and gas industry that does not consume freshwater supplies. This study will perform comprehensive chemical characterization of both an RO reject concentrate stream and hydraulic fracturing flowback water, and also will perform a geochemical modeling analysis to assess the down-hole scaling potential associated with the RO concentrate if used as hydraulic fracturing fluid in the Eagle Ford.

BACKGROUND

Fresh Water Use for Hydraulic Fracturing in Eagle Ford

Natural gas production in the Eagle Ford Shale is projected to last well past 2050, and natural gas will replace coal as the largest source of U.S. electricity by 2040, contributing to energy-related carbon emissions in the U.S. remaining below 2005 levels through 2040 (U.S. EIA, 2013).Water is a key factor in the development of the oil and gas industry in Texas. For example, recent estimates predict that over the next 15 years between 20,000 and 30,000 wells will be drilled for hydraulic fracturing in the Eagle Ford Shale, and that each of these wells will require 10000-25000 m^3 of water. Overall, it is estimated that the water utilization for development of the Eagle Ford

Shale will account for approximately 5-7% of the total water use (including agricultural, industrial, and municipal) within the main 16-county area (Jester, 2011). Unfortunately, the Eagle Ford Shale boom has coincided with severe drought in Texas. For example, 2010-2011 was the most intense one-year drought in Texas since at least 1985 when statewide weather records began (Nielsen-Gammon, 2011). Thousands of Texas farmers, including those in Matagorda County, did not receive water for irrigation this year because lakes and rivers remain low after more than a year of drought (Washington Post, 2012). A recent study determined that if Texas were to experience drought of record conditions, available sources of fresh water would not meet residential, industrial and agricultural demands (Ward, 2011). Of 11,634 shale wells in Texas in 2013, 5,891 (51%) were in high or extremely high water stress areas ("extremely high water stress" means over 80 percent of available water is already being withdrawn for municipal, industrial and agricultural purposes) (Freyman and Salmon, 2013). It is thus not surprising that the Texas legislature is pursuing measures such as mandatory flowback water recycling requirements (Boman, 2013), while the Texas Railroad Commission recently changed permitting requirements to make it easier to treat and recycle flowback water (TRC, 2013).

Although hydraulic fracturing operations have been estimated as having consumed less than 3% of the total annual water supply in the Dallas-Fort Worth area (Fry *et al.,* 2012), a recent study projected that hydraulic fracturing operations in the Eagle Ford Shale could be as high as 89% of the total annual water consumption in La Salle County by 2019 (Nicot and Scanlon, 2012). This indicates that freshwater consumption by the oil and gas industry could significantly compete with other uses, particularly if drought conditions persist. This concern is especially relevant in the Eagle Ford Shale, where fresh surface water is scarce and fresh groundwater from the Corrizo-Wilcox aquifer has a limited yield (Hanson, 2009).

The development of shale gas formations has realized a secure natural gas supply for decades to come. However, to minimize competition between the oil and gas industry and other users for fresh water resources in draught stricken regions like South Texas, non-potable water supplies – particularly brackish water – should be substituted for freshwater for hydraulic fracturing operations whenever possible. Although data related to water use for shale energy extraction is improving (FracFocus, 2013), information about the sources of water used, amount of water withdrawn from each source, and the volume and quality of flowback and produced water returned to the surface is sparse (Freyman and Salmon, 2013). While flowback recycling rates are estimated to be as high as 40% in the Marcellus Shale (Lutz *et al.,* 2013), recycling rates in the Eagle Ford remain at below 5%. However, use of saline water for hydraulic fracturing in the Eagle Ford Shale was estimated to be about 20% (Nicot *et al.,* 2012).

Brackish Groundwater in the Eagle Ford Shale Region

Although fresh groundwater resources are limited in Texas, the State has significant brackish groundwater resources (defined as between 1,000 and 10,000 mg/L of total dissolved solids). The largest amount of brackish groundwater (514 billion m^3) in Texas is present in the Region L (South Central Texas) water planning region, and

most of this (113 billion m^3) has a TDS of less than 3,000 mg/L (Kalaswad *et al*., 2004). Region L also contains ten counties at the center of the Eagle Ford Shale activity (i.e., Atascosa, DeWitt, Dimmit, Frio, Goliad, Gonzales, Karnes, La Salle, Wilson and Zavala). The productivity of the Corrizo-Wilcox aquifer, one of the best potential sources of brackish groundwater in Texas, is high (where productivity is a relative measure of the ease at which groundwater can be produced from an aquifer). However, because depths to brackish groundwater may range from 900 to 1,800 meters, costs to produce brackish groundwater from the Corrizo-Wilcox are projected to be relatively high. The Goliad Coast aquifer, located at the southern end of Region L in Karnes and Goliad counties, also has high productivity and low production costs for brackish groundwater (LBG-Guyton, 2003).

In 2010, Region L had approximately 10 percent of the state's population, and it is projected that by 2060 its population will increase by 75 percent. The Region's water demands are projected to increase 32 percent during this time, with municipal water use constituting the greatest increase. In 2013, Region L faced water supply needs of 215 million m^3 per year, and by 2060 water needs are projected to increase to 164 m^3 per year and to be dominated by municipal water use. Recommended water management strategies for meeting the Region L water supply includes 16.5% desalination by 2060 (TWDB, 2012).

Desalination Concentrate Use for Hydraulic Fracturing

Although freshwater resources are currently predominantly used for hydraulic fracturing operations, freshwater resources in the Eagle Ford Shale region are scarce. However, there are abundant supplies of brackish groundwater in South Texas (Chowdhury and Mace, 2007). Moreover, there is general consensus within the oil and gas industry that alternatives to freshwater need to be developed in the face of uncertain drought conditions and regulatory environment; indeed, the API *Water Management Associated with Hydraulic Fracturing Manual* states that non-potable water should be used "whenever practicable" (API, 2010). The proposed study will evaluate some of the geochemical aspects that may affect the potential for using brackish groundwater desalination concentrate streams as hydraulic fracturing fluid. This concept has the advantage of reducing the consumption of freshwater for hydraulic fracturing while simultaneously providing desalination facilities with a low-cost, or even profit-making, alternative for concentrate disposal (Burnett and Bateman, 2012).

Although the availability of fresh surface water and groundwater in Texas has declined with increasing population, installed brackish desalination capacity has increased by 445% since 1999 (Ward, 2011). Consequently, brackish groundwater desalination is becoming an important "drought resistant" source of fresh water, especially in coastal areas where fresh groundwater availability is limited, and is projected to supply 11% of the "new" water supply in Texas by 2060 (Arroyo, 2011). Of particular interest, the San Antonio Water System (SAWS) plans to complete a full-scale 38000 m^3/day brackish groundwater desalination plant (with a 12500 m^3/day brine reject stream) in 2016. Current plans are to dispose of the saline

concentrate stream using deep injection wells located in southern Bexar County near the center of the Eagle Ford Shale, at a cost of millions of dollars (SAWS, 2012).

The primary environmental concern associated with desalination is concentrate disposal (UNEP, 2008; Gamboa & Clapp, 2012). One alternative for RO desalination concentrate disposal in Texas is to use it as hydraulic fracturing for hydraulic fracturing operations. This would have two synergistic advantages (1) elimination of desalination concentrate discharges to surface waters, (2) provision of a low-cost source of water for the oil and gas industry that does not consume freshwater supplies. The oil and gas industry is moving towards treatment and reuse of flow back water, largely because treatment-and-reuse strategies are economically competitive with current deep-well injection methods. However, flowback water typically constitutes only 20-40% of the injected fluid and consequently, even if 100% of the flowback water were treated and reused, there would still be need for significant volumes of supplemental water. Fortunately, frac water does not have to be fresh water; rather, the best water for fracturing is clean salt water with low concentrations of multivalent cations and bacteria. Recent studies have indicated that increasing the chloride concentration in fracturing water actually boosts gas production (Jenkins, 2012).

Other potential advantages of using desalination concentrate instead of, or in addition to, treated and recycled flowback water include: (1) lower TDS (~12,000 mg/L); (2) significantly less variability in overall water quality; (3) lower concentrations of problematic scale-forming ions like barium and strontium; (4) lower microbial and suspended solids concentrations due to desalination pretreatment steps (e.g., 5-μm cartridge filters); and possibly (5) residual scale inhibitor (added to the desalination feed water to prevent scale forming on the RO membranes).

A potential problem with using desalination concentrate for hydraulic fracturing fluid is that when high-salinity water (particularly with high multivalent cation concentrations) is injected into shale formations, it will interact with the host rock at the increased temperature and pressure, often resulting in scaling that can lead to formation damage and diminished gas recovery (Alotaibi and Nasr-El-Din, 2009; Burnett and Veil, 2004). Although calcite ($CaCO_3$) precipitation can be minimized through pH control, precipitation of gypsum ($CaSO_4$), barite ($BaSO_4$), celestite ($SrSO_4$) and other scale-forming minerals are much harder to control and can significantly decrease the hydraulic conductivity of shale formations during hydraulic fracturing operations (Blauch, 2010). In addition, injection of slick water fracturing fluids can potentially mobilize clayey materials and fines, which can also damage the formation (Nicot and Chowdhury, 2005). Unfortunately, commercially available chemical additives (e.g., friction reducers, surfactants, clay stabilizers, scale inhibitors, and biocides) do not all perform well in waters with high salinity, and particularly in waters with high divalent cations like calcium and magnesium.

To overcome the limitations of commercially available chemical additives when used with brackish water, chemical manufactures and service companies are developing high-brine tolerant additives). For example, Chesapeake Energy, Inc., has developed salt-tolerant friction reducers and cross-linked gels as part of their Green Frac® program (Chesapeake Energy, 2012). In some cases studies have found significant improvement of slick water treatments where high brine water is used in shale fracturing. For example, use of brackish water can eliminate the

necessity of adding 2% KCl as a clay stabilizer (Paktinat *et al*., 2011). However, due to the geological complexities of each shale formation, it is necessary to assess chemical additives on a case-by-case basis to avoid incompatibilities (e.g., hardness will affect various polyacrylamide friction reducers differently).

RESEARCH OBJECTIVES

The main research objective of this study is to investigate the feasibility of using brackish groundwater desalination concentrate streams as hydraulic fracturing fluid in the Eagle Ford Shale. This objective will be achieved by initially performing the following tasks:

1. Performing a comprehensive time-series chemical characterization of the concentrate stream from a brackish groundwater reverse osmosis (BWRO) desalination plant in the City of Kenedy in Karnes County, Texas;
2. Performing a thorough chemical characterization of frac flowback water generated from hydraulic fracturing operations in the Eagle Ford Shale in Karnes County.
3. Performing a geochemical modeling analysis (using the PHREEQC software package [Parkhurst, 2013]) to assess the down-hole scaling potential associated with: (i) the desalination concentrate alone, (ii) the frac flowback water alone (assuming it is treated to remove suspended solids, oil, and grease), and (iii) blended desalination concentrate and treated frac flowback water.

RESEARCH METHODS

Chemical Characterization of RO Concentrate

The City of Kenedy is the largest community in Karnes County, which is in the middle of the Eagle Ford Shale play. A brackish water reverse osmosis (BWRO) desalination plant was constructed on the south side of the city in 1995, and was expanded in 2005. It is currently operated by Veolia Water for the City of Kenedy. In 2007, actual permeate production was 2700 m^3/day and actual concentrate discharge was 1350 m^3/day. The facility discharges the concentrate through a pipe to the abandoned arm of Escondido Creek. A comprehensive chemical time-series characterization of the City of Kenedy RO reject concentrate stream will be performed for the water quality parameters listed below (under "Analytical Methods"). The research team is currently coordinating with Veolia Water and the City of Kenedy to set up a schedule for collecting concentrate samples once per month over a 12-month period.

Chemical Characterization of Flowback Water

Pioneer Natural Resources has a number of drilling permits in the Eagle Ford Shale located within a few kilometers from the BWRO desalination plant in Kenedy County (Fig. 1). Each one of these wells is expected to produce roughly 1900 m^3 of

flowback water. The research team is currently coordinating with Pioneer Natural Resources to set up a schedule for collecting hourly grab samples of flowback water over two days at a minimum of two hydraulic fracturing sites. The collected samples will be analyzed for the water quality parameters listed below (under "Analytical Methods") to characterize the quality of the flowback as a function of time.

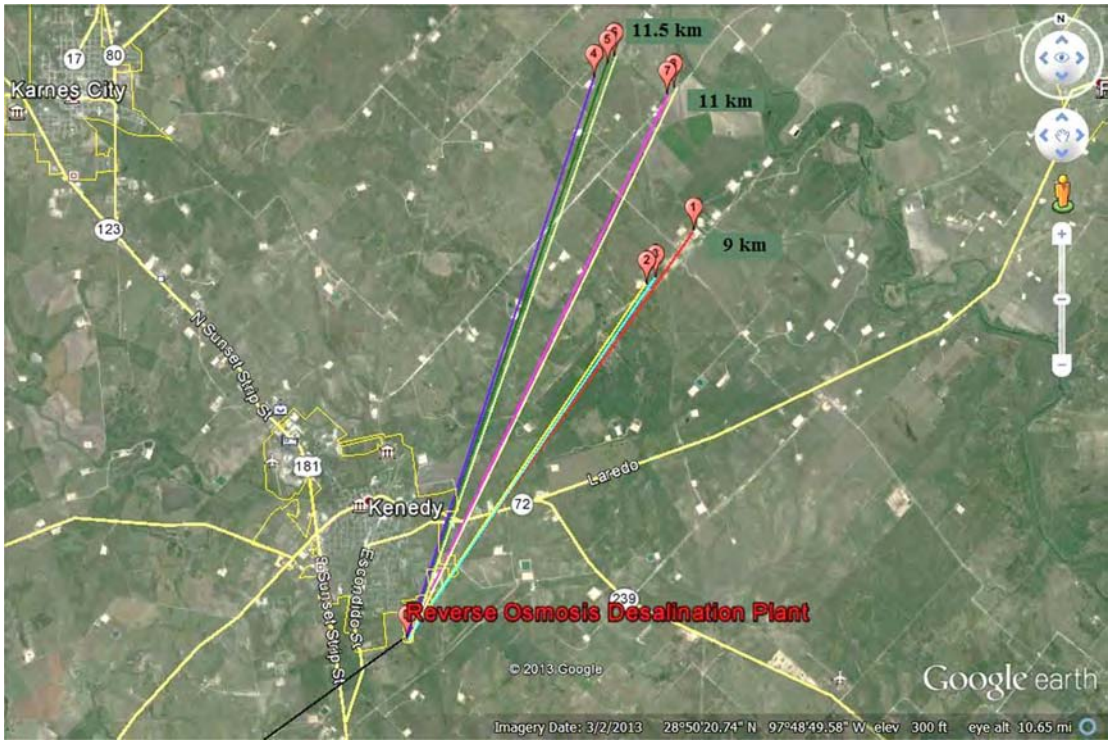

FIG. 1. Location of eight Pioneer Natural Resources drilling sites and their proximity to the brackish groundwater RO desalination plant in the City of Kenedy (Mineral Rights Forum, 2013). *Source:* "Kenedy, Texas." 28°50'20.74"N and 97°48'49.58"W. Google Earth. March 2, 2013.

Analytical Methods

The collected RO concentrate and flowback water samples will be analyzed for the following constituents:

- Dissolved oxygen (DO), pH, conductivity and temperature will be measured in the field (both at RO desalination plant and hydraulic fracturing sites) using a calibrated YSI 6920 Multi-parameter Water Quality Sonde.
- Alkalinity will be measured by titration with standardized H_2SO_4. Carbonate and bicarbonate concentrations will be calculated from the alkalinity and pH.
- Dissolved sulfide will be measured in the field using the methylene blue spectrophotometric method.

- The residual phosphonate-based antiscalant in the concentrate stream will be determined using ASTM Method D6501-09: *Standard Test Method for Phosphonate in Brines* (ASTM, 2013).
- Total dissolved solids (TDS) and total suspended solids (TSS) will be measured gravimetrically.
- An inductively coupled plasma – mass spectrometer (ICP-MS) will be used for dissolved cation analyses (Ca, Mg, Na, K, Fe, Ba, Sr, Si, As, B). Samples will be filtered through as 0.45-µm nylon filter and acidified to pH below 2 using nitric acid before analysis. Samples for total iron analysis will be prepared by dissolving the sample in 1 N H_2SO_4 before filtration.
- An ion chromatograph (IC) will be used for anion (Br^-, Cl^-, F^-, NO_3^-, SO_4^{2-}, and PO_4^{3-}) analyses. Samples will be filtered through as 0.45-µm nylon filter before analysis.
- Standard Methods 1020 and 1030 (APHA, 1998) will be followed to assure appropriate QA/QC methods are followed.

CONCLUSIONS

Using reject concentrate streams from groundwater RO desalination plants located within the Eagle Ford Shale region as hydraulic fracturing fluid could have two synergistic advantages: (1) elimination of brackish desalination concentrate discharges to surface waters, and (2) provision of a source of water for the oil and gas industry that does not consume freshwater supplies. This research will identify opportunities and obstacles for using brackish groundwater desalination concentrate for hydraulic fracturing operations. Lessons learned can be applied to other brackish water sources, including cooling tower blow down from refineries and power stations. It is also expected that the water characterization and subsequent geochemical modeling studies will complement ongoing frac water treatment research, and will contribute towards forging productive collaboration between the oil and gas industry, the industrial water treatment industry, municipalities and academia in South Texas.

ACKNOWLEDGMENTS

This research is supported through a grant from the Texas General Land Office's Coastal Impacts Technology Program (CITP), which is administered by the Houston Advanced Research Center (HARC), with additional seed funding from the Texas A&M University-Kingsville University Research Council.

REFERENCES

Alotaibi, M.B., and Nasr-El-Din, H.A. (2009). "Chemistry of injection water and its impact on gas recovery in carbonate and clastic formations." SPE paper 121565, presented at the *2009 SPE International Symposium on Oilfield Chemistry* held in The Woodlands, Texas, April 20-22, 2009.

American Petroleum Institute (API). (2010). *Water Management Associated with Hydraulic Fracturing*. API Guidance Document HF2, First Edition, June 2010.

American Public Health Association (APHA). 1992. *Standard Methods of Water and Wastewater*. 22nd ed. American Public Health Association, American Water Works Association, Water Environment Federation publication. APHA, Washington D.C.

ASTM International (2013). *Standard Test Method for Phosphonate in Brines (Method D6501-09)*.

Arroyo, J. *Desalination: Where Do We Go From Here?* Texas Water Development Board. Accessed from http://www.twdb.state.tx.us/innovativewater/desal/docs.asp on May 1, 2013.

Blauch, M.E. (2010). "Developing effective and environmentally suitable fracturing fluids using hydraulic flowback waters." SPE paper 131784, presented at the *SPE Unconventional Gas Conference,* Pittsburgh, PA, February 23-25, 2010.

Boman, K. (2013). "Legislation targets mandates for water recycling in oil, gas industry," *Rig Zone*, April issue.

Burnett, D.B., and Bateman, Z. (2012). *Hydraulic Fracturing and Brackish Groundwater Desalination: How Each Can Benefit from the Other*. Accessed from http://www.pe.tamu.edu/gpri-new/home/Publications.htm on May 1, 2012.

Burnett, D.B. and Veil, J.A. (2004). "Decision and Risk Analysis Study of the Injection of Desalination By-products into Oil- and Gas-Producing Zones." SPE paper 86526. Presented at *SPE Formation Damage Conference* held in Lafayette, LA, February 13-14.

Chesapeake Energy, Inc. (2012). "Green Frac." Accessed from www.chk.com on May 29, 2012.

Chowdhury, A. and Mace, R.E. (2007). *Groundwater Resource Evaluation and Availability Model of the Gulf Coast Aquifer in the Lower Rio Grande Valley of Texas*. Report 368, Texas Water Development Board.

FracFocus (2013). Accessed from http://www.fracfocusdata.org/ on December 21, 2013.

Freyman, M., Salmon, R. (2013). *Hydraulic Fracturing & Water Stress: Growing Competitive Pressures for Water*. Ceres, May 2013.

Fry, M., Hoeinghaus, D.J., Ponette-Gonzalez, Thompson, R., and La Point, T.W. (2012). "Fracking vs faucets: Balancing energy needs and water sustainability at urban frontiers." *Environmental Science & Technology,* 46: 7444-7445.

Gamboa, Y. and Clapp. L.W. (2012). "Characterization of brackish groundwater desalination concentrate discharge impacts on water quality in a Texas coastal area." (D. Ramirez, J. Ren, K. Jones, and H. Lamm, Eds.). In *Environmental Sustainability Issues in the South Texas – Mexico Border Region*. Springer.

Hanson, G.M. (2009). "Water: A natural resource critical for development of unconventional resource plays." *Transactions of the Gulf Coast Association of Geological Societies,* 59: 325-328.

Jenkins, S. 2012. "Frac water reuse." *Chemical Engineering,* February 2012, pp. 16-16.

Jester, S. (2011). *Eagle Ford Shale Water Supply and Demand*. Accessed from http://www.eaglefordshale.com/files/2011/11/Eagle-Ford-Water-Supply-and-Demand-10252011.pdf/ on March 7. 2012.

Kalaswad, S., B. Christian, & R. Petrossian (2004). *Brackish Groundwater in Texas*. Texas Water Development Board.

LBG-Guyton Associates. (2003). *Brackish Groundwater Manual for Texas Regional Water Planning Groups*. Prepared for the Texas Water Development Board, February, 2003.

Lutz, B.D., Lewis, A.N., Doyle, M.W. 2013. "Generation, transport, and disposal of wastewater associated with Marcellus Shale gas development." *Water Resources Research,* 49: 647-656.

Mineral Rights Forum (2013). "Permit Approved to Drill – 07/08/2013." Retrieved on-line from http://www.mineralrightsforum.com/group/eagle-ford-shale-karnes-county-tx/forum/topics/permit-approved-to-drill-07-08-2013 (last accessed on 7/15/13).

Nicot, J.-P., and Scanlon, B.R. (2012). "Water use for shale-gas production in Texas, U.S." *Environmental Science & Technology,* 46: 3580-3586.

Nicot, P.E.,J.-P., Reedy, R.C., Costley, R.A, Huang, Y. (2012). *Oil and Water Use in Texas: Update to the 2011 Mining Water Use Report*, Bureau of Economic Geology, Jackson School of Geosciences, University of Texas, Austin, September 2012.

Nicot, J.-P. and Chowdhury, A.H. (2005). "Disposal of brackish water concentrate into Depleted Oil and Gas Fields: A Texas Study." *Desalination,* 181: 61-74.

Nielsen-Gammon, J.W. (2011). *The 2011 Texas State Drought: A Briefing Packet for the Texas Legislature*. Texas State Climatologist, October 31, 2011.

NRS Consulting Engineers (2009). *Preliminary Engineering Assessment – Kenedy Brackish Desalination Plant, Karnes County, Texas*. Prepared for San Antonio River Authority.

Paktinat, J., O'Neil, B., Aften, C., and Hurd, M. (2011). "Critical evaluation of high brine tolerant additives used in shale slick water fracs." SPE paper 141356, presented at the *SPE Production and Operations Symposium*, Oklahoma City, OK, on March 27-29.

Parkhurst, D. (2013). *PHREEQC (Version 3)--A Computer Program for Speciation, Batch-Reaction, One-Dimensional Transport, and Inverse Geochemical Calculation*. Retrieved on-line from http://wwwbrr.cr.usgs.gov/projects/GWC_coupled/phreeqc/(last accessed on 7/14/13).

San Antonio Water System (SAWS). 2012. "Brackish Groundwater Desalination: Developing an Untapped Resource for the Benefit of the Entire Region." (Available from http://www.saws.org/Your_Water/WaterResources/projects/desal.cfm on November 4, 2012).

Texas Railroad Commission (TRC). (2013). *TRC Adopts New Hydraulic Fracturing Wastewater Rules*, Press release, March 26, 2013.

Texas Water Development Board (TWDB) (2012). *Water for Texas 2012 State Water Plan*. January, 2012.

United Nations Environmental Programme (UNEP). 2008. *Desalination: Resource and Guidance Manual for Environmental Impact Assessments*.

U.S. Energy Information Administration (U.S. EIA). (2013). *2014 Annual Energy Outlook – Early Release Overview*. Accessed from http://www.eia.gov/forecasts/aeo/er/index.cfm on December 21, 2013.

U.S. Geological Survey (USGS). 2011. *PHREEQC (Version 2) – A Computer Program for Speciation, Batch-Reaction, One-Dimensional Transport, and Inverse Geochemical Calculations*. Accessed from http://www.cpc.ncep.noaa.gov/products/Drought/ on March 7. 2012.

Ward, J.K. (2011). *Overview of TWDB's Brackish Groundwater Desalination Efforts*. Accessed from http://www.multi-statesalinitycoalition.com/summit-past/ on March 5, 2012.

Washington Post. 2012. "For first time, drought keeps thousands of Texas rice farmers from getting irrigation water." March 2.

Evolution of Best Management Practices and Water Treatment in High Volume Hydraulic Fracturing Operations

J. Daniel Arthur[1], P.E., SPEC, Brian Bohm[2], P.G., and Damian Zampogna[3], P.G.

[1]President/Chief Engineer, ALL Consulting, 1718 S. Cheyenne Ave., Tulsa, OK 74119, U.S.A., E-mail: darthur@all-llc.com.
[2] Professional Geologist, ALL Consulting, 1718 S. Cheyenne Ave., Tulsa, OK 74119, U.S.A., E-mail: bbohm@all-llc.com.
3 Professional Hydrogeologist, ALL Consulting, 1718 S. Cheyenne Ave., Tulsa, OK 74119, U.S.A., E-mail: dzampogna@all-llc.com.

ABSTRACT: Best water management practices (BMPs) and water treatment technologies in unconventional oil and gas development operations have been evolving since the late 1990s. That evolution underwent two major accelerations: the first started around 1999 when coal bed natural gas water production was climbing and disposal options in several western states was limited and the second started in 2005 with the growing adoption of high volume hydraulic fracturing (HVHF). Well drilling, completions and production operations of modern horizontal drilled unconventional plays require large volumes of water during the well lifecycle. The lifecycle cost of water alone for a Marcellus Shale well can exceed $1 million (Shauk 2012). Economic and environmental concerns have provided impetus for a "paradigm shift" toward the development of pre-planned water management programs that cover the full lifecycle of a field. The goal of such programs is to minimize fresh water use, optimize environmental and safety effects, and reduce costs. This paper will focus on trends in water management programs, water treatment technologies, and water best management practices.

INTRODUCTION

Best practices in water management are essential components of a cost-effective, environmentally friendly hydraulic fracturing program. In fact, industry and government work groups have set forth general best water management practices that have in some cases become part of the rapidly evolving regulations for high volume hydraulic fracturing (HVHF) operations (API n.d.). Lifecycle water planning and management for shale plays has expanded to include altering produced water for re-use, employing on-the-fly treatment technologies during completions jobs to reduce chemical loading, and conditioning recycled fluids by removing wastes that could impact completion activities. This paper looks at key aspects of produced water

management for HVHF projects and how best management practices (BMPs) are being applied to overcome water quality restrictions to facilitate re-use and recycling.

The production of shale gas has become economically viable through the adoption of two technologies: horizontal drilling and HVHF. Both of these processes utilize water as the source fluid for drilling mud and the carrier fluid for the proppant placed in the formation during the fracture job. The volume of water needed to drill and fracture a horizontal shale gas well generally ranges from about 2 million to 10 million gallons, depending on the formation characteristics. With potentially hundreds of wells to be drilled each year as development proceeds, these water demands can be significant; thus, water management issues associated with shale gas development impact operator's costs and can affect the ability to get permits.

Water management issues include more than identifying the volume of water needed, procuring that water, transporting it to the well pad, providing on-site storage, treating or conditioning the water as necessary, and eventually disposing of produced water; management must assess the potential for impacts from these activities. In addition to actual management of the water, there are public concerns of potential environmental and community impacts. These concerns can be directly related to water resources or more indirectly related to water management (e.g., potential traffic and roadway impacts that may result from the trucks used to haul water).

BASELINE WATER SAMPLING

Water management strategies are best formed through the use of historic data, current operations, and planned future development. Each of these strategies falls into the benchmarking process of establishing baseline conditions, an important practice for assessing how operations will evolve and affect future water demand. Baseline sampling ahead of development is critical to any post-development activity assessment and is also a crucial operational BMP for water treatment and for understanding how mixed waters in a re-use program may interact.

Establishing baseline water quality conditions before drilling is becoming standard industry practice to defend against groundwater or surface water contamination claims (Leatherbury and Denson 2012). Understanding the source of various chemical constituents that can be present in groundwater (including methane) can be complex. Water sampling establishes a snap shot of "Pre-Drill" water quality data that can also be applied to comprehend how source waters will interact with recycled water. Water sampling can also be used to "fingerprint" water sources and various water chemistry models can be used to evaluate scale tendency and other compatibility concerns related to the frac fluid being utilized in the job.

Some states are beginning to require baseline water sampling. For example, Ohio requires exploration and production (E&P) companies to collect water samples from water sources on properties that are within a 1,500-foot radius of a proposed well location prior to commencement of drilling (ODNR 2012). Colorado requires collection of baseline surface water data consisting of a pre-drilling surface water sample collected immediately downgradient of the oil and gas location and follow-up surface water data consisting of a sample collected at the same location three months

after the conclusion of any drilling activities, operations, or completion (COGCC 2013). In Pennsylvania, a well operator who wants to prove that pollution of a water supply existed prior to the drilling of the well must conduct a pre-drilling survey (PACODE 2011). Many other states are also considering proposed rules that would require operators to collect baseline samples from available water sources (Puls 2013).

WATER SOURCING, STORAGE, AND TRANSPORTATION

Because of the water needs of HVHF, water management planning is a critical part of the planning of any shale development project. This BMP includes issues related to water sourcing, well drilling, well completions, flowback water and produced water, and water requirements for production operations.

In the pre-completion stage, the focus is on the withdrawal source, transport and storage of water. Options available to meet water needs for drilling and fracturing include surface water, groundwater, municipal water, recycled produced water, collected water (e.g., precipitation, top-hole water), and private water purchases.

In evaluating these sources a recommended best management practice is to understand the existing regional water uses and how those uses may potentially impact or be impacted by shale play withdrawals. Water withdrawals for HVHF are often seen as a concern for both communities and the environment. For many individuals, talk of "millions of gallons" of water being withdrawn sounds ominous because they are not aware of the size of other large volume withdrawals such as for municipal public water distribution systems or agricultural, recreational, industrial, or power generation needs. Figure 1 is an example comparison showing existing sources and how the development of the Eagle Ford Shale compares to these other sources. It shows how shale gas production is less than 1.5% of total withdrawals on a regional basis.

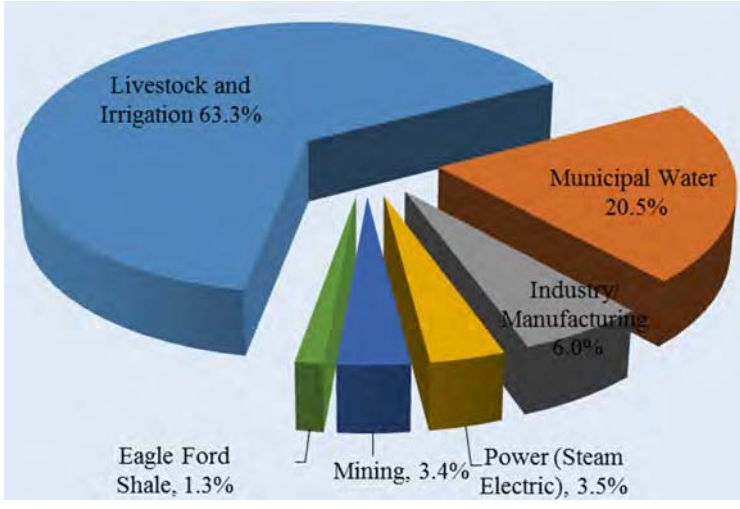

FIG. 1. Eagle Ford Shale Regional Water Uses (9000,000 ac-ft per year)
Source data: TWDB 2011, Jester 2013

However, operators are still developing and utilizing BMPs that are designed to limits impacts from surface water withdrawals. Some of the BMPS are designed to affect individual events, while others are designed to minimize the impact of cumulative activities. Without thorough planning and applying treatment technology BMPs, withdrawals from small and large rivers and streams can reduce stream flow, harming aquatic life and local recreation, especially during periods of low flow or in periods of prolonged drought. These impacts can be minimized through the application of BMPs that designate how and when water is pulled from these sources. Therefore, planning is essential to control impacts to the environment, and having more than one option for water sourcing is advantageous from both an impact and economic perspective.

For E&P companies, BMPs must also account for operational concerns. The pace of development varies, but BMPs that provide timely access to the water and flexibility in when water can be accessed, and that can be permitted to utilize different sources, are most effective. The economics of access to these different source options are also important; the cost of sourcing the water, the cost of transportation and storage of the water, and potential road and community impacts are all issues that may need to be remediated through BMPs are all going to factor into the applicability of the BMP.

Other BMPs related to storage of water for fracturing operations are important to alleviate limitations in water availability associated with variable flow volumes in surface water and with the lack of nearby groundwater sources. Storage BMPs include well-specific impoundments, temporary storage tanks, or a centralized facility that includes tanks or impoundments. Centralized impoundments that can be used to feed multiple wells on a single well pad or multiple well pads are being used to store large volumes of water. These centralized facilities allow for withdrawals in wet weather periods; use of smaller, more frequent withdrawals that occur over long periods of time; and, if regulations allow, withdrawals from multiple watersheds.

HVHF FRACTURE FLUID CHEMICALS

Fracturing fluid makeup technology has also advanced with BMPs that include source water mixing modeling (ALL 2010), the use of “greener” treatment chemicals to support advanced fracturing technologies to optimize production (Fisher 2012), and an overall reduction in the number of chemical additives used and chemical volumes.

Operators have started applying BMPs to the chemicals used for hydraulic fracturing by identifying ways to reduce and/or eliminate certain chemicals. Instead, operators are utilizing chemicals that are considered more environmentally friendly and are capable of utilizing brines or lower quality source waters. The chemical composition of HVHF fluids has evolved as service companies develop chemical BMPs and operators evaluate mixed fluid compatibility allowing for a reduction in the chemicals utilized in a treatment. Figure 2 provides an overview of the composition and percent by volume of chemicals for an average formula of HVHF fluid (note that less than 1% of the fluid composition is chemicals).

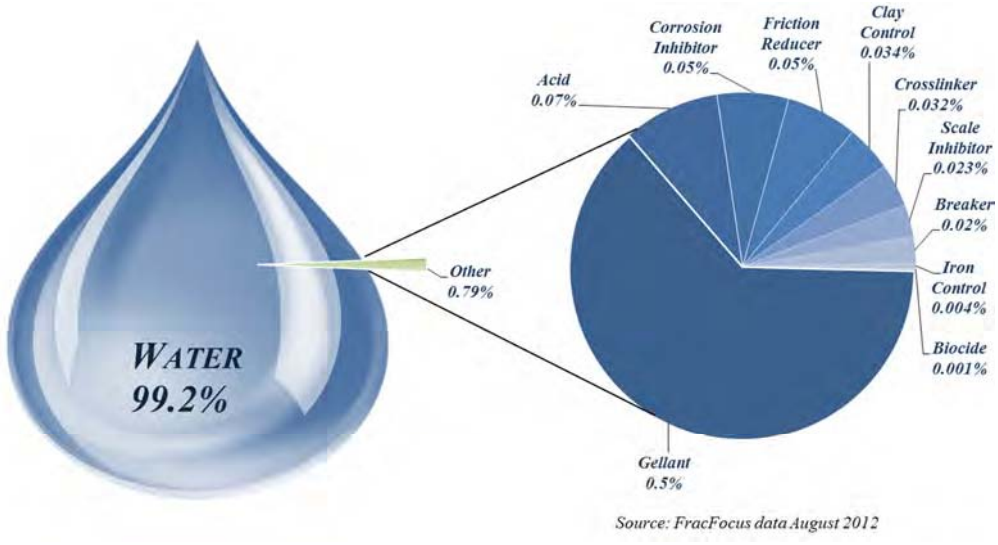

FIG. 2. Average Hydraulic Fracturing Fluid Composition for U.S. Shale Plays

Despite the very low percentage of chemicals in the average fracturing fluid, the public has focused on the potential for this low volume of chemicals from hydraulic fracturing to contaminate groundwater. Meanwhile, regulators and industry have focused on more likely impacts, including the potential for surface water contamination from chemical spills during handling and transportation, spills of produced water that contains small amounts of residual fracture fluid chemicals, and well equipment failures that could result in surface discharges of chemicals and produced water. However, even while operators focus on BMPs to address the more likely routes of contamination, the BMPs applied are also providing protections to groundwater.

Industry has even developed BMPs to address the concerns of disclosure of the chemicals present in HVHF fluids and changing regulations to chemical disclosure requirements. With disclosure requirements expanding, industry made a conscious effort to alleviate the public's concerns related to the composition of hydraulic fracturing fluids with the development of a national chemical disclosure registry, FracFocus. Today, 14 states require that companies use the website to publicly disclose the chemicals used in each new well that is hydraulically fractured (FracFocus.org 2014). The registry currently provides public access to disclosure of hydraulic fracturing chemical additives used in more than 55,000 wells by over 600 companies for hydraulic fracturing treatments completed in the United States since April 2011 (Arthur et. al. 2014). As of October 2013, operators had entered close to 1.5 million individual ingredients into FracFocus.

Companies have also been implementing BMPs for "greener" alternatives for select processes that were previously achieved by chemical additives for hydraulic fracturing. One example is Halliburton, which has invested considerable resources to develop greener fracturing systems. Halliburton's CleanStim® Formulation is a line of chemical additives comprised of materials sourced entirely from the food industry. The company is also using UltraViolet (UV) light instead of chemical additives for bacteria control with a system that treats wastewater at the well pad location during

the fracture stimulation. This treatment allows produced water from flowback operations to be reused and recycled by the operator, thus significantly reducing the need for freshwater (Halliburton 2013).

Other examples are operators like Southwestern Energy and Chesapeake Energy Corporation, both of which have instituted initiatives related to chemical usage. Chesapeake Energy Corporation has a Green Frac initiative that evaluates each chemical additive to determine its environmental friendliness. This initiative and others that are similar are being used by industry to assess the necessity of additives and their overall usefulness in facilitating and improving well production to understand the relative returns in cost compared to gas recovery volumes. To date, Chesapeake has eliminated 10-25% of the additives previously used in its hydraulic fracturing fluids (Chesapeake n.d.). Review of FracFocus data from plays like the Fayetteville Shale over time shows that Southwestern Energy has developed optimization BMPs in completion design that have allowed the company to reduce the number of chemical additives in fracture stimulations to 5-6 chemicals, water and sand.

PRODUCED WATER MANAGEMENT

Best Management Practices for HVHF have changed the produced water management landscape over the past 7 years. BMPs for produced water management and disposal have been developed for three general areas: reuse-recycling, treatment, and disposal. While produced water ratios to gas or oil production from shale plays may be small with produced volumes ranging in volume from 15 to 50% (or more) of the volume of the fracture fluid volume when compared to conventional water production profiles where the volume can exceed stimulation volumes by 10 fold or more, (GWPC and ALL 2009, ALL 2005) the larger volumes of fluids utilized in unconventional play development result in large volumes of fluids to be managed. This management as currently applied typically utilizes BMPs from all three produced water management areas.

Disposal

Oil and gas produced water in the United States has generally been disposed of through underground injection but even with injection disposal, BMPs are being developed to optimize this process. Even though underground injection is the most common disposal method, it is not always feasible as local geology does not always provide formations suitable for the large-volume disposal needed for unconventional plays.

When on-site underground injection is not an option, operators may have to transport produced water to other sites or facilities, incurring higher operating costs. To avoid this, many operators are treating and reusing/recycling produced water of varied quality from one well in the fracture fluid at another well.

Water Treatment

During the early days of treatment, there were three primary treatment needs for produced water: 1) reducing TDS (desalination) for discharge, beneficial use, or reuse; 2) reducing the volume for disposal; and 3) removing suspended solids and reducing scaling and bio-fouling potential in reuse applications (Parker et. al 2003; Arthur et. al. 2009, Gaudlip et.al 2008). In these early years, the BMP for produced water treatment for some shale plays was to send the water to municipal treatment plants where it would then be discharged to surface water bodies (C&EN 2013). Assessment of this treatment indicates that Publicly Owned Treatment Works (POTWs) may not have truly treated the water but merely diluted the produced water before release resulting in this process being stopped (EPA 2009).

"This loss of POTW treatment as a BMP coincided with the development of HVHF chemical fluids that could utilize higher salinity source waters. These two changes prompted treatment processes once considered pretreatment for desalination to become viable BMP treatment technologies to condition produced water for re-use. The concentration of TDS in produced water, which varies within and between plays and over time, could not only limit its potential uses but also dictate treatment options (GWPC and ALL 2009, Kuijenhoven et al 2013)."

Without POTW treatment, high TDS concentration waters were limited to Reverse Osmosis (RO) and thermal distillation/evaporation treatment technologies. RO, which forces water through an osmotic membrane, is generally limited to those produced waters where TDS concentrations are below 40,000 ppm (parts per million) (ALL Consulting 2005). Above these TDS concentrations, membrane fouling and replacement is a costly concern so alternative flow-through processes were developed. Thermal evaporation using Mechanical Vapor Recompression (MVR) has become the more common treatment process for TDS removal in high salinity waters. While MVR can be effective, there are still concerns with corrosion and scale can be cause operations issues. Still, MVR can handle TDS values up to about 200,000 mg/L (ALL Consulting 2005), but applications still need to balance the effectiveness with the cost of operations.

Crystallization has also been used successfully and can be cost effective, but much of the cost recovery comes from the sale of commodity chemical byproducts. Crystallization treatment benefits from no limit on TDS and is a zero-liquid-discharge system. However, crystallization still has a required disposal cost of the resultant solid waste that cannot be sold. Typical commodity byproducts include distilled water, calcium chloride liquid and sodium chloride dry salt (CDM Smith 2013).

Other modern treatment systems involve removal of suspended solids such as organics and fines, the deactivation/removal of scale-forming multi-valent ions, and the neutralization of bacteria. Technology improvements range from equipment to management of higher salinity fluids to new applications of existing water treatment technologies. Table 1 describes some typical treatment process and identifies the constituents the systems are capable of removing from produced water.

Table 1. Typical Water Treatment Systems and the Constituents Removed

Water Treatment Process	Organics	Suspended Solids	Biologics (bacteria & algae)	Low TDS (<10,000 mg/L)	Med TDS (<50,000 mg/L)	High TDS (>50,000 mg/L)	Metals
Thermal Distillation/ Evaporation	X		X	X	X	X	X
Crystallization	X		X	X	X	X	X
Reverse Osmosis		X		X	X		X
UV Sterilization	X		X				
Ozone			X				
Ultrasound		X	X				X

Depending on the primary treatment system, pretreatment or condition may still be needed. Pretreatment can include flocculation for removal of suspended solids, scale inhibitors and pH adjustments. Biocides may also be needed (Platt et. al. 2011, Geza et. al 2013). Typical biocides are liquid chemical biocides (Glutaraldehyde being one of the most commonly used), but can also be non-liquid chemicals such as Ozone, Ultraviolet light, or ultrasound. However, each of these has limitations:

- Ozone is affected by the Chemical Oxygen Demand (COD) of the water being treated and has only a limited residual kill (has a short half-life about a half hour in the atmosphere).
- Ultraviolet Light has no residual kill as the technology is only effective when the light is being applied.
- Ultrasound can reduce biological growth, but is limited because of secondary water characteristics which reduce its effectiveness. Ultrasound tends to target heavy metals, Total Suspended Solids (TSS) and turbidity in produced water first, which reduces its effectiveness in the treatment of biological growth.

To be economic, the cost of produced water treatment for reuse must be less than the cost to dispose of the water via underground injection plus the cost of sourcing and transporting an equal volume of fresh water. In addition, many of these technologies still produce a reject stream or solids that must also be account for in the cost analysis of the BMP. In areas where naturally occurring radioactive material (NORM) is a concern, solids may need to be tested prior to disposal in a landfill. If NORM exceeds state standards, special disposal options may be required.

Water Reuse and Recycling

Many people in the industry believe reuse/recycling of produced water is key to the future of unconventional oil and gas production and have invested resources into the development of BMPs. The overriding goal of water re-use is to minimize freshwater use, protect water resources, and maximize the recycling of produced water. In order to reduce current and future freshwater demands, produced water return volumes are being treated and made available for reuse and recycling. Many operators are applying the BMP of reuse of produced water by blending it with fresh water for use in subsequent fracturing operations. Blending can reduce the cost of fresh water sourcing and treatment.

Recycling is not simply a decision to haul water to a production pad instead of a disposal well; there are several factors to take into consideration when attempting to recycle produced water. While there are benefits of recycling that include the reduced cost for water sourcing and a reduction in the volume of water for disposal, other economic factors like storage, transport, and timing must also be considered in the overall economics to ensure a cost savings. An evaluation of recycling as a BMP needs to include assessment of the volume of produced water available, the quality and characteristics of the water, treated effluent requirements, storage needs and regulatory requirements, and site-specific considerations that may add cost.

There are several caveats to recycling/re-use:

- In some play areas, water is plentiful and treatment costs can greatly exceed the cost of sourcing fresh water.
- Blended water must be suitable for fracture fluid; high TDS concentrations may affect friction-reducing additives.
- Some friction reducers can work with higher TDS water, but there is a trade-off with increased chemical costs.
- Operators have to consider scale tendencies and the risk of bio-fouling with recycled waters.
- Recycling produced water typically requires separate storage facilities, since produced and fresh water should be stored separately.
- Some states have different requirements for ponds that hold low-quality water, which also may require additional site controls such as berms, lined pits, lined pads, tanks, leak prevention, spill control and cleanup measures.
- Additional containment may be required in case of berm failure, and additional monitoring may be required for permit compliance.

CONCLUSION

Shale Gas is going to remain an important source of energy; large volumes of water are necessary for production of that shale gas. Best management practices can conserve source water and reduce waste streams, but BMPs are more than simple desalination treatment. Reuse of produced water is becoming a critical BMP component of water management planning and appears to be the direction of the future for the unconventional development industry. While BMP treatment technologies are advancing and changing, the application of treatment for shale gas

produced water continues to change as more technologies come to market and plays mature. Operators have migrated away from treating produced water to fresh water quality, and the BMP play book has opened up options for treatment technologies that previously were limited by the low quality of produced water from many shale plays. Industry is also developing BMPs that include hydraulic fracturing treatment designs and identification of fracturing chemical additives that are more tolerant of lower quality source water but still efficient when used with higher TDS fluids. As these chemicals are developed, the options for treatment BMPs will continue to open up and expand. As such, it could be expected that the service industry of water treatment for shale gas produced water will also expand and those companies with successful treatment technologies will grow.

REFERENCES

ALL Consulting. (2005). "Technical Summary of Oil & Gas Produced Water Treatment Technologies." <http://www.all-llc.com/publicdownloads/ALLConsulting-WaterTreatmentOptionsReport.pdf> (Mar. 28, 2014).

ALL Consulting. (2010). "Water Mixing and Scale Affinity Model Quick Use Guide." Groundwater Protection Council and Southwestern Energy. <http://www.all-llc.com/projects/produced_water _tool/page.php?11> (Dec. 27, 2013).

American Petroleum Institute (API). (n.d.). "API HF2, Water Management Associated with Hydraulic Fracturing, First Edition/June 2010." *American Petroleum Institute*. <http://www.api.org/policy-and-issues/policy-items/hf/api_hf2_water_management.aspx > (Dec. 5, 2013).

Arthur, J.D., Bohm, B.K., Coughlin, B.J., and Layne, M. (2009). "Evaluating the Environmental Implactions of Hydraulic Fracturing in Shale Gas Reservoirs." SPE Paper 121038-MS, SPE Americas E&P Environmental and Safety Conference, 23-25 March 2009, San Antonio, Texas.

Arthur, J.D., Hochheiser, H.W., Layne, M., and Arthur, R. (2014). "Overview of FracFocus and Analysis of Hydraulic Fracturing Chemical Disclosure Data." SPE Paper 168461-MS, SPE International Conference on Health, Safety, and Environment, Mar. 17-19, 2014, Long Beach, California.

CDM Smith. (2013) "Key Considerations for Frac Flowback / Produced Water Reuse and Treatment." *http://nywea.org*. <http://nywea.org/meetings/ConfPres/KeyConsiderationsShaleGasWasteWaterReuseTreatmentMcLaughlin_a%20.pdf> (Dec. 5, 2013).

Chemical & Engineering News (C&EN). (2013). "Sewage Plants Struggle To Treat Wastewater Produced by Fracking Operations." *http://cen.acs.org* (Mar. 18, 2013). <http://cen.acs.org/articles/91/web/2013/03/Sewage-Plants-Struggle-Treat-Wastewater.html> (Dec. 18, 2013).

Chesapeake. (n.d.). "Green Frac Inititative." *Chesapeake Energy Corp*. <http://www.chk.com/Corporate-Responsibility/EHS/Environment/Green-Frac/Pages/Information.aspx> (Dec. 5, 2013).

Colorado Oil and Gas Compact Commission (COGCC). (2013). Rule 318A. e. (4) Groundwater Baseline Sampling and Monitoring. <http://cogcc.state.co.us/RR_Docs_new/rules/300Series.pdf> (Dec. 30, 2013).

Fisher, Kevin. (2012). " 'Green' Frac Fluid Chemistry Optimizes Well Productivity, Environmental Performance." *American Oil & Gas Reporter*. <www.flotekind.com/Assets/march-2012-aogr-article.pdf> (Dec. 30, 2013).

FracFocus.org. (2014). "Find Regulations for Your State- Interactive Map." <http://fracfocus.org/regulations-state> (May 31, 2014).

Gaudlip, A.W, Paugh, L.O., and Hayes, T.D. (2008). "Marcellus Shale Water Management Challenges in Pennsylvania." SPE Paper 119898-MS, SPE Shale Gas Production Conference, 16-18 November 2008, Fort Worth, Texas, USA.

Geza, M., Cath, T.Y., Xu, P., and Drewes, J.E. (2013). "Decision Support Tool (DST) for Characterization, Treatment, and Beneficial Use of Unconventional Gas Frac Flowback and Produced Water." SPE Paper 168895-MS, Unconventional Resources Technology Conference, Aug. 12-14, 2013, Denver, Colorado, USA.

Ground Water Protection Council (GWPC) and ALL Consulting. (2009). *Modern Shale Gas Development in the United States: A Primer*. Prepared for the Department of Energy Office of Fossil Energy and National Energy Technology Laboratory, Washington, DC.

Halliburton. (2013) "Case Study: Effective fracturing with recycled water." *www.halliburton.com*. <http://www.halliburton.com/public/pe/contents/Case_Histories/web/A_through_R/H09855.pdf> (Dec. 17, 2013).

Jester, Stephen. (2013). "Eagle Ford Shale Water Supply and Demand." Presentation the Environmental Protection Agency as part of the EPA's Study of Hydraulic Fracturing and Its Potential Impact on Drinking Water Resources. <http://www2.epa.gov/hfstudy/eagle-ford-shalewater-supply-and-demand-stephen-jester-pe> (Mar. 21, 2014).

Kuijvenhoven, C., Fedetov, V., Gallo, D., and Hagemeijer, P. (2013). "Water Management Approach for Shale Operations in North America." SPE Paper 167057-MS, 2013 SPE Unconventional Resources Conference & Exhibition - Asia Pacific, Nov. 11-13, 2013, Brisbane, Australia.

Leatherbury, R., and Denson, B.B. (2012). "Strategic Baseline Groundwater Sampling for Shale Exploration." SPE Paper 158381-MS, SPE Annual Technical Conference and Exhibition, Oct. 8-10, 2012, San Antonio, Texas, USA.

Ohio Department of Natural Resources (ODNR). (2012). "Best Management Practices for Pre-Drill Water Sampling (Sep. 2012)." *Ohio ODNR*. <http://www.ohiodnr.com/Portals/11/oil/pdf/BMP_PRE-DRILLING_WATER_SAMPLING.pdf> (Dec. 5, 2013).

Pennsylvania Administrative Code (PACODE). (2011). Section 78.52 of Subchapter C of the Environmental Protection Performance Standards. Code amended Feb. 5, 2011, and effecive Feb. 5, 2011.

Parker, M., Slabaugh, B., Walters, H., Hart, T., Walsh, F.H., Haley, W., Harper, J., and Weaver, J. (2003). "New Hydraulic Fracturing-Fluid Technology Increases Production in Barnett Shale and Reduces Impact on the

Environment." SPE Paper 80912-MS, SPE Production and Operations Symposium, Mar. 22-25, 2003, Oklahoma City, Oklahoma.

Platt, F.M., Burnett, D.B., Eboagwu, U.M., and Vavra, C.J. (2011) "Pre-Treatment Options for Frac Flow Back Brines: Laboratory and Pilot Plant Testing of Oil Removal Materials." SPE Paper 147417-MS, Canadian Unconventional Resources Conference, Nov. 15-17, 2011, Alberta, Canada.

Puls, Robert. (2013). "Overview of State Pre-Drill Water Quality Testing." Presented at the GWPC Annual Forum 2013, Sep. 23-25, 2013, St. Louis, MO.

Seth, K., Shipman, S., McCutchan, M., and McConnell, D. (2013). "Maximizing Flowback Reuse and Reducing Freshwater Demand: Case Studies from the Challenging Marcellus Shale." SPE Paper 165693-MS, 2013 SPE Eastern Regional Meeting, 20-23 August 2013, Pittsburgh, Pennsylvania, USA.

Shauk, Z. (2012). "Drillers Looking at Curring Need for Lots of Water." *My San Antonio* (Sep. 19, 2012). <http://www.mysanantonio.com/business/article/Drillers-looking-at-cutting-need-for-lots-of-water-3878703.php> (Dec. 20, 2013).

Texas Water Development Board (TWDB). (2011). State Water Use Snapshot, Regional Water Planning Water User Group.<http://www2.twdb.texas.gov/ReportServerExt/Pages/ReportViewer.aspx?%2fWU%2fSumFinal_WUGSum&rs:Command=Render> (Mar. 14, 2011).

U.S. Environmental Protection Agency (EPA). Region 3 (2009). "Requests for Information from Publicly Owned Treatment Works (POTWs) Taking Oil and Gas Waste." *Key Documents about Mid-Atlantic Oil and Gas Extraction*. <http://www.epa.gov/region3/marcellus_shale/> (Mar. 29, 2014).

Recycling of Produced and Flowback Water in Oil and Gas Drilling Operations through Hydraulic Fracturing in Texas

Mehmet A. Boz[1], Ph.D., P.E., M.ASCE

[1]Project Manager, AECOM Technical Services Incorporated, 112 E Pecan St, Suite 400, San Antonio, TX 78205, U.S.A., E-mail: mehmet.boz@aecom.com.

ABSTRACT: The process of hydraulic fracturing is a popular method for extracting oil and gas in Texas. It is estimated that approximately 4 to 8 million gallons of water is utilized per each well that is drilled and developed; the increase in hydraulic fracturing activity in Texas has led to an increase in the amount of water used by the oil and gas industry, from 44 million cubic meters (36,000 acre-feet) in 2008 to 100 million cubic meters (81,500 acre-feet) in 2011. The multi-year long drought, increasing pressure to regulate water usage, and desire to achieve greater water conservation has pushed some policymakers in the State of Texas to consider mandating the recycling of produced and flowback water from drilling operations. This paper focuses on the statewide water needs in Texas, the story of the legislative mandate, and the implications of such mandate on future hydraulic fracturing operations across the country.

INTRODUCTION

Texas is one of the fastest growing states in the United States. It is projected that the population of the state will reach past 45 million people before 2060. The projected population rates, along with increased industrial attention and activity, makes water supply one of the leading issues in planning for the future growth needs of the State. The State Water Plan estimates that the state wide water 2010 supply need of 4.4 billion cubic meters (3.6 million acre-feet) will increase to nearly 10 billion cubic meters (8.3 million acre-feet) by 2060 (TWDB, 2012).

Texas has always been at the center of the oil and gas activity in the United States, the recent center of growth being the Eagle Ford Shale area of South Texas and the increased output in the Permian Basin. According to Perry, after a sustained oil production of about 159,000 cubic meters (one million barrels) per day for about a decade, since 2010, oil production in Texas has increased by an unprecedented 75% through the middle of 2012, with production levels reaching approximately 318,000 cubic meters (two million barrels) of crude oil per day in the month of July 2012 (Perry, 2012). Figure 1 shows the top four oil producing states in the United States. Figure 2 shows a summary of the oil and gas activity in the Eagle Ford Shale.

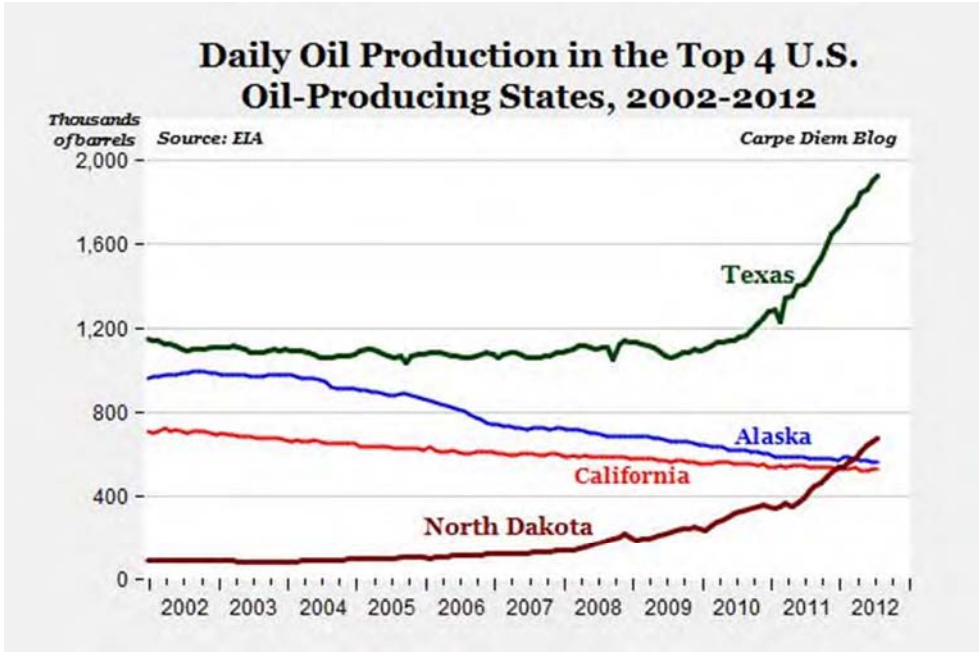

FIG. 1. Daily Oil Production in the Top 4 U.S. Oil-Producing States, 2002-2012 (Perry, 2012)

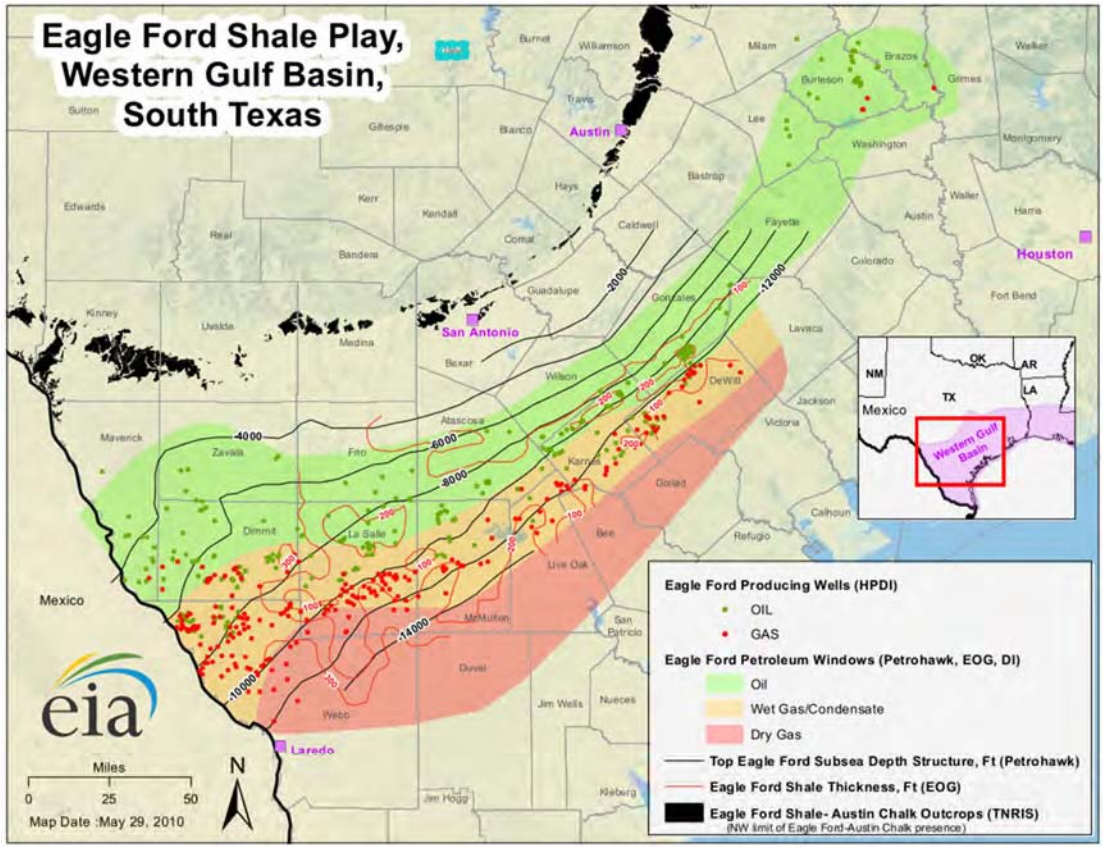

FIG. 2. Oil and Gas Activity in the Eagle Ford Shale (EIA, 2010)

Water Needs in Hydraulic Fracturing:

The mining industry uses water to drill and fracture wells and for recovery processes, to dewater and depressurize pits, and for dust control purposes (Nicot et al, 2011). Figure 3 below shows the estimated water consumption by various segments of the mining industry.

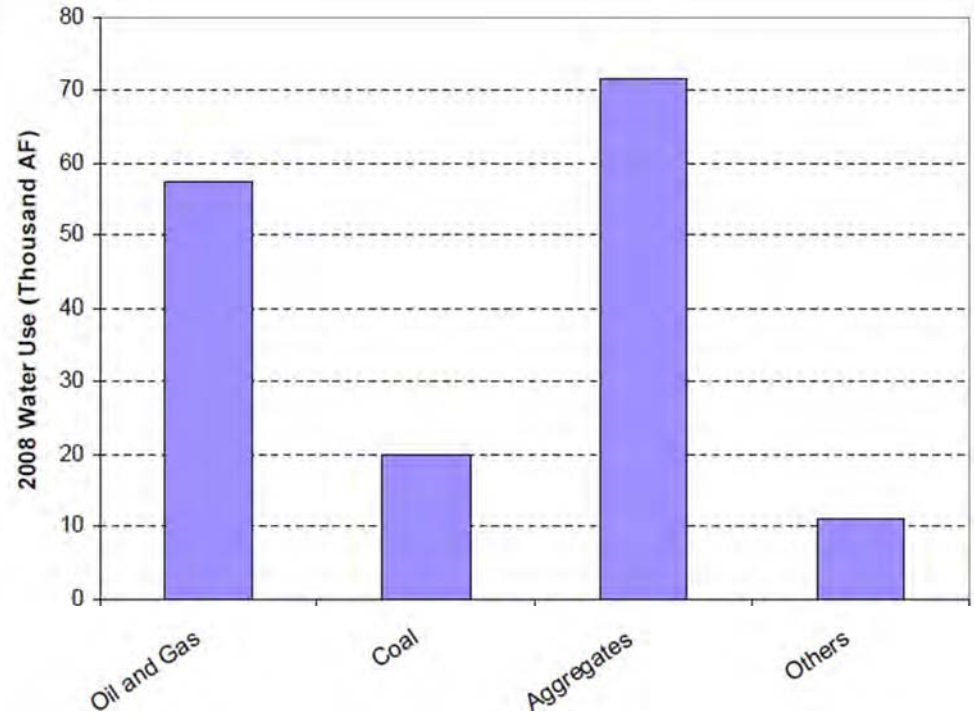

FIG. 3. Summary of Estimated Water Use by Mining Industry Segment (Nicot et al, 2011)

The increase in the oil and gas activity in Texas has intensified the spotlight on hydraulic fracturing and the effects thereof. The general process of hydraulic fracturing includes application of a pressurized hydraulic fracturing fluid into the well-bore, which propagates fractures in the target geologic formation and enhances the production of oil and gas. The size of these man-made fractures is approximately half the diameter of a human hair (Porter, 2013).

While the total water use in hydraulic fracturing activities in Texas has increased from 44 million cubic meters (36,000 acre-feet) in 2008 to approximately 100 million cubic meters (81,500 acre-feet) in 2011, the estimates indicate that the reuse of drilling water has also increased 21% to approximately 21 million cubic meters (17,000 acre-feet) in 2011 (Nicot et al, 2012). The total statewide mining water use, including hydraulic fracturing, represents only 1.6% of the statewide water use, with mining activities and water use concentrating in and around the Eagle Ford Shale, in Webb, Karnes, Dimmit, and La Salle Counties (Porter, 2013). Hydraulic fracturing alone represents 0.5% of the total state water use (Nicot et al, 2012). Estimates indicate between 20,000 and 25,000 new wells in the Eagle Ford Shale within the next 10 to 20 years, resulting in 370 million cubic meters (300,000) to 462 million

cubic meters (375,000 acre-feet) of cumulative future water use, not taking into account recycling, reuse, and brackish water use (Porter, 2013).

Water Recycling and Reuse:

The majority of hydraulic fracturing flowback water in Texas is disposed of in permitted disposal wells, with methods that will not cause pollution of surface and subsurface water supplies. The amount of flowback water that can be reused in a hydraulically fractured well varies, as does the quality of this flowback water. In some cases there is very little treatment required, which involves basic filtration and blending, and in other cases more sophisticated treatment techniques and processes are needed. Taking the added cost of the use of the recycled water in drilling activities, some have turned to other sources of recycled water, such as municipal treatment facilities (Porter, 2013).

Table 1. Estimated water use for hydraulic fracturing (Nicot et al, 2012)

Play / Region	*Type*	*Current (2011)*
Permian Far West	Recycled/reused	0 %
	Brackish	80 %
	Fresh	**20 %**
Permian Midland	Recycled/reused	2 %
	Brackish	30 %
	Fresh	**68 %**
Anadarko Basin	Recycled/reused	20 %
	Brackish	30 %
	Fresh	**50 %**
Barnett Shale	Recycled/reused	5 %
	Brackish	3 %
	Fresh	**92 %**
Eagle Ford Shale	Recycled/reused	0 %
	Brackish	20 %
	Fresh	**80 %**
East Texas Basin	Recycled/reused	5 %
	Brackish	0 %
	Fresh	**95 %**

While the amount of fresh water used is well-documented and varies from 20% in Far-West Texas to nearly 100% in East Texas, the amount of recycled water received from municipal treatment facilities is unknown. However, the Texas Commission on Environmental Quality (TCEQ) lists nearly 30 municipal and industrial facilities located in the Barnett Shale and Eagle Ford Shale areas that provide water to the oil and gas industry (Nicot et al, 2012). Table 1 shows the estimated water use by category in the hydraulic fracture activity areas.

As shown on Figures 4 and 5, the oil and gas activity in the Eagle Ford Shale

continues to rise. Estimates by the National Petroleum Council place the number of wells that will be hydraulically fractured in the next decade to 80 percent of the total wells that will be drilled. Assuming that each well uses an average of 23,000 cubic meters (6 million gallons) of water, which is equivalent to nine Olympic sized pools, and disposal costs run $9.43 to $12.58 per cubic meter ($1.50 to $2 per barrel), and transportation costs up to $25.16 per cubic meter ($4 per barrel), on-site recycling is attractive, not only for environmental reasons but also for the financial planning of oil and gas operations (Cockrell School of Engineering, 2013).

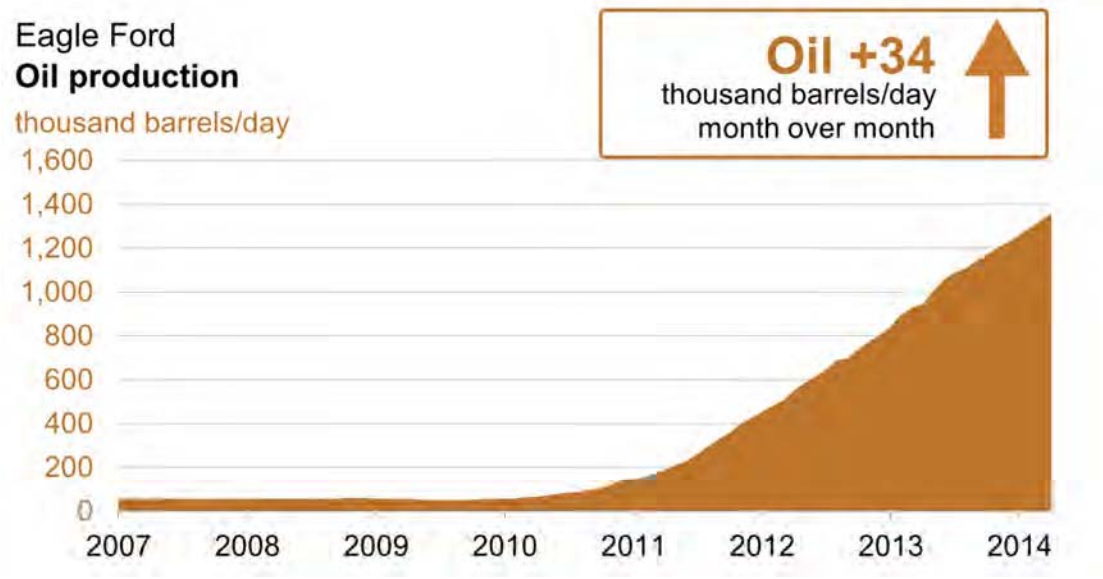

FIG. 4. Eagle Ford Oil Production (2007-2014) (EIA, 2014)

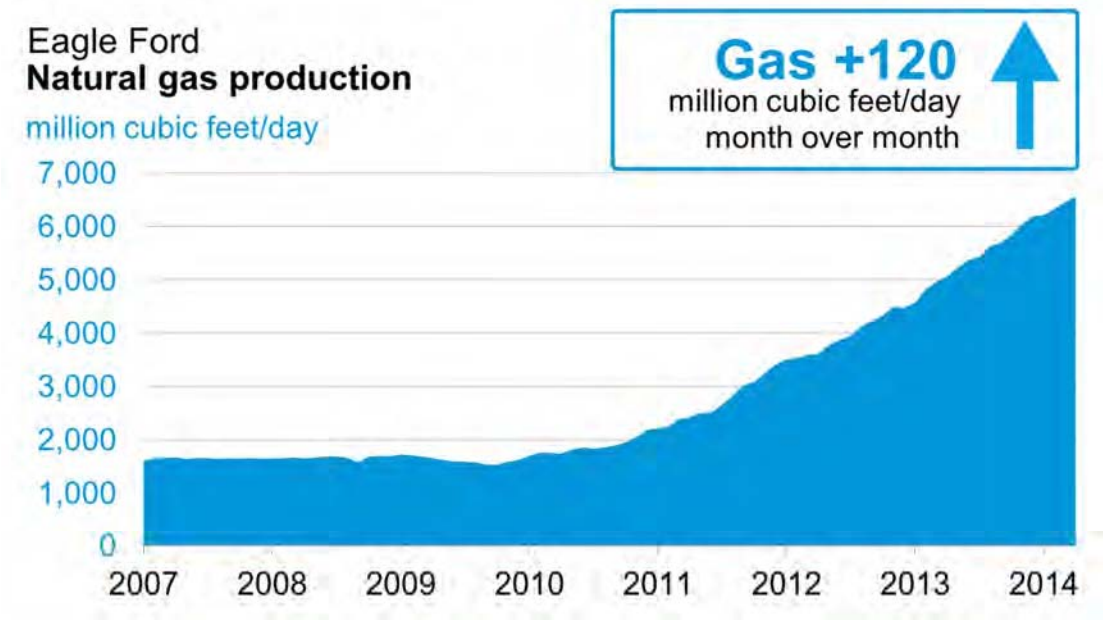

FIG. 5. Eagle Ford Natural Gas Production (2007-2014) (EIA, 2014)

Texas Legislative Story:

In Texas, the State owns and manages the waters flowing in the rivers, creeks, and bays and a water right is required to divert such surface waters. This authorization is granted by the State through TCEQ. Groundwater ownership rights are regulated and managed by the courts and the State Legislature, though landowners may choose to pump as much water as they would like under the "Rule of Capture" without the liability of depleting other surrounding wells (SARA, 2012).

Over the years, many water related issues have been brought to attention at the legislative level, one of the latest efforts being the mandated recycling of flowback water from hydraulically fractured wells. The increased activity in the Eagle Ford and the Permian Basins has raised concerns over the availability and the effects on the local water supplies.

In early 2013, the Texas Railroad Commission (TRC) issued a new set of rules that encourage recycling of drilling water by streamlining the permitting process, eliminating the permits for on-lease fluid recycling, and clarifying rules for operators to obtain Commission permits. These new set of rules establish spill protection rules for storage of fluids, allow the operators to store and recycle drilling fluids on leased properties, and allow the operators to recycle other operators' fluids (Rigzone, 2013).

Texas House Bill 2992 "Relating to the reuse, discharge, or disposal of fluid produced from certain oil or gas wells on which a hydraulic fracturing treatment has been performed", introduced by Rep. Tracy O. King (D-Batesville) attempted to prohibit flowback fluids and water produced by hydraulic fracturing from being injected into a disposal well if the fluid can be treated (Rigzone, 2013). Also included in the bill was a new set of rules to establish standards to determine the quality of flowback water that could be injected in a disposal well. The bill was considered in public hearing and discussed in committee but no decision has been made (Texas Legislature, 2013).

TRC estimated that this new bill would require a new series of expenditures and required funding, including an additional 16,200 inspections, 21 (twenty-one) new full-time employees, two new full-time inspectors at each of the agency's nine district offices, and new computerized water tracking system to determine water treatment and disposal, which would all total to approximately $1.4 million per fiscal year, and an initial capital expenditure of nearly $500,000 (Rigzone, 2013).

As of mid-2013, the rules and regulations for existing commercial recycling rules considered only two types of recycling facilities: mobile and stationary. Nevertheless, there have been many recycling permit applications that do not fit in these two categories, thus considerations are being made to consider up to five different types of recycling facilities in the permitting process. TRC has so far issued permits to 14 mobile recycling facilities and one stationary facility; all of the permitted operators, except two, are allowed to conduct business statewide. TRC is also reviewing permit applications for six more mobile processes (Porter, 2013).

CONCLUSIONS

The water use that can be attributed to oil and gas activities is hard to predict because of the dispersed nature of industry facilities. Also, generally, the water use is

transient and temporary, and there is a great lack of data for actual water needs in field operations. Another reason it is difficult to project a water need for hydraulic fracturing is because the oil and gas industry might have hydraulically fractured more formations that can be placed into the tight oil and gas category. Nonetheless, even when other oil and gas industry water uses, such as water flooding and drilling, are included, the projected water need for the oil and gas industry in Texas is approximately 222 million cubic meters (180,000 acre-feet) per year in the 2020s, which is only a small fraction of the projections for the total state water need. On the other hand, while the water used in oil and gas activities do not represent a large percentage of the statewide water needs, the isolated nature of hydraulic fracturing operations may mean that the localized water needs and projections can be much higher (Nicot et al, 2012).

Also, operational experience as well as advancements in filtering and treatment technologies can bring about an economic reason for on-site recycling of flowback fluids sooner than any state regulation would. As previously discussed, transporting and disposing of water can be costly; thus, any cost-effective approach to reduce fresh water use would be welcomed by the industry. An example of this is an operational trend that is starting to catch on in Texas, Oklahoma, Colorado and other places, where a biocide used to kill the corrosion causing bugs in the water is allowing field personnel to reuse the water four to five times instead of once before disposal. In addition, while initial recommendations placed the water quality needed for hydraulic fracturing at 25,000 to 40,000 parts per million (ppm) total dissolved solids (TDS), field experience has shown that these levels can be as high as 285,000 ppm TDS (Rigzone, 2013).

The Texas example provides a good set of experiences and examples for other hydraulic fracturing operations in the nation. The water question, as it relates to water supply needs and the recycling and on-site storage of flowback fluids remains to be a question of not only regulations but also economics. While authorities push for regulations that require recycling and reuse in an attempt to curb the volume of fresh water use in field operations, the industry has also been trying to find ways to recycle and reuse to cut operational costs. The trend shows that recycling of flowback fluids is likely to remain an operational objective of the industry for economical purposes as hydraulic fracturing activities continue, and the much-needed regulatory requirements will speed up this process.

ACKNOWLEDGMENTS

The author thanks the American Society of Civil Engineers and the ASCE Shale Energy Conference in their efforts to bring attention to the issues surrounding the shale energy plays.

REFERENCES

Cockrell School of Engineering (2013). *Engineers Improve Recycling System in Hydraulic Fracturing to Save Water and Energy*. Accessed from: http://www.engr.utexas.edu/news/releases/recycling-fracking-water on August 28,

2013

Nicot, J.-P., Hebel, A., Ritter, S., Walden, S., Baier, R., Galusky, P., Beach, J., Kyle, R. Symank, L., Breton, C. (2011). *Current and Projected Water Use in the Texas Mining and Oil and Gas Industry*. Bureau of Economic Geology, Jackson School of Geosciences, University of Texas, Austin, June 2011.

Nicot, J.-P., Reedy, R.C., Costley, R.A, Huang, Y. (2012). *Oil and Water Use in Texas: Update to the 2011 Mining Water Use Report*. Bureau of Economic Geology, Jackson School of Geosciences, University of Texas, Austin, September 2012.

Perry, M. J. (2012). *Energy chart of the day: Shale oil production in North Dakota and Texas has boosted US oil production to a 17-year high*. Accessed from http://www.aei-ideas.org/2012/10/energy-chart-of-the-day-shale-oil-production-in-north-dakota-and-texas-has-boosted-us-oil-production-to-a-17-year-high/ on December 27, 2013.

Porter, D. (2013). *Eagle Ford Shale Task Force Report*. Railroad Commission of Texas, March 2013.

Rigzone. (2013). *Legislation Targets Mandates for Water Recycling in Oil, Gas Industry*. Accessed from: http://www.rigzone.com/news/oil_gas/a/125794/Legislation_Targets_Mandates_for_Water_Recycling_in_Oil_Gas_Industry on August 28, 2013.

San Antonio River Authority (SARA) (2012). *Best Practices Handbook to Assist Communities in the Eagle Ford Shale, 2nd Edition, Identification and Implementation of Best Practices*. 2012

Texas Water Development Board (TWDB) (2012). *Water for Texas 2012 State Water Plan*. January, 2012.

Texas Legislature (2013). *83(R) Relating to the reuse, discharge, or disposal of fluid produced from certain oil or gas wells on which a hydraulic fracturing treatment has been performed*. Accessed from: http://www.legis.state.tx.us/BillLookup/History.aspx?LegSess=83R&Bill=HB2992 on November 14, 2013.

U.S. Energy Information Administration (EIA) (2010). *Eagle Ford Shale Play, Western Gulf Basin, South Texas*. Accessed from: http://www.eia.gov/oil_gas/rpd/shaleusa9.pdf on March 31, 2014.

U.S. Energy Information Administration (EIA) (2014). *Drilling Productivity Report for Key Tight Oil and Shale Gas Regions*. Accessed from: http://www.eia.gov/petroleum/drilling/pdf/dpr-full.pdf on March 31, 2014.

Review of Flowback and Produced Water Management, Treatment and Beneficial Use for Major Shale Gas Development Basins

Guanyu Ma[1], Mengistu Geza[2], Pei Xu[3]

[1] Department of Civil Engineering, New Mexico State University, Las Cruces, NM 88003-8001, U.S.A., E-mail: gyma@nmsu.edu
[2] Research Assistant Professor, Department of Civil and Environmental Engineering, Colorado School of Mines, Golden, CO 80401-1887, U.S.A., E-mail: mgezanis@mines.edu
[3] Assistant Professor, Department of Civil Engineering, New Mexico State University, Las Cruces, NM 88003-8001, U.S.A., E-mail: pxu@nmsu.edu

ABSTRACT: Produced water management is a major challenge to oil and natural gas exploration and production, in particular for unconventional gas development. Rapid development of shale gas production, regulations, water scarcity, concerns of environmental impacts, and limited disposal options are driving operators to consider, plan and change their current hydraulic fracturing and produced water management methods. Development of beneficial use of produced water has become a new trend for sustainable shale gas production. Treatment and beneficial use of flowback and produced water can enhance gas recovery and economic viability of gas production. It also minimizes potential environmental impacts, reduces demands on local water supplies, and meets regulatory requirements. However, there are many factors affecting the feasibility of beneficial reuse including water quality and quantity, appropriate treatment technologies, economics, disposal options and capacities, environmental impact, and regulations. This study evaluated the challenges and prospect of beneficial use through review of existing studies on flowback and produced water management in major shale plays. Currently, operators in Marcellus Shale are reusing over 90% of flowback and produced water, mainly for hydraulic fracturing. Barnett Shale, Eagle Ford Shale, Fayetteville Shale and Haynesville Shale, are using deep well injection as their primary disposal method. However, produced water beneficial use potential in Barnett, Eagle Ford and Fayetteville is expected high due to new regulations and water shortage due to droughts.

INTRODUCTION

Shale gas, known as natural gas production from hydrocarbon-rich shale formations, has become one of the most rapidly expanding energy resources today. According to the Energy Information Administration Annual Energy Outlook Report (EIA, 2012), shale gas production in the U.S. is projected to increase from 23% in 2010 to 49% in 2035. Conventional oil and gas has been produced from permeable geological formations for decades, which is still playing an important role; however, the advances in directional drilling and breakthroughs in hydraulic

fracturing have allowed expansion of unconventional gas production from deep and less permeable shale formations. This new gas development has brought changes and challenges to many relevant fields, including environmental issues, which is a particular concern to producers, regulators and the public. Most unconventional gas wells in both mature and new plays are using hydraulic fracturing as a technique for stimulation, which involves injection of water containing additives under high pressure. After the drilling process when the pressure is released, the injected water comes out from cracks in deep shale formations, with minerals, organic matters, salts, and added chemicals, which is called flowback and produced water.

Flowback and produced water are the largest volume byproducts associated with oil and gas exploration and production, which can either be a waste or a resource, depending on how they are managed. Current shale gas well drilling requires approximately 246 to 2,270 m^3 of water, and hydraulic fracturing requires 11,356 to 22,712 m^3 of water, of which 15% to 85% flows back to the surface and becomes flowback (short-term) and produced (long-term) water, which is estimated to be in the range of 2.4 to 3.2 billion m^3 per year in the U.S. (Clark and Veil, 2009). Due to its highly variable quality (salts, petroleum hydrocarbons, metals, chemical additives, suspended and colloidal solids) and quantity, flowback and produced water management poses significant challenge to both producers and regulators. Depending on availability, economics and regulatory requirements, currently there are four major produced water management options, including 1) deep well injection, 2) discharge to nearby surface water bodies, 3) disposal of commercial or municipal wastewater treatment facilities, 4) reuse for a future hydraulic fracturing job, with or without treatment.

Water shortage has been affecting many regions in the U.S., which also leads to water availability challenges to oil and gas industry. Continuous drought in southwestern U.S. has affected oil and gas production significantly, because drilling and hydraulic fracturing operations demand substantial amount of water. Water conflicts between Barnet Shale and Eagle Ford Shale is one example of the challenges, as they share the same surface water system (Arthur, 2011).

Beneficial reuse of flowback and produced water is in great need. In New Mexico, producers are taking flowback and produced water as a resource of water for well development because it costs much less than using freshwater for hydraulic fracturing and drilling. Further northeast, Marcellus Shale now reuses over 90% flowback and produced water for future fracturing jobs. All evidences demonstrate the urgent need to reuse flowback and produced water, as water shortage has become a critical factor for oil and gas exploration and production.

There are many factors affecting the decision on beneficial reuse of flowback and produced water, including suitable technologies for water treatment, freshwater availability and location, flowback and produced water quality and quantity, and availability of commercial treatment and disposal facilities. Generally, flowback and produced water is treated with oil/water separation before any other operations. Majority of beneficial use of flowback and produced water is for future fracturing job, after mixing the treated water with freshwater to meet the injection standard.

OBJECTIVE

This paper aims at understanding the challenges of flowback and produced water management in major basins by looking into detailed site conditions, and investigating the prospect of beneficial reuse of flowback and produced water.

METHODOLOGY

A comprehensive literature review was conducted for data and information collection, including peer-reviewed journal articles, white papers, conference proceedings and presentations, webpages, news release, technical reports, government documents, and data from research institutions and producers. Five major shale gas-producing basins are studied, including Marcellus, Fayetteville, Haynesville, Barnett and Eagle Ford.

RESULTS AND DISCUSSION

Considered as the largest volume of waste byproduct from shale gas industry, flowback and produced water was historically managed to be disposed of rather than beneficial reuse. Management of flowback and produced water depends on a variety of factors, including the quality and quantity of the waste stream, the type and location of infrastructure, the availability of injection wells and treatment facilities, regulations related to wastewater discharge and transportation, and the overall shale gas development (Rahm et al., 2013).

In recent years, beneficial reuse of flowback and produced water has increased. This trend is driven by fresh water shortage, nationwide drought, increased fresh water demand for hydraulic fracturing, regulations and policies, environmental concerns, rapid development of unconventional gas production, and public perception. In this paper, wastewater management, treatment options and challenges are analyzed and discussed for major shale gas producing plays.

Marcellus Shale

The Marcellus Shale is the largest natural gas producing play in the U.S., and is rapidly growing in recent years, especially in Pennsylvania. New wells drilled in Pennsylvania have been rapidly increasing since 2007, when breakthrough on hydraulic fracturing techniques occurred (Veil, 2013). Total shale gas producing wells in Pennsylvania was 6,391 as of Oct. 10, 2013 (Amico et al., 2013).

Along with the rapid growth of shale gas production comes an increasing amount of water demand, mainly for hydraulic fracturing, resulting in a substantial amount of flowback and produced water. Average fresh water demand for drilling a new well is 300 to 322 m^3, while hydraulic fracturing needs vary from 12,500 to 20,820 m^3, according to shale gas producers in the Marcellus Shale play. Produced water production raised from 2,158,781 m^3 in 2009 to 1,278,330 m^3 in the first half of 2013 (approx. 2.35 million m^3 annually) (Mantell, 2011).

Flowback and produced water quality from the Marcellus Shale is relatively well characterized by lab testing in the past few years. Flowback water coming out immediately after fracturing has a moderate to poor quality, with high total dissolved solids (TDS) at approximately 40,000 ppm to 90,000 ppm but low total suspended solids (TSS) (approx. 160 ppm). Hardness varies from moderate to

high concentrations. Long-term produced water also has a high TDS at over 120,000 ppm (Mantell, 2011).

Flowback and produced water management in the Marcellus Shale region has been successful. As shown in Table 1, compared to 2009 when reuse ratio of wastewater was only 15% to 20%, around 90% of the flowback and produced water are reused/recycled in the year 2013, mainly saved for new well drilling (Veil, 2013). Beneficial reuse of the wastewater makes up to approximately 10% of the water needed for hydraulic fracturing job for a new well.

Flowback and produced water needs to be treated before reuse or disposal. In Marcellus Shale areas, reuse for hydraulic fracturing needs oil/gas-water separation, filtration, and dilution as treatment methods. Dilution of the wastewater is aimed at decreasing contaminant concentrations to an acceptable level for hydraulic fracturing, and is the most common way to treat flowback and produced water for beneficial reuse. Disposal well injection is also in use in Marcellus, with annual volume of approximately 397,400 m^3.

Table 1. Comparison of Wastewater Management Options on Marcellus Shale between 2009 and 2013

Wastewater Management Options	Flowback Water (%)		Produced Water (%)	
	2009	2013	2009	2013
Reuse	21.3	26.8	15.3	75.1
Centralized Treatment for Recycle	0.0	70.1	0.0	12.8
Injection Wells	0.2	2.7	0.7	12
Discharge	78.5	0.4	84	0.1

Source: data adopted from (Veil, 2013)

Barnett Shale

During its development, the Barnett Shale became a leading shale gas production field in the U.S. in 2008, when horizontal drilling techniques were first adapted and refined. By the end of September 2013, there are in total 17,332 shale gas wells in Barnett Shale, producing more than 150 million m^3 shale gas per day (RRC, 2013a, b).

Drilling new wells in Barnett Shale requires around 950 m^3 of water per well, and hydraulic fracturing requires 14,385 m^3 per well, all of which come from groundwater (Mantell, 2011). Current fresh water availability in Barnett Shale is not a limiting factor for oil and gas production, because of the abundant surface and ground water resources in Texas.

In Barnett Shale, initial return rate of hydraulic flowback water is relatively small, gradually increasing over a long period of time. Due to its formation characteristics, high volume of natural formation water exists near the shale play, which would flow into the well site becoming produced water. Flowback and produced water in Barnett Shale has relatively low TSS, TDS and chlorides, however, increasing significantly over time, from 50,000 and 25,000 ppm in the beginning to 140,000 and 80,000 ppm at the end of well lifetime, respectively (Mantell, 2011).

Disposal well injection is the most common choice for Barnett Shale producers, because of its economics and availability. Some producers are reusing a small amount of wastewater, but many have just started considering beneficial use options. The Railroad Commission of Texas recognizes concerns over water use by the oil and gas industry and encourages recycling projects aimed at reducing the amount of fresh water used in exploration and production (RRC, 2013c). Besides, nationwide drought in the U.S. is also an incentive for beneficial use, with potential water conflicts between shale plays within Texas, such as in the Eagle Ford.

Fayetteville Shale

Fayetteville Shale is an unconventional natural gas producing shale in Arkansas with a steady increase in production since 2009. Total number of wells completed in 2010 was 3,017 (AGS, 2010, Veil, 2011).

Water required by well drilling in Fayetteville is 227 to 246 m^3 per well, and hydraulic fracturing requires 10,978 to 18,549 m^3 per well. Annual water demand is estimated to be 15.5 to 22.0 million m^3 per year (Veil, 2011). Generally, water supply should be sufficient to support the development of Fayetteville, although water restriction may exist in different areas and seasons (Veil, 2011). There are also water storages that producers collect and store water during times of abundance, and save for drought periods (Veil, 2011).

Flowback and produced water quality in Fayetteville Shale is better than that from other shale plays, with TDS between 10,000 to 20,000 ppm and chlorides 10,000 ppm (Mantell, 2011). Most of the wastewater is injected by disposal wells.

Haynesville Shale

Haynesville Shale locates in northern Louisiana (65%) and eastern Texas (35%). By mid-2011, approximately 1820 shale gas producing wells had been drilled in Haynesville Shale. With more than 3,048 m depth of the shale formation, drilling water demand is significantly higher than other shale plays, from 2,271 to 3,785 m^3 per well (Nicot and Scanlon, 2012). Hydraulic fracturing water demand is about 19,000 m^3 per well (Mantell, 2011).

Initial flowback water is less significant, at around 950 m^3 per well, but with poor quality (high TDS, TSS and chlorides). Scaling tendency is also very high, with calcium approximately 8,000 ppm and magnesium approximately 500 ppm (Mantell, 2011). Very poor flowback and produced water quality makes it very unattractive for treatment and reuse, both short and long term. Drilling mud, however, has a relative high quality and larger volume, which makes it more feasible for reuse.

Eagle Ford Shale

Eagle Ford Shale is a relatively new shale gas-producing field in Texas, with a rapid development. Starting from 2008 when the discovery well was drilled, 1040 wells had been drilled and producing shale gas in Eagle Ford Shale by 2012 (Nicot and Scanlon, 2012).

Drilling in Eagle Ford Shale requires 473 m^3 of water per well, and hydraulic fracturing requires between 7,570 to 51,860 m^3 per well (Arthur, 2011, Nicot and Scanlon, 2012). Annual net water use was 100 million m^3 in 2012.

Wastewater quality in Eagle Ford Shale is still under evaluation, but preliminary study showed the potential for beneficial use. Even though fresh

water availability has not yet become a major issue, nationwide drought has already showed potential water conflicts between Eagle Ford Shale and Barnett Shale. During the 2011 drought, many operators in Eagle Ford Shale were forced to "buy water from farmers, irrigation districts and municipalities" (Wang and Krupnick, 2013). And with the startup of Eagle Ford Shale, water shortage in Texas is very likely to occur (Wang and Krupnick, 2013).

SUMMARY AND CONCLUSION

Shale gas is becoming an important energy source for the U.S., as predicted to grow from 23% of total energy supply in 2010 to 49% in 2035. The rapid growth has caused water issues, with both fresh water uses and wastewater management. Table 2 summarizes gas production, water demand and quality, management options, and potentials for beneficial use in five major shale plays.

There are four options that are most widely adopted for flowback and produced water management. Currently, operators in Marcellus Shale are reusing over 90% of flowback and produced water, mainly saving for future hydraulic fracturing jobs; 10% of the water for drilling new wells comes from the reused water. Shale plays in Texas, including Barnett Shale, Eagle Ford Shale and Haynesville Shale, are using disposal injection as their primary choice, mainly due to economic consideration and availability of disposal wells. Many operators, however, are considering beneficial reuse because of potential water shortage. In addition, federal, state and local agencies are or have been making regulations and policies on oil and gas wastewater management (Rahm and Riha, 2012, Clark et al., 2012). Under Clean Water Act and Safe Drinking Water Act, the U.S. Environmental Protection Agency (EPA) is developing a proposed rule to control flowback and produced water management (USEPA, 2013). Besides, state governments and agencies are also developing regulations, to better manage oil and gas operations. Regulations and policies differ significantly among states, due to different situations and water issues (Tiemann and Vann, 2013).

Flowback and produced water management is facing significant challenges, involving regulatory, economic and technical factors, such as:

- Both rapid development of shale gas production and nationwide droughts have challenged fresh water availability for exploration and production. Without proper management, availability of fresh water will hinder future oil and gas production due to increasing water demands for drilling and hydraulic fracturing.
- Disposal options and capacities are limited. Regulated by Underground Injection Control Program via the Safe Drinking Water Act (SDWA), only eight deep-injection wells in Pennsylvania are permitted to take oil and gas waste, and only five of them are active (Philips, 2012). Besides, earthquakes are recorded triggered by deep injection wells in Texas, New Mexico, New York, Nebraska, Colorado and Ohio, and possibly in Oklahoma, Louisiana and Mississippi (Nicholson and Wesson, 1951). Therefore, the currently available disposal options may not be able to meet the projected shale gas growth in the future.
- Cost-effective and viable technologies are in urgent needs to treat flowback and produced water with high TDS, organics, TSS and scaling tendency. Current commercially available treatment technologies are energy intensive and often

cost inhibitive. Innovative technical solutions need to be developed to tackle the difficult-to-treat flowback and produced water.

- It is critical to thoroughly understand and characterize the water quality of shale gas wastewater. The flowback and produced water quality is highly variable yet complex, also due to the chemicals added for drilling and hydraulic fracturing. In addition, advanced analytical methods need to be developed and standardized for accurate measurement of the contaminants in a highly saline environment, in particular organic contaminants, for which very limited information is available.
- Beneficial reuse requirements need to be well understood and developed. Potential beneficial use options such as hydraulic fracturing, irrigation, industrial uses, have the water quality requirement based on conventional water supplies. The water quality requirements may need modification to adapt to produced water and flowback water. These standards dictate the selection and design of treatment processes.
- Environmental and health impact of beneficial use applications (e.g., irrigation, municipal and industrial uses) needs to be evaluated in order to reduce the liability issues and protect environment and public health.

Treatment and beneficial use of flowback and produced water is becoming a viable solution for sustainable development of shale gas resources. The challenges with respect to technologies, economics, environment, and regulations however should be addressed for beneficial use to be technically viable and economically attractive.

ACKNOWLEDGEMENT

The authors thank Dr. Engle Mark (USGS), John Veil (Veil Environmental, LLC), Corrie Clark and Christopher Harto (Argonne National Laboratory) for technical advices. This study is funded by the Research Partnership to Secure Energy for America (RPSEA) program (Grant #11122-53).

Table 2. Summary of produced water management in major shale plays

Shale Plays	Marcellus	Barnett	Fayetteville	Haynesville	Eagle Ford
Production Wells	Total wells: 9,715 by Oct 2013; Rapid growth in Pennsylvania since 2008	Total wells: 17,332 by Oct 2013; steady growth since 2009	Total wells: 3,017 by 2010; rapid growth since 2007	Total wells: 1,820 by mid 2011	Total wells: 1,040 by 2012. New shale play, rapid growth
Water Demand per well	300 - 320 m^3 for drilling; 12,500 – 20,800 m^3 for fracturing	950 m^3 for drilling; 14,400 m^3 for fracturing	225 to 250 m^3 for drilling; 11,000 to 18,550 m^3 for fracturing	2,270 – 3,800 m^3 for drilling; 19,000 m^3 for fracturing	50 m^3 for drilling; 7,570-51,860 m^3 for fracturing
Water Quality	TDS: 40 - 90 g/L short term, 140 g/L long term; TSS: 160 ppm; Scaling tendency: moderate	TDS: 50 – 140 g/L; TSS: low; Scaling tendency: moderate; Cl^-: 25 – 80 g/L	Good quality. TDS: 10 – 20 g/L; TSS: Low; Cl^-: 10 g/L.	Very poor quality. High; TDS & TSS: High; High scaling tendency	Under evaluation, high beneficial use potential according to preliminary studies
Current Status of Disposal	Disposal well injection, a small portion to wastewater treatment plant	Disposal well injection for most flowback and produced water			
Current Reuse and Potential	Over 90% of flowback and produced water are reused, most of which are stored for future hydraulic fracturing.	No reuse, but have a high potential because of new regulations and potential water shortage due to droughts	No reuse, but have a high potential because of new regulations and potential water shortage due to droughts	No reuse. Poor quality makes it less attractive. Drilling mud is more feasible for reuse for its relative high quality	No reuse, but have a high potential because of new regulations and potential water shortage due to droughts
Current Treatment Technology for reuse	Oil/gas - water separation; filtration; dilution with freshwater	Not available			

REFERENCES

AGS (2010) Arkansas Geological Survey. Microsoft Excel spreadsheet containing Fayetteville Shale well information updated through December 2010. Available at: <http://www.geology.ar.gov/xl/Fay_Wells.xls>; accessed January 6, 2011.

Amico, C., DeBelius, D., Detrow, S. and Stiles, M. (2013) Shale Play Natural Gas Drilling in Pennsylvania. Available at: <http://stateimpact.npr.org/pennsylvania/drilling/%3E. [cited on: September 12, 2013].

Arthur, J.D. (2011) Water Management Planning in the Eagle Ford Shale Play. Presented at the Society of Petroleum Engineers Eagle Ford Technical Workshop. August 24-26, 2011. Available at: <http://www.all-llc.com/publicdownloads/ALLEagleFordWMP082411.pdf%3E. [Cited on December 1, 2013].

Clark, C., Burnham, A., Harto, C. and Horner, R. (2012) Hydraulic Fracturing and Shale Gas Production: Technology, Impacts, and Policy. Argonne National Laboratory. September 10, 2012. Avaiable at: <http://www.ourenergypolicy.org/wp-content/uploads/2012/10/Hydraulic_Fracturing_and_Shale_Gas_Production.pdf%3E. [Cited on August 22, 2013]

Clark, C.E. and Veil, J.A. (2009) Produced Water Volumes and Management Practices in the United States. ANL/EVS/R-09/1. Prepared for U.S. Department of Energy, Office of Fossil Energy. National Energy Technology Laboratory under Contract DE-AC02-06CH11357.

EIA (2012) Annual Energy Outlook 2012 Early Release Overview. Report #:DOE/EIA-0383ER(2012). Release Date: January 23, 2012. Available at: <http://www.eia.gov/forecasts/aeo/er/executive_summary.cfm> Retrieved: Feb, 23, 2012., U.S. Energy Information Administration.

Hayes, T. (2010) Produced water reserch projects. RPSEA Unconventional Gas Conference. Available at: <http://www.rpsea.org/files/2028/%3E. [Cited September 1, 2013].

Mantell, M.E. (2011) Produced water reuse and recycling challenges and opportunities across major shale plays. EPA. 2011. Presentation at the EPA Hydraulic Fracturing Study Technical Workshop #4 Water Resources Management. March 29-30, 2011. Available at: <http://www2.epa.gov/sites/production/files/documents/09_Mantell_-_Reuse_508.pdf%3E. [Cited on September 1, 2013].

Nicholson, C. and Wesson, R.L. (1951) Earthquake hazard associated with deep well injection - a report to the U.S. Environmental Protection Agency. U.S. Geological Survey (USGS). Available at: <http://pubs.usgs.gov/bul/1951/report.pdf%3E. [Cited on December 9, 2013].

Nicot, J.-P. and Scanlon, B.R. (2012) Water Use for Shale-Gas Production in Texas, U.S. Environmental Science and Technology 46(3580−3586).

Philips, S. (2012) Deep injection wells in Pennsylvania. Pennsylvania State Impact: Energy. Environment. Economy. Available at: <http://stateimpact.npr.org/pennsylvania/maps/location-of-deep-injection-wells-in-pennsylvania/> [Cited December 11, 2013].

Rahm, B.G. and Riha, S.J. (2012) Toward strategic management of shale gas development: Regional, collective impacts on water resources. Environmental Science & Policy 17, 12-23.

Rahm, B.G., Bates, J.T., Bertoia, L.R., Galford, A.E., Yoxtheimer, D.A. and Riha, S.J. (2013) Wastewater management and Marcellus Shale gas development: trends, drivers, and planning implications. J Environ Manage 120, 105-113.

RRC (2013a) Barnett Shale Information. Updated: November 20, 2013 by Railroad Commission Texas. Available at: <http://www.rrc.state.tx.us/barnettshale/index.php%3E. [Cited on December 1, 2013].

RRC (2013b) Barnett Shale Information. Oil and Gas Production Data Query System (PDQ). Railroad Commission of Texas. Available at: <http://webapps.rrc.state.tx.us/PDQ/home.do%3E. [Cited December 1, 2013].

RRC (2013c) Water Use in Association with Oil and Gas Activities. Railroad Commission of Texas. Available at: <http://www.rrc.state.tx.us/about/faqs/wateruse.php - 6>. [Cited on December 9, 2013].

Tiemann, M. and Vann, A. (2013) Hydraulic Fracturing and Safe Drinking Water Act Regulatory Issues. Congressional Research Service. 7-5700. Available at: <http://www.fas.org/sgp/crs/misc/R41760.pdf%3E. [Cited Decmber 10, 2013]

USEPA (2013) Unconventional Extraction in the Oil and Gas Industry. United States Environmental Protection Agency. Available at: <http://water.epa.gov/scitech/wastetech/guide/oilandgas/unconv.cfm%3E. [Cited on December 6, 2013].

Veil, J. (2011) Water Management Practices Used by Fayetteville Shale Gas Producers. Report prepared for U.S. Department of Energy, Office of Fossil Energy, and National Energy Technology Laboratory. ANL/EVS/R-11/5. Available at: < http://www.veilenvironmental.com/publications/pw/Water_Mgmt_in_Fayetteville_Shale.pdf%3E. [Cited August 3, 2013].

Veil, J.A. (2013) Shale gas water management - experiences from north America. Lecture for the Society of Petroleum Engineers.

Wang, Z. and Krupnick, A. (2013) A Retrospective Review of Shale Gas Development in the United States. 2013 Resources for the Future. Available at: <http://www.rff.org/RFF/documents/RFF-DP-13-12.pdf> [Cited December 2, 2013]

Characterization of Waste Waters from Hydraulic Fracturing

Paul F. Ziemkiewicz[1], PhD, Yongtian He[2], PhD and John D. Quaranta[3], PhD, P.E.

[1] Director, West Virginia Water Research Institute, West Virginia University, P.O. Box 6064, Morgantown, West Virginia
[2] Research Chemist, West Virginia Water Research Institute, West Virginia University, P.O. Box 6064, Morgantown, West Virginia
[3] Assistant Professor, Department of Civil and Environmental Engineering, West Virginia University, P.O. Box 6103, Morgantown, West Virginia

ABSTRACT: Large-scale development of the Appalachian Basin shale gas resources began in 2008. Waste water, its characterization and handling have emerged as critical components in the industry's environmental management strategy. This study summarizes the literature on flowback characterization: organic, inorganic and radioactivity.

We found that inorganic constituents were dominated by extremely high concentrations of Na, Cl, Ca, Mg, Br, Ba and Sr with total dissolved solids concentrations approaching 200,000 mg/L. While many organic compounds were found at high concentrations, only benzene was consistently found in excess of its drinking water standard (MCL 5 μg/L). Normally occurring radioactive materials (NORMs) were also examined and α, β, ^{226}Ra and ^{228}Ra were consistently found above their primary drinking water MCLs in flowback water.

Concentrations of all of these constituents increased during the flowback cycle and concentrations of nearly all measured parameters were much higher in flowback water than in the injected hydraulic fracturing fluids. This indicates that the bulk of measured constituents, including benzene, are acquired through fluid contact with the formation and not from the injected hydraulic fracturing fluid.

INTRODUCTION

In the shale gas context, well completion refers to the process of drilling and stimulating a well in preparation for hydrocarbon production. Hydraulic fracturing is a well stimulation process in which a high volume mixture of water, sand and chemical additives are injected into a geologic formation at high pressures thereby opening or enlarging fractures in the rock (US EPA 2010). Combined with horizontal drilling and development of lateral well bores in excess of 1,000 m long, hydraulic fracturing technology makes the development of shale gas economically viable.

Hydraulic fracturing requires significant quantities of water: Requirements commonly range from 11,000 to 19,000 m^3 for a horizontal well, but volumes as high

as 34,000 m^3 have been reported (Xu et al., 2011; Lewis, 2012; Bai et al., 2013). Fracturing fluid typically consists of between 80 to 90 percent water; 8 to 15 percent proppant while the remaining 0.5- 1 percent consists of chemical additives. Commonly used additives include about 11 chemicals with different functions such as friction reducers, biocides, scale inhibitors, clay stabilizers, and surfactants (URS, 2011; McCurdy, 2011).

Figure 1 shows the general processes of fluid flow during hydraulic fracturing and gas production. During well completion, hydraulic fracturing fluids are injected into the target formation and the injected fluids return to surface via the well bore as flowback. Produced water is the fluid returned via the well bore along with gas during production phase. The distinction between flowback and produced water is not well defined and these two terms are sometimes used interchangeably in the vernacular.

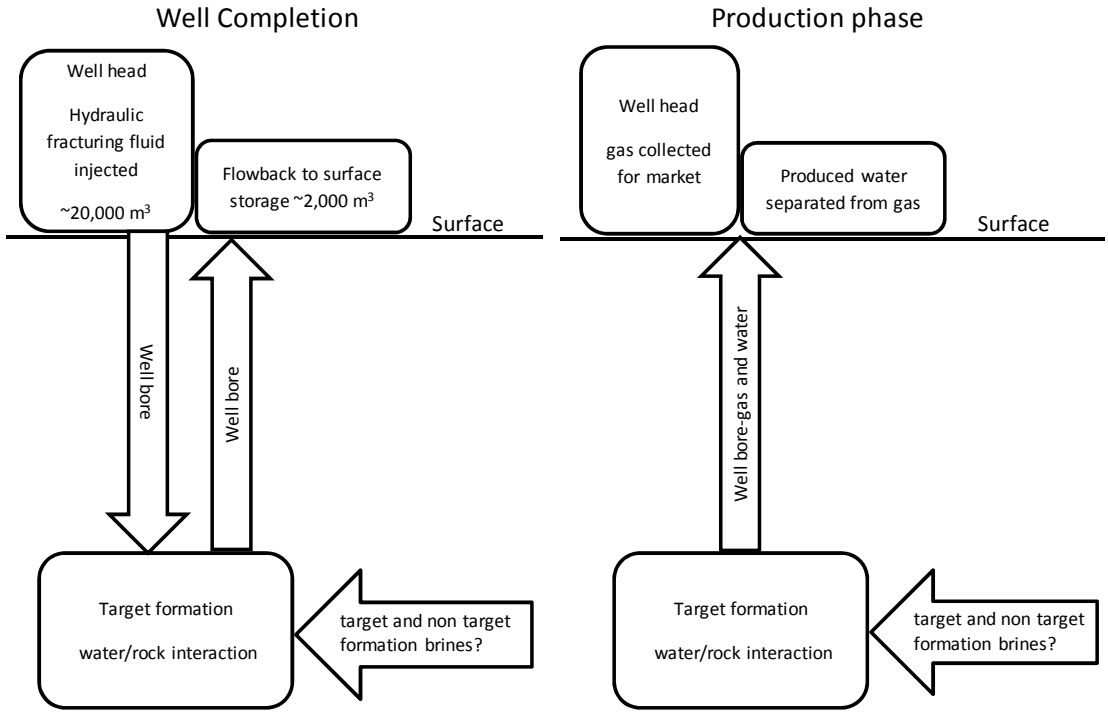

FIG. 1. Flow of fluids during the well completion (hydraulic fracturing) and production phases of well operations.

There is growing concern over the composition, environmental impact, and fate of **Flowback and Produced Water (FPW)**. Typical FPW disposal methods include dilution and re-use at subsequent wells completions, haulage to approved treatment facilities or class II underground injection wells. However, each of these options has its limitations and present different challenges. Leakage is possible at any stage in the handling of FPW with the potential to affect surface water or shallow groundwater through accidents or improper handling. If the integrity of the well's production casing is compromised, leakage of methane and FPW to shallow aquifers could result. Better understanding of FPW genesis, and chemistries will assist in the development of effective handling, recycling, treatment and disposal methods However, there is

little published literature on the mineralogy of the Marcellus formation or the genesis of FPW chemistry. The composition of FPW and the factors that control its composition are not well characterized and not well understood.

The objectives of this manuscript are to: 1) review and characterize FPW composition focusing on the Marcellus shale, 2) understand the processes and mechanisms that contribute to FPW composition, and 3) identify the environmental implications related to FPW management.

FLOWBACK/PRODUCED WATER VOLUME TRENDS AND COMPOSITION

Flowback and produced water volume trends

The volume of FPW recovered from a shale gas well varies with the characteristics of a particular shale formation, the depth and age of the well, drilling and well completion methods. Hydraulic fracturing is most successful in desiccated and thus brittle shale formations. Typically 10-40% of injected fluids returns to the surface as flowback and produced water in the Marcellus formation, but a much wider range 5-80% is reported across U.S. shale formations (USDOE 2009; URS, 2011; Lutz et al., 2013). Some of the discrepancies of reported range may be related to how flowback are defined and whether flowback is distinguished from produced water.

The literature contains few examples of measured long term flowback trends. The authors obtained gas industry operating estimates for Marcellus FPW return volumes for a ten year period. The data are based on a total fluid injection of 16,000 m^3 (Figure 2). The projections can be approximated using the following power functions:

$$y=0.0871x^{0.2541},\ R^2=0.986 \quad (1)$$

Where: y= cumulative percent FPW returned and x=months since initial flowback

$$y=382.64x^{-0.723},\ R^2=0.904 \quad (2)$$

Where: y=FPW generated per month and x=months since initial flowback

Fluid return during the first month was 1,569 m^3 declining to 54 m^3/month or 1.8 m^3/day after the first year. Using equation 1 to extrapolate cumulative FPW returns to 100 years suggests production of only 54% of injected fluid. It is not at all certain that the wells would still be functional at extended time frames, therefore, using 10 years as a practical cutoff for FPW returns, about 4,800 m^3 or 30% of the initially injected fluid would ultimately be produced. Of that amount, about 2,600 m^3 or 51% would be produced in the first year. Bai et al. (2013) pointed out that with more water used in the process and longer flowback time, horizontal wells have a higher water production rate than vertical wells, and horizontal wells also have a faster decay in the first year of operation because of the large volume of flowback generated in the first year. URS (2011) indicated, based on daily time series data, that approximately 60 percent of the total FPW occurs in the first four days after fracturing and that most FPW was recovered in the first 1 to 2 weeks. During the gas production phase, aqueous and non-aqueous liquid was produced at the surface in much lower volumes

(2–8 m^3/day) over the lifetime of the well. Bai et al. (2013) developed a model to

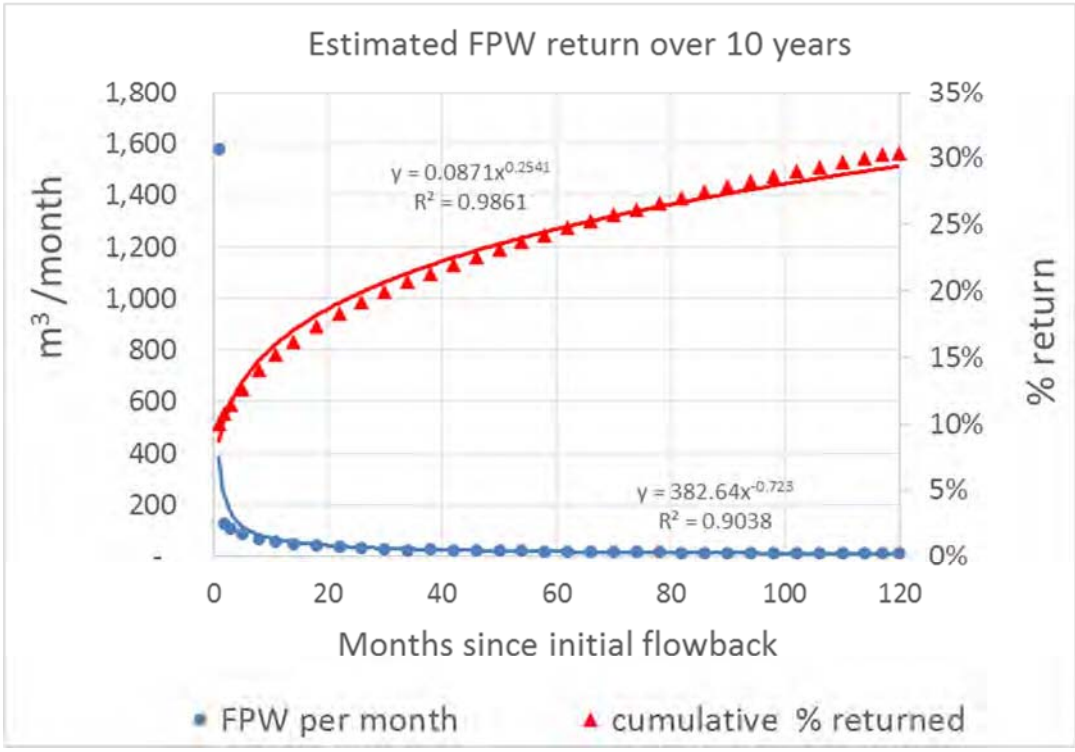

predict flowback and

FIG. 2. Volume trends for flowback and produced water in Marcellus shale gas wells. Prediction equations and resulting curves (solid lines) are included (from Ziemkiewicz et al. 2014).

produced water flow volumes from the Wattenberg oil and gas field in Colorado. They used an exponential curve for flowback and the harmonic curve for produced water.

FPW composition and trends

The composition of FPW is a function of makeup water quality, hydraulic fracturing fluid additives, formation geology (geologic age, depth and mineralogy), contact of hydraulic fracturing fluid with the formation and the time the fluid spends both underground and on the surface after hydraulic fracturing (Horner and Slutz, 2011). While chemical concentrations vary among FPW samples the major ions are broadly similar. Figure 3 shows the typical concentration trends of major constituents in FPW. Similar trends have been shown in Barbot et al. (2013) and Haluszczak et al. (2013). The general increase in dissolved constituents in FPW corresponds with a decrease in flow volume. Figure 3 is plotted using the average value of data collected from 19 wells across the Marcellus formation (Hayes, 2009). The makeup water injected into these wells had a median TDS of less than 1,000 mg/L, but within 90 days

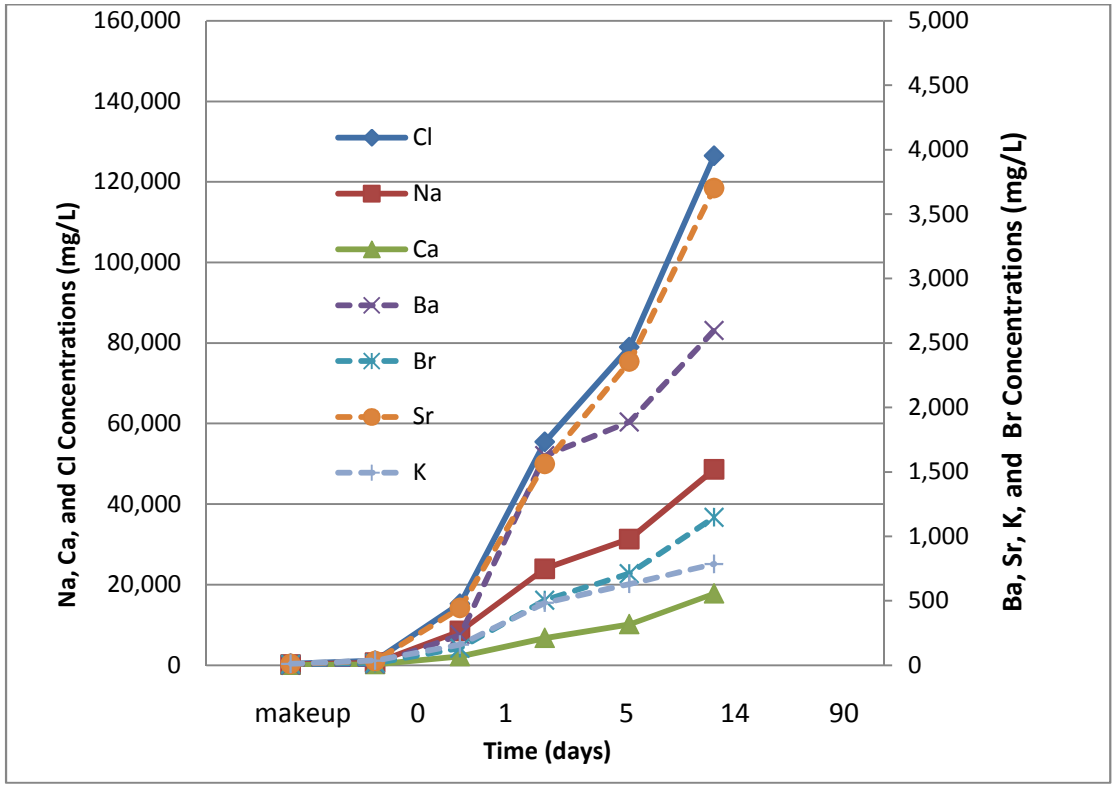

FIG. 3. Major FPW constituent concentration trends over time (Data from Hayes, 2009)

the salinities had increased to a median value exceeding 200,000 mg/L TDS. Hayes (2009) suggested that the marked increase in salinity with time is likely due to a decreasing proportion of the lower salinity injected fluid and an increasing proportion of the saline formation water returning to the surface. Salinity/TDS levels in FPW vary widely across the Marcellus Shale, from less than 1,500 mg/L to greater than 300,000 mg/L. Typically, early FPW emerging soon after well completion is relatively low in TDS and reflects the chemistry of the injected fluids. Later FPW is more influenced by formation brines. The upper end of the TDS range is comparable to brine waters produced from the underlying Lower Devonian and older reservoirs as well as some of the overlying Devonian reservoirs (Rowan et al., 2010).

In addition to the constituents shown in Figure 3, other minor components such as Fe, trace metals, naturally occurring radioactive materials (NORMs), and organic compounds also increase over time during flowback. Some constituents may result from higher ratio of mixing with formation brine in the later flowback, while other constituents may result from interaction of hydraulic fracturing fluid with formation minerals. On the other hand, the sulfate concentration has been observed to decrease over time in flowback (Haluszczak et al., 2013).

Key components of FPW

FPW chemistry is dominated by inorganic salts, metals, NORMs, and a wide variety of organic compounds. Table 1 summarizes several recent reports on chemical

composition of FPW in the literature. Hayes (2009) reported a comprehensive sampling study of FPW in 19 wells across Marcellus shale in PA and WV. The data from this study is also used in several recent studies (Barbot et al., 2013; Haluszczak et al, 2013). URS (2011) reported values of up to 193 samples from PA and WV including inorganics, a few organics and NORMs. Haluszczak et al. (2013) compiled analytical data of 22 samples from Bureau of Oil and Gas Management (BOGM), Pennsylvania Department of Environmental Protection (PADEP) and 7 samples from Hayes (2009). Barbot et al. (2013) also summarized data of up to 159 samples from more than 40 sources from PADEP and Marcellus Shale Coalition sampling from several wells reported by Hayes (2009).

Most of these studies rely on datasets that focus on major inorganic constituents such as Cl, Na, Ca, Ba and Sr. However, there is very little information on organics and trace metals in FPW. Information on NORMs in FPW in these analyses is also very limited.

Sulfates or carbonates in the fluid may lead to formation of a number of precipitates including $CaCO_3$, $BaSO_4$, $SrSO_4$. FPW is generally sufficiently alkaline that, upon oxidation, $Fe(OH)_3$ may form. Table 2 summarizes the solubility of common cations found in FPW and their chloride, sulfate and carbonate minerals. The low values for strontium and barium sulfates and carbonates indicate a strong tendency to precipitate and form scale at atmospheric pressures and temperatures. Precipitation is expected to be more pronounced at elevated temperature and pressure. However, behavior of these constituents at the elevated pressures and temperatures of a deep, horizontal well are poorly documented. These precipitates could occur in the fractures, perforations or the production casing, reducing permeability and ultimately gas production. Precipitates can also occur in pumps, tanks and other equipment which can reduce functionality (Horner and Slutz, 2011).

NORM

The most abundant radioactive isotopes FPW are ^{226}Ra and ^{228}Ra. Radium is derived from the radioactive decay of ^{238}U and ^{232}Th, which commonly occur in sandstones and shales in sedimentary settings such as hydrocarbon reservoirs (Kraemer and Reid 1984; Michel 1990; Neff et al., 2011). In surface and shallow subsurface environments, radium can be relatively soluble in groundwater over a range of pH and Eh (redox) conditions (Langmuir and Riese, 1985; Sturchio et al., 2001). Fisher (1998) found factors favoring Ra release to fluids include a large surface-to-volume ratio of U- and Th-containing materials, well-connected pore spaces, the presence of U and Th near grain surfaces and water filled pore spaces.

Rowan et al. (2011) indicated higher NORM in Marcellus shale than other shale formations. The range of radium activities for Marcellus Shale core samples (less than detection to 18,000 picocuries per liter (pCi/L)) overlaps the range for non-Marcellus reservoirs (less than detection to 6,700 pCi/L), and the median values for Marcellus and non-Marcellus shale are 2,460 pCi/L and 734 pCi/L, respectively. However, Fisher (1998) explored natural controls on radioactivity based on NORM in produced waters from oil, gas and geothermal operations in several locations across the U.S. He found

Table 1. Reported chemical composition of FPW in the literature

source		URS, 2011			Gaudlip et al., 2008			Blauch et al., 2009			Barbot et al., 2013			Haluszczak et al., 2013 a			Haluszczak et al., 2013b		
analyte	units	min	median	max	min	median	max	min	median	max	min	mean	max	min	median	max	min	median	max
TDS	mg/L	1530	63800	337000	9751	110847	200006	1850	20900	219000	680	106390	345000	3010	157000	228000	7510	42200	197000
TSS	mg/L	16	129	2080							4	352	7600	17	209	1150			
Hardness	mg/L	203	11354	98000				500	2500	32400				630	34000	95000			
pH			6.6	8.58	5.83	5.93	7	6.17	7.5	10.1	5.1	6.56	8.42	5.8	6.2	6.6	5.1	7.4	11.6
Alkalinity	mg/L	0	9485	48336				54	138	236	7.5	165	577	26	71	95	29	212	607
Cl	mg/L	287	56900	228000	5000	68000	125000	815	12400	169000	64.2	57447	196000	1070	98300	151000	390	24900	105000
SO_4	mg/L	0	1	1270	10	20	60	63.4	205	1010	0	7.1	763	0.8	<50	89.3	<5	51	420
Br	mg/L	11.3	607	3070				25.4	356	688	0.2	511	1990	16	872	1190	<2..2	233	613
Na	mg/L	83.1	23500	96700	1477	34548	54629	386	4340	69800	69.2	24123	117000	1100	36400	44100	1210	9530	37800
Ca	mg/L	29.9	4241	123000	241	6800	15680	176	739	8610	37.8	7220	41000	204	11200	14800	112	1350	17900
Mg	mg/L	9	177	3190	49	1707	6062	7.11	51.9	927	17.3	632	2550	22	875	1800			
Sr	mg/L	0.5	1115	5841				13	22	1800	0.59	1695	8460	46	2330	5350	6	213	3570
Ba	mg/L	0.55	1450	15700	1	112	547				0.24	2224	13800	76	1990	13600	4	314	6270
Fe	mg/L	0	29.2	810	4	92	1274	0.37	2.35	202	2.6	76	321	14	47	59			
Mn	mg/L	0.15	1.89	97.6	1.4	1.8	99.6	0.25	2.42	20.5				1.2	5.6	8.4	0.28	1.67	29.4
Pb	mg/L	0.008	0.035	27.4				<0.01	0.02	0.07									
Ni	mg/L	0.03	0.072	0.113				<0.01	0.09	0.16									
Zn	mg/L	0.07	0.07	0.07										0.07	0.09	0.14			
Oil/grease	mg/L	5	17	1470							4.6	74	802	4.6		103			
Benzene	µg/L	15.7	479.5	1950															
Phenols	µg/L	50	191	440															
^{226}Ra	pCi/L	2.58	4.67	33							2.75	623	9280				40	262	5830
^{228}Ra	pCi/L	1.15	4.66	18.41							0	120	1360				0	30	710
Sample size		varies, up to 193			5			7			varies, up to 159			7			22		

Note: URS, 2001 is based on samples from Pennsylvania and West Virginia (maximum sample size for each analyte is 193).

Gaudlip et al., 2008 from randomly selected 5 samples, Blauch et al., 2009 from 7 analysis of Marcellus Shale flowback water delivered to a POTW.

Barbot et al., 2013 used data from PADEP Bureau of Oil and Gas Management of analysis of flowback/produced water from more than 40 sources and Marcellus Shale Coalition analysis (Hayes 2009.),Haluszczak et al., 2013a, data from 7 horizontal wells of Marcellus Shale Coalition sampling (Hayes 2009.), Haluszczak et al., 2013b, data from PADEP Bureau of Oil and Gas I

Table 2. Estimated mineral solubility of cations common in FPW and their chloride, sulfate and carbonate minerals.

chlorides		sulfates		carbonates	
mineral	solubility (mg/L)	mineral	solubility (mg/L)	mineral	solubility (mg/L)
a) NaCl	360,000	a) Na_2SO_4	281,000	a) Na_2CO_3	307,000
a) $MgCl_2$	560,000	a) $MgSO_4$	357,000	a) $MgCO_3$	390
a) $CaCl_2$	813,000	a) $CaSO_4$	2,505	b) $CaCO_3$	5.8
a) $SrCl_2$	547,000	b) $SrSO_4$	108	b) $SrCO_3$	3.5
a) $BaCl_2$	370,000	b) $BaSO_4$	2.4	b) $BaCO_3$	10
a) $RaCl_2$	245,000	b) $RaSO_4$	2.1	c) $RaCO_3$	insoluble

a) from solubility table

b) derived from K_{sp}

c) reported insoluble, no K_{sp} available

Note: A solubility table from Handbook of Chemistry and Physics (93rd web version) was used for the more soluble minerals while K_{sp} values were used to calculate values for the less soluble minerals. All estimates were based on 20 ºC.

no regional control on Ra activity, but his study does not include samples from the Marcellus formation.

Radium has been documented in formation waters in many sedimentary basins (Rowan et al., 2011; Dresel and Rose, 2010), and it has been measured in the water co-produced with gas and oil from Devonian (Marcellus) age rocks in the Northern Appalachian Basin. Like organic and inorganic compounds, NORMs tend to increase during the flowback cycle. Mobilized radionuclides found in flowback depend on the geologic formation from which the water is produced (Ray et al. 1992). Levels of NORM in Marcellus Shale FPW tend to be relatively low, with increasing concentration through the flowback cycle. McElreath (2011) reported a range of gross alpha and beta from 620 to 4,000 pCi/L (mean value 1,750 pCi/L), and 250 to 1,200 pCi/L (mean value 760 pCi/L), respectively. Ziemkiewicz et al. (2013) reported gross alpha and beta ranged from 8.69 to 965 pCi/L and 34 to 317 pCi/L from 13 FPW samples, respectively; while ^{226}Ra and ^{228}Ra ranged from 15.4 to 1,194 pCi/L and 4.99 to 216 pCi/L, respectively.

Organic compounds

Information on organic compound concentrations in FPW is very limited. There is no agreement regarding which organic compounds should be routinely determined in order to characterize risk in FPW.

The most consistently detected volatile organic compounds (VOC) were benzene, toluene, ethyl benzene and xylenes (BTEX), naphthalene, acetone, phenol, and methyl chloride (Coleman, 2011; Hayes, 2009; Ziemkiewicz et al., 2013). These compounds may originate from naturally hydrocarbons in the formation, but they may also originate from drilling activities and hydraulic fracturing fluids additives.

However, Ziemkiewicz et al. (2013) reported that all four BTEX compounds increased during the flowback cycle from below detection to 100s-1000s µg/L suggesting a formation source.

Similar to metals, concentrations of VOCs in FPW are generally low. Benzene is a known carcinogen, with an primary drinking water limit of 5 µg/L. URS (2011) reported benzene detection in 14 of 35 collected samples, ranging from 15.7 to 1950 µg/L, with a median value of 479.5 µg/L. Hayes (2009) reported that approximately 96% of VOCs were found at non-detectable levels, 0.5% of the compounds with the higher concentrations reported in the 1-2 mg/L range. Nearly all of the semi-volatile organic compounds (SVOC) determinations were either non-detect or at trace levels, only bis(2-chloroethyl) ether and pyridine were measured at levels greater than 1 mg/L. Oil and grease range from 4.6 to 655 mg/L, with median value of 6.3 mg/L (Hayes, 2009). Other organic compounds such as ethylene glycols, 2-Butoxy ethanol, and 2,2-Dibromo-3-nitrilopropionamide (DBNPA) are thought to be biodegradable and unlikely to persist in the environment (McGrath, 2011). The toxicity and health risk associated with some organic constituents in FPW highlight the need for improved characterization.

CONCLUSIONS

We found that the inorganic fraction was dominated by extremely high concentrations of Na, Cl, Ca, Mg, Br, Ba, Sr with total dissolved solids concentrations approaching 200,000 mg/L. While many organic compounds were found at high concentrations, only benzene was consistently found in excess of its drinking water standard (MCL 5 µg/L). Naturally occurring radioactive materials (NORMs) were also examined and α, β, ^{226}Ra and ^{228}Ra were consistently found above their primary drinking water MCLs in flowback water.

Concentrations of all of these constituents increased during the flowback cycle and concentrations of all measured parameters were much higher in flowback water than in the injected hydraulic fracturing fluids. This indicates that the bulk of potential contaminants are acquired through fluid contact with the formation and not from the injected hydraulic fracturing fluid.

Chemical composition of FPW: its major constituent ions was consistent among studies. Concentrations, however, were highly variable. The few time series collected during the flowback cycle suggest that much of that variability reflects temporal changes.

REFERENCES

Bai, B., Goodwin, S., and Carlson, K. 2013. Modeling of frac flowback and produced water volume from Wattenberg oil and gas field. Journal of Petroleum Science and Engineering. http://dx/doi.org/10.1016/j.petrol.2013.05.003.

Barbot, E. Vidic, N. S. Gregory, K. B. Vidic, R. D. 2013. Spatial and Temporal Correlation of Water Quality Parameters of Produced Waters from Devonian-Age Shale following Hydraulic Fracturing. Environmental Science and Technology 47, 2562-2569.

Blauch, M.E., Myers, R.R., Moore, T.R., Lipinski, B.A., and Houston, N.A., 2009. Marcellus shale post-frac flowback waters-where is all the salt coming from and what are the implications? SPE International SPE 125740.

Coleman, N.P., 2011. Produced formation water sample results from shale plays. Proceedings of the Technical Workshops for the Hydraulic Fracturing Study: Chemical and analytical methods. EPA 600/R-11/066.

Dresel, P. E., and Rose, A. W. 2010. Chemistry and origin of oil and gas well brines in western Pennsylvania: Pennsylvania Geological Survey, 4th ser., Open-File Report OFOG 10–01.0, pp.48

Fisher, R.S., 1998. Geologic and geochemical controls on naturally occurring radioactive materials in produced water from oil, gas and geothermal operations. Environmental Geosciences 5, 139-150.

Gaudlip, A.W. and Paugh, L.O. 2008. Marcellus shale water management challenges in Pennsylvania. SPE International SPE 119898.

Haluszczak, L. O. Rose, A. W. Kump, L. R. 2013. Geochemical evaluation of flowback brine from Marcellus gas wells in Pennsylvania, USA. Applied Geochemistry 28, 55-61.

Hayes, T., 2009. Sampling and analysis of water streams associated with the development of Marcellus shale gas. Final report prepared for Marcellus Shale Coalition, Gas Technology Institute, Des Plaines, IL 60018.

Horner, P. and Slutz, J., 2011. Shale gas water treatment value chain- A review of technologies, including case study. SPE International SPE 147264.

Kraemer, T.F., Reid, D.F. 1984. The occurrence and behavior of radium in saline formation water of the U.S. Gulf coast region. Chemical Geology 2,153–174

Langmuir, D. and Riese, A.C., 1985, The thermodynamic properties of radium. Geochimica et Cosmochimica Acta 49, 1593–1601.

Lewis, A. 2012. Wastewater generation and disposal from natural gas wells in Pennsylvania. Master Thesis. Duke University.

Lutz, B.D., Lewis, A.N., and Doyle, M.W., 2013. Generation, transport, and disposal of wastewater associated with Marcellus shale gas development. Water Resources Research. 49, 647-656.

McCurdy, R. 2011. High rate hydraulic fracturing additives in non-Marcellus unconventional shales. Proceedings of the Technical Workshops for the Hydraulic Fracturing Study: Chemical and Analytical Methods. EPA 600/R-11/066.

McElreath, D., 2011. Comparison of hydraulic fracturing fluid composition with produced water following fracturing-Implications for fate and transport. Proceedings of the Technical Workshops for the Hydraulic Fracturing Study: Fate and Transport. EPA 600/R-11/047.

McGrath, A.E., 2011. Fate and transport of select compounds of potential concern in hydraulic fracturing fluids. Proceedings of the Technical Workshops for the Hydraulic Fracturing Study: Fate and Transport. EPA 600/R-11/047.

Michel, J. 1990. Relationship of radium and radon with geological formations. In: Cothern CR, Ribers PA (eds) Uranium in drinking water. Lewis Publishers, Chelsea, MI, pp 83–95

Neff, J., Lee, K., DeBlois, E.M., 2011. Chapter 1 Produced water: overview of composition, fates, and effects. P. 3-54. In *Produced water* K. Lee and J. Neff (eds.).

Ray, J.P. and Engelhardt, F.R. 1992. Produced Water – Technological/Environmental Issues And Solutions. Eds.; Plenum Press, New York & London.

Rowan, E.L., Engle M.A., Kirby, C.S. 2010. Inorganic Geochemistry of Formation Waters from Devonian Strata in the Appalachian Basin – Preliminary Observations from Pennsylvania, New York, and West Virginia. Geological Society of America Abstracts with Programs, Vol. 42, No. 5, p. 487. http://gsa.confex.com/gsa/2010AM/finalprogram/abstract_174638.htm

Rowan, E.L., Engle, M.A., Kirby, C.S., and Kraemer, T.F., 2011, Radium content of oil- and gas-field produced waters in the northern Appalachian Basin (USA)—Summary and discussion of data: U.S. Geological Survey Scientific Investigations Report 2011–5135, p.31

Sturchio, N.C., Banner, J.L., Binz, C.M., Heraty, L.B., and Musgrove, M., 2001, Radium geochemistry of ground waters in Paleozoic carbonate aquifers, midcontinent, USA. Applied Geochemistry 16, 109–122.

US Department of Energy (USDOE), 2009. Modern shale gas development in the United States: A primer. DOE-FG26-04NT15455, pp.166. Washington, D.C.

U.S. Environmental Protection Agency (USEPA), 2010. Office of Research and Development. Hydraulic Fracturing Research Study. Retrieved on May 2011, from http://www.epa.gov/safewater/uic/pdfs/hfresearchstudyfs.pdf

URS, 2011. Water-related issues associated with gas production in the Marcellus shale. NYSERDA contract PO number 10666, Fort Washington, PA.

Xu, P., Cath, T., and Drewes, J.E., 2011. Novel and emerging technologies for produced water treatment. US EPA Technical Workshops for the Hydraulic Fracturing, Arlington, VA.

Ziemkiewicz, P.F, Hause, J., Gutta, B., Fillhart, J., Mack, B. and O'Neil. M. 2013. Assessing environmental impacts of horizontal gas well drilling operations. Final report to West Virginia Department of Environmental Protection.

Ziemkiewicz, P.F., Quaranta, J.D., Darnell, A. and Wise, R. 2014. Exposure pathways related to shale gas development and procedures for reducing environmental and public risk, Journal of Natural Gas Science and Engineering, Volume 16, January 2014, Pages 77-84, ISSN 1875-5100, http://dx.doi.org/10.1016/j.jngse.2013.11.003.

Ziemkiewicz, P.F., Quaranta, J.D. and McCawley, M. 2014. Practical measures for reducing the risk of environmental contamination in shale energy production. Environ. Sci: Processes Impacts. DOI:10.1039/C3EM00510K.

Electrodialysis Treatment of Flow-Back Water for Environmental Protection in Shale Gas Development

Maria Peraki[1], Ehsan Ghazanfari[2]

[1]PhD Student, Civil and Environmental Engineering Program, University of Vermont, Burlington VT; Email: mperaki@uvm.edu
[2]Assistant Professor, Civil and Environmental Engineering Program, University of Vermont, Burlington VT; Email: ehsan.ghazanfari@uvm.edu

ABSTRACT: In the domain of shale gas extraction, water is used during the process of fracturing the shale in order to retrieve the gas trapped in the formation. A portion of the injected water is recovered during the initial extraction of the gas, which is known as flow-back water. Electrodialysis is an alternative for onsite treatment (or pre-treatment) and recycling of the flow-back water, which has gained more attention in recent years. The method is based on an electrically assisted membrane process for separation of salts from the water. Flow-back water has very high concentrations of dissolved solids (e.g. calcium, barium, magnesium, and iron) and electrodialysis is highly susceptible to these cations and has great potential to be used as a desalination process in such aggressive environment. In this study, the efficiency of the electrodialysis as a desalination process for flow-back water was investigated using samples of flow-back from Marcellus shale wells in the laboratory scale. The preliminary findings in the experimental evaluation of the method indicated a removal of total dissolved solids of more than 90%.

INTRODUCTION

The Marcellus shale gas play is among the largest and most active natural gas plays in United States. One of the major processes involved in the extraction of natural gas, is the hydraulic fracturing of the shale formation (Hayes et al., 2012). The main supplies of water for hydraulic fracturing are surface water, groundwater, or recycled water (Arthur et al., 2011). The volume of injected water in the Marcellus play varies between 10,000 and 30,000 cubic meter per well (Rahm et al., 2013). Almost 90% of the injected volume remains bound to the dry shale matrix and only 10-20% is recovered as wastewater stream, known as flow back water (Rahm et al., 2013; Arthur et al., 2011; Veil et al., 2010).

Flow-back water is considered as a mixture of hydraulic fracturing fluids returning to the surface, which also contains chemical constituents originating from the shale formation (Rahm et al., 2013; Arthur et al., 2011). The flow-back water contains various natural inorganic and organic compounds such as sodium, calcium,

magnesium, chloride, sulfate, barium, iron and several others (Arthur et al., 2011; Castle et al., 2013). It also contains chemical additives used during the drilling, fracturing and operation of the well and in some cases naturally occurring radioactive materials (Arthur et al., 2011; Hayes et al., 2012; Castle et al., 2013). The predominant constituents of flow-back water are the dissolved salts that can be identified using conductivity, salinity, or total dissolved solids (TDS) measurements. The concentration of TDS in the flow-back water for the Marcellus play varies between 30,000 mg/L and 200,000 mg/L (Arthur et al., 2011; Castle et al., 2013; Hayes et al., 2012; Lutz et al., 2013). With a production of 21 billion barrels per year in the USA (2007), flow-back water consists the largest byproduct stream of the shale gas extraction (Arthur et al., 2011). In Marcellus play the water demand, and therefore, the volume of the wastewater stream has increased during the past years (Rahm et al., 2013). Although, the Marcellus play has access to sufficient water supplies, the treatment and disposal of the flow-back water represent a major cost item (Godec et al., 2007; Hayes et al., 2012; Veil et al., 2010).

The common practice in shale gas extraction for the management of flow-back water, is the disposal in deep wells (Class II wells). In the Marcellus shale play, there are only 7 Class II wells. In Pennsylvania, about 87 % of the flow-back water was transported to commercial wastewater treatment plants that operate under the permission of the state environmental protection agency (Arthur et al., 2006; Hayes et al., 2012; Lutz et al., 2013; Veil et al., 2010). However, after the recent earthquakes in the state of Ohio that are linked with the injection of waste water in deep wells, the amount of flow back water that is recycled has increased from 11% prior 2011 to 56% in 2011 (Lutz et al., 2013). The industry standards for acceptable recycle water concerning the TDS level, is maximum 50,000 mg/L (Ziemkiewicz et al., 2012). However, limits for acceptable reuse may vary widely depending on the driller. In some cases water with TDS level greater than 50,000 mg/l has been used. Most companies apply a basic settling and filtration of the flow back water which is subsequently mixed with fresh water in order to reduce the TDS levels to be reused for other fracturing jobs (Arhtur et al., 2011; Veil et al., 2010). Since May 2010, the state of Pennsylvania has established more stringent discharge requirements for the TDS concentrations and shale gas industry is in search of efficient and economical remediation technologies (Veil et al., 2010).

Various technologies have been developed and tested over the past years for treatment of flow-back water. Examples of those technologies are thermal treatment, membrane treatment, and various hybrid and advanced treatment technologies. Most of these technologies are unable to treat wastewater with high TDS levels. Therefore, a need for development of pre-treatment methods to reduce the TDS level has arose (Ahmadun et al., 2009; Arthur et al., 2011, Hayes et al., 2012). A membrane treatment technology called electrodialysis could be implemented for the reduction of TDS levels (Godec et al., 2007; Hayes et al., 2012).

Electrodialysis combines the application of a Direct Current (DC) electric field with the use of ion selective membranes. The method has been used for over 50 years for desalination of brackish water (Strathmann et al., 2010). The principle of the method is the preferential transport of ions through the ion selective membranes under the influence of the applied electrical field. The products of the method are two

different outflows, the dilute flow with lower TDS level than the inflow, and the concentrated flow with higher TDS level than the inflow (Banasiak et al., 2007; Hayes et al., 2012; Sonune and Ghate, 2004; Strathmann et al., 2010). The performance of the electrodialysis method depends on various parameters such as the properties of the membranes, the composition of the inflow, and the design parameters of the equipment (Lee et al., 2002). The main investment cost of the method is the membranes and it depends on the required membrane area. After the initiation of the operation, the costs are mainly determined by the energy requirements for the application of the DC electric field (Lee et al, 2002).

The ion selective membranes are basically ion exchange resins in a form of a film. They have evolved from a laboratory tool to an industrial product. The two main categories are the cation and the anion selective membranes. The cation selective membranes include negatively charged groups (e.g. $-SO_3^-$, $-COO^-$, $-PO_3^{2-}$) that allow the movement of the cations only. In contrast, the anion selective membranes allow the movement of the anions using positively charged groups (e.g. -NH3+, $-NRH_2^+$, PR_3^+). The desired properties of the ion selective membranes are high permselectivity, low electrical resistance, high mechanical, thermal and chemical stability and low cost of production (Kariduraganavar et al., 2006; Strathmann et al., 2010; Xu, 2003).

This paper investigates the efficiency of the electrodialysis method as a desalination process for flow-back water taken from Marcellus shale wells in the laboratory scale. It should be noted that the results presented in this paper are based on initial investigation. We are continuing our investigation on efficiency of the method and the results of the comprehensive investigation will appear in future publications.

EXPERIMENTAL PROGRAM

The experimental set up consisted of the electrodialysis device, the peristaltic pump, the power supply for application of the DC electric field, and the container for the electrolyte. The device was built in the prototype lab of the Engineering Department at University of Vermont. The design of the device was based on the principle of electrodialysis as shown in Figure 1. Two pairs of anion and cation selective membranes were used with properties given in Table 1. The role of the central membranes was to trap the anions and the cations of the feed (flow back water) in the concentrated chambers. The two external membranes were used to protect the electrolyte from the ions of the feed.

The device consisted of five chambers including two electrode chambers, two chambers for the concentrated outflow, and one chamber for the dilute outflow as shown in Figure 2(a). The chambers were made of propylene to prevent reactions caused by application of the electrical field. The dimensions of the device were 30cm x 9cm x 9cm. The titanium electrodes were placed in the chamber using four titanium bolts that were also used for the connection of the electrodes to the power supply. Bolts that penetrated the frame of all the chambers were placed in the perimeter to keep the device sealed and prevent leakages. A peristaltic pump was used for injection of the feed to the three central chambers and then for circulation of the

electrolyte within the electrodes chambers.

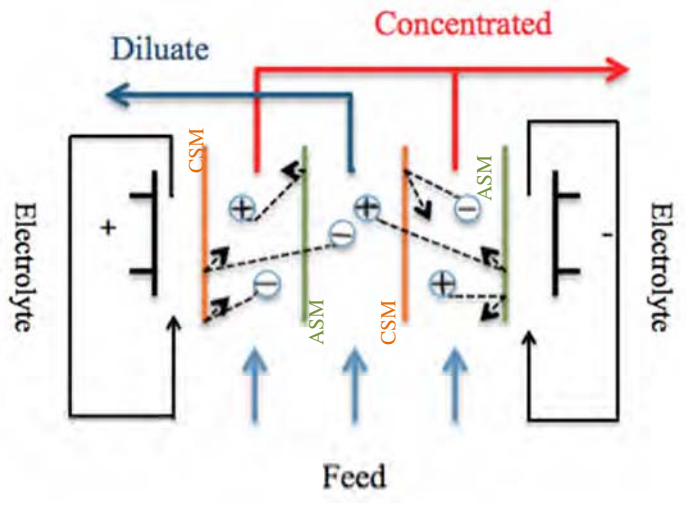

FIG. 1. Schematic of electrodialysis (CSM: Cation Selective Membrane; ASM: Anion Selective Membrane)

Table 1. Properties of the ion selective membranes (as given by the manufacturer)

Property	Anion selective membrane	Cation selective membrane
Technical Specification	AMI-7001S	CMI-7000S
Functionality	Strong Base Anion Exchange Membrane	Strong Acid Cation Exchange membrane
Polymer Structure	Gel polystyrene cross linked with divinylbenzene	Gel polystyrene cross linked with divinylbenzene
Functional Group	Quaternary Ammonium	Sulphonic Acid
Standard thickness (mm)	0.45	0.45
Chemical Stability Range (pH)	1-10	1-10

As shown in Figure 2(a), fittings were placed in all the inlets and outlets of the chambers. All fittings were connected with hoses. For the three central chambers, the hoses were used to inject the feed in each chamber and to obtain the samples after a certain time of operation (flow back treatment). Flow only existed in the chambers of the electrodes and the batch system was used for the central chambers. As shown in Figure 2(b), the device was placed in a vertical position to facilitate the injection from the bottom of the device and to remove existing air in the chambers from the top.

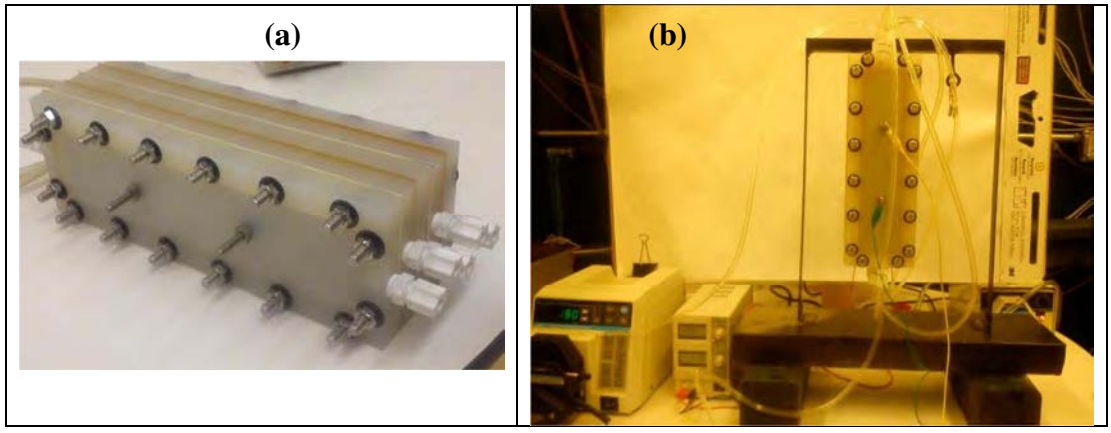

FIG. 2. (a) Electrodialysis device, (b) Experimental set up

A power supply device capable of applying 18 volts or 2 amps was used to apply the electric field. Readings of the current and the voltage between the top and the bottom bolts connected to the electrodes every taken during the experiment.
The electrolyte used was a brine solution with a concentration of 1.5 M NaCl. Two trials were conducted using the same type of electrolyte and their results are presented in the following section. The pH, conductivity, and TDS level of the original and treated flow back sample was measured during the experiment following the standard method. As stated above, two trial experiments were conducted in order to evaluate the effectiveness of electrodialysis in removing the TDS from samples of flow-back water. The samples were originated from wells in the Washington County in Pennsylvania. The initial TDS level was at around 70,000 mg/L. The results of the trials are presented in the following section.

RESULTS AND DISCUSSION

For the two trials presented in this paper, a brine solution was used as electrolyte. However, the very first trial was conducted using deionized water as electrolyte. The changes in the TDS levels of flow back specimen in different chambers of this specific trial were not significant, and therefore, they are not presented here. The main impact of using brine solution on TDS removal efficiency was the increase in the current due to its higher conductivity compared with the deionized water.

For both trials presented here, the brine solution had a concentration of 1.5M NaCl and the flow rate within the electrode chambers was set to 180 – 200 ml/min. A higher flow rate was tried which resulted in leakages. During the first trial no problems were observed, however, after the second hour of electric field application in the second trial, corrosion of the electrode was observed. Each of the two trial experiments was performed for 6 hours under the same applied electric field. According to the hourly measurements, a relatively constant voltage gradient of 1.9 V/cm (current of about 2 Amp) was applied to the sample.

Figure 3 shows the change in the TDS level at three chambers. As evident in Figure 3, the TDS level significantly decreased at the middle chamber (diluted) from around 70,000 mg/L to 1,400 mg/L with the TDS removal of about 98%. As expected, the TDS level increased in the two chambers near the electrodes. These results clearly indicated the high efficiency of the method in TDS reduction for the flow-back water.

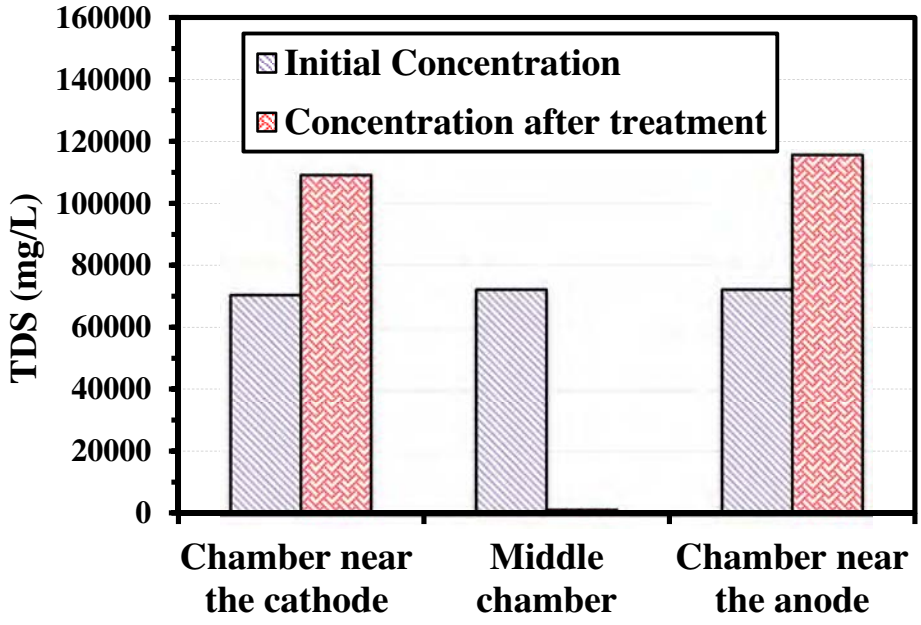

FIG. 3. TDS concentrations before and after treatment for first trial

Figure 4 shows the measured conductivity values for the flow back specimens before and after treatment. Due to the direct correspondence between the TDS level and the conductivity, the results of the conductivity followed the same pattern as those of the TDS. As it can be seen in Figure 4, the conductivity of the dilute sample was reduced from 82 mS to 2.6 mS. The measured conductivity values before and after treatment supported and validity of the changes in the TDS levels.

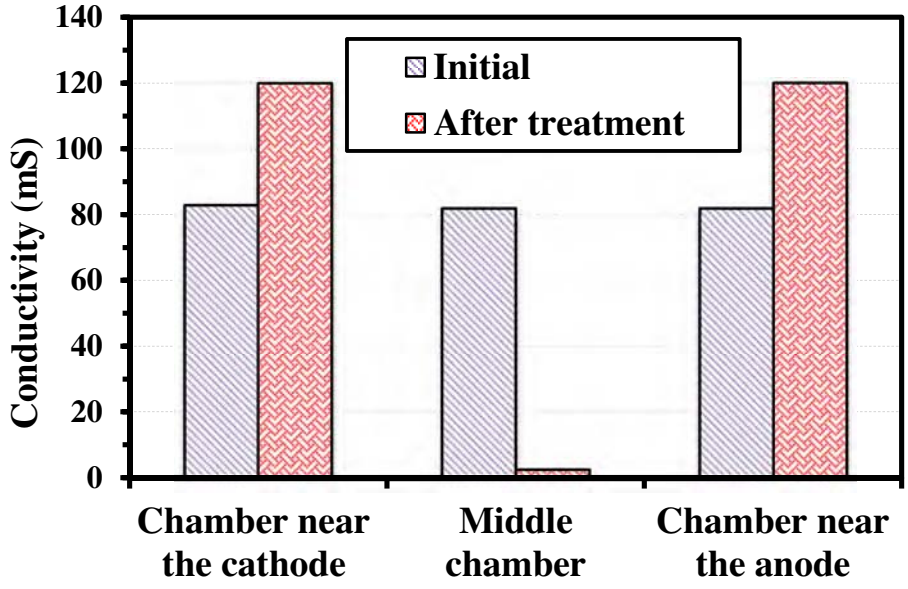

FIG. 4. Conductivity before and after treatment for first trial

The pH dropped in all three chambers as shown in Figure 5. This is attributed to the chemical reactions caused by the application of electrical field to fluids with high concentrations of ions, especially the brine electrolyte. An indication of the role of the brine electrolyte in the reduction of the pH was the chlorine production that was noticed in the chambers close to the electrode chambers and also in the hoses that were used for circulation of the electrolyte.

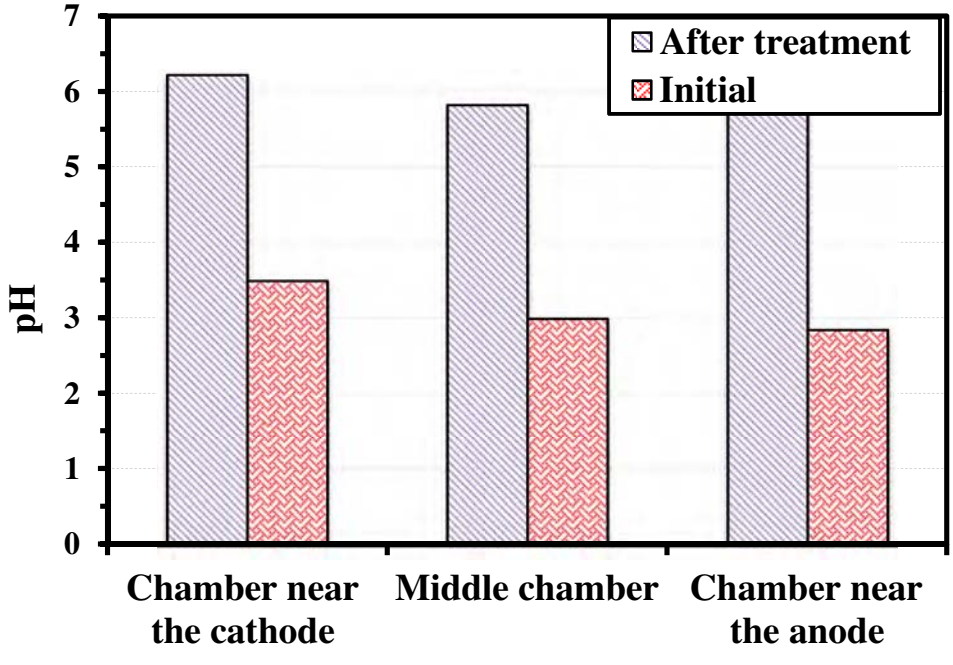

FIG. 5. pH before and after treatment for first trial

To confirm the findings of the first trial, the second trial was performed with the same parameters (applied voltage gradient, electrolyte concentration, initial TDS level, time duration). Figure 6 shows the change in TDS level of the specimens. As observed in Figure 6, the TDS levels in the middle chamber (dilute) were reduced significantly, similar to first trial. The TDS level reduction for the second trial was 92.3%. The changes in the conductivity for each sample are consistent with the results for the TDS level change as evident in Figure 7. Obviously, these results confirmed the significant reduction of the TDS level at the middle chamber.

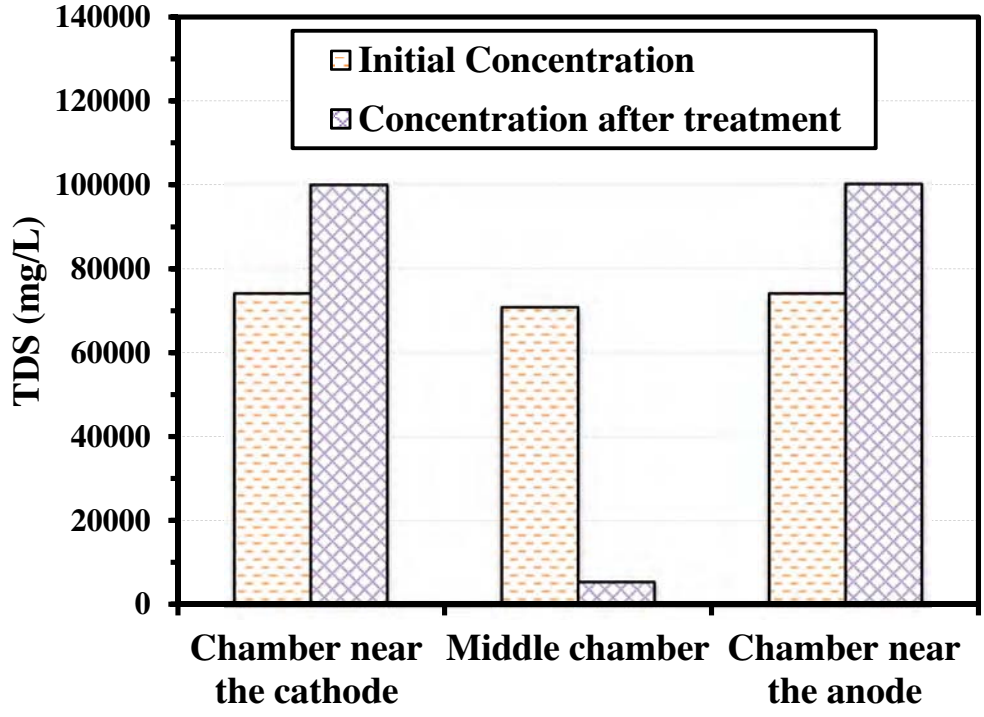

FIG. 6. Concentrations before and after treatment for second trial

Figure 8 compares the results from the two trials. The removal of TDS for the first trial is higher than the corresponding removal for the second trial. This might be due to corrosion of the anode electrode after application of the electrical field, which in turn might have reduced the applied electrical field to the specimens. Another contributing factor might be the exhaust of the membranes after several runs. In the second trial, an extra sample was obtained after 3 hours of operation from the middle chamber. The TDS level was measured as 40,000 mg/L corresponding to a TDS level reduction of 43%. Although, the investigation of the energy efficiency of the method was not a primary focus of this paper, the amount of kWh consumed per pounds of TDS removal from the samples was calculated. The corresponding value for the trials is at around 3.8 kWh/lb of TDS removed. This is a rather high value, however, additional research will be conducted to improve the efficiency of the method

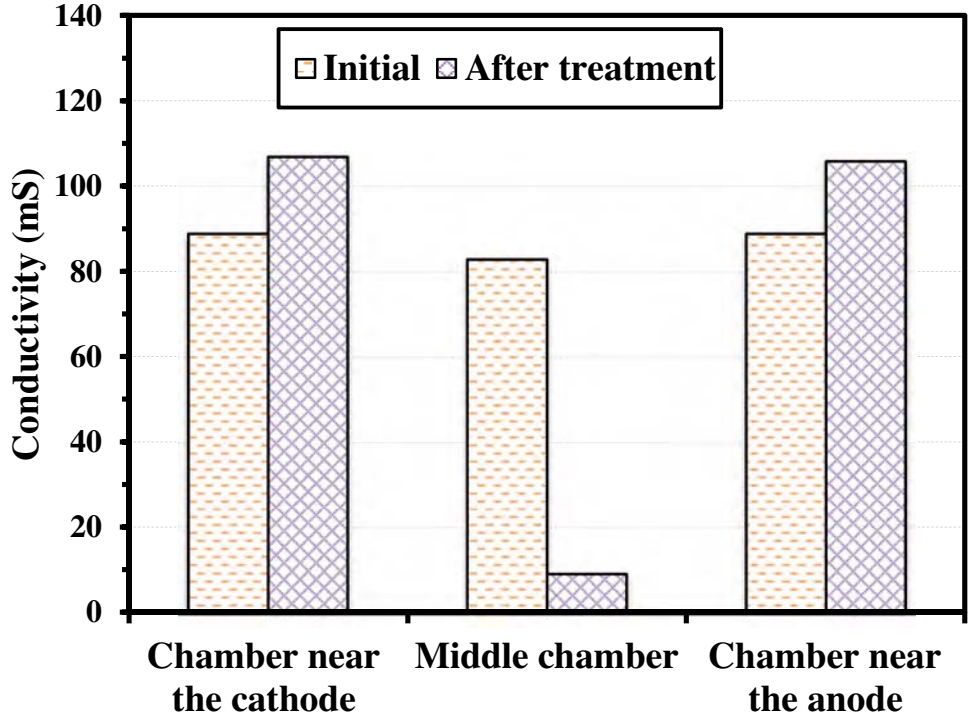

FIG. 7. Conductivity before and after treatment for second trial

.

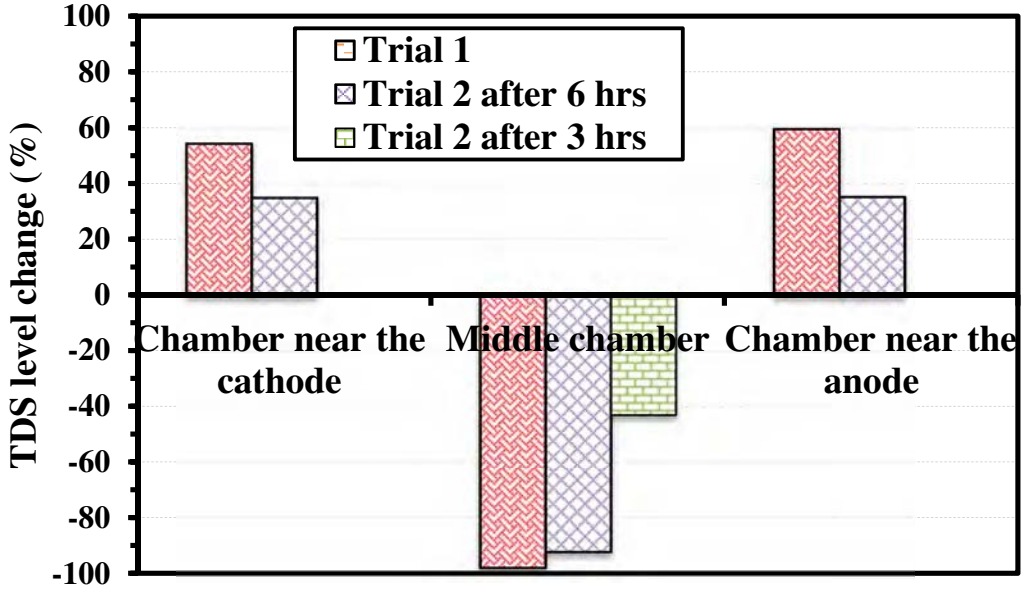

FIG. 8. TDS level change for the two trials

CONCLUSIONS

Efficiency of electrodialysis as a pre-treatment option for flow back water from shale gas wells was investigated through laboratory scale experiments. Electrodialysis was found to be an effective method for TDS level reduction from flow-back water. The TDS level reduction of more than 90% after 6 hours of low direct current electric field application was found to be promising. However, the results presented in this paper are part of a preliminary investigation and we are conducting further experiments to evaluate the impact of various parameters on the efficiency of the method to be used in field scale applications.

AKNOWLEDGEMENTS

The authors would like to thank Dr. George Pinder from the University of Vermont for his valuable contributions to this study. Also, we would like to thank Mr. James Locke from CONSOL Energy Inc. for providing flow back samples from Marcellus wells.

REFERENCES

Ahmadun F.R., Pendashteh A., Abdullah L.C., Awang D.R., Madaeni S.S., Abidin Z.Z. (2009). "Review of technologies for oil and gas produced water treatment", Journal of Hazardous Materials, 170, 530-551.

Banasiak L.J., Kruttschnitt T.W., Schafer A.I. (2007)."Desalination using electrodialysis as a function of voltage", Desalination, 205, 38-46.

Castle J.W., Rodgers J.H., Jr., Alley B., Beebe A., Coffey R., Jurinko K., Pardue M., Ritter T., Spacil M.M. (2013). "Innovative Water Management Technology to Reduce Environmental Impacts of Produced Water", Clemson University, SC.

Godec M., Van Leeuwen T., Kuuskraa V. (2007). "Economics of Unconventional Gas" OGJ Unconventional Gas.

Hayes T., (2012). "Barnett and Appalachian water management and reuse technologies", Research Partnership to Secure Energy for America (RPSEA) Report.

Kariduraganavar M.Y., Nagarale R.K., Kittur A.A., Kulkarni S.S. (2006). "Ion-exchange membranes: preparative methods for electrodialysis and fuel cells applications", Desalination, 197, 225-246.

Lee H.J., Sarfert F., Strathmann H., Moon S.H. (2002). "Designing of an electrodialysis desalination plant." Desalination, 267-286.

Lutz B.D., Lewis A.N., Doyle M.W. (2013). "Generation, transport, and disposal of wastewater associated with Marcellus Shale gas development", Water Resources Research, 49, 647-656.

Rahm B.G., Bates JT., Bertoia L.R., Galford A.E., Yoxtheimer D.A. (2013). "Wastewater management and Marcellus Shale gas development: Trends, drivers, and planning implications", Journal of Environmental Management,

120, 105-113.
Sonune A., Ghate R. (2004). "Developments in wastewater treatment methods", Desalination, 167, 55-63.
Strathmann H. (2010) "Electrodialysis, a mature technology with a multitude of new applications", Desalination, 264, 268-288.
Arthur D.J. (2011). "Management of produced water from oil and gas wells", Working document of the NPC North American Resource Development Study Report
Veil J.A., Argonne National Laboratory (2010). "Water Management Technologies used by Marcellus Shale gas producers", Office of Fossil Energy, Argonne, IL.
Xu T. (2005). "Ion exchange membranes: State of their development and perspective." Journal of Membrane Science, 263, 1-29.

Conversion of Marcellus Production Wastewater into Salable Products

Timothy Keister[1], CWT, F.AIC, SM.AIChE

[1]Chief Chemist/President, ProChemTech International, Inc., 51 ProChemTech Drive, Brockway, PA 15824, U.S.A., E-mail: tek@prochemtech.com

ABSTRACT: By 2016 development of the Marcellus shale gas play in the Northeast will generate an estimated 227 million liters (60 million gallons) per day of hydrofracture flowback and production wastewater. This wastewater is close to saturation with sodium, calcium, magnesium, strontium, and barium chlorides as major constituents. Discharge of such wastewater into surface waters has been effectively outlawed in Pennsylvania, leaving deep well injection and treatment for recycle/reuse as current disposal options. Resource recovery via the processes of precipitation and fractional crystallization, which produces salable products from the wastewater, has been developed as an economic, environmentally superior, disposal method for Marcellus wastewaters.

INTRODUCTION

Development of horizontal drilling combined with hydrofracture technology has enabled the gas production industry to develop the enormous gas reserves locked in dense shales. One of the largest such shale gas developments is the Marcellus shale play, centered in Pennsylvania. Hydrofracture technology produces two wastewaters, flowback and production. Flowback is that portion of the water used in the hydrofracture that is removed from the gas well immediately after hydrofracture and amounts to 10 to 30% of the 19 to 38 million liters (5 to 10 million gallons) injected into the well. Flowback does not present a major disposal problem during play development as gas well drillers have learned to filter and reuse it for makeup of new hydrofracture water in amounts up to 30% by volume of the total needed.

Production wastewater (PW) is produced at rates of 1,514 to 15,142 lpd (400 to 4,000 gpd) for the life of the gas well. In marked contrast to production wastewaters from other gas shale plays, Marcellus PW has a very high level of dissolved solids with large amounts of barium, calcium, magnesium, sodium, and strontium chlorides; with many other constituents, such as bromine and lithium, present in lesser quantities. Accordingly, disposal of Marcellus PW presents a significant challenge as it is a near saturated salt solution containing significant amounts of toxic barium. The following Table 1 is an analysis of a typical Marcellus production wastewater, Sample 18. Note that total dissolved solids range from 250,000 to 350,000 mg/l.

Table 1. Typical Marcellus Production Wastewater Composition

Parameter	result as mg/l	Parameter	result as mg/l
barium	7,700	bromide	1,070
calcium	30,400	chloride	180,000
iron	167	lithium	234
magnesium	2,100	manganese	13
sodium	52,000	strontium	3,720

By 2016 development of the Marcellus shale gas play in Pennsylvania will generate an estimated 227 million liters (60 million gallons) per day of PW. PW is a "dispersed" wastewater source; the wells producing it are geographically spread over wide areas with low daily flows. Management of this wastewater will require well site tankage and tank truck based collection to convey it to either transshipping locations for transport to injection wells, out of state treatment; or to central resource recovery facilities**.** Disposal of PW in an environmentally acceptable manner is costly and is a major roadblock to development of the Marcellus gas shale to its full potential.

Historically, such saturated brines have been considered an economic resource with production of sodium chloride (table salt) from brine dating back several thousand years. Currently, in addition to "salt", production of chemical commodities like bromine, lithium, calcium chloride, and potash from brines is a major business for many firms such as Dow Chemical, OxyChem, Dead Sea Bromine, and Albemarle.

Recognizing an opportunity to dispose of PW by resource recovery, ProChemTech has developed a precipitation fractional crystallization (PFC) process (Keister 2009 and 2011) to produce salable products from PW. Laboratory scale PFC bench studies on fourteen (14) different PW has produced barium sulfate (barite), sodium chloride (table salt), and calcium chloride solution which meet various specifications for sale of these materials as commodities. All three products are currently marketed and utilized in large amounts in the United States. No significant amount of waste, requiring subsequent costly disposal, is produced by the PFC process

A PFC operational spreadsheet has been developed and output shows that a PFC facility would produce an operating profit solely from sale of commodity chemicals; a disposal tipping fee simply improves the economics of the facility. Several in-house engineering studies show that the cost of such a facility can be returned in time periods ranging from 1.5 to 2.1 years.

CHEMISTRY

Precipitation

In the PFC process precipitation step; barium, radium, iron, manganese, suspended solids, and most organics are either destroyed by oxidation or removed by precipitation. The major component removed, barium, is precipitated by reaction with added sulfate ion to form insoluble barium sulfate. The conditions of the reaction are an oxidizing environment with pH in the range of 3.0 to 4.0 so as to reduce co-precipitation of calcium and strontium sulfates. An over stoichiometric level of sulfate ion, based on the combined level of barium and strontium in the PW, must be provided at a ratio of 1.5 to 1.8 to remove the barium to levels below 10 mg/l in the resulting clarified brine. Over one hundred (100) treatability studies have been done to confirm the reaction conditions required to obtain this barium level while minimizing co-precipitation of calcium and strontium.

Radium, present in most Marcellus PW at low levels, is co-precipitated as an insoluble sulfate and incorporated into the barium sulfate crystal matrix. Incorporation of the radium into a barium sulfate matrix addresses the radioactive emissions from radium as one use of barium is as a radiation shielding material.

Potassium permanganate is added to create and maintain an oxidizing reaction condition during the precipitation. Both iron and manganese are oxidized under these conditions and co-precipitate with the barium sulfate. The amounts are minor in comparison to the amount of barium precipitated, generally under 1% by weight.

Many of the organics in the PW, represented by the typically high chemical oxygen demand of the wastewater, are destroyed by oxidation under these reaction conditions.

Suspended solids present are also removed by the barium sulfate precipitation and following addition of an anionic flocculant prior to gravity separation of solids.

Fractional Crystallization

The clarified brine resultant from the precipitation step is then heated to remove water and concentrate the soluble salts present. Due to the different solubilities of salts present, as the clarified brine concentrates, fractional crystallization occurs. As shown in the following Table 2, Three Phase Aqueous Solubility, developed from an American Chemical Society publication (Linke 1958), fractional crystallization should be capable of separating both sodium and magnesium chloride from the other components of PW so as to produce to produce salable products, sodium and magnesium chloride, and calcium chloride solution.

Table 2. Three Phase Aqueous Solubility Data

Calcium chloride	Magnesium chloride	Sodium chloride
33.8	8.4	2.3
52.9	8.2	0.9
60.1	0	0
60.2	0	0

% by wt @ 95 C, ACS tables

This published data shows that sodium and magnesium chloride can be recovered from clarified brine by increasing the calcium chloride concentration above 60.1% by evaporating water from the clarified brine. To confirm this literature data, a large number of laboratory bench scale fractional crystallization studies were undertaken on various clarified brine samples. The following Table 3 notes the results from four (4) such studies on Sample 18. Note that the studies are reported in order of increasing density (specific gravity) achieved by evaporation.

Table 3. Fractional Crystallization Results

Parameter	Study 4	Study 3	Study 1	Study 7
density	1.28	1.36	1.42	1.49
calcium chloride - %	33.24	41.55	60.94	78.95
magnesium chloride - %	3.73	4.22	6.55	6.47
sodium chloride - %	5.28	2.49	0.75	0.42
lithium mg/l	1,100	1,480	1,720	2,470
strontium mg/l	5,116	9,800	11,700	3,300
barium mg/l	--	< 5	< 5	<5
bromide mg/l	4,740	5,910	10,360	11,400

As shown in Table 3, sodium chloride can be fractionally crystallized from clarified brine while, contrary to published data, magnesium chloride cannot. We believe this deviation from the published literature is due to the evaporation temperature required to remove water from clarified brine, 110 C, which is higher than the 95 C reported for the solubility data.

PROCESS DESIGN, EQUIPMENT, AND OPERATION

Our current PADEP permitted, General Permit WMGR123NW002, design for a PFC facility incorporates the following equipment and operations.

Primary Treatment

As PW is unloaded from tanker transport it will pass through a gravity separator for removal of gross solids and floating oil, exiting into a pump station well. PW is then pumped, via a coalescing oil and solids separator for further removal of any free oils and smaller solids, to one of two (2) aerated storage tanks. Recovered oil will be sold while

any solids would be disposed of by dewatering and landfill. Based on the PW samples studied to date, free oil and solids will be a minor concern.

Aerated Storage Tanks

Due to the known variability of PW, two (2) aerated holding tanks, volume of each equal to one (1) days plant flow, are provided to obtain chemical equalization and keep the PW in an aerobic condition. Chemical equalization is required to minimize chemical analysis and adjustment of the chemical additions in the chemical precipitation process to a once a day process. This allows the chemical precipitation process to operate on a continuous basis for 24 hour periods in spite of any variation in delivered PW composition. PW is aerated in storage to prevent formation of noxious odors due to biological degradation of organic content and to reduce the subsequent feed of potassium permanganate.

Chemical Addition and Mix

In the first chemical addition and mix tank, sulfuric acid and potassium permanganate solution are added. As noted, sufficient sulfuric acid is added to obtain an over stoichiometric level of sulfate ion calculated on the combined level of barium and strontium in the PW. It has been found that a ratio of 1.5 to 1.8 is needed and that this typically results in a pH of less than two (2). Potassium permanganate is added to obtain a faint pink color, indicating excess and an oxidizing environment. Design retention time is five (5) minutes with high energy, 5 hp/1000 gallons, mixing

The pH of the solution is increased to 3.0 to 4.0 in the second mix tank by addition of sodium hydroxide solution, addition controlled by a pH meter control circuit. A higher pH is required to complete the various precipitation reactions and obtain a pH suitable for polymer flocculation of the precipitates. Design retention time is five (5) minutes with high energy, 5 hp/1000 gallons, mixing

In the third mix tank, a high molecular weight anionic polymer has been discovered to provide good flocculation of the precipitate at 5 to 15 mg/l dosage. Design retention time is thirty (30) minutes with low energy, 3 hp/1000 gallons, slow speed mixing, and provision of a VFD drive on this mixer to allow for optimization of flocculation.

Clarification and Barium Sludge

Liquid flows by gravity from the third mix tank into a ProChemTech design inclined plate clarifier where the flocculated precipitate is removed as sludge. Sludge is transferred to a sludge thickener; then filter pressed, washed in the press, and discharged as a solid wet cake. Dependent upon customer requirements, the barium sludge may then be further processed by drying and pulverization.

Clarified brine flows from the clarifier into a clarified brine storage tank. Note that clear filter press supernatant and filter cake wash water are also discharged to the clarified brine storage tank to recover soluble salts.

Fractional Crystallization

Clarified brine is pumped to the steam heated evaporator where water is removed by evaporation. A significant discovery during laboratory bench testing is that by providing high energy mixing in the evaporator, the common problem of scale formation on heating surfaces is eliminated.

When the clarified brine reaches approximately 30% by weight calcium chloride, sodium chloride begins to fractionally crystallize as a pure salt. A continuous side stream from the evaporator is passed through a horizontal vacuum belt filter to remove the sodium chloride crystals. Stripped brine, with sodium chloride removed and within defined specific gravity levels, is routed to a calcium chloride solution storage tank. Stripped brine not meeting the specific gravity levels is routed back to the evaporator for further concentration.

Sodium chloride crystals are washed with a saturated sodium chloride solution to remove calcium, magnesium, lithium, and strontium chlorides, unwanted impurities in the produced sodium chloride. The purified sodium chloride is then dried. Wash water is returned to the evaporator for recovery of soluble salts.

Water vapor from the evaporator will be condensed as distilled water by passage through a heat exchanger operating counter current with incoming clarified brine. This operation recovers as much of the evaporation energy as possible and provides a source of pure water for facility process use.

Please note that the evaporation process can also be conducted on a batch basis rather than the above detailed continuous basis. Engineering studies to date have been limited to the continuous process.

As the stripped brine exceeds the common commodity level of 30% by weight calcium chloride, produced distilled water will be used for dilution. In addition to this use, distilled water will be used for preparation of potassium permanganate solution, washing of the barium sulfate press cake, preparation of saturated sodium chloride brine, polymer makedown, and makeup to facility boiler and cooling tower units.

With careful selection of operating parameters, the entire process can be operated with no discharge of water derived from the influent PW. Significant water losses are from drying of produced barium sulfate and sodium chloride, operation of the cooling tower and boiler, and calcium chloride solution dilution.

PRODUCTS

Produced products will consist of the following commodities.

Barite (Barium Sulfate)

The biggest use (95%) of this product is preparation of gas and oil well drilling mud with smaller uses in glass manufacture, molding compounds, rubber manufacture, and pigments. Annual US estimated use of barite is 2,430,000 metric tons (2,700,000 tons), with 80% imported from China. A 946,352 lpd (250,000 gpd) PFC facility using Sample 26 wastewater as influent would produce about 11.7 metric tons (13 tons) per day of barite.

Typical API specifications for barite are compared to laboratory bench study produced material in the following Table 4.

Table 4. API Barite Specifications Compared to a PFC Laboratory Sample

Parameter	API Specification	Test Result
Density g/cc	minimum 4.2	4.1
Water soluble alkaline mg/kg as Ca	maximum 250	< 150
Residue > 75 u	maximum 3.0% wt	< 0.1%
Residue < 6 u	maximum 30.0% by wt	> 80%
Moisture content	maximum 1%	< 1% *
Bulk density kg/m3	2100 – 2300	

The major deviation from API specifications is the particle size of produced barite, produced barite having a much smaller particle size profile as it is produced by chemical precipitation rather than grinding. It is believed that the small particle size produced in our laboratory studies is a result of rapid reaction of barium with sulfate ion, forming small barium sulfate crystals which cannot grow due to total removal of soluble barium in a short time period. It is expected that full scale plant operations, which will incorporate barium sulfate sludge recirculation to the second mix, will result in somewhat larger barite crystals.

A recent patent states that smaller barite particle size produces a superior drilling mud, thus our smaller particle size barite may end up being a premium product.

While the laboratory produced product does not meet the density specification of 4.2, at 4.1 it is close. Due to recent shortages of barite (RIGZONE 2011), the API has modified the specification and now accepts a density of 4.1 for drilling mud preparation. We believe the lower density of produced product is the result of co-precipitation of strontium sulfate with the barium sulfate.

We note that Halliburton Baroid 41 and Advantage Barite both have a listed density of 4.1, so our laboratory bench produced product is marketable. We have engaged Westminster College, using senior chemistry majors - senior projects, to more closely explore the relationship between pH, sulfate ion content, ORP, barium concentration, and strontium concentration to maximize barium precipitation while minimizing strontium co-precipitation. A secondary part of these multiple projects will be to explore precipitation of the strontium as an additional product.

Sodium Chloride

Annual US estimated use of sodium chloride is 45,000,000 tons, produced by seawater evaporation, mining, and brine mining followed by evaporation. A 250,000 gpd PFC facility using sample 26 wastewater as influent would produce an estimated 170 tons tons/day of sodium chloride. ASTM Standard specification for sodium chloride, D632-12, shows only a single chemical standard for sodium chloride, a minimum content of 95% as NaCl.

Sodium chloride produced from Sample 15, experiment 3, and Sample 18, experiment 3 were analyzed with the results shown in Table 5.

Table 5. PFC Sodium Chloride Analytical Results

Parameter	Sample 15	Sample 18
sodium chloride % by wt	99+	99+
calcium mg/kg	1,535	172 mg/kg
magnesium mg/kg	107	396
barium mg/kg	60	-

The chemical industry is a potential large customer for PFC sodium chloride as it consumes about 39% of the sodium chloride produced in the United States. Table 6 compares a typical chlor-alkali specification for sodium chloride with product produced by laboratory scale PFC.

Table 6. Chlor-alkali Specification and PFC Sodium Chloride Results

Parameter	IS-797:1982 Specifications	Sample 15
sodium chloride	minimum 98.5%	99+%
calcium as Ca	maximum 0.20%	0.154%
magnesium as Mg,	maximum 0.10%	0.011%
sulfate as SO4	maximum 0.6%	none detected
water insolubles	maximum 0.2%	none detected
moisture	maximum 2.5%	< 2.5%
iron as Fe	20 mg/l	none detected

Based on the results obtained to date, produced sodium chloride is a high quality product suitable for chemical industry use as well as use in regeneration of residential, commercial, and industrial water softeners.

Calcium Chloride Solution

US estimated annual use of calcium chloride solution is 4,200,300 metric tons (4,667,000 tons) as 30% calcium chloride solution. A 946,353 lpd (250,000 gpd) PFC facility using Sample 26 wastewater as influent would produce about 432 metric tons (480 tons) per day of calcium chloride solution.

Calcium chloride is a highly deliquescent salt commercially supplied as a 28 to 42% solution, most common 28 to 35%. Some typical specifications are shown in the following Table 7 as compared to diluted Sample 18, study 1.

Table 7. Calcium Chloride Specifications and PFC Product Results

Parameter	Dow Chemical	Solvay	study 1
Density	1.32	1.36	
Calcium chloride as $CaCl_2$	32%	35 to 37%	32
Sodium chloride as %	0.58	1.07	0.4
Iron as mg/kg	no specification	0.3	not detected
Sulfate as SO_4 - g/kg	no specification	0.1	not detected
Alkalinity as $Ca(OH)_2$ as %	maximum 0.2	0.04	<0.04

Various samples of all three produced products have been subjected to the USEPA TCLP procedure with the result that none were found to be characteristic hazardous materials.

ECONOMICS

Using conservative product sales prices and current costs for chemical reagents, energy, and estimated labor costs; we have constructed a MS Excel spreadsheet to examine the economics of various PW compositions and facility sizing. Running the spreadsheet with laboratory developed data for a PFC facility operating three shifts, five (5) days per week at 246,052 lpd (65,000 gpd) treating PW Sample 18, we find that daily operating cost would be $9,033.34, sales of produced chemical commodities would total $16,018.79 giving an operating profit of $6,985.45.

The majority of the PW compositions, with various sized facilities, examined using this spread sheet have shown an operating profit resultant from sale of produced chemical commodities.

Current disposal costs for PW are in the range of $0.15 to $0.35/gallon. Using a “tipping fee” of $0.15/gallon would add $9,750 to the daily profit and result in an annual profit of $3,347,090. Our estimate is that such a facility could be constructed and brought on-line at a cost between $5 and 7 million dollars, giving a simple return on investment of between 1.5 and 2.1 years.

FUTURE R&D

Calcium chloride solution produced by the PFC has significant amounts of bromide, lithium, magnesium, and strontium present. Several bench studies have shown that a second sulfate precipitation can remove significant amounts of strontium from the clarified brine. Further work is needed to define reaction

conditions, determine product purity, and ascertain if the recovered strontium has sufficient economic value to cover the costs of recovery.

Work with Westminster College (Murtagh and Boylan 2013) has shown that the bromine can be recovered by electrolysis. Definition of capital and operating costs, which will require larger than laboratory bench amounts of stripped brine, will determine if recovery of this product is viable.

In theory, nanofiltration may be used to recover lithium from the calcium chloride solution. As with the recovery of bromine, a substantial amount of stripped brine will be required to first determine if such a separation is possible, and then what the capital and operating costs are to ascertain the economics.

CONCLUSIONS

Laboratory bench scale processing of fourteen (14) different PW samples using the described precipitation fractional crystallization process has been successful in making three salable commodity chemical products. Spreadsheet analysis of the operating costs for commercial sized facilities shows that a positive cash flow is obtained even in the absence of a disposal "tipping fee".

Engineering studies using the described design and equipment have concluded that capital costs for commercial facilities can typically be recovered in 1.5 to 2 years with a tipping fee of $0.15/gallon. Given that current disposal costs for PW are in the range of $0.15 to $0.35/gallon, the precipitation fractional crystallization process is an environmentally superior, cost effective means to dispose of PW.

REFERENCES

Keister, T. (2009 and 2011), "Treatment of Gas Well Production Wastewater", US Patent Office applications 12/620,019 and 13/222,481

Linke, W. (1958). "Solubilities of Inorganic and Metal Organic Compounds", Fourth Edition, American Chemical Society

Murtagh, D. and Boylan, H., (2013). "Optimizing Resource Recovery from Produced Water Treatment", Summer Report, 10/06/2013, Westminster College

RIGZONE, (2011), "Barite Market Tight as China Supply Decreases", www.rigzone.com/news/article

Regulation of TDS and Chloride from Oil and Gas Wastewater in Pennsylvania

Eric H. Chase[1], P.G.

[1]Research Scientist, Matson & Associates, Inc., 331 East Foster Ave., State College, PA 16801, USA, E-mail: echase@matson-associates.com.

ABSTRACT: The recent boom in unconventional natural gas (UNG) production from the Marcellus Shale Formation in Pennsylvania has brought challenges of how to treat the large volumes of wastewater produced during drilling and hydraulic fracturing. In the late 2000s, capacity at permitted wastewater treatment facilities was quickly overwhelmed and drilling companies began sending their wastewater to Publicly Owned Treatment Works (POTW) that were not designed or permitted to treat wastewater high in Total Dissolved Solids (TDS) and chloride. Recognizing the need for wastewater effluent standards that specifically targeted TDS and chloride the Pennsylvania Department of Environmental Protection (DEP) added new effluent standards under 25 Pa. Code § 95 in August 2010. The new effluent limits for TDS and chloride were set at 500 mg/L and 250 mg/L, respectively. Under 25 Pa. Code § 95, facilities permitted to treat oil and gas wastewater prior to August 2010 were exempt from the new effluent limits. Although much progress has been made in reducing TDS and chloride loads from UNG wastewater through regulation and voluntary agreements, the exemption in 25 Pa. Code § 95 still exists for conventional oil and gas drilling wastewater, allowing the continued discharge TDS and chloride at hundreds of times greater than the new limits. An overview of Chapter 95 is provided, along with two case studies of wastewater treatment facilities that highlight the regulatory successes and failures in reducing TDS and chloride discharges to Pennsylvania's rivers.

INTRODUCTION

Recent advances in horizontal drilling and hydraulic fracturing (fracking) have led to a new frontier of exploration and production of unconventional natural gas (UNG) from the Marcellus Shale Formation in Pennsylvania and surrounding states. This technology has also led to new environmental challenges, including how to handle and dispose of large quantities of water produced during well drilling, fracking and gas production. The process of fracking is water intensive and each well can require over four million gallons of water to develop, with approximately 10% - 20% of the volume returning to the surface as flowback water that needs to be properly disposed of through treatment, deep well injection or recycling (Abdalla et al 2011, Hoffman

2010, Maloney and Yoxtheimer 2012). The water that returns to the surface with the flow of natural gas, commonly known as production water, also requires proper disposal. The treatment of Marcellus Shale wastewater (fracking and production water) is complicated by the high levels of total dissolved solids (TDS) and chloride which tend to be in the range of 10,000 to >300,000 mg/L and 5,000 to >150,000 mg/L, respectively (Hayes 2009, Yoxtheimer 2011, Maloney and Yoxtheimer 2012). In comparison, conventional oil and gas wastewater in Pennsylvania ranges from 68,000 to 350,000 mg/L and 40,000 to 130,000 mg/L for TDS and chloride, respectively (Dresel and Rose 2010).

These high levels of TDS and chloride are a concern if discharged untreated to surface waters due to their toxicity to aquatic life and the potential to impact drinking water supplies. Currently, EPA guidance for protection of aquatic life sets the maximum one-hour average chloride limit at 860 mg/L for acute exposures and 230 mg/L for chronic exposures (USEPA 1988). For drinking water the EPA has established a secondary drinking water regulation limiting chloride to 250 mg/L and TDS to 500 mg/L (USEPA 2009).

Historically, wastewater treatment facilities designed to treat industrial wastewater, known as centralized waste treatment (CWT) facilities, received wastewater from oil and gas wells associated with conventional vertical well drilling (Veil 2010, Wilson and VanBriesen 2012). When Marcellus Shale gas exploration and production ramped up in the late 2000s, CWT facilities began accepting flowback and production waters from UNG wells and soon became overwhelmed by the quantity of wastewater requiring treatment. In addition to the large volume of water being treated, most CWTs were not designed to remove the high levels of TDS and chloride found in oil and gas wastewater (Abdalla et al 2011, Veil 2010). By 2011, the volume of UNG generated wastewater was over five times the amount of wastewater produced from conventional oil and gas exploration: approximately three million cubic meters compared to over five hundred thousand cubic meters (Lutz et al 2013). The lack of capacity at CWT facilities led UNG drilling companies to begin sending their wastewater to publically owned treatment works (POTW) that were not permitted or designed to treat wastewater with high TDS, chloride, radioactive elements and petroleum products associated with oil and gas drilling (Veil 2010, Abdalla et al 2011, Lutz et al 2013). As a result, receiving streams were becoming negatively impacted by the effluent from the POTWs and State regulators were left scrambling as to how to update regulations concerning treatment and discharge of UNG wastewater (Wilson and VanBriesen 2012).

In 2008, low flows in the Monongahela River coupled with high effluent TDS loads from inadequately treated UNG wastewater raised concern about the impairment of Pennsylvania's surface water quality. Follow-up studies indicated that wastewater high in TDS from UNG activity was being discharged to the river without effective treatment by the POTWs (PA DEP 2011a, Tetra Tech 2009). In response, the Pennsylvania Department of Environmental Protection (DEP) requested the POTWs along the river reduce the amount of UNG wastewater they accepted and treated. In 2009, DEP proposed wastewater treatment effluent standards for POTWs and CWT plants specifically targeting TDS, chloride and other constituents related to all natural gas exploration and production wastewaters (Veil 2010, EQB 2010). Upon

approval by the Pennsylvania Environmental Quality Board the amended rules went into effect August 21, 2010 under 25 Pa. Code § 95.10, commonly known as Chapter 95.

Although researchers have explored water quality impacts of oil and gas wastewater disposal, have compared waste quantities in relation to source (UNG vs. conventional oil and gas), disposal practice, and changing regulations in Pennsylvania, and have delved into State and Federal regulations of oil and gas wastewater, the impact of exemptions in Chapter 95 on conventional oil and gas wastewater treatment has not been fully investigated. This paper focuses on TDS and chloride discharges from exempt CWTs in the Allegheny River watershed (Fig.1) and how the regulation of exempt facilities has led to continued high levels of TDS and chloride entering Pennsylvania's rivers. Two case studies are presented to help clarify the issues surrounding Chapter 95 and how regulators have tried to address discharges of TDS and chloride from exempt CWTs.

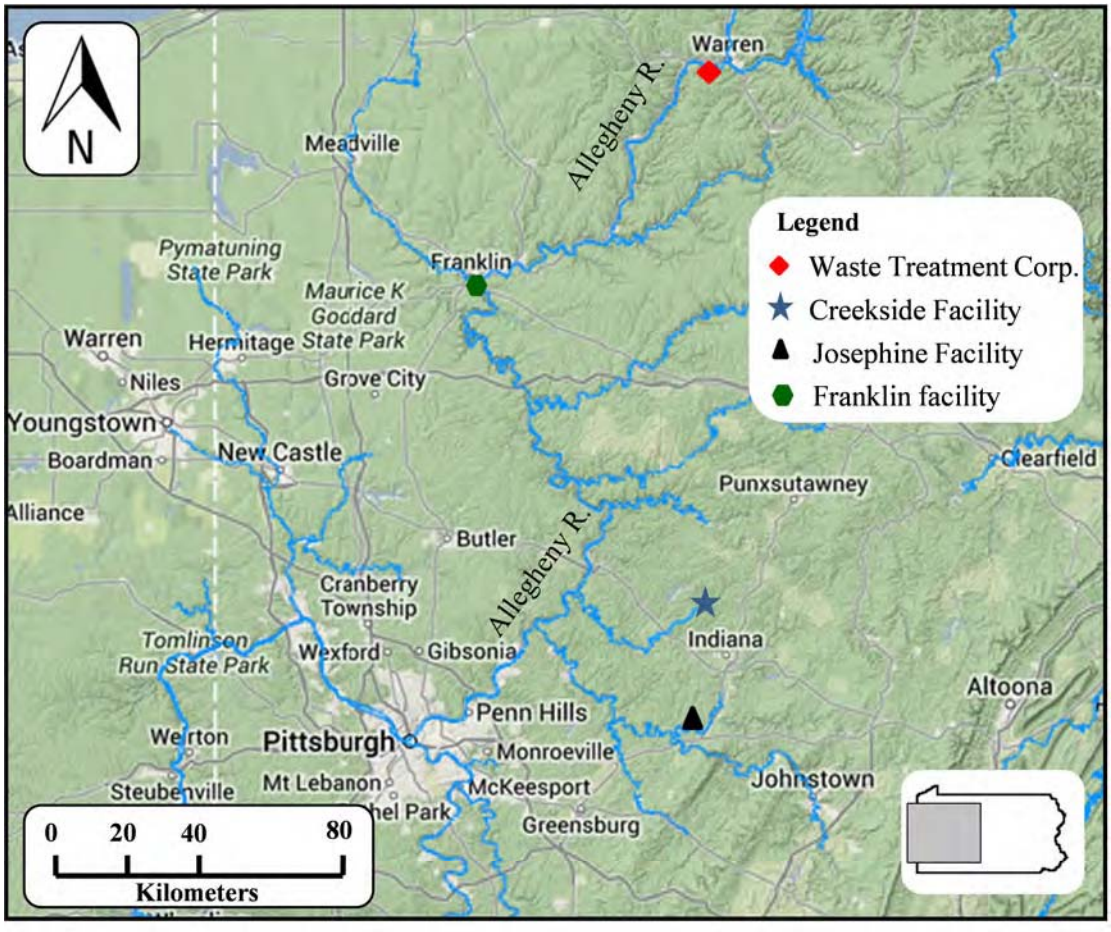

FIG. 1. Location map of four exempt centralized waste treatment facilities in the Allegheny River watershed.

REGULATORY FRAMEWORK

Chapter 95 was historically enacted to define effluent standards for industrial wastewater treatment facilities and included pH, oil, and dissolved iron. In 2010, Chapter 95 was amended to address new or expanded TDS and chloride loads from "natural gas" production. The effluent limitations under Chapter 95 Section 10 for facilities with new or expanded discharges were set at 500 mg/L of TDS, 250 mg/L of total chlorides, 10 mg/L of total barium and 10 mg/L of total strontium on a monthly average (25 Pa. Code § 95.10). Existing facilities permitted to treat oil and gas wastewater prior to the amendments of Chapter 95 were exempt from the new limitations. This exemption allowed these facilities to continue accepting both UNG and conventional wastewater resulting in the discharge of effluent high in TDS and chloride, often at hundreds of times the new limits. Chapter 95 also set forth a "wastewater source reduction strategy" that required UNG drillers to track flowback volumes and TDS concentrations, and to implement recycling and reuse of flowback water (25 Pa. Code § 95.10).

CWTs are exempt from Chapter 95 if they operate under a valid NPDES permit for oil and gas wastewater authorized prior to August 21, 2010 and they have not subsequently expanded their TDS mass loading by more than 2,268 kg (5,000 lb) as an annual average daily load. For expanded discharges after August 21, 2010, only the expanded portion of the load is classified as a new discharge and subject to Chapter 95 effluent limits. The existing permitted discharges are still considered exempt. As a result, a CWT plant that expands would still be permitted to discharge effluent with total TDS loads greatly exceeding the new regulation. POTWs, which typically handle municipal wastewater, are exempt from the regulations if they are operating under permits authorized to treat oil and gas wastewater prior to August 21, 2010 and have not expanded their TDS mass loading. For new or expanded NPDES applications, POTWs are not allowed to accept or treat flowback or produced water unless the water is pretreated by a CWT facility. Applications for new or expanded discharges of TDS mass loads from wastewater associated with industries or exploration other than natural gas are limited to 2,000 mg/L as a monthly average, unless a variance is granted (25 Pa. Code § 95.10).

Technical guidance drafted by DEP for implementing the new regulations under Chapter 95 provides multiple examples of how the exemption applies to CWTs and POTWs that were permitted prior to the promulgation of the regulations (PA DEP, 2011b). Examples presented in the guidance document demonstrate how exempt facilities are allowed to continue discharging TDS and chlorides to the waters of the State at levels hundreds of times higher than allowed under Chapter 95. For example, a CWT facility permitted to treat oil and gas wastewater prior to August 2010 that historically discharged 75,000 mg/L (150 times the Chapter 95 limits) of TDS as a monthly average would be allowed to discharge effluent at these high concentrations in perpetuity.

In May 2011, due to continuing problems with stream pollution from inadequate treatment of UNG wastewater, the oil and gas industry voluntarily agreed to DEP's request to stop sending wastewater from UNG wells to fifteen wastewater treatment facilities (nine POTWs and six CWT facilities) that were discharging high levels of

TDS and chlorides (Klaber 2011, Krancer 2011). DEP then sent a letter on July 11, 2011 to eighty-eight gas drilling companies working in Pennsylvania asking each to certify under penalty of law they would abide by the agreement (PA DEP, 2011c).

In July 2011, the US Environmental Protection Agency (EPA) notified fourteen POTWs in Pennsylvania that their acceptance of flowback or production wastewater may be considered a "substantial change in the volume or character of the pollutants being introduced" and would not be allowable under their existing NPDES permit (USEPA 2011a). This action was taken under EPA's authority as the regulator of Pennsylvania's pretreatment program for POTWs that accept industrial waste. The pretreatment program regulates waste streams from "industrial users which may pass through or interfere with POTW treatment processes or which may contaminate sewage sludge" (USEPA 2011b).

Since April 2011, there has been a coordinated effort by DEP, EPA and UNG drillers to recycle, deep well inject or send flowback and production water to facilities designed to properly treat the wastewater. These efforts have led to significant decreases in the amount of UNG wastewater being sent to CWTs and POTWs in 2011 compared to previous years (Wilson and VanBriesen 2012, Maloney and Yoxtheimer 2012, Hammer and VanBriesen 2012, Lutz 2013). This decrease has led to the public perception that discharges of oil and gas wastewater into Pennsylvania's streams and rivers have been effectively addressed by voluntary actions and the enforcement of regulations. Despite the cooperation among the agencies, drillers and the treatment facilities, the exemption in Chapter 95 allows treatment facilities accepting wastewater from conventional oil and gas drilling to discharge high levels of TDS and chloride to streams and rivers under their existing permits. In addition, the July 2011 voluntary agreement letter from DEP to the drillers validated the exemption when it restricted only flowback and production water from UNG to these exempt facilities (PA DEP, 2011c).

The specific targeting of TDS and chloride in wastewater from UNG exploration and production was a major factor in reducing water quality problems; however, the regulations and voluntary efforts failed to reduce TDS and chloride in wastewater effluent from conventional oil and gas drilling operations. Between 2010 and 2011 there was little decline in the volume of wastewater sent to CWTs from conventional oil and gas drilling (Wilson and VanBriesen 2012). A study examining effluent discharges from three wastewater treatment facilities (two POTWs and one CWT) found significant improvements in effluent water quality from the POTWs that stopped accepting UNG wastewater, while the CWT facility that stopped accepting UNG wastewater, but continued to accept large quantities of conventional oil and gas wastewater was releasing high levels of TDS and chloride (Ferrar et al, 2013). The two POTWs studied were able to meet the Chapter 95 effluent limits after discontinuing acceptance of UNG wastewater. In contrast, the CWT plant that primarily treated conventional oil and gas wastewater was discharging a mean of 160,000 mg/L of TDS and 68,000 mg/L chloride, which is over 250 times the effluent limits (for both TDS and chloride) for facilities required to comply with Chapter 95 (Ferrar et al, 2013). The CWT plant discharging high levels of TDS and chlorides was recently part of an administrative order between its parent company, Fluid Recovery Services, and EPA due to NPDES violations.

EXEMPT CENTRALIZED WASTE TREATMENT FACILTIES

Fluid Recovery Services

Fluid Recovery Services recently acquired ownership of three CWT facilities known as Hart Resource Technology Creekside Facility (Creekside), Pennsylvania Brine Treatment Josephine Facility (Josephine) and Pennsylvania Brine Treatment Franklin Facility (Franklin). These facilities historically treated conventional oil and gas wastewater under their respective NPDES permits and discharged their effluent into the Allegheny River watershed. With the increase in Marcellus Shale exploration in the late 2000s the facilities began treating UNG wastewater under their existing permits. When the Chapter 95 wastewater treatment regulations were amended in 2010 the facilities continued to operate as exempt facilities receiving UNG and conventional oil and gas wastewater. In May 2011, Creekside and Franklin were on the list of the fifteen facilities that DEP asked drilling companies to stop using for the disposal of UNG flowback and production water (PA DEP 2011c).

On September 19, 2011, Paul Hart, the President of Creekside, Josephine and Franklin, notified existing customers that the three facilities would comply with DEP's request for exempt facilities to stop accepting wastewater related to exploration and production of Marcellus Shale. Mr. Hart also stated that "[o]ur facilities will continue to accept and process wastewater produced by conventional oil and gas industry, as permitted in each plant's NPDES permit" (Hart, 2011). In addition, his letter made clear that the facilities were in the process of applying for new permits and making modifications to their facilities to comply with Chapter 95 regulations in order to resume accepting UNG wastewater in the future.

On September 28, 2011, EPA sent a Findings of Violation Order for Compliance and Request for Information to the three facilities. This order outlined NPDES effluent violations at the facilities, requested information on waste acceptance, effluent sampling, and required a representative for each facility to sign a certification that the facility would not accept any oil and gas wastewater without EPA and DEP approval (USEPA 2011c). At the time, the facilities either lacked effluent limits for TDS and chloride, or in the case of the Franklin facility there was an effluent limitation only for chloride, set at 85,000 mg/L or approximately 340 times the limit set in Chapter 95.

In May 2013, Fluid Recovery Services signed an Administrative Order for Compliance on Consent (AOCC) with EPA to settle historic and ongoing violations of NPDES permit effluent limitations at the Creekside, Josephine and Franklin facilities. As part of the AOCC, Fluid Recovery Services was required by EPA to renew or modify the NPDES permits for the facilities and follow all effluent limits set forth in Chapter 95 when their permits were renewed (USEPA 2013).

Effluent monitoring data as recently as August 2013 indicate that all three facilities are continuing to discharge wastewater containing TDS levels between 250 and 400 times the limit set in Chapter 95 and chlorides are being discharged at levels between 100 and 400 times the limit. While facilities owned by Fluid Recovery Services are in the process of making facility upgrades to treat TDS and chloride, another CWT

facility owned by Waste Treatment Corporation (WTC) is continuing to discharge approximately 80,000 mg/L of chloride to the Allegheny River (PA DEP 2013a).

Waste Treatment Corporation

The WTC facility in Warren, Pennsylvania discharges to the Allegheny River and has been in operation since the late 1980s. The facility is currently operating under a NPDES permit that was granted in 2003 and administratively extended in 2008. On its 2003 permit renewal application, WTC specifically requested to be listed as a Subcategory A - Metals and a Subcategory C - Organics facility and stated that "we have determined that we are not capable and chose not to direct any of our operations under the Sub-category B – Oils Waste Stream" (NOI Appendix M). The final 2003 permit included effluent limits and sampling requirements for the special condition that WTC could only accept Subcategory A – Metals wastes, municipal wastes and stormwater (PA DEP 2003).

In May 2008, DEP denied WTC's application to renew and modify its NPDES permit to only accept oil and gas wastewater including Marcellus Shale wastewater and instead administratively extended WTC's permit with the 2003 conditions. In November 2008, DEP was notified during an inspection that WTC was accepting oil and gas production related wastewater under its administratively extended NPDES permit. WTC subsequently amended its 2008 permit application to address deficiencies and the updated permit was treated as a historically exempt permit under Chapter 95 and noticed to the public in February, 2011 with a TDS limit of 100,000 mg/L (176,508 lb/day) and no chloride limitations (PA DEP, 2011d). In July 2011, WTC was one of the fifteen facilities that DEP asked oil and gas companies to stop sending UNG wastewater to; however, the facility has continued to accept conventional oil and gas wastewater and as of August 2013 it was still discharging chloride over 350 times the Chapter 95 limits (PA DEP 2013a). Back in August 2011, WTC entered into a Consent Order and Agreement with DEP to settle historic violations of its 2003 permit. This Agreement did not include the authority to treat any oil and gas wastewater or approve the permit renewal application or modify the permit conditions from 2003.

In fall 2012, DEP's sampling results for macroinvertibrates, sediment and water from the Allegheny River revealed that discharges from WTC's outfall were having a negative impact on the aquatic communities downstream, but DEP did not make any specific recommendation to reduce or limit discharges from the WTC outfall (PA DEP 2013b). The non-profit organization, Clean Water Action, sent a Notice of Intent to File a Citizen Suit (NOI) to WTC on July 18, 2013 for "significant and ongoing violations of the Clean Water Act (CWA), the Pennsylvania Clean Streams Law (CSL), and the federal Endangered Species Act (ESA)." The alleged violations stemmed from WTC's acceptance and discharge of oil and gas wastewater which was not explicitly part of its NPDES permit conditions. The notice additionally stated that the facility's "effluent discharge to the Allegheny River has resulted in significant habitat modification and degradation that is likely to kill and injure the northern riffleshell, a federally listed endangered freshwater mussel species" (Clean Water Action 2013). On October 28, 2013, after the 60 day period in which WTC could

respond to the allegations and attempt to settle the claims elapsed, CWA filed the citizen lawsuit in the U.S. District Court for the Western District of Pennsylvania. Then on November 25, 2013 DEP announced that it has reached a proposed consent decree with WTC to settle ongoing NPDES violations and require upgrades to meet Chapter 95 discharge requirements for TDS and chloride by January 2016.

DISCUSSION

The CWT case studies above show that the efforts of regulators and industry have been critical to reducing discharges of UNG wastewater, but discharges of conventional oil and gas wastewater continue to impact streams. Scientific studies analyzing UNG wastewater disposal practices show that in 2011 there was a significant shift toward deep well injection and recycling, which led to reduced UNG discharges to surface waters; however, discharges to Pennsylvania's waters remain above pre-Marcellus development levels. (Wilson and VanBriesen 2012, Maloney and Yoxtheimer 2012, Lutz 2013). The trend toward increased recycling continued into 2012 as a cost effective alternative to deep well injection (Dave Yoxtheimer, personal communication, February 29, 2012). The changes in disposal practices in 2011 can be attributed to the strengthened Chapter 95 regulations enacted in 2010 and the voluntary agreements put into place in 2011 (Fig. 2). Additionally, the DEP and EPA have been working to limit discharges through the use of consent orders and agreements (Fig. 2). However, the continued impact of conventional oil and gas wastewater on Pennsylvania's waters noted in the case studies indicates the need to strengthen effluent and instream water quality regulations.

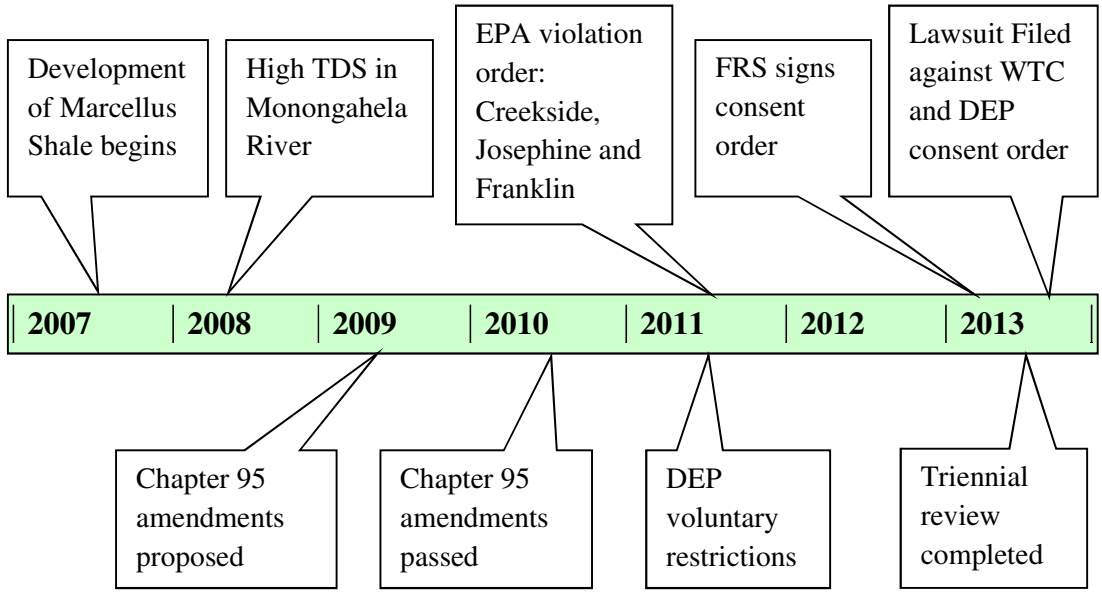

FIG. 2. Timeline of Marcellus Shale related regulatory developments and wastewater treatment facility enforcements.

Despite a long history of conventional oil and gas development and wastewater treatment, Pennsylvania currently lacks an instream water quality standard for both TDS and chloride. In 1988, EPA established water quality guidelines for chloride and many states across the country either adopted EPA's guidelines or developed their own chloride limits to protect aquatic life. In 2008, the Iowa Department of Natural Resources (Iowa DNR) did a comprehensive review of chloride toxicity information available and then collaborated with EPA to fill in data gaps through toxicity studies. The efforts by Iowa DNR and EPA showed that water chemistry parameters such as hardness and sulfate influence the toxicity of chloride (Iowa DNR 2009). In 2009, Iowa adopted equation based chloride criteria that takes into account hardness and sulfate when calculating chloride limits for individual streams.

During Pennsylvania's 2010 triennial review of water quality, DEP proposed adopting EPA's 1988 guideline for chloride which sets the maximum one-hour average chloride limit at 860 mg/L (Eldridge et al 2010), but it failed to include the limit in the final version of the standards that were adopted by the Environmental Quality Board. In 2013, DEP had another opportunity to strengthen water quality standards during the triennial review and this time proposed using Iowa's chloride criteria equations (PA DEP 2012). Despite known water quality problems due to high chloride loads from UNG and conventional oil and gas wastewater, DEP again failed to include chloride in the final version of the standards that were adopted in June 2013. DEP has said it plans to continue to review and evaluate a new aquatic life based standard for chloride during the next triennial review period.

As more facilities are required to comply with Chapter 95 regulations, the oil and gas wastewater industry has been exploring alternative treatment and disposal options to meet the needs of drillers. Traditional treatment options utilized by CWTs and POTWs for treating high TDS and chloride loads include reverse osmosis, distillation and crystallization, but these options can be prohibitive due to the high cost per gallon of water treated. In recent years, the oil and gas industry has been turning to recycling and reuse of wastewater as a cost effective alternative to traditional treatment of wastewater containing high levels of TDS and chloride. Lutz et al (2013) reported that prior to 2011 only 13 percent of wastewater from UNG was recycled, but in 2011 Maloney and Yoxtheimer (2012) noted that the number had grown to approximately 70 percent. In 2012 it was estimated that upwards of 75 percent of wastewater from UNG was being recycled (Dave Yoxtheimer, personal communication, February 29, 2012). The noted increase in recycling has in part been spurred by effluent standards imposed on treatment facilities under Chapter 95, and the additional Chapter 95 requirement that natural gas drilling companies develop a wastewater source reduction strategy to "maximize the recycling and reuse of flowback or production fluid" by August of 2011 (25 Pa. Code § 95.10).

A number of wastewater recycling facilities (zero discharge) are now in operation to serve the needs of the expanding UNG industry. Onsite recycling and reuse of UNG wastewater has also become popular with some drillers due to the cost savings compared to trucking wastewater to centralized recycling facilities. Newly proposed DEP regulations would allow oil and gas drillers to process and reuse wastewater onsite or at a subsequent site where the processed wastewater will be reused. As part of the proposed rules, drillers are required to develop a reuse plan for fracking

wastewater under their general site water management plan (25 Pa Code § 78). The reuse plan encourages drillers to recycle and reuse wastewater and ties directly in with the wastewater source reduction strategy outlined in Chapter 95. These changes in UNG wastewater management and disposal have helped to mitigate the water quality impacts of Marcellus Shale development in Pennsylvania, but as Wilson and VanBriesen (2012) show, TDS loads are still higher than prior to the development of the Marcellus Shale.

CONCLUSIONS

The volume of wastewater associated with the boom in Marcellus Shale natural gas production has brought challenges of oil and gas wastewater treatment and disposal to the forefront. In 2008, water quality issues began to surface in the Monongahela River and high concentrations of TDS were noted. Over time, increased TDS and chloride loads have led to the degradation of stream health due to the limited assimilative capacity of the streams and rivers. In response to concerns over water quality impacts from wastewater discharges the DEP enacted updated wastewater treatment effluent standards under Chapter 95, which set the stage for more regulatory oversight of both POTWs and CWTs.

TDS and chloride loads discharged to Pennsylvania's streams and rivers from UNG wastewater have been reduced through the efforts of State and Federal agencies and oil and gas drillers, but without more stringent rules on the conventional oil and gas industry, high loads of these harmful constituents will continue to be discharged. As shown in the case studies above, DEP and EPA continue to enforce the current regulations, but due to the exemption in Chapter 95 they have been forced to use alternate means to address wastewater discharges that may harm aquatic ecosystems. Through consent orders and agreements related to NPDES violations, EPA and DEP have required exempt facilities to meet the new TDS and chloride limits. Facilities that are exempt from Chapter 95 and operating in compliance with their permit conditions are permitted to discharge high TDS and chloride loads indefinitely under the current regulations. This loophole in Chapter 95 highlights the need for tighter effluent water quality regulation on the entire oil and gas wastewater treatment industry in order to improve water quality. In addition to closing the Chapter 95 loophole, enacting an instream water quality standard for chloride during the next triennial review would constitute a significant step toward continued improvement of stream health.

ACKNOWLEDGMENTS

The author would like to thank the staff at Matson & Associates for their ideas, support and critical review, especially Wendy Pearson. The author gratefully acknowledges the many researchers who took the time to wade through the DEP oil and gas production and wastewater reports, these efforts helped make this paper possible.

REFERENCES

Abdalla, C. W., Drohan, J. R., Blunk, K. S., and Edson, J. (2011). "Marcellus Shale Wastewater Issues in Pennsylvania – Current and Emerging Treatment and Disposal Technologies." Penn State University Cooperative Extension, 9 p.

Clean Water Action (2013). "Notice of Intent to File a Citizen Suit for Ongoing Violations of the Clean Water Act, the Pennsylvania Clean Streams Law, and the Endangered Species Act at Waste Treatment Corporation's Plant in the City of Warren, Warren County, Pennsylvania." July 18.

Dresel, P. E., and Rose, A. W. (2010). "Chemistry and Origin of Oil and Gas Well Brines in Western Pennsylvania." Pennsylvania Geological Survey, 4th ser., Open-File Report OFOG 10–01.0, 48 p.

Environmental Quality Board (EQB) (2010). "Water Treatment Requirements, 25 PA. Code Ch. 95." 40 Pa.B. 4835, August 21.

Eldridge, W. H., Arscott, D. B., Jackson, J. K. (2010). "Stroud Water Research Center Expert Report on the Proposed Rulemaking by the Pennsylvania Environmental Quality Board for Ambient Water Quality Criterion; Chloride." Stroud Water Research Center, Stroud Report #: 2010004, 38 p.

Ferrar, K. J., Michanowicz, D. R., Christen, C. L., Mulcahy, N., Malone, S. L., and Sharma, R. K. (2013). "Assessment of Effluent Contaminants from Three Facilities Discharging Marcellus Shale Wastewater to Surface Waters in Pennsylvania." *Environ*. *Sci*. *Technol*., 47 (7), 3472–3481.

Hart, P. (President, Pennsylvania Brine Treatment and Hart Resource Technologies) (2011). Letter to Marcellus Shale Customers. September 19.

Hayes, T. (2009). "Sampling and Analysis of Water Streams Associated with the Development of Marcellus Shale Gas." Gas Technology Institute, Prepared for Marcellus Shale Coalition.

Hoffman, J. (2010). "Susquehanna River Basin Commission Natural Gas Development." *Science of the Marcellus Shale Symp*., Lycoming College, Williamsport, PA, January 29. <http://www.srbc.net/programs/projreviewmarcellustier3.htm> (Aug. 19, 2013).

Iowa Department of Natural Resources (Iowa DNR) (2009). "Responsiveness Summary, Chloride, Sulfate and TDS Revisions." August 24, 23 p.

Klaber, K. Z. (President, Marcellus Shale Coalition) (2011). Letter to Michael Krancer (Secretary, PA DEP). April 20.

Krancer, M. L. (Secretary, PA DEP) (2011). Letter to Shawn Garvin (Regional Administrator, US EPA). July 26.

Lutz, B. D., Lewis, A. N., and Doyle, M. W. (2013). "Generation, transport, and disposal of wastewater associated with Marcellus Shale gas development." *Water Resources Research*, 49, doi:10.1002/wrcr.20096, 647-656.

Maloney, K. O., and Yoxtheimer, D. A. (2012). "Production and Disposal of Waste Materials from Gas and Oil Extraction from the Marcellus Shale Play in Pennsylvania." *Environmental Practice*, 14(4), 278-287.

Pennsylvania Department of Environmental Protection (PA DEP) (2003). Letter to Waste Treatment Corporation. November 19.

PA DEP (2011a). "Pennsylvania Environmental Quality Board Final Amendments to Regulations on Wastewater Treatment Requirements." Plain Language Summary, 3 p.

PA DEP (2011b). "Policy and Procedure for NPDES Permitting of Discharges of Total Dissolved Solids (TDS) -- 25 Pa. Code §95.10." 31 p.
PA DEP (2011c). Letter to 88 Gas production Operators. July 11.
PA DEP (2011d). "Applications for National Pollution Discharge Elimination System (NPDES) Permits and Water Quality Management (WQM) Permits." 41 Pa.B. 735, February 5.
PA DEP (2012). "Rationale for the Development of Ambient Water Quality Criteria for Chloride Protection of Aquatic Life Use." Bureau of Point and Non-Point Source Management, 5 p.
PA DEP (2013a). "PA DEP's Electronic Discharge Monitoring Reports (eDMR) System." <http://www.ahs.dep.state.pa.us/NRS/ > (Nov. 29, 2013).
PA DEP (2013b). "Aquatic Biology Investigation Warren City Wastewater Treatment Plant (PA0027120) Waste Treatment Corporation (PA0102784) Allegheny River (Stream Code 42122) City of Warren, Warren County." PA DEP Northwest Regional Office, January 10.
Tetra Tech, (2009). "Evaluation of High TDS Concentrations in the Monongahela River." Pittsburgh, PA, 127 p.
US Environmental Protection Agency (USEPA) (1988). "Ambient Water Quality Criteria for Chloride – 1988." Office of Water, Regulations and Standards Criteria and Standards Division, Washington, DC.
USEPA (2009). "National Secondary Drinking Water Regulation." EPA 816-F-09-004, 4 p.
USEPA (2011a). Letter to 14 POTWs, Acceptance of Oil and Gas Waste. July 13.
USEPA (2011b). "Introduction to the National Pretreatment Program." Office of Wastewater Management, EPA-833-B-11-001, 91 p.
USEPA (2011c). "Findings of Violation Order for Compliance and Request for Information, Docket No. CWA-03-2011-0274DN." USEPA Region III, Philadelphia, PA.
USEPA (2013). "Administrative Order for Compliance on Consent, Docket No. CWA-03-2013-0051DN." USEPA Region III, Philadelphia, PA.
Veil J. A. (2010). "Water Management Technologies Used by Marcellus Shale Gas Producers." United States Department of Energy, Argonne National Laboratory, 56 p.
Wilson, J. M., VanBriesen, J. M. (2012). "Oil and Gas produced Water Management and Surface Drinking Water Sources in Pennsylvania." *Environmental Practice*, 14(4), 288-300.
Wilson, J. M., VanBriesen, J. M. (2013). "Oil and Gas produced Water Management and Surface Drinking Water Sources in Pennsylvania." *Environ. Sci. Technol.*, 47 (21), 12575-12582.
Yoxtheimer, D. A. (2011). "Potential Surface Water Impacts from Natural Gas Development." PowerPoint Presentation, <http://www.marcellus.psu.edu/resources/PDFs/Halfmoon%208-24-11.pdf> (Aug. 30, 2013).
25 Pa. Code § 95 (2010). "Chapter 95 Wastewater Treatment Requirements." August 21.

Management of Produced Water in Pennsylvania: 2010-2012

Jeanne M VanBriesen[1], Ph.D., P.E., M.ASCE, Jessica M Wilson[2], Ph.D., and Yuxin Wang[3], S.M.ASCE

[1]Professor, Department of Civil and Environmental Engineering, Carnegie Mellon University, 5000 Forbes Avenue, Pittsburgh PA 15213, E-mail: jeanne@cmu.edu.
[2]Assistant Professor, Department of Civil and Environmental Engineering, Manhattan College, 4513 Manhattan College Parkway, Riverdale, NY 10471, E-mail: jessica.wilson@manhattan.edu.
[3]Research Assistant, Department of Civil and Environmental Engineering, Carnegie Mellon University, 5000 Forbes Avenue, Pittsburgh PA 15213, E-mail: yuxinw@andrew.cmu.edu.

ABSTRACT: Produced water from development of oil and gas resources, especially development of unconventional resources using hydraulic fracturing, requires management to avoid unintended environmental impacts. The recent rapid expansion of development in Pennsylvania's Marcellus Shale formation has led to significantly higher volumes of produced water requiring management. Conventional produced water management frequently involves treatment at centralized brine treatment plants that provide partial treatment and release into surface waters through NPDES permits that are exempt from salt limits, although use of this treatment option has declined from 3.18 to 2.27 Mbbls from 2006 to 2012. Reuse of conventional produced water increased significantly in 2012 (to 43% of the total volume). Although representing a small fraction of total water under management (less than 10%), use of surface-discharging publically owned treatment plants that do not remove salt has increased for conventional produced water (from 0.35 Mbbls in 2006 to 0.77 Mbbls in 2012). Unconventional (shale gas) produced water is predominately managed through recycling and reuse. Use of surface-discharging plants has significantly declined between 2006 and 2012 (from 5.81 Mbbls to 0.62 Mbbls), while underground injection and treatment at facilities that return treated water for reuse have both increased.

INTRODUCTION

Pennsylvania has been an oil and gas producing state for almost 200 years (Harper, 2008); however, recent activities to develop deep shale resources for natural gas and associated liquids have increased concerns regarding environmental protection during these activities.

Oil and gas extraction produces wastewaters that are typically high in dissolved solids, often dominated by simple salts. Some waters co-produced with the hydrocarbons are associated with the formation rock while others are the product of the use of hydraulic fracturing to increase formation permeability. For natural gas wells in low permeability shales, the spent hydraulic fracturing fluid that returns to the surface during the early flowback period can have a large volume but low salt concentration. During hydrocarbon production the produced formation water is usually a small volume but with significantly higher salt concentrations. Oil wells on the other hand generally produce from formations with significant formation water, and show increasing volumes of produced water over their lifetime,

All produced water from oil and gas wells requires management; in addition to salts it often contains naturally occurring radioactive materials (NORMs), hydrocarbons, and chemicals used in the hydraulic fracturing process. Produced water can be managed through reuse, disposal in underground injection wells, or treatment for reuse or discharge.

The present work examines the management of produced water in Pennsylvania during the recently natural gas boom, from 2010 to 2012. The analysis presented here is an update to earlier work (Wilson and VanBriesen, 2012).

METHODS

Data for the present analysis were acquired from the Pennsylvania Department of Environmental Protection (PADEP, 2012). Data for 2006 predate significant development in the Marcellus shale formation and thus are considered baseline for conventional produced water in the present analysis. Data for 2008 and 2009 are not included as the PADEP did not differentiate between conventional and unconventional wells for the produced water data that was reported at that time. Downloaded data were manipulated as described in Wilson and VanBriesen (2012).

The produced water data in the PADEP database have undergone some reclassification over the years. Table 1 identifies the categories used by PADEP in their database in different time periods. The categories used in this analysis are shown in the final column. There are significant misclassifications in the database, which were corrected for the present analysis. Reclassification was based on permit number and facility names. Errors are particularly common in earlier years and in classification of centralized waste facilities and publically owned treatment plants. Also, PADEP does not distinguish among centralized brine treatment facilities that treat water for reuse and those that treat for surface discharge under exemptions to new state TDS discharge standards. The exempt plants do not have a limit on salt discharges, and thus, it is important to evaluate this management option separately. The present analysis makes this distinction. Plants with current exemptions include: PA Brine Josephine (PA0095273), PA Brine Franklin (PA0101508), Hart Resource Technologies (PA0095443), Tunnelton Liquids (PA0091472), Advanced Waste Services of PA

(PAR0051 and PAR00002), McCutcheon Enterprises (PAD013826847), Waste Treatment Corporation (PA0102784), and Sunbury Generation (PA0008451).

Table 1. Classification of Produced Water Management Options

PADEP (2010 and earlier)	PADEP (2011 and 2012)	The Analysis
Injection Disposal Well	Injection Disposal Well	Injection Well (UIC)
Brine or Industrial Waste Treatment Plant	Centralized Treatment Plant for Recycle	Exempt Centralized Treatment Plants; *and* *separately* Centralized Treatment Plants for Recycle
Municipal Sewage Treatment Plant	Public Sewage Treatment Plant	Municipal Sewage Treatment Plant (POTW)
Surface Impoundment	Storage pending disposal or reuse	Reuse and Storage within Operations
Reuse other than Road Spreading	Storage pending disposal or reuse	Reuse other than Road spreading
Treated on site	Other	Other
NPDES discharge	Other	Other
No method entered	Identify method in comments	Other
Landfill	Landfill	Other
Road Spreading	(none entered with this classification)	Other

The present analysis builds on the work of Wilson and VanBriesen (2012), using the same method of assigning volumes to different management options. However, recent work by Lutz et al (2013) calls these methods into question. Lutz et al (2013) suggest that the PADEP database contains records that are effectively replicates, leading to significant over reporting of volumes of produced water when using the data as reported. If this is an accurate assessment of the data, the true volume taken to different facility types would be unknown, and the present analysis could not be undertaken. In order to compare the current work with our prior work, we have used the same methodology as reported in Wilson and VanBriesen (2012). Lutz et al (2013) suggests that this method will over estimate wastewater volumes, particularly Marcellus volumes. However, the alternative method of dividing large volumes uniformly among management options is likely to bias the results significantly since some management options (e.g. POTWs and CWTs) have restricted capacities. The present work should therefore be considered the worst-case volumes as it assumes all volumes reported for each management option are correct and do not represent double-counting of wastewater volumes.

RESULTS and DISCUSSION

Figure 1 shows results for total produced water for Pennsylvania, with 2006 as the pre-shale gas baseline. Significant increases are observed in total produced water requiring management as shale gas development proceeded (from 6.6 Mbbl in 2006 to 36.2Mbbl in 2012). This represents relatively small changes in produced water from conventional sources (6.5% increase), and large increases in unconventional sources. Year over year increases in produced water from unconventional sources are significant with a nearly doubling from 2010 to 2011 (11.7 to 20.2 Mbbl), and a further 44% increase from 2011 to 2012 (20.2 to 29.2 Mbbl).

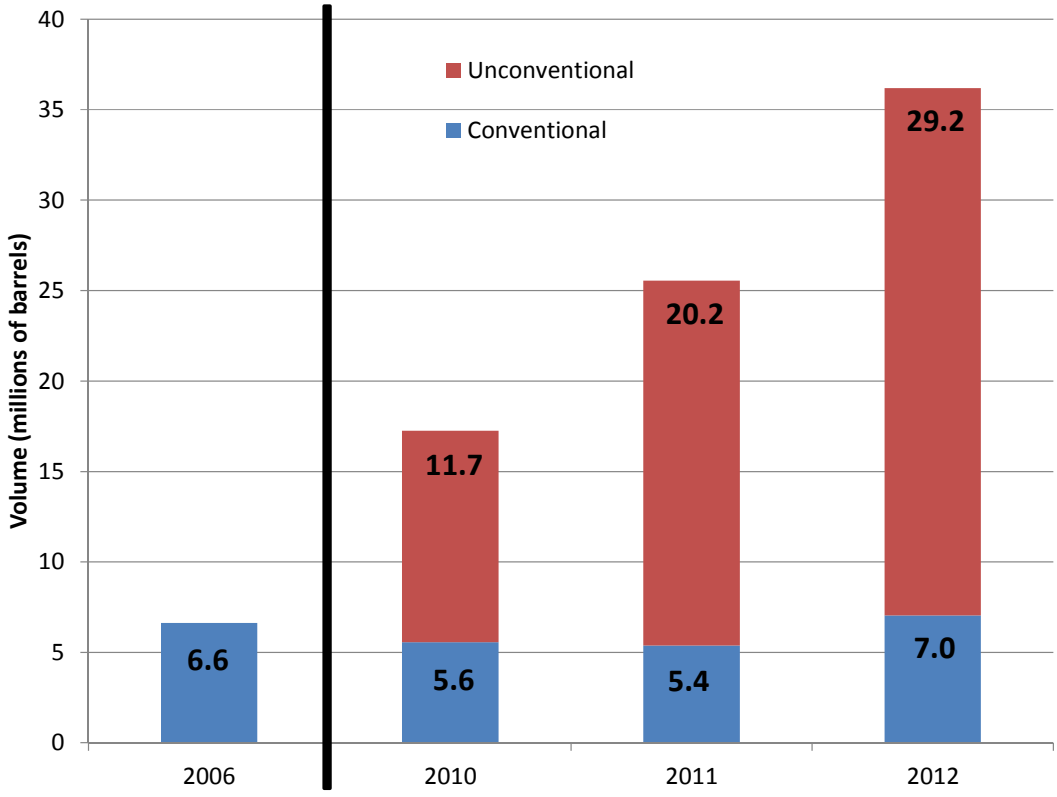

FIG. 1. Produced Water in Pennsylvania by Type for 2010 – 2012. Total for 2006 (assumed to be all conventional) shown for baseline.

Figure 2 shows management option changes for *conventional* produced water from 2010 to 2012, again with 2006 used as a baseline year. As shown in Figure 1, overall volumes of produced water from conventional sources have not changed significantly; however, Figure 2 shows an increase in detailed reporting (a decrease in the category 'other', which contained many unspecified entries for 2006). A decrease in the use of exempt centralized treatment plants from 3.18 Mbbls to 2.27 Mbbls is also notable, as is an increase in use of municipal sewage treatment plants (from 0.35Mbbls to 0.77 Mbbls). From 2011 to 2012 there is also a significant increase in storage and reuse of conventional produced water; from a baseline of 0.26 Mbbls in 2006 to 2.98 Mbbls in 2012 (more than a 10 fold increase). This is

likely associated with increased potential for reuse of produced water with the increase in activities associated with shale gas development. A small increase in the use of injection wells for disposal is also seen (from 0.39 to 0.62 Mbbls from 2006 to 2012). Although not shown in the Figure, the raw data indicate a significant increase in use of conventional oil and gas produced brines for dust control via road spreading between 2010 and 2012 (from 175,969 bbls in 2010 to 265,965 bbls in 2012; 50% increase).

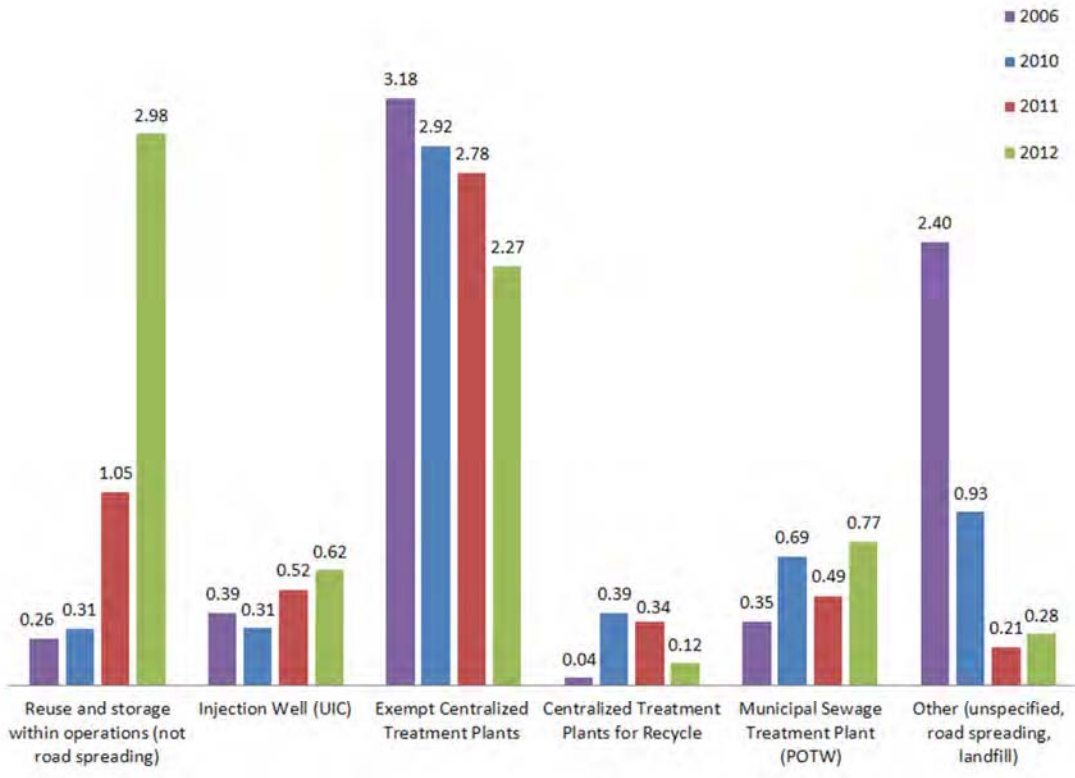

FIG. 2. Management options selected for *conventional* produced water in Pennsylvania (2010-2012). All values are in millions of barrels. 2006 is shown as a baseline, pre-shale gas development.

Figure 3 shows management option changes for *unconventional* produced water from 2010 to 2012. As shown in Figure 1, overall volumes of produced water from unconventional sources have increased significantly over the past three years. The storage and reuse category has increased most rapidly, with approximately a tenfold increase of water reported as reused or stored between 2010 and 2012 (from 2.39 Mbbls to 20.67 Mbbls). As expected, a significant decrease in the use of surface-discharging, partial-treatment options was observed following the request from PADEP to shale gas drillers to stop taking produced water to Chapter 95 exempt facilities. The use of exempt brine treatment plants decreased from 5.14 Mbbls in 2010 to less than 50,000 bbls in 2012. The use of publically-owned wastewater treatment plants decreased from 617,693 bbls in 2010 to zero in 2012. Significant increases in the use of injection wells for produced water from unconventional sources are also clear (from 0.4 Mbbls to 3.61 Mbbls from 2010 to 2012). Unlike the

conventional, very small amounts of unconventional produced water are reported to be spread on roads for dust control (e.g, 425 bbls in 2012). The bulk of the 'other' category is landfill for the unconventional produced water.

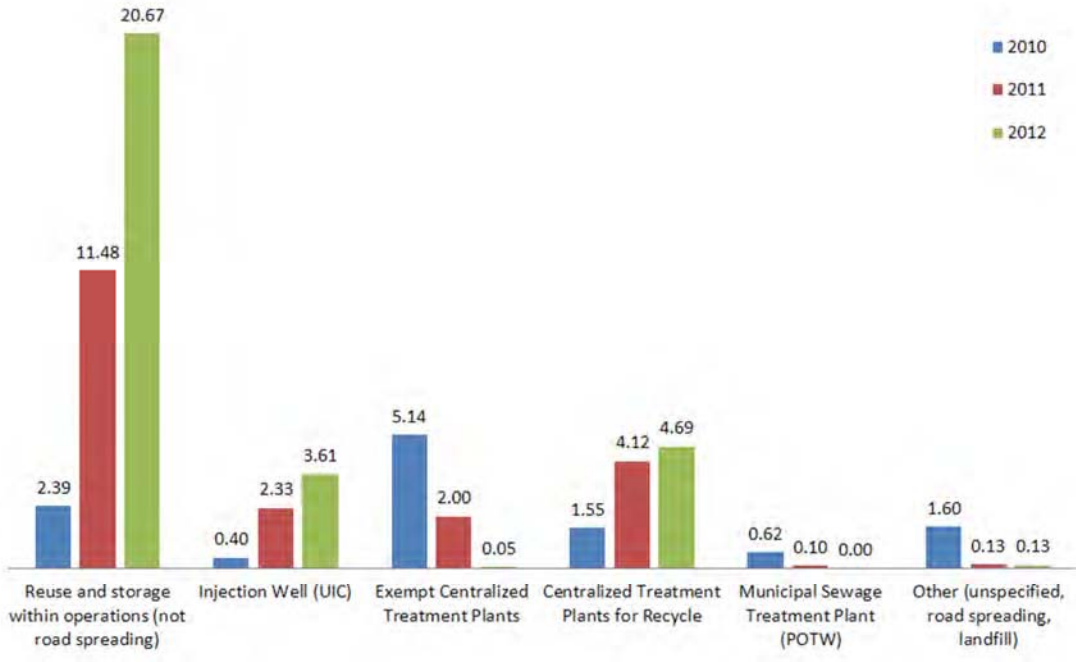

FIG. 3. Management options selected for unconventional produced water in Pennsylvania (2010-2012). All values are in millions of barrels.

CONCLUSIONS

The management of produced water from natural gas production in Pennsylvania has significantly changed due to expansion of unconventional development in the Marcellus Shale formation. Overall, the total volume of produced water increased from 6.6 to 36.2 Mbbls between 2006 to 2012. The use of exempt centralized brine treatment plants that discharge salt water to the environment decreased for conventional and unconventional produced water, while increases were seen in the use of centralized treatment plants which treat to either recycle or discharge unconventional produced water. Recycling and reuse for all produced water increased from 2010 to 2012.

ACKNOWLEDGMENTS

The authors gratefully acknowledge the funding support provided for this work, as well as related work, by the Colcom Foundation, the Heinz Endowments, the Achievement Rewards for College Scientists (ARCS) Foundation, the Steinbrenner Institute for Environmental Education and Research (SEER) and the Center for Water Quality in Urban Environmental Systems (Water QUEST) at Carnegie Mellon University.

REFERENCES

Harper, J.A. (2008). The Marcellus Shale: An Old "New" Gas Reservoir. *Pennsylvania Geology* 38 (1):2–13. Available at http://www.dcnr.state.pa.us/ topogeo/pub/pageolmag/pdfs/v38n1.pdf accessed November 11, 2012!.

Lutz, B.D., Lewis, A.N., Doyle, M.W. (2013) "Generation, transport, and disposal of wastewater associated with Marcellus Shale gas development," Water Resources Research, 49: 647-656.

Pennsylvania Department of Environmental Protection (PA DEP) (2012) *PA DEP Oil & Gas Reporting Website: Statewide Data Downloads*. PA DEP, Harrisburg, PA. https://www.paoilandgasreporting.state.pa.us/publicreports/ Modules/DataExports/DataExports.aspx . Accessed May 1, 2012 for 2006-2011 data; accessed November 15, 2013 for 2012 data.

Wilson, J.M., and VanBriesen, J.M. (2012) "Oil and gas produced water management effects on surface drinking water sources in Pennsylvania," *Environmental Practice,* 14(1): 1-13.

Evaluating Leachability of Residual Solids from Hydraulic Fracturing in the Marcellus Shale

Stephanie Countess[1], Gregory Boardman[2], Richard Hammack[3], Alexandra Hakala[4], Shekar Sharma[5], and Jeffrey Parks[6]

[1]Graduate Research Assistant, National Energy Technology Laboratory (NETL) – Regional University Alliance (RUA), Virginia Tech Department of Civil and Environmental Engineering, 418 Durham Hall, Blacksburg, VA 24061, U.S.A., E-mail: scount@vt.edu.
[2]Professor, NETL-RUA, Virginia Tech Department of Civil and Environmental Engineering, 417 Durham Hall, Blacksburg, VA 24061, U.S.A., E-mail: gboard@vt.edu.
[3]Research Group Leader, NETL, 626 Cochrans Mill Road, Pittsburgh, PA 15236, U.S.A., E-mail: richard.hammack@netl.doe.gov.
[4]Geochemist, NETL, 626 Cochrans Mill Road, Pittsburgh, PA 15236, U.S.A., E-mail: alexandra.hakala@netl.doe.gov.
[5]Graduate Research Assistant, NETL-RUA, Virginia Tech Department of Civil and Environmental Engineering, 418 Durham Hall, Blacksburg, VA 24061, U.S.A., E-mail: shekars@vt.edu.
[6]Research Scientist, Virginia Tech Department of Civil and Environmental Engineering, 408 Durham Hall, Blacksburg, VA 24061, U.S.A., E-mail: jparks@vt.edu.

ABSTRACT: The purpose of this research is to characterize residual solids from hydraulic fracturing in the Marcellus Shale to predict leaching behavior in the natural environment for elements of concern. Solid samples were subjected to strong acid digestions to determine the total environmentally available concentration of elements and to weak acid digestions with various extraction fluids (reagent water, inorganic acid, organic acid, and synthetic municipal landfill leachate) to determine worst-case leaching potential in various disposal environments. Comparing these results, it is possible to determine the effect of extraction fluid and sample characteristics on the leaching potential of select elements. This may be further developed to determine best management practices for the disposal of hydraulic fracturing residual solids.

INTRODUCTION

The process of natural gas extraction through hydraulic fracturing produces large quantities of water with total dissolved solids frequently exceeding 200,000 mg/L due to the elevated presence of naturally-occurring salt, radionuclides, and heavy metals (Chapman, 2012). This produced water is typically stored onsite in earth impoundments or temporary containers before being reused in subsequent well completions or being transported to a dedicated facility to undergo treatment (Hammer, 2012). The purpose of this research is to characterize the solids resulting from hydraulic fracturing operations and produced water treatment in the Marcellus

Shale in order to predict the leaching behavior of heavy metals and other elements of concern when residual solids are buried or disposed of in a municipal landfill.

Four types of samples were collected from a 1.2 MGD dedicated treatment facility in Pennsylvania, owned and operated by Reserved Environmental Services. These samples included: (1) drilling mud from well construction, (2) sludge resulting from the physiochemical treatment of process waters, (3) raw solids from the gravity thickening of produced water, and (4) sludge solidified with cement kiln dust (CKD) prior to disposal in a municipal landfill. After initial characterization, these samples were subjected to various digestion techniques to determine the potential for release of over thirty elements.

The elements of concern were identified based on previous research regarding produced water composition, Marcellus Shale geochemistry, and regulatory requirements for solid waste and wastewater. Naturally occurring elements found in the Marcellus Shale include major components, such as barium, chloride, sodium, calcium, strontium, and bromide (Chapman, 2012). Previous research concerning hydraulic fracturing wastewater has also focused on common elements like aluminum, boron, iron, lithium, magnesium, manganese, phosphorus, and potassium (Haluszczak, 2013).

Multiple methods of strong acid digestion were performed to determine the total composition of "environmentally available" elements capable of leaching under worst-case environmental conditions. Open vessel digestions were performed on a laboratory hot plate with a reflux system (USEPA, 1996) and closed vessel digestions were performed in a microwave unit for direct energy coupled extraction (USEPA, 2007). These digestion methods were performed with various extraction fluids to determine a suitable or preferred digestion method for all elements of concern.

Weak acid digestions were used to predict the leaching potential of these solids under simulated environmental conditions. EPA's Toxicity Characteristic Leaching Procedure (TCLP) was used to simulate disposal in a municipal landfill and determine if a waste is classified as hazardous based on its inorganic elemental leaching behavior (USEPA, 1992). Similar experiments were also performed using an ASTM method with modifications for an acidic extraction fluid (ASTM, 2012) in order to determine the effect of extraction fluid on leaching potential.

The results from strong and weak acid digestions were compared in an effort to better understand the types and quantity of materials that will likely leach from the various samples under environmental conditions.

METHODOLGY

To determine the environmentally available composition of samples, open vessel digestions were performed following EPA 3050B – Acid Digestion of Sediments, Sludges, and Soils. During this process, trace metal grade nitric acid and hydrogen peroxide (30%) are added to digest residual solids and release bound elements. In an optional step, trace metal grade hydrochloric acid is added to the final extract and refluxed to dissolve precipitates and complete the digestion process. The digestate is filtered and analyzed to determine the soluble composition.

In an alternate method, closed vessel digestions were performed following EPA

3051A – Microwave Assisted Acid Digestion of Sediments, Sludges, Soils, and Oils with a CEM Mars Extractor microwave unit. During this process, a sample of residual solids is placed in a glass vessel with either concentrated trace metal grade nitric acid or, alternatively, a nitric acid and hydrochloric acid mixture. The sample is digested following a 10 min extraction procedure, reaching temperatures up to 175°C. The digestate is then filtered and analyzed to determine the soluble composition.

Weak acid digestions of samples were performed using standard methods including EPA 1311 – Toxicity Characteristic Leaching Procedure (TCLP) and ASTM 3987 – Standard Procedure for Shake Extraction of Waste with Water. ASTM 3987 was also performed with modifications for an acidic extraction fluid to study the effect of fluid aggressiveness on leaching behavior.

TCLP is performed with an extraction fluid of either buffered or unbuffered acetic acid (pH 4.93 / 2.88) depending on sample alkalinity. Prior to analysis, samples are vacuum filtered to determine the solid portion of waste. Due to a limited sample volume, this experiment was performed with 5 g of solid sample and 100 mL of extraction fluid to maintain the desired 20:1 (mL:g) extraction ratio. The sample and extraction fluid were placed in a rotary tumbling device for 18 hours, and the resulting leachate was filtered through a 0.7 μm filter and analyzed.

ASTM 3987 does not require initial sample preparation. In this procedure, residual solids are agitated with reagent water (distilled/deionized) using proportions and agitation techniques similar to TCLP. The resulting extract is filtered through a 0.45 μm filter to obtain the soluble portion and analyzed.

A modified ASTM 3987 was performed with acidic extraction fluids including: (1) acid rain (pH 4.2) prepared with nitric/sulfuric acid (USEPA, 1994); (2) acetic acid (pH 2.88) prepared based on TCLP standards; and (3) oxygen-sensitive synthetic landfill leachate developed by Stanforth *et al*. (1979) to simulate the maximum aggressiveness of municipal landfill leachate. The constituents of this leachate include acetic acid as a representative volatile acid, sodium acetate as a pH buffer and for monovalent ionic strength, glycine for organic nitrogen, pyrogallol as a complexing agent, and ferrous sulfate for divalent ionic strength (Stanforth, 1979). The oxygen sensitive leachate was purged with nitrogen gas to avoid precipitation of iron; however, the procedure was otherwise performed as specified by ASTM 3987. It is generally assumed that digestion with reagent water or acid rain can be used to determine the leaching of residual solids during onsite burial, while procedures with acetic acid or synthetic leachate simulate disposal in a municipal landfill.

Samples from strong and weak acid digestions were analyzed with inductively coupled plasma-mass spectrometry (ICP-MS) for elements of concern.

RESULTS AND DISCUSSION

In order to highlight the overall results from this research, examples of experimental data for selected major elements of concern are provided below.

Multiple strong acid digestion techniques were used to determine the preferred method of quantification for elements of concern in hydraulic fracturing residual solids. Variations in results between methods may be due to the use of a closed vessel system which can prevent loss of volatiles or from the optional addition of

hydrochloric acid which can contribute to stabilization of select elements (USEPA, 2007). A comparison of the four strong acid extraction procedures used to determine the elemental composition (g/kg dry) of residual solids is outlined in Figure 1.

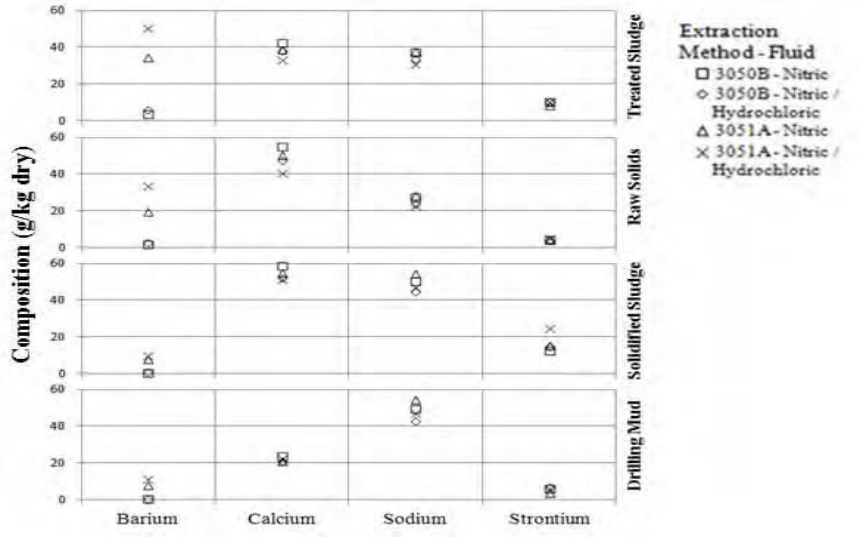

FIG. 1. Strong acid digestion results for environmentally available composition (g/kg dry) of barium, calcium, sodium, and strontium in residual solids.

From these results, it was observed that the characterization and quantification of environmentally available elements can vary considerably based on the extraction technique. Results for barium had the most notable variations, indicating that the method of extraction is important to accurately quantify residual solids. In general, the microwave assisted digestion of residual solids, which was expected to be a more rigorous and complete procedure, resulted in the greatest quantification for elements of concern. However, calcium is one example where improved quantification was observed through less rigorous digestion techniques and extraction fluids.

In order to determine the leaching behavior of residual solids in the presence of various extraction fluids, Figure 2 provides results for the extract concentration (mg/L) from weak acid digestions following the modified ASTM 3987 procedure. From these results, it was determined that the leaching of calcium is positively affected by the presence of acetic acid, both the unbuffered solution and the synthetic municipal landfill leachate. Contrarily, sodium has the highest leaching potential with reagent water and is considerably mitigated by the synthetic leachate which was developed to simulate the worst-case aggressive nature of a municipal landfill leachate. This indicates that certain disposal environments may be better suited to mitigate the risk of leaching for elements of concern. While these results help to predict the quantities of elements that will leach under various environmental conditions, it is also important to consider the total composition of these residual solids to determine the leaching potential of each element.

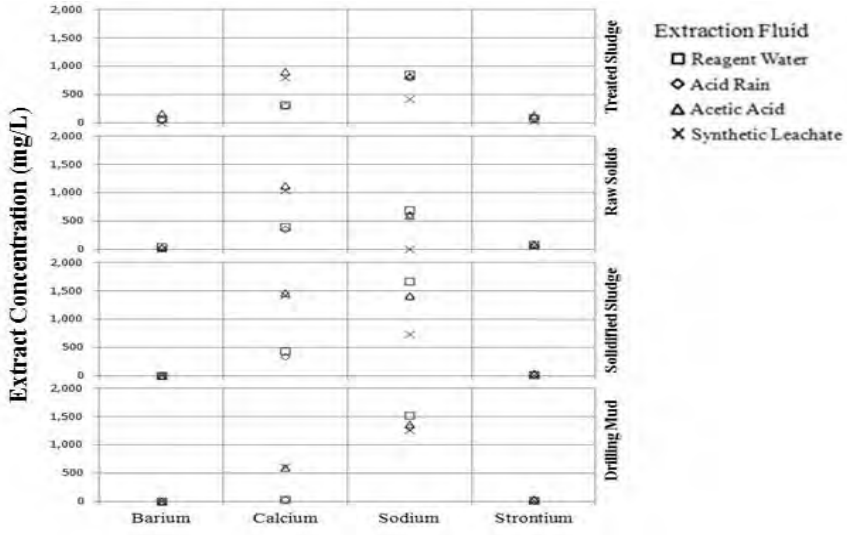

FIG. 2. Extract concentration (mg/L) from weak acid digestion of residual solids with modified ASTM 3987 for barium, calcium, sodium, and strontium.

Extract concentrations from weak acid digestions were compared to the maximum observed residual solid composition for each element of concern to determine the leaching potential (% of composition). The results from this analysis are presented in Figure 3. From these results, it was determined that elements such as strontium may be leaching at low concentrations, but as much as 70% of the amount present in the sample is observed to leach under worst-case conditions. In contrast, barium has a relatively low leaching potential in all residual solids regardless of the extraction fluid. This analysis is important in that it can be used to predict how loosely or tightly bound elements of concern are in hydraulic fracturing residual solids.

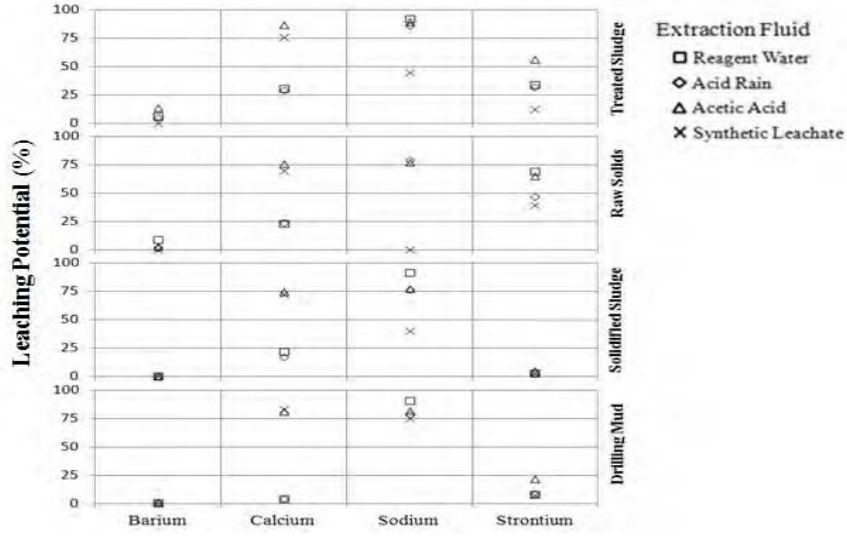

FIG. 3. Leaching potential (%) based on results from modified ASTM 3987 weak acid digestions and the highest observed composition from strong acid digestions of residual solids for barium, calcium, sodium, and strontium.

From Figure 3, it is also possible to recognize the effect of acetic acid on the leaching potential of strontium, which in the case of treated sludge is considerably more aggressive than the synthetic municipal landfill leachate. Another notable observation from this comparison indicates the solidification process employed by Reserved Environmental Services before the disposal of sludge in a municipal landfill is effective in reducing the release of strontium.

Note that the values presented in this research letter have been adjusted to remove baseline interferences determined from the control samples. However, some values may be approximations if the element was detected in control samples at trace amounts below the minimum reporting level (MRL).

CONCLUSIONS

Residual solids from hydraulic fracturing operations in the Marcellus Shale have complex compositions of naturally-occurring elements which may react and migrate differently, depending on environmental conditions. In this experiment to study the worst-case leaching potential of solids, it was determined that extraction fluid and sample characteristics can make a considerable difference on the leaching potential of elements. This information may be further developed and used by industry leaders to determine best management practices for residual solids in order to mitigate the risk of leaching for elements of concern in the natural environment during disposal.

ACKNOWLEDGEMENTS

As part of the National Energy Technology Laboratory's Regional University Alliance (NETL-RUA), a collaborative initiative of the NETL, this technical effort was performed under RES contract DE-FE0004000. The authors would also like to acknowledge and thank Reserved Environmental Services for providing samples and Julie Petruska and Jody Smiley of Virginia Tech for their technical assistance.

DISCLAIMER

Neither the United States Government nor any agency thereof, nor any of their employees, nor URS Energy & Construction, Inc., nor any of their employees, makes any warranty, expressed or implied, or assumes any legal liability or responsibility for the accuracy, completeness, or usefulness of any information, apparatus, product, or process disclosed, or represents that its use would not infringe privately owned rights. Reference herein to any specific commercial product, process, or service by trade name, trademark, manufacturer, or otherwise, does not necessarily constitute or imply its endorsement, recommendation, or favoring by the United States Government or any agency thereof. The views and opinions of authors expressed herein do not necessarily state or reflect those of the United States Government or any agency thereof.

REFERENCES

American Society for Testing and Materials (2012). Designation 3987: Standard Practice for Shake Extraction of Solid Waste with Water.

Chapman, E. C., Capo, R. C., Stewart, B. W., Kirby, C. S., Hammack, R. W., Schroeder, K. T., and Edenborn, H. M. (2012). "Geochemical and Strontium Isotope Characterization of Produced Waters from Marcellus Shale Natural Gas Extraction." *Environmental Science & Technology* 46(6): 3545-3553.

Haluszczak, L. O., Rose, A. W., and Kump, L. R. (2013). "Geochemical evaluation of flowback brine from Marcellus gas wells in Pennsylvania, USA." *Applied Geochemistry* 28(0): 55-61.

Hammer, R., and VanBriesen, J. (2012). "In Fracking's Wake: New Rules are Needed to Protect Our Health and Environment from Contaminated Wastewater." Natural Resources Defense Council.

Stanforth, R., Ham, R., Anderson, M., and Stegmann, R. (1979). "Development of a Synthetic Municipal Landfill Leachate." *Water Pollution Control Federation 51(7): 1965-1975*.

U. S. Environmental Protection Agency (1992). Method 1311: Toxicity Characteristic Leaching Procedure.

U. S. Environmental Protection Agency (1994). Method 1312: Synthetic Precipitation Leaching Procedure.

U. S. Environmental Protection Agency (1996). Method 3050B: Acid Digestion of Sediments, Sludges, and Soils.

U. S. Environmental Protection Agency (2007). Method 3051A: Microwave Assisted Acid Digestion of Sediments, Sludges, Soils, and Oils.

The Role of Shallow Surface Investigations in the Appalachian Shale Energy Development

John T. Henning[1], PE, M. ASCE and Steven Ladavat[2], P.G.

[1]Associate, Dawood Engineering, Inc., 11 Grandview Circle, Suite 116, Canonsburg, PA 15317, jhenning@dawood.cc
[2]Project Geologist, Dawood Engineering, Inc., 11 Grandview Circle, Suite 116, Canonsburg, PA 15317, sladavat@dawood.cc

ABSTRACT: Engineers and geologists within the Appalachian Basin encompassing the Utica and Marcellus Formations focus on the location and composition of shale layers located thousands of feet below the Earth's surface. However the soil and rock encountered within the top 30 meters (100 ft) can have a direct impact on the ability of the resources to be developed. A properly designed geotechnical investigation consisting of site reconnaissance, geophysics and/or geotechnical drilling can assist in identification of and anticipatory design for geohazards from the construction phase through lifetime of a well pads, water impoundments, midstream transmission systems, or access roads. This paper presents three case studies of geotechnical investigations for midstream operations that were performed during the preliminary design phase of the projects. Case Study #1 consists of a geophysical investigation performed on sensitive federal land in conjunction with geotechnical drilling operations in order to identify the appropriate geometry for a horizontal directional drill (HDD) installation of a 0.61 m (2 ft) diameter pipeline. Case Study #2 discusses a geotechnical drilling investigation and foundation design performed for the construction of a natural gas transmission facility. Case Study #3 presents the geotechnical drilling investigation for the design of a structure to support a natural gas transmission line/state route crossing located in an area that is to be subjected to longwall mining in the near future.

INTRODUCTION

Ranging in depth from 600 m to 2750 m (2000 to 9000 ft), the Marcellus and Utica Shale gas plays follow the Appalachian Basin stretching from the Adirondacks in Upstate New York into northern Tennessee. In order to access the substantial reservoir of natural gas below the surface and bring the resource to market, significant development is required. Upstream development includes the construction of access roads, water impoundments, water lines and well pads. Midstream development activities consist of the construction of gathering pipelines, transmission

pipelines, compressor stations, metering pads, and additional access roads. Downstream development, such as cracker plants, will continue to evolve as various industries enter into the area due to the increased abundance of natural gas.

State regulations have been developed in order to safely develop the vast natural resources below the surface while protecting the environmental resources and wellbeing of the public. As a result of these regulations, a multitude of services are required prior to the permitting of a new industry development including environmental investigations and permitting, hydrogeological studies, and site civil design, among others. The ever-evolving state regulations and industry advances in technologies and techniques have led to significant improvements in the safe development of the natural gas plays. However, unknown geotechnical hazards continue to cause damage to environmental resources and delays in production resulting in higher financial costs to Owners and operators.

A properly performed subsurface investigation can assist in evaluating the site for geotechnical issues that may be encountered during and after construction. Utilizing geotechnical professionals to perform a literature review and site visit can provide insight into potential geotechnical hazards. Upon completion of the initial site evaluation, the geologist or engineer can determine if a geotechnical or geophysical investigation is necessary for the site. The investigation can be tailored to investigate the extent of a geotechnical hazard or to optimize site design.

The majority of the geographic region encompassing the Marcellus and Utica Shale gas plays is located within landslide prone areas as well as other geohazards. The purpose of this paper is to summarize the geotechnical hazards relevant to the Marcellus and Utica gas play regions and to introduce three case studies of how a properly designed geotechnical investigation can assist in avoiding costly failures during development of natural gas resources.

GEOLOGICAL HAZARDS

Located at depths ranging from 610-2743 m (2,000-9,000 ft) below the surface, the footprint of the Marcellus and Utica Shale Gas Plays stretches from the Adirondacks in Upstate New York into northern Tennessee. Closely following the footprint of the natural gas reservoirs is the Appalachian Plateau Physiographic Region, the surficial materials of the region mainly consist of alluvial deposits in the valleys and residual soils or bedrock in the upland areas. Bedrock close to the surface consists of sedimentary rock from the Permian and Pennsylvania Periods. Despite the relatively horizontal bedding of the bedrock, numerous geological hazards are prevalent throughout the region and can have a significant effect on land development projects. These hazards include landslides, surficial and deep mining, settlement, and artesian aquifers.

Landslides

Due to the moderate to steep topography and the surficial materials, landslides have historically been a major issue to development sites throughout the region. Problem strata such as the Pittsburgh Redbeds have caused significant landslides that have

affected roadways and developments throughout Western Pennsylvania and the surrounding areas. Additional causes of landslides that have affected economic development are weathering bedrock overlain by weather-resistant bedrock and development on historical landslide colluvium.

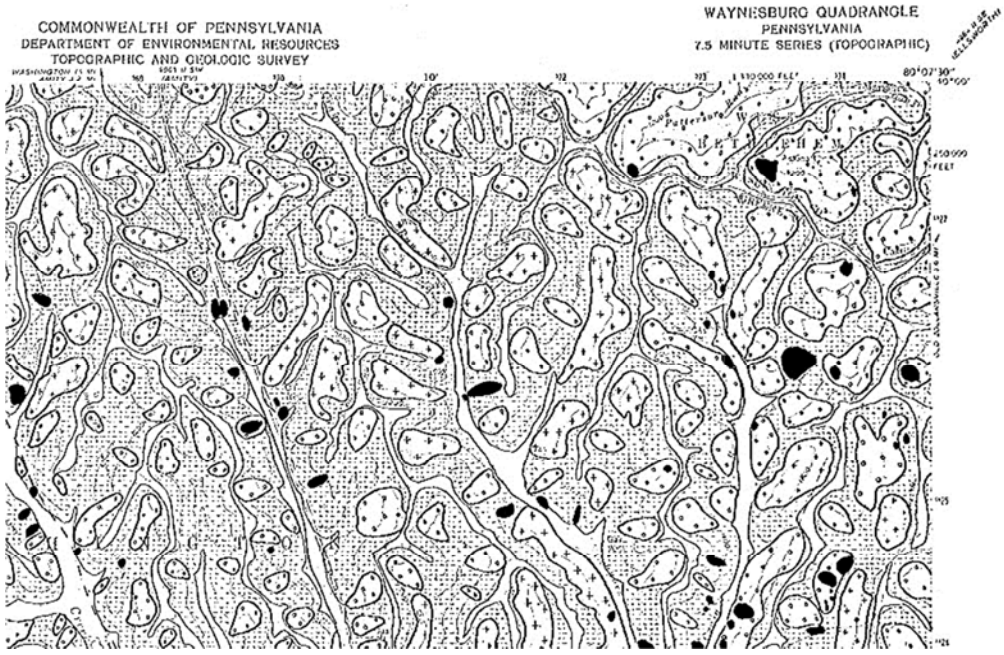

FIG.1 DCNR Landslide Feature Map on USGS Waynesburg Quadrangle (Hackman 1978)

The DCNR has annotated the USGS quadrangles throughout Western Pennsylvania and West Virginia to identify the historical landslides and related features throughout the states. Figure 1 indicates the areas with active landslides (black), historic landslides (white with circles) and landslide susceptible soils and rock (gray hatched area). As indicated by the portion of the Waynesburg Quadrangle provided, nearly 95% of the area has experienced landslide activity or is highly susceptible to landslides.

The susceptible areas to landslides are not confined to Western Pennsylvania and West Virginia. The USGS and the National Atlas prepared Figure 2 below. The red areas on the map indicate locations that have a very high susceptibility to landslides. Yellow indicates high susceptibility, while green indicates moderate potential. The areas covered by red encompass a majority of the region where Marcellus and Utica Shale developments are occurring.

Surficial and Deep Mining

Economically viable bituminous coal seams are prevalent throughout the Appalachian Plateau Region. In Western Pennsylvania and Northern West Virginia, the Pittsburgh Coal of the Conemaugh Group has been extensively mined. Additional seams that have been mined consist of the Freeport, Kittanning, Sewickley and Waynesburg coals. Coal fields extensively mined in Southern West Virginia consist

of Winding Gulf, New River, Flat Top-Pocahontas, Kanawha-Coal River, Greenbrier, Logan and Williamson. A significant amount of the coal has been extracted via deep mining consisting of room-and-pillar, retreat and longwall mining. Upland areas throughout the region where coal seams were exposed have been strip mined.

FIG. 2 USGS Landslide Susceptibility Map (from the National Atlas and USGS, http://maps.redcross.org/website/Maps/Images/NationalLevel/landslides_hires.jpg)

Development on land that has been undermined may be susceptible to subsidence issues. Two main factors that contribute to the potential for surficial mine subsidence are the depth of the mine below the surface and the height of the mined seam. As the mine extends deeper below the surface, the area of influence at the surface increases. Therefore, a larger surficial area may be affected if a deep mine collapse occurs. However, the amount of overburden rock separating the surface and the mine directly affects the likelihood of the surface experiencing any subsidence. The ratio of overburden height to mined seam thickness determines the extent of surficial development. Longwall mine subsidence can extend further than room and pillar mine subsidence due to complete roof collapse.

Another item of concern related to deep mining and surficial mining activities is the existence of acid mine drainage. Acidic mine drainage can result from water encountering coal strata, coal waste or overburden rock. The acidic nature of the drainage is caused by oxidation of the mineral pyrite.

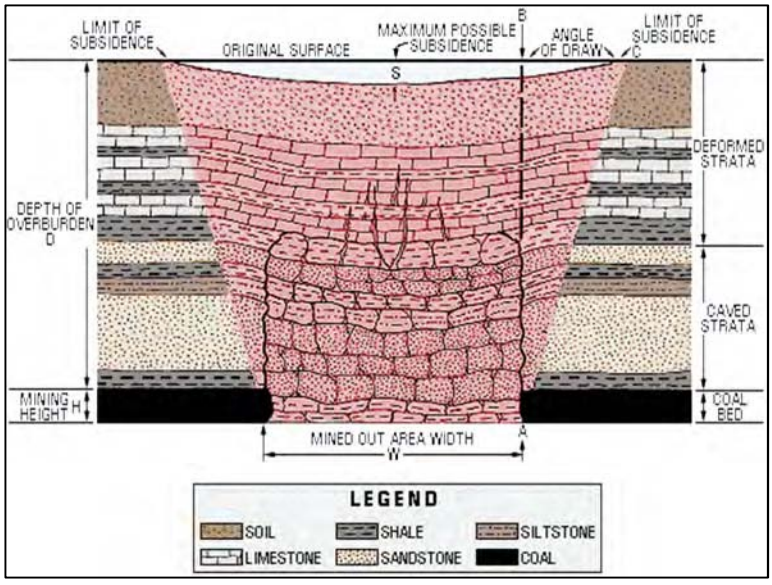

FIG.3 West Virginia Geological and Economic Survey Homeowners Guide to Geological Hazards - Mine Subsidence (adopted from Tandanand and Powell, 1983)

Aretesian Aquifers, Glacial Deposits, and Heterogeneous Alluvial Deposits

Artesian groundwater conditions, glacial deposits, and heterogeneous alluvial deposits can pose significant threats to the success of an HDD bore operation. Glacial deposits and artesian groundwater conditions can be observed in Ohio and Pennsylvania in areas that have been subjected to glacial activities during the Wisconsinian and Illinoian Age. Glaciolacustrine deposits, glacial outwash deposits, and artesian groundwater systems can create conditions that are prohibitive to steering an HDD drill bit and maintaining an open borehole with adequate drilling fluid circulation. Heterogeneous alluvial deposits and glacial till deposits that contain boulder sized fragments also pose threats to the accuracy of HDD bore operations. Boulders can be very difficult to penetrate when they are present in a soft matrix of soils. Boulders can also have the tendency to influence the direction of the drill bit, decreasing accuracy. Mapping of these areas are critical to designing a successful HDD bore.

CASE STUDY #1: HDD CROSSING - INDIANA AND WASHINGTON COUNTIES, PENNSYLVANIA

Case Study #1 consists of the geotechnical exploration for a 1935.5 m (6,350 ft) long, 0.61 m (24 in) diameter natural gas pipeline to be installed utilizing HDD methods. The crossing presented numerous challenges, including a meandering river approximately 70 m (230 ft) elevation below the exit point, approximately 488 m (1600 ft) of floodplain, limited access Army Corps of Engineers property, and a rails-

to-trails property. A subsurface exploration plan was tailored to the project site's unique limitations.

GEOLOGY

According to the Engineering Characteristics of the Rock of Pennsylvania by Gyeyer and Wilshusen (1982), the Conemaugh River Crossing is underlain by the Casselman and Glenshaw Formations of Pennsylvanian Age. The Casselman Formation typically contains cyclic sequences of shale, siltstone, sandstone, red beds, thin impure limestone, and thin, non-persistent coal. Red beds can be associated with landslides. The base of the Casselman is at the top of the Ames Limestone marker bed. The Glenshaw Formation typically contains cyclic sequences of shale, sandstone, red beds, thin limestone, and thin coal. The base of the Glenshaw is the top of the Upper Freeport Coal. The Conemaugh River is a meandering river with a large floodplain, terminating approximately 488 m (1800 ft) from the bank of the river.

SUBSURFACE EXPLORATION PLAN

The subsurface exploration plan was split up in to two parts, geotechnical drilling and geophysical exploration. Geophysical exploration was utilized due to access restrictions imposed by the Army Corps of Engineers. The Army Corps permitted mobilization of geotechnical drilling rigs to areas on their property that did not require heavy clearing or the use of machinery to create access. Access to heavily forested areas was permissible only with hand clearing. The Conemaugh River floodplain was the heavily forested area on the Army Corps property. According to the Army Corps representative, the floodplain was also very sensitive to water level fluctuations. Access to the floodplain was proposed by floating a drill rig on a barge to the project site, however, sufficient docking was not present within a reasonable distance from the project site.

A geophysical analysis was performed at the project site from July 30 to August 1, 2012. Seismic refraction analysis was performed at the project site to determine top of bedrock depth. Seismic refraction measures the transmission of sound waves through the subsurface generated with a sledge hammer blow on the surface. Individual subsurface layer depths and thicknesses can be estimated based on the analysis of sonic wave arrival times. Top of bedrock elevation data in the floodplain was critical due to the potential variability of alluvial soil composition, particularly the presence of boulders and non-cohesive granular material.

Geotechnical drilling was performed at eight locations along the crossing. Borings were drilled for the following purposes: to identify top of bedrock elevation, characterize subsurface conditions, obtain unconfined compressive strength samples to be tested in the laboratory. Unconfined compressive strength samples are used to determine the shear strength of the rock units that the HDD bore will be penetrating. In the event that bedrock units have greater than 206,842 kPa (30,000 psi) compressive strength, the HDD contractor will need to utilize stronger drill bits that can cut through these rock types. Soil was sampled using Standard Penetration

Testing (SPT) methods in 1.5 m (5 ft) intervals. Rock coring was performed using an NX diameter core barrel.

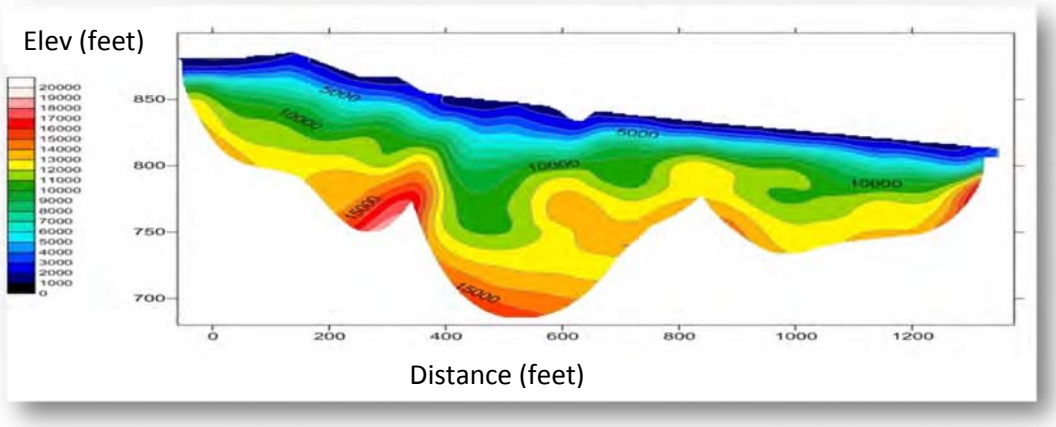

FIG. 4 Seismic Refraction Results (from Dawood Engineering, Inc.)

Subsurface information from the Conemaugh River through the initial 244 m (800 ft) of floodplain could have been useful in providing a more complete estimation of the subsurface conditions; however, barge access to the river was limited. Also, the initial 244 m (800 ft) of the floodplain was not accessible without heavy clearing.

RESULTS

Geotechnical drilling results are summarized in Table 1. Laboratory testing was conducted on 59 samples from the crossing. The lab results indicated the unconfined compressive strength of the rock samples ranged from 10,121 kPa (1,468 psi) to 113,811 kPa (16,507 psi) with an average of 55,482 kPa (8,047 psi).

The seismic analysis revealed that the top of bedrock depth reached a maximum of 10.7 m (35 ft) below ground surface to the end of the line at approximately station 2848+60. Boring data from B-6 indicates that bedrock was encountered at a depth of 4.7 m (15.4'). The top of bedrock encountered in B-6 correlates with approximately 1524 m/sec (5000 ft/sec) from the seismic data, as the data collection areas overlapped.

TABLE 1. Geotechnical Drilling Summary, Conemaugh River HDD Crossing

Boring	Approx. Elevation Meters (ft)	Bedrock Depth Meters (ft)	Top of Bedrock Unit	Approx. HDD Depth Meters (ft)	Proposed HDD Unit
B-1	347.5 (1140)	3.3 (10.8)	SANDSTONE	Exit Point	Lean Clay with gravel
B-2	335.3 (1100)	6.1 (20.0)	Sandy SILTSTONE	35.2 (115.5)	N/A
B-2A	332.3 (1090)	5.9 (19.2)	SANDSTONE	33.5 (110)	SHALE
B-6	297.2 (975)	4.7 (15.4)	SILTSTONE	51.8 (170)	SILTSTONE with interbedded claystone
B-9	295.7 (970)	3.1 (10.2)	SILTSTONE	50.3 (165)	Shaley SANDSTONE
B-10	286.5 (940)	1.6 (5.4)	SANDSTONE	18.3 (60)	SHALE
B-11	294.1 (965)	3.5 (11.4)	CLAYSTONE	7.6 (25)	CLAYSTONE
B-12	304.8 (1000)	6.4 (21.0)	SILTSTONE	Entry Point	Clayey Silt with sand and organics

CASE STUDY #2 WELLSVILLE INTERMODAL FACILITY- WELLSVILLE, OHIO

Case Study #2 (Figure 5) consists of the geotechnical design services for the Wellsville Intermodal Facility in Wellsville, Ohio. The purpose of the facility is to unload crude oil from approximately 120 tanker trucks per day into Lease Activated Custody Transfer (LACT) units and transferred to gathering lines terminating at a barge terminal. Approximately 75.7 kL (20,000 gallon) of oil were estimated to be transferred per day.

Geotechnical design services required included building and above ground storage tank foundations, 37.9 kL (10,000 gallon) oil-water separator foundation, and infiltration testing. Geotechnical investigation services provided for the facility included subsurface drilling consisting of soil sampling as well as laboratory testing. The final foundation types designed for the facility included spread footings for canopy piers, oil storage tanks, and an oil-water separator. Challenges include a shallow groundwater depth, nearby proximity to the Ohio River, and presence of heterogeneous fill material.

FIG. 5 Construction Photo of Wellsville Intermodal Facility (Photo from Dawood Engineering, Inc.)

GEOLOGY

The location of the Wellsville Intermodal Terminal was underlain by the Allegheny and Pottsville Groups (undifferentiated) of Upper Pennsylvanian Age. These groups consist of shale, siltstone, sandstone, conglomerate, limestone, underclay, coal, and flint. The top of the unit is mapped at the top of the Upper Freeport Coal bed. No bedrock was encountered during the subsurface exploration.

SUBSURFACE EXPLORATION PLAN

The subsurface exploration plan consisted of ten geotechnical test borings. The borings were advanced using SPT procedures at 0.9 m (3 ft) intervals. Shelby tubes were advanced in areas containing cohesive soils. The borings were advanced in the areas of proposed substructure units and roadways. Laboratory testing was provided in order to characterize the soils encountered in the subsurface exploration. Lab testing procedures included California Bearing Ratio, soil classification, consolidation, and corrosion testing.

Additional environmental services were required during construction because of potential mine drainage encountered when groundwater infiltrated a foundation excavation. The water infilling the excavations needed to be analyzed before it could be disposed. All water samples were analyzed by a Myron Ultrameter for specific conductance, temperature, and pH.

RESULTS

Table 2 provides a summary of the boring information obtained during the subsurface exploration. Table 3 provides a summary of the N-values encountered during the subsurface exploration which identifies the relative density of the potential foundation soils encountered during the investigation.

TABLE 2. Geotechnical Drilling Summary, Wellsville Intermodal Facility

Boring	Substructure	Total Depth Meters (ft)	Depth to Natural Soil Meters (ft)	Groundwater Level After Drilling Meters (ft) 0 Hr./24 Hr.
B-1	Offloading Facility	9.1 (30)	6.1 (22)	6.6 (21.7)/ NA
B-2	Roadway	3.0 (10)	N/A	Dry/Dry
B-3	Offloading Facility	9.1 (30)	3.5 (11.5)	Dry/ 3.6 (11.7)
B-4	Office/Warehouse	9.1 (30)	5.2 (17)	7.5 (24.5)/ N/A
B-5	Storage Tanks	11.4 (37.5)	4.4 (14.5)	6.6 (21.7)/ N/A
B-6	Offloading Facility	9.1 (30)	6.2 (20.5)	7.2 (23.6)/3.0 (9.8)
B-7	Roadway	3.0 (10)	N/A	Dry/Dry
B-8	Roadway	3.0 (10)	N/A	Dry/Dry
B-9	Offloading Facility	9.1 (30)	3.5 (11.5)	Dry/4.9 (16.2)
B-10	Office/Warehouse	9.1 (30)	3.5 (11.5)	5.9 (19.4)/ N/A

TABLE 3. N-Value Distribution, Wellsville Intermodal Facility

Depth m (ft.)	B-1	B-2	B-3	B-4	B-5	B-6	B-7	B-8	B-9	B-10
0.5 (1.5)	13	11	13	9	7	4	15	6	13	9
1.4 (4.5)	9	12	8	17	10	11	10	18	15	10
2.3 (7.5)	9	14	8	8	8	6	6	7	6	8
3.2 (10.5)	10	7	5	5	14	5	8	5	15	5
4.1 (13.5)	7		8	6	8	11			10	5
5.0 (16.5)	4		8	8	4	7			6	3
5.9 (19.5)	13		9	15	3	10			9	6
6.9 (22.5)	6		8	6	7	5			3	11
7.5 (25.5)	4		6	7	14	5			13	8
8.7 (28.5)	0		11	30	11	3			16	4
9.1 (30)	5		6	13	15	6			23	4
10.1 (33)					41					
11.0 (36)					27					
	Fill	Avg. N	**9.2**							
	Alluvial	Avg. N	**9.7**							

Individualized foundation designs were provided for each substructure unit due to the heterogeneous nature of the fill material and the differences in loading that each substructure was projected to receive. The canopy piers were divided into three categories depending on the amount of loading that they were projected to receive. The foundation sizes for each of the three pier groups varied, with foundation size increasing with projected load.

Several foundation options were considered for the oil tank pad. The pad was designed to support 3-500 barrel and 1-210 barrel oil storage tanks. Foundation options explored included a mat foundation with columns at the corners, a strip footing for the pad, individual ram aggregate piers for each tank, strip footings for each tank, or a massive mat foundation. Consolidation settlement was evaluated for each foundation type. The foundation type chosen was a mat foundation with columns supporting the corners. Pavement design recommendations were also provided for all of the access roads and parking lots.

CASE STUDY #3 NATURAL GAS TRANSMISSION LINE/STATE ROUTE CROSSING LOCATED ABOVE PROPOSED LONGWALL MINING OPERATION – GREENE COUNTY, PENNSYLVANIA

Case Study #3 consists of the collaboration of many different entities. The pipeline owner has several existing lines in Greene County, PA that are affected by scheduled longwall mining operations. The major issue is the effect of subsidence on integrity on the pipeline due to excessive stresses placed on the pipe. The pipe line is generally excavated in the area of the longwall mining and strain gages attached. However, the pipe runs under two active roadways on which traffic must be maintained. Additionally, the pipeline owner has required that the pipeline be able to resist loads while remaining within the required strain parameters for an unsupported pipe length of 15.2 m (50 ft). The solution to this issue required traffic, structural and geotechnical input. The excavation and construction required a detour of approximately 80.5 km (17 mi.) on roads that included restricted structures. As the time during which subsidence was to be monitored was approximately three months, it was necessary to be able to excavate the pipeline quickly and then provide a long term means to carry traffic over the road and remove the detour.

GEOLOGY

Engineering Characteristics of the Rocks of Pennsylvania by Geyer and Wilshusen (1982) indicates the project site is underlain by the Greene Formation of the Permian Period. The formation consists of shale, some siltstone and sandstone, and minor amounts of shaly limestone, claystone, carbonaceous shale, and thin coal. Shale is locally interbedded with siltstone and sandstone. Sandstone locally occurs as channel-fill deposits. The base of the formation is at the top of the Upper Washington Limestone. Thickness of the Greene Formation is variable and may be 152.4 m (500 ft). The depth of the Pittsburgh Coal (the seam to be longwall mined), is approximately 182.9 m (600 ft) below ground surface of the project site.

SUBSURFACE EXPLORATION PLAN

The subsurface exploration consisted of two borings drilled within the vicinity of the existing pipeline in order to obtain information about the subsurface conditions. The borings were advanced utilizing SPT methods at 0.9 m (3 ft) intervals.

RESULTS

Geotechnical drilling results indicated that a small amount of fill was present at the road surface, underlain by colluvium to a depth of 1.8-2.7 m (6.0-9.0 ft). Residual material was then encountered to spoon refusal at depths of 3.7 m (12.3 ft). The residual material consisted of clayey shale fragments and top of bedrock surface is anticipated at the refusal depths. There were also some shale outcrops present along the roadway in the project area.

Two general alternatives were examined. One alternative required that the pipeline be excavated, and lightweight fill material replaced then paved, with traffic running directly on the light weight fill and pipeline. This alternative was rejected as even small loads due to pavement structure and traffic only allowed an unsupported length of 7.6 m (25 ft). The second alternative required that the pipeline under the road be excavated and remain uncovered, while using either a temporary bridge or steel plates. For the temporary bridge alternative, geotechnical analysis of the bridge foundations was required. As the invert of the pipe is 2.7-4.0 m (9-13 ft) below existing grade, the use of temporary excavation support or sloping of the excavation sides was analyzed. Due to skewing of the roadways requiring a relatively long bridge, it was determined that the open cut would be approximately 6 feet wide with temporary excavation support and steel plate integrated into the support system. Lateral earth pressure parameters were determined and the temporary excavation support (TES) designed. One aspect of the design included external bracing between the parallel temporary retaining walls located at the top of the TES. This bracing reduced moments and deflections in the TES elements, while also providing a stiffened “bridge” structure on which the steel plates could be secured.

The open cut structure allows for examination of the pipeline after longwall mining subsidence, as well as providing access for shoring the pipeline to relieve increased stresses in the pipe due to subsidence.

REFERENCES

Geyer, A. R. and Wilshusen, J. P., (1982). “Engineering Characteristics of the Rocks of Pennsylvania”, Pennsylvania Geological Survey.

Hackman, R. J. (1978). “Landslides and Related Features of the Waynesburg, PA Quadrangle”, *USGS Open File Map 78-1056* (H-15).

Tandanand, S., and Powell, L.R. (1982).“Assessment of Subsidence Data from the Northern Appalachian Basin for Subsidence Prediction”, U.S. Bureau of Mines Report of Investigations 8630, Access from: http://www.wvgs.wvnet.edu/www/geohaz/geohaz3.htm.

Geomechanical Characterization of Shale Formations for Sustainable Production

Rafael Villamor Lora[1], S.M. ASCE, and Ehsan Ghazanfari[2], M.ASCE

[1]PhD Student, Civil and Environmental Engineering Program, University of Vermont, Burlington, VT 05405, U.S.A., E-mail: rvillamo@uvm.edu
[2]Assistant Professor, Civil and Environmental Engineering Program, University of Vermont, Burlington, VT 05405, E-mail: ehsan.ghazanfari@uvm.edu

ABSTRACT: Hydrocarbon production from unconventional shale gas reservoirs has become more common in recent years. Characterization of organic-rich shale formations is an important task because deformational properties not only control the success of hydraulic fracturing process, but also how transport properties are changed during production. A common problem encountered by the industry is that these deformational properties cannot be captured by geophysical techniques, which can only measure elastic properties. Therefore, it is very important to understand how deformational properties are related to elastic properties. In particular, the relationship between ductile deformation and elastic properties, and relations between elastic stiffnesses and clay/organic content of the shale formation are of significant importance. In order to investigate these relationships, laboratory experiments were conducted on shale gas samples taken from a Marcellus outcrop at State Game Lands 252, located in Lycoming and Union counties, Allenwood, Pennsylvania. Laboratory results show that the nonlinear nature of these rocks makes the characterization challenging. Appreciable differences were found between dynamic and static properties measured under the same stress conditions and directions.

INTRODUCTION

Hydrocarbon production from unconventional shale gas reservoirs has attracted more attention in recent years due to its notable contribution to the increase of the nation's gas proved reserves (EIA, 2013). Advances in technology, especially in horizontal drilling and hydraulic fracturing, have enabled economic production from these formations. These unconventional reservoirs are characterized by extremely small grain sizes, elevated total organic carbon, and low natural permeability, which usually range in the nano-Darcy scale (Vermylen, 2011; Ghassemi and Suarez-Rivera, 2012). Therefore, achieving economic gas production requires hydraulic fracturing stimulation of the reservoir to create a large surface area for gas to flow to the wellbore. Optimizing this production strongly depends on the ability of the hydraulic stimulation to activate an extensive fracture network (Maxwell, 2011). The

major problem here is the variability and unpredictability of the outcome from these fracturing operations. Current industrial practice involves the evaluation of the brittleness of the shale formation as a deciding factor for identifying prospect intervals for fracturing stimulation (Rickman et al., 2008). However, this practice is not based on the geomechanical behavior of shale reservoirs, which ultimately is controlled by the conjunction of in-situ state of stresses and deformational properties.

Characterizing these organic-rich shales is an important and challenging task because geophysical investigations or well logging cannot capture deformational properties. From a geomechanical perspective, linking between the small-strain elastic properties and the large-strain deformational properties of shale gas is crucial for the exploitation of shale gas reservoirs. The short-term brittle deformation of shales affects the fracturing pattern of the formation during the hydraulic fracturing operation. Additionally, the long-term ductile deformation significantly controls the transport properties of the formation during the production stage. Therefore, it is very important to understand how these deformational properties are related to the elastic properties.

One of the major concerns about hydraulic fracturing is the possibility for fractures to extend to the deepest aquifers causing groundwater contamination. During fracturing operations, fractures propagate in the direction perpendicular to the minimum principal stress. In addition, a significant number of shear failures are generated in the surrounding intact reservoir rock (Vermylen, 2011). Despite this basic framework, the mechanism of hydraulic fracturing is poorly understood, and mathematical models cannot yet precisely predict fracture growth (Davies et al., 2012, Vermylen, 2011). In fact, the knowledge about the propagation of fractures at in situ conditions comes from industry experience (King et al., 2008; Davies et al., 2012). Furthermore, rock fracture is also controlled by the in situ state of stresses, estimation of which is challenging and cannot be completely accomplished by direct means. Here, the role of geomechanics is the determination of the growth pattern and extent of hydraulically induced fractures in shale formations under a range of conditions and material properties. Thereby, before we can accurately predict the facture network resulting from a specific injection, we need to understand the factors and rock properties that control the variability in hydraulic fracture networks (Maxwell, 2011).

Another issue that has a major economic impact on gas production is the loss of productive fracture area and fracture conductivity in shale formations (Ghassemi and Suarez-Rivera, 2012). As gas is initially produced, pore pressure is drawn down resulting in an increase in the effective pressure that eventually leads to the closure of fractures and microfractures resulting in a reduction of permeability on multiple scales (Vermylen, 2011; Ghassemi and Suarez-Rivera, 2012). On the other hand, creep deformation also affects the transport properties in the long term as well as the regional stress state that has a major impact in hydraulic fracturing success. Therefore, understanding the causes and the rate of decline of production/permeability is a key factor in the management and operational design of shale gas reservoirs.

To date, many researchers have pointed the importance of understanding deformational properties to better optimize operational procedures in shale gas

reservoirs (Sone, 2012; Ghassemi and Suarez-Rivera, 2012; Britt and Schoeffler, 2009; Jacobi et al., 2008, Yale and Jamieson, 1994). Sone (2012) conducted a series of triaxial tests on shale samples in order to study the correlation between deformational properties and elastics properties, as well as their relationship to anisotropy. Elastic properties of gas shales were reported to be strongly anisotropic, and the degree of anisotropy found to be correlated with the clay and organic content of the rock (Sone, 2012). In these studies (Sone, 2012; Yale and Jamieson, 1994), elastic properties were studied using both static and dynamic methods. Moduli derived from dynamic techniques have shown monotonic stiffening against pressure, while static moduli exhibited a first stage of rapid stiffening followed by second stage of material degradation, perhaps due to additional energy-dissipative inelastic deformation during the triaxial stage (Zoback and Byerlee, 1975). Differences in the value of Young's modulus during the 1st-loading and the unloading/reloading were reported, being the latter 20% lower on average (Sone, 2012). P-wave and S-wave velocity relations were also studied to some extent, however no clear mechanical explanation was provided, and it is a topic that is still under debate (Lucier et al., 2011).

Ghassemi and Suarez-Rivera (2012) and Sone (2012) also investigated deformational properties of shale formations through characterization of the viscoelastic-plastic behavior of these formations. They found that creep strain is correlated with Young's modulus, and clay and organic content. However, Sone (2012) pointed that there is no universal inter-reservoir trend for clay and organic content. Results from these studies showed that creep behavior can be described using a power-law strain-time model during both hydrostatic and triaxial stage (Equation 1).

$$\varepsilon^c = k\sigma t^n \tag{1}$$

Where ε^c is the time-dependent component of the creep only. Nevertheless, during triaxial stage creep behavior is better described by a mechanical system known as Burgers model (Findley et al., 1976), which response can be modeled by Equation 2. This system is composed of a series of springs (E_1,E_2) and dashpots (η_1, η_2), which are able to reproduce the elastic and viscous response of creep.

$$\varepsilon = \frac{\sigma}{E_1} + \frac{\sigma}{\eta_1}t + \frac{\sigma}{E_2}\left(1 - e^{-\frac{E_2}{\eta_2}t}\right) \tag{2}$$

Both studies also observed that creep strain is smaller in the radial direction indicating a volume loss, most likely accommodated by microcrack and pore closure.

The objective of this study was to further investigate the relationship between ductile deformation with elastic properties, and relations of elastic stiffness with clay/organic content of the shale formations. For this purpose, a series of laboratory experiments were conducted on shale gas samples taken from a Marcellus outcrop at State Game Lands 252, located in Lycoming and Union counties, Allenwood, Pennsylvania.

METHODOLOGY

Sample Characterization

The samples used in this study were taken from a Marcellus outcrop from an average depth of 400 ft. The estimated overburden stress is about 5 MPa based on the bulk density of minerals and well log. In our experiments, saturation is considered low enough so that poroeslastic effects are considered negligible. Mineralogy and petrological properties were studied via X-ray diffraction (XRD), thin section and Scanning Electron Microscope (SEM) testing.

Laboratory Procedures

A series of triaxial experiments where cylindrical samples of 2-inch diameter and 2.5-inch length rock plugs were deformed under hydrostatic and triaxial pressure conditions were conducted. All the specimens were drilled perpendicular to the bedding, hindering characterization of anisotropy. Experiments were performed in a fully servo-controlled triaxial apparatus AutoLab 1500 (Figure 1a). Deformation was measured by two axial and one radial strain gauges installed on a copper sleeve as shown in Figure 1b. This copper sleeve also acts as a barrier between the sample and the confining fluid. P-wave and cross-polarized S-wave velocities were measured by ultrasonic transducers at various stress levels during the experiment. The frequency used for these dynamic measurements was ~750 kHz. Triaxial tests were run under undrained conditions.

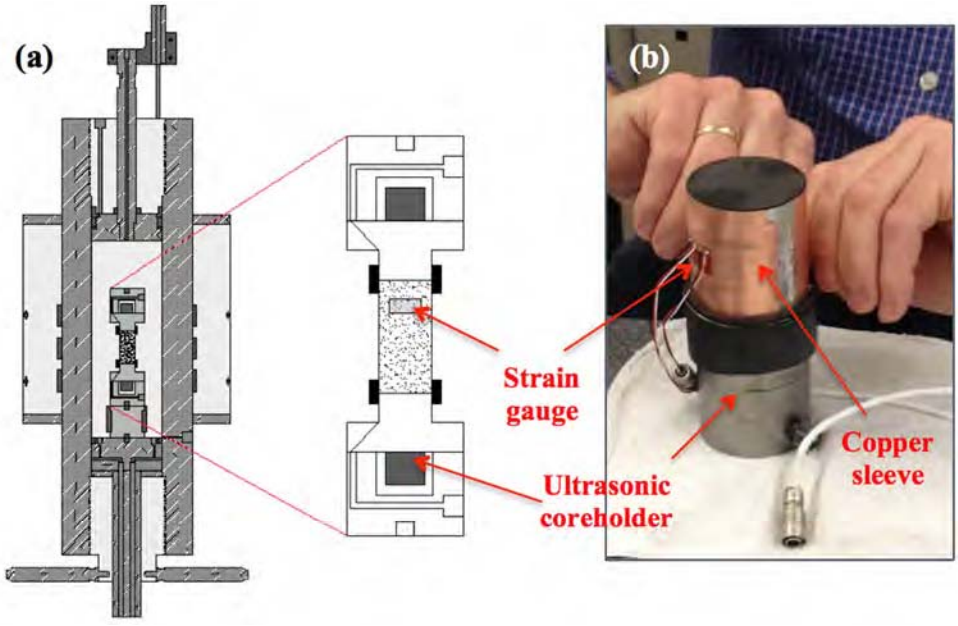

FIG. 1. (a) Schematic of the triaxial apparatus used in the experiments. (b) Two axial and one radial strain gauges were installed on a copper sleeve that separates the sample from the confining fluid. Ultrasonic coreholders measured wave velocities at various stress levels.

An example of the multistage stress path followed during the experiments is shown in Figure 2. During the hydrostatic stage, confining pressure, *CP*, was applied in 2-4 steps. After the target confining pressure was reached, deviatoric stress, *DS*, was applied in 2-4 steps. For each step, pressure was increased at a rate of 0.03 MPa/sec, then it was held constant for 1 hour to observe the creep response, and finally it was partially decreased and increased again at the same rate of 0.03 MPa/sec to measure the unloading/reloading constants. When testing non-linear materials, it is recommended to preform these unloading-reloading cycles at different stress levels so the sample is well characterized within the elastic range (Fjær et al., 2008). Dynamic and static properties were measured at the same direction and the same stress states, which enabled the comparison between both.

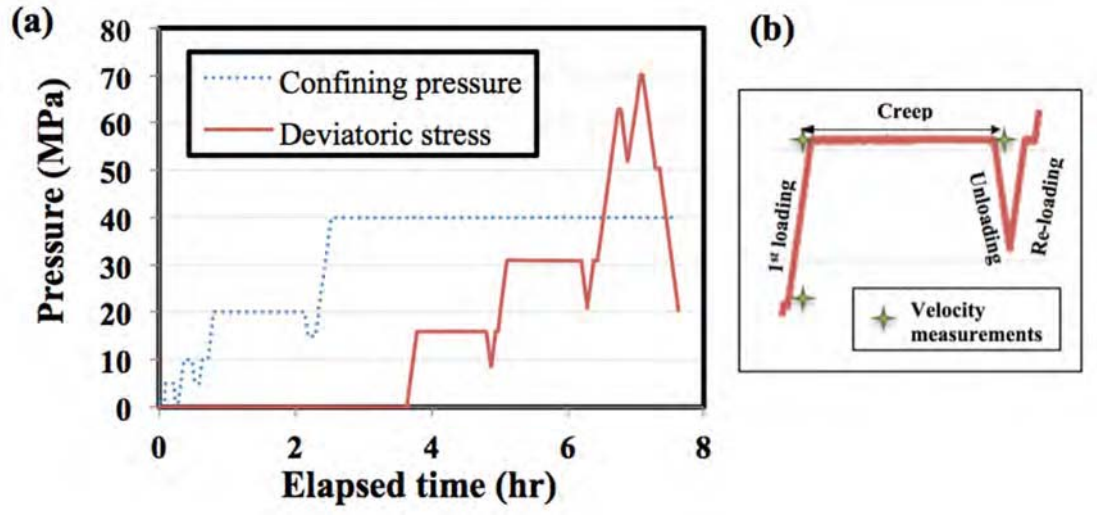

FIG. 2. (a) Example of a multistage loading followed during the experiments. (b) Static properties were estimated for all the 1st-loading and the unloading-reloading cycles. Dynamic properties were obtained at discrete points, always before and after the creep.

RESULTS AND DISCUSSION

Static and Dynamic Elastic Properties

The ultimate aim of this work is to understand how deformational properties affects ductile deformation of shale formations. Characterizing deformational and ductile properties will enable us to predict how transport properties and the effectiveness of hydraulic fracturing will change over time. Shale gas rocks are known to be non-linear materials (Fjær et al., 2008; Sone, 2012). Therefore, the characterization of their static properties requires performing unloading-reloading cycles at different stress levels in order to interpret the elastic moduli from the stress-strain response (Fjær et al., 2008). Rock cores are the principal sources for such characterization. However, they are not always available since their extraction is complicated. Also, they do not fully represent the target formation as they come from discrete levels.

Instead, in the field, elastic properties are often measured by dynamic techniques, which are capable to characterize large areas. With this in mind, we performed a series of experiments to measure static and dynamic properties in an attempt to develop a correlation between them as the first step to study deformational properties from seismic exploration or well logging. In this paper, results from the stress path followed in Figure 2 are presented.

During the hydrostatic stage, bulk modulus was measured for the 1st loading and unloading-reloading stages. Figure 3 shows an increase in stiffness for both 1st loading and unloading-reloading stages as expected from the consolidation process and the closure of microcracks. A more rapid increase in bulk modulus is observed around 5 MPa reflecting the closure of soft pore spaces and microcracks that may have opened as a result of the stress and pore pressure release during core extraction and sample preparation. Due to their extremely low permeability, fractures are likely to occur in shales during coring and retrieval, leading to macroscopically and/or microscopically fractures that significantly affect rock properties (Fjær et al., 2008).

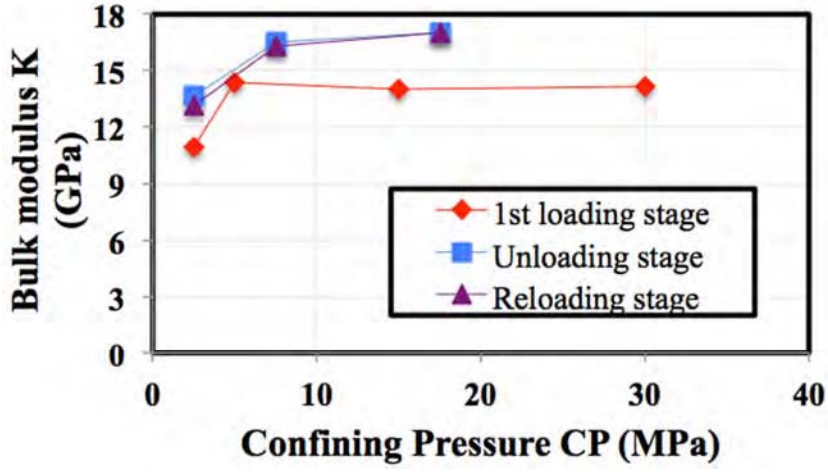

FIG. 3. Bulk modulus vs. Confining pressure during the hydrostatic stage. Four pressure steps are reported in this figure. An increase in bulk modulus is observed with increasing confining pressure. Results for the 1st loading and unloading-reloading stages are plotted separately, showing different tends and being the latter higher.

Figure 4 shows results for dynamic elastic properties of the shale specimen. Both, Young's modulus (E_{dyn}) and Poisson's ratio (ν_{dyn}) were measured under hydrostatic and triaxial conditions, and no abrupt changes were observed between stages. As evident by experimental data, there exist a monotonic stiffening against axial stress, with higher rates at pressures below the closure pressure. This, in fact, is in accordance with the behavior reported by Sone (2012). Again, this transitional behavior is a result of the closure of soft pore spaces and microcracks as explained above.

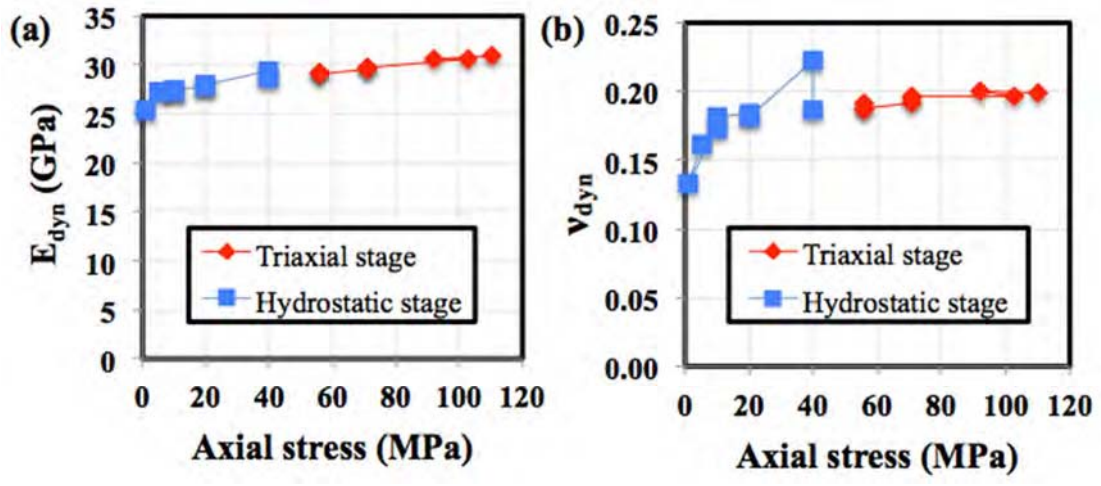

FIG. 4. (a) Dynamic Young's modulus and (b) Poisson's ratio vs. Total axial stress. Data from hydrostatic and triaxial stages are presented separately, no abrupt changes are observed between stages. Monotonic stiffening with axial stress occurs for both stages.

Static Young's modulus (E_{stat}) was only measured during the triaxial stage. Figure 5a presents Young's moduli values against axial stress; data from 1st loading and unloading-reloading stages are shown separately. Sone (2012) found that the static young moduli presents a stage of rapid stiffening against axial stress at pressures below in-situ effective stress. However, this pattern was not observed in our experiment, since the closure pressure of samples was below the initial axial stress.

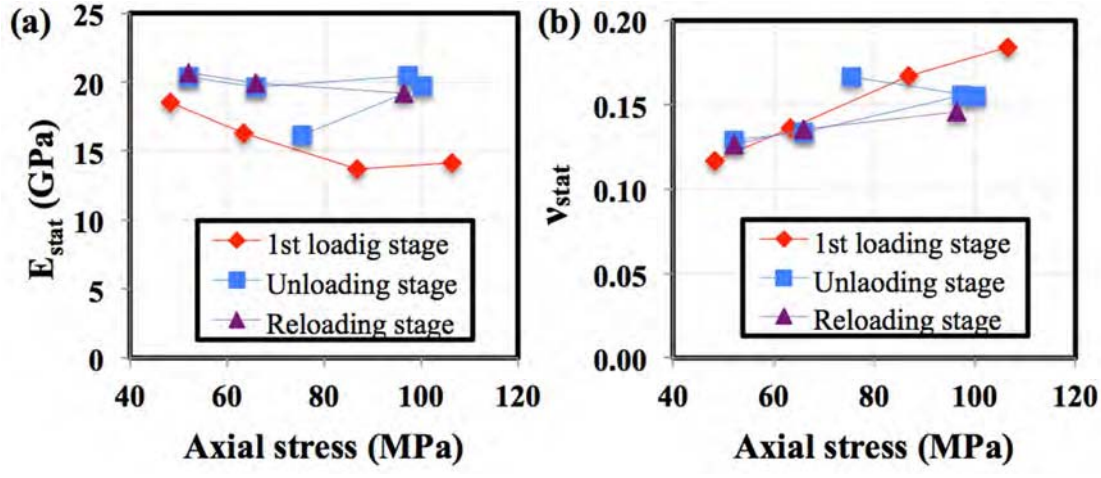

FIG. 5. (a) Static Young's modulus and (b) Poisson's ratio vs. Total axial stress. Values from 1st loading and unloading-reloading stages are shown separately, and different trends can be observed for those set of data for both properties. Static parameters have been estimated by linear regression and the average axial stress was chosen for each step.

Notwithstanding, our laboratory results showed decreasing Young's modulus against axial stress. Other researchers (Zoback and Byerlee, 1975; Sone, 2012) have pointed that not only mineral elastic deformation occurs during static measurements, but also energy-dissipative inelastic deformation is induced as a result of frictional sliding and microcrack growth. This additional plastic deformation clearly changes the structure of the rock, softening the Young's modulus and reflecting material degradation. Two different trends have been found for 1st loading and unloading-reloading stages respectively. While Young's modulus values from 1st loading decreases with axial stress, unloading-reloading values do not show such decrease (at least for small changes in stress). In fact, Young's modulus appears to be constant for unloading-reloading cycles. When elasto-plastic materials start to be deformed under stress, they start to move within the elastic region until they reach the elastic limit, then they deform plastically with a decreasing Young's modulus. If at a certain point the material is unloaded, it will deform following a stress-strain branch parallel to the elastic one until it would be reloaded again to the stress level it was unloaded to previously (Beer et al., 2009). This stress-strain behavior for elasto-plastic materials may explain the results of Figure 5a. We plan to run additional experiments with larger stress cycles necessary to confirm this.

As for the static Poisson's ratio (ν_{dyn}) data, Figure 5b shows a monotonic increase for both 1st loading and unloading-reloading trends. This enhancement of lateral material extrusion, is also indicative of the material degradation mentioned above (Sone, 2012). As it occurs for the Young's modulus, the Poisson's ratio value for the last unload step (which is around 75 MPa) does not follow the general trend for the unloading-reloading data. This particular value is measured along a step with a large change in stress where additional inelastic deformation, such as microcrack growth, may have occurred, and therefore it presents a different magnitude.

Comparing Figures 4 and 5, we can observe a significant difference between the elastic moduli obtained from acoustic velocities and those obtained from stress and strain measurements. Moduli measured from dynamic techniques are generally larger than those estimated by static means (Fjær et al., 2008). In this work, static moduli have been measured as slopes of stress-strain curves by linear regression. The strain amplitude during static measurements is about 4 orders of magnitude larger than for the corresponding dynamic ones. Plasticity and nonlinear effects explain to some extent the difference between these moduli. In addition, the heterogeneous microstructure of the rocks is also related to this discrepancy (Fjær et al., 2008).

Ductile Deformation

As discussed in the introduction, the characterization of the viscoelastic-plastic behavior of shale gas formations is important for production. Creep deformation affects the transport properties in the long term as well as the regional stress state that has a major impact in hydraulic fracturing success in the short term. For this purpose, creep deformation was measured under different stress conditions during hydrostatic and triaxial stages.

Figures 6 shows the laboratory results for 1-hour creep at two different confining pressures during the hydrostatic stage. Although it is generally assumed that creep is proportional to the deviatoric stress and that hydrostatic stresses alone will not produce creep effects (Fjær et al., 2008; Sone, 2012), laboratory results from shale tests (Ghassemi and Suarez-Rivera, 2012) have shown that this is not always true. It is known that local shear stresses can be developed in a sample subject to external hydrostatic loading due to inhomogeneities in the material (Fjær et al., 2008).

Figure 6a illustrates the visco-elastic behavior of the creep, which is the instantaneous plus the delayed response (total strain). Figure 6b shows creep strain as a result of the time-dependent component of deformation only. As observed in Figure 6b, creep strain at a given time can be described using a power-law strain-time model as reported by Ghassemi and Suarez-Rivera (2012). Moreover, creep strain in the radial direction seems to be much lower than the creep in the axial direction. This is attributed to the fact that our samples axis were oriented perpendicularly to the bedding, so this difference in creep means that the layered nature of the samples enhances the creep in the direction perpendicular to bedding.

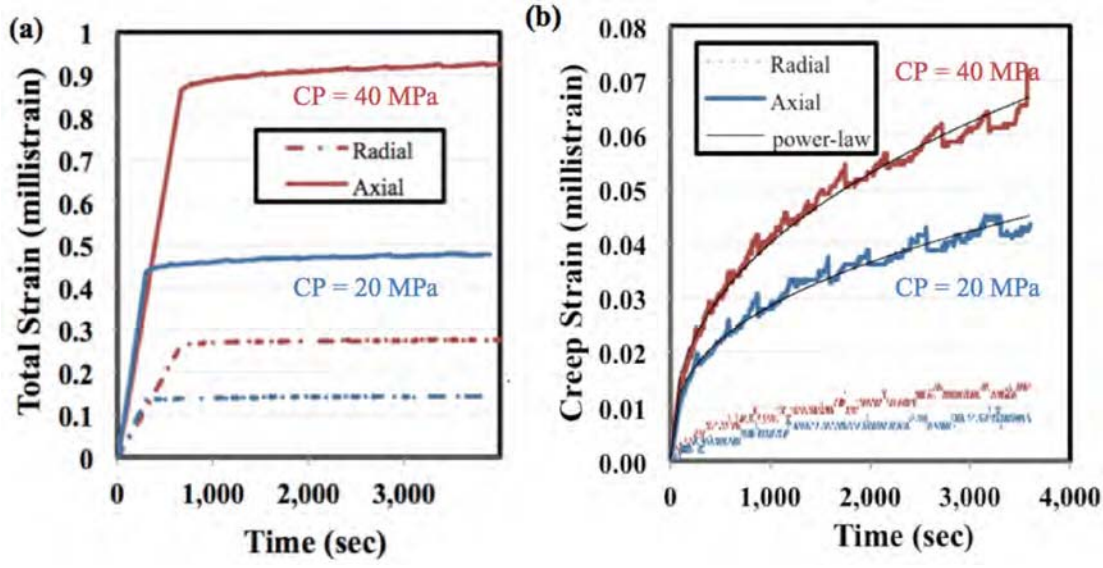

FIG. 6. (a) Hydrostatic stage immediate strain + 1-hour creep at different confining pressures. Both radial and axial strains are consistent with what would happen during a regular hydrostatic experiment, i.e. they shrink. (b) Hydrostatic stage 1-hour creep. Creep strain was fitted to a power-law strain-time model ($k=3.8938\cdot10^{-8}$, n=0.3802).

Figure 7 presents the data from the triaxial stage. Creep deformation is shown for two pressure steps at different deviatoric stress levels. Many features observed during the triaxial stage are similar to what was observed for the hydrostatic stage. However, now the sample dilates in the radial direction as is expected from a regular triaxial experiment. The fact that lateral deformation is still much lower than axial deformation implies a volume loss, which is thought to be accommodated by microcrack closure and compaction of the organic matter (Ghassemi and Suarez-

Rivera, 2012; Sone, 2012). For the triaxial stage, creep behavior can also be modeled by a power law as well (Ghassemi and Suarez-Rivera, 2012; Sone, 2012), but is better expressed by the Burger's model (Ghassemi and Suarez-Rivera, 2012). Fitting parameters for the power-law model (k, n) are in the range as those reported by Ghassemi and Suares-Rivera.

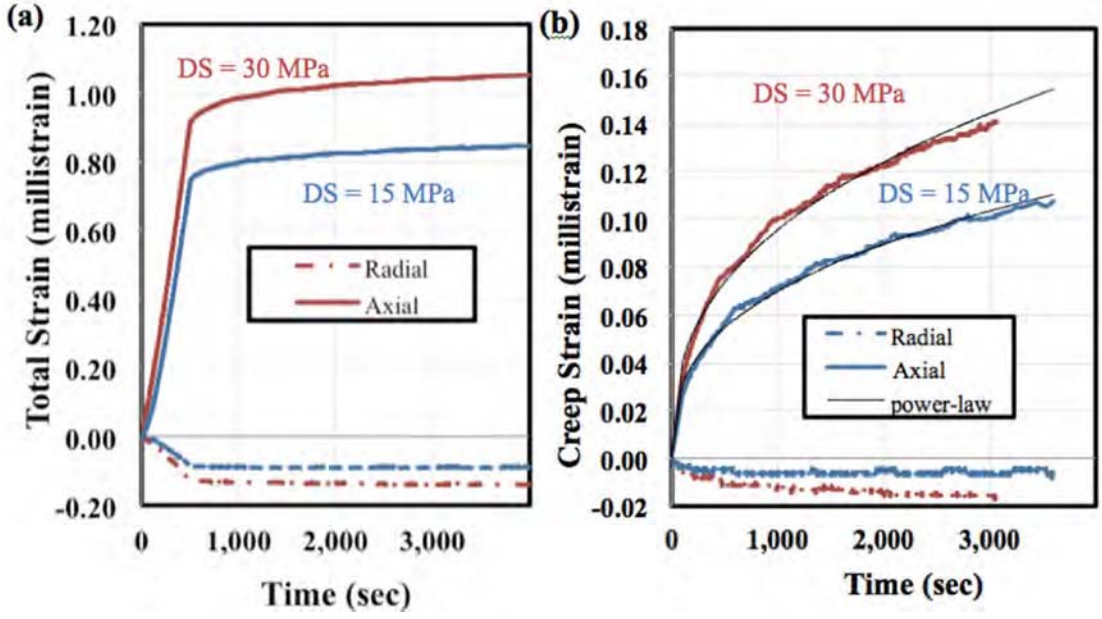

FIG. 7. (a) Triaxial stage immediate strain + 1 hour-creep at deviatoric stresses. The sample dilates in the radial deformation as is expected from a regular triaxial experiment. (b) Triaxial stage 1-hour creep. Creep strain was fitted to a power-law strain-time model ($k=1.0478\cdot10^{-7}$, $n=0.3645$)

CONCLUSIONS

Geomechanical characteristics of shale specimens taken from Marcellus shale were investigated and presented in this paper. Bulk modulus was measured during hydrostatic stage and found to be directly correlated with increasing confining pressure. Young's modulus and Poisson's ratio were investigated using both static and dynamic methods, ranging between 14-20 MPa, and between 25-31 MPa for the static and dynamic measurements respectively. Ductile deformation was characterized by 1-hour creep measurements under different stress conditions and creep strain was found to be proportional to the deviatoric stress. Experimental results indicated that due to the nonlinear nature of these formations, multiple unloading-reloading cycles at different stress levels are required to characterize the sample within the full elastic range. We are running additional experiments to gain more insight into relationships between dynamic and static properties of these formations.

REFERENCES

Beer, F.P., Johnston, R., DeWolf, J.T., and Mazurek, D.F. (2009). *Mechanics of*

Materials. McGraw-Hill, New York, NY

Britt, L.K., and Schoeffler, J. (2009). "The Geomechanics of a Shale Play: What Makes a Shale Prospective." *SPE Eastern Regional Meeting,* SPE, Charleston, WV

Davies, R.J., Mathias, S.A., Moss J., Hustoft, S., and Newport, L. (2012). "Hydraulic fractures: How far can they go?" *Journal of Marine and Petroleum Geology*, (37), pp. 1-6

Energy Information Administration, EIA (2013). *U.S. Crude Oil and Natural Gas Proved Reserves*. U.S. Department of Energy, Washington, DC

Findley, W. N., Lai, J. S., and Onaran, K. (1976). *Creep and Relaxation of Nonlinear Viscoelastic Materials: With an Introduction to Linear Viscoelasticity*. Dover Publications, Mineola, NY

Fjær, E., Holt, R.M., Horsrud, P., Raaen, A.M., and Risnes, R. (2008). *Petroleum Related Rock Mecanics*. 2nd Edition, Elsevier, Amsterdam

Ghassemi, A., and Suarez-Rivera, R. (2012). "*Sustaining fracture area and conductivity of shale gas reservoirs for enhancing long-term production and recovery"*. Research Partnership to Secure Energy for America, 08122-48, College Station, TX

Jacobi, D., Gladkikh, M., LeCompte, B., Hursan, G., Mendez, F., Longo J., Ong, S., Bratovich, M., Patton, G., Hughes, B., Shoemaker, P. (2008). "Integrated Petrophysical Evaluation of Shale Gas Reservoirs." *CIPC/SPE Gas Technology Symposium 2008 Joint Conference*, SPE, Calgary, Alberta (Canada)

King, G.E., Haile, L., Shuss, J., and Dobkins, T.A. (2008). "Increasing Fracture Path Complexity and Controlling Downward Fracture Growth in the Barnett Shale." *Shale Gas Production Conference*, SPE, Fort Worth, TX

Lucier, A. M., Hofmann, R., and Bryndzia, T. (2011). "Evaluation of variable gas saturation on acoustic log data from the Haynesville shale gas play." *The Leading Edge*, 30, 300-311.

Maxwell, S. (2011). "Microseismic hydraulic fracture imaging: The path toward optimizing shale gas production." *The Leading Edge*, 30, 340-346.

Rickman, R., Mullen, M., Petre, E., Grieser, B., and Kundert, D. (2008). "A practical use of shale petrophysics for stimulation design optimization: All shale plays are not clones of the Barnett Shale." *Annual Technical Conference and Exhibition*, SPE, Denver, CO

Sone, H. (2012). "Mechanical properties of shale gas reservoir rocks and its relation to the in-situ stress variation observed in shale gas reservoirs." PhD dissertation, Stanford University, Stanford, CA

Vermylen, J. (2011). "Geomechanical Studies of the Barnett Shale, Texas, USA." PhD dissertation, Stanford University, Stanford, CA

Yale, D.P. and Jamieson, W.H. (1994). "Static and Dynamic Rock Mechanical Properties in the Hugoton and Panoma Fields, Kansas." *SPE Mid-Continent Gas Symposium,* SPE, Amarillo, Texas

Zoback, M. D., and Byerlee, J. D. (1975). "The effect of cyclic differential stress on dilatancy in Westerly Granite under uniaxial and triaxial conditions." *Journal of Geophysical Research*, 80, 1526-1530.

Comminution of Solids Due to Kinetic Energy of High Shear Strain Rate: Implications for Shock and Shale Fracturing

Zdeněk P. Bažant[1], Hon.M.ASCE and Ferhun C. Caner[2]

[1]Distinguished McCormick Institute Professor and W. P. Murphy Professor of Civil Engineering, Mechanical Engineering, and Materials Science, Northwestern Univ., Evanston, IL 60208, USA E-mail: z-bazant@northwestern.edu.
[2]Associate Professor, Institute of Energy Technologies, School of Industrial Engineering, Univ. Politecnica de Catalunya, Campus Sud, 08028 Barcelona, Spain, E-mail: ferhun.caner@upc.edu.

ABSTRACT: This paper outlines the basic idea of a macroscopic model on the dynamic comminution or fragmentation of rocks, concrete, metals, and ceramics. The essential idea is that the driving force of comminution under high-rate shear and compression with shear is the release of the local kinetic energy of shear strain rate. The density of this energy at strain rates >1,000/s is found to exceed the maximum possible strain energy density by orders of magnitude, making the strain energy irrelevant. It is shown that particle size is proportional to the −2/3 power of the shear strain rate and the 2/3 power of the interface fracture energy or interface shear stress, and that the comminution process is macroscopically equivalent to an apparent shear viscosity that is proportional (at constant interface friction) to the −1/3 power of this rate. A dimensionless indicator of the comminution intensity is formulated. The theory was inspired by noting that the local kinetic energy of shear strain rate plays a role analogous to the local kinetic energy of eddies in turbulent flow.

INTRODUCTION

The previous studies of high-rate dynamic fracture of rocks, concretes, ceramics, composites and metals have dealt mainly with the nucleation, propagation and branching of a dynamically propagating crack, their interference with elastic or shock waves, and the mechanism of development of the zones of densely distributed fractures, called the Mescall zones (Mescall and Weiss 1984, Freund 1990, Doyoyo 2002, Deshpande and Evans 2008, Wei et al. 2009). However, a comminution model in the form of a macroscopic constitutive equation that could be used in large dynamic finite element programs for global response of structures had been lacking until a fundamentally new kind of approach, based on the release of kinetic energy of shearing, was proposed in 2013 (Bažant and Caner 2013a). This paper reviews the new approach and discusses its application to shale fracturing. Application to missile impact will appear in detain in Bažant and Caner (2013b).

THEORETICAL FORMULATION

Main assumptions and analogy with turbulence

We begin with the analysis of a simple idealized process in which the solid is comminuted to identical particles (Fig. 1). In the plane of maximum shear, we assume a regular hexagonal subdivision because it gives the smallest surface-to-volume ratio (Fig. 1a) and thus requires the minimum energy to form. In the direction normal to the hexagons, we assume the particles to be prismatic.

Consider that, at a certain moment, the strain rate (shown in Fig. 1b as a displacement regarded as infinitesimal) becomes high enough for the kinetic energy of shear strain rate to suffice for creating the fractures and interface slips that separate the particles of as yet unknown size. As that happens, the particles release their local kinetic energy, slip against each other, and regain their original undeformed shape, while the particle centers conform to the same macroscopic velocity field (Fig. 1c).

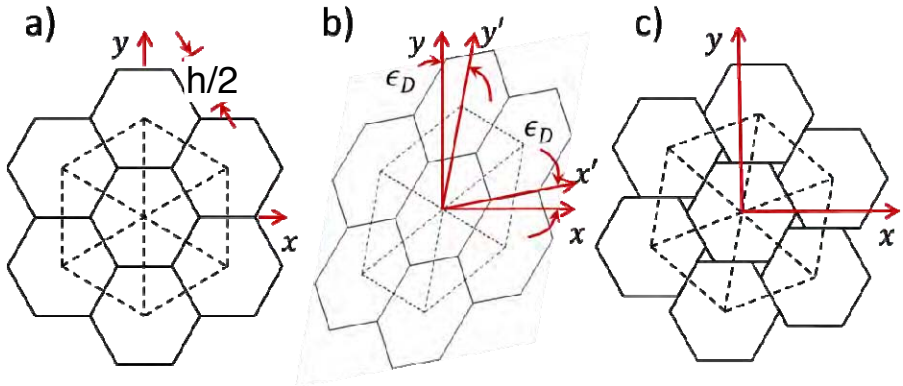

FIG. 1. Example of comminution of material into prismatic hexagonal particles; the velocities are shown as infinitesimal displacements (in which case the gaps at the hexagon corners are second-order small and thus negligible). (a) Undeformed material, (b) sheared material, and (c) comminuted material.

Assuming particle symmetry with respect to axes x and y, the drop of kinetic energy of the hexagonal prisms per unit volume due to comminution is:

$$\Delta\mathcal{K} = -\frac{h}{V_p}\int_A \frac{\rho}{2}\left(\dot{u}^2+\dot{v}^2-(\dot{u}^+)^2-(\dot{v}^+)^2\right)\mathrm{d}x\mathrm{d}y = -c_k\rho h^2\dot{\epsilon}_D^2 \qquad (1)$$

where A = particle area, ρ = mass density, $c_k = I_p/(2hV_p)$, $V_p = (3\sqrt{3}/8)h^3$ = particle volume, and $I_p = (5\sqrt{3}/128)h^4$ = polar moment of inertia of each hexagonal prism of side h. It is interesting that the kinetic energy $\mathcal{K}_{shear}$ of a particle deforming by pure shear at rate $\dot{\epsilon}_D$ happens to be the same as the kinetic energy $\mathcal{K}_{eddy}$ of an eddy rotating as a rigid body of the same size at angular rate $\dot{\omega} = \dot{\epsilon}_D$. In both comminution and turbulence, the micro-level kinetic energy augments the kinetic energy of the macro-level motion.

Comminuted particle size distribution

In this work, particle sizes h are considered to vary randomly, according to the following cumulative distribution (Schuhmann 1940, Charles 1957, Cunningham 1987, Ouchterlony 2005):

$$F(s) = \frac{s^k - h^k}{H^k - h^k} \quad [s \in (h, H), \quad F(s) \in (0, 1)] \tag{2}$$

where k = empirical constant ($k \approx 0.5$), s = variable particle size; and h, H = minimum and maximum particle sizes (usually H/h = 10 to 100). It should be noted that the strain softening damage, which precedes the fracture of concrete and absorbs part of the kinetic energy, is automatically simulated by the microplane constitutive model M7. This model capture comminution into particles of the same size as in static testing, i.e., into fragments not smaller than about 1 cm in size. Since the macroscopic quasi-static constitutive law with non-localized strain softening includes the energy dissipation corresponding to material crushing into particles of the size d_a of the largest material inhomogeneities, H should considered to be one order of magnitude smaller, i.e., about $0.1d_a$ (Caner and Bažant 2013). Now, the combined interface area per unit volume can be expressed as $S = C_s/h$ while the loss of kinetic energy of the shear strain rate of the particles of all sizes per unit volume is $\Delta\mathcal{K} = -\int_{s=h}^{H} c_k \rho s^2 \dot{\epsilon}_D^2 \mathrm{d}F(s) = -C_k \rho h^2 \dot{\epsilon}_D^2$ where $\bar{c}, C_s$ and C_k are dimensionless constants.

Assuming that all of a kinetic energy decrement $\mathcal{K}$ is dissipated by an interface fracture energy increment $\Gamma \Delta S$, the interface fracture (or frictional slip) can occur when:

$$-\frac{|\Delta\mathcal{K}|}{S} = -\frac{|\Delta\mathcal{K}|/h}{\mathrm{d}S/\mathrm{d}h} = \Gamma \tag{3}$$

After substitutions into Eq. (3) one gets:

$$h = \left(\frac{C_a \Gamma}{\rho \dot{\epsilon}_D^2}\right)^{1/3} \tag{4}$$

where C_a is a dimensionless constant.

It is worth noting here that $h \propto \dot{\epsilon}_D^{-2/3}$. This result is in agreement with what Grady (1998) verified empirically (though not theoretically) for the impact of missiles and it serves as one experimental verification of the present theory (Eq. 4).

Energy dissipation owing to comminution and implementation in macroscopic structural analysis

Substitution of Eq. (4) into (1) further yields:

$$\Delta\mathcal{K} = -(C_0 \Gamma^2 \rho)^{1/3} \dot{\epsilon}_D^{2/3} \tag{5}$$

where C_0 is a certain dimensionless constant. This expression suggests how to implement the energy sink due to comminution in macroscopic structural analysis. Note that $\Delta\mathcal{K}$ has the dimension of a stress and can be interpreted as such.

To obtain a three-dimensional generalization, it is convenient to introduce an equivalent viscosity η_D such that the viscous stress strain relation $s_{ij}^A = \eta_D \dot{\epsilon}_{Dij}$ would give the same energy dissipation density as Eq. (5) for any deviatoric strain rate tensor in the variational sense; here s_{ij}^A is the additional deviatoric stress caused by the comminution.

Since 1) the energy density is the same as the stress, 2) s_{12}^A must be equal to $\Delta\mathcal{K}$ when all other tensorial components vanish and 3) $\Delta\mathcal{K}$ must be a tensorial invariant, it is necessary that $-\Delta\mathcal{K} = \sqrt{s_{ij}^A s_{ij}^A/2}$. Accordingly, the energy sink due to the comminution process may be modeled by the equivalent viscosity:

$$\eta_D = (C_0 \Gamma^2 \rho)^{1/3} \dot{\epsilon}_D^{\,-1/3} \tag{6}$$

where $\dot{\epsilon_D} = \sqrt{\dot{\epsilon}_{Dij}\dot{\epsilon}_{Dij}/2}$.

Viscosity η_D can easily be implemented in the constitutive relation in a finite element program. It may be noted that the enhancement of dissipative viscous resistance to shearing is again a feature analogous to the enhancement of viscous resistance to flow due to turbulent eddies.

Finite element simulations indicate that, in practical applications such as impact, the rate of expansive volumetric strain rate, ϵ_{Ex}, plays no significant role. For explosions in a shale mass, though, the rates of shear strain and of volumetric expansion may both be important. One can show that, in that case, the foregoing theory can be easily generalized; e.g., $\dot{\epsilon}_D^{\,-1/3}$ in Eq. (6) needs to be replaced by $(\dot{\epsilon}_D^2 + \dot{\epsilon}_V^2)^{\,-1/6}$.

Introduction of a dimensionless indicator of the comminution intensity

In view of the partial analogy with turbulence we introduce a dimensionless indicator of comminution intensity. The strain energy density $\mathcal{U}$ that is stored in the material may be expressed as $\mathcal{U} = \tau^2/2G$ where G is the elastic shear modulus and τ is the shear stress. When $\Delta\mathcal{K} \gg \mathcal{U}$, then obviously the comminution cannot be caused by the release of strain energy and the release of kinetic energy is the only possible energy source for the comminution. Therefore, we may define the dimensionless number: $B_a = -\Delta\mathcal{K}/\mathcal{U}$ or:

$$B_a = \frac{G}{C_g \tau^2}\,(\Gamma^2 \rho\, \dot{\epsilon}_D^{\,2})^{1/3} \tag{7}$$

which has the property that the comminution is:

$$\begin{array}{l} \text{kinetic energy driven if} \quad B_a \gg 1 \\ \text{in transition if} \quad B_a \approx 1 \\ \text{static or absent if} \quad B_a \ll 1 \end{array} \tag{8}$$

The equivalent viscosity may also be uniquely expressed in terms of B_a.

RESULTS AND DISCUSSION

The most intriguing application of dynamic comminution modeling may be the fracturing of gas or oil shale by electro-hydraulic pulsed arc (Maurel et al. 2010) or by chemical explosion in the pipe of a horizontal borehole. However, since no data exist in the public domain, a confirmation of the present comminution model can be obtained by fitting the data on the measured exit velocity, v_e, of projectiles penetrating concrete walls of different thicknesses.

One such set of data (Adley et al. 2012) is shown in Fig. (2), which shows v_e as a function of the thickness D of the wall. The entry velocity of the missile is 310 m/s. The v_e values are computed with an explicit dynamic finite element program using the microplane model, first under the assumption that the only rate effects are the quasistatically calibrated rate effects, which consist of viscoelasticity of intact concrete between the cracks and of the rate of bond breakage at the fracture front controlled by activation energy (Bažant and Caner 2013, Caner and Bažant 2013). As seen, this simple assumption leads to a gross overestimation of the exit velocities. However, when the presently formulated equivalent viscosity due to kinetic comminution is included, the data for the two thicker walls are fitted perfectly.

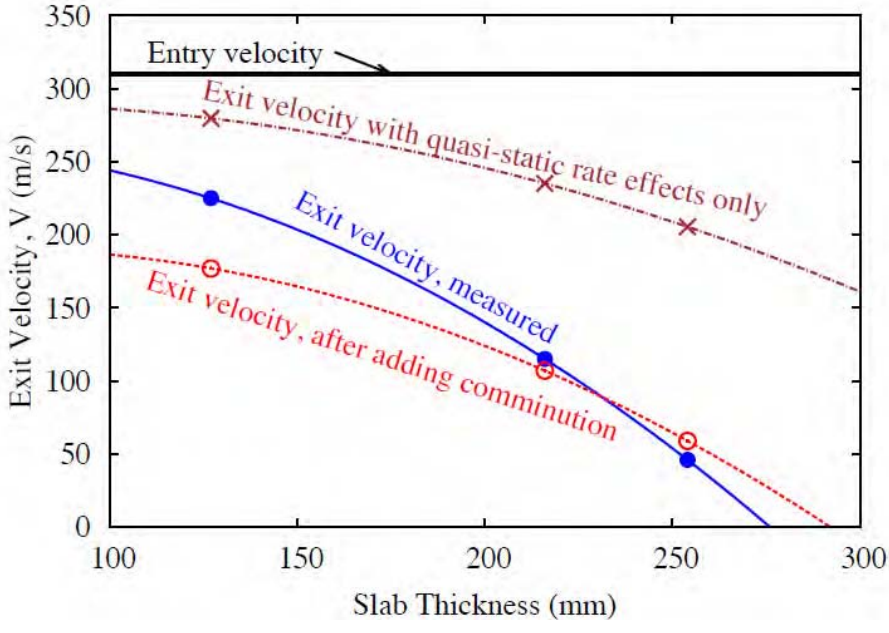

FIG. 2. Comparison of measured exit velocities and predictions by model M7 using only quasi-static strain rate effect and both quasi-static strain rate effect and effect of comminution of concrete.

For the thinnest wall, the exit velocity is still overestimated (Fig. 2). However, this is likely explained by differences in the specific moisture contents in the nanopores of

concrete. For a lower moisture content, Hopkinson bar experiments have shown a lower strength in high-rate shear, and this is the case for the thinner wall since it dries faster. A more detailed description of the reasons for underestimating the exit velocity of the thinnest slab are explained in detail in Caner and Bažant 2013.

CONCLUSIONS

In this paper, a macroscopic model on the dynamic comminution or fragmentation of rocks, concrete, metals, and ceramics is presented. The main assumption is that the driving force of comminution under high-rate compression is the release of the local kinetic energy of shear strain rate. The present theory indicates that the density of kinetic energy available for comminution is proportional to the (2/3) power of the shear strain rate, the particle size or crack spacing is proportional and the (−2/3) power of that rate, and the energy dissipation by comminution is equivalent to a shear viscosity decreasing as the (−1/3) power of that rate. Confirmation of the theory is provided by fitting the data on the measured exit velocity, v_e, of projectiles penetrating concrete walls of different thicknesses. The formulation can be applied to the fracturing of gas or oil shale by electro-hydraulic pulsed arc or by chemical explosion in the pipe of a horizontal borehole.

ACKNOWLEDGMENTS

This work was supported by Agency for Defense Development, Korea Grant 32788 from Daejeon University and initially by US Army Research Office, Durham Grant W911NF-09-1-0043, both to Northwestern University.

REFERENCES

Adley MD, Frank AO, Danielson KT (2012) “The high-rate brittle microplane concrete model: Part I: Bounding curves and quasi-static fit to material property data”. Comput Concr 9(4):293–310.

Bažant Z.P., Caner, F.C.. (2013a) “Comminution of solids caused by kinetic energy of high shear strain rate, with implications for impact, shock and shale fracturing." Proc., National Academy of Sciences 110 (48), 19291--19294.

Bažant Z.P., Caner, F.C.. (2013b) “Impact comminution of solids due to local kinetic energy of high shear strain rate: I. Continuum theory and turbulence analogy” J Mech Phys Solids, doi: http://dx.doi.org/10.1016/j.jmps.2013.11.008. In press.

Charles RJ (1957) “Energy-size reduction relationships in comminution”. Min Eng 9:80–88.

Cunningham CVB (1987) “Fragmentation estimation and the Kuz-Ram model—four years” on. Proceedings of the 2nd International Symposium on Rock Fragmentation by Blasting, eds Fourney WL, Dick RD (Society for Experimental Mechanics, Bethel, CT), pp 475–487.

Mescall J, Weiss V (1984). “Materials behavior under high stress and ultrahigh loading rates—Part II”. Proceedings of the 29th Sagamore Army Conference (Army Materials and Mechanics Research Center, Watertown, MA).

Deshpande VS, Evans AG (2008) “Inelastic deformation and energy dissipation in

ceramics: A mechanism-based constitutive model". J Mech Phys Solids 56:3077–3100.

Doyoyo, M. (2002). "A theory of the densification-induced fragmentation in glasses and ceramics under dynamic compression" Int J Solids Structures, 39, 1833-1843.

Caner F.C. Bažant Z.P. (2013) "Impact comminution of solids due to local kinetic energy of high shear strain rate: II. Microplane model and verification" J Mech Phys Solids, doi : http://dx.doi.org/10.1016/j.jmps.2013.11.009. In press.

Freund LB (1990) "Dynamic Fracture Mechanics" (Cambridge Univ Press, Cambridge, UK).

Grady DE (1998) "Shock-wave compression of brittle solids". Mech Mater 29:181–203.

Maurel O, et al. (2010) "Electrohydraulic shock wave generation as a means to increase intrinsic permeability of mortar". Cement Concr Res 40:1631–1638.

Ouchterlony F (2005) "The Swebrec function: Linking fragmentation by blasting and crushing". Mining Technology 114(March):A29–A44.

Schuhmann R, Jr. (1940) "Principles of comminution, I. Size distribution and surface calculation". The American Institute of Mining, Metallurgical, and Petroleum Engineers (AIME) Technical Publication 1189 (AIME, Englewood, CO).

Wei Z, Evans AG, Deshpande VS (2009) "The influence of material properties and confinement on the dynamic penetration of alumina by hard spheres". J Appl Mech 76: 051305-1–051305-8.

Guided Ultrasonic Waves For The Nondestructive Evaluation Imaging Of Pipes

Piervincenzo Rizzo, Abdollah Bagheri S.M.ASCE, and Kaiyuan Li

Laboratory for Nondestructive Evaluation and Structural Health Monitoring Studies,
Department of Civil and Environmental Engineering, University of Pittsburgh, Pittsburgh, PA 15261, U.S.A., E-mail: pir3@pitt.edu.

ABSTRACT: This paper presents the results of a numerical study where guided ultrasonic waves (GUWs) are used for the structural health monitoring of pipes. The method hypothesizes the generation and detection of longitudinal, torsional, and flexural waves from each transducer of two annular arrays located inside the pipe. The signals are processed using continuous wavelet transform and Hilbert transform to extract two damage-sensitive features. The estimation of the features for healthy condition is formulated in terms of an optimization problem based on the imperialist competitive algorithm. Finally, a probabilistic approach is used to create an image of the pipe in search for possible structural anomalies. A commercial finite element code is utilized to model the presence of eight ultrasonic transducers in contact with the interior wall of a pipe. Each transducer acts either as actuator or as a sensor. The time waveforms associated with all possible actuator-sensor pairs are processed using the algorithms proposed here. The results indicate promise and future studies should focus on the experimental validation of the methodology.

INTRODUCTION

It is known that guided ultrasonic waves (GUWs) are feasible for the structural health monitoring (SHM) of piping systems (Hayashi and Murase, 2005; Rizzo et al., 2005; Kim et al., 2012) or structures that contain pipe-like elements (Zhu et al. 2010). In nondestructive evaluation and SHM applications, the use of guided waves is often combined with signal processing to extract damage-sensitive features able to estimate the location, severity, and typology of damage. Signal processing may include short-time Fourier transform (Kannan et al., 2007) and wavelet transform (Rizzo et al., 2005; Ahmad et al., 2009; Sale et al. 2011). Most of the damage detection methods compare newly measured data to reference data that, ideally, include scenarios under all possible environmental conditions, so they require the knowledge of a baseline.

In this study, a baseline-free method is proposed for the detection and localization of damages in pipes. The method consists of three steps: feature extraction, baseline computation, and mapping. Ultrasonic signals are processed by means of the continuous wavelet transform (CWT) to extract a damage-sensitive feature that is fed

to a colonial competitive algorithm (CCA), which mimics socio-political dynamics. The ICA serves to establish the baseline dataset. The baseline is then used into a probabilistic approach utilized to create an image of the pipe in search of damage. The proof-of-concept is proven simulating the propagation of guided waves with a commercial finite element code. Two rings of transducers 200 mm apart are modeled by considering four nodes, equally spaced in the circumferential direction, of the mesh. Each node is subjected to a time-dependent force orthogonal to the pipe surface. The ultrasonic signals generated and detected by all the possible transducer (nodes) pairs are processed according to the scheme summarized above.

NUMERICAL SIMULATIONS

The propagation of guided waves in a 40 mild steel pipe was numerically simulated by using a time-transient analysis run under ANSYS v.13.0. The pipe was 600 mm long, 50 mm in external diameter, and 5 mm thick. For the mild steel we considered: density ρ=7932 kg/m^3, Young's modulus E=216.9 GPa, shear modulus G=84.3 GPa, and Poisson's ratio ν=0.2865. Two damage scenarios were considered: 1) through-thickness hole with diameter 20.93 mm; 2) 2 mm thick circular internal corrosion with diameter 10 mm. The geometry of the pipe and the first damage scenario are shown in Fig. 1(a). The pipe was discretized using the three-dimensional 8-node "SOLID185" element having three degrees of freedom per node.

The presence of two rings of transducers was simulated (Fig. 1(b)). The rings were 200 mm apart and each ring consisted of four points equally spaced in the circumferential direction. In the model, the position of these eight transducers coincided with the nodes of the elements. The nodes were located on the inner wall of the pipe in order to simulate the excitation of the wave from the inside.

In the analysis, an unconditionally stable implicit Newmark procedure with a decay factor of 0.005 and integration parameters α≈0.252 and δ=0.505 was used to perform the time integration. A small numerical damping was added to avoid undesirable levels of noise that the higher frequencies generated in the structure can produce.

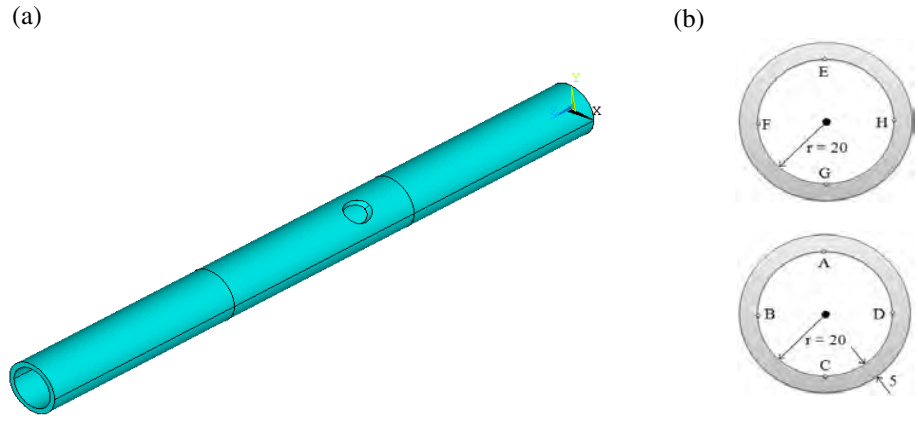

FIG. 1. (a) The geometry of the pipe and the location of damage in the first damage scenario. (b) Two rings of transducers. (Dimensions in mm)

In order to achieve good special and temporal resolution (Bartoli et al., 2005), the integration time step Δt was set equal to 0.5 μsec which corresponds to a 2 MHz sampling frequency, and the maximum mesh size was equal to 1 mm.

Guided waves were excited by imposing a modulated 3-cycle tone burst forcing function perpendicular to the pipe surface. The tone burst was centered at 100 kHz and applied at each of the eight nodes discussed before.

The simulation was such that while node A acted as actuator, the remaining nodes acted as receivers and the radial displacement was measured. This was repeated for all eight transducers. Thus, 56 measurements were taken according to the sensing paths listed in Table 1.

The time-history of the radial displacement at node F for the first damage scenario is presented in Fig. 2(a). Figure 2(b) shows the corresponding CWT scalogram of the time-history showed in Fig. 2(a). The out-of-plane axis of the scalogram indicates the energy of the nodal displacement. As expected, the main energy is located around 100 kHz.

Table 1. Sensing paths and the geometric distances for each path.

Actuator – sensor distance *d*(mm)	Sensing paths
31.40	AB, AD, BC, CD, EF, EH, FG, GH (and viceversa)
62.80	AC, BD, EG, FH (and viceversa)
200.0	AE, BF, CG, DH (and viceversa)
202.5	AF, AH, BE, BG, CF, CH, DE, DG (and viceversa)
209.6	AG, BH, CE, DF (and viceversa)

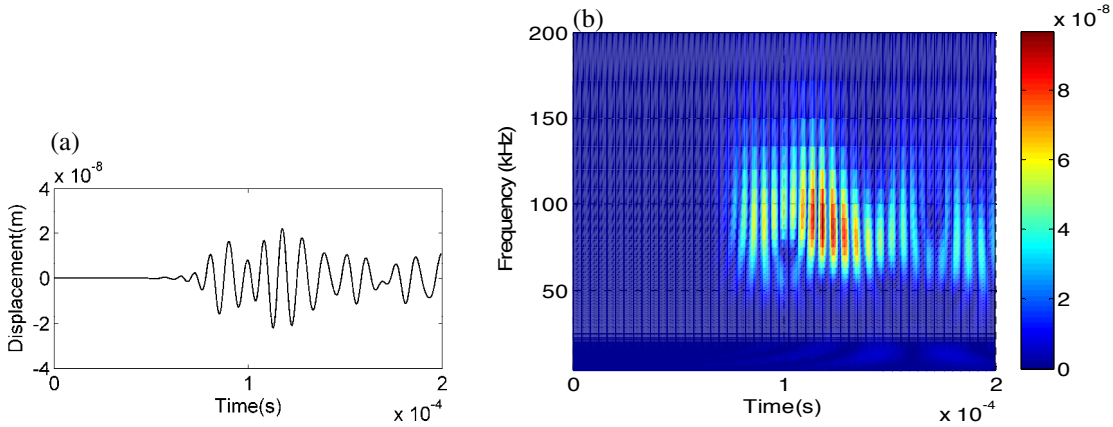

FIG. 2. (a) The time-history of radial displacements for the first damage case at node F when the 3-cycle tone burst was applied at node A, and (b) CWT associated with the time-history shown in Fig. 2(a).

DAMAGE DETECTION METHOD

From the scalogram **W** of each waveform, the wavelet energy spectrum **E**:

$$\mathbf{E}_j^i = \left|\mathbf{W}_j^i(t, f)\right|^2; i = 1,2,...,5;\ j = 1,2,..., m(i) \tag{1}$$

was calculated. In Eq. (1), the index i referees to the i-th sensing path length according to the groups de-fined in Table 1. The counter variable m is equal to 8 when i is equal to 2, 3, and 5, whereas it is equal to 16 when i is equal to 1 and 4 and it represents the number of wave paths having the same distance, i.e. the number shown in the third column of Table 1.

By using the wavelet energy spectrum the following feature was computed:

$$F_j^i = \sum_t \sum_f \mathbf{E}_j^i(t, f) \tag{2}.$$

Wave propagation properties in pipes are extremely complicated. This is due to the presence of at least three modes at any given frequency and to mode conversion that occur in presence of certain types of defects. In this study, the CCA was applied to find features for healthy status using the values of the defined feature in the previous section. The CCA is an optimization method inspired by the socio-political process of imperialist competition (Atashpaz-Gargari and Lucas, 2007). As any optimization algorithm, the objective of the CCA is to find an optimal solution, usually the minimum, of the argument x of a cost function $f(x)$.

The following relationship associated with the j-th guided wave signal associated with the i-th sensing path can be defined as:

$$e_j^i F_j^i - F_h^i = 0 \tag{3}$$

in which e is a coefficient and the subscript h indicates the value of the feature associated with a wave path that is not affected by the presence of the defect. The aim is to find those parameters e and F_h that minimize an objective function. Expanding Eq. (3) to all of the guided waves related to the same i-th path distance, we lead to this equation:

$$\mathbf{e}^i\mathbf{F}^i - F_h{}^i\mathbf{I} = 0 \tag{4}$$

where e^i is a diagonal matrix, and $\boldsymbol{I}$ is an identity vector. We can define a cost function in terms of the Euclidean length as follows:

$$f(e_1^i, e_2^i, ..., e_m^i, F_h^i) = \left\|\mathbf{e}^i\mathbf{F}^i - F_h{}^i\mathbf{I}\right\|^2 \tag{5}$$

subjected to the following constraints:

$$\min \mathbf{F}^i \le F_h^i \le \max \mathbf{F}^i, \quad \frac{\min \mathbf{F}^i}{\max \mathbf{F}^i} \le e_j^i \le \frac{\max \mathbf{F}^i}{\min \mathbf{F}^i} \tag{6}$$

To minimize the cost function, the CCA is applied to find the feature' value associated with a healthy status.

In the imaging method, the pipe is divided into a uniform 1 mm×1 mm pixel and the probability $P(x, y)$ that damage occurred at a grid node position (x, y) is defined as:

$$P(x,y) = \sum_{i=1}^{5} \sum_{j=1}^{m} \left| \frac{F_j^i - F_h^{\,i}}{F_h^{\,i}} \right| W_{i,j}\left[r_{i,j}(x,y) \right] \tag{7}$$

where $W_{i,j}[r_{i,j}(x, y)]$ is the probabilistic weight for the j-th guided wave signal at the i-th sensing path at (x, y), and $r_{i,j}(x, y)$ is the relative distance of the node (x, y) to the actuator and to the sensor associated with the j-th guided wave signal at the i-th sensing path. The Gaussian function was selected as the probabilistic weight as:

$$W_{i,j}\left[r_{i,j}(x,y) \right] = \exp\left[-\left(\frac{r_{i,j}(x,y)}{\beta} \right)^2 \right] \tag{8}$$

where β is a constant coefficient which determines the size of monitoring area. In this study, it is equal 0.02, which allowed for covering the entire monitoring area of the tube. This coefficient proved to be a good trade-off between sensitivity to damage and broad coverage area.

Then, the damage index DI at a given node (x, y) of the grid is defined as:

$$DI(x,y) = \frac{P(x,y) - \mu_D}{\sigma_D} \tag{9}$$

in which μ_D and σ_D are, respectively, the mean and standard deviation value of $P(x, y)$. In the last step, the damage index is normalized to the maximum value, and a threshold is applied such that all the values below the threshold are set to zero.

RESULTS

Figure 3 shows the values of the CWT-based features relative to the damaged pipe in the first damage pattern. In this scenario, the histograms are not constant which suggests that some wave paths were affected by the hole. In order to determine the constants the CWT-based feature associated with the undamaged path, the CCA was used. Figure 4 shows the values of the CWT-based feature associated with the undamaged path as a function of the travel distance. These values identify pristine conditions encountered by the guided waves as they travel the damaged pipe.

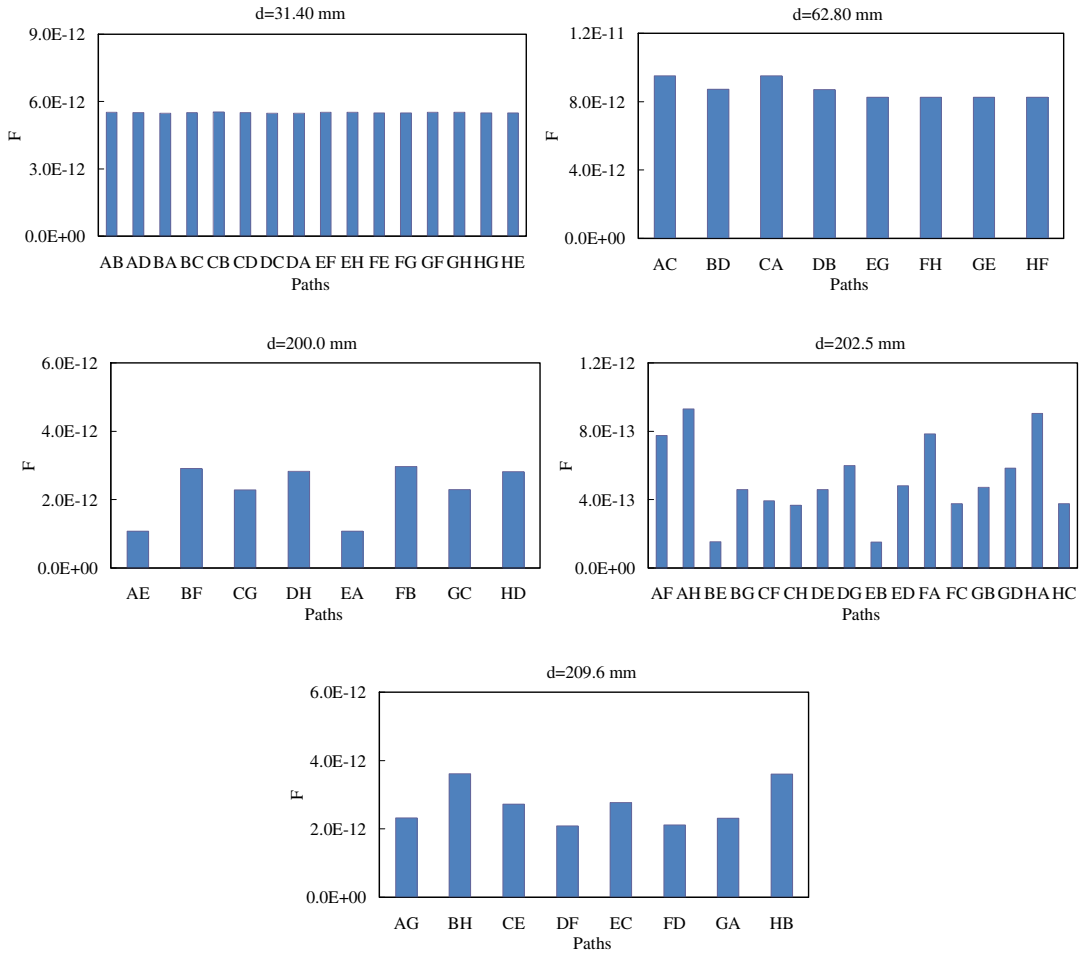

FIG. 3. Values of the CWT-based feature as a function of the travel distance for damage scenario 1.

The extracted features can found the presence of some damage, but they are not able to determine the size and the location of defect in the pipe. We employed the imaging algorithm described in the previous section to detect the location of defects. Figure 5(a) shows the image of the pipe for the first damage scenario when the CWT-based feature was considered. The contour plot describes the amplitude of the damage index DI and the white circle superimposed to the image represents the position of the hole. Owing to the threshold set in this study, the contour plot goes from 0.7 to 1 and all the DI below 0.7 were set to zero. The aim for considering a threshold 0.7 for the damage index is related to detect sever defects in the monitoring area of the pipe. As we did not use any data generated from the pristine pipe, the results presented in Fig. 5(a) demonstrate that the algorithm does not need to reference data. The damage index computed under the internal corrosion as the second damage pattern is shown in Fig. 5(b). The true position of the corroded areas is superimposed and it is within the area having the large damage index values.

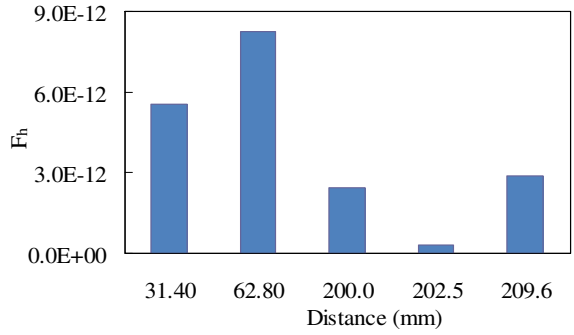

FIG. 4. Values of features associated with healthy paths.

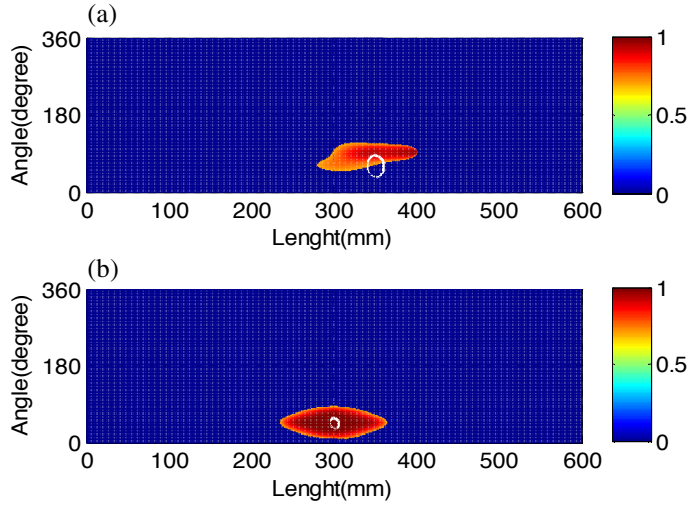

FIG. 5. Mapping of damage index for: (a) the first damage scenario and (b) the second damage scenario.

CONCLUSIONS

A reference-free imaging algorithm for the structural health monitoring of pipes by means of guided ultrasonic waves and signal processing was presented in this article. The method includes the extraction of a damage-sensitive feature from the signals processed using wavelet transform. Then, an optimization formulation was presented based on the colonial competitive algorithm to estimate those feature's values that are associated to wave paths that are not affected by damage. These values represent the baseline of the pipe. With respect to existing non reference-free algorithms, the proposed method does not need data from a pristine structure. In the last step, a probabilistic approach was employed to compute a damage index that maps the structure under monitoring.

The efficiency of the presented imaging algorithm was demonstrated using the simulation of a mild steel pipe a commercial finite element code. Two kinds of defects were simulated in terms of isolated through-the-thickness hole and internal corrosion. The features extracted from CWT were able to identify the presence of the damages. This was possible because some of the actuator-sensor paths were not

affected by damage and the amplitude associated with the sensing path having same distance was identified. This implies that the proposed health monitoring scheme is reference free provided the material is isotropic, i.e. the attenuation is not dependent on the direction of propagation, and the sensitivity of the probing devices is very similar.

ACKNOWLEDGMENTS

This study was funded by the Center for Energy at the University of Pittsburgh's Swanson School of Engineering and by the U.S. National Science Foundation, grant CMMI-1029457.

REFERENCES

Ahmad, R., Banerjee, S., and Kundu, T. (2009) "Pipe wall damage detection in buried pipes using guided waves," *J. Press. Vess. T. ASME*, 131, 011501.

Atashpaz-Gargari, E., and Lucas, C. (2007) "Imperialist competitive algorithm: an algorithm for optimization inspired by imperialistic competition," *IEEE Congress on Evolutionary Computation*, Singapore.

Bartoli, I., Lanza di Scalea, F., Fateh, M., and Viola, E. (2005) "Modeling guided wave propagation with application to the long-range defect detection in railroad tracks," *NDT&E Int.*, 38, 325-334.

Hayashi, T., and Murase, M. (2005) "Defect imaging with guided waves in a pipe," *J. Acoust. Soc. Am.*, 117(4), 2134-2140.

Kannan, E., Maxfield, B.W., and Balasubramaniam, K. (2007) "SHM of pipes using torsional waves generated by in situ magnetostrictive tapes," *Smart Mater.* Struct., 16, 2505-2515.

Kim, H.W., Lee, H.J., and Kim, Y.Y. (2012) "Health monitoring of axially-cracked pipes by using helically propagating shear-horizontal waves," *NDT&E Int.* 46, 115-121.

Rizzo, P., Bartoli, I., Marzani, A., and Lanza di Scalea, F. (2005) "Defect classification in pipes by neural networks using multiple guided ultrasonic wave features extracted after wavelet processing," *J. Press. Vess. T. ASME*, 127, 294-303.

Sale, M., Rizzo, P., and Marzani, A. (2011). "Semi-Analytical Formulation for the Guided Waves-Based Reconstruction of Elastic Moduli," *Mech. Syst. Sig. Proc.*, 25(6), pp. 2241-2256

Zhu, X., Rizzo, P., Marzani, A., and Bruck, J. (2010). "Ultrasonic guided waves for nondestructive evaluation/structural health monitoring of trusses," *Meas. Sci. Techn.*, 21, 045701.

Mechanical Behaviors of An Anisotropic Shale Rock

Q. Gao[1], J.L Tao[2], J.Y. Hu[3] and X. Yu[4*]

[1] Graduate Assistant, Department of Civil Engineering, Department of Electrical Engineering and Computer Science (Courtesy Appointment), Case Western Reserve University, 10900 Euclid Ave, Bingham 203, Cleveland, OH 44106.
[2]Assistant Professor, Department of Civil Engineering, the University of Akron, Akron, OH
[3]Graduate Assistant, Department of Civil Engineering, Department of Electrical Engineering and Computer Science (Courtesy Appointment), Case Western Reserve University, 10900 Euclid Ave, Bingham 203, Cleveland, OH 44106
[4*]Associate Professor, Department of Civil Engineering, Department of Electrical Engineering and Computer Science (Courtesy Appointment), Case Western Reserve University, 10900 Euclid Ave, Bingham 206, Cleveland, OH 44106. Ph. 216-368-6247; email: xxy21@case.edu

ABSTRACT: Shale gas is becoming an increasingly important energy source worldwide. The geomechanical properties of shale rocks can have a major impact on the efficiency of shale gas exploration. This paper studies the mineralogical and mechanical characteristics of a typical gas shale in Ohio, USA. Scanning electron microscope (SEM) with Energy Dispersive X-ray (EDX) analyses were employed to measure the microstructure and material composition of the shale rock. The anisotropic behaviors of shale rock, including compressive and tensile strength, were experimentally measured. The effects of anisotropy on the observed strength behaviors and failure patterns were discussed. The characteristics of shale rock are also studied by non-destructive wave speed measurements. The shale demonstrated strong anisotropic behaviors with the tensile strength perpendicular to the bedding plane around 300-360 times of that parallel to bedding plane. Results of ultrasonic testing indicated that both compression and shear wave velocities show strong anisotropic patterns. The compression wave speed was smallest in the direction perpendicular to the bedding plane, while the shear wave speed was smallest in the direction parallel to the bedding plan. The ratio of wave speed anisotropy is around 1.3-1.4 times for compression wave. The ratio of wave speed anisotropy is more diverse for shear wave.

INTRODUCTION

Shale gas, one type of natural gas formed in shale strata, has aroused significant interests worldwide as a major source of natural gas. Places with shale gas potentials are widely distributed including the U.S. (Peebles 1980, Donohue et al. 1981, Richard 2012), UK (Brooks et al. 2001, Swann and Munns 2003, Richard 2012), and China (Zou et al. 2010, Chen et al. 2011, Huang 2012), etc. Effective recovery of shale gas

needs to address technical issues such as wellbore instability, optimization of hydraulic fracture, etc. All of these are related to the mechanical properties of the shale rocks surrounding the wellbores (Horsrud et al. 1998, Talal et al. 2008) and therefore it is required to study their mechanical behaviors and failure mechanisms.

This paper is to study the anisotropic behaviors of shale rocks at both small strain and large strain levels. Anisotropic compression and tensile strengths of shale rocks were measured by uniaxial compression test as well as the direct and indirect tensile tests. Directional compression wave velocities of shale were measured using ultrasonic technology. The mechanical properties of shale rock helps to understand and predict the fracture behaviors under field operational conditions.

Materials Origin and Mineral Analyses

Samples used in this study are typical gas shale rock obtained from northeastern Ohio region. Scanning electron microscope (SEM) with Energy Dispersive X-Ray Analyses (EDX) was employed to measure its surface topography, microstructure and chemical composition. Figure 1 shows the SEM images of typical shale sample. The crystals tend to be in platy structure, which might correspond to the direction of the bedding plane. Element composition of the sample was analyzed with EDX module , which indicate that Oxygen (O), Silica (Si) and Ferrum (Fe) are the primary elements in this shale rock, accounting for nearly 90% of the gross weight. Other elements, such as Aluminum (Al), Potassium (K) and Calcium (Ca) can be also observed but with low concentration. No appreciable organic components were observed, possibly due to the fact the entrapped gas might have escaped during storage.

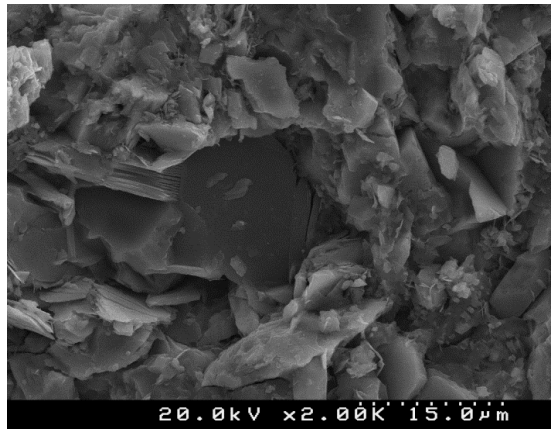

FIG. 1. SEM images of shale specimen

Experiment Design for Mechanical Testing

Specimen preparation

Three types of specimens were prepared for different types of destructive or nondestructive mechanical tests. According to ASTM D3967 and D4543, cylindrical specimens with height-diameter ratio of 2:1 and 1:2, were prepared for direct- and

indirect- tensile test, respectively. According to the standards, for diameter of the cylindrical specimens of 5 cm, the height of specimens for direct- and indirect- tensile tests needs to be at least 10 cm and 2.5 cm, respectively. The anisotropic properties (specially the extremely low interlaminar strength) of this type of shale make it very difficult to prepare testing specimens with the exact required length. Therefore, the height of prepared specimens for uniaxial compression test and direct tensile test were within the range of 80 to 100 mm. Prismatic specimens were prepared for wave velocity measurements. The top and bottom surface of the specimens were prepared as smooth and flat as possible so that both ends were parallel to each other. Three duplicate specimens were prepared for each type of test. The average density of the shale rock was measured to be around 2.503 g/cm^3.

Testing Program

A series of laboratory mechanical tests were conducted on the prepared shale rock specimens, including uniaxial compression tests, direct tensile tests, and indirect tensile tests. The strengths and stress-strain relationships were obtained from the experimental data. A MTS testing system was employed for the testing. The loading rate was set as 0.002 mm/s in both compression and tensile testing. Superglue was applied on both end of the specimen during direct tensile tests.

The wave speeds in the specimens were measured by nondestructive ultrasonic measurements. Both compression and shear wave types of ultrasonic transducers were used to measure the compression and shear wave velocities respectively. Wave velocities parallel and perpendicular to bedding plane were measured to evaluate the anisotropic behaviors of the shale rock. The setup of ultrasonic measuring system includes a pulse transmitter, an ultrasonic transducer (with frequency of 0.5 MHz), and a PC oscilloscope. Through-transmission mode of the ultrasonic system is used in this study, where two ultrasonic transducers served as transmitter and receiver, respectively. The transmitter sends a wide-band acoustic signal into the testing specimen from one surface, which propagates in the testing material and is picked by the receiver on the opposite surface of the testing specimen. From these, the travelling time of the acoustic signal in the testing specimen was determined. The wave velocity can then be calculated from the travel time and the thickness of the specimen. For compression wave testing, the ultrasonic tests were conducted underwater to facilitate the coupling with the testing specimens. For shear wave testing, a special couplant for shear wave transducers was used.

Experimental Results and Analysis

Triaxial compression test

Uniaxial compression tests were performed on three groups of specimens. The stress-strain curves are shown in Figure 2a. With the increment of compression strain, stress increases to a peak and then decreases rapidly. The average peak strength is 47.9 MPa.

Figure 2b shows the crack patterns at the failure. As can be seen, the crack patterns in anisotropic shale under compression loads are more complex than those observed in a homogeneous specimen. In general, the initiation and propagation of cracks play a significant role in the failure behaviors of the anisotropic shale samples. The direction of cracks can be initialized along the circumferential or perpendicular to the bedding plane. As stress increases, more microcracks initiated and propagated in the specimens. When the number of microcraks in the sample exceeds the threshold, the microcracks started to connect with each other, and the whole sample would break into pieces. This corresponds to the collapse failure point in stress-strain curves.

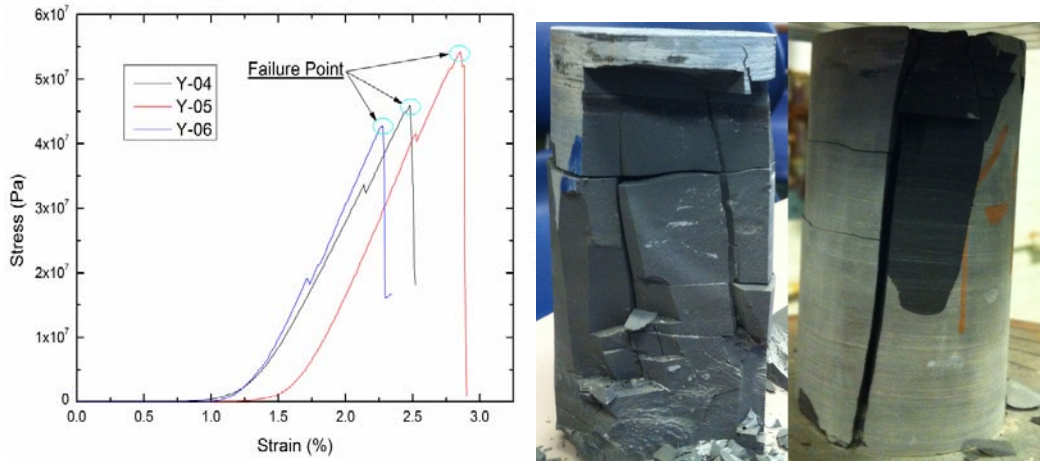

FIG. 2. (a) Stress strain curve of shale samples under uniaxial compression; (b) Typical failure mode of samples.

Direct tensile test

Figure 3a shows the measured stress strain curves. All curves show brittle types of failure. With the increases of loading strain, stress increases to a peak and then decreases. The following failure mode were observed during the testing process: with the increases in the axial loading, a microcrack firstly occurred at a certain location in the specimens, the crack then propagate along the circumference and from the outer circumference to the center of the specimens until the specimen is split into two parts (Figure 3b).

There were significant variations in the tensile strength, which is possibly due to the intrinsic variability of rock specimens resulting from the geological process or sample coring procedures. The average tensile strength is 25.0 kPa, which is the average adhesion strength along the bedding plane. The tensile strength is significantly lower than the compression strength.

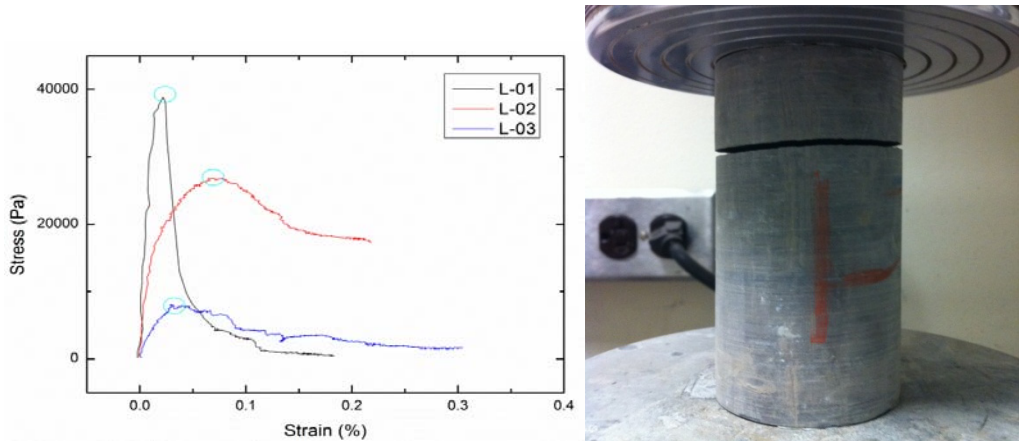

FIG. 3. (a) Stress-strain curves of specimens under direct tensile test; (b) typical failure mode of specimens after direct tensile test

Indirect tensile test

Two groups of specimens (each with 4 duplicates) were prepared for indirect tensile tests. The first group (P-02, P-03, P-04, P-05) was performed without loading beams at the top or bottom of the specimens; whereas the second group (P-07, P-08, P-09, P-10) were tested with the use of loading beams at both the top and bottom of the specimens. The measured indirect tensile strengths were 7.4 MPa and 9.1 MPa respectively for testing without or with the use of loading beams. These are around 300-360 times of the average tensile strength perpendicular to the bedding plane.

Figure 4 shows the measured load-displacement curves with loading beam. The observed failure trends are similar to that of direct tensile tests and compression tests, i.e., the specimens showed brittle types of failures.

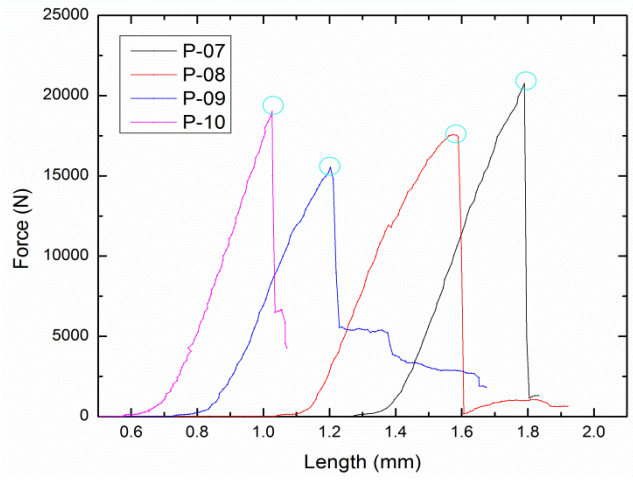

FIG. 4. Load displacement curves for indirect tensile tests

The failure mode of anisotropic shale (due to the low interlaminar strength) under indirect tensile loading is different from and much more complex than that of isotropic rocks (Erarslan and Williams 2011). Figure 5 shows photos of representative types of failure modes. Based on Hooke's law, compression stress σ_1 along the radius direction will lead to tensile stress in the direction perpendicular to the loading direction, i.e., in directions of σ_2 and σ_3 shown in Figure 7A. Both can lead to failures in respective directions. Therefore, besides the typical failure pattern of split tensile tests (Figure 5B), split cracks and failure between layers are intertangled in anisotropic shale (Figure 5C, D and E). It was observed in the tests that the cracks or failure parallel to the bedding layers tends to slightly reduce the measured indirect tensile strength. Therefore it is very difficult to accurately determine the indirect tensile strength of anisotropic shale rock by indirect tensile tests without observing/specifying the actual fracture patterns. The fracture mechanism of anisotropic shale under complex stress conditions is a challenging topic that deserves further investigations.

FIG. 5. Typical failure mode of specimens after indirect tensile tests

Ultrasonic wave velocity measurement

Four prismatic specimens were prepared for ultrasonic measurements on the wave speeds of the shale rock. The two surfaces perpendicular to the bedding plane were marked as 1-1 and 2-2, whereas the surface parallel to the bedding plane was marked as 3-3. Wave velocity from three pairs of surfaces was measured with ultrasonic technology as described previously.

Figure 6 plots the measured travel time of compression wave as a function of the travel distance (or the dimension of the specimen) in each direction. From this, the average compressional wave velocity in the shale rock along each direction can be easily calculated from the slope of the fitting the line. Similar analyses were conducted on the shear wave signals. Reverse polarity method was used to identify the arrival shear waves.

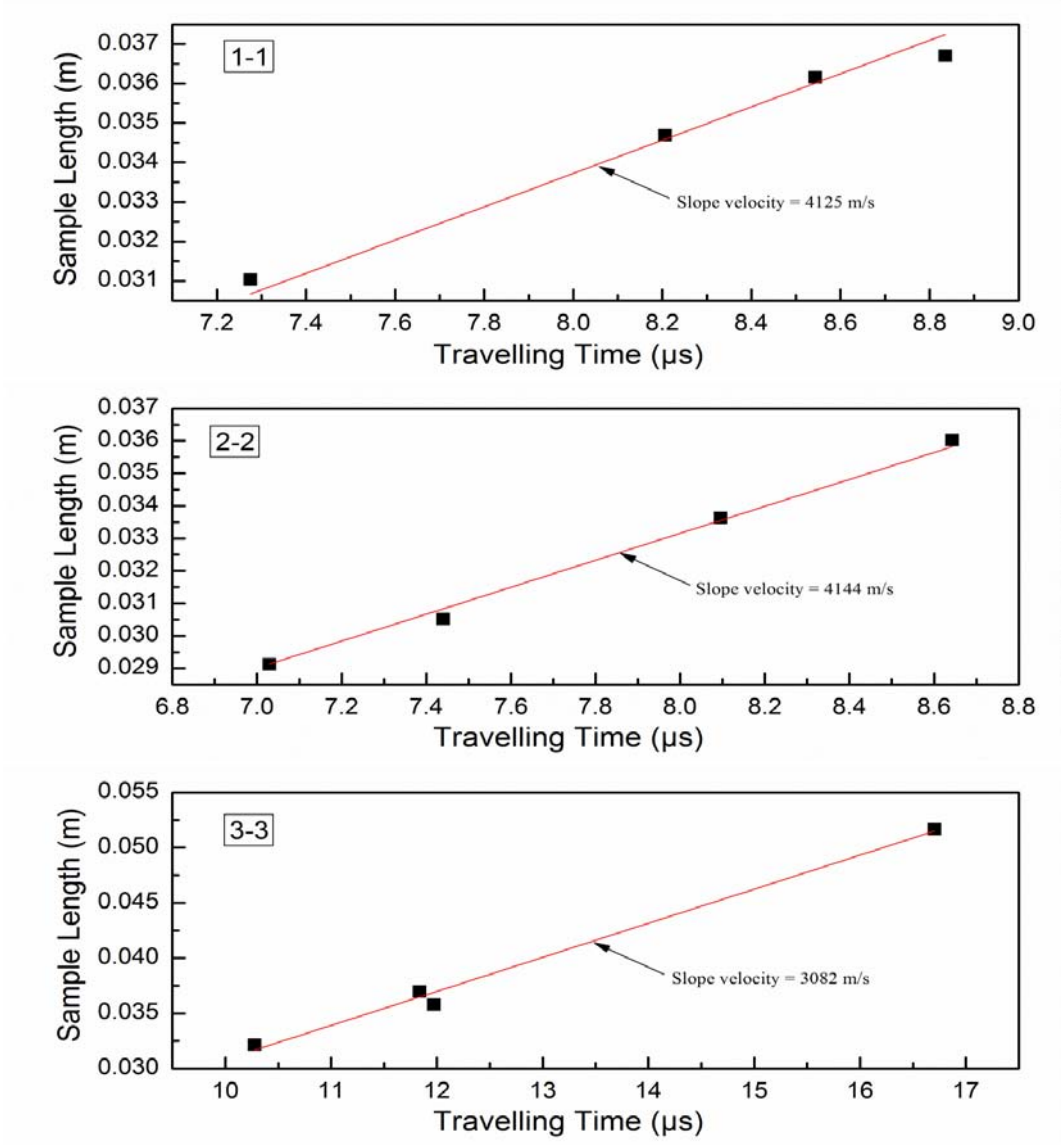

FIG. 6. Measured travel time as a function of the travel distance (or the dimension of the specimen) in each direction

The results of compression and shear wave velocities are summarized in Table 1. From the table it can be seen that the compression wave velocities in the direction parallel to the bedding plane, i.e., 1-1 and 2-2 directions, are similar. They are typically 1.3-1.4 times of that perpendicular to the bedding plane, i.e., 3-3 direction. The measured shear wave velocity however is smallest in the 2-2 direction (one of the directions parallel to the bedding plane). The ratios of wave speed in different directions are more diverse. That is possibly due to the relatively weak bonding between bedding layers, history of geological formation, etc. The fundamental mechanism for the observed anisotropic wave speed patterns needs to be further understood.

Table 1. Summary of shear and compression wave velocity measurement

Sample No.	V_p (km/s)	V_s (km/s)	$V_p/V_{p,min}$	$V_s/V_{s,min}$
B-1-1	4.227	2.288	1.37	1.00
B-2-2	4.154	2.292	1.34	1.00
B-3-3	3.093	2.492	1.00	1.09
C-1-1	4.265	x	1.43	x
C-2-2	4.168	x	1.39	x
C-3-3	2.990	x	1.00	x
D-1-1	4.233	2.833	1.35	1.43
D-2-2	4.101	1.983	1.31	1.00
D-3-3	3.128	2.406	1.00	1.21
E-1-1	4.154	2.621	1.33	1.59
E-2-2	4.144	1.647	1.33	1.00
E-3-3	3.122	2.487	1.00	1.51

Note: $V_p/V_{p,min}$ is the ratio of measured compression wave velocity to the smallest compression wave velocity in three directions; $V_s/V_{s,min}$ is the ratio of measured shear wave velocity to the smallest shear wave velocity in three directions

CONCLUSIONS

This paper studied the anisotropic behaviors of shale by laboratory experiments. The compression and tensile strengths were measured by uniaxial compression tests and direct/indirect tensile tests. From these, the stress-strain behaviors and strength characteristics along different directions were assessed. In general, the compression strength of shale is found to be much higher than tensile strengths. The failure pattern under compressive loads is more complex than those observed in a homogeneous specimen. Besides, the tensile strengths of shale rocks are different in the direction parallel to the bedding layers versus perpendicular to the bedding layers. From the results of direct and indirect tensile tests, the tensile strength inside the bedding layer is around 300-360 times of that perpendicular to the bedding layer. The phenomena observed from indirect tensile disk test revealed that the tensile strength along the bedding plane might be underestimated due to the influence of interlaminar failure along the bedding plane. Results of ultrasonic testing indicated that both compression and shear wave velocities show strong anisotropic patterns. The compression wave speed is smallest in the direction perpendicular to the bedding plane. The shear wave speed, however, is smallest in the direction parallel to the bedding plan. The ratio of wave speed anisotropy is around 1.3-1.4 times for compression wave. The ratio of wave speed anisotropy is more diverse for shear wave. The fundamental mechanism of the observed anisotropic wave speed patterns and the implications for the engineering practice needs to be further studies.

REFERENCES

Brooks JRV, Stoker SJ, Cameron, TDJ (2001) Hydrocarbon exploration opportunities in the twenty-first century in the United Kingdom. In: Downey MW, Threet JC, Morgan WA (Eds.), Petroleum Provinces of the Twenty-First Century. AAPG Memoir 74

Chen SB, YM Zhu, HY Wang (2011) Shale gas reservoir characterization: A typical case in the southern Sichuan Basin of China. Energy 36(11): 609-616

Donohue D, Anstey N, Morrill N (1981) Shale Gas in the Southern Central Area of New York State. U.S. Dept. of Energy, Morgantown. Vol (4)

Horsrud P, Sqonstebo EF, Boe R (1998) Mechanical and petrophysical properties of North Sea shales. Int. J. Rock Mech. Min. Sci. Vol. 35(8): 1009-1020

Huang JL, Zou CN, Li JZ, Dong DZ (2012) Shale gas generation and potential of the lower Cambrian qiongzhusi formation in the southern Sichuan basin, China. Petroleum exploration and development 39(1):75-81

Peebles MHW (1980) Evolution of the Gas Industry. New York University Press, New York.

Richard CS (2012) UK shale gas: the story so far. Marine and petroleum geology 31(1): 100-109

Sayers CM (1999) Stress-dependent seismic anisotropy of shales. Geophysics Vol. 64, 93–98.

Swann G, Munns J (2003) The hydrocarbon prospectivity of britain's onshore basins. DTI, London. 17

Talal AB, Zhang JG, Martin EC, Mukul MS (2008) Factors controlling the compressive strength and acoustic properties of shale when interacting with water-based fluids. Int. J. Rock Mech. Min. Sci. Vol. 45: 729-738

Zou CN, Dong DZH, Wang SHJ (2010) Geological characteristics and resource potential of shale gas in China. Petroleum exploration and development 37(6): 641-653

Shale Fracturing for Energy Recovery: Current Issues and Review of Available Analytical and Computational Models

Giuseppe Buscarnera[1], Ph.D., Aff.M.ASCE, Gianluca Cusatis[2], Ph.D., M.ASCE, Aleksander Zubelewicz[3], Ph.D., M.ASCE and Zdeněk P. Bažant[4], F.ASCE

[1]Assistant Professor, Northwestern University, Department of Civil and Environmental Engineering, 2145 Sheridan Road, Evanston, IL, 60208, U.S.A., E-mail: g-buscarnera@northwestern.edu
[2]Associate Professor, Northwestern University, Department of Civil and Environmental Engineering, 2145 Sheridan Road, Evanston, IL, 60208, U.S.A., E-mail: g-cusatis@northwestern.edu
[3]Research Scientist, Los Alamos National Laboratory, Los Alamos, New Mexico, 87545, U.S.A., E-mail: alek@lanl.gov
[4]Professor, Northwestern University, Department of Civil and Environmental Engineering, 2145 Sheridan Road, Evanston, IL, 60208, U.S.A., E-mail: z-bazant@northwestern.edu

ABSTRACT: The paper reviews some of the major scientific challenges faced in the field of non-conventional energy production. Particular attention is given to shale rocks, in which the production of hydrocarbons involves hydraulic fracturing, fracture connectivity, multiphase flow, and reactive-transport. In regard to these problems, the paper describes a series of analytical and computational models to study fracturing in quasi-brittle solids and capture failure events in multi-phase geomaterials subjected to simultaneous changes in stress state, fluid pressure, moisture content, thermal and chemical conditions. Advantages and limitations of the different techniques are discussed, setting a vision for a new generation of multi-scale/multi-physical models for shale that can be used to support the optimization of the extraction processes, as well as to address industrial needs and mitigate the risks of environmental hazards, groundwater contamination and induced seismicity.

INTRODUCTION

Most of the world's energy comes from fossil fuels hosted in the shallow crust. As a result, now and for the foreseeable future, human activities depend on our ability to extract these resources in an effective, safe and sustainable manner. The strategic role of extraction techniques has gained prominence over the last decade, mostly because of the unprecedented ability to recover fossil fuels from previously inaccessible areas, and hence referred to as unconventional resources (Law and Curtis, 2002). While this is a paradigm shift for the energy market, it carries considerable uncertainties about how the rocks react to these technologies, as well as for the risk of contamination and induced seismicity (Shapiro and Dinske, 2009; Osborn et al., 2011).

In this context, tight shale gas is an unconventional energy source that is setting the foundations for US energy independence, with reserves projected to last for many

decades to come. Although these aspects are already changing the energy landscape, the mechanics of oil/gas extraction from shale rocks is not yet fully understood. More specifically, the production of hydrocarbons from low permeability shale involves the underground pressurization of the injected fluids with the purpose to enhance fracture connectivity and stimulate the flow of the fluids hosted in the rock pores. The main challenges derive from the complex field conditions under which the process is conducted, as well as from the uncertainties about the response of fractured rocks. Characterization, simulation and prediction of shale is a major challenge, as these naturally occurring solids are heterogeneous, porous, multiphasic and chemically active. In addition, they contain flaws at all scales and are characterized by a variable response, which largely depends on the state of stress and the conditions at the site.

It is therefore arguable that, unless a new generation of characterization techniques, predictive theories and computational models is developed, it will not be possible to quantify the environmental, societal and industrial impacts of the future large-scale implementation of shale fracturing technologies. For this reason, this paper aims to provide a review of existing modeling approaches that can contribute to a quantitative understanding of fracture in quasi-brittle media subjected to multi-physical processes. The objective is to identify critical research areas that require a better understanding of the mechanics of fracturing in shale rocks for oil/gas extraction purposes.

MODELS FOR FRACTURE PROCESSES

The following sections outline the characteristics of different types of models able to simulate complex fracturing processes in geological materials. A detailed description of such models is available in Bazant and Caner (2013), Caner and Bazant (2013a,b), Cusatis et al. (2011a,b); Schauffert and Cusatis (2012); Schauffert et al. (2012), Alnaggar et al. (2013), Zubelewicz (2008, 2009) and Zubelewicz et al. (2013).

Microplane Model and Dynamic Comminution of Shale

Like all geomaterials, including the artificial one—concrete, the high strains in gas shale produce first distributed damage of microcracks and micro-slips, which later coalesce in distinct cracks. At the front of such cracks there is a propagating fracture process zone (FPZ) of a finite length and width which consists of distributed damage. To model the fragmentation of the gas shale, a realistic damage constitute model is required. Based in previous experience with concrete and some other geomaterials, the most realistic model is the microplane model, in which the material constitutive law is described in terms of stress and strain vectors, rather than tensors, acting on a generic plane, called the microplane, of arbitrary orientation within the material. The strain vectors on the microplanes are considered to be the projections of the macroscopic strain tensor, and the stress tensor is obtained from the microplane stress vectors by integration according to the virtual work principle.

Why microlane approach? Note that the internal friction in materials is usually modeled as a relation between the first stress invariant and the second deviator invariant, without any reference to the direction of slip. This is not realistic. The plastic or frictional slip occurs in fact only on planes of a certain specific orientation.

Likewise, almost all of the other inelastic deformations in geomaterials, including concrete, such as tensile cracking and compressive axial splitting, occur on planes of specific orientations. These orientations can be captured by the idea of G.I. Taylor in 1938, who proposed to formulate the constitutive law in terms of the vectors of stress and strain acting on planes of various orientations in the material. Taylor's idea was first developed for plasticity of polycrystalline metals under the name of slip theory of plasticity and has by now led to powerful plasticity models called the Taylor models. In these models, the stress vectors on the slip planes are the projections of the continuum stress tensor, which is called the static constraint, and the plastic slips on all the slip planes are simply superposed.

In the early 1980s, it was realized that Taylor models are unstable in the case of strain-softening damage, due to diffuse microcracking. To ensure stability, the static constraint had to be changed to the kinematic constraint, in which the strain vector is the projection of the strain tensor onto a generic plane of any orientation in the material microstructure, called the microplane. Also the elastic deformation had to be included on the microplane level. The static equivalence of the stress tensor with stress vectors on microplanes of all possible spatial orientation was enforced by the principle of virtual work, which gives the continuum stress tensor:

$$\sigma_{ij} = \frac{3}{2\pi}\int_{\Omega}\left(\sigma_N N_{ij} + \sigma_L L_{ij} + \sigma_M M_{ij}\right)d\Omega \tag{1}$$

This is an integral over a unit hemisphere Ω, in which σ_{ij} = stress tensor, $\sigma_N, \sigma_L, \sigma_M$ = normal and two shear components of the microplane stress vector, and N_{ij}, L_{ij}, M_{ij} = geometrical coefficients defined later. This integral is evaluated approximately according to an optimum Gaussian integration formula as a weighted sum over all the discrete microplanes whose normals are chosen to correspond to the integration points of this formula. According to the kinematic constraint, the normal component of the strain vector on a generic microplane of orientation defined by its unit normal n_i is $\epsilon_N = n_i n_j \epsilon_{ij} = N_{ij}\epsilon_{ij}$ where subscripts i, j = 1,2,3 refer to Cartesian coordinates x_i. The in-plane shear strain vector on each microplane is represented by its two in-plane orthogonal components in the directions of unit in-plane coordinate vectors ***m, l*** that are generated randomly on each microplane. These components are

$$\varepsilon_M = \frac{1}{2}\left(n_i m_j + n_j m_i\right)\varepsilon_{ij};\ \varepsilon_M = M_{ij}\varepsilon_{ij};\ \varepsilon_L = \frac{1}{2}\left(n_i l_j + n_j l_i\right)\varepsilon_{ij} = L_{ij}\varepsilon_{ij} \tag{2}$$

To be able to model the pressure-sensitive compressive behavior of concrete, it is necessary to split the microplane normal strains and stresses into their volumetric and deviatoric parts: $\epsilon_N = \epsilon_V + \epsilon_D;\ \ \sigma_N = \sigma_V + \sigma_D$ where $\epsilon_V = \epsilon_{kk}/3$ and $\epsilon_D = (N_{ij} - \delta_{ij}/3)\epsilon_{ij}$; σ_V, σ_D are computed from ϵ_V and ϵ_D by the microplane constitutive law. In contrast to previous microplane models, this split is in M7 introduced only for inelastic compressive behavior, and not for the elastic part of response. This change greatly improved the triaxial tensile softening representation.

The inelastic softening behavior is in the microplane model best characterized by

means of separate strength limits, or stress-strain boundaries, on the microplane stress components. Within the boundaries, the behavior is considered to be elastic, and it should be noted that in spite of that the macroscopic response represents the pre-peak nonlinearity because different microplanes enter the strain softening behavior at different moments of loading. The inelastic behavior, defined on the microplanes in terms of σ_N in tension and in terms of σ_V and σ_D in compression, can simply be specified as functions of the corresponding ϵ_N, ϵ_V and ϵ_D, while the shear stress components σ_M, σ_L are limited by boundaries depending on σ_N and ϵ_V.

Compared to the classical tensorial constitutive models based on tensorial invariants, the microplane concept has a number of advantages: 1) It is conceptually simpler, since the strain vectors on the microplanes can be intuitively related to crack opening and slip; 2) The orientation of cracking and slip can be captured; 3) The so-called vertex effect is automatic, while being beyond the capability of the tensorial constitutive models; 4) Apparent deviations from normality in the sense of tensorial plasticity models are represented, thanks to the fact that the microplane model is equivalent to a large set of simultaneously active yield surfaces intersecting at the same point of the stress space, for each of which the normality rule can be satisfied (this is articularly important for dynamic or shock wave loading, producing with highly nonproportional loading paths); 5) The kinematic constraint of the microplanes of different orientation automatically simulates the cross effects such as the shear dilatancy and pressure sensitivity; 6) Combinations of loading and unloading on different microplanes provide a complex path dependence and automatically reproduce the Bauschinger effect and the hysteresis under cyclic loading; 7) The dependence of the current yield or strength limits on the strain components (rather than scalar on a hardening-softening parameters) is easy to take into account; 8) In cyclic loading, fatigue is automatically simulated by accumulation of residual stresses on the microplanes after each load cycle; 9) And finally, anisotropy can be easily captured, which is important for shale.

Early on, the microplane model was computationally too demanding for full structures. But thanks to the phenomenal rise of computer power, the microplane model is now being used in systems with tens of millions finite elements. Many progressively improved versions of the microplane model, now labeled M1, M2,...M7, have been developed for concrete, and other variants for fiber-reinforced concrete, fiber-polymer composites, sandstone, shale, clay, rigid foam, shape memory alloy and some soft tissues. Model M4 was used with success in large-scale simulation of various explosions and groundshock, and with partial success in missile impact and penetration of concrete walls. The new model M7 brings about further significant improvements. It eliminates unrealistic lateral strains in postpeak tensile softening, gives damage dependent unloading, and works even for cyclic loading with softening.

Based on extensive calibrations on test data for many concretes, the stress-strain boundaries are in recent microplane models (such as M7) characterized by five free parameters k_i (i = 1 ,2,...5), which can be easily adjusted according to basic data from uniaxial and triaxial compression tests and uniaxial tensile tests and notched fracture test (for M7 for concrete, the definitions of the boundaries include about twenty fixed parameters, which can be considered the same for all concretes; they have been

identified by computer optimization of the fits of numerous data of different types.

Adaptation to shale (which is in progress at the time of writing) requires introduction of orthotropy, caused by bedding planes in the shale. Compared to some fiber-polymer composites, for which the ratio of in-plane stiffness to transverse stiffness or shear stiffness can exceed 1000:1, for shale this ratio is much smaller, generally <<10:1. This means the orthotropy is weak, which simplifies modeling. To generalize the microplane for a weak orthotropy, it may suffice to replace $d\Omega$ with $f(\theta,\phi)d\Omega$ where $f(\theta,\phi)$ is an orthotropic weight function varying ellipsoidally with spherical angles θ,ϕ. This behavior may be improved or modified by varying simultaneously or alternatively the normal stiffness E_N on the microplanes, again in the ellipsoidal way. Also the same can alternatively be applied to the shear stiffness E_T. Another way is the to omit the weight function and ellipsoidal corrections and introduce an increased stiffness only to the microplanes for in-plane normal strains, a stiffness equal to the difference between the in-plane and transverse elastic moduli, In the case of highly orthotropic fiber composites, there is a more fundamental way to introduce orthotropy into the microplane model—obtain the eigenvalues and eigenmodes of the symmetric elastic 6 x 6 matrix of the elastic moduli tensor, and then write the overall response as a linear combination of these eigenmodes. A similar extension for orthotropy needs to be applied to the normal or shear stress-strain boundaries, or both, to capture capture the strength orthotropy. The difference in normal strength between the in-plane and directions and the transverse direction is stronger than it is for stiffness.

Dynamic Comminution Shale by Shock Waves.

The modeling of high velocity impact into brittle or quasibrittle solids is hampered by the unavailability of a constitutive model for finite element codes capturing the effects of material comminution into very fine particles. Another paper at this conference (by Bažant and Caner, this issue) will describe a recent general formulation of such a model, usable in finite element programs. It is found that the comminution at very high strain rates can dissipate a large portion of the kinetic energy of a shock wave. The model is inspired by analogy with turbulence. In high velocity turbulent flow, the energy dissipation rate gets enhanced by the formation of micro-vortices (eddies) which dissipate energy by viscous shear stress. Similarly, here it is assumed that the energy dissipation at fast deformation of a confined solid gets greatly enhanced by the release of kinetic energy of the motion associated with a high-rate shear strain of forming particles. Equating the release rate of kinetic energy of shear to the interface fracture energy per particle gives the particle size (or range of particle sizes) also yields an apparent 'comminution viscosity' providing energy dissipation equal to the dissipation by interface fracturing. Dynamic finite element simulations with 'comminution viscosity' are conducted to study the effect of shock waves emitted by explosions in a blocked section of a horizontal borehole. Single or properly timed multiple explosions could be generated by pulsed arc electro-hydraulic discharge in the borehole section. If these prove sufficient to produce fine comminution of shale layer within a sufficently large zone, there would be negligible discharge of contaminated water to the surface, It seems more likely that subsequent

additional fracturing would be have to be produced hydraulically in the way well established by now, using water with suitable proppants and dispersants. In that case, there would still be discharge of contaminated water to the surface, but the amount would be reduced, perhaps greatly reduced, which would be environmentally very beneficial. The present theory promises to explore many more alternative than possible experimentally, at a much reduced cost, and much more quickly.

Constitutive Modeling of Dynamic Behavior and Fracture in Geomaterials

A mechanisms-based fracture model applicable to a broad class of Earth and Earth-like materials is describes as presented in Zubelewicz et al. (2013). The model captures several features and among them material's anisotropy, rate sensitive directional fracture, dilatational friction. Also, the model captures the contribution of dynamic overstress in loading extremes, where the rate of supplied energy is not fully compensated by the rate of the energy redistribution and release. Lastly, the model incorporates scalable stochasticity of the material's resistance to fracture. In comparison with more traditional descriptions, the strength and universality of the proposed approach lies in our tensor representation theory, which allows for converting the observed deformation and fracture mechanisms into a mathematically precise description. We illustrate the concept on the basis of generic geomaterials.

Friction-induced visco-plasticity: The frictional (plastic) deformation consists of slippages along crack surfaces and dilatation due to crack roughness (asperities). The shear strain rate is constructed with the use of a flow tensor M_{ij} such that

$$\dot{\varepsilon}^{p}_{ij} = \frac{1}{2} M_{ij} \dot{e}^{p}_{eq} \tag{3}$$

The tensor M_{ij} is defined in terms of stress deviator S_{ij}, the second invariant of stress deviator $J_2=S_{ij}\ S_{ij}/2$, and includes the dilatational part scaled through the internal friction parameter q, which is a function of the second invariant of stress deviator and its magnitude is affected by grinding of the asperities under compression. In the next step, we develop a constitutive relationship between the equivalent stress and strain rate. In here, the relationship is proposed in a pseudo-linear form as

$$\dot{e}^{p}_{eq} = \dot{\Lambda}_{p} \frac{\sigma^{p}_{eq}}{\sigma^{p}_{0}} \tag{4}$$

where the material's strength consists of static strength and the dynamic overstress. The dynamic overstress kicks in when the rate of the energy delivered to the material is comparable with the rate of the energy redistribution, dissipation and conversion; all the processes are caused by the propagating cracks. A similar problem has already been solved for metals, where the energy redistribution has been linked to the mobility of dislocations (Zubelewicz, 2008, 2009). The linear strain rate dependence in Eq. (2) can also be corrected to be non-linear if needed.

Fracture Tensor

In geomaterials, the fracture processes occur in tension, compression and shear.

Tensile micro-cracks are forming on micro-planes, which are predominantly aligned with the direction of maximum tensile stress. The extent of the damage is closely correlated with the amount of work required for the micro-crack to become fully opened (Zubelewicz and Bazant, 1987). In order to keep track of the damage processes, we introduce a fracture tensor, whose rate is defined as follows

$$\dot{\Omega}_{ij} = \dot{G}_f N_{ij}^{\sigma} \tag{5}$$

where the shape tensor $N_{ij}^{\sigma} = n_i n_j$ is aligned with the direction of the current maximum tensile stress. The fracture energy is equivalent to the work needed for opening the cracks, thus $\dot{G}_f = l_c \sigma_{nn} \dot{\varepsilon}_{nn}^{e}$. The normal component of the traction is $\sigma_{nn} = N_{ij}^{\sigma} \sigma_{ij}$ and the rate of crack opening displacements is $\dot{\varepsilon}_{nn}^{e} = l_c N_{ij}^{\sigma} \dot{\varepsilon}_{ij}^{e}$. Lastly, the characteristic fracture length l_c is correlated with the Stochastic Volume Element (SVE) of the material. The rate of work is accumulated only during active fracture process. The fracture tensor retains the fracture history and is $\Omega_{ij} = \int_{t_0}^{t} \dot{\Omega}_{ij}(s) ds$.

Underground Explosive Event in a Generic Isotropic Geomaterial

We apply the model to the study fracture processes in a generic geomaterial subjected to an underground explosion at 400m below the surface. It is an axisymmetric boundary value problem, where the high explosive charge is modeled using a Jones-Wilkins-Lee type of equation of state (Lee et al., 1973). The yield of the explosion is set to one kiloton (TNT-equivalent).

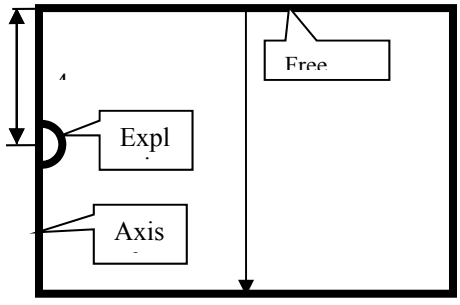

(a)

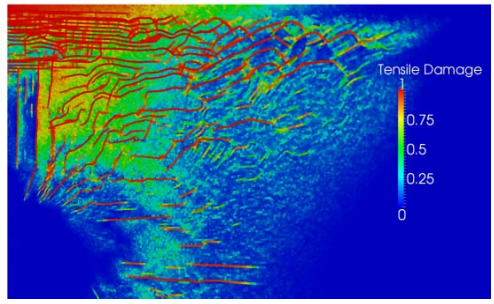

(b)

FIG. 1: (a) Sketch of the underground explosive event. (b) Underground high explosive charge: Tensile damage at 0.2 s after explosion

The contours of wave velocity (Fig. 1b) and the crack patterns are plotted at t=0.2s when the surface spallation is pronounced. Tensile cracks form a network, which stretches from the central point above the explosive and covers a significant area. In this plots, the tensile fracture is scaled from zero to one.

Lattice Discrete Particle Models

The simulation of shale fracturing for oil and gas recovery requires the accurate description of various fracture phenomena including crack initiation, propagation along complex three-dimensional paths, interaction and coalescence of distributed

multi-cracks into localized continuous cracks, effect of the confining pressure, interaction between fractured and unfractured material. These phenomena occur at multiple spatial scales ranging from the atomistic scale (~10^{-10} m) to the macroscopic scale (>10^{2} m). Atomistic simulations, in which the atomistic behavior drives the macroscopic, are impracticable at this point in time because reliable models for shale at that scale do not exist yet. However, accurate and reliable mesoscale (~10^{-4} m) modeling is possible by virtue of a recently formulated discrete model called the Lattice Discrete Particle Model (LDPM).

The Lattice Discrete Particle Model (LDPM) simulates the mesostructure of geo-materials by taking into account only the coarse material heterogeneities. The mesostructure is constructed through the following steps: 1) the coarse aggregate pieces, whose shapes are assumed to be spherical, are introduced into the volume of interest by a try-and-reject random procedure; 2) zero-radius nodes are randomly distributed over the external surfaces; and 3) a three-dimensional domain tessellation, based on the Delaunay tetrahedralization of the generated particle centers, creates a system of cells interacting through triangular facets. A vectorial constitutive law governing the behavior of the model is imposed at the centroid of the projection of each single facet (contact point) onto a plane orthogonal to the straight line connecting the particle centers (edges of the tetrahedralization). The projections are used instead of the facets themselves to ensure that the shear interaction between adjacent particles does not depend on the shear orientation. The straight lines connecting the particle centers define the lattice system.

Rigid body kinematics describes the displacement field along the lattice struts and the displacement jump, $[\mathbf{u}_C]$, at the contact point. The strain vector is defined as the displacement jump at the contact point divided by the inter-particle distance, L. The components of the strain vector in a local system of reference, characterized by the unit vectors $\boldsymbol{n}$, $\boldsymbol{l}$, and $\boldsymbol{m}$, are the normal and shear strains: $\varepsilon_N=\mathbf{n}^T[\mathbf{u}_C]/L$; $\varepsilon_M=\mathbf{m}^T[\mathbf{u}_C]/L$; $\varepsilon_L=\mathbf{l}^T[\mathbf{u}_C]/L$. The unit vector $\boldsymbol{n}$ is orthogonal to the projected facet and the unit vectors $\boldsymbol{l}$ and $\boldsymbol{m}$ are mutually orthogonal and lie in the projected facet.

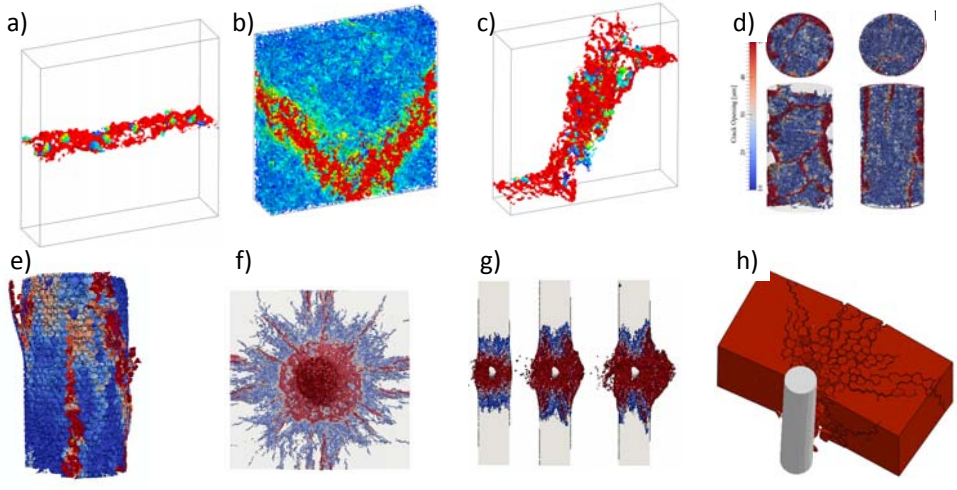

FIG. 2: LDPM simulates complex fracturing paths under quasi-static and dynamic loading conditions.

The elastic behavior is described by assuming that the normal and shear stresses are

proportional to the corresponding strains: $\sigma_N=E_0\varepsilon_N$; $\sigma_M=\alpha E_0\varepsilon_M$; and $\sigma_L=\alpha E_0\varepsilon_L$. where E_0 is the effective normal modulus, and α is the shear-normal coupling parameter. The parameters E_0 and α are assumed to be material properties. Detailed description of model behavior in the nonlinear range can be found in Cusatis et al., 2011a, and Cusatis et al., 2011b. The current LDPM formulation is implemented in MARS, a multi-purpose computational code for the explicit dynamic simulation of structural performance (Pelessone, 2012).

LDPM has been extensively calibrated and validated for concrete in the last few years and it has shown superior capabilities in reproducing and predicting qualitative and quantitative fracturing behavior under a wide range of loading conditions. Fig. 2a show a mode tensile crack pattern developed orthogonal to the applied load. Fig.2b shows the formation of shear bands at failure for a prismatic concrete specimen subjected to unconfined compression. Fig. 2c shows the LDPM capability of handling complex three-dimensional fracture paths with multiple branching and crack coalescence. Fig 2d shows simulated damage crack distribution due to the fect on an internal expansive pressure without (left) and with (right) longitudinally applied load. The model can capture automatically the effect of existing applied loads on thecrack patterns associated with loading conditions similar to hydraulic fracturing. Fig. 2e demonstrates the ability of simulating splitting cracks developing parallel to a compressive applied load in brittle materials. Figs. 2f and g presents the LDPM damage distribution and crater formation for a simulation of projectile penetration through a concrete slab. Finally, is relevant to the impact of a steel rod onto a concrete block. The simulations show, as observed in reality, that the number fragments generated by the impact increase with the impact velocity and there is a transition from failure with localized cracks to failure with complete fragmentation.

MODELS FOR MULTIPHYSICAL PROCESSES

Despite crack propagation in dry rocks has been widely studied, the role of fluids in propagating fractures has received little attention. Since it is well-known that such inelastic deformations depend on environmental conditions, multi-physical models for geomaterials offer new opportunities to design efficient fracturing procedures.

An active areas of research in this domain has been the study of the response of clays for the construction of multi-barrier nuclear waste repositories (Hueckel and Borsetto, 1990; Laloui and Francois, 2009; Gens, 2010). In these applications, the non-isothermal response of rocks is modeled via non-mechanical hardening-softening effects in a thermoplastic formalisms. Similar methods have been used to capture the effect of chemical and hydrologic conditions, which also induce shrinkage, swelling and compaction of mineral aggregates (Alonso et al., 1990; Nova et al., 2003; Hu and Hueckel, 2007; Buscarnera and Nova, 2009).

Nevertheless, little attention has been given to other aspects of relevance, such as formation of discontinuities due to non-mechanical forcing. Despite this, several studies show that chemical ageing, dissolution and precipitation affect stresses and mechanical properties, being a source of discontinuities (Hueckel et al., 2001; Shin et al., 2010). Recent studies to overcome such limitations have combined multi-physical models with the bifurcation theory (Buscarnera and Nova, 2011; Buscarnera and di

Prisco, 2012; 2013). Such works show that failure in porous media subjected to fluid injection and extraction depends on the energy supplied to each constituent of the mixture. In addition, solid-fluid interactions have implications for the robustness of the algorithms used to predict deformations (Mihalache and Buscarnera, 2013; Buscarnera, 2014), and the mathematical study of inelastic models is a potential tool to monitor site-specific conditions during shale fracturing for oil/gas extraction.

Another aspect of relevance for the mechanics of shale is the co-evolution of stress conditions and microstructural attributes, such as pore sizes and tortuosity, as well as crack size, orientation and density. While such microscopic features control virtually any property of rocks, few mechanical models account for evolving microstructural attributes. Thus, there is a tremendous need for approaches able to relate micro- and macro-scale properties. Recent attempts to bridge micro- and macro- scales in continuum models have used thermodynamic frameworks to incorporate structural descriptors (i.e., the statistics of particle grading, pore and/or crack size distributions). An example is the model for crushable media developed by Buscarnera and Einav (2012), who showed that the signatures of multi-physical coupling can be reconciled with their microscopic origin by incorporating these attributes in the formulation. This approach has been able to capture the effects of capillarity in multi-phasic solids (Buscarnera and Einav, 2012) and of chemical degradation (Buscarnera, 2012). In both cases, micro-scale effects were averaged via statistical homogenization and encapsulated in stress-strain models, showing that the coupling between yielding and non-mechanical agents can be reproduced as an emergent property. These modeling trends offer tremendous opportunities to understand inelastic deformation in reservoir rocks and derive quantitative models for site-specific reservoir rocks.

CONCLUSIONS

The last decades have seen remarkable advances in computational methods for rock mechanics, epitomized by numerous approaches based on continuum and/or discrete mechanics. Despite such advances, models are not yet accurate to cope with the unconventional resources, and major questions emerge from the mechanics of shale, a class of rocks likely to play a key role in the energy market for the decades to come.

This review paper has discussed a range of open issues and a series of methods to simulate rock fracturing in oil/gas reservoirs. While the paper focused on oil and gas extraction, developments in this area can impact a large number of technologies, such as geothermal energy, hazardous waste storage, and geologic sequestration of carbon dioxide. Hence, sustained efforts in this field of mechanics are likely to have long-term effects for a safe and sustainable use of the natural resources of the planet.

ACKNOWLEDGMENTS

We acknowledge Esteban Rougier of Los Alamos National Laboratory for the model implementation to a hydrocode and the subsequent analysis presented in this paper. The Northwestern University work presented in this paper was performed under the auspices of the Center for Sustainable Engineering of Geological and Infrastructure Materials (SEGIM).

REFERENCES

Alnaggar, M. Cusatis, G., and Luzio, G. D. (2013) Lattice discrete particle modeling (LDPM) of alkali silica reaction (ASR) deterioration of concrete structures. Cement and Concrete Composites, 41, 45-59.

Alonso, E. E., Gens, A., & Josa, A. (1990). A constitutive model for partially saturated soils. Géotechnique, 40(3), 405-430.

Bažant, Z.P., and Caner, F.C. (2013). "Comminution of solids caused by kinetic energy of high shear strain rate, with implications for impact, shock and shale fracturing." Proc., National Academy of Sciences 110 (48), 19291-19294.

Buscarnera, G., & Nova, R. (2009). An elastoplastic strainhardening model for soil allowing for hydraulic bonding–debonding effects. International journal for numerical and analytical methods in geomechanics, 33(8), 1055-1086.

Buscarnera G., Nova R. (2011) Modelling instabilities in triaxial testing on unsaturated soil specimens, Int. J. Numer. Anal. Meth. Geomech.; 35: 179–200

Buscarnera G., di Prisco C. (2012) Discussing the definition of second-order work in unsaturated soils, Int. J. Numer. Anal. Meth. Geomech., 36: 36-49.

Buscarnera G., di Prisco C. (2013) Soil stability and flow slides in unsaturated shallow slopes: how can saturation events trigger liquefaction processes? Géotechnique, 63(10), 801 –817.

Buscarnera, G. (2013) Uniqueness and existence in plasticity models for unsaturated soils. Published online in Acta Geotechnica, DOI 10.1007/s11440-013-0261-4.

Caner, F.C., and Bažant, Z.P. (2013a). "Microplane Model M7 for Plain Concrete: I. Formulation." ASCE J. of Engrg. Mechanics 139 (12), Dec., 1714-1723.

Caner, F.C., and Bažant, Z.P. (2013b). "Microplane Model M7 for Plain Concrete: II. Calibration and Verification." ASCE J. of Engrg. Mechanics 139 (12), Dec., 1724-1735

Cusatis, G., D. Pelessone, and A. Mencarelli. (2011a) Lattice Discrete Particle Model (LDPM) for Con-crete failure Behavior of Concrete. I: Theory. Cem. Concr. Compos., 33(9), 881-890.

Cusatis, G., Pelessone, D., Mencarelli, A., and Baylot, J. (2011b) Lattice discrete particle model (LDPM) for failure behavior of concrete. II: Calibration and validation. Cem. Concr. Compos., 33(9), 891–905.

Dewhurst, D. N., Jones, R. M., and Raven, M. D. (2002). Microstructural and petrophysical characterization of Muderong Shale: application to top seal risking. Petroleum Geoscience, 8(4), 371-383.

Einav, I. (2007). Breakage mechanics, part I – theory. J. Mech. Phys. Solids, 55(6), 1274–1297.

Gens, A. (2010). Soil–environment interactions in geotechnical engineering. Géotechnique, 60(1), 3-74

Hu, L. B., & Hueckel, T. (2007). Coupled chemo-mechanics of intergranular contact: Toward a three-scale model. Computers and Geotechnics, 34(4), 306-327.

Hueckel, T., & Borsetto, M. (1990). Thermoplasticity of saturated soils and shales: constitutive equations. Journal of Geotechnical Engineering, 116(12), 1765-1777.

Hueckel, T., Cassiani, G., Tao, F., Pellegrino, A., & Fioravante, V. (2001). Aging of oil/gas-bearing sediments, their compressibility, and subsidence. Journal of geotechnical and geoenvironmental engineering, 127(11), 926-938.

Lee, E., Finger, M., and Collins, W. (1973) JWL equation of state coefficients for high explosives, UCID-16189, Lawrence Livermore National Laboratory, Livermore, California.

Laloui, L., & François, B. (2009). ACMEG-T: Soil thermoplasticity model. Journal of engineering mechanics, 135(9), 932-944.

Law, B. E., and Curtis, J. B. (2002). Introduction to unconventional petroleum systems. AAPG bulletin, 86(11), 1851-1852.

Nova, R., Castellanza, R., & Tamagnini, C. (2003). A constitutive model for bonded geomaterials subject to mechanical and/or chemical degradation. International Journal for Numerical and Analytical Methods in Geomechanics, 27(9), 705-732.

Mihalache, C., Buscarnera, G. (2013). Mathematical identification of diffuse and localized instabilities in fluid saturated sands. Published online in Int. J. Numer. Anal. Meth. Geomech, DOI: 10.1002/nag.2196.

Osborn, S. G., Vengosh, A., Warner, N. R., and Jackson, R. B. (2011). Methane contamination of drinking water accompanying gas-well drilling and hydraulic fracturing. proceedings of the National Academy of Sciences, 108(20), 8172-8176.

Pellessone, D. (2012) MARS, modeling and analysis of the response of structures.. User's manual, ES3, San Diego, CA. http://www.es3inc.com/marssolver/.

Shapiro, S. A., and Dinske, C. (2009). Fluid induced seismicity: Pressure diffusion and hydraulic fracturing. Geophysical Prospecting, 57(2), 301-310.

Shin, H., Santamarina, J. C., & Cartwright, J. A. (2010). Displacement field in contraction-driven faults. Journal of Geophysical Research: Solid Earth (1978–2012), 115(B7).

Schauffert E. A., Cusatis, G. (2012) Lattice discrete particle model for fiber-reinforced concrete. I: theory. Journal of Engineering Mechanics ASCE, 138(7), 826-833.

Schauffert E. A., Cusatis, G., Pelessone, D., O'Daniel, J. L., and Baylot, J. T. (2012) Lattice discrete par-ticle model for fiber-reinforced concrete. II: tensile fracture and multiaxial loading behavior. Journal of Engineering Mechanics ASCE, 138(7), 834-841.

Zubelewicz, A., Rougier, E., Ostoja-Starzewski, M., Bradley, C., Knight, E.E., and Viswanathan, H.S. (2013). Dynamic behavior and fracture in geomaterials, Los Alamos National Laboratory, Report LA-UR 13-25656.

Zubelewicz, A. (2008). Metal Behavior at Extreme Loading Rates: Thermodynamics, Physical Review B, 77, 214111-1-8.

Zubelewicz, A. (2009). Metal Behavior at Extreme Rates, Mechanics of Materials, 41, 969-974.

Zubelewicz, A. and Bazant, Z.P. (1987) Constitutive Model with Rotating Active Plane and True Stresses, ASCE Journal of Engineering Mechanics, 113, pp. 398-416.

Particle Stacking Model to Simulate Sedimentary Rock Microcracks

Sangho Lee[1], Ph.D., P.E., M.ASCE

[1]Senior Engineer, GESTRA Engineering Inc., 1626 W. Fond Du Lac Ave., Milwaukee, WI 53217 U.S.A., E-mail: slee@gestrainc.com.

ABSTRACT: Author invented a proto-type 2-D discrete element program to simulate granular particle structure in different packing environments of sedimentary rocks. All particle shapes are assumed square to realize angular coarse particle depositions and limit simulation process time. However, this angular particle shape can enhance developments of potential internal microcracks/discontinuity or hidden pore structures inherited from the grain size difference. Stagnant packing mode simulated a lake or low tide sea environment where granular particles settled under a stagnant water condition and only allowed vertical movement. The packing was performed one dimensionally with no lateral agitation allowed. Reciprocal packing mode simulated severe tidal action during particle sedimentation in a marine valley environment with alternative deposition orientations/sequences. Densely packing mode simulated a pore structure to produce the maximum unit weight for discrete particle group different in size and number. Oversized void, or discontinuity was not generated in this mode to produce the minimum porosity of sedimentary rocks. Based on simulation results, well graded or poorly sorted discrete particles produced more various pore size distribution and more extensive microcrack generation in both stagnant and dynamic settlement modes. Program is able to count the individual pore/crack numbers and sizes after the packing simulation. Although the program did not handle self-healing or re-closure of unrealistic large cracks or discontinuity which would not take place in nature environment, simulation outputs of microcrack and discontinuity orientation still can help understand the tendency of anisotropic fracture development associated with fracking/ well stimulation for shale gas/oil production.

INTRODUCTION

Fracture and discontinuity development degree of source and cap rocks is closely related to oil and gas reservoir productivity. Beside geologic joints and faults in macro scale, pore connectivity and microcracks within sedimentary rocks in micro scale are also concerned in oil/gas industry especially for feasibility study of hydraulic fracturing (fracking) or other well stimulations.

Clastic sedimentary rocks (conglomerate, sandstone, siltstone, shale, and mudstone) bear characteristics of anisotropic and scale dependent permeability due to

numerous bedding and transverse joints originated from deposition process, foliation and/or non-conformity during sedimentation/metamorphic process, shear, dilation, hybrid and sheeting joints by tensional or shearing stress during geological formations (fault, thrust and fold) and columnar joints by thermal stress (Singal and Gupta, 2010). Among the various influencing factors on the sedimentary rock permeability, author is interested in the settling process of quartz rich sedimentary rocks and contribution of grain size gradation and packing process related to the microcrack development which possibly impact artificial fracture generation within the clastic sedimentary rock associated with fracking or other well stimulations.

Although intact (igneous or metamorphic) rocks do not look like granular material, series of mineral crystallization at different temperatures produced lattices between mineral crystals. The presence of submicron discontinuity in the rock matrices induces brittle behaviors (cleavage) of rocks by simulating the initiation, propagation and interaction of local defects. In general, sedimentary rocks contain more microcracks and larger discontinuity compared to the intact rocks because numerous pore spaces between discrete particles and discontinuities between bedding planes had been formed during the deposition process and was weakly consolidated through cementation process not as much as foliation or recrystallization with metamorphic process. Thus, the material property of clastic sedimentary rocks needs to be related to grain size gradation, grain shapes and particle array at settling process and bonding strength at cementation process (Price, 2009).

Discrete Element Method (DEM) is known capable of simulating pore structure and discontinuity of granular materials under various external loads. Most of DEMs use disks in two dimension or spherical elements in three dimension because only a single value, the diameter is required to define the geometry of the discrete elements and there is only one possible type of contact among particles, which can be detected easily (Donze *et al*, 2008). In general, there exist two different DEM approaches; either a dynamic algorithm or a geometric algorithm. The dynamic method uses Newton's second law of motion to determine the trajectory and the particle final positions inside a container whereas the geometric method generates particle packing which uses geometric functions applied on disks or spheres. The advantage of using geometric methods over dynamic methods to generate dense polydisperse packing is to lower the computation time (Donze *et al*, 2008). Among the geometric algorithms, Al-Raoush and Alsaleh (2007) developed a most updated algorithm using tetrahedral meshes to generate dense isotropic arrangements of non-overlapping spheres of different particle sizes which enables faster computation and more accurate generation of composite media.

DEM models are frequently used to investigate densely packing structure and lump sum porosity estimation based on a round shaped particle. However, actual shapes of sedimentary rock grains are closer to polygon or angular shape rather than sphere or round one. Thus, a new DEM model capable of simulating various packing modes and counting individual pore sizes between discrete elements will be required to simulate actual pore structures of sedimentary rock.

METHODOLOGY

Author invented a proto-type two dimensional simulation program to investigate pore and internal microcrack structures of quartz-rich (siliceous) sedimentary rock formation in stagnant (no lateral agitation allowed), reciprocal (tidal or alternate deposition direction) and dense (constraint for a minimal pore volume) deposition environments. All particle shapes are assumed with square rather than genuine polygon due to limited advancement of multi-directional packing algorithm and to save computation time in a PC environment. However, this square shape of particle is considered to enhance discrepancy of microcracks/discontinuity or pore structures inherited from non-homogenous grain sizes and shapes of sedimentary rocks. Figure 1 presents conceptual scheme of model to generate two dimensional pore structure of sedimentary rock.

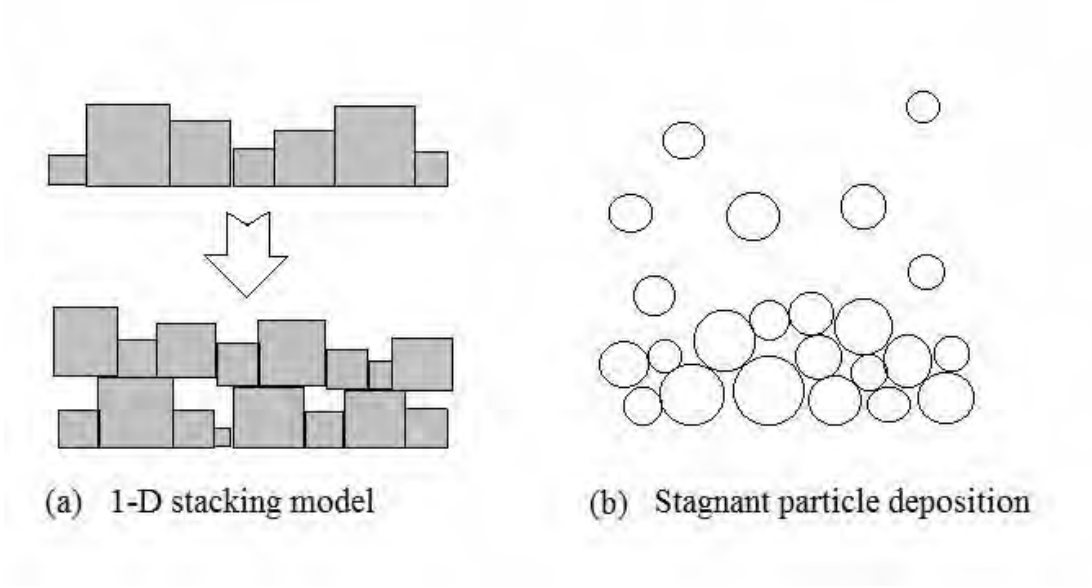

FIG. 1. Schematic plot of vertical stacking under stagnant deposition

In program, up to 10 discrete particle size and number ratio between grain sizes can be assigned as input parameters. This program is not using dynamic equations which find force and momentum equilibriums during particle deposition but using a geometric method which control uniformness and randomness of size/number distribution of discrete elements in light of statistical and probabilistic aspects.

This prototype program is a particle stacking simulator in two dimension. Thus, user should convert mass or volume based GSD (grain size distribution) into area based GSD using proportional relationship between number ratios of discrete particle sizes in a fractal scale. Particle numbers are limited to consider array capacity and computation time of the program. If user selects 1,2,3,4 and 5 discrete square sides with a number ratio of 10:5:3:2:1, program will pack 441 particles (21^2), consisting of 210 particles of square area 1, 105 particles of square area 4, 63 particles of square area 9, 42 particles of square area 16, 21 particles of square area 25. Program first determines the optimal initial particle coordinates to meet stochastic prerequisites, uniformity and randomness of discrete particle positions through an iterative

optimization prescreening process with statistic control parameters. This prescreening process prevents simulation from producing extreme deposition cases severely skewed with respect to either uniformity or randomness in individual particle positions. In general, the un-skewed stochastic prerequisites become more critical as analysis domain expands since the feature of micro-pore and extended discontinuity will be magnified by a large scale simulation. Figure 2 demonstrates the feature of pore structure dependent on analysis scale.

Stagnant packing mode simulates an alluvial/fluvial sediment condition where granular particles settled under stagnant water and only allowed for vertical stacking. Packing is performed one dimensionally with no lateral movement allowed.

Reciprocal packing mode simulates aerial or tidal deposition condition at basin region with alternative deposition sequence in alternative directions perpendicular to each other. Unrealistic large void and discontinuity can be generated from the simulation while self-healing (re-closure) of large discontinuity would take place during sedimentation process in nature.

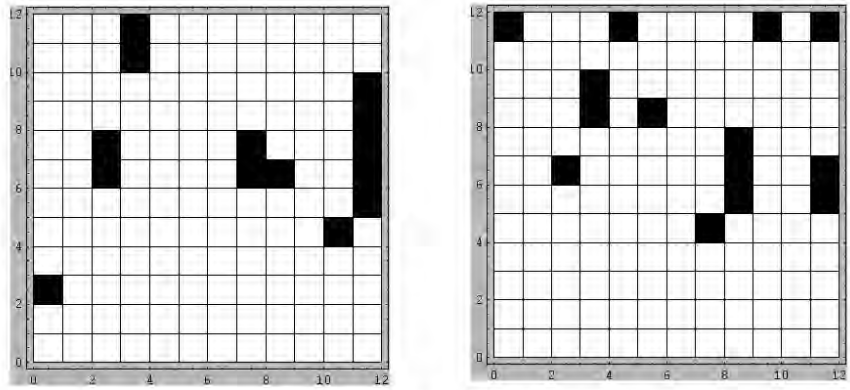

(a) Small scale model with paricle size 1d:2d

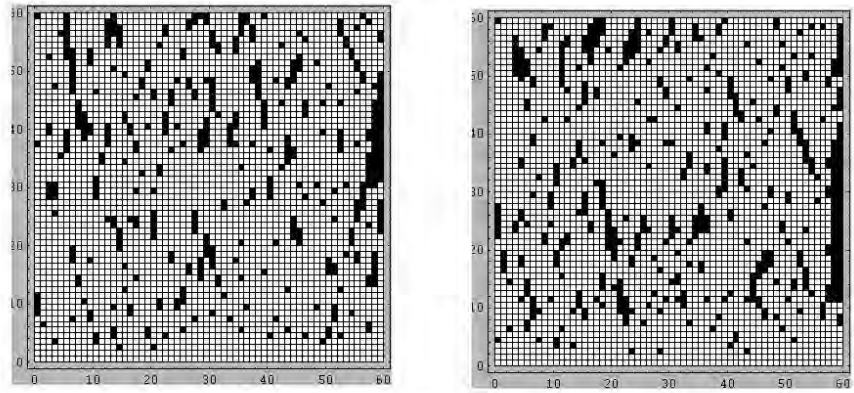

(b) Large scale model with particle size 1d:2d

FIG. 2. Scale effect on discrete element model especially in term of discontinuity

Dense packing simulates a pore structure with the minimum void area based on given particle size and number ratio. Enlarged void or discontinuity cannot be

observed in the outputs due to simulation of fully constrained packing environment under significant confining stress in geologic formation. For the same grain size distribution, Figure 3 compares the pore structure bearing various micro-cracks produced from stagnant deposition environment with the theoretically densest packing pore structure allowing no internal microcrack.

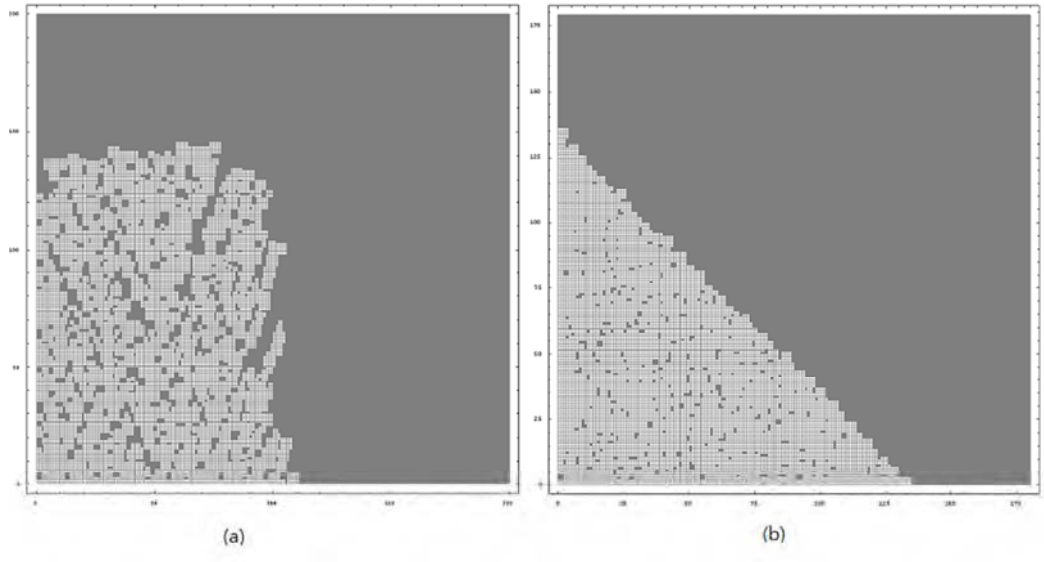

FIG. 3. Simulated pore structure of sedimentary rock with discrete grain size (number ratios of 2d:3d:4d = 10:10:10 where 2d, 3d and 4d are relative particle sizes in diameter) in (a) stagnant deposition and (b) densely packing structure

RESULTS

Sedimentary rock microcracks inherited from particle size difference and settling environment would produce anisotropic hydraulic permeability associated with prevailing orientation of microcracks. Figures 4 (a) and (b) compares different features of sedimentary rocks in intensity and orientation of the microcracks, associated with the change in particle size and deposition process. In the simulation, well graded particles produced enlarged discontinuity compared to the poorly graded or well sorted particles. This can be identified in Figures 4 (c) and (d) of polarizing microscopic photos for actual sandstones showing different grain size gradations.

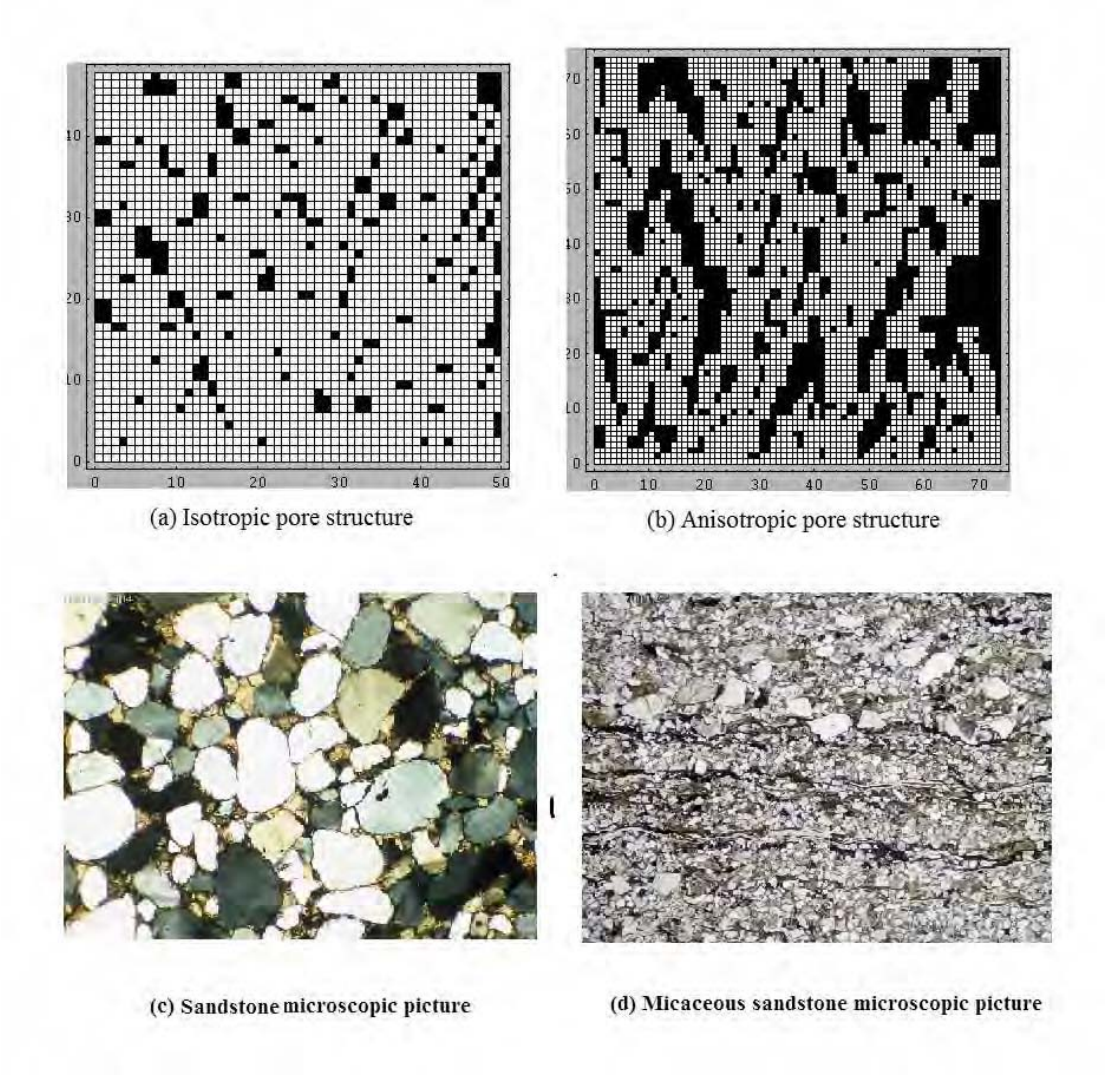

FIG. 4. Isotropic and anisotropic hydraulic properties of sedimentary rock with microcracks due to difference in grain size and deposition environment ((a) and (b) present the simulated results, and (c) and (d) present the actual polarizing microscopic photos of sandstone (from http://www.earth.ox.ac.uk/~oesis/micro/).

Simulation outputs of Figure 5 support above finding as the intensity of micro-cracks is proportional to fine grain content within sedimentary rock. As the content of fine grain increases, the discontinuity and porosity also increase in both number and size for either stagnant or reciprocal packing mode. The aperture width of microcracks also increases as the density of microcrack is intensified, which need be verified by more refined simulation in future or further microscopic investigation on actual loosely packed sedimentary rock matrix.

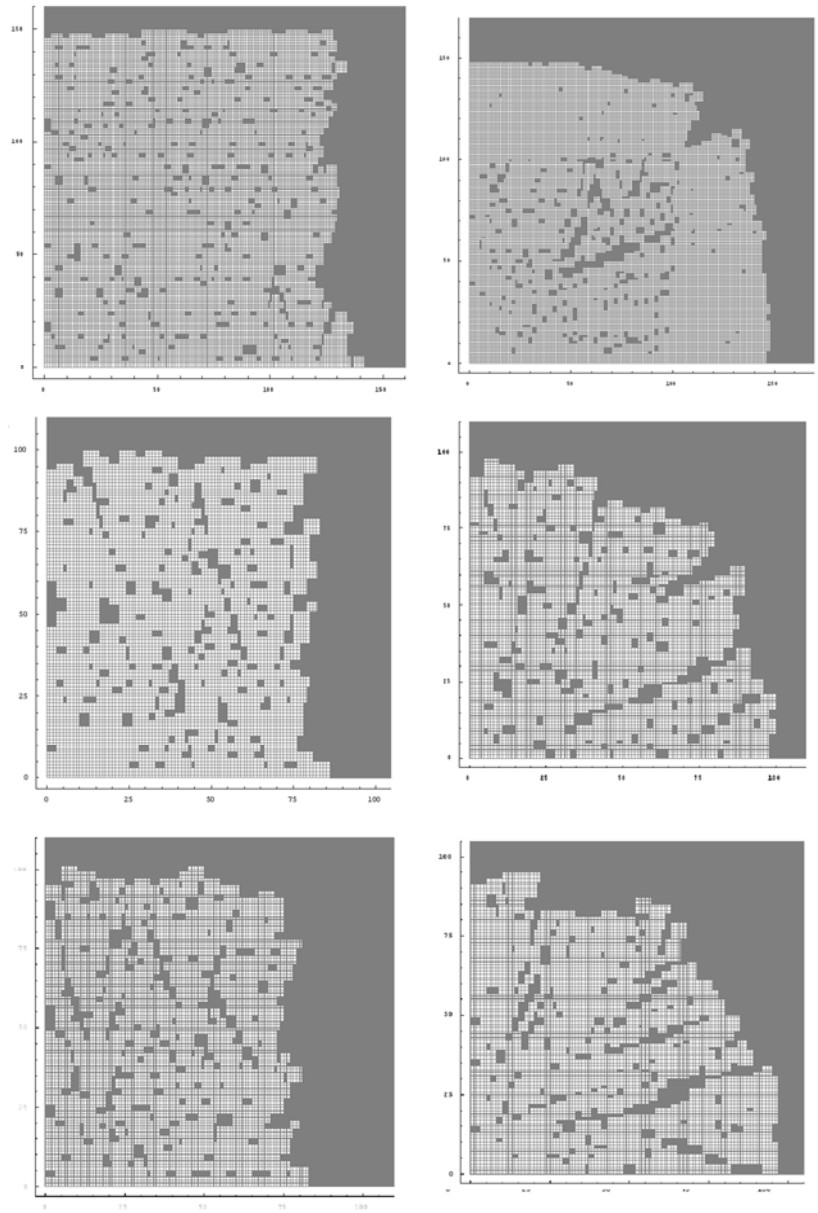

FIG. 5. Tendency of microcrack generation within quartz rich sedimentary rock dependent on composition ratio of fine and coarse grains whereas stagnant deposition outputs in left column and reciprocal deposition outputs in right column, and different number ratios between fine and coarse particles, 3d:5d=10:20 (upper row); 10:10 (middle row); 14:7 (bottom row) where 3d and 5d are relative particle sizes in diameter.

Compared with dual grain size model in Figure 5, more intensive microcrack structures were generated as the fine grain content increases in triple grain size model (Figure 6).

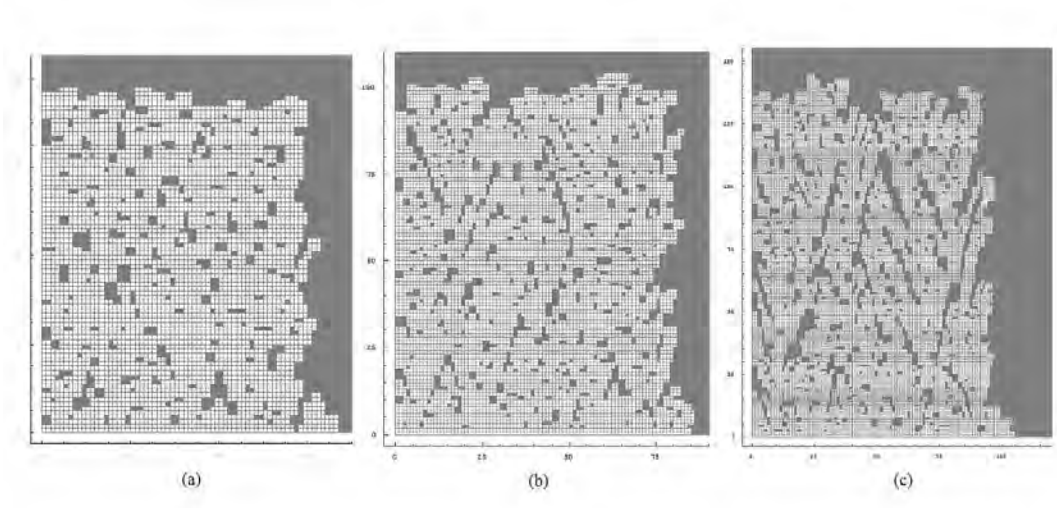

FIG. 6. Grain size gradation effect on microcrack production for the different composition ratios of grain sizes (2d:3d:4d= (a) 10:7:5, (b) 15:10:5 and (c) 20:10:5 where 2d, 3d and 4d are relative particle sizes in diameter)

The magnified discontinuity of sedimentary rock is likely to prevail in a larger scale model as shown in Figure 7. Both results were based on the same number ratio of discrete particle size (2d:3d:4d=1:1:1), but different particle numbers such as 225 (=15^2) and 900 (=30^2) were used in the stagnant deposition simulation.

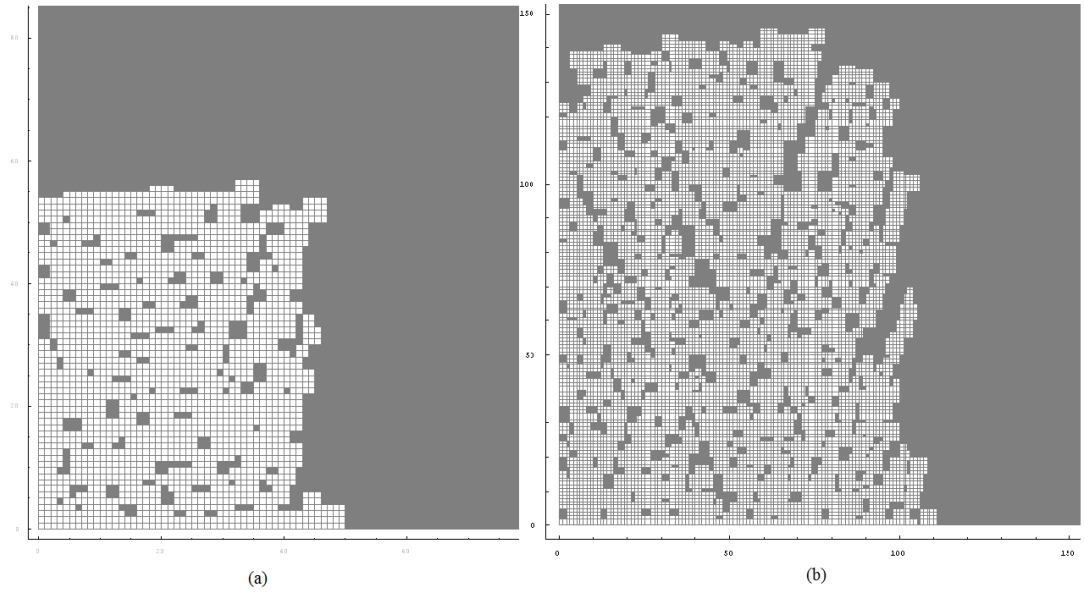

FIG. 7. Scale effect on microcrack propagation for the same composition ratio of grain sizes (2d:3d:4d= (a) 5:5:5 and (b) 10:10:10 where 2d, 3d and 4d are relative particle sizes in diameter)

The number of microcracks turned out to be proportional to total particle number used in packing simulation. Thus, individual void sizes including microcracks were analyzed and the void numbers were counted based on the several simulation outputs. Table 1 indicates the model porosity defined as counted void area divided by analysis area converged to a limiting value (0.2) as the model scale increases.

Table 1. Scale Effect on Porosity of Microcracks Based on Simulation Outputs (Particle diameter ratio=1d:2d:3d)

ϕ1:ϕ2:ϕ3	N1 : N2 : N3			**Analysis area**	**Counted pore area**	**Porosity**
multiplier	5	6	4			
1	5	6	4	225	36	0.125
2	10	12	8	900	192	0.152
3	15	18	12	2025	445	0.171
4	20	24	16	3600	888	0.192
5	25	30	20	5625	1452	0.201

The above scale effect becomes more evident in gap or poorly graded case which presented a tendency of porosity increment proportional to the analysis scale as shown in Figure 8. Thus, a large particle number should be used in the DEM simulation when a sedimentary rock contains a relatively small content of fine grain. In Figure 8, large values of porosity were also produced from the cases containing a relatively large content of fine grain, which is consistent to the previous finding that enlarged discontinuities were found for the simulation output from broad range of grain size.

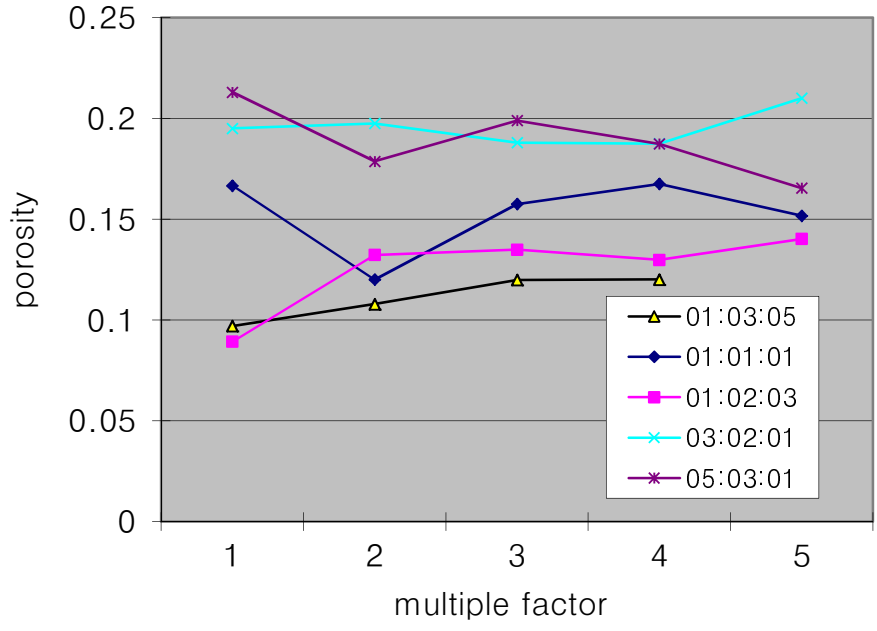

FIG.8. Relationship between porosity variation by grain gradation versus analysis domain size (numbers corresponding to 1d, 2d and 3d in particle size)

The size of microcrack was also analyzed with number frequency of each individual pore size counted from the void size analyzer embedded in the program. Poorly graded case (Cu=1.5) exhibited relatively high frequency of small sized pore (such as pore size equal to or below 4) whereas relatively high frequency of microcracks (such as pore size equal to or greater than 5) was observed in well graded case (Cu=4).

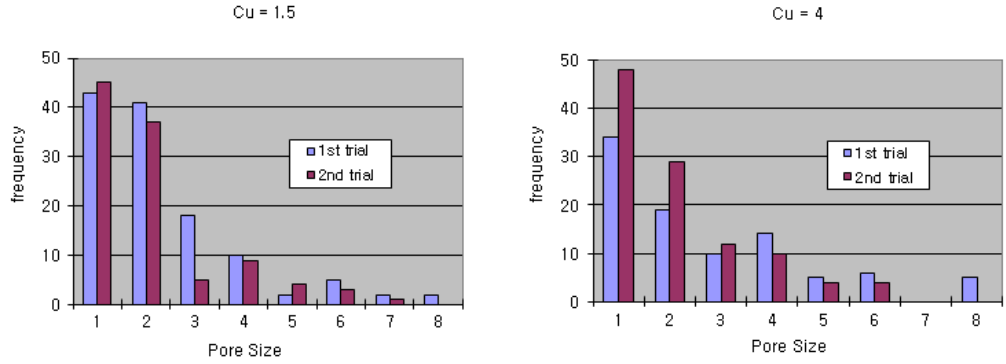

FIG. 9. Differentiation of pore size distribution based on grain gradation of quartz rich sedimentary rock (Cu: uniformity index defined by D_{60}/D_{10}, the particle sizes of which correspond to 60% and 10% of GSD)

CONCLUSIONS

Simulation outputs for well graded sedimentary rocks produced more various pore size distribution and larger microcrack/discontinuity in both stagnant and reciprocal deposition environments. Orientations and extents of microcracks presented in the outputs were clearly differentiated by grain size gradation and packing mode. Some simulation outputs revealed unrealistic pore structure features containing extremely large discontinuities between grain matrices. While this proto-type program did not encompass self-healing process or re-closure of unrealistic voids/discontinuities associated with the stagnant and dynamic packing modes, which would take place in nature sedimentation environment, the simulated outputs still can envision tendency of micro-crack development in quartz rich sedimentary rock and metamorphic cleavage features inherited from the grain size difference. This microcrack study can contribute to sophisticate geomechanical analysis on the production rock formation in conjunction with prevailing fracture/joint system identified from the field investigations to improve efficiency of new fracture generation associated with the fracking and other well stimulations.

REFERENCES

Al-Raoush, R., and M. Alsaleh (2007) "Simulation of random packing of polydisperse particles", Powder Technology, Vol. 176, pp. 47-55.

Donze F.V., V. Richefeu & S.A. Magnier (2009), "Advances in Discrete Element Method applied to Soil, Rock and Concrete Mechanics", in State of the art of geotechnical engineering, Electronic Journal of Geotechnical Engineering, p. 44,

Price, David George (2009) "Engineering Geology, Principles and Practice", Michael Freitas (Ed.), Springers, Chapter 2, pp. 21-61.

Singhal, B.B.S. and Gupta, R.P. (2010) "Applied Hydrology for Fractured Rocks", Second Edition, Springers, Chapter 2, pp. 13-24

Fracture Mechanics Evaluation of Parameters Associated with Horizontal Hydrofracturing

Luis E. Vallejo[1], Ph.D., M.ASCE and Jason Shamrock[2], M.S.

[1]Professor, Department of Civil & Environmental Engineering, University of Pittsburgh, Pittsburgh PA 15261, U.S.A., E-mail: vallejo@pitt.edu
[2]Former Graduate Student, Department of Civil & Environmental Engineering, University of Pittsburgh, Pittsburgh, PA 15261, U.S.A.

ABSTRACT: The horizontal portion of the borehole used to extract gas from shale deposits is made of an annulus of cement and a metal casing. This annulus has a series of diametrically opposed cracks made by a perforating gun. The annulus with the cracks is subjected to a fluid pressure or hydrofracturing. Little is known about the influence of the number, depth, and separation of the cracks on the fluid pressure efficiency in cracking the shale. The main objective of this study is to use fracture mechanics theory to evaluate the effect of the number, separation and depth of the gun induced cracks on the hydrofracturing of the shale. The level of tensile stress induced by the hydrofracturing fluid is a function of the Mode I stress intensity factor K_I . This study indicated that K_I was the highest for the case of two single diametrically opposed vertical cracks. K_I was found to decrease in value as the number of diametrically opposed cracks increased in number and decreased in separation. Also, regardless of the number of the gun induced cracks, as the depth of these cracks increased in value, the K_I value generally increased in value.

INTRODUCTION

To utilize the extensive natural gas resources in the Appalachian region, horizontal hydraulic fracturing has been developed. Fig. 1 outlines the method. First, a vertical well is drilled in the area above the Marcellus shale using a drill bit located at the tip of a drill pipe. The drilling is made to a depth of about 450 meters. This point is known as the "kick off" point. When this point is reached, the vertical drilling is forced to proceed in a curve until it reaches the Marcellus shale. At the shale location (at depth that varies between 1,980 to 4,500 meters), the drilling becomes horizontal (Fig. 1). After the drilling is complete, the drill pipe is removed and a casing is inserted in the borehole. Then, cement is pushed into the casing until it reaches the end of the drilling borehole. When the cement reaches the end or tip of the casing, it flows through an opening in the casing and into the interface between the casing and the shale. Thus, the borehole is sealed by an annulus made of cement and the casing.

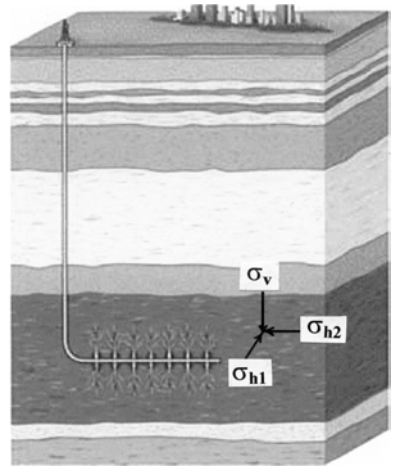

FIG. 1. Horizontal hydrofracturing of shale deposits

The annulus has a thickness that varies between 2.54 and 5.08 cm. The next step is the introduction of a perforating gun into the casing. This perforating gun uses remote controlled charges to produce small holes (cracks) in the annulus and the adjacent shale. The perforating gun develops these holes (cracks) in sections 15 to 24 meters in length. After the holes (cracks) in the casing and the adjacent shale are made, the perforating gun is removed. The horizontal portion of the borehole is ready for hydrofracturing.

Next, a fluid made of water, sand and additives is pushed under high pressures into the vertical and horizontal sections of the borehole. This fluid under pressure moves through the holes in the annulus and the adjacent shale and induces further cracking of the shale. These cracks are normal to the smallest horizontal, lateral stress in the shale (σ_{h1} or σ_{h2} in Fig. 1). This stress is smaller than the vertical overburden stress, σ_v (Soliman, et al., 1990; Soliman and Boonen, 2000). This smaller horizontal stress can be obtained from the vertical overburden stress (σ_v) by using the relationship $\sigma_h = [\nu/(1 - \nu)][\sigma_v]$, where ν is the Poisson's ratio. The vertical overburden stress $\sigma_v = \gamma h$, where γ is the average unit weight of the rock layers above the Marcellus shale. The height h varies between 1,980 and 4,500 meters.

Very little has been published about the mechanics of the horizontal hydrofracturing of shales. For example, little has been published about the effect that the number, extension and separation of the gun induced cracks have on the efficiency of the fluid pressure used to cause hydrofracturing of the shale. Also, very little is known about the state of the stresses near the tip of the induced cracks (Soliman et al., 1990; Soliman and Boonen, 2000). The main objective of this study was to clarify the above issues using linear elastic fracture mechanics theory.

FRACTURE MECHANICS EVALUATION OF HORIZONTAL HYDROFRACTURING

Fracture mechanics analysis of a circular hole with two single opposed cracks under an effective tensile stress

If the horizontal stress σ_{h1} is the smallest of the two horizontal stresses shown in

Fig. 1, the bore hole with the two opposing cracks will look like in Fig. 2. The two opposing cracks will grow in the direction normal to σ_{h1} (Fig. 1).

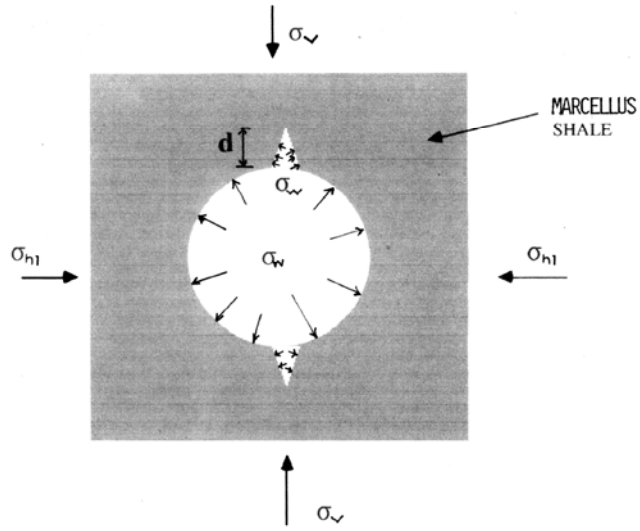

FIG. 2. Stresses on the horizontal borehole with two single opposed cracks

The shale with the annulus and two single cracks are subjected to a vertical overburden pressure σ_v and a lateral horizontal stress σ_{h1}. As explained in the previous section, $\sigma_{v} > \sigma_h$ and their values can be easily calculated using the known values for the depth of the annulus in the shale, the unit weight of the sedimentary rocks above the annulus, and the Poisson's ratio of the shale.

After the hydro-fracturing fluid is injected under pressure in the annulus, this pressure will produce a fluid pressure, σ_w , on the walls of the circular annulus and the small angular holes induced in the annulus by the perforating gun (Fig. 2). The fluid pressure, σ_w , will have to overcome the shale lateral pressure σ_{h1} and the tensile strength of the shale T_0 . In other words, the fluid pressure for hydrofracturing to take place should be:

$$\sigma_w > \sigma_{h1} + T_0 \qquad (1)$$

Thus, in order for the cracks in the annulus and the adjacent shale to propagate further into the shale in a direction normal to the minor lateral stress, σ_{h1} , an overall tensile effective stress, σ_{e1} , should be effective. Fluid induced crack propagation in the shale will take place when (Fig. 3):

$$\sigma_{e1} = \sigma_w - \sigma_{h1} - T_0 \qquad (2)$$

When the tensile effective stress, σ_{e1} , acts on the shale enclosing the annulus and the two cracks**,** hydrofracturing induced propagation of the cracks will develop in the shale. Because of lack of published data about the value of the effective stress σ_{e1} that causes the propagation of the two cracks, a value of σ_{e1} = 7 MPa will be used in

this study. Using this value for σ_{e1} and the fracture mechanics approach developed

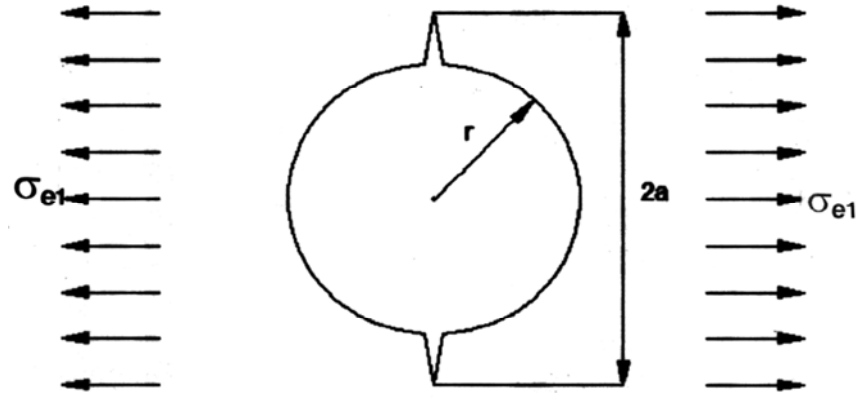

FIG. 3. A horizontal borehole with two cracks subjected to an effective tensile stress σ_{e1}.

by Simha (2001) (Fig. 3), one can obtain the stress intensity factor, K_I, induced in the shale by the circular borehole and the two opposing cracks. This stress intensity factor, K_I, has the following value (Fig. 4):

$$K_I = \sigma_{e1} (\pi a F)^{1/2} \quad (3)$$

Where a is the length shown in Fig. 3, and F is a parameters that can be obtained from the following relationship Simha (2001):

$$F = (1 - \sin\frac{\pi r}{a})[1 - (\frac{r}{a})^5]^{0.78} + 1.23(\sin\frac{\pi r}{a})(\frac{r}{a})^{0.19} \quad (4)$$

where r is the radius of the circular borehole (Figs. 2 and 3).

Using Eq. (3) the values for K_I were obtained. To obtain these values of K_I, a value for $\sigma_{e1=}$ 7 MPa was used. For the borehole radius a value of r = 12.7 cm was used. For the crack depths, d (Fig. 2), the values used varied between 0 and 20 cm. Using the values for these parameters and using Eqs. (2) and 4), a plot of the K_I values in function of the crack depths, d, is shown in Fig. 4 (Simha , 2001).

An analysis of Fig. 4 indicates that the stress intensity factor K_I increases with the initial depth d of the two cracks [Figs. 2 and 3 and Eq. (3)]. Since crack propagation takes place when the stress intensity factor K_I is equal to or greater than the critical stress intensity factor K_{IC} (Jayatilaka, 1979), crack propagation is influenced by either the initial depth d of the cracks, or the value of the effective tensile stress σ_{e1}. Typical values of K_{IC} for the Marcellus shale have recently been published in a report by Engelder (2012).

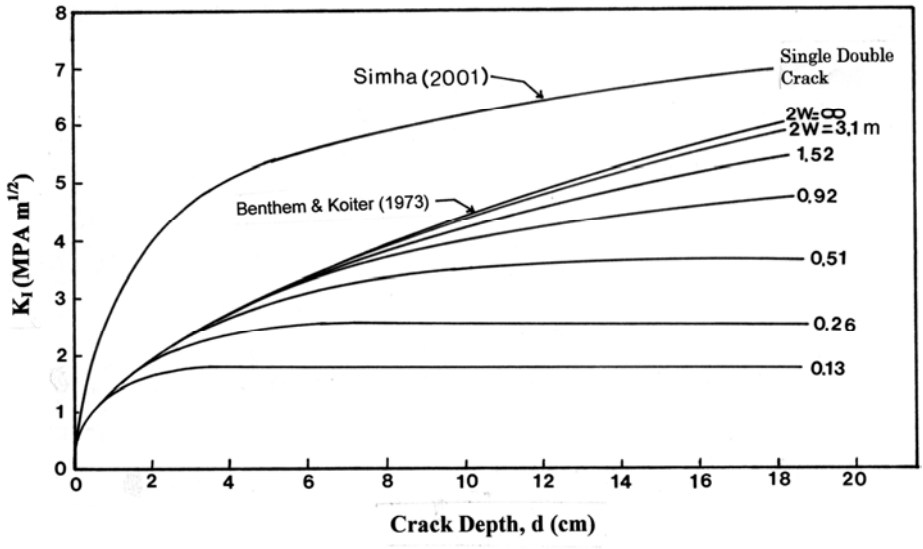

FIG. 4. Stress intensity factor KI in function of crack depth, d, and crack separation W.

Fracture mechanics evaluation for a series of aligned cracks under a tensile stress

If the horizontal stress σ_{h2} is the smallest of the two horizontal stresses shown in Fig. 1, the bore hole with the gun induced cracks will look like in Fig. 5. This figure shows the aligned cracks before (Fig. 5) and during (Fig. 6) the hydrofracturing process.

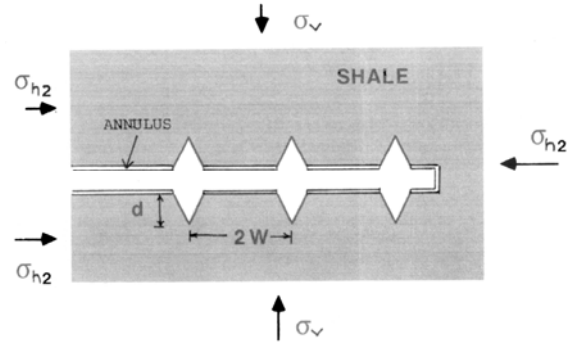

FIG. 5. A group of three cracks aligned normal to σ_{h2} in Fig. 1 before the hydrofracturing process.

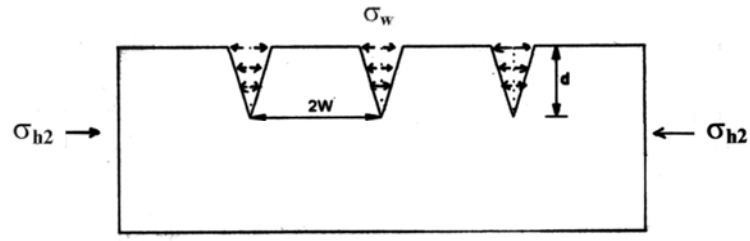

FIG. 6. A group of three cracks aligned normal to σ_{h2} in Fig. 1 during the hydrofracturing process.

An analysis of Fig. 6 indicates that the fluid pressure, σ_w acting during the hydrofracturing process on the two intermediate shale blocks cancel each other. That is, the fluid pressure σ_w acting on the first, second and third cracks are of equal magnitude and opposite direction. Therefore, they cancel each other. The only fluid pressures effective in Fig. 6 are the fluid pressure σ_w on the first and third cracks. This fluid pressure act in opposite direction to the horizontal shale pressure σ_{h2}. Thus, the three aligned cracks will be subjected to a resultant effective tensile stress σ_{e2} (Fig. 7) that can be obtained from the following relationship:

$$\sigma_{e2} = \sigma_w - \sigma_{h2} - T_0 \quad (5)$$

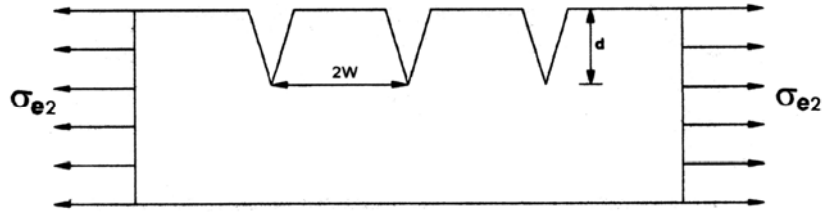

FIG. 7. A group of three aligned cracks subjected to an effective tensile stress σ_{e2}

For the case of Fig. (7) the stress intensity factor KI can be obtained from the following relationship (Benthem and Koiter, 1973):

$$K_I = \sigma_{e2} \ (\pi \, d \, S)^{1/2} (D) \quad (6)$$

where S and D can be obtained from the following relationships

$$S = \frac{1}{1 + \frac{d}{W}} \quad (7)$$

$$D = \frac{1}{(\pi)^{0.5}}\left[1 + \frac{1}{2}S + \frac{3}{8}S^2 + \frac{5}{16}S^3 + \frac{35}{128}S^4 + \frac{63}{256}S^5 + \frac{231}{1024}S^6\right]$$

$$+ 22.501S^7 - 63.502S^8 + 58.045S^9 - 17.577S^{10} \quad (8)$$

In Eqs (6), (7), and (8) d and W are the depth and half the separation of the cracks (Fig.7), and S and D are parameters that are function of d and W.

Using Eqs. (6) to (8), the value of the stress intensity factor K_I was plotted against the depth of the cracks, d, for different values of the cracks' separation, W. The resulting curves are shown in Fig. 4. To obtain these curves of K_I versus d, a value for $\sigma_{e2=}$ 7 MPa was used. For the crack depths, d (Fig. 7), the values used varied between 0 and 20 cm. The values of 2W used in the plots varied in value between 0.13 meters and an infinite value (which represents the case of a single crack) (Benthem and

Koiter, 1973).

An analysis of Fig. 4 indicates that the stress intensity factor K_I increases with the initial depth d of the cracks for values of 2W equal or greater than 0.92 m. For values of 2W smaller than 0.92 m, the value of the stress intensity factor K_I reaches a maximum value at small values of d and then remain constant after that. Fig. 4 also indicates that the separation of the cracks W has a detrimental effect on K_I. The closer the cracks are, the lower is the value of K_I. This result indicates that the fluid pressure is less efficient in causing crack propagation in the shale with cracks closely spaced.

Since crack propagation takes place when the stress intensity factor K_I is equal to or greater than the critical stress intensity factor K_{IC} (Jayatilaka, 1979), crack propagation is influenced by the initial depth d of the cracks, their separation W, and the value of the effective tensile stress σ_{e2} [Eq. (6)]. Typical values of K_{IC} for the Marcellus shale have recently been published in a report by Engelder (2012).

State of stresses at the crack tips

The stresses near the tips of the cracks shown in Figs. 3 and 7 are shown in Fig. 8.

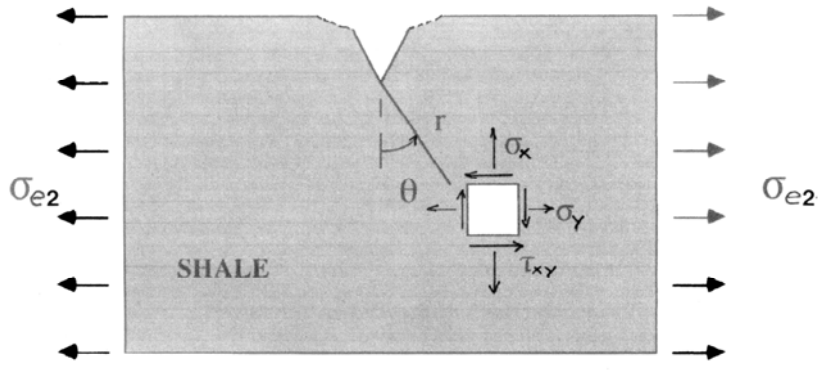

FIG. 8. Stresses near the tip of a crack

According to Jayatilaka (1979) the stresses σ_x, σ_y, and τ_{xy} can be obtained from the following relationships (Fig. 8):

$$\sigma_x = \frac{K_I}{(2\pi r)^{1/2}} \cos\frac{\theta}{2}\left(1 - \sin\frac{\theta}{2}\sin\frac{3\theta}{2}\right) \quad (9)$$

$$\sigma_y = \frac{K_I}{(2\pi r)^{1/2}} \cos\frac{\theta}{2}\left(1 + \sin\frac{\theta}{2}\sin\frac{3\theta}{2}\right) \quad (10)$$

$$\tau_{xy} = \frac{K_I}{(2\pi r)^{1/2}} \cos\frac{\theta}{2}\left(\sin\frac{\theta}{2}\cos\frac{3\theta}{2}\right) \quad (11)$$

where the value of K_I can be obtained from Eq, (6) and the rest of the terms are shown in Fig. 8.

Using the values of σ_x, σ_y, and τ_{xy} one can obtain the value of the magnitude and direction of the principal stresses near the tip of the crack (Vallejo, 1986, 1987; Vallejo and Liang, 1994). The principal stresses σ_1 and σ_3 as well as their directions can be obtained from the following relationships:

$$\sigma_{1,3} = \frac{(\sigma_x + \sigma_y)}{2} \pm [(\frac{\sigma_x - \sigma_y}{2})^2 + (\tau_{xy})^2]^{1/2} \quad (12)$$

$$\psi = (1/2)\tan^{-1}(\frac{2\tau_{xy}}{\sigma_x - \sigma_y}) \quad (13)$$

$$\lambda = \psi + \frac{\pi}{2} \quad (14)$$

where ψ is the angle that the direction of σ_3 makes with the vertical line in Fig, 8, and λ is the angle that the direction of σ_1 makes with the vertical line in Fig. 8.

Using Eqs. (6) through (14), the principal stresses and their directions are plotted near the tip of a crack as shown in Fig. 9. The values of the magnitude and direction of the principal stresses can be used to determine the direction of secondary cracks that develop in the shale surrounding the original gun induced cracks (Vallejo et al., 2013).

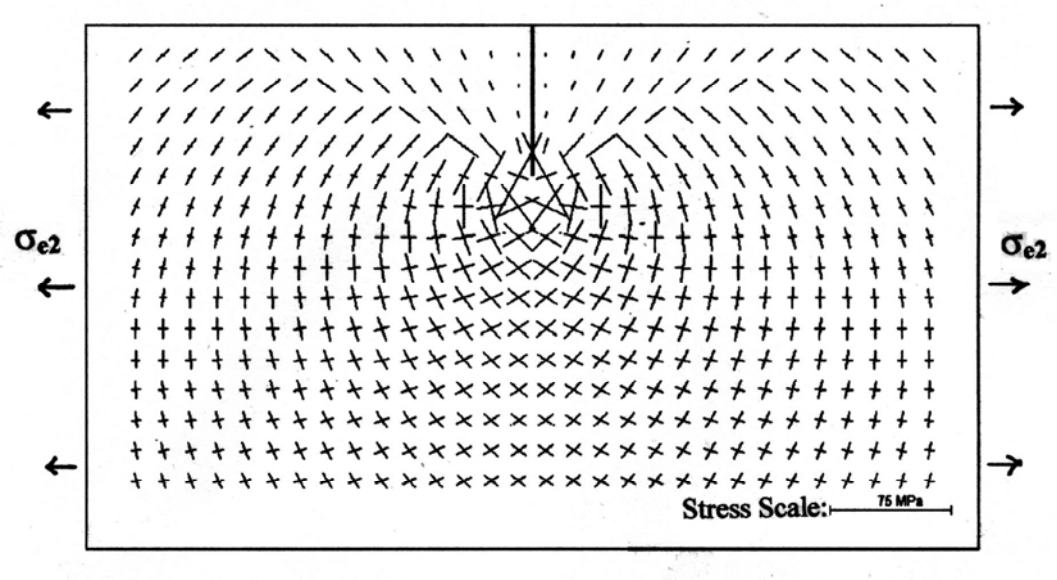

FIG. 9. Magnitude and direction of the principal stresses σ_1 and σ_3 (both in tension) for the case of a crack with d = 12.7 cm and σ_{e2} = 7 MPa.

CONCLUSIONS

From this study the following conclusions can be reached:

(1) Linear Elastic Fracture Mechanics (LEFM) theory was determined to be an excellent theoretical tool to analyze the way cracks associated with horizontal hydrofracturing propagate in shale deposits.

(2) The cracking efficiency of the fluid pressure associated with horizontal hydrofracturing was found to depend on the size of the perforating gun induced cracks. The larger the size of the cracks, the more efficient the hydrofracturing method,

(3) The separation of the multiple cracks induced by the perforating gun associated with horizontal hydrofracturing was also found to have and influence on the efficiency of the hydrofracturing method. The larger are the separation between the gun induced cracks, the more efficient is the fluid pressure used in cracking shale deposits.

ACKNOWLEDGMENTS

The work described in this study was partially supported by Grant No. ECE-8414931 to the University of Pittsburgh by the National Science Foundation, Washington D.C. This support is gratefully acknowledged.

REFERENCES

Benthem, J.P., and Koiter, W.T. (1973). "Asymptotic approximations to crack problems." In: *Mechanics of Fracture, Vol. I, Methods of Analysis and Solutions of Crack Problems,* Sih, G.C. (Ed.), Noordhoff, Leiden, the Netherlands, 131- 178.

Engelder, T. (2012). *Geomechanical Model for Gas Shale Based on the Integration of Stress Measurements and Petrophysical Data from Greater Marcellus Gas System*. Report RPSEA Contract 09122-32 to Pennsylvania State University, 13 p., http://www.netl.doe.gov/technologies/oil-ga

Jayatilaka, A. (1979). *Fracture Mechanics of Engineering Brittle Materials*. Applied Science Publishers, Barking, Essex, England.

Simha, K.R.Y. (2001). *Fracture Mechanics For Modern Engineering Design*. University Press, Hyderguda, Hyderababd, India.

Soliman, M.Y., Hunt, J.L., and El Rabaa, A.M. (1990). "Fracturing aspects of horizontal wells." *Journal of Petroleum Technology,* **42**(8): 966-973.

Soliman, M.Y., and Boonen, P. (2000). "Rock mechanics and stimulation aspects of horizontal wells. *Journal of Petroleum Science & Engineering,* **25**: 187-204.

Vallejo, L.E. (1986). "Mechanics of crack propagation in stiff clays." In: *Geotechnical Aspects of Stiff and Hard Clays,* R.P. Khera, and W. Lovell, Eds., Geotechnical Special Publication No. 2, ASCE Press, New York, pp. 14-27.

Vallejo, L.E. (1987). "The influence of fissures in a stiff clay subjected to direct shear." *Geotechnique,* **37**(1): 69-82.

Vallejo, L.E., and Liang, R. (1994). *Fracture Mechanics Applied to Geotechnical Engineering*. Geotechnical Special Publication No. 43, ASCE Press,

Reston, VA.
Vallejo, L.E., Shettima, M., and Alaasmi, A. (2013). "Unconfined compressive strength of brittle material containing multiple cracks." *International Journal of Geotechnical Engineering,* **7**(3): 318-322.

Numerical Simulation of Simultaneous Growth of Multiple Interacting Hydraulic Fractures from Horizontal Wells

Andrew P. Bunger[1], Ph.D., and Anthony P. Peirce[2], Ph.D.

[1]Assistant Professor, Department of Civil and Environmental Engineering, Swanson School of Engineering, University of Pittsburgh, 3700 O'Hara Street, Pittsburgh, PA 15261, USA, email: bunger@pitt.edu
[2]Professor, Department of Mathematics, The University of British Columbia, #121-1984 Mathematics Road, Vancouver, B.C. V6T 1Z2, Canada, email: peirce@math.ubc.ca

ABSTRACT: The technique of multistage hydraulic fracturing from horizontal wells is universally credited with enabling the economical production of hydrocarbon resources from shale formations. The method almost always entails the injection of fluid through the wellbore with the potential to create hydraulic fractures from multiple reservoir entry points, typically clusters of wellbore perforations, that are spaced out along the wellbore within a section that is colloquially referred to as a "stage". Arguably the most basic question about this situation is how many perforation clusters within a given fracturing stage can be expected to produce growing hydraulic fractures. This paper presents a numerical investigation of this issue that employs a newly-developed, fully coupled parallel planar 3D hydraulic fracturing simulator that features: implicit time stepping, an implicit level set scheme to locate the propagating hydraulic fracture fronts that respond to their regimes of propagation and enables highly accurate simulations using a very coarse mesh, and the capability to dynamically partition the fluid among multiple, simultaneously growing hydraulic fractures in parallel, overlapping planes. Our results demonstrate the dependence of the energetically preferred number of growing hydraulic fractures on the length of the isolated zone, the height of the reservoir, and the relative importance of the fluid viscosity. In particular, we show that reservoirs with effective height containment and injection strategies that ensure substantial viscous dissipation will promote growth of multiple simultaneous hydraulic fractures rather than localization to just one or two dominant fractures.

INTRODUCTION

Multistage hydraulic fracturing from horizontal wells is currently the petroleum industry's most important reservoir stimulation technology; without it, hydrocarbons from shale reservoirs could not be produced economically (e.g. King 2010). However, production logging often shows that more than half of perforation clusters are non-producing (Miller and Waters 2011).

This failure to generate uniformly distributed production highlights two issues that

are currently detrimental to optimal recovery. The first is failure to adapt the well completion strategy in the light of variability in reservoir properties, including the in-situ stress, along the well (e.g. Baihly et al. 2011). The second is the propensity of hydraulic fractures (HFs) to exert stresses on each other thereby suppressing the growth of some or most of the HFs attempting to extend from an array of entry points such as perforation clusters. This phenomenon, called "stress shadowing", has been studied using multiple fracture models for well over a decade (e.g. Gemanovich et al. 1997, Olson 2004, Fisher et al. 2004, Abass et al. 2009, Meyer and Bazan 2011).

These two issues, and their management, are at the core of mechanically-justified engineering decisions - such as length of each stimulation interval and spatial distribution of perforation clusters within the interval - which will have a first order effect on the productivity of the well. It is therefore vital to improve on the current situation wherein these critical engineering decisions are often made with little guidance from models that rigorously capture the essential physical mechanisms that determine the impacts of these decisions on HF growth.

Recognizing the value of simulations that capture the complexity that can be generated through the interaction of multiple, simultaneously growing hydraulic fractures (e.g. Germanovich et al. 1997, Olson and Dahi-Taleghani 2009, Damjanac et al. 2010, Cipolla et al. 2011, Nagel et al. 2011, Meyer and Bazan 2011, Kresse et al. 2013, McClure and Horne 2013), a different and complimentary approach has recently been developed that uses simple analytical models to clarify the basic contributors to the energy balance of a system of multiple, simultaneously growing and parallel HFs (Bunger 2013). The analysis is built on the premise is that, given a well interval of a certain length with multiple entry points, the number of HFs that will actually grow corresponds to the number that minimizes the required energy input. The resulting analytical models show how the required energy input depends on the number of HFs and how this dependence is affected by HF geometry, fluid viscosity and injection rate, mechanical properties of the rock, and perforation geometry (Bunger 2013, Bunger et al. In Press).

The analytical modeling has therefore proven useful for discerning the mechanisms that control the overall behavior of the system. But the approach is restrictive on both the geometry and the number of coupled phenomena that can be considered. Hence there is a need for a new, fully-coupled numerical simulator that can systematically test the analytical predictions and that can be progressively enhanced to capture increasingly more complex behavior. Such a model can therefore be seen as providing bridge between theory and the predictions of design-oriented HF simulators that prioritize rapid computation enabled by substantial simplifications of the underlying mechanical model, which almost always include a local treatment of the elasticity equations according to the so-called pseudo 3D approach (e.g. Meyer and Bazan 2011, Kresse et al. 2013).

As a first step in this reconciliation between theory and numerical simulation, this paper presents a comparison between the analytical predictions of Bunger (2013) and a newly-developed, fully coupled parallel planar 3D hydraulic fracturing simulator. This new simulator features an implicit level set scheme to locate the propagating hydraulic fracture fronts that respond to their regimes of propagation and enables highly accurate simulations using a very coarse mesh, and the capability to

dynamically partition the fluid among multiple, simultaneously growing hydraulic fractures in parallel, overlapping planes. Consistent with the predictions of Bunger (2013), these simulations demonstrate that two factors, substantial dissipation of energy through viscous fluid flow and effective containment of height growth, are critical to promoting simultaneous growth of multiple hydraulic fractures.

SUMMARY OF ANALYTICAL PREDICTIONS

Bunger (2013) and Bunger et al. (In Press) discovered that there are 3 critical factors that determine the propensity for multiple hydraulic fractures to growth simultaneously. These are: 1) HF geometry, 2) perforation pressure loss, and 3) dissipation of energy through viscous fluid flow. Hence we can contrast arrays of plane strain (2D), radial (penny-shaped), and blade-like (or "PKN") HFs, each of which gives strikingly different predicted behavior. For a start, the 2D cases always favor growth of one HF regardless of the number of and/or spacing between the entry points. Because this geometry is common for modelling but not very representative even of idealized HFs in the field, we conclude that 2D simulators will overstate the tendency of HFs to localize.

In contrast, arrays of penny-shaped hydraulic fractures favor growth from all perforation clusters as long as viscous dissipation of energy dominates the energy dissipation associated with breakage of the rock. Radial fractures will persist until their radius is around 0.8 times the spacing, at which point the elastic interaction or "stress shadow" effect causes a progressive localization to fewer HFs. If rock fracture dominates the energy balance, penny-shaped HF arrays will immediately favor growth of a single HF.

For height limited HFs that attain a PKN geometry the behavior is different again. Here the model predicts an energetically preferred spacing that results from a competition. On the one hand, minimization of the viscous energy dissipation drives the system to favor very closely spaced HFs, as was shown for the penny-shaped case. On the other hand, the stress shadow energetically penalizes the system when the HFs are close together. In the PKN case these competing processes result in an energetically-preferred spacing that is around 2.5 times the HF height in the absence of perforation losses and can be as little as 1.2 times the HF height with large perforation losses.

DESCRIPTION OF THE NUMERICAL MODEL

The numerical model assumes that fractures are propagating within parallel planes that are spaced h_k apart in a perforation stage of length Z within a pay zone of height H (see Fig. 1). The numerical model uses the Implicit Level Set Algorithm (ILSA) (Peirce and Detournay, 2008) to model the propagation of fractures with arbitrarily shaped boundaries within each of the parallel planes, which are assumed to be perpendicular to the minimum principal stress direction. The fractures are assumed to propagate in a three dimensional elastic medium at a rate that is sufficiently slow for the elastic medium to be in a state of static equilibrium. For details see Peirce and Bunger (In Review).

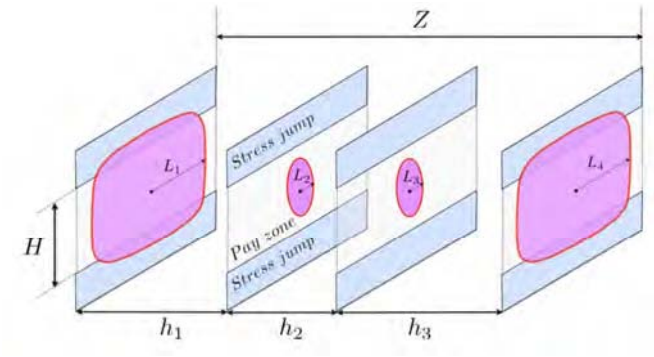

FIG. 1. Geometric configuration of the experimental perforation stage of length *Z* within a pay zone of height *H* in which h_k is the fracture spacing. After Peirce and Bunger (In Review).

NUMERICAL RESULTS

Radial Growth in Toughness Dominated Regime

Firstly we simulate simultaneous injection into 5 entry points spaced uniformly at 30 m so as to cover a 120 m interval of the wellbore. Injection parameters are chosen so that the total simulation time satisfies (e.g. Detournay 2004)

$$t_{TOT} >> \left(\frac{\mu' Q_o^3 E'}{K'^{18}} \right)^{1/2}$$

The typos in the powers of mu and E need to be fixed

where Q_o is the volumetric injection rate and 1) $\mu' = 12\mu$ for the fluid viscosity μ, 2) $E' = E/(1-\nu^2)$ for the Young's modulus E and Poisson's ratio ν, and 3) $K' = (32/\pi)^{1/2} K_{Ic}$ for the rock fracture toughness K_{Ic}. This constraint provides a convenient definition of the so-called toughness dominated regime for radial HFs. Consistent with this constraint, the following parameter values are chosen for this example:

$$E = 9.5\,GPa \qquad \nu = 0.2 \qquad K_{Ic} = 1.5\,MPa.m^{1/2}$$
$$\mu = 0.001\,Pa.s \qquad Q_0 = 0.0265\,m^3/s \qquad Z = 120\,m$$
$$\sigma_{zz}^0 = 70\,MPa \qquad \Delta\sigma_{zz}^0 = 0\,MPa$$

Fig. 2a shows a snapshot of the 5 HFs when the outer 2 have reached a radius of about 30 m. The inner HFs are clearly suppressed. Fig. 2b shows that the inner HFs grow uniformly with the outer HFs until their radius is about 0.15 times they spacing. Localization then commences favoring the outer HFs while the inner HFs attain a radius around 0.2 times the spacing and do not grow any further over the duration of the simulation.

Radial Growth in Viscosity Dominated Regime

As in the previous case, here we simulate simultaneous injection into 5 entry points spaced uniformly at 30 m so as to cover a 120 m interval of the wellbore. However, here the injection parameters are chosen so that the simulation is run in the so-called viscosity dominated regime for radial HFs. Within this constraint, the following parameters are chosen for this example:

$$E = 9.5\,GPa \qquad \nu = 0.2 \qquad K_{Ic} = 0MPa.m^{1/2}$$
$$\mu = 1\,Pa.s \qquad Q_0 = 0.1\,m^3/s \qquad Z = 120\,m$$
$$\sigma^0_{zz} = 70MPa \qquad \Delta\sigma^0_{zz} = 0MPa$$

Fig. 3a shows a snapshot of the 5 HFs when the outer 2 have reached a radius of about 30 m. The inner HFs are somewhat suppressed in their growth, although not nearly as strikingly as in the toughness dominated case. In fact, as shown in Fig. 3b, even after the outer HFs begin to be favored when the radius attains about 0.3 times the spacing, the inner HFs continue to grow and only trail the outer HFs by about 20% when the radius of the outer HFs is approximately equal to the spacing. Hence we observe that for viscosity dominated HFs the localization commences later than in the toughness dominated regime (here "later" means that the radius attains a larger value relative to the spacing). Furthermore the localization is less pronounced once it commences.

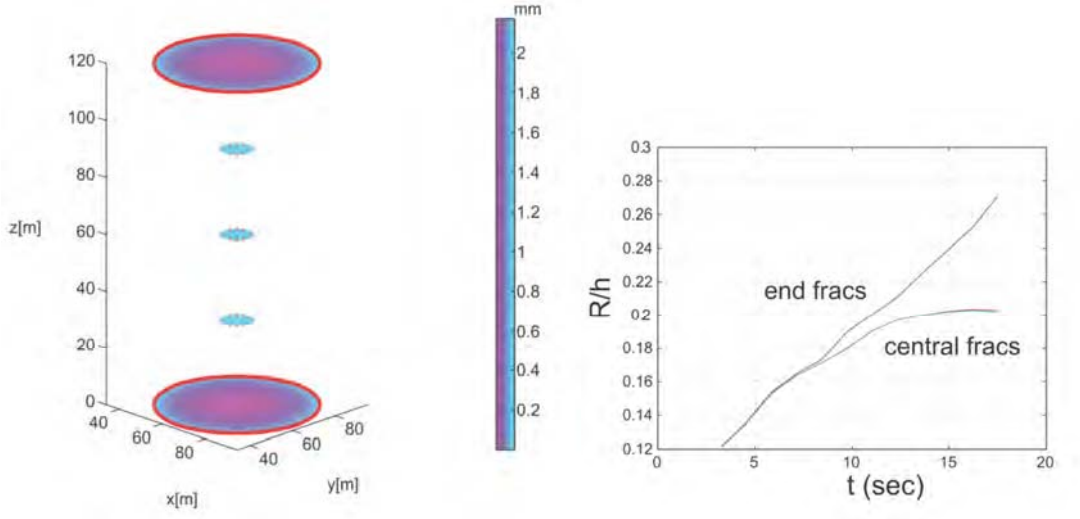

a) **b)**

FIG. 2. Radial toughness regime. a) 5 hydraulic fractures with contours corresponding to opening. b) Evolution of the radius of the fractures normalized by the spacing between them.

Blade-like Growth with Stage Length Greatly Exceeding HF Height

Here we simulate simultaneous injection into 7 entry points spaced uniformly at 20 m so as to cover a 120 m interval of the wellbore. Here we ensure growth that is strictly in the viscosity dominated regime by setting the rock fracture toughness to be small and the viscosity and pump rate to be relatively large. The set of parameters for this example are otherwise chosen as:

$$E = 9.5\,GPa \qquad \nu = 0.2 \qquad K_{Ic} = 0.157MPa.m^{1/2}$$
$$\mu = 1\,Pa.s \qquad Q_0 = 0.0265\,m^3/s \qquad Z = 120\,m$$
$$\sigma^0_{zz} = 70MPa \qquad \Delta\sigma^0_{zz} = 5\,MPa \qquad H = 12\,m$$

The main difference between this case and the radial viscosity-dominated case is there here we have imposed the condition that the injection takes place within a 12 m wide strip of low stress so that height growth is naturally limited.

Fig. 4a shows a snapshot of the 7 HFs when they have reached a length of about 40 m. In this case the array is nearly uniform; the inner HFs trail behind in terms of length by only a few percent as shown in Fig. 4b. We observe, then, that height constraint promotes extensive uniform growth when the spacing is on the order of 2 times the HF height.

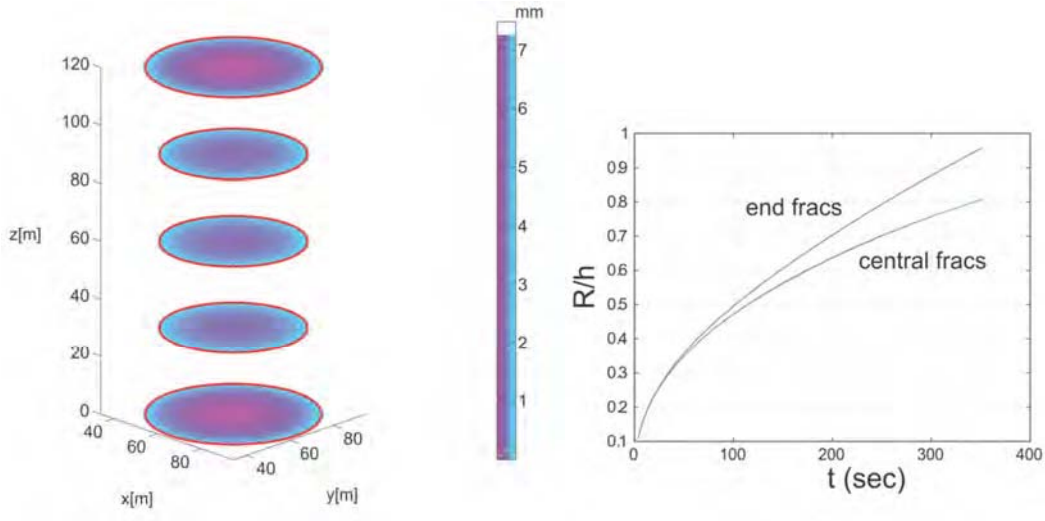

a) **b)**

FIG. 3. Radial viscosity regime. a) 5 hydraulic fractures with contours corresponding to opening. b) Evolution of the radius of the fractures normalized by the spacing between them.

Blade-like Growth with Stage Length Equal to HF Height

The previous case showed the propensity of height limited HFs to extensively grow simultaneously in the viscosity dominated regime as long as their separation is large enough relative to their height. In contrast, we finally simulate 5 HFs with a uniform spacing of 5 m so as to cover a 20 m interval within a 20 m high zone of low stress that limits height to approximately the same value. We ensure growth that is strictly in the viscosity dominated regime by setting the rock fracture toughness to zero. The set of parameters for this example are otherwise chosen as:

$$E = 9.5\ GPa, \quad \nu = 0.2, \quad K_{Ic} = 0\ MPa{\cdot}m^{1/2}$$
$$\mu = 1\ Pa{\cdot}s, \quad Q_0 = 0.1\,m^3/s, \quad Z = 20\,m$$
$$\sigma_{zz}^0 = 70\,MPa, \quad \Delta\sigma_{zz}^0 = 5\,MPa, \quad H = 20\,m$$

Fig. 5a shows the suppression of the inner HFs, consistent with a number of similar simulation results (e.g. Gemanovich et al. 1997, Olson 2004, Fisher et al. 2004, Abass et al. 2009, Meyer and Bazan 2011). However, somewhat surprisingly the suppression of the inner HFs can be mitigated, as shown in detail by Peirce and Bunger (In Review). Using the same pumped volume as that in the uniformly spaced array shown in Fig. 5a but with the entry points placed at z=0,3.5,10,16.5, and 20 m instead, we obtain a completely different HF growth pattern as shown in Fig. 5b.

Hence we find that specific non-uniformly spaced arrays can promote multiple simultaneous HF growth. In this example, as pointed out by Peirce and Bunger (In Review), the fracture surface area shown in Fig. 5b exceeds the fracture surface area in Fig. 5a by about 50%. If primary hydrocarbon recovery scales with surface area, then recovery rates could be improved by as much as 50% through modification of the entry-point locations.

DISCUSSION

The overall contrasting behaviors are: 1) growth of only the outer HFs in the array for toughness dominated radial hydraulic fractures and for uniformly-spaced arrays of PKN hydraulic fractures, 2) growth of all HFs in an array for radial growth in the viscosity dominated regime until the radius is 0.5-1 times the spacing, 3) persistent growth of multiple HFs for arrays of PKN fractures that are either spaced more widely than their height or that are strategically non-uniformly spaced according to the method of interference fracturing proposed by Peirce and Bunger (In Review).

The observations from these numerical experiments are consistent with the analytical predictions of Bunger (2013) with respect to the critical role of viscosity and geometry on the propensity for multiple simultaneous HF growth. Pressure loss through the perforations has not yet been implemented in the simulator so its role, as predicted by Bunger et al. (In Press), cannot yet be tested through numerical experiments with this simulator.

The simulations do, however, provide insight to the importance of the end effects of the array. That is, the array is not strictly uniform as in the analytical model of Bunger (2013) and Bunger et al. (In Press), but instead the outer HFs experience a different stress state than the inner HFs because they have one side that is not subjected to any stress shadow. In the case of widely-spaced PKN HFs the impact is that the outer HFs grow a few percent more rapidly than the inner HFs; from the perspective of estimating overall behavior this is arguably a negligible impact. For the radial viscosity-dominated and the short PKN array, the end effects apparently determine which HFs are favored by localization, but the basic prediction of Bunger (2013) of the presence and timing of localization is supported.

From the perspective of overall behavior, the only variation from the analytical predictions of Bunger (2013) is relatively subtle and is found in the radial toughness-dominated case. Bunger (2013) predicts immediate localization and Bunger et al. (In Press) show that this immediate localization can be mediated by perforation losses such that all HFs can grow to a radius around 0.2 times the spacing. However, the numerical model shows an early period where all HFs grow until the radius becomes 0.1-0.2 times the spacing in the absence of perforation losses. Furthermore, as pointed out by Bunger (2013), the analytical model cannot discern whether localization will favor growth of 1 or 2 HFs. The numerical experiments indicate localization to 2 HFs rather than 1. The dominant factor in this 2 way partitioning of fluid rather than strict localization to a single HF is probably driven by the small but finite contribution of viscous dissipation for the numerical simulations in the toughness dominated regime. This small contribution is ignored by the analytical model. However, including it in order to better predict the nature of localization to 1 versus 2 HFs generally and early-time localization in the radial toughness-dominated cases specifically should be

relatively straight forward and will comprise a useful extension of these research efforts.

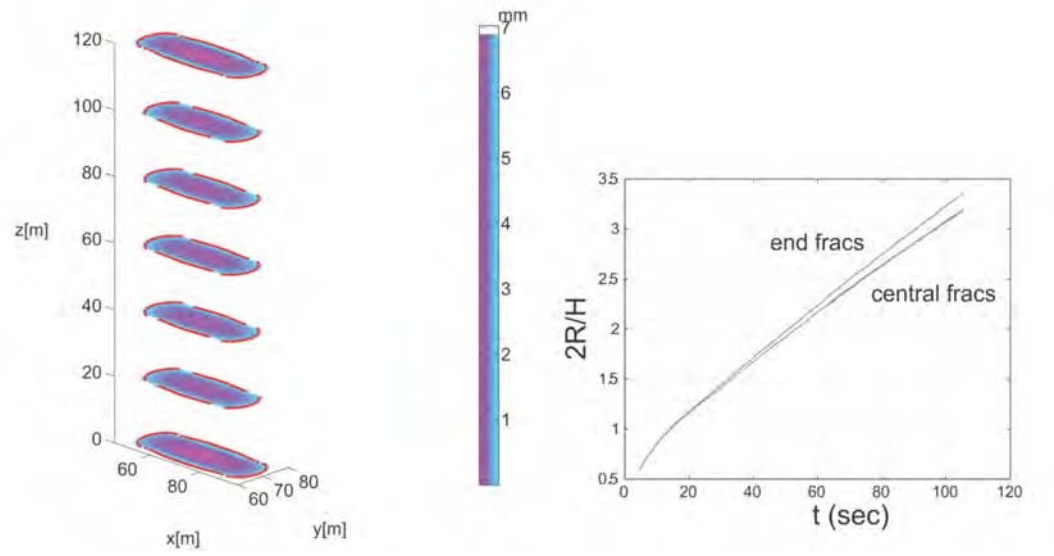

a) b)

FIG. 4. Height limited hydraulic fractures with spacing larger than the height. a) 7 hydraulic fractures with contours corresponding to opening. b) Evolution of the radius of the fractures normalized by the spacing between them.

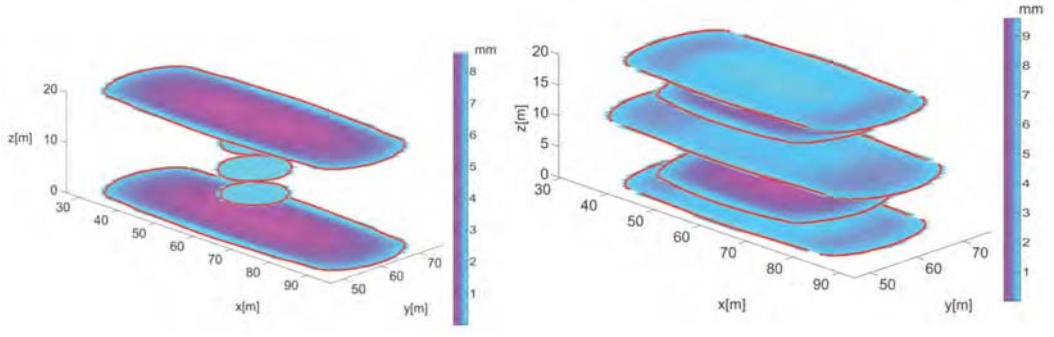

a) b)

FIG. 5. Height limited hydraulic fractures with spacing smaller than the height. a) Uniformly spaced HFs. b) Non-uniformly spaced HFs after Peirce and Bunger (In Review).

CONCLUSIONS

The basic conditions that promote or suppress multiple simultaneous HF growth from arrays of entry points (i.e. perforation clusters) along horizontal wells are critical for design. Recent analytical models (Bunger 2013, Bunger et al. In press) are aimed at providing basic insights into this issue, while, on the other hand, design-

oriented numerical models (e.g. Damjanac et al. 2010, Cipolla et al. 2011, Nagel et al. 2011, Meyer and Bazan 2011, Kresse et al. 2013, McClure and Horne 2013) are concerned with demonstrating details of the complexity that can characterize the problem. Here we present a new numerical model that aims at bridging the gap between theory and simulation. This fully-coupled, parallel planar 3D model has been used here to perform numerical experiments testing the predictions of Bunger (2013), namely that multiple simultaneous growth will be promoted by large viscous dissipation and height constraint. Both of these overall predictions of the theory are supported by the numerical experiments. Furthermore, we have observed some behaviors related to toughness-dominated HFs with small but finite viscous dissipation, as well as systems with 2 growing HFs, could be of practical importance and should be considered in future theoretical developments. Finally, we present an example showing that the complicated nature of systems of multiple HFs can lead to surprising results and unexpectedly simple strategies for promoting simultaneous growth that entail moderate perturbations to the locations of the perforation clusters.

ACKNOWLEDGMENTS

The authors appreciate the support of the International Engineering Foundation, the University of Pittsburgh Center for Energy, and the Natural Sciences and Engineering Research Council of Canada (NSERC).

REFERENCES

Abass, H. H., Soliman, M. Y., Tahini, A. M., Surjaatmadja, J., Meadows, D. L., and Sierra, L. (2009). Oriented fracturing: A new technique to hydraulically fracture an openhole horizontal well. Proceedings SPE Annual Technical Conference and Exhibition, New Orleans, LA, USA. SPE 124483.

Baihly, J. D., Malpani, R., Edwards, C., Han, S. Y., Kok, J. C. L., Tollefsen, E. M., and Wheeler, C. W. (2010). Unlocking the shale mystery: How lateral measurements and well placement impact completions and resultant production. Proceedings SPE Tight Gas Completions Conference, San Antonio, Texas, USA. SPE 138427.

Bunger, A. P. (2013). Analysis of the power input needed to propagate multiple hydraulic fractures. *Int. J. Solids Struct.*, 50, 1538–1549.

Bunger, A. P., Zhang, X., and Jeffrey, R. G. (In Press). Constraints on simultaneous growth of hydraulic fractures from multiple perforation clusters in horizontal wells. *Soc. Pet. Eng. J.*

Cipolla, C., Weng, X., Onda, H., Nadaraja, T., Ganguly, U., and Malpani, R. (2011). New algorithms and integrated workflow for tight gas and shale completions. Proceedings SPE Annual Technology Conference and Exhibition, Denver, Colorado, USA. SPE 146872.

Damjanac, B., Gil, I., Pierce, M., Sanchez, M., van As, A., and McLennan, J. (2010). A new approach to hydraulic fracturing modeling in naturally fractured reservoirs. Proceedings 44th U.S. Rock Mechanics Symposium, Salt Lake City, Utah, USA. ARMA 10-400.

Detournay, E. (2004). Propagation regimes of fluid-driven fractures in impermeable rocks. *Int. J. Geomechanics*, 4(1), 1–11.

Germanovich, L. N., Ring, L. M., Astakhov, D. K., Shlyopobersky, J., and Mayerhofer, M. J. (1997). Hydraulic fracture with multiple segments II: Modeling. *Int. J. Rock Mech. Min. Sci*., 34(3-4), 472.

King, G. E. (2010). Thirty years of gas shale fracturing: What have we learned? Proceedings SPE Annual Technical Conference and Exhibition, Florence, Italy. SPE 133256.

Kresse, O., Weng, X., Gu, H., and Wu, R. (2013). Numerical modeling of hydraulic fractures interaction in complex naturally fractured formations. *Rock Mechanics and Rock Engineering*, 46(3), 555–568.

McClure, M. W. and Horne, R. N. (2013). *Discrete Fracture Network Modeling of Hydraulic Stimulation: Coupling Flow and Geomechanics*. Springer Briefs in Earth Sciences. Springer, New York.

Meyer, B. and Bazan, L. (2011). A discrete fracture network model for hydraulically induced fractures-theory, parametric and case studies. Proceedings SPE Hydraulic Fracturing Technology Conference and Exhibition, The Woodlands, Texas, USA. SPE 140514.

Miller, C. and Waters, G. (2011). Evaluation of production log data from horizontal wells drilled in organic shales. Proceedings SPE North American Unconventional Gas Conference and Exhibition, The Woodlands, Texas, USA. SPE 144326.

Nagel, N., Gil, I., Sanchez-Nagel, M., and Damjanac, B. (2011). Simulating hydraulic fracturing in real fractured rocks - overcoming the limits of pseudo3D models. Proceedings SPE Hydraulic Fracturing Technology Conference and Exhibition, The Woodlands, Texas, USA. SPE 140480.

Olson, J. E. (2004). Predicting fracture swarms – the influence of subcritical crack growth and the crack-tip process zone on joint spacing in rock. The initiation, propagation, and arrest of joints and other fractures, , J. W. Cosgrove and T. Engelder, eds., Geological Society, London, vol. 231, 73–87.

Olson, J. E. and Dahi-Taleghani, A. (2009). Modeling simultaneous growth of multiple hydraulic fractures and their interaction with natural fractures. Proceedings SPE Hydraulic Fracturing Technology Conference and Exhibition, The Woodlands, Texas, USA. SPE 119739.

Peirce, A. and Detournay, E. (2008). An implicit level set method for modeling hydraulically driven fractures. *Computer Meth. Appl. Mech. Eng*, 197, 2858–2885.

Peirce, A. P. and Bunger, A. P. (In Review). Interference fracturing: Non-uniform distributions of perforation clusters that promote simultaneous growth of multiple hydraulic fractures. *Soc. Pet. Eng. J*. pre-print available at: http://hdl.handle.net/2429/45492.

Subcritical Crack Propagation Enhanced by Chemical Injection

M.M. Hu[1] and T. Hueckel[2]

[1]Ph.D Candidate, Department of Civil & Environmental Engineering, Duke University, Durham, NC 27708, U.S.A., E-mail: manman.hu@duke.edu.
[2]Professor, Department of Civil & Environmental Engineering, Duke University, Durham, NC 27708, U.S.A., E-mail: hueckel@duke.edu.

ABSTRACT: This paper studies the conditions of crack propagation in a subcritically stressed rock subject to chemically aggressive environment, which is often encountered in technologies of oil/gas extraction from low-permeability reservoirs. Frequently, matrix acidizing is employed, upon which mineral mass is dissolved and washed away by fracturing fluids. Such a mineral mass removal weakens the material mechanically and causes crack propagation and eventually permeability changes in the medium. The crack process zone is modeled mathematically using a recently developed chemo-plasticity coupling model. The coupling is established between mineral dissolution and a yield limit of rock matrix via chemo-plastic softening function. The rate of dissolution is a function of a rate constant and variable internal specific surface area, which is in turn affected by the initial void ratio as well as dilatant micro-cracking induced by irreversible damage (treated as a plastic strain). Numerical simulations for such a coupled system are performed under simplified boundary conditions.

INTRODUCTION

The use of hydraulic fracturing is becoming more and more common across the globe due to its efficiency in creating fractures in the rock formation, which dramatically enhances rock permeability and increases the subsequent oil/gas production (Jackson et al., 2011, Rahman, 2008). Recently, attention has shifted towards enhancing the fracture propagation by acidizing the rock, especially as it applies to carbonate reservoirs with low permeability. The most recent examples in the literature include a German study on the application of matrix acidizing for the enhancement of a geothermal system (Zimmermann et al., 2010), a Regular Mud Acid (RMA) stimulation that was applied to a Soultz Enhanced Geothermal System (EGS) reservoir in France (Portier and Vuataz, 2010), and a study by He et al. (2010) that investigated the creation of wormholes by acidizing tight carbonate reservoirs.

However, the actual process is very complex and has several different coupled mechanisms, which has caused the modeling of fracture enhancement to fall far

behind its practice. Additionally, there has been a heated debate on the use of acidizing for hydraulic fracturing due to the potential harm that could be caused by the disposal and transport of the toxic wastewaters, which could include formaldehyde, boric acid, hydrochloric acid, and isopropanol (Coffman, 2009). Poorly controlled hydraulic fracturing, likely caused by an inadequate understanding of the acid-rock interactions, may not only pose a threat to the environment but also generate unnecessary costs and lower productivity.

This paper investigates the possible chemo-mechanical mechanisms of rock/shale weakening and how these mechanisms enhance the fracture propagation. A crack tip case study is considered in which the degradation is caused by advanced irreversible deformation, modeled as a swarm of mode I micro-fissures, around the crack tip. The chemically induced propagation of a crack under stress is investigated by implementing an extension of the Cam-Clay model into a chemical model (Hueckel, 2002); in particular, the model couples chemical softening with the irreversible deformation (Hueckel et al., 1998, Hueckel and Hu, 2009).

MODEL DESCRIPTION

We consider a crack that is under pressure from a pressurized fluid that pushes against the crack walls and whose surrounding material is being chemically weakened. The fluid pressure causes dilatant damage near the edges of the crack that causes local chemo-mechanical coupling. The stress at the crack-tip is particularly significant due to the stress concentration at that location. The extended Johnson approximation (Johnson, 1970), which reduces the stress distribution to an axially symmetric system (see e.g. Collins and Stimpson, 1994 or Bigoni and Laudiero, 1989), is used to analyze the stress evolution coupled with the chemical weakening.

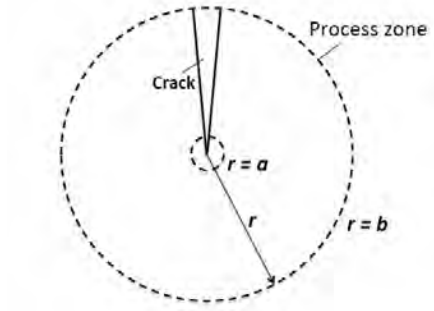

FIG. 1. Process zone simplified by the extended Johnson approximation

Only plane strain is considered, as the fracture toughness of soil or soft rock is assumed to be independent of the width of the crack. With the Johnson approximation, all the fields involved are assumed to be axisymmetric around the crack tip point, which features a small cylindrical cavity (as shown in Fig. 1). The boundary conditions for the system are a constant radial stress in the cylindrical cavity that represents the fluid pressure and zero stress at the external boundary:

$$\sigma_r|_{r=a} = P_a\ (const.); \qquad \sigma_r|_{r=b} = 0 \tag{1}$$

The equilibrium equation and kinematic relationships in polar form are given by

$$\frac{d\sigma_r}{dr} + \frac{\sigma_r - \sigma_\theta}{r} = 0;\ \dot{\varepsilon}_r = -\frac{d\dot{u}}{dr},\ \dot{\varepsilon}_\theta = -\frac{\dot{u}}{r} \tag{2, 3}$$

where θ is the circumferential coordinate, r is the radial coordinate, u is the displacement in the radial direction, and an overdot denotes a time derivative. r and u are defined to be positive in the outward direction. The circumferential displacement is null due to the assumed axial symmetry.

A linearized Cam-Clay yield locus (Fig. 2) and a rigid-plastic strain hardening rock behavior are assumed for simplicity (see Hueckel and Mróz (1973)). Tensile stress and strain are assumed to be negative; hence, the yielding process initiates in the 4th quadrant (as shown in Fig. 2b). The locus segment BC determines the relationship between σ_{r0} and $\sigma_{\theta 0}$ when the crack first yields:

$$\sigma_{\theta 0} = tan(\pi/4 - \vartheta)\sigma_{r0} - (tan(\pi/4 - \vartheta) + tan\varphi)\sigma_{01}$$

where ϑ, φ and σ_{01} are constant rock characteristics that are shown in Fig. 2b.

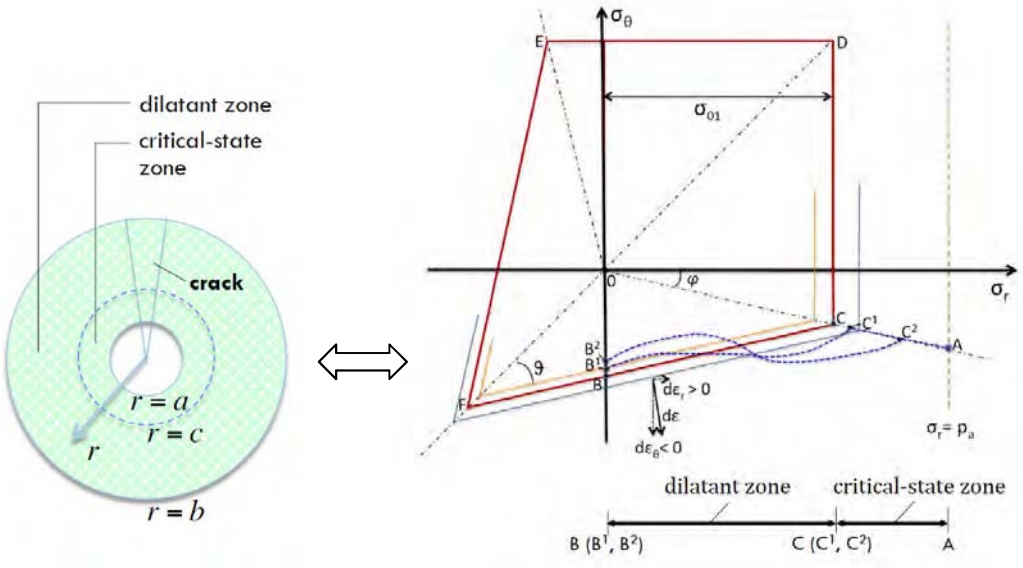

FIG. 2. Sketch of (a) two-zone model; (b) evolving stress profiles

The yield condition for the yielding stress state in a segment of the cylinder evolves through time (B^iC^i, i=1,2,3…) and is affected by the hardening or softening of the surrounding material. The relationship between the circumferential and axial stress in the yield state is given by

$$\sigma_\theta = tan(\pi/4 - \vartheta)\sigma_r - \left(tan\left(\frac{\pi}{4} - \vartheta\right) + tan\varphi\right)\sigma_{01} * (1 + H) \quad (4)$$

where H denotes the hardening parameter that is affected by both chemical softening and strain hardening, as specified below.

The stress state at r = b is represented by the intersection between the FC segment of the original yield locus (evolving in the process) and the σ_θ axis. For r = a, the radial stress at yielding must be equal to P_a in the critical state zone (Fig. 2), which is the zone where the stress state of the material is assumed to evolve along OCA in Fig. 2b. In order to satisfy both the boundary conditions, the system needs a two-zone stress state, as shown in Fig. 2a. The inner zone is a critical-state zone, C^iA, and the outer zone is a dilatant zone, B^iC^i (i=1,2,3…). The dilatant zone evolves according to eqn. (4) either inside or outside of the initial yield locus depending on whether strain hardening or chemical softening is the dominating mechanism.

The chemo-plasticity model adopted here was developed by Hu and Hueckel (2007a, b) and modified by Hu and Hueckel (2013) and by Ciantia and Hueckel (2013); in this model the hardening parameter is assumed to behave linearly:

$$H = \alpha\varepsilon_q^{irr} - \beta\xi \quad (5)$$

where α and β are constant coefficients controlling strain hardening and chemical weakening, respectively. The deviatoric strain ε_q^{irr} is chosen to control the degree of strain hardening; its rate is related to the rate of displacement through Eqn. 3 and through $\dot{\varepsilon}_r = -\dot{\varepsilon}_\theta \tan(\pi/4 - \vartheta)$, which can be determined from Fig. 2. ξ denotes the accumulated loss of mineral mass relative to the original mass, which represents the chemical softening effect. The different signs in the equation indicate that the increase of shear strain and the chemically induced loss of mass are competing to make the material harder or softer.

After iterating through equations (2, 3 and 4) a few times, P_a takes a value that is greater than σ_{01}; in other words, $\sigma_r = P_a$ is no longer inside the initial yield locus (Fig. 2b). The stress continuity between the two zones requires that at r = c

$$\sigma_r^{inner}\big|_{r=c} = \sigma_r^{outer}|_{r=c} \quad (6)$$

The evolution of curve BCA for the resulting stress profile is indicated in Fig. 2b by a dashed curve. The axial stress component σ_z is assumed to not influence yielding in plane strain rate conditions.

If we adopt the hexagonal crystal assembly model (Hu and Hueckel, 2007b) and neglect the precipitation effect, the mass removal rate can eventually be expressed as

$$\dot{\xi} = K \int |\varepsilon_v^{irr}|\, dt + K_c t \quad (7)$$

Hence, the hardening rule can be rewritten as:

$$H = \alpha \varepsilon_q^{irr} - K \int |\varepsilon_v^{irr}| \, dt - K_c t \tag{8}$$

where ε_v^{irr} denotes the irreversible volumetric strain, which is hypothesized to be a function of the internal specific surface area. K and K_c represent the overall chemical softening rate coefficients and are associated with newly generated micro-cracks and the initial void ratio, respectively. With this equation, an initial dissolution that is proportional to a constant specific surface area associated with the initial porosity can eventually cause plastic yielding, even for a low stress; this is accomplished through the slow mass removal and a corresponding shrinking of the yield locus. Plastic yielding occurs when $f = 0$ around the initially subcritical crack. At that point, $\dot{\xi} > 0$ due to the continuation of the reaction, but the coupled process is significantly intensified by the progressive micro-cracking, as manifested by $\dot{\varepsilon}_v > 0$.

SIMULATION RESULTS

Numerical solutions were obtained by solving the above-mentioned system of equations using *Matlab ©*, given the initial conditions and boundary conditions specified above. The input parameters for the model are $\alpha = 5$, $\beta = 1$, $\vartheta = \pi/6$, $\tan\varphi = 0.2$, $b/a = 10$, and $K_c = 1.0 \times 10^{-7} s^{-1}$. The value for K is set to be $1.0 \times 10^{-6} s^{-1}$ unless it is the subject of a parametric study. The dimensionless form of the displacement of the inner cavity of the process zone, u_a/a, is used to represent the crack propagation and its evolution as a function of time is shown in Fig. 3a for various levels of the chemical softening coefficient K. Increasing the value of K by a factor of 5 causes the displacement u_a to grow exponentially within about 10 days, indicating an accelerated crack propagation that underlines the importance of damage-dissolution coupling. The dependence on the chemical softening is less marked when plotted versus the total mass removal (i.e. integrated dissolved mass over time and radius), as is shown in Fig. 3b because the mass removal also accelerates with time. Fig. 4a and Fig. 4b show the evolution of the volumetric strain distribution and the mass dissolution, respectively, along the radius of the crack. Significant changes in the volumetric strains are confined to the area near the crack tip. It is worth noting that the absolute values of the volumetric strain and mass dissolution are both significantly higher at the interface between the critical-state zone and the dilatant zone, which is the location of the most severe irreversible damage/deformation. This is due to the fact that it is also the location of the largest tensile circumferential stress, as shown in Fig. 5. The radial stress is almost frozen during the process.

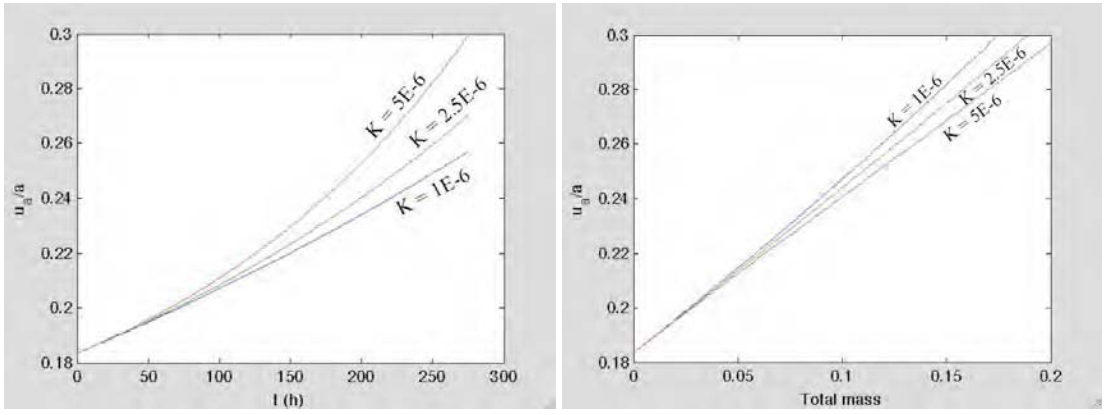

FIG. 3. Crack propagation versus (a) time and (b) total mass dissolved for varying values of the chemical softening coefficient

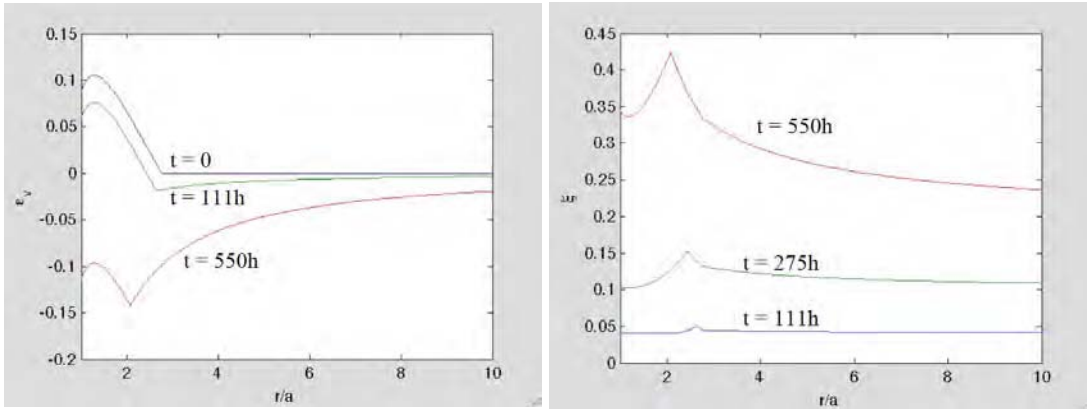

FIG. 4. (a) Evolution of the distribution of volumetric strain as a function of radius; (b) Evolution of the distribution of mass dissolution as a function of radius

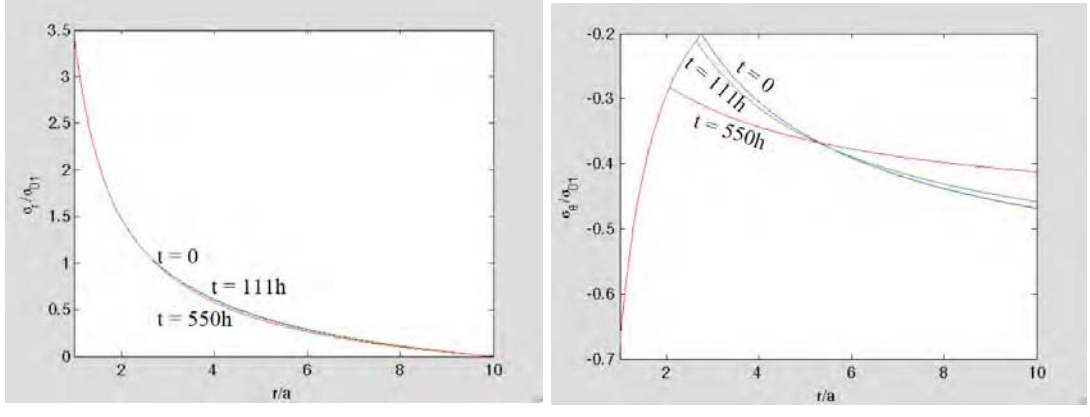

FIG. 5. Evolution of stress components along the radius

CONCLUSIONS

This study investigates a scenario of crack propagation in a pre-stressed geomaterial using the theory of damage-enhanced reactive chemo-plasticity. The presented simplified model is able to demonstrate the compensatory character of coupling between strain hardening and chemical softening in the material and to correlate the propagation of a single crack with the intensity and the location of chemical mass removal inside its process zone. A calibration against available data will follow a series of experiments to simulate a real case scenario.

REFERENCES

Bigoni, D. & Laudiero, F. (1989). The quasi-static finite cavity expansion in a non-standard elasto-plastic medium. *Int. J. of Mech. Sciences* **31**, No. 11-12, 825-837.

Ciantia M. and Hueckel, T. (2013). Weathering Of Stressed Submerged Calcarenites: Chemo-Mechanical Coupling Mechanisms, *Geotechnique* **63**, No. 9, 768-785.

Coffman, S. (2009). The Safety of Fracturing Fluids - A Quantitative Assessment. *Committee to Preserve the Finger Lakes*. Print.

Collins, I. F. & Stimpson, J. R. (1994) Similarity Solutions For Drained and Undrained Cavity Expansions in Soils *Geotechnique* **44**, No. 1, 21-34.

He, C., Guo, J., Wang, W., Liu, C. (2010). Study on acidizing wormhole of tight carbonate reservoir. *Duankuai Youqitian (Fault-Block Oil & Gas Field)* **17**, No. 2, 235-238.

Hu, L. B. & Hueckel, T. (2007 a). Creep of saturated materials as a chemically enhanced rate-dependent damage process. *Int. J. Numer. Anal. Meth. Geomech* **31**, 1537-1565.

Hu, L. B. & Hueckel, T. (2007 b). Coupled chemo-mechanics of intergranular contact: Toward a three-scale model. *Computer & Geotechnics* **34**, No. 4, 306-327.

Hu M. M. and Hueckel, T. (2013). Environmentally Enhanced Crack Propagation in a Chemically Degrading Isotropic Shale, *Geotechnique* **63**, No. 4, 313-321.

Hueckel, T. and Mróz, Z. (1973). Some boundary value problems for variable density materials. *Problèmes de la Rhéologie*, PWN , Warsaw, 173-191.

Hueckel, T., Pellegrini R., and Del Olmo, J. C. (1998). A Constitutive Study of Thermo-Elastoplasticity of Deep Carbonatic Clays, *I. J. Numer. Anal. Meth. Geomech*. **31**, 1537-1565.

Hueckel, T. (2002). Reactive plasticity for clays during dehydration and rehydration. Part I: concepts and options. *Int J Plast*. **18**, No. 3, 281-312.

Hueckel T. and Hu, L. B. (2009). Feedback mechanisms in chemo-mechanical multi-scale modeling of soil and sediment compaction, *Computers and Geotechnics* **36**, 934-943.

Jackson, R. B., Pearson, B. R., Osborn, S. G., Warner, N. R., and Vengosh, A. (2011). *Research and Policy Recommendations for Hydraulic Fracturing and Shale Extraction*. Center on Global Change, Duke University: Durham, NC.

Johnson, K. L. (1970). The correlation of indentation experiments. *J Mech Phys Solids* **18**, 115-126.

Portier, S. & Vuataz, F. D. (2010). Developing the ability to model acid-rock interactions and mineral dissolution during the RMA stimulation test performed at the Soultz-sous-Forêts EGS site, France. *C.s R. Geoscience* **342**, 7-8, 668-675.

Rahman, M. M. (2008). Constrained hydraulic fracture optimization improves recovery from low permeable oil reservoirs. *Energy Sources,* Part A **30**, 536-551.

Zimmermann, G., Blöcher, G., Reinicke, A., Brandt, W. (2011) Rock specific hydraulic fracturing and matrix acidizing to enhance a geothermal system - Concepts and field results. *Tectonophysics* **503**, No. 1-2, 146-154.

Numerical Analysis on Deformation Behavior of Expandable Casing and Contact Evaluation of Its Threaded Connection

Xinpu Shen[1] and Guoyang Shen[2]

[1]Senior Technical Advisor, Halliburton Consulting, 2107 City West Blvd, Houston, TX, USA, E-mail: Xinpu.shen@halliburton.com
[2]Student, University of Houston, 4800 Calhoun Rd Houston, TX 77204, USA, E-mail: gshen2@uh.edu

ABSTRACT: Numerical simulations were performed for the expansion of expandable casing with a threaded connection. Specific concerns that were focused on include evaluating the contact between the pin thread and the box thread, as well as predicting the driving force applied to the mandrel cone. The results indicate 1) with a specific value for the axial velocity of the mandrel cone, the connection surfaces between the pin thread and box thread maintain good contact in most areas after expansion; 2) during most of the expansion process, the values of the driving force applied to the mandrel cone are less that 1×10^6N. However, the maximum value can be as high as 2.03×10^6N; 3) the contact status between the pin thread and the box thread can be estimated with reasonable accuracy using coarse mesh. However, finer mesh can more accurately identify the localized peak value of the contact stress and that of the equivalent plastic strain at the root of the pin thread. This can also result in a higher driving force applied to the mandrel cone because of the plastic hardening property; 4) the rate of axial compaction after radial expansion is 1.45%.

INTRODUCTION

Expandable casing has been used as the primary method for remediation of old and eroded casing sections of production wells since the 1950s (Murchey and Zulia, 1955). With the development of ultradeep wells, expandable casing technology is not only used for remediation but also for drilling holes that have the same hole size for a long true vertical depth (TVD) interval. This use can be significantly more economical than conventional drilling technology.

Research and applications of expandable casing have been reported by various authors (Vincent and Jennings, 1962; Kemp, 1963; Robert and Fischer, 2003; Neely, 1985; Stewart et al., 1999; Sanders et al., 2012; Bufalini et al., 2012; Berge et al., 2013). Hilbert and Bergstrom (2004) presented their work on evaluating the sealing integrity of an expandable casing section, with specific focus on the sealing ring. However, they didn't investigate in detail the behavior of the threaded connection after expansion.

The expandable casing investigated here is made of ductile steel, the M20Cr, which

is a kind of Ductile Chromium alloy (American Society for Metals, 1957). Its maximum strain is 35% or even higher. Before installation, its sectional area is circular, and it remains circular after being installed downhole and expansion. However, during the process of expansion, the material will experience significant finite plastic strain. Thus, the history of the plastic deformation of the casing is significant for estimating its bearing capacity (i.e., the plastic strain hardening property of the material) after it is installed and expanded. In addition, the sealing contact on the threaded connection will change as a result of the finite plastic deformation. Therefore, it is essential to perform three-dimensional (3D) numerical simulations on the expansion process.

The finite element method was used to numerically simulate the expansion process of a section of expandable casing. The threaded connection was included in this model. However, the effect of the threaded helix was omitted for simplicity. One quarter of the geometry was used in the model for symmetry. Contact pairs of surfaces were modeled between mandrel cone and pin thread, pin thread and box; as well as pin thread –box thread and thread enhancement ring, totally 4 pairs of contacts within the model. The principal results obtained from this numerical analysis include 1) maximum value and distribution of equivalent plastic strain after expansion within the casing, 2) deformed casing shape, 3) maximum value and distribution of contact force at contact surface between the pin thread and box thread, and 4) a variation in values of the driving force of the mandrel cone during the expansion process.

Constrains provided by the borehole is not included in the model. Reason of this is because the study is focused on the sealing property without borehole constraint and this is required by the manufacturer.

Two different meshes were used in these calculations to investigate the mesh-sensitivity of the numerical solution obtained with the model.

FINITE ELEMENT MODEL

Geometry and Mesh

In this model (shown in Fig. 1), the following components are included: mandrel cone, pin thread, box thread, and enhancement ring. Influence of the borehole and other downhole environmental factors are omitted. An analytical rigid model was adopted to model the behavior of the mandrel cone. A model of elastoplastic material was used to model the casing, and von Mises strain hardening constitutive model was adopted. More details are shown in Fig. 2, which is an axial sectional view of the casing shown in Fig. 1. Fig. 2 is zoomed in to show details of the contact relationship between various components of the threaded connection.

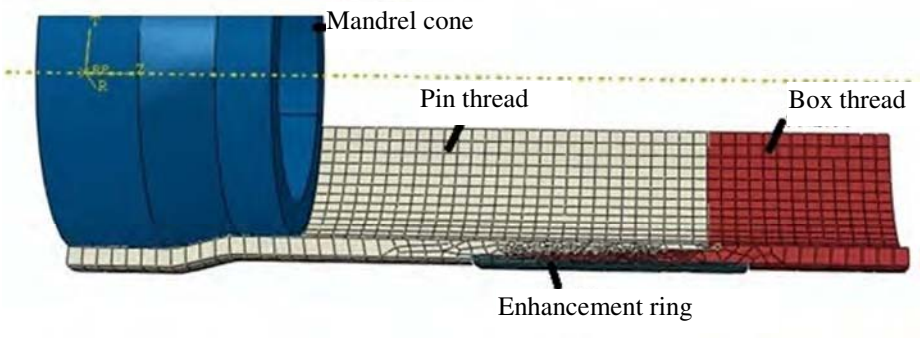

FIG. 1. Assembly of the expandable casing with the threaded connection and coarse mesh.

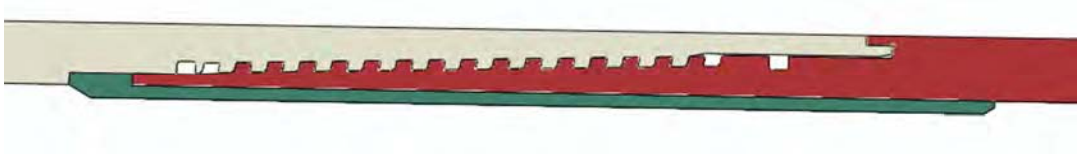

FIG. 2. Zoomed in view of the threaded connection.

The geometric parameters are

- Initial inner diameter of casing = 0.183 m
- Wall thickness = 0.01 m
- Length = 0.5 m
- Outer diameter of mandrel cone = 0.178 m for the thinner end (right side) and 0.198 m for the thicker end (left side)
- Thickness of the enhancement ring = 0.002 m

Two different meshes were used in the model. Discretization of the coarser mesh used 11,949 8-noded linear brick element which is named as C3D8R and 16,956 nodes (see Fig. 1). The details of the assembly relationship at the threaded connection are shown in the zoomed axial sectional view in Fig. 2. The finer mesh used 45,380 8-noded linear brick element, as well as 59,669 nodes (see Fig. 3). The analytical rigid model of the mandrel cone does not require meshing.

The frictional coefficient between the mandrel cone and the inner casing surface was set as 0.15.

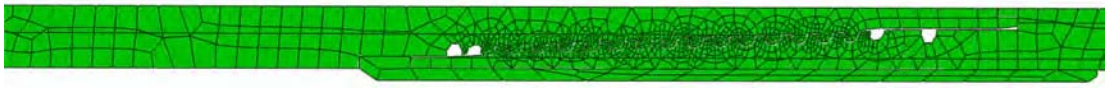

FIG. 3. The finer mesh.

Values of Material Parameters

The material used for expandable casing was ductile M20Cr, the Ductile Chromium alloy. The values of the elasticity parameters provided by the

manufacturer are shown in Table 1. In order to accurately obtaining the behavior of the structure, laboratory test was done with a piece of alloy provided by the manufacturer. A graph of the plastic strain hardening vs. stress obtained in the text is shown in Fig. 4. This diagram given in Fig.4 defines the strain hardening law in tabular form.

Table 1. Values of elasticity parameters of M20Cr

Name	Young's Modulus (MPa)	Poisson's Ratio	Density (kg/mm^3)
M20Cr	188 000	0.3	0.0078

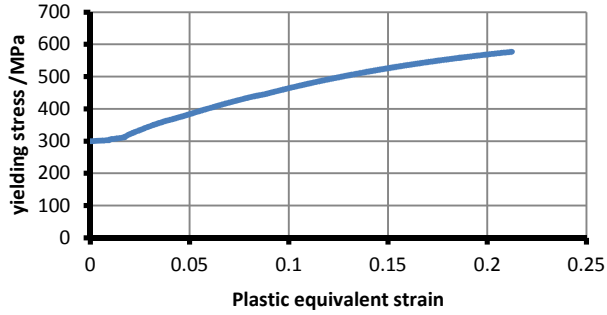

FIG. 4. Graph of plastic strain hardening vs. stress.

Initial Condition and Boundary Conditions of the Model

As shown in Fig. 5, zero normal displacement constraints were applied to the lateral surfaces of the casing. These lateral surfaces were symmetrical planes. The outer surface was a free surface. However, the inner surface was a contact surface and in contact with the moving mandrel cone during expansion. The bottom surface was fixed, and the top surface was free in the z-direction, which allowed the casing to be elongated or shortened, if necessary. The initial velocity of casing was zero, and the initial velocity of the mandrel cone was 0.225 m/s along the axial direction from left to right.

The density of the casing material is shown in Table 1, but the gravity load was ignored in this model for brevity. Density provided here is for use of dynamic calculation.

Contact properties setting for this model are: tangential frictional coefficient is 0.15. No penetration is allowed in normal direction to the contact surface.

Load of force applied to the model is thus to be determined by calculation of reaction with reference to the displacement boundary condition and initial condition on the mandrel.

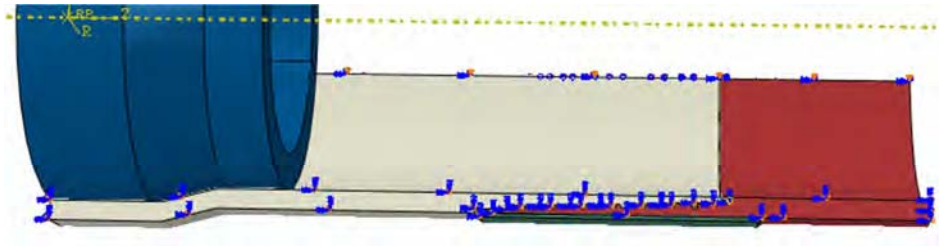

FIG. 5. Boundary condition of the model: displacement constraints.

NUMERICAL RESULTS OF CASING EXPANSION

With the finite element model defined above, the numerical solutions of the mechanical variables are shown in Figs. 6, 7, and 8. Fig. 6 shows the deformed shape of the expandable casing. The coarser mesh is used here. Fig. 6 also shows the contour of the equivalent plastic strain. The axial sectional view is used to show the details of deformation at the threaded connection. The maximum value of the equivalent plastic strain was approximately 0.3, and it occurred at the root of the male thread. Fig. 7 shows the zoomed axial sectional view of the right end of the threaded connection. It shows that most of the pin thread and box thread are in contact. Also, it shows that the plastic strain occurring at the tooth of the thread is less than that occurring in the area away from the tooth. There is a small part of the connected thread that separated instead of remaining in contact. Fig. 8 shows the left part of the threaded connection and is a zoomed axial sectional view. It shows that most of the left part of the thread has lost contact between the two parts of thread.

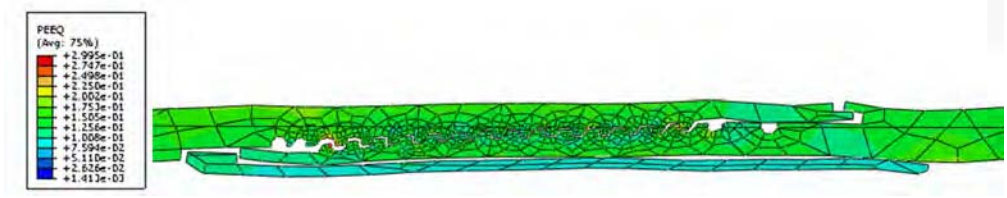

FIG. 6. Deformed shape after expansion and the contour of the equivalent plastic strain.

FIG. 7. Zoomed view of the right end of the threaded connection showing the deformed mesh.

FIG. 8. Zoomed view of the deformed mesh and the contour of equivalent plastic strain.

The contour of the contact stress which is the surface stress normal to the contact surface (units in MPa) is shown in Fig. 9. Dark blue indicates the area where there is zero contact stress, and the bright blue indicates the places where there is non-zero contact stress. Non-zero contact stress means actual contact. Because the surface geometry of the thread is complicated, the contact stress distribution is difficult to visualize clearly in one figure. However, it can be observed in Fig. 9 that there are regions of bright colors, which indicate that region is in actual contact. Fig. 10 shows the contour of the equivalent plastic strain within the box thread, and it can be observed that the maximum value of the equivalent plastic strain is approximately 0.3. Fig. 11 shows the contact stress on the surface of the box thread. The bright colors there also show that the same regions as those shown in Fig. 9 have good contact.

A diagram of the force applied to the mandrel cone is shown in Fig. 12. It can be observed that the peak value of force on the mandrel cone is 1.6×10^{6}N, which occurred at the moment when the entire mandrel cone entering the casing interval was covered by the enhancement ring.

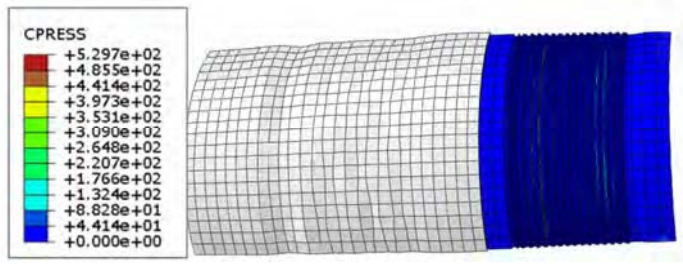

FIG. 9. The contour of the contact stress (in MPa).

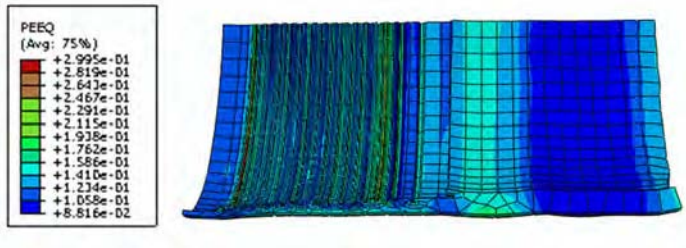

FIG. 10. The contour of the equivalent plastic strain within the pin box after expansion.

FIG. 11. The contour of the contact stress distribution on the surface of the box thread after expansion.

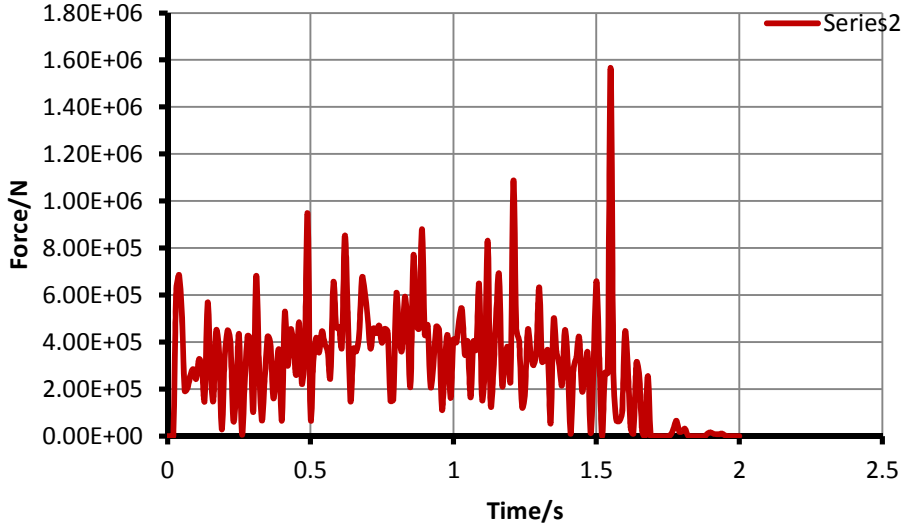

FIG. 12. Variation of the force applied on the mandrel cone over time.

NUMERICAL RESULTS OBTAINED WITH FINER MESH

To investigate the impact of mesh density on the numerical results, the finer mesh shown in Fig. 3 was used to simulate the expansion of an expandable casing section with a threaded connection.

Fig. 13 shows an axial sectional view of the deformed mesh and the contour of the distribution of the plastic strain. Compared with the results shown in Fig. 6, the result shown in Fig. 13 has a maximum value of 0.425, which is higher than that shown in Fig. 6. One possible reason is that the finer mesh can catch the localization phenomenon of the plastic strain occurring at the root of the pin thread, but the coarse mesh cannot. This indicates that using the finer mesh in the model is important for accurately estimating the integrity of the threaded connection if the plastic damage property is included in the material behavior parameters. Even for the plastic deformation analysis, the finer mesh is important to the accuracy of the numerical solution.

Fig. 14 shows an axial sectional view of the contact stress distribution between the pin thread and the box thread obtained using the finer mesh. The maximum value of

the contact stress here is 718.2 MPa, which is higher than the 529.7 MPa shown in Fig. 9 with the coarse mesh density. Fig. 15 shows the contour of the contact stress distribution at the surfaces of the threaded connection for both the pin thread and the box thread. By comparing Fig. 15 with Fig. 9, it can be observed that the regions with bright colors resulting from the finer mesh are larger than those obtained with the coarse mesh. This indicates that the finer mesh model performs better at modeling the contact force distribution than the coarse mesh model. Because the shape of the pin thread surface is complicated, the contact stress on the left side of the casing can be clearly visualized in the left side of Fig. 15, but the contact stress on the right side of the casing can only be visualized clearly in the right side of Fig. 5, which is rotated from its initial position of the view on the left.

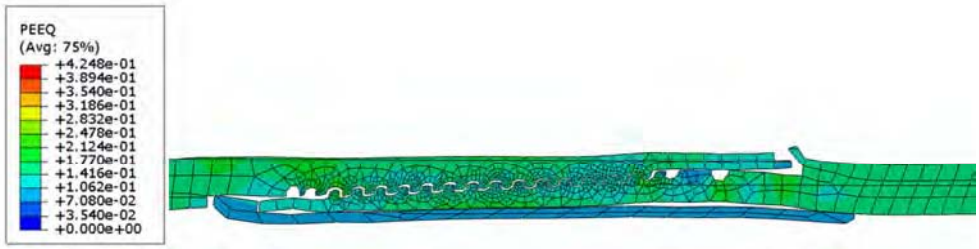

FIG. 13. Axial sectional view of the deformed mesh and the contour of the plastic strain distribution.

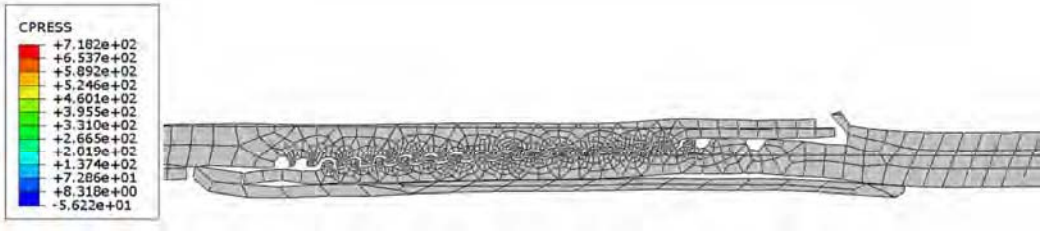

FIG. 14. Axial sectional view of the contact stress distribution between the pin thread and the box thread.

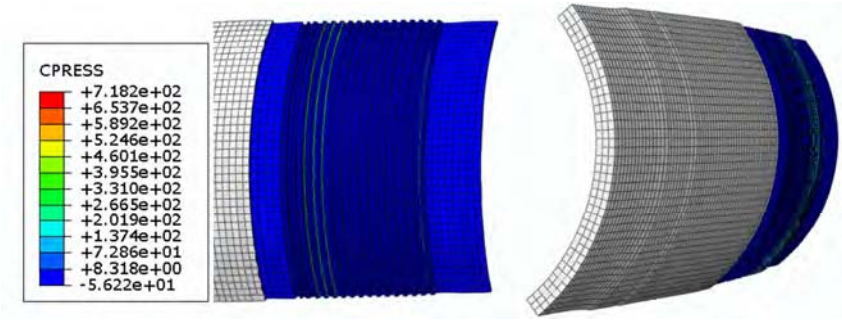

FIG. 15. Contour of the contact stress distribution at the surfaces of the threaded connection.

Figure 16 shows a diagram of the forces applied to the mandrel cone during

expansion obtained with both the coarse mesh and the finer mesh. It can be observed that the numerical results of the driving forces applied to mandrel cone are fairly similar. However, the maximum value of the driving force obtained with the finer mesh is 2.03×10^6N, and the maximum value with the coarse mesh is only 1.57×10^6N. The reason for this phenomenon is the plastic strain hardening of the material—the maximum value of the plastic strain obtained with finer mesh is higher than that obtained with the coarse mesh. Consequently, the extent of plastic strain hardening obtained with finer mesh is stronger than that obtained with coarse mesh.

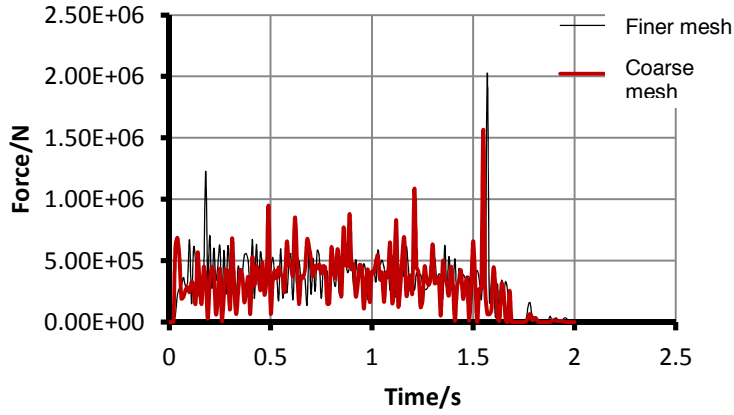

FIG. 16. Comparison of the forces applied to the mandrel cone from the coarse mesh and finer mesh.

NUMERICAL RESULTS ON DEFORMATION BEHAVIOR

Figures 17 and 18 show numerical results of the axial deformation and radius deformation after expansion obtained using finer mesh, respectively.

From Fig.17, it can be observed that the axial displacement on the free end of this casing section is 0.0055 m. Divided by the length of the deformed part of this casing section, which is 0.380 m, its nominal average strain is 0.0145. This means that the rate of axial compaction after radius expansion is 1.45%. For a 200-m section of wellbore that requires enhancement with expandable casing, the total length of casing sections necessary will be 202.9 m, which is the minimum value to satisfy practical requirements.

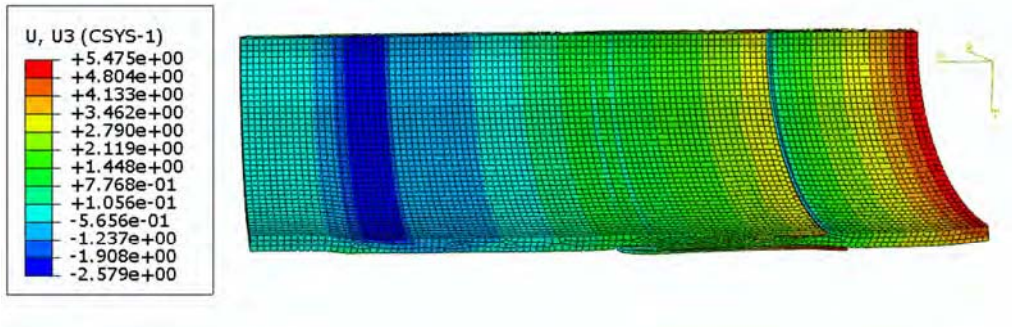

FIG. 17. Axial deformation after expansion (in mm).

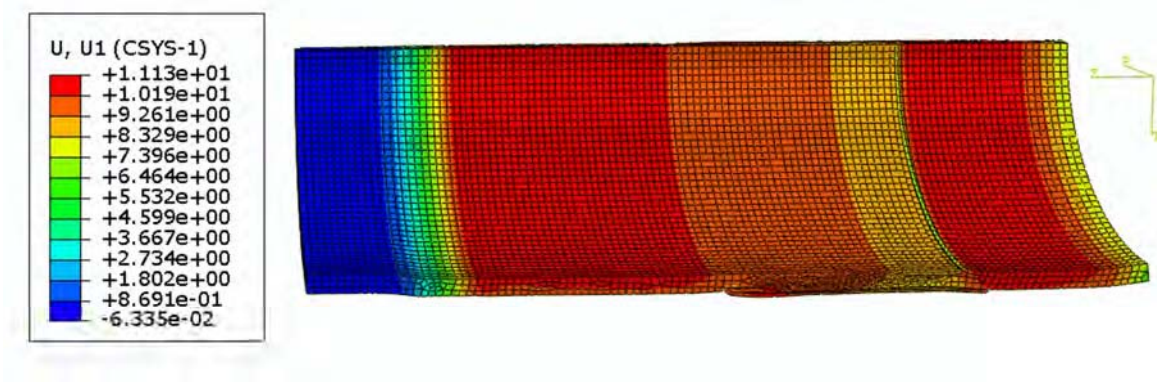

FIG. 18. Radius deformation after expansion (in mm).

From Fig.18, it can be observed that the minimum value of outward radius displacement occurs at the inner edge of the upper/left part of connection box and is 0.005 m. This value determines that the radius of net space in casing is 0.188 m after expansion.

CONCLUSIONS

Numerical simulations were performed for the expansion of expandable casing with a threaded connection. Specific areas of concern were evaluating the contact between the pin thread and box thread, as well as predicting the driving force applied to the mandrel cone and the deformation quantities after expansion. The results indicate the following:

- With a specific value of axial velocity of the mandrel cone, the connection surfaces between the pin thread and box thread maintain good contact at most areas after expansion.
- During most of the expansion process, the values of the driving force applied to the mandrel cone are less that 1×10^6N. However, the maximum value can be as high as 2.03×10^6N.
- The contact status between the pin thread and box thread can be estimated with reasonable accuracy using the coarse mesh. However, the finer mesh can more accurately identify the localized peak value of the contact stress and that of the equivalent plastic strain at the root of the pin thread. This can also result in a higher driving force applied to the mandrel cone because of the plastic hardening property.
- Numerical results of deformation after expansion are the following: rate of axial compaction after radial expansion is 1.45%, and the radius of net space in casing is 0.188 m after expansion with the current design.

REFERENCES

American Society for Metals, (1957): Ductile Chromium & Its Alloys. American Society for Metals. Cleveland, Ohio.

Berge, T., K.D. Mathisen, O. Storebo, and M. Muir: *Expandable Liner Hanger*

Milling: North Sea Case Histories, SPE/IADC 163568, The SPE/IADC Drilling Conference and Exhibition, Amsterdam, The Netherlands, March 5-7, 2013.

Bufalini, A., R. Morana, P.I. Nice, and M Bailey: *Assessment of Post Expanded Mechanical Performance of Materials and Evaluation of Material Expandability Limit,* SPE 159694, The SPE Annual Technical Conference and Exhibition, San Antonio, Texas, USA, October 8-10, 2012.

Hilbert Jr., L.B. and J.S. Bergstrom: *Evaluation Pressure Integrity of Polymer Ring Seals for Threaded Connections in HP/HT Wells and Expandable Casing*, IADC/SPE 87214, The IADC/SPE Drilling Conference in Dallas, Texas, USA, March 2-4, 2004.

Kemp, G.: *Field Results of the Stressed Steel Liner Casing Patch,* Casing Repairs, 1964, vol. 2, 147-149, SPE 0663.

Murchey, G.N. and L.E. Zulia: *Problems in Casing Collapse,* 519-G, The 30th Annual Fall Meeting of the Petroleum Branch of the American Institute of Mining and Metallurgical Engineers. New Orleans, Louisiana, October 2-5, 1955.

Neely, J.D.: *The Use of Casing Patches to Improve Workover Success Rates,* SPE 13996, Offshore Europe, Aberdeen, United Kingdom, September 10-13, 1985.

Robert, E.S. and P.A. Fischer: *Expandable Technology Growth Is Changing Drilling Practices,* World Oil, vol. 224, no. 7, July 2003.

Sanders T., C. Hogg, P. York, and F. Tompek: *Integration Optimized Casing Exit and Solid Expandable Technology,* SPE 160839, The SPE Saudi Arabia Section Technology and Exhibition, Al Khobar, Saudi Arabia, April 8-11, 2012.

Stewart, R.B., F. Marketz, W.C.M. Lohbeck, F.D. Fischer, W. Daves, F.G. Rammerstorfer, and H.J. Böhm: *Expandable Wellbore Tubulars, Quest for Solutions in a Changing Industry*, SPE 60766, The 1999 SPE Technical Symposium, Dhahran, Saudi Arabia, October, 1999.

Vincent, R.P. and E.R. Jennings: *Stressed Steel Liner Yields Stronger Casing Repairs,* Petroleum Equipment, December, 1962, 1337-1341, SPE 278.

Hydro-Mechanical Coupled Model of Hydraulic Fractures using the eXtended Finite Element Method

D.J. Youn[1], S.M.ASCE and D.V. Griffiths[2], F.ASCE

[1]Ph.D. candidate, Department of Civil and Environmental Engineering, Colorado School of Mines, 1500 Illinois street, Golden, CO 80401, U.S.A., E-mail: dyoun@mines.edu.
[2]Professor, Department of Civil and Environmental Engineering, Colorado School of Mines, 1500 Illinois street, Golden, CO 80401, U.S.A., E-mail: vgriffit@mines.edu.

ABSTRACT: This paper describes a hydro-mechanical coupled model for hydraulic fractures using the eXtended Finite Element Method (XFEM). To analyze the non-linear coupling behavior of hydraulic fractures, the XFEM uses local enrichment functions within a regular finite element framework. Thus, the mechanical behavior of a domain with fractures can be efficiently estimated by the method without explicitly meshing the discontinuities as would be necessary in other numerical techniques. The governing equations and coupling algorithms are presented as well as the required assumptions for hydraulic fractures. The 2D coupled XFEM program is validated by a numerical example study and shows coupled flows and their influence on stresses and fracture deformations.

INTRODUCTION

The role of hydraulic fracturing for enhanced recovery of unconventional oil and gas has grown dramatically in recent years. Realistic modeling of fracture and fluid flow in these systems is sought in order to improve physical understanding and efficiency. Such modeling remains highly challenging however, due to a number of factors including material heterogeneity, complex fracture propagation mechanisms, coupled behavior of rock stresses and fluid pressure, and interactions between pre-existing natural and artificially initiated hydraulic fractures.

For the numerical analysis of the hydraulic fractures, the discrete fracture network model (DFN) has been widely used (e.g. Xu and Dowd, 2010; Azadi and Khoei, 2011). However the numerical technique is computationally expensive to consider the moving boundary of the fracture propagation, since the fractures must be explicitly modeled as additional finite meshes. Therefore when the fractures and its geometry evolve, the entire model must be re-meshed and the global matrices reassembled and factorized in standard FE schemes.

A relatively new technique for finite element modeling of fractures without re-meshing developed by Belytschko and Black (1999) and Moës *et al*. (1999) has great promise and is explored in this paper. This technique named the eXtended Finite

Element Method (XFEM) involves a standard displacement-based approximation, enriched near a fracture and a tip. Discontinuous basis functions are added to standard shape functions for nodes that belong to the enriched elements. A major advantage of the XFEM is that the finite element mesh does not need to be updated to track the discontinuous path. The addition of a discontinuous field allows for the entire fracture geometry to be modeled independently of the mesh, and completely avoids the need to re-mesh as the fracture propagates.

XFEM has been successfully applied in various branches of engineering regarding fractures. The method was further developed by incorporating extensions known as weak and strong discontinuities which represent the continuous and discontinuous strain distribution along fracture boundaries (e.g. Sukumar and Prevost 2003) and by considering cohesive fracture propagation, where the non-linear behavior of fracture is caused by increased strength of material and dissipation of energy at the fracture tip (e.g. Bellec and Dolbow 2003). XFEM has also been adopted for modeling plasticity and large deformation (e.g. Fagerström and Larsson 2006), composite materials (e.g. Ashari and Mohammadi 2011), and fatigue fracture elongation and failure (e.g. Pais *et al*. 2012).

The main objective of this paper is to present the advanced coupled finite element program for hydraulic fractures. An XFEM scheme is developed based on the public domain software of Smith and Griffiths (2004) allowing for representation of fractures without any need for re-meshing. The 2D XFEM studies examine the fractured system can be deformed and coupled flows and their influence on stresses and fracture deformations. Since the surrounding rock is assumed to be very tight, fluid flow may only get through the fracture, and fluid leak off to the surrounding rock is neglected.

MECHANICAL BEHAVIOR OF FRACTURE USING THE XFEM

The XFEM uses local enrichment functions to enhance the traditional finite element shape functions, making the approximated displacement field and its derivatives discontinuous within an element. Once the fracture geometry and location are defined, different enrichment terms are selectively applied to the different element groups, namely elements divided by a fracture, or elements containing a fracture tip (See Fig. 1).

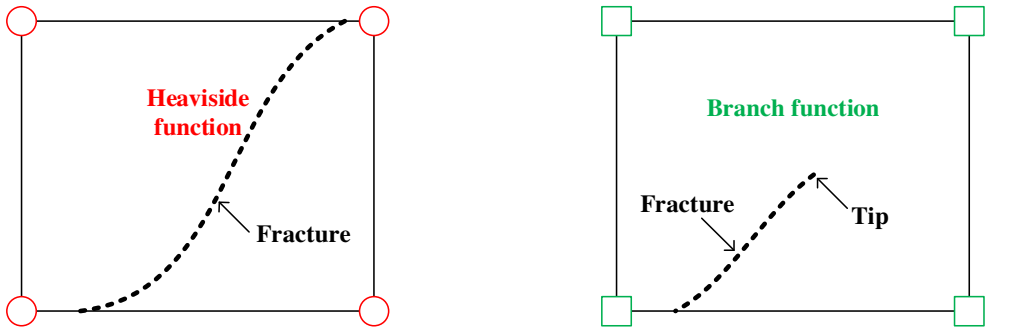

(a) Element divided by a fracture **(b) Element containing a fracture tip**

FIG. 1. Example of enriched elements

The enrichment functions include modified Heaviside and Branch functions that represent normal displacement of the fracture surfaces and the fracture tip asymptotic fields based on the Westergaard solution (Moës *et al*., 1999), respectively. The Heaviside function is first applied to elements entirely cut by a fracture and is given as below in Eq. (1).

$$H(\mathbf{x}) = \begin{cases} +1 & \varphi(\mathbf{x}) \geq 0 \\ -1 & \varphi(\mathbf{x}) < 0 \end{cases} \tag{1}$$

where $\varphi(x)$ is the signed distance function normal to the fracture. Branch functions are used to enrich elements that contain fracture tips and are given as in below.

$$\left[\Phi_\gamma(\mathbf{x})\right]_{\gamma=1}^{4} = \left[\sqrt{r}\sin\frac{\theta}{2}, \sqrt{r}\cos\frac{\theta}{2}, \sqrt{r}\sin\theta\sin\frac{\theta}{2}, \sqrt{r}\sin\theta\cos\frac{\theta}{2}\right] \tag{2}$$

where r and θ are the polar coordinates of the point x in the coordinate system centered at the tip of the fracture with the *x*-axis aligned to the fracture direction. The sum of the Heaviside and Branch enrichment terms results in the following displacement field within a discontinuous domain:

$$\mathrm{u}(\mathbf{x}) = \sum_{I\in\mathcal{N}} N(\mathbf{x})\mathrm{u}_I + \sum_{J\in\mathcal{N}_{fr}} N(\mathbf{x})\left[H\big(\varphi(\mathbf{x})\big) - H\left(\varphi\big(\mathbf{x}_J\big)\right)\right]\mathrm{a}_J + \sum_{K\in\mathcal{N}_{tip}} N(\mathbf{x})\sum_{\gamma=1}^{4}\left[\Phi_\gamma(\mathbf{x}) - \Phi_\gamma(\mathbf{x}_K)\right]\mathrm{b}_{\gamma k} \tag{3}$$

COUPLING ALGOLITM FOR A FRACTURE

For coupling purposes, a 1D fluid flow model is added to the XFEM program, and a sequential coupling scheme as suggested by Yew (1997) and Dahi (2009) using Picard iteration is applied. For the simplification of the model, an incompressible Newtonian fluid is assumed, and fluid leak off to the surround rock mass and fracture propagation are not considered. Those assumptions are reasonable when the surrounding rock has very small pore size and thus has almost zero permeability.

The weak form of the fluid mass balance equation (*e.g*. Rungamornrat *et al*. 2005; Segura and Carol 2008; Chen 2013) is applied to calculate the hydraulic pressure to the fracture and is presented as Eq. (4).

$$\int_L \frac{\Delta w}{\Delta t} N_i(x)dx + \int_L q_L(t)N_i(x)dx = \frac{1}{12\mu}\int_0^L \frac{\partial}{\partial x}\left(w^3\frac{\partial P}{\partial x}\right)N_i(x)dx \tag{4}$$

Although q_L is the fluid leak-off rate along the fracture surface, it is neglected due to the assumption that the surrounding rock is nearly impermeable. Boundary conditions are applied at each end of the fracture, for fluid injection at the wellbore

and zero fracture opening at the fracture tip. The boundary conditions are summarized in Eqs. (5) and (6).

$$\frac{1}{12\mu}\left(w^3\frac{\partial P}{\partial x}\right)N_i(x)\Big|_{well} = Q_i N_1(0) \tag{5}$$

$$P|_{tip} = 0 \tag{6}$$

Once the fluid pressure along the fracture is estimated, it is then applied to the global force vector, and the modified force vector is used by the XFEM program to calculating the trial solution of fracture aperture. The explicit fracture opening may be estimated using the additional degrees of freedom as suggested by Dahi (2009) and Chen (2013)

$$w(x) = \begin{cases} 2\sum_{J\in\mathcal{N}_{cr}} N(x)\mathrm{a}_J, & \text{For fracture body} \\ 2\sqrt{r}\sum_{K\in\mathcal{N}_{tip}} N(x)\mathrm{b}_{1K}, & \text{For fracture tip} \end{cases} \tag{7}$$

The entire process is repeated for each time step, and the resulting two trial solutions (w_k and $w_{k+1/2}$) for the fracture opening are compared with each other to enable an updating as shown in Eq. (8).

$$w_{k+1} = (1-\alpha)w_k + \alpha w_{k+1/2} \tag{8}$$

Convergence is determined by comparing the relative error between w_k and w_{k+1} for all elements along the fracture as shown in Eq. (9).

$$\varepsilon \geq \frac{\sum|w_{k+1} - w_k|}{\sum|w_k|} \tag{9}$$

Iterations stop when the relative error is less than 10^{-6}, at which time the fracture aperture and fluid pressure are taken as the converged solution.

SIMULATION RESULTS AND VALIDATION

A simple hydraulic fracturing example is presented in this section. The coupled fracture model analyzes only the half of the original fracture geometry due to the horizontally symmetric fracture shape, and the fracture tip is located at the center of the domain. Rollers are used to constrain lateral deformations along the left and right edges of the entire domain, and the right bottom corner is fully fixed. The details of the example model including the problem mesh, boundary condition, selection of the enriched nodal points are presented in Fig. 2.

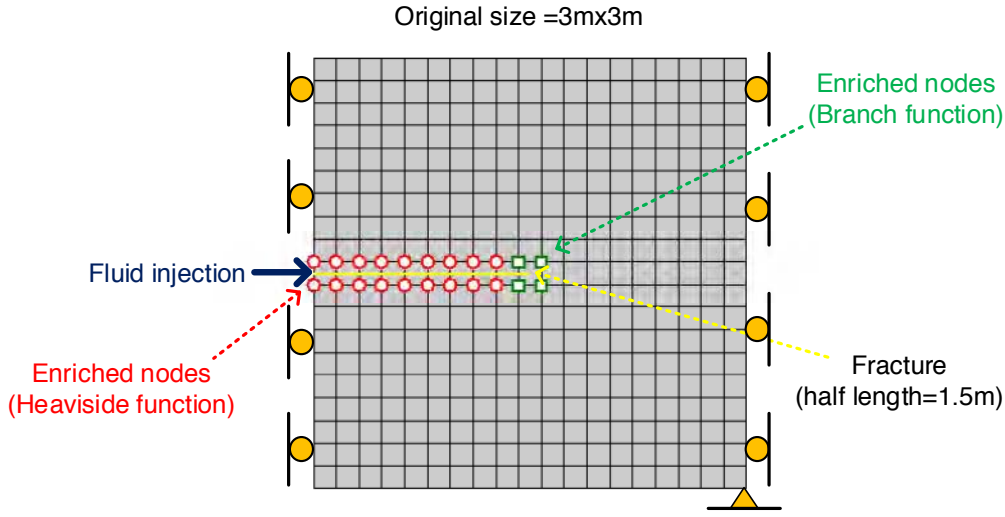

FIG. 2. Finite mesh for the example study

The hydraulic pressure is applied along the fracture and yields additional displacements along the enriched elements successfully. The recommended range of the Picard iteration coefficient ($0.1 < \alpha < 0.3$) reported by Yew (1997) and Dahi (2009) should be maintained, otherwise convergence may be slowed down or not achieved at all.

Table 1. Input Parameters

Young's modulus E	Poisson's ratio ν	Injection rate Q_i	Fluid viscosity μ
$4 \times 10^6 \mathrm{Pa}$	0.25	$5 \mathrm{m}^3/\mathrm{min}$	$2 \times 10^{-5} \mathrm{Pa} \cdot \mathrm{min}$

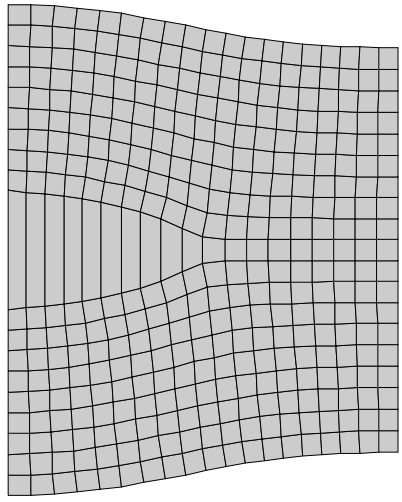

FIG. 3. Deformed mesh (deformation scale factor=200)

Figure 4 presents the fracture aperture convergence in the example study. The convergence coefficient is equal to 0.25, and it takes a total of 17 iterations, with the final relative error of about $6.30 \cdot 10^{-7}$.

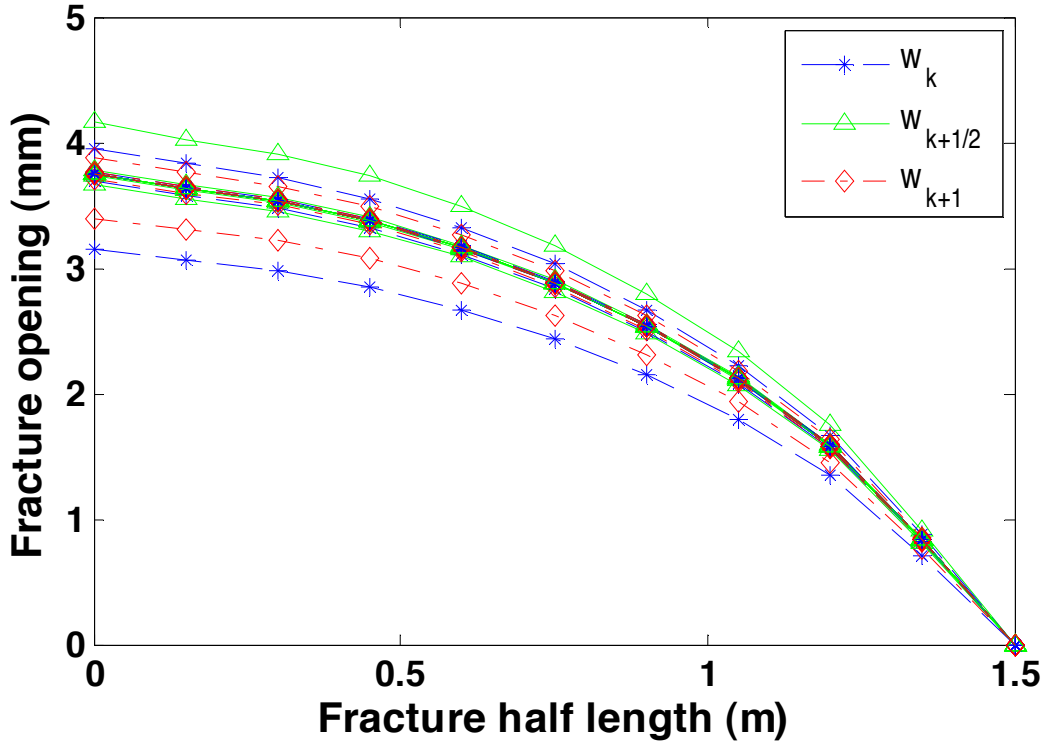

FIG. 4. Convergence of the fracture aperture

For the validation of the current numerical program , the fracture opening at the injection point from the simulation is compared to the analytical solution as in Eq. (10) given by Geertsma and de Klerk (1969). The simulation results matched quite well (the relative error is about 1.62%).

$$w_{well}^{anal}(t) = \left(\frac{5376}{\pi^3}\frac{\mu q_0^3}{E'}\right)^{\frac{1}{6}} t^{\frac{1}{3}} = 2.36\left(\frac{\mu q_0^3}{E'}\right)^{\frac{1}{6}} t^{\frac{1}{3}} = 3.69\ \text{mm} \tag{10}$$

$$w_{well}^{XFEM}(t) = 3.75\text{mm} \tag{11}$$

Figures 5 and 6 show the converged fluid pressure and fracture opening after the convergence, respectively.

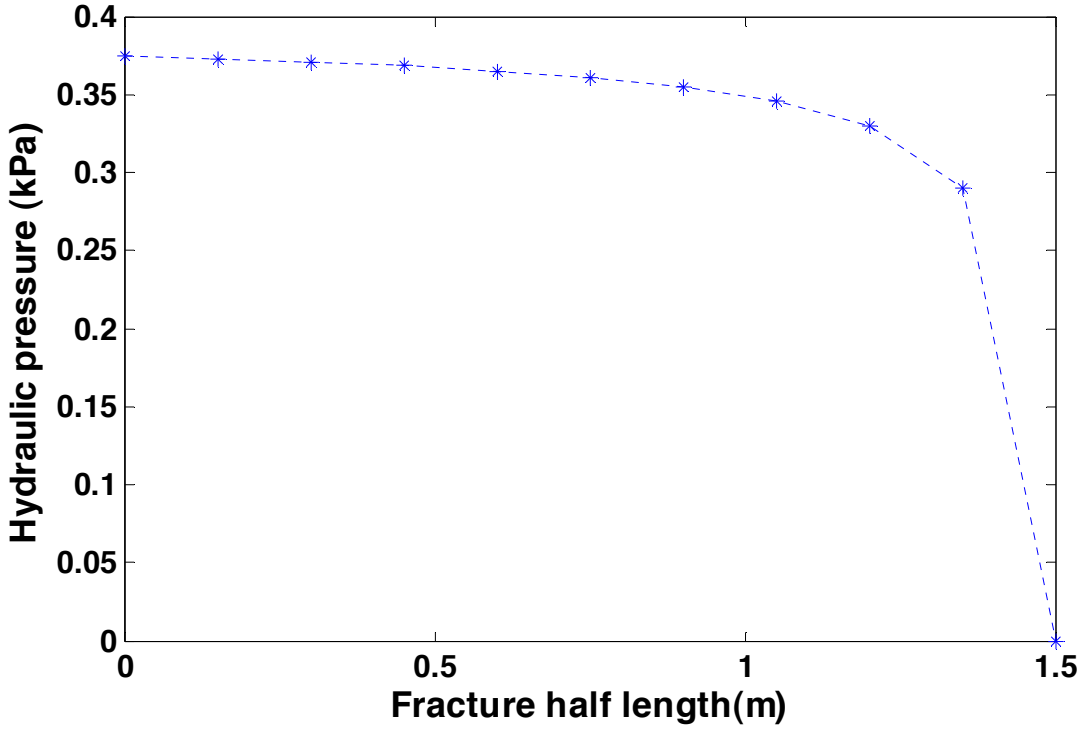

FIG. 5. Converged hydraulic pressure along the fracture

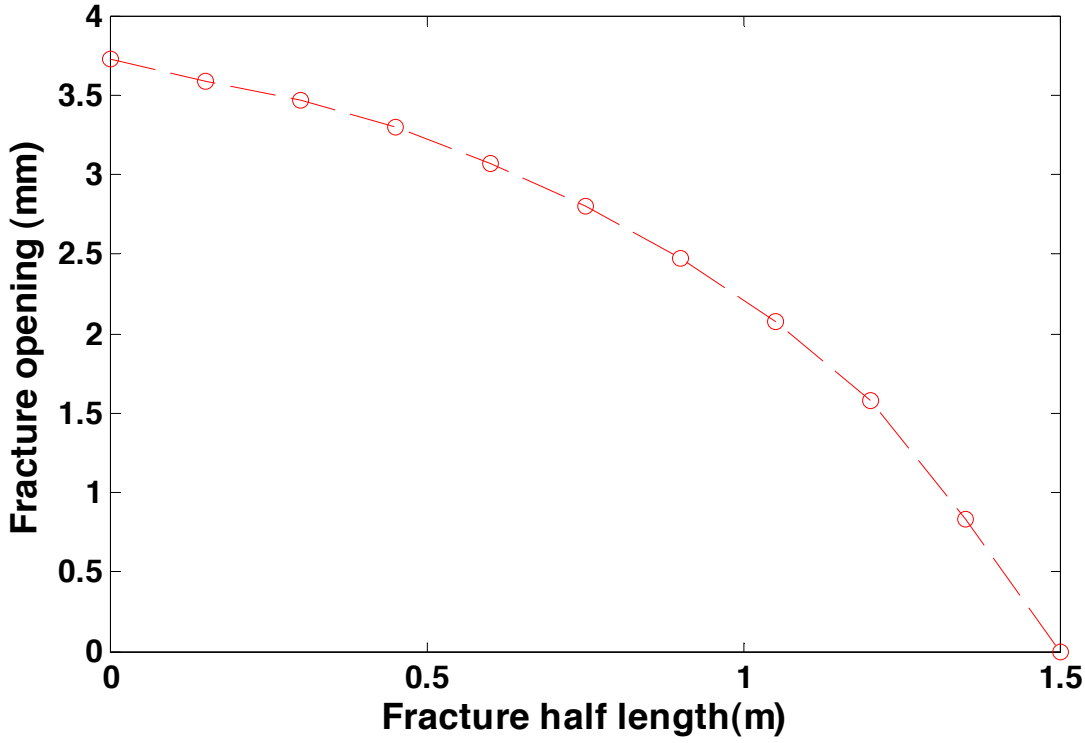

FIG. 6. Converged fracture aperture distribution

CONCLUSIONS

An algorithm for hydro-mechanical sequential coupling has been successfully developed, and the simulation results presented. This numerical model yields reasonable estimation of the key parameters, fluid pressure and fracture opening without compromising computational efficiency which can be easily caused by other numerical technique such as DFN. For the examples presented, convergence was achieved in a acceptable number of iterations by starting with a reasonable initial guess as to the fracture aperture and fluid pressure.

ACKNOWLEDGMENTS

The authors wish to thank Shell International E&P Inc. for permission to publish this conference proceeding.

NOTATION

a_J: additional degrees of freedom matched to Heaviside enrichment function
$\mathrm{b}_{\gamma K}$: additional degrees of freedom matched to Branch enrichment function
E and v: Young's modulus and Poisson's ratio
E': effective Young's modulus
$H(x)$: Heaviside enrichment function
I, J and K: order of nodes
L: fracture domain
m: number of element in each element
N: shape function
$\mathcal{N}$, $\mathcal{N}_{fr}$ and $\mathcal{N}_{tip}$: groups of regular, Heaviside enriched and Branch enriched nodes
P: hydraulic pressure
Q_i: fluid injection rate at wellbore
q_L: fracture surface leak-off rate
q_0: fluid injection rate over fracture height
r: fracture tip distance in polar coordinate system
t: time
u: displacement (standard degrees of freedom)
$\mathrm{u}(x)$: displacement approximation from the XFEM program
w: fracture aperture
w_k: k^{th} trial solution of fracture aperture
w_{well}^{anal}: fracture opening at well bore measured from the analytical solution
w_{well}^{XFEM}: fracture opening at well bore measured from the XFEM program
x: 1D coordinate along fracture
x: Cartesian coordinate vector = (x, y)
α: convergence coefficient for Picard iteration
ε: convergence criterion
θ: fracture tip angle in polar coordinate system
μ: fluid dynamic viscosity

$\varphi(x)$: signed distance function normal to the fracture
$\Phi_\gamma(x)$: Branch enrichment function

REFERENCES

Ashari, S.E. and Mohammadi, S. (2011) "Delamination analysis of composites by new orthotropic bimaterial extended finite element method." *Int. J. Numer. Methods Eng*., 86 (13): 1507–1543.

Azadi, H., and Khoei, A. R. (2011) "Numerical simulation of multiple crack growth in brittle materials with adaptive remeshing." *Int. J. Numer. Methods Eng*., *85*(8), 1017–1048.

Bellec, J. and Dolbow, J.E. (2003) "A note on enrichment functions for modelling crack nucleation." *Communications Numer. Methods Eng*., 19(12):921–932.

Belytschko, T. and Black. T. (1999) "Elastic crack growth in finite elements with minimal remeshing". *Int. J. Numer. Methods Eng*., 45(5):601–620.

Chen, Z. (2013) "An ABAQUS implementation of the XFEM for hydraulic fracture problems." *Effective and Sustainable Hydraulic Fracturing*, Dr. R. Jeffrey eds., InTech, 725-740

Dahi, A. (2009) "Analysis of hydraulic fracture propagation in fractured reservoirs : an improved model for the interaction between induced and natural fractures." PhD thesis, University of Texas at Austin

Fagerström, M. and Larsson, R. (2006) "Theory and numerics for finite deformation fracture modelling using strong discontinuities." *Int. J. Numer. Methods Eng*., 66(6): 911–948.

Geertsma, J. and de Klerk, F. (1969) "A rapid method of predicting width and extent of hydraulically induced fractures." *J. Petr.Tech*., 21:1571-81.

Moës, N., Dolbow, J., and Belytschko, T. (1999) "A finite element method for crack growth without remeshing." *Int. J. Numer. Methods Eng*., 46(1):131–150.

Pais, M.J., Yeralan, S.N., Davis, T.A. and Kim, N.-H. (2012) "An exact reanalysis algorithm using incremental Cholesky factorization and its application to crack growth modeling." *Int. J. Numer. Methods Eng*., 91(12):1358–1364.

Rungamornrat, J., Wheeler M., and Mear M. (2005) "A numerical technique for simulating non-planar evolution of hydraulic fractures." *SPE Annual Technical Conf. and Exhibition*, Society of Petroleum Engineers, Dallas, TX.

Segura, J. M., and Carol, I. (2008) "Coupled HM analysis using zero-thickness interface elements with double nodes. Part I: Theoretical model." *Int. J. Numer. Anal. Methods Geomech*., 32(18), 2083–2101.

Smith, I.M. and Griffiths, D.V. (2004) "Programming the Finite Element Method." John Wiley & Sons, Inc., Hoboken, NJ USA.

Sukumar, N. and Prévost, J.-H. (2003) "Modeling quasi-static crack growth with the extended finite element method Part I: Computer implementation." *Int. J. Solids Struct.,* 40(26):7513–7537.

Xu, C., and Dowd, P. (2010) "A new computer code for discrete fracture network modelling." *Computers & Geosciences*, *36*(3), 292–301.

Yew, C. H. (1997) "Mechanics of Hydraulic Fracturing." Gulf Professional Publishing, Houston, TX.

Modeling Flow Regime in Shale using Isogeometric Analysis

Shahriar Shahrokhabadi[1], S.M.ASCE, Farshid Vahedifard[2], M.ASCE, Ehsan Ghazanfari[3], M.ASCE

[1] Ph. D. Student, Department of Civil and Environmental Engineering, Mississippi State University, Mississippi State, MS 39762. email: ss2804@msstate.edu
[2] Assistant Professor, Department of Civil and Environmental Engineering, Mississippi State University, Mississippi State, MS 39762. email: farshid@cee.msstate.edu
[3] Assistant Professor, Civil and Environmental Engineering program, University of Vermont, Burlington, VT. email: Ehsan.Ghazanfari@uvm.edu

ABSTRACT: Fluid flow regime strongly affects fracture formation and growth in shale formations. The interaction between solid and fluid parts in a predefined discontinuity should be considered. Moreover, the fluid regime should be accurately monitored in every solution step. This study uses Isogeometric analysis (IGA), a recently developed numerical method, for modeling 1D fluid flow in shale medium. Splines, the functions commonly used in Computer-Aided design (CAD), are employed to model the geometry as well as to approximate solution results. Consequently, IGA eliminates the need for computationally-expensive remeshing which is a time consuming step in the finite element method. A benchmark problem was simulated using the proposed method and the results showed that IGA is a robust tool to model fluid flow in shale.

INTRODUCTION

Since the fluid flow regime strongly affects deformation of saturated porous media, accurate flow calculation in cohesive crack propagation is crucial and has been extensively investigated for simulation of the hydraulic fracturing process (e.g., Borden et al., 2012; Chen et al., 2010; Ghanizadeh et al., 2014). The Finite Element (FE) and Finite Difference (FD) methods have been commonly used to model fractures in porous geomaterials (Boone and Ingraffea, 1990). By taking crack propagation into account, the geometry of the problem is dynamic and an adaptive mesh FE can provide a compatible solution for crack tracking (Secchi et al., 2007).

FE formulations have been developed to predict crack growth in fully saturated porous media (e.g., De Borst et al., 2006; Segura and Carol, 2008). However, the remeshing process required to capture the dynamic geometry of fracturing is still recognized as a challenging step in the classic FE method. Even for simple linear-elastic problems, 80% of the computational time is generally spent for mesh generation to create an analysis-ready model (Simpson et al., 2013). Isogeometric

analysis (IGA) is a recently developed numerical method and has been found viable for simulation of complicated and mesh-dependent problems (Borden et al., 2012; Cottrell et al., 2009; Evans & Hughes, 2013; Irzal et al., 2013). IGA is developed based on splines, commonly Non-Uniform Rational Basis Functions (NURBS), which make the definition of geometry simple. The geometry can be built using Computer-Aided design (CAD) programs avoiding the need for mesh generation. Moreover, the derived basis functions for the geometry composition are also used to solve governing equations (Beer et al., 2013). By introducing the new concept of IGA, CAD and the FE method will be integrated and subsequently the discretization error will be omitted (Wang and Zhang, 2014). In comparison with the classic FE method, the smoothness of basis functions and accuracy of geometry modeling altogether make IGA a strong and accurate tool in computational mechanics.

This paper presents preliminary results from our ongoing effort for using IGA in hydraulic fracturing simulations. In the current paper, IGA is employed for solving 1D-flow problems. For this purpose, the Darcy's law is studied in an existing crack. It should be considered that the flow analysis is an important step which directly impacts the accuracy of hydraulic fracturing simulation results. A brief description of governing equations for fluid flow in a fully saturated medium is presented followed by basic definitions of B-splines and NURBS. Eventually, results and pertinent discussions for a benchmark problem are presented.

GOVERNING EQUATIONS FOR 1D FLOW

The momentum equation for steady-state flow is expressed as (Connor and Brebbia, 1976):

$$-\frac{1}{\rho}\frac{\partial p}{\partial x}+\frac{1}{\rho}\frac{\partial}{\partial x}\tau_i+b_i=0 \tag{1}$$

where ρ is the density of fluid, p is the pore pressure, τ_i is the friction term, and b_i is the body force in the x direction. For a homogenous, frictionless, and incompressible flow, Eq. 1 can be written based on Darcy's law as:

$$-k\nabla^2\varphi=c \tag{2}$$

where k is the permeability coefficient and φ indicates the flow pressure, and c is a constant value. Eq. 2 should meet the following boundary conditions:

$$p=\overline{p_f}\ \ on\ \Gamma_p \tag{3}$$
$$n_t.q=\overline{q}\ \ on\ \Gamma_q \tag{4}$$

where Γ_p is the essential boundary condition and Γ_q is the natural boundary condition. In Eqs. 3 and 4, $\Gamma_p \cup \Gamma_q = \Gamma$ and $\Gamma_p \cap \Gamma_q = \emptyset$. $\overline{p_f}$ and $\overline{q}$ denote the pore pressure and flux of fluid flow, respectively.

ISOGEOMETRIC ANALYSIS

The concept of IGA was initially developed based on B-splines and NURBS definitions (Cottrell et al., 2009). B-splines divide the parameter space to patches rather than elements. In the conventional FE method, every element usually has its own mapping from the parameter space. In IGA, however, a single B-spline map takes the patch from the parameter space to the physical space. Moreover, the FE method is based on polynomial interpolations while B-spline basis functions are recursive piecewise constants. The linear combination of piecewise basis functions for a set of control points forms a B-spline curve in the physical space. NURBS is basically derived from B-splines. The basis functions of B-splines are defined by a specific vector of weights. The weight vector consists of the $d + 1^{th}$ component of the control points set in R^{d+1}, where R is the physical space and d depicts the dimension of R (Cottrell et al., 2009).

KNOT VECTORS

A knot vector, Ξ, is a set of non-decreasing positive integers, ξ. That is, $\Xi = \{\xi_1, \xi_2, \xi_3, \dots, \xi_{n+p+1}\}$ where p shows the order of splines and n is the number of basis functions (Cottrell et al., 2009). The parameter space, Θ, is partitioned to several segments in which every non-zero length referred to as an element. The basis functions, $N_{i,p}(\xi)$, are defined as:

$$N_{i,p}(\xi) = \begin{cases} 1 & \xi_i < \xi < \xi_{i+1} \\ 0 & Otherwise \end{cases} \qquad \text{If } p = 0 \qquad (5a)$$

$$N_{i,p}(\xi) = \frac{\xi - \xi_i}{\xi_{i+p} - \xi_i} N_{i,p-1}(\xi) + \frac{\xi_{i+p+1} - \xi}{\xi_{i+p+1} - \xi_{i+1}} N_{i+1,p-1}(\xi) \qquad \text{If } p > 0 \qquad (5b)$$

Eqs. 5 are based on the Cox-De Boor recursion formula (Cox, 1972; De Boor, 1972). The advantageous property of B-spline functions is their C^{p-1} continuity over the element boundaries by considering the non-multiplicity of internal knots. The continuity of B-spline functions can also be controlled by the repeated internal knot vectors. Using B-splines facilitates fracture modeling since they possess continuity in higher-order derivatives. Moreover, the basis functions are desirable to have higher-order continuity to model fluid flux established by Darcy's law since they can ensure mass balance across element boundaries (De Borst et al., 2006).

If the variable ξ is considered in any position in the parameter space ($\xi_0 < \xi < \xi_{n+p+1}$), the corresponding point in the physical domain will be found by the following mapping functions:

$$C(\xi) = \sum_{i=1}^{n} N_{i,p}(\xi) B_i \qquad B_i \in \boldsymbol{B} = \{B_1, B_2, B_3, \dots., B_n\} \qquad (6)$$

where $\boldsymbol{B}$ is the control points set including nodes in the physical domain.

NON-UNIFORM RATIONAL B-SPLINES

NURBS is projection of B-splines from R^{d+1} to R^{d}. The projection is accomplished by dividing both basis functions and control points by weight functions (w). The weight function can be the $d+1^{th}$ component of the control points.

For a given B-spline curve and its associated set of control points, the components of control points for the NURBS curve are:

$$(B_i)_j = \frac{(B_i^w)_j}{w_i} \qquad j = 1,2,\ldots\ldots,d \tag{7}$$

Consequently, the NURBS basis functions can also be defined as follow:

$$R_i^p(\xi) = \frac{N_{i,p}(\xi)w_i}{W(\xi)} = \frac{N_{i,p}(\xi)w_i}{\sum_{i=1}^{n} N_{i,p}(\xi)w_i} \tag{8}$$

BENCHMARK EXAMPLE

The accuracy and convergence of the proposed numerical method were studied by solving 1D flow, which is applicable to fracturing simulation. The model geometry is shown in Figure 1. The IGA results are verified with the exact solution. The knot vectors and control points were chosen in a fashion to satisfy the Dirichlet boundary conditions. The second order NURBS (i.e., p = 2) was used to perform numerical simulations. In order to investigate the role of knot vectors in the solution accuracy, the problem was solved with two different knot vectors: $\xi_I = \{0,0,0,0.5,1,1,1\}$ and $\xi_{II} = \{0,0,0,0.25,0.5,0.75,1,1,1\}$. The control points used in the analysis were:

$$B_I = \left\{\begin{bmatrix}0\\0\end{bmatrix}, \begin{bmatrix}0.2\\0\end{bmatrix}, \begin{bmatrix}0.8\\0\end{bmatrix}, \begin{bmatrix}1\\0\end{bmatrix}\right\} \qquad B_{II} = \left\{\begin{bmatrix}0\\0\end{bmatrix}, \begin{bmatrix}0.2\\0\end{bmatrix}, \begin{bmatrix}0.4\\0\end{bmatrix}, \begin{bmatrix}0.6\\0\end{bmatrix}, \begin{bmatrix}0.8\\0\end{bmatrix}, \begin{bmatrix}1\\0\end{bmatrix}\right\}$$

The parameter space was partitioned by the number of knot vectors (i.e., 3 and 5 knot vectors). Increasing in the number of knot vectors has the equivalent function as refining mesh in the classic FE method.

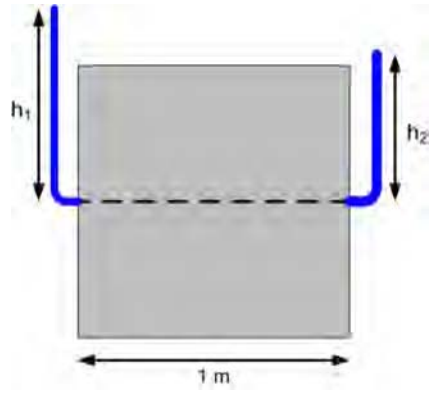

FIG. 1. 1D Flow Problem in porous media.

The shale medium is assumed to be fully saturated with water considering the gas

saturation is zero. The material has a porosity of $n = 0.1$ and permeability of $k = 0.2 \times 10^{-7}\ \frac{mm}{s}$. Two examples were considered: Example 1 includes $h_1 = 0$ and $h_2 = 0$ and Example 2 has $h_1 = 0$ and $h_2 = 100\ m$ (see Figure 1 for h_1 and h_2). The weight function, w, for all control points was 1 and the problem was solved using NURBS.

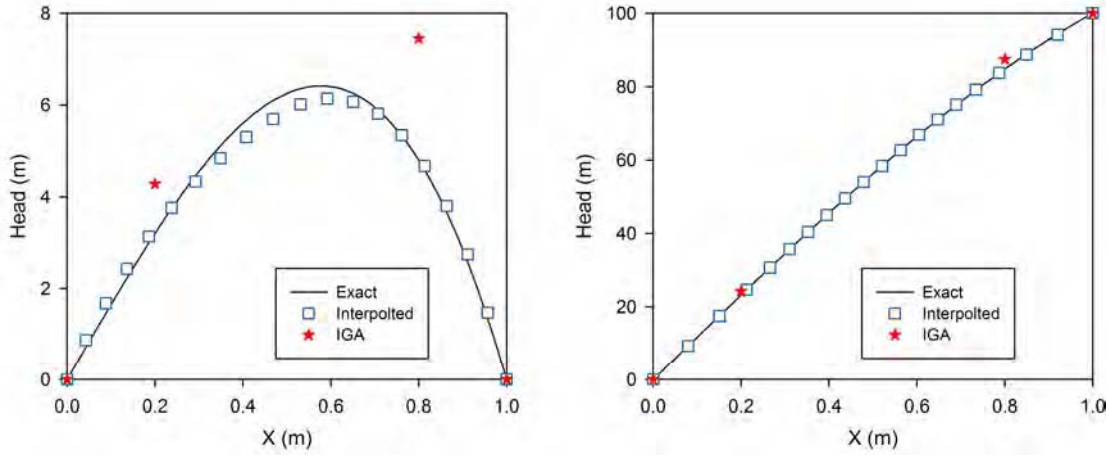

FIG. 2. Results of 1D flow simulation: (a) Example 1: imposing zero boundary condition at h_2 (b) Example 2: non-zero boundary condition at h_2.

Figure 2(a) shows the head along the crack length when the crack tips were not exposed to external pressures (Example 1). It is observed that the maximum pressure head occurs at the middle of crack length. As observed in Fig. 2, the IGA solution reasonably agrees with the exact solution for this example. Figure 2(b) depicts the pressure profile for Example 2 when the crack tip at $x = 1\ m$ is forced to external pressures. Again here, the IGA solution closely matches with those of the exact solution.

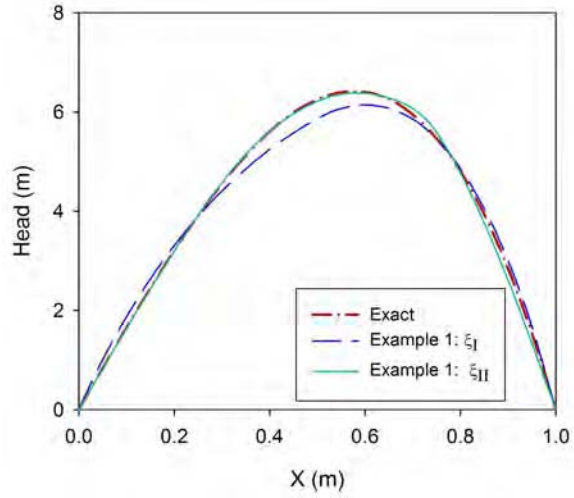

FIG. 3. Comparison of pressure heads for Example 1 for different knot vectors ($\xi_I = \{0, 0, 0, 0.5, 1, 1, 1\}$ and $\xi_{II} = \{0, 0, 0, 0.25, 0.5, 0.75, 1, 1, 1\}$).

The effect of control points and knot vectors was also investigated and the results are shown in Figure 3. It can be seen that increasing the number of knot vectors improves the accuracy of the solution. Moreover, mesh generation is not difficult anymore which is promising especially in 2D and 3D problems. It can be concluded from Figure 3 that the solution accuracy strongly depends on the knot vector formation. The difference between the exact solution results and the interpolated results is considerable at the middle of fracture where the effect of boundary conditions does not apply.

CONCLUSIONS

The 1D flow problem in shale was formulated based on isogeometric analysis (IGA). The performance of the proposed method was investigated through a simple benchmark problem. NURBS basis functions were used to simulate the hydraulic pressure through a fracture and it was shown that the hydraulic pressure is higher in the middle of fracture when the fracture tip is not exposed to an external head. In order to investigate the role of knot vectors in the solution accuracy, two different knot vectors were applied to a same problem. Results showed that for a given knot vector increasing the number of knots improves the accuracy of results. Since the effect of boundary conditions is lower in the middle of fracture in comparison with the vicinity of both ends, the effect of knot vectors on the results is obvious at the middle of fracture length. Generally, more knot vectors will lead to more accurate results. It was shown that this method is able to simulate 1D flow in fractured porous media even with a few number of knot vectors.

REFERENCES

Beer, G., Marussig, B., Duenser, C. (2013). "Isogeometric boundary element method for the simulation of underground excavations". *Géotechnique Lett*. 3, 108-111.

Boone, T. J., Ingraffea, A. R. (1990). "A numerical procedure for simulation of hydraulically driven fracture propagation in poroelastic media". *Int*. *J*. *Numer*. *Anal*. *Methods Geomech* 14, 27-47.

Borden, M. J., Verhoosel, C. V., Scott, M. A., Hughes, T. J. R., Landis C. M. (2012). "A phase-field description of dynamic brittle fracture". *Comput*. *Methods Appl*. *Mech*. *Engrg*. 217-20, 77-95.

Chen, G., Ewy, T. R., Yu, M. (2010). "Analytic solutions with ionic flow for a pressure transmission test on shale". J. Pet. Sci. Eng. 72, 158-165.

Connor, J. J., Brebbia, C. A. (1976). "Finite element techniques for fluid flow". London, Newnes-Butterworths. 317 p. 1.

Cottrell, J. A., Hughes, T. J., Bazilevs, Y. (2009). *Isogeometric analysis: toward integration of CAD and FEA*. John Wiley & Sons.

Cox, M. G. (1972). "The numerical evaluation of B-splines". *IMA J*. *Appl*. *Math*. 10, 134-149.

De Boor, C. (1972). "On calculating with B-splines". *J*. *Approx*. *Theory* 6, 50-62.

De Borst, R., Réthoré, J., Abellan, M.-A. (2006). "A numerical approach for arbitrary cracks in a fluid-saturated medium". *Arch*. *Appl*. *Mech*. 75, 595-606.

Evans, A. J., Hughes, T. J. R. (2013). "Isogemetric divergence-conforming B-splines for the unsteady Navier-Stokes equations". *J. Comput. Mech* 241, 141-167.

Ghanizdeh, A., Gasparik, M., Hildenbrand, A. A., Gensterblum, Y., Krooss, B. (2014). "Experimental study of fluid transport processes in the matrix system of the European orgnic-rich shales: I. Scandinavian Alum Shale". Mar. Pet. Geol. 51, 79-99.

Irzal, F., Remmers, J. J. C., Verhoosel, C. V., de Borst, R. (2013). "An isogeometric analysis approach to fluid flow in a fractured porous medium". *Poromech. ASCE.* 872-882.

Secchi, S., Simoni, L., A Schrefler, B. (2007). "Mesh adaptation and transfer schemes for discrete fracture propagation in porous materials". *Int. J. Numer. Anal. Methods Geomech* 31, 331-345.

Segura, J., Carol, I. (2008)." Coupled HM analysis using zerothickness interface elements with double nodes. Part I: Theoretical model". *Int. J. Numer. Anal. Methods Geomech* 32, 2083-2101.

Simpson, R., Bordas, S., Lian, H., Trevelyan, J. (2013). "An isogeometric boundary element method for elastostatic analysis: 2D implementation aspects". *Comput. Struct*. 118, 2-12.

Wang, D., Zhang, H. (2014). "A consistently coupled isogeometric–meshfree method". *Comput. Method. Appl. Mech. Eng*. 268, 843-870.

Towards a Real-Time Forecast of Induced Seismicity for Enhanced Geothermal Systems

Dimitrios C. Karvounis[1], Ph.D., Valentin S. Gischig[2], Ph.D. and Stefan Wiemer[3], Prof., Ph.D.

[1]Post-doctoral Researcher, ETH Zürich, Schweiz. Erdbebendienst (SED), Sonneggstrasse 5, NO H 62, 8092 Zuerich, dkarvoun@ethz.ch
[2] Post-doctoral Researcher, ETH Zürich, Schweiz. Erdbebendienst (SED), Sonneggstrasse 5, 8092 Zuerich, gischig@sed.ethz.ch
[3]Director SED, ETH Zürich, Schweiz. Erdbebendienst (SED), Sonneggstrasse 5, NO H 61, 8092 Zuerich, stefan.wiemer@sed.ethz.ch

ABSTRACT: The development of novel technologies such as Enhanced Geothermal Systems (EGS) has been decelerated due to induced seismicity. Sophisticated traffic light systems, which assess the seismic hazard in time for taking precautionary measures, can assist in the successful development of EGS sites close to urban areas. We present here the modeling approach for a hybrid model that can be used in such a traffic light system. This hybrid model combines the HFR-Sim software with stochastic models that have been used for forecasting induced seismicity. HFR-Sim is an EGS simulator, which can model flow inside dynamically changing fracture networks. It offers discrete representation of fractures, and can be used for simulating a wide range of three dimensional problems, which are related to the design, creation and operation of an EGS reservoir. Here, the coupling of HFR-Sim with a stochastic seed model is explained. Exemplary simulations are performed with the resulting software and the results obtained by those simulations are discussed.

INTRODUCTION

Many deep reservoir engineering projects require fluid injection, which results to human-induced earthquakes, increases the earthquake rate at those locations (Ellsworth 2013) and thus, can cause public anxiety and, in some occasions, may be a potential hazard for the local population and structures. This induced seismicity hazard is one of the main reasons for the deceleration of Enhanced Geothermal Systems (EGS) development, a novel technology for electrical power generation that aims to exploit the abundant deep geothermal resources and which, if it is successfully developed, can provide up to 70 GWe installed capacity by the year 2050 (Bertani 2012).

EGS technology relies on artificially enhancing the permeability of naturally fractured reservoirs. High pressure cold fluid is injected through each well into the

hot reservoir and hydro-shearing occurs, which reduces the overall reservoir impedance. These reservoir stimulations can be considered successful when the resulting reservoir allows the production of hot fluid at commercially interesting flow rates and the induced seismicity is neither a nuisance nor a hazard. The latter is important because felt earthquake events may occur, as was the case for the induced 3.4 magnitude earthquake event in Basel (Switzerland) in 2006, which resulted in the cancelation of the EGS project there (Kraft et al. 2009). It becomes clear that only if the induced seismicity hazard is kept low, the technology can be applied in urban environments, where the waste heat could also be used for heating.

For that reason, sophisticated traffic light systems are required, which operate in real time during the stimulation of an EGS reservoir. Such tools assess the hazard and the risk of the planned stimulation strategy and return these results to the reservoir operators in time for altering the implemented stimulation strategy. Bachmann et al. (2011), and Mena et al. (2013) have tested different statistical methods that were partly able to forecast expected seismicity for six hours in advance and are based on the applied injection rates. Such methods are solely data-based and do not include any physical process that is relevant for injection-induced seismicity. Goertz-Allmann and Wiemer (2013), and Gischig and Wiemer (2013) attempt to avoid this drawback and couple the stochastic processes to pressure solutions and form the so-called hybrid approaches. The former use the analytical pressure solution for a point source linear problem and the latter uses the numerical solution for a line source non-linear problem. In both cases, seismicity is modeled using the so-called 'seed points', which are potential earthquake locations and can be triggered only by enhanced fluid pressure.

These modeling approaches reproduce both the wellhead pressure curve and the seismicity characteristics of the Basel stimulation experiment in 2006. However, in these approaches the pressure solution is solved for reservoirs of reduced dimensions, where permeability is initially isotropic, homogeneous and can increase only in an isotropic manner. As a result, the pressure fronts for highly heterogeneous 3D reservoirs cannot be captured representatively, while rarely show up the fine spatial pressure variations, due to the large fractures. Important information, such as the position and the orientation of the fractures that have been penetrated by the well, is neglected.

In order to develop a hybrid model that does not suffer from the above mentioned limitations, the seed model needs to be extended into three dimensions and a discrete fracture model (DFM) should be employed for the flow and heat transport modeling. DFMs can be divided into two categories: the conforming and the embedded approaches. Conforming DFMs, such as the one suggested by Kohl et al. (1995), the DFM used by McClure and Horne (2011), and the one employed by the CSMP++ code (Matthai 2005, Geiger et al. 2006), discretize the medium around the complex shaped fractures with a grid that conforms to the complex shape of those fractures. Consequently, for performing probabilistic ISHA, all foreseeable fractures need to be prescribed and discretized, independently of whether they participate in the flow or not. This computational cost could be avoided with the use of embedded approaches that employ a structured grid for the matrix that surrounds the large discrete fractures. The DFM employed by the EGS simulator HFR-Sim (Karvounis and Jenny 2011,

Karvounis 2013) is one of those. In HFR-Sim the pre-description of all fractures is not necessary.

Here, we present the modeling framework for a hybrid model that aims to combine the seed model approach with more realistic solutions for the pressure field inside an EGS reservoir. The seed model by Gischig and Wiemer (2013) is extended into three dimensions and it bases the decision to trigger a seed point upon the transient pressure solution that is returned by HFR-Sim. Triggered seeds are modeled by HFR-Sim as additional discrete fractures. This new hybrid model will be used in the future for real time probabilistic seismic hazard assessment (PSHA) and is currently under development. Issues regarding maximum magnitude of induced earthquakes are not considered here. In principle, and with few modifications, such hybrid models can be employed for forecasting induced seismicity in a wide range of sites where fluid is injected (e.g. shale gas reservoirs or waste water disposal sites).

MODELING FRAMEWORK FOR THE HYBRID MODEL

A near real-time traffic light system is currently under development by the Swiss Seismological Service (SED). Every few hours the induced seismicity hazard is assessed for a period of hours up to several days into the future. For this, seismicity and hydraulic data that has been measured up to that time is used for calibrating the employed models. Hence, the model improves at each new calibration, which reduces the uncertainty range for the subsequent estimate of induced seismic hazard. Figure 1 illustrates the framework for the traffic light system that is under development and the central role that hybrid models have for performing PSHA there.

The hybrid model, that is presented here, is needed both for calibrating the employed reservoir models towards observed real-data ('history matching') as well as for PSHA estimate for the future time periods. During the 'history matching' process, the hybrid model is used numerous times until a set of hydraulic parameters matching the observed seismicity, focal mechanisms and well data is located. During the PSHA calculations, the model is used numerous times until a large number of equally probable synthetic catalogs are produced. Then, the probability of inducing a seismic event of magnitude larger than a certain magnitude can be estimated.

The hybrid model consists of the HFR-Sim software and the stochastic 'seed model', which are loosely coupled to each other. At each time step, HFR-Sim returns an approximation of the pressure distribution and subsequently, the seed model performs all the geomechanical modeling; i.e. the seed model decides 1) which seeds are saturated with fluid of pressure high enough to trigger them and 2) what is the fracture network that HFR-Sim needs to simulate at the next time step.

Stress interaction between fracutres, gravitational phenomena and thermal effects are not considered here. Single phase flow is modeled everywhere and permeability does not increase aseismically. Without loss of generality, hydro-shearing is the only earthquake mechanism that is considered here.

Flow Calculations with HFR-SIM

Henceforth, single phase Darcy flow is assumed everywhere and the Boussinesq

approximation is employed. The density of the fluid ρ and the viscosity of the fluid μ are assumed constant. The reservoir is characterized by a porosity φ and a permeability tensor $\underline{\underline{k}}$, which can change dynamically, e.g. when the permeability of fractures increases due to hydro-shearing.

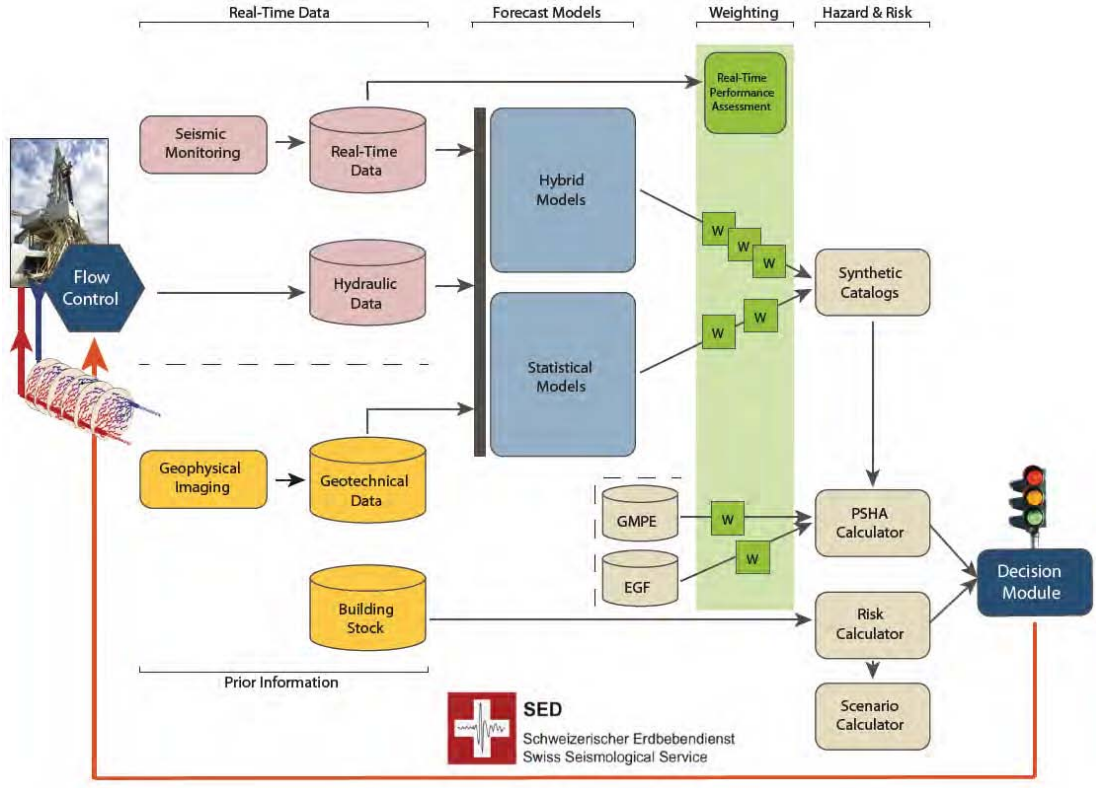

FIG. 1. The algorithmic framework for the real time traffic light system is illustrated above. The hybrid and the statistical models, post-process the real time data and prior information, in order to return synthetic catalogs. These catalogs are used for performing PSHA and for changing the injection rate accordingly. The image is adapted by the webpage of the Induced Seismicity group in SED.

Mass conservation in a Cartesian grid can now be expressed as

$$\frac{\partial \varphi}{\partial t} - \nabla \cdot \left(\frac{\underline{\underline{k}}}{\mu} \cdot \left(\nabla p - \rho \underline{g} \nabla z \right) \right) = q, \tag{1}$$

where p is the fluid pressure, $\underline{g}$ the vector for gravitational acceleration, z the depth and q a source term. This governing equation is here solved with HFR-Sim.

HFR-Sim uses an embedded DFM, where discrete fractures are treated as lower dimensional manifolds. It employs a hierarchical fracture representation where large, dominant fractures are treated by a discrete representation and the cumulative effect

of the small fractures is captured by a continuum description of the so called 'damaged matrix'. A rather coarse and structured grid can be used for the damaged matrix and a structured grid can be also employed for each one of the discrete fractures. A simple well model is employed, where the fluid pressure along the open case of the well is considered constant and thus, each open case well corresponds to only one control volume.

Once the discrete fractures, the damaged matrix and the wells have been divided into smaller control volumes, a node is assigned to each control volume and connections are added between nodes, where mass exchange can occur. Obviously, mass exchange can only occur between volumes that have a common interface; i.e. adjacent damaged matrix cells, adjacent cells from the same discrete fracture grid, intersecting cells from two different discrete fractures, intersecting cells, where the one belongs to the damaged matrix, and the other to a discrete fracture and finally, all the cells that are penetrated by the well volume. Eventually, a graph is obtained that resembles to a tube network.

This tube network is adaptive to dynamic changes in the network of discrete fractures. New discrete fractures can be added to the computational domain without the need of re-meshing, since the structured grids employed for the discrete fractures do not need to conform to the boundaries of any other employed grid.

Equation (1) can now be solved inside this tube network. The transmissibility $C_{M,J}$ is computed at each tube, such that volume flux from node M to volume J equals $F_{M,J} = C_{M,J}(P_M - P_J - (Z_M - Z_J)\rho|\underline{g}|)$, with P_M corresponding to the mean volume pressure, Z_M the average depth of the volume and $C_{M,J}$ is derived by applying the finite volume method to Eq. 1. If volume M or J is a well volume, then transmissibility $C_{M,J}$ is computed similarly to how Peaceman (1978) computed the production index of a well. Now, the equation of mass conservation results into a discretized system of N equations, where N is the total number of control volumes and each equation M is

$$\frac{\partial V_M}{\partial t} + \sum_{J=1}^{N} C_{M,J}(P_M - P_J - (Z_M - Z_J)\rho|\underline{g}|) = Q_M, \tag{2}$$

where Q_M is the rate of the injected fluid and V_M is the size of the volume M, which is a function of the pressure distribution.

Henceforth, it is assumed that $\frac{\partial V_M}{\partial t} = 0$ if M is a well volume and $\frac{\partial V_M}{\partial t} = S_M \frac{\partial P_M}{\partial t}$ otherwise, where S is the average storativity of the volume M for an incompressible fluid.

Finally, it is noted that HFR-Sim uses an efficient linear system solver, i.e. an algebraic multigrid (AMG) solver with a Gauss-Seidel method as a smoother. As a result, the convergence rate for solving the system of equations described by Eq 2 scales linearly with the size N.

Seed Model

We consider a number of N_s seeds distributed in space. Each seed is a potential earthquake location, thus it is assumed that they all lay on faults. For the i-th seed, which in a Cartesian system is located at $\underline{x}^i=(x^i,y^i,z^i)^T$, we assume that the seed is located on a fault with pole unit vector $\underline{P}^i$, we assign to it three principal compressive stress vectors $\underline{\sigma}_1^i$, $\underline{\sigma}_2^i$ and $\underline{\sigma}_3^i$ representative of the ambient stress field, as well as, friction coefficient μ_c^i and cohesion C^i.

For each seed point *i* the values of the normal stress σ_n^i and of the shear stress τ_n^i are analytically computed. The value of the effective normal stress equals to

$$\sigma_{n,eff}^i = \sigma_n^i - p\left(\underline{x}^i\right), \tag{3}$$

where the pressure of the fluid at each seed point can be interpolated from the solution returned by HFR-Sim. According to the Mohr-Coulomb failure criterion, a fault slips around the seed point when the ratio

$$(\tau_n^i - C^i)/\sigma_{n,eff}^i \tag{4}$$

exceeds the frictional strength μ_c^i.

Here, it is assumed that when a seed slips, an earthquake is triggered. A b^i value (describing a Gutenberg-Richter distribution) is assigned to this seed point by using a negative linear relationship with the differential stress $\Delta\sigma = \left(\left|\underline{\sigma}_1^i\right| - \left|\underline{\sigma}_3^i\right|\right)$; i.e. the b^i value increases as the differential stress Δσ decreases. Afterwards, a random magnitude M_w^i is drawn from a Gutenberg-Richter distribution with the b-value b^i accordingly and a 'new' discrete fracture is introduced into the HFR-Sim model. This fracture has the shape of a circle which is centered in $\underline{x}^i$ and the vector $\underline{P}^i$ is normal to this fracture. The sampled magnitude M_w^i is converted to moment M_0^i by using the Hanks and Kanamori (1979) relationship

$$M_0^i = 10^{1.5(M_w^i+6.03)} \tag{5}$$

Note that $[M_0^i]$=N×m. The stress drop of the earthquake is here considered constant for all earthquake events, i.e. $\Delta\tau^i=\Delta\tau$= 3.0 MPa and thus, the radius size r^i of the fracture is computed by the relationship given by Eshelby (1957)

$$r^i = \sqrt[3]{\frac{7M_0^i}{16\Delta\tau}}\,. \tag{6}$$

The hydraulic aperture b_h^i of the new fracture is considered constant thus, all new fractures have the same permeability.

The N_s seeds are uniformly distributed inside the domain. The directions of the principal stresses are kept constant for all seeds and a Gaussian distribution is employed for sampling their values. The pole of each seed is uniformly distributed around a mean pole direction and with a maximum acceptable dilation angle from this mean pole direction. More than one sets of seeds can be employed, where each set of seeds *j* has N_S^j seeds, its own mean pole vector and maximum dilation angle.

EXEMPLARY SIMULATION

Here, a fictional three-step stimulation scenario is simulated, where stimulation starts with an injection rate of 5.0 *l/s* which increases by 5.0 *l/s* every 36 hours. The injection scenario is plotted in Figure 2a. The simulated EGS reservoir has the shape of a cube, where each of its sides is 1.28 *km* long and the bottom of the reservoir is located at 5.6 *km*. A 50×50×50 orthogonal grid is employed for this three dimensional domain. Inside the reservoir lies the open case of the injection well, which has its bottom at 5.0 *km*, it is 368.0 *m* long and it has a radius of 0.18 *m*. The well is considered a straight horizontal line that goes through the center of the cubical EGS reservoir. Two discrete fractures, which are identical, penetrate the well at 4.681 *km* of depth and 4.881 *km* of depth, respectively. These two fractures are parallel to each other and they have the shape of a circle, which is centered on the well and the vector $(-0.447214,0,0.894428)^{\mathrm{T}}$ is normal to these two circles. The length of the radius of these circles is 223.607 *m* and the permeability for both fractures is considered equal to 1.041×10^{-14} m^2. It is noted that this fracture permeability corresponds to a hydraulic aperture of approximately 50 μm. The permeability at the rest of the domain equals to 2×10^{-16} m^2 and the value of storativity is set to 10^{-11} m^3/Pa both for the continuum domain and for the two discrete fractures. The density and the viscosity of the fluid are considered constant and equal to 10^3 kg/m^3 and 10^{-3} $Pa{\cdot}s$, respectively. Gravitational effects are neglected.

In total 10,000 seed points are sampled inside the reservoir. They are uniformly distributed in space, the pole vectors sampled to them may have any orientation and the axis of the principal stresses are considered parallel to the system of coordinates; i.e. $\underline{\sigma}_1^i = (0, 0, \left|\underline{\sigma}_1^i\right|,)^{\mathrm{T}}$, $\underline{\sigma}_2^i = (0, \left|\underline{\sigma}_2^i\right|, 0)^{\mathrm{T}}$ and $\underline{\sigma}_3^i = (\left|\underline{\sigma}_3^i\right|, 0, 0)^{\mathrm{T}}$,. Three normal distributions are employed for the values of the principal stresses; i.e. $\left\langle\left|\underline{\sigma}_1^i\right|\right\rangle = 185.0\,\mathrm{MPa}$, $\left\langle\left|\underline{\sigma}_2^i\right|\right\rangle = 90.0\,\mathrm{MPa}$ and $\left\langle\left|\underline{\sigma}_3^i\right|\right\rangle = 75.0\,\mathrm{MPa}$, while each standard deviation is equal to the 10% of the mean principal stress to which it corresponds. The hydrostatic pressure of the reservoir is assumed equal to 45.0 MPa and thus, stresses lesser than 45.0 MPa are not allowed. Without loss of generality, the maximum stress value allowed is 232.0 MPa. For all seeds cohesion is 7.0 MPa and the friction coefficient is 0.85. Re-sampling is applied to the seeds that would satisfy the Mohr-Coulomb failure criterion if their friction coefficient was 0.8. The b value

ranges from 1.0 to 1.8 and the magnitude M_w^i of the earthquakes that occur is sampled from 0.85 to 6.0. In Figure 2c the normal stress σ_n^i is plotted versus the shear stress τ_n^i for all the seeds that are eventually used by the hybrid model. It is noted that M_w^i can be sampled from any range of magnitudes wanted. Also, the model that is considered here has not been calibrated with any real data. However, the employed settings are similar to other models of the EGS reservoir in Basel.

The simulated well pressure is plotted in Figure 2c, while Figure 2d shows the magnitude of the triggered seeds and when they are triggered during the simulation. Discrete fractures are added only for earthquakes that have magnitude above the straight horizontal line (approximately $M_{w\,\min}^i$=1.36). This lower limit ensures that all discrete fractures penetrate more than grid-blocks from the employed orthogonal grid. Here, the rest of the earthquakes are considered to have a negligible effect on the flow and re-triggering is not allowed.

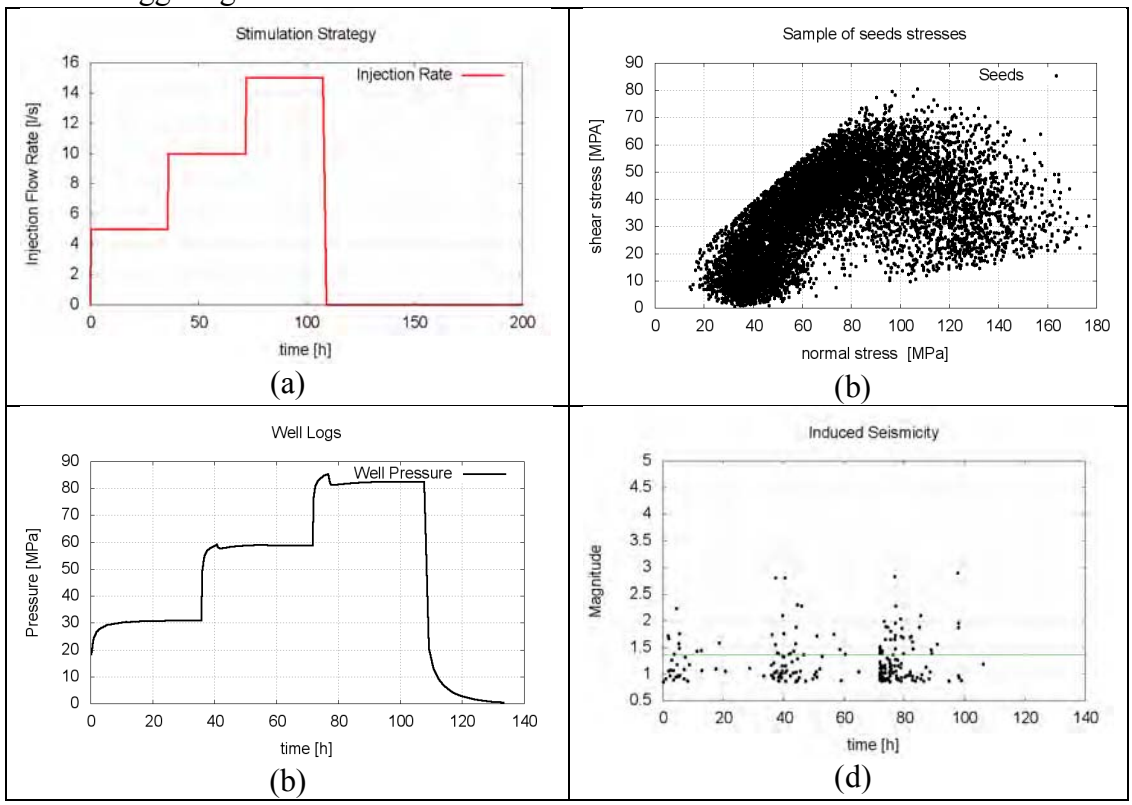

FIG. 2. In (a) the assumed injection strategy is shown. In figure (b) the sampled normal stress is plotted versus the sampled shear stress for all the employed seeds. The evolution of the simulated well pressure is plotted in (c). The magnitude of the induced seismicity versus time is plotted in (d). Here, each dot corresponds to a seed which is triggered at that moment and produces an earthquake of that magnitude. The seeds above the thin green line introduce discrete fractures to the flow model of HFR-Sim henceforth.

According to the model, the rate of induced seismicity increases when the injection

rate increases. This rate decreases while the injection rate remains constant thus, the pressure field in the model approaches its steady state pressure solution. This rapid approach to the steady state solution, as well as the rapid well pressure drop after the injection shut-in, can be explained by the low value of storativity that is chosen for this exemplary simulation. The impedance of the well is in overall reduced. Initially, the impedance of the well is 6.0 MPa/(l/s) and after the shut-in the impedance is dropped to approximately 5.3 MPa/(l/s). Out of the four earthquakes with magnitude above 2.5, three of those caused the largest reduction of the impedance.

CONCLUSIONS

A hybrid model has been presented, which is under development and it combines modeling of flow with stochastic geomechanic considerations. The EGS simulator 'HFR-Sim' is used for modeling flow inside an EGS reservoir. HFR-Sim employs a discrete fracture representation for large fractures and it adds new fractures to the employed meshed model, whenever the stochastic model triggers an earthquake. At each iteration step, the pressure field is approximated by HFR-Sim, the synthetic catalog of events is updated by the stochastic seed model and the fracture EGS model is updated with new discrete fractures. Exemplary simulations that have been performed with this novel hybrid model have been presented and discussed.

ACKNOWLEDGMENTS

The authors appreciate the support of Geo-Energie Suisse in the development of the near real time traffic light system and Delano Landtwing for his assistance.

REFERENCES

Bachmann C., Wiemer S., Woessner J., Hainzl S. (2011). Statistical analysis of the induced Basel 2006 earthquake sequence: Introducing a probability-based monitoring approach for Enhanced Geothermal Systems. Geophys. J. Int. (2011) 186, 793–807.

Bertani, R. (2012). Geothermal power generation in the world 2005–2010 update report. Geothermics, 41, 1–29. doi:10.1016/j.geothermics.2011.10.001

Ellsworth, W. L. (2013). Injection-induced earthquakes. Science (New York, N.Y.), 341(6142), 1225942. doi:10.1126/science.1225942

J. D. Eshelby (1957). The Determination of the Elastic Field of an Ellipsoidal Inclusion, and Related Problems, Proceedings of the Royal Society of London. Series A, Mathematical and Physical Sciences , Vol. 241, No. 1226 (Aug. 20, 1957), pp. 376-396

Gischig, V. S., & Wiemer, S. (2013). A stochastic model for induced seismicity based on non-linear pressure diffusion and irreversible permeability enhancement. Geophysical Journal International, 194(2), 1229–1249. doi:10.1093/gji/ggt164

Goertz-Allmann, B. P., & Wiemer, S. (2013). Geomechanical modeling of induced seismicity source parameters and implications for seismic hazard assessment. GEOPHYSICS, 78(1), KS25–KS39. doi:10.1190/geo2012-0102.1

Geiger, S., Driesner, T., Heinrich, C. A., & Matthäi, S. K. (2006). Multiphase

Thermohaline Convection in the Earth's Crust: II. Benchmarking and Application of a Finite Element – Finite Volume Solution Technique with a NaCl–H2O Equation of State. Transport in Porous Media, 63(3), 435–461. doi:10.1007/s11242-005-0109-y

Hanks, T. C., & Kanamori, H. (1979). A moment magnitude scale. Journal of Geophysical Research, 84(B5), 2348. doi:10.1029/JB084iB05p02348

Karvounis, D., & Jenny, P. (2011). Modeling of Flow and Transport in Enhanced Geothermal Systems. Thirty-Sixth Workshop on Geothermal Reservoir Engineering. Stanford University, Stanford, California, USA.

Karvounis, D. C. (2013). Simulations of enhanced geothermal systems with an adaptive hierarchical fracture representation. ETH. doi:10.3929/ethz-a-009967366

Kraft, T., Mai, P. M., Wiemer, S., Deichmann, N., Ripperger, J., Kästli, P., Bachmann, C., et al. (2009). Enhanced Geothermal Systems: Mitigating Risk in Urban Areas. Eos, Transactions American Geophysical Union, 90(32), 273. doi:10.1029/2009EO320001

Kohl, T., Evansi, K. F., Hopkirk, R. J., & Rybach, L. (1995). Coupled hydraulic, thermal and mechanical considerations for the simulation of hot dry rock reservoirs. Geothermics, 24(3), 345–359. doi:10.1016/0375-6505(95)00013-G

McClure, M. W., & Horne, R. N. (2011). Investigation of injection-induced seismicity using a coupled fluid flow and rate/state friction model. GEOPHYSICS, 76(6), WC181–WC198. doi:10.1190/geo2011-0064.1

Matthäi, S. K., Mezentsev, A., & Belayneh, M. (2005). Control-Volume Finite-Element Two-Phase Flow Experiments with Fractured Rock Represented by Unstructured 3D Hybrid Meshes. Proceedings of SPE Reservoir Simulation Symposium. Society of Petroleum Engineers. doi:10.2118/93341-MS

Mena, B., Wiemer, S., & Bachmann, C. E. (2013). Building Robust Models to Forecast the Induced Seismicity Related to Geothermal Reservoir Enhancement. Bulletin of the Seismological Society of America, 103(1), 383–393. doi:10.1785/0120120102

Peaceman, D. W. (1978). Interpretation of Well-Block Pressures in Numerical Reservoir Simulation(includes associated paper 6988). Society of Petroleum Engineers Journal, 18(3), 183–194. doi:10.2118/6893-PA

Predicting the Seismic Hazard Due to Deep Injection Well Induced Seismicity

Ali Fatehi, Ph.D.[1], Richard Quittmeyer, Ph.D.[2], Melih Demirkan, Ph.D., P.E.[3], Jose Blanco, Ph.D.[4], Jeffrey Kimball[5]

[1]Technical Director, Paul C. Rizzo Associates, Inc., 500 Penn Center Blvd., Suite 100, Pittsburgh, PA 15235 Email: ali.fatehi@rizzoassoc.com
[2]Vice President Seismology, Paul C. Rizzo Associates, Inc., 500 Penn Center Blvd., Suite 100, Pittsburgh, PA 15235 Email: richard.quittmeyer@rizzoassoc.com
[3]Managing Principal, Paul C. Rizzo Associates, Inc., 500 Penn Center Blvd., Suite 100, Pittsburgh, PA 15235 Email: melih.demirkan@rizzoassoc.com
[4]Technical Director, Paul C. Rizzo Associates, Inc., 500 Penn Center Blvd., Suite 100, Pittsburgh, PA 15235 Email: jose.blanco@rizzoassoc.com
[5]Principal Seismologist, Paul C. Rizzo Associates, Inc., 500 Penn Center Blvd., Suite 100, Pittsburgh, PA 15235 Email: jeffrey.kimball@rizzoassoc.com

ABSTRACT: Disposal of flow-back and produced waters in deep injection wells is known to induce earthquakes in a small number of cases. While many of these induced earthquakes are small (less than moment magnitude [M_W] 5), some are in the M_W 5 to 6 range and, potentially, can be a significant contributor to seismic hazard at a nearby site. Assessing seismic hazard from disposal-induced earthquakes is complicated by uncertainties in the characteristics of the events. Probabilistic seismic hazard analysis (PSHA) provides a way to incorporate these uncertainties. As a first step, this paper identifies some issues in characterizing disposal-induced seismicity for PSHA and discusses approaches that may be used to address them. Issues discussed are characterization of the rate of recurrence, maximum magnitude, ground motion prediction, and focal depth.

INTRODUCTION

Various human activities are known to induce seismic activity. Some of these activities include reservoir impoundment, natural gas and hydrocarbon extraction, mining, hydraulic fracturing, waste water disposal, and geothermal energy development (e.g., Gupta, 1992; Grasso, 1992; Davis and Frohlich, 1993; Talwani, 1997; Phillips et al., 2002; Gupta, 2005; Suckale, 2009). While, in general, induced earthquakes are relatively small ($M < 5.0$), larger magnitude events ($M \geq 6.0$) are known to have been induced by reservoir impoundment (e.g., Gupta, 2005; Suckale, 2009). There are also controversial cases of larger magnitude induced events attributed to human activities in hydrocarbon fields (See Suckale, 2009 for a summary).

This paper deals with the case of induced seismicity due to deep fluid injection and the assessment of its associated hazard. The proposed methodology for assessing the hazard, however, can be applied to other cases of induced seismicity with or without slight modifications.

INDUCED SEISMICITY DUE TO DEEP FLUID INJECTION

While infrequent, in some cases deep fluid injection induces earthquakes. Kim (2013) summarizes several recent cases of earthquakes in the U.S. that are thought to be induced by fluid injection into subsurface strata through disposal wells. These events are summarized in Table 1 (Kim, 2013). The largest of these events (the 2011 M_W 5.7 earthquake in Prague, Oklahoma) occurred within the Wilzeta oil field and at a distance of 180 km from the closest known Quaternary-active fault (Keranen et al., 2013).

Table 1. Recent Cases of Potentially Induced Earthquakes in the United States (Kim, 2013)

Date	Lat. (°N)	Lon. (°W)	Depth (km)	Magnitude (M_W)	Location
2011-11-06	33.53	96.77	5	5.7	Prague, OK
2011-08-23	37.06	104.70	4	5.3	Trinidad, CO
2011-10-20	28.86	98.08	5	4.8	Fashing, TX
2012-05-17	31.93	94.37	5	4.8	Timpson, TX
2011-02-28	32.57	92.34	3	4.7	Guy, AR
2011-09-11	32.85	100.77	5	4.3	Snyder, TX
2011-12-31	41.12	80.68	5	3.9	Youngstown, OH
2009-05-16	32.97	97.02	4	3.3	Dallas-Fort Worth, TX

In general, the impact of ground shaking from the induced seismicity due to deep fluid injection is minimal due to the small magnitudes of the induced events. However, the possible link between the 2011 M_W 5.7 Oklahoma earthquake and deep fluid injection indicates the potential for larger-magnitude induced earthquakes. It is desirable, therefore, to study the characteristics of such induced seismicity and quantify its impact on seismic hazard.

This paper identifies and discusses issues in using the Probabilistic Seismic Hazard Analysis (PSHA) methodology (e.g., Cornell, 1968; Reiter, 1990; McGuire, 2004) to quantify the impact of induced seismicity due to deep fluid injection. PSHA has become the standard approach for the assessment of seismic hazard due to natural seismicity. It has also begun to be applied in the assessment of seismic hazard due to induced seismicity (e.g., Lasocki, 2005; Van Eck et al., 2006; Convertito, et al., 2012).

The mechanism of induced seismicity is discussed extensively in the literature. For detailed discussions on the mechanisms of induced seismicity, the reader is referred to Grasso (1992), Talwani (1997), and Suckale (2009).

PSHA METHODOLOGY

Probabilistic Seismic Hazard Analysis determines the annual frequency or rate of exceedance of some level of an earthquake ground motion measure, such as peak ground acceleration (PGA), at a specific site. This result can alternatively be viewed as the average return period for exceedance of the ground motion level. A seismic hazard curve shows the variation in annual frequency of exceedance as a function of the level of ground motion.

A key aspect of PSHA is the incorporation of epistemic (knowledge) uncertainty and aleatory (random) variability in characterization of seismic sources and ground motion. For epistemic uncertainty, a logic tree format is often used to represent weighted alternative interpretations of parameter values. Hazard is calculated for each combination of alternatives. Aleatory variability is typically represented by continuous or discrete probability distributions and included in the integration carried out to determine each hazard curve. The final results of the PSHA are used in the design of buildings, lifelines and other critical structures.

The PSHA process (Figure 1) can be summarized in the following steps:

- Identification of earthquake (seismic) sources judged to be capable of generating significant ground motions at the site
- Determination of annual rates of earthquakes of different magnitudes within each seismic source, including the maximum magnitude that can occur
- Predicting the earthquake ground motion at the site resulting from earthquakes for each seismic source
- Combining uncertainties in earthquake location, size, and ground motion and calculating annual rates of exceedance for different levels of ground motion at the site.

Mathematically, the process is expressed as:

$$\nu(z) = \sum_i \alpha_i(m_0) \int f_i(m)[\int f_i(r|m)P(Z > z|r,m)dr]dm \quad (1)$$

in which Z is a measure of ground motion (e.g., PGA, or Spectral Acceleration, SA, at a prescribed response frequency); $P\ (Z>z|m,r)$ is the conditional probability that Z will exceed value z for earthquake magnitude, m, and distance, r; $f(m)$ and $f(r|m)$ are probability density functions for magnitude and for distance given magnitude; and $\alpha_i(m_0)$ is the number of earthquakes per year above a prescribed minimum magnitude, m_0, for the i-th seismic source.

For each seismic source, the integration over magnitude is performed from m_0 to the maximum magnitude, M_{max}. Integration over distance is carried out to a sufficient distance such that significant contributors to hazard are included.

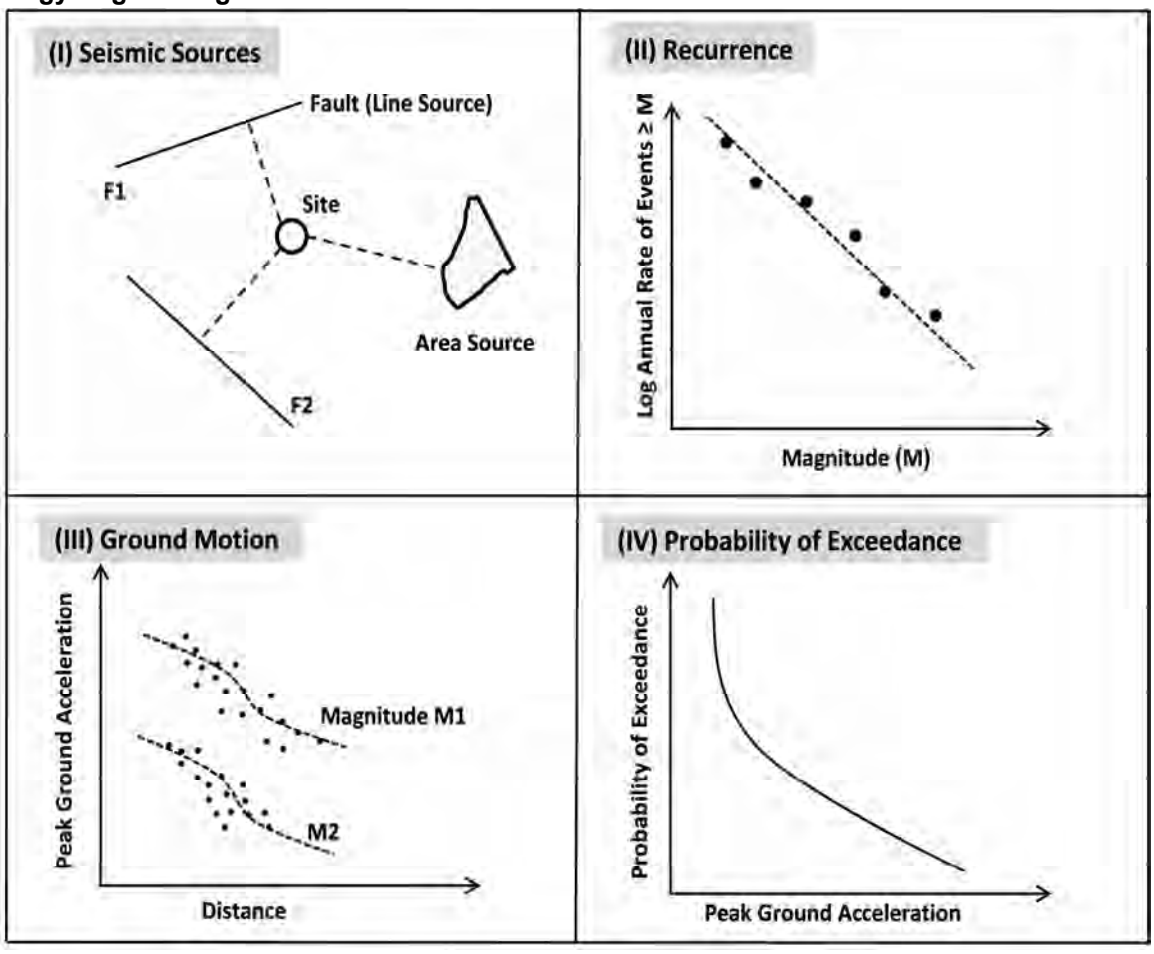

FIG. 1. Basic Steps of Probabilistic Seismic Hazard Analysis

PSHA INPUT

Inputs to a PSHA consist of a seismic source characterization model and a ground motion characterization model. The seismic source characterization model describes the location of future earthquakes and their magnitude-frequency distribution, including the maximum magnitude that can occur. For naturally occurring seismicity, the magnitude-frequency distribution is often represented with an exponential model that, in its simplest form, is given as:

$$\log \lambda_m = a - bm \tag{2}$$

in which λ_m is the rate of earthquakes with magnitudes greater than m, and a and b are constants that are determined by regression based on the observed seismicity using a maximum likelihood method.

The ground motion characterization model predicts the ground motion level expected to occur for an earthquake of a given magnitude occurring at a given distance from the site. The prediction may also depend on other parameters such as the style of faulting and the site condition. In its simplest form a ground motion prediction equation (GMPE) has the following form:

$$\log Y = f(m,r) + \varepsilon\sigma \quad (3)$$

in which $\log Y$ is the logarithm of ground motion, $f(m,r)$ is a function of magnitude and distance, σ is the standard deviation of log Y, and ε is a standard normal random variable that represents the observed variability in log Y (Baker, 2008). The standard deviation of log Y is typically assumed to be normally distributed.

EXTENSION OF THE PSHA METHODOLOGY TO THE CASE OF INDUCED SEISMICITY

Incorporation of the hazard from induced seismicity into a PSHA needs to take into account characteristics of induced seismicity that differ from those of natural seismicity. Some of these differences are described below.

Earthquake Recurrence Model

In general, a Poissonian earthquake recurrence model for naturally occurring earthquakes is used in PSHA. In this model, the average rate of occurrence, α_i, is constant over time. In the case of seismicity induced by deep fluid injection, however, this rate may vary in time due to changes in, for example, injection rate, and, therefore, the assumption of a stationary recurrence rate may not be valid.

To account for time dependence in the recurrence of induced earthquakes, Convertito et al., (2012) modify the hazard equation by making α (Eq. 1) and b (Eq. 2) time dependent. They derived recurrence parameters over specific time periods and calculated Eq. 1 for each period, thereby producing "time-dependent" hazard maps.

In some cases of induced seismicity, a time-dependent rate may not be appropriate. Van Eck et al. (2006) assume a stationary process for induced seismicity recurrence based on the assumption of a long-term steady gas exploitation rate.

For the case of deep fluid injection, previous examples of induced seismicity, the distribution in space and time of the induced earthquakes as a function of magnitude, and their relation with injection rates need to be studied to understand whether a Poissonian model is appropriate to describe their recurrence. Alternative models of earthquake recurrence, such as those in which recurrence varies with time, can also be examined, but use of such models may require estimates of additional parameters that are not well constrained from available data.

Lower and Upper Bound Magnitudes

As for PSHA of naturally occurring seismicity, the lower-bound magnitude for a PSHA that takes into account induced events is based on an assessment of the magnitude threshold for earthquakes that can cause damage to engineered structures. A moment magnitude of 5 is often used for the lower bound. This value should be appropriate for PSHA involving induced seismicity as long as there is no reason to expect ground motion from induced seismicity will be more damaging than from naturally occurring earthquakes.

The upper bound (i.e., maximum) magnitude determination can be challenging for induced events related to fluid injection. One can use the methodology of Markopolus and Burtun (1983) as done by Van Eck et al. (2006) and Convertito et al., (2009), in which the maximum magnitude is determined from the cumulative energy release in the area. One problem with this and other statistical methods is that sufficient induced seismicity data need to exist at a site to make a site-specific assessment.

Alternatively, McGarr (2014) has shown that for earthquakes induced by fluid injection, the upper bound magnitude appears to be directly related to the volume of fluid injected. In a PSHA, uncertainties in assumptions made by McGarr (e.g., *b* in Eq. 2 is 1.0) can be incorporated by representing maximum magnitude with a discrete probability distribution based on alternate assumed values.

Ground Motion Prediction Equations

Ideally, selection of a GMPE(s) to represent ground motion from fluid-injection induced earthquakes would be based on comparison of recorded data with the predictions. However, because most fluid-injection induced earthquakes are small ($M_W < 5$), comparisons must be made using extrapolation of the predicted ground motions to levels below those constrained by data. Most GMPEs are based on data from M_W 4 to 5 and larger earthquakes.

Also, ground motion data from fluid-injection induced earthquakes is limited because seismic monitoring often is not implemented until after a significant earthquake occurs. Recorded data from fluid-injection induced earthquakes is needed to evaluate whether ground motion from such earthquakes systematically deviates from median predictions based on data from naturally occurring earthquakes. The sparse data from induced events leads to significant uncertainty in ground motion predictions. Use of the probabilistic approach allows the uncertainty to be appropriately incorporated in seismic hazard analysis.

Empirical GMPEs have a limited range of applicability usually defined by the ranges of magnitudes and distances used to derive the GMPEs. These GMPEs are not constrained for small magnitudes, very close (less than 10 km) and very large distances. A problem that is frequently encountered in the PSHA studies is that the GMPEs have to be significantly extrapolated beyond their ranges of applicability. GMPEs based on the stochastic simulations also have a limited range of applicability, although compared to empirical GMPEs, they can be applied to far greater distances (up to 1000 km). The lower bound magnitude for which many of the empirical GMPEs are applicable is in the range M_W 4.0-5.0.

If sufficient data from induced earthquakes exist, developing a GMPE from induced seismicity may be feasible. For example, Douglas et al. (2013) have developed empirical and stochastic GMPEs for application in geothermal fields. They have analyzed near-source seismograms of small events induced by geothermal activity or gas extraction, and some data from naturally occurring seismicity. Similarly, ground motion data from deep fluid injection sites can be analyzed for evaluation of existing GMPEs or to develop new GMPEs. Seismograms from near-source small earthquakes can be collected during microseismic monitoring in the vicinity of fluid injection sites.

Focal Depth

One aspect of fluid-induced earthquakes that may systematically differ from naturally occurring earthquakes is the focal depth at which they occur. Fluid injection induced earthquakes are typically shallow compared to naturally occurring earthquakes. For example, focal depths of potentially induced earthquakes in Table 1 range from 3 to 5 km. Therefore, an appropriate focal depth distribution needs to be included in the PSHA for induced seismicity.

CONCLUSIONS

While PSHA typically is used to determine seismic hazard from naturally occurring earthquakes, hazard from fluid-injection induced earthquakes can also be incorporated. In carrying out this incorporation, differences between the characteristics of fluid-injection induced and naturally occurring earthquakes must be taken into account. Characterization of fluid-injection induced earthquakes is subject to large uncertainties because of the limited number of case histories and sparse recorded ground motion data. PSHA is an appropriate methodology for dealing with these uncertainties.

PSHA inputs for fluid-injection based seismic sources that likely require modification from the typical characterization approach include:

- Recurrence parameters (α_i in Eq. 1; a and b values in Eq. 2), which may need to take into account time-dependency related to, for example, fluid injection rate or fluid injection cumulative volume
- Maximum earthquake magnitude, which may be related to activity rate or cumulative injected volume
- GMPEs, which may require adjustments if ground motion from fluid-injection induced earthquakes differs systematically from median values for GMPEs determined on the basis of naturally occurring seismicity
- Focal depth, which may have a shallower distribution for fluid-injection induced events than for naturally occurring earthquakes

If fluid-injection induced seismicity basically reflects the triggered, time-shifted release of tectonic stress, it is reasonable to use GMPEs derived based on naturally occurring earthquake data to model their attenuation with distance, taking into account any adjustment for systematic differences in depth. It is, therefore, important to look at the ground motion data from induced events to evaluate the applicability of existing GMPEs for the hazard assessment from induced seismicity. If sufficient data exist, specific GMPEs may be developed for deep fluid injection seismicity. However, if they are empirically based, the range of magnitude and distance of such GMPEs will be very limited.

The current state of knowledge limits the ability to *a priori* determine which fluid-injection well operations will produce induced seismicity. The probability of having induced seismicity can be characterized based on empirical assessments of regional observations, or as case histories provide better insight into the conditions controlling induced events (e.g., injection rates and duration, depth of injection wells, distribution

of preexisting shallow faults, and current state of stress), based on detailed characterization of individual sites. For the present and foreseeable future, however, assessment of seismic hazard from fluid-injection induced seismicity will be subject to uncertainty and random components. A PSHA is an appropriate tool that takes into account the uncertainty and randomness in the input.

REFERENCES

Baker, J. W. (2008). "An introduction to Probabilistic Seismic Hazard Analysis (PSHA)." Version 1.3, Stanford University, 72 pp.

Davis, S. D., and Frohlich, C. (1993). "Did (or will) fluid injection cause earthquakes?- criteria for a rational assessment." Seismological Research Letters, 64(3-4), 207-224.

Convertito, V., Maercklin, N., Sharma, N., and Zollo, A. (2012). "From induced seismicity to direct time-dependent seismic hazard." Bulletin of Seismological Society of America, 102 (6), 2563-2573.

Cornell, C. A. (1968). "Engineering seismic risk analysis." Bulletin of Seismological Society of America, 58(5), 1583-1606.

Douglas, J., Edwards, B., Convertito, V., Sharma, N., Tramelli, A., Kraaijpoel, D., Cabrera, B. M., Maercklin, N., and Triose, C. (2013). "Predicting ground motion from induced earthquakes in geothermal areas." Bulletin of Seismological Society of America, 103(3), 1875-1897.

Grasso, J. R. (1992). "Mechanics of seismic instabilities induced by the recovery of hydrocarbons." Pure and Applied Geophysics, 139(3-4), 507-534.

Gupta, H. K. (1992). "Reservoir-induced earthquakes." Current Science, 62(1-2), 183-198.

Gupta, H. K. (2005). "Artificial water reservoir-triggered earthquakes with special emphasis at Koyna." Current Science, 88(10), 1628-1631.

Keranen, K. M., Savage, H. M., Abers, G. A., and Cochran, E. S. (2013). "Potentially induced earthquakes I Oklahoma, USKA: Links between wastewater injection and the 2011 M_W 5.7 earthquake sequence." Geology, 41, 699-702.

Kim, W.-Y. (2013). "Induced seismicity associated with fluid injection into a deep well in Youngstown, Ohio." Journal of Geophysical Research, Solid Earth, 118, 3506-3518.

Lasocki, S. (2005). "Probabilistic analysis of seismic hazard posed by mining induced events." In: Potvin, Y. and Hudyma, M. (Eds.), Proceedings of 6th International Symposium on Rockburst in Mines, Controlling Seismic Risk, ACG, Perth, 151-156.

Markopoulos, K. C., and Burton, P. W. (1983). "Seismic risk of Circum-Pacific earthquakes, I. strain energy release." Pure and Applied Geophysics, 121(2), 247-267.

McGarr, A. (2014). "Maximum magnitude earthquakes induced by fluid injection." Journal of Geophysical Research, Solid Earth, 119, doi: 10.1002/2013J010597.

McGuire, R. K. (2004). "Seismic hazard and risk analysis." Electric Power Research Institute Monograpgh MNO-10, Oakland California.

Phillips, W. S., Rutledge, J. T., House, L. S., and Fehler, M. C. (2002). "Induced microearthquake patterns in hydrocarbon and geothermal reservoirs: Six case studies." Pure and Applied Geophysics, 159, 345-369.

Reiter, L. (1990). "Earthquake hazard analysis, issues and insights." Columbia University Press, New York, 254 pp.

Suckale, J. (2009). "Induced seismicity in hydrocarbon fields." Advances in Geophysics, 51 (Ch. 2), 55-106.

Talwani, P. (1997). "On the nature of reservoir-induced seismicity." Pure and Applied Geophysics, 150, 473-492.

Van Eck, T., Goutbeeck, F., Haak, H., and Dost, B. (2006). "Seismic hazard due to small-magnitude, shallow-source, induced earthquakes in the Netherlands, Engineering Geology, 87, 105-121.

Numerical Simulation of Induced Seismicity due to Hydraulic Fracturing of Shale Gas Reservoirs

Kimia Mortezaei[1], S.M.ASCE, Farshid Vahedifard[2], M.ASCE

[1] Ph.D. Student, Dept. of Civil and Environmental Engineering and Center for Advanced Vehicular Systems (CAVS), Mississippi State University, Mississippi State, MS 39762.
Email: km1745@msstate.edu
[2] Assistant Professor, Dept. of Civil and Environmental Engineering and Center for Advanced Vehicular Systems (CAVS), Mississippi State University, Mississippi State, MS 39762.
Email: farshid@cee.msstate.edu

ABSTRACT: Microseismic events in shale-gas hydraulic fracturing are due to propagation of induced fractures. Larger and noticeable seismic events are less likely to occur but the probability of occurrence will increase in the presence of a pre-stressed fault. Intersection of an undetected and pre-existing fault/fracture with the production well is the main cause for upward extension of induced fractures. This upward extension of fractures may lead to reactivation of existing faults and can increase the induced seismicity potential. This study investigates the induced seismicity and fault reactivation potential associated with hydraulic fracturing operations when a limited-dimension fault exists close to the fracturing site. For this purpose, a 2D fully coupled hydro-mechanical numerical model was developed to simulate changes in the stress distribution in the fractured zone and fault. The results obtained from the numerical simulations were used to determine the fault responses. Seismological theories were adopted along with the fault slips obtained from the numerical simulations to estimate the magnitude of induced seismic events. Parametric study was performed to investigate the impact of injection rate and fault permeability on the magnitude of induced seismic event. In all cases which were examined, the magnitude of induced earthquake was very low and never reached to the level of a noticeable seismic event.

INTRODUCTION

Possibility of gas extraction from shale basins has tremendously increased estimates of the U.S. natural gas reserves. The U.S. Energy Information Administration predicts that 46% of the U.S. natural gas supply by 2035 will come from shale basins (Stevens 2012). Shale gas, as low-carbon energy, will decrease the nation's dependence on oil and will decrease excessive carbon emissions to the atmosphere (Flavin and Kitasei 2010). Shale gas extraction has become economically

and technically feasible by employing recent advances in horizontal drilling and hydraulic fracturing technologies. The hydraulic fracturing technology, however, has faced with some social, technical and environmental concerns. Among others, two main concerns associated with the hydraulic fracturing process are groundwater contamination and induced microseismic events (Zoback et al. 2010, Arthur et al. 2008). Although the probability of the first risk is low, low-depth producing zones and pre-existing faults can increase the probability of such risk (Zoback et al. 2010). However, Fisher and Warpinski (2012) showed that fractures do not threaten groundwater since fractures do not move vertically several thousands of feet to infect groundwater. Microseismic events are due to propagation of induced fractures by the hydraulic fracturing process (Fisher & Warpinski 2012). The magnitude of induced seismic events may slightly increase if the injection leads to reactivation of a nearby pre-existing fault. Several low magnitude seismic events recently reported in Texas, Oklahoma, Arkansas and Ohio have been controversially attributed to hydraulic fracturing operations or deep disposal of hydraulic fracturing waste water in nearby areas (e.g., Casselman 2009, Kim 2013).

Despite controversy regarding main triggering factors, there is consensus that high pressure fluid injection can significantly change pore pressure and effective stress distributions in the reservoir rock. This change in the pore pressure may lead to reactivation of favorably oriented pre-existing faults. The frictional resistance along the fault will decrease when the fluid in a pressurized fault escapes or accumulates (e.g., Rice, 2006). Fault rupture initiates when the shear stress on the fault plane exceeds the shear strength of the fault (Miller et al., 1996; Streit and Cox, 2001).

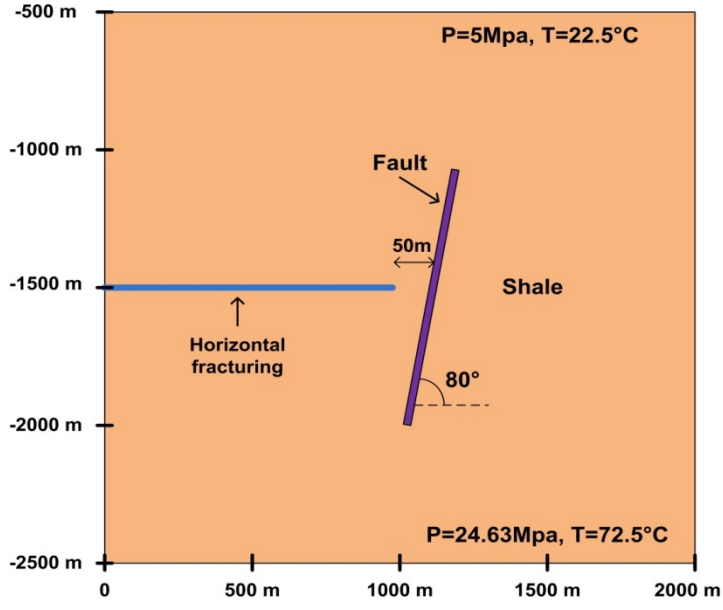

FIG. 1. Model geometry used in numerical simulations.

This study investigates the potential of induced seismicity associated with shale-gas hydraulic fracturing for a scenario where a limited-length fault exists near the fracturing site. We determine the magnitude of earthquake corresponding to the

injection-induced fault slip. The effect of injection rate and permeability of the fault on the magnitude of seismic events is evaluated.

COUPLED HYDRO-MECHANICAL MODELING

In this study, a 2D finite element model coupling single-phase flow and poroelasticity was built in COMSOL Multiphysics.

The governing equations of single phase flow and geomechanics associated with the poroelasticity. According to the poroelasticity theory and Darcy's law, the hydro-mechanical coupling can be expressed as follows:

$$G\nabla^2 u + \left(k_d + \frac{G}{3}\right)\nabla.(\nabla u) = \alpha\nabla p_f \tag{1}$$

$$\frac{1}{M}\frac{\partial p_f}{\partial t} - \nabla\left(\frac{k}{\mu}(\nabla p_f - \rho_f g\nabla z)\right) = -\alpha\frac{\partial(\nabla.u)}{\partial t} \tag{2}$$

where G is the shear modulus of the solid part, k_d is the drained bulk modulus and u is displacement. M is the Biot's Modulus which is defined as:

$$\frac{1}{M} = \frac{\alpha - \varphi}{k_s} + \frac{\varphi}{k_f} \tag{3}$$

The model, inspired by the work done by Rutqvist et al. (2013), was used to determine the fault slip due to hydraulic fracturing operations. Rutqvist et al. (2013) used TOUGH-FLAC (Rutqvist et al., 2002) for coupled fluid flow and geomechanical modeling and estimated the magnitude of induced seismic events under the assumption that the fracturing well intersects the fault. This study investigates the influence of the injection rate and permeability of fault on the earthquake magnitude for a model where a fault is located 50 m away from the end of the horizontal fracturing well.

GEOMETRY AND INPUT PARAMETERS

Fig. 1 shows the model geometry that was used in simulations. The model is a square of 2 km by 2 km. The overburden layer, from the ground surface to the depth of 500 m, was not included in the model geometry and instead, equivalent vertical and horizontal pressures were applied on the top and right boundaries, respectively. Ratio of 0.7 was used to calculate initial horizontal stresses from corresponding vertical stresses. The model includes a 1-km long fault starting from the depth of 1,000 m going down with 80º inclination to the horizon. The length of horizontal fracturing well is 1 km. Properties of the shale and fault are given in Table 1.

Considering the mechanical boundaries, no movement was allowed at the bottom boundary where only the horizontal movement was restrained for the left and right boundaries. All the boundaries were assigned no-flow condition. As shown in Fig. 1, the fault is located 50 m away from the end of the horizontal fracturing well. The fault has an initial offset displacement of 10 m. The initial temperature at the top boundary was 22.5 ºC and it linearly increased versus depth with a thermal gradient

of 0.025 °C/m. The model was conducted in an isothermal mode which means the thermal gradient doesn't change from the initial condition during the course of the simulation (Rutqvist et al., 2013).

Table 1. Material Properties

Parameter	Shale	Fault
Young's modulus, E (GPa)	30	5
Poisson 's ratio, ν	0.2	0.25
Friction angle, φ′ (deg.)	-	25
Density (kg/m^3)	2,700	2,700
Permeability, k (m^2)	1×10^{-19}	Variable
Porosity, ∅	0.01	0.01
Biot's coefficient	1	1

DETERMINATION OF EARTHQUAKE MAGNITUDE FROM FAULT SLIP

Fault geometry and seismic moment can be defined by the orientation of the fault, direction of fault movement, and size of an earthquake. The seismic moment, M_0, can be calculated by the following equation (Hanks and Kanamori, 1979):

$$M_0 = \eta dA \tag{4}$$

where η is the shear modulus of the faulted rock, d is the average displacement on the fault surface, and A is the area of the fault-surface rupture. In this study, $\eta = 3\times10^9$ and for simplicity, it was assumed that the fault is circular which is consistent with that in Rutqvist et al. (2013). The diameter of the circle is equal to the length of rupture obtained from the numerical modeling. The magnitude of earthquake, M, can be expressed as (Wells and Coppersmith, 1994):

$$M = \frac{2}{3}[\log_{10}(M_0) - 9.1] \tag{5}$$

In the next section, the results obtained from the numerical simulations will be used to determine the fault response under different conditions. The fault slip obtained from the numerical model will be used along with Eqs. 1 and 2 to estimate the magnitude of induced seismic events.

EFFECT OF INJECTION RATE

One of the controlling parameters in the hydraulic fracturing operation is the injection rate. In this study, fluid injection was molded through several point sources located at the end and along the length of the horizontal fracturing well. Three different values for the injection rate were examined: 0.0001, 0.005, and 0.001 kg/s. The difference between the shear stress after injection and the shear strength was

quantified by a parameter named "fail". Fig. 2 shows the distribution of this parameter after hydraulic fracturing with the injection rate of 0.001 kg/s. The "fail" parameter was calculated by the following equation:

$$\text{fail} = (\sigma_3 + \text{p}) - \left(\frac{1+\sin\varphi}{1-\sin\varphi}\right)(\sigma_1 + \text{p}) + \frac{\cos\varphi}{1-\sin\varphi}\,\text{c}\left(1 + \frac{\sigma_2+\sigma_1}{\sigma_3-\sigma_1}\right) \qquad (6)$$

where c is the cohesion and φ is the friction angle. In this equation, fail = 0 indicates the beginning of rock failure, fail < 0 denotes catastrophic failure, and fail > 0 demonstrates stability. As shown in Fig. 2, the area between the fracturing well and fault reached failure after injection (i.e., fail < 0).

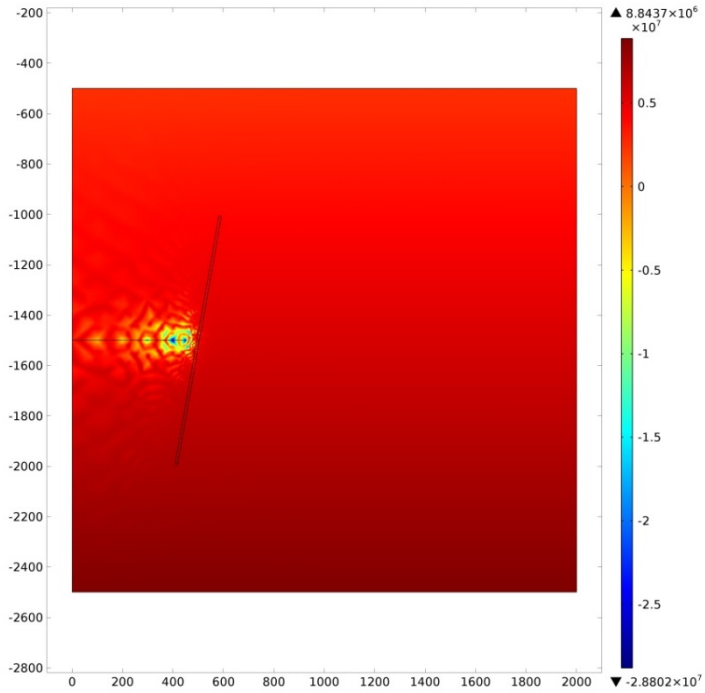

FIG. 2. Failure for injection rate of 0.001 kg/s.

Fig. 3 shows the amount of slip after 20 days of injection. For this case, rupture did not happen with the injection rate of 0.0001 kg/s. The fault slip started and increased as the injection rate was increased resulting in 4.5 cm slip at the injection rate of 0.001 kg/s. Based upon Eqs. 1 and 2, this fault slip can cause a seismic event with magnitude of 0.81. As shown, the overpressure for the injection rates which were examined never reached to a value that can induce a noticeable earthquake.

EFFECT OF FAULT PERMEABILITY

Fault properties can impact formation and growth of an induced fracture as well as the amount of fault slip. In this study, three different values for the fault permeability, k_f, were investigated: 10^{-19}, 10^{-18}, and 10^{-17} m^2. For all three models, the injection rate was kept constant at 0.001 kg/s. Fig. 4 depicts the slip along the fault surface for different k_f values. As shown, for the model with least permeable fault (k_f = 10^{-19}

m^2), the rupture happened after 5 days of injection and it induced a 0.95 magnitude seismic event. The magnitudes of induced seismic event for the models with $k_f = 10^{-18}$ m^2 and $k_f = 10^{-17}$ m^2) were 0.9 and 0.81, respectively. These events occurred after 12 and 20 days of injection for the medium- ($k_f = 10^{-18}$ m^2) and highly-permeable ($k_f = 10^{-17}$ m^2) faults, respectively. A higher permeable fault will allow quicker dissipation of excess pore pressures along the fault surface. Consequently, it will increase the effective stress in this area and will delay the rupture occurrence.

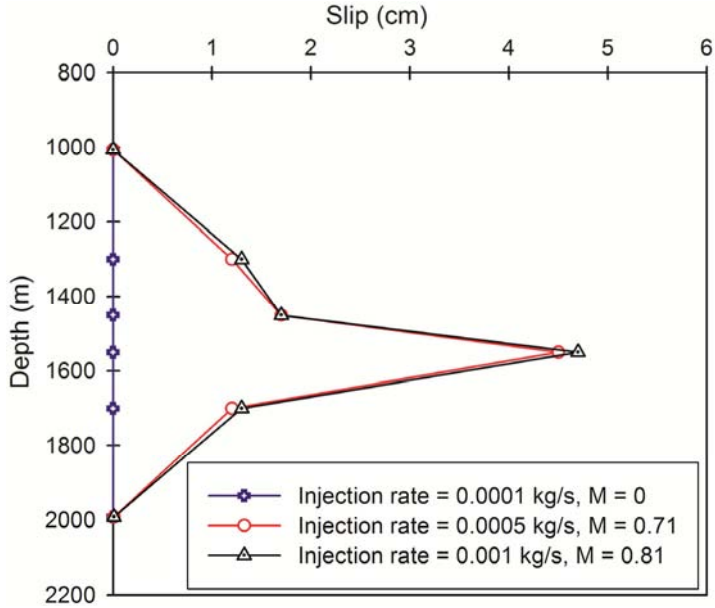

FIG. 3. Slip along fault for different injection rates. Rupture occurred after 20 days of injection.

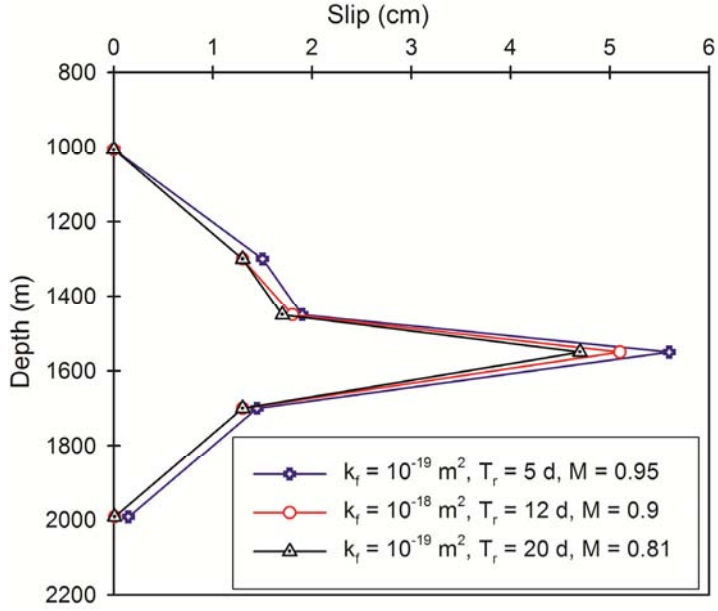

FIG. 4. Slip along fault for different fault permeability values. T_r is the time when rupture happens.

CONCLUSIONS

Induced seismicity due to hydraulic fracturing or due to deep disposal of hydraulic fracturing waste water is one of the major concerns associated with natural gas extraction from shale basins. In this paper, we studied the seismicity induced by high pressure fluid injection during hydraulic fracturing operations. 2D fully coupled hydro-mechanical numerical modeling was conducted to simulate changes in the stress distribution in the fracture zone and fault. The fault slips obtained from the numerical simulation were used along with seismological equations to estimate the magnitude of induced seismic events. Two variables of injection rate and permeability of the fault were investigated. No rupture occurred at the injection rate of 0.0001 kg/s. The amount of slip increased to 4.5 cm by increasing the injection rate to 0.001 kg/s. Among the models which were simulated, rupture occurred in shorter period of time in the faults with lower permeability. In all cases which were examined, the magnitude of induced earthquake was very low and never reached to the level of a noticeable seismic event. It can be concluded that, under controlled conditions, the hydraulic fracturing operation can only induce very small seismic events.

REFERENCES

Arthur, J. D., Bohm, B., & Layne, M. (2008). "Hydraulic fracturing considerations for natural gas wells of the Marcellus Shale." *In Groundwater Protection Council Annual Forum*. Cincinnati. Available from: http://www.dec.ny.gov/docs/materials_minerals_pdf/GWPCMarcellus.pdf.

Casselman, B. (2009). "Temblors rattle Texas town." *Wall Street Journal*. Available from: http://online.wsj.com/news/articles/SB124476331270108225.

Fisher, M., & Warpinski, N. (2012). "Hydraulic-fracture-height growth: Real data." *SPE Production & Operations*, 27(1), 8-19.

Flavin, C, and Kitasei S. T. (2010). "The role of natural gas in a low-carbon energy economy" Worldwatch Institute, Washington, DC, Available from: www.worldwacth.org.

Hanks, T.C., and H. Kanamori. (1979). "A moment magnitude scale." *Journal of Geophysical Research*, 84, 2348-2350.

Kim, W.-Y. (2013). "Induced seismicity associated with fluid injection into a deep well in Youngstown, Ohio." *Journal of Geophysical Research*, Solid Earth, 118, 3506-3518.

Miller, S.A., Nur, A., Olgaard, D.L. (1996). "Earthquakes as a coupled shear stress-high pore pressure dynamical system." *Geophys*, 23, 197–200.

Rice, J.R. (2006). "Heating and weakening of faults during earthquake slip." *Journal of Geophysical Research*, 111.

Rutqvist, J., Wu, Y.-S., Tsang, C.-F., Bodvarsson, G. (2002). "A modeling approach for analysis of coupled multiphase fluid flow, heat transfer, and deformation in fractured porous rock." *International Journal of Rock Mechanics and Mining Sciences* 39, 429–442.

Rutqvist, J., Rinaldi, A. P., Cappa, F., & Moridis, G. J. (2013). "Modeling of fault reactivation and induced seismicity during hydraulic fracturing of shale-gas reservoirs." *Journal of Petroleum Science and Engineering*. 107, 31-44.

Streit, J. E., Cox, S.F. (2001). "Fluid pressures at hypocenters of moderate to large earthquakes." *J. Geophys*, 106, 2235–2243.

Stevens, P. (2012). "The shale gas revolution: Developments and changes". *Chatham House*. Available from: http://www.chathamhouse.org/sites/default/files/public/Research/Energy,%20Environment%20and%20Development/bp0812_stevens.pdf.

Zoback, M., Kitasei, S., Copithorne, B. (2010) . "Addressing the environmental risks from shale gas development." *Natural Gas and Sustainable Energy Initiative*, Worldwatch Institute, Washington, DC, Available from: www.worldwacth.org.

Rock Excavation Index Approach for Estimating Blast Rock for Shallow Pipeline Construction

Jeffrey R. Keaton[1], Ph.D., P.E., D.GE, ENV SP, F.ASCE and
Luther H. Boudra[2], P.E., D.GE, F.ASCE

[1]Principal Engineering Geologist, AMEC Americas, 6001 Rickenbacker Road, Los Angeles, CA 90040 U.S.A., Email: jeff.keaton@amec.com
[2]Principal Engineer, AMEC Americas, 4000 Meadow Lake Drive, Suite 125 Birmingham, AL. 35242-5427 U.S.A., Email: Luther.Boudra@amec.com

ABSTRACT: Pipeline construction can be disruptive for rural communities in the vicinity of shale energy development and expensive for the pipeline companies, particularly if unanticipated blasting for excavating shallow pipeline trenches causes construction delays. A rock excavation index can be defined based on subsurface conditions interpreted from digital topography, geology, and soils data. Topographic data provide slope steepness and down-slope direction needed for evaluating sidehill conditions. Rock factors ranging from 0 for uncemented soil to 3 for nearby rock outcrop, weathered rock near top of ditch, or unweathered rock at any ditch depth can be created with GIS utilities as "rock factor" polygons along the pipeline centerline. Ground-condition variability requires subjective assessment and can be addressed in a limited way with use of seismic refraction surveys at truly random locations along the pipeline or at selected locations based on rock excavation factors. Rock excavation can be estimated using length-based and area-based percentages for ditch rock and right-of-way grading rock. Blasting details from actual construction records are needed to improve the accuracy of rock excavation estimation.

INTRODUCTION

Shale energy development requires new pipelines for gathering and transmitting natural gas or oil. In many places, blasting is required for right-of-way grading on sidehills, as well as for excavating ditches, where rock formations are encountered; sidehill conditions primarily are issues for midstream transmission pipelines in rural areas. Experienced construction personnel commonly use judgment to estimate the extent of rock excavation. A simple procedure based on engineering geology supplemented by seismic refraction surveys was developed in an attempt to improve reliability of estimated shallow rock conditions along pipeline alignments (Keaton et al., 2012). Geotechnically based estimates of total excavation volume and rock excavation volume can be developed with an office study using readily

available digital topography, geology, and soils data in geographic information system (GIS) platform. Geologic observations made in the field and non-invasive geophysical measurements can improve the confidence in the office-based estimates, which can be further refined by drilling a few borings, excavating a few test pits, or driving a few dynamic cone penetrometer soundings.

After a project concept has been defined and approved, reasonably accurate forecasting of rock excavation requirements is consistent with the principles of sustainability that balances the "triple bottom line" of economy, environment, and society (Elkington, 1997). The economy aspect is straightforward to understand: more accurate rock excavation forecasting results in more efficient construction, less construction delay, and better implementation of plans to move in required equipment and handle excavated materials. The environment, from a narrow viewpoint, benefits from the construction efficiency, the speed of completing the construction, or possibly from adjustments in the pipeline alignment, if the rock excavation forecasting is preformed early enough in the pipeline process. Society, also from a narrow viewpoint, benefits from efficient construction that minimizes traffic disruption, as well as from well-planned blasting performed by a qualified contractor working under a reasonably negotiated contract that includes all of the provisions for safe blasting that minimizes disruptions of noise, vibration, and fly rock.

CALCULATIONS ALONG A PIPELINE CENTERLINE

In addition to the location of a proposed pipeline centerline, three types of digital data are needed for the office-based calculations: topography, geology, and soils. Digital elevation model (DEM) topographic data are available at a resolution of 10 m in many places in the United States. A resolution of 10 m is reasonably detailed, yet computationally efficient; therefore, this resolution was maintained for conversion of geology and soils vector data into raster data for use with GIS tools. ESRI ArcGIS platform was used for these calculations, but other GIS software would produce the same or comparable results. Keaton et al. (2012) used the phrase "virtual geologic field reconnaissance" for the process of a professional geologist using Google Earth Pro as part of an office study that includes a detailed examination of the visible conditions along the pipeline corridor. ESRI shape files can be opened directly in Google Earth Pro to facilitate the virtual geologic reconnaissance.

The virtual geologic reconnaissance is supplemented by geologic maps that provide general information about rock type and geologic structure. State-scale digital geologic maps are available in ESRI shape-file format. In the state of Pennsylvania, the geology polygons were developed from a geologic map (Berg et al., 1980) that was digitized by the State of Pennsylvania and made accessible in a state-scale series on a U.S. Geological Survey website (http://pubs.usgs.gov/of/2005/1325/#PA).

The state-scale geologic map information is generalized, but suitable for the office-based study. Digital soil survey data is more detailed but limited in its vertical extent; a soil survey represents the upper 150 cm (60 in., 1.5 m, 5 ft) of the soil profile. Major transmission pipelines can extend nominally to depths of 2 to 2.6 m (6 to 6.8 ft). Soil survey data are available for the entire United States at a convenient website maintained by the National Resources Conservation Service (NRCS) of the U.S.

Department of Agriculture (http://datagateway.nrcs.usda.gov/). The geology and soils GIS polygons are interpreted by a professional geologist and assigned numerical scores representing rock factors. Rock factors used by Keaton et al. (2012) denote uncemented soil (score = 0), cemented soil (score = 1), weathered rock near ditch bottom (score = 2), or nearby rock outcrop, weathered rock near top of ditch, or unweathered rock at any ditch depth (score = 3). Once the rock factor scores are assigned to the geology and soils polygons, the polygons are converted to GIS grids at a 10-m pixel spacing to match the available topography data.

The office-based procedure using GIS tools converts the pipeline centerline from a line into points spaced 10-m apart, and includes a point at the beginning (i.e., MP 0) and at the ending of the line. A point-spacing of 10 m in excavation calculations is expressed as 10.936 yd because right-of-way grading volumes in the United States are expressed in cubic yards. Values of elevation can be extracted from the digital topography data layer at each pipeline centerline point to produce an elevation profile along the pipeline alignment. An example graph of the elevation profile and other calculated values is presented in Figure 1. The horizontal length of the pipeline is calculated easily with GIS tools; the slope length is easily calculated with a spreadsheet application. The rock factors are used as a basis for estimating the length of pipeline ditch which will require rock blasting; typically rock excavation in the United States is paid by ditch length in units of feet.

Pipeline alignments that are oriented directly up and down slopes have no sidehill conditions and, therefore, no need for significant right-of-way grading. In most cases, however, sidehill conditions exist and grading is needed to provide a safe working pad for the construction equipment. The calculation to estimate the volume of right-of-way grading uses the construction right-of-way width (typically 33.5 to 45.7 m, 110 to 150 ft, for transmission pipelines) and the apparent slope of the sidehill perpendicular to the pipeline alignment. Keaton et al. (2012) describe the geometry details for the sidehill calculations which involve the following parameters:

1. Azimuth of the pipeline alignment referenced to increasing pipeline station,
2. Gradient and aspect of the topographic slope at each pipeline centerline point,
3. Width requirements based on where excavation spoil will be placed, and
4. Steepness of the back-cut slope angle.

The geometry is straightforward and sidehill conditions and associated volumes can be calculated efficiently with GIS tools. Ground slope, apparent slope across the pipeline right-of-way, rock excavation factor, total right-of-way grading, and estimated rock excavation volumes are plotted in Figure 1.

DISCUSSION

Geologic knowledge of the pipeline area is helpful in the subjective assessment of ground-condition variability. For example, the effects of continental glaciations can result in essentially unweathered rock exposed at the ground surface or present at shallow depth. This geologic knowledge can be considered for each of the rock excavation factors using length-based percentages for ditch rock and area-based percentages for right-of-way grading rock. Rock excavation factor 0, uncemented soil

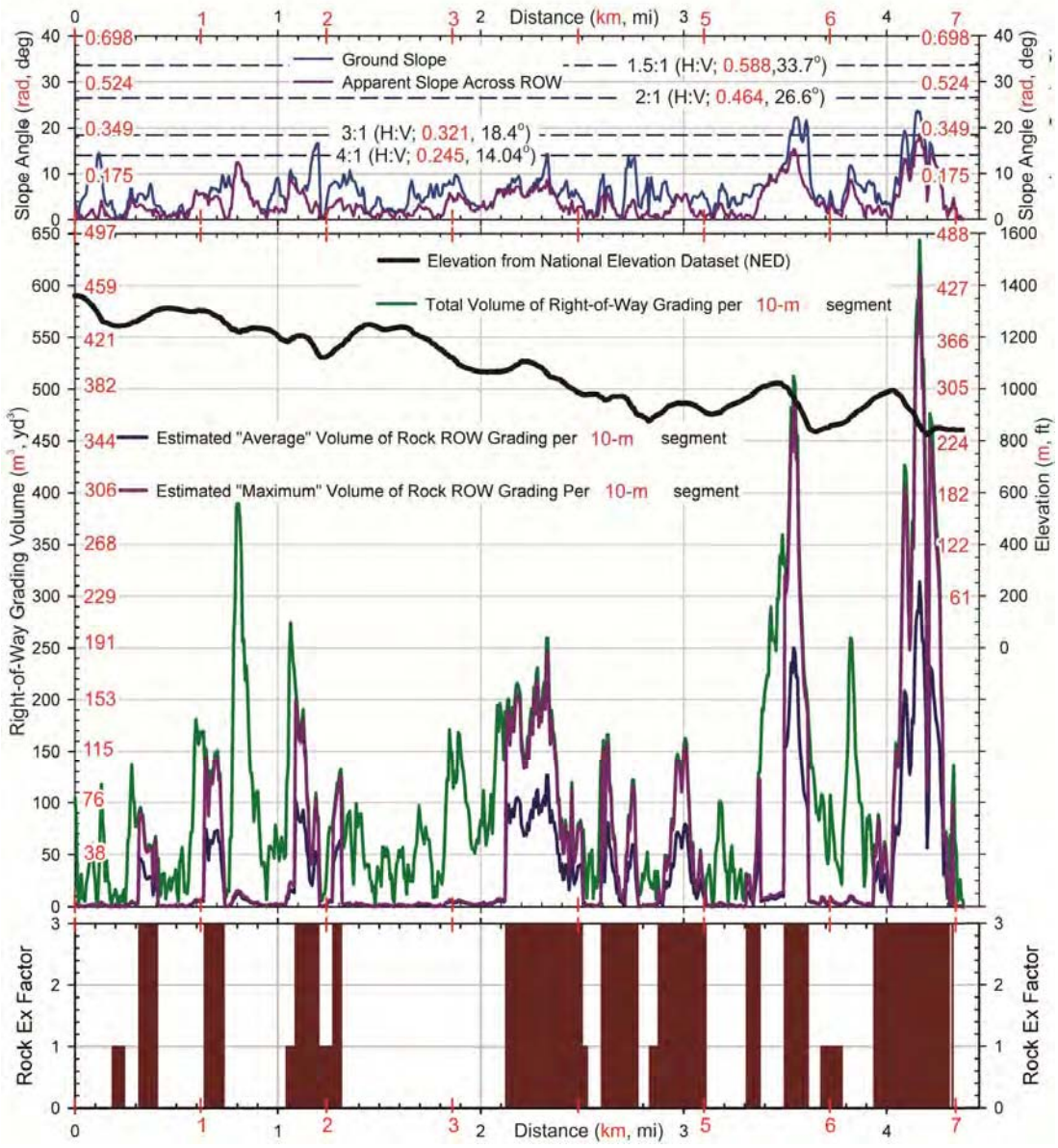

FIG. 1. Graph of example data used for estimating pipeline rock excavation requirements.

can include areas where rock is close enough to the ground surface to be encountered in a pipeline ditch excavation, whereas rock excavation factor 3, nearby outcrop or unweathered rock at ditch depth, can include reaches of uncemented soil. Rock excavation percentages are estimated for "average" and "maximum" conditions using judgment for both ditch and right-of-way grading conditions.

Rock excavation estimates are expressed as ranges based on "average" and "maximum" length or volume (Table 1). Ditch rock is a length factor, whereas right-of-way rock is an area factor. Rock condition ranges are appropriate for the rock excavation index categories for several reasons, such as 1) associations of two or

three soil series represent a single soil survey map unit, 2) a single map unit contains ranges of soil conditions, including depths of soil horizons, and 3) the underlying geology is concealed by sediment that has formed on the rock as residual soil or has been deposited on the rock (alluvial, colluvial, eolian, or glacial deposits).

The projected ditch rock excavation values (Table 2) are estimated by summing the pipeline centerline length for each rock excavation index factor and multiplying by the corresponding expected rock excavation percentage from Table 1 for both "average" and "maximum" rock conditions. Similarly, projected volumes of right-of-way rock excavation (Table 2) are estimated by multiplying the area of excavation in a vertical cross-section across the right-of-way by the 10-m (10.936-yd) incremental length of pipeline centerline and summing the volume for each rock excavation index factor and then multiplying by the rock excavation percentages from Table 1 for both length and area for both "average" and "maximum" rock conditions. The length-based percentages address variability along the pipeline alignment, whereas the area-based percentages address variability across the pipeline right-of-way. The volume of total right-of-way grading for each 10-m increment is plotted in Figure 1, as are the estimated volumes of "average" and "maximum" right-of-way rock excavation; ditch rock values are not plotted. The projected ranges of rock excavation volumes are summed from the values for each rock excavation index factor for both ditch and right-of-way conditions.

TABLE 1. Expected length- or area-based percentages of rock excavation.

Rock Excavation Index Factor	Ditch (Length) Rock		Right-of-Way (Area) Rock	
	"Average" Rock Condition	"Maximum" Rock Condition	"Average" Rock Condition	"Maximum" Rock Condition
0	5%	10%	2.5%	5%
1	20%	25%	10%	15%
2	40%	60%	20%	30%
3	75%	90%	40%	75%

TABLE 2. Example summary of estimated rock excavation length and volume. Note: Excavation volume in the US is paid per 1 yd^3 = 0.7646 m^3.

Rock Excavation Index Category	Pipeline Length (km)	Average Rock Excavation Length (km)	Maximum Rock Excavation Length (km)	Estimated Total ROW Excavation Volume (m^3)	Average ROW Rock Excavation Volume (m^3)	Maximum ROW Rock Excavation Volume (m^3)
0	6.373	0.322	0.644	49,330	81	247
1	3.782	0.756	0.950	14,575	381	547
2	0.000	0.000	0.000	---	---	---
3	2.945	2.205	2.655	25,037	9,824	16,900
Total =	13.115	3.283	4.233	88,942	10,286	17,693

Rock excavation volumes for right-of-way grading can be calculated using an alternative approach that assumes the top of bedrock is parallel to the ground surface projected across the pipeline right-of-way as part of the GIS calculations. Experience gained from seismic refraction surveys conducted on pipeline projects in Pennsylvania and New Jersey suggests that this approach is reasonable. Depths to the top of blast rock could be based on judgment, or a range of depths could be used in a sensitivity analysis. Higher confidence in depths to rock and in the variability of depth could be obtained from measurement of seismic velocities along the alignment.

The office-based identification of locations where rock blasting is likely to be required can be used to identify targets for short seismic refraction surveys (a typical seismic refraction survey uses a linear array of 12 or 24 geophones with uniform spacing of 1.5 or 3 m [5 or 10 ft] for survey line lengths of 16.8 to 73.2 m [55 to 240 ft]). Rock requiring blasting in trench excavations was assumed to have seismic velocities above 1,220 to 1,370 m/s (4,000 to 4,500 ft/s) based on the size of trackhoe excavators typically used for pipeline construction.

Seismic refraction uses acoustic energy (typically a sledgehammer striking a metal plate that is placed on the ground surface); the speed of sound in water is about 1,500 m/s (4,900 ft/s); therefore, geologic experience is needed to interpret seismic velocities that are in the range of 1,500 to 1,680 m/s (4,500 to 5,500 ft/s) where shallow groundwater may be present. It should be noted that seismic refraction surveys are performed with portable equipment that can be carried by a crew of two to four, depending on the number of geophones used, to locations that are not accessible to vehicles. Each geophone has a nail-like metal spike on its base that allows it to be pushed into firm contact with the ground; the extent of ground disturbance is so slight that special use permits normally are not needed. A single seismic refraction survey line can be laid out, data collected, and picked up within a period of 7,200 to 10,800 s (2 to 3 hr). Thus, seismic surveys are economical for collecting valuable subsurface information relevant for blasting evaluations.

Seismic refraction survey lines traditionally are oriented along the pipeline alignment where the ditch excavation will be made. Several seismic lines positioned to provide subsurface information over a longer stretch of alignment to help quantify ditch rock variability. Additional seismic survey lines would be helpful where sidehill conditions exist to characterize depth to rock along lines perpendicular to the pipeline alignment or parallel to the pipeline alignment in the uphill direction from the pipeline centerline. Excavation typically is not needed in the downhill direction from the pipeline ditch to provide a level working pad for the construction equipment.

The ground-condition variability is important where projected “blast rock” seismic velocities are shallower than pipeline ditch depth. The accuracy of rock excavation estimation procedures needs to be improved by collecting and analyzing actual construction records of blasting. The construction records need to have sufficient detail that the actual “as-built” rock blasting can be compared directly to the rock excavation forecasting estimates essentially at or better than a resolution of 10 m. Pipeline construction contracts tend to pay for ditch rock on the basis of length regardless of where in the ditch blast rock is encountered; shooting the bottom 0.3 m (1 ft) of the ditch pays the same amount as shooting the entire ditch depth. In contrast, pipeline construction contracts tend to pay for area rock on the basis of volume.

Pipeline construction inspectors have not needed to document blast rock in particular detail beyond what is needed for payment. Improved detail regarding locations where rock required blasting for excavation in needed for validating and refining the rock excavation index approach for estimating blast rock requirements on pipeline projects.

CONCLUSIONS

Rock excavation index factors can be used to estimate blasting requirements along pipeline alignments using office-based GIS procedures and readily available digital data. Well-planned pipeline projects can reduce the disruption caused by unanticipated blasting for excavating shallow trenches for pipeline construction. Subsurface conditions are interpreted from digital topography, geology, and soils data by geology professionals. Variability of ground conditions is assessed subjectively and can be quantified to some extent by results of seismic refraction surveys at locations along the pipeline selected randomly or on the bases of rock index factors. Rock excavation is estimated using length-based terms for ditch excavation and area-based terms for right-of-way grading. Rock excavation estimation procedures could be validated and refined if actual construction records with detailed information of the locations where blasting was needed could be obtained from pipeline projects. Improvements in accuracy are needed, but they are challenging because of the number and variety of sources of ground-condition variability at pipeline depth.

Rock excavation index factors and the estimated volume of excavation could be applied as an office-based study to alternative alignments for pipeline route selection. The procedure as described in this paper would be suitable for developing rock excavation estimates for alternative alignments without the validation and refinement from actual construction records provided that the procedure was implemented in the same way on all alternative alignments being compared. Not all alignments will have a potential for encountering rock that might require blasting. A simple office-based screening of a pipeline alignment by a qualified geologist will identify alignments that warrant further evaluation with the rock excavation index procedure.

REFERENCES

Berg, T.M., and others. (1980). *Geologic map of Pennsylvania*. Pennsylvania Geological Survey, Harrisburg, PA. Map 1. scale 1:250,000.

Elkington, J. (1997). *Cannibals with forks: Triple bottom line of 21st Century business*. Capstone Publishing, North Mankato, MN.

Keaton, J.R., Parks, T.H., Boudra, L.H., and Walker, L.D. (2012). "Enhancing pipeline project management with improved rock excavation forecasting." *Proceedings of the 9th International Pipeline Conference*. September 24-28, 2012, Calgary, Alberta, Canada, ASME Digital Collection, CD Paper IPC2012-90143, 8 p.

Rock Behavior under High Pressure and High Temperature (HPHT)

Mudasar Zahoor[1], PhD

[1]Engineering Associate II, Paul C. Rizzo Associates, Inc., 500 Penn Center Blvd, Pittsburgh PA 15235, USA., E-mail: mudasar.zahoor@rizzoassoc.com.

ABSTRACT: The concept of pure damage or the nucleation and evolution of voids is the primary phenomenon responsible for rock failure. However, the behavior of rocks under HPHT is very different than under the conditions of normal pressure and normal temperature. HPHT conditions occur at depths of around 3,000 *m* or below. A rock, which is otherwise a brittle material, behaves more like a metal showing ductile behavior under HPHT conditions. Due to confinement, the fragments can stay together and flow like a continuum thus demonstrating ductile behavior. In this study, a ductile damage model was developed to examine the behavior of rocks under these special conditions. The model includes two coupled theories; the elasto-plasticity theory and the damage evolution theory. Two main problems that were studied are: the un-constrained uniaxial compression and the completely constrained uniaxial problem. The results focus on the effect of confining pressure on rock failure.

INTRODUCTION

Pure Damage is defined as the nucleation and growth of voids/cracks in a body. It is the primary phenomenon responsible for failure of brittle materials like concrete and rocks. A rock is a brittle material under normal conditions. However, under the conditions of High Pressure and High Temperature (HPHT), it behaves more like a metal showing ductile behavior. This is attributed to the confinement, due to which, fragments stay together and flow like a continuum thus demonstrating ductile behavior. This behavior prompts the study of ductile damage. It must be noted that voids can play a role in metal behavior (Horstemeyer, M.F., Gokhale, A.M. 1999) as well; however, most studies do not consider the effect of voids.

The damage process can be accurately represented by non-local material modeling. The conventional models and theories have no intrinsic material length scale, thereby, predicting deformation bands of zero thickness, which is physically incorrect. Runicki and Rice (1975) introduced the concept of bifurcation as a condition for localization into mainstream solid mechanics. Pijaudier-Cabot and Bazant (1988) provide the first non-local damage model. Historically, this is an important paper as it showed that non-local damage mechanics could be formulated and implemented in a robust and relatively simple manner. Mediavilla, J. et al (2006) developed damage

Laplacian based gradient damage model for ductile failure. The Laplacian model of nonlocality is the most convenient for numerical implementation and works robustly down to failure. In the context of the scope of this paper, only local analysis is presented with the main focus on the effect of confinement.

The ductile damage model comprises of the coupling of the plasticity theory and the damage evolution theory. It is assumed that the damage is activated and controlled by plasticity. This assumption is fair in the sense that under extremely high pressure, it is at the onset of plasticity that the material flows like a continuum and therefore initiating damage.

The physical body containing voids is thought of as a set of points. Each point is endowed with a void volume fraction attribute, defined physically as the limit of the ratio of the volume of voids in a region to the volume of the region, as the volume of the region goes to zero (Acharya 2009). The void volume fraction field on the body naturally varies with time. This field is identified as the damage variable of the model, physically representative of a density of microcavity volume in the material. The void volume fraction, defined as above, is a volumetric density. Therefore, its evolution can be expressed as a balance law.

The governing equations for the ductile damage phenomenon in 1D are presented below:

a) Balance of linear momentum equation (Acharya 1999):

$$\rho \frac{\partial v}{\partial t} = \frac{\partial \sigma}{\partial x} \tag{1}$$

b) Damage evolution equation:

$$\frac{\partial \varphi}{\partial t} = \frac{\partial f}{\partial x} + s \tag{2}$$

where, ρ is the mass density, v is the velocity, σ is the stress, φ is the void-volume fraction, $f \cdot \hat{n}$ is the inward flux of void-volume through the surface with a unit outward normal $\hat{n}$ and s is the source term. The damage evolution equation is derived from the concept of free energy and the second law of thermodynamics. The damage driving variable is dependent upon plastic strain and is related through a relation by Mediavilla, J. etal (2006). It may be noted that more emphasis is laid on the results that will be presented later than the mathematical formulation of the model to keep this paper within the recommended scope.

The model developed was verified before implementation to any physical problem. The balance of linear momentum equation was verified for material behavior and governing equation verification respectively. For the governing equation verification, equation (1) can be reduced to a second order wave equation, which can then be verified using a well-known D'Alembert's solution. The damage evolution equation is essentially a diffusion equation (Farlow, S.J. 1993), which when reduced to a heat equation with constant coefficient of diffusion can be verified. During verification, since both equations (1) and (2) are coupled, one of the governing equations was deactivated while verifying the other and vice versa.

In order to verify the balance of linear momentum equation (1), an initial

displacement in the form of a smooth Gaussian is considered with prescribed initial velocity equal to zero. The classical D`Alembert solution for the given problem is of the form (Graff, K.C. 1991):

$$u(x,t) = \frac{1}{2}[f_d(x-ct) + f_d(x+ct)]$$

where f_d is the initial displacement profile. This describes two waves of same amplitude traveling in opposite directions at exactly same velocities emerging from a single disturbance of double their amplitude. Figure 1 shows the initial and resultant displacement that was achieved numerically at a certain time. It is clear that the result is a perfect representation of the above mentioned D`Alembert solution.

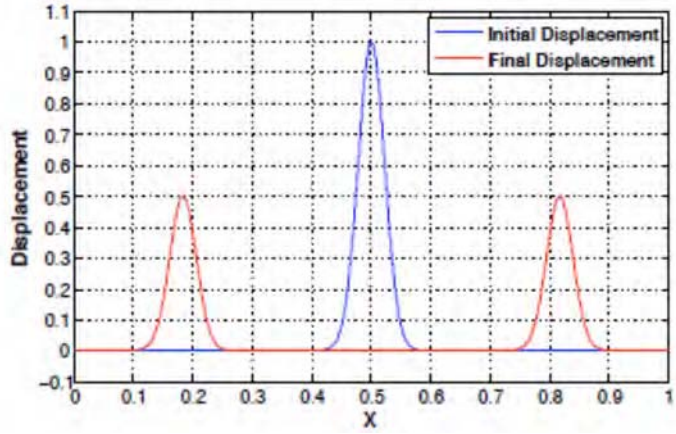

FIG. 1. Verification of D`Alembert solution (Non-dimensionalized)

In the verification of the damage evolution equation (2), the source term is ignored and the diffusion coefficient kept constant. The property of the heat equation is that, it diffuses an initial variable with a certain rate of diffusion depending upon the diffusion coefficient of the equation. Figure 2 shows how diffusion equation smoothes out the solution progressively over a period of time.

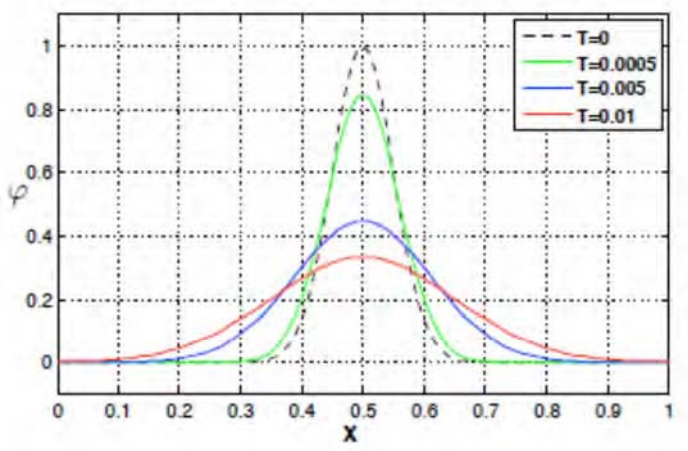

FIG. 2. Verification of the Damage Evolution equation (Non-dimensionalized)

UNIAXIAL COMPRESSION PROBLEM

A full-scale coupled pure uniaxial compression problem with both the governing equations (balance of linear momentum and damage evolution equations) active was solved. The damage as mentioned earlier is controlled by plasticity or in other words, the damage shall propagate or evolve at the onset of plasticity. Figure 3 shows the setup for the uniaxial compression test.

Individual cases of unconstrained and completely constrained setups with respect to applied boundary conditions and loading conditions are discussed in detail. However, in both the cases it was assumed that there is some initial uniform distribution of voids, which is represented as void-volume fraction (number of voids per unit control volume) in the model. For the problem under consideration, 10% initial void-volume fraction was used. The problem was simulated for unconstrained as well as completely constrained cases respectively.

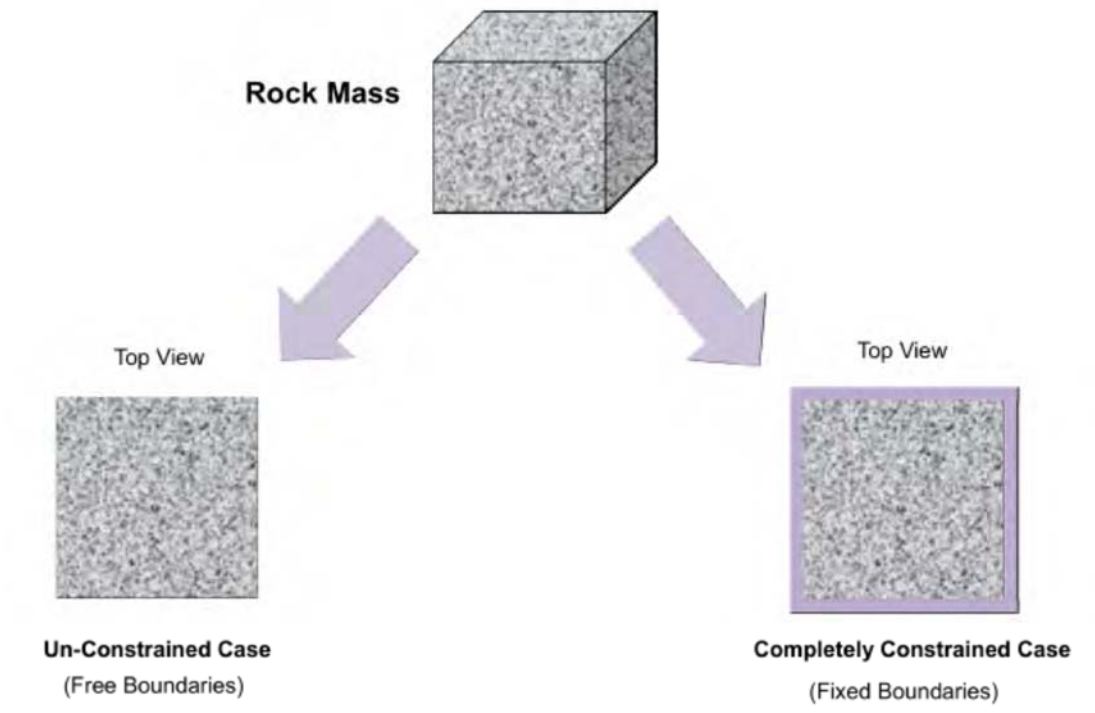

FIG. 3. Uniaxial Compression Setup

The following list shows the materials properties for the specimen considered:

- Material Type = Rock (sandstone)
- Density = $2500\ kgm^{-3}$
- Young's Modulus = $4.3 \times 10^{9}\ Nm^{-2}$
- Poisson's Ratio = 0.25
- Yield Strength = $14 \times 10^{6}\ Nm^{-2}$
- Friction Coefficient = 0.6
- Dilatancy Coefficient = 0.5

Unconstrained Case

Figure 4 gives the details of the loading and boundary conditions for the unconstrained compression case. As is clear from the figure, the boundaries are free complementing the unconstrained setup with a fixed base. The loading is uniform over the top face.

Figure 5 shows the results for the unconstrained case. Two mesh sizes (40×40×1 and 50×50×1) were used. The plot compares the average stress versus average strain curves for the two mesh sizes mentioned above. The simulations for both the mesh sizes were allowed to run up to 100% void-volume fraction. As is clear from Fig.5, the curves show convergence.

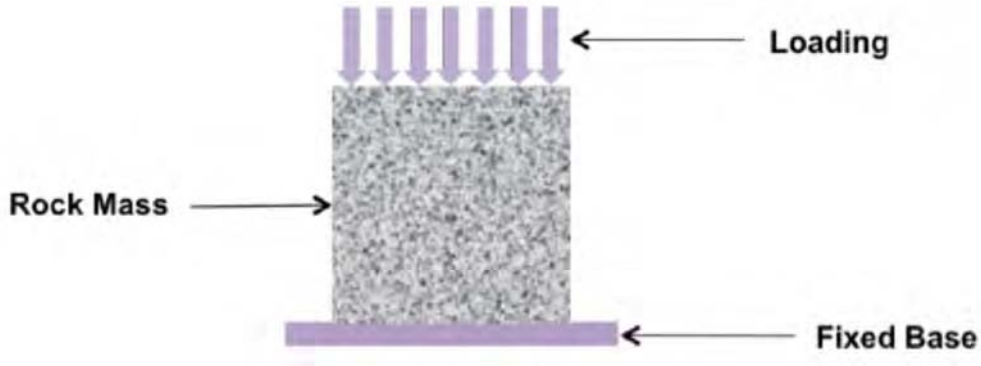

FIG. 4. Uniaxial Unconstrained Compression Setup

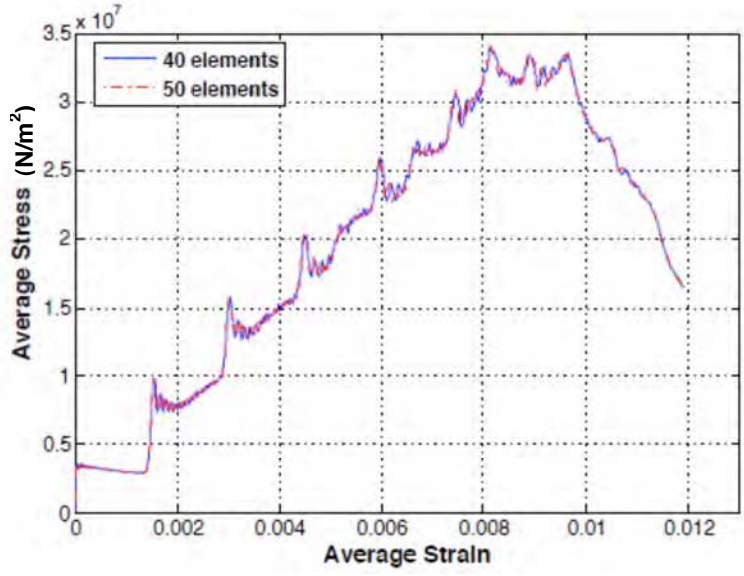

FIG. 5. Av. Stress versus Av. Strain – Unconstrained

Completely Constrained Case

The details of the loading and the boundary conditions for the completely constrained case are shown in Fig. 6. The lateral constraints are provided in the form of rigid displacement control. Visually, lateral constraints can be inferred as the lateral pressure that the rock mass experiences under the conditions of High Pressure.

Figure 7 shows the results for the completely constrained case two mesh sizes (40×40×1 and 80×80×1). The plot compares the average stress versus average strain curves for the two mesh sizes. In the completely constrained case, the simulations were allowed to run up to 100% void-volume fraction. The results from the two mesh sizes are converged.

Further, it can be inferred from the figure the earlier claim that rocks behave like metals under HPHT conditions. It is indicated by work hardening as seen in Fig. 7 between strains 0.05 and 0.09 approximately. On the contrary, there is little or no hardening in the unconstrained case.

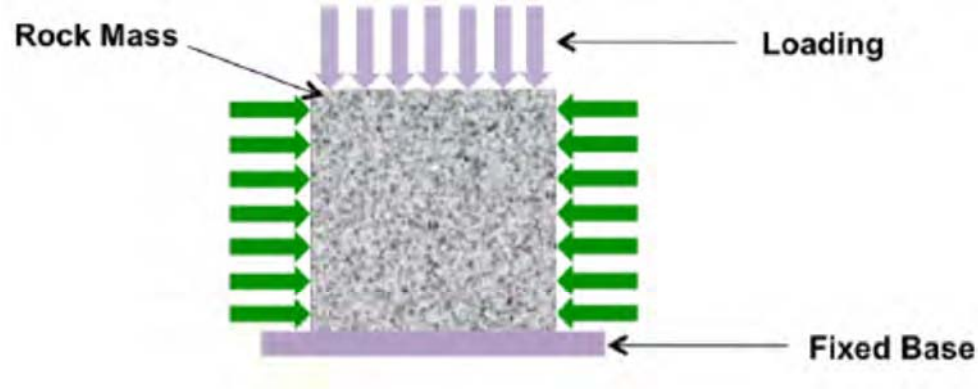

FIG. 6. Uniaxial Constrained Compression Setup

Unconstrained versus Completely Constrained

A comparison between the unconstrained and completely constrained cases is presented as follows. Figure 8 shows the comparison between the unconstrained and the completely constrained cases respectively. Again, the comparison is based on average stress versus average strain plots for both the cases.

The figure gives a clear indication of what it means dealing with the conditions of High Pressure. The curves are plotted at a maximum vertical pressure of approximately 310 *MPa*. There is an exorbitant difference in the failure strains between the constrained and the unconstrained cases. In other words Fig. 8 gives an indication of the difficulty in drilling deep inside the earth's crust where High pressures increase the failure strains by huge margins.

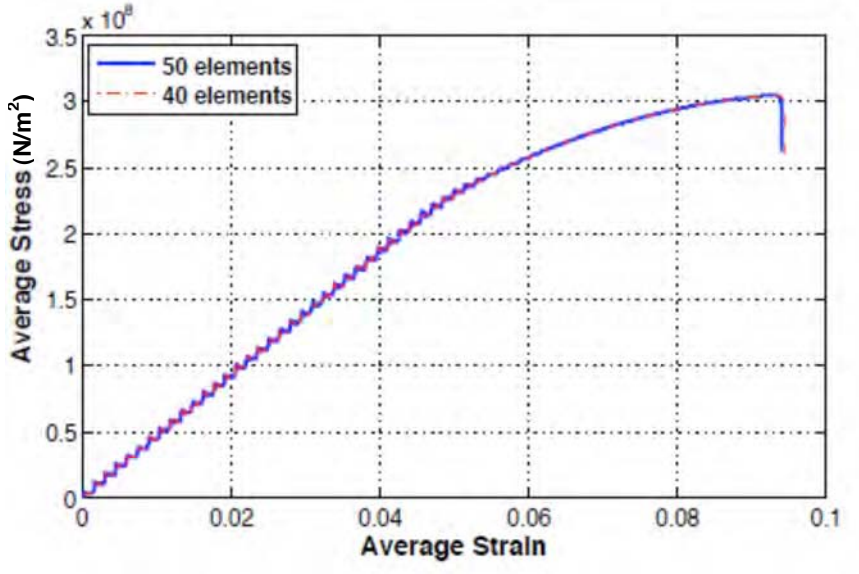

FIG. 7. Av. Stress versus Av. Strain – Constrained

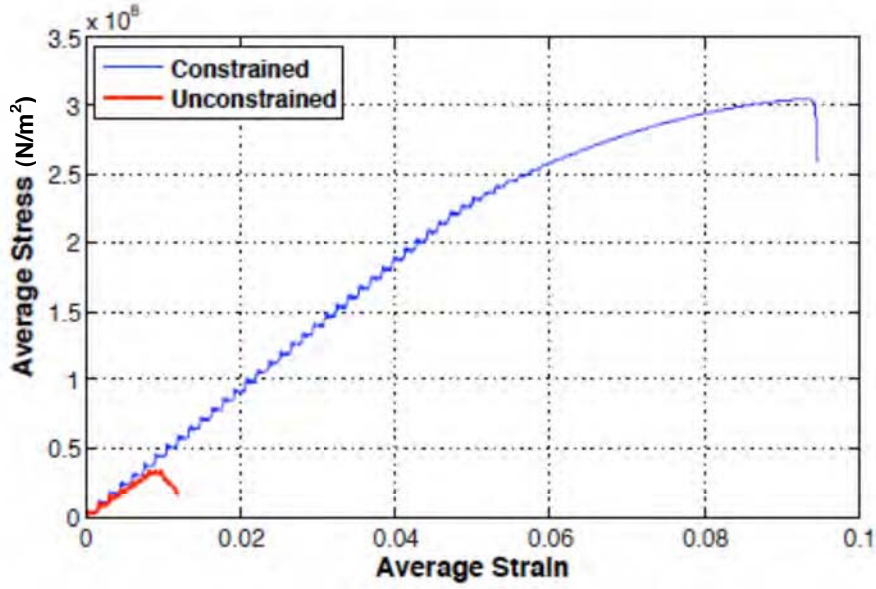

FIG. 8. Av. Stress versus Av. Strain – Constrained versus Unconstrained

It may be noted that the results presented in this paper are from simulation carried on Local plasticity models. Non-Local plasticity models are more realistic and model the physical phenomenon more accurately. This is imperative in case of any perturbations or numerical singularities, where a non-local model is stable while a local model solution becomes asymptotic.

As far as the Shale industry is concerned, this study is mostly applicable to deep sites like the Haynesville. Therefore, in order to effectively implement this numerical

model to sites like Haynesville, some experimental results may be required to get certain material specific parameters to be used in the proposed numerical model.

CONCLUSIONS

The results presented above give a quantitative as well as a qualitative representation of the effect of the conditions that exist deep inside the earth's crust. It also confirms the statement made at the start of this paper about the different behavior demonstrated by rocks under HPHT. It is, therefore, established numerically that rocks display behavior similar to metals under HPHT conditions. However, as mentioned above, in order to model rock failure accurately, non-local modeling scheme needs to be employed.

REFERENCES

Horstemeyer, M.F., Gokhle, A.M. (1999). "A void-cracking nucleation model for ductile metals." *International Journal of Solids and Structures*. Vol 36(3), 5029-5055

Rudnicki, J.W. and Rice, J.R. (1975). "Conditions for the localization of deformation in pressure-sensitive dilatant materials." *Journal of the Mechanics and Physics of Solids*. 23, 371-394

Pijaudier-Cabot, G. and Bazant, Z.P. (1988). "Non-local continuum damage, localization instability and convergence." *Journal of Applied Mechanics*. 55, 287-293

Acharya, A. (2009). "Use of Thermodynamic Formalism in Generalized Continuum Theories and a Model for Damage Evolution." *J. Engrg. Mech*. 135(3), 171-177

Acharya, A., H.P. Cherukuri, and R.M. Govindarajan. (1999). "A new proposal in gradient plasticity: theory and application in 1-D quasi-statics and dynamics." *Mechanics of cohesive frictional materials*, 4, 153-170

Mediavilla, J., Peerlings, R. H. J., and Geers, M. G. D., 2006. "A nonlocal triaxiality depenent ductile damage model for finite strain plasticity." *Comput. Methods Appl. Mech. Engrg*. 195, 4617-4634

Graff, K.C. (1991). "Wave Motion in Elastic Solids." *Dover Publications, New York.*

Farlow, S.J. (1993). "Partial Differential Equations for Scientists and Engineers." *Dover Publications, New York.*

Influence of Mineralogy on the Index Properties and Durability of Crushed Shales

L. Sebastian Bryson[1], Ph.D., P.E., M. ASCE and Isabel Cristina Gomez-Gutierrez[2], S.M. ASCE,

[1]Hardin-Drnevich-Huang Associate Professor, Department of Civil Engineering, 161 Raymond Bldg., University of Kentucky, Lexington, KY 40506, USA, email: bryson@engr.uky.edu
[2]Research Assistant, Department of Civil Engineering, 161 Raymond Bldg., University of Kentucky, Lexington, KY 40506, USA.

ABSTRACT: Weak shale formations in oil shale production are the primary cause of instability in drill holes due to sloughing and swelling. During and after the drilling, shales continuously absorb water and consequently deteriorate with time. The effect of the deterioration results in the transformation of a hard rock with high cohesion and frictional resistance to a soft fine-grained mass without cohesion, lower shear strength, and high swelling susceptibility. As a result, the shales swell and slough into the hole. Shales are primarily composed of varying amounts of clay minerals (i.e. chlorite, mixed layer illite-smectite, illite, and kaolinte), quartz, and other minerals such as carbonates, pyrite or iron oxides. In particular, understanding the influence of clay minerals on the shale is crucial to understanding the mechanical behavior of shales. This is because clays are highly reactive minerals in the presence of water. Due to this reactivity, shales tend to be highly susceptible to deterioration. This paper investigates the association between shale mineralogy and mechanical characteristics. For this study, shale samples were collected from a variety of location in Kentucky. The specimens were assumed to be representative of hard and soft shales with high, medium, and low durability. These samples were crushed and laboratory testing was performed. The lab tests included index tests, mineralogical tests, and durability tests. It was observed from the results of this study that the mineralogy explained the activity and variations in several index properties, as well as the durability of the samples.

INTRODUCTION

Weak shale formations in oil shale production are the primary cause of instability in drill holes due to sloughing and swelling. During and after the drilling, shales continuously absorb water and consequently deteriorate with time. The effect of the deterioration results in the transformation of a hard rock with high cohesion and frictional resistance to a soft fine-grained mass without cohesion, lower shear strength, and high swelling susceptibility. As a result, the shales swell and slough into

the hole. Shales are primarily composed of varying amounts of clay minerals (i.e. chlorite, mixed layer illite-smectite, illite, and kaolinte), quartz, and other minerals such as carbonates, pyrite or iron oxides. In particular, understanding the influence of clay minerals on the shale is crucial to understanding the mechanical behavior of shales. This is because clays are highly reactive minerals in the presence of water. Due to this reactivity, shales tend to be highly susceptible to deterioration. This study investigated the association of the mineralogy of shales and mechanical characteristics. For this study, shale samples were collected from a variety of location in Kentucky. The specimens were assumed to be representative of hard and soft shales with high, medium, and low durability. These samples were crushed and laboratory testing was performed. The laboratory tests included specific gravity, grain size analysis, Atterberg limits, X-ray diffraction and durability tests. All tests were conducted to the applicable ASTM standards.

STUDY SHALES

Various methods were used to sample shale formations throughout Kentucky. The goal was to obtain five shale samples of diverse durability, geological age, and formations. Typically, shale samples were obtained from ongoing highway construction sites containing prevalent shale deposits. Four samples were collected from new excavations and one sample was obtained via surplus core taken from a proposed mining location. Table 1 includes the geologic and location information of the samples used for this study.

Table 1. Geological and Location Information

Geologic name	Geologic Period	Location
Grundy	Pennsylvanian	Clay County, KY
Carbondale	Pennsylvanian	Webster County, KY
Tradewater	Pennsylvanian	Philpot, KY
Bull Fork	Ordovician	Boone County, KY
Fort Payne	Mississippian	Taylor County, KY

Figure 1 shows the approximate locations where the shale specimens were obtained. Samples were obtained from three major geologic periods as outlined in Table 1. The Grundy, Carbondale, and Tradewater formations are Pennsylvanian formations deposited in transitional environment. The Grundy formation consists of sequences of gray siltstone and shale, and minor amounts of limestone. The Tradewater formation is composed of about equal amounts of sandstone, siltstone, and shale, and contains several beds of limestone. The Carbondale formation consists of siltstone, shale, and some locally prominent sandstone units. The Bull Fork formation is an upper Ordovician formation that outcrops in central and north-central Kentucky. It was deposited in shallow marine water and is composed of fossiliferous limestone interbedded with shale in approximately equal amounts. The Fort Payne formation is a Mississippian formation that outcrops over much of south-central Kentucky. It was deposited as marine basin fill. It consists of gray to black dolomitic siltstone and cherty, dolomitic limestone (McDowell, 1986).

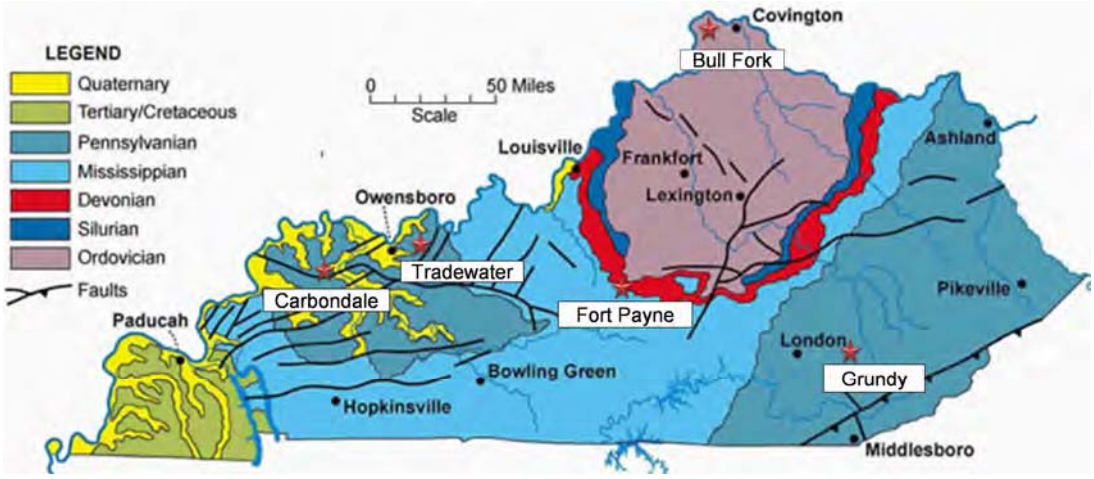

FIG 1. Kentucky map with highlighted sample locations.

LABORATORY TESTING

Sample Preparation

The shale specimens used in this research were subjected to two crushing phases. A jaw crusher was utilized in the reduction of the initial shale specimens obtained from the field. After initial crushing, 1000 g of crushed shale was passed through an 8 mm sieve and retained in No. 4 (4.76 mm) sieve. The sieved sample was then further crushed in a standard Proctor mold (volume = 944 cm^3) using a modified Proctor hammer (weight = 44.5 N) for 100 blows. All tested samples were crushed using identical techniques. Thus, the crushing process was repeatable and provided unique grain-size distributions for the individual shales.

Index Testing

After the samples were crushed, the grain size distribution (GSD) of the sample was calculated in accordance with ASTM D422. A hydrometer test was performed for samples that passed the No. 200 sieve. Table 2 shows the results of the grain size analysis. Is should be noted that the values presented in the table reflects that grain size data after crushing. The table includes, Fines (percent passing the No. 200 sieve), clay fraction, CF (portion smaller than 0.002 mm in diameter), uniformity coefficient, C_u ($=D_{60}/D_{10}$), and the coefficient of gradation, C_c ($=D_{30}^2/D_{60}D_{10}$).Table 2 also shows the results of the Atterberg limit testing. The tests were performed according to ASTM D4318 on the crushed specimens. The silty nature of the crushed shales can be recognized from the low plasticity indices ranging from 2 to 8. All the shales were classified as low plasticity clays or silts over the A-line, with the exception of Fort Payne which was classified as low plasticity silt under the A-line. The specific gravities of the samples ranged from 2.64 to 2.77.

Table 2. Summary of Index Properties of the Crushed Samples

Geologic name	Fines (%)	CF (%)	C_u	C_c	LL	PI	G_s
Grundy	4.3	0.97	9.7	2.7	23	4	2.74
Carbondale	3.7	1.07	8.2	2.5	24	5	2.77
Tradewater	4.2	1.52	12.7	2.4	29	8	2.68
Bull Fork	5.8	2.09	21.8	2.7	26	7	2.65
Fort Payne	4.8	1.42	15.3	2.6	25	2	2.64

LL = liquid limit; PI = plasticity index; G_s = specific gravity.

MINERALOGY TESTING

X-ray diffraction (XRD) tests were performed in order to identify and quantify the minerals in the shale samples. Fine-size crushed samples (i.e. passed through a No. 200 sieve) were used to perform powder XRD. The scan range was 2° to 60° at 1°/minute and a step size of 0.1°. The XRD spectra were analyzed using the *Traces* program, version 6.4.0 (Diffraction Technology, Pty, Ltd). The interpretation of the spectrum was performed by looking for the minerals that presented the d-spacing patterns observed in the spectrum. Table 3 shows the quantification of the primary minerals in the study shales.

All the samples contained clay minerals (i.e. chlorite, illite, kaolinite, and mixed layer illite-smectite), carbonates (i.e. calcite, dolomite, and siderite), and quartz. Illite and kaolinite were the predominate clay minerals in the study shales, which is indicative of shales deposited in marine and transitional environments. However, Bull Fork and Fort Payne had higher percentages of non-clay minerals (i.e. quartz and carbonates) than clay minerals. In particular, the Fort Payne shale had less than 16 percent total clay minerals in the crushed fraction. Also shown in Table 3, Fort Payne contained approximately 3.55 percent of gypsum. It is therefore possible that the Fort Payne sample was a siltstone rather than shale.

Table 3. Summary of Shale Mineralogy

Shale	Ch (%)	I-S (%)	I (%)	K (%)	Q (%)	C (%)	D (%)	S (%)	G (%)
Grundy	6.98	1.33	35.07	21.73	16.27	4.43	5.35	6.15	ND
Carbondale	7.63	0.31	37	23.28	19.08	6.76	ND	ND	ND
Tradewater	4.32	0.23	30.43	22.06	24.06	3.63	ND	12.06	ND
Bull Fork	4.78	ND	11.13	8.56	12.26	44.76	14.95	ND	ND
Fort Payne	2.38	0.44	9.03	3.41	28.75	3.35	42.86	ND	3.55

Ch = chlorite; I-S = mixed layer illite-smectite; I = illite; K = kaolinite; Q = quartz; C = calcite; D = dolomite; S = siderite; G = gypsum; ND = Not detected.

Figure 2 presents a further analysis of the mineralogy. The figure shows the occurrence of illite and kaolinite in the samples, as well as a comparison of the total clay minerals to the total carbonates.

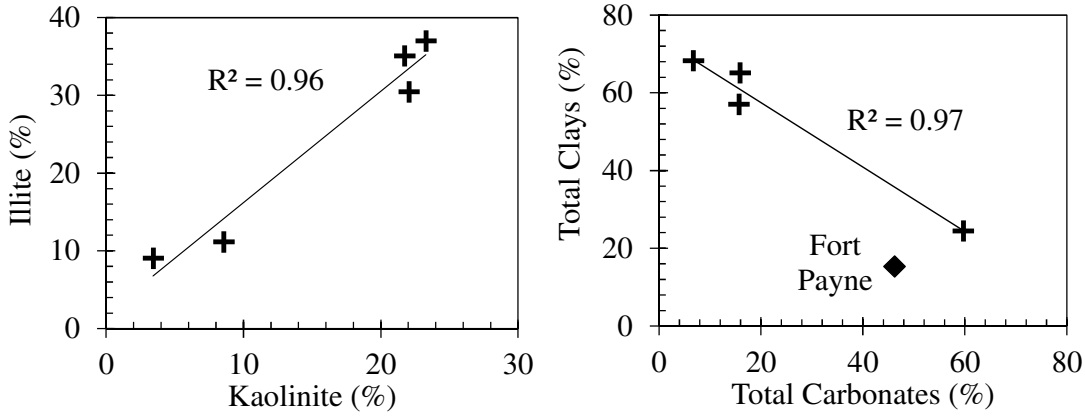

FIG. 2. Primary mineralogical relations for study shales.

Although it must be acknowledged that this mineralogy was obtained from the fraction of the crushed sample that passed the #200 sieved (as opposed from the fraction smaller than 0.002 mm), these data are useful in analyzing mineralogical influences. Figure 2 shows that the amount of illite minerals is proportional to the kaolinite minerals for all samples. The relation between the total clay minerals and the total carbonates is inversely proportional; with total clay minerals decreasing with increasing total carbonates. If it is assumed that material properties and engineering behavior of shales are influenced by the mineralogy, then the relatively smooth transition from one set of minerals to another would indicate that variations in material properties and engineering behavior will be reflected in variations in illite and kaolinite content, and in the total carbonate and clay amounts. The exception is the Fort Payne, which has a large amount of non-clay minerals (i.e. carbonates, gypsum, and quartz) relative to the clay minerals. The implication is that Fort Payne will most likely behave more like a cemented silt than a shale.

Durability Data

Durability of shales is often quantified using the slake durability index, I_{d2} in accordance with ASTM D4644. This test provides an index that is representative of the portions of sample remaining after two wetting and drying cycles, with 10-min cycle durations. Bryson et al. (2012) proposed a slake loss test that follows the same procedure as the slake durability test with the difference being only one wetting and drying cycle is required and the procedure is done for 10, 25, 60, and 120-min cycle durations. The result of this test is the lost slake index, LSI, which represents the logarithmic decay of durability with the time of cycling. Table 4 shows the LSI of the crushed shales as compared to the slake durability index. The insitu water contents of the shales are also shown in Table 4. These water contents are the oven-dried water contents at the time of sampling. From a general comparison of the durability indices in Table 4, it is observed that the greater the rate of loss (ie. rate of deterioration), the greater the LSI, and consequently, the less the durability.

Table 4. Summary of LSI and Id2 values

Geologic Name	Water Content (%)	LSI (%)	I_{d2} (%)
Grundy	1.3	0.07	96.51
Carbondale	2.89	0.155	94.74
Tradewater	5.24	0.497	80.81
Bull Fork	3.29	0.219	77.17
Fort Payne	4.4	0.074	92.62

OBSERVATIONS AND DISCUSSION

Grain Size Parameters and Mineralogy

Grain size parameters obtained for a crush sample must be used with caution. The obvious concern is that different crushing techniques will produce different grain sizes and different size distributions (Bohloli et al., 2001). Thus while the crushing procedures used for this study will not produce the actual fractional components of the shale, they did produce indices that were useful in evaluating the mechanical properties of shale. For example, less durable shales tend to produce more silt size and clay size particles than more durable shales.

Figure 3 shows the variation of fine grain fraction of the crushed samples with some of the mineralogical characteristics. Specifically, the percent fines of the crushed samples are plotted against the total carbonate contents and the clay fraction is plotted versus the illite/kaolinite ratio.

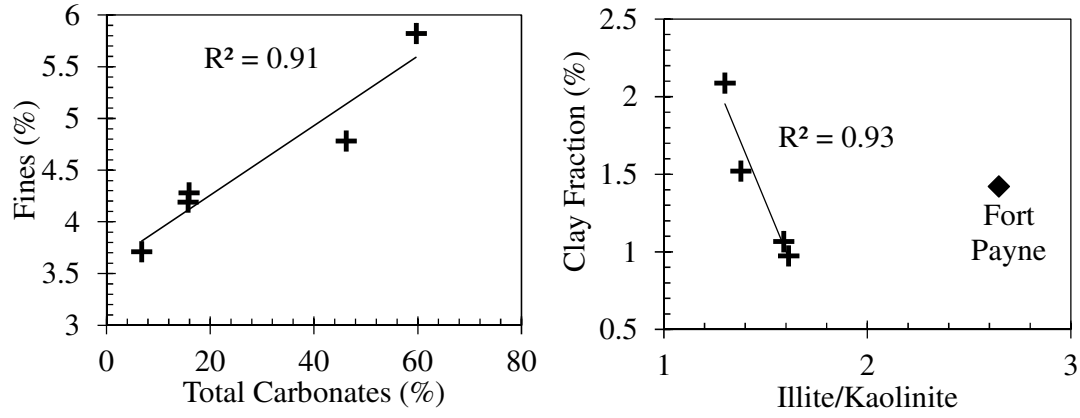

FIG 3. Variation of the fine grain fraction with mineralogical characteristics.

Figure 3 shows the fines content increases with the carbonate content. This is because the carbonate minerals are water soluble and thus can be transported by pore water where they precipitate in soil and become cementing agents. For samples subjected to mechanical crushing only (i.e. no chemical dissolution), the carbonates will occur as bulky, silt sized particles. As was mentioned earlier, the more durable

shales produce smaller amounts of silt sized (i.e. fines) and clay sized (i.e. clay fraction) particles. Therefore, the implication is that the less durable shales will tend to have greater quantities of carbonate minerals.

The intent of the illite/kaolinite ratio used in Figure 3 was to expressed the dominate clay minerals as a ratio of the more active mineral relative to the less active mineral. The kaolinite clay minerals are 1:1 phyllosilicates, consisting of alternating silica and alumina sheets. Kaolinite is a very stable non-expanding clay mineral. Illite is a 2:1 clay mineral consisting of two silica sheets to one alumina sheet. Although illite is not subject to expansion when exposed to water, the chemical bonds in the crystal structure are weaker than those in kaolinite. However, because the more durable shales produced smaller quantities of silt and clay sized particles, the clay fraction is shown to actually decrease with increasing illite/kaolinite ratio. This observation is counter to clay mineralogy and cannot be used for a strict mineralogical analysis of the shale samples. However, the findings do strongly suggest that shale durability in a crushed sample roughly decreases with increasing illite/kaolinite content relative to the percent of clay sized particles. In addition, the durability of shales is observed to be approximately inversely proportional to the clay fraction produced by crushing. The Fort Payne sample is again the exception to the observation because of the high content of quartz and carbonate minerals.

Figure 4 shows the variation of the coarse grain fraction with the mineralogical characteristics. In the figure, the coarse grain fraction is represented by the coefficient of uniformity and the coefficient of curvature. The total carbonate content and the percentage of quartz minerals are used to reflect the mineralogical characteristics.

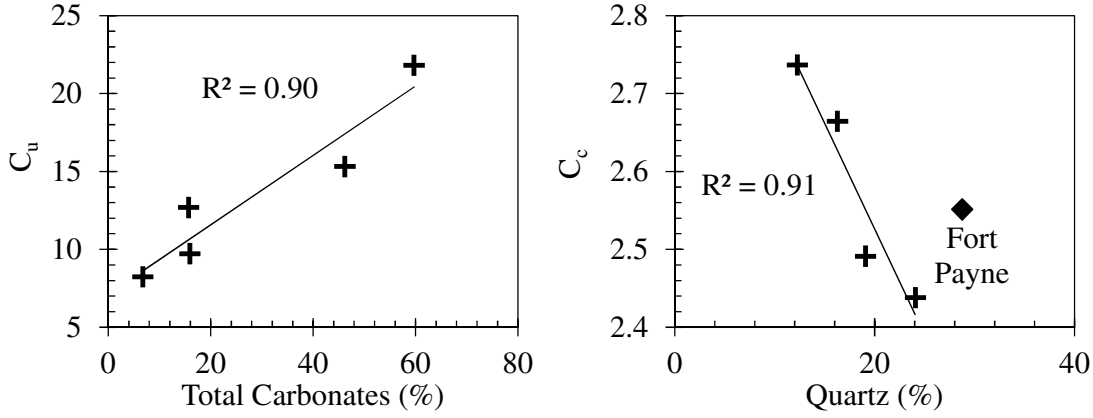

FIG 4. Variation of coarse grain fraction with mineralogical characteristics.

Figure 4 shows the coefficient of uniformity strongly trends with the total carbonates. As the name implies, the coefficient of uniformity is an index used to quantify the uniformity of the sample's gradation; the smaller the number, the more uniform the gradation. For example, a coefficient of uniformity equaled to one would be a sample with only one grain size. Clay minerals are flat with very small variations in size. Therefore samples with a high clay mineral content would tend to have lower coefficient of uniformity values. However, carbonate minerals are more bulky and have much greater variations in size. Thus, Figure 4 shows that the coefficient of

uniformity increases with amounts of carbonate minerals present in the crushed sample.

The coefficient of uniformity has been shown to be reflective of specific surface (Santamarina et al., 2001), which is the surface area-to-mass ratio of clay particles. Clay minerals that have the greatest specific surface also have the greatest affinity to absorb water. This affinity to absorb water tends to be an indicator of the mechanical behavior of shale. Specifically, shales that have a high affinity to absorb water tend to have lower shear strengths, be more likely to swell in the presence of water, and be more prone to weather. Conversely, shales with low affinity to absorb water will tend to be non-expansive, have higher shear strengths, and be more durable. Thus, by extension of the relation between the coefficient of uniformity and the specific surface, it can be loosely stated that shales with high C_u values will exhibit poorer mechanical characteristics than shales with low C_u values.

The coefficient of curvature is a grain size parameter used as a measure of the shape of the grain size distribution curve. When plotted against the quartz content, the coefficient of curvature is observed to be loosely trend with durability. Softer shales subjected to mechanical crushing produce more fines with greater occurrences of quartz minerals. As the quartz content goes up, the sample tends to be dominated by one grain size and the coefficient of curvature tends to decrease. Unfortunately, the crushing procedures used for this study produced grain size curves with relatively the same shape. Thus, there is very little variation in the range of Cc values.

Index Properties and Mineralogy

Figure 5 shows the variation of the plasticity index with the illite/kaolinite ratio and the variation of the activity with the occurrence of kaolinite minerals.

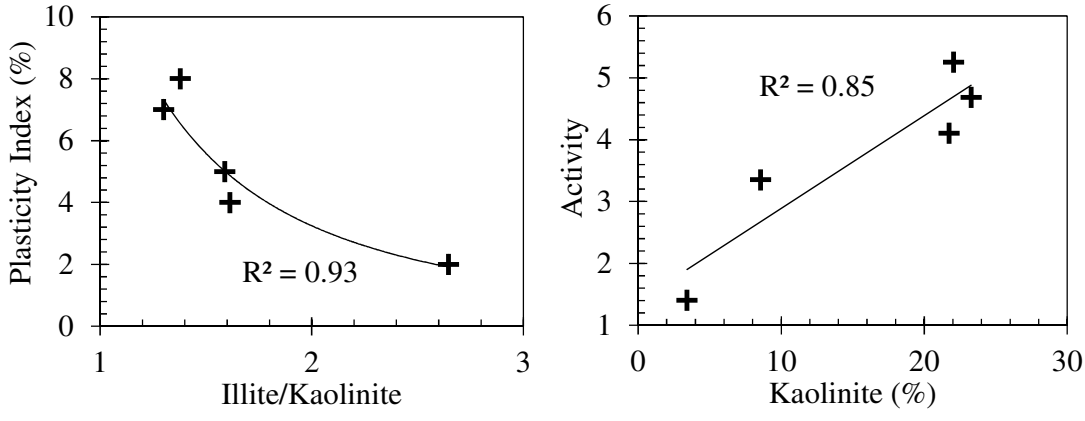

FIG 5. Variation of Atterberg data with mineralogy.

Activity is defined as the plasticity index divided by the clay fraction. It is noted that illite is a 2:1 clay mineral, which support substitution of water molecules between the silica sheets, while kaolinite is a 1:1 clay mineral. This would imply that as the illite/kaolinite ratio increases, the samples have more capacity to absorb water

and thus the plasticity of the samples should increase. However, as was discussed previously, the crushing procedure used for this study produced decreasingly less silt and clay sized particles for increasingly more durable shales. Consequently, the plasticity index actually decreases with increasing illite/kaolinite ratio because there is less clay and silt sized material. The plot of the plasticity index versus the illite/kaolinite ratio for this study serves as indication of the importance of the crushing procedure, not the strict influence of mineralogy.

The data presented in Figure 5 suggest that the study shales are susceptible to shrinking and swelling behavior. A loose relation is seen between activity and durability of shales; more durable shales have lower activity and kaolinite content and less durable shales have higher activity and kaolinite content. This observation better agrees with commonly excepted clay mineralogy. Consequently, Figure 5 may suggest that the relationship between the activity and the kaolinite mineral content is somewhat independent of the crushing procedure. Nevertheless, caution should be used when attempting to quantify durability of a shale with just one clay mineral.

Durability and Mineralogy

As has been discussed throughout this paper, durability was quantified using the loss slake index (LSI) developed by Bryson et al. (2012). Figure 6 shows the LSI value plotted directly against the ratio of chlorite plus illite to kaolinite, (Ch+I)/K. Chlorite is a 2:1:1 mineral. It consists of repeating layers of silica sheet, an alumina sheet, another silica, and then a brucite sheet. Thus, the (Ch+I)/K ratio represents the sum of the 2:1 clay minerals over the 1:1 clay mineral.

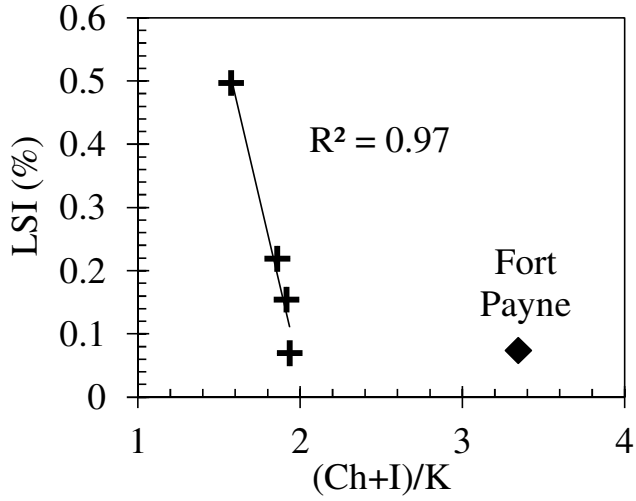

FIG 6. Variation of LSI with mineralogical characteristics.

The LSI is an engineering behavior parameter that gives an indication of the accumulation of silt and clay sized materials due to mechanical deterioration. The direct impact of mineralogy on the LSI is not easily defined because the index considers both structure (i.e. the lattice size and geometric arrangement of the mineral grains) and mineralogy (i.e. particle size and interparticle forces). However, Figure 6

suggests that there is somewhat of a relationship between the clay mineral content and the LSI. But as has been discussed throughout this paper, the relation observed in the figure more reflects the crushing procedure, as opposed to strict clay mineralogy.

Future research is recommended whereby various crushing techniques are evaluated to assess the most appropriate methodology for preparing the samples. Also, future research is recommended that utilizes the true mineralogical characteristics (i.e. analysis of the fraction less than 0.002 mm) of the samples shales, for the analyses.

CONCLUSIONS

This study investigated the association between shale mineralogy and mechanical characteristics. It was generally found that mechanical characteristics of shales are loosely reflected in variations in illite and kaolinite content, and in the total carbonate and clay minerals content. More importantly, the crushing methods used to prepare the samples have a significant impact on the resulting test data. However, regardless of the crushing methodology, less durable shales tended to produce more silt size and clay size particles than more durable shales. This study also found that the less durable shales tended to have greater quantities of carbonate minerals. The evaluation of the coarse grain fraction of the shale samples suggested that shales with high C_u values will exhibit poorer mechanical characteristics than shales with low C_u values. An evaluation of the fine grain fraction indicated that more durable shales will most likely have lower activity and kaolinite contents than less durable shales. Future research into the influence of mineralogy is warrented.

ACKNOWLEDGEMENTS

The authors would like to thank Mr. Jordan Kirkendoll for his efforts in collecting the shale samples and performing the durability tests. The authors would also like to thank the Kentucky Geologic Survey (KGS) and the Kentucky Transportation Cabinet (KYTC) for help with identifying sample sites.

REFERENCES

Bohloli. B., Gustafson. G., Ronge. B. (2001). “A laboratory study on reducing the quantity of rock fines at failure: application to rock blasting and crushing.” *Bulletin of Engineering Geology and the Environment,* 60(4), 271-276.

Bryson, L. S., Gomez-Gutierrez, I. C., and Hopkins, T. C. (2012). “Development of a new durability index for compacted shale.” *Engineering Geology,* 139-140, 66-75.

Franklin, J.A. (1981). Shale Rating System and Tentative Applications to Shale Performance. *Transportation Research Record*, 790, 2-12

McDowell, R. (1986). “The Geology of Kentucky – a text to accompany the Geologic Map of Kentucky.” <http://pubs.usgs.gov/prof/p1151h/contents.html> (2013).

Santamarina, J.C., Klein, K. and Fam, M. (2001). *Soils and Waves*, John Wiley and Sons, Ltd., Chichester, England, 488 pp.

Interpretation Challenges for In Situ Stress from Mini-Frac Tests in Soft Rocks/Hard Soils

Nadia ShafieZadeh[1] and Rick Chalaturnyk[2], Ph.D, P.Eng., M.ASCE

[1] PhD candidate University of Alberta, E-mail: shafieza@ualberta.ca.
[2]Professor, Geotechnical Engineering, 3070 NREF, Dept of Civil and Env. Engineering, University of Alberta, Edmonton, AB, Canada, T6G 2W2, E-mail: rjchalaturnyk@ualberta.ca

ABSTRACT: The importance of measuring in-situ stresses as an essential input factor to caprock integrity analysis is realized for both the technical management of SAGD and CCS projects (design of optimal operating pressure) and environmental reasons (loss of caprock containment). A common technique to carry out stress tests in impermeable and weak rocks like clay shale is to combine sleeve fracturing with micro-hydraulic fracturing test for which premature initiation of the fracture at the packer level can be avoided. Following a brief introduction of the micro-hydraulic fracture technique, field data obtained from a micro-hydraulic fracturing test program completed to assess the far field in-situ stress state for a proposed low pressure Steam-Assisted Gravity Drainage (LP-SAGD) pilot project located southeast of Fort McMurray, Alberta, Canada has been analyzed. Pressure analyses during and after micro-hydraulic fracturing are used to compute the minimum in situ stress at depth and illustrate the wide variability in the results. Issues surrounding stress alterations in the near wellbore region, low permeability and low injection volumes are shown to contribute to incorrect estimates of the far field minimum in situ stress.

INTRODUCTION

Measurement of the magnitude and orientation of the minimum horizontal stress is a key element in determining the far field stress distribution in the subsurface. For thermal oil recovery projects such as steam assisted gravity drainage (SAGD), where steam is injected at elevated pressures, knowledge of in situ stresses, particularly the minimum horizontal stress, within the overlying seals of the reservoir or caprock is critical for selecting the maximum steam injection pressure. Micro-hydraulic fracturing tests or mini-fracs are the most common methods used for stress measurement in borehole at depth. These tests generate a pressure response obtained during the cyclic fluid injection/shut-in periods that allow interpretation of the initiation, propagation and closure of an induced hydraulic fracture. The pressure response is generated by injecting fluids at a constant rate into a region of the borehole sealed between two inflatable packers.

For SAGD projects in the northeastern region of Alberta, the Clearwater Formation is generally identified as the caprock. The Clearwater Formation consists primarily of black and green shale, with some interbedded grey and green sandstone and siltstone (Glass, 1997). The properties of these lithologies place them in the complex transitional range of geological materials described as either "hard soils" or "soft rocks" (HSSR). An appropriate classification for HSSR can be found in Hawkins and Pinches (1992).

Mini-frac testing within these HSSR lithologies can sometimes be difficult. Occasionally, the induced fractures will migrate along the packer elements used to seal the testing interval. To alleviate issues such as this, field test procedures have been implemented where an initial "induced" fracture at the borehole wall is created using the inflation of one of the packers – typically referred to as a "sleeve" fracturing stage. The intent of this process is to create a discontinuity at the borehole wall that will serve as the initiation point for the hydraulic fracture generated during the mini-frac test. These multiple test stages within an HSSR lithology have unfortunately lead to complex stress paths around the borehole, complex behavior during fluid injection and difficulty in interpreting the fracture closure pressure, which is required for interpreting the minimum in situ stress. For following sections discuss a series of mini-frac tests conducted using the multistage packer technique for in situ stress measurement test performed in Clearwater Formation and highlights the issues surrounding the interpretation of the minimum in situ stress.

GEOLOGICAL DESCRIPTION OF SAGD PROJECT

In northeast Alberta, bitumen resources are at relatively shallow depths located about 100 meters below ground surface. The stratigraphic section in the project area consists of Devonian, Cretaceous, and Quaternary sediments overlying the Precambrian basement. The Devonian-aged strata underlie the prospective Cretaceous reservoir sediments, and are separated by the sub- Cretaceous unconformity. The Cretaceous sediments are in turn overlain by a thin veneer of Quaternary sediments. The characteristics of these stratigraphic units are described in detail by Andriashek (2003), Bachu et al (1993) and Porter et al (1982). The stratigraphic and geomechanical unit of interest is the Clearwater Formation, defined as the caprock for this project, and which is subdivided into the lower Wabiskaw Member and the Clearwater shale. This unit is lower Cretaceous-aged, and conformably overlies the McMurray Formation (reservoir).

According to project operator (AOS, 2010), the Clearwater shale is pervasive in this area, conformably overlying the Wabiskaw Member, and is unconformably overlain by Quaternary sediments. The top of the Clearwater shale occurs at depths of 10 to 14 meters with the thickness of the Clearwater shale in the Project area typically ranging from 52 to 56 meters. The Clearwater shales are thick and laterally extensive throughout this area, and are expected to provide an excellent cap rock for SAGD production.

IN SITU STRESS TESTING PROCEDURE

Micro-frac testing conducted in this project were performed with a multiple packer tool that allowed both the sleeve and hydraulic fracturing stages of the micro-frac test to be conducted with a test interval or depth. Figure 1 illustrates the configuration of the packer tool during these stages. The hydraulic fracturing stage of the micro-frac test consisted of a series of injection/shut-in cycles. The following provides a summary of the test stages:

- Sleeve Fracturing Cycle
- Packer Inflation
- Leak-Off Cycles
- Hydraulic Fracturing Cycles

INTERPRETATION METHODOLOGY

A variety of interpretation techniques have been developed to estimate the magnitude of the minimum principal stress from the pressure records obtained during the mini-frac test. The following pressures (if measurable) are used in these interpretation techniques: breakdown pressure, propagation pressure, instantaneous shut-in pressure (ISIP), closure pressure, reopening pressure, and rebound pressure.

The goal of stress testing with the micro-hydraulic or mini-frac techniques is to create a fracture that provides an estimate of the closure stress as close as possible to the minimum in situ stress. Theoretically, the width of the created fluid-filled fracture will become zero if the pressure of the fluid in the fracture is equal to the total stress acting on the fracture surface. The value of this pressure is called the closure stress and would ideally equal the in situ minimum stress. Unfortunately, measurement or interpretation of the closure stress is challenging since constant fluid pressure in the fracture cannot be attained in practice. What is measured is the pressure at which the fracture initiates, propagates, closes and opens in the near-well region of the borehole. Consequently, estimates of the closure stress (or pressure) are detected by examining the flow regimes associated with the abrupt changes in fracture conductivity when the fracture opens or closes over the several stages of the testing program. At each stage, various estimates of the closure pressure are determined. Reconciling estimates over all cycles provides an estimation of the closure stress and the minimum in situ stress.

Various pressure-time data analysis methods used in this research for determination of the minimum in situ stress, as listed below:

- Pressure versus square root of shut-in time
- Tandem square root or linear flow plot
- Log pressure versus time since shut-in
- Log ΔP versus log Δt plot
- Pressure decay rate
- Fracture reopening test
- Horner plot

A description of the methodology followed for each of these methods can be found in Barree et al. (2009).

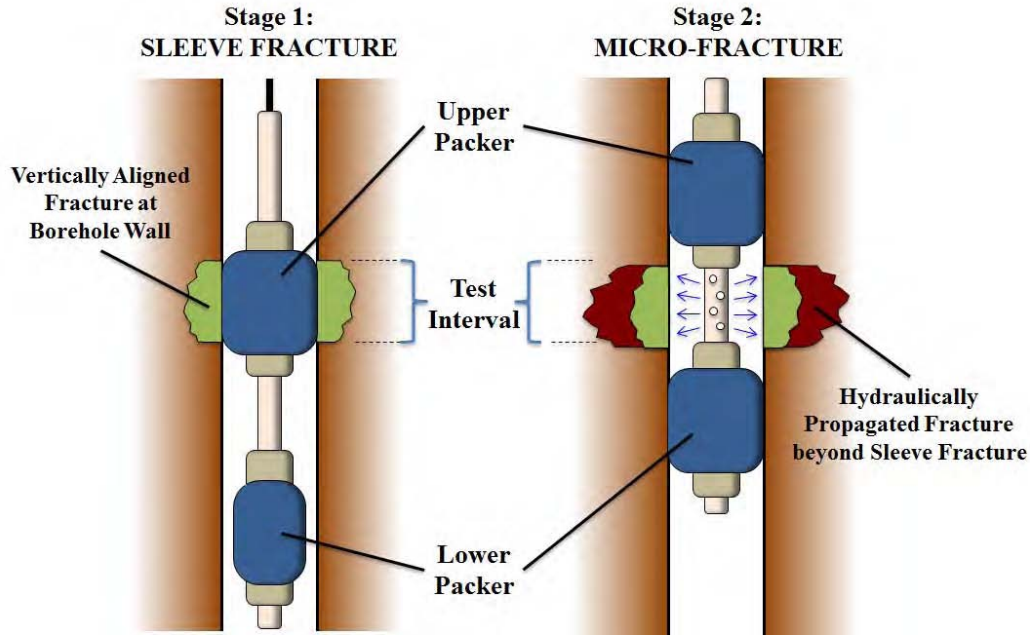

FIG. 1. Arrangement of packers during the sleeve fracture and micro-frac tests stages

RESULTS FROM MICRO-FRAC TEST CONDUCTED IN HSSR

To illustrate the issues with micro-frac testing in HSSR, the following section will describe and interpret the results obtained from a micro-frac test conducted at a depth of 63 m in Well AA/03-22-088-08W4. The test consisted of two stages: 1) sleeve fracturing and 2) hydraulic fracturing and each stage are discussed below.

1) Sleeve fracturing

Figure 2 provides a summary plot of the complete pressure history during the sleeve fracturing stages of the micro-frac test. This figure also illustrates the slope change in the pressure-time plot for two cycles, which are used for interpreting the potential formation breakdown pressure. As noted in Figure 2, the breakdown pressures were estimated to range from 13.5 MPa and 14.2 MPa.

One of the issues that may complicate stress interpretations during this stage of the test in HSSR materials is creep and stress relaxation processes. The Clearwater Formation shales within this test interval, like many soft shales, when subjected to a sustained loading can undergo significant creep strains. Conversely, stress relaxation may occur if the inflated packers are held constant for a period of time and under a fixed deformation, there is a time-dependent reduction in stress. Stress relaxation can be considered as the reverse of creep and conceptually, creep is pressure controlled and relaxation is volume controlled. As noted in Figure 2, eleven points were identified in the two sleeve fracturing stages where both creep and/or stress relaxation effects may play a role in modifying both boundary conditions of the test.

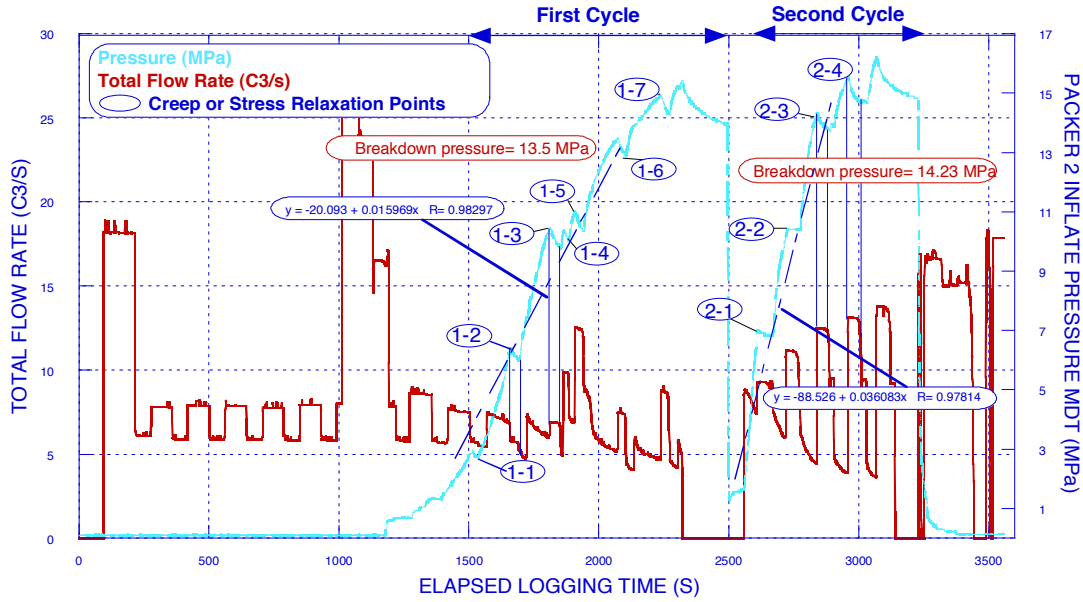

FIG. 2. Complete packer inflation pressure time record for sleeve fracturing stages of micro-frac test

2) Micro-hydraulic fracturing

After the sleeve fracturing stage, the upper and lower packers of the tool are moved to straddle the 63 m depth to perform leak-off and micro-frac tests. One leak-off test was performed with relatively slow leak-off, which indicated low formation permeability. Figure 3 illustrates the injection rate and pressure versus time record for the micro-frac test. The micro-frac test sequence analyzed in this paper comprised two fracturing cycles. The initial leakoff test, the first injection and fall off test, the second injection and fall off test and the first and second rebound stages of the test are summarized in Figure 3. The first and second injection cycles have been analyzed using the methods listed above to determine the reopening, fracture propagation, ISIP and fracture closure pressure. Figures 4 and 5 illustrate the results for the first cycle obtained from application of the pressure-time data analysis methods mentioned previously.

DISCUSSION ON INTERPRETATION METHODS

A review of the flow regime identification methodologies is beyond the scope of this paper but understanding flow regimes is an important element in understanding the downhole formation response to fluid injection. Increasingly more sophisticated pressure transient analysis techniques are being utilized for estimating ISIP and fracture closure pressures (Powless, 2013). One fundamental method for detecting flow regimes in the presence of the fracture is by plotting the log of pressure versus the log of time. For both cycles, the unit, half and almost zero slope could be observed (Figure 4a) which indicated the wellbore storage and skin effect, fracture/formation linear flow and bilinear or pseudoradial flow regime respectively.

Although the reopening pressure normally considers as an upper bound of

minimum stress (Ratigan 1992, Ito et al. 1993, Detournay et al. 1994), the use of this pressure as a measure of σ_{min} can be unreliable especially in nearly impermeable materials. Sensitivity of the reopening pressure to the pumping rates and the residual permeability of the existing fracture, assuming it was formed during the sleeve fracturing stage and that it was mechanically closed during the previous shut-in period are the factors that can influence the reopening pressure and result in an overestimate of σ_{min}.

All data obtained from various methods of interpretation are summarized in Table 1 and Figure 6, which allow estimating the lower and upper limits of minimum in situ stress and its gradient. Fracture closure pressure is the most suitable measurement for estimating σ_{min} and as shown in Figure 6, ranges between 2.03 to 2.53 MPa in the 1st cycle and 2.09 to 2.47 MPa in the 2nd cycle. Assuming equal validity for each of the interpretation methods, σ_{min} (1st) = 2.33 ± .20 MPa and σ_{min} (2nd) = 2.31 ± .14 MPa. Recalling that the test depth interval was 65 m, this stress estimate can be converted to a stress gradient. Based on all the closure measurements, the stress gradient computed for this test interval is σ_{min} = 35.6 ± 2.5 kPa.

The magnitude of this estimate for σ_{min} is problematic. Based solely on formation bulk density estimates alone, the gradient of the in situ vertical stress will be approximately 21kPa/m. If both horizontal stresses are substantially higher than the vertical stress, than the micro-frac test should have yielded an estimate of σ_{min} close to 21kPa/m. If one of the horizontal stresses was less than the vertical stress, than the micro-frac test should have yielded a minimum stress gradient estimate lower than 21kPa/m. Clearly, this is not the case over the two cycles analyzed in this test and this result has been found in many other tests deploying the same multi-packer technique in HSSR.

There are several hypotheses for why such high minimum in situ stress gradients are generated. For instance, impermeable formations pose several challenges for stress testing. First, as mentioned previously, a fracture must be initiated in the interval during sleeve fracturing test which itself induces stresses in vicinity of the borehole wall. The area of influence of this stress change may extend out as far as ten times the borehole radius. Second, classic test interpretation methods may be no longer valid because it is based on the assumption that sufficient fluid will leak from the fracture face(s) to close it during the limited time of shut-in periods. If the formation has very low permeability, the fracture may not close during the test.

Based on regional data for the Clearwater Formation, permeability would be approximately 10-15 μD, which is a low permeability. In such cases, a pressure decrease is still observed after shut-in, as in a typical hydraulic fracturing cycle, but it corresponds only to the dissipation of stored energy to further extend the fracture and cannot be directly interpreted for the estimation of closure pressure.

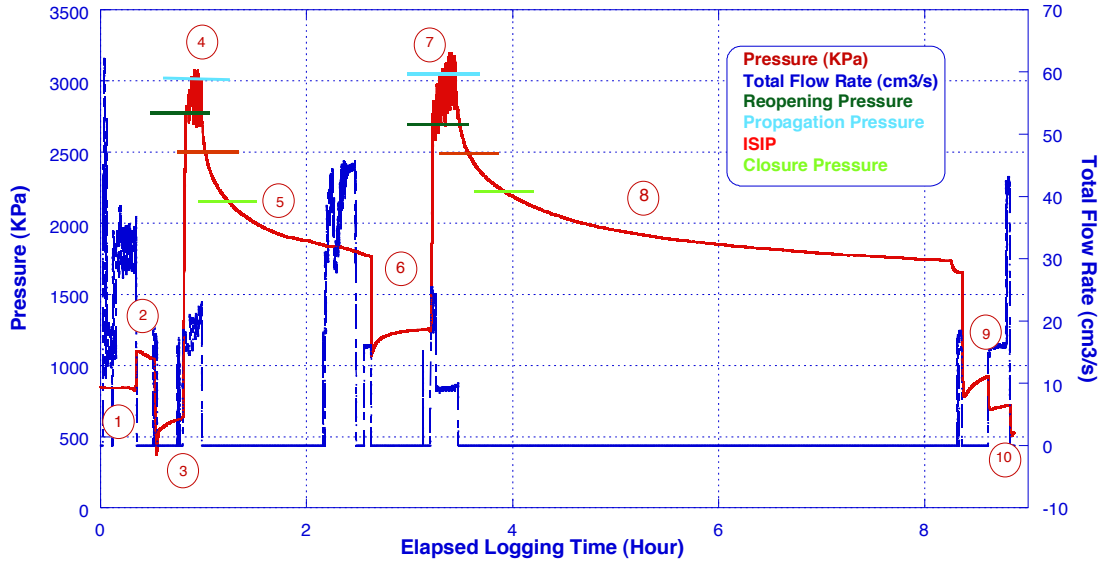

FIG. 3. Recorded pressure history during the micro-frac test in Clearwater Formation at 63 m depth. Circles refer to the following stages: 1) upper and lower packer inflation, 2) leakoff test, 3) drawdown, 4) first cycle, 5) first falloff, 6) flowback, 7) second cycle, 8) second falloff, 9) flowback and 10) packer deflation

For example, even if closure of the fracture for these two test cycles can be identified at 2.3 or 2.5 MPa, the pressure decline exhibits a peculiar behavior of shale which does not lend itself to an explicit determination of the closure pressure, at least not with the range of interpretation methods used in this analysis.

As well, during pumping cycles following fracture creation, the pressure record may exhibit features similar to those characteristics of the reopening of a closed fracture. These features, however, correspond only to the loading of an already open fracture before propagation and cannot be directly interpreted for σ_{min} .

Furthermore, stresses around the borehole are higher than the far-field in-situ stress condition as a result of induced stresses from the drilling phase and also sleeve fracturing stage. Therefore, a proper micro-fracturing test should inject enough volume of fluid to ensure fracture propagation extends beyond this altered-stress zone. For the current micro-frac test, a relatively small volume of 30 L of fluid was injected into the formation. This small injection volume did not extend the fracture beyond the altered stress zone and is likely the main reason for incorrect high fracture closure pressure, reflecting the near well stress field rather than the far field stress state.

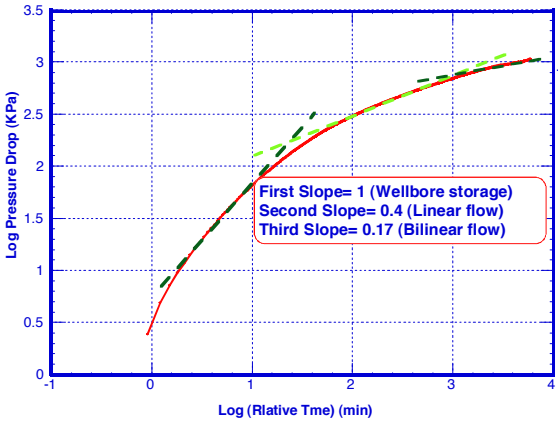

(a) Schematic plot of mini-frac pressure fall-off data showing various flow regimes- first cycle

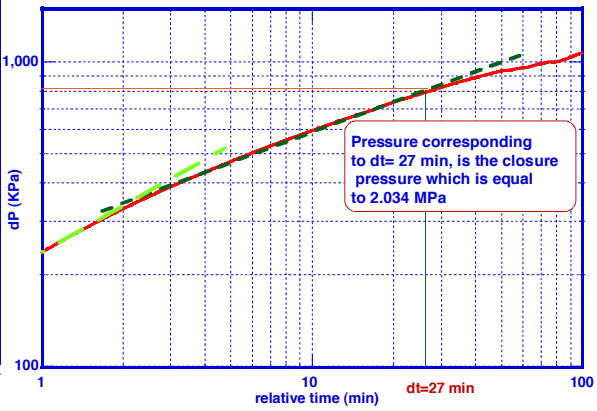

(b) Log-log scale of dP versus dt, closure pressure corresponds to a value where fracture linear flow deviates from a straight line-first cycle

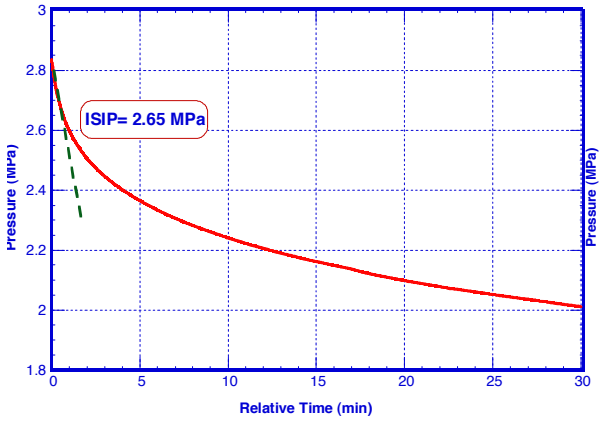

(c) Interpretation of ISIP from change in slope of pressure versus shut-in time

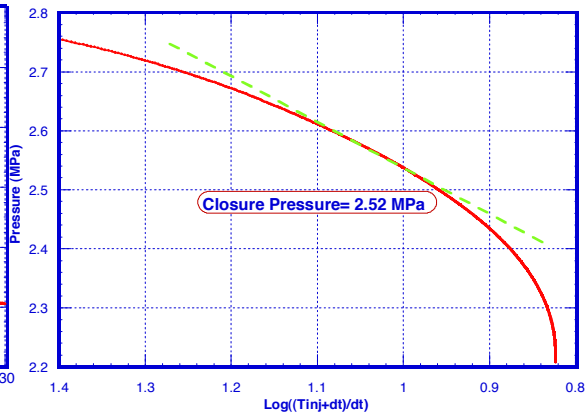

(d) Determination of in-situ minimum stress from the slope of a Horner plot- first cycle

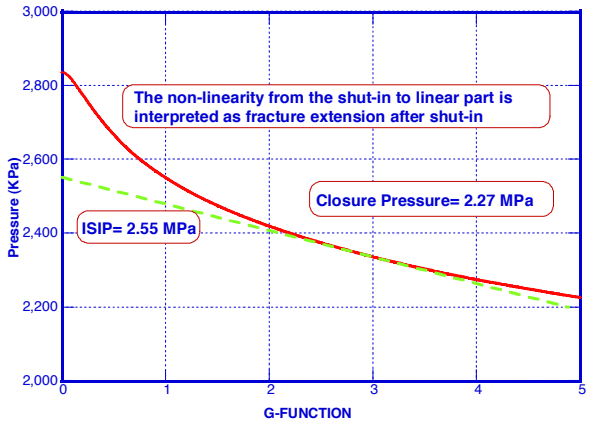

(e) Pressure versus G-Function plot- first cycle

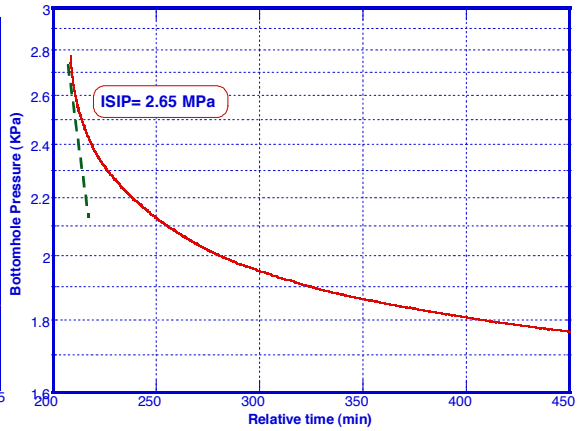

(f) Determination of ISIP from Log P versus Relative Time- first cycle

FIG. 4. Data interpretation using different classical methods for determination of ISIP, reopening pressure and closure pressure, First cycle

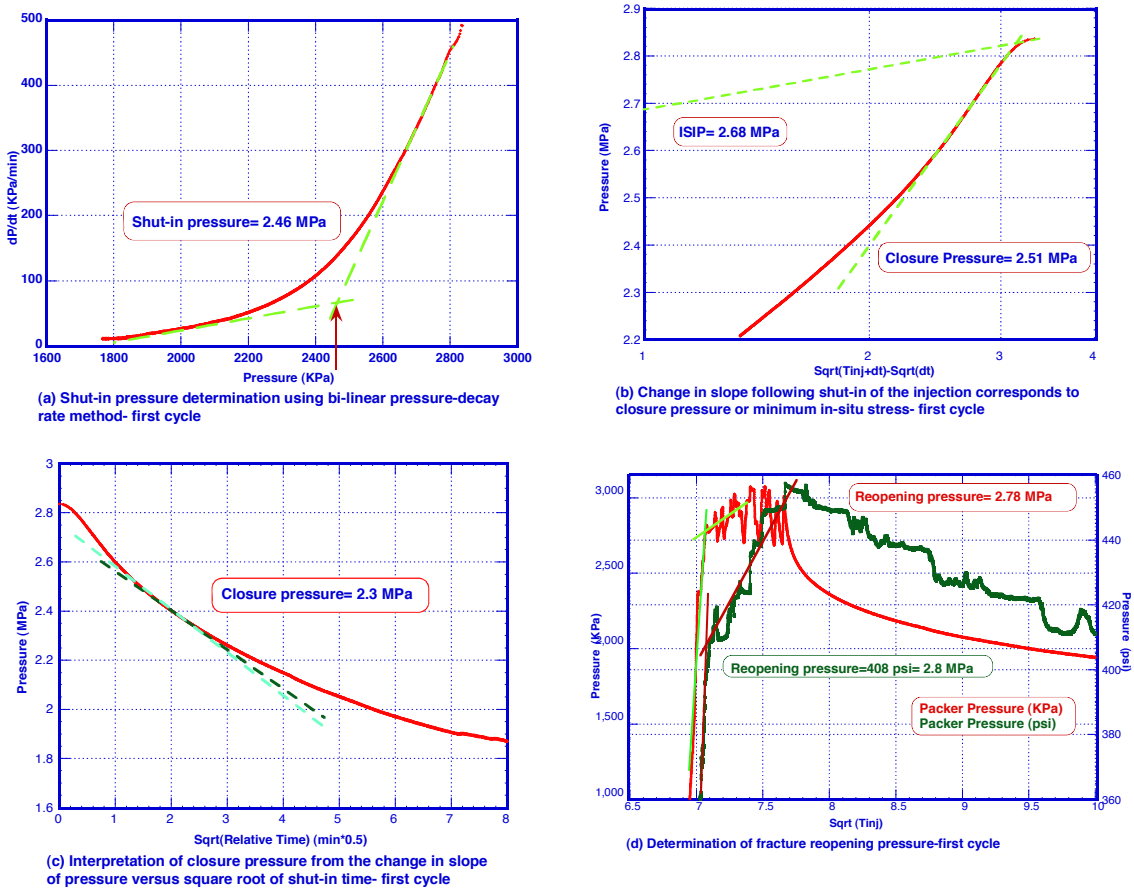

FIG. 5. Data interpretation using different classical methods for determination of ISIP, reopening pressure and closure pressure, First cycle

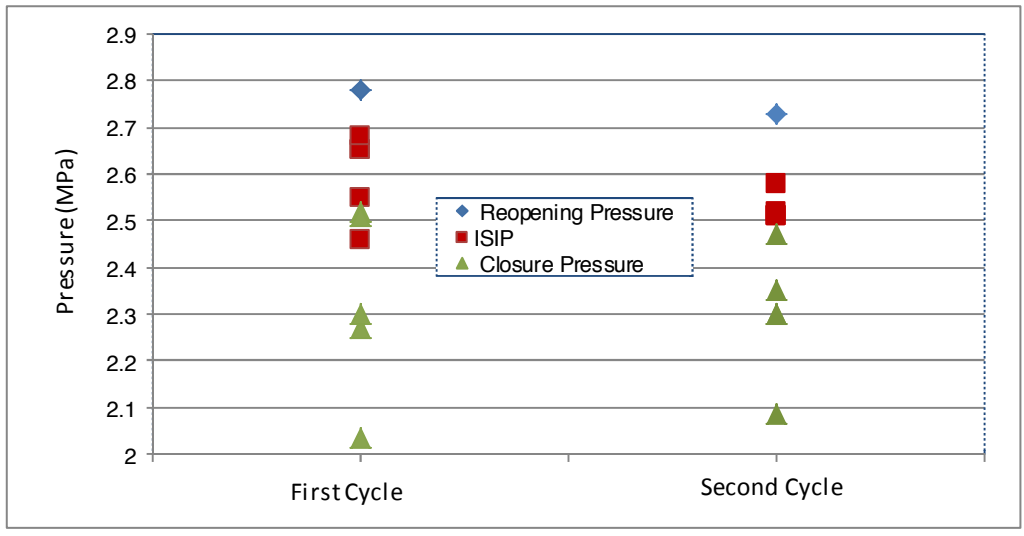

FIG. 6. Reconciliation plot of all data obtained from various methods of interpretation

Table. 1. All the data obtained from various methods of interpretation of micro-hydraulic fracturing test

Method of Interpretation	First Cycle			Second Cycle		
	Reopening Pressure (MPa)	ISIP (MPa)	Closure Pressure (MPa)	Reopening Pressure (MPa)	ISIP (MPa)	Closure Pressure (MPa)
P-Sqrt (Tinj)	2.78	-	-	2.73	-	-
P- dt	-	2.65	-	-	2.52	-
Log dp- Log dt	-	2.65	-	-	2.51	-
Horner Plot	-	-	2.52	-	-	2.47
Log dp- Log dt	-	-	2.034	-	-	2.086
dP/dt - P	-	2.46	-	-	2.51	-
P- G Function	-	2.55	2.27	-	2.58	2.3
Tandem plot	-	2.68	2.51	-	2.51	2.3
P-Sqrt(dt)	-	-	2.3	-	-	2.35

CONCLUSION

The data acquired from a multi-packer micro-hydraulic fracture test was analyzed and discussed. The results demonstrate that although the micro-frac tests are regularly used in the petroleum industry, special attention must be paid to the unique conditions of the caprock in the oilsands development and consequent demands for high quality data and accurate interpretation. Issues surrounding stress alterations in the near wellbore region, low permeability and low injection volumes were shown to contribute to incorrect estimates of the far field minimum in situ stress.

Inversion with a fully coupled hydraulic fracturing model will be conducted to investigate the hypotheses concerning the minimum in situ stress estimates. A second approach consists of conducting a flow-back/rebound cycle at the end of each hydraulic fracturing cycle. When the pressure stabilizes at the end of the rebound part of the cycle, the pressure in the fracture is closer to the closure pressure and is the best estimate for the closure stress in such formations. Multiple cycles and flow-back technique can specifically help to define the closure pressure for low permeability materials like clay shale.

ACKNOWLEDGEMENTS

The authors would like to acknowledge the financial support provided by the Helmholtz Alberta Initiative (HAI) for this study.

REFERENCES

Alberta Oil Sands Inc., (2010), "Application for Alberta Oil Sands Inc. Clearwater West LP-SAGD Pilot Project", Website:http:/www.aboilsands.ca

Andriashek, L.D., (2003), "Quaternary geologic setting of the Athabasca oil sands in situ area, Northeast Alberta", EUB/AGS Earth Sciences Report, 2003-03, 83 p.

Bachu, S., U nderschultz, J.R., Hitchon, B., Cotterill, D., (1993), "Regional-scale subsurface hydrogeology in Northeast Alberta", Bulletin No.6, Alberta Geological Survey (AGS), Alberta Research Council (ARC), 49 p.

Barree, R.D, V.L. Barree and D.P. Craig, 2009. Holistic Fracture Diagnostics: Consistent Interpretation of Prefrac Injection Tests using Multiple Analysis Methods. SPE J. Production and Operations, SPE 107887, pp. 396-406.

Castillo, J.L., (1987), "Modified fracture pressure decline analysis including pressure-dependent leakoff", SPE 16417, 9 p.

Glass, D.J. (editor) 1997. Lexicon of Canadian Stratigraphy, vol. 4, Western Canada including eastern British Columbia, Alberta, Saskatchewan and southern Manitoba. Canadian Society of Petroleum Geologists, Calgary, 1423 p. on CD-ROM. ISBN 0-920230-23-7

Detournay, E., Carbonell, R., (1994), "Fracture mechanics analysis of the breakdown process in minifrac or leak-off tests", Proc. of the joint ISRM/SPE conference Eurock'94, August, Delft, pp. 399-407

Desroches, J, and A. Kurkjian, 1999. "Applications of Wireline Stress Measurement", SPE Reservoir Eval. & Eng., Vol 2, No. 5, SPE 58086, pp. 451-461.

Dubost, F.X. Zheng, S.Y. Corbett, P.W.M., (2004), "Analysis and numerical modelling of Wireline pressure tests in thin bedded turbidites", Journal of petroleum science and engineering, pp. 247-261.

Hawkins, A.B., and Pinches, G.M. (1992). Engineering description of mudrocks. Quarterly Journal of Engineering Geology. Vol. 25, pp.17-30

Ito, T., Hayashi K., (1993), "Analysis of crack reopening behavior for hydrofrac stress measurement", Int. J. Rock Mech. Min. Sc. Geomech. Abs. , 30, 7: pp. 1235-1240.

Lee, M.Y., Haimson, B.C., (1989), "Statistical evaluation of hydraulic fracturing stresses measurement parameters, Int. J.Rock Mech.Min. Sci., Geomech. Abstr. Vol.26, No.6, pp. 447-456.

McLennan, J.D., Roegiers, J.C., (1981), "Do ISIP accurately represent the minimum principal stress?", USGS Workshop on hydraulic fracturing stress measurement, Monterey, California. 11 p.

Notle, K.G., (1982), "Fracture design considerations based on pressure analysis", SPE Production Engineering. February, SPE 10911, pp. 22-30.

Notle, K.G., (1979), " Determination of fracture parameters from fracturing pressure decline", paper SPE 8341. 16 p.

Porter, I.W., Price. R.A., McCrossan, R.G., (1982), "The Western Cnanadian Sedimentary Basin: Philosophical transactions of the Royal Society of London, Series A, V:305, pp. 169-182.

Powless, K., 2013. The Use of Pressure Transient Analysis Tools To Interpret Mini-

Frac Data in Alberta Oilsands Caprocks. SPE Heavy Oil Conference, SPE 157843, Calgary, 8 p.

Ratigan, J.L. (1992), "The use of fracture reopening pressure in hydraulic fracturing stress measurements", Rock. Mechanics and Rock Engineering, Vol. 25, No. 4, pp. 225-236.

Syfan, F.E., Newman, S.C., Meyer, B.R., Behrendt, D., (2007), "Case history: G-Function analysis proves beneficial in Barnett shale application", SPE 110091, 10 p.

Warpinski, N.R., (1989), "Determination in-situ stress from hydraulic fracturing through perforations", Int. J.Rock Mech.Min. Sci., Geomech. Abstr. Vol.26, No.6, pp. 523-531.

Field Borehole Testing of Anisotropic Shale Rock

X. Yu[1]

[1]Associate Professor, Department of Civil Engineering, Department of Electrical Engineering and Computer Science (Courtesy Appointment), Case Western Reserve University, 10900 Euclid Ave, Bingham 206, Cleveland, OH 44106. Ph. 216-368-6247; E-mail: xxy21@case.edu

ABSTRACT: This paper describes a group of field testing to study the characteristics of shale rock that shows strong anisotropic behaviors. Field borehole geophysical testing were performed at three locations to depth up to 280 ft. Based on the site investigation program, most subsurface rock consists of shale with thin clay seams embedded at certain depths. Borehole geophysical testing performed at the site include: 1) Borehole caliper, 2) Natural Gamma and Electrical Resistivity, 3) Acoustic Televiewer. The purpose was to characterize the geological structures, especially the major joint planes in rock formation. Borehole seismic testing includes seismic downhole testing, which determined the shear wave velocity of rock at different depths typically at 5 ft interval. A specially design seismic cross hole testing was conducted, where the shear wave excitation was generated by striking the steel tube. Simplifications are made to interpret the crosshole signals where the rock is assumed to be consistent of a uniform heterogeneous material. The results indicate that the shear wave velocity in the inclined direction is typically much larger than the shear wave velocity in the vertical direction. The speed typically decreases as the inclination angle increases. This is consistent with commonly observed anisotropic behaviors in sedimentary rocks with horizontal bedding plan.

INTRODUCTION

The anisotropic mechanical behaviors of shale rock has been studied in a number of previous investigations (i.e., Sarout et al. (2007); Sarout and Guéguen (2008); Herwanger and Horne (2009); Ciz and Shapiro (2008); Kuila et al. (2011); Verdon (2012); Wang (2002); Vernik and Liu (1997); Vernik and Nur (1992)). The work presented in this paper was initialized as part of the efforts to understand the anisotropic mechanical properties of shale rock for the design of underground pump station. The depth of investigation ranged up to 85.3m (280ft) under the ground. A variety of borehole geophysics testing were conducted in the field to determine the physical and geological properties of shale rock. For mechanical properties measurement in the field, seismic downhole and cross hole measurements were performed using unconventional setup to measure the shear and compression wave

velocities in the horizontal and vertical directions, as well as the wave speeds along inclined directions. From these, the anisotropic mechanical properties of shale rock were determined. While the study was primarily for designing of underground pump station, the testing performed provided an opportunity to study the anisotropic behaviors of in situ shale rock, the popular shale gas bearing material.

Field Conditions and Borehole Geophysical Testing Program

Field borehole geophysical testing were performed at three borehole locations designated as TDPS-1, TDPS-2 and TDPS-3, close to the location of the underground pump station (Figure 1).

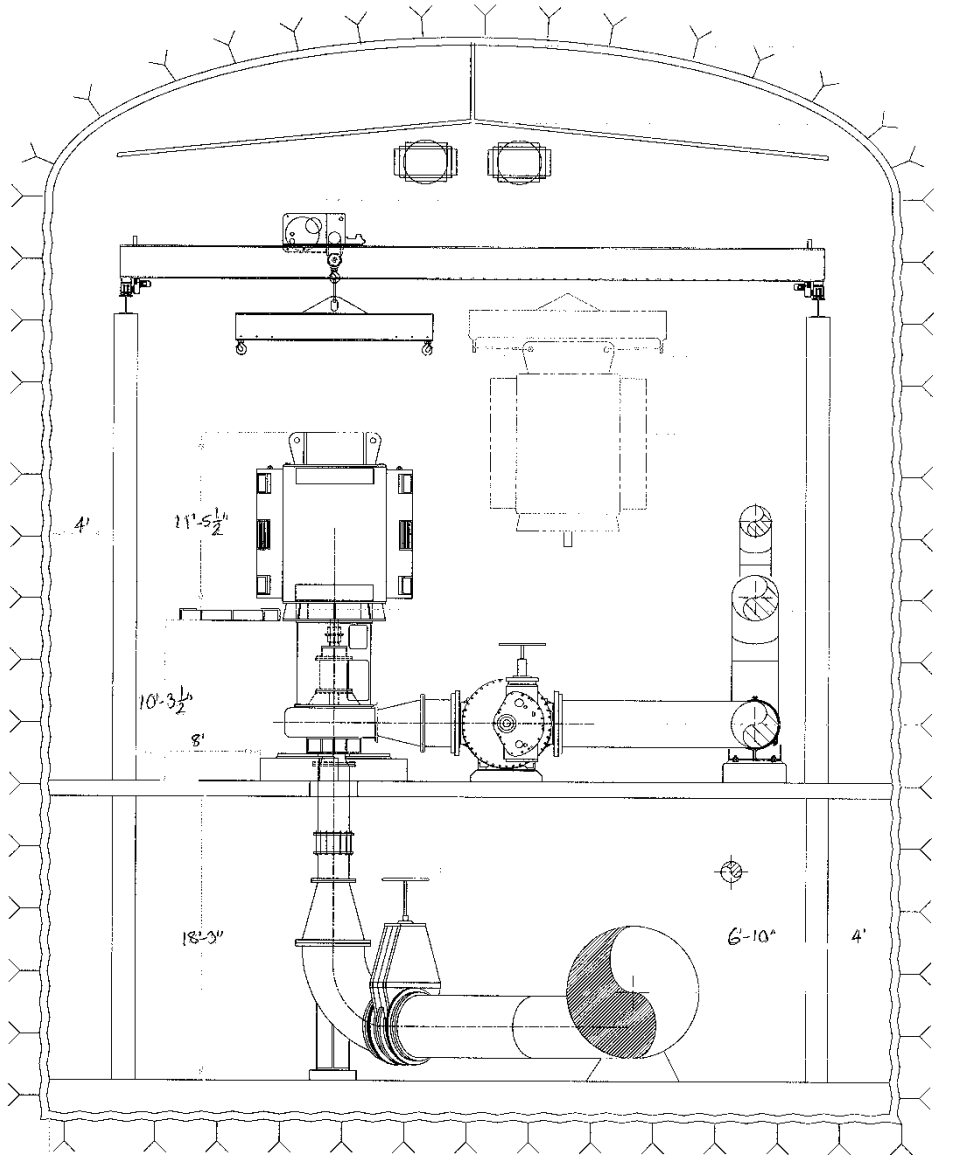

FIG 1 Schematic of the location of the pump station in underground shale rock (the top of the tunnel is 51.51m (169 ft) under the ground, 18.29m (60 ft) in width, 21.95 m (72 ft) in height)

Distance between TDPS-1 and TDPS-2 is 50.3m (165 ft). The distance between TDPS-2 and TDPS-3 is 49.53m (162.5ft). The depth of boreholes was around 85.3m (280ft), including around 18.28-27.4m (60-90ft) in soil layers. The section of borehole in the soil layers was encased with steel tube. Based on the site investigation program conducted by Resource International Inc. and URS Inc., most subsurface rock consist of shale with thin clay seams embedded at certain depths.

At the request of the design firm, borehole geophysical testing performed at the site include: 1) Borehole caliper, 2) Natural Gamma and Electrical Resistivity, 3) Acoustic Televiewer. The purpose of these geophysical testing is to characterize the geological structures, especially the major joint planes in rock. The borehole caliper uses a multiple armed tripod to measure the diameter of the hole. The integrated inclinometer together with the borehole caliper provide quality assessment on the borehole. The natural gamma probe measures the radioactivity in soils, based on the phenomena that rock seams with high clay content and shale produces high level of gamma radiation. The acoustic televiewer uses a focused acoustic beam to scan around the borehole and measure the shape of the hole from the time or amplitude of reflected signals. It is used to measure the geological features such as strike and dip of structural joints.

From borehole caliper data, the boreholes diameters are typically between 9-10 cm. The size of the borehole appears to be slightly smaller with increasing depth (however, this might be caused by the off-center of the caliper as discussed in the previous note). From the tilt measurement built into the acoustic televiewer, the tilt angle of the boreholes along the depth are typically within 1°. The quality of boreholes should be of high quality.

From the natural gamma measurement, the magnitude of natural gamma in rock is typically large (around 150 cps). The current consensus among geologists are sand and sand stone has low natural gamma values (less than 50 cps), clay and shale has higher natural gamma values (larger than 100 cps). The relatively consistent large value of natural gamma in the rock layer confirms the observation from the drilling log, i.e., the rock are mostly shale and embedded with clay seam. Occasionally the shale is embedded with thin layer of sand stone. Due to the thin thickness of these layers, the natural gamma count did not have the resolution to clearly identify these layers, i.e., the natural gamma values are the averaged value of shale and sand stone/clay, and are therefore larger than that observed in a pure sand layer.

The acoustic televiewer was conducted at TDPS-1 and TDPS-2. As the steel casing on TDPS-3 was pulled out for other drilling activities, acoustic teleiviewer testing was not able to be conducted at this location. The acoustic televiewer clearly identifies a variety of embedded layers or fractures along the borehole. 3D view of the borehole is generated from the acoustic televiewer data.

The results of these testing are presented in the project report and not discussed in detail here since they are not the focus of this paper.

Borehole Seismic Testing

Borehole seismic testing include seismic downhole testing and a specially design seismic cross hole testing. The seismic downhole test determines the shear wave

velocity of underground soils at different depths. In this testing program, shear waves were generated on the surface of ground by use of a sledge hammer to hit a wood block horizontally. Seismic signals at different depths were collected (typically at 1.52m (5 ft) interval).

The seismic excitation for the crosshole testing was generated by striking the steel tube encased in soil layers (Figure 2). Due to the large separation of more than 45.72m (150ft) (the standard cross hole testing requires testing holes to be within around 2.74m (9 ft) distance), refraction of wave might occur and could lead to deviation from a liner travel path assumption.

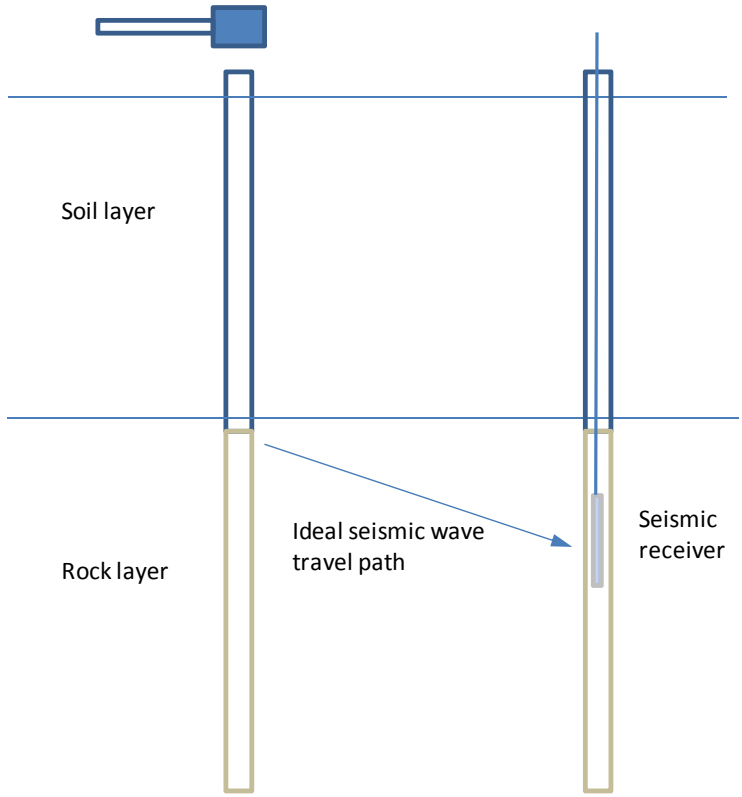

FIG. 2. Schematic of large separation cross hole testing

Results and Analyses

Distribution of vertical compression wave velocity versus depth from downhole testing

Figure 3a summarizes the measured compression wave velocity distribution from three testing locations. The results were organized in terms of average, maximum and minimum velocities. Figure 3b summarizes the measured shear wave velocity distribution from three testing locations. The results were organized in terms of average, maximum and minimum velocities. The Poisson's ratio at different depth can be calculated from the measured shear wave and compression wave speeds.

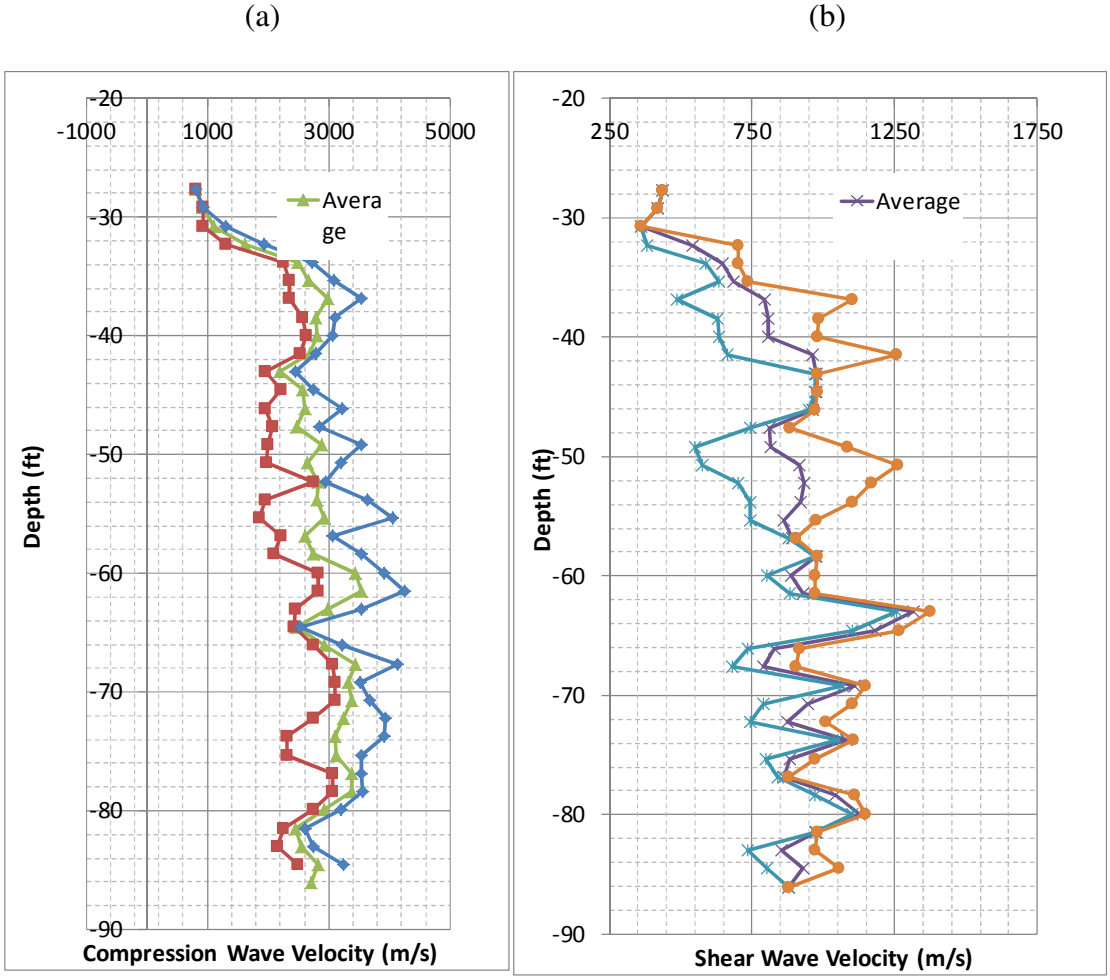

FIG. 3. (a) Compression wave velocity with depth; (b) Shear wave velocity with depth

Variation of shear wave velocity in the inclined direction from crosshole testing

As described in the early context of this paper, the shear wave excitation was generated by striking the steel tube. The wave scattering process would become rather complex. Considering the fact that the average vertical shear wave velocity does not appear to change significantly (at least between 42.67m to 85.34m (140ft to 280 ft)). A simplification is made to interpret the crosshole signals. The rock is assumed to be consistent of a uniform heterogeneous material.

Figure 4(a) summarizes the variation of average shear wave velocity in the inclined direction from crosshole testing. Compare figure 4(a) and Figure 3, the shear wave velocity in the inclined direction is typically much larger than the shear wave velocity in the vertical direction. This is consistent with commonly observed anisotropy in sedimentary rocks.

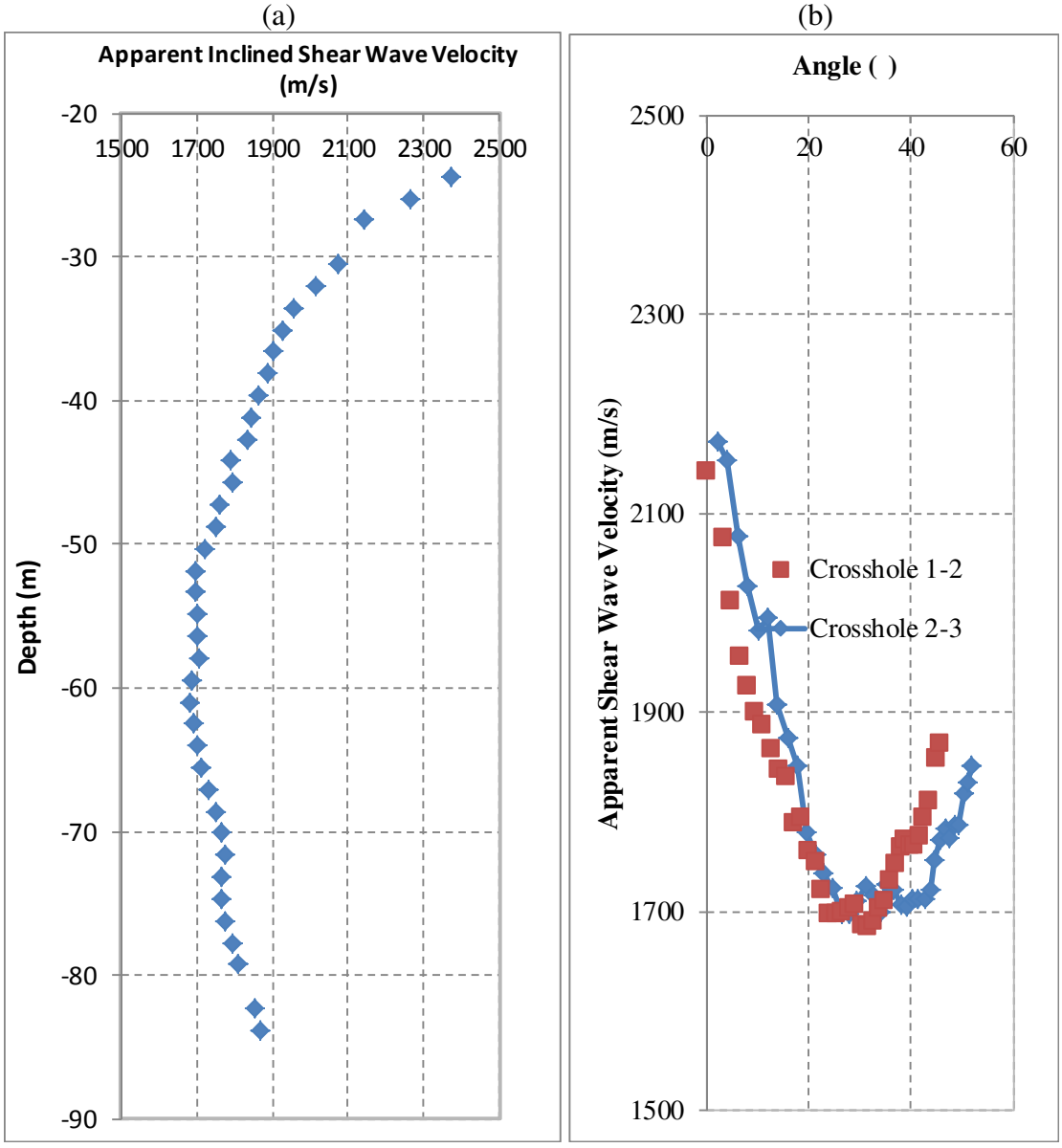

FIG. 4. (a) Average shear wave velocity in the inclined direction from crosshole testing; (b) Variation of average shear wave velocity with angle (0 degree is parallel to the horizontal bedding)

Figure 4(b) plots the variation of the average shear wave velocity with inclination angle. The wave speed is largest when closing to horizontal direction (using the convention of inclination angle, which is defined with the horizontal direction as reference). The speed typically decreases as the inclination angle increases. Besides, the results measured at two different locations are consistent with each other.

CONCLUSIONS

A group of field tests were conducted to measure the anisotropic mechanical properties of shale rock. Field borehole geophysical testing were performed between at three locations to depth up to 85.34m (280 ft). These tests determine the physical and structural characteristics of shale rock, particularly the clay seams and major structural joints. Borehole seismic testing includes seismic downhole testing were conducted using unconventional setup to measure the shear and compression wave velocity of rock in the vertical direction. A specially design seismic cross hole testing was conducted, where the shear wave excitation was generated by striking the steel tube. A simplified method was used to interpret the crosshole signals under the assumption that the rock layers as a uniform heterogeneous material. The results indicated that the shear wave velocity in the inclined direction is typically much larger than the shear wave velocity in the vertical direction. The variation of the shear wave velocity with inclination angle was determined, where the speed typically decreases as the inclination angle increases.

ACKNOWLEDGEMENTS

Assistance from engineers of the Resource International Inc. and MWH Global Inc. are highly appreciated.

REFERENCES

Ciz, R., & Shapiro, S. A. (2008). Stress-dependent anisotropy in transversely isotropic rocks: Comparison between theory and laboratory experiment on shale. Geophysics, 74(1), D7-D12.

Herwanger, J. V., & Horne, S. A. (2009). Linking reservoir geomechanics and time-lapse seismics: Predicting anisotropic velocity changes and seismic attributes. Geophysics, 74(4), W13-W33.

Kuila, U., Dewhurst, D. N., Siggins, A. F., & Raven, M. D. (2011). Stress anisotropy and velocity anisotropy in low porosity shale. Tectonophysics, 503(1), 34-44.

Verdon, J. P. (2012). Generating Anisotropic Seismic Models Based on Geomechanical Simulation. In Microseismic Monitoring and Geomechanical Modelling of CO2 Storage in Subsurface Reservoirs (pp. 107-139). Springer Berlin Heidelberg.

Vernik, L., & Liu, X. (1997). Velocity anisotropy in shales: A petrophysical study. Geophysics, 62(2), 521-532.

Vernik, L., & Nur, A. (1992). Ultrasonic velocity and anisotropy of hydrocarbon source rocks. Geophysics, 57(5), 727-735.

Wang, Z. (2002). Seismic anisotropy in sedimentary rocks, part 2: Laboratory data. Geophysics, 67(5), 1423-1440.

Sarout, J., Molez, L., Guéguen, Y., & Hoteit, N. (2007). Shale dynamic properties and anisotropy under triaxial loading: experimental and theoretical investigations. Physics and Chemistry of the Earth, Parts A/B/C, 32(8), 896-906.

Sarout, J., & Guéguen, Y. (2008). Anisotropy of elastic wave velocities in deformed shales: Part 1-Experimental results. Geophysics, 73(5), D75-D89.

Yu, X. (2011). Report on The Borehole Geophysical Testing for Sewer District Pump Station Project, Project Report for the Resource International Inc.

Numerical Estimation of Casing Integrity under Injection Pressure for Fracturing of Shale Gas Formation

Xinpu Shen [1]

[1]Senior Technical Advisor, Halliburton Consulting, 2107 City West Blvd, Houston, TX USA., E-mail: Xinpu.shen@halliburton.com

ABSTRACT: Injection pressure is a key factor in the design of a successful formation stimulation treatment of shale gas—the higher the pressure, the larger the stimulated volume. However, if the pressure is too high, the risk of compromising casing integrity during the injection process is also high. This paper analyzes a practical case of casing integrity problem resulting from injection in a field in southwest China. The purpose is to investigate the relative importance of the factors that influence casing integrity in a horizontal well section, and to determine the upper bound of the safe injection pressure. Calculations were performed by using porous elastoplastic model with finite element method. Anisotropy caused by non-uniform distribution of natural fractures is also included. For the specific casing and formation environment, it was found that casing integrity mainly depends on these three parameters: injection pressure, casing strength, and cement quality. The maximum inward displacement of casing can reach 16 mm and results in serious ovalization under 90 MPa injection pressure, given non-uniform distribution of natural fractures and poor cementing quality. But plastic deformation disappears with 80 MPa injection pressure when all other factors remain unchanged. Consequently, the upper bound of safe injection pressure is set as 80MPa.

INTRODUCTION

Shale gas is a major type of unconventional oil and gas resource, and it is currently in full-scale development, both in the US and abroad. Compared with the scale and history of international development, especially in the North American region, shale gas development in China is still under developing (Shen, 2012; Chen, 2011).

Chinese shale gas reserves are abundant in the southwest region, where many drilling exploration and development projects are ongoing. Because of the complex geological structure and relatively deep location, there are various problems associated with drilling exploration and mining projects. Here, only the issue of casing integrity as it relates to fracturing is discussed.

Fracturing is required to exploit shale gas and oil resources where low permeability exists. Using higher fracturing pressure during the stimulation process ensures that a

larger crack zone range results from the fracturing treatment, which, correspondingly, provides a greater oil and gas yield. However, when the fracturing pressure is too high, and there are other unfavorable conditions, the casing can become seriously deformed, and further construction, even the whole engineering outcome, can be affected. Therefore, the mechanical behavior of the casing under given conditions should be forecast with a numerical simulation to predict casing deformation in advance, achieve further integration with the actual control measures, and select a rational fracturing pressure, which will greatly influence the project's progress.

Based on the case of an actual project for Petro China, a simplified mechanical model for the fracturing of the horizontal well section reservoir stratum of a shale gas resource is discussed in this paper. The factors that can impact the casing integrity were studied and assessed one-by-one through numerical simulation; finally, the major factors were identified according to the results of the numerical simulation.

MECHANICAL MODEL

Based on the information of a real case of shale gas formation fracturing, the research adopts a plane strain model to simulate the horizontal well section as well as casing and its cement ring and shale formation. The corresponding finite element mesh is shown in Figs. 1 and 2. The model is 500-m high and 1000-m wide. The true vertical depth (TVD) of the top surface is 2100 m, and the surface load is also the corresponding gravitational load of 2100 m. The lower left part of the model is the naturally cracked zone, where a lower Young's modulus will be assigned. Because of the possibly uneven distribution of the crack, two types of materials are used here to simulate the two regions of both formations.

Fig. 2 is the zoomed view around the casing in Fig. 1. This figure shows that the innermost layer is the casing and that the external cement sheath is divided into two parts to simulate the uneven inner sheath property distribution caused by the potential well cementation mass difference.

FIG. 1. Mesh: overall mesh, simplified plane strain model.

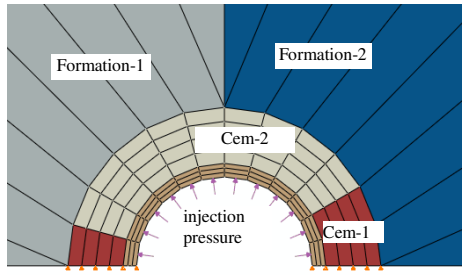

FIG. 2. Mesh: zoomed view around casing of the mesh.

The input data of the model include the following: 1) initial geostress field: sequence and direction of principal stress; 2) casing: geometric parameters, material parameters; 3) cement sheath: geometric parameters, material parameters; 4) mechanical properties of the rock formations; 5) injection pressure; and 6) initial pore pressure. The specific values of the parameters are provided in the following paragraphs.

Initial Geostress Field: Sequence and Direction of Principal Stress, and initial pore pressure

The TVD of the casing is 2600 m, the vertical stress is Sig_v=63 MPa, the minimum horizontal principal stress is Sh=66.2 MPa, and the maximum horizontal principal stress is SH=66.6 MPa. The direction of the maximum horizontal principal stress (SH) is parallel to the wellbore axis. The initial pore pressure is set as 30 MPa.

In the process of determining values of geostress, density logging data shown in Fig. 3 is used. Reverse fault stress pattern was found in practice for geostress distribution in this region.

Casing: Geometric Parameters, Material Parameters

The inner diameter of the casing is 0.1214 m, the wall thickness is 0.0091494 m, the material density of the P110 steel of which the casing is made is 7922 kg/m^3, and the intensity is 758 MPa. The modulus of elasticity is E=206 GPa, the modulus of shearing is G=79.38 GPa, and the Poisson's ratio is 0.3. In the calculation, the ideal elastoplastic model is used to simulate plastic deformation (Dassault Systems, 2008) of the casing material.

Cement Sheath: Geometric Parameters, Material Parameters

The inner diameter of the cement sheath is 0.1397 m, the outer diameter is 0.2159 m, the material density is 1900 kg/m^3, the modulus of elasticity of regular cementing material is E=27.2 GPa, and the Poisson's ratio is 0.3. To simulate the unevenness of the cement sheath filling caused by poor well cementation quality, the dark (Cem-1) and light (Cem-2) parts of the cement sheath material in the figure are respectively given different modulus values of elasticity. In detail, Young's modulus given to Cem-1 is the original regular value of E=27.2 GPa. And the value for Cem-2 which is the weaker one is E1=60% of E =16.32GPa.

Mechanical Properties of the Rock Formations

Logging data shown in track-1 and track-2 in Fig.3 has been used to derive the mechanical properties of this well. 1-D analysis has been done with Drillworks™. Fig. 3 shows the Poison's ratio (track-3), Young's modulus (track-5), and overburden stress gradient (track-4).

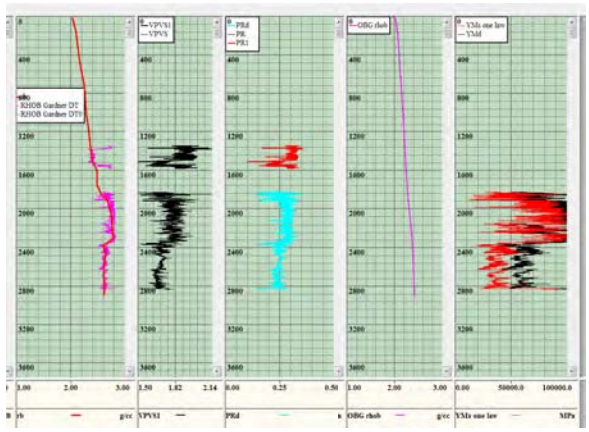

FIG. 3. Illustration of logging data and mechanical properties derived with Drillworks™.

The rock density used in the model is 2650 kg/m^3, the modulus of elasticity is E=40 GPa, and the Poisson's ratio is 0.25. To simulate the unevenness of the natural fracture distribution, the blue and grey parts of the formation material in the figure are respectively given different modulus values of elasticity.

Microseismic monitoring has been done for this project in this field. The monitored micro seismic data shown in Fig.4 appears significant asymmetry to the axial direction of the given horizontal wellbore. This asymmetry was interpreted as a result of asymmetric distribution of initial natural fracture.

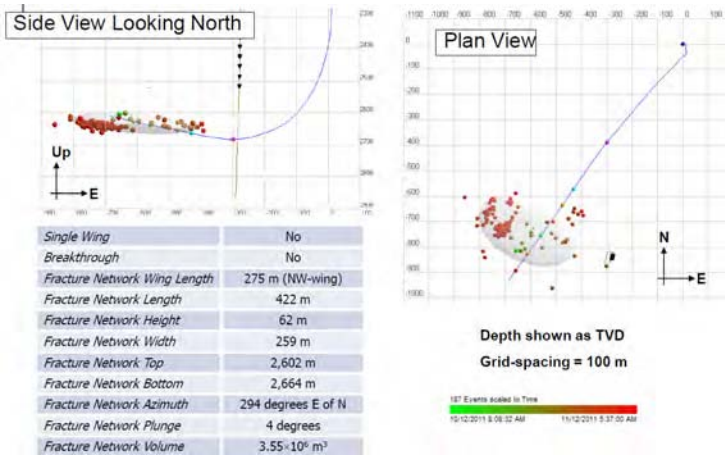

Single Wing	No
Breakthrough	No
Fracture Network Wing Length	275 m (NW-wing)
Fracture Network Length	422 m
Fracture Network Height	62 m
Fracture Network Width	259 m
Fracture Network Top	2,602 m
Fracture Network Bottom	2,664 m
Fracture Network Azimuth	294 degrees E of N
Fracture Network Plunge	4 degrees
Fracture Network Volume	3.55×10^6 m^3

FIG. 4. Illustration of non-uniform distribution of monitored micro-seismic activities.

In order to take into account of the asymmetric distribution of natural fractural as well as induced fracture shown in Fig.4, non-uniform distribution of mechanical properties. This is modeled by using two different sets of values of material property parameters: formation-1 and formation-2 shown in Fig.2.

Due to injection stimulation, formation of shale gas reservoir was fractured. Consequently, values of the Young's modulus of this fractured formation will be degraded from its original value E0 to a smaller value E.

Reference has been made two the works reported in (Xinpu Shen, 2012; Xinpu Shen, 2014). To simulate the crack phenomenon during fracturing, the elastic-plastic damage constitutive model (Lubliner et al., 1989; Lee and Fenves, 1998) was adopted as formation material. The continuum damage used there is a representation of degradation of Young's modulus. In the work reported there, maximum value of Young's modulus degradation within formation around the wellbore is 40%. Accordingly, values of Young's modulus used in this model are: E0 for formation-1; and 65% of E0 is set for E of formation-2.

Injection Pressure

The bottom-hole injection pressure of the fracturing process is calculated from pumping pressure with the assumption of no friction drag. The peak value of fluid pressure applied on the inner surface of the casing is P=90 MPa.

Boundary Conditions

The boundary conditions of the model are set up as follows: normal zero displacement constraint on both lateral surfaces as well as the bottom surface, with the surface pressure load on top, which simulates the overburden gravity load.

NUMERICAL RESULTS

The Abaqus finite element software is used here in the calculation. Fig. 5 shows the casing deformation and stress distribution within the casing obtained from the numerical calculation, under the injection pressure P (P=90 MPa). For clear illustration, the figure only shows the casing and its deformation and conceals the formation and cement sheath. The color image in the figure is the casing position after deformation, and the monochromatic image is the casing position before deformation. The figure indicates significant horizontal deformation of the casing under the injection pressure. The maximum value of von Mises equivalent stress within the casing is up to 800 MPa, which exceeds the initial yield limit and results in significant plastic deformation.

Figure 6 shows the horizontal displacement of the casing under an injection pressure of P=90 MPa. From this figure, it can be observed that the maximum value of displacement is 16.2 mm, and the maximum value of vertical deformation is less than 1 mm, which is very small. Therefore, the major deformation occurs in the horizontal direction. An interpretation of this displacement result is that: total value of overburden doesn't change during the injection process; therefore, little

deformation occurs in vertical direction. On the other hand, both value and direction of horizontal stress will change due to variation of pore pressure as well as fracture development, displacement in horizontal direction will be the major deformation component.

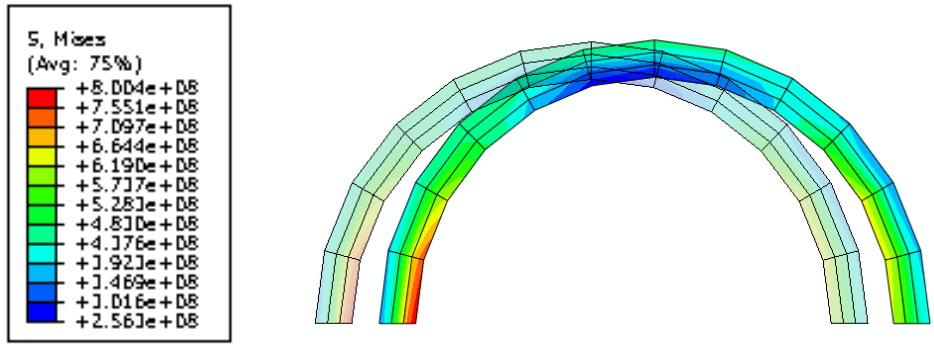

FIG. 5. Casing deformation and stress distribution, with maximum injection pressure of P=90 MPa.

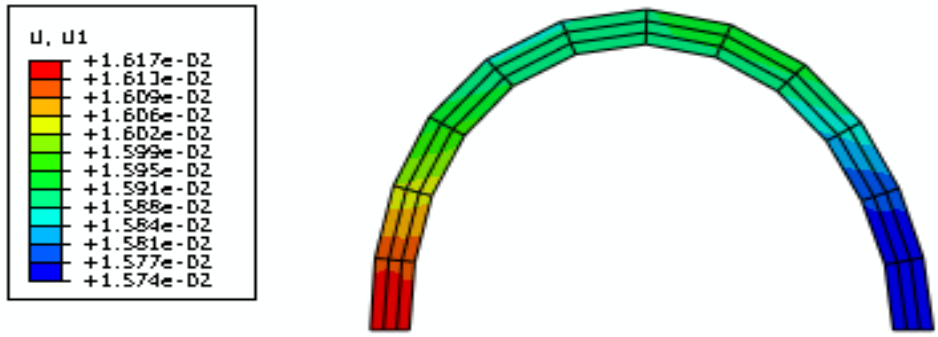

FIG. 6. Casing deformation and displacement (components distribution), with maximum injection pressure of P=90 MPa.

Various combinations of values of injection pressure and natural fracture distribution, as well as non-uniform distribution of Young's modulus within the concrete ring, are simulated in this calculation. Values of maximum von Mises equivalent stress within the casing that correspond to each set of a combination of parameter values are obtained (Table 1).

Table 1 shows that, when the bottom-hole pressure (BHP) is BHP=80 MPa and if the uneven distribution of the cement sheath material is only the result of well cementation quality, the maximum equivalent stress within the casing is 608 MPa; meanwhile, if there is also an uneven distribution of the formation's natural fracture, the stress can be up to 720 MPa with the same injection pressure of 80 MPa.

When the internal casing pressure, corresponding to the injection pressure, is BHP=90 MPa and the formation has uneven material properties and poor well cementation sheath quality, the maximum equivalent stress within the casing is 800

MPa, which exceeds the initial intensity and can result in serious deformation.

Table 1. Maximum values of von Mises equivalent stress within the casing corresponding to each set of input data

Injection Pressure /MPa	Maximum value of von Mises Stress within Casing /MPa	Strength of P110 /MPa	Distribution of Asymmetric Properties	
			Natural Fractures	Cement Sheath Properties
90	800	758	Asymmetric	Asymmetric
90	688			
90	791		Asymmetric	
90	726			Asymmetric
80	608			
80	720		Asymmetric	Asymmetric

CONCLUSIONS

The work reported here is based on a real case of shale gas stimulation in the southwest region of China. A simplified mechanical model was built for casing integrity assessment under fracturing pressure. In this calculation, the factors that can impact casing integrity were investigated and evaluated one-by-one through numerical simulation. According to the results of the numerical simulation, the major factors that impact casing integrity were identified as follows:

- The significant ovalization of the casing's cross-sectional is the result of the joint action of high injection pressure and non-uniform distribution of the natural fracture within the formation.
- To ensure the casing integrity during the formation stimulation process, casing deformation should be strictly monitored during the process of injection. When an obvious casing deformation tendency is detected, injection pressure should be immediately reduced to avoid serious casing integrity problems.
- Upper bound of injection pressure window is determined with given material properties of casing, cementing as well as formation. Degradation of Young's modulus caused by injection fracturing is modeled with simplified method.

It should be noticed that injection pressure window proposed here is an important concept for the design of stimulation work. This window actually defines a reasonable range of the value of injection pressure: its lower bound is the value below

which the formation cannot be fractured, and its upper bound is the value above which the casing will lose its integrity. Here only the upper bound of the injection window is investigated.

REFERENCES

Chen, M. (2011). Scientific assessment of horizontal well reservoir transformation and control fracturing technology, In: *Complex Structure Static Optimization Design and Drilling Completion Control Technology* Gao, D. (Editor). China University of Petroleum Press, Dongying, Shandong Province, 118-169.

Dassault Systems. (2008). *Abaqus Analysis User's Manual*. Vol. 3: Materials, Version 6.8, Vélizy-Villacoublay, France: Dassault Systems, 19.3.1-17 – 19.3.2-14.

Lee, J. and G.L. Fenves. (1998). Plastic-damage model for cyclic loading of concrete structures. ASCE *J. Engng Mech*. (124) 8: 892-900.

Lubliner, J., J. Oliver, S. Oller, and E. Onate. (1989). A plastic damage model for concrete. *Int. J. Solids & Struct*. (25) 3: 299-326.

Shen, X. (2012). Cohesive crack for quasi brittle fracture and numerical simulation of hydraulic fracture. In: *Drilling and Completion in Petroleum Engineering-Theory and Numerical Application*. Shen, X., Bai, M., and Standifird, W. (Editors). CRC Press Taylor & Francis, London, UK, 175-191.

Xinpu Shen (2012). Modelling fractures with continuum damage and its numerical application to stimulation estimates. Paper No: ARMA 12-196. *The 46th US Rock Mechanics / Geomechanics Symposium* held in Chicago, IL, USA, 24-27 June 2012, 1-7.

Xinpu Shen (2014). Numerical analysis on the interaction between two zipper frac wells using the continuum damage method. OTC -24975, presented at *the Offshore Technology Conference Asia (OTC Asia)*, 25-28 March 2014, Malaysia, 1-11.

Analysis of Hydraulic Fracturing Chemical Disclosure Data from FracFocus

J. Daniel Arthur[1], P.E., SPEC, H. William Hochheiser[2], Roy Arthur[3]

[1]President, ALL Consulting, 1718 South Cheyenne, Tulsa, OK, 74119, U.S.A., E-mail: darthur@all-llc.com.
[2]Senior Manager, ALL Consulting, 8401 Spain Rd. NE, Albuquerque, NM, U.S.A., E-mail: bhochheiser@all-llc.com
[3] IT Director, ALL Consulting, 1718 South Cheyenne, Tulsa, OK, 74119, U.S.A., E-mail: rarthur@all-llc.com.

ABSTRACT: The FracFocus chemical disclosure registry provides public disclosure of hydraulic fracturing chemical additives used in nearly 55,000 wells by over 600 companies. ALL Consulting developed and manages the FracFocus database and web site. This database represents a treasure trove of information on the use of hydraulic fracturing fluids. This paper will analyze the disclosures in the FracFocus chemical disclosure registry database to give insight into the additives that are used in hydraulic fracturing in the United States. The large number of well sites that have been entered into the registry present a rich population of hydraulic fracturing jobs over a wide geographic area and spanning a period of more than two years. From this database, it is possible to look at the breadth of chemicals used, their uses and variations in how they are listed, how the number and mixes of additives vary by service company and/or operator, and how geology/geography affects the composition and volumes of hydraulic fracturing fluids. The paper will also present time trends over the period in which FracFocus has been active.

INTRODUCTION

Oil and gas production from shale formations has increased dramatically in the United States in the past several years. As a result, this country is now the largest oil producer in the world, surpassing even Saudi Arabia (Reuters 2013). This development has been made possible by the twin technologies of horizontal drilling and high volume hydraulic fracturing. The widespread use of the later technology has led to public concern about the need for information on the chemicals being used in the process. This concern, and the political attention it has garnered, has threatened to become an obstacle to continued widespread application of the process. As a result, the oil and gas industry sponsored the Ground Water Protection Council (GWPC) and the Interstate Oil and Gas Compact Commission (IOGCC) to host a website and database, called FracFocus, to provide the public with information on the specific chemicals that are included in the fluids pumped into individual hydraulically

fractured wells.

The FracFocus national chemical disclosure registry was officially launched in April 2011 (GWPC & IOGCC 2011). Initially, disclosure of fracture fluid chemicals by operators was voluntary. However, once FracFocus was established and industry was submitting their information regularly, several states adopted laws and regulations requiring operators to enter data into the registry to publicly disclose the chemicals used in each new well that was hydraulically fractured. As time progressed, more states passed such laws and today 15 states require such disclosure (GWPC & IOGCC 2013). An additional eight states require submission of hydraulic fracturing data to state agencies but not to FracFocus.[1] However, companies in those states have the option of submitting data to FracFocus as well as to the state. Agencies can also upload disclosures directly to FracFocus if the operators have not done so. In other states, disclosure of hydraulic fracturing chemicals is voluntary and some operators do submit their data in the interest of full disclosure, which is the objective of FracFocus. As a result, at the time of this publication, the FracFocus database contains submissions on more than 55,000 wells from over 600 operators.

The FracFocus system has evolved over time to meet expanding needs. The original FracFocus system (known as FracFocus 1.0) used a Microsoft Excel template as the entry form. Operators entered data onto the Excel template on their own computers then uploaded each spreadsheet to the website. The system created disclosures in a PDF format from this data. As the database grew, states passed laws that not only required chemical disclosure but also required additional data elements. It became clear that the system's capabilities had to be expanded to meet these requirements. In November 2012, FracFocus 2.0 was launched to fulfill these needs. This new version uses the Extensible Markup Language (XML) platform. This allows the FracFocus system to validate many more data elements and potentially identify errors in those data before being submitted to the public database.

On June 1, 2013, FracFocus 1.0 was turned off and 2.0 became the only active system for hydraulic fracturing chemical disclosure. FracFocus 2.0 also enhanced distribution options of the data to state agencies in a format that can be imported into their database systems and their work flow processes. FracFocus can now better meet the needs of the state agencies that want to use it for regulatory reporting and compliance.

As FracFocus evolved, the authors conducted an internal company project to compile the disclosures into a database format more suited to analysis. Company staff has used the resulting database to analyze a variety of research questions about hydraulic fracturing and related environmental and public disclosure issues. As part of that effort, they have also compared FracFocus data to information on service company websites and researched information on the chemicals being reported. This has increased understanding of the water volumes and chemical additives used in hydraulic fracturing, as well as how fracturing practices have evolved over time.

[1] The states that require disclosure using FracFocus are (from east to west) Pennsylvania, West Virginia, Ohio, Tennessee, Alabama, Mississippi, Louisiana, North Dakota, South Dakota, Kansas, Oklahoma, Texas, Montana, Colorado, and Utah. The additional states that require chemical disclosure are New York, Michigan, Indiana, Illinois, Arkansas, Wyoming, New Mexico, and Idaho.

DATA ISSUES AND ANALYSIS

Analysis of the information in FracFocus is not just a matter of creating a database from the PDF disclosures and sorting the data to get information on water and chemical use. The authors have found that the analysis is not so straightforward and has entailed considerably more effort and research. First of all, different companies present the same data differently in their submissions, and some make data entry errors, or put information in the wrong format. FracFocus 1.0 had very limited data validation capabilities so that submissions made in that system were more prone to errors. The increased error checking capability of FracFocus 2.0 has improved the quality of the data in disclosures submitted to that system. Second, the process of converting the data from pdf files to a relational database can introduce errors and the results must be carefully checked.

One goal of the analysis of FracFocus data is to understand the "recipes," or mix, of additives that are used in fracturing fluids. In this paper, the term "additive" is used to designate a chemical or mixture of chemicals with a single purpose, such as a surfactant or a biocide. This is called a "Purpose" in the FracFocus disclosure. In the pie charts that are presented in the next section, the number of additive categories is limited to the top 15 by percentage mass in the database as a whole. Most additives can be assigned to one of these categories. Additives that could not be so assigned are lumped in the "Other" category. Generally, but not always, this category constitutes less than 0.1% of the mass of the fracture fluid. An example of additives that could not be assigned is a mixture of additives where the proportions of individual components were impossible to determine.

Presentation of Data and Results

Once the well disclosure data have been processed, a number of interesting analyses can be performed. The following discussion and figures give some examples of what can be done with the data, from simple statistics on the disclosures in the database, to geographic distribution of wells by company, to variations in water use and chemical recipes across states, plays, and counties. For example, looking at the distribution of submissions, we can see which companies have made the most submissions, and in what states those submissions are located. The following analyses use submissions for hydraulic fracturing jobs that were performed from January 2011 through November 2013. Figure 1 shows the number of disclosures in the database by state for the top 10 states.

Texas, a state that requires the use of FracFocus and also has multiple producing shale plays, stands out as having by far the most disclosures with over 28,000, over half the disclosures in the database. New Mexico is the only state that appears in the top 10 which does not require the use of FracFocus. It is important to note that FracFocus disclosures are for all wells that are hydraulically fractured. Therefore, wells completed in the tight sands of Wyoming and Colorado, for example, are included in the database along with wells drilled in shale formations. As discussed earlier, FracFocus does not contain information on the geologic formation that is fractured.

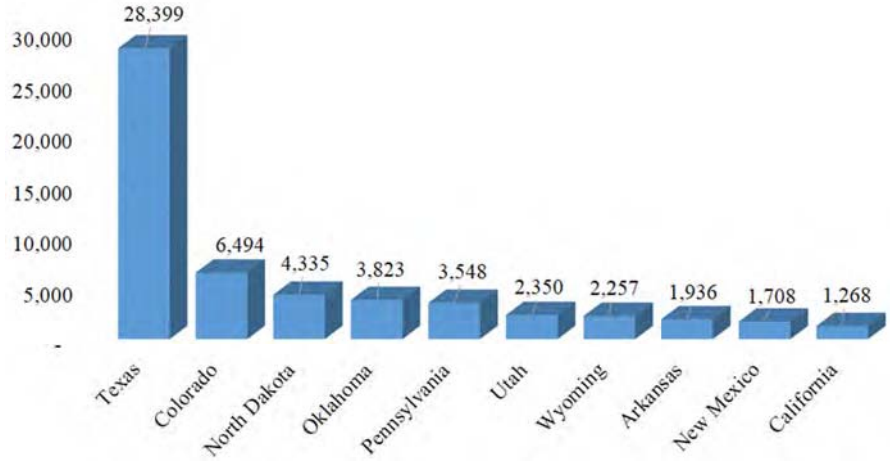

Source: ALL Consulting FracData system as of 11/30/2013

FIG. 1. Number of FracFocus Disclosures in the Top 10 States, Jan. 2011-Nov. 2013

Figure 2 shows the top 10 shale plays in terms of number of disclosures. The Eagle Ford, Marcellus, Bakken, and Barnett plays, all very well known active areas, figure prominently in this list. The Niobrara play has had a spate of recent activity, moving this play up from fifth to third place just since May 2013.

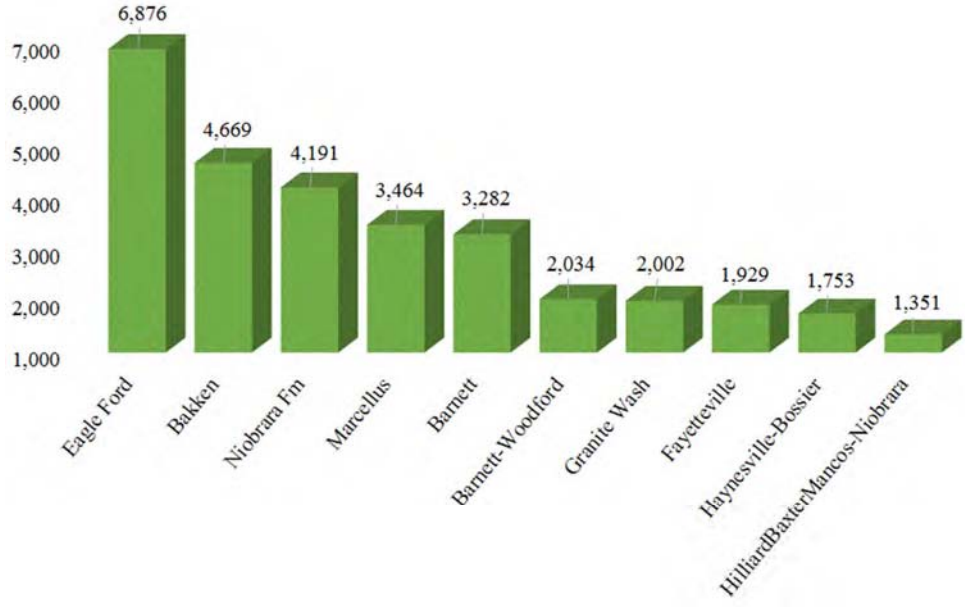

Source: ALL Consulting FracData system as of 11/30/2013

FIG. 2. Number of disclosures in the Top 10 Shale Plays, Jan. 2011-Nov. 2013

Figure 3 displays the top 10 operators by number of disclosures. Chesapeake and Anadarko stand out as reporting the most wells by far.

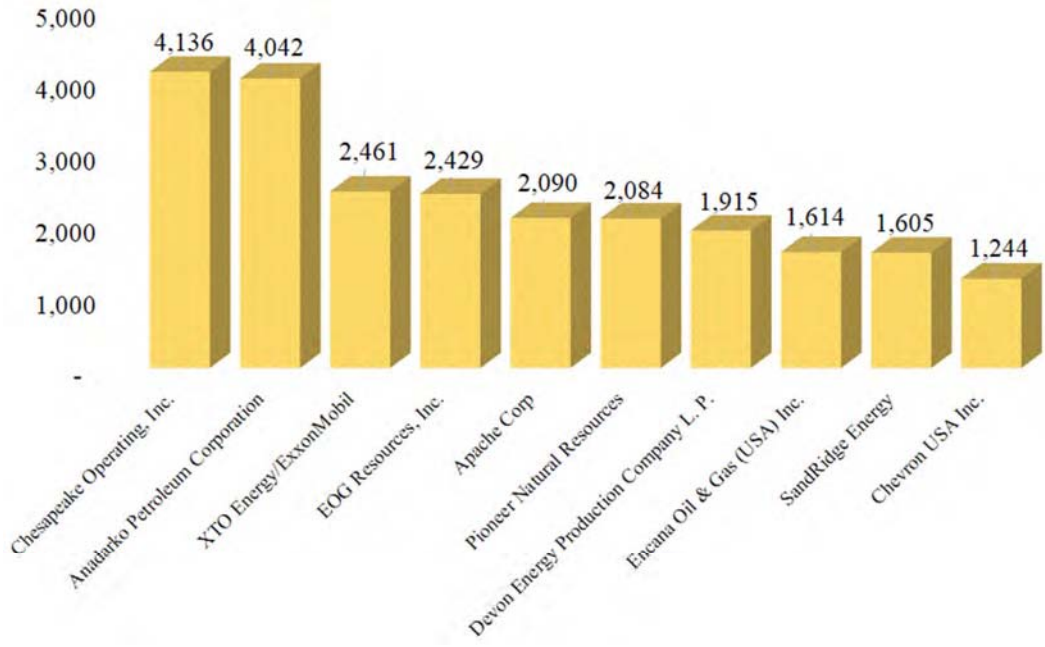

Source: ALL Consulting FracData system as of 11/30/2013

FIG 3. Number of Disclosures in the Top 10 Operators, Jan. 2011-Nov. 2013

FracFocus disclosures include the water volumes used in each fracture job. (All other ingredients are giving only in terms of mass.) From those data, we can look at a geographic area (e.g., a state) and see both the total amount of water used, as well as the average volume of water per job within that area. This can be analyzed both by area (state, play, county, census tract) and by company. It can also be displayed over time. Note that the total water used in an area is dependent on the number of submissions. Since submissions are voluntary in some states, and some states do not require the use of FracFocus even though they do require disclosure, this does not represent all the water used in some areas. Therefore, average water volume per job is more meaningful for comparison and time trend analysis.

Figure 4 shows the average water per job in the 10 shale plays with the highest water volume per job. These plays are different from the top 10 plays by number of disclosures shown in Figure 2. For example, the Tuscaloosa play has few disclosures in the database, only 29. However, the average fracturing job there uses over eight million gallons of water. The situation is similar for the Utica play, which has had a lot of recent activity, with 840 disclosures. The Bakken play, which has the second largest number of disclosures, does not appear in Figure 4 because the average amount of water used in that play per job is less than 3 million gallons.

Each well in FracFocus has an associated latitude and longitude, as well as a state and county designation in the API well number. (The system checks that the lat-long location is within the designated county.) Since location data are included in the FracFocus well disclosures, the data can be mapped to show differences in fracture jobs between different states and plays, as well as to show trends within states and plays. The following maps are examples of this kind of analysis.

Play	Disclosures
Tuscaloosa	29
Utica	840
Woodford	484
Cana Woodford	601
Haynesville-Bossier	1,739
Fayetteville	1,927
Eagle Ford	6,858
Marcellus	3,358
Antrim	16
Excello-Mulky	12

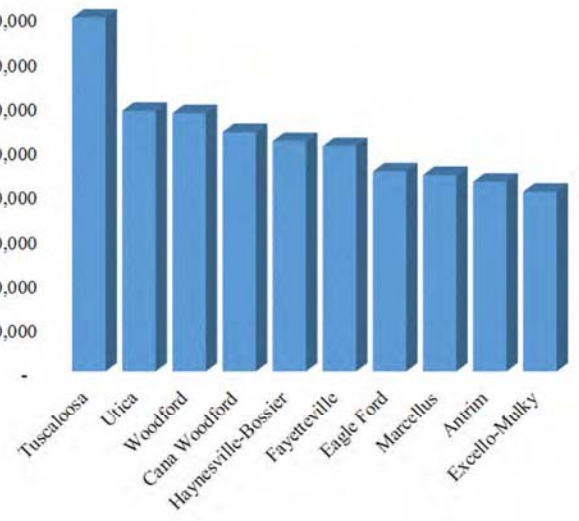

Source: ALL Consulting FracData system as of 11/30/2013

FIG. 4. Average Water Per Job for the Top 10 Plays with Highest Water Volume, Jan. 2011-Nov2013

Figure 5 is a "bubble map" of average water use per job in Texas. Each bubble represents one well. The size of each bubble represents the volume of water used to fracture that well. The map shows differences in water use among the various shale plays in Texas. For example, one can see the predominance of large volume fracture jobs in the Haynesville-Bossier Play, as compared to wells in West Texas.

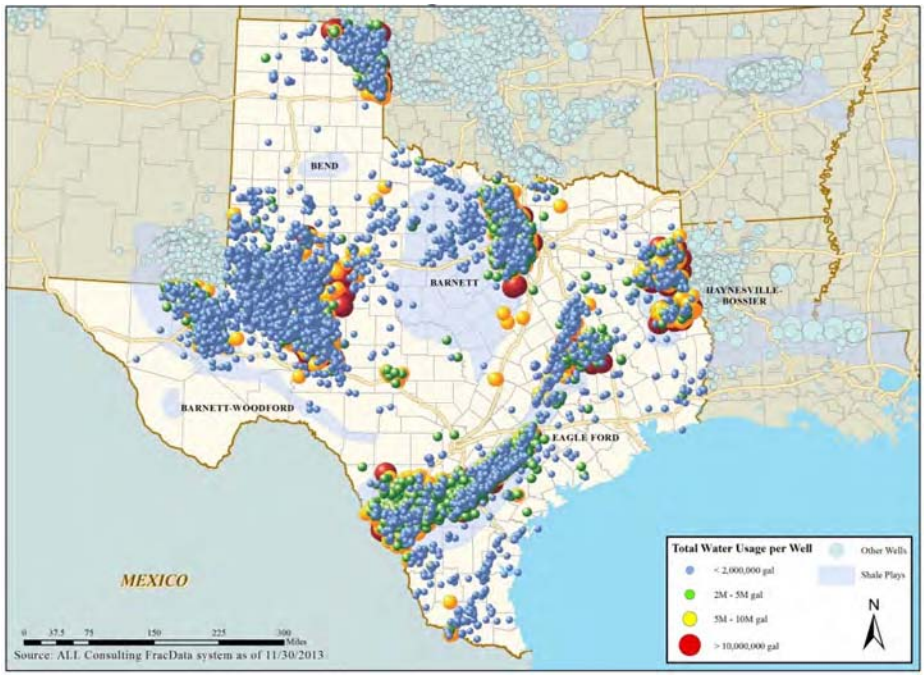

FIG. 5. FracFocus Wells: Water Usage for Texas, Jan. 2011-Nov. 2013

Variations within plays are also apparent. Within the Eagle Ford play, for example, trends in water use can be seen, with lower volumes per job generally used toward the northeast and larger volumes toward the southwest part of the play.

The data can also be used to map water use by service company, as shown in Figure 6 for Ohio. The top 10 service companies in the state, by number of disclosures, are shown. Both their operating locations and volumes of water used are easily seen in this kind of display. For example, the relatively large volume fracture jobs of some companies, e.g., companies one and six, stand out visually. This kind of analysis can also be done by operating company to show their producing areas and differences among or similarities in operator practices, as shown in Figure 7.

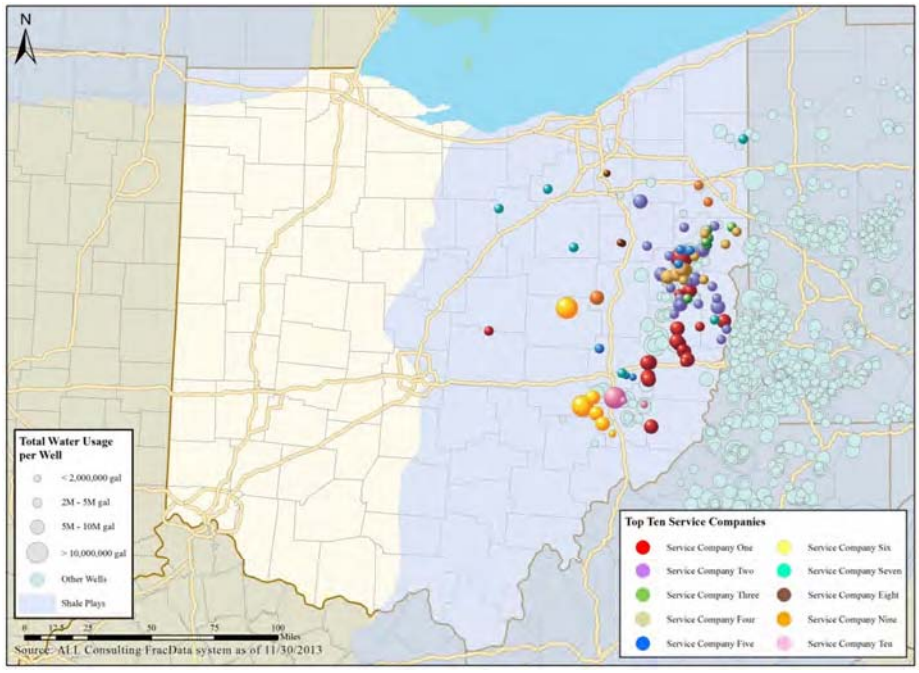

FIG. 6. FracFocus Wells: Top Ten Service Companies for Ohio by Disclosures, Jan. 2011-Nov. 2013

Analysis of the additives listed in the FracFocus disclosures can show how the chemical recipes used by operators and service companies differ among plays, within plays, and by company.

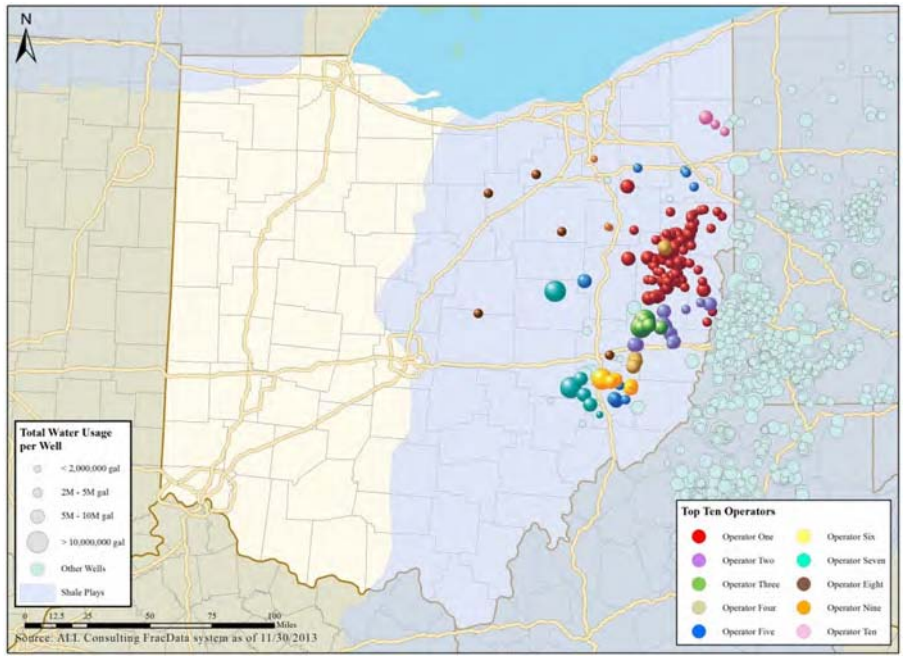

FIG. 7. FracFocus Wells: Top Ten Operators for Ohio by Disclosures, Jan. 2011-Nov. 2013

For example, Figure 8 displays the additive mix in pie charts for three prominent shale plays: the Eagle Ford, Bakken, and Utica. Each pie chart represents the additives in the fracture fluid other than the carrier fluid (usually water) and the proppant. The percentage of the mass of the fluid made up of carrier fluid and proppant, and the percentage mass of the additives are shown in the table to the left of each pie chart. First, it is evident that there are differences in the proportion of the fluid consisting of chemical additives, ranging from 0.39 percent in the Utica to 2.24 percent in the Eagle Ford, a five-fold difference. Second, the makeup of the additives differs from play to play. For example, acid makes up a much larger percentage in the Utica play compared to the others, while clay control is more important in the Eagle Ford. Comparisons among companies in the same location can also be performed with this kind a display. Figure 9 shows the additive distributions for three service companies in the Bakken play. One can see large differences among companies in the use of such additives as surfactants, scale inhibitors, and crosslinkers/breakers/catalysts. Such differences can be the result of a number of factors, such as the location/geology within the play, the design of the well, or company approach to hydraulic fracturing.

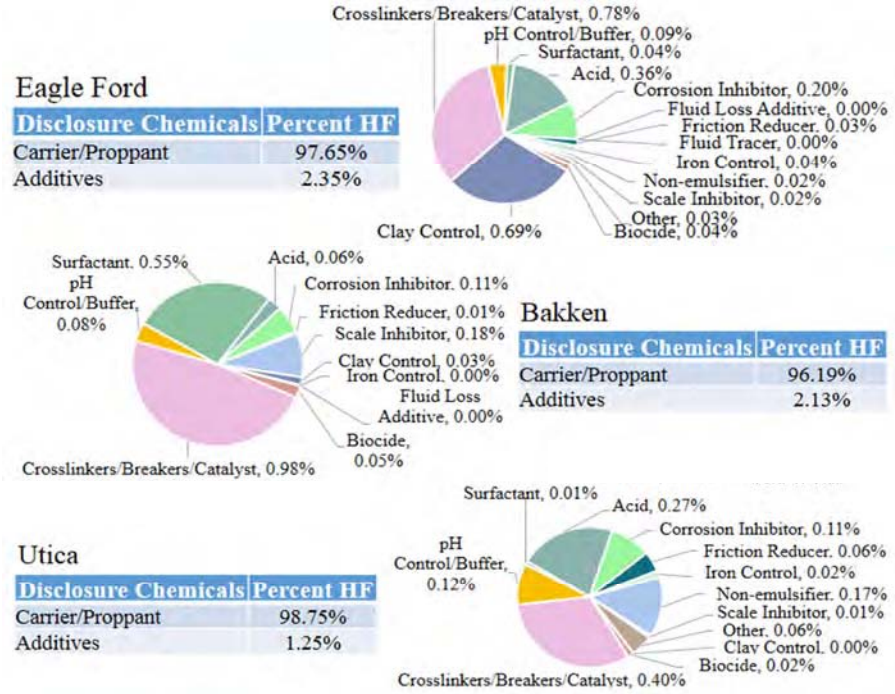

Source: ALL Consulting FracData system as of 11/30/2013

FIG. 8. Average Fracture Fluid "Recipes" in Three Shale Plays, Jan. 2011-Nov. 2013

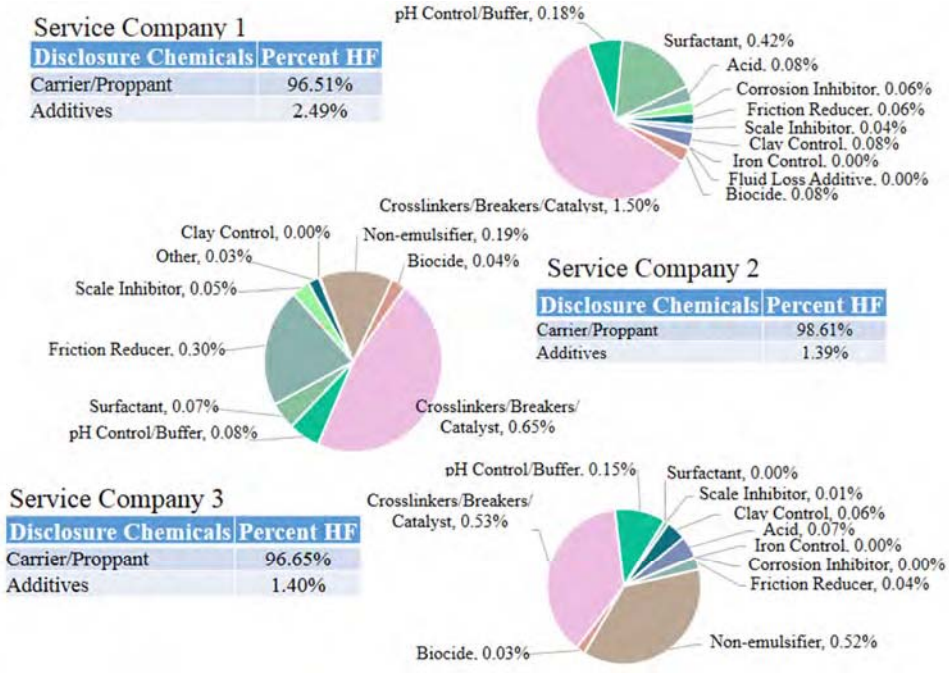

Source: ALL Consulting FracData system as of 11/30/2013

FIG 9. Average Fracture Fluid "Recipes" for Three Service Companies within the Bakken Shale Play, Jan. 2011-Nov. 2013

One point of concern that continues to be expressed by environmental groups, researchers, and the public is the designation of some products used in fracturing as proprietary or trade secret. State and federal laws provide for companies to maintain trade secrets as a way to promote investment and competition. These provisions of law extend to all industries, including the oil and gas industry. Contrary to some reports, a relatively small percentage of the chemical ingredients in FracFocus are listed as proprietary.

As of October 2013, almost 600 different operators had entered close to 1.5 million individual ingredients into FracFocus. Of those, approximately 200,000, or 13 percent, were labeled as proprietary as shown in Figure 10. This number remains fairly stable over time and does not vary much across plays, ranging from 10 percent in the Barnett to 17 percent in the Granite Wash Play.

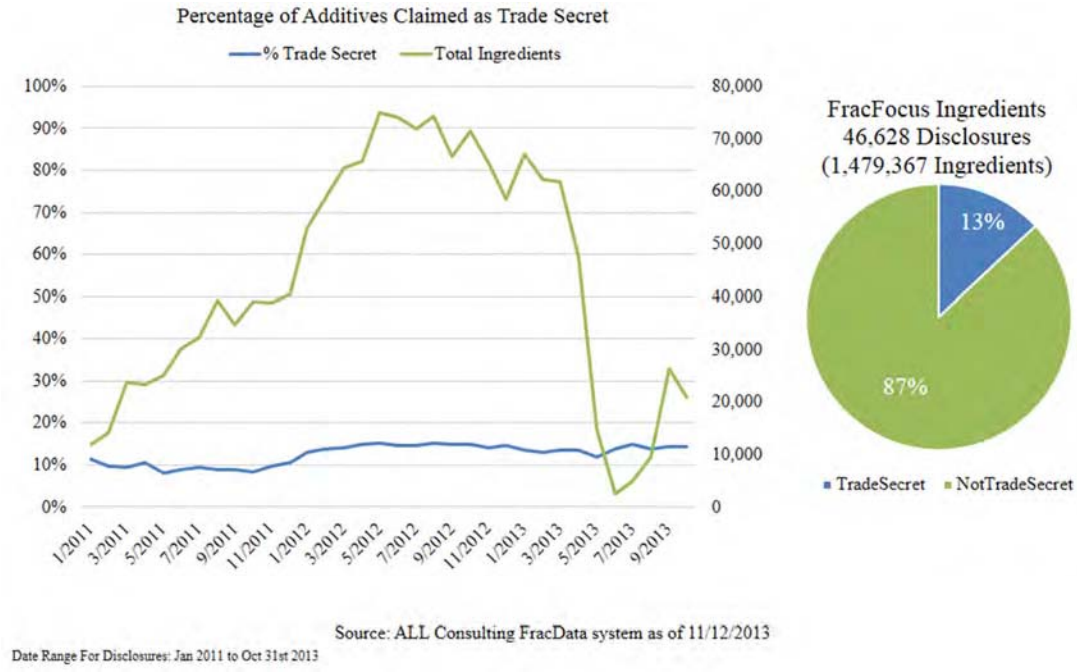

FIG. 10. Percentage of Additives in FracFocus Claimed as Proprietary, Jan. 2011-Oct. 2013

CONCLUSION

The large number of well sites that have been entered into the FracFocus registry present a rich population of hydraulic fracturing jobs over a wide geographic area and spanning a period of almost three years. The disclosures include data on well locations, fracture dates, operators and service companies, water use, and chemical additives in the fracture fluid for each well. This allows a variety of analyses to be performed to answer research questions about the process of hydraulic fracturing and its variations across locations, time, and industry segments. Among these analyses are differences in water use, chemical use, and the designation of proprietary

ingredients.

FracFocus data does require significant processing to be fully useful as an analytical tool and it will benefit from additional research on the disclosed and proprietary chemicals listed. In the future, combining the FracFocus data with additional information from service companies, state files, and other information sources will allow for more in-depth analysis of the chemicals used in hydraulic fracturing, their application, their relative volumes, and their use by different companies. It will also provide the opportunity to look at "green" chemicals and more specifics about the chemicals being used by each of the major service companies. Screening for higher risk chemicals can also be performed and can provide an aid to planning and risk management for operators and service companies. Ultimately, the analysis of data from FracFocus can help bring a data-driven, scientific approach to addressing many of the topics of discussion that have engaged the public, non-profit organizations, and regulatory agencies regarding hydraulic fracturing.

REFERENCES

Ground Water Protection Council (GWPC) and Interstate Oil and Gas Compact Commission (IOGCC). (2013). FracFocus Chemical Disclosure Registry/About Us. <http://fracfocus.org/welcome> (Nov. 4, 2013)

Ground Water Protection Council (GWPC). (2013). Groundwater Communique, October 2013, p.6.

Reuters. (2013). U.S. surges past Saudis to become world's top oil supplier –PIRA (Oct. 15, 2013). <http://www.reuters.com/article/2013/10/15/us-oil-pira-idUSL1N0I51IX20131015> (Nov. 7, 2013)

Erosion and Sediment Controls

Lauren R. Parker, P.E., M.S., CPESC, CESSWI, CPSWQ[1]

[1]Project Manager, Civil & Environmental Consultants, Inc., 333 Baldwin Road, Pittsburgh, PA 15205, U.S.A., E-mail: lrparker@cecinc.com.

ABSTRACT: This topic will cover erosion and sediment control for natural gas well pads, facilities, and pipelines. Proper erosion and sedimentation control design and implementation is a critical part of the development process for operators in the Appalachian Basin. The Clean Water Act (CWA) was enacted in 1972, and Section 402 of the Act established the National Pollutant Discharge Elimination System (NPDES). Oil and natural gas projects became exempt from NPDES permits through the Energy Policy Act of 2005, which was published as a final rule by the Environmental Protection Agency (EPA) on June 12, 2006. However, many states are beginning to implement their own requirements for these activities despite the federal exemption. For example, Pennsylvania has an oil and gas specific Erosion, Sediment, and Stormwater General Permit (ESCGP-2) that adopted many of the NPDES regulations. WV requires an Erosion and Sediment Control Plan be submitted with the well drilling permit package for review and approval. At this time, Ohio does not have a specific earth disturbance permit for natural gas projects. Typical erosion controls used on natural gas projects include rolled erosion control blankets, sprayed hydromulch, water bars, proper stream and wetland crossing methods, and temporary vegetation. Typical sediment controls used on a natural gas well pad or other permanent facilities can include diversion channels, sediment traps, sediment basins, compost filter sock sediment trap, compost filter sock, silt fence, and rock construction entrance. Typical sediment controls used on a natural gas pipeline project can include compost filter sock, silt fence, and rock construction entrances. This paper includes example projects and photographs of the controls used.

INTRODUCTION

Erosion and sediment (E&S) control design for natural gas well pad, facilities, and pipelines is an important piece of the development process for this industry. This paper will cover the background on permitting and plan requirements, proper project planning, E&S design, E&S installation, and E&S maintenance.

Permitting and Plan Requirements

Many Acts, Regulations, Laws, and Guidance documents have been issued by both Federal and State Agencies which dictate the permitting requirements and the extent to which E&S controls must be used and designed. Knowledge of these items is integral to the design process in that it allows the design professional to meet the expectations of the agencies responsible for E&S plan review and field implementation.

The first of many Acts created by the Federal Government was The Water Pollution Control Act of 1948. The Water Pollution Control Act authorized the Surgeon General of the Public Health Service to prepare comprehensive programs for eliminating or reducing the pollution of interstate waters and tributaries and improving the sanitary condition of surface and underground waters.

The second act created by the Federal Government was the CWA. The industrial development in the US over many years created pollution issues throughout the country that included contamination of many rivers and lakes. The pollution drastically impaired these waters with oils, chemicals, and sewage. The combustible characteristics of certain chemicals results in fires occurring on the rivers, including the Chicago, Buffalo, and Rouge Rivers. After the Cuyahoga River in Cleveland, Ohio (tributary of Lake Erie) caught fire in 1969, the Federal Government determined that action was necessary. The CWA was enacted in 1972 with the intent of restoring and maintaining the chemical, physical, and biological integrity of the waters of the United States (U.S.). The program is administered by the EPA. The NPDES was established as part of the CWA. Stormwater runoff from construction activities became a regulated activity covered by the CWA in 1987. The regulated activities that required a NPDES permit were any construction activity that would disturb more than 5 acres or any construction activity that disturbed between 1 and 5 acres and had a point source discharge. The program has since become more stringent in that any construction activity disturbing 1 acre of more, regardless of the existence of a point source or not, is required to obtain an NPDES permit.

The final act covered in this paper and the one that has had the greatest impact on the natural gas industry, is the Energy Act of 2005. The Energy Act was published as a final rule by the Environmental Protection Agency (EPA) on June 12, 2006. One piece of the Energy Act to be highlighted is that the Act amended the NPDES regulations and exempted stormwater discharges associated with oil and gas exploration, production, processing, or treatment operations or transmission facilities from being required to obtain an NPDES permit for their construction activities.

Since 2006 when the Energy Act was enacted, certain states have created regulations which require the Natural Gas Industry to obtain permits for their construction activities.

Project Planning

A critical part of the planning process is the proper routing of a pipeline and siting of a well pad or facility. Up front avoidance and minimization of stream and wetland impacts, steep slopes or other difficult topographic, geologic formations such as

shallow depth to bedrock, rock outcrops, coal, karst soils, and historic landslides, forest areas, for example, may eliminate future problems related to erosion and subsequent sedimentation. In many cases, it is difficult to avoid these areas due to other constraints, such as Owner/Operator requirements, unavailability of alternate routes, landowner requirements, or agreements with other subsurface mineral owners.

E&S Design

Upon completion of pipeline and well pad planning for the project, E&S design commences. Construction of pipelines and well pads requires the removal of vegetation and other ground cover, leaving bare soil exposed to the elements. Erosion of the bare soil can be caused by wind, rain, snow melt or any other surface water runoff. Once the soil has eroded from the surface, it is then transported and finally deposited, more often than not, in a nearby stream and known as sedimentation. The design of controls should be specific to each site and be focused on reducing erosion to the extent practicable. Methods used to prevent erosion include:

Construction Schedule

Consideration should be given, where possible, to the time of year in which construction will occur. This is quite often impossible due to drilling schedules, the need to keep the drill rig active, and the need to gather natural gas from drilled wells as soon as they begin producing. However, where possible, earth disturbance activities should be avoided in winter and early spring. It is difficult to prevent erosion due excessive surface runoff caused by snow melt and rainfall. The best time for construction is during dry seasons.

FIG. 1. E&S controls impacted by spring rainfall.

Construction Sequencing

By providing a detailed construction sequence, the amount of disturbed area at any given time can be reduced. For example, rather than clearing and grubbing an entire right-of-way for a 6 mile pipeline before beginning trenching operations, the project can be phased into manageable overlapping segments that allow for a majority of

construction tasks to be completed in one segment before disturbing the adjacent segment. In the case of a pipeline installation, the survey, clearing and grubbing, trenching, pipe installation, revegetation, etc. should progressively follow each other, as cars in a train, to reduce areas of disturbed land.

FIG. 2. Cleared pipeline right-of-way. No crews are working on the project; it is not stabilized and erosion rills can be observed.

Stabilize Immediately

A majority of earthwork operations require that existing topsoil be stripped and stockpiled on site prior to excavation, trenching or fill placement. Topsoil cannot and should not be used as structural fill. Additionally, many sites located in sloping topography where the quantity of excavation and quantity of fill placement need to be balanced from a cut and fill standpoint will require soil material stockpiles. As cut and fill operations are completed, topsoil should be spread and the completed surfaces or slopes should be stabilized immediately. Covering the soil with a blanket or other protective erosion surface measure reduces the potential for rain droplets hitting the bare soil to break soil particles from the group. These stockpiles should also be stabilized immediately using erosion control blankets, hydromulching and seeding, and standard mulch and seed.

FIG. 3. Well Site with slopes covered in erosion control blanket and vegetation starting to establish.

Cleanwater Diversion Channels

The incorporation of cleanwater diversion channels will minimize clean surface water runoff from upslope, undisturbed areas from entering the project limit of disturbance, thereby reducing the potential for erosion of site soils from the project area.

Trench Plugs

Trench plugs are installed inside the pipeline trench surrounding the pipeline itself. The plugs reduce the length in which groundwater in the trench backfill material can flow along the pipeline. By reducing the travel length, the potential for 'piping' of soils from the trench backfill is reduced, which in turn will reduce the potential for settlement and the creation of rills and ruts, which promote erosion.

Waterbars

Waterbars are constructed on the ground surface to break up slope lengths so that treatment of sediment laden runoff can be accomplished on a smaller scale. Additionally, by breaking up the slope length, the risk of runoff becoming channelized and creating ruts and rills is reduced. Waterbars are typically used on pipeline right-of-way projects. They are low height, rounded earthen berms that allow for vehicular crossing and that extend across access road right-of-ways. They are vegetated and direct runoff to the side of the right of way where compost filter sock, straw bales, rock filters, or other treatment controls can be located.

FIG. 4. Waterbar directing runoff off of the right-of-way to a compost filter sock for treatment.

Reduced Right-of-way at Stream and Wetland Crossings

For pipeline projects and access roads, reducing the width of the right-of-way, or limit of disturbance, at stream and wetland crossings can reduce the risk of erosion and subsequent sedimentation into the resource. Where possible, this should always be done.

FIG. 5. Timber mat stream crossing with reduced right-of-way at the stream.

Even the best schedule, construction sequence and stabilization methods are unable to prevent all erosion from construction sites. Proper control of eroded soils is key to prevent sediment laden discharges from occurring into nearby streams, wetlands, and other water bodies. Sedimentation controls should be site specific.
Typical sediment controls used on Natural Gas projects include:

Compost Filter Sock and Silt Fence

Both of these controls are used as a final barrier to delay sediment laden runoff

from leaving the project area and act as a filter and can be used on both well pad and pipeline projects. These controls are installed parallel to contour with each end turned upslope. This allows the runoff to pond behind the barrier where heavy sediments will drop out of the runoff. As the water travels through the barrier, the sock or fence acts as a filter to remove additional particles of sediment. It is imperative that these controls be installed as described above, and additionally, be installed in accordance with their manufacturer's specifications. For compost filter sock, this includes proper sizing and staking of the sock. For silt fence, this includes proper sizing, trenching in the bottom of the fence, and staking of the fence. Maintenance of both controls is necessary to ensure proper performance. Sediment build-up should be removed when it reaches half the height of the controls, unless otherwise specified in the State or Local Erosion and sediment Control Manual, if available.

FIG. 6. Silt Fence at the perimeter of earth disturbance.

Rock Construction Entrance

Used at all exit points from the construction area into public roadways. The rock construction entrance serves to knock dirt off of vehicles as they leave the construction area and prevent it from entering the public roadway. Often, rock construction entrances may include a wash rack or wash station to aid in removal of sediment from the vehicles.

FIG. 7. Rock construction entrance.

Collector Channels

Utilized to collect sediment laden runoff from the construction area and direct it to another control for treatment. Collector channels are not typical on pipeline projects due to the need for a larger treatment facility. Channels should be sized based on their tributary drainage area and a liner selected based on the shear stress that the runoff will cause within the channel. The channel should be inspected to make sure overtopping if not occurring and that the installed liner is providing adequate protection against erosion.

FIG. 8. Vegetated Channel.

Sediment Traps/Basins

Utilized to treat sediment laden runoff from construction areas. In certain states, sediment traps are used to treat smaller drainage areas while sediment basins are used to treat larger drainage areas. There are slightly different criteria for each; however, the overall goal is to provide time for the sediment to drop out of the water, prior to the water being discharges from the trap or basin. The sediment trap can consist of an

earthen embankment trap or a compost filter sock trap. If the site topography permits the earthen embankment trap, this option is more desirable from a cost standpoint. For projects with difficult terrain and steep topography, compost filter sock traps are often the only option in order to prevent large cuts and fills from occurring to construct an earthen embankment.

FIG. 9. Compost Filter Sock Sediment Trap.

FIG. 10. Embankment Sediment Trap.

Filter Bag

A filter bag can be used to remove sediment from runoff. These are typically used in conjunction with a pump. A trench, excavation, or bore pit that has filled with water can be pumped out and into the filter bag. Filter bags are placed in well vegetated areas and provide both time for the sediment to drop out of the water, as well as, a filter to grab smaller particles. Sediment from filter bags should be spread out in upslope areas and immediately stabilized.

CONCLUSIONS

Design professionals practicing in the oil and natural gas industry have many federal, state, and local regulations they need to be aware of and very familiar with. Up front planning and proper design by design professionals is paramount to assisting the oil and natural gas industry in completing their projects in a timely and environmentally sound manner.

ACKNOWLEDGMENTS

I would like to acknowledge Dustin Kuhlman, Pat Sullivan, Rick Celender, Tara Kirkman, and Emily Chiodo of Civil & Environmental Consultants, Inc., and Will Ratcliffe of Access Midstream Partners for providing photographs, diagrams, input, and feedback on this technical paper.

REFERENCES

United States Environmental Protection Agency, 33 U.S.C., 1251 et seq., Washington, D.C., 1972.

United States Environmental Protection Agency, Energy Act, June 12, 2006.

Commonwealth of Pennsylvania, Department of Environmental Protection, Office of Water Management, Erosion and Sediment Pollution Control Program Manual, Harrisburg, Pennsylvania, March 2012.

Commonwealth of Pennsylvania, Pennsylvania Code Title 25, Environmental Resources, Department of Environmental Protection, Chapter 102: Erosion and Sediment Control, Harrisburg, Pennsylvania, November 19, 2010.

Stormwater Runoff and the Oil and Gas Industry: A State-by-State Review of Regulations and Surface Water Quality Impacts

Megan Walsh[1], P.E., C.F.M and Christine Pomeroy[2], Ph.D., P.E., Kirsten Eliassen[3]

[1]Graduate Research Assistant, Department of Civil and Environmental Engineering, University of Utah, 110 S. Central Campus Drive Suite 2000, Salt Lake City, UT 84112, U.S.A., E-mail: megan.walsh@utah.edu.
[2]Associate Professor, Department of Civil and Environmental Engineering, University of Utah, 110 S. Central Campus Drive Suite 2000, Salt Lake City, UT 84112, U.S.A., E-mail: christine.pomeroy@utah.edu.
[3]Contributing Author, Department of Civil and Environmental Engineering, University of Utah, 110 S. Central Campus Drive Suite 2000, Salt Lake City, UT 84112, U.S.A., E-mail: kirsteneliassen@gmail.com.

ABSTRACT: The Ninth Circuit Court of Appeals opinion effectively exempted oil and gas operations from National Pollutant Discharge Elimination System (NPDES) permit requirements for construction activities unless there is a discharge of a reportable quantity of oil or hazardous substance or a violation of a water quality standard. As a result, many oil and gas operations (including unconventional drilling operations for shale oil and gas development) are largely unregulated in terms of stormwater runoff, despite construction of large well pads (approximately 1 to 5 acres) and miles of unpaved roads that have the potential to significantly impact surface water quality. This paper focuses on a broad review of literature regarding stormwater permitting of the oil and gas industry on a state-by-state basis. This paper also provides an overview of studies conducted that have examined the potential impacts that oil and gas development has on surface water quality.

INTRODUCTION

The United States has recently experienced an increase in oil and gas development due to technological advances that have made hydraulic fracturing and horizontal drilling more cost-effective. However, many oil and gas operations (including hydraulic fracturing of shale formations) are largely unregulated with respect to stormwater runoff. The Ninth Circuit Court of Appeals opinion vacated the U.S. Environmental Protection Agency's (U.S. EPA) 2006 oil and gas construction stormwater regulation. This decision exempts oil and gas operations from construction stormwater permit requirements unless there is a discharge of a reportable quantity of oil or hazardous substance or a violation of a water quality standard (U.S. EPA, 2009; Williams et al., 2008).

Research on the surface water quality effects of the oil and gas industry is limited. Two published studies have illustrated that stormwater runoff from oil and gas activities contributes a significant amount of sediment to receiving streams (McBroom et al., 2012; Williams et al., 2008). It is difficult to quantify the water quality impacts resulting from oil and gas industry construction activities through in-stream sampling. It is even more difficult to determine if a violation of a water quality standard has taken place due to the limited amount of water quality sampling instruments in streams that receive runoff from oil and gas development activities. Sedimentation is one of the nation's leading causes of stream impairment (U.S. EPA, 2013). With the anticipated increase in oil and gas drilling, impairment of streams due to sediment loading will most likely occur unless erosion and sediment controls are widely applied to oil and gas sites.

A review of studies that have quantified sediment runoff on water quality impacts from oil and gas development is presented in this paper. Several research studies have taken place at a site-scale, meaning at well pads and roads (Bloser et al., 2012; McBroom et al., 2012; Williams et al., 2008) and some have taken place on a more regional scale (Buto et al., 2010; Entrekin et al., 2011; Olmstead et al., 2013). The methodologies and results of these surface water quality studies are presented in the following section.

To further our understanding of state construction stormwater permitting, individual state regulations were reviewed to determine whether or not stormwater permits where required for the construction of oil and gas well pads and supporting infrastructure, such as roads. Up to this point, a summary of construction stormwater permitting requirements for the oil and gas industry where unconventional drilling is taking place has not been documented on a state-by-state basis. Stormwater construction permit requirements for the oil and gas industry vary widely by state. A state-by-state review and synthesis in a single paper will hopefully serve as a useful reference for agencies and decision makers considering possible changes to policy and permitting requirements.

REVIEW OF OIL AND GAS IMPACTS ON SURFACE WATER QUALITY

A review of literature regarding unconventional oil and gas development's impact on surface water quality was undertaken in the fall of 2013. While there was a substantial body of published research pertaining to shale oil and gas drilling effects on subsurface water, studies on surface water effects were limited. Six (6) studies were identified and reviewed for this paper; their findings related to primarily sediment parameters, total suspended solids (TSS) and turbidity in particular, are highlighted. It is expected that increased sediment loading to streams will result where stormwater construction permits and erosion and sediment control plans are not required or enforced. This is a concern because sedimentation is one of the nation's leading causes of stream impairment (U.S. EPA, 2013). Excess sedimentation causes stream instability, negative impacts on aquatic organisms and vegetation, increased stream temperatures, and can compromise the functionality of a stream in terms of its beneficial use designation.

Each of the six studies reviewed for this paper was classified as one of two study types: 1) site-scale studies meaning studies conducted on oil and gas development sites such as well pads or roads, and 2) large-scale studies that took place within a watershed or a region. Table 1 outlines the six studies that were reviewed.

Table 1. Shale Oil and Gas Impacts on Water Quality Studies Summary

Authors	Location	Constituent	Findings
Williams et al., 2008	TX	Sediment	Average sediment loading rate of 48,988 kg/ha/year from gas well sites
McBroom et al., 2012	TX	Sediment	Sediment loading rate of 16,896 kg/ha/yr from natural gas site with no BMPs
Bloser & Scheetz, 2012	PA	Sediment	24.7 lbs/30-minute rain interval/100-ft length of unpaved road
Olmstead et al., 2013	PA	Sediment & Chlorophyll	5% increase in TSS concentrations when the average density of wells increased by 1 standard deviation
Entrekin, et al., 2011	PA, WV, OH, AR, NY	Turbidity	Positive correlation between well density and turbidity measurements
Buto, et al., 2010	WY, CO, UT, NM, AZ	Dissolved Solids	Estimated land disturbance from O&G development does not significantly contribute to dissolved solids loading

Site-Scale Studies

Williams et al. (2008) looked at five sites in Denton County, Texas (three well sites and two control sites) to investigate sediment runoff from natural gas well sites. Catchment traps, bed load traps and weirs installed near gas well sites and the control sites were used to determine the amount of sediment runoff from each site. Rill traps were installed in overland flow paths between the sites and receiving streams in order to determine if runoff and sediment from the drilling sites were reaching the streams. Estimated erosion rates included both bed load plus suspended sediment, as the two were not separated. Sediment was measured from storm events taking place between March 2005 and May 2006. Automated rain gauges were installed near each weir for precipitation measurements. The investigators indicated that measured sediment loads did not include all of the suspended solids produced at each site since some suspended sediment was carried over the weirs by storm flow, thus not being recorded in the measurements. All three gas sites showed decreasing trends in sediment load, reflecting the “first flush” or “site stabilization” effect. The study results showed that natural gas well sites have the potential to increase erosion and sediment runoff beyond what is expected for undisturbed sites. The study also

illustrated that sediment from the natural gas well sites did reach nearby streams. Finally, a potential sediment loading rate of 54 tons/hectare/year (48,988 kilograms/hectare/year) was estimated from the study results, which is within EPA's sediment loading range of small construction sites, and therefore the authors suggested that gas well sites should be subject to similar erosion and sediment control regulations as small construction sites.

McBroom et al. (2012) quantified stormwater concentrations and losses of sediment, nutrients, and metals from natural gas well sites in an experimental watershed in East Texas. Two natural gas well pads were constructed: one 1.4 hectare (ha) well pad was constructed in an intermittent stream channel (site F1) while the second 1.1 ha well pad was constructed 15 meters away from an intermittent stream (site F2). Water quality and sedimentation were measured at both sites using V-notch weirs placed approximately 80 meters downstream of both constructed well pads. Streamflows for both study sites were estimated using ArcAPEX models and precipitation measured using rain gauges. Coarse sediments that were deposited in the drop box section on the floor of the weir were removed and weighed after each storm event to determine the amount of sedimentation occurring in the stream channel. The authors found that regardless of season, site F1 produced significantly greater water than site F2. Also, runoff as a percentage of precipitation was different for the two sites, site F1 being 33% and site F2 being 12.3%. Sediment yield was also significantly greater at site F1 compared to site F2. Annual sediment losses calculated over the 19-month period of the study were 16,896 kilograms/hectare/year for site F1 and 1,087 kilograms/hectare/year for site F2. Although sediment yield was significantly different for each site, there was no significant difference in TSS concentrations. The authors found that the use of a 15 meter riparian buffer at gas well sites reduced sedimentation up to 94% when compared to gas well sites that did not employ a riparian buffer.

In 2010, the Center for Dirt and Gravel Road Studies (CDGRS) looked to quantify the amount of sediment runoff (TSS) produced from unpaved oil access roads (Bloser & Scheetz, 2012). Fourteen 100-foot segments of unpaved access roads were selected across a wide variety of terrain. Four of the fourteen sites were sampled after aggregate had been placed on the road segments to determine the percent TSS reduction after paving the road segments. Sampling events were carried out using a portable rainfall simulator that produced 0.61 inches of precipitation in a 30-minute rain event, equating to an approximate return interval of less than two months. The average amount produced over the fourteen unpaved 100-ft long road segments was 24.7 pounds of TSS over a 30 minute period. The four sites that were treated with aggregate yielded an average of 14.3 pounds of TSS for each 30 minute period.

Large-Scale Studies

Olmstead et al. (2013) performed a large-scale study which analyzed chloride and TSS water quality data from Pennsylvania using U.S. EPA's Storage and Retrieval Data Warehouse (STORET) database, well spatial data, drilling and completion dates of wells, drilling wastewater shipment information to permitted treatment facilities, and precipitations data. The study objective was to determine surface water quality

impacts from shale gas development. Both the impacts from the actual location of the wells and the impacts from waste disposal facilities were considered. The authors found that TSS concentrations were not affected by the density of shale wastewater treatment facilities upstream. However, Olmstead, et al. did find that TSS concentrations were correlated with the presence of shale gas wells in that watershed. Furthermore, a 5% increase in TSS concentrations were observed when the average density of wells increased by 1 standard deviation in that watershed. According to the authors, clearing the land for drilling infrastructure may have resulted in the increased TSS concentrations; however, the particular mechanisms for transporting TSS to surface waters could not be determined by this study.

Entrekin et al. (2011) studied the threats that oil & gas development pose to surface water. According to the authors, concerns about the effects of unconventional drilling on surface waters and terrestrial ecosystems have largely been overlooked. In an effort to demonstrate potential surface water impacts, Entrekin et al. looked at well density and proximity of wells to streams in the Fayetteville and Marcellus shale formations. Since 2005, wells have increased from 60 to 2,834 in the Fayette formation. As of summer 2010, the Marcellus formation had 3,758 natural gas wells. The Marcellus shale formation overlays sensitive watersheds, including the Delaware River and Chesapeake Bay watersheds. Using the National Hydrography Dataset (NHD) stream line data mapped at 1:24,000, wells in both formations were found to be located an average of 252 meters and 230 meters away from stream lines in the Marcellus and Fayetteville shale formations respectively. The authors felt that this was a conservative value since NHD underestimates the density of headwater streams. Using 10-meter digital elevation models (DEMs), drainage area lines were generated using the ArcHydro extension in ArcGIS with a stream threshold of 50,000m^2. Using the ArcHydro tools yielded average well proximities of 153 meters and 130 meters respectively. The authors hypothesized that stream turbidity measurements are positively correlated with well density in the Fayetteville shale formation. Well location data from the Arkansas Oil and Gas Commission and seven stream drainage areas delineated using ArcHydro in ArcMap 9.3.1 were used to develop well density data. When density data was compared with turbidity measurements taken with a Hach Lamotte 2020 meter during high spring flow throughout April of 2009, Pearson product moment correlations identified a positive relationship between in-stream turbidity and well density. Entrekin et al.'s work illustrated the proximity, on average, in which wells are built to streams and their measurable effects (in terms of turbidity) in receiving streams. The authors concluded that regulations which consider the proximity of oil and gas wells to receiving streams are needed, as well as further ecological research on the impacts from oil and gas well development.

The United States Geological Survey (USGS) used the Spatially Referenced Regressions on Watershed Attributes (SPARROW) surface water-quality model to assess the statistical significance land disturbance associated with the oil & gas industry on total dissolved (TDS) concentrations of streams in the Upper Colorado River Basin (Buto et al., 2010). According to the USGS study, land disturbance from oil & gas development was estimated using GIS analysis. The estimated land disturbance was put into the Upper Colorado River Basin dissolved solids

SPARROW model to assess the statistical significance. The sparrow model is a surface water-quality model relates measured chemical constituents at monitoring stations to upland catchment attributes, such as land use, land cover, or geology (Smith et al., 1997). According to the USGS, the model results were zero, meaning the estimated area of lands disturbed by oil and gas development was not statistically significant as a contributor of dissolved solids in streams. However, the authors point out that the model results were affected by the available monitoring data, distribution of monitoring sites with respect to land disturbance, the total area of disturbed lands associated with oil & gas within the entire basin and the reaches used for calibration, and the potential yield of dissolved solids from the disturbed lands compared with the natural yield. Furthermore, the authors emphasize that the study was an observational study, not an experimental study, and that the study was limited to the available data (Buto et al., 2010).

STATE CONSTRUCTION STORMWATER PERMITTING REVIEW METHODOLOGY

The methodology used to determine the current state of construction stormwater regulation for the oil and gas industry included two steps. The first was determining which states hydraulic fracturing activities are taking place. Once these states in were identified, state stormwater regulations were reviewed to determine if there are any additional state stormwater permit requirements for the oil and gas industry in regards to construction activities. These additional state requirements of interest would be in addition to federal permitting requirements, which exempt the oil and gas industry unless there is a reportable quantity release or a contribution to a water quality violation (U.S. EPA, 2009).

The state agency tasked with enforcing the National Pollutant Discharge Elimination Systems (NPDES) program within that state, and thus in charge of enforcing construction stormwater permits was identified, and the presence of permits recorded, along with the permit name and number. If the state construction permit did not specify an oil and gas exemption, it was assumed that the oil and gas industry did not need a permit in that state. Some states only require an Erosion and Sediment (E&S) plan, which means that no additional permit is required. The state stormwater permitting agency was documented as well as any websites, contacts, and the date this information was accessed. The shale formation where drilling takes place was recorded for every state in which hydraulic fracturing activity was confirmed as taking place.

STATE CONSTRUCTION STORMWATER PERMITTING REVIEW RESULTS

Out of twenty-four states that were indicated to have unconventional shale oil and gas drilling activities, thirteen (13) states require that a stormwater construction permit for oil and gas drilling activities be obtained. Figure 1 depicts whether or not the states require stormwater construction permits from oil and gas activities. The minimum size of the construction project that required a permit differed between

states, being either 1-acre or 5-acres. Eleven (11) states do not require oil and gas drilling activities to obtain a permit. However, some states (such as Michigan) did require an E&S plan be completed before construction begins.

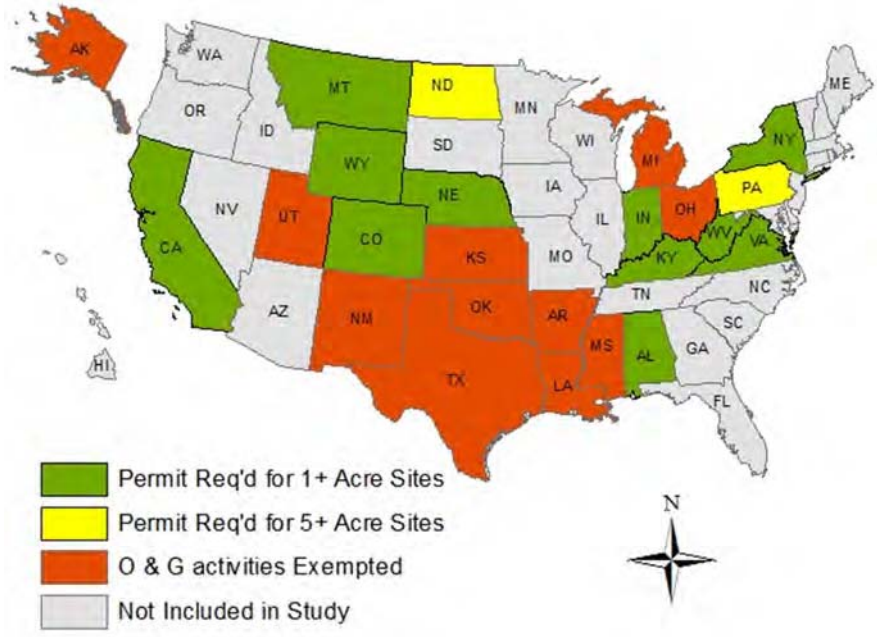

FIG. 1. States that enforce construction stormwater permitting requirements in addition to the National Pollutant Discharge Permit requirements as of November, 2013.

SUMMARY AND CONCLUSIONS

Studies have demonstrated that oil and gas construction sites have the potential to produce as much sediment as other types of construction sites (McBroom et al., 2012; Williams et al., 2008). Furthermore, well density has been found to be positively correlated with in-stream turbidity measurements (Entrekin et al., 2011) and an increase in TSS concentrations have been found to occur when the density of wells increased (Olmstead et al., 2013). The USGS SPARROW model results indicated that oil & gas development did not significantly contribute to dissolved solids loads of receiving streams; however, the authors concluded that emphasize that the study was an observational study and that the study was limited to the available data (Buto et al., 2010). The state-by-state review of construction stormwater permitting requirements for the oil and gas industry demonstrated significant differences in permitting requirements across the twenty-four states reviewed. Although the U.S. EPA does not require an NPDES permit for oil and gas construction activities, thirteen states have employed stricter stormwater permitting requirements than that of the national government.

Despite inconsistent regulation of construction stormwater runoff among states, studies have shown that when best management practices (BMPs) are put in place at oil and gas sites, a reduction in sediment loading to streams is observed (Bloser & Scheetz, 2012; Entrekin et al., 2011; Williams et al., 2008). Employing BMPs, ranging from using aggregate on unpaved access roads, limiting well density, or establishing a buffer between sites and receiving streams, were shown to reduce the impacts of oil and gas construction activities on surface waters. McBroom et al. (2012) noted that although construction of gas well pads is not currently regulated in the State of Texas, other unregulated industries, such as the forest management industry, have successfully promoted the use of voluntary BMPs without regulation. They went on to explain that in the mid-1980's, voluntary BMPs that restricted harvesting activities along streams were adopted by the forest industry in Texas after research showed that clear-cutting had significant impacts on water resources (Ice, 2004). By 2011 approximately 98% of forestry activities in Texas retained streamside buffers after an extensive education and outreach campaign (Simpson et al., 2011).

Although a handful of studies have quantified sediment loading at oil and gas well and access road sites in Pennsylvania and Texas, similar studies in semi-arid regions such as Utah has not been published. This research gap is important because the shale oil and gas industry is currently growing rapidly in Utah and other western states. Furthermore, the landscape and precipitation patterns in semi-arid regions differ greatly than in Texas and Pennsylvania, and results are expected to be different. Similar sediment loading quantification studies are needed in Utah to determine the effects of converting land to support oil and gas activities as well as how that conversion will impact the surface water quality of receiving streams.

ACKNOWLEDGMENTS

We would like to thank innovative Urban Transitions and Arid-region Hydro-sustainability (iUTAH), the University of Utah's Global Change and Sustainability Center, and the Utah Chapter of the Advancement Rewards for College Scientists (ARCS) for providing funding which enabled the literary exploration into this field. Furthermore, we would like to thank the support that has been provided by the University of Utah Urban Water Group.

REFERENCES

Bloser, Steven, & Scheetz, Barry E. (2012). Sediment Production from Unpaved Oil Well Access Roads in the Allegheny National Forest.

Buto, Susan G, Kenney, Terry A, & Gerner, Steven J. (2010). Land Disturbance Associated with Oil and Gas Development and Effects of Development-Related Land Disturbance on Dissolved-Solids Loads in Streams in the Upper Colorado River Basin, 1991, 2007, and 2025: U. S. Geological Survey.

Entrekin, Sally, Evans-White, Michelle, Johnson, Brent, & Hagenbuch, Elisabeth. (2011). Rapid expansion of natural gas development poses a threat to surface waters. *Frontiers in Ecology and the Environment, 9*(9), 503-511. doi: 10.1890/110053

Ice, G. (2004). History of innovative best management practice development and its role in addressing water quality limited waterbodies. *Journal of Environmental Engineering, 130*(6), 684-689. doi: 10.1061/(ASCE)0733-9372(2004)130:6(684)

McBroom, M., Thomas, T., & Zhang, Y. (2012). Soil erosion and surface water quality impacts of natural gas development in East Texas, USA. *Water, 4*(4), 944-958. doi: 10.3390/w4040944

Olmstead, Sheila M., Muehlenbachs, Lucija A., Shih, Jhih-Shyang, Chu, Ziyan, & Krupnick, Alan J. (2013). Shale gas development impacts on surface water quality in Pennsylvania. *Proceedings of the National Academy of Sciences of the United States of America, 110*(13), 6.

Simpson, Hughes, Coup, Chuck, & Duncan, Chris. (2011). Voluntary Implementation of Forestry Best Management Practices in East Texas: Texas Forest Service: Lufkin, TX, USA.

Smith, Richard A, Schwarz, Gregory E, & Alexander, Richard B. (1997). Regional interpretation of water-quality monitoring data. *Water Resources Research, 33*(12), 2781-2798.

U.S. EPA. (2009). Regulation of Oil and Gas Construction Activities. Retrieved August 14, 2013, from http://cfpub.epa.gov/npdes/stormwater/oilgas.cfm

U.S. EPA. (2013). National Rivers and Streams Assessment: A Collaborative Survey. Washington, DC 20460: US Environmental Protection Agency (USEPA) Office of Wetlands, Oceans and Watersheds, Office of Research and Development.

Williams, H. F. L., Havens, D. L., Banks, K. E., & Wachal, D. J. (2008). Field-based monitoring of sediment runoff from natural gas well sites in Denton County, Texas, USA. *Environmental Geology, 55*(7), 1463-1471. doi: 10.1007/s00254-007-1096-9

Subpart W – Past, Present, and Future

David J. Larson[1] and Kristian A. Macoskey,[2] QEP

[1]Project Manager, Environmental Practice, Civil & Environmental Consultants, Inc., 333 Baldwin Road, Pittsburgh, PA 15205, U.S.A., E-mail: dlarson@cecinc.com.
[2]Principal, Environmental Practice Lead, Civil & Environmental Consultants, Inc., 333 Baldwin Road, Pittsburgh, PA 15205, U.S.A., E-mail: kmacoskey@cecinc.com.

ABSTRACT: The *Mandatory Greenhouse Gas Reporting* Rule (GHG Rule), 40 CFR 98 *Subpart W – Petroleum and Natural Gas Systems,* affects eight segments of the petroleum and natural gas industry. Starting in 2011, operators in the oil and gas production segment were required to correlate well locations with corresponding oil and gas fields for tracking and reporting purposes; delineate well locations within facilities, basins, and fields; and aggregate greenhouse gas (GHG) emissions to determine applicability. Strategies had to be developed for recording data, estimating emissions, and reporting. Data was collected on production rates, equipment counts, well venting durations, gas compositions, and other parameters needed to estimate emissions. If producers could not fully comply with Subpart W requirements, the Environmental Protection Agency (EPA) allowed for use of best available monitoring methods, providing unique or unusual circumstances could be justified. Producers subject to Subpart W first had to report annual GHG emissions in September of 2012. Many shale oil and gas producers were not prepared to cope with the GHG Rule and many still may not be in full compliance. The authors discuss the requirements, challenges, and potential future implications of GHG monitoring and reporting for oil and gas producers.

INTRODUCTION/HISTORY

Many of the activities related to the oil and gas industry were not historically subject to federal regulation. For example, the Energy Policy Act of 2005 (frequently referred to as the Halliburton Loophole) exempts hydraulic fracturing from the federal Safe Drinking Water Act of 1974 and exempts oil and gas construction from the federal Clean Water Act.

Following the 2008 Consolidated Appropriations Act (H.R. 2764; Public Law 110–161), the Environmental Protection Agency (EPA) released the Mandatory Reporting of Greenhouse Gases Rule (74 FR 5620), then the *Mandatory Greenhouse Gas Reporting* Rule (GHG Rule), 40 CFR 98 on October 30, 2009, and subsequently 40 CFR 98 *Subpart W – Petroleum and Natural Gas Systems,* on November 30, 2010. The GHG Rule applies to natural gas sources and suppliers that emit greenhouse

gases (GHGs) totaling 25,000 metric tons or more of carbon dioxide equivalent (CO_2e) per year. Affected industry segments, as defined by EPA, include: onshore production, offshore production, natural gas processing, natural gas transmission, underground natural gas storage, natural gas distribution, liquefied natural gas import/export, and liquefied natural gas storage, along with other oil and gas combustion. This paper focuses on the onshore production industry and how the GHG Rule has influenced operations, the steps owners/operators have taken to facilitate compliance, and some potential future implications.

REQUIREMENTS

Onshore production facilities, including conventional and unconventional (shale) wells, were required to estimate annual GHG emissions beginning in calendar year 2011. GHG emissions data had to be recorded, aggregated, and reported by facility, basin, and field.

Applicability of Subpart W is based on facility-wide GHG emissions, so one of the first things onshore producers had to do was determine how many wells they had within each hydrocarbon basin to delineate their facilities. Facility is defined by Subpart W (§98.238) as *"…all petroleum or natural gas equipment on a well pad or associated with a well pad…under common ownership or common control including leased, rented, or contracted activities by an onshore petroleum and natural gas production owner or operator and that are located in a single hydrocarbon basin as defined in § 98.238. Where a person or entity owns or operates more than one well in a basin, then all onshore petroleum and natural gas production equipment associated with all wells that the person or entity owns or operates in the basin would be considered one facility."* According to this definition of Facility, many onshore production companies may own and operate multiple well pads that constitute a single facility.

The next step was to estimate total facility emissions. EPA created a Microsoft Excel Screening Tool (available at: http://www.epa.gov/ghgreporting/help/tool/index.html) that could be used to estimate the collective equipment leaks, vented emissions, and combusted emissions (including flares, workover equipment, and wellhead compressors) for comparison to the 25,000-metric ton CO_2e threshold. If the onshore production owner/operator concluded that reporting was not required, then he/she may have simply documented the assessment and stopped there. Most shale-gas producers with a well or two likely exceeded the reporting threshold and had to proceed to the next phase of planning.

Onshore production facilities that were required to report had to develop and implement a Greenhouse Gas Monitoring Plan (40 CFR 98.3(g)(5)), which requires operators to specify the methods and procedures that will be used to ensure that data, calculations, and reports are consistent with applicable requirements of the GHG Rule. Through the process of developing monitoring plans, some producers discovered that they had not been recording all of the information required, or that the information recorded did not meet the monitoring and quality requirements. The amount of information needed depended on the types of activities or sources of emissions present at each well location. Sections (a) through (z) of 40 CFR 98.233

identify very specific activities or emission sources related to venting, storing, flaring, leaking, and combusting natural gas that need to be considered.

Onshore production facilities reported annual aggregated carbon dioxide (CO_2), methane (CH_4), and nitrous oxide (N_2O) mass emissions expressed as metric tons of each GHG and in metric tons of CO_2e in accordance with the definitions and data reporting methods outlined in the GHG Rule. Conversion of CO_2, CH_4, and N_2O emissions to CO_2e was in accordance with Equation A-1 of 40 CFR 98.2(b)(4) as follows:

$$CO_2\text{e} = \sum_{i=1}^{n} \text{GHG}_i \text{ x } GWP_i$$

Where:
CO_2e = carbon dioxide equivalent (mt/yr);
GHG_i = mass emission of each greenhouse gas (mt/yr);
GWP_i = global warming potential for each greenhouse gas as follows:
CO_2 = 1;
CH_4 = 21;
N_2O = 310; and
n = 3 (the number of GHGs emitted).

Finally, after the annual facility GHG emissions were aggregated, facilities had to report the estimates to EPA using the Electronic Greenhouse Gas Reporting Tool (e-GGRT), available at: https://ghgreporting.epa.gov/ghg/login.do.

CHALLENGES

The first task facing the onshore production segment was to determine whether the GHG Rule applied to its operations. As described above, companies could use the EPA's applicability Screening Tool, however, the disclaimer infers that the GHG Rule governs and that EPA will not guarantee that use of the spreadsheet will result in an official determination of applicability. As a result, companies may have implemented costly data collection and emission estimation procedures in accordance with the regulation only to find that they were exempt from reporting.

For those companies that determined they would be subject to the rule, the implementation of their Greenhouse Gas Monitoring Plan involved a significant data collection, compilation, and management effort. Many facilities had to develop field data forms to uniformly collect required parameters, such as counts of high, low, and intermittent bleed devices for pneumatic device venting, or counts of equipment, such as pressure relief valves, pumps, and flanges. Well tenders had to be trained to identify the components and record required information. Production supervisors, operations managers, and environmental professionals had to work together to match the data required by the GHG Rule with the data they already were tracking. Data may have been tracked by a number of different individuals, recorded, and saved in multiple locations and formats.

Thus, companies faced logistical challenges of streamlining data collection, entry, and recordkeeping. Consultants and software developers created new systems and databases aimed at helping the natural gas industry comply with these new information challenges. In the end, each company had to develop and implement appropriate compliance solutions.

To allow facilities time to implement their monitoring plans and develop appropriate data collecting and recording methods, EPA allowed owners or operators to use best available monitoring methods (BAMM) for parameters that could not reasonably be measured through December 31, 2011. To use BAMM beyond December 31, 2011, companies had to submit requests to EPA detailing the sources involved and the unique or unusual circumstances leading to the need for BAMM. By submitting a BAMM request by March 30, 2012, facilities were automatically authorized to use BAMM through June 30, 2012, but EPA approval was required to use BAMM beyond that date. Therefore, the BAMM approval process left some facilities in the awkward position of not knowing if their request for BAMM would be accepted or denied for the second half of 2012.

The last step was to report the GHG data to EPA through e-GGRT. Reporting required that facilities follow the prescribed methodologies for estimating emissions, summarize the total GHG emissions by CO_2, CH_4, N_2O, and CO_2e, and assign a Designated Representative to certify the data on behalf of the company. Companies could manually input the data into the e-GGRT web forms or upload data using the Extensible Markup Language (XML) reporting schema. Regardless of which reporting method was selected, each facility had to invest time and resources to adequately compile, review, and summarize the data before it was ready to submit. Many companies assigned this responsibility to internal staff, but many others sought external assistance from consultants, attorneys, and software developers. Understanding the GHG Rule and adhering to the data quality requirements proved to be a substantial undertaking for onshore production companies.

FUTURE IMPLICATIONS

Global Warming Potential

Because methane is the principle component of natural gas, and each metric ton emitted is equivalent to 21 metric tons of CO_2e due to methane's GWP of 21, any increase in the GWP will have a direct impact on GHG from this industry sector. EPA issued a final rule (78 FR 230) on November 29, 2013, which raised the GWP for methane from 21 to 25 (a 19% increase). It is believed that the Intergovernmental Panel on Climate Change (IPCC) 5^{th} Assessment may result in another increase of the GWP for methane to 28 (a 33% increase from 21). These 19 to 33% increases in the GWP factor could have a significant influence on the number of facilities that exceed the 25,000 mt/yr reporting threshold. Facilities that were just below the reporting threshold may be required to revisit their estimates. The natural gas industry is already the largest source of methane emissions in the United States, and the higher GWP for methane will further highlight that fact.

Possible Uses of Reported Data

Possible uses of reported data are a concern to the industry. GHG information submitted to EPA is available to the public unless the information qualifies for treatment as confidential business information (CBI). Due to the volume of information involved and confidentiality concerns raised by the industry, EPA is working on determining what information will be kept confidential under 40 CFR Part 2, Subpart B, instead of evaluating individual CBI requests. EPA already has made some information public through the Facility Level Information on GreenHouse gas Tool (FLIGHT), which allows users to download files and search by state, facility, or industry (refer to: http://ghgdata.epa.gov). EPA also released GHG information by means of the ENVIROFACTS database (www.epa.gov/enviro), which offers users additional searching and analyzing capabilities. Public access to operational and production data used to generate emission estimates produces the potential for unintended uses.

Potential Emission Fees

As early as 2008, the Bay Area Air Quality Management District (BAAQMD) of California had adopted a fee on GHG emissions from stationary sources in the amount of 4.8 cents per metric ton. This fee was adopted to "…recover the costs associated with its [the Air District's] Climate Protection Program activities related to stationary source." (BAAQMD, 2008). For a source emitting 100,000 metric tons of GHG, the fee amounted to $4,800 per year.

The authors are not aware of any other regions of the U.S. where a GHG emission fee has been incorporated into the annual emission fee program, but the merits of assessing fees and ascribing value to GHG emissions as a policy tool associated with responses to global climate change concerns have been discussed for several years. While a cap-and-trade or "carbon tax" program has not been implemented in the U.S., the precedent for carbon management exists in the European Union and the infrastructure has been established in the U.S. with entities such as the Chicago Climate Exchange, which currently operates as an offsets registry program. According to a recent Reuters article (Volcovici 2013), some U.S. companies, such as Wal-Mart, ExxonMobil, and Google, have incorporated GHG or carbon values ranging from $6 to $60 per ton into their internal strategic plans. If fees of that magnitude were assessed for a 100,000-ton-per-year facility, annual costs could be significant.

Potential Source Aggregation

Air quality regulators employ a three-pronged test to determine if emissions from multiple facilities should be aggregated for permitting and comparison to major source thresholds. First, do the industrial activities share the same first two-digit Standard Industrial Classification (SIC) code? Second, are the activities located on one or more contiguous or adjacent properties? Third, are the activities under common control?

According to the Tailoring Rule (EPA 2010a), newly constructed sources that are not major sources for another pollutant would be subject to Prevention of Significant Deterioration (PSD) rules if they have the potential to emit more than 100,000 metric tons per year of CO_2e. In addition, an existing major source would be subject to PSD if a modification caused GHG potential emissions to increase by more than 75,000 metric tons per year of CO_2e. While Subpart W reporting addresses actual emissions and PSD applicability addresses maximum potential emissions, because the definition of a facility can encompass thousands of individual well pads, the question arises: could GHG emissions from a "Facility" as defined by Subpart W trigger PSD permitting under the Tailoring Rule? A few rules of thumb derived from EPA's Screening Tool (EPA 2010b) may be instructive, as summarized in Table 1.

Table 1. Screening Level Well Pad CO_2e Emission Rates

Source Category	Number of Units	CO_2e (t)
Gas well venting during well completions	1	4,086
Reciprocating compressor (leaks for rod packing)	1 (operating 8,760 hours)	2,471
Reciprocating compressor (combustion emissions)	1 million horsepower-hours	1,043

While the assumptions underlying EPA's estimates are conservative, they can be used to evaluate the potential for multiple well pads to accumulate up to 75,000 or 100,000 metric tons per year of CO_2e. For instance, if a "Facility" included 24 gas wells vented during well completions in one year, combined emissions would exceed 100,000 metric tons of CO_2e. Similarly, one 145-horsepower compressor engine operating about 100% of the time (about 1.3 million horsepower-hours) will generate about 3,800 metric tons of CO_2e. With only 27 such engines operating at the same rate, more than 100,000 metric tons of CO_2e would be generated.

Because all of the well pads would have the same two-digit SIC code and be under the common control of the reporting company, if the Subpart W definition of "Facility" established that all well pads were contiguous, it is feasible that many facilities could be determined to be major sources. These simple examples point out the potential for a significant compliance and permitting burden should the Subpart W facility definition be used to establish a basis to aggregate multiple well pads for purposes of Tailoring Rule applicability determinations.

Potential Emission Offset Credits

If future policy limits GHG emissions at the facility level and establishes mandatory use of GHG (carbon or CO_2e) offsets to drive industry to reduce or avoid emissions, then onshore producers will have to evaluate their business options. Information collected from Subpart W reporting could lead to creation of a carbon cap for this or other industry segments. Existing companies with producing wells and no plans to expand may be able to sell credits as their well production declines. New

or expanding companies would seek to buy offsets from existing companies or invest in carbon reduction projects, such as reforestation, renewable energy, landfill gas, or carbon sequestration.

Depending on how offsets are valued, GHG reporting under Subpart W may become more or less onerous. If EPA has enough data after a few years to better gauge and predict the emissions from a facility, it is conceivable that reporting requirements could be reduced. Alternatively, if offsets become scarce or highly valued, industry may prefer detailed reporting for accounting purposes, and seek ways to gain competitive advantage by minimizing emissions, increasing the efficiency of production and completion methods and technology, and banking offsets for future use or sale.

CONCLUSIONS

Subpart W is complex, and onshore producers had to overcome significant challenges and expense to comply. Subpart W has also been a moving target, having been amended and revised nine times in under four years to address industry comments and concerns and improve clarity of requirements. If the past and present of Subpart W indicate the future, we can expect continuing challenges to comply.

REFERENCES

U.S. EPA. (November 29, 2013). "2013 Revisions to the Greenhouse Gas Reporting and Final Confidentiality Determinations for New or Substantially Revised Data Elements; Final Rule." *Federal Register*, Volume 78, Number 230, 71904-71981 <http://www.gpo.gov/fdsys/pkg/FR-2013-11-29/pdf/FR-2013-11-29.pdf> (December 2013).

Bay Area Air Quality Management District, 2008. "Fact Sheet – Proposed Bay Area Air Quality Management District Greenhouse Gas Fee Schedule – February 5, 2008." <http://www.baaqmd.gov/Divisions/Planning-and-Research/Rules-and-Regulations.aspx> (December 2013).

Bay Area Air Quality Management District, 2012. "Regulation 3-334, Schedule T - Greenhouse Gas Fees." <http://www.baaqmd.gov/Divisions/Planning-and-Research/Rules-and-Regulations.aspx> (December 2013).

U.S. EPA, 2010a. (June 3, 2010). "Prevention of Significant Deterioration and Title V Greenhouse Gas Tailoring Rule; Final Rule." *Federal Register*, Volume 75, Number 106, 31514 <http://www.gpo.gov/fdsys/pkg/FR-2010-06-03/pdf/2010-11974.pdf> (December 2013).

U.S. EPA, 2010b. Greenhouse Gas Reporting Program: Applicability Tool Onshore Petroleum & Natural Gas Production, <http://www.epa.gov/ghgreporting/help/tool/step2a.html> (December 2013).

U.S. EPA. Greenhouse Gas Reporting Program. <http://www.epa.gov/ghgreporting/index.html> (December 2013).

U.S. Government Printing Office. (December 5, 2013). U.S. EPA. 40 CFR 98 Subpart W – PETROLEUM AND NATURAL GAS SYSTEMS.

<http://www.ecfr.gov/cgi-bin/text-idx?c=ecfr&tpl=/ecfrbrowse/Title40/40cfr98_main_02.tpl> (December 2013).

Volcovici, Valerie. (December 5, 2013). "Major companies plan for U.S. carbon emissions fee, report says." Reuters. <http://www.reuters.com/article/2013/12/05/usa-energy-carbon-idUSL2N0JK0V220131205> (December 2013).

Effective Use of Cementitious Materials, Ground Granulated Blast Furnace Slag, and Bentonite in Treating Contaminants on Polluted Land

Mary Allagoa[1]

[1]Postgraduate Researcher, University of Aberdeen, Environmental Science, Aberdeen, AB24 3FX, United Kingdom, E-mail: maryallagoa@gmail.com

ABSTRACT: This study focuses on pollutant stabilisation by the formation of less mobile, less toxic and less bio available contaminant binding forms which protects humans, health and the environment. This treatment involves mixing a binding agent into the contaminated media by immobilizing hazardous constituents within the treated material. Cementitious materials such as CEM I, ground granulated blast furnace slag (GGBS), and bentonite are the predominate material choices because of their low associated processing costs, compatibility with a wide variety of disposal scenarios and the ability to meet stringent processing and performance requirement. The aim requires selection of immobilising agents based on a set of physico-chemical test designed to provide understanding of the processes involved in a particular stabilisation scheme, durability of its products and environmental impacts. Laboratory treatability studies are a fundamental part of the design process to assess mix, design and demonstrate that a binder can be selected to achieve remedial objectives for the design life of the remediation. The composition of the mixes were similar but the difference is the percentage of water applied. A more comprehensive treatability study is proposed for ensuring that the study accurately reflects anticipated on-site conditions and the chosen binder satisfies the remedial objectives.

INTRODUCTION

Solidification/stabilization (S/S) is a term normally used to designate a technology employing additives to alter hazardous waste to make it non-hazardous or acceptable for current land disposal requirements. The use of this technology to treat hazardous waste may become more important as regulations restrict the use of land for disposing of hazardous waste. Solidification refers to a process in which materials are added to the waste to produce a solid is referred to as solidification. It may or may not involve a chemical bonding between the toxic contaminant and the additive.

Stabilization refers to a process by which a waste is converted to a more chemically stable form. The term includes solidification, but also includes use of a chemical reaction to transform the toxic component to a new non-toxic compound or substance.

The broad objective of S/S technology is to contain a waste and prevent it from entering the environment. In practice this broad objective may be

realized by several mechanisms which lead to factors important in assessing S/S technology(Wiles, 1987). These are:

a. produce a solid
b. improve handling characteristics of the waste,
c. decrease the surface area across which the transport of the contaminant may occur, and
d. limit the solubility of the contaminant when exposed to leaching fluids. Idealistically, the objective is to completely transform the potentially toxic contaminant into a non-toxic form. S/S treatment consists of mixing the waste with waste-specific reagents and water, according to the formulation specified by the laboratory (Klein and Magne 2005).

A wide range of binders have been used in S/S treatments, below is a brief description of those which are used in the research reported here. These include Portland cement, Ground granulated blast furnace slag and bentonite.

Portland cement (PC) is a conventional binder that is derived from clay or shale and limestone which are calcareous and contain alumina and silica. PC has proved to be the material that has the widest applicability for treating wide forms of hazardous waste enabling improvement in both the physical (solidification) and chemical (stabilisation) characteristics (Banaszkiewicz and Marcinkowski 2007) and has been used widely in soil mix technology(Topolnicki 2004). Heavy metals are best suited in PC stabilisation. This is because cement is highly alkaline, that enhances chemical fixation and physical encapsulation of the heavy metals found in the waste mainly through the precipitation of the hydroxides (LaGrega et al. 1994). The poor performance of PC in some organic contaminant stabilisation has investigated other binders for their feasibility in soil stabilisation including modified clays (LaGrega et al. 1994).

Ground granulated blastfurnace slag (GGBS) is a by-product of the manufacture of the steel industry with chemical compositions similar to that of PC and containing silica, alumina and lime. GGBS usually needs an activator like PC and Lime to speed up the production of its hydration cementitious properties since it is latent hydraulic cement. GGBS is commonly used in cement replacement and its use is well established as a binder in many cement applications where it is known to provide enhanced durability.

There is very little reference in this literature to the treatment of contaminants using GGBS. Since, NaOH is an activator and highly alkaline when mixed with GGBS, NaOH affect the formation of CSH (a hydrate). Allan and Kukacka (1995) studied the effect of blasfurnace slag in Chromium contaminated soil using in-situ stabilisation. The leaching resistance improved with increasing slag replacement level. The results showed that soil contaminated with trivalent and hexavalent chromium can be stabilised and solidified with cement-based grouts containing ground granulated blast furnace slag.

Bentonite is montmorillonite clays, and hence has high surface area and cation exchange capacity compared to the clays which provide high adsorption capacity of various contaminants. Clays are aluminosilicates with sheet like structure and usually absorbed water which contains exchange cations hence are usually effective with heavy metals and are fast less effective with organics particularly those which are hydrophobic. This has led to recent developments in clay modifications.

Design Criteria and Treatability Study

Design criteria provide the insight towards the performance of the binders and hence the effectiveness of the use of S/S treatment technology. These criteria are categorised into physical and chemical test (Harris et al. 1995). Physical tests determine the quality of the binders, the quantity required to be used and homogeneity in mixing. This test includes durability, permeability and strength. Chemical test involves determining the leaching behaviour of stabilised material (Harris et al. 1995). The chemical test is mainly leachability test. The actual values required depend on the end use application following treatment:

a. durability testing is carried out to assess the ability of solidified materials to resist freezing/thawing and repeated drying/wetting. As well the long term performance of the stabilised material is been checked.

b. unconfined compressive strength test is used to determine the ability of the S/S stabilised material to resist mechanical stresses (Stegemann and Cote 1990 and 1991). There are different factors that affect the strength of the materials stabilised with binders as shown in Table 1.

c. Permeability is defined as the tendency of a fluid to pass into a material. The permeability limit should be between 10^{-8} to 10^{-9}m/s for the material to be disposed in landfill or be used for in-ground treatment (Al-Tabbaa and Evans 1998). Additional, the material must be able to resist stresses from the environment.

d.leachability is the ability of a stabilised material to be leached into the environment. Leaching is the process by which the stabilised soil is been immersed into a liquid to remove the minerals. The liquid is called the leachant and the solid is the leachate in solution. Leachability of a material generally depends on the physical and chemical properties of the stabilised material. Important variables that determine the level of leaching of a stabilised materials in the leachate are analysis of the leachate, leachate-solid separation, temperature, contact time, leachant renewal, liquid-solid ratio(L/S), mode and method of contact, leachant composition and sample preparation(LaGrega,1994). Alkalinity of the stabilised material, tortuosity, diffusion and the surface –to-volume ratio of the stabilised material are the major factors that affect the leachability of the stabilised material (Van der Sloot et al. 1989). There are two main classification of leaching test. These are extraction and dynamic leaching test (Lewin et al. 1994, Conner 1990). Extraction test are the most common which are subdivided into agitated and sequential chemical extraction test while dynamic test is sub-divided into serial batch tests (most popular), chloride permeability, flow through and flow around test.

Table 1. Main Factors Affecting the Observed Strength of Stabilised Soil (Topolnicki 2004)

Source	Specific items
Physical and chemical properties of the soil to be treated	Grain size distribution, mineralogy, natural water content, Atterberg limits, organic matter content, reactivity and pH of pore water
Binder, additives and process water	Type and quality of hardening agent(s), binder composition, quantity of binder and other additives, quality of mixing water
Installation technique and mixing conditions	Tool geometry, installation process, water/binder ratio, energy of mixing, time lag between overlaps and working shifts
Curing conditions, time	Curing time, temperature(heat of hydration in relation to treated volume), humidity, wetting/drying and freezing/thawing cycles, long-term strength gain and/or deterioration
Testing and sampling	Choice of testing method, type of test, sampling techniques, sample size, testing conditions(stress path and drainage conditions, confining pressures, strain rate, method of strain measurement)

The design is usually based on laboratory based treatability study work in which samples from the field soil and groundwater are tested in the laboratory with a number of binders and binder dosages to arrive at the optimum binder for the field application. As the performance is complicated by the high degree of variability in soil and contaminant conditions, this leads to differences between the laboratory and field performance. Hence establishing a correlation between the laboratory and field performance will help in achieving better design criteria.
The original intention of this work presented here was to be able to perform comparison between binders and composition between the curing days of the mixes.

MATERIALS AND METHODS

Soil Physico-Chemical Characterisation

Made ground soil were homogenised in the laboratory. An aliquot of the soil was used for the determination of the physico – chemical characteristics including moisture content, bulk density, and Liquid limit, and Plastic limit, total concentration of the contaminant, Strength and chemical properties.

Binder Material

Binders used where Portland cement, GGBS and Bentonite.

a. Portland cement (PC) is the most conventional and commonly used binder in soil mixing applications and it was hence chosen as the primary binder in order to study the relative performance of other binders in soil stabilisation/solidification. PC was obtained in 25kg bags from Blue Circle, Lafarge, UK, and it is classified as CEM 1 according to BS EN 197-b.

b. Ground granulated blast furnace slag (GGBS) - The GGBS used was obtained from Civil and Marine Ltd, UK. In this study GGBS is either used in a blend with CEM I, in the form of CEM III in 1:1 ratio, and other ratios or in a blend with magnesia as its activator.

Historically Contaminated Soils

Made ground soil was obtained from the contaminated Castleford Site used for the SMiRT project. The soil was a mixture of clayey silt and sandy clay which were homogenised in the laboratory and had a water content of 25%, a Liquid Limit of 30% and a Plastic Limit of 24%. The made ground soil is contaminated by a cocktail of toxic chemicals including lead, zinc, copper, cadmium, nickel, analines, chloroanalines, nitrobenzene and dinitrotoluene.

Soil-Binder Mixes

The soil- binder mixes used for the laboratory treatability study are presented in table 1. These table shows the composition of the mixes.

Table 2. Composition of CEM III and Bentonie Based Mixes Produced in the Laboratory Treatability Study

Mix	Binders	water:binder	Slurry (%)	Soil (%)	Water (%)	CEMI (%)	GGBS (%)	B (%)
WL1	CEM III:B (4:1)	1.8:1	42	58	27	6	6	3
OL1	CEM III:B (4:1)	1.0:1.0	20	80	10	4	4	2
OL2	CEM III:B (4:1)	1.9:1	29	71	19	4	4	2

Sample Preparation

For soil mixing, a more powerful mechanical mixer with a K blade was used. The mixer was stopped every 2-3 minutes and the material was remoulded with a spatula to make sure lumps do not form. Every Batch was mixed for approximately 15 minutes and the homogeneity of the mix was censured by physical observation. After preparing the soil and grout separately, they were mixed together for another 15minutes with 3 stopping's for remoulding by using a spatula. This mixing was carried out by the same mixer which was used for soil mixing. The homogenous soil-grout mix is then poured in three equal layers into cylindrical moulds of 50mm diameter and 100mm height. Every layer was compacted by an 8mm diameter steel rod for moderate compaction and to remove any air bubbles trapped in to the mix. The samples were then remoulded a few days later, examples of samples are shown in Figure 3.2b. The prepared samples were placed in a sealed plastic container in which the relative humidity was maintained at around 98% and kept in a constant temperature room of 20^0C. Once the samples were strong enough to withstand remoulding, they were remoulded and placed back in the container for curing.

FIG.1. a) Mechanical mixer used for soil and soil-binder mixing and (b) typical prepared samples.

Testing Procedures

Unconfined Compressive Test

Unconfined compressive Strength test is the most common test in assessing the strength soil-binder mixes because of its rapidity. The UCS is a measure of the un-drained shear strength of cohesive material ranging from soft clay to concrete and represents the material's resistance to failure by shear whilst under rapid loading. In addition to Strength, UCS also provides an indication of the ductility/brittleness of the material. The UCS test specimens were 50mm in diameter and 100mm in height. Both ends of specimens were made flat to within ± 0.05mm. The vertical load was applied axially at a constant rate of strain of 1.14mm per minute until failure from which the strength was calculated.

The Batch Leachability Test

The Batch Leachability test was used. The duration of the test was 24hrs to ensure that equilibrium condition are reached to make the comparison applicable to a wider variety of materials. The experimental protocol followed British Standard BS 12457-2. The liquid to solid ratio (L/S) was kept at 10:1. The pH of the de-ionised water was between 6 to7 and CO_2 were added. The bottles containing the liquid to solid ratio (L/S) of 10:1 were placed on a roller table (rotation speed 10rpm) for 24hours at 20^0C. After the test, the bottles were left on the table to allow the suspended solid of sorbent to settle. Once the sorbent settled the pH was measured with a Fisher Scientific Accumet Ap-71. Then supernatant was filtered in a 0.45m filter and syringe.

Heavy Metals and organics Extraction

pH meter were used to read the leachate pH. A syringe and filter were used to extract the heavy metal contained in the bottle. The inductively coupled plasma machine was used to analyse the metal. In addition, Hydrochloric Acid (5ml) serves as an acid catalyst while the dichloromethane (30ml) acts as the solvent used to extract the solute (organics) from the solution. These were done three times per sample, empty bottle of the container were weighed before the organics was poured into the bottle.

RESULT AND DISCUSSION

A set of physical and chemical tests was conducted on the different mixes. These are presented in separate section below.

Density and Unconfined Compressive Strength

The bulk densities of all the laboratory prepared mixes are presented respectively in Figure 2 and 4 and show an average margin of error of ±1%. Except for mix WL1 which contained higher water content and the density decrease after increase in curing days, the other mixes behave differently as there was an increase in density after increasing the curing days.

A summary of the UCS at 7 – 90 days is presented in Figure 2, for mix WL1. The result has an average margin of ±12%. The UCS increase as the curing days increases which ranges from 200kPa to 400kPa respectively for mix WL1, 600kPa for OL1 and 250kPa for OL2 in figure 3 at 7days of curing. Depending on the management scenario of the treated material, different threshold values of UCS apply. For the burial purposes the UCS value can be as low as 140kPa (Meegoda et al. 2003), for the production of blocks and bricks and for load bearing concrete materials the values would be much higher at 3MPa and 7MPa respectively (Johnson, 2004). Lower UCS values could find applications in areas where low-grade materials are acceptable or simply to be used as stabilised ground. Given the very wide range of UCS values above, all the mixes, based on their UCS values, are likely to find suitable applications.

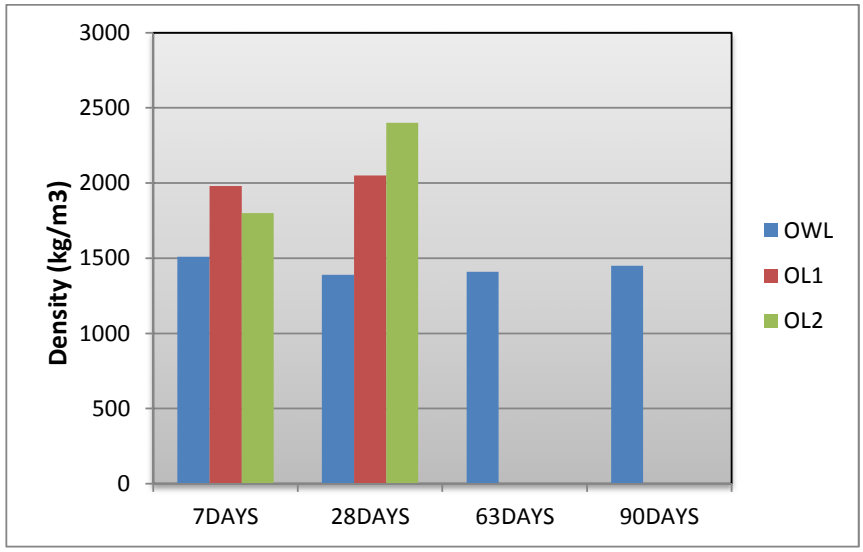

FIG.2. Showing the mean value of all the result of the mixes at various curing days.

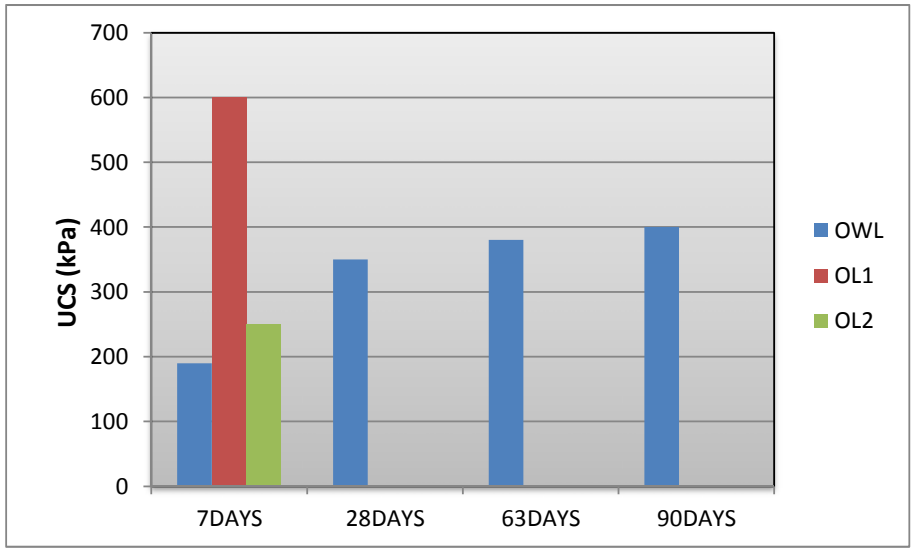

FIG. 3. Showing the mean value of all the result of the mixes at various curing days.

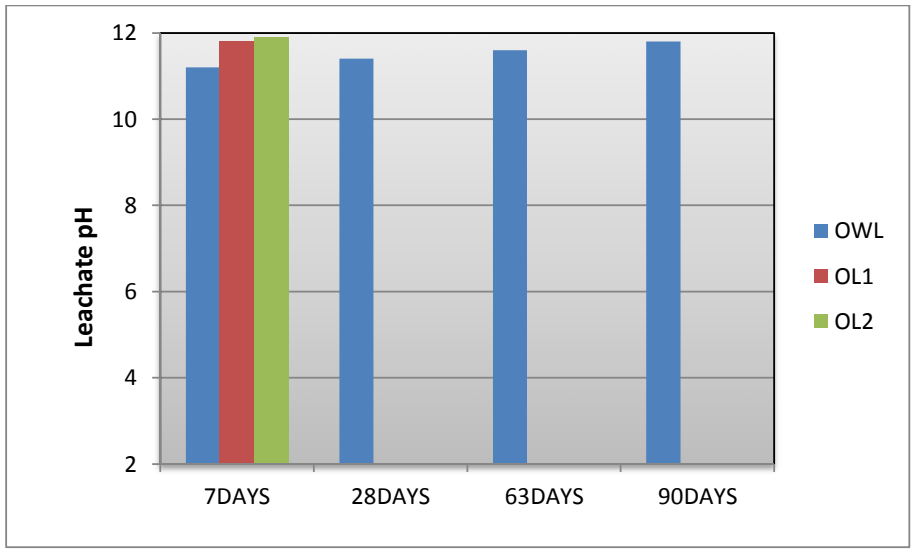

FIG. 4. Showing the mean value of all the result of the mixes at various curing days.

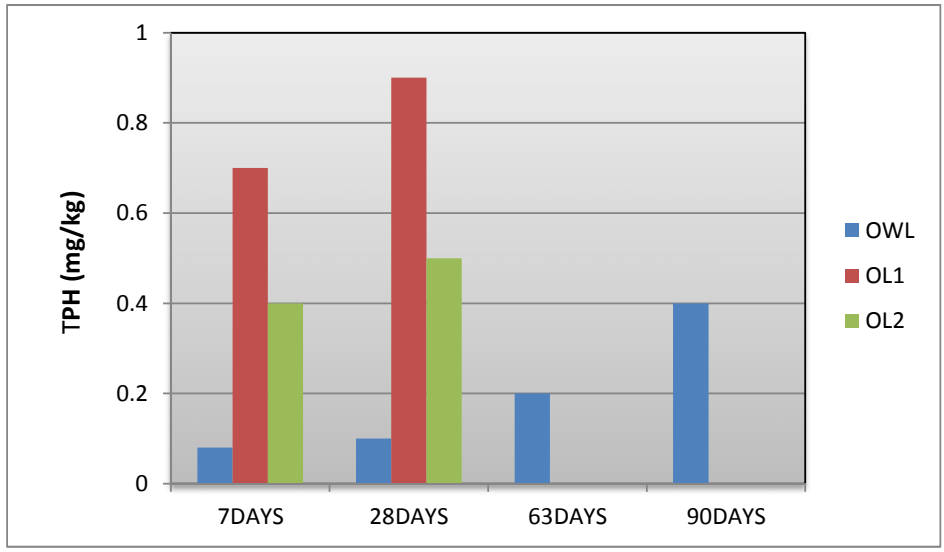

FIG. 5. Showing the mean value of all the result of the mixes at various curing days.

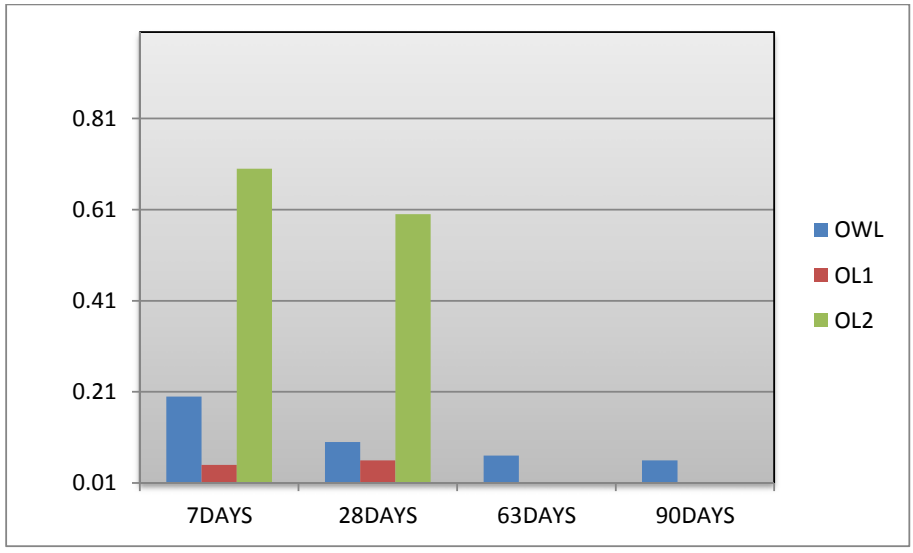

FIG. 6. Showing the mean value of all the result of the mixes at various curing days.

Leachability and Leachate pH

The leachate pHs for all the mixes was higher alkaline ranges from 10.5 to 12 and show a maximum margin of error of ± 0.1. The corresponding TPH value decrease with an increase in curing days for mix WL1 while the reverse was the case of OL1and OL2 mixes. The total Heavy metal (THM) was all much lower and generally under 1.0mg/kg and shows a maximum margin of error of ±3%.

CONCLUSION

It is clear that the total metal concentration leached were extremely low. The mixes satisfied the threshold value required and it is expected that longer period of curing will bring about higher UCS values. Further investigations should be carried out to assess the adsorptive capacity of the different binders and their performance at different binder content. Further investigation should also be carried out to examine means of improving the leachability of the binders. While the original intention of this work presented here was to be able to perform comparison between binders and composition, this was not directly possible given the various differences between the curing days of the mixes.

REFERENCES

Allan, M.L. and Kukacka, L.E. (1995). 'Blastfurnace slag-modified grouts for in-situ stabilisation of chromium contaminated soil'. Waste Management: 15(3):193-202.

Al-Tabbaa, A. and Evans, C.W. (1998). Pilot in situ auger mixing treatment of a contaminated site. Part 1: treatability study. Proceeding of the institution of Civil Engineers, Geotechnical Engineering. Vol. 131, pp 52-59.

Conner, J.R. (1990) Chemical Fixation and Solidiifcation of Hazardous wastes, Van Nostrand Reinhold.

Banaszkiewicz, K.P and Marcinkowski , T.(2007). Studies on solidification of wastes from metal Coating. Polish Journal of chemical Technology, Vol. 9,3, pp. 51-55.

Harris. M.R,Herbert, S.M. and Smith, M.A. (1995). Remedial treatment for contaminated land, Vol. IX: In-situ methods of remediation. Construction Industry Research and Information Association. Special Report No. 109, pp 121-131.

Johnson, D. 2004. Personal Communication

LaGrega, M.D., Buckingham,P.L& Evans, J.C. (1994) Hazardous Waste management, McGraw-Hill.

Lewin, K.,Bradshaw, K., Blakey,N.C., Turrell, J.,Hennings,S.M and Flavin,R.J.(1994) Leaching tests for assessment of contaminated land:Interim NRA guidance, *NRA R&D Note 301*,Bristol,UK.

Meegoda, J.N., Ezeldin, A.S., Fang, H.Y and Inyang, H.I. 2003. Waste immobilization Technologies, Practice Periodical of Hazardous, Toxic and Radioactive Waste Management 7, No. 1, 46-58.

Stegemann, J.A and Cote, P.L.(1990).Summary of an investigation of test methods for solidified waste evaluation. Waste management 10:41-52.

Stegemann, J.A and Cote, P.L. (1991).Investigation of test methods for solidified waste evaluation.Appendix B: Test methods for solidified waste evaluation. Environment Canada

Topolnicki, M., (2004),"In situ Soil Mixing, Chapter 9 in Ground Improvement book" Editors Moseley, M. and Kirsch, K., Spon Press, pp. 331-428, 2004.

Van der Sloot, .H.A., de Groot G.J and Wijkstra .J. (1989). 'Leaching Characteristics of Construction Materials and Stabilization'.

Wiles. C.C. 1987. A Review of Solidification/Stabilization Technology. Journal of Hazardous Materials, 14: 5-21.

VOC Emission Monitoring at Eagle Ford Shale Drill Sites using Wireless Sensor Network for Understanding Emission Generation and Dispersion

Nikhil Mantrawadi[1], Mais Nijim[2*], David Ressegiue[3], Gerald Ogumerem[4]., Lee Clapp[5], Ph.D., Alvaro Martinez[6], Ph.D.

[1]Research Assistant, Texas A&M University-Kingsville, TX 78363, U.S.A., E-mail: nikhil.mantrawadi@students.tamuk.edu
[2]Associate Professor- Department of Electrical Engineering & Computer Science, Texas A&M University-Kingsville, TX 78363, U.S.A., E-mail: mais.nijim@tamuk.edu
[3]Research Staff- Computational Science and Engineering Division, Oak Ridge National Laboratory, TN 37831, U.S.A., E-mail: resseguiedr@ornl.gov
[4]Research Assistant, Texas A&M University-Kingsville, TX 78363, U.S.A
[5]Associate Professor- Department of Environmental Engineering, Texas A&M University-Kingsville, TX 78363, U.S.A., U.S.A., E-mail: lee.clapp@tamuk.edu
[6]Associate Professor- Department of Environmental Engineering, Texas A&M University-Kingsville, TX 78363, U.S.A., U.S.A., E-mail: alvaro.martinez@tamuk.edu

ABSTRACT: With the exploration of the Eagle Ford Shale challenges come in disguise. The emission of Volatile organic compounds (VOC's) may have serious environmental and health impacts. High level of exposure to VOC can also happen at high traffic areas and cities having larger percentage of older vehicles.

This paper presents methods used for development of improved understanding of VOC sources and dispersion at hydraulic fracturing sites.

A coherent infrastructure is needed to treat sensors and the generated data in an interoperable, platform independent and uniform way. The composite ambient air non-methane hydrocarbons (TNMH) levels can be effectively monitored. We also integrate a weather station to gather information on wind speed/direction at the fracturing site to build a correlation between the VOC and its dispersion in surrounding air.

The ability to efficiently and effectively measure the concentrations of VOCs helps to better our understanding in reducing the VOC imprint and its adverse effect on individuals working at the drill site.

INTRODUCTION

The Eagle Ford Shale (EFS) is conceivably the largest single economic advancement in the history of the State of Texas and is also the largest oil and gas

development in the world based on capital invested (Duke, 2012). It has engendered a lot of changes, ranging from an exponential population increase within the region to environmental impacts associated with such heavy drilling activity. Among the environmental issues are air emissions of reactive volatile organic compounds (VOCs). The oil and gas industry is the largest industrial source of VOCs emission [1]. EPA recently issued a NSPS rule for gas wells and related operations that will take effect on January 1, 2015. The rule requires operators to develop detection and repair programs for fugitive emissions (EPA, 2012). In the past, monitoring of VOC air emissions at drilling sites was limited due to high costs. However, with the recent availability of low-cost photo-ionization detectors (PIDs), with detection limits down to the low ppb range, it is now easier to implement continuous VOC monitoring at drilling sites.

EQUIPMENT

We have integrated sensing technology with ambient air sampling canisters and a weather monitoring station, supported by specialized devices capable of carrying out EPA's TO-15 gas chromatography-mass spectrometry (GC-MS) method. Figure 1 shows the ppbRAE PID 3000 sensors kit used to identify and measure volume of VOC emissions.

FIG.1. ppbRAE PID 3000 sensor with its RAE link telemetry equipment.

Figure 2 shows the Anemometer and weather station, which helps us determine the dispersion of VOC emissions during a given time sample.

FIG.2. Weather station

METHODS, STUDY AREA AND DATA SOURCE DESCRIPTION

The monitoring equipment will be deployed at several hydraulic fracturing sites. Baseline data will be collected before drilling starts, and will continue during the drilling, fracturing, completion, and production stages. To date, two sites have been visited. The first site (in La Salle Co.) was already in the production phase. The second site (in DeWitt Co.) is a private property surrounded by six well pads, all in the drilling stage. At both sites the weather station was set up (with a solar panel as the power source) to record the wind speed and direction. The PID detectors and related telemetry were set up at different locations to continuously monitor VOC concentrations. The PID sensors used have a detection limit of approximately 1 ppb (with a range of 1 to 10,000 ppm), a three-second-response time, and humidity compensation. The data was gathered for a sample time of two hours with time duration of 1 minute. A summa canister was deployed next to one PID detector to collect time-averaged ambient air samples for subsequent GC-MS analyses back at the lab. The coordinates of the weather station and PID detectors were recorded using a GPS receiver.

RESULTS

The preliminary deployment of sensor at the La Salle County and DeWitt County drilling sites show a promising future for the use of wireless sensors for extensive monitoring of frack sites.
Figure 3 shows the placement of the sensors at an actual drill site.

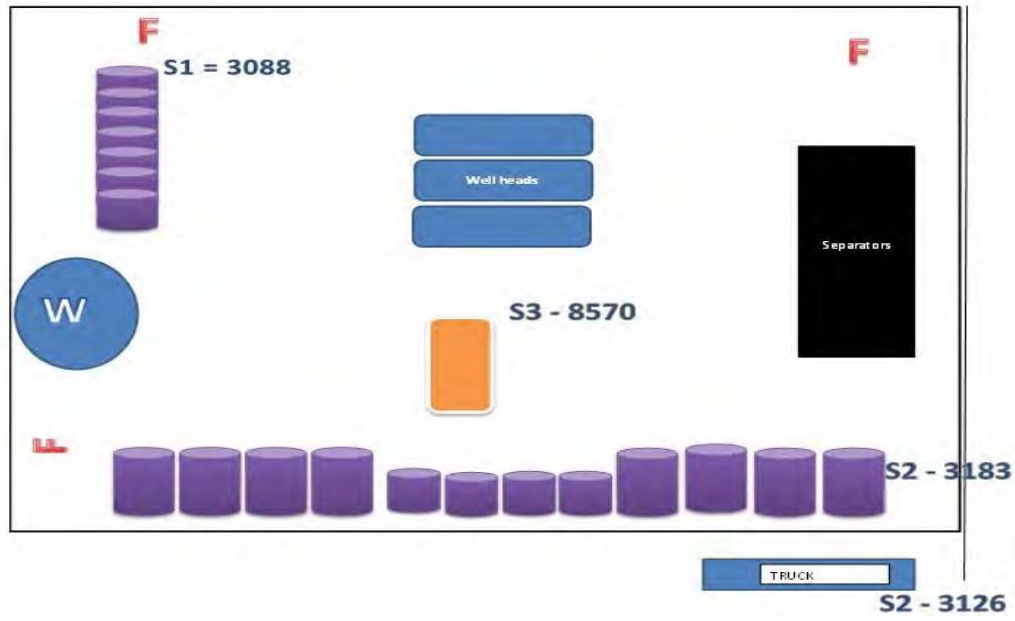

FIG.3. LaSalle County drill site schematic

The PID data represents 10 minute averages.

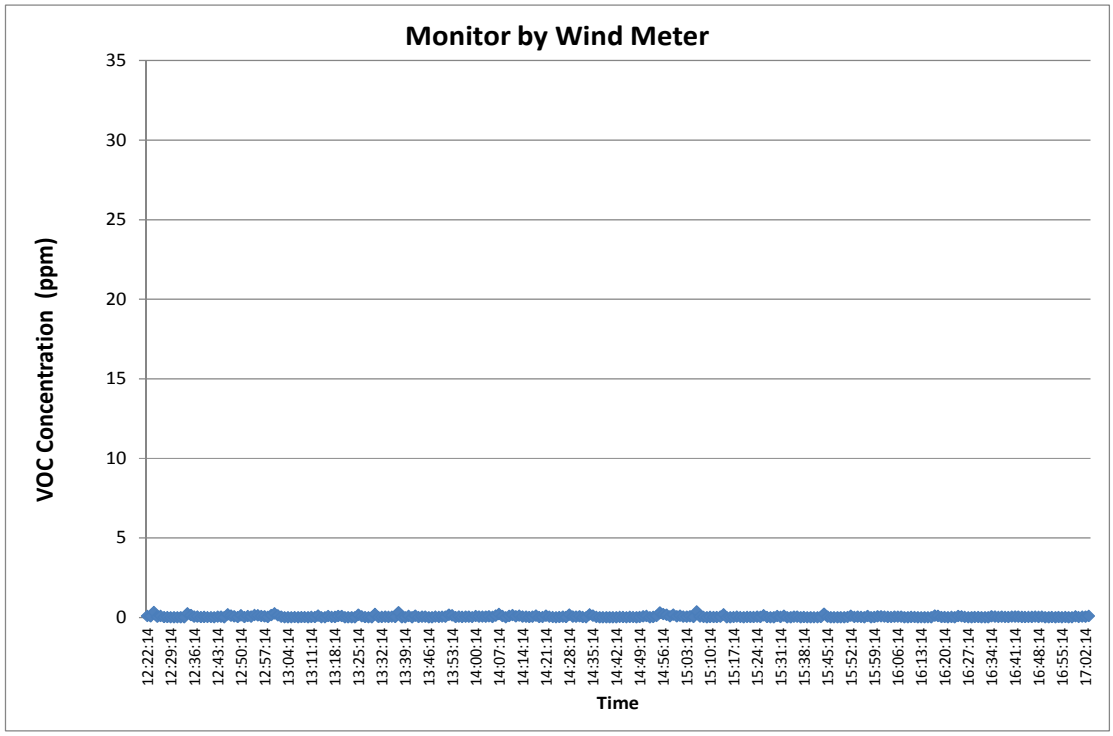

FIG. 4. VOC measurement by sensor 3126 placed on weather station

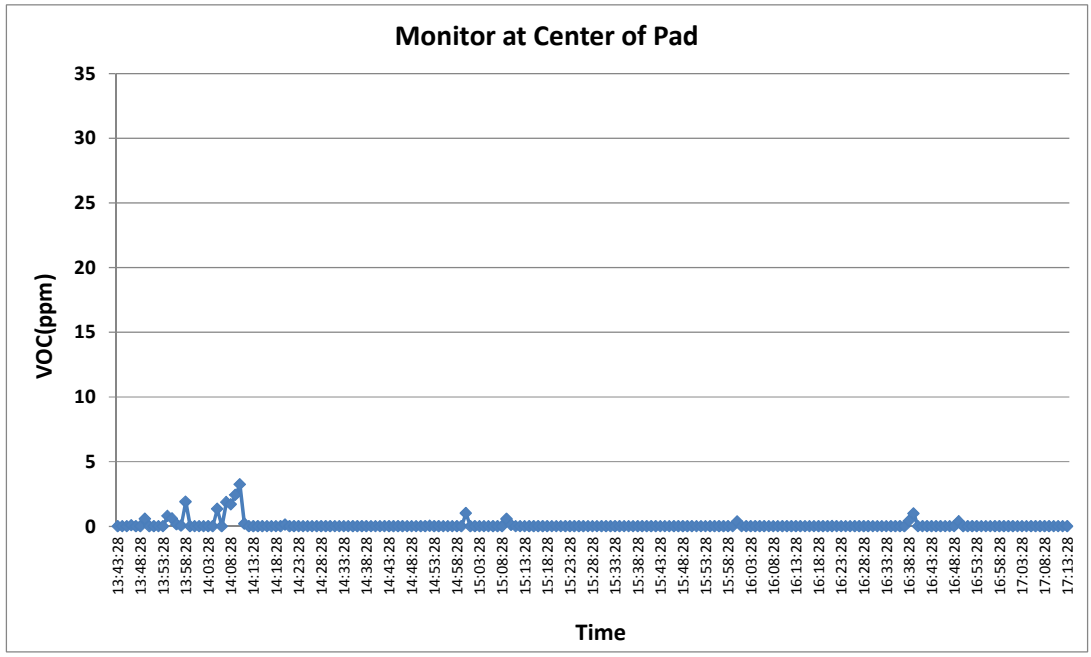

FIG. 5. Sensor data from middle of pad 8570

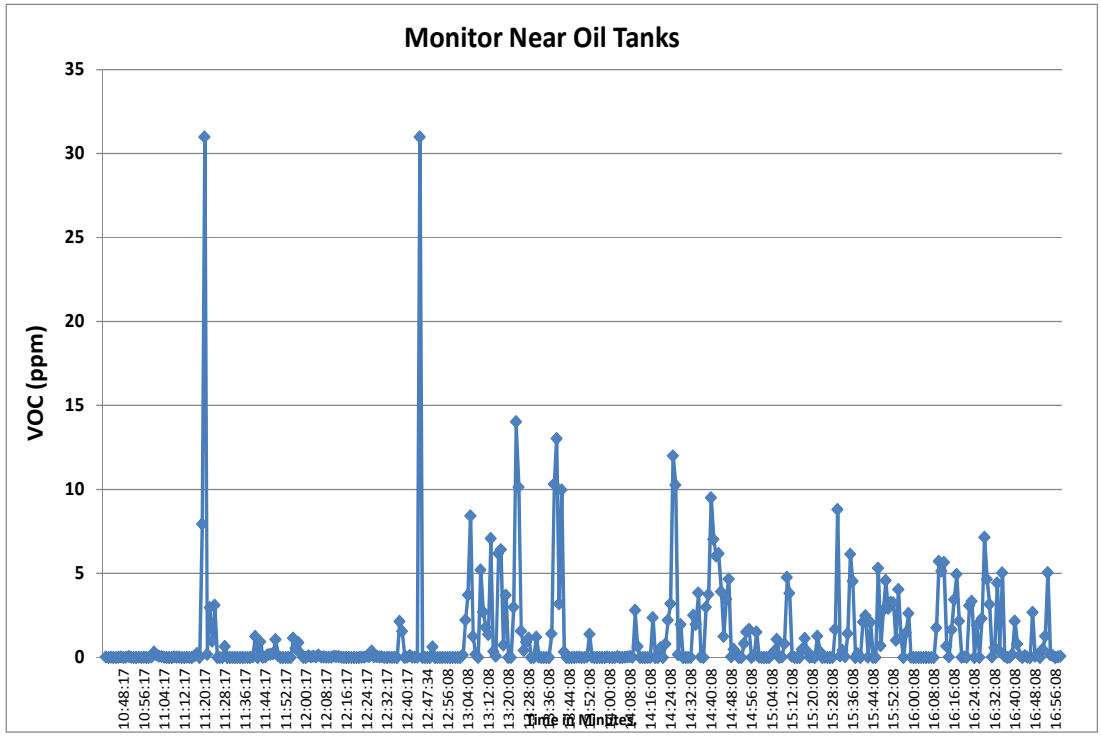

FIG. 6. Sensor values for 3088 near oil tanks on pad

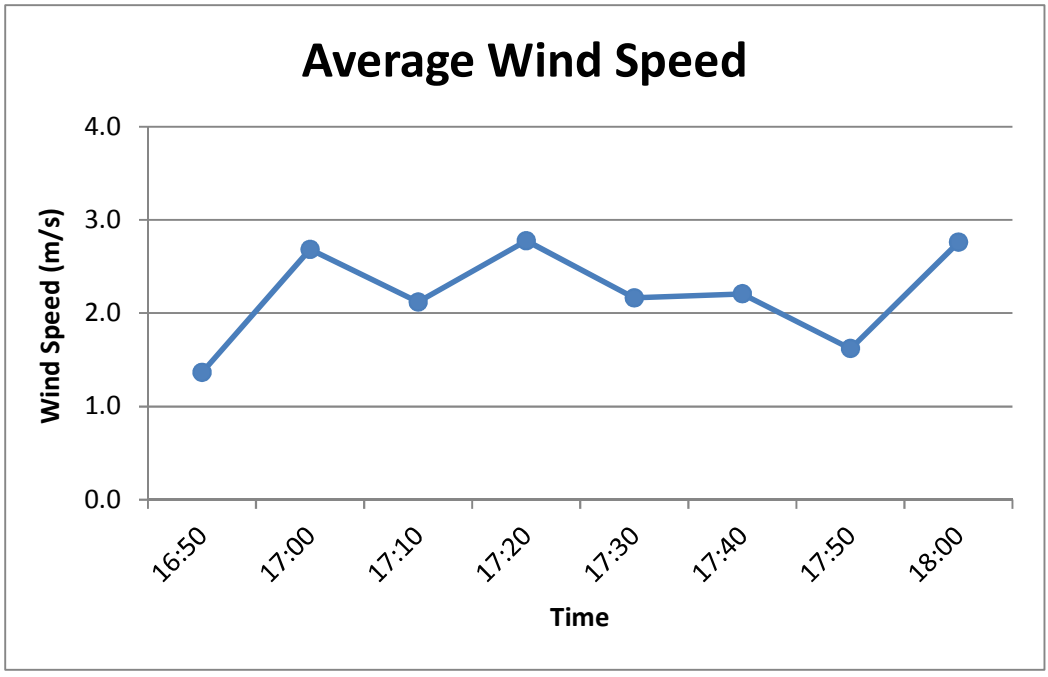

FIG. 7. Wind speed analysis on LaSalle county to understand VOC dispersion

Figure 8 through Figure 10 shows the graphical representation of wind speed, wind direction and VOC emission on the DeWitt County drill site.

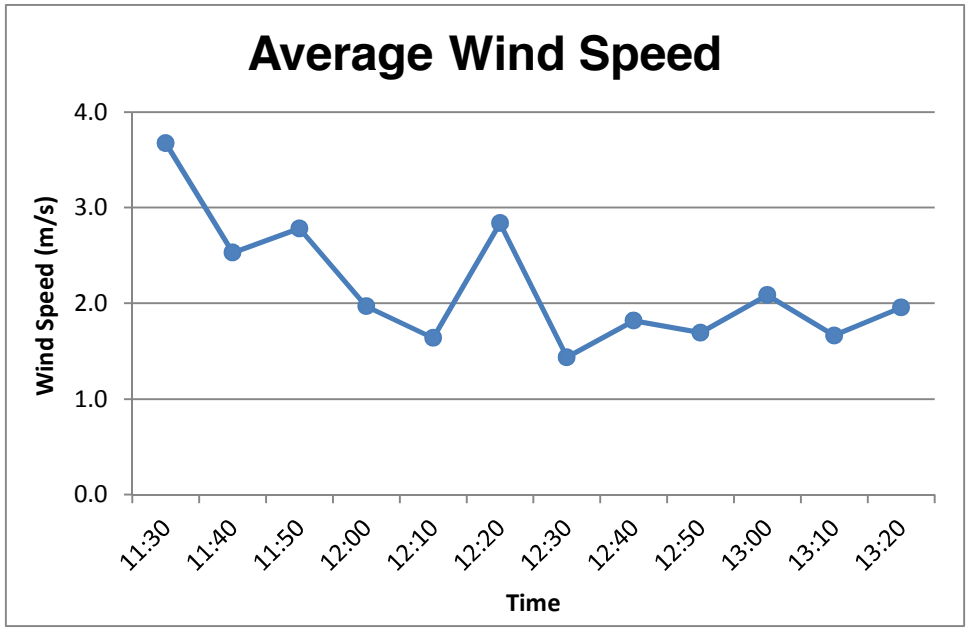

FIG.8. Average wind speed over 2-hour duration on site

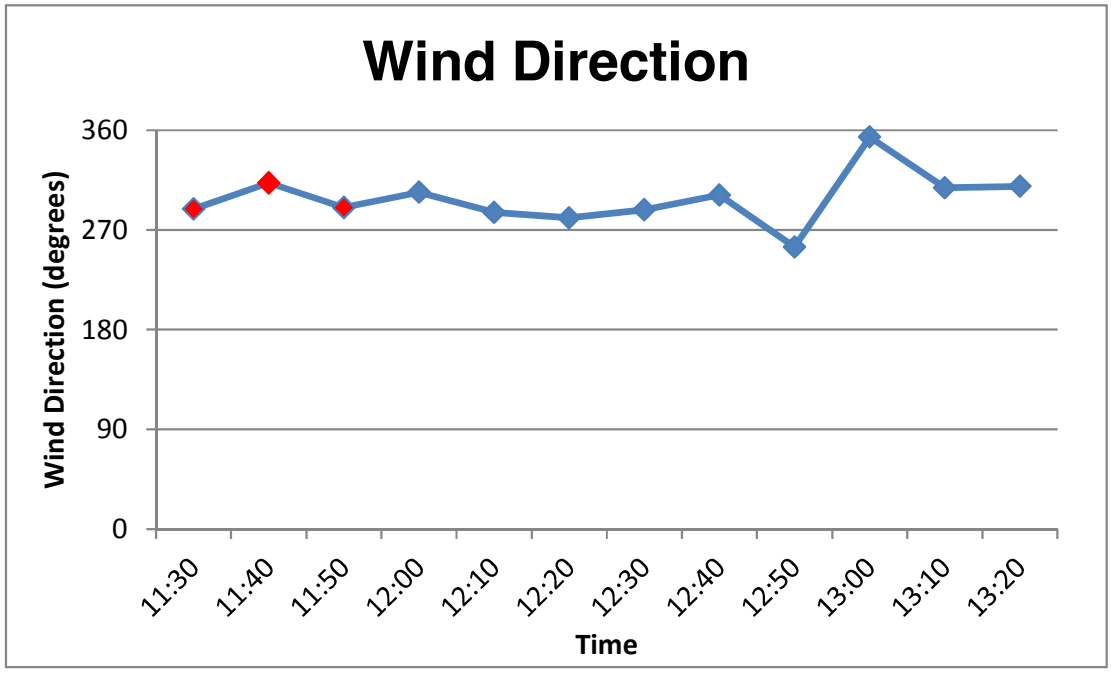

FIG.9. Direction of wind on pad over 2 hour sample period

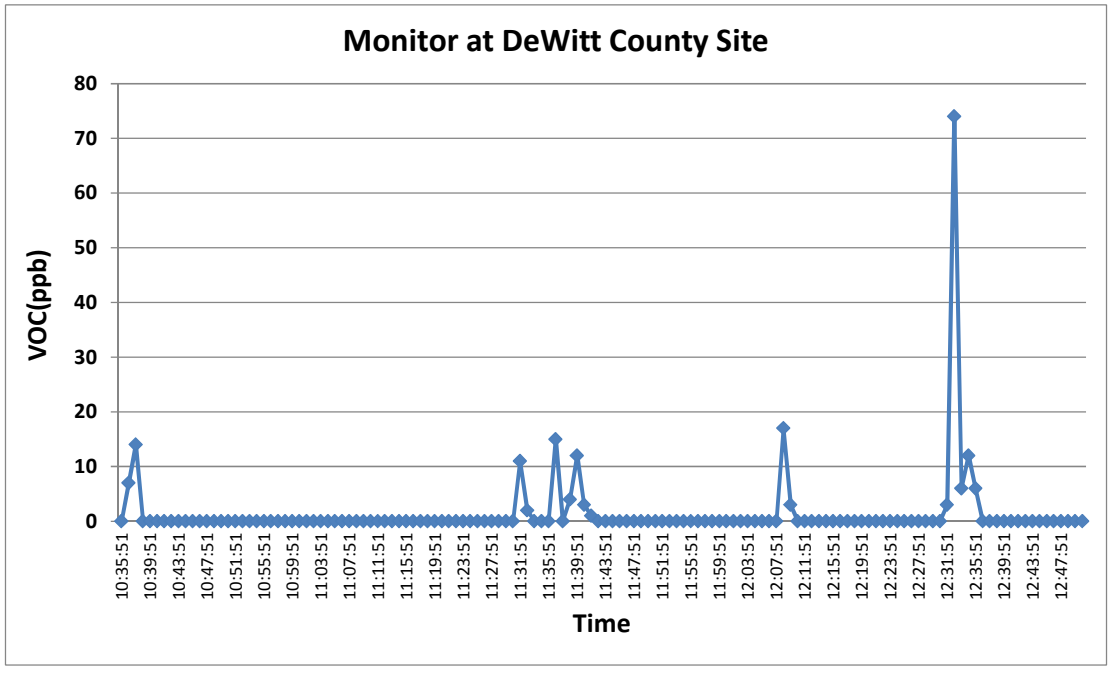

FIG.10. VOC emissions on DeWitt county site over two hour sample time

FUTURE WORK

Results obtained so far are positive and promising. The hydraulic fracturing sites are remote and hence it is impossible to man the sensors round the clock. However, it is imperative to continuously monitor VOC emissions from the drilling sites to meet

pending EPA regulations. The integration of wireless sensor data with a real time framework would enable sensor data to reach labs for analysis and facilitate real time monitoring of VOC emissions from the sensed drilling pad.

One method proposed is the use of a platform named "Sensorpedia". Sensorpedia is a program initiated by Oak Ridge National Laboratory (ORNL) that utilizes Web 2.0 and social networking principles for organizing and providing access to online sensor network data and related data sets. Sensorpedia can be used to share and discover a variety of sensor information online. It would facilitate statistical tools for visualization of data. The transport of data from remote drilling sites is a two-step process. In the first phase, near real time emission data from the on-site computer is transferred to the TAMUK server. Figure 11 below shows example data from the sensors saved in an Excel file format. This file is sent every 12 hours to the Texas A&M University- Kingsville lab for further processing. In the second phase, the data is translated and sent to ORNL's Sensorpedia server from TAMUK.

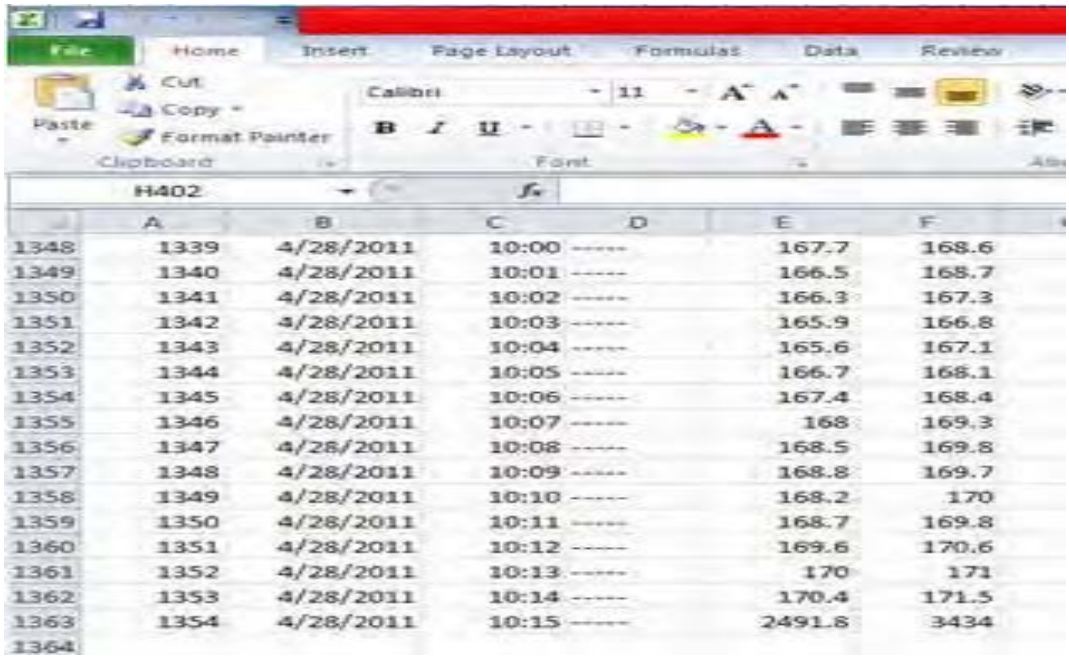

	A	B	C	D	E	F
1348	1339	4/28/2011	10:00	-----	167.7	168.6
1349	1340	4/28/2011	10:01	-----	166.5	168.7
1350	1341	4/28/2011	10:02	-----	166.3	167.3
1351	1342	4/28/2011	10:03	-----	165.9	166.8
1352	1343	4/28/2011	10:04	-----	165.6	167.1
1353	1344	4/28/2011	10:05	-----	166.7	168.1
1354	1345	4/28/2011	10:06	-----	167.4	168.4
1355	1346	4/28/2011	10:07	-----	168	169.3
1356	1347	4/28/2011	10:08	-----	168.5	169.8
1357	1348	4/28/2011	10:09	-----	168.8	169.7
1358	1349	4/28/2011	10:10	-----	168.2	170
1359	1350	4/28/2011	10:11	-----	168.7	169.8
1360	1351	4/28/2011	10:12	-----	169.6	170.6
1361	1352	4/28/2011	10:13	-----	170	171
1362	1353	4/28/2011	10:14	-----	170.4	171.5
1363	1354	4/28/2011	10:15	-----	2491.8	3434
1364						

FIG.11. Sensor data saved as a Microsoft Excel spreadsheet file.

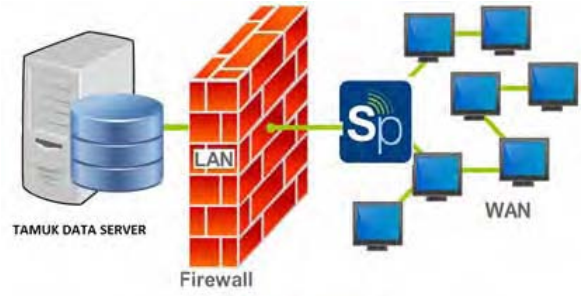

FIG. 12. Framework for uploading near real time VOC data to Sensorpedia.

Figure 12 below shows the architecture for transfer of data from TAMUK lab to ORNL's Sensorpedia for study, analysis and real time hosting. Sensorpedia is comprised of two parts: the Web application itself and the underlying Web services. The Web application helps to explore information within the Sensorpedia framework. The end user can search for sensor data and view information from multiple sources and sensors side-by-side on a geo-referenced map supported by Google.

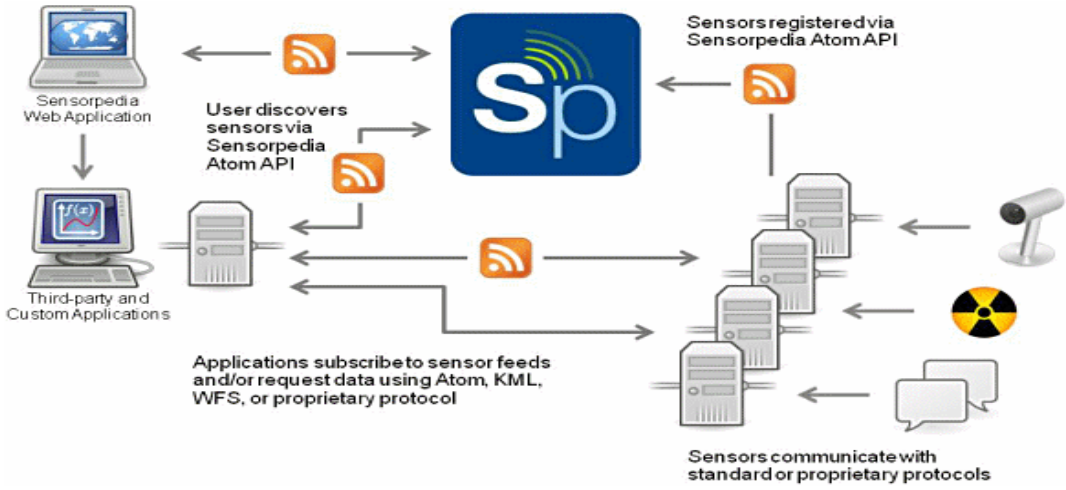

FIG.13. User interface for Sensorpedia

Sensorpedia has been designed to work with both legacy and standards-based sensors such as those that support the Open Geospacial Consortium's Sensor Web Enablement (SWE) suite of standards. Figure 14 demonstrates the use of a SWE-to-Sensorpedia translation tool for registering one or more SWE sensor systems with Sensorpedia [sensormag]. This approach would enable the expansion of monitoring efforts in the future through the inclusion of standards-based sensor data.

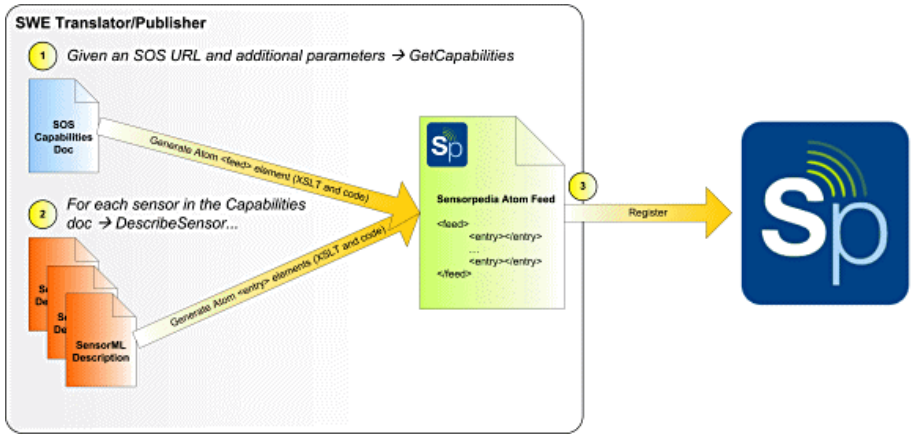

FIG.14. Translator tool maps SWE sensor information into Sensorpedia formats.

The final step would be developing a data visualization module for graphical

display of sensor information that supports policy making to reduce VOC emissions.

CONCLUSIONS

The results from the field trial conducted show a significant amount of VOC emissions traced on an Eagle Ford shale site. We have presented methods that may be used to improve understanding of VOC sources and dispersion at hydraulic fracturing sites. The field trials started by sample data collection from the oil pads. A more extensive deployment of sensors covering the entire drill operation process from initiation to post recovery of oil would be extremely beneficial to trace the VOC gas imprint on the adjoining community of the Eagle Ford Shale gas site. A rapid development of web interface technology discussed in Future Work needs to be tested and deployed to help retrieve data on a regular basis from the drilling pad.

ACKNOWLEDGMENTS

The authors appreciate the support of the Houston Advance Research Center (HARC) Environmentally Friendly Drilling Systems program and the Department of Energy for funding and support the research program.

REFERENCES

U.S. Environmental Protection Agency(2012) http://www.epa.gov/airquality/oilandgas/basic.html

The Eagle Ford Shale – News, MarketPlace, Jobs (2012). Retrieved on July 17, 2012

Duke, R. (2012). Eagle Ford Shale Play. San Antonio, TX: http://eaglefordshale.com/.

Arkansas Department of Environmental Quality (2011). Emissions Inventory & Ambient Air Monitoring of Natural Gas Production in the Fayetteville Shale Region**.**

U.S. Environmental Protection Agency (2012). "EPA Issues Final Air Rules for the oil and Natural Gas Industry." Retrieved on July 17, 2012 from http://www.epa.gov/airquality/oilandgas/actions.html .

McKenzie, L. M. (2012). Human health risk assessment of air emissions from development of unconventional. *Science of the Total Environment*, 79-87.

Lee Clapp, Mais Nijim. (2012). Wireless Sensor Network for Monitoring VOC Levels near Drilling Operations. Kingsville, TX: Environmental Friendly Drilling Kick-Off Meeting (San Antonio, TX).

http://www.sensorsmag.com/networking-communications/unifying-isolated-sensor-systems-using-web-20-and-open-stand-7107

Life Cycle Assessment of Air Toxics for Natural Gas Production, Transport and Power Generation in the Marcellus Shale Region.

David D. Good[1,2], Jorge Abad[3], Ph.D., and Vikas Khanna[4], Ph.D.

[1]Air Pollution Control Engineer, Allegheny County Health Department, 301 39th St., Pittsburgh, PA 15201, U.S.A., E-mail: dgood@achd.net.
[2]Graduate Student, Department of Civil & Environmental Engineering, University of Pittsburgh, 742 Benedum Hall, 3700 O'Hara Street, Pittsburgh, PA 15261, U.S.A., E-mail: ddg14@pitt.edu.
[3]Assistant Professor, Department of Civil & Environmental Engineering, University of Pittsburgh, 742 Benedum Hall, 3700 O'Hara Street, Pittsburgh, PA 15261, U.S.A., E-mail: jabad@pitt.edu.
[4]Assistant Professor, Department of Civil & Environmental Engineering, University of Pittsburgh, 742 Benedum Hall, 3700 O'Hara Street, Pittsburgh, PA 15261, U.S.A., E-mail: khannav@pitt.edu.

ABSTRACT: Fossil fuel power generation technologies offer a number of alternatives, which involve different fuel supply, production, power generation, and pollution control devices with varied environmental impacts. The holistic approach to examining these impacts through Life Cycle Assessment (LCA) can help decision makers to quantify the many emissions trade-offs inherent in any change to the fuel supply and power production systems and ensure that a change in fuel or fuel sourcing does not result in increases of other environmental and health impacts. Besides endpoint emissions exiting from a smokestack in natural gas-fueled power generation, air toxics such as formaldehyde, benzene and xylenes are also generated through the supply chain from compressor engines, oil/condensate tanks, as well as intermittent sources such as well drilling and fracturing engines, well completions, gas processing, and also fugitive emissions from production and transmission. These emissions sources differ in quantity, species, spatially and in overall risk to the surrounding population. People exposed to air toxics at sufficient concentrations and durations may have an increased risk of developing cancer or experiencing other serious health effects. The purpose of this paper is to identify the appropriate air toxics emission factors for natural gas production and utilize a LCA approach to quantify the "cradle-to-gate" air toxics emissions in terms of one (1) kWh of electricity generated.

INTRODUCTION

Besides endpoint smokestack emissions in natural gas-fueled electricity generation such as cadmium, nickel and dioxins, air and water emissions are generated throughout the entire supply chain. Water discharge emissions such as lead, arsenic and beryllium are released during the drilling and processing of natural gas. Air toxics emissions such as formaldehyde, benzene and xylenes are also generated through the supply chain from compressor engines, oil/condensate tanks, as well as intermittent sources such as well drilling and engines, well completions, gas processing, and also fugitive emissions from production and transmission. The methodology to arrive at these estimates comes into question as many of the emission factors used to derive these estimates are poorly rated, out of date, incongruent with shale gas formations, or simply ignored because of the uncertainty attributed to them (Stuver et al., 2012). Additionally, control technologies and regulations (NSPS, NESHAP) that minimize the generation of air toxics have not been fully explored.

Similarly, the air emissions exiting from a smokestack in coal-fueled electricity generation include metals of arsenic, lead and selenium. Additional processes of coal-fueled electricity generation like crude oil production, natural gas extraction and diesel fuel combusted at industrial boilers create additional air and water emissions (Meij et al., 2007). These emissions from various sources differ in quantity, species, phase, spatially and in the overall increased risk to the surrounding population.

The purpose of this project is to identify and compare the complete spectrum of air and water emissions for natural gas and bituminous coal-fueled electricity production and utilize a LCA approach to quantify the "cradle-to-gate" human health impact in terms of one (1) kWh of electricity generated (kg/kWh). Carcinogenic and non-carcinogenic impacts are measured by characterizing the air and water emissions as benzene and toluene equivalents, respectively. Further examination, speciation, characterization and comparison of the air emissions has also been performed. This paper will serve to generate an inventory of emissions and also be of use to future studies interested in identifying environmental 'hot spots', optimizing the capture and control of emissions, and modeling the spatial distribution of health risk from exposure to emissions along the supply, transmission and generation chains of electricity generated from natural gas and coal.

System Description

Natural Gas

Natural gas-fueled electricity generation processes include gas extraction, gas processing, pipeline transmission and electricity generation. Gas extraction includes processes such as well construction, vertical drilling, and venting and flaring of the gas as needed. Natural gas and diesel fuel are used to power the engines that provide the power needed to extract raw gas from the subsurface. Processing includes compressing, dehydrating and acid removal necessary to make the gas into a commercial pipeline quality fuel. Transmission delivers the fuel to the point of electricity generation by way of a pipeline. Finally, the electricity generation process

combusts the natural gas in a turbine or boiler to produce steam and create electrical power. Air and water emissions are generated by the combustion of the gas, extraction and the subsequent treatment of the effluent waste streams.

Bituminous Coal

Bituminous coal-fueled electricity generation processes include coal extraction, transportation, and power generation (primarily combustion). Coal extraction involves the mining of bituminous coal from seams well below the surface. Transportation processes deliver the fuel to the point of electricity generation by way of a barge, railroad car, or truck. Finally, the electricity generation process combusts the coal in a chamber connected to a boiler to produce steam and create electrical power. Significant air and water emissions are generated by the combustion of the coal and the subsequent treatment of the effluent waste streams.

Goal and Scope

The findings of this study are intended to help improve external public communication regarding the benefits and risks of deriving energy from natural gas or bituminous coal. The goal of this LCA is to identify all emissions from the process supply chain of natural gas and typical bituminous coal energy production from extraction of fuel to electricity generation (cradle to gate) and quantify their impact on human health. The results are to serve as a basis for further research into the spatial distribution of carcinogenic and non-carcinogenic risk from both fuel supplies.

The system boundaries for each fuel are the primary processes to extract and process the fuels along with the transportation and power generation processes. They are further defined above in the System Description section. Secondary processes to create the fuel and power necessary to extract and transport the fuels were also included. More exhaustive processes such as infrastructure development and all processes after electricity generation were not considered in this study.

The environmental impacts examined in this study were the carcinogenic and non-carcinogenic human health impacts from the air and water emissions generated during natural gas and bituminous coal-fueled electricity production. The emissions were quantified and then further characterized in terms of kg of benzene and toluene equivalents for carcinogenic and non-carcinogenic health effects, respectively. The functional unit chosen for these emissions is one (1) kWh of electricity generated.

METHODS AND DATA SOURCES

The method used in this study is process-based Life Cycle Assessment, which has been codified by ISO's 14040 standard (ISO, 2006). In this method, the product system (natural gas and bituminous coal electricity generation) is broken down into individual unit processes (UP) where input and output data are quantified. Elementary flows are aggregated from other data sources to provide average input and output data for each UP. The system boundary specifies which unit processes are included as part of the product system and prevents infinite data disaggregation and computations by ultimately restricting the scope of the study.

Life Cycle Inventory (LCI) for this study was generated through the commercial software program SimaPro7. The data sources used for the product system and unit processes are from USLCI and are incorporated into SimaPro7 (USLCI, 2012). The unit processes are based on data derived from sources in the United States. The inventory results, therefore, should be interpreted to be relevant to electricity generation in the USA.

Life Cycle Impact Assessment (LCIA) was performed using the Tool for the Reduction and Assessment of Chemical and Other Environmental Impacts (TRACI) LCIA method through SimaPro7. TRACI LCIA was developed by USEPA to provide characterization factor units for different impact category indicators (Bare, 2002). The category indicators evaluated in this study are Human Health Cancer and Human Health Non-cancer and the characterization factor units are benzene equivalents/kg emission and toluene equivalents/kg emission, respectively. The characterization factors used for this study are based on data from TRACI 2 version 3.01.

RESULTS

Inputs and Outputs

The inputs for natural gas-fueled electricity generation were 0.323 m^3 of natural gas, 0.0025 kg crude oil and 0.0045 kg of coal (26.4 MJ per kg). All inputs were assumed to be "in ground" elementary flows. The outputs were the chosen functional unit of 1 kWh of electricity, 0.645 kg of air emissions an 0.101 kg of water emissions.

The inputs for coal-fueled electricity generation were 0.0015 m^3 of natural gas, 0.008 kg crude oil and 0.5185 kg of coal (26.4 MJ per kg). All inputs were assumed to be "in ground" elementary flows. The outputs were the chosen functional unit of 1 kWh of electricity, 1.047 kg of air emissions an 0.0034 kg of water emissions.

Life Cycle Inventory

209 unique air and water emissions were identified in the LCI for both product systems. 110 of the compounds were air emissions and 63 of those meet the definition of "Air Toxic", in that they have a defined inhalation toxicity value by the USEPA Integrated Risk Information System (EPA IRIS), CalEPA or Provisional Peer Reviewed Toxicity Values Database (PPRTV). 51 of the 110 air emissions had a TRACI characterization factor for either carcinogenic or non-carcinogenic human health impact.

The majority of the emissions released from the natural gas and bituminous coal product systems are air emissions. Air emissions represent 86.5% of total emissions from natural gas and 99.7% of the total emissions from bituminous coal, by weight. Fig. 1 below compares the air emissions to the total emissions.

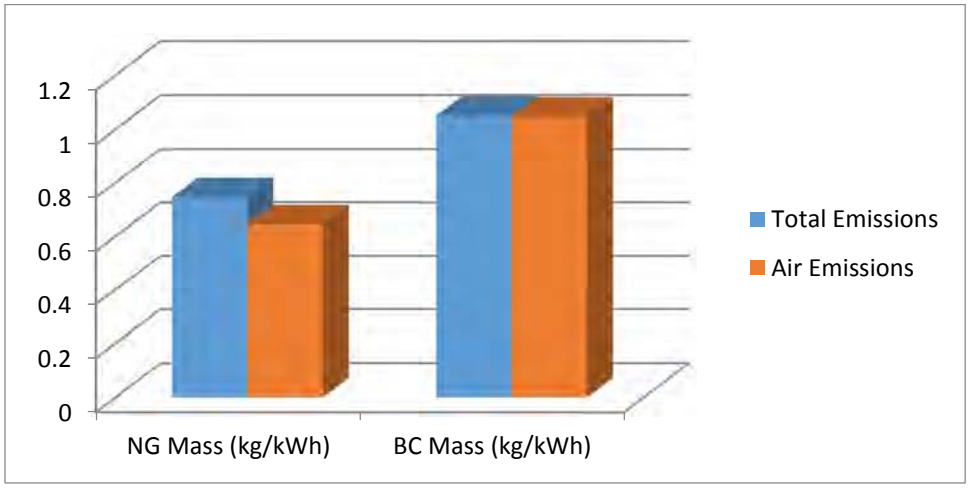

FIG. 1. Mass of air emissions compared to mass of total emissions.

The largest air emissions for coal are carbon dioxide, sulfur dioxide, nitrogen oxides, methane and unspecified particulates. The largest air emissions for natural gas are carbon monoxide, sulfur dioxide, methane, nitrogen oxides and carbon monoxide. In Fig. 2 it is shown that Air Toxics only make up 0.001% of the total air emissions from natural gas and 0.03% of the total air emissions from coal, by weight. TRACI LCIA emissions characterizations were not able to quantify all air emissions. Characterization could only be made for 35.1% of the air toxics for natural gas and 87.1% of the air toxics for bituminous coal, by weight.

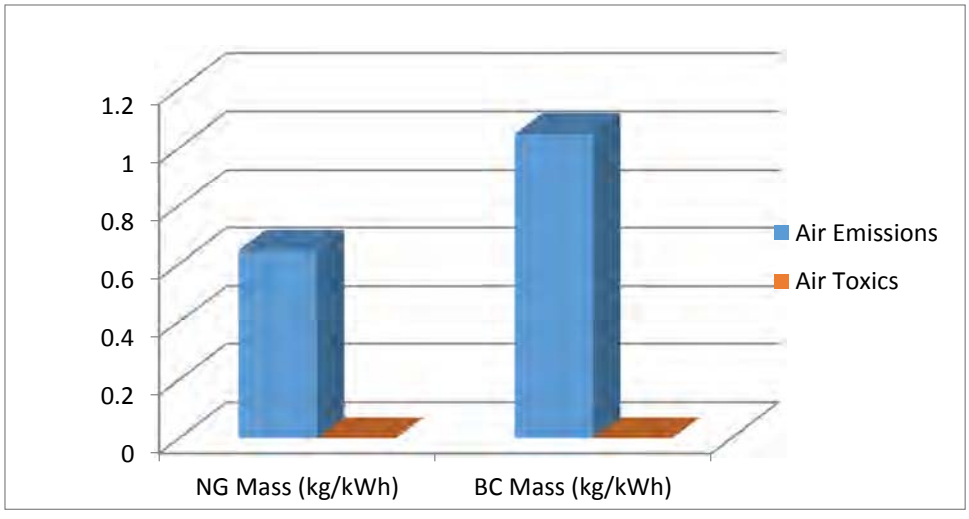

FIG. 2. Mass of air toxics emissions compared to mass of total air emissions.

The largest water emissions for coal are dissolved solids, chloride, sodium ion, suspended solids and calcium ion. The largest water emissions for natural gas were dissolved solids, chloride, sodium ion, calcium ion and lithium ion. The total mass of water emissions was significantly larger (27.7 times) for natural gas than bituminous coal, as seen in Fig. 3.

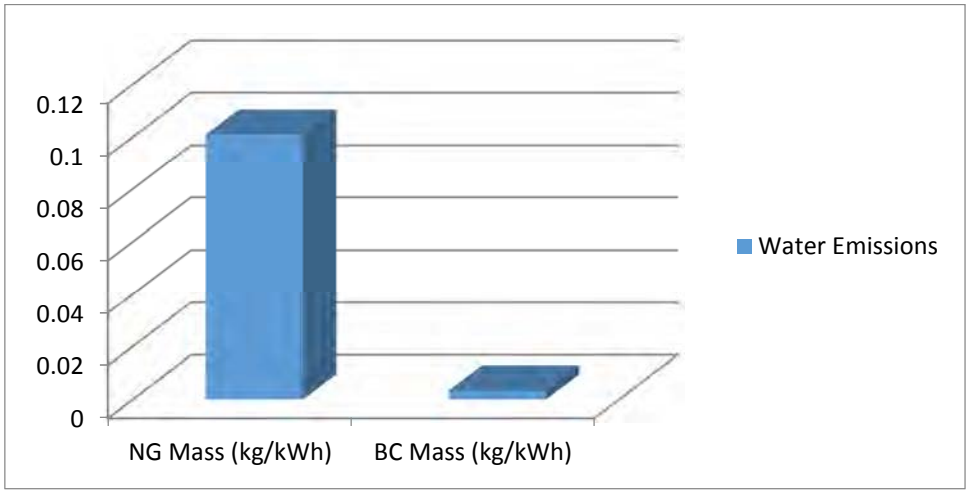

FIG 3. Mass of water emissions.

Life Cycle Impact Assessment

The life cycle human health impacts are summarized in Fig. 4 below. Carcinogenic impact is 4.3 times higher for bituminous coal than natural gas, as seen in Fig. 5. Non-carcinogenic impact is 6.7 times greater for natural gas, as seen in Fig. 6.

Impact Category	Unit	Electricity, natural gas (kg/kWh)	Electricity, bituminous coal (kg/kWh)
Carcinogenics	kg benzene eq	0.00020	0.00086
Non carcinogenics	kg toluene eq	3.85	0.58

FIG. 4. Carcinogenic and non-carcinogenic human health impact.

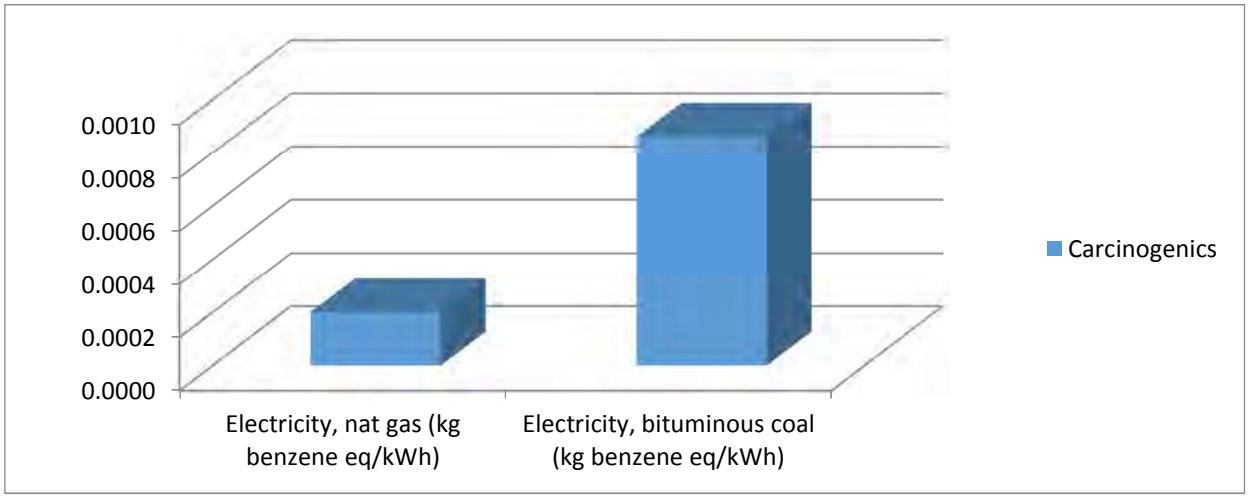

FIG. 5. Carcinogenic human health impact in kg benzene eq/kWh.

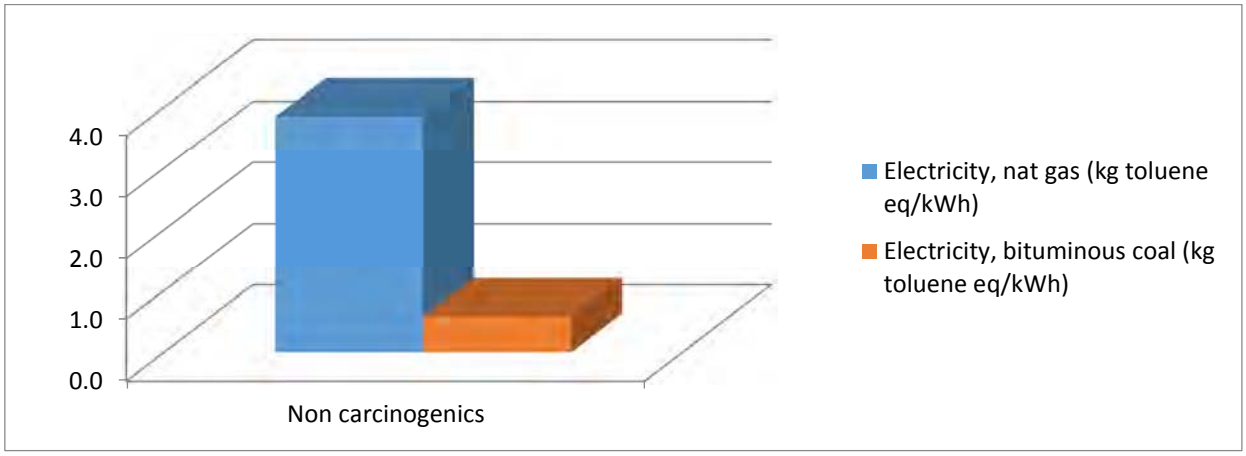

FIG. 6. Non-carcinogenic human health impact in kg toluene eq/kWh.

Carcinogenic Impact Assessment of Natural Gas and Bituminous Coal

A contribution analysis of natural gas carcinogenic impact shows that lead, arsenic ion, and arsenic emissions make up the majority of the carcinogenic impact. A dominance analysis as to what parts of the life cycle yield the greatest carcinogenic impact shows that extraction makes up the majority of the carcinogenic impact. Emissions from natural gas and bituminous coal electricity generation are the processes with the next highest impacts.

A contribution analysis of bituminous coal carcinogenic shows that arsenic, dioxins and lead emissions make up the majority of the carcinogenic impact. Emissions from the coal combusted at the point of electricity generation make up almost the entirety of the carcinogenic impact.

Non-Carcinogenic Impact Assessment of Natural Gas and Bituminous Coal

Lead, cadmium ion, and barium emissions make up the majority of the non-carcinogenic impact for natural gas. Extraction emissions make up almost the entirety of the non-carcinogenic impact. Emissions from natural gas electricity generation are less than the process with the next highest impact (crude oil production).

A contribution analysis of bituminous coal non-carcinogenic impact is shows that lead, dioxins, arsenic and selenium emissions make up the majority of the non-carcinogenic impact. A dominance analysis shows emissions from coal combusted at the point of electricity generation make up most of the non-carcinogenic impact. The crude oil production process also makes a significant impact.

Air and Water Emissions Impacts

In addition to species and process dominance, the human health impacts of the natural gas and bituminous coal-fueled electricity generation are also dominated by phase. Carcinogenic health impact varies considerably between air and water emissions. The carcinogenic air impact is from natural gas is 9.8% as large as the

water impact. Conversely, the carcinogenic water impact is only 1.1% as large as the air impact for bituminous coal, as seen in Fig. 7 below.

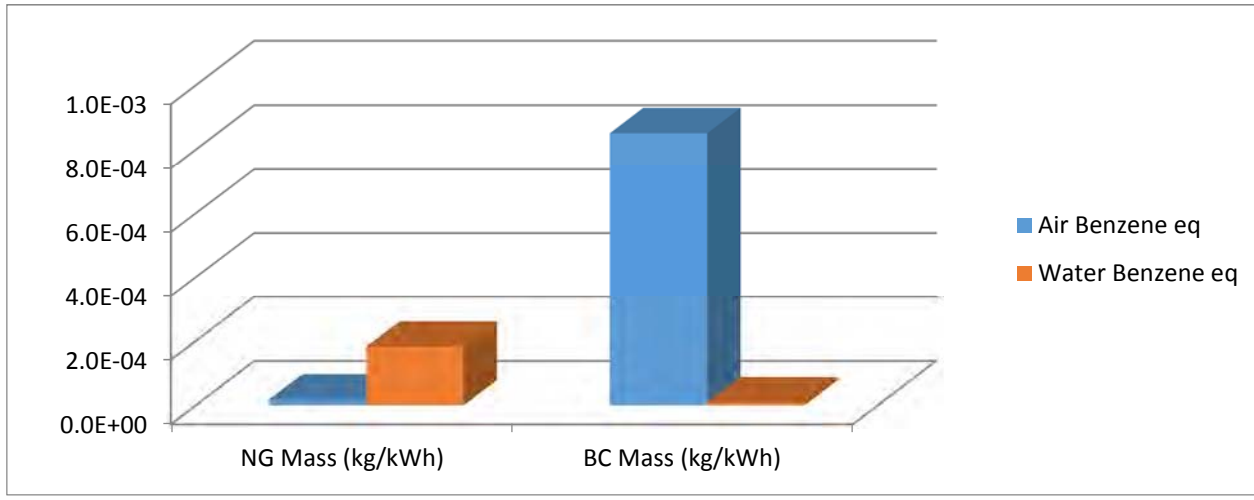

FIG. 7. Air and water carcinogenic health impact.

The non-carcinogenic health impact also varies considerably between air and water phase emissions. The non-carcinogenic air impact is from natural gas is only 0.4% as large as the water impact. Conversely, the non-carcinogenic water impact is 59% as large as the air impact for bituminous coal, as seen in Fig. 8 below.

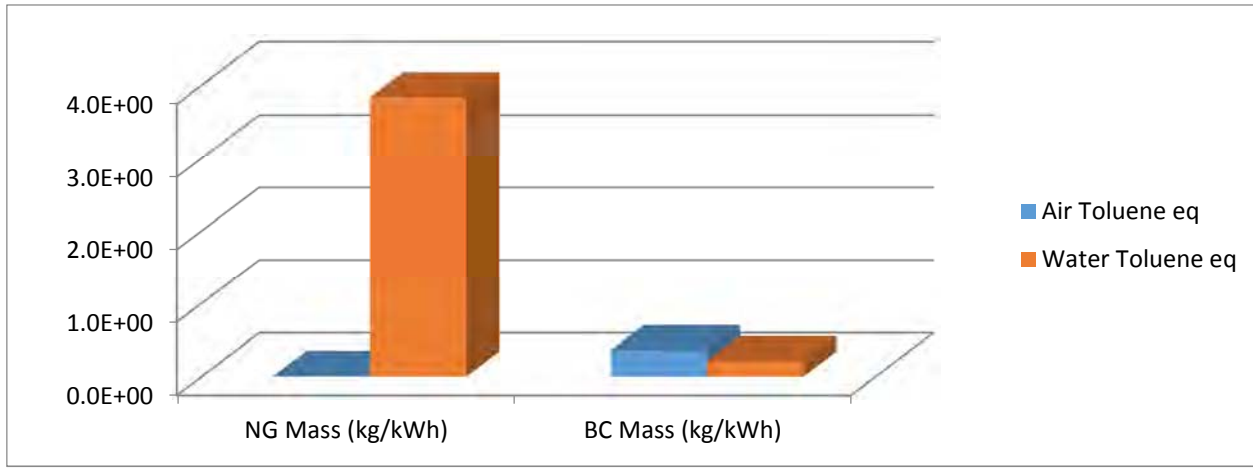

FIG. 8. Air and water non-carcinogenic impact.

Air Emissions Impacts

Since air emissions have a higher potential towards human exposure, they are evaluated separately in this study (McKenzie et al., 2012). Carcinogenic human health impact was found to be 47 times greater for air emissions from bituminous coal than from natural gas-fueled electricity generation, as seen in Fig. 9. The majority of the air emissions impacts from both product systems are from arsenic.

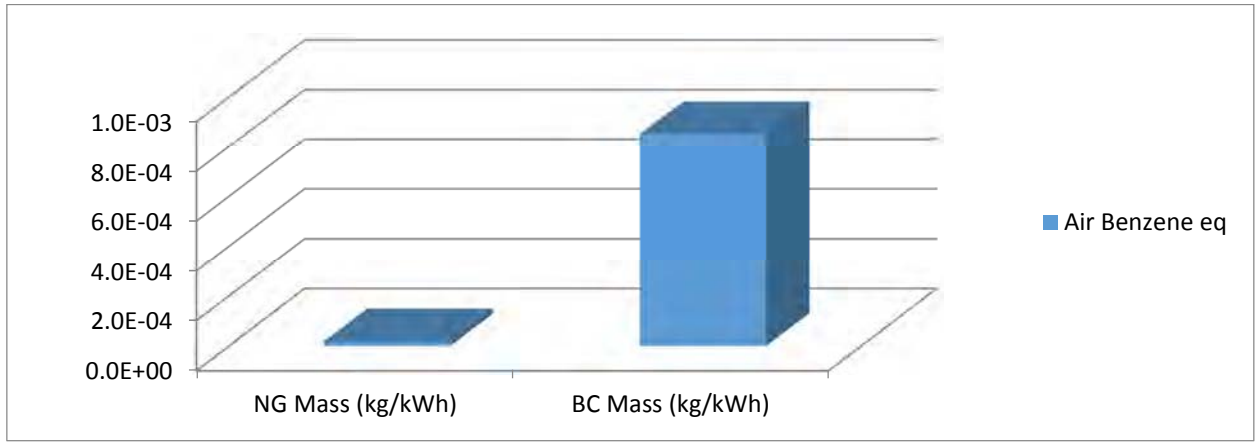

FIG. 9. Carcinogenic impact from air emissions.

Non-carcinogenic human health impact is 27 times greater for air emissions from bituminous coal than from natural gas-fueled electricity generation, as seen in Fig. 10. Most of the air emissions impacts from both product systems are from lead, but there are also significant contributions from arsenic and dioxins.

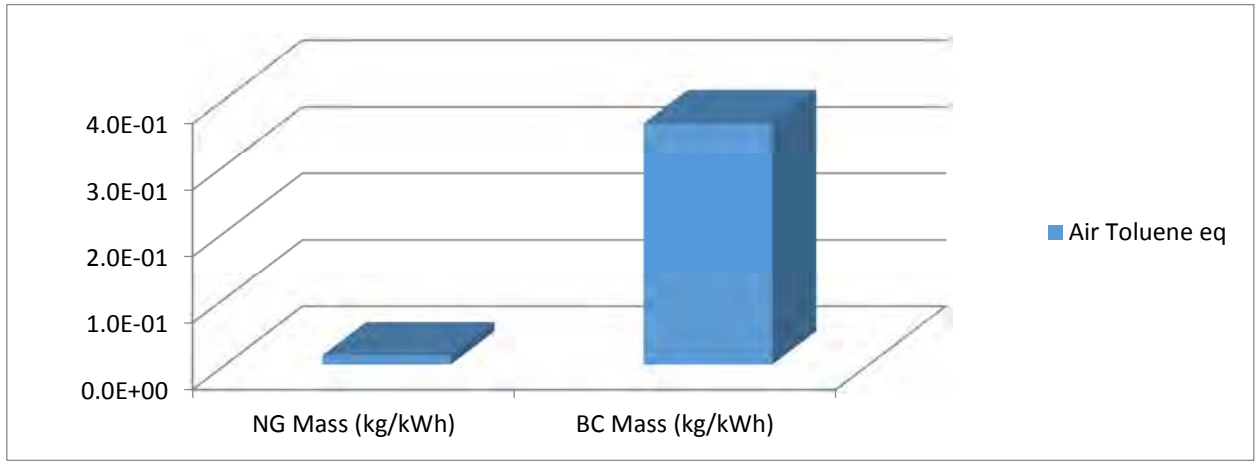

FIG. 10. Non-carcinogenic impact from air emissions.

DISCUSSION, CONCLUSIONS AND RECOMMENDATIONS

Natural gas has a lower carcinogenic health impact and higher non-carcinogenic impact than coal. Water emissions contributed to the majority of the health impact for natural gas and occurred mostly during extraction. Air toxics had the greatest health impact for bituminous coal and occurred mostly during electricity generation. The two product systems greatly differ by health impacts in terms of category indicator, species, phase and spatial and temporal patterns. Greenhouse gasses, not evaluated in this study, were found to be lower for natural gas in other studies (Dale et al., 2013).

The air emissions human health impacts were significantly higher for bituminous coal-fueled electricity generation than that of natural gas. Carcinogenic health

impacts were 47.5 times greater for bituminous coal and the non-carcinogenic health impacts were 26.7 times greater. That result has to be taken with a major qualifier since, as demonstrated earlier, the entire spectrum of air emission impacts were not able to be evaluated due to the lack of appropriate TRACI LCIA characterization factors for some emissions. This disproportionally affected natural gas air emissions in this study and is likely a major reason why the differences in human health impacts from air are so stark between the two fuels.

With those differences in mind, it would thus be useful to look closer at the toxicity of the indicator species itself to help determine which impact is greater. Benzene has a 1 in 100,000 cancer risk level for a continuous lifetime (70 year) inhalation exposure to the range of 1.3 to 4.5 $\mu g/m^3$ (EPA IRIS). Toluene carries a risk of non-carcinogenic neurological health effects for a continuous lifetime (70 year) inhalation exposure of 5,000 $\mu g/m^3$ (EPA IRIS). Looking exclusively at air emissions impacts, it might be fair to say that the carcinogenic health impact from bituminous coal is more significant, but the study also evaluated water impacts, which are scaled differently than air emissions. The water oral carcinogenic risk (1 in 100,000) is 0.1 to 1.0 mg/L and the oral RfD is 0.08 mg/kg-day for toluene (EPA IRIS).

LIMITATIONS AND FUTURE WORK

The results presented tell an incomplete picture because of the missing TRACI LCIA characterization factors. More than 65% (by weight) of the air toxics for natural gas-fueled electricity generation and 13% of the bituminous coal-fueled electricity generation are unaccounted for. These air toxics include hydrogen fluoride, aldehydes and others. This partially explains the extremely high contrast between air emissions from each product system.

The study assumed linear scaling of the 1 kWh functional unit. The efficiencies and environmental flows could certainly change dramatically based upon the size of the power plant. Additional spatial changes could occur due to the geographical location and its proximity to fuel source. Lastly, power generating facilities can use different feed stocks for their fuel and vary by region. Likewise, coal electricity generation can use coal sourced from open pit mining, such as that of the Powder River Basin and will see its environmental flows and emissions altered (Whitaker, et al., (2012).

Future work will be to further refine emission factors for unconventional natural gas production in shale formations. These have been demonstrated through emissions testing and ambient air sampling to be different from those of conventional formations (Armendiaz, 2009). The latter serve as the basis for most emissions inventories, such as EPA's AP-42 and Fire 5.0 databases (Grant et al., 2009). Recently, the EPA has developed a new Oil & Gas tool to assist local regions in finding better estimates of emissions related to unconventional gas wells (a previous tool had already been released for conventional formations). Incorporating those findings into an LCIA study to help better the evaluation of the potential environmental effects compared to traditional natural gas sourcing. Additionally, Air Toxics "hot spots", in terms of quantity, species and overall risk, can be identified along the production chain and can serve to possibly develop better operating practices or control technology to minimize their release to the atmosphere.

REFERENCES

Stuver, S., Alonzo, J., Holditch, S., Mills, S. (2012). "Getting ahead of the regulators by building your own emissions profile." *Society of Petroleum Engineers annual technical conference and exhibition*, SPE, San Antonio, TX.

Meij, R., Te Winkel, H. (2007). "The emissions of heavy metals and persistent organic pollutants from modern coal-fired power stations." *Atmospheric Environment*., 41, 9262-9272.

ISO. (2006). "14040: 2006 Environmental Management: Life Cycle Assessment: Principles and Framework." International Organization for Standardization, Geneva, Switzerland, 2006.

USLCI. (2012). "U.S. Life Cycle Inventory Database." *National Renewable Energy Laboratory,* 2012.

Bare, J. (2002). "Developing a consistent decision-making framework by using the U.S. EPA's TRACI." *US Environmental Protection Agency,* Cincinnatti, OH.

EPA IRIS: http://www.epa.gov/iris/

CalEPA: California EPA Office of Env. Health Hazard, http://www.oehha.ca.gov/

PPRTV: http://hhpprtv.ornl.gov/index.html

Dale, A., Khanna, V., Vidic, R., Bilec, M. (2013). "Process based Life-Cycle Assessment of natural gas from the marcellus shale." *Environmental Science & Technology*., 47, 5459-5466.

McKenzie, L., Witter, R., Newman, L., Adgate, J. (2012). "Human health risk assessment of air emissions from development of unconventional natural gas resources." *Science of the Total Environment*., 424 (2012) 79-87.

Whitaker, M., Heath, G., O'Donoughue, P., Vorum, M., (2012). "Life Cycle Greenhouse Gas Emissions of Coal-Fired Electricity Generation." Journal of Industrial Ecology, 16 (S1), S53-S72.

Armendiaz, A. (2009). "Emissions from natural gas production in the Barnett Shale area and opportunities for cost-effective improvements." *Report for Ramon Alvarez, Ph.D.,* Environmental Defense Fund, Austin, TX.

Grant, J., Parker, L., Bar-Ilan, A., Kemball-Cook, S., Yarwood, G. (2009). "Development of Emissions Inventories for Natural Gas Exploration and Production Activity in the Haynesville Shale." Prepared for The East Texas Council of Governments, Kilgore, TX.

Effect of Fractures on Methane Migration in Shallow Groundwater Aquifer

Liwei Zhang[1], Ph.D., M. ASCE, Nicole Anderson[2], and Daniel J. Soeder[3]

[1]National Energy Technology Laboratory (Pittsburgh Site), 626 Cochrans Mill Road, Pittsburgh, PA 15236, U.S.A., E-mail: liwei.zhang@netl.doe.gov
[2]National Energy Technology Laboratory (Pittsburgh Site), 626 Cochrans Mill Road, Pittsburgh, PA 15236, U.S.A., E-mail: Nicole.Anderson@contr.netl.doe.gov
[3]National Energy Technology Laboratory (Morgantown Site), 3610 Collins Ferry Rd, Morgantown, WV 26507, U.S.A., E-mail: daniel.soeder@netl.doe.gov

ABSTRACT: There is a great concern on methane contamination in shallow groundwater aquifers as a result of drilling operations at unconventional natural gas reservoirs to produce natural gas. The presence of fractures in shallow groundwater aquifer is expected to accelerate the migration of methane in the aquifer. In this study, time needed for methane to be detected at a monitoring well 500 m away from a leaking point in a shallow groundwater aquifer was determined. Both scenarios (with and without fractures) in the aquifer were studied with the use of a numerical simulation code (TOUGH 2), so as to determine the effect of fractures on methane migration. For CH_4 volume fraction detection, it would take 10.4 days to detect a significant CH_4 volume fraction increase at the monitoring well if the aquifer was homogeneous, while it would only take 2 hours to detect a significant CH_4 volume fraction increase at the monitoring well if the aquifer is a fractured aquifer.

INTRODUCTION

The development of unconventional natural gas reservoirs has become economically feasible in the U.S. (Jackson et al., 2013), and a boom of natural gas production from unconventional natural gas reservoirs has been seen in Ohio, Pennsylvania, New York, Maryland and West Virginia (Kargbo et al., 2010). To produce trapped natural gas from unconventional natural gas reservoirs, advanced drilling technologies, namely horizontal drilling and hydraulic fracturing, are applied. However, there has arisen concern by public that pre-existing fractures and faults in the formations above unconventional natural gas reservoirs can be expanded by horizontal drilling and hydraulic fracking, and natural gas can migrate from deep unconventional natural gas reservoirs to shallower groundwater aquifers through those fractures and faults. This study aims to investigate the pace of natural gas migration in a shallow groundwater aquifer if a natural gas leakage results in entry of natural gas into the groundwater aquifer, so as to determine the range of the affected region if a leakage does occur.

In this paper, the speed of natural gas migration in shallow groundwater aquifer is studied by a quantitative modeling approach. TOUGH 2 (Transport of Unsaturated Groundwater and Heat) coupled with the GUI code PetraSim is used as the modeling tool in this study (Yamamoto, 2008). The reliability of TOUGH 2 has been tested by comparison with many different analytical and numerical solutions, with results from laboratory experiments, and with field observations (see e.g., Moridis and Pruess 1992; Finsterle and Pruess 1995; Pruess et al. 1996; Kiryukhin et al. 2007; Müller et al. 2009; Pruess et al. 2012). TOUGH 2 has the capability to model both homogeneous porous media flow and fracture flow. The code employs the integral finite difference method (IFDM) and Multiple Interacting Continua (MINC) method which facilitate the preprocessing of geometric data to implement double- and multiple-porosity methods for fractured media.

To specify the components to be incorporated into the model, TOUGH 2 provides multiple equation-of-state (EOS) modules, which define phases and related thermophysical properties (such as density, viscosity and enthalpy) of the fluid mixture. The chosen EOS module EOS7C is linked to the TOUGH 2 core, which solves two-phase mass and energy balance equations involving methane, brine, non-condensable gas (NCG) and tracer (Oldenburg et al. 2004). In this study the module EOS7C was utilized to model flow and transport of methane in a confined groundwater aquifer at given temperature and pressure.

METHODOLOGY

The system that was modeled is a confined groundwater aquifer with a constant methane injection (representing natural gas leakage from a deep unconventional natural gas reservoir to an overlying groundwater aquifer) at the bottom of the aquifer. The model set up can be seen in Figure 1, and a list of important modeling parameters can be seen in Table 1.

The model had a total of 3724 polygonal cells. The cells were automatically generated by the code with a maximum cell area of 320 m^2. The cells close to the leaking point and the monitoring well were with a lower maximum area (16 m^2), so as to assure the accurate prediction of methane volume fraction changes at the leaking point and the monitoring well. The confined layers (Layers 1 and 3 in Figure 1-a) were modeled by a single layer of polygonal cells in Z direction, and the groundwater aquifer (Layer 2 in Figure 1-a) was modeled by 5 layers of polygonal cells in Z direction. Boundary cells (see Figure 1-b) were assigned a very large volume (10^5 times larger than the volume of normal polygonal cells), so as to ensure free migration of methane out of the model domain.

This work applies the MINC (Multiple Interacting Continua) approach to model flow in fractured groundwater aquifer. Details about the MINC approach can be found on the webpage of PetraSim Resources (Thunderhead Engineering Consultants, Inc. 2013). The fractures accounted for 5% of the total volume, had a fracture spacing of 5m (in X, Y and Z directions), and had a permeability of 2 D (To reduce the simulation time, this work assumes no flow in aquifer rock matrix, and all flows can only be seen in fractures).

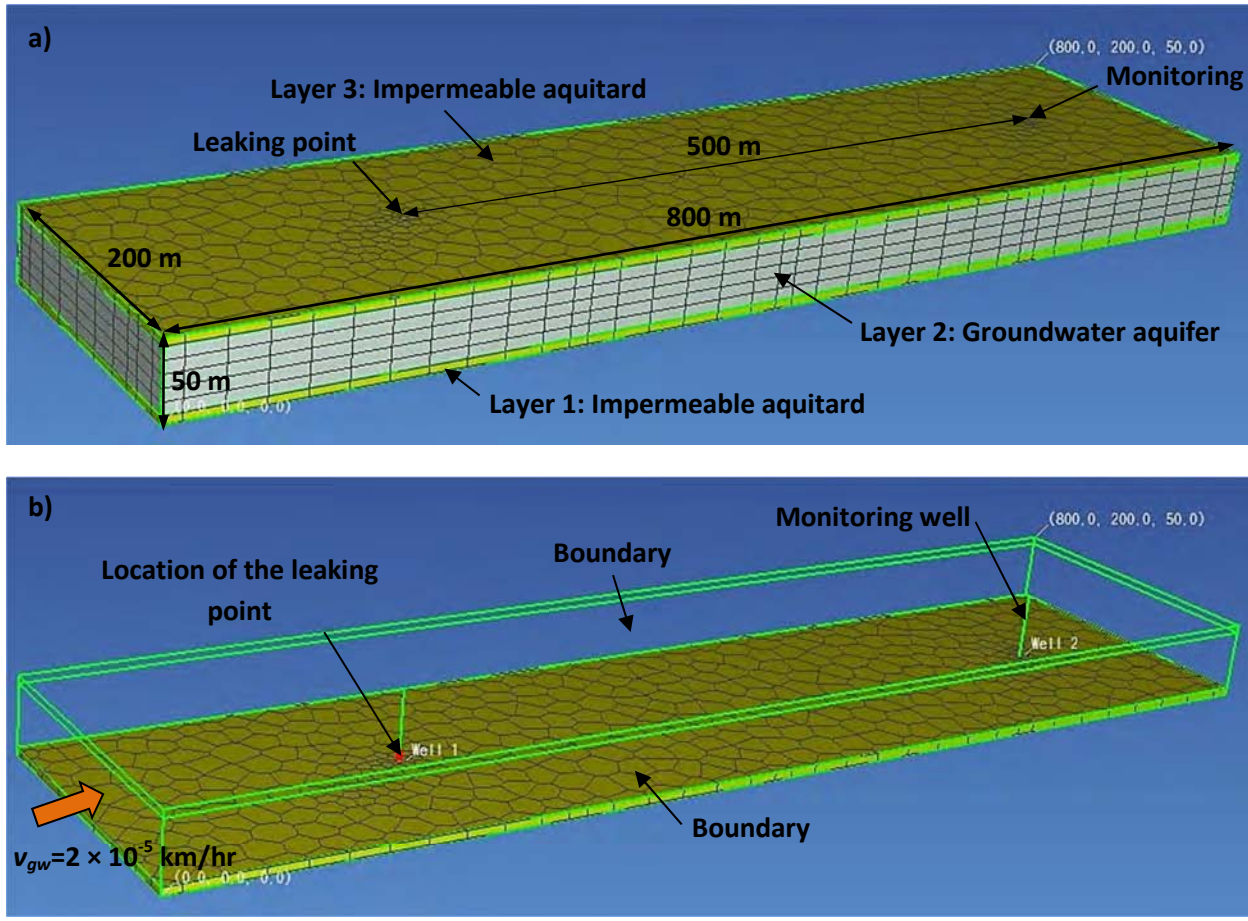

FIG. 1. a) Model set up. The modeling domain is an 800 m × 200 m × 50 m rectangle. A methane leaking point is located 200 m away from the left boundary of the domain, and a methane monitoring well is located 500 m away from the leaking point. The groundwater flows at a velocity of 2 × 10^{-5} km/hr toward the monitoring well. b) Image showing the exact location of the leaking point (at the bottom of the groundwater aquifer), boundaries of the model domain (with large volume boundary cells), and the flow direction of groundwater.

Table 1. Modeling Parameters Used for the Scenario with No Fractures

Parameter	Value	Parameter	Value
Density of rock in Layers 1-3	2600 kg/m^3	Layer 2 thickness	40 m
Initial pressure in Layer 2	1.5x10^5 Pa	Layers 1 and 3 thickness	5 m
Temperature	25 ^{o}C	Methane leaking rate	0.001 kg/s
Horizontal permeability (Layer 2)	200 mD	Porosity (Layer 2)	0.3
Vertical permeability (Layer 2)	200 mD	Porosity (Layers 1 and 3)	0.2
Horizontal permeability (Layers 1 and 3)	10^{-3} mD	Maximum simulation time	579 days
Vertical permeability (Layers 1 and 3)	10^{-3} mD	Indicator of significant methane leakage (methane volume fraction)	0.05
Simulation time step	Automatic adjustment (initial step = 100 s)		

RESULTS AND DISCUSSION

Figure 2 shows the distribution of water saturation (note that water saturation is the same as volume fraction of water in the two-phase system, and volume fraction of methane is equal to 1 – water saturation) as a function of simulation time (no fractures). Due to buoyancy, methane migrated to the top of the groundwater aquifer from the leaking point and was moved by groundwater flow toward the monitoring well. As a result, the top of the monitoring well was the location that was able to detect methane leakage at the shortest time. With the increase of the simulation time, there was an accumulation of methane at the top of the aquifer, and the water saturation was significantly decreased at the top of the aquifer.

Figure 3 shows the time needed to detect significant amount of methane at the top of the monitoring well (hereby a criterion of less than 95% water saturation is used to indicate the presence of significant amount of methane). The time needed to detect significant amount of methane was 10.4 days.

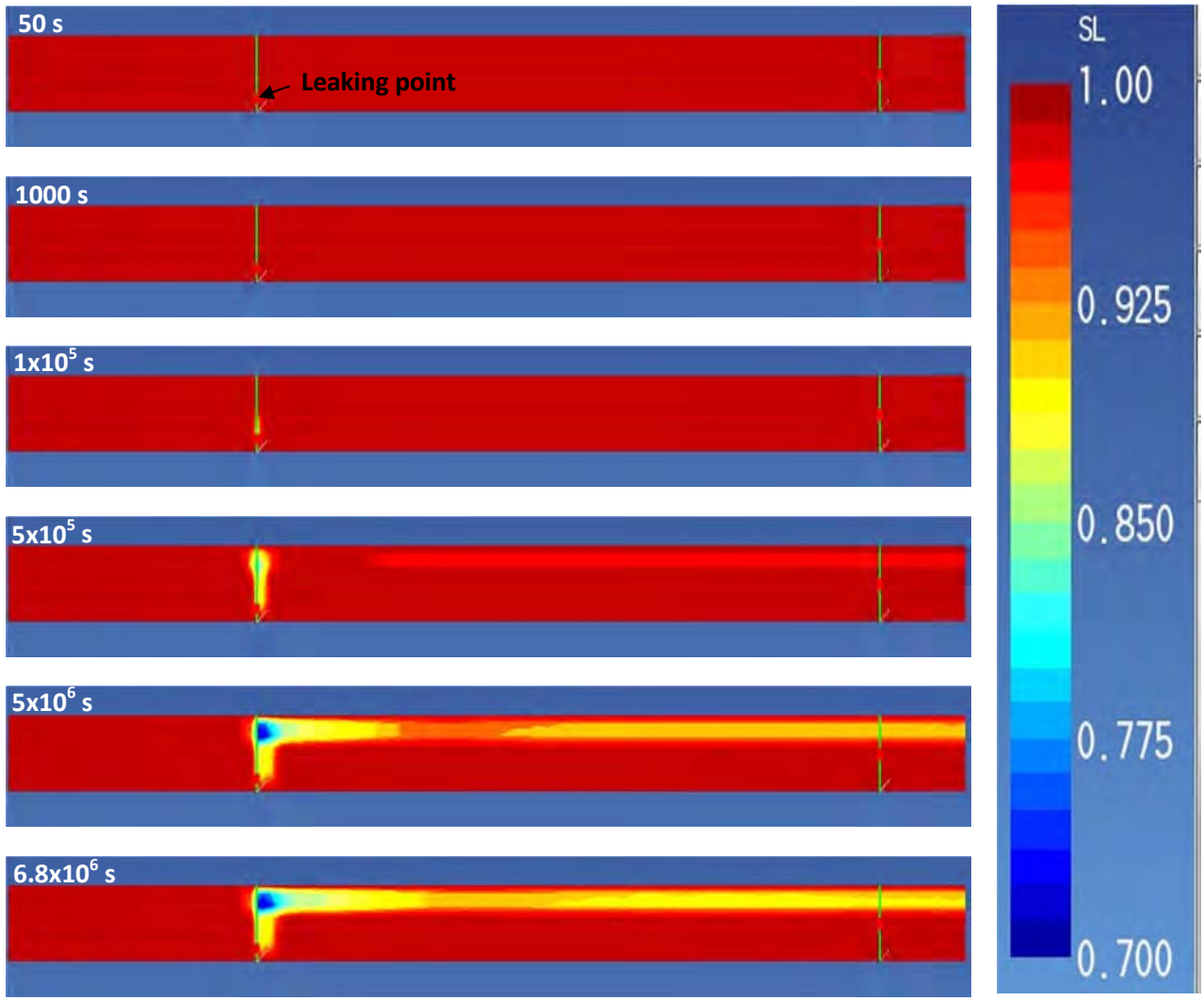

FIG. 2. Distribution of water saturation showing methane migration as a function of time (no fractures).

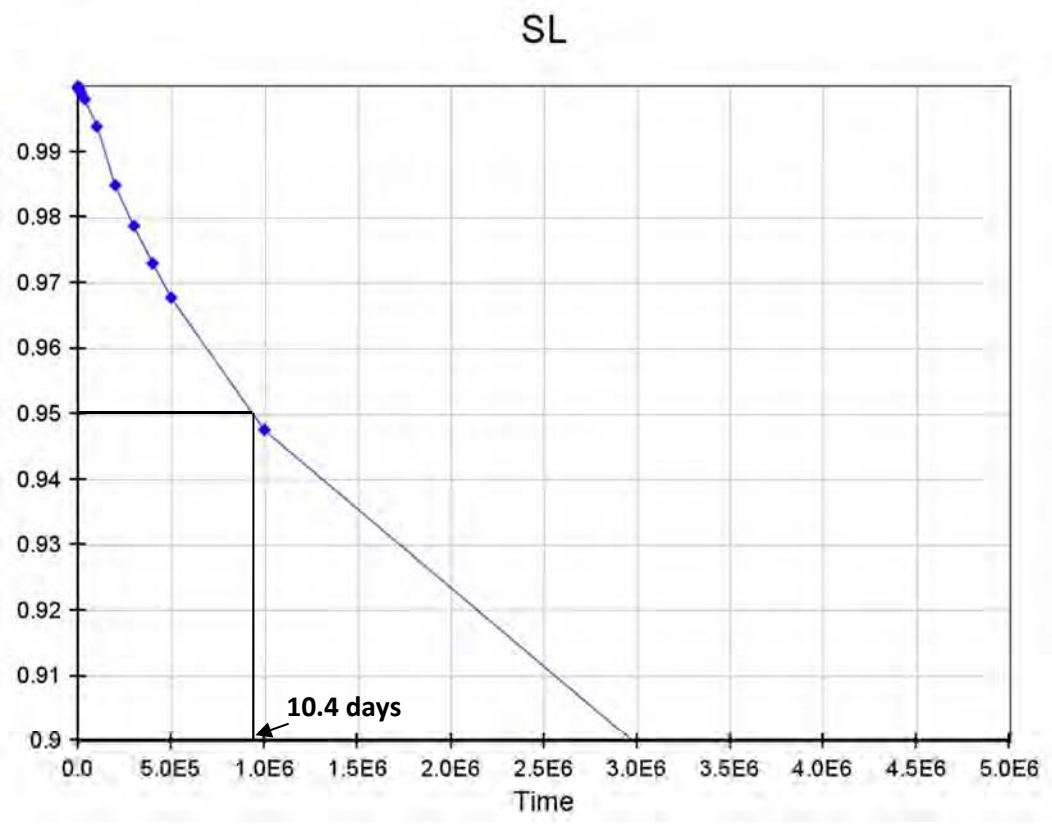

FIG. 3. Water saturation as a function of time at the top of the monitoring well.

Figure 4 shows the distribution of water saturation as a function of simulation time (with fractures). Compared with Figure 2, methane was able to migrate to the top of the groundwater aquifer and to the monitoring well with much less time than the time needed in the scenario with no fractures. To be specific, it only took 7100 s (about 2 hours) to detect significant amount of methane at the monitoring well after the leakage (Figure 5), while it took 10.4 days to detect significant amount of methane at the monitoring well after the leakage if there were no fractures. Therefore, if methane leaks into a shallow fractured groundwater aquifer, it will migrate in a fast speed and cause impact on a large area.

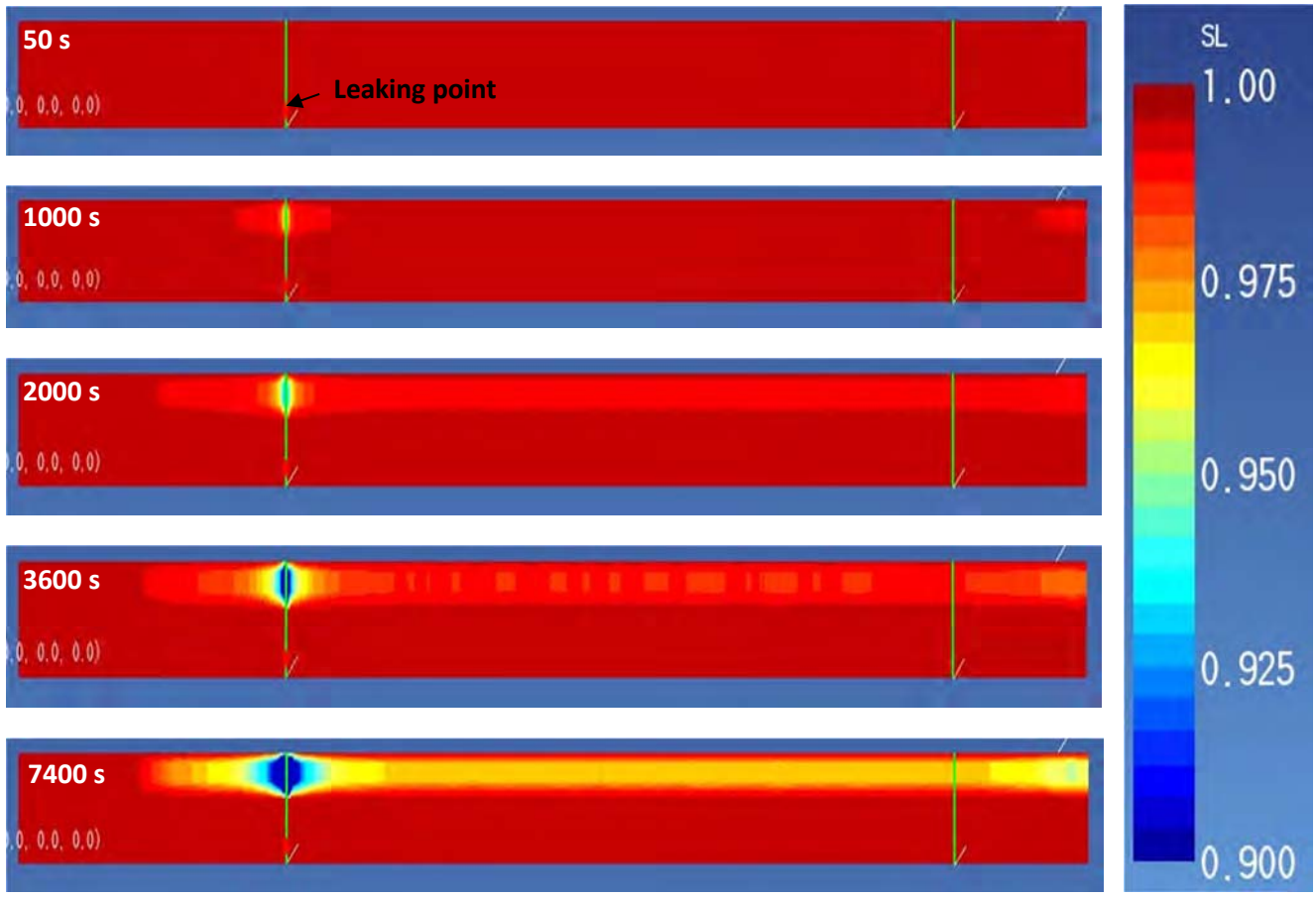

FIG. 4. Distribution of water saturation showing methane migration as a function of time (with fractures).

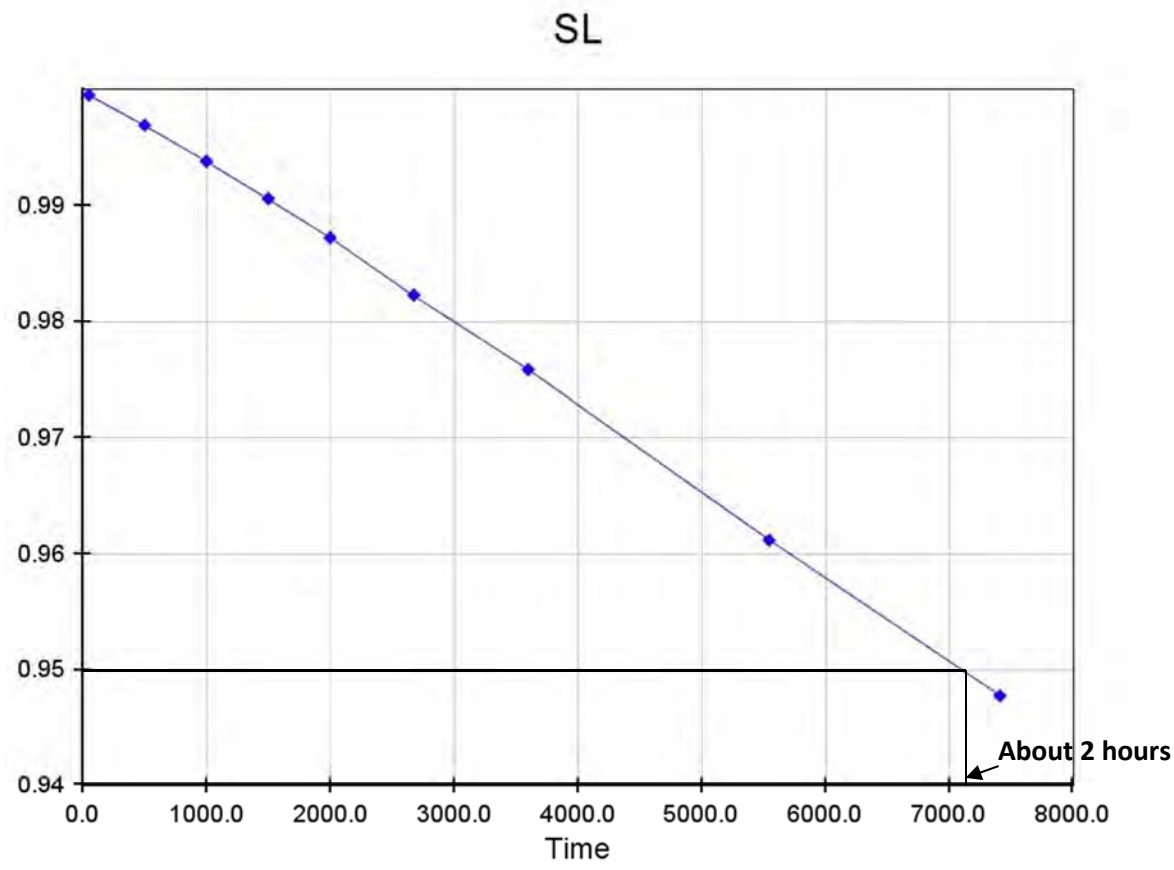

FIG. 5. Water saturation as a function of time at the top of the monitoring well (with fractures).

CONCLUSIONS

Methane migration in a homogeneous groundwater aquifer and a fractured groundwater aquifer is modeled by TOUGH 2 (Transport of Unsaturated Groundwater and Heat) coupled with the GUI code PetraSim. The modeling work aims to determine the time needed to detect significant amount of methane at a monitoring well 500 m away from the leaking point. The time needed to detect significant amount of methane is 10.4 days if the groundwater aquifer is homogeneous (no fractures), while the time needed to detect significant amount of methane is only two hours if the groundwater aquifer is with fractures. Model simulation results show that methane is able to migrate in a fast speed in a fractured groundwater aquifer, and the area that is impacted by methane leakage in a fractured groundwater aquifer is much larger than the area in a homogeneous groundwater aquifer.

ACKNOWLEDGMENTS

This work was completed as part of National Energy Technology Laboratory (NETL) research for the Department of Energy's Research and Development

Program under Section 999 of the Energy Policy Act of 2005. The authors would like to thank the Office of Research and Development at NETL for funding support and providing access to research article databases, computing devices, etc. The authors also would like to acknowledge Alison Alcott and Michael Devine at RockWare, Inc., Golden, CO for programmatic guidance, direction, support, and helpful discussions.

REFERENCES

Finsterle, S. and Pruess, K., (1995). "TOUGH2: Solving TOUGH Inverse Problems. Paper presented at the TOUGH workshop '95." Earth Sciences Division, Lawrence Berkeley National Laboratory, Berkeley, CA.

Jackson, R. E., Gorody, A. W., Mayer, B., Roy, J. W., Ryan, M. C., & Van Stempvoort, D. R., (2013). "Groundwater Protection and Unconventional Gas Extraction: The Critical Need for Field-Based Hydrogeological Research." *Groundwater*, 51(4), 488–510.

Kargbo, D. M., Wilhelm, R. G., and Campbell, D. J., (2010). "Natural gas plays in the Marcellus shale: Challenges and potential opportunities." *Environ. Sci. Technol.*, 44(15), 5679-5684.

Kiryukhin, A. V., Kaymin, E. P., and Zakharova, E. V., (2007). "Using TOUGHREACT to Model Laboratory Tests on the Interaction of $NaNO_3$-NaOH Fluids with Sandstone Rock at a Deep Radionuclide Repository Site." *Nucl. Technol.*, 164, 196-206.

Moridis, G., and Pruess, K., (1992). "TOUGH Simulations of Updegraff's Set of Fluid and Heat Flow Problems." Lawrence Berkeley Laboratory Report LBL-32611, Berkeley, CA.

Müller, W., Alkan, H., Xie, M., Moog, H., and Sonnenthal, E. L., (2009). "Modeling of the reactive transport for rock salt-brine in geological repository systems based on improved thermodynamic database". American Geophysical Union Fall Meeting, San Francisco, CA.

Oldenburg, C., Moridis, G., Spycher, N., Pruess, K., (2004). "EOS7C Version 1.0: TOUGH2 Module for Carbon Dioxide or Nitrogen in Natural Gas (Methane) Reservoirs." Lawrence Berkeley National Laboratory, <http://escholarship.org/uc/item/3wm703z2> (Mar. 2, 2014).

Pruess, K., Simmons, A., Wu, Y. S., and Moridis, G., (1996). "TOUGH2 Software Qualification." Lawrence Berkeley National Laboratory Report LBL-38383, Berkeley, CA.

Pruess, K., Oldenburg, C., and Moridis, G., (2012). "TOUGH2 User's Guide, Version 2." Earth Sciences Division, Lawrence Berkeley National Laboratory, Berkeley, CA.

Thunderhead Engineering Consultants, Inc., 2013. "Understanding and Using MINC." <http://www.thunderheadeng.com/downloads/petrasim/Understanding%20and%20Using%20MINC.pdf> (Mar. 15, 2014).

Strategies for Sustainable Management of Oilfield Wastes and Wastewaters in Shale Resource Plays

J. Daniel Arthur[1], P.E., SPEC, and B. Greg Casey[2], P.E.

[1]President/Chief Engineer, ALL Consulting, 1718 S. Cheyenne Ave., Tulsa, OK 74119, U.S.A., E-mail: darthur@all-llc.com.
[2]Principal Engineer, ALL Consulting, 1718 S. Cheyenne Ave., Tulsa, OK 74119, U.S.A., E-mail: gcasey@all-llc.com.

ABSTRACT: Management of exploration & production (E&P) industry waste and wastewaters has evolved rapidly over the last dozen years, driven by greater scrutiny of waste management practices by state and federal regulatory agencies, the public, and environmental groups. The evolution of waste management has accelerated with the focus on unconventional oil & gas plays and use of multiple horizontal well completions from a single pad. The use of multi-well pads and rapid development of regional areas has resulted in large, localized volumes of waste materials and water not seen before in the industry. This paper provides a comprehensive summary of the types of wastes that may be generated during shale resource development and reviews regulatory requirements for waste management, recycling and disposal. It also discusses the importance of developing a "cradle to grave" waste management plan covering a project from exploration and development through production of oil & gas and eventually to site closure.

INTRODUCTION

Management of exploration and production (E&P) industry waste has evolved rapidly over the last dozen years, driven by greater scrutiny of waste management practices by state and federal regulatory agencies, the public, and environmental groups. That evolution has accelerated with the focus on unconventional oil and gas plays and use of multiple horizontal well completions from a single pad. The use of multi-well pads and rapid development of regional areas has resulted in large, localized volumes of waste materials not seen before in the industry.

As a result, waste management programs have become an essential and integral part of planning an oil and gas project from exploration and development through production and eventual site closure. Because waste management can be a drain to the bottom line of a project, a "cradle to grave" approach is needed to minimize risks, liability, and costs associated with waste materials.

Each well site produces a broad variety of waste types (e.g., produced water, drilling fluids, waste oils, etc.), each with its own handling and disposal requirements. Also,

each phase of exploration and production produces its own set of wastes. For instance, construction sites should manage stormwater runoff and construction wastes; drilling produces drill cuttings and spent drilling muds that should be recycled or disposed of; hydraulic fracturing operations must manage large volumes of fluids that flow back up the well and are produced; and produced water may continue to be co-produced with oil and gas throughout the life of the well. In addition, there are smaller volumes of other wastes such as tank bottoms, contaminated soil, and even trash that should be managed and disposed of or recycled.

Waste management should be included early in the planning phase of field development. Goals and objectives generally include the following:

- Complying with regulatory and community requirements;
- Minimizing the quantity of wastes produced;
- Implementing effective programs to reuse or recycle on site;
- Minimizing waste transportation costs;
- Avoiding creation of hazardous wastes;
- Minimizing safety, environmental, and cost risks; and
- Managing liability associated with generating and disposing of wastes.

The planning process must have buy-in from management and operations staff to be successful. It includes an assessment of current and evolving regulations and community requirements, and the necessary permitting (with time frames for obtaining permits). The process should establish project/operating boundaries and identify types and quantities of wastes to be generated, opportunities to reduce waste quantities, choices of reuse, recycling and disposal for each type of waste, decisions regarding on-site vs. off-site disposal, waste transportation options, and types and locations of approved commercial waste management and/or disposal sites.

TYPICAL OILFIELD WASTES

There are many oilfield wastes and other waste types that might be found at a well site. These generally include the following:

- Non-hazardous oilfield waste (NOW): Exempt waste under the Resource Conservation and Recovery Act (RCRA), Subtitle C; which is essentially a waste that comes up from "down hole" such as drill cuttings and produced brine, and also includes tank bottoms and pit contents;
- Non-exempt industrial waste: Examples include lube oils, unused chemicals, paint waste, scrap metal, and trash;
- Special wastes: Naturally occurring radioactive materials (NORM) and Technologically Enhanced, Naturally Occurring Radioactive Materials (TENORM); and
- Hazardous Wastes: Many of the above wastes can be classified as hazardous if mismanaged. For example, unused chemicals dumped in a drill cuttings pit might result in the entire pit contents being labeled as hazardous.

The wastes from drilling, completions, work overs and production operations are classified for the most part as NOW. For example, wastes from oilfield operations are identified in each waste category for Texas E&P operations with the Texas Railroad Commission (RRC), in a Memorandum of Understanding by the Texas Commission

on Environmental Quality (TCEQ) and the RRC (e.g., TAC 1998, TCEQ 2006, EPA 1993). Additionally, methods of determination for hazard classification are provided by the United States Environmental Protection Agency (EPA) for producing states which have primary regulatory authority under RCRA (TAC 1996). Waste classifications are generally categorized as presented below:

NOW (Non-hazardous/Exempt Oilfield Waste)

- Drill solids/fluids – used water and oil-based
- Drill fluids – un-used water and oil-based
- Produced water – flowback fluids from fracturing
- Rig wash
- Spent acid treatment wastes from gas plant
- Spent dehydration unit wastes – glycol, caustics, and amines from gas plant
- Spent adsorbents and catalysts – i.e., activated carbon from gas plant
- Tank bottoms (including pigging solids) – produced solids with sand, paraffin, scale, and basic sediment and water (BS&W)
- Work over/completions produced wastes

Industrial (Non-Exempt Oilfield Wastes)

- Construction debris – cement, wood, etc.
- Contaminated soils – chemicals, hydrocarbons
- Lube oil – contaminated soils, engine filters, oily rags, adsorbents
- Paint waste (non-liquid)
- Sewer and lagoon wastes
- Special rig wastes (lubricants, etc.)
- Unused and used chemicals – lab solvents, anti-freeze, treating chemicals

Industrial Recycle

- Batteries
- Oils – used lubricating and hydraulic
- Scrap metals – pipe, vessels, drums, wire
- Scrap plastics

Trash

- Construction debris
- Trash including recycle materials

Special Wastes

- NORM
- Technically-Enhanced NORM

In addition to the above, stormwater discharges require management. Although oil and gas well sites are exempted from stormwater rules under the Federal Clean Water Act, various state and/or local requirements may apply. Furthermore, best practices for most areas prompt the need for stormwater management. This may range from preparing Storm Water Pollution Prevention Plans (SWPPPs), Sediment and Erosion Control Plans, or simply using applicable Reasonable and Prudent Practices (RAPPs) as defined by groups such as the Independent Petroleum Association of America (IPAA).

REDUCE, RECYCLE, REUSE

As a project is being developed and planned, waste management should be integrated into the design with the specific goal to reduce the amount of waste materials generated and to recycle and reuse as much material as possible.

Improvements in techniques and technologies have made oil and gas recovery more efficient and less costly while also improving environmental performance. The result is less waste and/or less costly waste management. For example, the chemicals used in hydraulic fracturing are evolving to be "greener" both to improve fracture effectiveness and to minimize risks to the environment during transport, use, and flowback/production operations. The centralization of wells and treatment systems also helps to reduce surface footprint and associated environmental impacts, and is an important waste minimization technique.

Treatment and recycling of produced water on site is becoming more common as treatment technologies evolve and fracturing fluid chemicals are improved to tolerate higher salinity fracturing fluids. The produced water then is recycled back into the hydraulic fracturing fluid for the next fracturing job, greatly reducing the high salinity waste volumes for transport and disposal.

PLANNING STEPS

Waste management programs should be developed during the project planning phase and implemented as field operations begin. To be effective, the plan should include detailed guidelines for managing each waste. The plans should be functional, containing information on responsible parties, approved vendors, applicable regulations and contact information. The processes should cover waste handling, recycling, hauling, disposal, and tracking.

Waste management planning should include these basic steps:

- Determine the probable wastes to be generated and their classification (i.e., NOW, Non-Exempt, etc.);
- Estimate the quantity and quality of each waste to be generated;
- Consider waste minimization options and determine if waste can be recycled or disposed on-site;
- Determine the regulatory regime (e.g., special wastes, RCRA exempt wastes, etc.);
- Find the regulatory agencies with jurisdiction for the wastes;

- Consider applicable requirements for each waste from generation to disposal;
- Find the closest disposal sites that meet company specified requirements;
- Audit the disposal sites to determine if they can accept and dispose of wastes safely;
- Compile a list of acceptable disposal sites with contacts and location;
- Prepare a list of permitted waste haulers;
- Set up a checklist for hauler inspection and waste documentation to be filled out prior to loading and leaving the site;
- Establish internal handling and storage procedures;
- Develop a working field manual for handling, storage, and disposal procedures;
- Develop waste tracking procedures and forms;
- Combine information from steps above into a comprehensive waste management plan;
- Gain management and operations approval for the plan;
- Train users and managers of the plan; and
- Develop a record management system for tracking and documenting implementation of the waste management plan.

After determining the probable wastes to be generated, the regulatory agencies and their applicable waste regulations should be found for each waste. This evaluation should cover the handling, storage, hauling, and disposal of each waste material. Wastes from oilfield E&P activities are regulated by Federal, state and/or local agencies. Additionally, community and social considerations can affect waste handling and disposal.

State agencies typically have primacy over waste management activities. For example, in Montana the Montana Board of Oil & Gas Conservation (MBOGC) has regulatory responsibility for most oilfield wastes such as NOW, and the Montana Department of Environmental Quality (MDEQ) regulates discharges and hazardous wastes. However, methods for determining hazard classification are provided by the U.S. EPA for producing states which have primary regulatory authority under RCRA.

If off-site disposal is necessary, handling and transportation should be planned. Handling processes on-site should be developed to ensure safety and initiation of waste tracking. Waste haulers should be inspected to help ensure safe delivery of the waste to the disposal site. A checklist documenting hauler approval to accept and transport the waste, as well as document the waste type and quantity, is useful.

Another important aspect of waste planning is to have a system to track all waste types from “cradle to grave” to minimize long-term liability and costs. Tracking of wastes documents the type and quantity of waste to its final disposal. This is essential to verify that the specific waste is delivered to its intended and approved disposal site. If the waste should be accidentally or purposefully released to the environment before reaching the intended disposal site, a good tracking system will allow reporting of the waste type and composition. That information can also be provided to guide proper cleanup.

Delivery of the wastes to the approved disposal site is tracked with chain-of-custody documentation that should begin as wastes destined for off-site disposal are loaded onto the trucks. The hauling checklist and chains of custody then should be

maintained on file long-term. In the event a disposal site has an unpermitted release, companies that have disposed of their wastes at the site could be liable for cleanup and damages. Therefore, it is in a company's best liability interest to document the quantity and quality of wastes disposed at the site.

The process for selecting an off-site disposal facility should begin with an audit to ensure the facility uses proper waste disposal practices and has current permits. Auditing of salt water disposal wells (SWDs), land farms, pits, and other facilities should be performed by a professional experienced with the technical and operational requirements of the specific type of facility. Approved sites should be chosen to minimize transportation (trucking or pipeline) distance from operating areas. To limit liability, a producer may want to minimize the number of facilities used.

STRATEGIES

Sustainable strategies for waste management are typically developed as part of a waste management planning process. As discussed above, the waste management plan for a specific shale development project takes into account the complex framework of drilling, completion and production operational criteria; waste streams; federal, state and local regulations; logistical considerations; and economic factors.

Strategies utilized will vary by location. Table 1 below illustrates, as a typical example, the strategies for the handling and disposal of select waste streams encountered in the Utica Shale in Ohio.

Table 1. Strategies for Handling and Disposal of Oilfield Waste

Waste Stream	Handling	Disposal
Drill cuttings	Solidified with bulking agent at the drilling rig; Transport using end dump trailers	Subtitle D landfill; Beneficial reuse with Ohio Department of Natural Resources (ODNR) approval
Synthetic oil base mud	Leased through mud company; Returned to mud company at end job for reconditioning and re-use	Spent mud is characterized for TENORM before solidification and landfill disposal
Produced water	Stored in production tanks at the well; Transported by 100-bbl capacity trucks	Class II disposal well; Exempt from TENORM characterization if disposed at Class II well
Produced solids	Stored in solids tank at the well. Cleanout of tank using vacuum truck into vac boxes	Characterize for TENORM and transport to landfill for solidification and disposal
Tank and container cleanouts	Power wash interior of tank and vacuum recovery of fluids and solids into vac boxes	Characterize for TENORM and transport to landfill for solidification and disposal
Contaminated soil	Excavate impacted area;	Characterization based on

and spill waste	Vacuum truck recovery of fluids may be applicable; Store in roll-off box	contaminant type; Generator knowledge or Material Safety Data Sheet (MSDS) may be sufficient in some instances; Dispose at landfill

The following examples provide more details on two strategies for waste handling and disposal. One example of a shale-play specific strategy would be the handling and disposal of drill cuttings for the Utica Shale. Ohio has very restrictive regulations for the disposal of TENORM; however, drill cuttings are specifically exempted from the definition of TENORM by the Ohio Department of Natural Resources (ODNR) and approved disposal is at a Subtitle D (non-hazardous waste) landfill. One beneficial re-use project is in current development under the Ohio Environmental Protection Agency-Voluntary Action Program (OEPA-VAP) and in coordination with the ODNR. The project would provide for the processing of drill cuttings from the non-oil based mud vertical section of the well bore into an inert fill/building-type material. The drill cuttings would be characterized and profiled before transport to the OEPA-VAP approved facility for processing. Drill cuttings properly managed for beneficial re-use within the regulatory requirements of the OEPA-VAP program would be indemnified as a proper management practice and eliminate regulatory risk to the shale developer. The VAP-approved facility is located within the active shale development area and will significantly reduce carbon emissions and transportation costs as compared to transport to the outlying Subtitle D landfills.

Another specific strategy utilized in Ohio is for the waste stream of produced solids consisting of fracture sands and formation solids. During well production, solids are separated from the hydrocarbon stream and routed to on-site storage tanks. The accumulation rate of the solids is monitored and at the proper time the solids are characterized for TENORM while in the storage tanks. Upon receipt of TENORM results, the storage tanks are cleaned out into vacuum boxes and transported for proper solidification and disposal at a Subtitle D landfill. The sustainable nature of this strategy is that equipment and transportation costs are optimized in order to reduce the carbon footprint of the regulatory compliant waste handling and disposal process.

CONCLUSIONS

Guidelines included in a waste management plan should provide for each waste, including the principal classification, description, disposal/recycling options, handling, packaging/labeling, required logs/notifications, approved vendors, and regulatory references.

A waste management program is an essential and integral part of planning an E&P development project. A well-developed plan can help minimize risks, liability, and costs associated with waste management. This requires planning related to the types of operations generating wastes, current regulations, disposal sites, potential liabilities, recycling and disposal options, and costs associated with various options and alternatives.

Elements of a functional and “operations friendly” waste management plan include

processes for achieving compliant, low-risk, and cost-effective waste management while also incorporating complete guidelines for each specific waste. To be successful, it should serve as a good reference tool for management, while being functional and easy to use for field operations.

REFERENCES

Environmental Protection Agency (EPA). (1993). "Clarification of the Regulatory Determination for Wastes from the Exploration, Development and Production of Crude Oil, Natural Gas and Geothermal Energy." *58 Federal Register* 15284-15287. March 22, 1993. <http://www.epa.gov/osw/nonhaz/industrial/special/oil/og93wp.pdf> (Dec. 5, 2013).

Texas Administrative Code (TAC). (1996). Title 16, Part 1, Chapter 3, Rule §3.98. Standards for Management of Hazardous Oil and Gas Wastes. <http://info.sos.state.tx.us/pls/pub/readtac$ext.TacPage?sl=R&app=9&p_dir=&p_rloc=&p_tloc=&p_ploc=&pg=1&ti=16&ch=3&rl=98> (Dec. 5, 2013).

Texas Administrative Code (TAC). (1998). Title 16, Part 1, Chapter 3, Rule §3.30. Memorandum of Understanding between the Railroad Commission of Texas (RRC) and the Texas Commission on Environmental Quality (TCEQ). <http://info.sos.state.tx.us/pls/pub/readtac$ext.TacPage?sl=R&app=9&p_dir=&p_rloc=&p_tloc=&p_ploc=&pg=1&ti=16&ch=3&rl=30> (Dec. 5, 2013).

Texas Commission on Environmental Quality (TCEQ). (2006). “Disposal of Special Wastes Associated with the Development of Oil, Gas and Geothermal Resources.” Regulatory Guidance RG-003.

The Impact of Shale Gas/Oil Waste on MSW Landfill Composition and Operations

Eric D. Chiado[1], P.E.

[1]Principal, Solid Waste Practice Lead, Civil & Environmental Consultants, Inc., 4000 Triangle Lane, Suite 200, Export, PA 15632, U.S.A., E-mail: echiado@cecinc.com.

ABSTRACT: This paper presents an overview of the weights and types of solid and semi-solid wastes generated from exploration and production (E&P) of Marcellus Shale in the Commonwealth of Pennsylvania, and the engineering and operational issues faced by operators of municipal solid waste (MSW) landfills that co-mingle these wastes. Since approximately 2009, the volume of Marcellus Shale drilling (MSD) waste being landfilled has increased substantially, becoming a significant component of the waste stream and an important revenue source. Our understanding of the physical and strength characteristics of MSD waste is relatively limited, raising questions concerning the stability of the landfill waste mass that incorporates this waste stream. This paper includes results from several field and laboratory studies performed to evaluate and develop physical and shear strength properties of MSD waste. Conclusions from these studies are provided, and general guidelines for incorporating MSD waste into an MSW landfill are provided.

INTRODUCTION

Since approximately 2005, industry has made substantial efforts to explore, develop and extract natural gas contained within the Marcellus Shale Formation. The geographic areas being explored and number of wells being drilled have increased substantially as gas reserves are proven and refined. Because of the considerable vertical depth (nominally 1,500 meters) to the formation coupled with the use of multiple horizontal bores within the formation, a sizeable volume of Marcellus Shale drill (MSD) cuttings are produced at each well pad. Typically, state regulatory agencies classify the cuttings as residual/industrial waste that requires disposal, which is primarily accomplished through landfilling.

Currently, MSD waste comprises approximately 5% of the total waste weight being landfilled in states located within the Marcellus Shale region (defined in this paper as Pennsylvania, West Virginia, Ohio and New York). However, only about 20% of all landfills within the region accept the majority of this waste due to their proximity to drilling pads. Consequently, at these landfills MSD waste has become a significant portion of the overall waste weight being accepted, ranging from 10% to 60% of the

total (PaDEP-1,2013). Figure (Fig.) 1 shows the number of landfills accepting MSD waste, and the approximate percentage of MSD waste being disposed relative to the total annual waste weight being disposed.

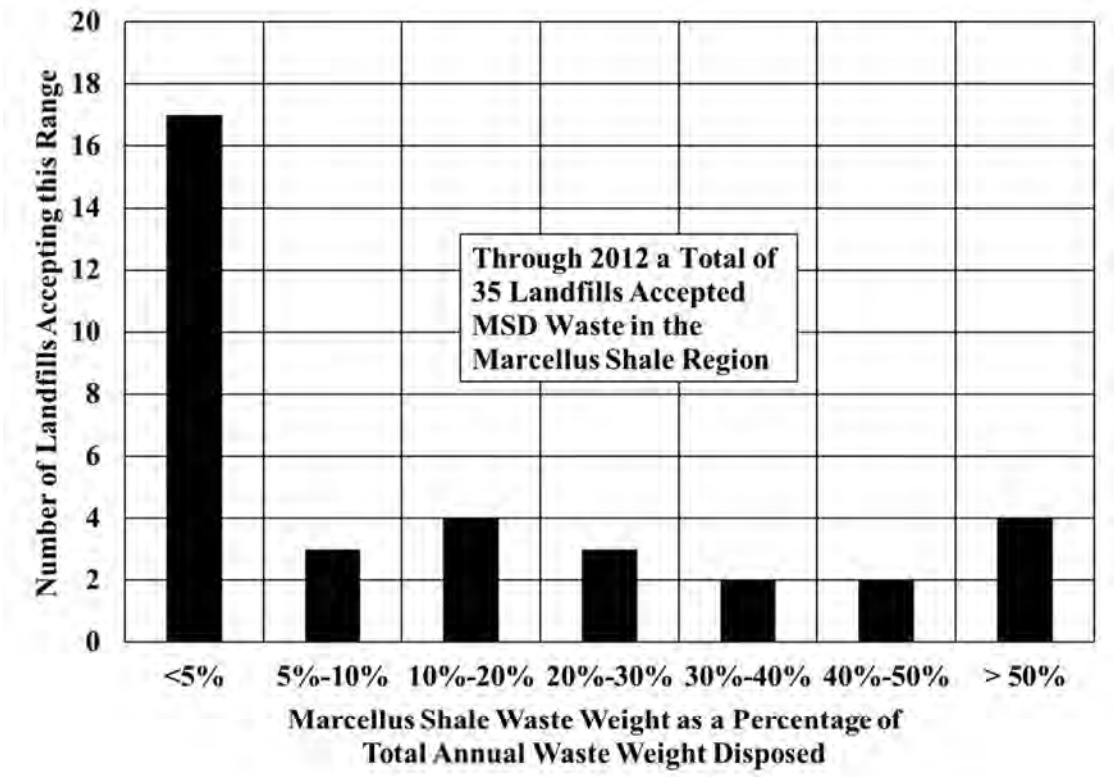

FIG. 1. Distribution of Landfills Accepting MSD Waste, End of 2012

These weights help offset a decreasing trend of MSW being disposed, as shown in Fig. 2 (for waste disposed in Pennsylvania), and provide a needed source of revenue for these landfills (PaDEP-2, 2013). MSD waste disposal as a percentage of the total waste weight should continue to increase for the near future, and will continue to represent a profitable waste stream for landfill owners.

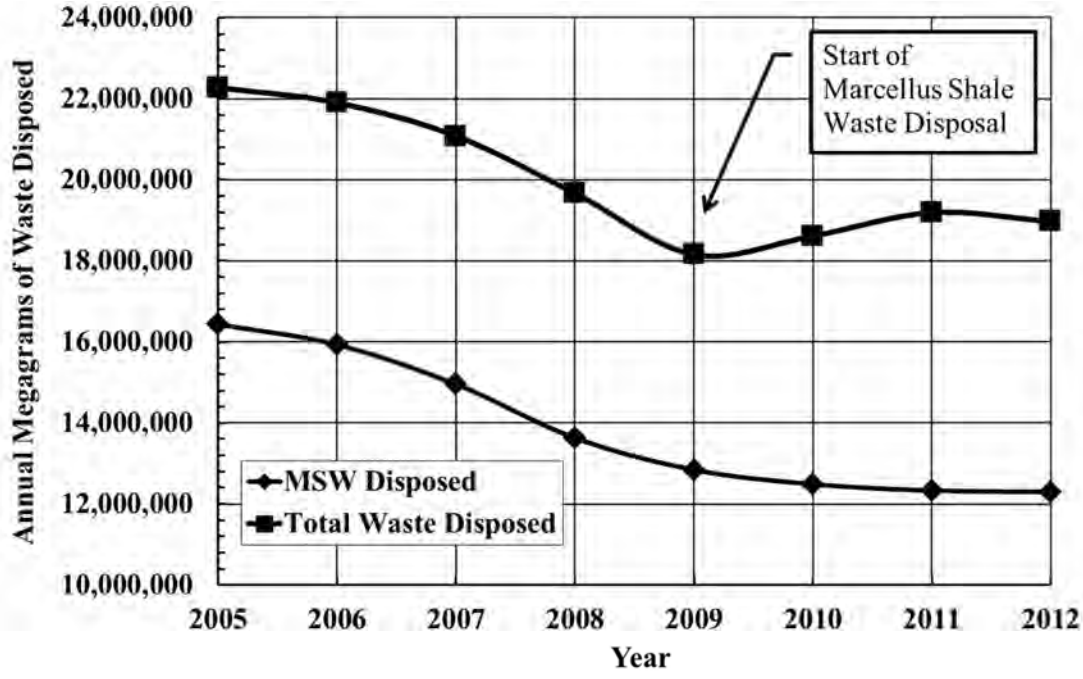

FIG. 2. Annual Municipal Solid Waste and Total Waste Disposed in Pennsylvania Landfills, End 2012

MSD WASTE GENERATION AND CHARACTERIZATION

MSD waste consists primarily of rock cuttings brought to the surface as the drill cutting head advances. Water and drilling mud entrain the cuttings and facilitate their transport to the surface. The resulting waste consistency ranges from liquid to semi-solid. Prior to disposal, the MSD waste is solidified at either the drill pad or the landfill through the addition of bulking agents. Closed-loop systems are also used at the drill pad to separate solids from liquids using various mechanical means, and produce a more soil-like waste.

Field Evaluations

The author has conducted several field and laboratory evaluations to characterize the physical and engineering properties of MSD wastes. Field evaluations have focused on obtaining representative samples using visual observations of moisture content to sort and choose samples; typically to obtain "wet" samples and "dry" samples. Pocket vane shear, pocket penetrometer, and slump cone tests have been used to refine the sample selection process, and to evaluate the ability for these relatively simple tests to field-screen MSD waste for disposal acceptance. General conclusions from field evaluations of MSD waste are:

- Moisture content is difficult to evaluate visually, and general field descriptions (i.e. dry, wet, very wet, etc.) do not correlate with laboratory-determined moisture content. In other words, it is difficult to accurately judge the moisture content of MSD wastes in the field;
- Moisture content does not correlate with laboratory-determined shear strength.
- Unconfined undrained shear strengths measured with a pocket vane shear tester range widely from approximately 9.5 kiloPascals (kPa) for wet MSD waste to 86 kPa for dry MSD waste;
- Shear strengths determined with a pocket vane shear tester correlate relatively well, in a qualitative sense, with laboratory-determined shear strength. Typically, low pocket vane shear strength corresponds to low consolidated undrained (CU) shear strength, and conversely, high pocket vane shear strength corresponds to high CU shear strength;
- Pocket penetrometer tests and slump cone tests are not useful for differentiating MSD waste consistency, are not overly sensitive to moisture content, and are not suitable for screening MSD waste; and
- There does not appear to be a simple field-based method to consistently screen MSD waste for suitability of disposal and/or determining the need for additional processing or solidification. The pocket vane shear tester provides the "best" method for field screening MSD wastes, but only in a qualitative sense, and cannot be used to accurately determine shear strength of these wastes.

Laboratory Evaluations

Laboratory evaluations of MSD wastes have focused on developing traditional geotechnical engineering properties. To date, approximately two dozen samples of MSD waste have been tested for grain size and hydrometer analyses, Atterberg limits, specific gravity, gravimetric water content, bulk unit weight, consolidated undrained (CU) triaxial shear strength, direct shear strength, one-dimensional consolidation, and permeability. Table 1 summarizes the test results (E. Chiado, unpublished internal report, December 2012).

Table 1. Summary of Laboratory Tests on MSD Wastes

Property	Average Value	Range	No. of Samples
Specific Gravity	2.56	2.15 – 2.85	21
% Fines (< 0.005 mm)	47	0 – 100	25
Atterberg Limits	LL 44, PL 31, PI 16	NP to LL 101, PL 88, PI 63	16
As-Received Moist. Cont. (%)	35	5 – 110	21
Wet Unit Weight (kg/m^3)	1,810	640 - 2,400	21

Table 1 (Cont.). Summary of Laboratory Tests on MSD Wastes

Property	Average Value	Range	No. of Samples
Permeability (cm/s)	7×10^{-6}	2×10^{-5} to 1×10^{-9}	6
CU Eff. Cohesion (kPa)	13	0 - 68	17
CU Eff. Friction Angle	34º	23º - 42º	17

Of the above samples, approximately two thirds possess a Unified Soil Classification System (USCS) classification of either low plasticity silt (ML) or low plasticity clay (CL). The remaining one third classify as either silty sand (SM) or clayey sand (SC). Relative to typical MSW properties, these test results indicate MSD waste is more fine-grained, generally wetter, approximately 2 to 2.5 times heavier, and approximately 100 times less permeable. Fig. 3 shows the effective shear strength of MSD waste is similar to that for MSW, or slightly higher. However, it must be realized the MSD waste samples were consolidated and drained prior to shearing, a condition that may or may not be achieved in a landfill setting.

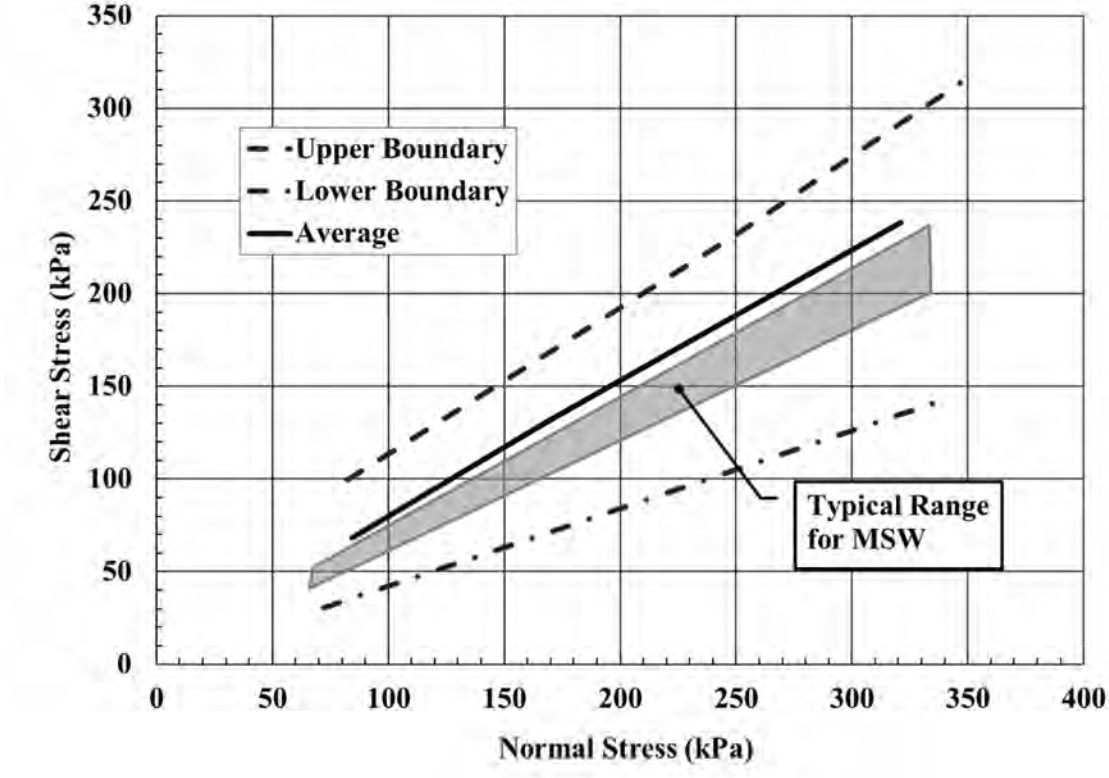

FIG. 3. MSD Waste Effective Stress Shear Strength

One dimensional consolidation tests indicate MSD waste volume decreases by approximately 5% under low normal loads, to 20% under high normal loads (E. Chiado, unpublished internal report, December 2012). Correspondingly, consolidation of MSD waste will likely release large volumes of water. Fig. 4 shows that on average, under normal loads typical of MSW landfills, each megagram (Mg) of MSD waste can potentially release approximately 0.05 to 0.15 cubic meters (m^3) of water over time, a substantial volume for which the landfill operator must plan.

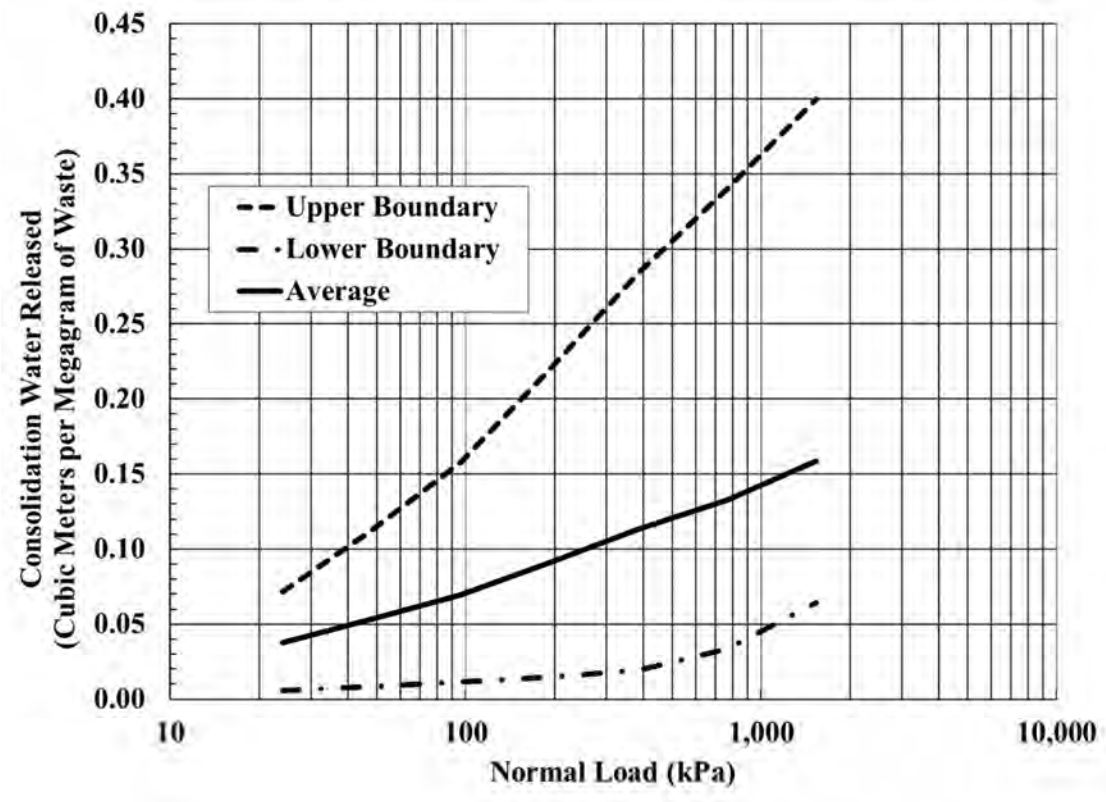

FIG. 4. MSD Waste Consolidation Water Volume as a Function of Normal Load

ENGINEERING AND OPERATIONAL CONSIDERATIONS

The consistency of MSD waste ranges from semi-solid to soil-like. Further, MSD waste is wetter and heavier than MSW, needs to consolidate and drain to possess adequate effective shear strength, is fine grained, and has low permeability. For landfills where MSD waste constitutes a substantial percentage of the total weight being disposed, potential effects on landfill operations should be considered. These include working face operations, waste mass stability, seepage, leachate quantity and quality, landfill gas (LFG) generation, and leachate and LFG collection.

Working Face and Waste Stability Considerations

Adding MSD waste into the landfill working face provides several positive benefits. These include the potential to enhance compaction by releasing water that softens and lubricates adjacent MSW, and by infilling voids within the MSW matrix with fine-grained material. Airspace utilization studies document landfill density increases between 0.36 Mg/m^3 to 0.59 Mg/m^3 when appreciable volumes of MSD waste are incorporated (E. Chiado, unpublished quarterly airspace utilization reports, 2009 through 2013).

However, because of MSD waste's relatively high moisture content, low to moderate unconfined unconsolidated shear strength, and low permeability, precautions should be taken at the working face. Perhaps most critically, MSD waste needs to be landfilled in a manner that promotes consolidation and drainage to develop adequate effective shear strength. If drainage is absent or ineffective, low strength conditions could result. This may lead to localized instability in the short-term, as evidenced by equipment becoming bogged-down in the working face, or instability of the overall waste mass in the long-term.

To achieve this end, MSD waste should not be segregated in large piles or lenses that are not eventually blended with MSW. Instead, MSD waste should be spread in thin lifts on top of MSW and be overlain by additional MSW to provide drainage paths and enhance absorption. Further, if working face conditions allow, MSD waste should be spread out to air-dry before incorporating it into the working face. Supplementary solidification agents can also be added to the MSD waste.

To minimize seepage MSD waste should be disposed in the interior of the daily working face, and should not be placed in or near the edge of interim slopes. In areas that will eventually contain final slopes MSD waste should not be graded parallel with the final slope to prevent near-surface lenses or planes. The percentage of MSD waste disposed relative to the total waste mass should be closely monitored. It is likely there is a percentage of MSD waste above which the MSD waste hydraulic and shear strength properties dominate. This could create undrained conditions regardless of operational processes undertaken to prevent this condition, resulting in an unstable waste mass.

A question to be addressed is whether the relatively high moisture content of MSD waste will affect the shear strength of MSW and the overall waste mass. MSW shear strength properties have been developed, in part, from tests and back calculations performed on unsaturated materials. With the addition of MSD waste, saturated conditions may eventually be present within the waste mass. Additional laboratory testing needs to be conducted to evaluate whether mixtures of MSD waste and MSW at various percentages and moisture contents possess different shear strengths.

Leachate Considerations

Routine landfilling of MSD waste has only occurred during the past several years, and there is little empirical data available to evaluate the effect, if any, on leachate quantity or quality. However, based on laboratory tests, on average 1 Mg of MSD waste can potentially release 0.05 to 0.15 m^3 of water, which is considerable in a

landfill environment. For example, landfilling 100,000 Mg of MSD waste per year, a rate that some sites are presently accepting, could release approximately 10,000 m^3 of consolidation water over time. This water will be absorbed by surrounding MSW and/or accumulate in the leachate collection system, and over time it is likely that unitized leachate volumes (i.e. m3/hectare) will increase.

Site personnel should evaluate the leachate collection system's ability to adequately collect, convey and remove potential increased volumes, and make system changes if warranted. Changes to enhance the leachate collection capacity could include using more permeable protective cover, and increasing pipe diameters and pump capacities. In a newly opened cell, operators should evaluate how closely to place MSD waste to the landfill base and leachate collection system. MSD waste's fines content, particularly silt, could migrate into the collection system and detrimentally affect flow capacity. Accordingly, vertical separation should be provided between the collection system and a waste lift that incorporates MSD waste.

LFG Considerations

Similar to leachate, there is little empirical data available to evaluate the effect, if any, that MSD waste may have on LFG quantity. Water released as MSD waste consolidates may promote quicker decomposition of the organic waste fraction, and thereby increase the LFG generation rate. However, this increase may be offset by the increased inorganic content provided by the MSD waste. Landfill Gas Emission Model (LandGEM) modeling indicates there is a percentage of MSD waste relative to the total waste mass below which LFG generation increases with increasing MSD waste content, and above which LFG generation decreases with increasing MSD waste.

Landfill operators should evaluate the LFG collection and control system's ability to adequately collect and convey potential increased LFG volumes, and make system changes if warranted. Changes to enhance LFG collection could include installing extraction wells earlier than planned, reducing the spacing between extraction wells, and performing more frequent maintenance of extraction wells and associated pump systems to remove water and fines.

CONCLUSION

Marcellus Shale waste is an economically attractive and growing waste stream for landfills located within the Marcellus Shale region. Volumes being disposed have increased significantly over the past several years, and this trend will likely continue in the near term. At some landfills, MSD waste comprises the majority waste type being disposed. The attraction to accept and dispose MSD waste is understandable. However, limited laboratory tests coupled with field observations indicate MSD waste possesses unique characteristics that could potentially affect both short and long-term landfill operations. Landfill owner and operators should evaluate these potential effects and determine if changes to daily operations and environmental control systems are warranted to mitigate these effects.

REFERENCES

Pennsylvania Department of Environmental Protection (PaDEP-1) (2013). "PaDEP Oil & Gas Reporting Website - Waste Reports - By Waste Facility." https://www.paoilandgasreporting.state.pa.us/publicreports/Modules/Waste/WasteByWasteFacility.aspx (Dec. 3, 2013).

Pennsylvania Department of Environmental Protection (PaDEP-2) (2013). "PaDEP Waste Management Website - Municipal Waste - MW Disposal Info." http://www.portal.state.pa.us/portal/server.pt/community/municipal_waste/14087/mw_disposal_info/589667 (Dec. 3, 2013)

Restoration of Streams and Wetlands Following Pipeline Construction Projects

Paul A. Kanouff[1]

[1]Project Manager, Civil & Environmental Consultants, Inc., 4000 Triangle Lane, Suite 200, Export, PA 15644, U.S.A., E-mail: pkanouff@cecinc.com.

ABSTRACT: Pipelines are routinely installed under streams and wetlands, resulting in temporary impacts to these resources. Section 404 of the Clean Water Act requires impacted streams, wetlands, and other waterbodies to be either restored or replaced. However, if the streams and wetlands are not restored correctly, the impacts can be permanent. The success of stream and wetland restoration is primarily dependent on returning the disturbed areas to pre-existing conditions and contours, which can be readily verified by monitoring construction activities or conducting post-construction monitoring. Recently, the U.S. Army Corps of Engineers (Corps) added a special permit condition to several linear projects in Pennsylvania requiring post-construction monitoring of restored streams and wetlands to ensure the success of the restoration efforts. The special permit condition required that a summary report of the monitoring be submitted to the Corps stating that excess fill material was removed and the site was restored to pre-existing conditions and contours. The report also needed to document the existence and relative success of revegetation efforts and installed erosion and sedimentation controls. The majority of stream and wetland permits for pipeline projects do not include a special condition requiring post-construction monitoring. Further, most natural gas operators do not typically conduct construction monitoring or post-construction monitoring to specifically review stream and wetland restoration efforts unless required as a permit condition. Without monitoring, easily avoidable and solvable problems could result in permanent stream and wetland impacts. As more pipelines are installed, stream and wetland restoration may become a primary environmental and regulatory concern and require more active construction monitoring by natural gas operators.

INTRODUCTION

Stream and wetland impacts resulting from the installation of pipelines should be temporary. However, if the restoration is not conducted properly or uncommon conditions are encountered, the impacts can become permanent. These impacts can result in the loss of stream headwaters, the isolation of stream sections, the introduction of non-native species, the loss of wetlands, and the conversion of scrub-shrub and forested wetlands to herbaceous wetlands. Most restoration problems can

be easily corrected during or shortly after the restoration is completed. However, the problems cannot be corrected unless they are identified. Since neither construction nor post-construction monitoring is required for most pipeline projects, these problems will only be identified through self-imposed monitoring or field reviews conducted by regulatory agencies.

This paper was written to assist natural gas operators with project planning, to provide instruction on restoration methods, and to stress the importance of restoration monitoring.

PROJECT PLANNING AND IMPACT MINIMIZATION

Corps Nationwide Permit General Condition 23 requires stream and wetland impacts to be minimized to the maximum extent practicable. Although this is a requirement, there is no guidance provided for determining the maximum extent. The Corps defines practicable as, "Available and capable of being done after taking into consideration cost, existing technology, and logistics in light of overall project purposes". However, the extent of minimization is typically more dependent on the construction standards adopted by each natural gas operator, which specify right-of-way widths and construction methods. Therefore, the degree of minimization is often left to the discretion of the natural gas operator or their consultant.

Besides being a requirement, minimizing impacts can be greatly beneficial to natural gas operators by reducing overall restoration efforts. Minimizing impacts also can benefit natural gas operators by reducing restoration costs, especially if the impacted areas must be revegetated with trees, shrubs, or a special seed mixture, or if the soil must be reconditioned or improved prior to restoration.

Impact minimization should be a fundamental part of project planning. Techniques include routing adjustments and construction right-of-way reduction at stream and wetland crossings, the latter of which can significantly minimize impacts for longer pipeline projects. Figure 1 shows an example of avoiding and minimizing impacts by adjusting the pipeline route and reducing the right-of-way.

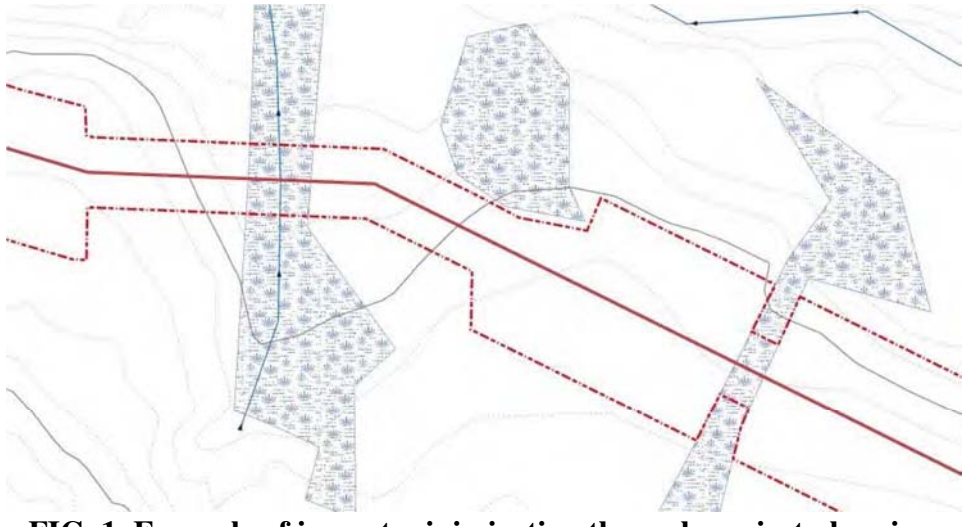

FIG. 1. Example of impact minimization through project planning.

Project planning should also include such details as the type and placement of pipeline and temporary road crossings of aquatic resources and the time of year that construction will occur. For instance, crossings should be conducted at the narrowest points of the resources and positioned within the right-of-way to facilitate vehicle traffic, reduce the amount of travel throughout the right-of-way, and minimize the number of repeated passes. Different types of construction equipment, such as low ground pressure equipment, can be used to lessen the compaction of wetland and stream bank soils and reduce rutting. Lastly, the time of year can greatly influence the amount of disturbance and either hasten or hinder restoration. The best time to conduct pipeline activities is dependent on the location, but "low flow" periods in late summer and frozen conditions in mid-winter are typically considered the best for minimizing impacts to aquatic resources (NHDRED 2010).

OPEN-CUT PIPELINE INSTALLATION IN STREAMS AND WETLANDS

The open-cut pipeline installation method involves the excavation of an open trench, the placement of the pipeline into the bottom of the trench, and the backfilling of the trench. This is the typical method used for pipeline installation for upland areas and is often used for stream and wetland crossings. However, open-cut pipeline installation in streams and wetlands should include additional steps specific to streams and wetlands to significantly improve the likelihood of successful restoration.

For streams, the existing substrate should be separated from the subsoils during excavation of the pipeline trench. Once the pipeline has been installed, the subsoils should be replaced and the stream channel re-graded. The existing substrate should then be placed back into the re-graded stream channel. The banks should be stabilized immediately, and all disturbed areas restored to approximate original contour, seeded, and mulched.

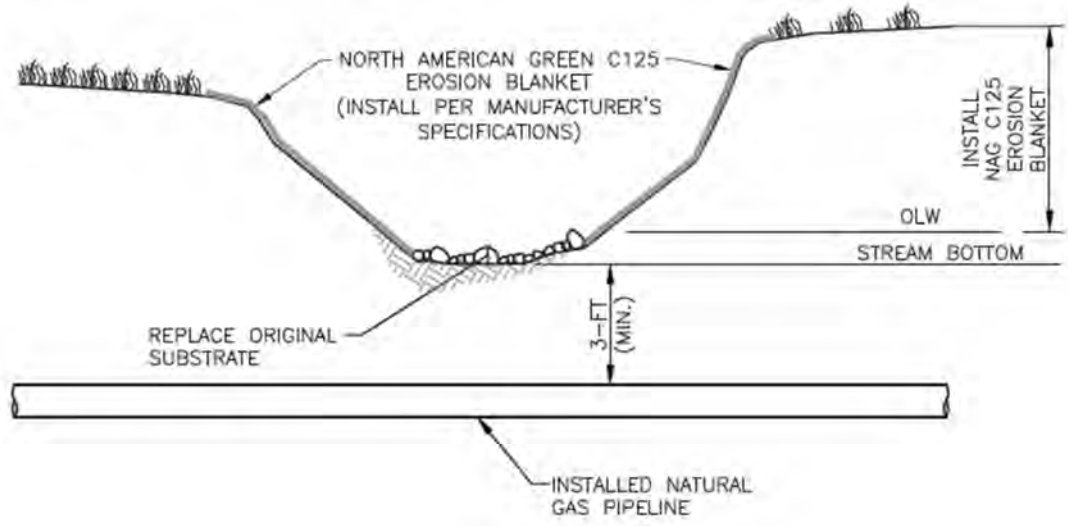

FIG. 2. Typical pipeline installation under a stream.

For wetlands, construction equipment should be operated on timber mats to

minimize disturbance to the wetland. The top 12 inches of soil should be segregated from the other soils during excavation of the pipeline trench. Clearing and grubbing should be limited to the extent possible, especially for scrub-shrub wetlands and forested wetlands. Once the pipeline has been installed and the subsoils replaced, the excavated 12 inches of wetland topsoil should be replaced into the top of the trench. The wetland should then be restored to approximate original contour, seeded and/or planted, and mulched.

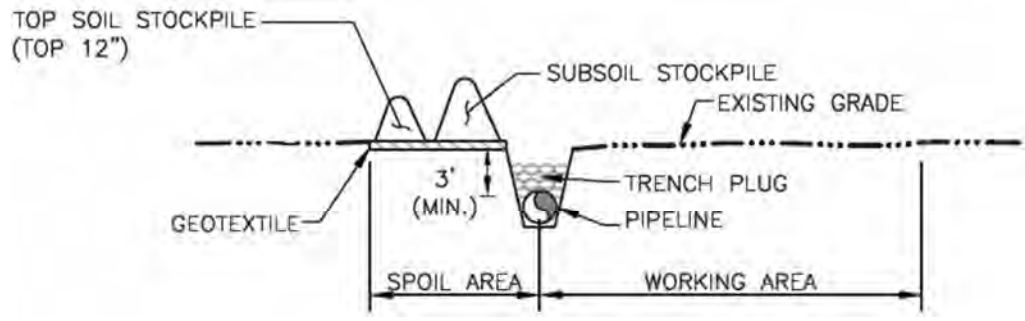

FIG. 3. Typical pipeline installation under a wetland.

The erosion and sediment controls used at stream and wetland crossings should consider factors such as anticipated stream flows and depths, bank grades, and the degree of saturation of the wetland soils. Additionally, trench plugs should be installed on both sides of all stream and wetland crossings to prevent the draining of the streams and wetlands, and to prevent changes to their hydrology (PADEP 2012).

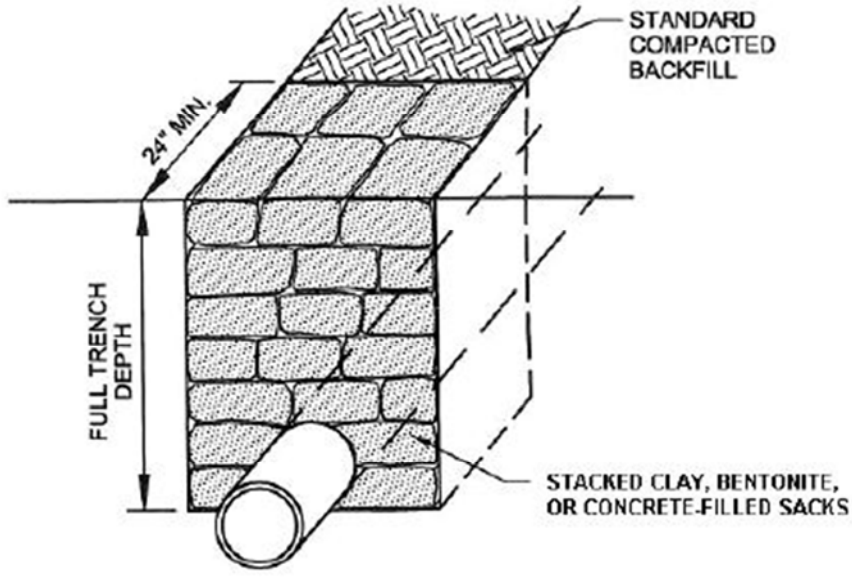

FIG. 4. Typical trench plug (PADEP 2012).

COMMON PROBLEMS

Problems Related to Construction

Changing the slope and contours of a stream or wetland can have a significant detrimental effect on restoration efforts. The success of stream and wetland restoration is primarily dependent on returning the disturbed areas to pre-existing conditions and contours. Wetlands that are restored to pre-construction grades are significantly more successful than wetlands that are not restored to pre-construction grades (FERC 2004). Figure 5 shows a depressional wetland area that was not restored to pre-existing contours and conditions following pipeline construction. The depressional area was located at the toe of the slope and was inadvertently filled because the contractor followed the existing contour from the upslope area instead of the pre-construction grade of the depressional area. In addition, a waterbar was added immediately upslope of the area. Due to the waterbar and the additional fill, upslope runoff was being diverted away from the area, and water from overbank flooding was no longer being trapped in the depressional area. As a result, the wetland did not fully recover following construction.

FIG. 5. A depressional wetland area that was not restored to pre-existing contours and conditions following pipeline construction. The red line represents the original toe of slope. The red arrow points to the waterbar that was added.

If construction monitoring is not an option, ample documentation ranging from photographs, delineation maps, and survey data should be provided to enable the pipeline contractor to restore the site to pre-construction grades. The correction of grading issues after initial restoration has occurred typically requires remobilizing

construction equipment and the re-seeding of the disturbed areas, which can increase restoration costs.

Improper placement or installation of temporary crossings and extensive vehicle traffic can cause soil compaction in wetlands and along stream banks, increasing surface water runoff and hindering revegetation. These effects will, in turn, lead to an increase in erosion and sedimentation. Soil compaction also can change wetland hydrology by decreasing the absorption and infiltration of surface water (Schipanski 2008).

Improper placement or installation of erosion and sediment controls can cause increased sedimentation in streams and wetlands. The additional sediment can reduce the amount of water storage provided by streams and wetlands, which decreases their ability to reduce flooding. Increased sedimentation also decreases species richness in streams (Newcombe 1991).

Problems Related to Types of Aquatic Resources

Some streams and wetlands have natural features that make restoration difficult. Bedrock substrates, braided stream channels, and frequently flooded areas may require different approaches or controls to enable successful restoration. Wetland borders and wetlands with poor characteristics are especially vulnerable to disturbances because they often barely meet the parameters to be designated wetlands. Therefore, slight changes to these areas can be detrimental and difficult to correct. Extremely wet areas present difficulties for both the pipeline installation and the restoration efforts. Special restoration measures or equipment may be needed in these areas.

CORPS SPECIAL PERMIT CONDITION FOR PIPELINE PROJECTS

The Corps recently added a special permit condition to linear projects, such as gas pipeline and sewer line projects, that are located in Pennsylvania and reviewed by the Corps under the Pennsylvania State Programmatic General Permit (PASPGP-4) and contain cumulative impacts. The special permit condition requires post-construction monitoring of restored streams and wetlands. According to the Corps, the condition was created in response to public concern over the growing number of pipeline projects and the need for the Corps to review cumulative impacts under the PASPGP-4. The submitted data will allow the Corps to assess whether these projects are having a cumulative effect on streams, wetlands, and overall watersheds. The Corps anticipates the special permit condition will continue to be added to projects for at least the next few years.

The special permit condition required the post-construction monitoring include two monitoring events. The first event was to be conducted one month after the authorized work was completed and the second event conducted at the end of the first full growing season, but no later than October 31. Summary reports were required to be submitted to the Corps within two weeks of each monitoring event. The reports had to contain a statement that all excess fill material was removed and the site was restored to pre-existing conditions and contours. In addition, the report had to document the existence and relative success of revegetation efforts and installed

erosion and sedimentation controls.

The special permit condition did not include performance standards nor has the Corps established general performance standards for restoration projects. Therefore, the restoration of temporary impacts for these pipeline projects will be considered a success if the site is restored to pre-construction conditions and contours. It must be assumed that post-construction measures of attributes such as percent vegetative cover and bank stability must match or exceed pre-construction conditions to be considered successful.

MONITORING

Pre-Construction Walkover

With the exception of Federal Energy Regulatory Commission (FERC) regulated waterbody crossings greater than 100 feet, site-specific restoration plans are not typically prepared for temporary pipeline impacts. Therefore, the pipeline installation should be conducted according to the typical methods described herein. Additional measures may be needed for certain sites, such as bedrock streams, braided stream channels, and frequently flooded areas. A pre-construction walkover could allow an experienced professional to identify these areas prior to construction and recommend additional measures, if needed.

Construction Monitoring

Construction monitoring is the on-site observation of pipeline installation and/or restoration activities during active construction. If restoration work is not successful, remedial work will be required, which may involve additional grading, seeding, planting, or installation of erosion and sediment controls. Active construction monitoring allows for identification and correction of problems as they occur and is particularly useful for areas that are difficult to access with equipment or materials. Although additional costs will be incurred to conduct the monitoring, restoration and post-construction expenditures may be substantially reduced. The construction monitoring technician should have wetland and stream experience and the knowledge and authority to identify problems and recommend corrective actions.

Post-Construction Monitoring

Post-construction monitoring is the on-site observation of site conditions after construction activities have been completed. The monitoring can be conducted at any time after construction, but should include at least two monitoring events. Issues identified during the first event should be corrected prior to conducting the second event. Post-construction monitoring should be completed on all projects to verify that streams and wetlands are restored to pre-existing conditions. Monitoring reports are a record of the restoration efforts and, if needed, can be used to verify that restoration efforts were successful. In addition, if the restoration is not successful due to outside circumstances such as ATV traffic, farming, logging, or

residential/commercial development, monitoring reports will also serve as a record of these activities.

CONCLUSIONS

Section 404 of the Clean Water Act requires the restoration of temporary impacts to streams and wetlands. However, if the streams and wetlands are not restored correctly, the impacts can be permanent. The success of stream and wetland restoration is primarily dependent on returning the disturbed areas to pre-existing conditions and contours, which can be confirmed by monitoring construction activities or conducting post-construction monitoring. A recent special permit condition added by the Corps to several pipeline projects required post-construction monitoring of restored streams and wetlands. A summary report of the monitoring had to be submitted to the Corps detailing the relative success of the restoration efforts.

Stream and wetland impacts should be avoided and minimized through project planning, and site-specific construction plans and methods should be used to further minimize impacts. Poor construction methods and inadequate erosion controls can impede the restoration of streams and wetlands. In addition, natural features of streams and wetlands may make restoration difficult and could require additional measures. A pre-construction walkover could identify these potential problem areas, and additional measures could be recommended. Construction and post-construction monitoring can identify and correct problems that could result in permanent stream and wetland impacts.

Post-construction monitoring of wetland and stream impacts is not required for most pipeline projects, and most natural gas operators do not typically conduct construction monitoring or post-construction monitoring to specifically review stream and wetland restoration efforts. As more pipelines are installed, stream and wetland restoration may become a primary environmental and regulatory concern and require more active construction monitoring by natural gas operators. To assist with this effort, the Corps should establish regional performance standards for the restoration of temporary stream and wetland impacts.

REFERENCES

Commonwealth of Pennsylvania, Department of Environmental Protection. (2012). "Erosion and Sediment Pollution Control Program Manual." Technical Guidance Number 363-2134-008. Harrisburg, PA.

Commonwealth of Pennsylvania, Department of Environmental Protection, Bureau of Oil and Gas Management. (2001). "Oil & Gas Operators Manual." Harrisburg, PA.

Commonwealth of Pennsylvania, Department of Environmental Protection, Bureau of Watershed Management. (2001). "Underground Utility Line Construction Typical Erosion and Sediment BMP's." Harrisburg, PA.

Cowardin, L. M., Carter, V., and Golet, F. C. (1979). "Classification of Wetlands and Deep Water Habitats of the United States." U.S. Department of the Interior, Fish and Wildlife Service. Washington, D.C. FWS/OBS-79/31.

Federal Energy Regulatory Commission (FERC). Office of Energy Projects. (2004). "Research of Wetland Construction and Mitigation Activities for Certificated Section 7(c) Pipeline Projects." Washington, D.C.

FERC. Office of Energy Projects. (2013). "Wetland and Waterbody Construction and Mitigation Procedures." Washington, D.C.

Newcombe, C.P. and MacDonald, D.D. (1991). "Effects of Suspended Sediments on Aquatic Ecosystems." *North American Journal of Fisheries Management*, 11(1), 72-82.

New Hampshire Department of Resources and Economic Development (NHDRED). (2010). "Best Management Practices Manual for Utility Maintenance in and Adjacent to Wetlands and Waterbodies in New Hampshire." Concord, NH.

Novitzki, R.P. (1979). "Hydrologic characteristics of Wisconsin's wetlands and their influence on floods, stream flow, and sediment." *Wetland functions and values: The state of our understanding*. Minneapolis, MN, 377-388.

Schipanski, N. GBH Environmental. (2008). "Wetland Protections in Tompkins County, New York: Existing Status, Gaps and Future Needs." Ithaca, NY.

U.S. Army Corps of Engineers Environmental Laboratory. (1987). "Corps of Engineers Wetlands Delineation Manual." Technical Report Y-87-1, U.S. Army Engineer Waterway Experiment Station, Vicksburg, MS.

U.S. Army Corps of Engineers. (2012). "Regional Supplement to the Corps of Engineers Wetland Delineation Manual: Eastern Mountains and Piedmont Region Version 2.0." ERDC/EL TR-10-9, U.S. Army Engineer Research and Development Center, Vicksburg, MS.

Ensuring Sustainable Development of Shale Gas Transmission Infrastructure by Applying State-of-the-Art Methods in Geomorphology

M. Logan Cline[1], Ph.D., K. Michael Cline[2], P.G., Daniel J. Barton[3], P.E., and Paul C. Rizzo[4], Ph.D., P.E.

[1]Senior Project Geoscientist, Paul C. Rizzo Associates, 500 Penn Center Boulevard, Penn Center East, Suite 100 Pittsburgh, PA 15235, E-mail: mlogan.cline@rizzoassoc.com
[2]Principal, Geosciences, Paul C. Rizzo Associates, 500 Penn Center Boulevard, Penn Center East, Suite 100 Pittsburgh, PA 15235
[3]Vice President, Earth and Environmental Sciences, Paul C. Rizzo Associates, 500 Penn Center Boulevard, Penn Center East, Suite 100 Pittsburgh, PA 15235
[4]President/CEO, Paul C. Rizzo Associates, 500 Penn Center Boulevard, Penn Center East, Suite 100 Pittsburgh, PA 15235

ABSTRACT: A boon in shale gas transmission infrastructure (SGTI) is underway due to the importance of shale gas as a critical global energy resource that can pave the way toward energy independence in the U.S. Because its importance, it is critical to develop SGTI in responsible and sustainable ways by mitigating risks associated with geological hazards, while simultaneously evaluating potential environmental impacts resulting from SGTI development. We describe a robust set of quantitative and qualitative geomorphic methodologies that relying on state-of-the art data and methods for evaluating geological hazards related to SGTI development. The methods include: 1) high-resolution spatial and temporal monitoring of (potentially) active slopes in true three-dimensional (3D) space; high-precision and accuracy measurements of both modern and long-term erosion rates at the basin-scale; and 3) the application of paleoflood hydrology for improving flood hazard evaluations.

INTRODUCTION

On August 13, a Marcellus Shale gas pipeline ruptured in Wetzel County, WV due to a landslide that was triggered during heavy rains. Approximately one month later, in Colorado, flooding caused at least two pipelines to rupture from flooding debris impacts, forcing a large shutdown of all operations. Events like these are costly for both the environment, as well as the gas industry; however, natural gas-rich geological deposits such as the Marcellus Shale are poised to pave the way toward energy independence in the U.S. This relatively new boon in energy resource development has been made possible by technological advances in resource extraction. In order to continue on a path forward, it is critical that the shale gas industry be better prepared to mitigate flood and slope hazards (herein referred to as

geological hazards), particularly in light of growing public concern over shale gas industry practices (e.g. various moratoriums on hydro-fracturing either in effect, or under consideration). The SGTI industry is in a position to alter negative public opinions of extraction and transmission practices, but to be successful they must demonstrate their commitment to environmental sustainability, in addition to their commitment to economic development.

One very significant way that the SGTI industry can demonstrate their sustainability commitment is through robust hazard and environmental mitigation practices. Geological hazards such as landslides and floods place SGTI at reasonably high risk, and the development of SGTI poses an environmental hazard to surface water in numerous ways, including sediment loading caused by excessive runoff and subsequent erosion. The hazards are particularly significant in areas where SGTI traverses steep terrain, waterfronts or seismically active zones.

METHOLOGICAL APPROACH TO ACCESSING GEOLGICAL HAZARDS

Topographic form is primarily governed by tectonics (mountain building) and climate (e.g. processes that produce relief). The processes of erosion, sediment transport and deposition are well-described by geomorphic equations (e.g. Dietrich, 2003, Bull 1999). Consequently landscape's form is semi-predictable, and in many cases self-organizing (Perron, 2009). As a result of its predictability and organization, information about the processes that form them can be deduced by carful geomorphic analysis. This is complicated, however, when the earth's surface is perturbed by seismicity episodic processes such as meteor impacts, anomalous large floods, and anthropogenesis, thereby leaving behind lasting features on the landscape that overprint the original, internal form of the landscape. In some cases the features have easily identifiable forms such as fault scarps or impact craters; however, in most cases the features are more subtle, requiring careful observation, measurement, and analysis. To ensure that the maximum number of relevant landscape features are be identified, high-resolution topographic should be exploited and the best methods that measure the rates of those processes should be used. We present several previously-developed methods for evaluating the landscape for landslide and flood hazards, as well as methods for evaluating and quantifying modern and paleo erosional impacts. We describe a robust set of quantitative and qualitative methodologies for evaluating geological hazards and erosional impacts related to SGTI, including:

- Flood hazard evaluation applying paleoflood hydrology methods
- Landslide hazard evaluation based on extremely high-resolution light detection and ranging (LiDAR) topographic data.
- High-resolution spatial and temporal scale monitoring of (potentially) active landslides and slopes in true three-dimensional (3D) space.
- Characterization of modern erosion rates resulting from SGTI development using, as well as paleo erosion rate measurements for background rate determination.

Results from these types of analyses can be used to protect infrastructure and assess future impacts to ecological resources, thereby providing a framework to responsibly develop shale gas that enjoy a higher level of support from the public. To better illustrate these approaches, we borrow several examples from our own work, as well as others that are presented here.

Flood Hazards

Floods pose a considerable risk to SGTI (e.g. Colorado Floods of 2013). The majority of our flood management practices are built around the way flood frequency-magnitude relationships are understood. High magnitude flood predictions are derived from straight-forward extrapolations of relatively small temporal records, and the magnitude-frequency relationships are assumed to be time-invariant (i.e. "stationary"). Because extreme events are rare in nature, they are infrequently captured by gaged records (Klemes, 1994; Baker, 2002) that in some cases only span a century. Fortunately, many extreme floods are recorded in the geological record. The study of these extreme floods is referred to as paleoflood hydrology (e.g. Kochel and Baker, 1982), and what we have learned from the field is that the stationarity assumption used to develop flood magnitude-frequency relationships is flawed. The paleoflood record, as well as recent extreme flooding has demonstrated that floods cluster in time and space (e.g. Ely et al., 1993), and as a result, the flood magnitude-frequency distribution of a given river basin is variable in time and space, dependent on the global, synoptic, regional and local-scale circulation patterns (Hirschboeck, 1988; Cline, 2010). Furthermore, peak meteorological floods result from combinations of incipient conditions that couple with unique meteorological events. While the signal of a meteorological events may be captured by the statistical description of surface hydrology (i.e. magnitude-frequency relationships), the incipient conditions are not, leaving a critical element out of the frequency magnitude analysis.

Some of these shortcomings are overcome with catchment runoff modeling approaches, although true empirically-derived data can be developed from paleoflood hydrology, and the data can "fill-in" the extrapolated part of the flood frequency analysis (FFA) curve with empirically-derived data. Paleoflood hydrology can typically extend a flood record several thousand to ten thousand years in bedrock-controlled rivers. The methods of paleoflood hydrology borrow from geology, engineering, and hydrology. It relies on the assumptions that the geomorphic positions of flooding evidence can be used to model peak discharge, and that their geomorphic evidence can be dated.

Paleofloods leave behind paleostage indicators (PSIs)—the geomorphic indices of flood-water levels (e.g. Baker 2006). The PSIs are either geological (sediment deposits or erosional features) or biotic (changes in growth patterns). Some PSIs may not be indicative of the maximum water surface during a flood, whereas others are well-known to demarcate the upper limit of a floods water surface, such as a slackwater deposit (SWD). In both cases, there are means to date virtually any of them analytically to derive high-precision ages. Given the right geological

preservation conditions (e.g. Ely et al., 1993) a suite of flood deposits, each representing a different age flood can be preserved on the landscape. If age control is developed along with paleodischarge estimates, then these data can be added to FFA. Figure 1 shown below is a slackwater deposit (SWD) that formed in a bedrock alcove along the San Miguel River in S.W. Colorado. The SWD is composed of sediments from at least five significant floods. Each of which dramatically exceeds the largest historical floods, including one from a dam break in 1923 (Cline, 2010).

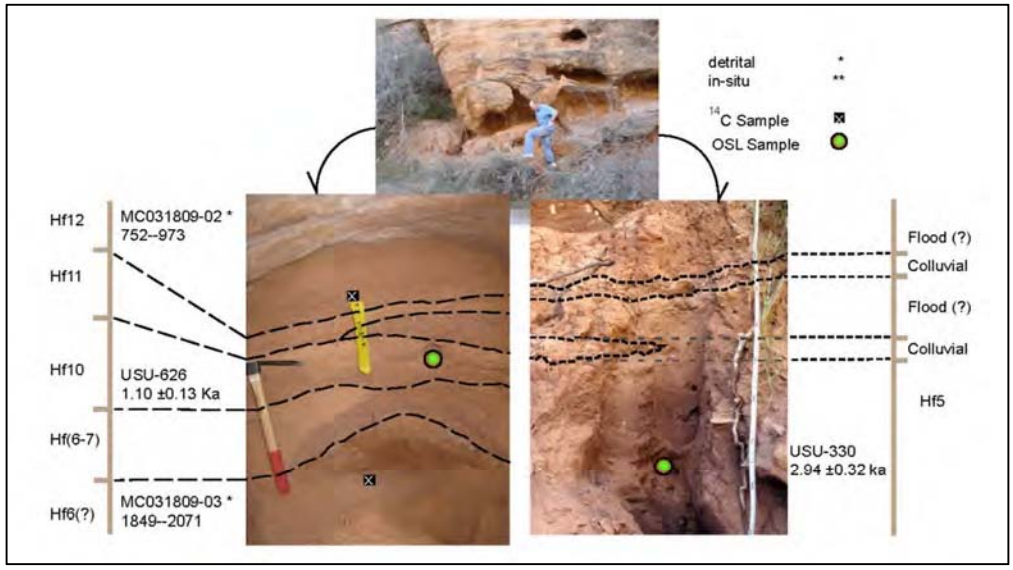

FIG. 1. Slackwater deposit along the San Miguel River in SW, Colorado, showing locations of various sampling methods (Cline, 2010). Individual flood units are delineated by dashed lines. Holocene floods (Hf) are noted. Black X's and green circles indicate sampling locations.

One-dimensional step-backwater models such as HEC-RAS are used to reconstruct paleoflood discharges by iteratively running steady flow simulations until the flood stages indicated from the PSIs are reached. By incorporating LiDAR data, much of the uncertainty in the topography is removed, and robust 1D discharge estimates are possible. The image below (Figure 2) shows an oblique view, looking upstream along the San Miguel River where the SWD shown in Figure 2 was excavated.

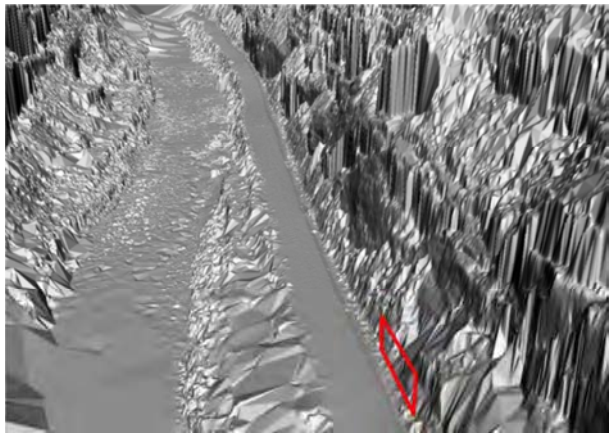

FIG. 2. Terrestrial LiDAR data of San Miguel River near the SWD shown in figure 1. The location of Figure 1 is shown by the red polygon. For near-field scale, the red polygon in 10 m in length.

As an illustrative example, below is an example of a flood envelope curve for the Upper Colorado River Basin (Figure 3). A flood envelope curve is an empirically-driven plot of peak discharges at given locations along a river, relative to their upstream contributing area. The upper bound represents the empirically-driven maximum flood when all data (recorded and paleoflood) are included. The data derived from the San Miguel River example are plotted for comparison, including the peak paleoflood and peak floods from the instrumental period. The San Miguel River has a limited flow record, and remains one of the few rivers in the western U.S. that flows (mostly) freely.

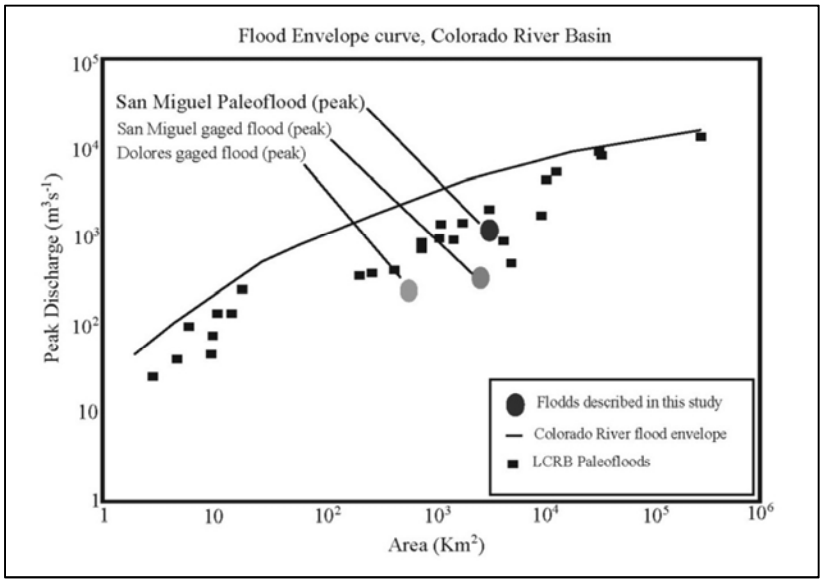

FIG. 3. Peak flood envelope (peak discharge vs. contributing area) for the Lower Colorado River Basin with San Miguel peak paleoflood and gaged flood plotted (From Cline, 2010).

Erosion Rate Measurements

Quantifying paleo-erosion rates has been an issue that has long-plagued the scientific community. There are many rudimentary methods available such as: 1) measuring sediment deposit thicknesses and correlating with other deposits; 2) measuring basin dissection; and 3) utilizing erosion "pins" such as hoodoos or other stable landscape features. Unfortunately the methods are quite limited and rely on significant assumptions. There are numerous methods for measuring modern erosion rates as well, and even most of those are rudimentary, most relying on various forms of sediment traps. These methods are not spatially uniform so significant assumption must be made to estimate erosion of broad catchments. But even with the best modern estimates, we still have very little constraint on past processes—those occurring prior to industrialization or even widespread shale gas extraction. As a result, it is difficult to assess the erosional impacts related to SGTI or any other impacts that may enhance or reduce erosion rates within a catchment. In this section we briefly describe a possible solution to his dilemma that includes high-resolution, modern erosion measurements and catchment-averaged paleo-erosion measurements.

Modern Erosion Measurements

An increasing number of states around the U.S. have LiDAR data resolved finer than 1 m^2 resolution. These data are often accurate to within a 15 cm, and their precision is extremely high. The state of PA has LiDAR coverage for nearly the entire state and these data can provide a baseline for new development of SGTI as a pre-erosion condition. Following development, additional LiDAR scans can be used to quantify the change with very high precision and accuracy, with complete spatial coverage so no spatial interpolation methods are required. The measurements derived from this method of change detection require far less time, and fewer resources, as they can be done remotely. For small basins (<4 km^2) repeated terrestrial (tripod- or vehicle-based) LiDAR scans can be performed at a very high rate (daily, weekly, monthly etc.) with a resolution on the order of a couple of a cm^2, and the temporal resolution required can meet the needs of any project (daily, weekly, annually, etc.). By combining these repeated LiDAR scans, real, meaningful change detection can be quantified. As such, the volumetric flux of sediment can be easily quantified with unprecedented accuracy (e.g. Delong et al., 2010).

An even newer and cheaper method—Structure From Motion (SFM)—provides a means of developing very high resolution terrain models, comparable to LiDAR data from the geometric sequencing of 2D photographs. The potential applications of this tool are extensive for geomorphologists for a number of reasons: the method often requires less lead time for planning data acquisition; it can be flown from remote controlled "toy" helicopters, kits, balloons, remote controlled airplanes etc. Furthermore, they only require simple cameras and softwares to process the data into extremely high resolution (a few cm^2). With proper ground control, accuracies of <10 cm can be achieved, and change detection of several cm vertically and a few tens of centimeters horizontally are possible.

To illustrate the level of detail provided by terrestrial LiDAR, Figure 4 highlights the accuracy of erosion measurements when proper field techniques and processing techniques are applied. The terrestrial scans were produced by DeLong et al., (manuscript in preparation) of the USGS in the summer of 2011, and spring of 2012. The first of five scans (each taking roughly 8 hours) was performed immediately after the Horseshoe 2 fire in the Chiricahua Mountains of southeastern AZ. The southwestern Monsoon season had not yet begun, so virtually no erosion had taken place prior to the initial scan. There were five scans in total, each occurring after significant storm events, and a final scan that occurred the next spring, prior to the onset of the 2011 Monsoon season. Rain gauges as well as time-lapse photos were deployed to further constrain the processes in the steep headwater catchment. Ultimately the data produced from this study resulted in an unprecedented level of detail, allowing for high accuracy and precision volumetric flux measurements. The LiDAR-measured flux was compared with empirical formulations developed by the USGS (Delong et al., (*in preparation*) noted a difference of roughly (+) 25% increase in actual flux than formulas predicted).

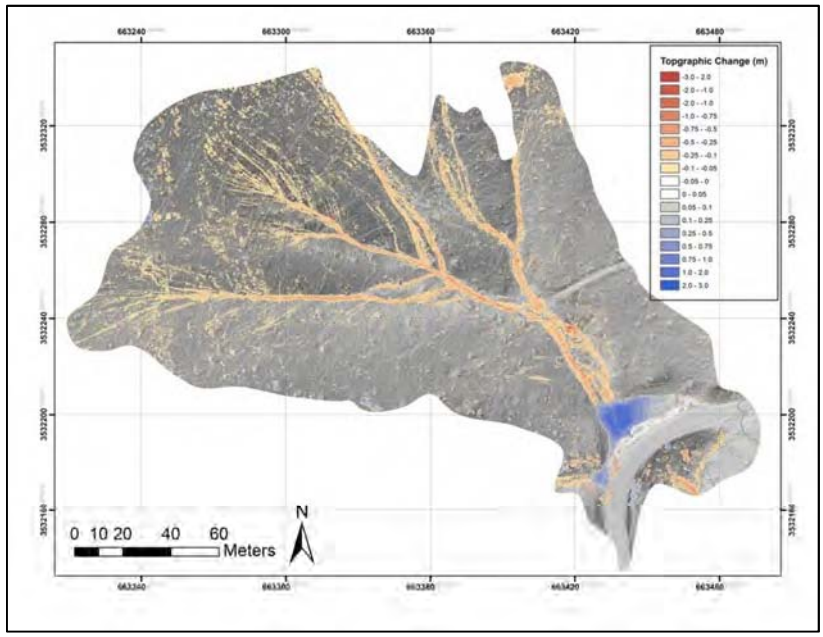

FIG. 4. The image is showing the result repeat measurements of terrestrial LiDAR scans, following bare earth extractions. Values on scale represent vertical change in elevation (*Delong et al., manuscript in preparation; with permissions*).

Paleo-Erosion Measurements

Regardless of how accurate the modern erosional measurements are, paleo-erosion must be estimated in order to make meaningful conclusion about the impacts of modern SGTI development to the sediment budgets. These measurements are

quantifiable by using in-situ cosmogenic nuclides that are produced when cosmic rays bombard the Earth, interacting with minerals within the upper part of the Earth's near-surface. By measuring cosmogenic nuclides on the sediments of active channels, we can now determine basin-averaged erosion rates. Basin-averaged erosion rates not only account for the vertical and lateral adjustments of developed channel networks, but also the surface denudation (aka lowering) of hillslopes. Most rocks that contain quartz or feldspar or calcium-bearing minerals that develop in-situ cosmogenic nuclides such as ^{10}Be and ^{36}Cl (there are others) when they are near the earth's surface. These unstable cosmogenic nuclides have well-constrained production and decay rates, and as a result, measuring their concentrations in active channels provides critical information about the rates of erosion within the basin for both the bedrock and sediments. In essence, low cosmogenic concentrations suggest erosion rates are high, and high cosmogenic concentrations suggest the erosion rates are low. The actual paleo-erosion values determined cosmogenic nuclide measurements can be compared with modern values to provide a broad constraint on the erosion rate changes due to the development of SGTI.

In coastal California near the San Andreas Fault, DeLong et al., (2012) measured erosion rates derived from cosmogenic ^{10}Be and compared them with erosion rates measured by differencing two LiDAR scans over four years. Figure 5 highlights these changes. Delong et al, (2012) were able to produce high-resolution, meter-scale, change detection maps of the surface topographic change, and calculate volumetric flux in true 3D space. The authors showed that the high-resolution topography produces a high-accuracy estimate of volumetric flux, and the cosmogenic ^{10}Be-derived measures were consistent with those values, suggesting that the long-term erosion rates (thousands of years) are consistent with the modern day sediment flux. Results from this study demonstrate the feasibility of utilizing CRN ^{10}Be to develop catchment-wide erosion rate measurements for engineering application.

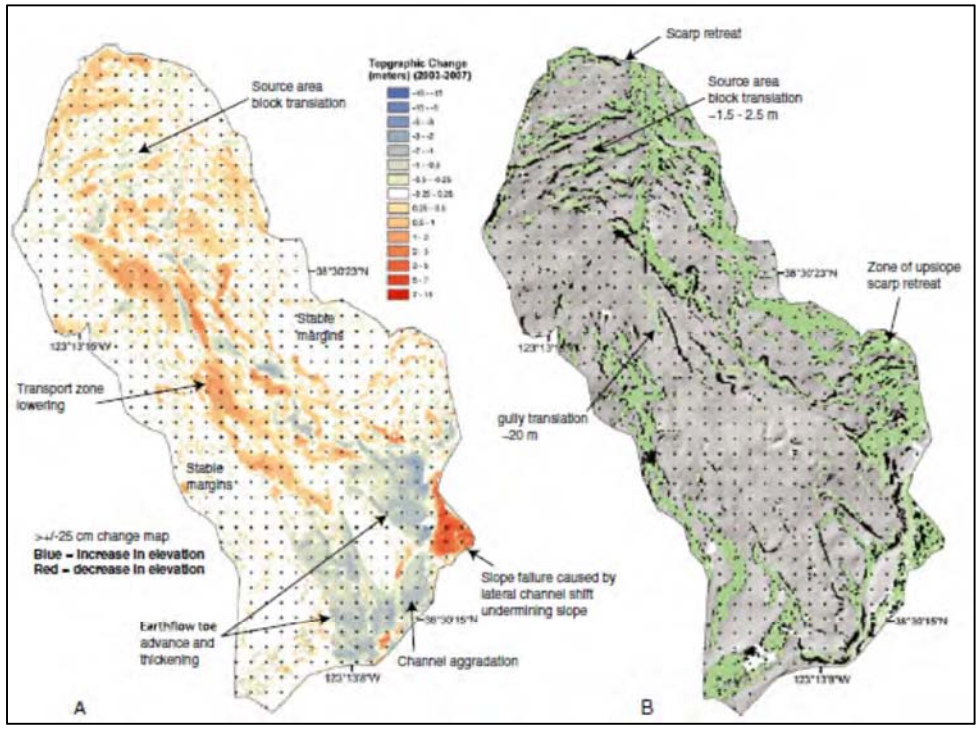

FIG. 5. Differencing of two LiDAR scans at 1 m resolution showing areas of aggradation and areas of denudation. Image on left shows areas of positive vertical change (red) and negative vertical change (blue). Image on right shows steep areas (<27 degrees) in 2007 (black) and in 2010 (green) to illustrate the downslope translation of material, and upstream migration of head scarps (*from Delong et al., 2011, with permissions*).

Landslide Monitoring and Detection

In areas with notable topographic relief, like much of Pennsylvania, mass wasting associated with hillslopes presents a significant hazard to infrastructures on or near slopes, particularly infrastructure such as highways and SGTI that may follow along slopes for extended distances. Much of the "High Risk" zone of slope hazards aligns with the part of the state that overlies the Marcellus Shale Formation.

Landslides and other mass movements down slopes are typically triggered during extreme precipitation events when the soil is saturated or when seismic shaking occurs, and a critical stability threshold is exceeded. While numerous equations exist for calculating factors of safety for hillslopes with different levels of sophistication, significant inhomogeneities exist in the subsurface, so in many cases, these calculations cannot adequately account for broad regions unless high-density borehole data exist, or high-resolution (e.g. 1:5000) Quaternary geological maps that contain information about the underlying structure and stratigraphy. Unfortunately, this level of detail is infrequently available and can be expensive to develop. In lieu of deterministic calculations of slope stability, slope hazard maps may help steer high-resolution mapping efforts to regions more vulnerable to slope hazards. As a

simple example, if a specific region shows evidence for paleo or historical slope failures, it is reasonable to assume that additional slope failures will continue to occur in that region. Even without detailed mapping or measurements, this "correlation" method should help to target high-risk zones. Unfortunately, in March, 2014 a landslide claimed dozens of lives in the state of Washington. Observation of LiDAR base maps suggest the disaster could have been avoided (Haugerud, R. A., 2014). Early response mapping performed by the USGS show that LiDAR data of the pre-slide conditions, clearly indicated an area of recent and high spatial-density landslides.

Fortunately the geological record preserves the evidence of slope failures on the earth's surface for extended periods of time (from hundreds to tens-of-thousands of years); however, in highly vegetated areas such as Pennsylvania, the morphological evidence is highly obscured by dense vegetation, limiting the utility of air photos. Furthermore, land access limitations and morphological scale issues may limit the feasibility of ground-based, geomorphic field mapping. As a result it is often the case that countless hours of field mapping, air reconnaissance surveys, and stereo imagery result in unmapped landslides (e.g. Schulz, 2007).

LiDAR can resolve the vast majority of the issues described above by virtually "deforesting" the landscape. This is done through a series of steps that are briefly described here. Raw data can be thought of as a cloud of points in XYZ space. The point cloud can then be processed and filtered so that only the ground points remain. An example is shown in Figure 6. The bare-earth topographic model that results from these data helps remove the vegetation bias of identifying landslides.

Geomorphic investigations are primarily interested in analyzing the earth's surface, so the ground points are the primary data of concern. After classifying the point clouds, the ground returns are used to produce a "Bare Earth" digital terrain dataset, which can be subsequently gridded to produce a digital elevation model (DEM). This presents an excellent opportunity to use LiDAR for rapid characterization of mass wasting. The application of LiDAR to understand mass wasting processes is already well-described in the literature. Analytical methods being applied to LiDAR range in sophistication, and several works highlight the identification (e.g. Schulz, 2007; Booth et al., 2009) and monitoring of landsliding processes (e.g. Delong et al., 2012; Baldo et al., 2009; Glenn et al., 2006); however, its use is not yet widespread in the public sector or private industry, much less the SGTI industry.

Figure 7 shows the location and series of LiDAR-derived topographic products from recent work we performed on from a hydropower project in the western foothills of Central Chile. After the LiDAR data were processed into a DEM, the slope hazards became clear, which caused the client to abandon the site and move it several hundred meters upstream, away from an active slide surface. To ensure it was in fact a large, deep seated landslide, several methods were applied to create derivatives of the topography. The delineated slides are shown in the figure 8. It is also worth noting that several teams of geologists had traversed this site in a mapping effort for the same project. They did not identify the mass movement from mapping efforts for reasons: heavy vegetation covered the area and the slide stratigraphy was

not highly deformed as compared to highly deformed (tightly folded and highly fractured) geologic units. As a result, the structural measurements from the slide did not stand out relative to the background.

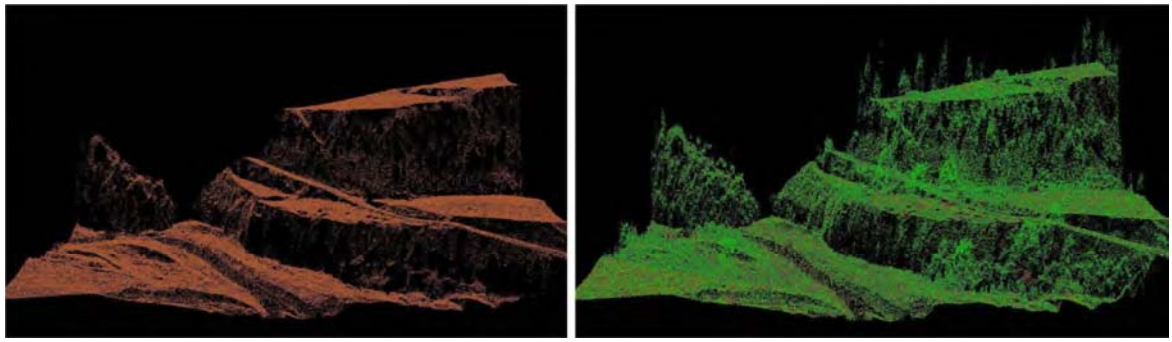

FIG. 6. Processed LiDAR 3D point cloud for a site near Coya, Chile. Top image shows only the bare earth points. Lower image includes all vegetation returns.

A second example that our group was involved in is shown in Figure 9. The site is in southern Slovenia in a region with high-density karst topography. The region is densely vegetated and the topography is very steep. This particular slope had been mapped in detail by numerous geologists for over ten years before it was recognized as a paleo-landslide. When the LiDAR was processed in 2012, the slide extent became immediately apparent. The image shown the hillshade LiDAR, superposed onto a hillshade of a conventional, high resolution 5.0 m DEM (Figure 9). Initial interpretations of the mechanisms driving the landslide were purely lithology-based (e.g. the presence of clays, etc) (i.e. Poljak and Ribičič, 2005); however, the LiDAR reveals the high density of the karst, suggesting it may impose some influence on the process. The solution weathering associated with Karst often leaves behind a clay residue, and the karstic dissolution acts as conduits for subsurface water flow, suggesting the karst processes may have played a significant role in the landslide formation as well.

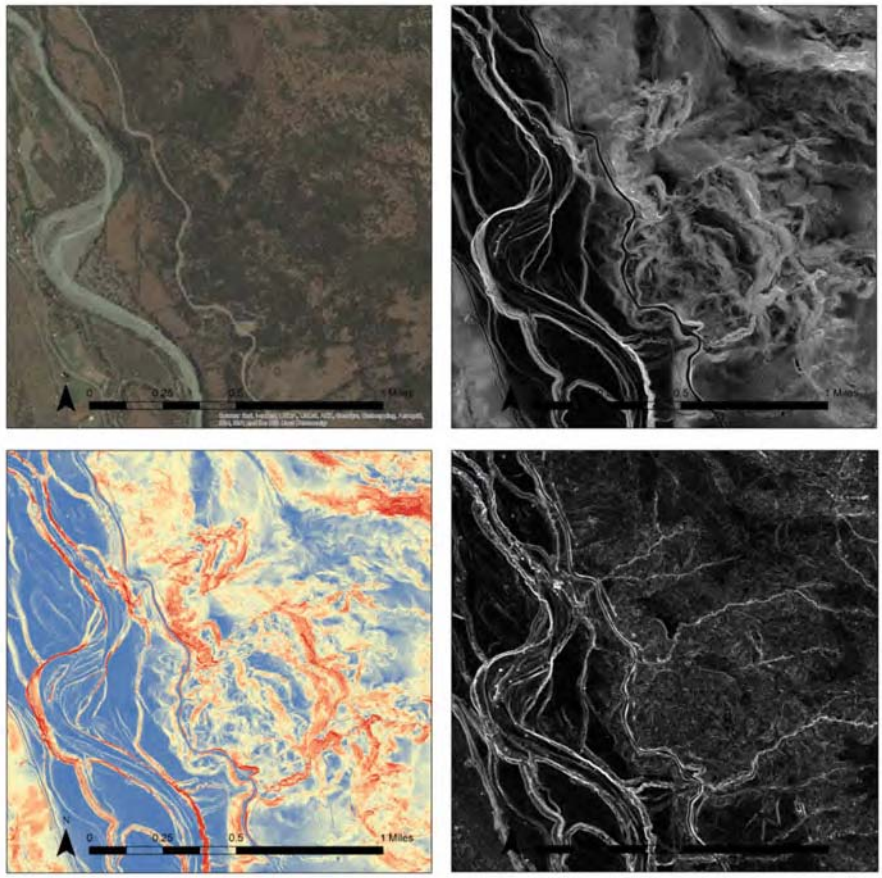

FIG. 7. Location map, showing moderate vegeatation coverage followed by derivative products of LiDAR topogrpay (upper left: 1.0 m orthophoto; upper right: Slopeshade for 1.0 m DEM; lower left; topographic profile curvature for 1.0 m DEM; lower right; topographic roughness on 2.0 m LiDAR DEM).

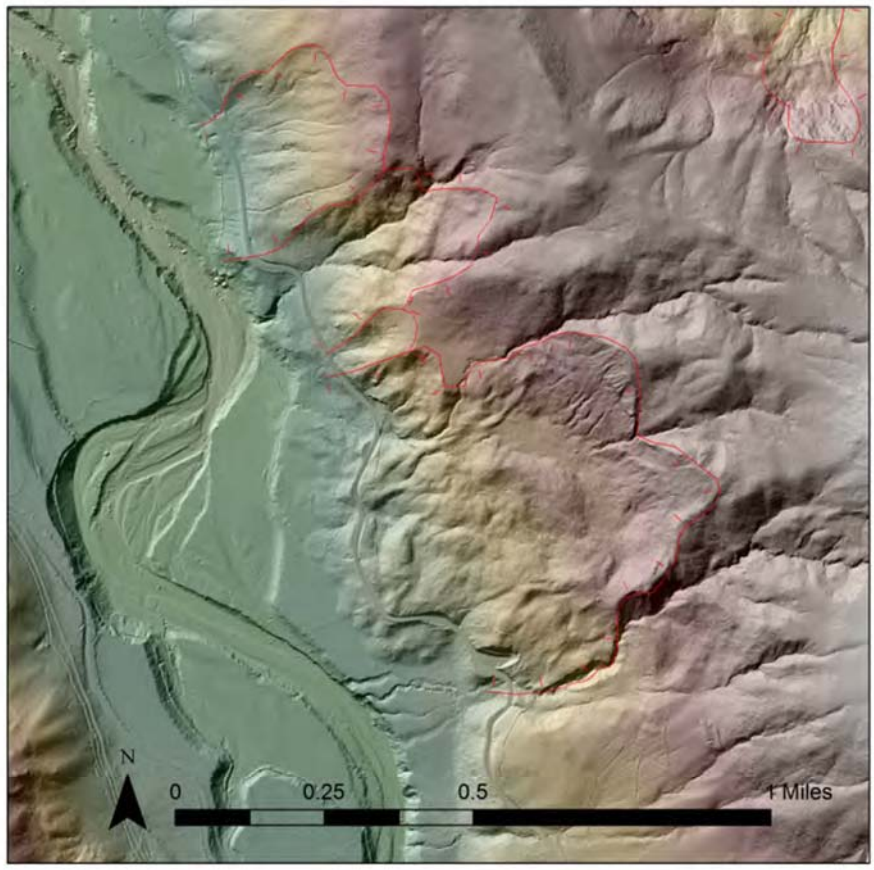

FIG. 8. Color hillshade of LiDAR DEM with landslide features delineated.

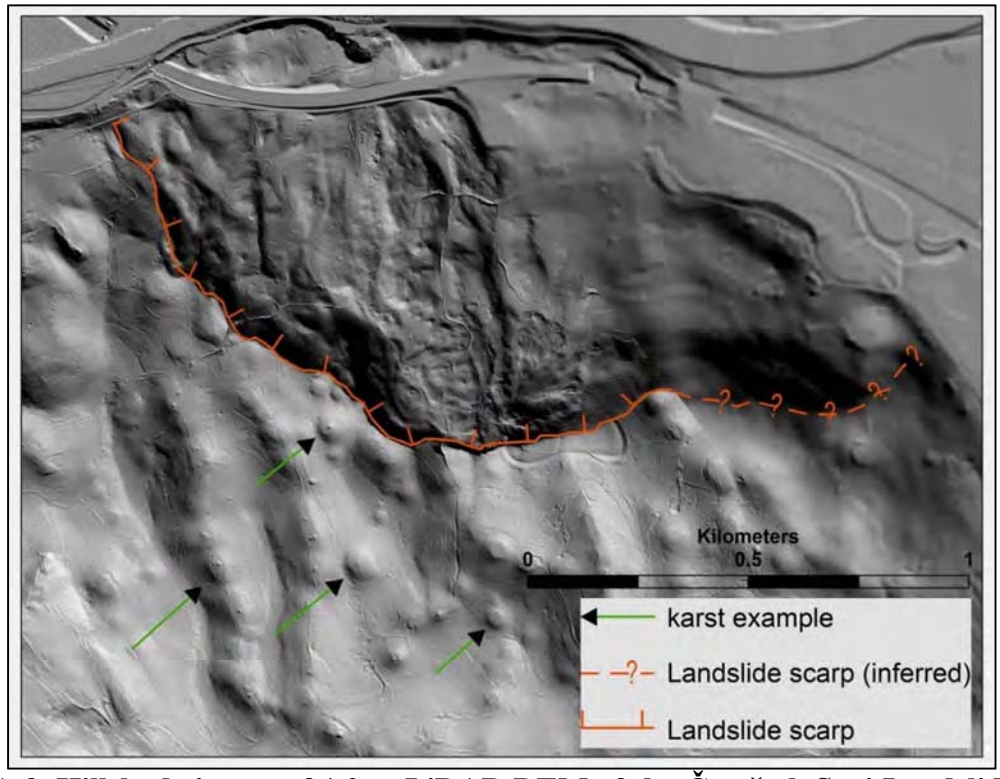

FIG. 9. Hillshade image of 1.0 m LiDAR DEM of the Čatež ob Savi Landslide in Slovenia. Examples of karst sinkholes are shown by green arrows. Within the slide area (delineated by orange line) there are numerous inset slides showing the complexity of the process. From RIZZO, 2012.

CONCLUSION

PA is poised to pave the way for incorporating stat-of-the-art hazard mitigation practices in the SGTI development. Remarkable access to low-cost LiDAR topographic data provides an excellent baseline for this. The methods summarized in this paper are only a sampling of many of the state-of-the-art methods for analyses of geologic hazards. Applying them not only provides a cost-effective and robust means of evaluating natural geological hazards, but they also add to the environmental quality of a region by more accurately assessing pre-industrial conditions. Therefore, applying these methods will improve the public image of the controversial practices of the shale gas industry. The examples described in this paper demonstrate their value in evaluating the geologic hazards of flooding, erosion, and landsliding. It is important to note that these methods do not provide cookie-cutter approaches—each method must be tailored to the specific hazard being addressed, and the area of the existing or planned development of the SGTI; however, we have demonstrated that the application of these methodologies will significantly contribute to the sustainable development of SGTI.

REFERENCES

Anders, N, R. Masselink, S. Keesstra; J. Suomalainen (2013) "High-Res Digital Surface Modeling using Fixed-Wing UAV-based Photogrammetry". Conference proceedings from Geomorphometry.

Baker, V.R., (2006). "Palaeoflood hydrology in a global context". Catena, 66(1-2): 161-168.

Baker, V.R., Webb, R.H. and House, P.K. (Editors), (2002). The scientific and societal value of paleoflood hydrology. Ancient floods and modern hazards, principles and applications of paleoflood hydrology, 4. American Geophysical Union, Water Science and Application Series, Washington, D.C., 1-19.

Baldo M, Bicocchi C, Chiocchini U, Giordan D, Lollino G (2009) "LiDAR monitoring of mass wasting processes: The Radicofani landslide, Province of Siena, Central Italy". Geomorphology (105)193-201.

Booth AM, Roering JJ, Perron JT (2009) "Automated landslide mapping using spectral analysis and high resolution topographic data: Puget Sound lowlands, Washington, and Portland Hills, Oregon". Geomorphology (109)132–147.

Bull, W. (1991), "Geomorphic responses to climatic change". Oxford University Press, Oxford.

Cline, M. L. (2010). "Extreme flooding in the Dolores River Basin, Colorado and Utah: Insights from paleofloods, geochronology and hydroclimatic analysis". University of Arizona, Ph.D. Dissertation.

DeLong, S. B., C. S. Prentice, G. E. Hilley, and Y. Ebert, (2012), "Multi-temporal ALSM Change Detection, Sediment Delivery, and Process Mapping at an Active Earth Flow," Earth Surface Processes and Landforms, 37(3), 262-272.

Delong et al., (2014). Manuscript in preparation and personal communications (2014)

Dietrich, W. E., D.G. Bellugi, L. S. Sklar, J. D. Stock, A. M. Heimsath and J. J. Roering, (2003), "Geomorphic Transport Laws for Predicting Landscape Form and Dynamics," Geophysical Monograph (135) 103-132.

Ely, L.L., Enzel, Y., Baker, V.R. and Cayan, D.R., (1993). "A 5000-year record of extreme floods and climate change in the southwestern United-States". Science, 262(5132): 410-412.

Glenn, N.F., Streutker, D.R., Chadwick, D.J., Thackray, G.D., Dorsch, S.J., (2006). "Analysis of LiDAR-derived topographic information for characterizing and differentiating landslide morphology and activity". Geomorphology (73) 131–148.

Haugerud, R. A., (2014) "Preliminary Interpretation of Pre-2014 Landslide Deposits in the Vicinity of Oso, Washington". U.S. Geological Society Open-File Report 2014–1065

Hirschboeck, K. Ed., (1988). "Flood hydroclimatology". Flood Geomorphology. John Wiley & Sons, 27‑49.

Kochel, R.C. and Baker, V.R., (1982). "Paleoflood Hydrology". Science, 215(4531) 353-361.

Klemes, V. (1994). ‘‘Statistics and probability: wrong remedies for a confused hydrologic modeller.’’ Statistics for the environment 2 Water related issues, V. Barnett and K. F. Turkman eds., Wiley, Chichester, U.K., 345–366.

PA Map LIDAR Pennsylvania Department of Conservation and Natural Resources. www.dcnr.state.pa.us/totpogeo/pamap

Perron, J. T., J. W. Kirchner, and W. E. Dietrich, (2009), “Formation of Evenly Spaced Ridges and Valleys”, Nature, 460(7254), 502-505.

Poljak, M and M Ribičič (2005), “Fossilni Kamninski Plan Pri Čatež ob Savi,” 17th Posvetovanje Slovenskih Geologov (18)

RIZZO, (2013), “Interim Technical Report: Geomorphic Analysis of Tectonic Features in the Krško Basin, Slovenia, Revision 0”, Paul C. Rizzo Associates, Inc., Pittsburgh, PA, USA, 21 December 2012.

Schulz, W.H., (2007), “Landslide susceptibility revealed by LIDAR imagery and historical records, Seattle, Washington”: Engineering Geology, v. 89, p. 67-87.

Best Management Practices for Access Roads for Shale Energy Development with Consideration to Surface Waterbodies

Elizabeth Myers Toman[1], Ph.D., and Gordon R. Keller[2], P.E., G.E., M.ASCE

[1]Visiting Assistant Professor, The Ohio State University, School of Environment and Natural Resources, 2021 Coffey Rd, Columbus, OH 43210-1085, U.S.A., E-mail: toman.11@osu.edu.
[2]Geotechnical Engineer, E-mail: gordonrkeller@gmail.com.

ABSTRACT: Access roads connect a drilling pad for shale energy with public roads and are most often constructed with unbound aggregate surfacing materials. With traffic volume averaged over the lifetime of the road, an access road may be considered as a very low-volume road (ADT ≤ 400); however, a majority of the traffic occurs over 2-3 month spans during the initial construction and drilling phase of each shale oil and gas well on the pad. Research suggests that roads built and used in this manner have a great potential to produce and transport fine sediments to surface water bodies where increased sedimentation can be deleterious to the health of the ecosystem. Here we present best management practices (BMPs), with consideration to traffic for shale energy development, for the design and use of access roads to minimize the production and transport of fine sediments. Emphasis is placed on adequate drainage features, quality maintenance practices, apposite materials, and proper traffic use.

INTRODUCTION

Recent advances in hydraulic fracturing and horizontal drilling technologies have facilitated substantially easier extraction of oil and gas from unconventional reserves in shale formations throughout the world (Vidic et al. 2013). Energy analysts project the extensive oil and gas contained in the global shale deposits will significantly impact the overall global energy market for decades to come (U.S. Energy Information Administration 2013). The development of shale energy requires high volumes of vehicles in a short time period (2 to 3 months) as trucks transport rock, drilling equipment, water, proppants, flowback water, and drill cuttings to and from the well site. It is estimated that the number of heavy trucks necessary for the drilling and fracturing of one well range from 890 to 1370 (Kuhn 2006; Nagle 2011). Additionally, passenger vehicles and light pick-up trucks related to the activities of shale energy development may contribute four times more vehicles than the number of heavy trucks (Mason 1981).

To access the well pad from a public road often requires the construction of a new

road or the improvement of existing driveways or farm roads on private land. These access roads are most often constructed with unbound aggregate surfacing materials following design procedures for low-volume roads. Following traditional methods for low-volume roads (e.g., AASHTO 1993; Bolander 1995) the unbound pavement structures are designed to withstand a defined volume of traffic over the pavement life, therefore the mechanical strength and structural integrity of the pavement is engineered based on the anticipated vehicle traffic. However, these methods do not consider the environmental impacts or integrity of the unbound aggregate pavement.

Unbound aggregate roads can produce a significant quantity of fine sediment, especially with heavy traffic use (Toman and Skaugset 2011; Foltz and Burroughs 1990; Reid and Dunne 1984). Where roads are connected to the surface water network, road runoff can transport and deliver sediment to streams (Wemple et al. 1996). Excessive sediment levels in streams can clog gills, reduce light available, and interfere with the foraging success of aquatic organisms (Davies-Colley and Smith 2001; Gordon et al. 1994); degrade aquatic habitat (Lisle 1989); reduce dissolved oxygen (Kumar et al. 2010); alter hyporheic exchange, connectivity, and hydrologic regime (Rehg et al. 2005); modify channel storage (Grant and Wolff 1991); and is a leading cause of stream impairment in the United States (USEPA 2006). Where streams enter lakes and reservoirs sediment can be deposited causing sedimentation of the reservoirs or increase turbidity impairing drinking water supplies (Marguis 2005). Road-related sediments may also carry heavy metals, petroleum hydrocarbons, and other hydrophobic pollutants that could further degrade water quality (Herngren et al. 2006; Pitt 1995; Ellis and Revitt 1991). Changes in surface water quality such as increased sediments, chemicals, and heavy metals can influence microbial communities, and consequently human health (Cheung et al. 2013).

The erosional losses from and deterioration of unbound aggregate pavements and the delivery of road runoff to surface waterbodies can be mitigated with best management practices (BMPs). While common BMPs for unbound aggregate pavements have been developed for roads with very low-volume traffic (i.e., ≤ 400 ADT (average daily traffic); AASHTO 2011), they are still relevant for access roads with higher volumes of traffic and may be even more important as the production of sediment from road surfaces has shown to increase with increasing traffic (Reid and Dunne 1984). Sediment production is likely accelerated due to heavy truck traffic.

Here we present BMPs for the design, maintenance, and use of unbound aggregate pavements to minimize the production and transport of fine sediments from access roads to surface water bodies with traffic use for shale energy development. While current literature and practice provide many examples of BMPs for unbound aggregate roads (see Keller and Sherar 2003; BLM 2007; Adams and Storm 2001, for examples), the practices presented here are tailored to meet the needs of roads used to access drilling pad locations with traffic characteristics specific to shale energy development.

Drainage Features

Access roads experience the greatest volume of traffic during the active drilling and hydraulic fracturing phases of shale development, which can last from 4 to 10 weeks.

For the first well at a drilling pad, this high volume of traffic typically occurs immediately after construction or rehabilitation of the access road. Luce and Black (2001) suggest that sediment production from unbound aggregate roads decreases with time and age of the road as road surface areas become armored and the fines are washed off. Bare soil cut slopes and fill slopes without vegetation or other erosion control measures are also a source of sediment. As new construction areas, the entire right-of-way of access roads will produce a significant volume of sediment. To minimize the environmental impacts from sediment production, it is paramount that the road is not hydrologically connected to a surface water body. Connection between a road structure and a stream network can occur directly where the road crosses and drains to a channel or indirectly where a gully forms between a culvert or drainage feature and the surface waters (Wemple 1994). An access road for shale development should be designed with adequate drainage features for the location to quickly divert runoff away from the road and onto vegetated surfaces. A crown or outslope pavement shape in cross section allows for rapid shedding of road surface runoff. Inboard ditches should be avoided to prevent the accumulation of significant volume and velocity of runoff and the subsequent formation of a gully between the ditch and a stream channel (Figure 1). Where an inboard ditch is necessary it should be designed in short segments with minimal spacing between cross-drain culverts or ditch outlets and discharge to vegetated or armored surfaces with sufficient infiltration capacity (Figure 2). Where ditches convey substantial volume of runoff, they should terminate at a sediment catchment basin.

FIG. 1. The inboard ditch of an access road in Ohio that will accumulate surface runoff from the road surface, cutslope, and upslope contributing areas.

FIG. 2. A leadoff ditch that is "disconnecting" the roadway ditch from a stream and moving sediment into a vegetated area.

Access roads for shale development will experience many heavy trucks and some over-sized vehicles as drilling equipment and the associated infrastructure are moved in and out of the well pad. Drainage features on the road surface such as rolling dips and rubber water diverters (water bars) are good options for access roads as they divert runoff from the road surface yet allow for a relatively smooth driving surface. Rolling dips (or broad-based dips, Figure 3) should only be used on roads with grades less than 12 % and the outlet of the dip should be armored with rock. With high truck volume and large, low trucks, the rolling dips will need to be constructed relatively long and flat to prevent damage or delays for the haul vehicles. Alternatively the rolling dips may be installed on the road after the short but intense haul period during well development. Long-term administrative and maintenance traffic can negotiate higher, more radical rolling dips.

Rubber water diverters can be used on any slope or road surface, are easy to install after the road has been constructed (to target problem areas), but are not easy to grade over (Figure 4). The objectives for any drainage feature are to prevent the concentration of surface runoff and the discharge of water onto erosive, unprotected soils. See Keller et al. (2011) for recommended shape and dimensions for rolling dips and the maximum recommended spacing between drainage features as a function of road grade and soil erodibility.

FIG. 3. A rolling dip constructed into an unbound aggregate road in Pennsylvania.

FIG. 4. Installation of a rubber water diverter (water bar) across an unbound aggregate road.

Construction and Maintenance Practices

Access roads are constructed with the primary objective of allowing vehicles required for shale development to gain access to the well pad. With this purpose in mind, access roads are designed for structural strength to bear over-weight, and over-size vehicles and to limit failures of the road structure. As such, the structural section

of access roads is thicker with greater depth of aggregate than the traditional low volume, unbound aggregate road. However, rutting in the wheel paths of all unbound aggregate roads can occur with time and traffic use (Douglas and McCormack 1997). Indeed, traditional methods for the design of unbound aggregate pavements plan for a specified rut depth at the end of the pavement life and make provisions for this in the design process (AASHTO 1993; Bolander 1995). Ruts in the surface of the road will allow water to pond, weaken the structural strength of the road structure, accelerate damage to the surface, and make driving difficult. In addition, ruts create a channelized flow pathway for surface runoff that collects a greater volume of runoff, which in turn provides more kinetic energy to detach and transport sediment particles from the road surface (Figure 5). Research on unbound aggregate roads give evidence that roads with wheel ruts produce two to seventeen times more sediment compared with similar roads without ruts (Toman and Skaugset 2011; Burroughs et al. 1984; Foltz 1995; Foltz and Burroughs 1990). Proper engineering and construction of the road, including use of high quality aggregate and adequate compaction measures, can limit the speed and degree of rut formation; however, routine maintenance is eventually needed on any unbound aggregate road to keep the integrity of the pavement shape and road drainage working properly. To minimize sediment production from access roads, a design rut depth should be reduced if not eliminated and routine grading of the road surface should be performed.

FIG. 5. Wheel ruts in an unbound aggregate road in Oregon have become "small streams;" channelized pathways for surface runoff.

Pavement Materials

While proper drainage features do not permit road runoff and sediment to reach surface waterbodies and road surface maintenance reduces the volume of sediment removed from a road surface, the quality and gradation of aggregate used in the unbound aggregate pavement plays a key role in the quantity of sediment available for transport from the surface of an access road. Especially important for access roads for shale energy development, adequate fines and a durable, dense, well-graded material are necessary for adequate compaction, stabilization, and to allow for a smooth running surface. However, excessive fines, particularly plastic fines, can contribute to high sediment runoff.

Design for bound aggregate pavements considers material that passes the 4.75-mm sieve to be fine aggregate and material that passes the 0.075-mm sieve to be mineral filler. Studies with aggregate local to Oregon, Idaho, South Dakota, and Washington, and California found that the most important particle size in surface aggregate for the production of fines is the percent passing the 0.6-mm sieve (Toman and Skaugset 2011; Foltz and Truebe 2003). These studies found that sediment production from unbound aggregate roads increased as the percentage of fines passing the 0.6-mm sieve in the surface aggregate increased. In particular, roads that contain aggregate with greater than 14% passing the 0.6-mm sieve had much higher rates of sediment production. Good road performance has been achieved with use of aggregate such as the US Forest Service Special Project Specification, Section 703.05 Grading F Surface Course Aggregate or the Penn State CDGRS specified 1.5-Inch Minus DSA (Driving Surface Aggregate) material (Bloser 2007; Bloser and Scheetz 2012).

Time of Traffic Use

The saturation of roadway materials, particularly the subgrade, from precipitation or freeze-thaw events greatly reduces bearing capacity and overall strength of the road. Traffic use of unbound aggregate roads in a saturated condition, especially with the high-volume of heavy vehicles characteristic of traffic for shale energy development, can produce dramatic road failures in the form of potholes and rutting that can quickly escalate to inoperable road conditions (Figure 6). Road failures of this sort result in high erosional losses of sediment from the road. A timeline for shale energy development typically involves an intense schedule of round-the-clock activity and material transport during the active drilling and hydraulic fracturing phases. Because it may be difficult to delay vehicles associated with shale energy development once drilling at a shale energy pad has begun, the entire operation should be scheduled to avoid periods of freeze-thaw and high rainfall to reduce the chances of road failure and associated sediment production. The alternative of wet weather or winter road use implies the need for a thicker aggregate structural section, more frequent maintenance, higher risk of problems and sediment production, and higher operational costs.

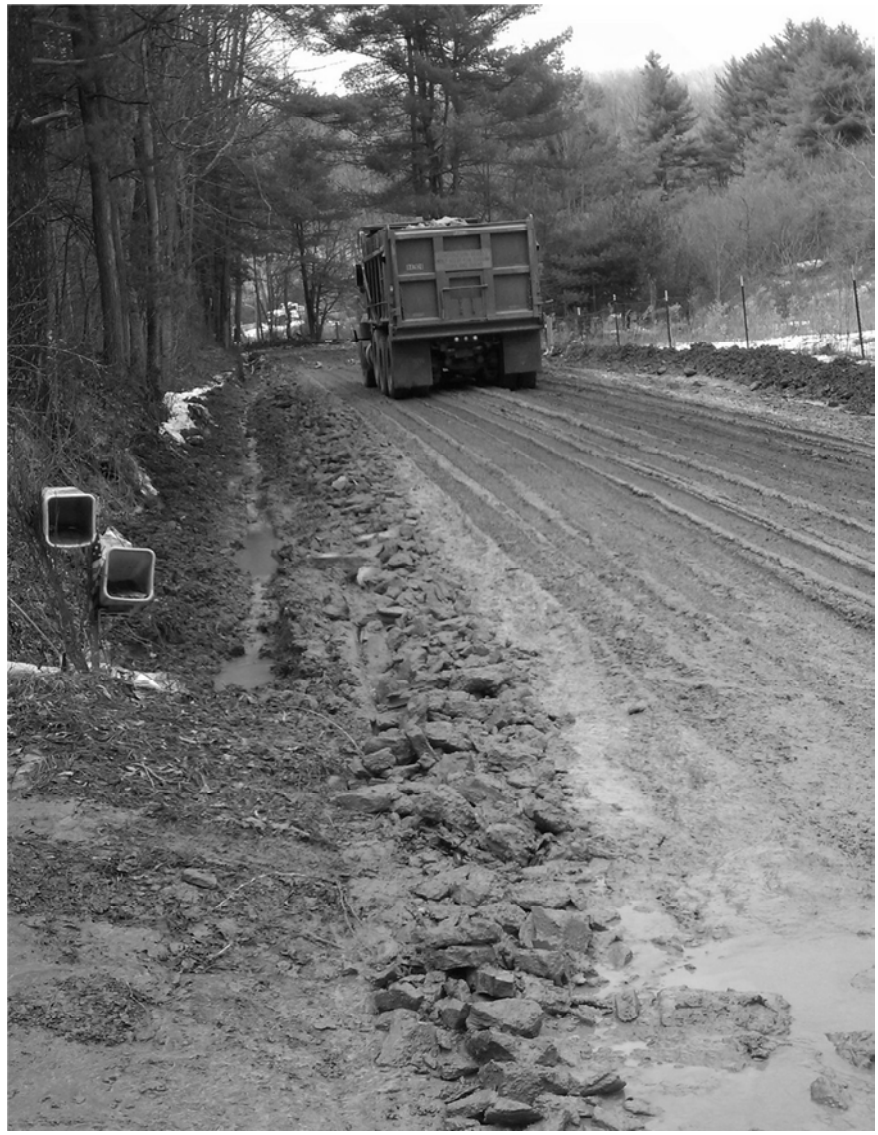

FIG. 6. Unbound aggregate road used for shale energy development in Pennsylvania with wet weather and saturated road conditions. (Photo courtesy Center for Dirt and Gravel Road Studies, Penn State).

CONCLUSIONS

Design of an unbound aggregate road for access to shale well pads can include both structural strength and environmental performance measures. With best management practices for access roads such as those presented here, sediment production from the road and delivery to surface waterbodies can be mitigated.

REFERENCES

Adams, P.W. and Storm, R. (2011). "Oregon's forest protection laws, an illustrated manual." Second edition. Oregon Forest Resources Institute.

American Association of State Highway and Transportation Officials (AASHTO) (1993). "Guide for Design of Pavement Structures." Washington, D.C.

AASHTO (2011). "Guidelines for Geometric Design of Very Low-Volume Local Roads (ADT ≤ 400)." Washington, D.C.

Bloser. S. and Scheetz. B. (2012). "Sediment production from unpaved oil well access roads in the Allegheny National Forest." State College, PA: The Pennsylvania State University, The Graduate School, College of Engineering. 62 p.

Bloser, S.M. (2007). "Comparative analysis of commonly used aggregate materials and placement methods for a surface wearing course on low-volume roads in Pennsylvania." Master of Science Thesis, State College, PA: The Pennsylvania State University, The Graduate School, College of Engineering. 75 p.

Bolander, P., Marocco, D., and Kennedy, R. (1995). "Earth and aggregate surfacing design guide for low volume roads." Report no. FHWA-FLP-96-001. United States Department of Agriculture, Forest Service in cooperation with the United States Department of Transportation Federal Highway Administration, Washington, D.C.

Bureau of Land Management (BLM). (2007). "Surface operating standards and guidelines for oil and gas exploration and development, the gold book." Fourth edition. Prepared by United States Department of the Interior, Bureau of Land Management and United States Department of Agriculture, Forest Service.

Burroughs, E. R., Jr., Watts, F. J., and Haber, D. F. (1984). "Surfacing to reduce erosion of forest roads built in granitic soils." *Symposium on effects of land use on erosion and slope stability*, Honolulu, Hawaii, 255-264.

Cheung, M.Y., Liang, S, Lee, J. (2013). Toxin-producing Cyanobacteria in Freshwater: A Review of their Problems, Impact on Drinking Water Safety, and Efforts for Protecting Public Health. *Journal of Microbiology*, 51(1): 1-10.

Davies-Colley, R.J., and Smith, D.G. (2001). "Turbidity, Suspended Sediment, and Water Clarity: A Review." *Journal of the American Water Resources Association*, 37(5): 1085-1101.

Douglas, R. A., and McCormack, R. (1997). "Pavement management applied to forest roads, Paper No. 975031." *ASAE Annual International Meeting*, Minneapolis, Minnesota.

Ellis J.B., and Revitt D.M. (1991). "Drainage for roads: control and treatment of highway runoff." Report NRA 43804/MID.012. National Rivers Authority, Reading, UK .

Foltz, R. B. (1995). "Sediment Reduction from the Use of Lowered Tire Pressures." *Central tire inflation systems: managing the vehicle to surface*. SP-1061, Society of Automotive Engineers, Warrendale, Pennsylvania, 47-52.

Foltz, R.B., and Burroughs, E.R., Jr. (1990). "Sediment production from forest roads with wheel ruts." *Proceedings of the Symposium on Watershed Planning and Analysis in Action*. Durango, Colorado, 266-275.

Foltz, R. B., and Truebe, M. A. (2003). "Locally available aggregate and sediment production." *Transportation Research Record,* Transportation Research Board, National Academies of Science, Washington, DC. 1819(2): 185-193

Gordon, N.D., McMahon, T.A. and Finlayson, B.L. (1994). "Chapter 7: Patterns of

shifting sand stream." *Stream Hydrology: An Introduction for Ecologists*. John Wiley and Sons, Chichester, 288-345.

Grant, G.E., and Wolff, A.L. (1991). "Long-term patterns of sediment transport after timber harvest, western Cascade Mountains, Oregon, USA." *Sediment and Stream Water Quality in a Changing Environment: Trends and Explanation*. IAHS Publ., Gentbrugge, Belgium, 31-40.

Herngren, L., Goonetilleke, A., and Ayoko, G.A. (2006). "Analysis of heavy metals in road-deposited sediments." *Analytica Chimica Acta*. 571(2): 270-278.

Keller, G.R. and Sherar, J. (2003). "Low-volume roads engineering, best management practices field guide." Conservation Management Institute, Virginia Polytechnic Institute and State University in cooperation with U.S. Agency for International Development and USDA Forest Service, Blacksburg, Va.

Keller, G., Wilson-Musser, S., Bolander, P., and Barandino, V. 2011. "Stabilization and rehabilitation measures for low-volume forest roads." 1177 1801—SDTDC. San Dimas, CA: U.S. Department of Agriculture, Forest Service, San Dimas Technology and Development Center. 333 p.

Kuhn, D.B. (2006). "Highway freight traffic associated with the development of oil and gas wells. (Report specifically details impact to the Uinta Basin)." Utah Department of Transportation internal report, Salt Lake City, Utah.

Kumar, B., Rai, S.P., Kumar, U.S., Verma, S.K., Garg, P., Kumar, S.V.V., Jaiswal, R., Purendra, B.K., Kumar, S.R., and Pande, N.G. (2010). "Iso-topic characteristics of Indian precipitation." *Water Resources Research*, 46(12): W12,548.

Lisle, T.E. (1989). "Sediment transport and resulting deposition in spawning gravels, north coastal California." *Water Resources Research*, 25(6): 1303–1319.

Luce, C.H., and Black T.A. (2001). "Spatial and Temporal Patterns in Erosion for Forest Roads." *Influence of Urban and Forest Land Uses on the Hydrologic-Geomorphic Responses of Watersheds* (M. W. Wigmosta and S. J. Burges, eds.), Water Resources Monographs, American Geo- physical Union, Washington, D.C., 2001, pp. 165–178.

Marquis, P. (2005). "Turbidity and suspended sediment as measures of water quality." *Streamline Watershed Management Bulletin* 9:21–23. <http://www.forrex.org/sites/default/files/publications/articles/streamline_vol9_no1_art4.pdf> (Oct. 4, 2012).

Mason, J.M. (1981). "Investigation of the effects of oil field traffic on low volume roadways." Doctorate of Philosophy Dissertation, Texas A&M University, College Station, Texas. 202 pp.

Nagle, L. C. (2011). "Impacts on community character of horizontal drilling and high volume hydraulic fracturing in Marcellus shale and other low-permeability gas reservoirs." Revised final report prepared for New York State Energy Research and Development Authority by NTC Consultants. <www.nyserda.ny.gov/Publications/Research-and-Development-Technical-Reports/Other-Technical-Reports/Natural-Gas-Enviromental-Impact.aspx> (November 25, 2013).

Pitt R.E. (1995). "Biological effects of urban runoff discharges." *Stormwater urban runoff, and receiving water systems*. Herricks EE (ed.), Lewis/CRC, Boca Raton,

FL, pp 127–162.

Reid, L.M., and Dunne, T. (1984). "Sediment production from forest road surfaces." *Water Resources Research*, 20(11): 1753-1761.

Toman, E.M. and Skaugset, A.E. (2011). "Reducing sediment production from forest roads during wet-weather hauling." *Transportation Research Record: Journal of the Transportation Research Board*, 2203(1): 13-19.

United States Energy Information Administration. (2013). "Technically recoverable shale oil and shale gas resources: an assessment of 137 shale formations in 41 countries outside the United States." <http://www.eia.gov/analysis/studies/worldshalegas/> (Sept. 11, 2013).

United States Environmental Protection Agency (USEPA). (2006). "Wadeable stream assessment: a collaborative survey of the nation's streams." Washington, DC: EPA. EPA 841-B-06-002.

Vidic, R., Brantley, S.L., Vandenbossche, J.M., Yoxtheimer, D., and Abad, J.D. (2013). "Impact of Shale Gas Development on Regional Water Quality." *Science* 340, 1235009(2013).

Wemple, B.C., (1994). "Hydrologic integration of forest roads with stream networks in two basins, Western Cascades, Oregon." M.S. Thesis, Oregon State University, Corvallis, Oregon.

Wemple, B.C., Jones, J.A., and Grant, G.E. (1996). "Channel network extension by logging roads in two basins, western Cascades, Oregon." *Water Resources Bulletin*, 33(6): 1195-1207.

Shale Gas Well Pad Air Quality Permitting in Ohio and West Virginia

Kristian A. Macoskey, QEP[1], Gerard G. Alberts[2],
Donald Gray[3], and Robert A. Bosiljevac, EIT[4]

[1]Vice President, Civil & Environmental Consultants, Inc., 333 Baldwin Road, Pittsburgh, Pennsylvania 15205, U.S.A., E-mail: kmacoskey@cecinc.com.
[2]Environmental and Regulatory Manager, Antero Resources Corporation, 1625 17th Street, Suite 300, Denver, Colorado 80202, U.S.A., E-mail: jalberts@anteroresources.com.
[3]Environmental and Regulatory Manager, Antero Resources Corporation, 1625 17th Street, Suite 300, Denver, Colorado 80202, U.S.A., E-mail: dgray@anteroresources.com.
[4]Project Consultant, Civil & Environmental Consultants, Inc., 333 Baldwin Road, Pittsburgh, Pennsylvania 15205, U.S.A., E-mail: rbosiljevac@cecinc.com.

ABSTRACT: Air permit application requirements and the resultant operating permit conditions for shale gas well pad production facilities differ from state to state. The lack of standardized permitting requirements and inconsistent permit conditions obliges applicants to evaluate and apply differing strategies from state to state to obtain approvals to install and operate the same equipment. Recent shale gas air permitting experiences in West Virginia and Ohio illustrate the differences between Ohio Environmental Protection Agency and West Virginia Department of Environmental Protection air permitting approaches. The unique characteristics of gas production decline curves and their impacts on the potential-to-emit of proposed operations present unique challenges. Differences in permit application requirements and the resulting operating permits in Ohio and West Virginia are highlighted and discussed.

INTRODUCTION

Production of natural gas present in the Marcellus and Utica shale gas formations requires installation and operation of specialized equipment at the well pad. Operation of that equipment and transport of byproducts generates atmospheric emissions that are subject to regulatory approvals. Companies operating in Ohio and West Virginia are required to obtain applicable construction and operating permits prior to installing and operating this equipment. Because permitting requirements vary, companies operating in both states can benefit from understanding the differences in the permit application process and the resulting permits. This paper presents an overview of shale gas well pad air quality permitting in Ohio and West Virginia.

SHALE GAS WELL PAD AIR EMISSION SOURCES

Production Equipment

At a typical shale gas well pad, natural gas and associated liquids flow from one or more wells through pipes and valves to well-specific gas production units (GPUs). GPUs use heat and pressure to separate the incoming gas stream into natural gas, hydrocarbon vapor, hydrocarbon liquid (condensate), and aqueous (produced water) fractions. From the GPU, product gas is piped to metering and then on to the pipeline. Condensate from the GPU is further processed in a low-pressure flash separator where entrained vapors are liberated and sent to a mechanical Vapor Recovery Unit (mVRU) for recompression and delivery to the sales gas pipeline. From the GPU, condensate and produced water are pumped to on-site storage vessels. The hydrocarbon vapors emitted from storage vessels are captured and conveyed to the mVRU or vented to a flare. After storage, the condensate and produced water are loaded onto trucks and hauled off-site for sale or disposal.

Fugitive Emissions

Volatile Organic Compounds (VOCs)

Fugitive emissions of VOCs occur where threaded connections, valve packings, flanges, seals, and other components that come in contact with hydrocarbon liquids and gases leak. Each well pad contains multiple components. Uncontrolled emissions from these sources can be significant.

Fugitive VOC emissions also occur during the transfer of produced water and condensate from storage vessels to tanker trucks. Depending on state requirements, transfer operations may require the use of vapor balancing equipment which enables the operator to transfer hydrocarbon vapors displaced from the tanker during filling back to the storage vessel and eventually to the mVRU or flare. In cases where vapor balancing equipment is not present, the displaced vapors from the tanker are released to the atmosphere.

Similarly, it is likely that less than 100% of the vapors that are piped to mVRUs for recompression and delivery to the sales gas pipeline are actually captured. The uncaptured fraction, which is emitted as fugitives, is often assumed to be 5% unless specialized systems and recordkeeping procedures are used (Texas Commission on Environmental Quality, 2012).

Particulate Matter

During operation of the well pad, tanker trucks used to transport condensate and produced water from on-site storage vessels typically access the facility from public roadways via an unpaved road. Particulate emissions are generated as a truck travels the unpaved road – the quantity of which depends largely on the moisture content of the road.

Storage Vessels

Storage vessels are sources of breathing, working, and flash emissions of VOCs. Breathing losses are generated by the evaporation of organic constituents from condensate in response to daily changes in air temperature and atmospheric pressure. Working losses are caused when organic vapors are displaced from inside the vessel as the liquid level rises and falls. Flash losses occur when there is a decrease of pressure exerted on the liquid, such as when it is transferred from the pressurized GPU to a storage vessel at atmospheric pressure. The pressure drop causes organic vapors present in condensate to rapidly volatilize or "flash." Working, breathing, and flashing emissions are typically captured and directed to an mVRU or flare.

Combustion Equipment

Internal Combustion Engines

Internal combustion engines (ICEs) are used to power mVRUs. In some cases, additional compressors are needed to raise the pressure of sales gas prior to delivering it to the downstream gathering lines. The ICEs are normally powered by natural gas generated on site, although diesel fuel is also used. The primary pollutants from these burners are combustion pollutants, including minor emissions of hazardous air pollutants (HAPs).

Flares

Depending on the needs of the well pad, one or more flares may be installed for control of VOCs produced during gas processing. In some configurations, flares are used as a backup VOC emission control device during maintenance or malfunction of the mVRUs.

THE SHALE GAS PRODUCTION CURVE

Unconventional gas wells in the Marcellus and Utica shale plays may have productive life spans in excess of 20 years. During that period, the average rate of gas production and the associated atmospheric emissions from a single well will asymptotically decrease to a long-term steady-state. This is contrary to the traditional behavior of industrial processes that maintain, if not increase, their permitted capacity over time. The rapid decline in gas production at shale gas wells presents a unique challenge for permit applicants, as well as state regulators.

Average daily gas production can decrease significantly in the initial several months of operation. From an air permitting perspective, this means that the facility initially has a much higher capacity to produce atmospheric emissions (termed its potential-to-emit) than it will have several months later. Because the facility operator is required to obtain a permit that accounts for the potential emissions from the site when it is first operated, this characteristic requires applicants to install equipment with capacities that may quickly be oversized. In some cases, it may be possible to

develop alternative operating scenarios for initial and later phases of pad development. In other cases, permit modifications may be needed to obtain approvals to replace high-capacity processing equipment with lower-capacity units or to remove a portion of the permitted equipment altogether.

WELL PAD PERMIT APPLICATION PROCESS

Ohio Environmental Protection Agency (OEPA)

In Ohio, applicants have two options to obtain an air permit for well pad operations: a general permit or an individual permit. The choice as to which permitting path to follow is primarily a function of the equipment and emission characteristics of each well pad. While both permits can be applied for electronically online, the general permit can be issued much more quickly because of the pre-established standard permit conditions. If the general permit Qualifying Criteria described below cannot be met, the applicant would need to apply for an individual Permit to Install and Operate (PTIO).

General Permit GP-12

General Permit GP-12 (*Oil and Gas Well Site Production Operations*) is applicable to the following equipment operating at the well pad:

1. Dehydration System;
2. Spark Ignition Internal Combustion Engines;
3. Compression Ignition Engines;
4. Flare/Combustor;
5. Equipment/Pipeline Leaks;
6. Unpaved Roadways and Parking Areas; and
7. Flash Vessel/Storage Tanks and Truck Loading for Liquids.

OEPA has established a list of twenty-one Qualifying Criteria that a site must meet to be eligible for permitting under the GP-12 (OEPA, 2012a). There are applicability limits on equipment capacities and overall emissions from the well pad. By establishing specific equipment thresholds and associated facility-wide emission limits, OEPA has streamlined the application preparation and review process. Specific streamlining examples include:

1. Emission calculations need not be submitted with the GP-12 application. If the applicant certifies that the facility will meet the emission thresholds established in the qualifying criteria document, it is not necessary to submit calculations unless the reviewing engineer requests additional information.
2. The GP-12 application can be submitted through an online database. OEPA's required forms are completed online, the application is validated for completeness, and separate files can be attached to provide site-specific information, such as process flow diagrams and site location maps.
3. Future GP-12 applications for similar facilities can be created with the help of OEPA personnel from an existing application. The process of cloning

subsequent well pad applications expedites the process of preparing and reviewing applications.
4. Because the permit conditions have already been reviewed and approved by a public comment process, no further time is required to solicit and respond to public comments on general permits. In the experience of the authors, GP-12 permits have been issued by OEPA in as few as 10 days after forms were submitted online.

Permit to Install and Operate

In cases where the proposed operations do not satisfy all of the Qualifying Criteria, a permit still can be obtained, but the PTIO process must be followed. The forms needed for the PTIO application are the same as those submitted for the general permit. Major differences between the GP-12 and the PTIO include:
1. The PTIO applicant must provide emission calculations.
2. Dispersion modeling may be required of a PTIO applicant if specific emission thresholds are exceeded.
3. The PTIO application review requires a public comment period.

West Virginia Department of Environmental Protection (WVDEP)

As of late October 2013, applicants in West Virginia also have two paths to obtain an air permit for well pad operations: a general permit or an individual permit.

General Permit G70-A

General Permit G70-A (*Operation of Oil and Natural Gas Production Facilities Located at the Well Site*) is applicable to oil and natural gas production facilities in West Virginia that operate the following equipment:
1. Natural Gas Well Affected Facilities;
2. Storage Vessels;
3. Gas Producing Units, In-Line Heaters, Heater Treaters;
4. Glycol Dehydration Units;
5. Pneumatic Controllers Affected Facilities;
6. Natural-Gas-Fired Compressor Engines; and
7. Tank Truck Loading Facilities.

The G70-A is applicable to facilities that fall under NAICS code 211111 (Crude Petroleum and Natural Gas Extraction) and/or SIC code 1311 (Crude Petroleum and Natural Gas) with the exceptions that the facility may **not**:
1. Be a major stationary source of air pollutants;
2. Be located in one of the five counties where VOC reasonably available control technology requirements apply (Putnam, Kanawha, Cabell, Wayne, and Wood);
3. Include any fuel-burning equipment that does not use natural gas;
4. Include any compression ignition engines (i.e., diesel-fired);

5. Include any gas processing, sweetening, transmission compression, or NSPS, Subpart Kb gas production activities; or
6. Include any NSPS, Subpart Dc steam generating unit.

In contrast to the streamlining procedures that OEPA has implemented, the WVDEP G70-A does not significantly reduce the application preparation. For example:

1. Detailed emission calculations are required for both general and individual permits.
2. The general permit application cannot be submitted through an online database, although a scanned version can be sent via e-mail.
3. Future applications for similar facilities cannot be created through a simple cloning process.
4. Despite the fact that the G70-A is a general permit, a public comment period still applies.

Regarding the general permit public comment period, a legal advertisement must be published in the newspaper most commonly read in the area where the well pad will be constructed. The affidavit of publication must be received prior to the end of the 30-day public comment period. As stated by the WVDEP on their website (WVDEP, 2013a), "By demonstrating compliance with the requirements and conditions of the general permit, general permit registration may be granted to the applicant in as little as 31 days."

Rule 13 New Source Review Permit

As is the case in Ohio with the PTIO, West Virginia has an individual permitting process for facilities that do not qualify for a general permit or where the applicant requires site-specific permit conditions. The WVDEP refers to their individual permit as a Rule 13 (R13) permit. Similar to the Ohio PTIO, the R13 permit application requires that the applicant provide a detailed description of the proposed processes, the associated emissions, and the applicable regulatory requirements.

Comparison of Ohio and West Virginia General Permit Applications

Table 1 identifies key differences between the Ohio and West Virginia general permits. In many cases, the application processes are similar in that they both require that the applicant provide engineering data that the permit reviewer can use to evaluate the emission characteristics or regulatory applicability of sources. In several cases, however, the OEPA GP-12 significantly simplifies the permit application process. Much of the GP-12 simplification is associated with the fact that detailed emission estimates are not requested as part of the application. This does not eliminate the need to prepare representative emission estimates for each well pad. The applicant must certify that the source will adhere to the facility-wide emission thresholds provided in the Qualifying Criteria, but the specificity with which those calculations must be prepared and documented is relaxed because they need not be

submitted with the application.

Table 1. Key Emission Unit Information Required by Ohio and West Virginia General Permit Applications for Shale Gas Well Pad Operations

Emission Unit	*Ohio GP-12*	*West Virginia G70-A*
Gas Wells	No well-specific information required	Must identify each well by API number
Natural Gas Fired Heaters	Number and Btu rating	Emission estimates
Flares	General process flow information with a narrative description	Detailed engineering information and emission estimates
Storage Vessels	No significant differences	
Tanker Truck Loading	General narrative description	Detailed engineering information and emission estimates
Dehydration Units	General process flow information with a narrative description	Detailed engineering information and emission estimates
Fugitive Equipment Leaks	General process flow information with a narrative description	Detailed inventory of all components in 10% or greater w/w VOC service
Internal Combustion Engines (natural gas-fired)	No significant differences	
Compression Ignition Engines (diesel-fired)	Detailed engineering information is required	Not allowed
Roadways and Parking	A separate general permit application is used to present fugitive particulate emissions from vehicle traffic	Emission estimates only
Other Control Devices (Condensers and Carbon Absorption)	If applicable, other control devices would be identified on the general process forms	Detailed engineering specifications needed to evaluate capture and control of VOCs
Mechanical Vapor Recovery Units	Treated as process equipment with 100% VOC capture efficiency	Justification required for VOC capture efficiencies greater than 95%
Other Requirements	1. Emission units with a requested allowable emission rate in excess of 10 tons/year must demonstrate that Best Available Technology will be used 2. A source aggregation discussion should be included	A source aggregation discussion should be included in the application

One aspect of the OEPA GP-12 application that is not required by the WVDEP G70-A application is that a best available technology (BAT) discussion be provided for sources that will emit more than 10 tons/year of a regulated pollutant. BAT commitments, such as watering or other dust suppression for unpaved roadways, are included as site-specific additional terms and conditions in the GP-12.

WELL PAD AIR PERMIT CONDITIONS

Table 2 compares general permit conditions for well pad operations in Ohio and West Virginia. This is not intended to be a complete or exhaustive summary, but instead an overview of key differences that are expected based on WVDEP's template permit (WVDEP, 2013b).

The primary difference between well pad general permit conditions in Ohio and West Virginia is that the Ohio conditions are established relative to specific maximum equipment capacities and facility-wide emission thresholds, while the West Virginia general permit allows for site-specific limits. Another significant difference is the prevalent reference to the NSPS Subpart OOOO requirements in the West Virginia general permit compared to a general statement requiring conformance with the requirements of NSPS Subpart OOOO "once it becomes rule" in the Ohio general permit (OEPA, 2012b). Given that the NSPS has been finalized, it is expected that GP-12s will contain Subpart OOOO requirements.

Operationally, the WVDEP permit offers the applicant greater flexibility. There are no specific equipment capacity limits or facility-wide emission thresholds to work within as there are with the OEPA GP-12. As long as the facility demonstrates that it will stay below major source thresholds (and that it will not need to be aggregated with one or more adjacent facilities, the combined emissions of which exceed the major source thresholds), then the applicant can request emission limits that are needed to operate the particular well pad.

Table 2. Permit Conditions Included in Ohio and West Virginia General Permits for Shale Gas Well Pad Operations

Emission Unit	*Ohio GP-12*	*West Virginia G70-A*
Gas wells	No specific requirements	NSPS Subpart OOOO requirements
Pneumatic Controllers	No specific requirements	NSPS Subpart OOOO requirements, as applicable
Natural gas-fired heaters	Generally classified as exempt sources due to negligible emissions	Natural gas fuel usage limits as established by the permit application emission estimates
Flares	1. Maximum heat input capacity may not exceed 250 MMBtu/hr 2. Flare may not be operated at more than 10 MMBtu/hr except during emergency 3. VOC, NOx, CO, and SO2 limits	1. No limits on heat input 2. NSPS Subpart OOOO requirements, as applicable 3. VOC, NOx, CO, and PM limits

Emission Unit	*Ohio GP-12*	*West Virginia G70-A*
Storage Vessels	1. Limits on the maximum size of each storage vessel (950 bbl) and the combined capacity of all condensate vessels (6,000 bbl) 2. VOC emission limits	1. No limit on individual storage vessel size or cumulative capacity 2. Emission limits and production throughputs are as stated in the application 3. NSPS Subpart OOOO requirements, as applicable
Tanker Truck Loading	Vapor balancing required if BAT applies	Produced water and condensate throughput limits
Dehydration Units	1. Allows for up to 2 units 2. VOC emissions may not exceed 5.0 tpy 3. Dehydration system flare maximum heat input limited to < 10 MMBtu/hr	1. No limit on number of units 2. Flow rates specified in the application will establish permitted throughput
Fugitive Equipment Leaks	1. VOC emissions may not exceed 10.6 tons per 12-month rolling period 2. Leaks shall be repaired as soon as possible following detection 3. Develop and implement a LDAR program with leak defined as 10,000 ppm total VOC based on Method 21 procedures	Permitted VOC emission rate is established by emission estimates presented in the application
Internal Combustion Engines (natural gas-fired)	1. Individual and combined horsepower limits 2. Performance testing required for engines > 500 hp purchased without an EPA certificate of conformity	Fuel consumption limits (MMcf/yr) consistent with permit application emission estimates
Compression Ignition Engines (diesel-fired)	1. Engines must be certified to meet EPA Tier 3 emission standards 2. Combined horsepower for all engines at the site may not exceed 250	Not applicable (diesel engines not provided for in the G70-A)
Roadways and Parking	Must employ best available control measures on all unpaved roadways and parking areas	Generally not addressed
Siting Criteria	No specific restrictions	Facility may not be located within 300 feet of any occupied dwelling, business, public building, school, church, community, institutional building, or public park
Facility-Wide Emission Limits	Qualifying Criteria establishes facility-wide limits	Source-specific emission limits (lb/hr and ton/yr) with facility-wide limits constrained to less than major source thresholds

CONCLUSIONS

As natural gas production companies evaluate the types of equipment that will be needed to produce gas over the productive lifetime of shale gas wells, they are faced with the unique permitting requirements of each state. While these requirements continue to evolve, this paper offers a snapshot of significant similarities and differences in the Ohio and West Virginia air permitting programs.

The permitting of shale gas well pad operations in Ohio is generally less cumbersome than in West Virginia. The electronic cloning and submittal processes, the fact that emission calculations need not be provided, and the lack of a public comment period enable applicants to submit and receive approvals to install and operate equipment in less than two weeks.

However, the flexibility afforded by the site-specific conditions that apply to the West Virginia G70-A offers operational benefits over the OEPA GP-12. Since the capacity of flares, the capacity of storage tanks, and the horsepower of internal combustion engines is not constrained by the G70-A, the applicant is free to design equipment configurations as needed, provided that the major source thresholds are not exceeded. If, either through site-specific needs or source aggregation, it is determined that the facility would exceed major source thresholds, the standard R13 permit is still an option for West Virginia operators.

REFERENCES

Ohio Environmental Protection Agency, 2012a. Model General Permit (MGP) Qualifying Criteria Document. Effective January 31.

Ohio Environmental Protection Agency, 2012b. Model General Permit - Oil and Gas Well-Site Production Operations (GP-12). Effective January 31.

Texas Commission on Environmental Quality, 2012. Vapor Recovery Unit Capture/Control Guidance. Revised February 2012.

West Virginia Department of Environmental Protection, 2013a. Division of Air Quality, "General Permit Registration," <http://www.dep.wv.gov/daq/permitting/Pages/airgeneralpermit.aspx> (December 2, 2013).

West Virginia Department of Environmental Protection, 2013b. Division of Air Quality, "DRAFT General Permit G70-A Registration," <http://www.dep.wv.gov/daq/permitting/Documents/G70-ARegistration.pdf> (November 21, 2013).

The Grey Science of Wetland Avoidance

William T. Acton[1], PWS

[1]Principal, Ecological Practice Lead, Civil & Environmental Consultants, Inc., 8740 Orion Place, Suite 100, Columbus, Ohio 43240, U.S.A., E-mail: bacton@cecinc.com.

ABSTRACT: Exact wetland boundaries often are not easily identified. Natural gas producers and midstream operators often operate under deadlines and restrictions that are not compatible with regulatory timelines. As a result, they must rely on their consultants to make black and white decisions about project siting and routing when the science and regulations may not fully support such a call, leaving room for further discussion and potential judgment calls, or "grey" areas. The outcome of similar situations can vary based on the geomorphic landscape, the environmental sensitivity of the general area, different regulatory agencies, and even differing opinions within the same regulatory agency. A comprehensive understanding of the 1987 U.S. Army Corps of Engineers (Corps) Wetlands Delineation Manual (Manual) and the Corps Regional Supplements, as well as state-specific water quality regulations are required to make defensible decisions in the field so that projects can proceed ahead of regulatory concurrence. This requires thorough documentation of questionable areas to address project pressures, while avoiding the inherent risks of differing opinions with regulators (who may not have the same history of the site as the consultant does) after costly design, construction schedules, or delivery contracts are in place. These decisions require frequent and open communication between the producer or midstream operator and the consultant.

INTRODUCTION

Impacts to wetlands can occur via permitted actions, direct or indirect impacts to hydrology, unintentional discharges, or naturally occurring processes. The oil and gas industry may have to prove after-the-fact avoidance or compliance with non-notifying (or blanket authorized) allowable impacts, or disprove perceived impacts that may be the result of seasonal weather patterns, unrelated activities in the watershed, or differences in regulatory interpretations between agencies. Realizing it is not possible for the regulatory community to verify most upland projects or situations that will not impact regulated ecological features, the industry is often forced to rely on its experts to provide firm and defensible delineations of wetlands in conjunction with expedited construction schedules, constantly changing construction corridors, and the aforementioned variables that cannot specifically be addressed by the Corps Manual or the Corps Regional Supplements. This paper explores some of the challenges (including the morphology of the local environs, seasonal changes, variations between specific regulators,

environmental sensitivity, and local ordinances) that the natural gas industry faces when attempting to comply with wetland and stream regulations without waiting for regulatory concurrence of the defined limits of hydrologic features.

MORPHOLOGY

The physical morphology of the landscape can contribute to varying seasonal conditions to create grey areas. Examples of landforms that are susceptible to grey areas include seasonal seeps, floodplains, and mature forested areas.

Seasonal seeps on slopes can create grey areas that often have an available seed bank of both wetland and upland species. These areas typically exhibit wetland vegetation and hydrology during wetter periods in the spring when most seeps are active. Hydrophytic vegetation adapted for growth in ephemeral seeps often rapidly reaches maturity, reproduces, and wilts (Lichvar 2013). Seasonal seeps typically dry quickly in the absence of sustained precipitation in part due to their well-drained position on slopes. The hydrophytic vegetation can then be quickly outcompeted and overgrown by pioneer upland vegetation. This creates significant difficulties in identifying these areas as wetlands during the middle to later parts of the growing season or during sustained dry periods. This cycle often repeats year after year due to the stress that the varying oxygen conditions in the soils presents to non-pioneer species that are better adapted to sustained wet or dry conditions.

Floodplains are another landform susceptible to grey areas. Low gradient floodplains with well drained soils (sandy or silty) can create similar difficulties to season seeps, such as rapid hydrophytic plant growth/hydrology cycles.

Mature forests also are prone to grey areas. These areas often harbor multiple poorly drained hummocks in small mosaic patterns due to soil heave associated with large, mature root systems and other drainage impediments. These same root systems help facilitate significant evapotranspiration in the forest during the growing season, which can significantly alter the surface hydrology during the growing season. Therefore, the wet, hummocky areas that exist in the spring are absent during the growing season. These grey areas can quickly become overgrown with upland vegetation similar to that of seeps, but adapted for lower light conditions. Therefore, these areas can be difficult to delineate based on one site visit.

FIG. 1. A seasonal seep located on a hillside in Washington County, Pennsylvania.

SEASONAL VARIATIONS

Industry experts and regulators realize that wetlands with marginal hydrology can appear vastly different during various times of the same year. Wetlands, by their definition, are areas that fall somewhere between uplands and deep water habitats. Obviously, perennial wetlands, streams, and clear uplands do not typically present issues to the seasoned professional. However, when planning a pipeline route, access road, or well pad during drier months, it is important to understand that clearing activities can alter hydrology. Whether hydrology is altered from the removal of evapotranspiration in forests, diversion or concentration of upland sheet flow, or even rutting from heavy equipment, these changes in conjunction with seasonal precipitation variation can combine to create suspect grey areas that may not have previously existed prior to development activities.

Groundwater tables, especially perched aquifers, can vary significantly by season and often rise and fall quickly in relatively permeable glaciated tills underlain by clay or bedrock. These areas often can exhibit apparent upland and wetland conditions at different times of the year and often exhibit soils with nearly equally oxidized and reduced matrices.

FIG. 2 AND FIG. 3: THIS SITE WAS LOCATED APPROXIMATELY 1.5 MILES SOUTH OF LAKE ERIE AND HAD A HIGH WATER TABLE THAT VARIED THROUGHOUT THE GROWING SEASON. FIGURE 2 SHOWS A WETLAND MOSAIC AREA IN APRIL (LOOKING WEST). FIGURE 3 SHOWS THE SAME PORTION OF THE FIELD IN OCTOBER (LOOKING NORTH). NOTE THE STANDING WATER AND HYDROPHYTIC VEGETATION (I.E., *JUNCUS EFFUSUS* AND *JUNCUS TENUIS*) APPARENT IN FIGURE 2. BY OCTOBER, THE WATER TABLE WAS LOWER AND THE FIELD WAS COVERED BY WHITE OLDFIELD AMERICAN ASTER (*SYMPHIOTRICHUM PILOSUM*), AN UPLAND PLANT. THE REMNANTS OF THE EARLY GROWING SEASON PLANTS COULD BE FOUND UNDERNEATH THE CANOPY OF THIS LATE-SEASON ASTER, HOWEVER, BY OCTOBER THERE WAS A PREDOMINANCE OF UPLAND VEGETATION EVEN THOUGH THE WATER TABLE WAS STILL PRESENT AT A DEPTH OF 10 INCHES. THE ENTIRE SITE (BOTH UPLAND AND WETLANDS) HAD HYDRIC SOILS.

REGULATORY VARIATIONS AND CLIENT EXPECTATIONS

Professional experience varies widely in both the regulatory and consulting sectors. Difficult, non-routine, and marginal areas may require judgment calls based on an individual's experience and training. Often times, the demands of the private sector require unique or specialized training, client-specific reporting formats, or varying levels of micro-delineation based on the client's needs. In some situations, a consultant may be instructed to avoid regulatory conflict by delineating all marginal areas as wetlands in response to flexible schedule or construction limits. Other times, work schedule or land restrictions require a strong grasp of technical, scientific, and legal concepts to delineate "tight" boundaries that will be subject to scrutiny and that will require significant documentation to defend. These areas often occur in situations described previously, forcing a consultant to draw upon his/her experience in the local area and in the industry to "predict" how the area may change throughout the season.

The demands of the private sector, as well as the frequency and nature of interaction between the consultant and regulator, must be managed to respect professional relationships, which are critical in maintaining integrity with the regulatory agencies while providing advocacy for a client.

While the oil and gas industry often has a complete understanding of a project site and history, regulators often are only afforded hours or minutes to assess a delineation for accuracy. Disagreements can result in requests for additional information, additional site visits, increased boundaries, or even lengthy appeals. During these delays, the aforementioned changes, in addition to regulatory personnel changes, can occur, leading to delays or additional boundary or classification changes.

ENVIRONMENTAL SENSITIVITY

Environmentally sensitive areas and targeted activism often increases scrutiny by multiple parties. Watersheds of known high quality streams or other high quality resources are protected and scrutinized at a higher level. Public lands and parks, as well as producing agricultural areas, mature forests, and areas in close proximity to urbanized areas, also require an increased level of environmental due diligence and precautions.

The oil and gas industry is currently the target of multiple and well-organized environmental groups. These groups can slow or stop development. Such extraneous pressures can be impossible to predict, have the potential to delay or block projects, and can influence political or regulatory decisions. Awareness, expertise, planning, and thorough documentation are crucial in these situations.

LOCAL ORDINANCES

Specific ordinances in states, counties, municipalities, and townships are becoming increasingly common. Accords between several entities that encompass larger watersheds also are becoming more frequent. These ordinances often go beyond state and federal regulations, and may include riparian setbacks, groundwater impacts and recharge zones, tree preservation, and additional upland buffers around wetlands, streams, and headwater areas that do not qualify as wetlands or steams. Specific knowledge of these local regulations and an understanding of how they may affect the project schedule are required. Some local or state ordinances include erosion and sedimentation controls and even speculative upland impacts. In some areas, the local ordinances require concurrence with wetland or stream delineation findings from the federal or state regulatory community that may otherwise not have required such concurrence. A request to a regulator to concur with an upland finding that does not require that specific agency to issue a permit often is a low priority. Projects requiring a permit from the Federal or State government often take priority since no action on their part is technically required. Specific knowledge of these local regulations and an understanding of how they may affect the project schedule are required.

TOOLS TO ADDRESS CHALLENGES

Challenges presented by regional morphology, seasonal variations, interpretations of regulators, environmental sensitivity, and local ordinances often require that additional information be taken into consideration when delineating wetlands.

An office review should be conducted prior to visiting the site. Analysis and understanding of the United States Department of Agriculture (USDA) Soil Maps and Soil Series Descriptions, the United States Fish and Wildlife Services (USFWS) National Wetland Inventory Maps, the United States Geological Survey (USGS) National Hydrology Dataset, and high resolution aerial photography often provide indications of potential seasonally wet areas. National Climatic Data Center (NCDC) Palmer Drought Indices also provide information on the monthly moisture levels in a region and the departure from normal, which can help guide field methodology. Background research of the site should be gathered as well.

The use of the sources stated above and other tools not only provides field methodology guidance, but can help build a defensible scientific conclusion that takes into account historical data and provides additional reliability in the event that unexpected conditions are encountered after the field work is completed.

CONCLUSIONS

While simple avoidance of wetlands and streams may seem like the best alternative, proceeding with projects without regulatory concurrence and involvement can present its own set of challenges above and beyond situations that require a permit for impacts. Some of the challenges that the natural gas industry faces when attempting to comply with wetland and stream regulations without waiting for regulatory concurrence of the defined limits of hydrologic features may include the morphology of the local environs, seasonal changes, variations between specific regulators, environmental sensitivity, and local ordinances. To effectively address these challenges, the following tools are beneficial: thorough documentation, office review of supplemental data, background research, familiarity with the seasonal variability of the study location, and expert understanding of the Corps Manual and Supplements. These tools combined with experience can create defensible decisions in regards to grey wetland areas.

ACKNOWLEDGMENTS

The author appreciates the support of Civil & Environmental Consultants, Inc.

REFERENCES

Cowardin, L. M., Carter, V., and Golet, F. C. 1979. Classification of Wetlands and Deep Water Habitats of the United States. U.S. Department of the Interior, Fish and Wildlife Service, Washington, D. C., FWS/OBS - 79/31.

Environmental Laboratory. 1987. Corps of Engineers Wetlands Delineation Manual, Technical Report Y-87-1, U.S. Army Engineer Waterway Experiment Station, Vicksburg, Mississippi.

Lichvar, R.W. 2013. The National Wetland Plant List: 2013 Wetland Ratings. Phytoneuron, 2013-49: 1-241.

National Oceanic and Atmospheric Administration (NOAA) National Climatic Data Center. 2013. Weekly Palmer Drought Indices.

Ohio Environmental Protection Agency (OEPA). Ohio Administrative Code, Chapter 3745-1: Ohio Water Quality Standards, Beneficial Use Designations.

United States Army Corps of Engineers (USACE) and Environmental Protection Agency (EPA). 2007. U.S. Army Corps of Engineers Jurisdictional Determination Form Instructional Guide Book.

USACE and EPA. 2012. Regional Supplement to the Corps of Engineers Wetlands Delineation Manual: Northcentral and Northeast Region (Version 2.0), J.S. Waleley, R.W. Lichvar, C.V. Noble, and J.F. Berkowitz, eds., ERDC/EL TR-12-1. U.S. Army Engineer Research Development Center, Vicksburg, Mississippi.

United States Department of Agriculture, Natural Resources Conservation Service (USDA, NRCS). 2010. Field Indicators of Hydric Soils of the United States Version 7.0, L.M. Vasilas, G.W. Hurt, and C.V. Noble. USDA, NRCS in cooperation with the National Technical Committee for Hydric Soils.

USDA, NRCS. 2013b. National List of Hydric Soils. USDA-NRCS Soils, <http://soils.usda.gov/use/hydric/> Accessed November 2013.

United States Fish and Wildlife Service (USFWS). National Wetlands Inventory. Data by State – Ohio. Revised 2012.

United States Geological Survey (USGS). National Hydrography Dataset (NHD), <http://nhd.usgs.gov/> Accessed November 2013.

Improving Impact Analysis of the Eagle Ford Shale Oil and Natural Gas Production on Regional Rural Communities

Gerardo J. Pinzon[1], P.E., Jianhong-Jennifer Ren[2], Ph.D., P.E., and Kim D. Jones[3], Ph.D., P.E.,

[1]Department of Environmental Engineering, Texas A&M University-Kingsville, MSC 213, Kingsville, Texas 78363, Phone: (956)740-9663, E-mail: gerardo.pinzon@students.tamuk.edu
[2]Department of Environmental Engineering, Texas A&M University-Kingsville, MSC 213, Kingsville, Texas 78363, Phone: (361) 593-2290, E-mail: jianhong.ren@tamuk.edu
[3]Department of Environmental Engineering, Texas A&M University-Kingsville, MSC 213, Kingsville, Texas 78363, Phone: (361) 593-2187, E-mail: kim.jones@tamuk.edu

ABSTRACT: The Eagle Ford Shale, a formation that is 80 kilometers wide by 640 kilometers long, and located in South Texas, was traditionally considered to be economically unfeasible as a potential natural gas and oil producing formation. Since the onset of hydraulic fracturing of the non-porous rock, the Shale has rapidly become one of the highest producing areas of natural gas and oil, with a positive economic impact on the communities located over it. Previous studies have shown both direct and indirect impacts of the Shale development on the regional communities. The intent of this study is to re-evaluate the overall impacts of the Eagle Ford Shale development in consideration of a set of extended components, in addition to the production, drilling, and related activities that have traditionally been considered. This paper presents the preliminary findings for Cotulla, Texas. The findings will provide more evidence supporting the importance of considering all extended factors to better illustrate the impact of shale development on rural communities.

INTRODUCTION

The Eagle Ford Shale (EFS) spreads across over 20 counties; however, its impact and economic boost extend well beyond its boundaries. For instance, both San Antonio and Laredo, which are not within the boundaries of the Shale, have experienced an increase in oil and gas related businesses such as service and pipeline companies, hotel industry and education. Study has shown that the EFS impact translated to a yield of more than $19.2 billion, supported 38,000 full-time jobs,

generated close to $10.5 billion in gross regional products, $211.0 million to local governments and $312 million to the state in revenues. By year 2021, these numbers could increase to $62.1 billion in yield, 82,600 full time jobs, $34.0 billion in gross regional product, $888 million for local government and $1.6 billion in state revenues (UTSA, 2013).

Cotulla, Texas, located to the east of Interstate Highway 35 and is in the heart of the EFS, has become a "model city" as it has a population of over 5,000 now. This population growth was estimated based on the number of water connections created in the last two years due to the economic boom caused by the oil and natural gas extraction (TEEX, 2013). Becoming a model city means the City of Cotulla may now establish its own city charter with a local government based on local needs and is no longer subject to a general law that relies on State government (TML, 2013).

Many studies have been undertaken with most highlighting the economic boost caused by the EFS development. Others are tackling issues and problems created by the rapid growth. For example, Palacios (2012) and the Texas Groundwater Protection Committee (TGPC, 2013) conducted water quality studies. Various water quantity studies were conducted by Freyman (2013), Palacios (2013), and Dale (2013). Studies on air quality have been ongoing (Bella, 2012, TCEQ, 2013), and studies dealing with indirect effects, such as earthquakes, that have allegedly been attributed to fracing have also been published (Frohlich, 2012).

The local governments in rural communities of the EFS were not prepared for the rapid growth. To better facilitate a balance between economy and natural resources, the intent of this study is to re-evaluate the impacts of the EFS development by considering a set of extended factors, in addition to the production, drilling, and related activities that have traditionally been considered. The extended impacts to be considered include what is known as soft infrastructure, which entails increased stress on government, law enforcement, by-products of oil production, transportation load increases and road damage, and stress on water resources and air quality.

THE SHALE

Several shale formations are producing oil and gas in Texas through hydraulic fracturing including the EFS, Permian Basin, Barnet Shale, Haynesville/Bossier Shale, and Granite Wash. The EFS is 80 kilometers wide and 640 kilometers long, extending from the Texas/Mexico border towards the northeast, ending just south of Dallas. It has varying depths of between 1,200 and 3,600 meters (STEER, 2013).

The impact of the EFS is evident through the drastic increase in the number of flares and lights in the EFS as seen from satellite images taken over the last decade (Figure 1). The success in the EFS is a direct outcome of horizontal drilling. In contrast to vertical drilling, horizontal drilling is capable of accessing natural gas/oil deposits as far as 90 meters from the well site in all directions. Thus, horizontal drilling is more cost efficient by reaching far more fuel with less wells drilled (GWPC, 2013). Because horizontal drilling requires fewer individual wells than vertical drilling, a dramatic drop in the number of drilling permits occurred after 2008, when horizontal drilling started in Texas (Figure 2).

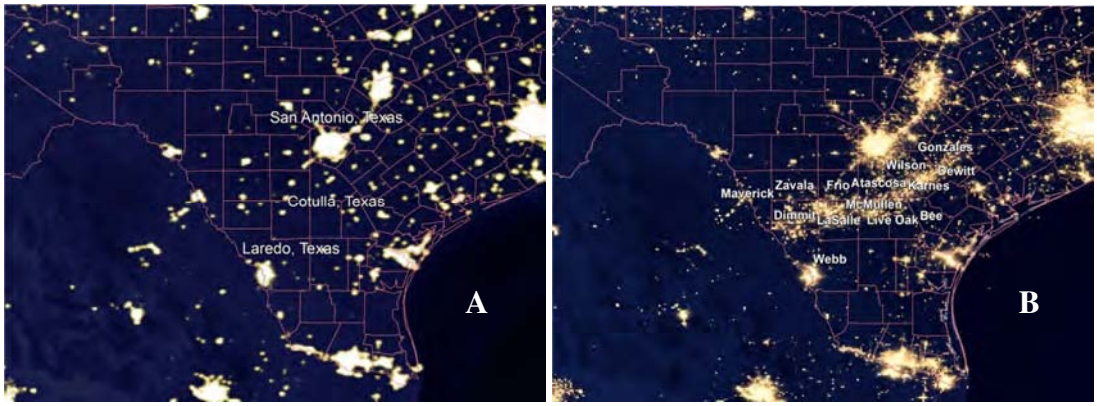

Source: NASA satellite images

FIG. 1 – Night Lights over the EFS in: A) 2000, and B) 2010

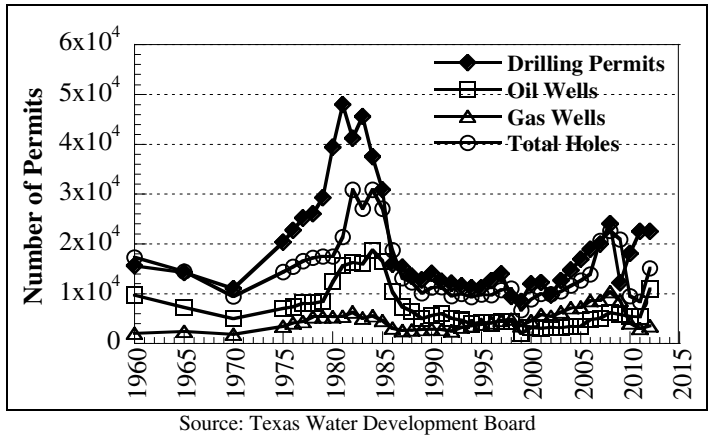

Source: Texas Water Development Board

FIG. 2 – Drilling Statistics in Texas

IMPACTS

Previous studies on EFS impacts have mainly considered the economic benefits. This study employs a new angle and chooses "balance" as its key word toward the goal of obtaining a sustainable system. This approach considers all impacts, whether positive or negative, to identify all factors that contribute to this "balanced" view of the sustainability of the EFS development.

Direct Economic Impacts

Shale gas production in North America is projected to grow exponentially. Shale gas extraction is expected to become the most prominent source of future gas production growing up to 924 billion cubic meters in the next 30 years (Figure 3). In South Texas, continuous shale extraction has permanently changed the region. Almost $30 billion was spent developing the prolific EFS in year 2013 and the economic outcome included more than $60 billion dollars and over 116,000 jobs. The EFS is expected to have an overall economic boost of $89 billion and over 127,000 jobs by the year 2022 (STEER, 2013).

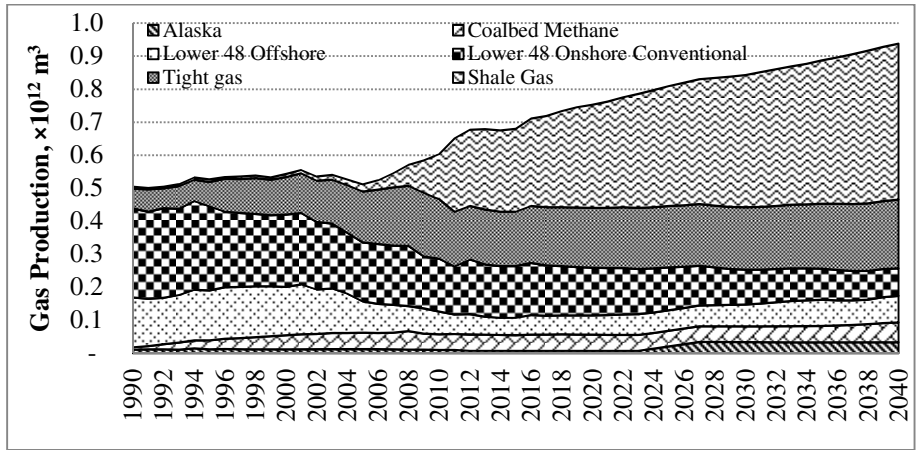

Source: U.S. Energy Information Agency

FIG. 3 – Gas Production in North America

Indirect Impacts

Social Issues

The indirect impacts of the EFS activity include expansions in law enforcement and social support services due to a rise in crime and social stress. There has been an increase in cases of domestic violence, child abuse, neglect, drug abuse, drinking under the influence (DUI), and racial tension. For instance, a recent review of domestic calls in some of the EFS counties showed a 30% increase to 911 emergency number that resulted in further investigations between 2011 and 2013. In Live Oak County, there has been a 400% increase in felony cases between 2012 and 2013 (Dugan, 2013). Although these data cannot be directly correlated to the EFS, the increase is significant compared to other counties not in the EFS.

Issues involving race are also of concern. According to La Salle County Judge Joel Rodriquez, the EFS is attracting workers from Canada, Louisiana and South Texas. They are brought here from all walks of life but mostly are skilled, yet uneducated workers that have very little knowledge of other races and cultures adding to the tensions of overworked and inhumane living conditions (Rodriguez, 2013).

Product Disposal Effect

According to Green (2013), the potential for aquifer contamination can occur as a result of migration of the injected salt water into the aquifer through nearby abandoned wells. This is because most of the abandoned wells are old and dilapidated where the steel casings have already ruptured, allowing the intrusion of salt water into the aquifer (Green, 2013).

Another area of concern is accidental spills during drilling or production. The Texas Railroad Commission (TRC) has the jurisdiction over all spills; however, the enforcement of spills is dependent only on the reporting by operators. Oil and gas operators are required to provide immediate notice of a fire, leak, spill or break to the appropriate commission district office (TCEQ, 2013). However, this requirement

only applies to a loss of five barrels (595 liters) in the aggregate. A visit and discussion with oil operators revealed that since it is the responsibility of the operator to report these violations, it is not customary to report them. Instead, they either clean them up or hide them with sand. The lengthy process required for spill notification and the lack of enforcement makes it very easy to ignore spills entirely. The impact of the common practice of ignoring spills at the drilling site can be amplified by the oil waste haulers spilling along the road, and/or oil spills from hundreds of miles of oil pipelines that go unreported.

Impact on Education System

Despite the fast growth in all aspects in the EFS communities, an assessment of the student enrollment of Cotulla, Texas, indicates that no significant impact is seen (Figure 4). This could be explained by the nomadic living of the oil workers. Most of the workers travel to the working sites on their own without their families and go back to their hometown during their off periods.

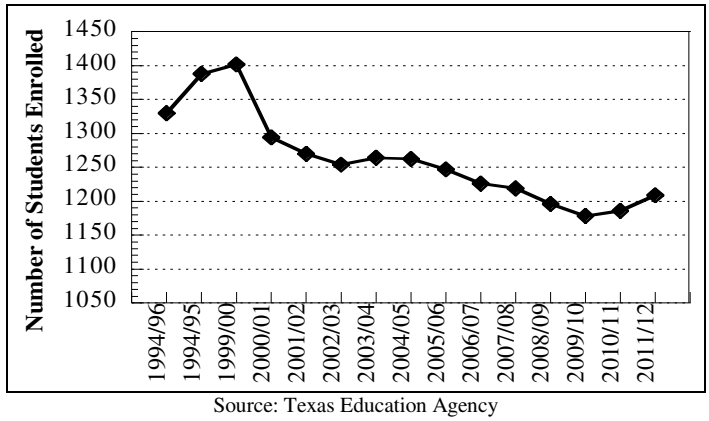

Source: Texas Education Agency

FIG. 4 – Student Enrollment Data for Cotulla, Texas

Impact on Transportation

According to the Texas Department of Transportation, it takes over 2,000 loaded trucks for an oil well to be brought up to production and for the maintenance and upkeep of the well for up to 5 years on the life of the well. This has reduced the lifetime expectancy of the Farm to Market (FM) Roads and resulted in well over $1 billion in increased maintenance and replacement costs annually to the FM road system in Texas just by the EFS (Barton, 2013).

The State of Texas approved $225 million to fix roads affected by the EFS (Porter, 2013). Government officials in the impacted communities must develop the engineering designs and proposals necessary to request the funds. Unfortunately, most of these small communities do not have the adequate administrative and technical personnel to prepare the considerable amount of research and paperwork required for accessing these funds.

Impact on Number of Crashes

The increase in vehicular traffic is of concern, particularly on the farm roads and in the surrounding rural communities. As shown in Figure 5, all key EFS counties had an increase in the number of total crashes. A recent study indicates that most car wrecks can be attributed to oil workers falling asleep while driving after long hours of work. Many workers neglect wearing their seatbelts, increasing the severity and/or fatality rates that occur with accidents in the region (Haley, 2013).

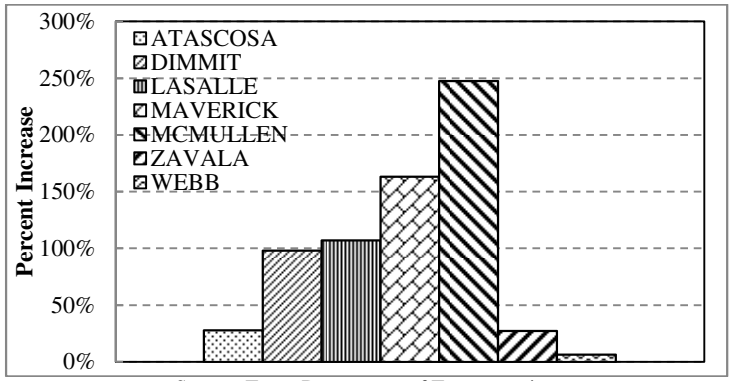

Source: Texas Department of Transportation

FIG. 5 – Percent Increase in Crashes by County between 2006 and 2012

Impact on Water

The EFS lies right beneath the Carrizo-Wilcox outcrop and subcrop. Based on the Texas Water Development Board (TWDB) daily average of hourly water depth data measured in various counties that are impacted by the EFS activities, Zavala's water level dropped from 116 m to 120 m (3%), La Salle dropped from 95 m to 147 m (54%), Frio dropped from 120 m to 124 m (3%) and Duval dropped from 77 m to 87 m (13%) from January 2011 to December 2013 (Figure 6).

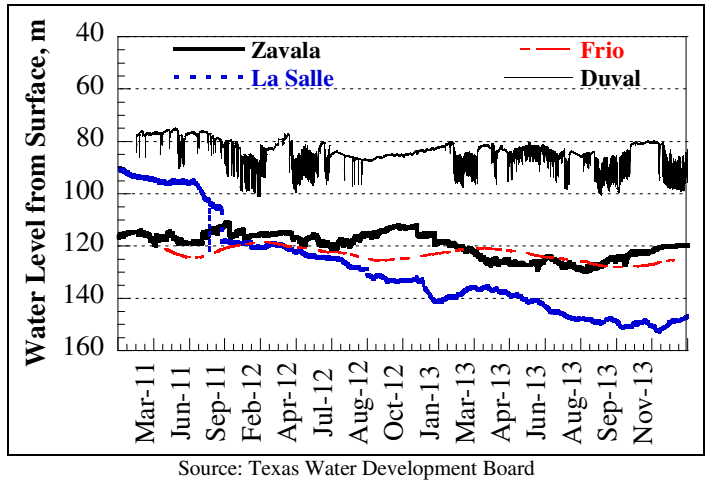

Source: Texas Water Development Board

FIG. 6 – Historic Water Well level by Counties that are Impacted by EFS

Groundwater

Obtaining water for fracing has been another major issue. In Texas, groundwater belongs to mineral rights owners; while surface water is owned by the State. Diverting surface water from its source requires authorization from the Texas Commission on Environmental Quality (TCEQ) according to the Texas Water Code, ch. 11.

The EPA recently studied the cause of the water contamination in Pavilion, Wyoming and claimed that this water contamination was due to fracing conducted in and below the drinking water aquifer and very close to drinking water wells. Such water contamination should not happen elsewhere since fracing is usually conducted far below the drinking water aquifer (TRC, 2012; EPA, 2013).

Drilling in the EFS is under the jurisdiction of the TRC in Texas. TRC regulations require all well casings be set below the depth of the water table aquifer to ensure the protection of groundwater. A groundwater advisory unit under the TRC enforces the groundwater protection by requiring several layers of steel casings and cement beyond the water table aquifer to the deepest useable quality groundwater level to serve as a protective sleeve (TRC, 2012). Protection is further secured by a second layer, which is the pipe placed in the wellbore to the well's total depth and permanently cemented in place. Some operators even add a third layer if the pressure of the fracturing process requires it. Monitoring gauges are usually placed at the surface to monitor these casings to quickly identify any downhole problems or leaks.

Groundwater is managed individually by landowners under the Rule of Capture and, in some cases, collectively by groundwater conservation districts. The "Rule of Capture" in Texas allows its mineral rights owner to pump as much water as they wish, as long as there is no liability to surrounding landowners or there is no complaint that surrounding landowners' wells are being affected (TCEQ, 2013). The only exception to this law is when a groundwater conservation district is approved by the legislature as authorized by the Texas Water Code, Chapter 36. By state law, the districts have the power to conserve, preserve, protect, recharge, and prevent waste of groundwater resources within their jurisdiction (TCEQ, 2013).

According to the TRC, no incidents have been reported to indicate contamination associated with hydraulic fracturing in Texas (TRC, 2013). FracFocus.org is a website established by the TRC for oil and gas operators to disclose chemical ingredients and water volumes used in fracing. This website is hosted by the Ground Water Protection Council (GWPC) and the Interstate Oil and Gas Compact Commission (IOGCC). The GWPC is a national association of state groundwater and underground injection control agencies. The IOGCC is a national commission whose members are governors and state regulators of oil/gas producing states (TRC, 2013).

Texas regulation does not require, but does encourage recycling of flowback fluid, the returned fluid from the fracing process. This fluid does not have the proper quality for reuse as stipulated by the Underground Injection Control Rule of the Safe Drinking Water Act. For this reason, the flowback water must be either recycled or disposed of in permitted and regulated disposal wells.

Recycling is currently being investigated and promoted because of the potential to reduce not only the amount of water used but also the cost associated with the production. However, drilling engineers do not want to change current drilling

practices (Dale, 2013). This leaves disposal as the most widely used method for disposition of the fracing fluids. Thus, the total water disposal has increased since the activity in the EFS. Frio County has received the bulk of the flowback fluids from the fracing activity in the EFS although there are not many oil wells drilled in this county. Thus, the disposal of flowback fluids in Frio County increased from an average of 3.6E+17 liters to 2.5+18 liters in 2013 (Figure 7).

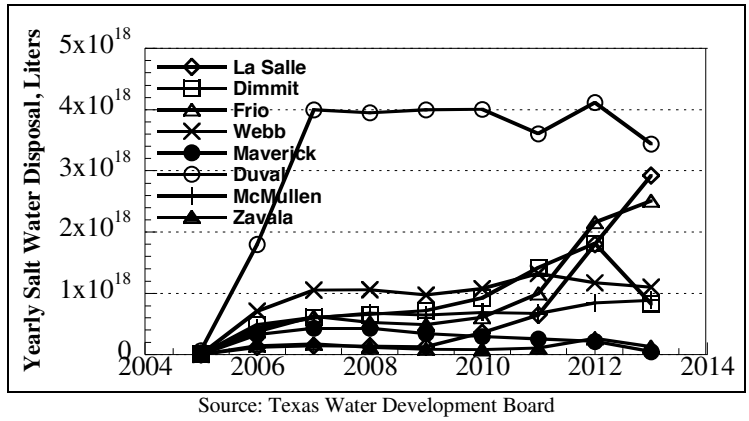

Source: Texas Water Development Board

FIG. 7 – Yearly Salt Water Disposal by County

Impact on Air Quality

The increased flares (Figure 1) in the EFS region could be emitting high levels of methane gas, hydrogen sulfide, and Volatile Organic Compounds, which have been known to cause leukemia (EPA, 2013). San Antonio, Texas, the largest city in the US with an attainment air quality status and located in close proximity to the EFS, is now at risk of losing this nationally acclaimed status. TCEQ, agency with jurisdiction for air quality, is overseeing the monitoring, investigating and conducting enforcement operations in the EFS to minimize potential negative impacts of oil/gas production on air quality in the region. During the summer of 2013, 286 aerial video images were compiled, where more than 10,000 individual farm water tanks were surveyed and approximately 5 percent were found to have some degree of emissions. Formal notices of violation have increased, reaching approximately 100 in 2013 (TCEQ, 2013).

A recent study published by Miller et al. (2013) shows that shale gas emissions of greenhouse gases were underestimated by as much as 20% than previously thought. Although emissions by the EFS flaring are legally allowed, the TRC only allows gas flaring to occur for ten days from the initial production. The TRC has the authority to grant an exception under certain circumstances (TRC, 2013).

Earthquakes

There have been some questions whether fracing may cause earthquakes. To date, no direct effect has been identified. However, the EPA recently published a study that relates earthquakes to disposal of salt water (EPA, 2013). There are more than

50,000 disposal wells in Texas and most of these wells use abandoned or old wells. Pumping disposal water into a well that is close to a fault can cause the fault to slip and shake, creating an earthquake (Gan & Frohlich, 2013).

CONCLUSION

This paper presents a comprehensive picture of the impacts created by the EFS. The data presented add to the knowledge of ongoing impacts; however, there is still a need to obtain more detailed data to improve our understanding on the level of impacts that each community is facing. The information presented provides insights for local governments on the types of data that they will need to collect and evaluate to gain a better assessment of the impact that the EFS gas and oil activities are causing in their jurisdictions. To manage these impacts, both traditional means for impacts mitigation/prevention and non-traditional techniques for quantification and analysis of each impact should be pursued.

ACKNOWLEDGMENTS

We would like to thank the City of Cotulla City Manager Larry Dovalina and the La Salle County Judge Joel Rodriguez for their time and openness to provide insights on their governmental duties and impacts on their communities due to the rapid growth of the EFS. Special thanks also go to colleagues at the Center for Earth and Environmental Studies, Texas A&M International University, particularly Arturo Diaz for assisting in the production of the NASA night light images.

REFERENCES

Barton, John A. (2013) TxDOT Deputy Executive Director "Presentation to House Appropriations Subcommittee Committee on Budget Transparency and Reform" March 11, 2013

Baker H., (2012). *Baker Hughes rotary rig count*. Retrieved from Baker Hughes website: http://phx.corporate-ir.net/phoenix.zhtml?c=79687&p=irol-rigcountsoverview.

Bella, P., Prepared for Alamo Area Council of Governments. (2012). *Ozone: Violations, nonattainment & our air quality future*. Retrieved from http://www.aacog.com/Document Center/View/8335.

Dale, W. (2013). *Green can be green*. Paper presented at the Supply, Flowback and wastewater treatment training course on hydraulic fracturing operations Workshop at Texas A&M University Kingsville, Kingsville, TX, Nov. 5 – 7.

Dugan, J. (2013) Community Educator, *Women Shelter of South Texas*.

Freyman, M. & Salmon, R. (2013). "Hydraulic fracturing & water stress: Growing competitive pressures for water". Retrieved from Ceres website: http://www.ceres.org/resources/reports/hydraulic-fracturing-water-stress-growing-competitive-pressures-for-water/view.

Frohlich, C. (2012). Two-year survey comparing earthquake activity and injection-well locations in the Barnett Shale, Texas. *Proceedings of the National Academy*

of Sciences of the United States of America, *109*(35), 13934–13938. doi:10.1073/pnas.1207728109.

Gan, W., & Frohlich, C. (2013). "Gas injection may have triggered earthquakes in the Cogdell oil field, Texas". *Proceedings of the National Academy of Sciences of the United States of America, 110*(47), 18786-18791. doi:10.1073/pnas.1311316110, #2600.

Green, R. (2013) Scientist, Southwest Research Institute, Presentation to Wintergarden Ground Water District, San Antonio.

Green, R. (2013) Scientist, Southwest Research Institute, as reported on Texas Tribune on Mar 2013.

GWPC (Groundwater Protection Council), 2013, Retrieved from FracFocus.org.

Haley, E., Business Development Manager, PEC Premier Safety Management Systems, Interviewed on Nov 13.

UTSA. (2013) Institute for Economic Development and the Center for Community and Business Research, *Economic Impact of the Eagle Ford Shale*. University of Texas San Antonio.

Miller, S.M., Wofsy, S.C., Michalak, A.M., Kort, E.A., Andrews, A.E., Biraud, S.C., Dlugokencky, E.J., Eluszkiewicz, J., Fischer, M.L., Janssens-Maenhout, G., Miller, B.R., Miller, J.B., Montzka, S.A., Nehrkorn, T., and Sweeney, C.(2013),"Anthropogenic emissions of methane in the United States", *Proceedings of the National Academy of Sciences,* vol. 110, pp. 20018-20022, 2013. http://dx.doi.org/10.1073/pnas.1314392110.

Palacios, V. (2012).*"Baseline groundwater quality testing needs in the Eagle Ford Shale region"* Duke University. Retrieved from http://hdl.handle.net/10161/5370.

Palacios, V. (2013). "In Texas, Freshwater Use for Oil and Gas Should be Reduced Strategically" Austin, Texas: Environmental Defense Fund. Retrieved from http://blogs.edf.org/energyexchange/2013/04/09/in-texas-freshwater-use-for-oil-and-gas-should-be-reduced-strategically/.

Porter, D. (2013) *Eagle Ford Shale Task Force Report*. Texas Railroad Commission.

Rodriguez, J., LaSalle County Judge, Interview, Oct. 2013.

STEER (South Texas Energy & Economic Roundtable), (2013), Retrieved from www.steer.com.

Texas Commission on Environmental Quality (TCEQ). (2013), Texas Administrative Code, 16 TAC §3.8, 2012.

Texas Commission on Environmental Quality (TCEQ). (2013). Oil and Gas Facilities Workshop. http://www.tceq.texas.gov/permitting/air/training/ogfacworkshop.html

Texas Commission on Environmental Quality (TCEQ). (2013). Texas Water Code.

Texas Department of Transportation (TxDot). (2013).

TEEX (Texas Engineering Extension Service), (2013), *Competitive Assessment of Cotulla, Texas*, TAMU, November 2013.

TGPC (Texas Groundwater Protection Committee) (2013). *Joint Groundwater Monitoring and Contamination Report — 2012*. Austin, Texas. Retrieved from http://www.tgpc.state.tx.us/AllPublications.php.

TML (Texas Municipal League) 2010, "Home Rule Cities", *Handbook for Mayors and Council Members, Texas Municipal League,* obtained directly from the website at http://www.tml.org/pdftexts/HRHForward.pdf.

SPCC Planning for Oil Drilling, Workover and Production Facilities

Martin J. Hamper, P.G.[1]

[1]GZA GeoEnvironmental Inc., 16 W. 241 S. Frontage Road, Burr Ridge, Illinois 60527
773-256-7718 martin.hamper@gza.com

ABSTRACT: The United States Environmental Protection Agency (US EPA) has issued a revised guidance manual on Spill Prevention, Control and Countermeasures (SPCC) plans in August 2013 for its Regional Inspectors. The manual also provides insights to the regulated community on achieving compliance with the largely performance-based SPCC regulations. The previous SPCC manual was published in November 2005. Since then there have been revisions to the SPCC regulations in 2006, 2008, 2009 and 2011 and these revisions have been incorporated into the 2013 SPCC guidance manual. The manual also includes expanded discussions of SPCC regulations that cover oil production, and oil drilling and workover facilities. In addition to meeting the general SPCC requirements, the main components for oil drilling and workover facilities include positioning equipment to prevent discharges, providing catchment basins or diversions structures to intercept discharges of oil, and installing a blowout prevention assembly and well control system. For oil production facilities in addition to the general SPCC requirements, there are requirements for bulk storage, flow-through process vessels, produced water containers, and transfer operations. Owner/operator self-certification of SPCC plans can be a cost-effective and flexible approach for the development of SPCC plans for facilities where the largest tank is either no greater than 18,900 L (5,000 gallons) (Tier I) or 37,800 L (10,000 gallons) (Tier II).

INTRODUCTION

Spill Prevention, Control and Countermeasures (SPCC) planning is not new to the oil industry as the SPCC rules were first effective on January 10, 1974. Nearly 40 years ago, existing facilities were required to have plans in-place by January 10, 1975 (38 FR 34164). These 1974 SPCC rules were not significantly modified until 2002. The modifications were largely in response to recommendations from the United States General Accounting Office (GAO) and the United States Environmental Protection Agency (EPA) 1988 SPCC Task Force.

In 1988, EPA organized an SPCC Task Force to review the SPCC program after a significant aboveground storage tank (AST) oil spill on the Mononagahela River (EPA 1988). Also in response to the Mononagahela River AST oil spill and to the Martinez, California AST oil spill, the GAO was requested by the United States Senate to assess federal aspects of AST regulation and certain elements of the oil spill program (GAO 1989). In 1991, the EPA proposed amendments to the SPCC regulations incorporating certain EPA SPCC Task Force and GAO recommendations.

One aspect of EPA's 1991 proposal was a reorganization of the SPCC regulations into five industry-specific groups to aid in the clarification of requirements for different types of facilities (56 FR 54612). Sections 40 CFR 112.9 (Onshore Oil Production Facilities) and 40 CFR 112.10 (Oil Drilling and Workover Facilities) were two of the five facility-specific sections included in the 1991 SPCC proposed rules. In addition to reorganizing the rules, additional industry-related sections and approaches were also added. These proposed rules were promulgated as a final rule in 2002.

The EPA developed the SPCC Guidance for Regional Inspectors guidance manual subsequent to the 2002 final rule (EPA 2005). The EPA revised the guidance manual in 2013 after an additional series of amendments to the SPCC regulations (EPA 2013). A more complete history of the SPCC regulations can be found in both the 2005 and the 2013 revised SPCC Guidance Manual for Regional Inspectors (EPA 2005; EPA 2013).

As noted above, the SPCC regulations have changed since their inception in 1974 including providing owners and operators the cost-saving option of developing and self-certifying SPCC plans for their oil production sites. Some owners and operators may not be aware of this option or know if their operations qualify for self-certification. Also, some owners and operators may not be aware that the SPCC regulations have been reformatted by industry type, which makes the requirements easier to understand. While the guidance manual is called the SPCC Guidance for Regional Inspectors, owners and operators will find the example plans and explanations helpful should they decide to develop and self-certify their SPCC plans. This paper provides an overview of the SPCC regulations for owners and operators and describes the types of facilities that may qualify for self-certification.

GENERAL REQUIREMENTS

Owners/operators of oil production facilities must prepare and implement SPCC plans within six months after beginning operations. SPCC plans must be in writing and designate a responsible person with the authority to commit the necessary resources to implement the plan. Certain facilities with the potential for substantial harm to the environment must also prepare a Facility Response Plan (FRP). The SPCC plan must include a certification by the owner/operator as to whether or not they must prepare an FRP. The presentation of topics in the SPCC plan must either follow the regulatory sequence or include a cross-reference between plan sections and the regulations. The plan can call for procedures, facilities, methods or equipment not yet operational as long as the installation and start-up details are provided.

The SPCC rules and guidance define an oil production facility to include all structures including wells, platforms, oil storage tanks, produced water tanks, separation facilities, flowlines, gathering lines, drilling and workover equipment used in the production, extraction, recovery, separation, lifting, stabilization, or treating of oil (including condensate) located in an oil or gas field (EPA 2013).

The general requirements for SPCC plans are found in 40 CFR 112.7. SPCC plans must include a description of the facility, types of oil stored, oil storage management practices, inspection and testing requirements, training program, discharge prevention measures, discharge controls, and discharge countermeasures for the discovery, reporting, coordination, response and cleanup. Oil production facilities, which as noted above include drilling and workover operations, are exempt from the general security requirements of 40 CFR 112.7 (g).

The owner/operator has flexibility in defining the extent of a facility. Fixed and portable oil storage container locations, transfer stations, equipment, flowlines and gathering lines must be depicted on the facility layout map. Factors considered in determining the boundaries of a facility include: ownership, management and operational control; operational similarities; proximity, and shared drainage paths. Typically, a well, flowlines and tank battery comprise an oil production facility. An owner/operator may wish to aggregate multiple wells, flowlines and tank batteries under common ownership or control or consider them as separate and distinct facilities, each with their own SPCC plans. Such decisions may also affect EPA jurisdiction over flowlines (i.e., inter-facility v. intra-facility flowlines).

The plan must provide for appropriate containment and diversionary structures. The design of general secondary containment system should address the typical failure mode and the most likely quantity of oil that may be discharged from areas such as oil transfer, piping, and process equipment. The design of specific secondary containment for bulk containers should address a major failure of the largest container plus precipitation freeboard. The containment system must be able to prevent the escape of oil prior to cleanup. Secondary containment systems may be either passive or active systems. Containment systems can include dikes, berms, retaining walls; curbing or drip pans, sumps and collection systems, culverts, gutters, or other drainage; weirs, booms, or other barriers; spill diversion ponds, retention ponds, or sorbent materials.

SELECTED OIL PRODUCTION FACILITY REQUIREMENTS

In addition to meeting the general requirements of 40 CFR 112.7, oil production facilities must meet the industry-specific requirements of 40 CFR 112.9. There are specific requirements for inspections, facility drainage, discharge prevention engineering practices, container compatibility, secondary containment, and alternative compliance approaches for flowline/intra-facility gathering lines, produced water, and flow-through process vessels.

Bulk storage containers are subject to specific secondary containment sizing requirements (i.e., largest container volume plus precipitation freeboard). Drainage from undiked areas must be confined to a catchment basin or holding pond. If secondary containment is not practicable, then the SPCC plan must require periodic

integrity testing of the containers, periodic integrity testing and leak testing for piping, and a 40 CFR Part 109 Oil Spill Contingency Plan.

Produced water containers and separation process vessels are also subject to the specific secondary containment sizing requirements. However, the regulations also provide an alternative compliance approach for these containers and vessels using the general secondary containment requirements with additional inspection and management activities designed to reduce the potential for releases.

Secondary containment requirements for oil production facilities are summarized in Table 1.

Table 1. Selected Secondary Containment Options for Oil Production Facilities

Unit or Process	**Secondary Containment Requirement**	**or**	**Alternate Compliance Approach**
Bulk Storage Containers	Largest container volume plus precipitation freeboard (40 CFR 112.9(c)(2))		_____
Flowlines and Intra-facility Gathering Lines	Most likely quantity of oil discharge (40 CFR 112.7 (c))	or	Provide an Oil Spill Contingency Plan meeting 40 CFR 109 (40 CFR 112.9 (d)(3)
Produced Water Containers	Largest container volume plus precipitation freeboard (40 CFR 112.9(c)(2))	or	Most likely quantity of oil discharge (40 CFR 112.7 (c)) and Inspection and Management Programs (40 CFR 112.9(c)(6)
Flow-through Process Vessels	Largest container volume plus precipitation freeboard (40 CFR 112.9(c)(2))	or	Most likely quantity of oil discharge (40 CFR 112.7 (c)) and Inspection and Management Programs (40 CFR 112.9(c)(5)
Other Areas with Potential for Discharge (transfer areas, mobile fueling areas, etc.)	Most likely quantity of oil discharge (40 CFR 112.7 (c))		_____

Bulk storage containers must be visually inspected periodically on a regular basis consistent with an industry standard such as "*Recommended Practice for Setting, Maintenance, Inspection and Operation and Repair of Tanks in Production Service*"

(API RP 12 R1). The tank battery must also incorporate good engineering practices to prevent discharges by:

- Size containers with extra capacity to prevent overfill if the pumper/gauger pick-up is delayed,
- Provide for overflow equalizing lines to prevent overfills by routing overflow to an adjacent container,
- Vacuum protection to prevent container collapse during removal of oil, and/or
- High level alarms for a computer controlled system.

A facility must institute a flowline and intra-facility gathering line maintenance program. The written maintenance program must provide procedures for:

- Ensuring compatibility of lines, valves and equipment with the produced fluids,
- Visually inspect and/or test lines and associated appurtances on a periodic and regular schedule,
- Repair/take corrective actions indicted by inspection and testing, or evidence of a discharge,
- Promptly remove or initiate actions to stabilize and remediate discharged oil.

Flowlines and intra-facility gathering lines are subject to the general secondary containment requirments of 40 CFR 112.7 (c). However, it is often impracticable to construct secondary containment for flowlines and intra-facility gathering lines. Accordingly, the SPCC rules provide for an alternative compliance approach without having to include an impracticability determination. The SPCC plan using an alternative compliance approach for flowlines/intra-facility gathering lines must include:

- A 40 CFR Part 109 Oil Spill Contingency Plan, and
- A written commitment of manpower, materials, and equipment to expeditiously control and remove any quantity of oil discharged that might be harmful.

SELECTED OIL DRILLING AND WORKOVER FACILITY REQUIREMENTS

In addition to meeting the general requirements of 40 CFR 112.7, oil drilling and workover facilities must meet the industry-specific requirements of 40 CFR 112.10. These requirements include locating the drilling and workover equipment to prevent a discharge; providing catchment basins or diversion structures to capture discharges of fuel, crude oil and oily drilling fluids; and installing a blowout prevention assembly and well control system.

Drilling and workover facilities are temporary and mobile. The SPCC regulations allow such mobile facilities to use a general SPCC plan rather than create a site-

specific plan for each new well location or amend the plan for each new well location. In the case of a workover, the oil production facility must maintain its SPCC plan for its facility during the workover operations.

SELF-CERTIFICATION

Previously, all SPCC plans were required to be reviewed and certified by a licensed Professional Engineer (PE). In 2006 and 2008, the SPCC rules were amended to include an option for an owner/operator of a *qualified facility* to self-certify the facility's SPCC plan and amendments thereof. *Qualified facilities* are facilities with limited capacity to store oil (i.e., less than 37,800 L or 10,000 gallons), and with no oil discharges above certain thresholds for the previous three years. *Qualified facilities* are divided into two groups: Tier 1 and Tier II. A Tier II facility is a facility that has an oil storage capacity of 37,800 L (10,000 gallons) or less, and in the past three years has had no single discharge exceeding 3,780 L (1,000 gallons), and no two discharges each exceeding 160 L (42 gallons) within any 12 month period in the past three years. A Tier I qualified facility is a facility that meets the requirements for Tier II, plus it does not have an oil storage container with a capacity greater than 18,900 L (5,000 gallons).

Tier I *qualified facilities* have three options for SPCC plan preparation:

- Follow the template provided in Appendix G of 40 CFR Part 112 (or prepare an equivalent plan with a cross-reference index), and self-certify, or
- Follow the requirements for Tier II facilities, and self-certify, or
- Follow the requirements in 40 CFR 112.7 and the applicable requirements in 40 CFR Part 112 Subpart B, and obtain a certification by a PE.
-

Tier I *qualified facilities* completing the Appendix G template must certify:

- Facility meets the Tier I *qualified facility* criteria,
- Familiarity with 40 CFR Part 112,
- Visited and examined the facility,
- Prepared the plan in accordance with accepted and sound industry standards and practices,
- Have established procedures for required inspections and testing in accordance with industry inspection and testing standards, or recommended practices,
- The plan does not deviate as allowed by 40 CFR 112.7 (a)(2) (equivalent environmental protection) and 40 CFR 112.7(d)(impracticability) or include measures pursuant to 40 CFR 112.9(c)6) for produced water or any associated piping,
- Commitment to fully implementing the plan, and
- The plan and the individual responsible for implementing the plan have the approval of management and the facility owner or operator has committed the necessary resources to fully implement the plan.

Tier II *qualified facilities* must prepare a plan meeting the requirement of 40 CFR Part 112.7 and 40 CFR Part 112 Subpart B with certain limitations. Tier II qualified facilities must certify:

- Facility meets the Tier II qualified facility criteria,
- Familiarity with 40 CFR Part 112,
- Visited and examined the facility,
- Prepared the plan in accordance with accepted and sound industry standards and practices, and the requirements of 40 CFR Part 112,
- The plan does not deviate as allowed by 40 CFR 112.7 (a)(2) (equivalent environmental protection) and 40 CFR 112.7(d)(impracticability) or include measures pursuant to 40 CFR 112.9(c)6) for produced water or any associated piping,
- Commitment to fully implementing the plan, and
- The plan and the individual responsible for implementing the plan have the approval of management and the facility owner or operator has committed the necessary resources to fully implement the plan.

If a Tier II *qualified facility* wanted to take advantage of the flexibility afforded by the SPCC regulations for environmental equivalence, impracticability or produced water, the facility may have a PE review and certify in writing such alternative procedures within the plan.

SUMMARY AND CONCLUSIONS

Certain oil drilling, workover and production facilities may qualify for self-certification of SPCC plans by the owner or operator. Owners and operators that take advantage of this option can save money. Qualified facilities are those that have:

- Storage capacities of 10,000 gallons or less,
- No oil discharges over the past three years exceeding 1,000 gallons, and
- No two discharges exceeding 42 gallons within any 12 month period in the last three years.

There is certain flexibility in defining the boundary of a facility which can be advantageous to some owners and operators by reducing the number of SPCC plans needed and potentially affecting EPA jurisdiction over flowlines. SPCC plans must include a description of the facility, types of oil stored, oil storage management practices, inspection and testing requirements, training program, discharge prevention measures, discharge controls, and discharge countermeasures for the discovery, reporting, coordination, response and cleanup. There are specific oil production facility requirements for inspections, facility drainage, discharge prevention engineering practices, container compatibility, secondary containment, and alternative compliance approaches for flowline/intra-facility gathering lines, produced water, and flow-through process vessels.

A facility must institute a flowline and intra-facility gathering line maintenance program. Flowlines and intra-facility gathering lines are subject to the general secondary containment requirments of 40 CFR 112.7 (c). However, it is often impracticable to construct secondary containment for flowlines and intra-facility gathering lines and so a facility may incorporate a 40 CFR Part 109 Oil Spill Contingency Plan into their SPCC plan in lieu of secondary containment.

Produced water containers and separation process vessels are also subject to the specific secondary containment sizing requirements. However, the regulations also provide an alternative compliance approach using the general secondary containment requirements with additional inspection and management activities designed to reduce the potential for releases.

The drilling and workover facility requirements include locating equipment to prevent a discharge, providing catchment basins or diversion structures to capture discharges of fuel, crude oil and oily drilling fluids, and installing a blowout prevention assembly and well control system. Drilling and workover facilities are temporary and mobile. The SPCC regulations allow such mobile facilities to use a general SPCC plan rather than create a site-specific plan for each new well location or amend the SPCC plan for each new well location. In the case of a workover, the oil production facility must maintain its SPCC plan for its facility during the workover operations.

.

REFERENCES

38 Federal Register 34164 Final SPCC Rule, December 11, 1973
56 Federal Register 54612, Proposed SPCC Rule, October 22, 1991
67 Federal Register 47042, Final SPCC Rule, July 17, 2002
40 Code of Federal Regulations Part 109
40 Code of Federal Regulations Part 112
API RP 12 R1, Recommended Practice for Setting, Maintenance, Inspection and Operation and Repair of Tanks in Production Service, American Petroleum Institute Recommended Practice 12 R1.
EPA (1988), The Oil Spill Prevention, Control, and Countermeasures Program Task Force Report, Interim Final Report, SPCC-IP-7-1, May 13, 1988.
EPA (2005) SPCC Guidance for Regional Inspectors, United States Environmental Protection Agency, EPA 550-B-05-001, Version 1.0, November 28, 2005
EPA (2013) SPCC Guidance for Regional Inspectors, United States Environmental Protection Agency, EPA 550-B-13-001, August 28, 2013.
GAO (1989) Inland Oil Spills, Stronger Regulation and Enforcement Needed to Avoid Future Incidents, United States General Accounting Office, GAO/RCED-89-65, February 1989.

A Review of NORM/TENORM in Wastes and Waters Associated with Marcellus Shale Gas Development and Production

Jeffrey P. Schubert[1], Michael F. Rosenmeier[2], PhD., and Mark P. Zatezalo[3], P.G.

[1]Managing Principal, Paul C. Rizzo Associates, Inc., Penn Center East, 500 Penn Center Blvd., Suite 100, Pittsburgh, PA 15235, U.S.A. E-mail: jeff.schubert@rizzoassoc.com.
[2]Senior Project Geoscientist, Paul C. Rizzo Associates, Inc., Penn Center East, 500 Penn Center Blvd., Suite 100, Pittsburgh, PA 15235, U.S.A. E-mail: michael.rosenmeier@rizzoassoc.com.
[3]Senior Project Hydrogeologist, Paul C. Rizzo Associates, Inc., Penn Center East, 500 Penn Center Blvd., Suite 100, Pittsburgh, PA 15235, U.S.A. E-mail: mark.zatezalo@rizzoassoc.com.

ABSTRACT: Marine black shales have long been known to contain elevated concentrations of uranium, thorium, and associated daughter products, commonly known as Naturally-Occurring Radioactive Material (NORM). Because uranium and thorium are only marginally soluble in near-neutral groundwater and formation waters typically associated with black shales, dissolved concentrations of these elements in produced waters (technologically-enhanced NORM [TENORM]) have not been considered a serious environmental issue. In contrast, radium-226 (^{226}Ra) and radium-228 (^{228}Ra) are much more soluble, particularly in formation waters with high concentrations of total dissolved solids (TDS). Total radium activities in formation and produced waters typically range from 30 to 5,000 picocuries per liter (pCi/L). While total radium activities in waters produced from Marcellus Shale gas wells are commonly less than 5,000 pCi/L, activities as high as 16,000 pCi/L have been reported. When produced water reaches the land surface, changes in pressure and temperature affect the solubility of dissolved gases, and subsequently affect the solubility of calcite, gypsum, and other minerals. These minerals commonly precipitate and form scale and sludges, which can accumulate on the inside surfaces of pipes, tanks, and other water-handling equipment. Radium isotopes co-precipitate and concentrate in these mineral deposits, thereby forming a residue with higher radioactivity values than the original water. The general occurrence and speciation of radionuclides in shale samples, produced waters, scale, and sludges associated with Marcellus Shale are presented and discussed in this paper.

INTRODUCTION

Uranium and thorium, their daughter products (progeny), and several other natural radionuclides are collective referred to as Naturally-Occurring Radioactive Materials (NORM). These nuclides are found in all geologic materials, animals, and

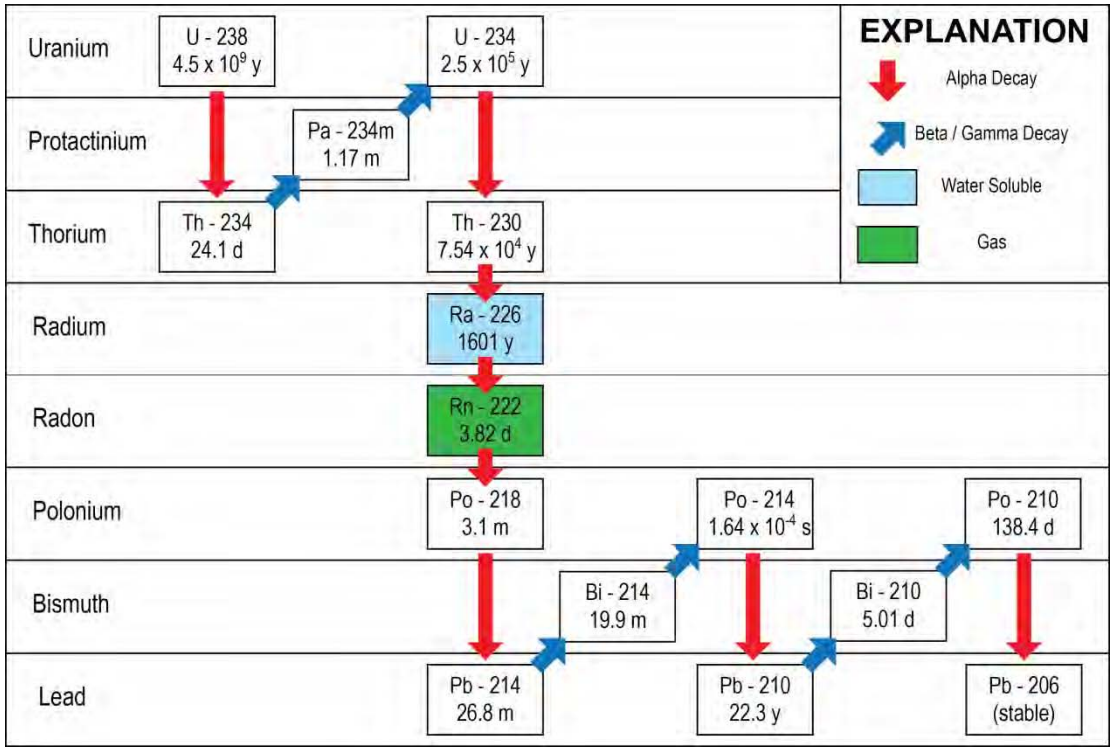

FIG. 1. U-238 Decay Series

plants, but usually at very low levels. They can, however, be found in higher concentrations in several types of geologic deposits, such as coal seams, sandstone, granite, some beach sands, and phosphate-rich marine deposits. Marine black shale is another type of geologic deposit that commonly contains above-average concentrations of uranium, thorium, and associated progeny.

Uranium-238 (^{238}U), uranium-234 (^{234}U), and thorium-232 (^{232}Th) are the most notable, naturally-occurring, long-lived radionuclides. ^{238}U has a very long half-life (4.5×10^9 years) and goes through a series of eight alpha and six beta decays (Fig. 1) before it finally results in the formation of stable lead-206 (^{206}Pb). The "uranium series" decay chain includes the formation of the following important isotopes: ^{234}U, thorium-230 (^{230}Th), ^{226}Ra, radon-222 (^{222}Ra), lead-210 (^{210}Pb), and polonium-210 (^{210}Po).

The "thorium series" decay chain (Fig. 2) starts with the long-lived ^{232}Th isotope (half-life = 1.4×10^{10} years), which undergoes a total of seven alpha decays and five beta decays before it reaches the stable ^{208}Pb isotope. Important isotopes created along this decay path include: ^{228}Ra, ^{228}Th, and ^{220}Rn.

Both the uranium and thorium decay series include radium isotopes (^{226}Ra and ^{228}Ra, respectively), which can be significant contributors to radiation dose in humans and the environment. Radium is one of the most soluble elements in these two decay chains, so it is not surprising that the two significant radium isotopes (^{226}Ra and ^{228}Ra) are the isotopes usually found in highest activities in groundwater and produced waters associated with black shales.

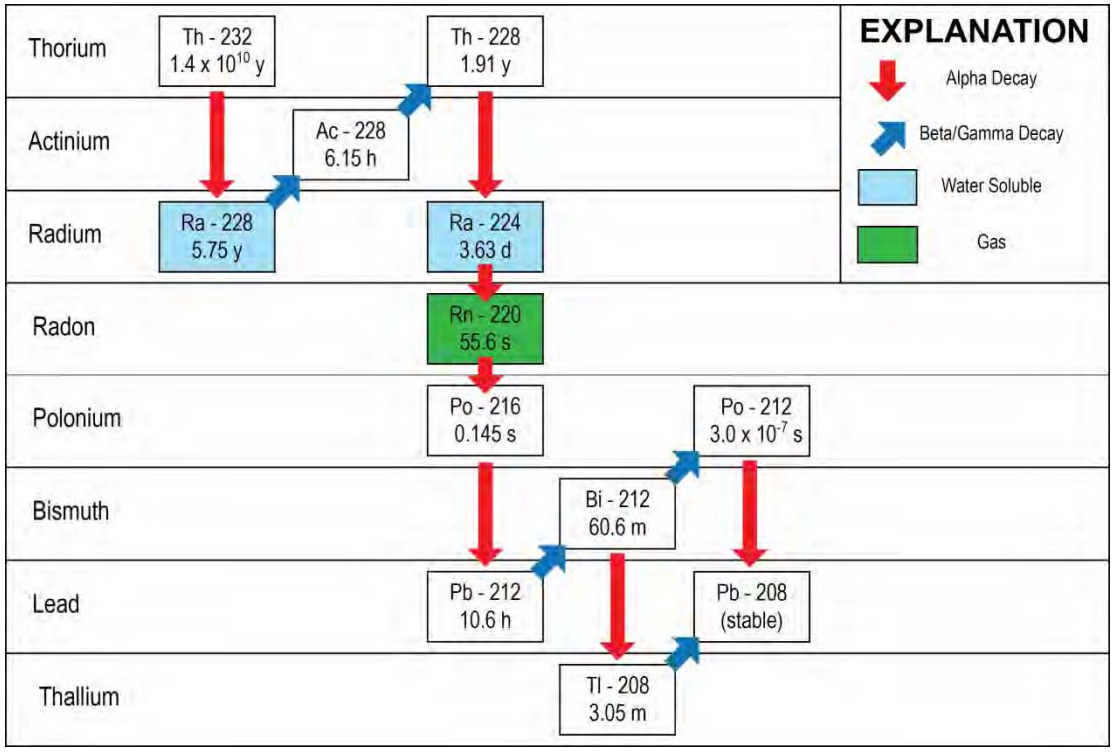

FIG. 2. Th-232 Decay Series

Also of significance are the radon isotopes (^{222}Rn and ^{220}Rn), especially ^{222}Rn because it is has a longer half-life (3.82 days) than ^{220}Rn (55.6 s). These isotopes are significant because they are the only gaseous isotopes within the uranium and thorium decay chains. This is a critical concern because radon isotopes can enter lungs when breathing air and subsequently decay internally (within the lungs), thereby causing greater potential radiation damage and health risks.

The U-235 (^{235}U) is another decay chain that contains similar types of radionuclides, However, their activities are roughly two orders of magnitude lower and are of lesser environmental and health risk concern.

Potassium-40 (^{40}K) is a radionuclide that is prevalent in marine shale deposits and is a significant contributor to total radioactivity present in shale.

Uranium and thorium are typically present at parts per million (ppm) concentrations in sedimentary rocks (Table 1). Higher concentrations of uranium have been found in some black shales, as shown in Table 1. Thorium concentrations can also be elevated in black shales.

URANIUM AND THORIUM IN MARINE BLACK SHALES

Based on microradiographs, the uranium and thorium contained in marine black shales are disseminated in the rock matrix. Many investigations over the past 70 years have been conducted to determine the levels of uranium and thorium in black shales, the factors that might have led to accumulation of these radionuclides in black shale, and the paleodepositional and geochemical factors that might be controlling

Table 1. Concentrations (ppm) of Uranium and Thorium in Sedimentary Rocks

Rock Type	U Range	U Mean	Th Range	Th Mean	Reference
Common Shale		3.7		12	Bell, 1978
Common Shale	3.0 – 4.0	3.5			Swanson, 1961
Common Shale	1 - 13	3.7	2 - 47	12	Adams et al., 1959
Claystone/Shale		4.4		11.5	Dypvik and Bue, 1984
Bentonite	1 - 21	5	6 - 44	24	Adams et al., 1959
Black Shale	1.4 - 80		2.8 - 28		Adams et al., 1959
Black Shale	3 - 250	8			Swanson, 1961
Black Shale		20			Bell, 1978
Siltstone		2.7		8.8	Dypvik and Bue, 1984
Phosphate Rock		245		3.9	Adams et al., 1959
Sandstone		2.4		8.0	Dypvik and Bue, 1984
Orthoquartzite	0.2 – 0.6	0.45	0.7 – 2.0	1.7	Adams et al., 1959
Carbonates	0.1 - 9		0.1 - 7	1.7	Adams et al., 1959
Chert	1.9 – 3.3		0.1 – 1.6		Adams et al., 1959
Halite	0.1 – 0.2		0.4 – 0.5		Adams et al., 1959
Anhydrite	0.1		0.15		Adams et al., 1959

their spatial distribution. Black shales owe their color and distinctiveness to finely disseminated organic matter. "Carbonaceous shale" for all practical purposes is synonymous with "black shale" (Swanson, 1961). Black shales of more than 200 formations were investigated in the United States from 1944 to 1957 during the search for uranium resources. Of all the shale beds tested, none was found to be rich enough to be mined and processed economically for uranium (Swanson, 1961).

The ultimate source of uranium and thorium in marine black shales is sea water. Sea water contains approximately 3 parts per billion (ppb) of uranium. The uranium in marine black shales and muds probably was concentrated in several forms and by several processes, but organic matter is directly or indirectly responsible for concentrating most of the uranium. Marine shales with low concentrations of organic matter generally contain only one to four ppm of uranium, most of which is residing in a small fraction of resistate minerals, such as zircon and sphene, and some of which is adsorbed onto clay minerals. If a shale contains two or more percent of organic carbon, it is considered a "black shale," and the uranium concentrations in these shales may be a few to as much as 250 times greater than non-carbonaceous marine shales (Swanson, 1961). Scientific evidence suggests that most uranium contained in black shales has accumulated due to one or more of the following processes: uranium is 1) uptake by algae and plankton, which then settle to the sea floor, 2) adsorption from sea water by dissolved and/or solid organic materials already accumulating on the sea floor, 3) coprecipitation as a sulfide mineral, 4)

coprecipitation as a phosphate mineral, and 5) adsorption to inorganic mineral surfaces such as clays (Swanson, 1961). The organically-bound uranium is usually the predominant form of uranium present in most black shales. These mechanisms require that the sea bottom conditions are anoxic at the time of deposition, so that organic matter can accumulate and be preserved.

Uranium content of about 90 ppm was consistently found in 47 samples collected over a distance of one mile in central Tennessee from a bed of Chattanooga Shale less than 2.5 cm thick. "The lateral changes in uranium content are very small over hundreds, even thousands, of square miles of Chattanooga Shale units several feet thick (Swanson, 1961)." These observations support the conclusion that the uranium was deposited concurrently and uniformly with the sediment at the time of deposition, and the only logical source of the uranium is the overlying column of sea water.

URANIUM IN THE MARCELLUS SHALE AND DRILL CUTTINGS

Drill cuttings (shale chips) are a waste product that is generated during drilling. The shale is broken up and brought to the ground surface. It is separated from drilling fluids and then requires disposal. Gamma ray measurements of core samples, outcrop samples, and drill cuttings of the Marcellus Shale show a rather uniform range of radioactivity (Fig. 3), ranging from approximately 0.005 to 0.09 milliRoentgens per hour (mR/hr). Interestingly, 97 percent of the approximately 5,900 NORM measurements in the Barnett Shale in Texas were below 0.047 mR/hr (RCT, 2010), which is very similar to the Marcellus measurements. According to the New York State Department of Conservation (NYSDEC, 1999, 2009), NORM in Marcellus Shale drill cuttings will not pose a public health threat.

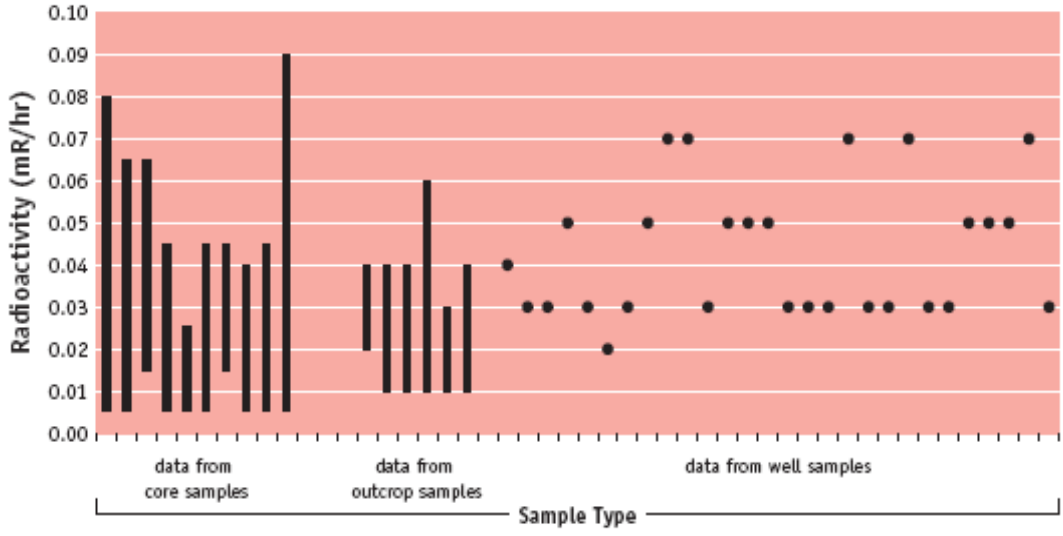

FIG. 3. Gamma Radiation Measurements of Marcellus Shale Samples (data from CoPhysics Corp., 2010; NYSDEC, 1999, 2009)

RADIUM IN OIL AND GAS FIELD BRINES

Water produced from oil and gas reservoirs can have relatively high levels of radioactivity. Uranium and thorium are essentially insoluble in oil and gas field brines, as predicted by thermodynamic data and demonstrated by exceedingly low concentrations measured in formation waters (Langmuir and Chatham, 1980; Kraemer, 1985; Kraemer and Kharaka, 1986; Zukin et al., 1987). The radioactive decay of uranium and thorium contained in geologic materials results in the formation of ^{226}Ra and ^{228}Ra, respectively. Radium is relatively soluble in water, more so than any of the other radionuclides in the uranium and thorium decay series. The radium isotopes are leached from the shale matrix and accumulate in pore waters associated with geologic strata containing the uranium and thorium. Thus, it is the radium isotopes that are causing most of the radioactivity in the brines.

The aqueous activities of parent uranium and thorium isotopes are insufficient to support the activities of daughter ^{226}Ra and ^{228}Ra, respectively, present in formation waters. The velocities of basinal brines are typically very low; on the order of centimeters per year in West Texas (Wirojanagud et al., 1986) and the Gulf Coast Basin (Harrison and Summa, 1991). The geologically short half-lives of ^{226}Ra and ^{228}Ra (1,601 and 5.75 years, respectively) coupled to the low flow velocities of brines lead to the conclusion that the radium isotopes in formation waters have not travelled long distances from their origin in the rock matrix.

Many studies have shown that the activities of radium isotopes in subsurface groundwater and brines increase as the level of salinity of the formation pore waters increase (e.g., Fisher, 1998; Sturchio et al. 2001; Rowan et al., 2011). Theoretically, radium is released directly into solution as thorium isotopes decay, and the radium stays in solution because the higher concentrations of other cations in the formation water (i.e., calcium, sodium, magnesium, barium, etc.) preferentially compete for adsorption sites on the aquifer matrix.

Elevated levels of radioactivity in oil field brines have been reported as long ago as 1904 in Canada (Wilson, 1994) and in the 1930s in Russia (Kolb and Wojcik, 1985). More recently, Fisher (1998) collected chemical and isotopic data for 215 produced water analyses from eight different geologic basins and reported ^{226}Ra activities ranging over three orders of magnitude, from 1.3 to 5,150 pCi/L. Specifically, Fisher (1998) noted that:

- 161 samples (74.9 percent) had ^{226}Ra activities less than 300 pCi/L,
- 23 samples (10.7 percent) had ^{226}Ra activities greater than 1,000 pCi/L, and
- ^{226}Ra and ^{228}Ra activities were generally equal in 20 samples (correlation line equaled 1.03, $r^2 = 0.96$).

In 13 produced water samples collected from oil and gas wells in southeastern Kansas and northern Oklahoma, Sturchio et al. (2001) found ^{226}Ra activities ranging from 573 to 17,005 pCi/L. In that study, 11 of the 13 samples had ^{228}Ra/^{226}Ra ratios less than 0.62, indicating that uranium was present in much greater quantities than thorium in the producing zones.

RADIUM IN PENNSYLVANIA AND NEW YORK OIL AND GAS FIELD BRINES

Sampling and analyses of radium isotopes in produced waters collected from oil and gas wells in Pennsylvania and New York have been conducted during several studies (PADEP, 1992; NYSDEC, 1999, 2009; Dresel and Rose, 2010; and Rowan et al., 2011). Total radium activities in all samples were generally less than 7,000 pCi/L (Fig. 4). The total radium activity in non-Marcellus samples (n=91) in these studies ranged from <1 to 6,723 pCi/L and the median value was 1,011 pCi/L. The total radium activity in Marcellus samples (n=52) ranged from <1 to 18,045 pCi/L; the median value was 2,460 pCi/L (Rowan et al., 2011). Thus, the total radium content of the Marcellus produced waters was generally more than two times the activities found in the non-Marcellus samples. It should also be noted that the Marcellus produced waters generally have higher radium activities than brines from other oil and gas fields around the world reported by Bou-Rabee et al. (2009). The median value of the $^{228}Ra/^{226}Ra$ ratio for Marcellus samples was 0.16, which indicates that uranium is much more prevalent than thorium in the shale matrix.

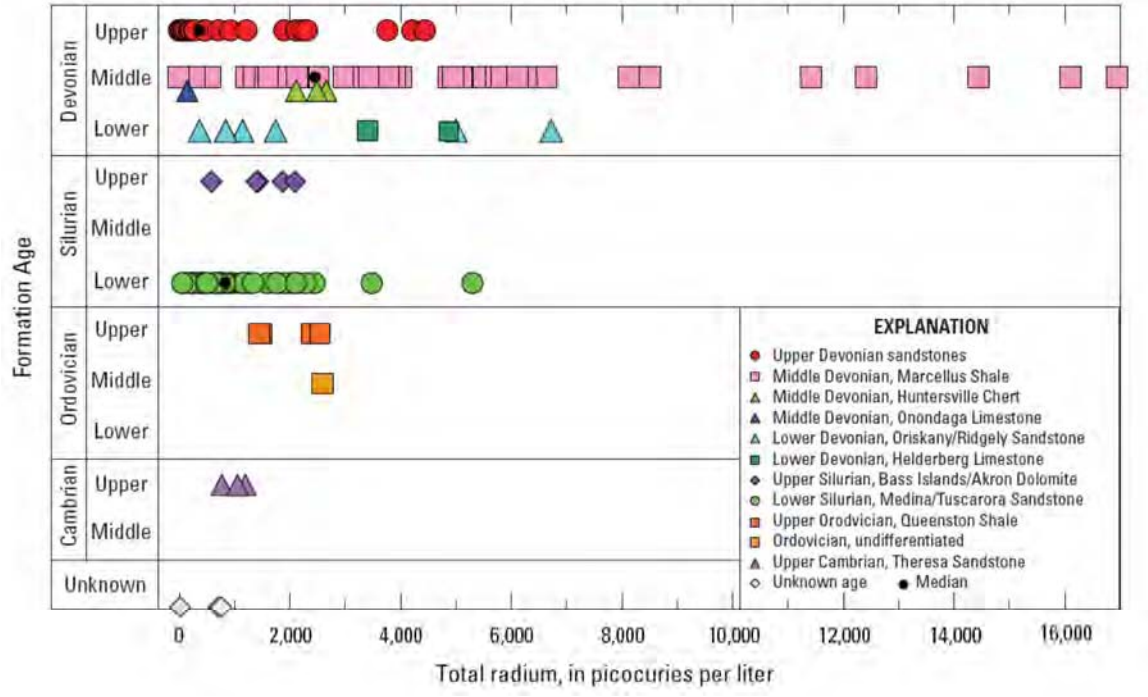

FIG. 4. Total Radium in Oil and Gas Produced Waters in Pennsylvania and New York (modified from Rowan et al., 2011).

SCALE FORMATION AND CONCENTRATION OF RADIUM

When produced water reaches the land surface, changes in pressure and temperature affect the solubility of dissolved gases, and subsequently affect the solubility of calcite, gypsum, barite, and other minerals. These minerals commonly precipitate and form scale, which can accumulate on the inside surfaces of pipes, tanks, and other water-handling equipment. Radium isotopes co-precipitate and concentrate in these mineral deposits, thereby forming a residue with higher radioactivity values than the original water. The principal minerals that form scale include calcite, barite, and possibly gypsum (USGS, 1999; Sturchio et al., 2001; Bou-Rabee et al., 2009).

Total radium activities in pipe scale associated with oil and gas production have been found as high as 154,000 pCi/g in Brazil and the United States (Scot, 1998; Gazineu et al., 2005, 2008; Bou-Rabee et al., 2009). More commonly, the total radium activities are less than 13,500 pCi/g (Bou-Rabee et al., 2009). These levels are still the most concentrated form of radioactive waste encountered in the oil and gas industry, and poses the greatest potential exposure to drillers and workers in the oil and gas industry. The exposure risk is due to gamma radiation from the scale and inhalation of radon daughter products, which subsequently decays within the lungs.

CONCLUSIONS

The presence of uranium, thorium, and associated daughter products is ubiquitous in black shale drill cuttings and water produced from oil and gas bearing formations. However, the levels of uranium in the Marcellus Shale and the levels of radium in brine produced from the Marcellus Shale are somewhat higher on average. Studies are currently underway to better quantify the levels of NORM/TENORM in all types of drilling and production wastes, and produced gas, from all Marcellus Shale activities. Radium isotopes and daughter products can accumulate on the inside of pipes, tanks, and pipelines that come in contact with produced waters and gas. These locations are where the greatest radiation exposure may exist for workers related to drilling, drilling equipment maintenance, pipeline maintenance, etc. Elevated radiation exposure or risks to the general public is not likely to occur. However, monitoring and added effort may be warranted for the handling and proper disposal of some of the more concentrated oil and gas related wastes (TENORM).

REFERENCES

Adams, J.A.S., Osmond, J.K., and Rogers, J.J.W. (1959). "The geochemistry of thorium and uranium." *Physics and chemistry of the earth,* L.H. Ahrens, ed., Pergamon Press, Oxford, 298-348.

Bell, R.T. (1978). "Uranium in black shales – a review." Short course handbook, Mineralogical Society of Canada, Ontario, 307-329.

Bou-Rabee, F., Al-Zamel, A.Z., Al-Fares, R.A., and Bem, H. (2009). "Technologically enhanced naturally occurring radioactive materials in the oil industry (TENORM). a review." *Nucleonika*, 54(1), 3-9.

CoPhysics Corporation. (2010). "Radiological survey report: Marcellus Shale drilling cuttings from Tioga and Bradford Counties, PA, and New England Waste Services of N.Y., Inc. landfill sites in Chemung, NY, Campbell, NY, and Angelica, NY", <http://www.co.chenango.ny.us/Planning/Radiological%20Survey%20Report%20-%20Marcellus%20Drill%20Cuttings%204-26-2010%201%20.pdf>

Dresel, P.E., and Rose, A.W. (2010). "Chemistry and origin of oil and gas well brines in western Pennsylvania." *Open-File Report OFOG 10-01.0*, Pennsylvania Geological Survey, 48 p.

Dypvik, H., and Bue, B. (1984). "The U, K, and Th distribution in black shales of the Janusfjellet Formation, Svalbard, Norway." *Chem. Geology*, 42, 287-296.

Fisher, R.S. (1998). "Geological and geochemical controls on naturally occurring radioactive materials (NORM) in produced water from oil, gas, and geothermal operations." *Environmental Geosciences*, 5(3), 139-150.

Gazineu, M.P.H., de Araujo, A.A., Brandao, Y.B., Hazin, C.A., and Godoy, J.M. (2005). "Radioactivity concentration in liquid and solid phases of scale and sludge generated in the petroleum industry." *J. Environmental Radioactivity*, 81, 47-54.

Gazineu, M.P.H., and Hazin, C.A. (2008). "Radium and potassium-40 in solid wastes from the oil industry." *Appl. Radiation Isot.*, 60, 90-94.

Harrison, W.J., and Summa, L.L. (1991). "Paleohydrology of the Gulf of Mexico Basin." *Am. J. Sci.*, 291, 109-176.

Kolb, W.A., and Wojcik, M. (1985). "Enhanced radioactivity due to natural oil and gas production and related radiological problems." *Science and the Total Environment*, 45, 77-84.

Kraemer, T.F. (1985). "Natural radioelement behavior in geopressured aquifers." *Geopressured-geothermal energy*." M.H. Dorfman and R.A. Morton, eds., Pergamon Press, New York, NY, 127-136.

Kraemer, T.F., and Kharaka, Y.K. (1986). "Uranium geochemistry in geopressured-geothermal aquifers of the U.S. Gulf Coast." *Geochim. Cosmochim. Acta*, 50, 1233-1238.

Langmuir, D., and Chatham, J.R. (1980). "Groundwater prospecting for sandstone-type uranium deposits: a preliminary comparison of the merits of mineral-solution equilibria and single-element tracer methods." *J. Geochem. Explor.*, 13, 201-219.

NYSDEC (New York State Department of Environmental Conservation). (1999). "An investigation of naturally occurring radioactive materials (NORM) in oil and gas wells in New York State." Albany, NY.

NYSDEC (New York State Department of Environmental Conservation). 2009. "Draft supplemental generic environmental impact statement on the oil, gas, and solution mining regulatory program." <http://www.dec.ny.gov/energy/58440.html>.

PADEP (Pennsylvania Department of Environmental Protection). (1992). "NORM survey summary," prepared Sept. 1, 1992; reproduced in *IOGA NEWS* (Independent Oil and Gas Association of Pennsylvania), April 1995;

<http://www.portal.state.pa.us/portal/server.pt/community/oil___gas_related_topics/20349/radiation_protection/986697> (18 Sept. 2013).

RCT (Railroad Commission of Texas). (2010). "NORM - naturally occurring radioactive material." <http://www.rrc.state.tx.us/environmental/publications/norm/index.php>

Rowan, E.L., Engle, M.A., Kirby, C.S., and Kraemer, T.F. (2011). "Radium content of oil- and gas-field produced waters in the northern Appalachian Basin (USA): summary and discussion of data", U.S. Geological Survey, *Scientific Investigations Report 2011-5135*.

Scot, M.L. (1998). "Naturally occurring radioactive materials in non-nuclear industry." *Proc., 2nd International Symp. On the Treatment of Naturally Occurring Radioactive Materials NORM II*, 10-13 November 1998, Klefeld, Germany, 163-167.

Sturchio, N.C., Banner, J.L, Binz, C.M., Heraty, L.B., and Musgrove, M. (2001). "Radium geochemistry of ground waters in Paleozoic carbonate aquifers, Midcontinent, USA," *Applied Geochemistry*, 16, 109-122.

Swanson, V.E. (1961). "Geology and geochemistry of uranium in marine black shales, a review", U.S. Geological Survey, *Professional Paper 356-C*, 112.

USGS (U. S. Geological Survey). (1999). "Naturally occurring radioactive materials (NORM) in produced water and oil-field equipment – an issue in the energy industry." USGS Fact Sheet FS-142-99.

Wilson, W.F. (1994). "*NORM: a guide to naturally occurring radioactive material*." PennWell Books, Tulsa, OK.

Wirojanagud, P., Kreitler, C.W., and Smith, D.A. (1986). "Numerical modeling of regional ground-water flow in the Deep-Basin Brine aquifer of the Palo Duro Basin, Texas Panhandle." The University of Texas at Austin, Bureau of Economic Geology, *Rept. of Inv. 159*.

Zukin, J.G., Hammond, D.E., Ku, T.-L., and Elders, W.A. (1987). "Uranium-thorium series radionuclides in brines and reservoir rocks from two deep geothermal boreholes in the Salton Sea geothermal field, southeastern California." *Geochim. Cosmochim. Acta*, 51, 2719-2732.

An Integrated Emergency Evacuation System for Real-Time Operations -- A Case Study of Eagle Ford Shale Gas Area, South Texas

Young Lee[1], Joon-Yeoul Oh[2], Nuri Yilmazer[3], Aritra Ghosh[4], Md Naim Hossain[5]

[1] Assistant Professor, Texas A&M University-Kingsville, young.lee@tamuk.edu
[2] Associate Professor, Texas A&M University-Kingsville, joon-yeoul.oh@tamuk.edu
[3] Associate Professor, Texas A&M University-Kingsville, nuri.yilmazer@tamuk.edu
[4] Graduate Student, Texas A&M University-Kingsville, aritra.ghosh@ students.tamuk.edu
[5] Graduate Student, Texas A&M University-Kingsville, md_naim.hossain@ students.tamuk.edu

ABSTRACT: Due to geographic position and rich natural gas reservoir, the Eagle Ford Shale (EFS) is vulnerable to natural disasters like wildfire, tornado, flooding and chemical or gas leakage. The EFS area also lacks effective disaster preparedness system to confront natural disasters. Timely disaster warning and evacuation guideline can save lives of the people. In addition, a worker or a tourist may face difficulties in finding safe area or shelter prior to the occurrence of natural and man-made disasters. For this reason, we have proposed a location based early disaster warning and evacuation system using Integrated Mobile Sensor Environment (IMOSE). Our system comprises a Disaster Management Server (DMS), android application, sensors and users. The sensors detect chemical or gas leak and send data on DMS. The disaster affected area is determined by ray casting algorithm. When our application detects the user is in disaster zone then application will disseminate evacuation guideline including shortest path to shelter or safe zone on the map of the application. In this paper, we describe the scenarios of the emergency evacuation by two case studies: gas leak and wildfire in eagle ford area.

INTRODUCTION

Natural Disaster is the consequence of natural hazards such as earthquake, tornado, flood, wild fire etc. Natural hazards generally end up with disasters where the affected areas are vulnerable. The report of United Nation's International Strategy for Disaster Reduction (UNISDR) on Mortality Risk Index (MRI) in 2009 ranks the Eagle Ford Shale Gas area as risk prone from tornado, gas explorer, chemical or gas leak.

Since Eagle Ford Shale is disaster-prone area, so prevention is necessary for protecting lives and properties. A worker, new comer or a tourist in a particular area may face the problem in finding safe area from his current position during disaster (Marathon Oil Corporation 2014). Hence, we have proposed a location based early

disaster warning and evacuation system on mobile phones using IMOSE which is mainly utilized to provide messages on the schematized map. IMOSE focuses on the manipulation of wireless sensors. It is capable of controlling any type of sensor. It is an application working on bidirectional communication, capable of reading sensor data as well as send command to remotely located robot to respond in various situations like Gas Explosion, Gas Leak, Hurricane, Flooding, Wild Fire, and Extreme Heat in Eagle Ford Shale area. IMOSE provides graphical user interface that allows users to write applications for controlling different types of wireless sensor networks. It is capable of communicating with multiple sensors simultaneously. IMOSE embeds all smart phone features with sensors to create a unique wireless sensor network. The visual editor is capable of creating any kind of sensor application and uploads it to wireless sensors or robots even at run-time.

The rest of the paper is organized as follows. In 2nd Section, we discuss about some related works and their shortcomings in brief. Then we present the description of our proposed location based system in 3rd Section. In 4th Section, system implementation details are described. Finally, we conclude this paper stating the future plan in 5th Section.

RELATED WORK

Disaster Warning and Evacuation System is very common disaster management approach in disaster-prone areas of the world. In recent years, efforts in disaster management have gained the impetus from unprecedented development of Mobile Technology (Cioca et al 2008). Currently, mobile phones provide vital support for disaster management in many ways: monitoring, communication, warning dissemination, evacuation, and rescue and relief aid. Moreover, the advent of smart phones supporting GPS functions assists in disaster management. To date, different researchers from all over the world have conducted decent number of researches about effective disaster management system. Among them, Short Message Service (SMS) is used to collect the upcoming flood warning and send back to all citizens from the server (Jayasinghe et al 2007). In this case, lots of SMS transfer can cause the network congestion which might impede the voice call communication through the same network and make the evacuation process more difficult. GSM alarm device for early disaster warning is proposed to place it in the local police station or fire brigade station. The device gets disaster warning from the weather office and makes three different types of warning. This alarm based early disaster warning system is not a faster way of evacuation though it can avoid the problem of network congestion (Wenzel 2012). Developed countries like Australia and South Korea are planning to use satellite communication for disaster management when the mobile network fails (Jeong 2009, Park 2006). This service will be more reliable, secure, efficient and robust. This service initialization and maintenance are expensive and cannot be affordable for developing areas like EFS. Very few researches have been carried out to provide location based services for disaster management on mobile phones (Aloudat and Michael 2011). Considering the facts, we have presented a location based warning and evacuation system. Our system will forecast impending disasters, disseminate understandable warnings to mobile users, and demonstrate evacuation

guidance along with the warnings.

PROPOSED WARNING AND EVACUATION SYSTEM

Our proposed system consists of a Disaster Management Server (DMS), and GPS supported android mobile phones with our proposed application installed on it. Fig. 1 demonstrates the workflow of our proposed warning and evacuation system. The DMS stores the map of disaster prone areas, sensor data, and the details about the users in its database. There are sensors for explosion, gas or chemical leak, fire etc. which can detect the occurrence and send the information to DMS. Through network provider or GPS provider, mobile phone gets the current location of its user and sends it to server. Using this current position, our system (IMOSE) determines whether the user is in probable disaster affected area or not. To do this, the system employs Ray Casting Algorithm. The user of our proposed application gets disaster warning message on map of the application. The user also gets the shortest path of safe area or shelter zone on the application. The special feature of IMOSE system is the extremely user-friendly Visual Editor that is used to design a unique sensor application which can be implemented on any type of sensor. The steps of our proposed system are as follows:

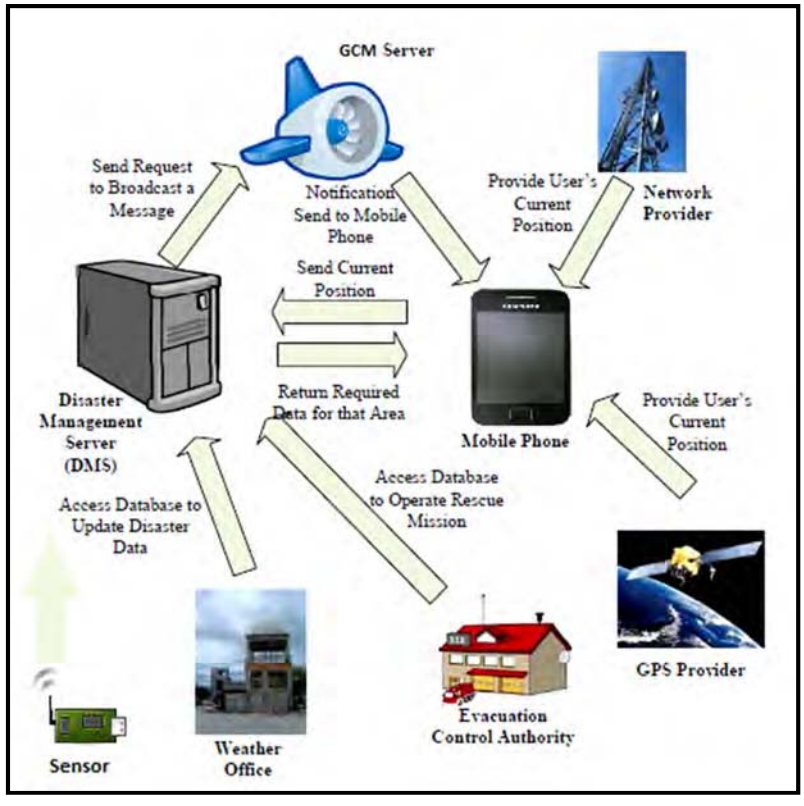

FIG. 1. Proposed location based early disaster warning and evacuation system. (IMOSE)

1) Communication with Disaster Management Server (DMS): Our application gets the current position through GPS or network provider from the user mobile phone and application communicates with DMS to send the latitude and longitude of user's current position. On the other hand, for registered user, when DMS needs to push a message to our android application, it requests to broadcast the message via an HTTP POST to Google's GCM server (Google Developers 2012). GCM server broadcasts the message to the device of the application. Afterwards, our android application fetches the data from DMS. And for unregistered user, our application receives the message when he wishes to from DMS. Fig. 2 illustrates the communication with Disaster Management Server (DMS).

2) Probable Disaster Affected Area Determination: The DMS server runs Ray casting algorithm to determine the probable disaster affected areas. If user's current position is in these areas, then server returns the feedback message to the device and in turn to the application. This is also shown in Fig. 2. The Ray casting algorithm is the most efficient algorithm among all point-in-polygon (PIP) algorithms (GNU Operating Systems 2014).

The algorithm counts the number of intersections for a ray passing from the exterior of the polygon to any point. If the count value is odd, it shows that the point is inside of the polygon. And if the count value is even, it shows that the point is outside of the polygon.

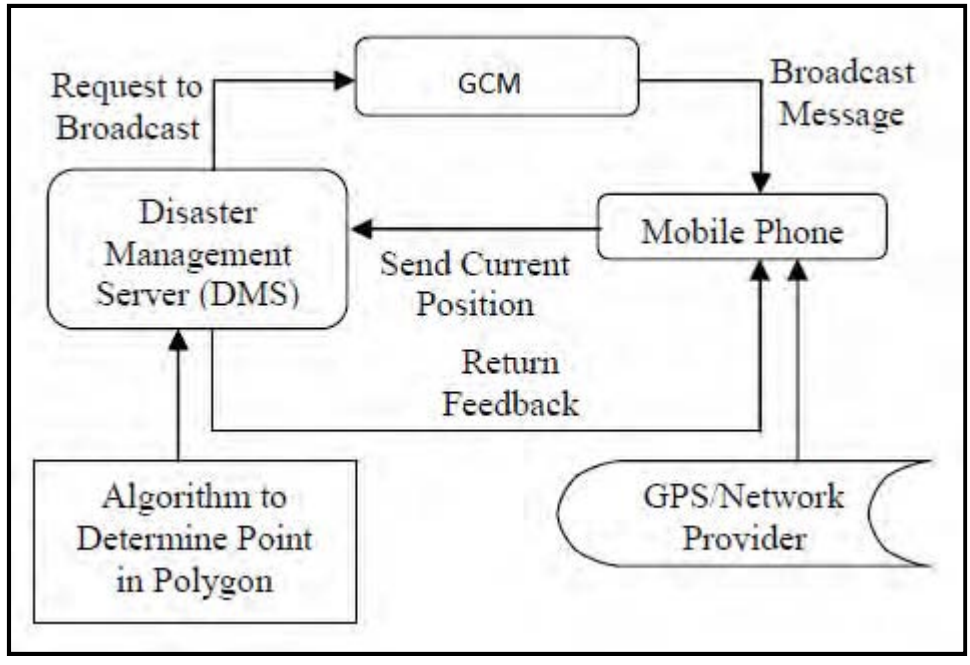

FIG. 2. Communication with disaster management server (DMS).

3) Dissemination of Disaster Warning and Evacuation Guideline: When the application finds its user in a disaster zone, the user of our application gets early disaster warning message on map of the application. Google Map Service, a geographic related service provider, provides necessary data so that the application

uses that data to draw the shortest path around the area of the user's current location and shelter or safe area with proper guideline. We have made our own schematized map algorithm for our application showing the two different places with different icon over the map. In Fig. 3, it presents the utilizing tools of the application to disseminate warning message and evacuation guideline. In Fig. 4, we are showing the evacuation process tracking.

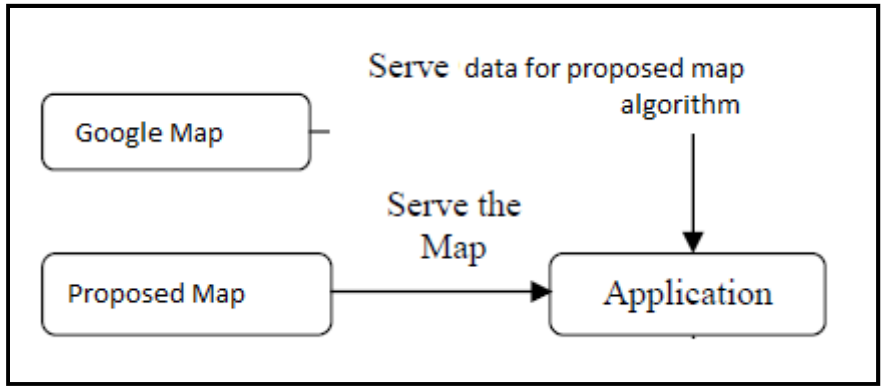

FIG. 3. Utilizing tools to disseminate warning message and evacuation guideline.

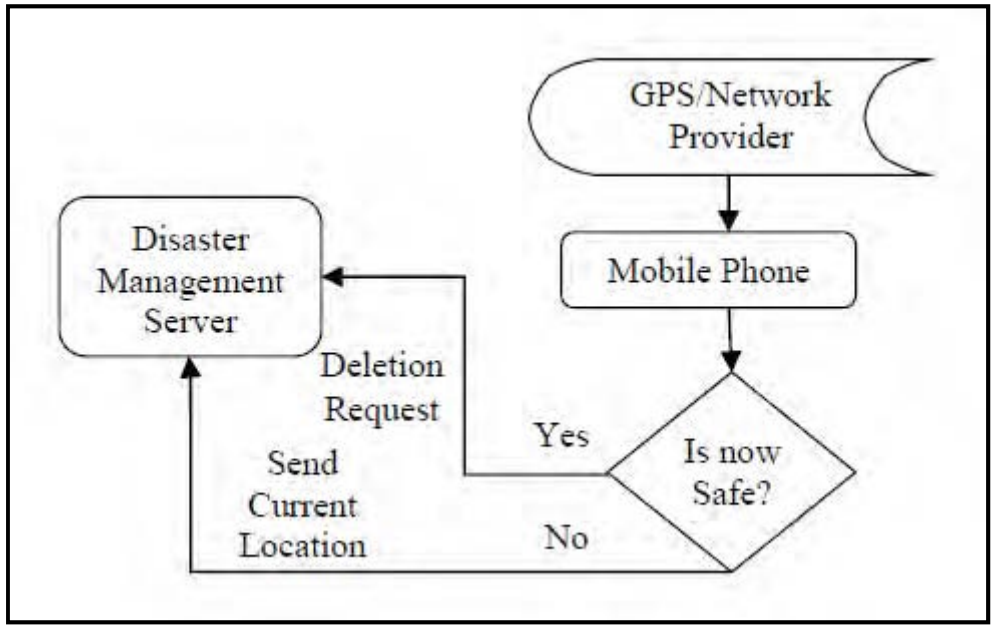

FIG. 4. Tracking evacuation progress.

4) Visual Editor: IMOSE provides extremely user friendly Visual Editor to program user-defined code and simulate or run it. This visual editor basically consists of different icons which we call blocks. Each block represents a unique task. For example, a delay block will give a specific amount of delay in the program. There are number of such blocks in the toolbar for programming. It is scientifically proven that graphical representation of anything is more resemble than textual version. So

keeping that thing in mind, in IMOSE user does not need to type any textual coding. One can do programming by just dragging and dropping such blocks from toolbar to the main workspace. Fig. 5 shows the functional diagram of IMOSE and Fig. 6 shows the configuration process.

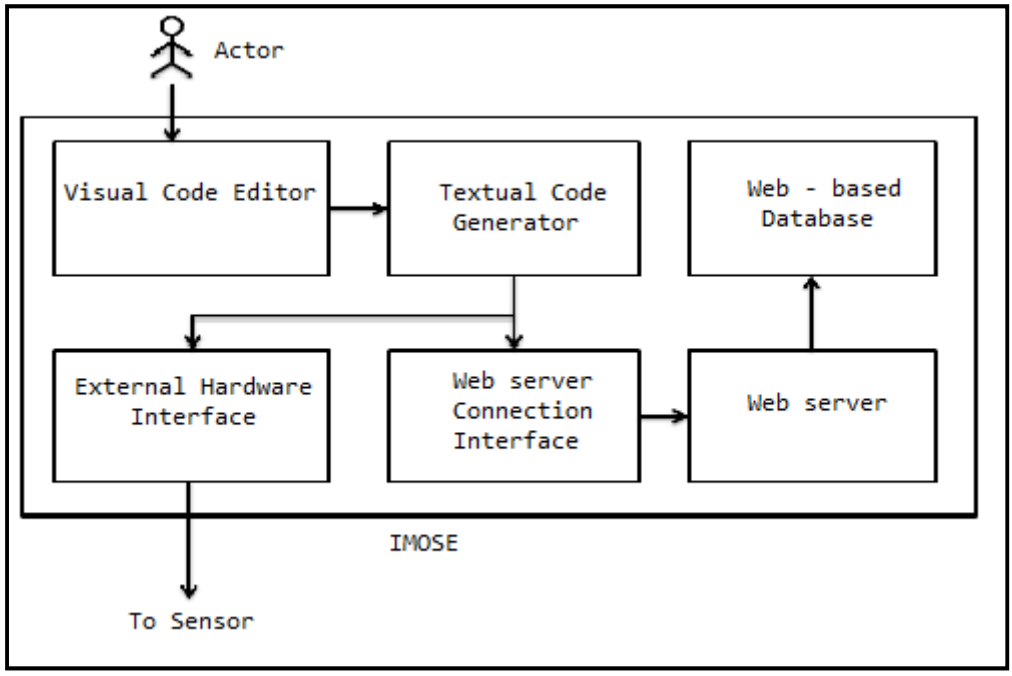

FIG. 5. Functional diagram of IMOSE comprising 4 different components.

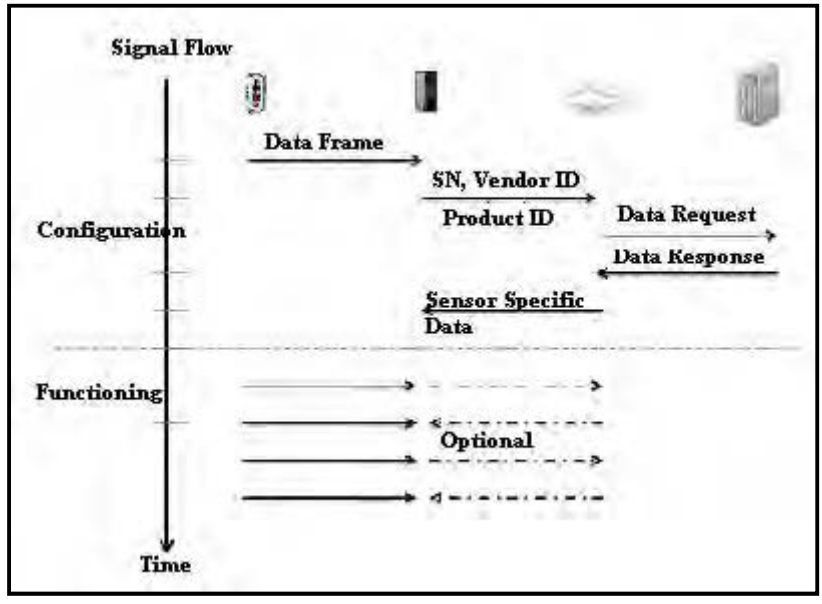

FIG. 6. Configuration process of an unknown sensor.

Visual Editor also supports saving and loading of previously made projects. In IMOSE new project and loaded projects works in two different ways. When user saves any project, only list of blocks, its location and data attached to it is saved in a textual file. When user loads previously saved project, the stored text file is opened and according to saved data, whole visual editor is created and code is written accordingly. The blocks in vertical direction represents order of the events, which will occur one after another. The blocks in horizontal direction represent simultaneous tasks, which will occur at the same moment of time.

IMOSE also supports text code. So when user creates visual code, in parallel screen, its text equivalent code is displayed for reviewing. So it is also helpful in learning embedded C language. As you can see, the notations used for textual programming is basically used for convenience. These notations are called Control Structure Diagram (CSD). It is intended to improve the comprehensibility of source code by clearly depicting control constructs, control paths, and the overall structure of each program unit.

Moreover, IMOSE has log window, which displays all log data from the beginning of the IMOSE operation. So while creating or simulation a code if error or malfunction occurs, one can easily review the log file and see what went wrong and he can rectify it. Simple routine log data is written in white colour. Warnings are written in orange colour. And errors occurred are reported in red colour. If a task went through successfully, 0 is returned and if operation was failed, a non-zero number is returned. As shown in figure, three different logs: routine, warning and error are reported to log in respectively white, orange and red colour font. Log file is stored as text file each time IMOSE is started.

SYSTEM IMPLEMENTATION

Utilizing our proposed Map and Disaster Management Server (DMS), we have developed an android-based mobile application mentioned before that provides disaster warning and evacuation facility. Our application will run on android 2.3.3 supported mobile phones and upgraded versions. The mobile phone should have GPS supported location identification facility. However, our application can identify the location of user through network provider of mobile operator. Our application has two major parts: (1) Early Disaster Warning and (2) Tracking Evacuee User.

A. Early Disaster Warning:

The application provides disaster warning in two ways:

1) *Automatic Warning Notification:* There is a toggle button in our application's homepage which starts or stops the service. When user starts the service as shown in Fig. 7(a), the application sends a registration request to the Disaster Management Server. It provides users an immediate notification on the application when there is any change in the server. The application in this case automatically starts a broadcast service that indeed communicates with the server determining user's current position to check whether current area of user is probable disaster affected area or not. If the

application finds the user within a vulnerable area to disaster then the application automatically notifies the user with a message which is demonstrated in Fig. 7(b).

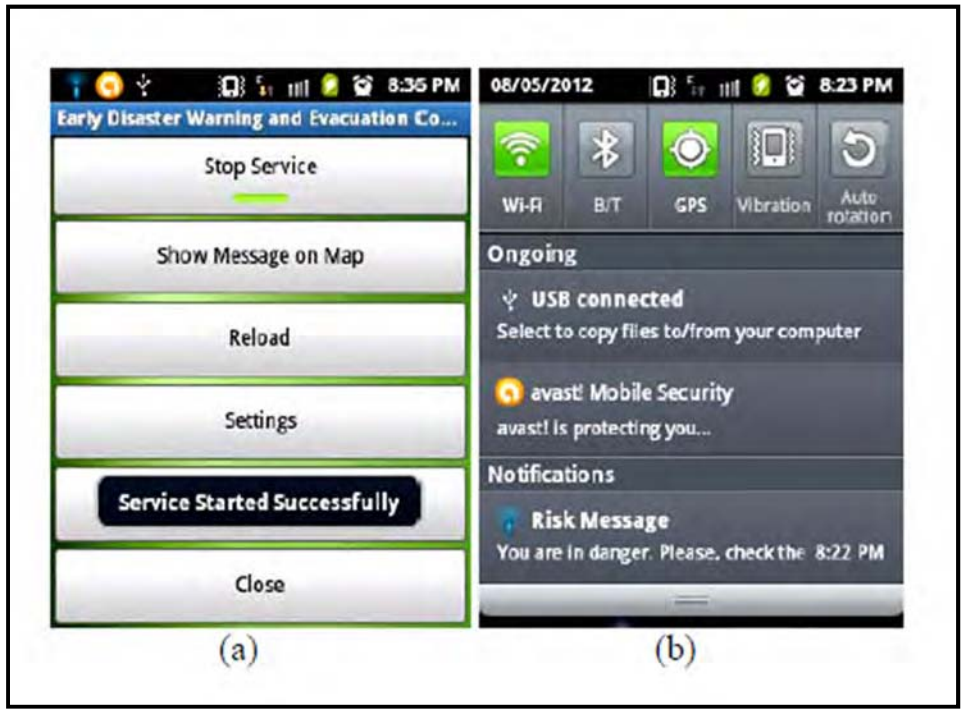

FIG. 7. (a) Starting service to notify automatic warning; (b) The notification status.

The gas leak incident can be detected using sensor and sensors will report to the DMS server. The DMS server will notify all the application user surrounding the disaster zone automatically and the users will be directed to evacuation or safer are showing an alternative path.

2) Manual Warning Notification: The application also has a reload button which connects application with the DMS and checks the current user area from the perspective of upcoming disaster. If there is any disaster out of reach of sensor, for example a wildfire incident, then the mobile application user can specify that area in the map using a button/icon and it will be updated in the DMS server and subsequently all the users in the surrounding area will be notified.

B. Tracking and Evacuating a User:

The service checks that if the user currently is in any probable disaster affected area. It sends the location of user to DMS when user changes his location. DMS stores the data in tracking of users as depicted in Fig. 8. We used Cotulla, TX as use case.

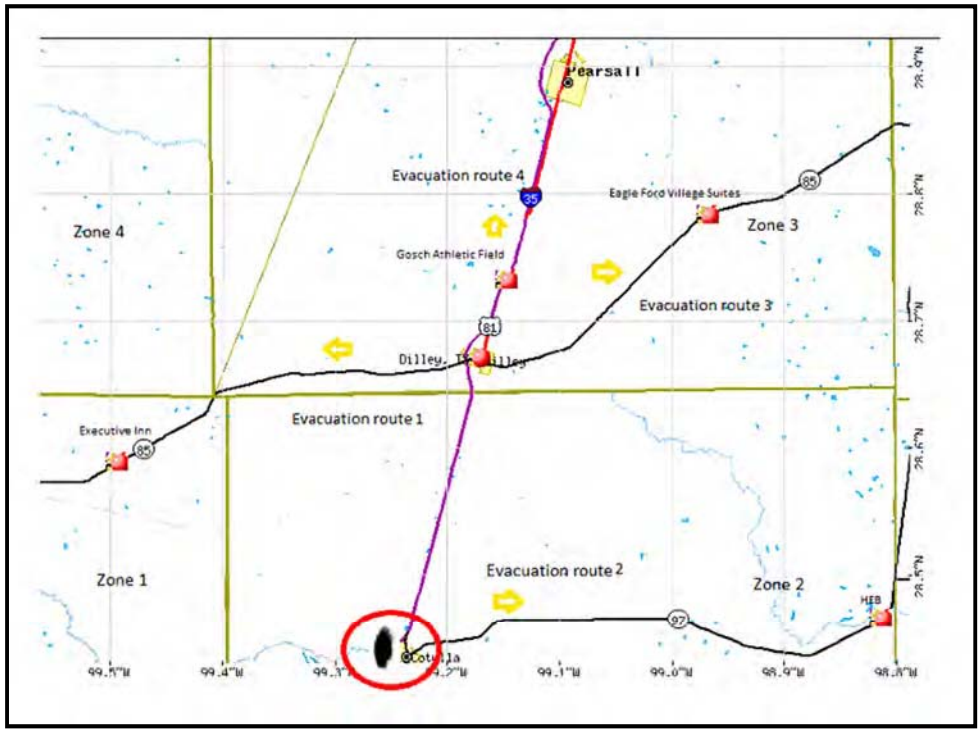

FIG. 8. Tracking and evacuating users.

Our application also has a button labeled as Show Message on Map. While the user presses that button it shows the map on the screen as given in Fig. 9, identifying user's current position and displaying shortest path to nearest shelter area.

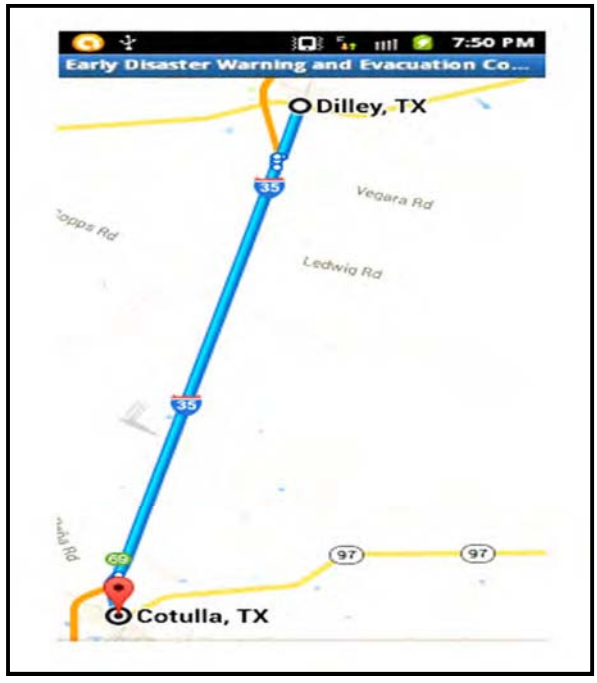

FIG. 9. Application shows the shortest path between current location and shelter

CONCLUSION

Our location based disaster management system is an android mobile phone application employing IMOSE user friendly visual editor which can communicate with all type sensors, Google Map, and Disaster Management Server (DMS). The application provides warning and evacuation help on the map of the application to user if the device user is in probable disaster affected area considering the user's current location. This helps the user to go to the safe area or shelter place prior to the disaster. Lack of details on map of Eagle Shale Ford area is the main challenge of our work. Moreover, we have a future plan to implement another application to assist in rescue and relief operation after the disaster and a better server side application to totally automate the system of detecting disaster prone area.

REFERENCES

Wenzel, Cortney, "A Case Study - Hydraulic Fracturing Geography: The case of the Eagle Ford Shale, TX, USA" 2012, retrieved on April 24, 2014 from https://digital.library.txstate.edu/handle/10877/4247.

Marathon Oil Corporation, Eagle Ford Oil and Natural Gas Fact Book, 2014, retrieved on April 24, 2014 from http://www.marathonoil.com/content/documents/news/eagle_ford_fact_book_final.pdf.

United Nations, United Nations International Strategy for Disaster Reduction Secretariat (UNISDR), Mortality Risk Index, 15 June 2009.

D. H. Jeong, "National Disaster Warning System in Korea," Sep. 2009, retrieved on April 24, 2014 from http://www.drs.dpri.kyotou.ac.jp/pw/workshop/pdfs/16dhj_national_disaster_warning_system.pdf.

Marius Cioca, Lucian-Ionel Cioca, and Sabin-Corneliu Buraga, "SMS Disaster Alert System Programming," *Second IEE International Conference on Digital Ecosystems and Technologies*. pp. 260-264, Feb. 2008.

Jayasinghe, Gamini, Fahmy, Farazy, Gajaweera, Nuwan, and Dias, Dileeka, "A GSM Alarm Device for Disaster Early Warning,", pp. 383- 387, May 2007. *1st IEEE international Conference on Industrial and Information Systems*.

Anas Aloudat and Katina Michael, "Toward the Regulation of Ubiquitous Mobile Government: A Case Study on Location-Based Emergency Service in Australia," *Journal of Electronic Commerce Research*, Vol. 11, Issue 1, Article 3, pp. 31-74, Jan. 2011.

Dugkeun Park, "One of the Nowcasting Applications: Early Warning Systems for Natural Disasters in Korea," Oct. 2006, retrieved on April 24, 2014 from https://www.wmo.int/pages/prog/amp/pwsp/documents/Dugkeun_Park_South_Korea_Paper.pdf.

Google Developers, Android Cloud to Device Messaging Framework, 2012, retrieved on April 24, 2014 from https://developers.google.com/android/c2dm/?csw=1

GNU Operating System, GNU Free Documentation License 1.2, 2014, retrieved on April 24, 2014 from http://www.gnu.org/licenses/fdl-1.2.html

Waters of the United States: Understanding Definitions and Jurisdictional Determinations Specific to Shale Resource Development

J. Daniel Arthur[1], P.E., SPEC; Jon Seekins[2]; David Winter[3]; and David Alleman[4]

[1]President/Chief Engineer, ALL Consulting, 1718 S. Cheyenne Ave., Tulsa, OK 74119, U.S.A., E-mail: darthur@all-llc.com.
[2]Senior Environmental Scientist, ALL Consulting, 1718 S. Cheyenne Ave., Tulsa, OK 74119, U.S.A., E-mail: jseekins@all-llcom.
[3]Biologist/Environmental Scientist, ALL Consulting, 1718 S. Cheyenne Ave., Tulsa, OK 74119, U.S.A., E-mail: dwinter@all-llc.com
[4]Senior Environmental Manager, ALL Consulting, 1718 S. Cheyenne Ave., Tulsa, OK 74119, U.S.A., E-mail: dalleman@all-llc.com.

ABSTRACT: Clean water is a valuable natural resource and is relied on for drinking, agriculture, recreation, manufacturing, energy development, tourism, and many other purposes that are essential to the public and the economy. The Clean Water Act (CWA) is the primary legislative instrument used to protect this resource but over the past decade, interpretations of Supreme Court rulings have clouded definitions of "waters of the United States" (WOUS) and caused confusion about which waters and wetlands remain under the jurisdictional control of the U.S Army Corps of Engineers (USACE) and the Environmental Protection Agency (EPA). To clarify protection of waters and wetlands the EPA and the USACE drafted guidance to sort out what the CWA covers and what may now lie beyond its reach. The guidance provides procedures for identifying waters and wetlands protected under the CWA with a focus toward protecting small waters that feed into large waters, so that downstream waters are safe from upstream pollutants. The guidance also reaffirms protection for wetlands that filter pollution and store water. The agencies propose to finalize the guidance and to continue work on a rulemaking. This paper will analyze the final guidance, definitions, and jurisdiction determination procedure and how these affect the development of well pads, impoundments, access roads and water used for oil and gas development within shale plays. The central subject of this paper is to what extent does the final guidance allow the CWA to cover "non-traditional, non-navigable" wetlands and streams within shale plays, and how such guidance can be used to determine jurisdictional authority using existing scientific literature and ground truthing tools. The paper is intended to assist operators faced with a jurisdictional question involving a wetland or stream to understand what factors will allow them to determine CWA jurisdiction.

INTRODUCTION

This paper examines the categories of waters that are considered to be "waters of the United States" (WOUS) by the Environmental Protection Agency (EPA) and the United States Army Corps of Engineers (USACE) under the EPA's "Draft Guidance on Identifying Waters Protected by the Clean Water Act" (2011) and the current process for conducting a jurisdictional determination under the USACE *Jurisdictional Determination Form Instructional Guidebook* (2007).

BACKGROUND

The Federal Water Pollution Control Act (FWPCA) was approved in 1948; the current version, commonly referred to as the Clean Water Act (CWA), is derived from broad amendments passed in 1972. Under the CWA, U.S. jurisdiction applies to "navigable waters," which is defined as WOUS.

The Supreme Court determined in the Rapanos et ux.,et al. V. United States (2006) that the phrase "waters of the United States" is unclear, and as a result the jurisdiction of the CWA has been restricted from its previous and traditional all-encompassing claim to waters. These cases involved wetlands lying near ditches or man-made drains (non-navigable tributaries) that eventually empty into traditional navigable waters and resulted in two different standards for determining waters under the CWA: the "significant nexus" test and the plurality opinion's two-part test.

The plurality standard recognizes those waters which have a "continuous surface connection to bodies that are water of the United States in their own right" (Rapanos v. U.S. 2006). However, the significant nexus test goes beyond the plurality's continuous connection and, as an alternative, acknowledges that wetlands are WOUS if they "either alone or in combination with similarly situated lands in the region, significantly affect the chemical, physical, and biological integrity of the covered waters more readily understood as 'navigable'" (Rapanos v. U.S. 2006). The Circuit Courts of Appeal have not agreed on which test to use; the Seventh, Ninth, and Eleventh courts have accepted the significant nexus test as the tightest definition, whereas the First and Eighth courts hold that either test may be used to determine CWA jurisdiction (e.g., Northern California River Watch v. City of Healdsburg 2007, U.S. v. Bailey 2009, U.S. v. Robinson 2007, U.S. v. Johnson 2006, U.S. v. Gerke Excavating 2006). Conspicuously, no court has held that the plurality standard is the only applicable standard.

Recognizing the confusion over these two tests, the EPA and the USACE released a draft guidance document in April 2011 to clarify the types of waters within the jurisdiction of the CWA. The 2011 Guidance encompasses several programs under the CWA, including:

- Section 311 Oil Spill Prevention Control and Countermeasure plans;
- Section 401 State Water Quality Certification requirements;
- Section 402 National Pollution Discharge Elimination System (NPDES) Permitting Program; and
- Section 404 Permits for Dredging and Filling into WOUS.

The 2011 Guidance has been under consideration by the U.S. Office of Management and Budget since February 2012 and has not yet been finalized.

CWA JURISDICTIONAL WATERS THAT DO NOT REQUIRE A SIGNIFICANT NEXUS

The 2011 Guidance stresses jurisdiction over the following waters without reference to the significant nexus test:

- Traditional Navigable Waters (TNW);
- Interstate Waters;
- Non-navigable Tributaries to TNW that are relatively permanent; and
- Wetlands that directly adjoin relatively permanent waters connected to TNW.

Traditional Navigable Waters

The legal definition of TNW is defined in Appendix D of the USACE Jurisdictional Determination Form Instructional Guidebook (2007) as "[a]ll waters which are currently used, or were used in the past, or may be susceptible to use in interstate or foreign commerce, including all waters which are subject to the ebb and flow of the tide." 33 C.F.R. § 328.3(a)(1); 40 C.F.R. § 230.3(s)(1). The guidance also states that, for purposes of the guidance, these "(a)(1) waters" are the "traditional navigable waters." These (a)(1) waters include all of the "navigable waters of the United States," defined in 33 C.F.R. Part 329 and by numerous decisions of the federal courts, plus all other waters that are navigable-in-fact (e.g., the Great Salt Lake, UT and Lake Minnetonka, MN).

The authority of the EPA and the USACE's jurisdiction over TNW is not questioned and therefore no further analysis of these waters is conducted.

Interstate Waters

The 2011 Guidance defines interstate waters to include all interstate wetlands, rivers, lakes, and other waters that flow across, or form a part of state boundaries, and all lakes, ponds, and similar lentic (still) water features crossing state boundaries.

Relatively Permanent, Non-Navigable Tributaries to TNW

The 2011 Guidance specifies that "relatively permanent" is indicative of a class of tributary that contains water at least seasonally. The 2011 EPA Guidance does not specify a time period for the seasonal flow, rather the guidance states that "the time period constituting 'seasonal' will vary across the country." An example is provided that states "seasonal flow in most of New Mexico and large portions of Arizona and Colorado would be during the period of two months" (EPA 2011, 28). The 2011 Guidance is vague as to what constitutes continuous seasonal flow, but emphasizes its consistency with the plurality standard, which requires a relatively permanent tributary to have seasonal continuous flow. The plurality standard alludes to what is considered sufficient continuous flow by stating a seasonal river "contain[s]

continuous flow during some months of the year but no flow during dry months" (Rapanos v. U.S. 2006). Note, the 2011 Guidance omits "ephemeral tributaries that flow only in response to precipitation" (EPA 2011, 27).

Wetlands that Directly Adjoin Relatively Permanent Waters

Under the 2011 Guidance, "wetlands with a continuous surface connection to relatively permanent, standing or continuously flowing bodies of waters" are jurisdictional under the plurality standard (EPA 2011, 15). According to the 2011 Guidance, "[a] continuous surface connection exists between the wetland and a relatively permanent tributary where the wetland directly abuts the water (e.g., they are not separated by uplands, a berm, dike, or similar feature)." The 2011 Guidance notes that a physical connection to the relatively permanent tributary must exist for the wetland to be considered jurisdictional under the plurality standard (EPA 2011, 15). Although a physical connection is required, the 2011 Guidance states that "a continuous surface connection does not require surface water to be continuously present in the connection between the wetland and the jurisdictional water."

JURISDICTIONAL WATERS IF THEY HAVE A SIGNIFICANT NEXUS TO TNW OR INTERSTATE WATERS

The 2011 Guidance recognizes the following waters as jurisdictional under the CWA if an analysis determines they have a significant nexus to TNW or interstate water:

- tributaries to TNW or interstate waters;
- wetlands adjacent to jurisdictional tributaries to TNW or interstate waters;
- ditches with a bed, bank, and Ordinary High Water Mark (OHWM); and
- other waters, both physically proximate and non-physically proximate to TNW and interstate waters (EPA 2011, 5).

Significant Nexus Test

Under the 2011 Guidance's significant nexus test, the agencies will consider "waters to have a significant nexus if they alone or in combination with other similarly situated waters in the same watershed have an effect on the chemical, physical, or biological integrity of [TNW] or interstate waters that is more than 'speculative or insubstantial'" (EPA 2011, 8). Noteworthy are several differences with this definition as compared to the significant nexus test set forth in the Supreme Court's ruling (Rapanos v. U.S. 2006).

The jurisdictional reach is essentially expanded by the use of the word "or" verses the original "and" that was used in Rapanos. This change results in waters meeting the significant nexus test that would not meet the test as stated originally. The change reduces the requirement that the water significantly affect all three components—chemical, physical and biological integrity. Thus, the agencies are asserting jurisdiction based on effects to one component instead of all three.

The jurisdictional reach further expands the original significant nexus when the 2011 Guidance lets any effects on chemical, physical, or biological integrity that are "*more than* 'speculative or insubstantial'" to be recognized as a significant nexus (EPA 2011, 8). The 2011 Guidance seems to accept that effects that are *slightly more than* speculative or insubstantial constitute a significant nexus. The plurality standard indicates that "it is unclear . . . [w]hen, exactly, does a wetland 'significantly affect' covered waters, and when are its effects 'in contrast . . . speculative or insubstantial.'" Therefore, it is understood that the significant nexus test is a more thorough analysis of whether the effects are slightly more than speculative or insubstantial (Rapanos v. U.S. 2006).

The 2011 Guidance recognizes waters to be jurisdictional if they have a significant nexus to interstate waters. This is the first time that interstate waters are equated to TNW. The basis for treating interstate waters as analogous to TNW under the CWA could not be identified in the Acts text. Additionally, interstate waters may be non-navigable and therefore were not used in interstate commerce.

Finally, the 2011 Guidance allows the agencies to combine all "similarly situated" waters in a watershed to decide if the similarly situated waters, as a whole, have a significant nexus to the nearest TNW or interstate water (EPA 2011, 8). A watershed is defined in the 2011 Guidance as the area draining into the nearest TNW or interstate water (EPA 2011, 8). This expands the significant nexus test, which found that wetlands are within CWA jurisdiction if they "alone or in combination with similarly situated lands in the region" have a significant nexus to TNW (Rapanos v. U.S. 2006). The basis for equating "region" with an entire watershed is not explained in the guidance. Furthermore, the 2011 Guidance appears to allow one significant nexus analysis to establish significant nexus for all "similarly situated waters" (EPA 2011, 1, 9). However, the Supreme Court's ruling set forth the significant nexus test as a case-by-case determination (Rapanos v. U.S. 2006).

Under this seemingly expanded significant nexus test, agencies' jurisdictional determinations could extend beyond the Supreme Courts intended limits of WOUS.

Categories of Waters Subject to a Significant Nexus Analysis

Non-relatively Permanent Tributaries

According to the 2011 EPA Guidance, the first step to determining whether a tributary has a significant nexus to TNW or interstate waters is to access the water for a bed and a bank and an OHWM. The next step is to decide if the tributary is part of a system connected to a TNW or an interstate water (EPA 2011, 13). If both criteria are met, then it is presumed that the tributary has a significant nexus to the downstream TNW or interstate water. However, the flow characteristics and functions of the tributary and its hydrologic relationship to the nearest downstream TNW or interstate water must be documented to show a significant nexus (EPA 2011, 14).

Adjacent Wetlands

To determine if a water is jurisdictional, one must undertake two separate investigations. Initially it must be determined if the wetland is adjacent to a recognized jurisdictional water other than another wetland (EPA 2011, 18). Second, one must decide if the wetland, either alone or in combination with other adjacent wetlands in the watershed, has a significant nexus to the nearest downstream TNW or interstate water.

Ditches with a Bed, Bank, and OHWM

The 2011 Guidance outlines criteria for determining if a ditch is a tributary. Under the 2011 Guidance, ditches are tributaries if they have:

- a bed, bank, and OHWM;
- connect directly or through other tributaries to a TNW or interstate water; and
- have at least one of the following four characteristics:
    - Natural streams that have been altered;
    - Ditches excavated in waters of the U.S. (i.e. wetlands)
    - Ditches that contain relatively permanent flowing or standing water; or
    - Ditches that connect two or more jurisdictional waters of the U.S. (EPA 2011, 12).

The 2011 Guidance states that "if a ditch is considered a tributary, it will be evaluated in the same manner as other tributaries (i.e., plurality standard or significant nexus test, as appropriate)" (EPA 2011, 12).

Other Waters

The 2011 EPA Guidance states that the agencies, on a case-by-case basis, "will make fact-specific determinations of jurisdiction for other waters that are in close physical proximity to traditional navigable waters, interstate waters, or their jurisdictional tributaries" and have a significant nexus to TNW or interstate waters. In addition, "non-physically proximate other waters [which] are isolated, intrastate, non-navigable waters and wetlands that would not meet the regulatory definition of 'adjacent' with respect to jurisdictional waters" may be found to meet the significant nexus test although it "may be more challenging" (EPA 2011, 20).

USACE JURISDICTION DETERMINATION PROCEDURE

As part of the Section 404 permitting process, USACE conducts a Jurisdictional Determination (JD) to establish whether or not the affected water body is subject to regulation under the Clean Water Act. The Jurisdictional Determination Form approved by EPA and USACE is provided in the USACE "Jurisdictional Determination Form Instructional Guidebook" (2007).

The Guidebook provides the regulatory and statutory definitions of the term "Waters of the U.S.," and provides an overview of the various Supreme Court decisions that have modified the definition of that term, and, therefore, have modified

the waters over which USACE can assert jurisdiction. The Supreme Court cases have primarily addressed the circumstances under which water bodies that are not TNW fall under CWA jurisdiction.

A key step in the JD process is the assessment of whether or not the tributary is a "relatively permanent water body" (RPW). The guidebook states that all RPWs and wetlands that abut RPWs are jurisdictional. A non-RPW must have a "significant nexus" with a TNW to be considered jurisdictional. The guidebook provides a detailed set of analyses to determine whether or not a non-navigable tributary to a TNW has a "significant nexus" with a TNW. The significant nexus analysis is further broken down into an analysis of the Physical, chemical, and biological nexus that the non-RPW has with a TNW.

The determination of whether or not wetlands associated with non-RPWs are jurisdiction is a multi-step process in the JD. The JD form addresses whether the water body meets the definition of a wetland, and then addresses whether the wetland abuts the non-RPW or is adjacent to it and provides definitions of each.

The Guidebook Provides a summary of jurisdictional findings for the various classes of water bodies as determined by the JD Form:

- TNWs and Adjacent wetlands are considered jurisdictional under the CWA.
- RPWs that flow into TNWs are considered jurisdictional under the CWA.
- Non-RPWs that flow into TNWs are considered jurisdictional if there is a significant nexus with a TNW.
- Wetlands directly abutting RPWs that flow into TNWs are considered jurisdictional under the CWA.
- Wetlands adjacent to, but not directly abutting, RPWs that flow into TNWs are considered jurisdictional under the CWA.
- Wetlands adjacent to non-RPWs that flow into TNWs are considered jurisdictional under the CWA.
- Impoundments of jurisdictional waters do not generally affect the water's jurisdictional status.

CONCLUSIONS

Many of the expansions in the 2011 Guidance do not have a clear basis in the text of the CWA, EPA, or USACE regulations, or the recent Supreme Court ruling. To the extent that the 2011 Guidance allows jurisdictional determinations that go beyond the limits of Supreme Court intention and the Commerce Clause, a court could find that the 2011 Guidance is unenforceable. The development of oil and gas facilities can be inhibited by the uncertainty of the status of intermittent streams, and associated wetlands pending a jurisdictional determination of the WOUS by both the USACE and EPA. Furthermore, the jurisdictional determination can be subjective depending on the agencies' interpretation of the draft guidance document. These jurisdictional determinations currently affect the construction of well pads, impoundments, and access roads needed for oil and gas development by reducing the land available for building needed infrastructure, delaying construction due to lengthy permitting procedures, and by increasing the cost of analyzing each infrastructure component in order to avoid potential regulatory missteps.

REFERENCES

Environmental Protection Agency (EPA). (2011). "Draft Guidance on Identifying Waters Protected by the Clean Water Act." <http://www.epa.gov/tp/pdf/wous_guidance_4-2011.pdf> (Jan. 21, 2014).

Northern California River Watch v. City of Healdsburg. (2007). 496 F.3d 993, 999 (9th Cir.).

Rapanos Et Ux., Et Al. V. United States. (2006). Certiorari To The United States Court Of Appeals For The Sixth Circuit, No. 04–1034. Argued February 21, 2006—Decided June 19, 2006.

U.S. Army Corps of Engineers (USACE). (2007). *USACE Jurisdictional Determination Form Instructional Guidebook*. <http://www.usace.army.mil/Portals/2/docs/civilworks/regulatory/cwa_guide/jd_guidebook_051207final.pdf> (Jan. 21, 2014).

United States v. Bailey. (2009). 571 F.3d 791, 799 (8th Cir.).

United States v. Robinson. (2007). 505 F.3d 1208, 1222 (11th Cir.).

United States v. Johnson. (2006). 467 F.3d 56, 64 (1st Cir.).

United States v. Gerke Excavating, Inc. (2006). 464 F.3d 723, 724 (7th Cir.).

How API's Shale Gas Standards and Best Practices support Sustainable Shale Gas Development

David Lee Miller[1], P.E., F.ASCE

[1]Director, Standards, American Petroleum Institute, 1220 L Street, NW, Washington, DC 20005, U.S.A, E-mail miller@api.org

ABSTRACT: Founded in 1919, the American Petroleum Institute (API) has a long history in the development of industry standards, starting with the first standards published in 1925 on drilling thread specifications to ensure safety in the production of oil and natural gas. Continuing on for nearly 90 years, API has led the development of petroleum, petrochemical and natural gas equipment and operating standards. These standards represent the industry's collective wisdom on subjects ranging from drill bits to environmental protection and embrace proven, sound engineering and operating practices and safe, interchangeable equipment and materials. API maintains more than 650 standards, many of which have been incorporated into state and federal regulations. API standards are also the most widely referenced oil industry standards cited by the international regulatory community.

API ensures the technical relevance of its standards by maintaining its status as an American National Standards Institute (ANSI) accredited standards developing organization. As an accredited body, API's standards program undergoes regular program audits to ensure it meets ANSI's "Essential Requirements" for openness, balance, consensus and due process.

API has also been the leader in the development of standards supporting sustainable shale gas development. API published its first of five specific shale gas standards in 2009 on well integrity, and subsequently developed standards on water resource management, environmental practices, and well cementing technology. This presentation will focus on the status of updates to these standards as well as a new standard on Community Engagement, being developed to ensure well operators, drilling and well servicing companies and the communities in where the shale gas is being developed fully understand the important aspects of operations taking place in and around their neighborhoods, towns, and cities.

INTRODUCTION

The American Petroleum Institute (API) is the U.S. Petroleum industry's primary trade association. Its membership of approximately 550 companies covers all aspects of the oil and natural gas industry, including exploration, production, and transportation, refining, and marketing. The development of consensus standards is one of API's oldest and most successful programs. Beginning with its first standards in 1925, API now maintains some 650 standards covering all segments of the oil and gas industry.

API STANDARDS AND STANDARDS DEVELOPMENT

API produces standards, recommended practices, specifications, codes and technical publications, reports and studies that cover all parts of the industry. For upstream, API publications cover offshore structures and floating production systems, tubular goods, valves and wellhead equipment, drilling and production equipment. In the downstream area, API publications address marketing and pipeline operations, and refinery equipment including storage tanks, pressure-relieving systems, compressors, turbines and pumps. API also has a number of publications in these areas that cut across industry sectors, covering fire and safety, environmental practices, and petroleum measurement.

Subcommittees and task groups made up of industry experts develop API standards. These groups identify the need, then develop, approve, and revise standards and other technical publications. New projects must be justified by valid business and safety needs. The standards-writing subcommittees and task groups are open to representatives of groups that are materially affected by the standards. These include oil and gas companies, manufacturers and suppliers, contractors and consultants, and representatives of government agencies and academia.

API standards writing groups do their work at meetings and by e-mail, net meetings and webinars and electronic collaborative authoring. API corporate membership is not a requirement for participation in the process. Representatives of "materially affected parties" may attend standards-writing meetings, and they may review drafts of standards and have their comments considered.

API standards at various stages of development – new project, draft ballot, and final ballot – are announced periodically in the American National Standards Institute's ANSI Standards Action, and on API's web page at www.api.org.

An important part feature of the API process is developing consensus. Consensus does not mean unanimous approval, but it requires that the directly and materially affected parties have reached substantial agreement. Consensus requires that views and objections be considered and that an effort be made to resolve differences. Because its process provides for consensus and other "due process" requirements of ANSI, API is recognized an ANSI accredited Standards Developing Organization. This means that API's standards procedures have been reviewed and approved by ANSI, and that API is regularly audited against those procedures to demonstrate compliance with them.

To keep API standards current with new technology developments and experiences in the field, they are reviewed at least every five years, and sometimes more

frequently, to determine whether or not they need to be revised, reaffirmed, or withdrawn. The API program also funds research on technology developments to improve API standards. API committees also respond to technical inquiries and requests for interpretations, many of which are then used to update the standards.

High quality, industry-specific API standards provide many benefits. By promoting safe and proven engineering practices in the design, fabrication, installation, and operation of materials and equipment in petroleum operations and facilities, they can:

- Improve safety
- Improve environmental performance
- Reduce engineering costs
- Improve equipment interchangeability
- Improve product quality
- Lower equipment costs

API also operates several quality, conformity assessment, and personnel qualification programs based on API standards for assuring competency of manufacturers, inspectors, and equipment. API is also a registrar under the ISO 9000 quality program.

Although API standards are developed, published, and implemented by industry on a voluntary basis, they are often incorporated into state and federal regulations. API standards are referenced in the regulations of the Coast Guard, Environmental Protection Agency, Federal Trade Commission, Pipeline and Hazardous Materials Safety Administration, Occupational Safety and Health Administration, Bureau of Safety and Environmental Enforcement, Bureau of Land Management, and in the fire, electrical and building codes of most states. In this way, API standards help to produce regulations that are based on sound science and engineering practices – a very important benefit for industry, the government, and the public.

API'S SHALE GAS STANDARDS AND BEST PRACTICES THAT SUPPORT SUSTAINABLE SHALE GAS DEVELOPMENT

Starting in 2009, API published a series of five standards that support sustainable shale gas development. Broadly speaking, these standards present industry best practices on well construction and integrity (HF1), water management (HF2), surface impact mitigation (HF3), environmental protection (51R) and cementing practices for isolating potential flow zones (65-2). A summary of each of these standards will be given as well as a key environmental section. All five standards are available for free online at www.api.org.

HF1, *HYDRAULIC FRACTURING OPERATIONS – WELL CONSTRUCTION AND INTEGRITY GUIDELINES*, 1ST EDITION, OCTOBER 2009

The first standard released in the API shale gas series is HF1, published in October 2009. This is the first standard published as the key to sustainable gas development is proper well design and integrity, and includes the following sections:

1. Scope
2. References
3. General Principles

4. Casing Guidance
5. Cementing and Casing
6. Well Logging and Other Testing
7. Well Construction Guidelines
8. Perforating, Data Collection
9. Analysis, and Monitoring

HF1's scope is as follows:

The purpose of this guidance document is to provide guidance and highlight industry recommended practices for well construction and integrity for wells that will be hydraulically fractured. The guidance provided here will help to ensure that shallow groundwater aquifers and the environment will be protected, while also enabling economically viable development of oil and natural gas resources. This document is intended to apply equally to wells in either vertical, directional, or horizontal configurations.

Many aspects of drilling, completing, and operating oil and natural gas wells are not addressed in this document but are the subject of other API documents and industry literature (see Bibliography). Companies should always consider these documents, as applicable, in planning their operations. Maintaining well integrity is a key design principle and design feature of all oil and gas production wells.

Maintaining well integrity is essential for the two following reasons.

1. *To isolate the internal conduit of the well from the surface and subsurface environment. This is critical in protecting the environment, including the groundwater, and in enabling well drilling and production.*
2. *To isolate and contain the well's produced fluid to a production conduit within the well.*

Although there is some variability in the details of well construction because of varying geologic, environmental, and operational settings, the basic practices in constructing a reliable well are similar. These practices are the result of operators gaining knowledge based on years of experience and technology development and improvement. These experiences and practices are communicated and shared via academic training, professional and trade associations, extensive literature and documents and, very importantly, industry standards and recommended practices.

A key environmental protection and sustainability section is 7, Well Construction Guidelines. It covers the four main components of conductor, surface, intermediate, and production casing. The various casing strings are used to ensure ground water protection. This section also notes that in addition to the recommendations, operators must be aware of local geological conditions and state regulations. Actual well casing depths are determined in advance as part of the drilling plan and are designed to assure zonal isolation, meet regulatory requirements, achieve well integrity, and contain well pressure. See Figure 1 for typical well design and construction.

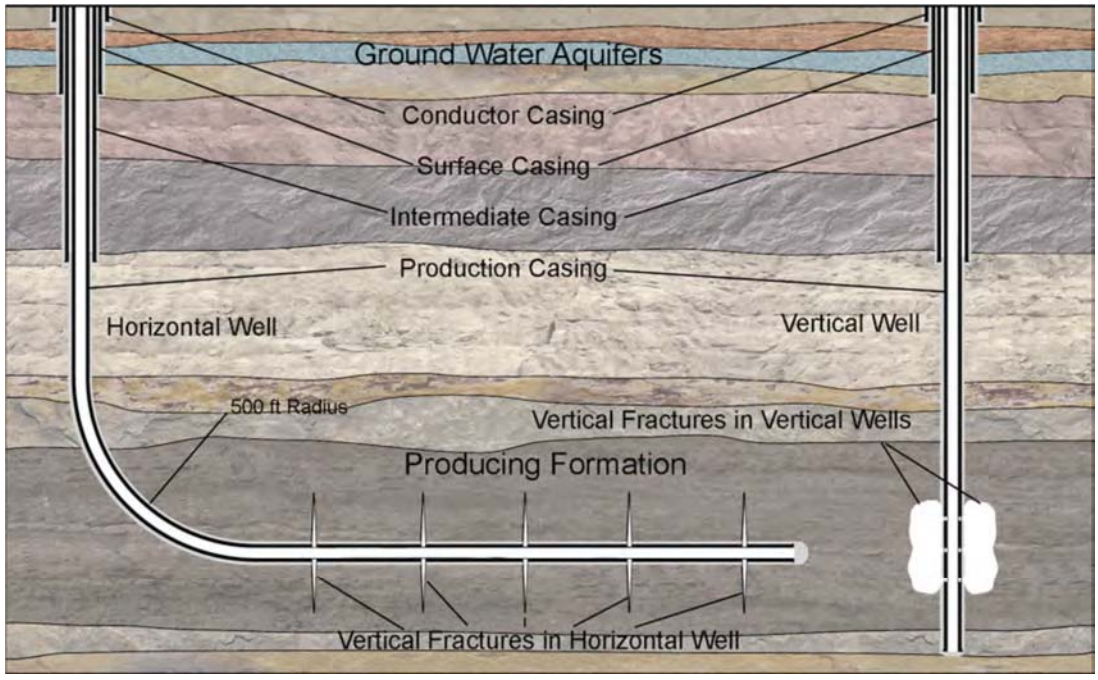

FIG. 1. Example of typical well design and construction

HF2, *WATER MANAGEMENT ASSOCIATED WITH HYDRAULIC FRACTURING*, 1ST EDITION, JUNE 2010

The second standard published in the API shale gas series was HF2 on water management and management of this extremely valuable resource is integral to sustainable gas development. This standard contains the following 7 sections:

1. Scope
2. Definitions
3. Introduction and Overview
4. Hydraulic Fracturing Process
5. Water Use and Management Associated with Hydraulic Fracturing
6. Obtaining Water Supply for Fracturing
7. Water Management and Disposal Associated with Hydraulic Fracturing

HF2's scope is as follows:

The purpose of this guidance document is to identify and describe many of the current industry best practices used to minimize environmental and societal impacts associated with the acquisition, use, management, treatment, and disposal of water and other fluids associated with the process of hydraulic fracturing. While this document focuses primarily on issues associated with hydraulic fracturing pursued in deep shale gas development, it also describes the important distinctions related to hydraulic fracturing in other applications. Moreover, this guidance document focuses on areas associated with the water used for purposes of hydraulic fracturing, and does not address other water management issues and considerations associated with oil and gas exploration, drilling, and production. These topics will be addressed in future API documents

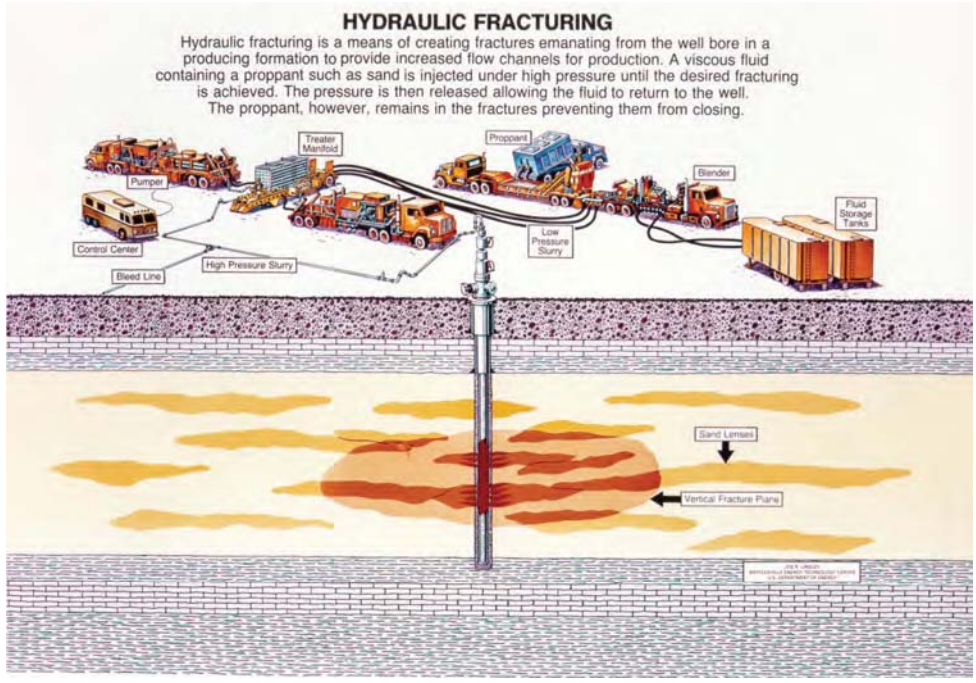

FIG. 2. Typical Well Site

A key environmental protection and sustainability section is section 7, Water Management and Disposal Associated with hydraulic fracturing. This section addresses well permits and the requirements for disposal of fracturing fluids and flow back water. Fracturing fluids and flow back water removal and disposal can include:

- UIC wells
- Treatment at a facility or on site
- Reuse/recycling

Operators should prepare for proper management and disposal by working with state, regional and local regulators to ensure surface and groundwater quality. Primary potential destinations for flow back/production fluids generally include the following: injection wells, which are regulated under either a state or federal UIC program; municipal waste water treatment facilities; industrial waste treatment facilities; other industrial uses; and fracture flow back water recycling/reuse. In many parts of the United States recycling is approaching 90% for flow-back water. See figure 2 for typical well site operations.

HF3, *PRACTICES FOR MITIGATING SURFACE IMPACTS ASSOCIATED WITH HYDRAULIC FRACTURING*, 1ST EDITION, JANUARY 2011

The third published standard in the API Shale Gas Series addressed mitigation of surface impacts. This standard contains 16 sections:

1. Scope
2. Terms & Definitions
3. Introduction & Overview
4. Stakeholder Engagement
5. Wide-scale Development

6. Selection of Hydraulic Fracturing Fluids
7. Management of Chemicals and Materials
8. Transport of Chemicals and other Materials
9. Pre-job Planning
10. Water Management
11. Maintaining Equipment & Facilities
12. Minimizing Surface Disturbance
13. Protecting Air Quality
14. Preserving Visual Resources
15. Mitigating Noise Impacts
16. Mitigating Road Use Impacts

HF3's scope is as follows:

The purpose of this guidance document is to identify and describe practices currently used in the oil and natural gas industry to minimize surface environmental impacts—potential impacts on surface water, soils, wildlife, other surface ecosystems and nearby communities—associated with hydraulic fracturing operations. While this document focuses primarily on issues associated with operations in deep shale gas developments, it also describes the important distinctions related to hydraulic fracturing in other applications.

A key environmental protection and sustainability section is section 7, Management of Chemicals and Materials, which states the following API Policy Position on chemical disclosure for hydraulic fracturing operations. In summary, API supports transparency regarding the disclosure of the chemical ingredients used in hydraulic fracturing operations to ensure that state regulators have the ability to assess potential incident response needs and plan accordingly, with appropriate confidentiality protections. Additionally, we endorse state programs that balance the need to protect oilfield service company confidential business information with the public's need to know. We endorse the use of the FracFocus website that companies use to disclose additives. This website, managed by the Ground Water Protection Council and the Interstate Oil and Gas Compact Commission, was launched in January 2011 and as of February 2014 had over 793 participating companies; 599 reporting companies; and over 65,600 wells included in the database. See figure 3 for the composition of typical hydraulic fracturing fluid.

The fourth standard published in the API sustainable shale gas series was API recommended practice 51R, a standard that had been originally published in the mid-1970s and was updated to address shale gas practices. The Recommended Practice contains 8 sections:

1. Scope
2. References
3. Acronyms and Abbreviations
4. Government Agencies
5. Lease Roads
6. Production, Injection/Disposal Wells
7. Lease Gathering and System Lines
8. Production and Water

FIG. 3. Typical Hydraulic fracturing fluid

51R, *ENVIRONMENTAL PROTECTION FOR ONSHORE OIL AND GAS PRODUCTION OPERATIONS AND LEASES*, 1ST EDITION, JULY 2009

51R's scope is as follows:

This standard provides environmentally sound practices for domestic onshore oil and gas production operations. It is intended to be applicable to contractors as well as operators. Facilities within the scope of this document include all production facilities, including produced water handling facilities. Offshore and arctic areas are beyond the scope of this document. Operational coverage begins with the design and construction of access roads and well locations, and includes reclamation, abandonment, and restoration operations. Gas compression for transmission purposes or production operations, such as gas lift, pressure maintenance, or enhanced oil recovery (EOR) is included; however, gas processing for liquids recovery is not addressed. Annex A provides guidance for a company to consider as a "good neighbor."

A key environmental protection and sustainability section is Annex A, API's "Good Neighbor Guidelines", which address the important relationship between the operator and the lease holder. API also recognizes the importance of the relationship between the operator and the community, and is developing standard HF4 on Community Engagement.

65-2, *ISOLATING POTENTIAL FLOW ZONES DURING WELL CONSTRUCTION*, 2ND EDITION, DECEMBER 2010

The fifth standard published in the API sustainable shale gas series was API standard 65-2 on isolating potential flow zones. The standard contains 7 sections:

1. Scope
2. Normative References
3. Definitions and Terms
4. Barriers
5. Cementing Practices and Factors Affecting Cementing Success
6. Casing Shoe Testing
7. Post-cement Job Analysis and Evaluation

65-2's scope is as follows:

This standard contains practices for isolating potential flow zones, an integral element in maintaining well integrity. The focus of this standard is the prevention of flow through or past barriers that are installed during well construction.

Barriers that seal wellbore and formation pressures or flows may include mechanical barriers such as seals, cement, or hydrostatic head, or operational barriers such as flow detection practices. Operational barriers are practices that result in activation of a physical barrier. Though physical barriers may dominate, the total system reliability of a particular design is dependent on the existence of both types of barriers.

A key environmental protection and sustainability section is section 5, Cementing Practices and Factors Affecting Cementing Success, which includes an Introduction and discussion of the following topics: Hole Quality, Drilling Fluid, Casing Hardware, Close-tolerance and Other Flow Restriction Considerations, Engineering Design, Slurry Design and Testing, Wellbore preparation and conditioning, Cement Job Execution and Post Cementing Operations.

FUTURE ACTIONS

Even though all of the hydraulic gas standards are current and within their five-year time horizons, due to the increased interest in the issue of sustainable shale gas development API has undertaken updates of the first three standards and initiated development of an additional standard. The current activity is as follows:

- RP 100-1 (formerly HF1), *Hydraulic Fracturing – Well Integrity and Fracture Containment*, 1st Edition
- RP 100-2 (formerly HF2 & HF3), *Environmental Aspects Associated with E&P Operations including Hydraulic Fracturing*, 1st Edition
- Bulletin HF4, *Community Engagement Guidelines*, 1st Edition

Bulletin HF4 is a new standard and has garnered interest from a diverse set of stakeholders. Its draft scope is as follows:

These guidelines outline what communities may expect from operators. Oil and gas operators acknowledge the challenges associated with development activities, which may include increased road traffic, noise and population fluctuations within a community. Principles of integrity, transparency and consideration for community concerns underpin responsible operations. Conscientious operators are committed to

helping communities leverage their industry's presence towards achieving positive and long-lasting benefits.

Both local stakeholders and operators can use this guidance. It is designed to acknowledge challenges and impacts that occur during the industry's presence in a given region. It provides flexible and adaptable strategies, recognizing that application will vary from operator to operator and community to community. Many operators already apply similar guidelines or processes within their operations. These guidelines are typical and reasonable and generally apply under normal operating circumstances. The use of these guidelines is at each individual operator's discretion. Operators do recognize that different stakeholders may have differing level of concerns and issues, which may also be in direct conflict with one another. Working together to resolve such conflicts is an important element of community engagement.

These guidelines are intended primarily to support onshore oil and gas projects in the United States for shale developments; however, they may be adapted to any oil and gas projects in the United States.

CONCLUSIONS

The development of shale gas has meant invaluable contributions to the economy and energy balance for the United States. Based on the U.S. Energy Information Agency's (USEA) Annual Energy Outlook: 2013 report, shale gas's contribution to the overall U.S. gas production is projected to be over 50% by 2040, with another 22% coming from tight gas formations. This is a significant increase from shale gas' current contribution of 35% of the overall U.S. gas production. Perhaps more notable is the fact that also according to USEA statistics natural gas production – which had been flat since 1975 – was surpassed in 2011 due to the contribution of shale gas and as stated above, is expected to continue to grow in the coming year. API's accredited standards program is an open, transparent process that ensures that its standards are updated on a regular basis to ensure they reflect industry best practices. These standards, widely cited by both Federal and State Governments, support sustainable shale gas development though the application of proven engineering and environmental practices.

REFERENCES

"States Experience with Hydraulic Fracturing, A Survey of the Interstate Oil and Gas Commission," July 2002.

Testimony Submitted To The House Committee On Energy and Commerce By Victor Carrillo, Chairman, Texas Railroad Commission, Representing The Interstate Oil and Gas Compact Commission. February 10, 2005. http://www.rrc.state.tx.us/commissioners/carrillo/press/energytestimony.html

Environmental Protection Agency, "Study of Potential Impacts of Hydraulic Fracturing of Coalbed Methane Wells on Underground Sources of Drinking Water," Office of Ground Water and Drinking Water report, June 2004, accessed December 6, 2006; Ground Water Protection Council, "State Oil and Gas Regulations Designed to Protect Water Resources," May 2009;

Ground Water Protection Council, "Inventory and Extent of Hydraulic Fracturing in Coalbed Methane Wells in the Producing States," 1998.

The Influence of Hydraulic Fracturing on the Water Market in Texas

Margaret A. Cook[1] and Michael E. Webber[2], Ph.D.

[1]Department of Civil, Architectural and Environmental Engineering, The University of Texas at Austin 301 E Dean Keeton St. Stop C1786, Austin, TX 78712-1173, U.S.A., E-mail: margaretcook@utexas.edu.
[2] Department of Mechanical Engineering, The University of Texas at Austin 204 E. Dean Keeton St. Stop C2200, Austin, TX 78712-1591, U.S.A., E-mail: webber@mail.utexas.edu.

ABSTRACT: Hydraulic fracturing, the injection of pressurized fluid, often water, to increase extraction rates and recovery of oil or gas, has become increasingly popular in combination with horizontal drilling, especially in shales in Texas. Hydraulic fracturing augments the flow of fossil fuel from a well, but requires a significant amount of water to do so. Thus, the growth in shale wells puts pressure on existing water resources, especially in drought-prone areas of Texas. Due to increased water demands in these areas that already have low water availability, current water users and landowners have begun to sell their water resources to supply industry needs. This analysis characterizes the current state of the water market in shale-rich areas of Texas, including water pricing, type of water used, source and end use location, original intended use, and current end use—all within the water policy framework of Texas. Between 1987 and 2008, prior to the increase in hydraulic fracturing in much of Texas, the median lease price was approximately $30 per thousand cubic meters (m^3) and the average price was approximately $100 per thousand m^3. In this preliminary analysis, we found that between 2009 and 2013, the median lease price was approximately $3,100 per thousand m^3 and the average price was $2,300 per thousand m^3, an increase of two orders of magnitude in the median price of water for mining water use. These prices and market trends open up the possibility for innovation and investments in technologies for water use efficiency in various sectors.

INTRODUCTION

Dwindling water supplies, change in climate, and increased demand on resources due to population and industry growth have led increased to water stress worldwide. More recently in Texas, hydraulic fracturing, the injection of pressurized fluid composed of water, sand, and proprietary chemicals to increase extraction rates and

recovery of oil or gas, has become increasingly popular in combination with horizontal drilling, including in shale formations in the state. Hydraulic fracturing requires a significant amount of water to augment the flow of fossil fuel from low permeability source rock. This intensive water requirement can inhibit production in places with low water availability such as drought-prone south and west Texas. With continued scarcity of water that threatens to restrict production, shale oil and gas fracturing companies have benefited from individual water leases and sales in these areas. This paper conducts a first-cut engineering analysis of the water market in Texas and the impact of the water demand for hydraulic fracturing in that market. Those trends and price impacts are relevant to the prospects to innovations in water efficiency. Thus, understanding the underlying dynamics is useful for identifying the potential for engineering solutions to mitigate the various water-related challenges. This paper does not explore possibilities for using brackish, saline, or reuse water for hydraulic fracturing, nor does it discuss potential optimization of water allocation through water marketing though these opportunities do exist.

WATER SCARCITY IN TEXAS

The 2010 United States census revealed that, over the last ten years, Texas received the largest increase in population of any state (U.S. Census Bureau, 2012). In the same period, Texas suffered more weeks of exceptional drought (the worst drought classification given by the National Drought Mitigation Center) than any other state in the union (National Drought Mitigation Center, 2013). In the last three years alone, Texas' water supplies have dwindled. Surface water levels reached their twenty-year low between February and October 2013. This scarcity is a motivating context for the research presented in this manuscript.

HYDRAULIC FRACTURING IN TEXAS

Shale formations have been an important aspect of the public policy dialog about energy recently because of their productivity. Shale production might also be an important part of the evolving water policy discussion as new users of water, and as a potential source of investment capital within the water market. Because oil and gas companies have significant capital to invest, because they require large quantities of water to fracture wells, and because they are willing to pay a higher price for water than conventional water purchasers, they can stimulate the water market, altering the current allocation of water and the implementation of technologies used for efficiency, reuse, or recycling.

Shale deposits are thin, sometimes relatively impermeable, layers of rock that contain significant quantities of natural gas or liquids and often cover a wide area underground. Hydraulic fracturing in combination with horizontal drilling has enabled economic extraction of the natural gas and petroleum liquids from the shale. The shale gas industry reportedly already employs more than half a million workers in the U.S. in 2010 alone and by 2015, could contribute $118 billion to the U.S. economy (Bonakdarpour 2012).

Texas has several shale plays, most notably the Barnett and Eagle Ford shales. For example, the Energy Information Administration (EIA) estimates the Eagle Ford shale holds about 595 billion cubic meters of shale gas, about 4.3% of the nation's 13.6 trillion cubic meters of total supply and about 3 billion barrels of shale oil, about 7% of nation's 24 billion bbl of total supply (U.S. EIA 2011). The past several years have seen high oil and gas production in Texas, but there is still room for growth.

Water Demand for Hydraulic Fracturing

While hydraulic fracturing brings some economic benefits to regions of high drilling activity, the process requires a significant amount of water to extract gas or liquids. In the area surrounding the Eagle Ford shale formation, for example, total water consumption is expected to increase from 7.15 million cubic meters (m^3) in 2010 to 55.2 million m^3 in 2020 due to oil and gas drilling (Lee 2011). These projections for high water use introduce a vulnerability and potential hindrance to increased hydraulic fracturing in Texas because the water might not be available due to prior allocation for other purposes, such as irrigation. Moreover, in certain areas of the state, water use for hydraulic fracturing has been banned. In the Barnett shale region, the City of Grand Prairie recently banned the use of municipal water for hydraulic fracturing. Similarly, in the Texas Panhandle, the Board of Directors of the High Plains Underground Water Conservation District Number 1—the officials governing water use in the Ogallala Aquifer in the area—included limits on water use for hydraulic fracturing when they approved restrictions in July of 2011 (Lee 2011).

For many other sectors, the price of water can be prohibitive; however, because of higher costs for other parts of the supply chain, and because water is used to produce an even higher-value product, water prices are unlikely to be a major hurdle for the oil and gas sector. To illustrate, the price of water is minimal compared to the cost to drill a well. Breitling Oil and Gas recently paid $68,000 for 13,000 m^3 of water—a mere 0.2% of the $3.5 million spent to hydraulically fracture the well, according to the CEO Chris Faulkner (Lee 2011). Thus, the price of water is not expected to be a key constraint at the current time for oil and gas producers.

By contrast, the physical unpredictability and scarcity of water could represent an important potential inhibitor to production. While Texas has an abundance of oil and gas-bearing shale, it has significant water scarcity in some regions that are geographically co-located with the shale. In particular, the Eagle Ford and Barnett shale regions overlap with areas of water scarcity, especially during the record-setting drought of 2011. In the midst of drought and added water restrictions, the increase in shale liquid and gas extraction might be stunted by lack of available freshwater. Thus, water sales and leases by oil and gas operators intending to shore up water supplies for hydraulic fracturing could play an important role in the market for water in these water-stressed areas of the state.

WATER ALLOCATION POLICIES IN TEXAS

Current water policies have slowed the impacts of drought and population growth in some areas and exacerbated them in others. Texas surface water is allocated under

the Doctrine of Prior Appropriation, where a permit to withdraw water is based not on land ownership but on the point in time at which the permit or "water right" was acquired (Getches, 2009). The doctrine of prior appropriation developed in western states where water scarcity led to the need for allocation. The system is often simplified as "first in time, first in right" because, upon application, a permitting authority gives a water right holder a priority date and an allocation amount that resides with the water right as long as it remains valid. Thus, water shortages fall on those who last obtained a legal right to use the water unlike Riparian water law, common in eastern states, where shortages are shared equally among landowners adjacent to the water source.

Users must prove their rights are being exercised and put to a beneficial use for the rights to remain valid. Otherwise, a right can be deemed abandoned or terminated. This principle creates an incentive for water rights holders to use all of their allotted water. For example, senior water rights holders, often irrigators in Texas, receive no benefit for conserving water. The water saved will go to the next-priority user while the irrigator receives no monetary reward or increase in water supply for later years. Instead, senior water rights holders in Texas are motivated to devote large quantities of water to beneficial uses like growing low-value crops (Brewer et al., 2008).

Because appropriative rights exist separate from land ownership, they can be bought, sold, leased, or transferred, forming the basis for a surface water market.

In contrast to its governance of surface water, Texas does not incorporate permitting or judgments on reasonable use of water into its groundwater policy. Groundwater in Texas follows the Rule-of-Capture, attributing the right to withdraw groundwater to the landowner residing above that water and providing that, absent malice or willful waste, landowners can withdraw as much water as they want without incurring liability even if that withdrawal will inhibit access to water by neighboring landowners (Potter, 2004). A groundwater conservation district (GCD) authorized by the Texas Legislature can protect and manage groundwater resources to maintain supplies in the area (Mittal & Gaffigan, 2009). These districts have the ability to require permits and to place reasonable restrictions on water withdrawals or well location (Mittal & Gaffigan, 2009).

Under the Rule-of-Capture, groundwater is an open-access good. Unless restricted by a GCD or other authority, landowner may withdraw as much water as they need and are inclined to overexploit it. No single user has an incentive to reduce exploitation due to knowledge that neighbors might exploit or sell water (Holland). Additionally, limited transferability of water rights could be economically inefficient, preventing redistribution of water to uses with higher monetary returns (Holland).

USE OF PRICING TO COMBAT SCARCITY

As with other commodities, a market could be used mitigate some of these issues of allocation and inefficiency by making water available to most economical purposes. Much of the economics literature emphasizes the economic gains from increased water trading. Howitt (1994) emphasized the role that the water bank in California played in alleviating the impacts of the 1991 drought (Howitt, 1994), and Loomis et al. asserted that markets can lead to smoother reallocation than non-voluntary

regulatory reallocation (Loomis et al. 2003).

A water market could create challenges for the state of Texas, though. In a market, water would move to its highest-valued uses, which might not be the most equitable allocation from a social justice or human rights perspective. Additionally, there are physical (lack of infrastructure for moving water, for example) and political barriers to implementation of water trading. Furthermore, the trade of water can inadvertently disturb multiple entities. For example, if water is transferred out of a basin, users who depended on the original return flow will not receive their original source water (Brewer et al., 2008).

Because buyers and sellers face uncertainty on efficient pricing, wholesale water prices do not always increase as water resources become scarcer (Brewer et al., 2008). Moreover, landowners and water rights holders already have inexpensive access to water, making water a low-cost product to market. However, in some cases, water scarcity, as well as intended use of the water, does influence price. Limited information on efficient pricing has slowed water transactions and restricted their ability to remedy water allocation issues.

WATER TRADING IN TEXAS

Despite the drawbacks to the current water trading system, water transfers have occurred in Texas for decades. These transfers fall into two categories: 1) transfers of water rights ownership, and 2) leases or contracts that grant the purchaser a specified volume of water for a limited term (Hansen, Howitt, & Williams, 2012). Leases can be short- or long-term and negotiated close to the time of transaction or planned far in advance of the water need (Hansen, Howitt, & Williams, 2012). Some users also pay for reservations of water for a future use. Leases and contracts might be for firm or interruptible supply. Purchasers desiring firm water supply pay a certain rate to receive their contracted amount while interruptible users pay a lower price, allowing the seller to reduce the interruptible user's water supply in a dry year to fulfill other contracts.

Usual transactions occur within the agriculture sector or from agriculture to non-agriculture users (Brewer et al., 2008). According to the Western Governors Association, Texas traded a total 3.5 billion m^3 between 1988 and 2009 at an average 10 million m^3 per year. Trades increased between 2007 and 2009 resulting in 185 million m^3 of transfers. However, the ongoing drought in Texas produced increased demand for water transfers across the state. During the drought in 2011, users sold or leased more than 21 million m^3 (Doherty & Smith, 2012).

In Texas, formal water markets have been slow to develop. Water scarcity is generally not an issue in the relatively wet eastern portion of Texas. Water is rarely traded across Texas due to the large size of the state and the lack of natural or man-made conduits for large water transfers like those in California (Brewer et al., 2008). Where water is traded, local markets prevail, specifically in the Lower Rio Grande Valley (in the Southern tip of Texas), over the Edwards Aquifer (in central Texas), and in Northwest Texas.

Water Trading in the Rio Grande Valley

Water transactions in the Rio Grande Valley below Amistad Dam became commonplace after the 1967 Water Rights Adjudication Act passed, imposing regulated scarcity where there was already physical scarcity and attributing value to water rights on the river (Chang & Griffin, 1992). The Act, stimulated by State of Texas v Hidalgo County Water Control and Improvement District 18, merged surface water claims into the state's water permit system (Chang & Griffin, 1992). Claims to water were adjudicated by 1971 (Chang & Griffin, 1992). Those that had previously applied for statutory water rights under the 1913 Irrigation Act were granted Class A water rights while others received Class B rights (Chang & Griffin, 1992). Class A water rights holders receive 1.7 times the water as that allocated to Class B water rights holders (Chang & Griffin, 1992). Because the system does not incorporate any priority assignment, shortages and surpluses are shared by all water rights holders (Chang & Griffin, 1992). The Rio Grande Watermaster's office administers water rights and transfers on the U.S. side of the river. About 99 percent of rights are designated for use in either municipal or irrigation activities.

Because Class A water rights holders are guaranteed more water, the rights can be traded at prices relative to the amount of water involved (Chang & Griffin, 1992). Usual trades in the area occur within the agriculture sector or from agriculture to municipal and industrial users. For example, in 2007, the City of Roma in Starr County was awarded $2.8 million from the Economically Distressed Area Program to purchase water rights. Rather than buying more water from the markets, the city engineers decided to make a trade for water rights with irrigation districts in Cameron County (Gerston 2002). The city funded improvements to irrigation canal conveyance efficiency within Irrigation District No. 2 and received the excess water rights in return. The City of Roma received the needed water supply, while the irrigation districts still received the water they needed and even had an additional savings of about 100,000 m^3/yr. This example demonstrates the potential for water treating with subsequent investments in water efficient technologies to achieve resource allocation that meets multiple needs.

Surface Water Outside of the Rio Grande Valley

In Texas, river authorities often own much of a river's water rights, operate some major reservoirs, and administer contracts for water supply to agricultural, municipal, industrial, recreational, or other uses (Griffin & Characklis, 2002). River authorities are water districts with service areas often covering the entire river basin. The authorities often channel their revenues into growing their service domain by purchasing facilities and water rights of smaller public and private water entities. Due to this relatively monopolistic control of water rights, traditional water trading is almost infeasible on these rivers (Griffin & Characklis, 2002). Water reallocation instead occurs within the river authorities through water supply contracts (Griffin & Characklis, 2002).

Water Trading in the Edwards Aquifer

The Edwards Aquifer is located in South Central Texas and resides beneath the City of San Antonio. The Edwards Aquifer Authority, created by the Texas Legislature through the Edwards Aquifer Authority Act in 1993, monitors groundwater withdrawals from the Edwards Aquifer (Supreme Court of Texas, 2010). The Authority issued permits for water withdrawal from the aquifer to persons who withdrew and beneficially used groundwater from the Edwards Aquifer on or before June 1, 1993 and based allocation on historical municipal, industrial, and irrigation water use between 1972 and 1993 (Edwards Aquifer Authority, 2014). Well owners could apply for water rights until December 30, 1996. The Act prohibits withdrawals without a permit with an exception for wells producing less than 25,000 gallons per day (gpd) for domestic or livestock use (Supreme Court of Texas, 2010), but the Act allows purchases or leases of groundwater rights excluding transfers outside the basin (Edwards Aquifer Authority, 2014). The Act included a provision granting existing irrigators permits to withdraw up to approximately 2,467 m^3/yr (2 acre-feet/yr) for each 4,046 m^2 (1 acre) historically irrigated (South Central Texas Regional Water Planning Area, 2010). Due to this provision, an irrigation permit holder cannot lease more than 50% of the initially permitted rights.

Active leasing has resulted in significant transfers from agricultural to municipal water use. For example, the San Antonio River Authority administers the Regional Water Resource Development Group (RWRDG) to purchase Edwards Aquifer groundwater rights for municipal use, providing several communities access to Edwards Aquifer groundwater (San Antonio River Authority, 2014). The South Central Texas Regional Water Planning Group, the entity responsible for planning for future water supplies for the area surrounding San Antonio, reported that sales and leases of Edwards Aquifer water rights in 2011 were made at rates ranging from $80 to $105 per thousand m^3/yr with lease terms of 5 to 10 years while water right purchase prices ranged from $4,500 to $5,300 per thousand m^3 (South Central Texas Regional Water Planning Area, 2010).

Groundwater Outside of the Edwards Aquifer

In Northwest and West Texas, water marketing takes the form of groundwater ranching (Chang & Griffin, 1992). Entities purchase land underlain with developable groundwater resources with the intent to lease the water or sell the land and underlying water rights to other users (Chang & Griffin, 1992). Because buyers often only desire the water underling the land, overlying land is sometimes leased for dryland production (Chang & Griffin, 1992). One recent example of this method of water prospecting occurred in 2011 when Mesa Water sold 850 square kilometers (km^2) of land underlain with about 15 billion m^3 of water for 103 million U.S. dollars to the Canadian River Municipal Water Authority and the City of Amarillo.

In much of Texas, groundwater conservation districts protect and manage groundwater resources to maintain supplies in the area, issuing permits and restricting water withdrawals (Mittal & Gaffigan, 2009). To preserve future water supplies within the Ogallala Aquifer, GCDs overlying the aquifer have limited groundwater

withdrawals in recent years. The Panhandle GCD, one of many districts that govern groundwater extractions from the aquifer, has limited withdrawals to 0.3 meters per year for every 4,046 square meters (m^2) of land owned (Patoski, 2001). Similarly, landowners wishing to export their water can only transfer 1,233 m^3/yr for every 4,046 m^2 of land owned (Patoski, 2001).

HYDRAULIC FRACTURING AND THE WATER MARKET IN TEXAS

With the surge in oil and gas drilling in the nearby Eagle Ford shale, energy companies have been buying or leasing water rights on the Rio Grande in South Texas (Doherty & Smith, 2012). One of the major irrigation districts in the Lower Rio Grande, Hidalgo County Irrigation District No. 2, has added diversion points in the Middle Rio Grande where water can be easily delivered to energy entities (Doherty & Smith, 2012). Landowners in other parts of the shale basin have sold water from their wells to oil and gas producers, sometimes requiring the producers desiring access to the land's mineral rights to also drill a water well on the property and purchase that water for fracturing any oil or gas wells. Landowners might sell their water through water marketing firms. One firm reportedly sold more than 220,000 m^3 to oil and gas companies (Muniz, 2014). Figure 1 shows these and other mining water transactions that occurred between 2009 and 2013.

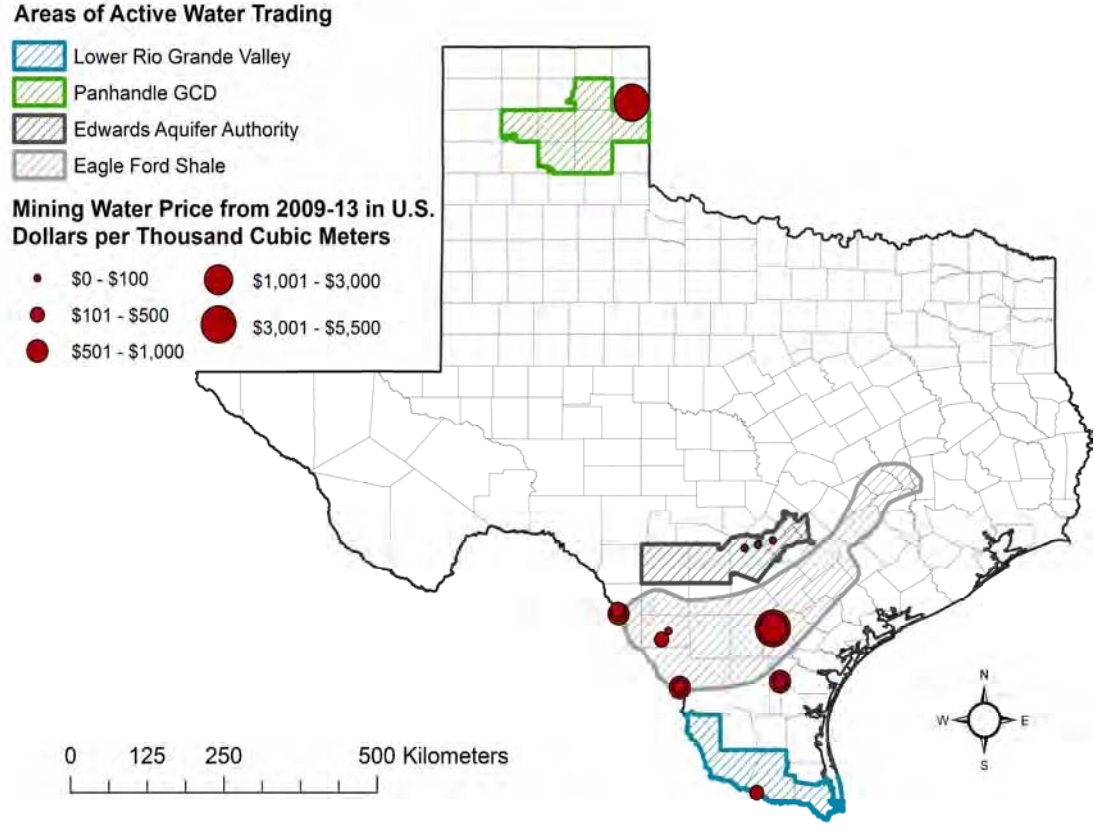

FIG. 1. Water transactions for mining have increased in price and volume in the Eagle Ford shale area. Water originates in the Rio Grande or in aquifers overlying the shale. Data were acquired from Donohew & Libecap 2009, TCEQ 2013, and Muniz 2014.

As the amount of mining transactions has increased, so has the price of water per cubic meter as shown in Figure 2. Between 1987 and 2008, prior to the increase in hydraulic fracturing in much of Texas, the median lease price was approximately $30 per thousand m^3 and the average price was approximately $100 per thousand m^3. Between 2009 and 2013, the median lease price was approximately $3,100 per thousand m^3 and the average price was $2,300 per thousand m^3. Surface water leases averaged $800 per thousand m^3. This change in price could be due to the spike in water demand for oil and gas drilling as well as the decrease in water supplies caused by the intense, state-wide drought that began in 2011, among other factors.

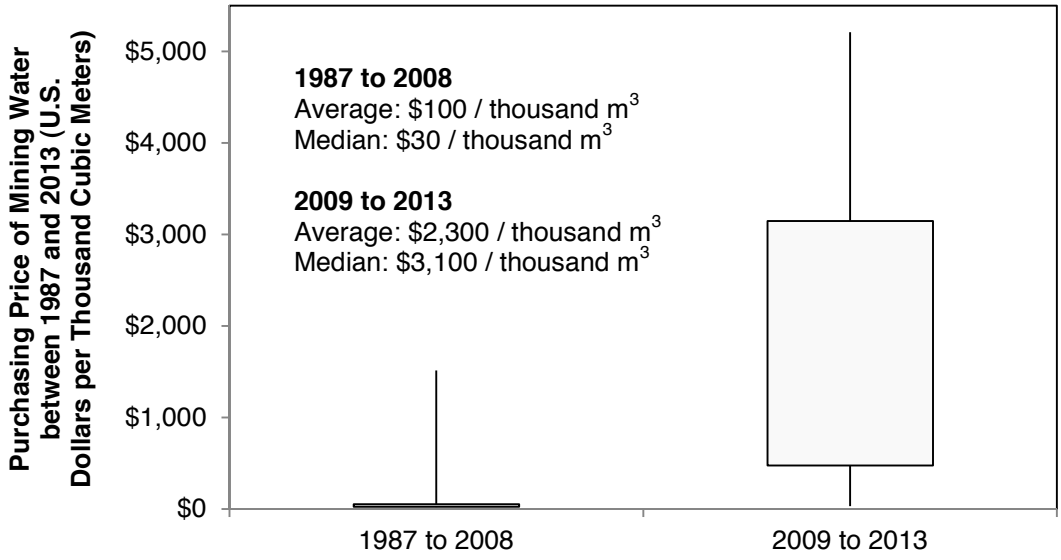

FIG. 2. Water prices in the mining sector increased dramatically since 2009. Between 1987 and 2008, the median lease price was approximately $30 per thousand m^3 and the average price was approximately $100 per thousand m^3. After 2009, the median lease price was approximately $3,100 per thousand m^3 and the average price was $2,300 per thousand m^3. Data were acquired from Donohew & Libecap 2009, TCEQ 2013, and Muniz 2014 and include approximately 30 transactions prior to 2009 and over 100 transactions after 2009.

With more market activity and higher prices, it is possible that sufficient capital will be available to agricultural and other industrial users to enable them to invest in water efficiency. That means, following the model of the experience in Roma, that with the right combination or trades and investments, there will be sufficient water for everyone. By implementing a combination of conservation methods, these users and their economic partners, which might include shale liquid and gas companies, can optimize their water efficiency, reuse, or recycling and achieve more water availability for themselves or the environment. In this energy-water partnership, this increased water availability would augment the ability to fracture more wells without hindering other production.

Alternatively, higher prices for water might encourage increased use of water efficiency, reuse, or recycling in the hydraulic fracturing process. Specifically, if the price of water exceeds the total cost to save, reuse, or treat water, these technologies might be implemented more often than they are currently used and overall water use in this industry could decrease. Understanding the water market helps determine potential implications such as those mentioned in both the buying and selling sectors.

CONCLUSIONS

The water market in Texas is heavily influenced by policy, water supplies, and demands from various sectors of water use. The market has historically been dominated by transactions within the agriculture sector and transactions between the agriculture and municipal sectors. However, between 2009 and 2013, the market experienced an increase in demand for water from the energy industry, particularly in the Eagle Ford Shale.

As the demand for water for mining increased, so did the price of water per cubic meter for the mining sector. In this preliminary analysis of the water market for oil and gas water use, we found that the median price of water increased by two orders of magnitude, from \$30 per thousand m^3 between 1987 and 2008 to \$3,100 per thousand m^3 after 2009. This change in price could be due to the increase in water demand for oil and gas drilling in the Eagle Ford shale and is probably exacerbated by the decrease in water supplies caused by the intense, state-wide drought that began in 2011.

This high price of water in the energy industry could encourage other changes in the water market in Texas including increases in welfare due to trading from less economically efficient uses of water to the energy industry or improvements in technology for water conservation, reuse, or recycling in the energy sector or in the selling sector. Consequently, future work could analyze the potential uptake of advanced technologies, refined market designs, and improved policy structures that might be enabled by the more active water markets.

ACKNOWLEDGEMENTS

This work was funded in part by the National Science Foundation's EFRI-RESIN program and the U.S. Department of Energy.

The authors would like to acknowledge Dr. Sheila Olmstead and Matt Muniz for their help with this work.

REFERENCES

Amarillo City Council. (2013). "Minutes." Amarillo, TX. http://www.amarillo.gov/departments/citymgr/2013/minutes/minutes_12_03_2013.pdf.

Brewer, J., R. Glennon, A. Ker, and G. Libecap. (2008). Water markets in the West: prices, trading and contractual forms. Economic Inquiry 46: 91-112.

Bonakdarpour, M and Larson, J. (2012). "The Economic and Employment

Contributions of Unconventional Gas Development in State Economies," IHS Inc., http://www.ihs.com/images/State_Unconv_Gas_Economic_ Contribution_Main.pdf.

Canadian River Municipal Water Authority. (2012). "Comprehensive Annual Financial Report." Sanford, TX. http://crmwa.com/wp-content/uploads/2013/02/FY-11-12-Audited-Financial-Statements-CAFR.pdf.

Caputo, Anton (2009). "Exelon Still Holding Onto Guadalupe Water." San Antonio Express-News. http://thearansasproject.org/basin-management/exelon-still-holding-onto-guadalupe-water/.

Chang, C., & Griffin, R. (1992, March). Water Marketing as a Reallocative Institution in Texas. Water Resources Research, 28(3), 879-890.

Doherty, T., & Smith, R. (2012). Water Transfers in the West 2012: Projects, Trends, and Leading Practices in Voluntary Water Trading. Denver, CO: Western Governors' Association.

Donohew, Z., & Libecap, G. (2009). California Water Transfer Records. Retrieved from Water Transfer Data: http://www.bren.ucsb.edu/news/water_transfers.htm.

Edwards Aquifer Authority. (2010). "Comprehensive Annual Financial Report." San Antonio, TX. http://data.edwardsaquifer.org/files/FY2010%20Comprehensive%20Annual%20Financial%20Report.pdf.

Edwards Aquifer Authority. (2011). "Comprehensive Annual Financial Report." San Antonio, TX. http://www.edwardsaquifer.org/files/download/3fdf1888cb38bda.

Edwards Aquifer Authority. (2012). "Comprehensive Annual Financial Report." San Antonio, TX. http://www.edwardsaquifer.org/files/2012_Comprehensive_ Financial _Annual_Report.pdf.

Edwards Aquifer Authority. (2013). "2013 Operating Budget." http://www.eaadevelopment.com/operating-budget/financial-overview.

Edwards Aquifer Authority. (2014). Groundwater. Retrieved from Managing Your Permit: http://data.edwardsaquifer.org/display_permit_portal_m.php?pg=permit_faqs/

Gerston, J., MacLeod, M., Jones, C. A. (2002). "Efficient Water Use for Texas: Policies, Tools, and Management Strategies." Environmental Defense Fund.

Getches, D. (2009). Water Law in a Nutshell. St. Paul, MN: West Publishing Co.

Griffin, R., & Characklis, G. (2002). Issues and Trends in Texas Water Marketing. Water resources Updated, 29-33.

Guadalupe-Blanco River Authority. (2011). "Minutes of the Board of Directors." http://www.gbra.org/documents/board/minutes/110518.pdf.

Hansen, K., Howitt, R., & Williams, J. (2012). An Econometric Test of Water Market Structure in the Western United States. Allied Social Science Associations Annual Meeting. Chicago, IL.

Holland, Stephen, and Michael Moore. (2003). Cadillac Desert revisited: property rights, public policy and water-resource depletion. Journal of Environmental Economics and Management 46: 131-155.

Howitt, R. E. ''Effects of Water Marketing on the Farm Economy,'' in Sharing Scarcity: Gainers and Losers in Water Marketing, edited by H. O. Carter, H. J. Vaux Jr, and A. F. Scheuring. Davis, CA: Agricultural.

Issues Center, 1994, 97–132.Kimmell, T. A., & Veil, J. A. (2009). Impact of Drought on U.S. Steam Electric Power Plant Cooling Water Intakes and Related Water Resources Management Issues. DOE/NETL-2009/1364.

Lee, M. (2011). "Parched Texans Impose Water-Use Limits for Fracking Gas Wells," Sept. 30, 2011, http://www.businessweek.com/news/2011-10-06/parched-texans-impose-water-use-limits-for-fracking-gas-wells.html.

Loomis, J. B., K. Quattlebaum, T. C. Brown, and S. J. Alexander. (2003). "Expanding Institutional Arrangements for Acquiring Water for Environmental Purposes: Transactions Evidence for the Western United States." Water Resources Development, 19, 21–8.

Mittal, A., & Gaffigan, M. (2009). Energy-Water Nexus: Improvements to Federal Water Use Data Would Increase Understanding of Trends in Power Plant Water Use. GAO.

Muniz, Matt. Personal Interview. 25 June 2012.

Muniz, Matt. Personal Interview. 9 January 2014.

National Drought Mitigation Center. (2013). "Current U.S. Drought Monitor." http://droughtmonitor.unl.edu/.

Nicot, J. P. and Scanlon, B. R. (2012)."Water Use for Shale-Gas Production in Texas, U.S." *Environmental Science & Technology*. 46, 3580-3586.

Olmstead, S. M., and R. N. Stavins (2009). Comparing price and nonprice approaches to urban water conservation, Water Resour. Res., 45, W04301, doi:10.1029/2008WR007227.

Patoski, J. (2001, August). Boone Pickens Wants to Sell You His Water. Retrieved from Texas Monthly: http://www.texasmonthly.com/story/boone-pickens-wants-sell-you-his-water.

Potter, I. H. (2004). History and Evolution of the Rule of Capture. Report 361, Rule of Capture Conference (pp. 1-9). Austin: TWDB.

San Antonio River Authority. (2014). Public Services. Retrieved from Regional Planning: http://www.sara-tx.org/public_services/water_planning/.

South Central Texas Regional Water Planning Area. (2010). 2011 Regional Water Plan Volume II: Technical Evaluations of Water Management Strategies.

The Supreme Court of Texas (2010). The Edwards Aquifer Authority and the State of Texas v. Burrell Day and Joel McDaniel, 08-0964.

Texas Commission on Environmental Quality. Public Information Request number (PIR number) 14509. 2013.

Texas Commission on Environmental Quality (TCEQ). (2009). "Rights to Surface Water in Texas," *GI-228*, http://www.tceq.texas.gov/publications/gi/gi-228.html/at_download/file.

Texas Natural Resources Information Services (TNRIS) of the Texas Water Development Board (TWDB). (2012). "Maps & Data," http://www.tnris.org/get-data.

U.S. Census Bureau. (2012). "The 2012 Statistical Abstract." http://www.census.gov/compendia/statab/ cats/population.html.

U.S. Energy Information Administration (U.S. EIA). (2011). "Review of Emerging Resources: U.S. Shale Gas and Shale Oil Plays," http://www.eia.gov/analysis/studies/usshalegas.

U.S. EIA. (2012). "AEO2013 Early Release Overview," *DOE Report Number: DOE/EIA-0383ER(2013),* http://www.eia.gov/forecasts/aeo/er/early_production.cfm.

U.S. EIA. (2012)."Maps: Exploration, Resources, Reserves, and Production," ftp://www.eia.doe.gov/pub/oil_gas/natural_gas/analysis_publications/maps/maps.htm.

Vaughan, E. G., Crutcher, J. M., Labatt III, T. W., McMahan, L. H., Bradford, B. R., Cluck, M. (2012). *Water for Texas 2012 State Water Plan* Texas Water Development Board, http://www. twdb.state.tx.us/publications/state_water_plan/2012/2012_SWP.pdf.

Water Data For Texas. (2014). Retrieved from Texas Reservoirs: http://www.waterdatafortexas.org/reservoirs/statewide.

Welch, Kevin. (2013). "City Might Sell Last of Hartley County Water Rights." http://amarillo.com/news/local-news/2013-12-02/city-might-sell-holdings.

Welch, Kevin. (2013). "Water Authority May Sell Lipscomb County Rights." Amarillo Globe-News. http://amarillo.com/news/local-news/2013-07-10/water-authority-may-sell-lipscomb-county-rights.

Investigation and Analysis of Social Impacts of Eagle Ford Shale on Local Communities

Hua Li[1], Ph.D., Jieming Chen[2], Ph.D., Jennifer E. Pearce-Morris[3], Ph.D., Brenda Hannon[4], Ph.D., Kai Jin[5], Ph.D., Lian Yang[6], Emilio Alaniz[7], M.S., Jaime Herrera[8], Ruth Zabelin[9]

[1]Assistant Professor, Mechanical and Industrial Engineering, Texas A&M University-Kingsville, 700 University Blvd, Kingsville, TX 78363, U.S.A., hua.li@tamuk.edu.
[2]Professor, Psychology and Sociology, Texas A&M University-Kingsville, 700 University Blvd, Kingsville, TX 78363, U.S.A., jieming.chen@tamuk.edu.
[3]Assistant Professor, Psychology and Sociology, Texas A&M University-Kingsville, 700 University Blvd, Kingsville, TX 78363, U.S.A., jennifer.pearce-morris@tamuk.edu.
[4]Assistant Professor, Psychology and Sociology, Texas A&M University-Kingsville, 700 University Blvd, Kingsville, TX 78363, U.S.A., brenda.hannon@tamuk.edu.
[5]Professor, Mechanical and Industrial Engineering, Texas A&M University-Kingsville, 700 University Blvd, Kingsville, TX 78363, U.S.A., kai.jin@tamuk.edu.
[6]Graduate Student, Mechanical and Industrial Engineering, Texas A&M University-Kingsville, 700 University Blvd, Kingsville, TX 78363, U.S.A., lianyang1949@gmail.com.
[7]Lecturer, Psychology and Sociology, Texas A&M University-Kingsville, 700 University Blvd, Kingsville, TX 78363, U.S.A., emilioalaniz3@hotmail.com.
[8]Graduate Student, Psychology and Sociology, Texas A&M University-Kingsville, 700 University Blvd, Kingsville, TX 78363, U.S.A., jaime11herrera@gmail.com.
[9]Graduate Student, Psychology and Sociology, Texas A&M University-Kingsville, 700 University Blvd, Kingsville, TX 78363, U.S.A., rzabelin@yahoo.com.

ABSTRACT: In a region traditionally known for agriculture, the Western Gulf Basin of South Central Texas has recently become a major player in the oil and gas industry. The shale gas and oil development in the area, now known as the Eagle Ford Shale region, has generated a significant boost to South Texas. However, the issue of whether the development has benefited all residents in the region, most of whom are Hispanic and low income, and how the development has affected the social life of the local communities in general, remains an unanswered question. To investigate the general economic and social impacts of the development to the local residents in the region, a research team at Texas A&M University-Kingsville has conducted a large-scale social survey in the region. Adopting a multi-stage probability sampling frame, the survey has randomly selected 1590 respondents in the region for interview. In the paper, we describe in detail the research design and survey instrument, and provide results of preliminary analysis of the data thus collected.

INTRODUCTION

Rapid growth of renewable energy industry in recent decades notwithstanding, oil, and to a lesser extent natural gas, continue to serve as the "lifeblood" of modern society. Oil and natural gas provide the bulk of energy to a number of important economic undertakings, including transportation, electricity generation, heating, and other industrial applications. However, oil and natural gas also create significant and varied negative impacts and costs to human health, cultures, and the environment in the production stage (O'Rourke and Connolly 2003). Thus, it is critical to evaluate the costs as well as the benefits of oil and natural gas, especially for the local communities living in the production sites.

In a region traditionally known for agriculture, the Western Gulf Basin of South Central Texas has recently become a major player in the oil and gas industry. The area now known as the Eagle Ford Shale has experienced many changes since the oil production began in 2010. The recent Eagle Ford Shale development has generated a significant economic boost to South Texas, and produced enormous economic impacts on local communities in the region. Some preliminary research has been carried out to examine some of the impacts, such as emerging employment opportunities, greater needs for housing, and traffic congestion and overuse of the highway systems in the region (UTSA 2012). However, the actual social impacts caused by the estimated economic boost have not been systematically investigated yet. According to Pleeter's definition (1980), economic impact analysis (EIA) normally examines the effect of a policy, program, project, activity or event on the economy of a given area, and measures the changes in economic growth (output or value added) and associated changes in jobs (employment) and income (wages). On the other hand, the social-economic impacts are the influences and changes on the social life of the region caused by economic development or changes (Cottrell 2009). To date, there is lack of a systematic approach to qualitatively and quantitatively evaluate social-economic impacts of the shale oil and gas development in the region. To fill the void, a research team was formed by several researchers of different disciplines at Texas A&M University-Kingsville to conduct a general assessment of the impacts on the local communities in the region. A large-scale social survey in the region has been carried out, and the data collection is still in progress. In this paper, we report the methodologies, survey process, and findings of preliminary analysis of the data thus collected.

RESEARCH DESIGN

The Eagle Ford Shale is arguably the single largest economic development in the history of Texas. With drilling activities in the region that is considered one of the most active, there is a question of whether the economic growth is sustainable in that it generates benefits to all in the region. For oil and gas production, we hold the view that sustainable development also involves equitable or "just" distribution of benefits for all people living the region of production, now and into the future. Given that the region of the Eagle Ford Shale region was economically depressed in the past, and most residents were economically disadvantaged vis-à-vis the national average, the

extent to which the oil and gas development impacts the social and economic conditions of the local communities in the region is our guiding question.

More specifically, the research team focuses on following impacts:

1) What are the general social-economic impacts of Eagle Ford Shale Development on local communities?

2) How the Eagle Ford Shale Development will affect home life of the local communities?

3) How the Eagle Ford Shale Development will affect STEM education potential and the need for STEM education in the local communities?

Therefore, the objectives of the study are multiple. First of all, we seek to gather data about the general impact of the oil and gas development, social as well as economic, to the local communities. This entails both factual data, such as income and employment change since the development, and opinions and subjective evaluations of local residents' sense of wellbeing. Secondly, because families continue to be the primary units around which members of the local communities organize their social life and pool their resources, we also plan to investigate the extent to which the economic develop impact the home life in the region. Lastly, as education is the major mechanism through which individuals of lower socioeconomic status achieve their upward social mobility, we also wish to examine the impact on both educational facilities and aspirations of local families, especially educational aspirations in science, technology, engineering, and mathematics (STEM).

To achieve these objectives, we chose to adopt survey research to collect data for the study. The target population included all non-institutionalized residents living in the Eagle Ford Shale region, we planned to use a probability sampling scheme to generate a sample of respondents, and conduct interview of those selected into the sample. Two major components of this plan were (1) questionnaire design, and (2) selection of respondents using a probability sampling frame.

QUESTIONNAIRE DESIGN

In order to gather data for the three major research questions mentioned above, a comprehensive questionnaire with about 65 questions was designed. The questionnaire consists of six sections: background, family and household conditions, education, employment, health conditions, and impact of the oil and gas industry. In the background section, the respondent's demographic information is collected, including age, gender, ethnicity, marital status, etc. The second section contains questions about household information and family relationships. Questions about education levels of the respondents and their family members are included in the education section. The respondent's expectation or plan for future education opportunities is also part of this section. In the employment section, current employment status and previous working experience are asked. In the last section, a series questions are designed to gauge the respondents' opinions and subjective evaluations of the impact of oil and gas industry.

Other than the demographic information that was inquired about in the background section, which will be used for description of the basic characteristics of the sample and will be used as control variables in multivariate analyses, the other topics listed above were included into the questionnaire because they will be used to address the

major research questions we set out to seek answers. Additionally, we created detailed questions on issues of home life, educational attainment and aspirations, and health conditions, for the purpose of conducting indepth analysis of racial/ethnic differentials in home life, educational attainment, and health conditions.

For instance, we propose that several pathways or mechanisms are at work in creating health disparities across different racial/ethnic groups (Braveman 2005; Adler and Rehkopf 2008). The first one is income differentials. In America as well as in almost all industrialized societies, income is one of the most powerful predictor of health, and those with higher incomes have better access to good quality food and doctors. Economic inequality contributes in a very direct way to the racial and ethnic differentials in health. The second mechanism that contributes significantly to health disparities is education differentials. The way that education influences health can be multifaceted: education attainment determines, directly or indirectly, life style, worldviews, health knowledge, and belief systems. All these lead to the general pattern that better educated tend to enjoy better health. The third one is differentials in access to health care, which is related with income and education, but has independent effect on health disparities. The Eagle Ford Shale region has historically been an economic depressed area. Ideally the economic development will benefit all in the region. As most residents in the region are Hispanic and poor, the improvement in average income, education, and health access will significantly improve the general health conditions, and hence reduce or eliminate health disparities. As identified by NIH, U.S.-Mexico Border region is one of four focused regions of the US for reducing the incidence and prevalence of health disparities. The development of Eagle Ford Shale may not only have social-economic impacts on local communities, it may also affect the health disparities in this region. So a separate section focusing on health conditions is included in the questionnaire.

SAMPLING FRAME AND SURVEY INSTRUMENT

Given the budgetary constraints, instead of selecting all 23 counties in the Eagle Ford Shale region as our target population, we chose to select residents in La Salle county, McMullen county, Dimmit county, Live Oak county, Karnes county, DeWitt county, and Bee county as our target population. The seven counties were selected based on two criteria: 1) the intensity of the oil and gas drilling; and 2) the physical proximity to our home institution. There are intensive oil and gas drilling activities in all seven counties selected, and all counties are within 2-3 hour driving distance from Texas A&M University-Kingsville, our home institution. According the 2012 population estimates, the population size for all seven counties is 98185.

For this project, we have adopted a two-stage area probability sampling framework, in which the county is the primary sampling unit (PSU), and the non-institutionalized adults (age 18 and above) who registered as voters in 2012 are the second sampling unit (SSU). Of the seven counties included in target population, as McMullen county has a population of only 726, it is combined with the adjacent La Salle county as one unit. The resulting six counties or combinations of counties were used for first stage sampling. For the first stage sampling, we used the method of probability proportional to size (PPS) by assigning different weights to counties of different sizes. Three

counties (combinations of counties) were selected using this method. These counties are: La Salle county +McMullen county, Karnes county, and Bee county. Of the three counties selected, we used the data from voter registration in the four counties. Systematic sampling method is used to select 530 respondents from each PSU. For each county selected, the sampling interval k is calculated as $k=N/n$, where N is the total number of residents in the voter registration data of the selected county, and n is the targeted number of selected respondents (530 in this project). Systematic sampling means that we randomly select one number form the first interval, and from then on, add the interval number to draw the next case, and so on and so forth (Doherty, 1994). The combined total will be 1590. For the voter registration list, we simply used the alphabetical order. Using this method, we presume that only one respondent from each household will be selected.

Assuming non-response rate of 25%, our targeted sample size will be in the range of 1200. In order to increase the response rate with the limited budget, a hybrid survey method with incentive (a free T-shirt for whom completes the questionnaire) was used, which consists of mail survey, online survey, and phone interview. We have mailed the cover letter to each selected respondent, in which a link to online survey is included. The respondents are encouraged to complete the survey online. However, hard copy of questionnaire is also available in both English and Spanish as mail-in option. Then, a pilot phone interview has also been conducted for 50 respondents. The phone interview will be extended in January 2014 in order to increase the response rate.

PRELIMINARY DATA ANALYSIS

By December 8, 2013, a total of 74 responses have been collected, where 62.9% is female and 37.1% is male. Of the 74 respondents, 36.5% are Hispanic, 58.7% are Non-Hispanic White, and 4.8% are other ethnic groups. In the paper, the authors focus on the last section of the questionnaire, i.e. Impact of the Oil and Gas Industry. Of the 74 respondents, 52 respondents have answered all the questions in the last section. The following data analysis is based on the responses from the 52 respondents.

Of the 52 respondents, 59.6% are female and 40.4% are male. About 41.5% of respondents currently work or have family members/relatives working in the oil and gas industry, and about 69.8% of respondents or their family members own mineral rights in the Eagle Ford Shale region. The summary of results is shown in Fig. 1-5 below.

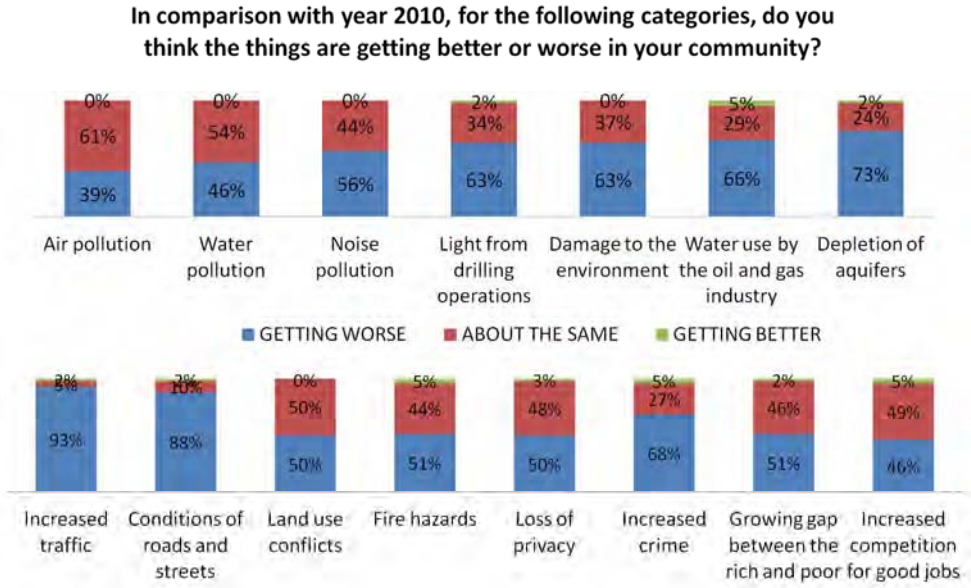

FIG. 1. Respondents' opinions about the changes in detailed categories compared with 2010.

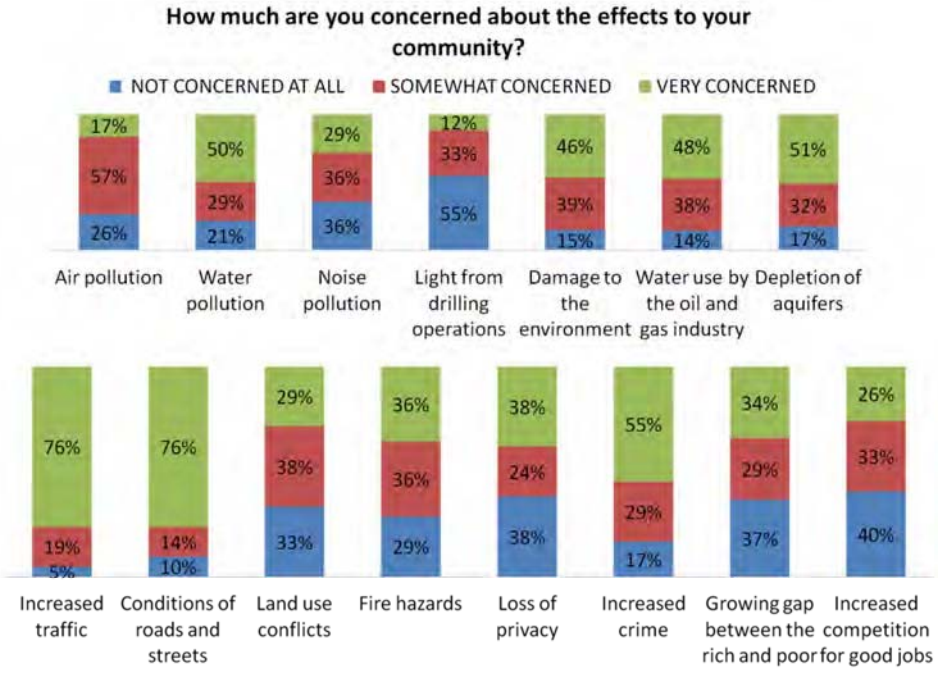

FIG. 2. Respondents' opinions about impacts caused by oil and gas industries in detailed categories.

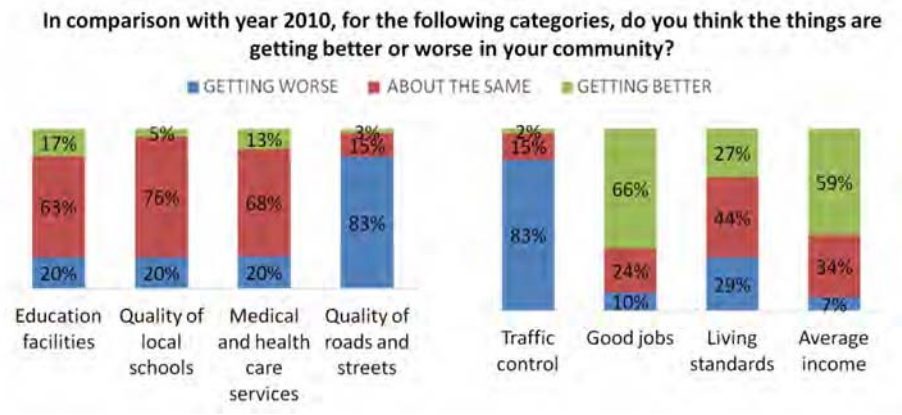

FIG. 3. Respondents' opinions about the changes in general categories compared with 2010.

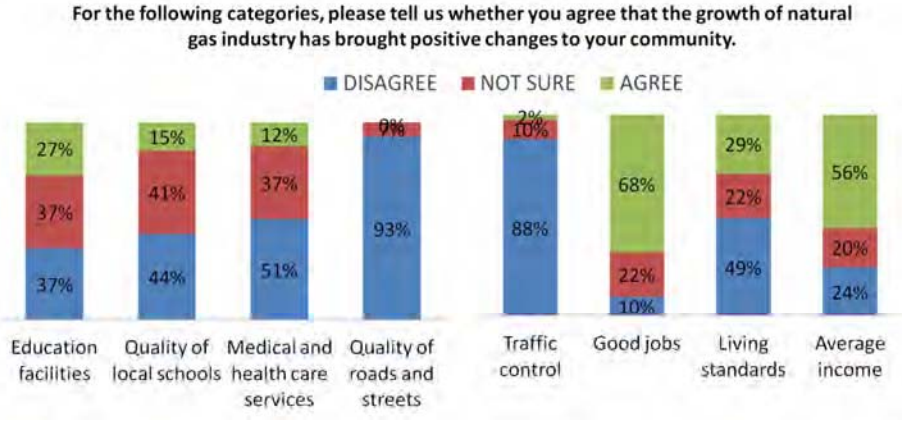

FIG. 4. Respondents' opinions about positive impacts caused by oil and gas industries in general categories.

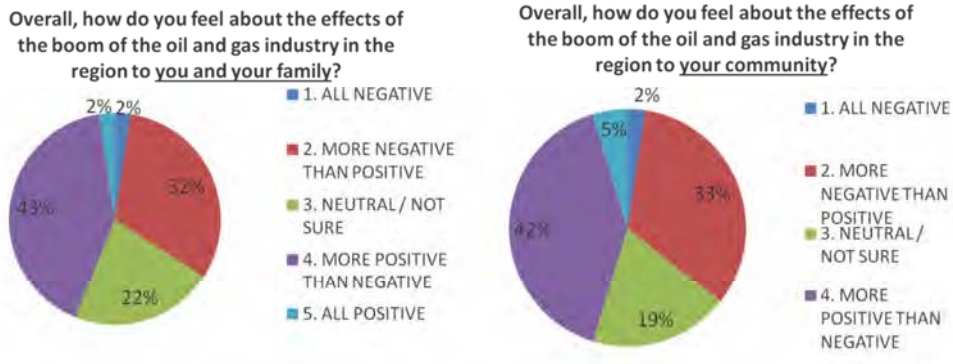

FIG. 5. Respondents' opinions about impacts caused by oil and gas industries to their families and community.

The results shown in Fig. 1 and 2 indicate that water, traffic and road condition, and environmental impacts are the major concerns. In these categories, majority of respondents think the situation are getting worse than 2010. Figures 3 and 4 further indicate that local residents believe traffic and road conditions are getting worse in this region. Local residents however also believe that the job market and average income have improved. Interestingly, respondents have different opinions about the living standards and education facilities. Although there seems to be a sizeable group who think it has more negative than positive coming from Eagle Ford Shale development, more respondents think oil and gas industries generate positive impacts on their families and communities in overall. In order to further analyze the reasons of causing different opinions among respondents, a correlation analysis has been conducted between gender/ethnicity/household income/working status/ownership of mineral rights and opinions of living standards/education facilities/overall effects on family and communities. The significant correlations (p-value < 0.05) are listed in Table 1 with corresponding Pearson correlation values and p-values.

Table 1. Correlation analysis among selected questions

	Living Standards	Education Facilities	Overall Effects on Family	Overall Effects on Community
Gender	-	-	-	-
Ethnicity	-	0.324 (0.022)	-	-
Household Income	0.458 (0.001)	0.386 (0.006)	0.473 (0.001)	0.364 (0.01)
Working Status	-	-	-	-
Ownership of Mineral Rights	-	-0.427 (0.002)	-0.343 (0.015)	-0.329 (0.021)

CONCLUSIONS

Based on the preliminary data collected, it shows that water and traffic and road conditions are the major problems caused by Eagle Ford Shale development in this region. It also shows that local residents have already identified positive economic impacts caused by the oil and gas industries. Both findings are consistent with the results from previous studies. However, local residents do have different opinions on several categories, including education facility, living standards, overall effects on family and communities. The correlation analysis shows that household income plays an important role. The positive correlations with all four categories suggest that the respondents with higher household income have more positive opinions about the Eagle Ford Shale development in all four categories. Furthermore, non-Hispanic respondents are likely than the Hispanic respondents to believe that the education facilities have improved. Also, residents who own or whose family members own mineral rights are more positive about the Eagle Ford Shale development in education facilities, overall effects on family and communities, suggesting their opinions are closely related with benefits they have received during the development. A more

comprehensive analysis will be conducted after sufficient number of responses have been collected.

ACKNOWLEDGMENTS

The authors are thankful to the support provided by College of Engineering, Office of AVP for Research, and Eagle Ford Center for Research, Education, and Outreach at Texas A&M University-Kingsville.

REFERENCES

Adler, N. E., and Rehkopf, D. H. (2008). US disparities in health: descriptions, causes, and mechanisms. *Annu. Rev. Public Health*, 29, 235-252.

Braveman, P. A., Cubbin, C., Egerter, S., Chideya, S., Marchi, K. S., Metzler, M., and Posner, S. (2005). Socioeconomic status in health research. *JAMA: the journal of the American Medical Association*, 294(22), 2879-2888.

Cottrell, F. (2009). *Energy & Society: The Relation Between Energy, Social Change, and Economic Development*. AuthorHouse.

Doherty, M. (1994). Probability versus Non-Probability Sampling in Sample Surveys, *The New Zealand Statistics Review*, March 1994 issue, pp 21-28.

Economic Impact of the Eagle Ford Shale. (2012). Report prepared by Center for Community and Business Research, *The University of Texas at San Antonio*, May 2012.

O'Rourke, D. and Connolly, S. (2003). Just oil? The distribution of environmental and social impacts of oil production and consumption. *Annual Review of Environment and Resources*, 28(1), 587-617.

Pleeter, S. (1980). *Economic impact analysis: Methodology and applications*. M. Nijhoff Pub.

Issues and Options for Oversize/Overweight Permitting of Petroleum-Related Trucks in a Performance-Based Regulatory Context: The Manitoba Experience

Mark J. Reimer, M.Sc. Student, EIT, S.M.ASCE[1],
Jonathan D. Regehr, Ph.D., P.Eng., A.M.ASCE[2], and Jan McKee[3]

[1]Research Associate, Department of Civil Engineering, University of Manitoba, E1-327 EITC, 15 Gillson Street, Winnipeg, Manitoba, Canada R3T 5V6, Email: umrei234@cc.umanitoba.ca
[2]Assistant Professor, Department of Civil Engineering, University of Manitoba. E1-310 EITC, 15 Gillson Street, Winnipeg, Manitoba, Canada R3T 5V6, Email: regehr@cc.umanitoba.ca
[3]Director, Trucking Relations, Manitoba Infrastructure and Transportation. 420-215 Garry Street, Winnipeg, Manitoba, Canada R3C 3Z1, Email: jan.mckee@gov.mb.ca

ABSTRACT: This paper presents a case study of the Manitoba experience in permitting petroleum-related oversize/overweight (OS/OW) truck traffic. In recent years, Southwest Manitoba, along with many regions throughout North America, has experienced rapid growth and change in the petroleum industry. This growth has fuelled economic development and also caused infrastructure challenges on rural roads that are being used by unique vehicle configurations, many of which are beyond basic truck size and weight (TSW) limits. Manitoba's OS/OW permitting program for these vehicles stems from the performance-based approach to TSW regulation being used in Canada since 1988 and relies on ongoing collaboration with the petroleum industry. Manitoba's experiences have led to several insights, which may be options for other jurisdictions facing similar issues related to OS/OW petroleum-related trucking. These insights include: (1) purposeful collaboration with the industry and officials in neighbouring jurisdictions to understand permitting needs and barriers; (2) supplementing qualitative understanding of the industry with quantitative data; and (3) identifying opportunities to expedite permitting procedures by issuing annual permits to routinely-configured vehicles, utilizing technologies to assist with TSW enforcement, and rationalizing permit fee structures.

INTRODUCTION

Southwest Manitoba, along with many regions throughout North America, has experienced rapid growth and change in the petroleum industry in recent years. This industry growth has been caused by technological improvements in extraction techniques, such as horizontal drilling and hydraulic fracturing, and advancements in geological exploration. The changes in the industry have helped stimulate regional economic development but have resulted in infrastructure challenges along rural, low-volume highways and roads. Historically, this rural infrastructure in Manitoba has served farm to market related truck trips which exhibit temporal patterns reflective of the seeding and harvesting seasons. While truck traffic volumes and vehicle types have gradually evolved for the agriculture industry, the recent and

growing freight transportation demands of petroleum development and production have resulted in marked increases in truck volumes, the introduction of new vehicle types, and unique spatial and temporal trip-making patterns which cause additional stress on rural highway infrastructure.

Certain vehicles required for moving equipment and product related to the petroleum industry do not comply with "basic" provincial truck size and weight (TSW) regulations in terms of dimensions, gross and axle weight, or axle configuration. In addition, trip origins and destinations and the temporal dynamics of industry operations commonly necessitate concentrated access for these vehicles on local road networks. Therefore, to facilitate petroleum industry operations and to encourage regional economic development, local road authorities (provincial and municipal) develop permitting programs and routing plans for industry-specific oversize/overweight (OS/OW) vehicles. These programs and plans aim to balance economic growth with public objectives of infrastructure protection and on-road operational safety.

The purpose of this paper is to present a case study of the Manitoba experience in permitting petroleum-related OS/OW truck traffic. Specifically, the objectives of this case study are to:

- Synthesize the Canadian performance-based approach to truck size and weight regulation and permitting;
- Highlight the unique challenges of permitting petroleum-related OS/OW truck traffic by characterizing the petroleum industry and transportation system in Southwest Manitoba, analyzing field data to demonstrate the prominence of permitting truck configurations in the region, and describing the petroleum-specific elements of the OS/OW permitting process in Manitoba; and
- Discuss insights and options concerning OS/OW permitting of trucks for the petroleum industry.

Components and details of this paper are specific to the Manitoba experience with permitting trucks for the petroleum industry. However, the findings from this paper can assist jurisdictions in developing public policy and support transportation engineering decision-making for pavement and bridge design and truck permitting and routing through improved understanding of OS/OW truck traffic characteristics of the petroleum industry.

CANADIAN APPROACH TO TRUCK SIZE AND WEIGHT REGULATION

In 1988, representatives from all Canadian provinces and territories signed the Memorandum of Understanding Respecting A Federal-Provincial-Territorial Agreement on Vehicle Weights and Dimensions. Colloquially, this is referred to as the RTAC MoU, which credits the organization overseeing the signing of the document, namely, the Roads and Transportation Association of Canada. This signing was the culmination of several years of technical research concerning the impacts of truck loads on pavements and bridges and the relationship between vehicle configuration (i.e., number of axles, axle spacing, trailer coupling devices) and dynamic stability and control. The main objectives of the MoU were to: (1) improve regulatory uniformity across jurisdictional boundaries; (2) enable economic

opportunity by purposely increasing truck productivity; and (3) ensure that the newly regulated, more productive vehicles met specified safety-related dynamic performance criteria (Woodrooffe et al. 2010; Regehr, Montufar, and Clayton 2009).

The RTAC regulations enabled truck productivity improvements on primary Canadian highways for both payload weight and cubic capacity. From a weight perspective, the current regulations limit axle weights as follows: 5,500 kg (12,125 lb) on the steer axle of a tractor; 9,100 kg (20,020 lb) on a single axle (dual tires); 17,000 kg (37,400 lb) on a tandem axle; and 21,000 to 24,000 kg (46,200 to 52,800 lb) on a tridem axle (depending on axle spread). Gross vehicle weights (GVWs) are normally the sum of axle load limits, though the gross weight for some configurations is capped. On RTAC (i.e., primary) routes, a standard five-axle tractor semitrailer is limited to 39,500 kg (86,900 lb), a six-axle tractor semitrailer is limited to 46,500 kg (102,300 lb), and an eight-axle B-train configuration is limited to either 62,500 or 63,500 kg (137,500 to 139,700 lb), depending on route and province. The introduction of the tridem axle group for use on both single-trailer and multiple-trailer trucks was a key aspect of the RTAC MoU. From a cubic perspective, tractor semitrailer and truck-trailer combinations are limited to 23 m (75 ft) and double-trailer trucks are limited to 25 m (82 ft). Trailer lengths are limited to 16.2 m (53 ft) (Woodrooffe et al. 2010; IBI Group and ADI Limited 1987).

For the most part, the regulations in effect today are the same as those originally envisaged by the MoU, though their applicability has broadened in terms of the extent of the highway network to which they apply. This network densification has occurred as communities and industries without connectivity to the RTAC (i.e., primary) network lobby for infrastructure upgrades to enable access for the most productive trucks. Minor modifications have occurred as jurisdictions continue to harmonize regulatory details and respond to dynamic industry needs.

The development and implementation of the RTAC MoU has gained international recognition as the first to apply a performance-based approach to truck size and weight regulation. In essence, the performance-based approach sought to regulate vehicles based on infrastructure impact and vehicle stability and control criteria such as braking, off-tracking, and roll stability. Based on a thorough engineering understanding of these impacts, truck size and weight "envelopes" providing a full vehicle specification of weight, axle configuration, and length limits were developed (Woodrooffe et al. 2010). In this regard, the Canadian approach departs from the somewhat more prescriptive approach to regulating truck size and weight in the United States (save for perhaps the Federal Bridge Formula, which can be understood as a performance-based regulatory approach). Notably, performance-based standards existing in Australia and elsewhere have extended the Canadian approach (Organisation for Economic Cooperation and Development 2011).

The foregoing discussion provides background concerning the Canadian approach to "basic" truck size and weight regulations. In other words, in general, trucks can operate on designated highway networks at these weight and length limits without a permit. Complexities do exist—for example, seasonal changes, trailer connections, tire size, vehicle age, *inter alia*—and these complexities have important operational impacts (Montufar and Clayton 2002). Beyond these basic limits, all provinces also permit OS/OW loads. These permits fall into two classifications: (1) annual "blanket"

permits, which are routinely issued to carriers for unlimited trips by "standard" OS/OW truck configurations on predetermined highway networks; and (2) single-trip permits issued on a trip-by-trip basis where the carrier seeks approval of a proposed route. In both cases, proposed truck configurations are typically subject to engineering analyses concerning pavement and bridge impacts and dynamic performance similar to the assessments done to support the RTAC MoU.

In many Canadian provinces, longer combination vehicles (LCVs) have become the most common type of vehicle operating under annual permits. These vehicles, which exceed basic vehicle length limits but operate within basic weight limits, are permitted on certain highways as standard configurations (namely, the Rocky Mountain double, the Turnpike double, and the triple trailer configuration). Permits are granted to these vehicles because of the cubic productivity benefits they provide. In contrast, carriers operating industry-specific vehicle configurations, such as those for use in the petroleum sector, must normally obtain single-trip permits. This relies on an administrative process between the carrier and the highway agency and requires engineering assessments.

PERMITTING OF PETROLEUM-RELATED TRUCK TRAFFIC IN MANITOBA

This section contains three sub-sections. The first sub-section characterizes petroleum industry activity and the transportation system in Southwest Manitoba, focusing particularly on issues that relate to OS/OW truck permitting in the Manitoba context. The second sub-section utilizes field data to demonstrate the types of vehicle configurations prominent within the petroleum-producing region of Manitoba. The third sub-section describes the permitting process used in Manitoba and specific efforts to accommodate the unique needs of the petroleum industry.

The Petroleum Industry and Transportation System in Southwest Manitoba

Over the last decade, Southwest Manitoba has seen considerable growth in petroleum well development and the production of petroleum products. This growth, depicted in Figure 1 in terms of annual well development, generates truck trips on local and regional transportation networks, with economic, infrastructure, and safety impacts. Manitoba has seen over 500 new wells drilled annually for the last three years, and currently has over 6400 producing wells. Like many other petroleum-producing regions where hydraulically fractured horizontal wells are used, well development and production in Manitoba can be divided into four broad stages: (1) site preparation; (2) drilling; (3) hydraulic fracturing; and (4) production. Understanding how these stages impact truck trip-making characteristics—such as origin-destination patterns, trip generation rates and temporal variations, vehicle configurations, and routing—is an important component of building a truck permitting program that responds to industry needs while also achieving public sector objectives.

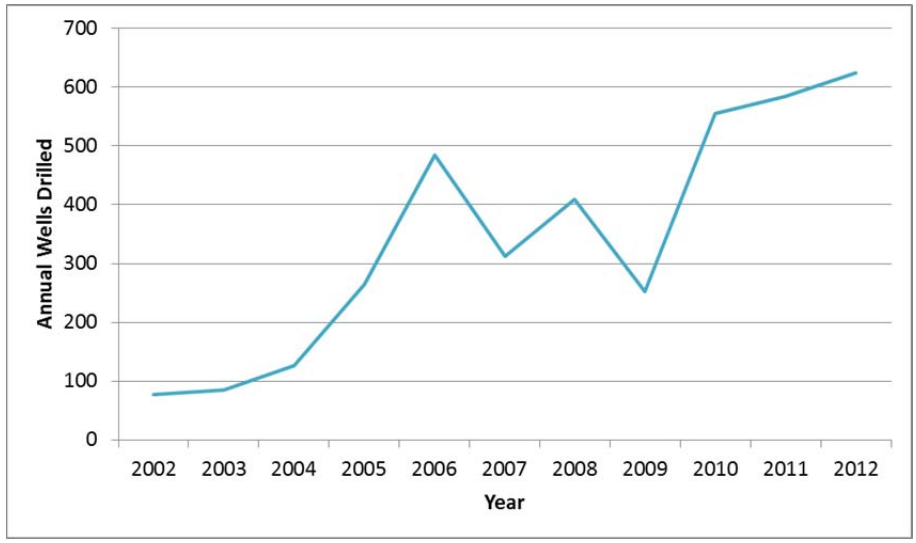

FIG. 1. Wells Drilled in Southwest Manitoba by Year.

Origin-destination patterns: A well serves as both a destination for inputs (such as freshwater, sand, and equipment) and as an origin of equipment, supplies, water, and oil once the well is producing. At a regional scale in Manitoba, both inputs and outputs are moved by truck, rail, pipeline, or a combination of these three modes, but movements to and from well sites are handled principally by truck. In certain more mature petroleum-producing areas utilize flowlines to transport water and petroleum products to and from well sites. Truck traffic trip lengths depend on the location of wells, materials and supplies, and transload facilities. Lengths can vary between 50 and 250 km (30 and 150 miles) and can change quickly as origins and destinations are dynamic. For example, while producers will attempt to minimize travel distance, the source locations for the water used in the fracturing process commonly change as withdrawal limits or disposal capacity limits are reached, leading to longer distances (Quiroga, Fernando, and Oh 2012).

Trip generation rates and temporal variations: The total number of truck trips generated by a well varies geographically as a function of the extraction process, geological conditions, well depth, horizontal length, and water requirements (Quiroga, Fernando, and Oh 2012). In Manitoba, the geological conditions are such that approximately 140 to 250 loaded trucks, of various configurations, are required to bring one well to production. In comparison, wells in New York and North Dakota can require up to 1100 loaded truck trips per well (Upper Great Plains Transportation Institute 2010). In all cases, the majority of truck trips involve moving water to and from the well during the fracturing process.

Trip generation also varies temporally. In Manitoba, it takes approximately 25 days to bring a well to completion, though duration of each stage of development varies and interruptions may occur between stages. Understanding and predicting when and where truck traffic trips are generated can be difficult given the sporadic timing of these stages. Adding to this complexity, horizontal wells can be re-fractured to increase productivity after a certain time period. The fracking process leads to concentrated truck trip generation over a short time period as the process, once

started, must continue uninterrupted until completed. Activity also fluctuates seasonally, as indicated by the number of active drill rigs in the region which ranges from zero during spring thaw to as many as 20 or 25 rigs in peak drilling periods.

Vehicle configurations: The petroleum industry requires unique vehicle configurations to transport various commodities and equipment to and from well sites; certain configurations fall beyond "basic" TSW regulations and must operate under OS/OW permits. In Manitoba, the following vehicle configurations are commonly used during the four stages of well development:

1. Site Preparation: heavy equipment movers (e.g., truck mounted cranes)
2. Drilling: drill rigs, open hole loggers, cementers, service rigs for completion
3. Hydraulic fracturing: coil tubing unit, blenders, pumper trucks, service rigs for completion
4. Well production: heavy equipment for lease return and pump-jack setting

Examples of non-standard configurations from these stages are shown in Figure 2.

FIG. 2. Examples of Permitted Vehicles, Clockwise from Top Left: Drill Rig; Truck Mounted Crane for Equipment Moving; and Service Rig

Routing: In Southwest Manitoba, truck routing occurs on a road network originally designed and maintained to support agriculture-related truck traffic. The network consists of paved highways (provincial jurisdiction), gravel roads (primarily municipal jurisdiction), and dirt roads (municipal jurisdiction). The provincially-managed road network has three load classes, RTAC, A1, and B1, with GVW limits (depending on configuration and season) of 62,500 kg (138,000 lbs), 56,500 kg (125,000 lbs), and 47,630 kg (105,000), respectively. This network is shown in Figure 3 along with the designated oilfields in the region.

As discussed, certain truck configurations operating in the oil and gas industry exceed weight limits on the highest rated roads (i.e., RTAC roads) and therefore may operate well beyond weight limits on the lower class roads that provide access to materials and wells. Effective permitting programs can help manage movements by these types of configurations and help reduce the proportion of illegally overloaded

trucks. Though no Manitoba-specific information is readily-available, in some North American petroleum producing regions, estimates are that up to 25 percent of trucks operating may be overloaded and unpermitted (Tolliver 2013).

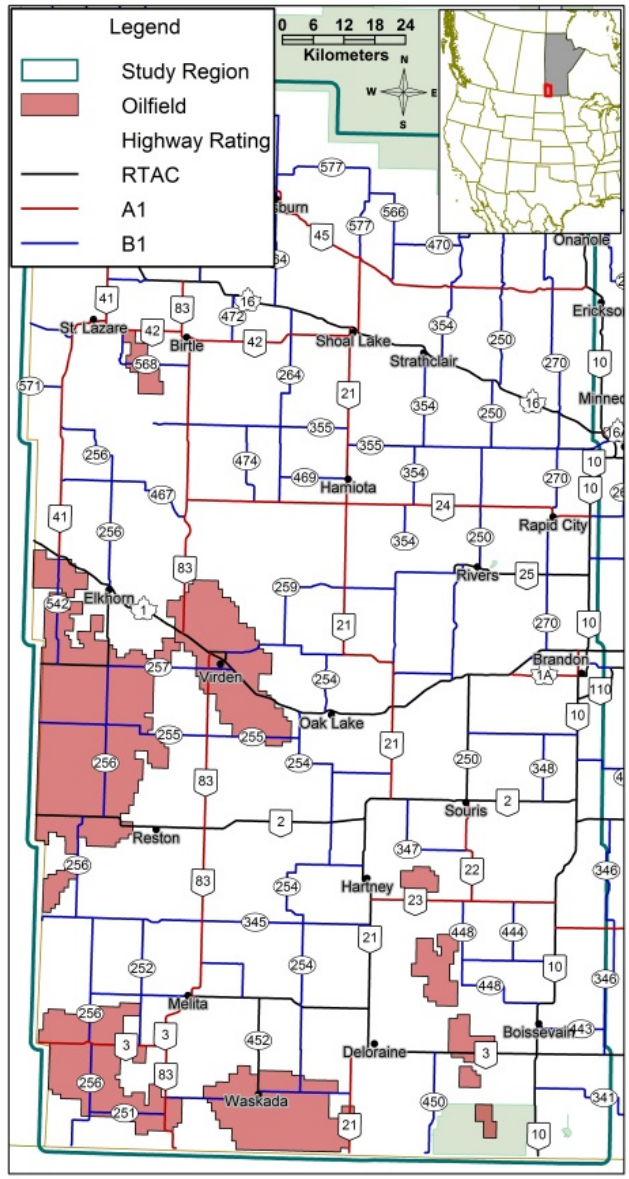

FIG. 3. Provincial Road Network by Load Class in Southwest Manitoba

Illustrative Analysis of Petroleum-Related Trucking in Manitoba

Manitoba has recently made efforts to improve understanding of petroleum-related truck activity—including OS/OW trucking—by developing data collection programs directed at characterizing truck traffic in the southwest region. Existing (total) traffic datasets provide evidence of general increases in annual average daily traffic (AADT) on many road segments in Southwest Manitoba. These increases reflect similar growth patterns found in other petroleum-producing regions, such as Pennsylvania

and North Dakota (Gannet Fellming 2011; Tidd 2013; Upper Great Plains Transportation Institute 2010; Upper Great Plains Transportation Institute 2013). In addition, readily-available industry information such as the number of wells being drilled each year and the number of active drill rigs in the region provides an indication of petroleum-related economic development. However, until recently there has been limited information about truck traffic available.

To fill this data gap, a short-term (48-hour) classification count program (among other data collection efforts) was designed and implemented in the summer of 2013. Count locations were manually selected based on total traffic volume changes, locations with recent and ongoing well development, and proximity to key terminals and facilities. Classification data were collected using the standard Federal Highway Administration (FHWA) 13-vehicle classification scheme, but raw data (in per-vehicle format) were also retained which provide details on the number and spacing of axles. While these counts do not capture temporal variations evident in the industry, the data do enable more robust analysis of the unique configurations serving the petroleum industry.

Figure 4 illustrates the capability of these data by showing the vehicle class distributions (VCDs) obtained from four 48-hour classification sites near the Pierson oilfield, adjacent to the Saskatchewan and North Dakota borders. The distributions shown are unique to oilfield activity in Manitoba, Saskatchewan, and Alberta, as evident by the high percent of class 10 trucks (Reimer and Regehr 2014).

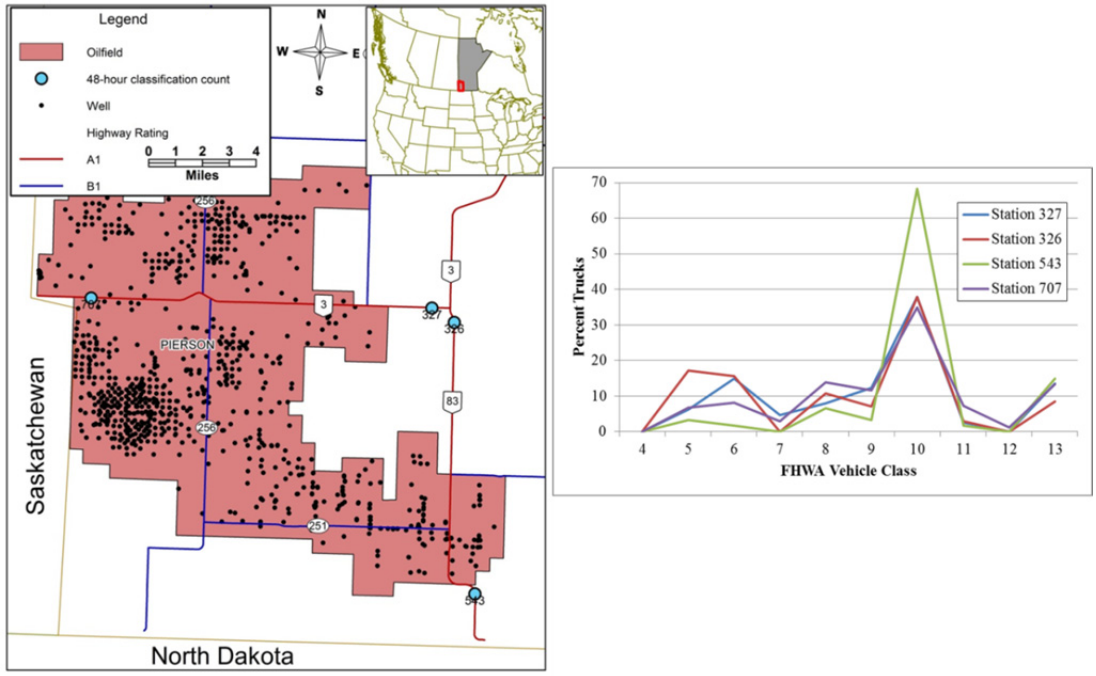

FIG. 4. Pierson Oilfield in Southwest Manitoba with Four 48-Hour Classification Counts and Their Corresponding Vehicle Class Distributions

A preliminary analysis of the raw data used to generate these VCDs indicates that between 10 and 20 percent of the truck traffic observed during the 48-hour count may require a permit. This range is derived based on an analysis of axle configurations only, and does not reflect overweight trucks (conventional or non-standard configurations) that may also require permits.

Table **1** provides sample data from these counts (in per-vehicle format) for the same three configurations shown in Figure 2, namely a drill rig, a crane, and a service rig. Each of these configurations would require a special permit because of their unique axle configurations, and possibly also because of axle loads.

The table shows the FHWA class assigned to these configurations using the standard classification algorithm. The drill rig falls into class 10 (six- or seven-axle single-trailer trucks), the crane falls into class 11 (five-axle double-trailer truck), and the service rig falls into class 8 (four-axle single-trailer truck). In the latter two cases, the presence of the tandem steer axle group appears to cause the standard algorithm to classify the vehicles differently than how one might classify them visually. This underscores the need for a thorough understanding of industry-specific configurations when interpreting the data and retention of the detailed axle spacing data.

Table 1. Sample Data Collected from 48-Hour Classification Counts

		Axle Spacing (cm)					
Vehicle	**FHWA Class**	**1 - 2**	**2 - 3**	**3 - 4**	**4 - 5**	**5 - 6**	**6 - 7**
Drill Rig	10	183	600	134	844	155	152
Crane	11	186	561	137	137		
Service Rig	8	183	728	168			

NOTE: 1 cm = 0.394 in.

Permitting of Petroleum-Related Trucks

Oversize and overweight trucks in Manitoba must follow an approval process defined by Manitoba Infrastructure and Transportation (MIT). All OS/OW vehicles must apply for permits. Application approval is based on an assessment of public safety impacts, current condition of infrastructure, characteristics of the vehicle, and the route proposed by the carrier. To apply for a permit, carriers submit information regarding a vehicle's dimensions, GVW, axle spacing, and axle weights. Permits may be granted with restrictions such as scheduling, speed reductions, designated travel lane, and escorts or inspections. Permits are issued in two categories:

- One move permits may be issued for OS/OW vehicles on specific routes when that vehicle's weight or dimensions are not normally allowed on the route. The movement of a drill rig is a common situation requiring one move permits in Southwest Manitoba. (Blanket permits valid for several months may be issued for OS/OW vehicles when a route will be regularly used by the same vehicle and an engineering analysis has been completed on the route).

- Annual permits are issued for routinely-configured OS/OW vehicles travelling on roads where the province is the traffic authority. Multiple trips can be made under an annual permit.

One move and annual permits may be issued without a bridge assessment for overweight truck configurations that fall within specified axle weight and/or GVW limits. These limits are:

- 21,960 kg (48,310 lb) for an eight-wheel tandem axle group (the maximum legal limit on RTAC roads is 17,000 kg);
- 27,500 kg (60,500 lb) for a 16-wheel tandem axle group, 12-wheel tridem axle group, and 24-wheel tridem axle group (the maximum legal limit for tridems on RTAC roads is 24,000 kg);
- 16,000 kg (35,200 lb) for a tandem steer axle group;
- 22,000 kg (48,400 lb) for a tridem drive axle group;
- 38,000 kg (83,600 lb) for the GVW of a non-articulated straight truck; and
- 60,000 kg (132,000 lb) for the GVW of articulated trucks.

Configurations exceeding these limits require bridge assessments, which in extreme cases may involve a detailed load rating on every bridge along a proposed route.

Currently, Manitoba has expedited the permitting process by developing and issuing annual permits for OS/OW vehicles routinely required by the petroleum industry. These annual permits can in some cases replace one move permits which are administratively burdensome. The annual permits most commonly issued for the industry include service rigs, winch-bed trucks, concrete trucks, and pumper trucks. These vehicles are straight trucks (non-articulated), exceed the axle or GVW limit on routes in the area, and have permanently mounted apparatus (PMA).

Figure 5 shows two examples of different petroleum-related trucks with PMA currently operating under annual permits in Manitoba. PMA trucks that operate with non-divisible loads, such as a service rig, are allowed a GVW and maximum axle group weights that are independent of highway load rating. When loads are divisible, such as the case for a winch truck, GVW and axle group weights vary by highway load class and the spread of the drive axle group. The legal and maximum permitted weights for axle groups of the trucks in Figure 5 are summarized in Table 2.

FIG. 5. Winch Trucks Operating Under Annual Permits in Southwest Manitoba

Table 2. Legal and Permitted Axle Loads for PMA Divisible Load Straight Trucks

	Legal Limit (kg)	Maximum Limit by Annual Permit (kg)
PMA divisible load straight truck with single steer and tridem drive		
Single steer axle	7300	9100
Tridem axle	17,000	22,000
PMA divisible load straight truck with tandem steer and tandem drive		
Tandem steer axle	7300	16,000
Tandem drive axle	17,000	21,960

CONLUDING REMARKS ON MANITOBA'S PERMITTING EXPERIENCE

Manitoba's experiences in permitting specialized vehicles serving its growing petroleum industry are shaped by Canada's performance-based approach to truck size and weight policy and collaboration with the industry. Examination of these experiences leads to the development of the following insights, which may provide options for other jurisdictions facing similar challenges.

- The rapid emergence of the petroleum industry in Manitoba using hydraulic fracturing and directional drilling techniques has necessitated a concerted public sector effort to understand the industry, its economic drivers, and its impacts on local and provincial economies, infrastructure, and the environment. To facilitate this understanding and foster dialogue, the province has initiated a standing stakeholder committee which seeks to find reasonable balances between the interests of the industry (including petroleum extraction companies and the companies that serve the industry) and the municipal and provincial agencies that oversee resource conservation, infrastructure and transportation, water resources, and planning. Better understanding of industry needs, including truck permitting needs, enables more cohesive delivery of relevant policies and programs.
- Related to the foregoing point, there is a need to support qualitative industry understanding with quantitative data. To this end, the provincial government has invested in developing targeted truck traffic data collection to better support infrastructure maintenance activities, planning decisions, and permitting practices. This data collection effort focuses on truck traffic volume, vehicle classification, axle and gross vehicle weight, commodity flows, and modal share (Reimer and Regehr, in press).
- Special permitting practices aim to balance the needs of industry with the objectives of infrastructure protection and on-road safety. To achieve this, the permitting process relies on engineering assessments of infrastructure impacts and vehicle performance; these assessments take time. Manitoba has expedited this process by issuing annual permits for commonly utilized OS/OW vehicles for the petroleum industry. The Manitoba experience

suggests that the straight trucks with permanently mounted apparatus be considered for these types of permits; additional configurations may also be candidates subject to further analysis. In addition, there may be opportunities to reduce barriers to interprovincial transportation by collaborating with neighbouring jurisdictions and to utilize technologies that facilitate self-issuance of permits. As with other routinely-permitted vehicles in Canada (e.g., LCVs), this process facilitates more timely administrative responses to industry needs while still holding true to the performance-based principles that underpin truck size and weight regulation in Canada.

- Jurisdictions with long-standing and extensive petroleum industry activity, such as Texas, have existing OS/OW permitting methods in place specific to trucks involved in oil and gas development. Reviewing established regions and practices can assist jurisdictions develop solutions to the issues introduced by the petroleum industry.
- The adage that "freight knows no boundaries, but trucks do" is apt for specially-permitted trucks serving the petroleum industry. In this context, "boundaries" arise between provinces, between a province and a municipality, and between countries when permitting practices are not harmonized between jurisdictions. The demand for cross-jurisdictional petroleum-related freight movement is evident, yet productivity is sometimes diminished by administrative inconsistencies. Manitoba collaborates with neighbouring provinces on size and weight issues in an effort to reduce barriers for cross-jurisdictional moves. Perhaps the performance-based regulatory approach offers a way forward to resolve these differences.
- When opportunities arise to issue routine special permits, jurisdictions may choose to attach conditions to the granting of this permit that enable the carrier to demonstrate compliance with relevant permit conditions, thus improving transparency and easing the burden of traditional on-road enforcement activities. Real-time demonstration of compliance using satellite-based tracking and vehicle monitoring systems, subject to occasional audits, is plausible in Manitoba.
- Like other jurisdictions experience with growth in petroleum-related truck traffic, the issue of establishing appropriate permit fees is one which has garnered considerable attention. While not the direct focus of this paper, Manitoba has considered various models for structuring special permit fees, principally options based on cost recovery principles. Related to this is the establishment several years ago of the Manitoba Truck Productivity Improvement Fund, which has as its intent to dedicate permit revenues for infrastructure upgrades (not necessarily only those related to the petroleum industry). Whatever approach is ultimately taken, rational and transparent fee structures are most likely to gain acceptance with industry.

The intent of providing the foregoing insights is to share Manitoba's experience concerning the permitting of petroleum-related trucks; these insights may bring forward options to consider in other jurisdictions facing similar challenges. As the petroleum industry continues to change (and change rapidly), these experiences also evolve and ongoing efforts are needed to balance private and public sector concerns.

REFERENCES

Reimer, M.J. and Regehr, J.D. (in press). "A framework for characterizing truck traffic related to petroleum well development and production in unconventional shale plays." *Transportation Research Record: Journal of the Transportation Research Board,* Transportation Research Board of the National Academies, Washington, D.C., 2013.

Montufar, J. and Clayton, A. (2002). "Seasonal weight limits on prairie region highways: Opportunities for rationalization and harmonization." *Canadian Journal of Civil Engineering*, vol. 29: 8-16.

Regehr, J.D., Montufar, J., and Clayton, A. (2009). "Lessons learned about the impacts of size and weight regulations on the articulated truck fleet in the Canadian prairie region." *Canadian Journal of Civil Engineering*, vol. 36: 607-616.

Woodrooffe, J., Sweatman, P., Middleton, D., James, R., and Billing, J.R. (2010). "Review of Canadian Experience with the Regulation of Large Commercial Motor Vehicles." *NCHRP Report 671*, Transportation Research Board, Washington, D.C.

IBI Group and ADI Limited. (1987). "Economics of Truck Sizes and Weights in Canada." Roads and Transportation Association of Canada, Ottawa, ON.

Organisation for Economic Cooperation and Development and the International Transport Forum. (2011). "Moving Freight with Better Trucks." Organisation for Economic Cooperation and Development, Paris.

Quiroga, C., Fernando, E., and Oh, J. (2012). "Energy Developments and the Transportation Infrastructure in Texas: Impacts and Strategies." *Report FHWA/TX-12/0-6498-1*, Texas Transportation Institute, College Station, Texas.

Upper Great Plains Transportation Institute (2010). "Additional Road Investments Needed to Support Oil and Gas Production and Distribution in North Dakota." North Dakota Department of Commerce.

Upper Great Plains Transportation Institute (2013). "Impacts to Montana State Highways due to Bakken Oil Development." Montana Department of Transportation.

Gannet Fellming (2011). "Marcellus Shale Freight Transportation Study." Northern Tier Regional Planning & Development Commission.

Tidd, L. (2013). "Consideration of Shale Gas Development Impacts in Long-Range Transportation Planning." *Proc., Transportation Research Board Annual Meeting*, Washington, D.C.

Tolliver, D. (2013). "Effects of Oil & Gas Development on Highway Infrastructure Investments: Case Study of the Bakken Shale," *Proc., Transportation Research Board Annual Meeting*, Washington, D.C.

Reimer, M. and Regehr, J.D. (2014). "A Hybrid Approach for Clustering Vehicle Classification Data to Support Regional Implementation of the Mechanistic-Empirical Pavement Design Guide." In *Transportation Research Record: Journal of the Transportation Research Board,* No. 2339 Transportation Research Board of the National Academies, Washington, D.C., 2014, pp. 112-119.

Geosynthetic Solutions for Paved and Unpaved Applications

D. Lipomi[1], M.B.A., E.I.T., ASCE, and M. H. Wayne[2], Ph.D., P.E., M. ASCE

[1,] Tensar International Corporation, 258 Strawberry Circle, Cranberry Township, PA 16066, U.S.A., E-mail: dlipomi@tensarcorp.com.
[2] Tensar International Corporation, 2500 Northwinds Parkway, Suite 500, Alpharetta, GA 30009, U.S.A., E-mail: mwayne@tensarcorp.com.

ABSTRACT: Geogrid use at current US drilling facilities within the Marcellus and Utica Shale regions, as well as lesser publicized shale formations, have given the Operators and Producers a way to increase the performance of their access roads and well pads. Within this market, the construction costs for these roads have increased dramatically as a direct result of the presence of areas of soft soil or unforeseen environmental impacts (e.g. cold weather). Since some of these companies have started to include geogrids into their road and well pad sections, the time for construction has been reduced, the road and well pad have been and remain stabilized, and most importantly, their construction costs have been greatly reduced. One producer in PA has saved $1.4 million in construction costs, and still maintains an incredible access road that requires little to no maintenance. This paper explains how geogrids enhance performance over conventional construction methods and documents this performance through the inclusion of case histories that will help more companies in the Oil and Gas Market better understand how they can utilize this same approach in their current operations.

INTRODUCTION

Throughout the United States, the recent drilling for natural gas, oil and other methods of energy have led to an explosion of design, engineering and construction, These services are necessary to support a number of different upstream applications, which is vital to unlock these energy resources within the earth. Unfortunately, these services add an incredible amount of expense to these companies. On top of this, midstream applications have similar expenses for its work in the Shale formations.

The objective of this research letter is to illustrate how the inclusion of a geogrid can greatly reduce the construction costs, as well as peripheral costs, while increases the performance of the roadway or well pad. This will be shown with real world data that an energy producer actually reported as an added savings to the conventional method of construction.

GEOGRID USE AS AN ALTERNATIVE

The conventional methods of construction of roads and well pads have been to use stone and, sometimes, a geotextile. While geotextiles are great for drainage and separation, Army Corp of Engineer (ACOE) states that no structural benefit shall be given to a roadway section for the use of a geotextile. Because of this, engineers have to design roadways with just stone in mind. A change in technology in the past forty years has been to use another geosynthetic whereby a contractor can install less stone and immediately improve the performance of a road.

Effort has to be taken to show why using massive amounts of stone alone are not the answer to many roads with unsuitable foundation soils. Dr. Kinney's work during his tenure at the University of Alaska, visually demonstrated unstabilized aggregate behavior. He placed colored aggregate on a Plexiglas sheet and filmed it from the bottom up. He then trafficked the colored aggregate with an Air Force C-130 tire. He noted that the aggregate moved in a fishhook pattern as illustrated in Figure 1 below.

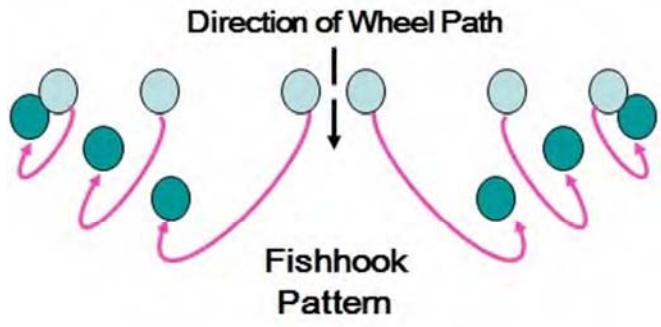

Figure 1 – Aggregate response to simulated traffic loading

This test verified that the downward and lateral movement of stone is detrimental to the performance of the road. In February of 2003, the USACOE released *Engineering Technical Letter (ETL) 1110-1-189* that added support to this work. In the ETL, three mechanisms are identified for stabilizing a road with a geosynthetic. They are: (a) lateral restraint, (b) improved bearing capacity, and (c) tensioned membrane effect. Further, the letter states that "in the early stages of research regarding geogrid reinforcement of pavement systems, the tensioned membrane effect was thought to be the primary reinforcement mechanism. However, subsequent investigations have shown that reinforcement benefits are obtained without significant deformation of the pavement section. Thus, lateral restraint has been identified as the primary mechanism.

What is required is a product that will lock the stone into place, not allowing it to move downward or laterally. This is where geogrid comes into play because of its main function of stabilization, which involves the mechanical interlock and confinement of aggregate. Interlock prevents aggregate from moving into a soft subgrade through downward movement. The confinement of aggregate within the geogrid apertures stabilizes the aggregate layer, preventing lateral movement while

being trafficked and increasing the load bearing capacity. The USACOE noted that tensile properties have very little to do with the performance of a geosynthetic within a roadway section. This is why the USACOE does not allow the thickness of stone to be reduced when using a product that quotes tensile properties alone. What is needed is a product that will keep the stone in place, allowing it to do the brunt of the work in supporting the traffic loads. A design methodology has been developed by Giroud and Han (2012a, b), the authors state that any geosynthetic using in this methodology requires proper validation and calibration. Because of this, geogrids need to be calibrated and validated for use of the Giroud-Han Design Methodology to determine the aggregate thickness required for subgrade improvement. The geogrid allows for stone thickness to be reduced in a road section giving the same performance as a section constructed with substantially more aggregate.

PROJECT OVERVIEW

In Clearfield County, Pennsylvania, an energy producer was building a number of well pads and associated access roads in the State Game lands. This area has roads that are governed and maintained by the Department of Conservation of Natural Resources (DCNR) and the Bureau of Forestry. The public roads were utilized by the energy producer with vehicles and equipment for construction, drilling, hydraulic fracturing, and other associated well activities. As part of the agreement between the Forestry Service and the energy producer, the roads needed to be built and maintained at the cost of the operator so the public is able to use the roadways. Building a nine and a half mile road that would be able to stand up the vehicular traffic would be incredibly expensive.

The site conditions were adding to the potential expense because of the climate and foundation soils. This region of Pennsylvania lies within the snowbelt. It sees a great deal of lake effect snow due to its proximity to Lake Erie. This causes the snow to accumulate on the roads, where trucks traffic the roads before the plows can clear them. As trucks drive on snow covered roads, 15.2 cm (6 in.) of snow can change to 5.1 cm (2 in.) of ice, in what is locally referred to as an ice lens. After that, more aggregate is brought in to maintain the roads, and then it snows which starts the cycle over again. The whole system is a lamination of ice and stone. The Forestry Service was concerned that arrival of the spring thaw would lead to an unstable mess.

Another concerning factor to local officials was the moisture that would be retained in the clay subgrade. This also leads to an unstable roadway when the spring-thaw hits. These two conditions would make roads impassable in the spring months.

CONTRACTOR CHALLENGE AND ASSOCIATED DESIGN

The operator needed the road to be properly stabilized because it would be incredibly expensive to maintain a conventional road. Moreover, the road needed to meet the Forestry Service's standards. The contractor did not have an answer other than laying on more stone. There was no geotechnical investigation of the subgrade soils, and they were losing a large amount of stone into the weak clay. The truck

traffic from the construction, drilling and fracking tallied up to 2500 trucks per month.

Since a geotechnical investigation was not performed for this site, a design was performed based on a worst-case scenario. The contractor provided to the geogrid representative a visual description of the site. The Giroud-Han design method was performed based on a number of input parameters that include: axle passes, axle load, tire pressure, maximum rut depth, aggregate properties and type of geogrid.

Axle passes equals the number of vehicle passes multiplied by the number of axles per vehicle. Thus, 400 passes of a 3 axle dump truck would represent 1,200 axle passes. For computational purposes, each axle is presumed to carry the same load, or (conservatively) the load of the heaviest axle. 10,000 axle passes was used for this design.

Axle load is an Equivalent Single Axle Load (ESAL) and is 80kN (18 kips). This value is used by default in the Giroud Han Method. However, modern vehicles often have axle loads of 89 kN (20 kips) or higher. An ESAL of 89 kN (20 kips) was used for this design to be conservative.

It is assumed in this method that the contact pressure on the pavement is equal to the tire pressure. In the United States, the tire pressure for the standard highway truck is 552kPa (80 psi), and this is used by default in this program. As with the ESALs, modern haul vehicles have higher tire pressure, in some cases up to 689 kPa (100psi) or greater. For this design, 827kPa (120 psi) was used to be conservative.

Rut depth describes the maximum surface deformation for an access road or well pad required to maintain serviceability. For this design, as with most permanent scenarios, a 40 mm (1.5 in) rut depth is appropriate.

The required thickness of the granular material calculated using this design methodology is very sensitive to the magnitude of the subgrade strength. When inputting this parameter, the value should be representative of the conditions likely to be experienced in situ during the life of the road. When onsite the contractor described the soil as weak and that he sank an inch standing on it with his own weight. A Guide for estimating Subgrade strength that was used is shown below:

Guide for Estimating Subgrade Soil Strengths (Fine-Grained Soils)

Estimated Consistency by:		Test by:				Correlates to:			
Feel	Equipment/Visual	Standard Penetration Test (SPT)	Dynamic Cone Penetrometer (mm/blow)			Shear Strength, C_u		R Value	CBR
			SC, SM, SP	CL	CH	(kPa)	(Kg/cm^2)		
Very Soft	Man standing sinks >75 mm	<2	–	–	–	<12	<0.122	–	<0.4
Soft	Man walking sinks ~50 - 75 mm	2 - 4	–	–	–	12 - 24	0.122 - 0.24	<0.36	0.4 - 0.8
Medium	Man walking sinks ~25 mm	4 - 8	–	>66	–	24 - 48	0.24 - 0.49	0.36 - 2.5	0.8 - 1.6
Stiff	Pickup truck ruts ~12 - 25 mm	8 - 15	>100	66 - 46	–	48 - 96	0.49 - 0.98	2.5 - 6.8	1.6 - 3.2
Very Stiff	Loaded dump truck ruts ~ 25 - 75 mm	15 - 30	100 - 56	46 - 33	>109	96 - 193	0.98 - 1.95	6.8 - 15.5	3.2 - 6.4
Hard	Insignificant ruts from loaded dump truck	>30	56 - 27	33 - 23	109 - 54	>193	>1.95	>15.5	>6.4

References: After Portland Cement Association, E.I. DuPont literature and McCarthy, David F. *Essentials of Soil Mechanics and Foundations*, 1977 & Tensar1998. Webster, Personal Communication 2001. DCP vs. CBR Correlations AASHTO, *1993 Guide for Design of Pavement Structures*, Van Till et al. NCHRP 128.

NOTE: For use with Tensar® TriAx® (TX) Geogrids shown and for preliminary analysis only. Final design and installation are the responsibility of others based upon site-specific conditions. Please see the Tensar TriAx Geogrid Installation Guide for complete installation procedures. Tensar International Corporation is not responsible for any use or misuse hereof. Thickness results shown on the reverse side are for the specific scenario indicated and are based on SpectraPave4™ PRO Software and the Giroud-Han Design Methodology. More comprehensive results, including cost savings, are available using Tensar International Corporation's SpectraPave Mobile App or SpectraPave4™ PRO Software. For other scenarios, contact your local TriAx Geogrid distributor or call toll TENSAR 1.

Figure 2 – Guide for the estimation of subgrade strength

From Figure 2, a CBR of 1.0 was assigned to this project based on visual observations in the field. It is important to note that with visual observations alone, all of the inputs were selected to yield a very conservative design. Site based Dynamic Cone Penetrometer (DCP) testing is recommended to better refine the input parameters but was unavailable for this project.

The aggregate fill CBR is used to describe the strength of the unbound aggregate following placement and compaction on the top of the proposed subgrade. The value may be significantly lower for a soft subgrade. In the Giroud-Han method, a maximum ratio of 5.0 is conservatively assumed for the moduli of the aggregate fill and the subgrade materials. While this is sensible for the unstabilized pavements and those stabilized by geotextiles and other geogrids, the USACOE has shown that this may be a conservative approach for roadways.

The stabilization benefit provided by a geosynthetic depends on numerous interaction factors, including: (1) geosynthetic type, (2) product geometry, (3) compatibility with fill aggregate, and (4) product quality. The quantification of the benefit can only be accomplished based on full scale testing of specific product and calibration to proper design methods. For this design, the heaviest weight TriAx® geogrid was used to maximize reduction of aggregate. These variables needed to be selected within the computer model shown in Figure 3. The results are shown in Figure 4.

DESIGN PARAMETERS

DESIGN REQUIREMENTS

Property	Value
Axle Load (kN)	89
Tire Pressure (kPa)	827
Axle Passes (Each)	10000
Maximum Rut Depth (mm)	40

PAVEMENT SOIL PROPERTIES

Property	Value
Aggregate Fill CBR (%)	20
Design Subgrade CBR (%)	1.0

Aggregate fill shall conform to following requirement:

D50 <= 27mm

Figure 3 – Input parameters for haul road design

RESULTS

Geosynthetic	Aggregate Fill Thickness (mm)		Aggregate Fill Thickness Savings (mm)	
	Calculated	Required	(mm)	(%)
Unstabilized	794.2	800	N/A	N/A
TX5	467.8	470	330	41
TX7	374.4	380	420	53

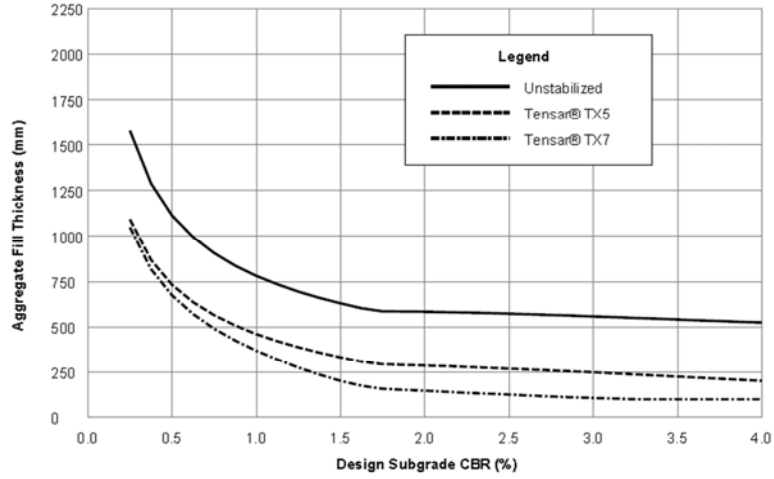

Figure 4 – Results for stabilized and unstabilized road sections

COST ANALYSIS

After determining the stone reduction, a cost analysis was prepared to illustrated the overall cost savings. The contractor provided information for the analysis:

1. Road was 15.3 km (9.5 miles), 6.7 m (22 ft) wide.
2. The in-place cost for the PennDOT 2a Modified aggregate was $21.68/tonne ($19.66/ton)
3. They were building on the subgrade without any excavation (this is important because it could add to the cost savings if there is a decrease in excavation).
4. The installation cost of the geogrid is usually $0.30/sm ($.25/sy).
5. The cost for the analysis for the TX 5 was $2.99/sm ($2.50/sy) and TX 7 was $5.08/sm ($4.25/sy) (the actual cost when purchased was lower but Tensar uses these values to be conservative).
6. The required overlap of the geogrid should be a minimum of 0.6 m (2 ft).

RESULTS

COST ANALYSIS PARAMETERS

PROJECT SIZE

Length(m)	15300
Width (m)	6.7

AGGREGATE INFORMATION

Total in place cost ($/Tonne)	21.68

TOP SURFACE CONSTRAINT

There are no restrictions on the top level of the pavement. Therefore, irrespective of the required fill thickness, there is no requirement for undercut of the existing formation.

GEOSYNTHETIC INFORMATION

	TX5	TX7
Material Cost ($/sq.m)	2.99	5.08
Roll Width (m)	4.0	4.0
Installation Cost ($/sq.m)	.30	.30
Minimum Overlap (m)	0.6	0.6

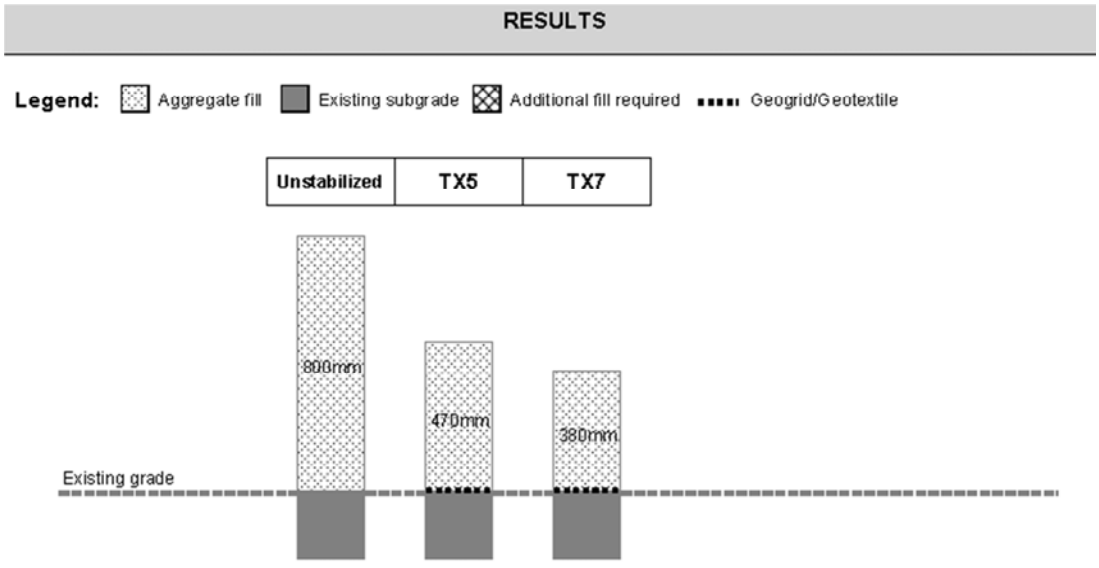

Aggregate costs	$3,788,770	$2,225,902	$1,799,666
Geosynthetic costs	$0	$387,847	$634,229
Undercut costs	$0	$0	$0
Additional fill costs	$0	$0	$0
Total project costs	$3,788,770	$2,613,749	$2,433,895
Overall project savings	$0	$1,175,021	$1,354,875
Percent savings	0%	31%	36%

Figure 5 – Cost Analysis Results of the Haul Road

INSTALLATION AND PERFORMANCE

Figure 6 – Entrance Road

The photograph in Figure 6 was taken in July of 2010 when installation started at the site. It shows the entrance of 4 Mile Road with the intersection of the SR 153 roadway. Notice that the stone has been brushed back to show the geogrid location

Figure 7 – In Service Performance of the Road

Figure 7 and 8, also used in the County Conservation District flyer, shows the roadway and how well it stood up to traffic. This photograph was taken in the fall of 2010.

Figure 8 – Post Construction County Conservation District Photo

Figure 9 – Spring Thaw Behavior of the haul road

One of the main concerns of the DCNR was the performance of the road throughout the spring thaw. The geogrid manufacturer went back to the site after the winter to see how the road was performing. Figure 9 was taken on March 24, 2011. Snow can be seen in the picture, and the performance was as expected during the spring thaw.

Figure 10 – Stabilized haul road and unstabilized well pad

Figure 10 shows the access road installed with geogrid. There is a dramatic contrast between the performance of the stabilized road and the unstabilized well pad. This is readily visible in the center of the photograph.

CONCLUSION

After three years of service, the roadway exhibited the ride quality experienced immediately after construction. The road requires minimal maintenance. In fact, maintenance costs for this section of road were far lower than expected because stone was not needed to fill in potholes after the spring thaw. To this day, the roadway out performs other roads that have been built with conventional methods of construction. The DCNR and Forestry Service have adopted geogrids as the standard for road construction, and the Dirt and Gravel Road Center at Pennsylvania State University have given the use of geogrids a full endorsement. The operator continues to design its roads with geogrid because they saved $1.4 million dollars on this project.

REFERENCES

Department of the Army, US Army Corps of Engineers (2003), "Use of Geogrids in Pavement Construction" Engineering Technical Letter (ETL) 1110-1-189, Washington, D.C.

Giroud, J.P. and Jie Han (2004), Closure to "Design Method for Geogrid-Reinforced Unpaved Roads. I: Development of Design Method" *Journal of Geotechnical and Geoenvironmental Engineering,* August 2004, Vol. 130, No. 8, pp. 775–786. DOI: 10.1061/_ASCE_1090-0241_2004_130:8_775_

Giroud, J.P. and Han, J. (2012a). The Giroud-Han design method for geosynthetic-reinforced unpaved roads. Part I The method development and its calibration. *Geosynthetics*, 30(1), 40-49.

Giroud, J.P. and Han, J (2012b). The Giroud-Han design method for geosynthetic-reinforced unpaved roads. Part II Recommendations for the proper use of the method. *Geosynthetics*, 30(2), 12-19.

The Positive Environmental and Cost Impact of Geosynthetics in Well Pad and Access Road Construction

Bruce A. Lacina[1], P.E., M.ASCE, John D. Herrmann[2], AffM.ASCE, and Monte Madsen[3]

[1]Roadway Reinforcement Technical Manager, TenCate Geosynthetics Americas, 365 S. Holland Dr., Pendergrass, GA 30567, U.S.A., E-mail: b.lacina@tencate.com
[2]Market Development Manager – Oil & Gas, TenCate Geosynthetics Americas, 637 Avondale Dr., St. Peters, MO 63376, U.S.A., E-mail: j.herrmann@tencate.com
[3]Completions Engineering Team Lead, Whiting Petroleum Corporation, 1700 Broadway, Suite 2300, Denver, CO 80290, U.S.A., E-mail: monte.madsen@whiting.com

ABSTRACT: The incorporation of high strength geosynthetics provide numerous benefits to oil and gas producers and the engineering consultants tasked with designing their well pads and access roads. This paper will present examples of the positive environmental impact and cost benefit high strength geosynthetics provide Whiting Petroleum Corporation in the Williston Basin of North Dakota and Montana, along with an example of a gas well pad and access road in central Pennsylvania stabilized with the same geosynthetic. Subgrade stabilization is often required for access roads leading to the well pad and the well pad itself. Leading methods include significant depths of aggregate, chemical stabilization and geosynthetic reinforced sections. General soft soil conditions and significant rain and snow events often require producers, engineering consultants and contractors to recommend additional aggregate to stabilize access roads and well pads. The need for additional aggregate contributes to higher traffic counts, increased CO_2 emissions and increased cost. Whiting Petroleum Corporation began exploring alternate means of stabilizing access roads and well pads in October of 2011. After reviewing various geosynthetic options and accompanying test data, the producer ultimately chose an innovative high strength woven geotextile to stabilize their sites. This has led to the elimination of future maintenance and has required no additional aggregate over the life of the road and well pad. This paper will present both laboratory and full scale test data on the performance of this innovative high strength geosynthetic. In addition, detailed cost savings associated with eliminating additional aggregate requirements will be presented, along with the environmental impact of eliminating additional aggregate hauling, placement and compaction. Case studies will be included along with photographs of well pad sites constructed both with and without this geosynthetic.

INTRODUCTION

The increased production of shale oil and gas in the United States has quickly led experts to predict U.S. energy independence in the not too distant future. Oil and gas producers have uncovered many challenges when constructing well pads and access roads. Drill rigs have to set up in optimal locations related to where the shale oil and gas reserves are located, anywhere from 1,524 m (5,000 ft) to over 3,048 m (10,000 ft) below the surface. Energy producers must work with land owners to minimize disturbances to the land owner's property. Poor subgrade conditions must be overcome, not bypassed in lieu of more ideal surface conditions for locating well pads.

Challenging subgrade conditions often warrant improvement. Subgrade improvement may include several millimeters of aggregate, chemical stabilization or the use of geosynthetics. Geosynthetics allow energy producers to either reduce the initial aggregate requirements or eliminate maintenance of the well pad and access road. Maintenance refers to the repeated placement of additional aggregate to fill in rutting and regain stabilization of the well pad and access road.

This paper will present laboratory and full scale test data of an innovative high strength geotextile used extensively in the Williston Basin by Whiting Petroleum Corporation. Whiting examines each well pad site prior to construction. If weak subgrade conditions exist, the use of a geosynthetic is installed to eliminate continued maintenance. A review of typical cost savings and reduced CO_2 emissions will be analyzed.

BACKGROUND

The Williston Basin area of North Dakota experienced up to 2,921 mm (115 in) of snow fall during the winter of 2010/2011. Following the spring thaw in 2011, Whiting Petroleum Corporation experienced numerous site challenges on their existing oil well pads and access roads. Severe rutting required substantial investments in additional aggregate to fill in ruts and stabilize these sites. On average, an additional 200 truckloads of aggregate were required to stabilize a typical well pad in addition to the original 100 mm (4 in) depth of aggregate originally installed per site. This resulted in a standard well pad requiring 3,652 m^3 (4,800 CY) of additional aggregate. Although aggregate costs are variable depending on distance from quarry to well pad, Whiting estimated aggregate at $46.00 per m^3 ($35.00 per CY) delivered, spread and compacted. Total aggregate cost for well maintenance averaged $168,000 per well pad, in addition to the original aggregate installed for $76,300.

WHITING PETROLEUM CORPORATION – INITIAL CONCERNS

In October of 2011, Whiting Petroleum Corporation began searching for more reliable means of stabilizing well pad and access road sites in the Williston Basin of North Dakota and Montana. Soil conditions, especially in areas north of the Missouri River, required more than traditional subgrade improvement solutions. TenCate

Geosynthetics offered several geosynthetic solutions, ranging from traditional slit tape geotextiles, nonwoven geotextiles and extruded biaxial geogrids to a new innovative high strength woven geotextile, Mirafi® RS580i. After reviewing much of the research and testing documented below, Whiting elected to test this new high strength geosynthetic on (3) well pad locations in North Dakota.

GEOSYNTHETIC BACKGROUND

Using geosynthetics to improve the performance of gravel surfaced roads, loading pads and in undercut and stabilization applications has been done in the United States since the 1970's. Much like today's geosynthetics, early geosynthetics were either woven or nonwoven geotextiles, or geogrids. Unlike today's design methods, most of the benefit from the geosynthetic was attributed primarily to tensile membrane support. The tensile membrane support function relies mainly on the presence of a geosynthetic in the cross section not as much on the reinforcement strength of the material used. The geosynthetic design tools created during this time reflected these concepts (e.g., Heukelom and Klomp 1962, Barenberg, et. al. 1975, Steward, et. al. 1977, Giroud and Noiray 1981).

Over time, engineers, contractors, owners and geosynthetic manufacturers have realized through continuous product development and improvement that newer geosynthetics with integrated mechanical properties can provide a measureable benefit over earlier geosynthetics used in these applications. As a result, there are currently many more types and strengths of roadway stabilization and reinforcement geosynthetics than were available in the 1970's. Modern design theories are able to incorporate the use of these newer geosynthetics when they have been properly calibrated to the performance of the material (Giroud and Han 2012).

Early geosynthetics included 136 g/m^2 and 271 g/m^2 (4 & 8 oz/yd^2) nonwovens and 890 N and 1.33 kN (200 & 300 lb) slit tape wovens. New geosynthetics were developed to fill the demand created by better/controlled filtration and drainage capacities, higher reinforcement capacities and the need for lower elongation under sustained loading conditions. Mirafi® N-Series nonwoven geotextiles were created to provide excellent separation, filtration and drainage capacities; Mirafi® FW-Series were created to provide controlled filtration and drainage using a woven geotextile structure; and Mirafi® HP-Series woven geotextiles were created to provide high tensile strength stabilization and reinforcement capacities. The newest Mirafi® RS*i*-Series roadway construction geosynthetics incorporate the improvements of more than forty years of product development and successful project histories.

Mirafi® HP-Series woven stabilization/reinforcement geotextiles were first developed in the nineteen eighties and continue to be improved and refined. HP-Series have a long history of high performance and significant cost savings in subgrade stabilization applications. Research into the functions and behaviors of these geosynthetics in these applications (Christopher and Lacina 2008) have led to the development of TenCate's current Mirafi® RS*i*-Series and H_2R*i* stabilization/reinforcement geotextiles. These new geosynthetics have optimum integrated functions of layer separation, reinforcement strength, filtration and drainage capacity, and soil / aggregate interaction.

LABORATORY GEOSYNTHETIC TESTING

Both small-scale and large-scale laboratory testing have been performed over the years on geosynthetics to determine their relative performance and behaviors in different soil and gravel fills. Small-scale laboratory testing includes cyclic and monotonic pullout interaction, direct shear interaction, and filtration and drainage capacity. Large-scale laboratory testing includes the application of simulated wheel loads from truck traffic to compare, refine and develop reinforcement/stabilization geosynthetics. An example of the relative performance of different geosynthetics as a function of surface rutting in large-scale big box cyclic load testing is shown in (Fig. 1).

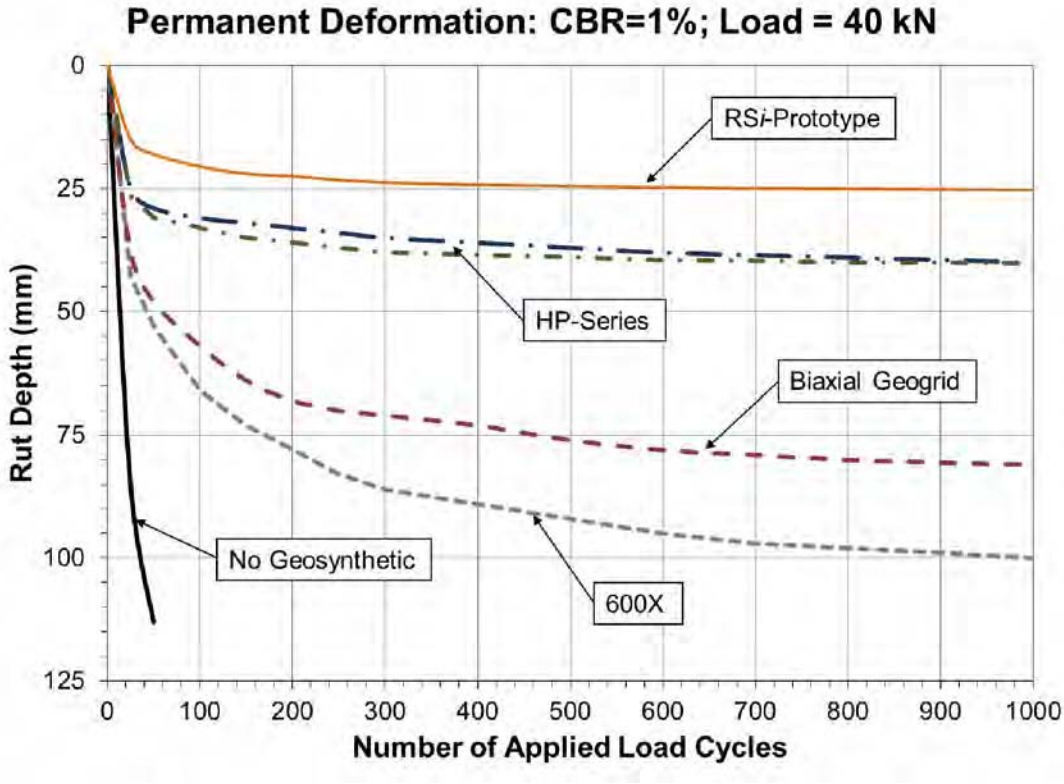

FIG. 1. Cyclic Load Testing Permanent Surface Deformations as a Function of Applied Loads.

Test sections were constructed in a 2 m X 2 m (6.5 X 6.5 ft) X 1.5 m (5 ft) deep test box with removable facing that provided access to the interior. A 300 mm (12 in) diameter steel plate placed on a rubber pad was used to simulate wheel loads that provided a more uniform contact pressure on the test section surface. The applied loads and load frequency simulated a 40 kN (9 kip) wheel load or 80 kN (18 kip) axle load. Another significant role geosynthetics contribute to subgrade stabilization is to quickly and efficiently dissipate pore pressures developed in the subgrade soil during dynamic loading as shown in (Fig. 2) (Christopher, et. al. 2009).

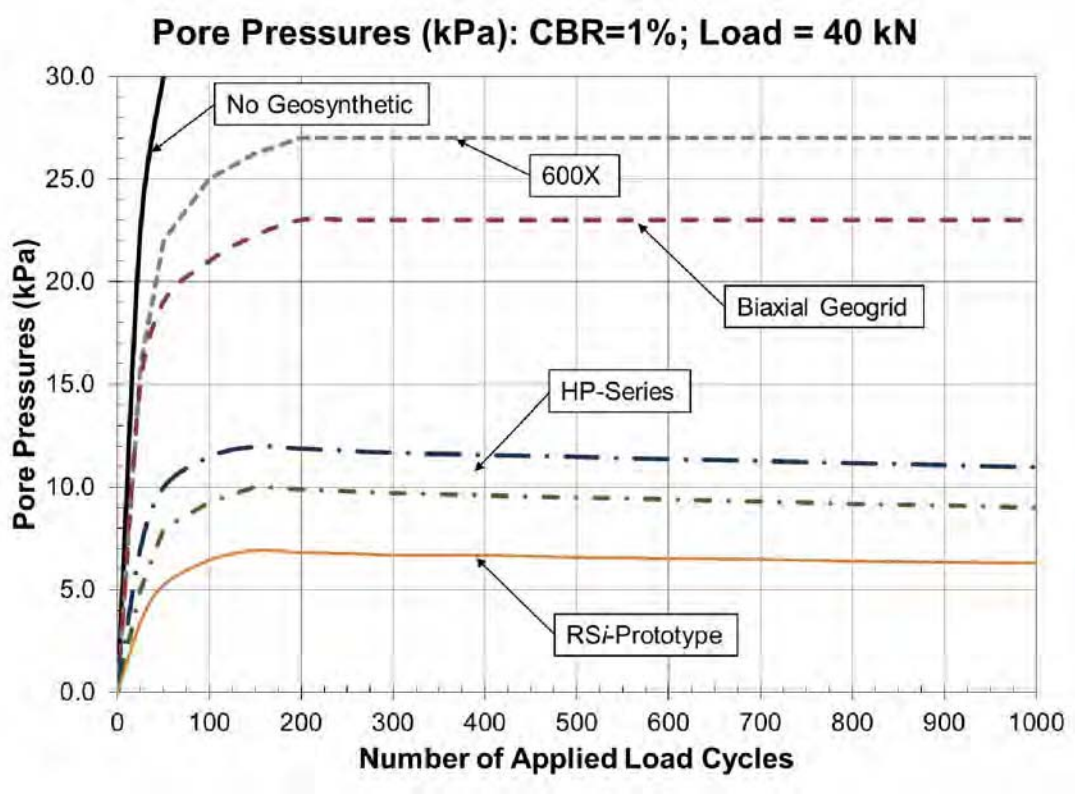

FIG. 2. Cyclic Load Testing Subgrade Pore Pressure as a Function of Applied Loads.

The loading and data collection software were set up to provide a linear load increase from zero to 40 kN (9 kips) over a 0.3 second rise time, followed by a 0.2 second period where the load is held constant, followed by a load decrease to zero over a 0.3 second period and finally followed by a 0.5 second period of zero load before the load cycle is repeated, resulting in a load pulse frequency of 0.67 Hz. The maximum applied load of 40 kN (9 kips) resulted in a pavement pressure of 552 kPa (80 psi). This load represents one-half of an axle load from an equivalent single axle load (ESAL). The load frequency is selected to allow the data acquisition system time to store data before the next load pulse was applied.

Large-scale lab testing of developmental RSi-Series geotextiles showed early reductions in surface rutting behavior in large-scale testing compared to HP-Series and X-Series. The prototype RSi-Series geotextiles also provided better pore pressure dissipation during dynamic load testing and higher pullout resistance in common roadway geotechnical fills than previous woven stabilization/reinforcement geotextiles. Continued testing, development, refinement and enhancement have led to the successful development of TenCate's current Mirafi® RSi-Series geosynthetics.

FULL-SCALE GEOSYNTHETIC TESTING

Full-scale testing has been performed by Kansas State University (KSU) and Louisiana Transportation Research Center (LTRC) to better determine the

reinforcement/stabilization benefits of Mirafi® RS*i*-Series geotextiles. The accelerated load frame (ALF) test sections were created to evaluate traffic benefit ratios (TBR) and aggregate base course and asphalt reductions using RS*i*-Series.

In the KSU testing, the reaction frame of the ALF machine covers a distance of 12.8 m (42 ft) and applies the axle load with air-bag suspension on dual tires. The wheel loading assembly is belt driven by a 20-HP electric motor, while the load is controlled by hydraulic pressure. The loading mechanism can be controlled via hydraulic pressure, tire pressure, and test speed. In this test, an 80-kN single axle load with air-bag suspension was applied on dual tires. The tire pressure was 620 kPa and testing speed was 11.3 km/h. It is possible to laterally wander wheel loading to model more realistic trafficking patterns. A ±150 mm wander was applied in a truncated normal distribution with 676 repetitions for one wander cycle. Rut measurements were recorded after every 50,000 wheel passes. Once the rut depth measurement met or exceeded 12.5 mm (0.5 in), the ALF test section was considered to have met the failure criterion. Graphs were then generated to show the actual rut depth recorded at each 50,000 pass interval. The number of truck passes corresponding to a rut depth of 12.5 mm (0.5 in) was estimated from the data plot.

ALF testing results show that Mirafi® RS*i*-Series provide a significant increase in the structural stability of roadway cross sections. They provide load support for more than twice the number of wheel loads applied to the unreinforced cross sections as shown in (Fig. 3).

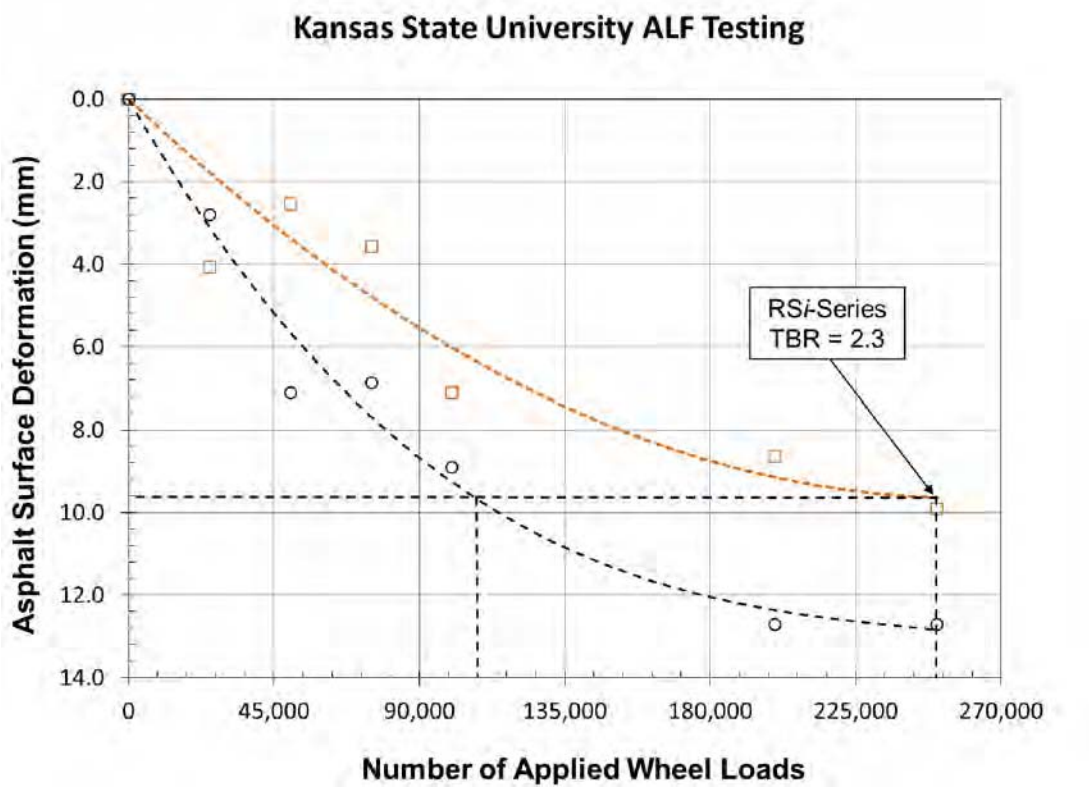

FIG. 3. ALF Testing Permanent Surface Deformations as a Function of Applied Loads.

WHITING PETROLEUM CORPORATION – CONSTRUCTION

After monitoring the successful performance of the geosynthetic on the (3) well pads chosen for testing, Whiting began utilizing Mirafi® RS580i on the most challenging well pad sites. Typical conditions where the geosynthetic is installed includes saturated soils, expansive clay soils and subgrade soils with a CBR less than 3.0% (Fig. 4). The geosynthetic is placed directly on the subgrade. It should be rolled out as flat as possible with minimal folds or wrinkles. Adjacent rolls and roll ends are overlapped 600 mm (24 in) (Fig. 5). 100 mm (4 in) minus scoria aggregate is placed directly over the geosynthetic in a 150 mm (6 in) lift. Rubber tired belly dump trucks can be driven over the geosynthetic to speed placement of the aggregate (Fig. 6). Motor graders spread the aggregate evenly over the geosynthetic (Fig. 7). No additional compaction methods are employed prior to the well pad receiving traditional drilling equipment, followed by hydraulic fracturing equipment. At this point, the well pad is constructed and ready for drilling operations.

FIG. 4. Soft subgrade condition requiring geosynthetic stabilization.

FIG. 5. Geosynthetic material installed and overlapped 600 mm (24 in).

FIG. 6. Aggregate placed onto the geosynthetic.

FIG. 7. Motor grader evenly spreads the aggregate.

WHITING PETROLEUM CORPORATION – PERFORMANCE

To date, over 1,254,191 m^2 (1,500,000 SY) of high strength geosynthetics have been installed on Whiting well pads and access roads. The geosynthetic has proven extremely durable and resilient to the challenging conditions of the Williston Basin. Whiting has received numerous benefits from the inclusion of the geosynthetic. In addition to the long term cost and environmental benefits detailed below, additional benefits include quicker well pad construction time versus thicker aggregate sections or chemical stabilization. Construction and stabilization of well pad sites can proceed in any weather conditions. A review of the financial impact of time delays is included in the conclusion.

Figure 8 below shows a well pad constructed in November 2011. The photograph is from April 2013. This well pad was constructed with the traditional 100 mm (4 in) aggregate placed directly on the subgrade. Severe rutting and displacement of the aggregate into the subgrade has left this well pad in need of maintenance. An additional 225 mm (9 in) of aggregate will be added to re-stabilize the well pad.

FIG. 8. Well pad constructed with aggregate only, in need of maintenance.

Figure 9 below shows a well pad constructed in November 2011. The photograph was taken in April 2013. The edge of this well pad is located approximately 30 m (100 ft) from the edge of the well pad in (Fig. 9). Similar subgrade conditions were present at both locations and both locations received similar construction, drilling and hydraulic fracturing wheel loads. Weather conditions and moisture content are also similar at both well locations. Performance of the geosynthetic stabilized well pad has been excellent. There is no maintenance anticipated on this well pad.

FIG. 9. Well pad constructed with geosynthetic stabilization.

WHITING PETROLEUM CORPORATION – COST BENEFIT

Table 1. Aggregate Only Stabilization Costs on a Typical Well Pad

	Unit Amount	Unit Cost	Total Cost
Initial 100 mm (4 in) thick aggregate section	1,658.70 m^3	\$46.00 / m^3	\$76,300
Additional 225 mm (9 in) thick aggregate section	3,652.17 m^3	\$46.00 / m^3	\$168,000
		Total Cost per Well Pad	\$244,300

Table 2. Geosynthetic Stabilization Costs on a Typical Well Pad

	Unit Amount	Unit Cost	Total Cost
Initial 150 mm (6 in) thick aggregate section	2,586.96 m^3	\$46.00 / m^3	\$119,000
Geosynthetic Installed	12,532.13 m^2	\$3.89 / m^2	\$48,750
		Total Cost per Well Pad	\$167,750

Aggregate savings per well pad has averaged \$76,550. This results in a 31.3% cost savings per well pad. The geosynthetic stabilization method has been utilized on approximately 30 well pads annually, with an annual savings of \$2,296,500.

WHITING PETROLEUM CORPORATION – ENVIRONMENTAL BENEFIT

Table 3. Carbon Footprint of Aggregate Only Stabilization on a Well Pad

	Aggregate Hauling	Number of Loads	Total Distance	CO_2 Emissions
Initial 100 mm (4 in) thick aggregate section	177 km (110 miles) round trip	91	16,107 km (10,010 miles)	15,554 kg [a]
Additional 225 mm (9 in) thick aggregate section	177 km (110 miles) round trip	200	35,400 km (22,000 miles)	34,185 kg [a]
Motor Grader Operation			60 hours	3,684 kg [b]
			Total CO_2 Emissions	53,423 kg

Table 4. Carbon Footprint of Geosynthetic Stabilization on a Well Pad

	Aggregate Hauling	Number of Loads	Total Distance	CO_2 Emissions
Initial 150 mm (6 in) thick aggregate section	177 km (110 miles) round trip	142	25,134 km (15,620 miles)	24,271 kg [a]
Motor Grader Operation			25 hours	1,535 kg [b]
Geosynthetic Manufacturing	30 rolls	188 kg per roll	5,640 kg of geosynthetic	15,228 kg [c]
Geosynthetic Transportation	2,811 km (1,747 miles)	0.286 loads [d]	804 km (500 miles)	777 kg [a]
			Total CO_2 Emissions	41,811 kg

[a] Material hauling calculated at a truck fuel consumption rate of 6.5 miles per gallon. CO_2 emissions calculated at a rate of 10.1 kg of CO_2 produced per gallon of fuel used.

[b] Motor grader operates at 190 HP with a fuel consumption rate of 0.032 gallons/hour/horsepower. CO_2 emissions calculated at a rate of 10.1 kg of CO_2 produced per gallon of fuel used.

[c] Geosynthetic manufacturing carbon footprint calculated at 2.7 kg of CO_2 per kg of material (Koerner 2013).

[d] 3.5 well pads worth of geosynthetic can be transported on one truck from the geosynthetic manufacturing facility to a storage yard near the well pad locations. Therefore, overall shipping distance is divided by 3.5 to calculate the CO_2 emissions produced by transporting the geosynthetic required for one well pad.

The carbon footprint associated with an individual well pad utilizing the geosynthetic stabilization method is reduced by 11,612 kg of CO_2 versus conventional aggregate maintenance. This results in a CO_2 emissions reduction of 21.7% per well pad. The geosynthetic stabilization method has been utilized on approximately 30 well pads annually, resulting in an annual carbon footprint reduction of 348,360 kg of CO_2.

MARCELLUS SHALE GAS WELL PAD CONSTRUCTION

Pursuant to meeting with an oil and gas producer in the Northern Tier of Pennsylvania, the field superintendent/manager asked for a site visit to provide recommendations for subgrade stabilization. The well pad location was cut into a

mountain side. There was continuous water seepage from the upslope side on to the northeast corner of the well pad area (Fig. 10).

FIG 10. Saturated subgrade at location of well pad.

This was also the location where the lease road connects the well pad. The primary concern was the anticipated truck traffic (aggregate hauling, rig mobilizing, water hauling, supply trucks, etc.) accessing that corner and turning out on to the pad. Due to the anticipated magnitude of truck traffic and given the continuously wet subgrade conditions, Mirafi® RS580i geosynthetic was installed on the northeast corner of the pad in February 2012 (Fig. 11). The geosynthetic was deployed directly upon the exposed subgrade where the lease road accessed the well pad.

FIG. 11. Geosynthetic installed at northeast corner of well pad.

The construction crew installed 600 mm (24 in) of bank run aggregate across the entire four (4) acre pad location. The bank run material, obtained from a nearby farm, was a mixture of aggregate ranging from boulder size to fine grained sand with some fines (Fig. 12). This material was placed on the geosynthetic and compacted. The balance of the well pad received the same aggregate material, but without the geosynthetic material for stabilization.

FIG. 12. Aggregate being installed on geosynthetic.

Following completion of the well pad, drilling commenced and the area stabilized with the geosynthetic performed well with no rutting or maintenance concerns. In December 2012, the well pad was revisited. Figure 13 shows the area of the well pad where the geosynthetic was utilized. Performance at this area compared to the area without geosynthetic stabilization is significantly improved.

FIG. 13. Following 10 months of wheel load and completion of the well.

CONCLUSIONS

The incorporation of high strength geosynthetics into the original construction of well pads and access roads have led to multiple benefits. Annual stabilization maintenance with the addition of aggregate to fill in wheel ruts has been eliminated. This has resulted in per well construction savings of 31.3%. Environmental impact has been reduced. The carbon footprint on each well pad utilizing the geosynthetic stabilization method has been reduced by 21.7%. Additional benefits to Whiting include the elimination of costly time delays. Well pads in the past constructed over soft, saturated subgrades without a geosynthetic could experience delays on average of 2 to 5 days. When a well pad had deteriorated to the point that additional aggregate was required to stabilize a site, drill rig and/or hydraulic fracturing mobilization and demobilization had to be delayed. Whiting estimated a financial burden of $100,000 every day a well pad could not be accessible.

The reduction of aggregate requirements benefits local municipalities, counties and states. A reduction in the number of trucks hauling aggregate reduces the stress placed on roadways. These roadways are often maintained by local authorities.

Reduced construction costs on well pads ultimately is reflected in reduced market prices for gasoline, heating oil, natural gas, plastics, cosmetics and all fossil fuel based products consumers purchase on a daily basis.

REFERENCES

Barenberg, E. J., et. al. (1975). "Evaluation of Soil Fabric-Aggregate Systems with Mirafi® 500X." *Civil Engineering Studies*.

Christopher, B.R. and Lacina, B. (2008). "Roadway Subgrade Stabilization Study", *Proceedings of GeoAmericas 2008*, Cancun, Mexico, International Geosynthetic Society, pp. 1013–1021.

Christopher, B. R., et. al. (2009). "Pore Water Pressure Influence on Geosynthetic Stabilized Subgrade Performance," *Proceedings, 2009 Geosynthetics Conference*, Salt Lake City, Utah.

Giroud, J.P. and Han, J. (2012). "The Giroud and Han design method for geosynthetic-reinforced unpaved roads, Part 1: The method development and its calibration", *Geosynthetics*, Vol. 30, No. 1, pp. 40-49.

Giroud, J. P.; Noiray, L. (1981). "Geotextile reinforced unpaved road design." Journal of the Geotechnical Engineering Division, 107(GT9): 1233-1254.

Heukelom, W. and G. Klomp, A. J., (1962). "Dynamic testing as a means of controlling pavements during and after construction." *Proceeding of International Conference on the Structural Design of Asphalt Pavements*, Ann Arbor, MI.

Koerner, R.M. (2013) "Carbon Footprint of Geosynthetics" *Geosynthetics*, October/November 2013, pg. 16.

Saghebfar, M., et. al. (2013). "Investigation of Bearing Capacity of Geotextile-Reinforced Paved Roads," *Mid-Continent Transportation Research Symposium*, Ames, IA.

Steward, J. E.; et al. (1977). Guidelines for use of fabrics in construction of low volume roads." FHWA-TS-78-205: *U.S. Department of Agriculture, Forest Service, Pacific Northwest Region*, Portland, OR.

Use of Geosynthetics for Reinforcing/Stabilizing Unpaved Roads under Full-Scale Truck Axle Loads

Xiaochao Tang[1], Ph. D., Murad Abu-Farsakh[2], Ph. D., P. E., Shadi Hanandeh[3] and Qiming Chen[4] , Ph. D., P. E.

[1]Assistant Professor, Department of Civil and Environmental Engineering, Widener University, One University Place, Chester, PA 19013; xtang@widener.edu
[2]Research Professor, Louisiana Transportation Research Center, Louisiana State University, 4101 Gourrier Ave., Baton Rouge, LA 70808; cefars@lsu.edu
[3]Graduate Research Assistant, Department of Civil and Environmental Engineering, Louisiana State University, Baton Rouge, LA 70808; shanan1@tigers.lsu.edu
[4]Research Associate, Louisiana Transportation Research Center, Louisiana State University, 4101 Gourrier Ave., Baton Rouge, LA 70808; qchen1@tigers.lsu.edu

ABSTRACT: The significant impact of the truck traffic associated with the shale energy developments on local roads, including many unpaved gravel roads has been a pressing issue while the regional economy benefits from the recent shale gas boom. In many cases, roads had to be reconstructed over a soft soil subgrade treated and stabilized by cement or lime. As an alternative, geosynthetics offer a potentially more cost effective solution for reinforcing/stabilizing roads on soft soil subgrade. This paper presents a study using a full-scale accelerated traffic load testing to evaluate two recently emerged geosynthetic products, a triaxial geogrid and a high-strength woven geotextile in unpaved roads built over soft soil subgrade. A total of six full-scale test sections were constructed, among which two sections were reinforced by one and two layers of triaxial geogrids, respectively; while high strength geotextiles were used to reinforce two of the other sections with different aggregate layer thicknesses. The rest of the two sections were left as control sections, of which one section was constructed over 30-cm thick sand embankment. The test sections were subjected to a full-scale moving wheel load applied by the Accelerated Loading Facility (ALF). A variety of instrumentations were used to measure the load-associated and the environment-associated responses and performance of the unpaved test sections. Results of the full-scale testing on the unpaved test sections demonstrate the benefits of geosynthetics in reducing the permanent deformation/rutting.

INTRODUCTION

In recent years, there has been a boom of shale gas energy development in some parts of the country. While the regional economy benefits from the shale gas energy, the significant impact of shale gas development-related activities on local roads has been a

pressing issue. The truck traffic associated with the shale gas development typically starts with the movement of the drill rig and equipment, which requires approximately 20 oversize and overweight truck permits (Kuhn, 2006). There is also truck traffic related to construction activities such as the transportation of construction equipment and materials for constructing the pad site and access road. Among all of the shale gas development-related activities, hydraulic fracturing generates the most truck traffic, which involves moving about 5 million gallons of water and delivering about 2500 tons of sands for a typical deep shale gas well (Cheasapeak Energy, 2012; Gannett Fleming, 2011).

It is often difficult to estimate and quantify the impacts on local roads from the truck traffic associated with the shale energy development since it requires detailed information such as the road structure and materials, truck traffic characteristics, and climate conditions of the region (Mason et al., 1982; Quiroga et al., 2012). Nonetheless, a theoretical study on highway roads has indicated that the shale gas development truck traffic could cause additional damage to the highway roads by a rate as high as 13% and a reduction of highway road service life by 29% (Banerjee et al., 2012). Particularly, in states such as Pennsylvania and New York where freeze-thaw cycles are frequently encountered in road subgrades, the heavy hauling truck load associated with the shale gas development has caused significant challenges to road maintenance and rehabilitation, especially during the spring season with the weakened soil subgrade. In many cases, roads had to be reconstructed over a stabilized subgrade treated by stabilizers such as cement and lime. As a mechanical stabilization of soil, geosynthetics offer an alternative solution for reinforcing/stabilizing roads built on soft soil subgrade.

Numerous studies have shown that geosynthetics provide benefits in roadway structures by either extending the roads' service life or reducing the structural layer thickness, especially the aggregate layer, with an equivalent performance (Barksdale et al., 1989; Al-Qadi et al., 1994; Perkins et al, 2004; Tang et al., 2008; Abu-Farsakh et al., 2012). Aimed to evaluate two recently emerged geosynthetic products, a triaxial geogrid and a high-strength woven geotextile, a full-scale accelerated pavement testing was conducted on a total of six test lane sections constructed over soft subgrade soil. Each section was instrumented by a variety of sensors to measure the critical responses and performance and the environmental factors that may affect the performance of test sections. The response and performance measurements are intended to be used to calibrate and/or develop ME models that can account for the effects of geosynthetics in pavement design.

TESTING PROGRAM

Full-Scale Test Section

A total of six test lane sections were constructed over soft soil foundation at an outdoor site located at the Pavement Research Facility (PRF) of Louisiana Department of Transportation and Development (LA DOTD) in Port Allen, LA. The dimension of each test section is 24 m (80 ft) long and 4 m (13 ft) wide. Fig. 1-a shows the cross sections of the six test lane sections, while Fig. 1-b shows a photo during the

construction of test sections. Section 1 and Section 4 are the control sections that were constructed without geosynthetic reinforcements, of which Section 1 was constructed over an embankment of 30 cm thick sand wrapped by nonwoven geotextiles. Section 4 is a typical control section without geosynthetics. Section 2 and Section 3 were reinforced/stabilized by the triaxial geogrid, GG, placed at the aggregate base - subgrade interface. An additional layer of geogrid, GG, reinforcement was also installed at the upper one-third of the aggregate base layer thickness in Section 2. The high strength geotextiles, GT, were used to reinforce/stabilize Section 5 and Section 6 with different aggregate layer thicknesses.

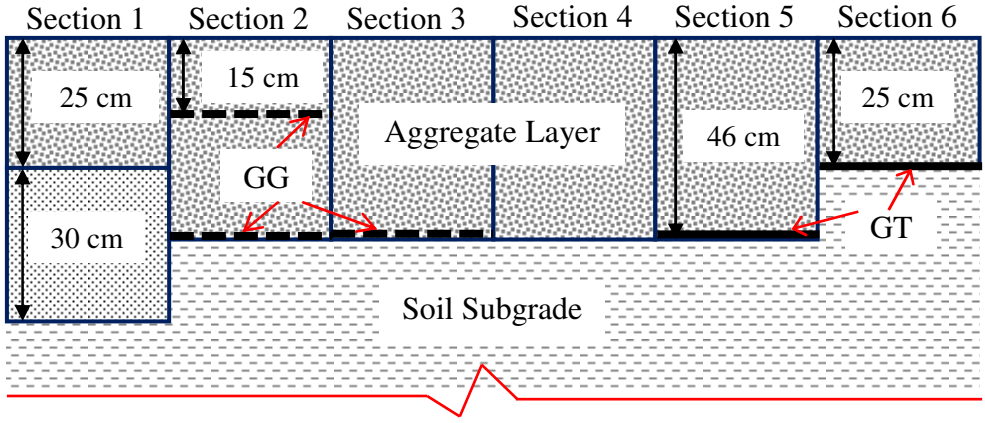

(a) Cross section of the test sections

(b) Construction of sections

FIG. 1. Test sections

The native subgrade soil in this study is classified as heavy clay (CH) per Unified Soil Classification System (USCS) or A-7-6 according to the American Association of State Highway and Transportation (AASHTO) classification system. The soil has a plasticity index, PI, of 55% with 96.6% passing the #200 sieve. The subgrade soil has an optimum moisture content of 29.5% and a maximum dry density of 1305 kg/m^3, according to the Standard proctor test. The aggregate used in this study is a dense-graded crushed limestone classified as GW or A-1-a. A modified Proctor test of the aggregate yields an optimum moisture content of 9.4% and a maximum dry density of 2066 kg/m^3.

Two recently emerged geosynthetic products, a triaxial geogrid and a high-strength woven geotextile, are selected for this study and are herein designated as GG and GT.

The triaxial geogrid was made by means of punching and drawing polypropylene (PP) sheets. The geotextile was made from high-tenacity polypropylene filaments that are formed into weaves.

Instrumentation

The test sections were instrumented by a variety of sensors to measure the load – and environment – associated pavement responses and performance. Spring-loaded LVDTs (RDP DCTH2000A) were customized to measure the total deformation of the subgrade. A thin yet rigid disk with a diameter of 5 cm (2 in) was attached onto the contact tip of the spring-loaded LVDT to provide sufficient contact area with the soil (Fig. 2-a). Potentiometers (Honeywell MLT-38000201) were customized to measure the strain at the mid-height of the aggregate layer. The potentiometer has a maximum travel distance of 25.4 mm (1 in). Two circular end plates with diameters of 5 cm were attached onto the potentiometer (Fig. 2-b).

(a) **(b)**

FIG. 2. Instrumentation sensors for the test lane sections: (a) LVDT; (b) customized potentiometer

The geosynthetics were instrumented with foil strain gauges installed in pairs on opposite sides of the geosynthetic. Other instruments including thermocouples to measure temperature variation and time-domain reflectometers (TDR) for monitoring the moisture contents were installed. Also, earth pressure cells (Geokon 3500) and piezometers (Geokon 3400) were installed at the top of the subgrade to measure the total vertical stress and possible excess pore water pressure generated by the cyclic wheel load.

Full-Scale Accelerated Testing

A full-scale accelerated load facility (ALF) was used to apply cyclic moving wheel loads on test lane sections. Fig. 3 shows a picture of the ALF with an insert of the dual-wheel assembly. ALF is a testing device that applies unidirectional trafficking to the test sections with a nominal speed of 16.8 km/h (10.5 mph) or 350 passes per hour. ALF has a due-tire axle consisting of two Michelin XZE-model truck tires and applies a 43.4-kN (9,750-lb) axle load, approximately representing half of the standard axle

load, the 80-kN (18-kip) single-axle load. ALF has the capacity of applying a normally- distributed wander covering a transverse distance of 76 cm (30 in) to simulate live traffic pattern. The wheel path generated by ALF is about 12 m (40 ft) long.

At the end of the testing, a total of 2000 passes were applied to the sections with geosynthetic reinforcements, while only 400 passes were applied to the two control sections. Using a laser profilometer, the transverse surface profile of the test sections were measured at selected intervals of load repetitions at 8 different locations along the wheel path.

FIG. 3. The accelerated load facility (ALF) with an insert of the dual-wheel assembly.

RESULTS AND ANALYSIS

Surface Rutting

Fig. 4-a presents the accumulation of the surface rutting/total permanent deformation along with the number of wheel passes for the six test lane sections. The total permanent deformation for each test lane section shown in Fig. 4-a is the average of the measurements taken at the different locations along the wheel path in each section. The control sections, Section 1 and Section 4, exhibited significantly greater total permanent deformation than the reinforced sections under the same number of wheel load passes, indicating the benefits of geosynthetics mobilization in reducing permanent deformation in unpaved roads built over soft soil subgrade.

Between Sections 2 and 3, Section 2 reinforced with two layers of geogrids showed less permanent deformation at the end of the testing. Furthermore, there is less deformation at the early stage of the traffic in Section 2, which is most likely due to the mobilization of the geogrid layer installed at the upper one-third of the aggregate layer in Section 2. The two control sections, Section 1 and Section 4 showed almost similar performance in terms of total permanent deformation.

Compared to the test sections (Sections 2 and 3) that are reinforced with triaxial geogrids (GG), the test sections (Sections 5 and 6) with high-strength geotextile (GT), showed less permanent deformations. It should be pointed out that, in addition to the presence of geosynthetics or geosynthetic types, there are other factors that can affect the performance of the test sections in terms of resisting the surface rutting. The deformations needed to mobilize the triaxial geogrids might be different than the

high-strength geotextile. The variations in construction such as degree of compaction may significantly affect the pavement performance. Although efforts were made to ensure consistent or similar testing conditions for all test sections, the possible change of the subgrade soil and aggregate layer conditions throughout the testing process may affect the sections' stiffness and strength, and thus their performance. In-situ tests conducted after the accelerated load testing, to be presented later, showed that the dry density and modulus at testing were higher for Section 5 and Section 6, which may attributable to that Section 5 and Section 6 had a less permanent deformation.

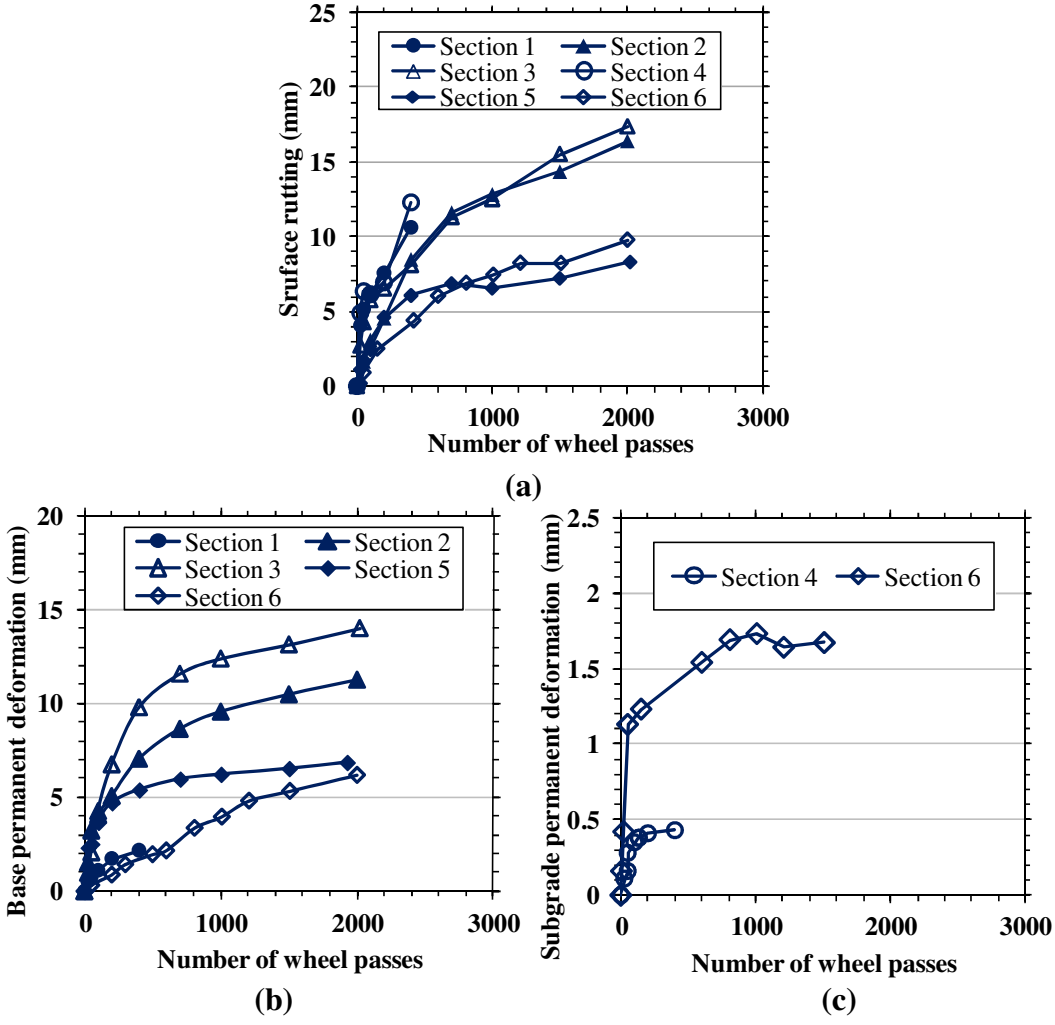

FIG. 4. Accumulated permanent deformation: (a) on the surface; (b) in aggregate layer; (c) in subgrade.

Permanent Deformation in Aggregate Layer and Subgrade

Two customized potentiometers were installed at the mid-height of the aggregate layer for each test section. Measurements from the potentiometer were relative distances between its two end plates. The change of the distance is converted into the compressive strain that is subsequently used to estimate the deformation of the

aggregate layer by multiplying with the overall thickness of the aggregate layer. The use of the potentiometer measurements for estimating the aggregate layer deformation is based on the assumption that the compressive strain of the aggregate layer is uniformly distributed and represented by the mid-height compressive strain. Fig. 4-b presents the derived permanent deformation of the aggregate layer for each test section except for Section 4 due to the potentiometer malfunction.

Sections 2 and 3 reinforced by GG exhibited more permanent deformation in the aggregate layer than Sections 5 and 6 reinforced with GT. Compared to Section 3, Section 2 with two layers of geogrids showed significantly less aggregate layer deformation. Unlike other test sections, Section 6 showed a nearly linear increase of the aggregate layer permanent deformation. Although Section 1 showed a higher total permanent deformation at the same number of wheel passes, the aggregate layer deformation in Section 1 is relatively smaller, indicating that the underlying sand embankment may significantly contribute to the overall permanent deformation in Section 1.

The LVDTs were mounted in a steel rod, which had one end relatively fixed to a great depth of the soil foundation. Therefore, the permanent deformation measured by LVDTs represented the overall deformation of the entire subgrade layer. Fig. 4-c shows the accumulation of subgrade permanent deformation along with the number of wheel passes for Section 4 and Section 6. LVDTs in other test sections were out of order during the accelerated pavement testing. As can be seen in Fig. 4-c, the control section (Section 4) has a significantly less deformation than Section 6 reinforced by the high-strength geotextile. This is likely due to the fact that the aggregate layer of Section 4 is 21 cm (8 in) thicker than that of Section 6, suggesting that the additional 21 cm (8 in) aggregate layer provides more protection to the subgrade than the high-strength geotextile layer does.

The total surface permanent deformation or surface rutting for each test section consists of permanent deformation in the aggregate layer and the subgrade permanent deformation. It is noted that the majority of the total permanent deformation is generally attributed to the permanent deformation in the aggregate layer. The load-induced permanent deformation is usually a result of material densification, shear-related deformation, or a combination of both, which can occur in any layer of the pavement system. Measurements of aggregate layer deformation demonstrate that the aggregate layer has the greatest relative layer contributions to the total permanent deformation.

Strain Developed in Geosynthetics

Foil strain gauges were installed on opposite surfaces at each location to measure tensile strains developed in geosynthetics with the repetitions of the traffic load. The measurements from strain gauges installed on opposite surfaces should be averaged to account for the flexural bending effects (Tang et al., 2013).

Fig. 5 shows the geosynthetic tensile strains measured at the centerline of the test sections. No reliable results from strain measurements were obtained in Section 5 due to the loss of strain gauges. Among the geosynthetics installed at the subgrade - aggregate base layer interface, the geotextile in Section 6 showed higher tensile strain

at the end of the loading. Between the two layers of geogrids in Section 2, the geogrid installed at the upper one-third of the aggregate layer developed the tensile strains that are more than twice as the geogrid installed at the subgrade-aggregate layer interface. Overall, Fig. 5 demonstrates that the geosynthetics were all mobilized at the end of the accelerated loading.

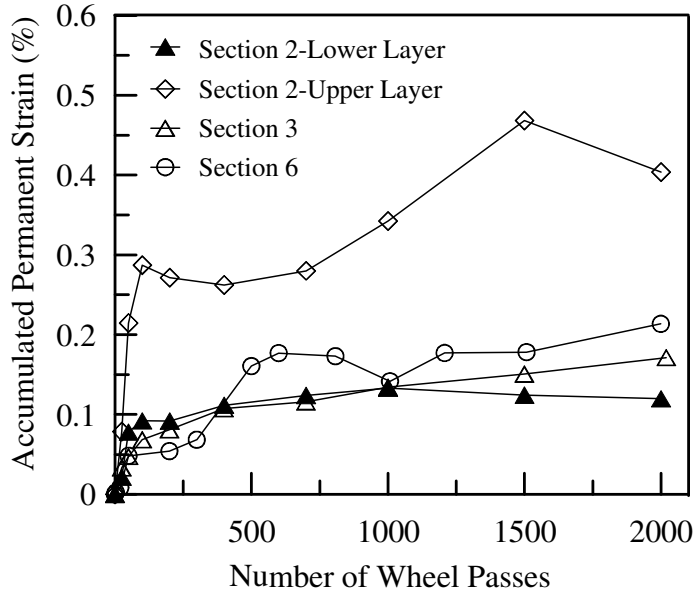

FIG. 5. Strains developed in geosynthetics at the center of test sections.

In-Situ Testing

In-situ tests were conducted upon the completion of accelerated testing on the aggregate layer along two locations: inside and 0.9 m (3 ft) outside the wheel path. The purpose of these tests is to characterize the respective site conditions before and after the traffic loading. For each test section, the in-situ testing was conducted at a minimum of five locations inside and outside wheel path, respectively. Table 1 presents the in-situ dry density and moisture content measured by the nuclear gauge. Section 6 showed the highest dry density in the aggregate layer followed by Section 3. Except for Section 4, there is a noticeable increase of dry density for locations inside the wheel path compared to locations outside the wheel path, indicating a further compaction of the aggregate layer from the repetitive wheel load.

Table 2 lists the aggregate layer moduli tested by different devices at locations inside and outside the wheel path. For the moduli tested by light-weight deflectometer (LWD) and GeoGauge, no significant difference was observed between the locations inside and outside the wheel path. Between the reinforced sections and comparable control section, e.g. sections 2, 3, and 4, no evident increase of resilient modulus was observed due to the geosynthetic reinforcements, which is in agreement with other study (Tang et al., 2014). Dynamic cone penetrometer (DCP) tests were conducted on the aggregate layer and results were converted into moduli based on a correlation model (Mohammad et al., 2008). The aggregate base moduli showed an overall increase for

locations inside the wheel path, which reflects the change of dry density measured by the nuclear gauge (Table 1). Additionally, among the different test sections, the DCP testing results showed a good correlation with the in-situ dry density. This suggests that measurements from the nuclear gauge density and DCP may be more reliable. Section 6 showed a higher DCP-derived aggregate layer modulus compared to other sections, which contributes to that Section 6 had relatively less surface rutting despite its thinner aggregate layer. Table 3 lists the subgrade modulus value from DCP tests. It can be seen that Section 6 had a higher in-situ subgrade modulus, which is also attributable to the less rutting observed in Section 6.

Table 1. Dry density and moisture content of the aggregate layer

Test Sections	Dry Density (kg/m^3)				Moisture Content (%)			
	Outside wheel path		Inside wheel path		Outside wheel path		Inside wheel path	
	Avg.	Stdv.	Avg.	Stdv.	Avg.	Stdv.	Avg.	Stdv.
1	1986.0	28.9	2017.0	19.3	6.1	0.3	5.8	0.3
2	1988.3	62.0	2002.7	33.8	5.7	0.8	6.0	0.6
3	2012.9	30.8	2038.1	21.0	5.6	0.2	6.3	0.4
4	1985.2	38.0	1949.0	33.5	5.9	0.3	5.5	0.4
5	2000.9	37.9	2036.8	26.4	7.6	0.3	7.1	0.4
6	2015.6	40.1	2040.7	30.3	5.5	0.2	5.3	0.2

Table 2. Resilient modulus for aggregate layer moduli outside and inside wheel path from LWD, GeoGauge, and DCP testing

Test Sections	LWD (MPa)				GeoGauge (MPa)				DCP (MPa)			
	Outside wheel path		Inside wheel path		Outside wheel path		Inside wheel path		Outside wheel path		Inside wheel path	
	Avg.	Stdv.	Avg.	Stdv.	Avg.	Stdv.	Avg.	Stdv.	Avg.	Stdv.	Avg.	Stdv.
1	51.8	2.8	51.7	3.4	70.5	12.0	72.2	4.8	37.4	0.9	39.6	0.5
2	49.6	1.8	50.7	3.6	71.5	43.9	68.3	16.9	36.0	1.1	38.8	0.9
3	52.0	15.1	50.2	14.9	75.8	26.4	72.4	11.4	38.7	1.6	40.9	0.5
4	50.6	4.3	49.6	1.3	72.5	35.4	69.2	19.4	34.9	0.3	37.0	0.7
5	52.4	4.4	51.2	3.4	75.4	22.9	72.1	24.4	38.0	1.0	41.2	1.7
6	45.8	18.7	45.3	11.1	77.7	38.3	69.9	13.1	41.1	1.8	41.9	2.0

Table 3. Subgrade modulus derived from DCP tests, units in MPa

Test Section	Inside Wheel Path		Outside Wheel Path	
	Avg.	Stdv.	Avg.	Stdv.
1	23.5	2.1	21.2	0.7
2	22.0	0.6	21.1	0.4
3	23.5	1.6	21.5	0.9
4	20.1	1.7	21.9	0.7
5	22.6	0.7	20.9	1.0
6	24.6	0.8	24.7	1.0

SUMMARY AND CONCLUSIONS

The truck traffic associated with the shale gas development has caused significant challenges to the maintenance and rehabilitation of local roads, including many unpaved gravel roads. Geosynthetics offer an alternative for reinforcing/stabilizing unpaved roads built over soft soil subgrade. A full-scale accelerated load testing was conducted to evaluate the benefits of using two recently emerged geosynthetics, a triaxial geogrid and a high-strength woven geotextile to reinforce/stabilize unpaved roads. A total of six test lane sections were constructed over soft subgrade soil, and were extensively instrumented to measure the critical pavement responses and performance. The findings and conclusions are summarized as follows:

1) Results of the full-scale accelerated load testing demonstrated the benefits of both geosynthetic products in significantly reducing the total permanent deformation/surface rutting of unpaved test sections. Likely due to the stiffer subgrade and aggregate layer, the two test sections with geotextile showed less permanent deformation than the sections with geogrids.
2) An important finding is that the majority of the surface permanent deformation was attributed to the aggregate layer, instead of the soft subgrade layer. The deformation in the aggregate layer is most likely due to further compaction and densification of the layer. However, Section 1 with a sand embankment showed less deformation in the aggregate layer, indicating that the sand embankment may contribute to the majority of the permanent deformation in Section 1.
3) Measurements from the strain gauges demonstrate that the geosynthetics were mobilized during the accelerated testing. In general, the permanent strain developed in the geosynthetic was around 0.2% at the end of the accelerated load testing. The geogrid installed at the upper one-third of the aggregate layer in Section 2 showed twice more tensile strains than that of the geogrid installed at the subgrade-aggregate layer interface in Section 2.
4) Extensive in-situ tests using various devices were conducted to characterize the site conditions before and after the accelerated load testing. No appreciable change of aggregate layer moduli before and after the accelerated load testing was observed from the non-destructive LWD and GeoGauge tests. The more reliable intrusive measurements by the nuclear gauge and DCP demonstrate that Section 6 had a relatively higher modulus in the aggregate layer and subgrade than other sections, which may be attributable to that Section 6 has relatively less rutting despite its thinner aggregate layer.

ACKNOWLEDGMENTS

The authors would like to acknowledge the financial support provided by the Louisiana Department of Transportation and Development (LA DOTD), Tensar International, and Mirifi TenCate.

REFERENCES

Abu-Farsakh, M. Y., Souci, G., Voyiadjis, G. Z., and Chen, Q. (2012). "Evaluation of Factors Affecting the Performance of Geogrid-Reinforced Granular Aggregate layer Material Using Repeated Load Triaxial Tests." *Journal of Materials in Civil Engineering*, 24(1): 72-83.

Al-Qadi, I.L, Brandon, T.L., Valentine, R.J., Lacina, B.A., and Smith, T.E. (1994). "Laboratory Evaluation of Geosynthetic-Reinforced Pavement Sections." *Transportation Research Record 1439*, Transportation Research Board, National Research Council, Washington D.C., 25-31.

Banerjee, A., Prozzi, J. P., Prozzi, J. A. (2012). "Evaluating the Effect of Natural Gas Developments on Highways: Texas Case Study" *Transportation Research Record 2282*, Transportation Research Board, Washington, D.C., 49-56.

Barksdale, R.D., Brown, S. F., and Chan, F. (1989). "Potential Benefits of Geosynthetics in Flexible Pavement Systems." *National Cooperative Highway Research Program Report No. 315*, Transportation Research Board, National Research Council, Washington D.C.

Chesapeake Energy (2012). *Water Use in Deep Shale Gas Exploration*. Chesapeake Energy Fact Sheet, May 2012.

Gannett Fleming (2011). *Marcellus Shale Freight Transportation Study*. Northern Tier Regional Planning & Development Commission.

Kuhn, D. (2006). *Highway Freight Traffic Associated with the Development of Oil and Gas Wells*. Utah Department of Transportation, Salt Lake City, Utah.

Mason, J. M., Metyko, M. J., and Rowan, N. J. (1982). The Effects of Oil Field Development on Rural Highways. *Report No. TTI-2-10-81-229-1*. Texas Transportation Institute, Texas A&M University System, College Station, TX.

Mohammad, L. N., Herath, A., Gudishala, R., Nazzal, M. D., Abu-Farsakh, M. Y., and Alshibli, K. (2008). Development of Models to Estimate the Subgrade and Subaggregate layer Layers' Resilient Modulus from In situ Devices Test Results for Construction Control. *Report No. 406*, Louisiana Transportation Research Center, Baton Rouge, LA 70808.

Perkins, S. S., Christopher, B. R., Cuelho, E.L., Eiksund, G. R. (2004). "Development of Design Methods for Geosynthetic Reinforced Flexible Pavements." *Report No. DTFH61-01-X-00068*, U.S. Department of Transportation, Federal Highway Administration, Washington, D.C.

Quiroga, C., Fernando, E., and Oh, J. (2012). Energy Developments and the Transportation Infrastructure in Texas: Impacts and Strategies. *FHWA/TX-12/0-6498-1*, Texas Department of Transportation, Research and Technology Implementation Office, Austin, TX.

Tang, X., Chehab, G.R., and Palomino, A.M. (2008). "Evaluation of Geogrids for Stabilizing Weak Pavement Subgrade." *International Journal of Pavement Engineering*, Vol. 9 (5): 413-429.

Tang, X., Palomino, A. M., and Stoffels, S. M. (2013). "Reinforcement Tensile Behavior Under Cyclic Moving Wheel Loads." *Transportation Research Record 2363*, Transportation Research Board, Washington, D.C., 113-121.

Tang, X., Stoffels, S. M., and Palomino, A. M. (2014). "Resilient and Permanent

Deformation Characteristics of Unbound Pavement Layers Modified by Geogrids." *Transportation Research Record 2369*, Transportation Research Board, Washington, D.C., 3-10.

Non-Destructive Evaluation and Reinforced Design of Gravel Heavy Haul Road Structures in Northern Alberta

Fadi M. Jadoun[1], Ph.D., P.E., P. Eng. Khaled Galal[2], Ph.D.,
Edward Wilson[3], M.Sc., P. Eng., Amr Ayed[4], M.Sc., P. Eng. and
Khaled Helali[5], Ph.D., P. Eng.

[1]Project Manager, Stantec Consulting, 200-325 25th Street SE, Calgary, AB, T2A 7H8 Canada, Email: fadi.jadoun@stantec.com.
[2]Manager, Pavement and Infrastructure Division, Engineering and Research International (ERI), Riyadh, KSA, Email: khaled.galal@eri-rgme.com.
[3]Principal Geotechnical Engineer, Private Consultant, 1520 Phoenix Drive, Vernon, BC, V1B4B3 Canada, Email: wilsoned@shaw.ca.
[4]Project Manager, Stantec Consulting, 49 Frederick Street, Kitchener, ON, N2H 6M7 Canada, Email: amr.ayed@stantec.com.
[5]Manager, Infrastructure Management and Pavement Engineering (IMPE), Stantec Consulting, 49 Frederick Street, Kitchener, ON, N2H 6M7 Canada, Email: khaled.helali@stantec.com.

ABSTRACT: A case study is discussed herein where non-destructive deflection testing was carried out to achieve three goals; first, to evaluate the performance of existing heavy haul roads in Northern Alberta, Canada; second, to backcalculate in-situ moduli of various materials used in the construction of these roads; and third is to develop a heavy haul road structural design methodology based on existing empirical and Mechanistic-Empirical design methods, while utilizing material moduli backcalculated using a thickness-independent backcalculation approach. Heavy Weight Deflectometer (HWD) equipment was used to impact the surface of granular roads constructed with and without geosynthetics. A total of 11 haul roads were evaluated. The road structures ranged in thickness between 1.0 and 2.6 meters. Heavy loads were applied that simulate the 105 ton wheel load of the Caterpillar 797F truck. Results suggest that incorporating geosynthetic reinforcement in gravel pavements can cause pavements to behave stiffer under heavier loads, i.e. stress hardening. Moreover, Geosynthetics can be used to reduce the thickness of the road structure and save the non-renewable aggregates. HWD testing is an effective way to evaluate structural capacity and to determine in-situ material properties. A methodology is developed and successfully implemented for the design of heavy haul roads.

INTRODUCTION

The Oil Sands industry in Alberta, Canada has been one of the major sources of wealth and jobs for Albertans in specific and for Canadians in general. According to the Government of Alberta website (2014), Alberta has oil reserves of approximately

170 billion barrels, the third largest proven crude oil reserve in the world after Saudi Arabia and Venezuela. Oil sands are located in three major areas in Alberta underlying approximately 140,000 square kilometres (14 million hectares); Athabasca oil sands; Peace River oil sands and Cold lake oil sands. The three major areas are located in the northern part of Alberta. Approximately 600 square kilometers of land has experienced oil sands mining activity to date. According to the government of Alberta website (2014), there are 101 active oil sands project in Alberta as of April 2012.

Oil sands mining projects rely on heavy haul trucks in their mining operations to move overburden material, ore, and waste material within the project area. Haul trucks have grown in size and payload capacity to accommodate the demand of heavy hauling. One of the heaviest trucks available nowadays and in operation at most of the oil sands projects in Alberta is the Caterpillar 797F truck. According to Caterpillar website (2014), this truck has a payload capacity of 400 short tons (0.8 million pounds) and a gross vehicle operating weight of approximately 687 short tons (1.37 million pounds). It is fair to assume that the oil sand projects will increase in number and size throughout the coming decades, hence, the demand for such larger trucks will increase.

Unlike typical paved roads, gravel/unpaved heavy haul roads don't currently have an established standard structural design procedure. While there are different approaches available for the design and analysis of haul road sections, each of these approaches/techniques has their own weaknesses and requirements that could be sophisticated to measure. Furthermore, the use of geosynthetic reinforcement materials in pavement design is becoming more and more popular, which highlights a need to study the performance of these materials in the field.

PROBLEM STATEMENT

Existing haul road design approaches are either; 1) empirical in nature, which restricts validity and applicability to materials, traffic loads, and construction practices under which the empirical formulae were developed; or 2) mechanistic-empirical (M-E), which requires accurate layer thickness and accurate material properties as inputs. With increased truck payload capacities up to 400 short tons, and while utilizing modern geosynthetic materials for reinforcement, empirical approaches by themselves don't work. Similarly, in the absence of accurate layer thickness and material properties information, the available M-E design approaches cannot be efficiently applied.

The obstacles and uncertainties associated with the evaluation of existing pavements and the constraints this places on the development of a design and pavement evaluation process raises the need to develop the knowledge of how to incorporate unknown in-situ subgrade and construction material properties, along with inconsistent specifications for the construction materials, into a well-structured design and evaluation process. The knowledge of how to develop a design process with unknown and/or inaccurate pavement layer thickness information, which is very critical for M-E design approach, is needed. Additionally, there is a need to develop the knowledge of how to incorporate important parameters such as variable traffic

loads, loading history, use of geosynthetic reinforcement material, and construction practice and season(s) into the design procedure.

OBJECTIVE AND SCOPE

The objective of this paper is a three-fold; first is to evaluate the performance of existing heavy haul roads in Northern Alberta, Canada; second is to backcalculate in-situ moduli of various materials used in the construction of these roads; and third is to develop a heavy haul road structural design methodology. The design methodology is based on existing empirical and M-E design methods, but also utilizes material moduli backcalculated using a thickness-independent backcalculation approach. The developed design methodology will be implemented to design a new short and long term heavy haul roads built on top of oil sands. These roads should be capable of accommodating the Caterpillar 797F truck without failing catastrophically.

HEAVY WEIGHT DEFLECTOMETER (HWD) TESTING

Heavy-Falling Weight Deflectometer (hereafter referred to as: Heavy Weight Deflectometer (HWD)) is an equipment that can apply an adjustable load pulse to the pavement surface that simulates the load produced under a truck rolling wheel. The heavy load is produced by dropping a weight that is transmitted to the pavement through a circular loading plate. A load cell mounted on top of the loading plate measures the actual applied load. Deflection sensors mounted at various radial distances from the center of the loading plate measure the deflection of the pavement surface in response to the load. In general, larger deflection values indicate a softer pavement structure. A schematic diagram of the HWD equipment and the measured deflections profile (deflection basin) is shown in (Fig. 1).

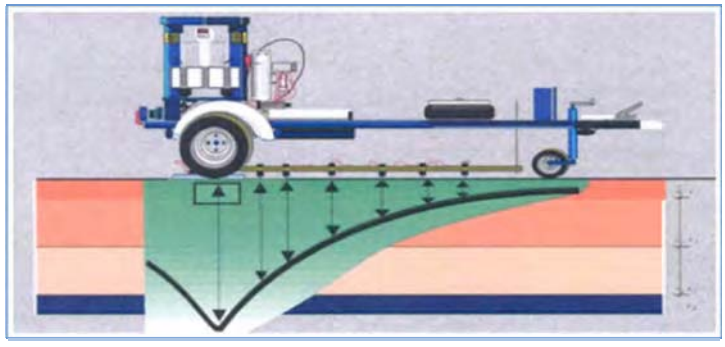

FIG. 1. Schematic of HWD Equipment and Deflection Basin

HWD testing was performed to initially determine the in-situ moduli of materials in various pavement cross sections. Design parameters (surface modulus, effective pavement layers modulus and subgrade resilient modulus) were then calculated for each homogeneous haul road section.

A loading plate with a diameter of 450 mm (18 inches) was used in this case study. Worth mentioning is that the HWD testing procedure is relatively fast; less than an

hour per kilometer in both directions. This minimizes disruptions and minimally affects haul productivity on mine haul roads.

Layer type and thickness information of the 11 evaluated roads is presented in Table 1 below. The information in Table 1 also indicates the presence or absence of geosynthetic reinforcement materials (e.g. geogrid and nonwoven geotextile) in the structure of each of the roads.

Table 1. Layer Type and Thickness Information of the Evaluated Roads

Road #	Pavement Layer Type and Thickness (mm)	Nonwoven Geotextile	TriAx® Geogrid
1	1,000 mm Pit Stripping and Pit Run Gravel	Yes	None
2	1,000 mm sand and 1,600 mm Glacial Gravel	Yes	4 layers
3	1,000 mm sand and 300 mm Glacial Gravel	Yes	None
4	1,000 mm to 1,400 mm sand and 450 to 575 mm Glacial Gravel	Yes	1 to 2 layers
5	1,000 mm sand and 350 mm Limestone	Yes	1 layer
6	1,800 mm Sand	None	None
7	1,000 mm to 1,300 mm sand and 550 mm to 850 mm Limestone	Yes	1 to 2 layers
8	1,000 mm sand and 850 mm Glacial Gravel	Yes	2 layers
9	1,000 mm sand and 450 mm Glacial Gravel	Yes	1 layer
10	1,000 mm sand and 800 mm Glacial Gravel	Yes	1 Layer
11	1,850 mm sand and 750 mm Glacial Gravel	Yes	2 layers

The HWD data was quality controlled, and then used to backcalculate structural layers and subgrade in-situ moduli using an Excel spreadsheet that was developed in-house for this work. The equations used within the spreadsheet are presented in subsequent sections of this paper.

While the other alternative of determining material moduli is to test field samples in the lab, there are multiple advantages of using HWD testing to determine pavement layer moduli. For example, the HWD approach accounts for in-situ conditions such as moisture content, construction practice, compaction history, and others. Additionally, the test is non-destructive, quick and was proven to be reliable and repeatable. Opposed to soil sampling, HWD testing can easily cover many more test points and locations across the site quickly and efficiently. Moreover, HWD testing of sections with geosynthetic materials allows for capturing the effect/contribution of the geosynthetic material to the overall stiffness of the tested section.

HWD Test Protocol

Table 2 summarizes the HWD testing protocols that were applied in this study. The loading protocol for each section was selected based on initial deflection measurements from the HWD seating drops. Seating drops help reduce the variability of the data by ensuring that the loading plate is in firm contact with the road and the deflection sensors are well seated. The selected HWD loads were designed to simulate the impact of wheel loads on heavy haul roads. Additionally, for each tested road section, the surface and air temperatures were measured and recorded.

Table 2. Heavy Weight Deflectometer Testing Protocols

Variable	Value
Loading Plate Diameter	450 mm (18 inches)
Sensor Spacing	0, 305, 610, 914, 1219, 1524, 1829, 2438 mm 0, 12, 18, 24, 36, 48, 60, 72, 96 inch
Loading[1,2,3]	**Loading Protocol 1** 89.0, 111.2, 155.7, 200.2 kN 20,000 – 25,000 – 35,000 – 45,000 lbf
	Loading Protocol 2 66.7, 89.0, 133.5, 177.9 kN 15,000 – 20,000 – 30,000 – 40,000 lbf
Drops / load level	Two
Tests / Section	Varies, section-dependent. Typically a test is performed every 200 m per lane

THICKNESS-INDEPENDENT APPROACH FOR BACKCALCULATING ELASTIC MODULI

Layer modulus information is one of the inputs required for a M-E analysis. To accurately backcalculate layer material moduli from HWD deflections, layer thickness information is needed. With missing and/or inaccurate layer thickness information, a thickness-independent backcalculation technique was implemented. The technique was introduced by Noureldin (1993). The proposed technique uses falling weight deflectometer (FWD) deflection bowl data to backcalculate the subgrade modulus (M_R) and the overall pavement layer modulus (E_p). According to Noureldin, this backcalculation scenario can be used when "thickness data are not available, not reliable or not representative". In 2004, Noureldin et al. (2004) expanded the methodology to handle a three-layer system for work done in Indiana.

This technique was developed originally for hard-surfaced pavements (asphalt concrete and Portland cement concrete) but has been applied in this case study to backcalculate in-situ subgrade and layer material moduli more accurately. While considering the large number of layers typically found in heavy haul roads (4 or more), the method of equivalent thickness (MET) or so-called; Odemark's method (covered later in this paper), is used to convert a multi-layer system into an equivalent system with fewer layers for use with the thickness-independent backcalculation technique.

Subgrade Resilient Modulus (M_R)

Resilient modulus (M_R) of the subgrade, at the time of testing, is calculated using Equation 1 as follows:

$$M_R = \frac{2149}{3 \cdot r_x \cdot D_x} \quad (1)$$

Where,

M_R = Subgrade soil resilient modulus (psi)
r_x . D_x = Largest radii-deflection multiplication (r_x in inches and D_x in mils)

Combined Pavement Modulus (E_p) Calculations

The combined pavement modulus (E_P) refers to the combined modulus of all road layers on top of the existing subgrade soil including granular layers and any engineered subgrade layers. E_P is typically calculated using Equation 2 based on the AASHTO 1993 design guide (1993). However, due to the lack of accurate layer thickness information, the thickness-independent formula shown in Equation 3 and recommended by Noureldin (1993) has been used instead to calculate E_p.

$$d_o = 1.5 \cdot P \cdot a \cdot \left\{ \frac{1}{M_R \sqrt{1+\left(\frac{D}{a} \cdot \sqrt[3]{\frac{E_P}{M_R}}\right)^2}} + \frac{1-\frac{1}{\sqrt{1+\left(\frac{D}{a}\right)^2}}}{E_P} \right\} \tag{2}$$

$$E_P = \frac{716 - \frac{2149}{r_X}}{D_0 - D_X} \tag{3}$$

Where,

E_p = Combined pavement modulus (psi)
D_0 = Deflection measured at the surface at the center of the loading plate
r_x . D_x = Largest radii-deflection multiplication (r_x in inches and D_x in mils)

Pavement Surface Modulus ($E_{surface}$) Calculations

The pavement surface modulus ($E_{surface}$) is a representation of the overall stiffness of a pavement structure, including the effect of subgrade. When testing on top of the subgrade, the surface modulus is a representation of the resilient modulus.

Surface modulus values are calculated using the Boussinesq's equations as reported by Ullidtz P. (1987) as follows:

Surface Modulus at Center of the Loading Plate:

$$E_0 = \frac{2 * P * \left(1 - \mu^2\right)}{\pi * a * d_0} \tag{4}$$

Surface Modulus at Distance ***r*** from the Center of the Loading Plate:

$$E_r = \frac{P * (1 - \mu^2)}{\pi * r * d_r} \quad (5)$$

Where,

E_o = Surface modulus at the center of loading plate (MPa or psi)
E_r = Surface modulus at a distance r from the center of loading plate (MPa or psi)
P = Applied load (kN or lbs)
μ = Poisson's ratio
a = Loading plate radius (mm or inch)
d_o = Deflection under the center of the applied load (mm or inch)
r = Radial distance measured from the center of the loading plate (mm or inch)
d_r = Deflection at distance r from the center of the applied load (mm or inch)

SUMMARY OF RESULTS

This section of the paper summarizes the results of the HWD testing. The goal here is to present to the readers actual test results and backcalculated performance parameters that can potentially become a point of reference when compared to the performance of similar-type structures. Note that each of the 11 roads in the following tables, except Road # 1, represents a group of sections. Sections of a road were grouped based on the testing directions (North Bound vs. South Bound or East Bound vs. West bound) but also based on differences in the road structure, with the material type being similar. Refer to Table 1 for layer type and thickness information. This section also summarizes the backcalculated modulus values of the limestone material; when positioned at different depths. This is of specific interest because the limestone material was used in the construction of heavy haul roads on oil sands foundation, as presented later in this paper.

Applied Loads and Measured Deflections

As mentioned earlier, the target loads are essentially determined based on the deflection results obtained from the seating drops. A target load protocol is then selected, see Table 2. Note that the actual load felt by the HWD load cell (sitting on top of the loading plate) is not always similar to the target load. The actual recorded loads reflect the pavement stiffness under the loading plate. Gravel roads typically have more variability in their performance compared to paved roads. The load protocol is changed within a section only if measured deflections get out of the calibration range, or are found to be very low. Table 3 provides a summary of the mean applied loads and corresponding deflections measured under the loading plate. The actual loads presented in Table 3 are the mean loads for all the sections within each road.

Table 3. Mean Applied Loads and Measured Deflections under Loading Plate

Road #	Actual Applied Load (kN)				Measured Deflections (micron)			
	Load Level 1	Load Level 2	Load Level 3	Load Level 4	D0-Load 1	D0-Load 2	D0-Load 3	D0-Load 4
1	68.1	93.4	122.3	156.6	1,524	2,032	2,667	2,870
2	63.6	90.3	138.8	168.6	1,473	2,007	2,896	2,972
3	67.4	93.4	137.7	172.6	927	1,257	1,715	2,019
4	67.4	94.6	137.4	173.3	993	1,273	1,750	2,022
5	66.4	94.0	135.3	172.3	879	1,153	1,556	1,835
6	77.4	108.3	154.6	199.7	584	800	1,156	1,435
7	68.3	96.5	150.6	192.2	876	1,194	1,715	1,994
8	68.3	96.3	139.4	175.3	737	965	1,295	1,524
9	73.2	102.3	153.0	192.2	737	991	1,435	1,715
10	72.7	100.5	145.2	184.4	546	762	1,105	1,384
11	72.9	102.3	147.7	185.9	457	610	864	1,016

Deflections measured under the loading plate are considered to be a quick indicator of the overall modulus of the pavement structure. For similar loads, smaller deflections under the loading plate indicate stiffer road structures.

Subgrade Modulus (M_R)

Table 4 ranks the different roads in an ascending order based on the mean backcalculated M_R values. Additionally, Table 4 shows the minimum, maximum, standard deviation and covariance values calculated for each road. The data suggests that the smallest mean M_R value is approximately 26 MPa (3.8 ksi), and the largest mean value is 85 MPa (12 ksi). Roads with lower M_R variability (represented by lower Standard Deviation and Covariance) typically indicate consistency in the in-situ subgrade materials and also in the construction technique. With the exception of Road # 1, which was built on top of Muskeg material, the in-situ subgrade soils underlying other roads are of the same type. However, differences may be attributed to a group of factors including; the season in which the roadbed was compacted/constructed, heavy truck traffic history and construction technique. The covariance results in Table 4 suggest a large variability in the subgrade stiffness on Road # 11. Detailed historical information of the aforementioned factors was unavailable, and hence, no clear explanation could be concluded.

Table 4. Statistics of Subgrade Modulus (M_R) by Road, MPa

Road #	Min.	Max.	Mean	Std. Dev.	Covariance
1	8.5	67.3	26.3	14.6	22.0%

2	15.4	45.8	27.9	7.2	35.1%
3	21.5	71.8	39.6	10.3	21.1%
4	26.8	57.9	43.7	7.3	22.9%
5	33.8	63.2	46.7	8.7	22.0%
6	31.5	68.7	47.0	9.8	48.8%
7	23.6	69.4	47.1	9.0	22.8%
8	23.1	91.3	48.3	12.7	23.8%
9	34.4	73.5	48.7	8.2	17.6%
10	55.6	110.2	83.4	11.1	30.4%
11	51.9	137.1	85.0	22.1	130.4%

Worth mentioning is that the data presented in Table 4 reflects the in-situ conditions of the soils at the time of testing. Factors that affect the backcalculated M_R include moisture content and compaction history, among other factors. Repetitive HWD testing can be used to assess the seasonal variability impact on the in-situ subgrade resilient modulus and is recommended.

Effective Pavement Layers Modulus (E_p)

Table 5 ranks the different roads in an ascending order based on their mean E_P. The table also presents the minimum, maximum, standard deviation and covariance values calculated for each road. The information in Table 5 suggests that the smallest backcalculated mean E_P is 123 MPa (18 ksi) and the largest is approximately 455 MPa (66 ksi). Note that roads with higher subgrade stiffness allow for a better compaction to be achieved for subbase and overlaying layers. Better compaction translates to a higher pavement modulus (E_P). This is to a large degree consistent with the M_R and E_P information presented in Table 4 and Table 5 respectively. In general, sections with higher E_P are those constructed on stiffer subgrade soils. Few exceptions can be noted.

Table 5. Statistics of Effective Pavement Layers Modulus (E_p) by Road, MPa

Road #	Min.	Max.	Mean	Std. Dev.	Covariance
2	41.6	208.1	123.0	28.3	23.0%
1	50.0	383.3	188.8	68.6	36.3%
4	109.6	346.7	220.0	50.7	23.0%
7	101.6	452.1	225.6	57.8	25.6%
5	155.4	391.0	248.5	64.0	25.8%
3	117.8	786.3	269.2	145.5	54.0%
8	131.1	514.5	292.8	77.3	26.4%
9	177.4	579.9	312.3	86.0	27.5%
10	204.2	508.8	337.9	67.0	19.8%
11	232.7	771.0	445.7	106.2	23.8%
6	205.3	710.2	454.2	156.2	34.4%

Surface Modulus ($E_{surface}$)

Table 6 ranks the different roads in an ascending order based on the backcalculated mean surface modulus values. The minimum, maximum, standard deviation and covariance statistics are also presented. The data in Table 6 suggests that the smallest mean surface modulus value is approximately 113 MPa (16 ksi) and the largest is approximately 400 MPa (58 ksi). As noted earlier, the $E_{surface}$ represents the overall stiffness of a road section as felt under the loading plate. The surface modulus can be looked at as a combined effect of the E_p and the M_R.

Table 6. Statistics of Surface Modulus ($E_{surface}$) by Road, MPa

Road #	Min.	Max.	Mean	Std. Dev.	Covariance
2	43.3	188.5	113.3	24.9	22.0%
1	39.5	259.7	119.1	41.8	35.1%
4	100.4	281.7	186.3	39.4	21.1%
3	97.6	513.1	200.9	88.5	43.3%
7	96.5	359.3	201.1	46.3	22.9%
5	133.5	298.8	201.8	45.3	22.0%
9	154.7	402.1	246.5	56.3	22.8%
8	113.7	409.7	248.5	59.2	23.8%
10	199.4	439.9	309.6	53.6	17.6%
6	180.1	520.4	342.7	104.5	30.4%
11	233.5	616.6	399.0	83.1	20.8%

BACKCALCULATED MODULUS OF LIMESTONE

The limestone material was used in the construction of a group of roads as shown in Table 1. The material was positioned at different depths in the pavement structure as it was used as subbase, base and surface layer. The surface layer consisted of 75 mm Nominal Maximum Aggregate Size (NMAS) whereas the base consisted of 150 mm NMAS material and the subbase was basically a quarry run limestone. Due to the paper size limits, only the final recommended results are presented below:

- 400 MPa is the recommended modulus for the 75 mm crushed surface;
- 300 MPa is recommended for the 150 mm crushed base; and
- 190 MPa is recommended for the subbase quarry run.

STRESS SENSITIVITY OF HAUL ROADS WITH GEOSYNTHETIC MATERIALS

Stress sensitivity is a term used to explain the stress hardening or the stress softening behavior of granular and/or fine soils under load. Stress hardening refers to an increased backcalculated modulus with increased applied load, whereas stress softening refers to a decreased backcalculated modulus with increased loads. In this

work, pavement moduli were backcalculated at each applied load level and the stress sensitivity of each pavement section was examined.

At the time of HWD data collection, some test sections were completely constructed while others were still in different construction stages. The opportunity to test incomplete pavement sections was invaluable, because it allowed for the evaluation of the effect of different layer materials and different number and location of geogrid reinforcement layers on pavement performance. In this work, Tensar TX-160 TriAx® geogrid was used. Additionally, Nilex 4553 nonwoven geotextile material was used as a separator between gravel/aggregate and engineered subgrade (silty fine sand).

HWD loads were applied on heavy haul road sections with and without geogrid reinforcement. Sections with geogrid reinforcement ranged in the number of geogrid layers used (from 1 layer up to 4 layers) as shown in Table 1.

Backcalculated pavement moduli, specifically the Effective Pavement Layer Modulus (E_p) suggest that the use of the Tensar TX-160® geogrid reinforcement causes stress-hardening behavior. Other types of geogrid materials have not been tested, and therefore, this conclusion should be expanded to cover all types of geogrid reinforcement materials.

REVIEW OF AVAILABLE HAUL ROAD DESIGN APPROACHES

Various methods/approaches have been utilized for the design of heavy haul roads; the CBR Curves method; the Modified CBR method and the M-E method are three examples. The following is a brief explanation of each of these methods.

CBR Curves Method

The California Bearing Ratio (CBR) Curves method is one of the first, and yet most commonly accepted haul road design methods. As the name implies, the CBR curves method is based on the CBR Parameter. The CBR is a simple strength indicator that compares the bearing capacity of sand or aggregate material with that of a standard well graded crushed stone with a CBR of 100%. Tannant and Regensburg (2001) reported that the first use of CBR values to calculate the required cover thickness over in-situ material was reported by the California Division of Highways during 1928-1929. In 1977, Kaufmann and Ault (1977) were among the first to apply the CBR method for the design of haul roads.

Being an empirical method, the CBR Curves method has several shortcomings that are mentioned in the literature. Three primary shortcomings are: 1) while the CBR Curves method does consider the wheel loading, it does not take traffic density and traffic volume into account; 2) the method does not consider the properties of the surface material, since the surface layer thickness is the last step of the design process that does not depend on the surface material CBR value; and 3) the CBR Curves method was developed to accommodate a maximum wheel load of approximately 80 metric tons, the maximum available at the time. With larger and heavier trucks in use nowadays, there is uncertainty as the design curves are extended without any supporting experience. Such is the case for the 400-Ton CAT 797F truck with a wheel load of 105 metric tons.

Modified CBR Method

A Modified CBR method was reported by Tannant and Regensburg (2001) which uses the modulus of the pavement, tire contact radius and pressure, wheel loading, as well as a deflection factor for designing haul road pavement structures. This Modified method takes into consideration the effect of axle geometry and different wheel loads on the pavement, by calculating the Equivalent Single Wheel Load (ESWL) instead of just relying on a single wheel load as is the case in the CBR Curves method. The logic behind this method is two-fold; first, the ESWL has the same circular contact area as that of the other wheel loads; and second, the maximum deflection generated by the ESWL is equal to the maximum deflection generated by the group of wheels.

While the Modified CBR method is an improvement over the CBR Curves method, it still depends on CBR as the basis for cover and layer thickness calculations. In addition, deflection factors will have to be developed for the 400-Ton haul trucks.

Mechanistic-Empirical Method

M-E design methods are based on the calculation of the developed stresses, strains and deflections in a layered haul road section under wheel loads. Pavement designs developed using such mechanistic approaches are typically affected by the following factors: 1) material properties, including elastic modulus and Poisson's ratio; 2) climatic effect on material properties; and 3) traffic loading conditions.

Roger Thompson (2011) presented a haul road pavement design methodology that is based on limiting the vertical compressive strains on haul road layers to maximum allowable values; less than 1000 microstrains for a 20-year design life; and less than 1500 microstrains for a 5-year design life. Vertical compressive strains on top of unbound layers affect permanent deformation, while radial strains in bound layers are responsible for cracking. Since haul roads are typically unpaved, the limiting vertical strain in the design of haul road sections is critical. In addition to the vertical compressive strain limits, the maximum stress levels experienced within each pavement layer should be smaller than the compressive strength of that layer.

While the M-E method by itself is an excellent design method, it still requires the resilient modulus of different layer materials as an input. Resilient modulus laboratory testing is expensive to perform and requires special equipment and skills. Moreover, this method requires monitoring/calibration with field performance data to verify the reliability of the method for each haul road conditions.

Equivalent Thickness Technique

While the Equivalent Thickness Technique is not an actual design method, it was still used as part of the haul road design approach for the work presented herein. The equivalent thickness approach, also known as the Odemark method, was originally developed by Odemark in 1949 to transform a multi-layer pavement structure into an equivalent one-layer structure that has a specific thickness and one elastic modulus, which corresponds to the unbound base material. The equivalent thickness approach

has been used in this work to manipulate the thickness of the different layers to optimize a fill thickness that can successfully spread the load and minimize the critical stresses on top of the natural subgrade soil.

HAUL ROAD DESIGN METHOD USED IN THIS WORK

The following four factors were considered in the development of the heavy haul road pavement design method that is used in this work:

1. The use of geotextile and geogrid materials in the haul road structures;
2. The designs were developed to handle the CAT 797F 400-Ton haul trucks, for which CBR curves are unavailable;
3. Despite some "noise" due to inaccurate subbase (engineered subgrade) sand layer thickness information, the Heavy Weight Deflectometer (HWD) data measured for the different sections (total of 35 homogenous haul road sections) were essential for backcalculating material moduli that are representative of field conditions at the time of testing; and
4. The uncertainties in the thickness data of the subbase (engineered subgrade) sand layers at different sections had triggered the need for utilizing a non-thickness based approach in combination with the method of equivalent thickness.

In conjunction with the aforementioned four factors, three primary design methodologies/references were considered for developing the haul road designs: first; *Guidelines for Mine Haul Road Design* by Tannant and Rogensburg (2001); second; *Design of Surface Mine Haulage Roads-A Manual* by Kaufman and Ault (1977); and third; *An Integrated Approach to Mine Haul Road Design* by Thompson R. (2011).

Design Method Used in This Work

Utilizing the authors' engineering experiences and information from the three sources mentioned above, the pavement designs presented in this paper were developed using a combination of the CBR Curves method, the M-E method, and the Equivalent Thickness Technique, while utilizing material moduli information that were calculated using a thickness-independent backcalculation approach. The CBR Curves method was modified in conjunction with the equivalent thickness technique to accommodate the wheel loading experienced from the CAT 797F haul truck for calculating the required fill covers. The mechanistic approach was utilized to check the critical responses developed within the pavement structures and to ensure that such responses are still within the allowable limits for proper pavement performance.

Once material properties (including the effect of geogrid material) are backcalculated using the non-thickness technique, the empirical design approach is used to estimate the overall cover thickness for a specific wheel load and material moduli. Thickness of individual layers with different material types is also approximated.

Backcalculated moduli are used in conjunction with the JULEA Multi-layer Elastic Analysis (MEA) program, developed by Uzan (1989), to refine and optimize the preliminary designs to ensure that critical responses due to truck wheel loads, mainly

compressive strains and vertical deformations, are still within the allowable limits based on traffic level.

Existing haul road design criteria suggest that the vertical compressive strain at any point in an unbound pavement structure should be in the range of 1,500 to 2,000 microstrains to avoid pavement structural failures. A more accurate calculation has been carried out in this work that utilizes existing formula for estimating the maximum allowable vertical strain based on the amount of hauled ore and overburden materials, truck payload capacities, and the desired design life of the pavement. For this work, a limit of 1,368 microstrains has been established as the design criterion for a pavement design life of 10 years. In addition, a general design/evaluation requirement is that the maximum vertical deformation at the pavement surface should be less than or equal to 6 mm, to maintain the integrity of the wearing/surface layer and to reduce the required maintenance.

HAUL ROAD STRUCTURAL DESIGN ON OIL SANDS SUBGRADE

This section presents the recommended pavement designs for short and long-term operations on haul roads constructed on oil sands subgrade. The recommended designs are developed to accommodate the Caterpillar 797F haul trucks throughout the design life of the haul roads without catastrophic failures.

Oil Sands Subgrade Modulus

Due to safety reasons, the oil sands subgrade locations could not be accessed for HWD testing. The design subgrade modulus value was estimated based on information reported by Joseph Anochie-Boateng (2007), who carried out a series of laboratory resilient modulus tests on different oil sand samples with different bitumen content and at different test conditions. The oil sands design modulus value was selected based on the following four test conditions: Bitumen content of oil sands samples = 8.5 %; Resilient modulus test temperature = 20°C; Loading pulse time = 0.5 sec; and Deviatoric stress/ Confinement pressure ratio = 4.5.

Based on the information above, a design modulus value of 105 MPa was selected for the design.

Design Traffic

Traffic volumes used for the design of short and long term pavement structures for this case study are calculated based on information received from the oil sands plant as follows:

$$\textit{Short Term} \left[\frac{10{,}000 \ \frac{tons}{hr} \times 20 \frac{hrs}{day} \times 350 \frac{days}{year} \times 2 \ years}{400 \ \frac{tons}{truck \ pass}} = 350{,}000 \text{ CAT 797F trucks} \right]$$

$$Long\ Term \left[\frac{10{,}000\ \frac{tons}{hr} \times 20\ \frac{hrs}{day} \times 350\ \frac{days}{year} \times 10\ years}{400\ \frac{tons}{truck\ pass}} = 1{,}750{,}000\ \text{CAT 797F trucks} \right]$$

Short- and Long-Term Pavement Design Recommendations

Table 7 provides a summary of the recommended pavement designs for the short-term (2-year life) and the long-term (10-year life) for the aforementioned traffic.

Table 7. Recommended Pavement Designs for Short and Long-Term Roads

Layer Material Type and Quality	Recommended Thickness (mm)	
	Long-Term Design (10-year)	Short-Term Design (2-year)
75 mm Crushed Limestone Surface E = 400 MPa, Poisson's ratio =0.35	800	300
150 mm Crushed Limestone Base E = 300 MPa, Poisson's ratio =0.35	1,100	500
Quarry Run Crushed Limestone Subbase E = 190 MPa, Poisson's ratio =0.35	1,200	600
Oil Sand semi-lean Subgrade E = 105 MPa, Poisson's ratio =0.35	Semi-Infinite	
Total Pavement Thickness (mm)	**3,100**	**1,400**

CONCLUSIONS AND RECOMMENDATIONS

The following conclusions and recommendations are drawn from this case study:

- Heavy Weight Deflectometer (HWD) is a non-destructive and convenient approach that can successfully be used on heavy haul roads to obtain in-situ material properties.
- HWD testing can successfully capture the differences in field performance due to variable field conditions. This was evident in the M_R results, where different stiffness values were backcalculated for similar subgrade soils.
- Deflections measured under the loading plate are found to correlate reasonably well with the backcalculated surface modulus of the pavement of heavy haul roads.
- The use of Tensar TX-160 TriAx® geogrid material is found to result in stress hardening effect, i.e. pavement stiffness increases under increased load levels.
- An approach is presented and implemented in this paper for the design of heavy haul roads utilizing backcalculated modulus results from HWD testing.
- In order to determine reasonable modulus values for different road construction materials, it is recommended that HWD testing be carried out in two different seasons; April to May is a thawing period under which the material is at its lowest stiffness and August to September is a time frame during which the material can show higher stiffness values.

REFERENCES

Government of Alberta website (2014). http://oilsands.alberta.ca/resource.html and http://www.oilsands.alberta.ca/FactSheets/Economic_FSht_May_2012_Online.pdf. Last Accessed January 13, 2014.

Caterpillar (2014). http://www.cat.com/en_US/products/new/equipment/off-highway-trucks/mining-trucks/18093014.html. Last Accessed January 8, 2014.

Noureldin, S. (1993) "New Scenario for Backcalculation of Layer Moduli of Flexible Pavements." Transportation Research Record, Vol. 1384, pp: 23-28, National Research Council, Transportation Research Board, Washington, DC.

Noureldin, S., Zhu, K., Harris, D., and Li, S. (2004). "Non-Destructive Estimation of Pavement Thickness, Structural Number, and Subgrade Resilience Along INDOT Highways." Final JTRP Report, Contract No.SPR-2408. Purdue University, West Lafayette, IN, 2004.

American Association of State Highway & Transportation Officials. (1993). "Guide for Design of Pavement Structures", Washington, DC.

Ullidtz P. (1987). "Pavement Analysis", Elsevier Science Publishers, New York.

Tannant, D. D. and Regensburg, B. (2001). "Guidelines for Mine Haul Road Design". Final Report, University of British Columbia - Okanagan, Kelowna, B.C. Canada.

Kaufman, W. W. and Ault, J. C. (1977). "Design of Surface Mine Haulage Roads – A Manual." Information Circular 8758, United States Department of the Interior, Bureau of Mines.

Thompson, R. (2011). "GSFM - An Integrated Approach to Mine Haul Road Design". Mine Road Workshop, Western Australian School of Mines, Curtin University. Kalgoorlie, Australia.

Uzan J. (1989). JULEA linear elastic analysis computer program. US army waterways experiment station, Vicksburg, Mississippi.

Anochie-Boateng J. K. (2007). "Advanced Testing and Characterization of Transportation Soils and Bituminous Sands". Dissertation. University of Illinois at Urbana-Champaign, Urbana, Illinois.

Confined-Aggregate-Concrete MEPCO Loading Dock Road, Morgantown, WV Case Study

Samuel G. Bonasso, P.E., F.ASCE

[1]President, Reinforced Aggregates Company, (www.mechanicalconcrete.com) P.O. Box 199, Morgantown, West Virginia 26507, U.S.A., E-mail: sam@reagco.com

ABSTRACT: Trucking from shale oil and gas development destructively impacts rural, low volume farm-to-market roads. The options for repair and reconstruction are relatively few and involve large quantities of new stone. An emerging aggregate confinement technology is being used on industrial roadways with significant success. This U.S. and Canadian patented technology trade named, Mechanical Concrete®, physically confines aggregates within a thin-walled structural cylinder, creating a confined-aggregate-concrete, CAC. It creates a road base with a collection of open ended, waste-tire-derived, cylindrical segments filled with crushed stone, i.e. tire-derived-geo-cylinders, TDGC. This physical confinement process creates a, porous, virtually solid material with a minimum, lab proof tested, load supporting capacity in excess of 1380 kPa (200 psi). On June 20, 2011, MEPCO Mining, Morgantown, WV, reopened a gravel surface road at its Mon River dock, reconstructed with a CAC base. This road handles three-hundred 36,364 kg (80,000 lb) coal trucks per day. Prior to reconstruction this road required approximately 2 truckloads of new crushed stone per week for maintenance. The new road has consistently been maintained with 2 truckloads of new stone per month; an over 75% reduction in maintenance costs. Stone filled tire-derived-geo-cylinders are a sustainable, economical alternative for reconstructing rural roads.

INTRODUCTION

MEPCO is an established mining company in the Morgantown, WV area associated with the Longview Electric Power Plant in Fort Martin, WV. It operates a loading dock nearby on a multi-acre site on the Monongahela River (39°41'6"N, 79°56'49"W). The Monongahela River and its basin are the remnants of a glacial lake. The name is from an American Indian word meaning 'falling and eroding banks'. The river's banks and those nearby live up to this name and are in a state of relatively frequent geologic movement.

In addition to a coal storage yard and a barge load out the site contains: a truck scale with a 135 m (450 foot) long stone surfaced access road and reinforced concrete

approach and exit ramps and an exit road. This truck scale access road and the scale approach ramps are the subjects of this paper.

For almost 30 years prior to the summer of 2011 MEPCO maintained this stone surfaced road utilizing stone mined from its coal operations and local quarries. The dock was formerly the Riverside private park and swimming pool. It was closed in the late 1970's and was purchased by mining interests and converted into a coal dock and river barge loading facility. The pool was filled in and the site was raised to its current elevation, approximately, 245 m (816 ft.)**,** with the addition of from 1.2 m to 4.8 m (4 to 16 feet) of rock fill from surface mining operations. In 2000 the site, scale and roads were upgraded and improved. It operated under this scenario until June 20, 2011, when the new stone filled, tire-derived-geo-cylinder based access road and reinforced concrete ramps were put into service along with some other facility modifications.

The highway and heavy project contractor, Laurita, Inc. of Morgantown, WV, is established and well known in northern West Virginia and southwestern Pennsylvania and provides services to the oil and gas industry. Laurita has provided support services to MEPCO for several years. In December, 2010, they were directed to reconstruct approximately 143 m (475 feet) of the nearby Dana Prime coal mine asphalt access road for MEPCO. They chose a Mechanical Concrete® base for a 10 inch reinforced concrete wearing surface. The construction success and performance of the new stone filled, tire-derived-geo-cylinder, TDGC, base on this road motivated Laurita personnel to consider the same process for the MEPCO coal loading dock access road.

Confined-aggregate-concrete construction technology applications are for load support and roadway bases, retaining and bearing walls and erosion control. It's been called an industrial strength version of the geocell, but with wider applications and at considerably less cost. It uses a waste auto or light truck tire with both sidewalls removed to create a tire-derived-geo-cylinder, TDGC, which when stone filled, rigidly confines and solidifies the stone aggregate which remains porous. See photo FIG. 1. It was discovered by the author in 2004 and has been in research, development and demonstration since 2005. The first test road is still in use. It was constructed in 2006 by the West Virginia Division of Highways in Doddridge County, WV, an area of significant Marcellus shale play activity. Since then road projects have been constructed in four other states, California, Arizona, Ohio and Texas. Reinforced Aggregates Company licenses this US and Canadian patented technology and provides technical support and training.

FIG. 1. Typical Tire-Derived-Geo-Cylinder-Confined Aggregate Concrete Cell

It is a uniquely sustainable technology, in constructing industrial road bases since it: 1. Environmentally Reuses waste tires without sidewalls in their basic original form, 2. Economically Provides a lower cost alternative to conventional construction methods, 3. Technically Offers a consistently stronger result than conventional construction methods without the need for testing and 4. Socially Uses less energy and material, smaller equipment, no water, and no specially trained personnel.

LABORATORY TESTS

Lab testing in late 2005 determined, for a variety of reasons which will be discussed, that the optimum material for use in the tire-derived-geo-cylinder was crushed stone graded to meet the AASHTO #57 gradation. These tests were to assess the performance of a range of aggregate materials when confined. Coarse sand, AASHTO #8, AASHTO #57, and a 20 mm, (3/4 inch) crusher run limestone gradation were confined and load tested in two, instrumented, 508 mm, (20 inch) diameter, steel cylinders—one 305 mm (12 inches) long and the other 914mm (36 inches). It was the object of these tests to determine if these materials while subjected to cylindrical confinement could achieve a load supporting pressure of 1389 kPa (200psi) from various size load heads without failure and how the lateral pressure was distributed, i.e. to assess Poisson's ratio. This 1380 kPa (200 psi) test pressure value is significant since it is two times the 690 kPa (100 psi) pressure of a heavy dump truck tire or over-the-road semi-truck tire.

Load tests on the aggregates in the steel cylinders were conducted with steel load heads of 152 mm (6 inch) diameter, 304 mm (12 inch) diameter and 456 mm (18 inch) diameter. With one exception the result of confinement allowed the aggregate materials to achieve the 1389 kPa (200 psi) objective. The exception was the 152 mm (6 inch) diameter load head on the coarse sand, which failed at the usual upper compression load limit for sands, around 414 kPa (60 psi). However, it is worth noting that the 304 mm (12 inch) and 452 mm (18 inch) load head tests on sand were

able to achieve 1380 kPa (200 psi), over 3 times the usual load supporting capacity for sands. See the References for a technical report with more detail on these tests.

In addition a separate lab load test was performed on a column made up of 6 stacked tire-derived-geo-cylinders filled with AASHTO #57 limestone. This was a similar load test and it was also able to achieve the 1380 kPa (200psi) loading, for the 452 mm (18 inch) diameter load head, which amounted to a 22,727 kg (50,000 lb) concentrated load.

TIRE AND TDGC STRENGTH CHARACTERISTICS

In general auto tires are designed for a maximum operating pressure of 304 kPa (44 psi). It is appropriate to assume a design factor exists on this *operating pressure* even though its value is not public knowledge. When a tire-derived-geo-cylinder is placed on the ground, filled with stone and a fully loaded truck tire passes over it; the calculated lateral pressure on the inside of the cylinder is between 55 and 83 kPa (8 and 12 psi) depending on the tire width and cylinder diameter. See Figure 2.

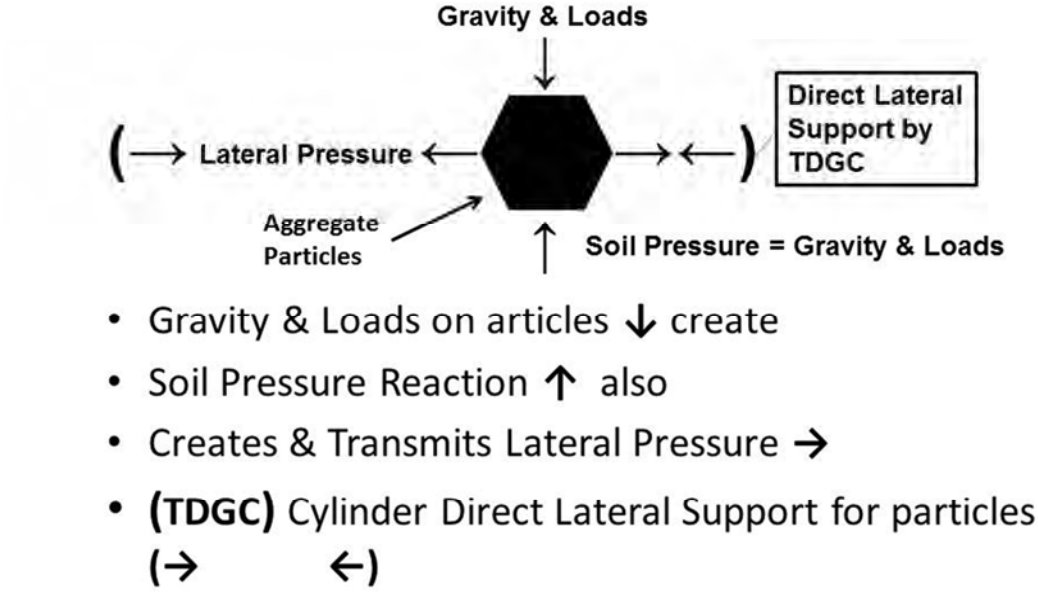

FIG. 2. Diagram of Aggregate /TDGC Loads

Assuming a relatively uniform pressure distribution, a typical calculation of the inner pressure on a tire-derived-geo-cylinder, TDGC, loaded with a truck wheel is as follows:

Surface Area tire-cylinder (SA) = Circumference x Tread Width= $\pi\ D\ W$

Lateral Force (LF) = Vertical Loads x Poisson's Ratio = $F * \mu$

$$(LPTCS)\text{Lateral Pressure Tire Cylinder Surface} = \frac{P}{A} = \frac{LF}{SA} = F\,\mu\,/\,\pi\,D\,W$$

E.g.—Tire Diameter 711mm (28”), Tire Tread Width 216mm (8.5”),
Wheel Load 9090 kg (20,000lb), Poisson’s ratio = 0.3
LPTCS = 20,000 x .3/ 3.1416 x 28 x 8.5 = 55.3 kPa (8.02 psi)

This indicates an operational design factor for stone filled, tire-derived-geo-cylinder of more than 3 against the tires original maximum operating pressure and more than 4 on its ultimate strength. This is significant since it means that in civil engineering applications stone filled, tire-derived-geo-cylinders are extremely strong and have the prospect of an indefinite, long term service life.

Tire-Derived-Geo-Cylinder Confinement, Geometry and Subgrade Effects

The geometry of the, TDGC, tire-derived-geo-cylinder also contributes to load distribution and the functioning of a confined aggregate concrete road base. A 711mm (28 inch) diameter tire tread generates a cylindrical area of approximately 3900 centimeters squared (600 square inches). A loaded truck tire with a 690 kPa (100 psi) tire pressure and a 9090 kg (20,000 pound) wheel load creates a foot print of 1300 centimeters squared (200 square inches). This ratio of 1300/3900 (200/600) indicates the load redistribution impact of a stone filled, tire-derived-geo-cylinder base to reduce the pressure on the subgrade material by at least half or as much as one third, from 690 kPa (100 psi) to approximately 233 kPa (34 psi).

This ‘snowshoe’ or ‘elephant foot’ load redistribution effect has functioned effectively on two very soft soils. First, on soft Appalachian clay subgrades with an approximately 138 kPa (20 psi) bearing strength and second, on extra fine sand in California’s Imperial Dunes with less than138 kPa (20psi) bearing strength. These are locations where stone filled, tire-derived-geo-cylinder road bases were built. Separation fabric was placed on these road subgrades and the stone filled, tire-derived-geo-cylinder base supports low volume road traffic.

THE MEPCO DOCK ROAD

West Virginia is a mountainous, mid Atlantic state subject to a true four season climate with an annual 1. average rainfall range from 1020 to 1524 mm (40 to 60 inches); 2, average snow fall range from 381 to 3810 mm (15 to 150 inches); and 3. a range of 15 to 25 freeze thaw cycles. It is a challenging place to construct unpaved roads particularly those subject to heavy industrial traffic. For unpaved gravel roads, maintenance is a given cost of operation, particularly in the energy industry. The only questions are how to quantify it and how to keep it to a minimum. Established WV mining companies like MEPCO understand this, plan for it and look for ways to optimize it; since road maintenance is an ongoing cost of doing business. The MEPCO dock handles approximately 300 coal trucks per day at 36,364 to 45,454 kg (80,000 to 100,000 lbs.) each, that’s 6,500 trucks per month (Figure 3).

FIG. 3. Typical Daily Traffic at the MEPCO Dock Road

CONVENTIONAL VS. STONE FILLED, TDGC APPROACH

The generally accepted conventional method of constructing an industrial roadway is: (1) on top of the prepared subgrade, to place a stone bridging layer of large diameter stone, i.e. +152mm (+6 inch) diameter material; then, (2) on top of the bridging layer, to install a compacted road base layer and finally, (3) install a stone or other type wearing surface. This conventional engineered reconstruction approach to this road would have included: (1) Preparing and compacting and perhaps even stabilizing the subgrade; (2) Constructing a 609 mm (24 inch) thick bridging layer of large size, 152 mm (6"+) stone material; (3) Topping this bridging layer with a 152 mm (6 inch) thick base course; and (4) topped with a 152 mm (6 inch) wearing surface of optimally compacted 38 mm (1.5 inch) crusher run fully graded limestone material. This result would have been a 914 mm (36 inch) section depth. The primary goal of this design depth is to spread out and redistribute the truck wheel loads on the subgrade, in order to optimally keep the subgrade load pressures below a certain value. See Figure 4.

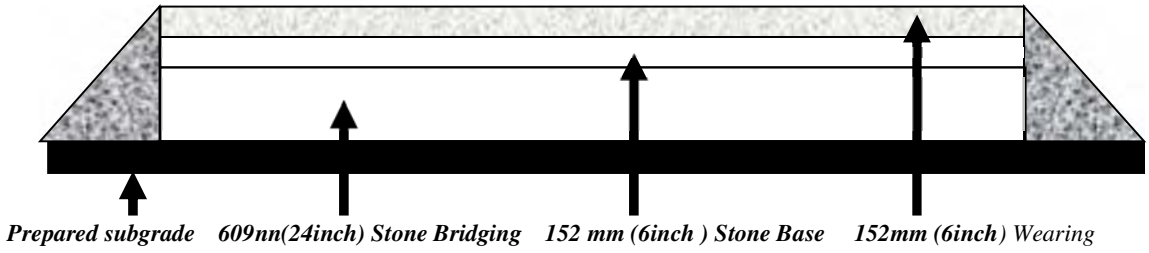

FIG. 4. Conventional 914 mm (36 inch) Cross Section

The 216 mm (8.5 inch) wide tire-derived-geo-cylinder with its load redistribution effectively creates the same or improved 'bridging' effect on the subgrade soils as the 609 mm (24 inch) conventional bridging layer and the base course. Therefore, one key reason for selecting stone filled, tire-derived-geo-cylinders was the reduction in the depth of the cross section and the associated reduction in industrial road construction cost.

THE MEPCO DOCK PROJECT ROAD DESIGN

The dock road cross section consists of a prepared and compacted subgrade for a 7.2 m (24 foot) wide roadway with 600 mm (2 ft) shoulders. The base consists of a 216mm (8 1/2 inch) base layer of stone filled, tire-derived-geo-cylinders. The 203 mm (8 inch) wearing surface layer is optimally compacted 38 mm (1.5 inch), well graded, crusher run, with a side slope, super-elevation of 12.7 mm per 305 mm (0.5 inch per ft) for drainage. See cross section FIG. 5.

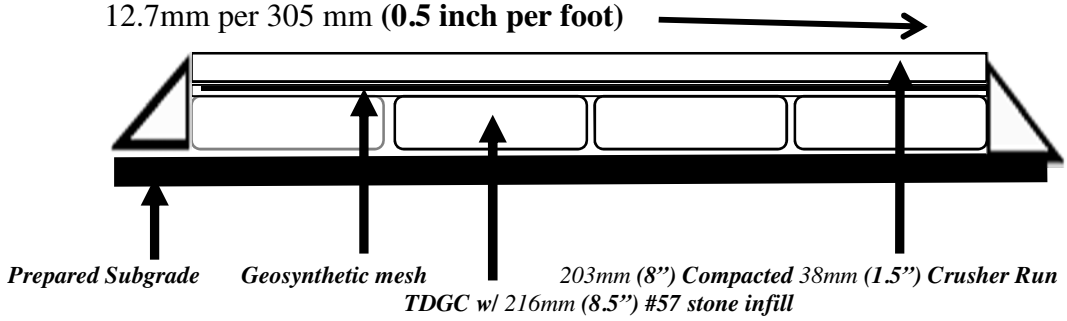

FIG. 5. Typical TDGC Dock Access Road 419 mm (16.5 inch) Cross Section

The detailed horizontal geometry for the roadway was provided by Triad Engineering, Morgantown, WV, mid Atlantic, regional civil and geo technical consultants. See roadway plan drawing Figure 6.

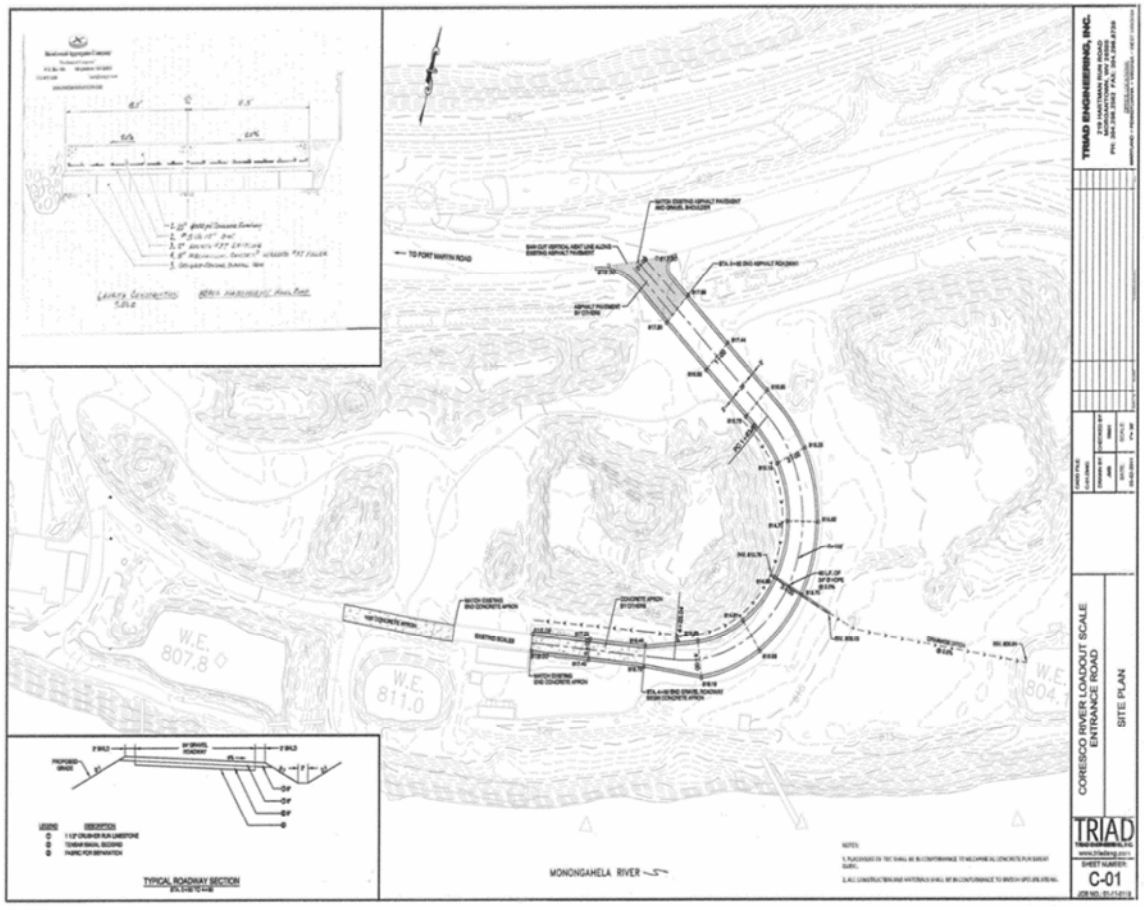

FIG. 6. TRIAD Engineering Layout of MEPCO Dock Road Project

CONSTRUCTION PROCESS

The contractor first installed all the, TDGC, tire-derived-geo-cylinders; then filled them with stone. For stabilization during the stone filling operation the tire-derived-geo-cylinders were temporary attached to each other with one screw. A power driven nail is also an option. This step is like wiring rebar and insures that the cylinders say in place and do not collapse during the stone dumping and spreading. See photo Figure 7.

FIG. 7. Dock Road Tire-Derived-Geo-Cylinder Layout and Stone Filling

Next they installed the 203mm (8 inch) stone wearing surface in two lifts; watering and compacting the material to optimum density. For additional wearing surface strength the contractor elected to place a layer of geosynthetic mesh between the stone surface layer and the TDGC base. See photos Figure 8 and 9.

FIG. 8. Geosynthetic Mesh on Stone Filled, Tire-Derived-Geo-Cylinder Base

FIG. 9. Typical Uncompacted Layer Wearing Surface Stone

Why AASHTO # 57 is Specified For TDGC Fill

Filling the tire-derived-geo-cylinder with AASHTO #57 limestone allows roadbuilding to be a more efficient manufacturing process. A truck load of new stone is backed up to the cylinder layout and dumped onto the leading edge cylinders. The stone is then pushed into the surrounding cylinders and leveled to their upper edge. See Figure 7. One of the key reasons AASHTO #57 stone is specified is it flows like a fluid. AASHTO #57 stone is primarily 12.7 mm to 19 mm (0.5 in to 0.75 in) sized stone. It is also a primary stone gradation used to make portland cement concrete. Because it is made up of similar size particles it naturally has a fluid like tendency to flow. This is particularly true when it is placed under pressure or load. So it pressurizes the tire-derived-geo-cylinder when a loaded truck passes over the stone base. This unique physical characteristic is the key reason the AASHTO #57 gradation is the preferred and specified stone material in Mechanical Concrete®. This also means when the stone is placed within the tire-derived-geo-cylinders it is at or very near its maximum density as a graded stone and little compaction is needed or possible. AASHTO #57, therefore, contributes to simplicity, quality and ease of use. It is also why, under normal construction conditions, stone filled, tire-derived-geo-cylinders are consistently the same each time they are made. It doesn't require the usual field testing to determine if it meets compaction specifications. Using AASHTO #57 stone, it's very difficult to incorrectly make Mechanical Concrete®. Other stone gradations may be used in the tire-derived-geo-cylinders but some compaction is required to achieve optimal density and load distribution.

REINFORCED CONCRETE SCALE APPROACH SLABS

The truck scale is a steel girder bridge with abutment supports which are instrumented to precisely measure the loading reactions when the loaded truck comes onto the scale. The concrete scale approach and exit ramps slop away from the scale and were constructed of a #57 stone filled, tire-derived-geo-cylinder base with a 254 mm (10 in) reinforced concrete slab with #5 rebar at 305 mm (12 in) each way. The 36m (120 foot) long entrance approach slab has 5 full depth construction joints without load transfer dowels and full depth expansion joint at the scale concrete abutment. The 195 m (65 ft) long exit ramp has 3 full depth construction joints without load transfer dowels and full depth expansion joint at the scale concrete abutment. Considering the daily coal truck traffic it is notable that there is no visible settlement at these joints in spite of their full depth and the rainy weather conditions of the region. See cross section Figure 10 and photo Figure 11.

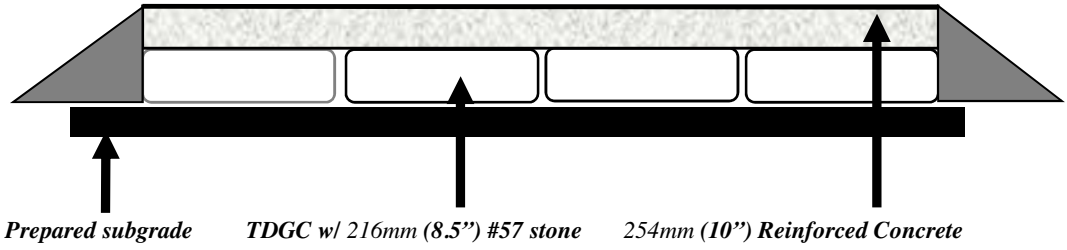

FIG. 10. Scale Approach and Exit Reinforced Concrete Dock Road Section

FIG. 11. Reinforced Concrete Scale Approach Slabs During Construction

ROAD DRAINAGE AND MAINTENANCE

In the mid-Atlantic region, drainage is a major concern on unpaved roads. To deal with this concern, knowledgeable designers specify these gravel roads to have a minimum side slope of 12.7 mm per 305 mm (0.5 in per ft) or slightly greater than 4%. A stone filled, tire-derived-geo-cylinder base with its lateral confinement mechanism and its 30 % to 40% porosity fill material behaves like a structural French drain; so water has insignificant impact on it. However, the 203 mm (8 inch) compacted stone surface is subject to water deterioration, so surface drainage is important.

Based on information provided by MEPCO Fuels and Logistics Manager, Jerry Swartz, on MEPCO's original stone surface roadway potholes and ruts were a weekly challenge requiring on average 2 truckloads of new stone each week to maintain the road. Potholes are generally caused by deep road base failure that is continuous and ongoing. On conventionally constructed gravel roads even with a well-drained surface eventually water gets into the road base. Most compacted stone bases are dependent on particle friction for their strength; so water is the enemy, since its presence reduces particle friction and eventually weakens the base.

On the new MEPCO dock road surface water is all drained toward the curve radius center and then transported to a settlement pond through a pipe. The road surface positive drainage design and the stone filled, tire-derived-geo-cylinders with their inherent lateral strength and load distribution capacity and their permeable structural properties are the primary reasons road maintenance has been reduced to two truckloads of stone per month—an over 75 percent reduction in maintenance. The principal areas for stone wearing surface maintenance are at the approach ends of the concrete scale ramps and near the center of the curve in the general location of the pipe drain which runs under the roadway. See Figure 12. Surface water drains down the concrete ramps directly on to the unpaved surface; so it is predictably a higher maintenance area.

FIG. 12. Final Gravel Surface Concrete Approach Slab Transition

TDGC ENVIRONMENTAL CONSIDERATIONS, AVAILABILITY, COST

State and federal environmental agencies are all challenged by the 300 million waste tires generated annually in the USA; that's one waste tire per person per year. They actively promote the beneficial reuse of waste tire derived materials in civil engineering applications, particularly when buried underground. Using these tire-derived-geo-cylinders in road bases is consistent with the specific beneficial tire reuse regulations of the WV Department of Environmental Protection.

Currently tire-derived-geo-cylinders are available anywhere in the US through the tire recycling industry in lane-mile quantities at a cost of approximately $2 each, which includes patent royalties. The average coverage rate per 3.6 m (12 foot) wide lane mile is 12,000 TDGC. Freight and installation costs average of 5 to 7 percent of the material cost and depend on the geographic location and size of project.

The TDGC costs on this project were $3 each due to the relatively small volume of 1920 TDGC. The comparable conventional industrial roadway section for this use would have included a stone bridge layer and a stone sub-base totaling approximately 761mm (30 inches) of new stone. The 216 mm (8 1/2 inch) base layer of stone filled, tire-derived-geo-cylinders reduced the excavation costs and the stone costs by more than 50%. See Conventional Cross Section Figure 4.

CONCLUSIONS AND TDGC LIFE EXPECTANCY

Over 180,000 coal trucks have passed over this dock road since June 20, 2011. By the owner's economic measures and by engineering assessments the stone filled, tire-derived-geo-cylinder base has performed well on this industrial roadway. The performance on both the base for the stone surface and the concrete surface has been exemplary. The elimination of deep potholes and ruts on the stone wearing surface is the key performance measure. On the concrete surface the cold joints have exhibited no relative movement on the approaches or at the abutments. This indicates unique performance stability which is rare in roadway concrete slabs without load transfer dowels on conventionally compacted stone bases.

This project clearly demonstrates that stone filled, tire-derived-geo-cylinders have the power to create an industrial roadway base with at least 50 percent less material, reduce subgrade loadings, and manage diverse climatic conditions without reduction in strength or performance.

One frequently asked question is "What is the expected life of a stone filled, tire-derived-geo-cylinder road base?" From an engineering perspective some facts to be considered in the answer are: 1. the rubber in which the tire's steel belts are imbedded and protected from deterioration is an inert hydrocarbon and does not deteriorate when buried under ground, and 2. the relatively large design factor on the tire-derived-geo-cylinder in this civil engineering use indicates that the material can withstand these types of repetitive loads indefinitely. Considering these facts it appears that as long as the subgrade does not fail, the stone filled, tire-derived-geo-cylinder base would have an indefinite life.

REFERENCES

Bonasso, Samuel G. (2008), The Effects of Aggregate Size and Gradation on Hoop Stresses in Steel Cylinders and the Reuse of Waste Tire Tread Cylinders for Aggregate Confinement in Confined Aggregate Concrete. http://66.147.244.58/~mechank5/wp-content/uploads/2011/07/technicalreport1.pdf

Leshchinsky, B. and Ling, H. (2013). "Effects of Geocell Confinement on Strength and Deformation Behavior of Gravel." *J. Geotech. Geoenviron. Eng.*, 139(2), 340-352.

Tanyu, B. F., Aydilek, A. H., Lau, A. W., Edil, T. B. and Benson, C. H. (2013). "Laboratory Evaluation of Geocell-Reinforced Gravel Subbase Over Poor Subgrades." *Geosynthetics International*, 20, No. 2, 47-61.

Road Impacts from Shale Energy Development

Paul W. Wilke[1], P.E., M.ASCE

[1]Principal Engineer, Applied Research Associates, Inc.;Tel: (717) 975-3550; Fascimile: (717) 975-3557, E-mail: pwilke@ara.com

ABSTRACT: In recent years, new hydraulic fracturing technologies have led to rapid shale oil and gas development. This development has included an unprecedented amount of heavy truck loading on low volume, rural roads, many of which were not built to withstand such loading. Many highway agencies are concerned about the impact of these loads on the life of their pavements and have had to adapt to this new paradigm by developing polices to protect their infrastructure. Pennsylvania has seen extensive development of the Marcellus shale formation in recent years, with significant impact to its road system. New York state has been preparing for future development of their Marcellus shale pending environmental reviews. This paper describes a variety of approaches used in Pennsylvania and New York to keep local roads safe during construction of these energy facilities and to provide fair reimbursement to municipalities for the loss in pavement service life that occurs from these activities. The engineering background is described for methods used to project long-term damage, quantify damage to specific roads, determine needs for pre-development pavement upgrades, and allocate damage costs to multiple users. The advantages and disadvantages of alternative approaches are discussed and provisions for Road Use Agreements are suggested.

INTRODUCTION

The development of natural gas wells utilizing hydraulic fracturing (or "fracking") requires a significant number of trips to each well site by heavy trucks. The most substantial trucking consists of 20,000 liter water trucks each weighing about (40,000 kilograms) to support the fracking process at each well site. This water requirement often results in large concentrations of water trucks traversing a single road each day (see Figure 1). Other truck trips (example- gravel, sand and other materials) are required for well pad construction and access. The combined trucking associated with a single well has been estimated to be approximately 1300 trips; many well sites contain more than one well. Most well sites are located in remote areas that are typically accessed by farm to market roads that were not designed to handle this level of heavy truck traffic. The cost of damage to such roads due to shale gas development can be severe (example-2 to 3million dollars/mile to reconstruct a failed pavement).

FIG. 1. Water trucks to support hydro- fracturing of oil and gas wells

PROJECTION OF OVERALL COST IMPACT

For government agencies that own road networks that are expected to be affected by significant energy development projects that will occur over many years or decades, it may be useful to estimate the overall impact of such developments on the road network in advance. If the impact in terms of additional road maintenance and reconstruction are known, it can be helpful to the agency in planning long term capital and maintenance budgets and/or assessment of some type of impact fee to help compensate for the expected road impacts.

A methodology is presented herein that may be used to develop broad, planning level estimates of the overall cost of shale energy project impacts to roadway pavements. The method essentially consists of comparing the projected truck traffic associated with shale energy development to the expected life of pavements in the agency's road network, determining the percentage of pavement life consumed by the development traffic, and estimating the cost of this consumed pavement life.

The proposed methodology is based on the American Association of State Highway and Transportation Officials (AASHTO) empirical models that relate pavement life to truck axle loads. The AASHTO road test (American Association of State Highway and Transportation Officials, 1962) showed that the relative damage to pavements depends on the weight of vehicles loading the pavement and on the number and spacing of axles over which the load is distributed. A method was developed to convert various truck axle configurations to one standard; an equivalent 80 kN single axle load (ESAL). Design procedures were developed to determine the pavement structure needed to support the projected traffic, in terms of ESALs. This process may be used in reverse to estimate pavement life (ESALs carried) for a known pavement structure. The details of this approach are provided in the eight steps described below:

Step 1. Estimate Truck Traffic Associated with Shale Development

First, the number of wells to be developed is estimated and the truck trips associated with each well is estimated. Projecting the number of gas wells is not precise, however, short term estimates of the number of wells may be made based on land leases or environmental permit applications available through public records. Longer term, the extent and geographic locations of future development is often estimated based on industry estimates of the location and volume of oil and gas deposits in economically viable reservoirs. Based on this information, the number of wells and general locations may be projected. Next the volume, weight, and axle configuration of heavy vehicles associated with each development is estimated.

Step 2. Convert Truck Fleet into ESALs

In order to determine the damage from a fleet of trucks with various weights and axle configurations, it is customary to determine the equivalent single axle loads (ESALs) for each truck type and add them together to determine the total ESALs anticipated to use the pavement. ESAL factors for each truck's axle type (example-single, tandem or triple) and axle weight are provided in Appendix D of the AASHTO Pavement Design Guide (American Association of State Highway and Transportation Officials, 1993). Alternatively, if weights are not known, average ESAL factors for each truck class may be used.

Step 3. Determine Representative Pavement Section for the Roads Expected to be Impacted by the Development

There may be several hundred kilometers of road expected to be used to develop the anticipated energy projects, and the pavement section is likely to vary significantly over this network of roads. In some cases it may be useful to divide the road network into classes and estimate an average or representative pavement section for each class. If an agency's pavement management system has good data on pavement composition it may be possible to extract pavement layer thickness for the network, or for each road class, and calculate an average thickness for each layer.

Step 4. Determine the Structural Number for each Pavement Section

A commonly accepted term used to quantify the overall strength and load carrying capacity of a pavement is the Structural Number (SN) as defined in the AASHTO Guide for Pavement Design (American Association of State Highway and Transportation Officials, 1993). The SN is determined by multiplying the structural layer coefficient (or contributing strength from each layer) by the thickness of each layer, then summing them together. Typical layer coefficients have been published widely; some transportation agencies have developed coefficients for their specific pavement materials. Applying the appropriate layer coefficients to the typical pavement sections identified in step 3, the SN is determined for the road network or for each road class if the analysis is done for separate classes.

Step 5. Determine the Pavement Life for each Pavement Section

The AASHTO design method calculates the required pavement structural strength (in terms of structural number, SN) for a given level of projected traffic, subgrade soil strength and other parameters. As noted above, the same design principles may be applied in reverse to determine the pavement design life (in terms of ESALs carried) for a known pavement strength (i.e. - structural number, SN). For this application it will be necessary to assume an average subgrade strength to calculate remaining life.

Step 6. Estimate Pavement Life Consumed by Heavy Vehicle Traffic

The portion of pavement life consumed by projected traffic associated with shale gas development projects is determined by dividing the projected ESALs applied (from step 2) by the ESAL life of typical pavements (from step 5).

Step 7. Determine Unit Cost for Pavement Replacement

The replacement cost is estimated for the typical pavement section referenced in step 3.

Step 8. Determine Pavement Replacement Cost due to Projected Traffic

The cost to replace pavements consumed by the projected traffic is determined by multiplying the portion of pavement life consumed by the replacement cost. The cost impact projected using this method may be used as the basis for a development impact fee or for maintenance and capital planning.

Example Applications of Cost Impact Projection

This process was used by the Pennsylvania Department of Transportation (PennDOT) near the beginning of the Marcellus shale development boom to estimate the overall damage to non-posted roads. Tompkins County, in New York state, is using this procedure to estimate potential damage from specific, proposed developments and to set bond amounts for use in road use permits.

ASSESSMENT OF DAMAGE TO SPECIFIC ROADS FROM SHALE GAS DEVELOPMENT

An alternative to assessing a development impact fee is to charge a user fee based on damage incurred on specific roads used by specific developers. Such an approach has been adopted by several agencies where developers are required to obtain a permit to haul heavy loads on low volume roads and to enter into a Road Use Agreement (RUA) as part of the process. The RUA typically requires the permit holder to make some type of improvement to roads they will use. Such

improvements may be required in advance and/or at the end of development. One approach used by several agencies is to perform a visual condition survey before and after development and to require that the developer repair visible damage (example-seal cracks, patch areas of base failure, and possibly resurface with a thin overlay). Alternatively, a more rigorous approach may be used that is based on more project specific data. Some agencies have found that in addition to estimating the pavement damage caused by development traffic, it is necessary to determine when pavement improvements should be made: before the start or after heavy hauling by the industry is complete. The procedures described below address both of these issues.

Procedures for determination of the need and financial responsibility for pre-development and post-development upgrades are outlined in five basic steps:

1. Projection of Truck Traffic
2. Pre-Development Assessment
3. Determination of Need for Pre-Development Upgrades
4. Post-Development Assessment
5. Assignment of Financial Responsibility

Step 1. Projection of Truck Traffic

a. Request that the developer provide their anticipated haul routes and a list of heavy vehicle types, volumes and axle configurations anticipated to use the permitted road(s) over the period of the permit.
b. Convert the truck fleet projected above to equivalent single axle loads (ESALs) using the axle equivalency factors provided in Appendix D of the AASHTO Guide (American Association of State Highway and Transportation Officials, 1993). The determination of axle equivalency factors requires the axle weight; if this is not known assumptions will need to be made. For example, it may be reasonable to assume that half of the projected trips are made with trucks loaded to the legal limit and half of the trips are made by an empty truck. Alternatively, the process may be simplified by multiplying the volume of trucks by an ESAL factor that converts truck trips to ESALs based on the axle configuration as discussed previously.

Step 2. Pre-Development Assessment

The condition of the existing pavement before the start of hauling by developers should be assessed in terms of its structural carrying capacity. This may be determined using non-destructive testing of the pavement structure and mechanistic pavement analyses. Alternatively, a simpler but more subjective procedure may be used based on pavement cores, visual assessment of pavement conditions and

empirical methods contained in the AASHTO Guide (American Association of State Highway and Transportation Officials, 1993).

The mechanistic approach consists of nominal pavement coring or ground penetrating radar testing to obtain pavement layer thicknesses, and non-destructive testing using a falling weight deflectometer (FWD) to determine pavement layer stiffness and subgrade soil strength. FWD testing consists of the application of a series of loads on the pavement surface and measuring the resultant pavement surface deflection with sensors placed on the pavement surface. Using this data, mechanistic analyses are performed using layered elastic theory to predict stresses and strains in the pavement and to compute the number of load applications (expressed in terms of ESALs) the pavement can withstand before failing (ie.- the remaining pavement life). The simpler empirical approach consists of coring and soil borings to determine pavement layer thicknesses and subgrade strength, combined with a visual assessment of pavement surface conditions. Correlations provided in Table 5.1 of the AASHTO Guide (American Association of State Highway and Transportation Officials, 1993) may be used to estimate the structural coefficient for each pavement layer based on the pavement's surface condition. As described above, the layer thicknesses and structural layer coefficients may be used to calculate the effective structural number (SN) for the pavement. This information combined with the subgrade strength determined from borings may be used in the AASHTO empirical design procedure to estimate the remaining pavement life in terms of ESALs.

Step 3. Determination of Need for Pre-Development Upgrades

Compare the projected truck traffic (ESALs) to the remaining life determined in Step 2. For this step, pre-existing traffic (ESALs) should be included. If the total projected ESALs (pre-existing and developer traffic) is expected to result in a remaining pavement life below some threshold, after a specific agency defined period (example- if remaining life is less than 2,000 ESALs after 6 months of hauling), it is recommended that the pavement be upgraded prior to the start of hauling. The upgrade should include a repair of any base failures and an overlay designed to carry the projected ESALs. The purpose of this evaluation is to prevent premature failures that have been known to occur that render the road unsafe for the traveling public.

Step 4. Post-Development Assessment

a. Conduct FWD testing, or pavement cores and a visual condition survey, as described in Step 2.
b. Determine the structural number, SN as described in Step 2.
c. Determine the pavement life consumed during the period of developer's hauling (remaining pavement life pre-development minus post-development, in terms of ESALs).
d. Determine the cost per ESAL for the pavement within the limits of the

permitted road. The cost is computed as follows: Unit Cost = (cost to construct a new pavement with the layers identified in the cores in Step 2 / ESAL life for new pavement).

Step 5. Assignment of Financial Responsibility

Determine cost impact = unit cost per ESAL x ESAL life consumed. The developer/permittee may pay the highway agency an amount equal to this cost impact or construct an upgrade that will consist of patching areas of base failure and a hot mix asphaltic concrete (HMA) overlay, full depth reclamation, or reconstruction that restores the SN to the effective SN at the pre-development stage.

It should be noted that in most cases, this method will result in a greater cost impact than the method currently being used by some highway agencies that requires the developer to repair only significant distress visible at the pavement surface. If FWD testing is used, any fatigue cracking that may be present in the bottom portion of the pavement that has not yet manifest itself at the road surface will result in lower pavement stiffness and less remaining pavement life. Although the more subjective empirical methods do not directly account for any fatigue cracking that may be present below the pavement surface, it does so indirectly by downgrading the effectiveness of the current pavement structure even if surface distress is below a threshold where crack filling or patching may normally be recommended. This downgraded pavement effectiveness will result in a lower remaining pavement life.

If the permittee constructed a pre-development pavement upgrade and the effective SN after development is greater than or equal to the effective SN pre-development, the agency may wish to waive any future upgrade or payment requirements.

Example Applications of Damage Assessment Procedures

To date, PennDOT has used the visual condition assessment approach for simplicity considering the significant number of roads impacted (note- PennDOT has jurisdiction over many local roads in the state, many of which are used for shale energy development). PennDOT's guidelines for pre-development road upgrades are based on the remaining pavement life procedure presented above.

Tompkins County, New York is using a hybrid approach to damage assessment. A visual condition assessment is used for developments with low projected truck traffic and roads in poor condition where most damage from the developer's hauling will be visible. For all other situations, the remaining pavement life approach is used.

ISSUES TO CONSIDER WITH MULTIPLE USERS OF PERMITTED ROADS

When applying the procedures discussed above, some special considerations may come into play if there are multiple developers using the same road segments. For example, in Pennsylvania it is common for roads under permit to be used by many different companies and road repair costs need to be allocated to each of these permitted haulers or road users. Two issues to be considered in assessing road

damage costs to multiple users of permitted roads are the relative damage caused by different types of trucks and the relative damage inflicted to roads during different times of year. Procedures to account for these two issues are presented below.

Accounting for Different Truck Types

Many different truck types with different weights and axle configurations are used in the development of shale energy and for other industries (example- timber). As discussed earlier, the AASHTO pavement design procedure converts all projected truck traffic to a common standard, the ESAL, to reflect the relative contribution of various truck types to pavement damage. For this reason, a fair and defensible method to allocate responsibility amongst multiple users of permitted roads is to apportion damage costs in relation to the number of ESALs applied to the road by each user.

This procedure is considered to be technically sound, however there is at least one practical issue to be handled if this method is used. In order to apply this procedure, the number of ESALs applied to the road by each user must be determined. One method, as is used in the state of Pennsylvania, is to require permittees to self-report their truck trips (truck type and weight). In order to determine the number of ESALs associated with each load, either the axle loads and configuration need to be known and the ESAL factor determined from Appendix D of the AASHTO Guide (American Association of State Highway and Transportation Officials, 1993) or average ESAL factors published by the highway agency may be used if the truck type (axle configuration) is reported.

Accounting for Relative Damage by Season

Many highway agencies have recognized that road damage from truck traffic is accelerated during the period of spring thaw. Water from thawing ice near the surface becomes trapped because it is unable to percolate downward through the soils that remain frozen. Subgrade soils directly below the pavement structure become saturated and weakened. The decreased subgrade support leads to increased deflection of the pavement layers which leads to fatigue cracking and/or rutting. Many northern U.S. state departments of transportation and Canadian provinces (Hein, et al 2002) place load restrictions on some vulnerable roads during spring thaw to address this issue.

In areas with substantial energy development activity, the highway agency may be reluctant to post spring load restrictions due its negative impact on the local economy. An alternative approach for roads with multiple haulers operating under a permit with the agency is to allow hauling during spring thaw but to seek additional compensation for the relatively greater road damage caused by those permitees that choose to continue hauling during spring thaw.

One method to account for the relative damage during spring thaw is to apportion road repair costs to multiple users based on each user's share of "equivalent ESALs" applied. The equivalent ESALs may be determined by multiplying the ESALs

applied during spring thaw by a spring thaw damage factor defined as the ratio of damage predicted, per ESAL, during the spring thaw period compared to the average damage throughout the remainder of the year.

Example Applications of Multi-User Cost Allocations

PennDOT is currently allocating road damage costs among multiple users based on each user's share of total ESALs. The ESALS are based on self-reporting of truck loads, truck types and weights. The application of the equivalent ESAL concept based on a spring thaw damage factor is currently being considered.

ADMINISTRATIVE CONSIDERATIONS

Many highway agencies have been dealing with heavy hauling, associated with the logging and mining industries, on low volume roads for decades. Many of these agencies have developed regulations, incorporated into their jurisdiction's highway law, that provide a mechanism to obtain compensation from heavy haulers for road damage. With the rapid increase in energy development projects throughout North American in recent years, more agencies are developing such regulations or modifying existing regulations to better address their concerns.

One common technique is to post low volume roads with a relatively low load limit (example- 10 tonnes) and to require companies that wish to haul heavier loads over these roads to enter into a Road Use Agreement (RUA). Typically the RUA address a wide range of issues including safety, hours of operation, noise, environmental restrictions, geometric restrictions on vehicles and others.

A few of the common pavement related issues addressed in RUA's are listed below:

- Performance bond required to help enforce RUA requirements including receipt of compensation for road damage or adequate repairs performed by the developer.
- Pre- and post-development road inspections to determine the extent of damage and/or extent of repairs required. Most RUA's require developer to pay for inspections; some have a maximum cap on the inspection cost.
- Requirement that damage causing an unsafe condition be repaired within 8 hours.
- Provision that allows the highway agency to make emergency repairs if in their opinion the road is not safe for the motoring public and to require the developer to pay for such repairs.
- Developer is required to perform any necessary road repair as a result of damages caused by developer and to provide a warranty of such repair work for a period of three (3) years after the date of final acceptance.

SUMMARY AND CONCLUSIONS

Roadway agencies that have experienced a significant increase in shale energy

development projects, applying heavy truck traffic to rural, low volume roads that were not intended for such traffic may wish to consider seeking compensation from developers for road damage incurred. This compensation could be in the form of a development impact fee based on the magnitude of the development such as the number of wells. Alternatively, the compensation could be in the form of a user fee based on damage to specific roads resulting from the developer's heavy hauling.

If a development impact fee is adopted, the basis for fees charged could be determined by the pavement life expected to be consumed by the truck traffic associated with the development. The method proposed in this paper requires an estimate of the truck traffic associated with the development. Ideally, truck axle configurations and weights would be included in the projection in order to convert the truck fleet to total ESALs. Additionally, reasonable assumptions need to be made regarding the typical pavement section and subgrade soil strength for the affected roads. Finally, the cost to construct this pavement section needs to be estimated.

If it is preferable to seek compensation from developers based on actual damage they cause to roads they use, a similar method is proposed. However, if this method is used it will be necessary to assess pavement conditions before and after use by the developer in order to objectively estimate the magnitude of damage associated with the developer's truck traffic. The simplest procedure involves a pre-development and post-development visual pavement surface condition survey and a requirement that the developer make repairs of visible damage beyond that present at the start of development. Such repairs may include crack filling, patching and perhaps resurfacing to restore ride quality. A more comprehensive approach may be taken that more accurately determines the true cost, to the highway agency, for allowing heavy hauling by the developer. The more comprehensive approach is based on an assessment of the cost of pavement life consumed by the developer's truck traffic.

If the highway agency adopts a policy such as that described above, thought should be given to how to handle cases where multiple companies are under permit for use of the same road. In such cases, it is recommended that the repair costs be allocated to each permit holder based on their percentage of the total ESALs applied to the pavement during the permit period. This procedure may be further refined by allocating costs based on equivalent ESALs that account for the relative damage caused by each ESAL in different seasons such as the vulnerable spring thaw period and the more forgiving winter freeze period. A method to account for this is provided in this paper.

REFERENCES

The AASHTO Road Test- Report 5- "Pavement Research", Highway Research Board, Special Report 61E, p. 107, 1962.

AASHTO Guide For Design of Pavement Structures, American Association of State Highway and Transportation Officials, Washington, D.C. 1993.

Hein, D.K., Olidis, C., and Cole, R., "*Establishment and Monitoring of Pavement Load Restrictions in the Province of British Columbia",* Annual Meeting of the Transportation Association of Canada, Winnipeg, Manitoba, 2002.

Assessing the Impacts of Shale Oil & Gas Developments on Rural Texas Highway Infrastructure

Timothy Miller[1], P.E. and James M. Sassin[2], P.E.

[1]Project Engineer, Fugro Roadware, Inc., 2420 Del Paso Road, Suite 250 Sacramento, CA 95834, U.S.A., Email: tmiller@fugro.com
[2]Senior Consultant, Fugro Roadware, Inc., 8613 Cross Park Drive, Austin, TX 78754, U.S.A., Email: jsassin@fugro.com

ABSTRACT: While shale oil and gas developments have been a boom for the Texas economy, these developments have taken a toll on low-volume roads. Impacts of truck traffic on roads in the Eagle Ford and Barnett Shale plays and the Permian Basin are obvious in the cracks, potholes, and other major distresses. Many of Texas' Farm-to-Market, Ranch-to-Market, and local county roadway systems are not designed to withstand the heavy loads and higher traffic volumes arising from energy development. Rapid development of energy resources will continue to strain agencies until measures are taken to implement infrastructure impact plans, road-user agreements, or other measures to rehabilitate effected roadways. This paper uses case studies to explore four approaches for partnerships between energy companies, county officials, and other organizations. The proactive, performance-based approach strengthens pavements prior to energy development. The reactive, performance-based approach assesses impact fees associated with road maintenance after the damage. The third approach assesses impact fees that are not attached to actual roadway deterioration. The fourth approach uses policy changes to the Texas Transportation Code, which allows counties to promote transportation infrastructure projects affected by oil and gas production activities. Funding for this approach arises from grants. The authors discuss what is currently being done in Texas and suggest recommendations for future work. With future exploration expected throughout, execution of agreements and creative reimbursement procedures will be critical to maintaining adequate levels of service and preserving working relationships between the energy industry and county governments charged with preserving roadway assets.

INTRODUCTION

The development of new energy resources has helped to buoy the economy of many communities throughout Texas. Energy companies have brought technical jobs to small communities while pledging to hire from local labor pools (AASHTO 2001). Rapid development in the oil and gas (O&G) energy sectors holds promise at boosting a struggling economy, promoting energy independence, improving national security, and keeping fuel costs low. Yet such developments occur against a backdrop of unintended consequences, as rural road networks and bridges bear the brunt of energy development activities.

Oil and gas discoveries in the Eagle Ford Shale play in south Texas and the Barnett Shale play in north central Texas represent areas of tremendous energy potential and economic growth. Texas energy production in May 2013 came from 155,983 oil wells and 91,437 gas wells (Railroad Commission of Texas 2013). Crude oil production has risen by 26 percent to 267,796,411 L per day, and natural gas production has also increased 9 percent to almost 15,621,176 m^3 compared to production a year ago (Railroad Commission of Texas 2013). Drilling permits in the Eagle Ford Shale play have increased exponentially since 2008, with 5459 permits issued through July 2013 (Railroad Commission of Texas 2013). An energy revolution is taking shape in Texas and in several states throughout the country, with profound impacts only now being realized. Figure 1 illustrates heavy truck traffic commonly seen on low-volume roads.

FIG. 1 An exploration truck passes testing equipment in Fayette County, Texas.

With production figures confirming that Texas is in the midst of an energy revolution, a rush to develop O&G resources has significantly affected transportation infrastructure in surrounding areas. Development of O&G wells demands the use of trucks to haul heavy loads of pipe, water, drilling equipment, heavy machinery, cranes and rigging, and construction materials to the drilling site (Railroad Commission of Texas 2013). Much of this activity is occurring in rural areas where existing infrastructure was originally designed to withstand low traffic volumes and few loading cycles of 36,320 kg trucks. Effected roads are often classified as very

low-volume local roads, which are designed to accommodate daily traffic volumes less than 400 vehicles per day (AASHTO 2001). These pavements frequently have under-designed base layers thicknesses that fail to provide adequate structural support for heavy truck traffic encountered on rural roads (Begley 2013).

The impacts of energy development on transportation infrastructure are far-reaching. O&G operations are consuming transportation infrastructure faster than it can be maintained and rehabilitated. In fact, the Texas Department of Transportation (TxDOT) has temporarily allowed some paved roads to regress to gravel roads (Senate Bill 1747 2013). The effects of development are felt on bridges, too, as counties are left with damages to bridge infrastructure resulting from O&G development. Damage to roadway networks due to heavy truck traffic creates safety, drainage, durability, and economic issues. These impacts must be balanced with the positive benefits of energy production. For example, Karnes County, TX is one of more than a dozen counties inundated with traffic from the Eagle Ford Shale energy boom. In the past three years, there has been an increase in traffic accidents of 216 percent, with 12 fatalities in 2012 in Karnes County alone. That is 12 times the number of fatalities reported to TxDOT in 2008, just as oil and gas drilling started to take off (Quiroga et al 2012). Safety is a primary concern for travelers and state officials alike (Quiroga et al 2012; Texas Transportation Researcher 2012; Wilke and Harrell 2011). Most rural roadway users are more accustomed to experiencing little vehicular traffic in the range of 400 vehicles per day of passenger vehicles and the occasional farm tractor, rather than the steady stream of 18-wheelers now using the facilities for O&G exploration and development.

Recent studies have investigated the economic impacts of O&G developments on transportation infrastructure. In a recent report from the Texas Transportation Institute, researchers studied 710 0.8-km sections for remaining pavement life in the Barnett Shale play (Quiroga et al 2012). Researchers found the cost of energy development impact on the Farm-to-Market (FM) System is, on average, experiencing an additional $890 million of maintenance needs annually. The overall cost is estimated to exceed $1 billion annually. The report estimates maintenance of other local county roads to cost an additional $1 billion, though actual figures may be higher. The Eagle Ford Shale play could present even greater challenges, as a pipeline has not been established and additional trucking and construction activities related to pipeline construction can have dramatic effects on pavement infrastructure. Costs of bridge damages are also growing.

The confluence of under-designed pavements and soaring truck traffic resulting from energy development is causing major damage to local roadway infrastructure. Questions about how to quantify damage and estimate impact are now being asked by those responsible for approving well permits and balancing county budgets (Sassin 2012). Developing infrastructure impact plans or roadway user and maintenance agreements that account for roadway damage without constricting operations remains a shared goal. Sustained growth in the energy sector will demand adequate infrastructure to support development but must not compromise existing synergies between local officials and energy companies. Thus, discussing and identifying appropriate strategies to plan roadway infrastructure to accommodate energy

developments remains an area worthy of investigation and analysis and is the focus of this investigation.

PARTNERSHIP MODELS

An assessment of the current Texas landscape suggests four strategies for dealing with deteriorated pavements resulting from energy resource development. While these strategies have yet to be formally adopted by county governments, they demonstrate the spectrum of policies currently being advocated. These strategies include:

- A *proactive, performance-based approach* that strengthens pavements prior to energy development in what can be called a preemptive upgrade in anticipation of the extra loadings due to heavy truck traffic prior to drilling operations;
- A *reactive, performance-based approach* that assesses impact fees associated with roadway maintenance after impacts of heavy truck traffic have already occurred;
- A *reactive, non-performance based approach* that assesses impact fees that are not related to actual roadway deterioration;
- A *long-term, performance-based* plan to upgrade roads with competitive grant funding from the DOT.

The proactive, performance-based approach aims to strengthen pavements prior to energy development in an effort to 'armor up' the roadway. This approach requires early coordination between stakeholders, particularly between energy companies and county governments. Due to the explosion of O&G exploration and development operations, there is little evidence of this method being applied in Texas, as most facility owners remain fully occupied with assessing present deterioration. Research by TxDOT suggests that a 7-to-1 cost benefit can be realized if roads are "armored up" prior to exposure to operator traffic (Wilson 2012). In other words, if funds are spent upfront to preserve pavements, spending will be reduced by 700 percent compared to situations in which a pavement is left to be damaged and rebuilt continuously in order to handle increased heavy truck traffic.

The authors have been involved in two separate energy plays in different areas of the country where the counties have chosen to do preemptive upgrades. The first is the Fayette County, Texas approach in the Eagle Ford Shale play and the other is the Guernsey County, Ohio approach located in the Utica Shale play that requires operators to submit and fund a full engineering report that identifies a pavement's structural properties prior to commencing drilling operations. This arrangement is known as a Roadway Use and Maintenance Agreement (RUMA) and is coordinated in conjunction with the issuance of a drilling permit. Per the lease agreement with Guernsey County, maintenance is required and paid for by the operator for the duration of the servicing process. Execution of such an agreement requires use of non-destructive, performance-based pavement testing methods to characterize baseline and post-development pavement structural properties.

A second approach utilizes a similar methodology of applying performance-based testing to assess impact fees associated with roadway damage, though this approach takes effect after the damage has already occurred. This reactive approach does not "armor up" the pavement before beginning operations, which often leads to rapid deterioration of the facility, significant distresses, and increased safety hazards as the pavement is consumed during the drilling and servicing processes. Measurements of the pavement's remaining life can be used to estimate the consumption of the pavement's useful life by the operator. This approach allows for impact fees to be assessed during drilling activities for the rebuilding of facilities, but may not portray an optimal maintenance schedule for the duration of the drilling activity. A similar approach was used effectively in New Orleans, LA to evaluate the impact of Hurricane Katrina on roadway infrastructure and to determine which roads required maintenance (Zhang et al 2008).

Another approach, even less proactive than the first two, is currently employed in the south Texas Eagle Ford Shale play and offers a third alternative. This strategy represents an unstructured approach that assesses impact fees at a flat rate without determining how much drilling operations have actually contributed to the roadway's deterioration. This approach attaches a road damage fee to each well permit but is not quantified by any value-added improvements to the infrastructure itself. This path is primarily used in the south Texas Eagle Ford Shale play and is the source of much discussion currently. Karnes County is using this approach.

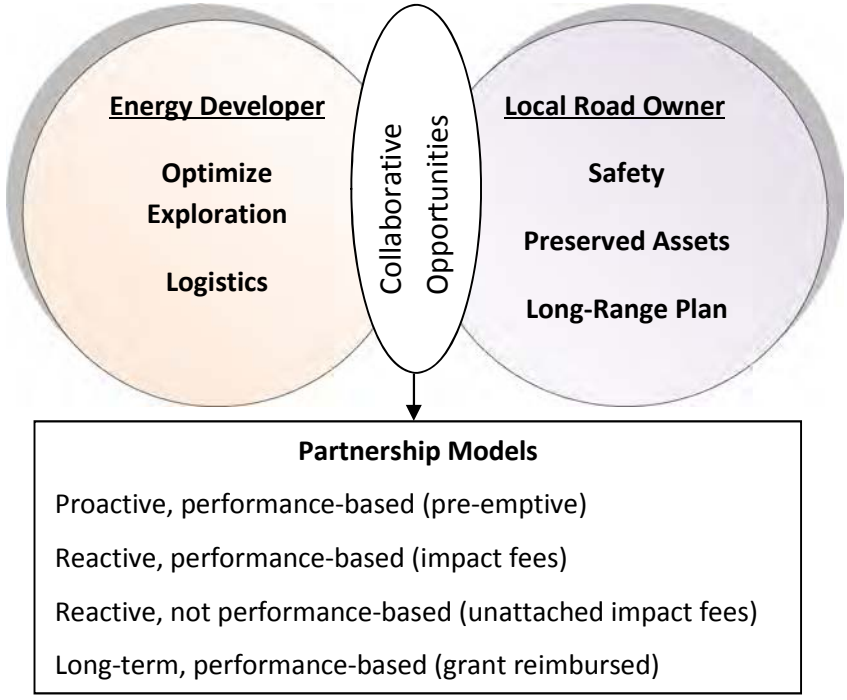

FIG. 2. Collaborative opportunities exist between the O&G industries and the counties and municipalities charged with maintaining rural road networks.

With a high cost for deferred maintenance looming for many counties, striking up mutually beneficial arrangements between counties and the O&G industry remains a priority. The best approach for achieving such arrangements remains the focus of much discussion. Figure 2 illustrates the competing desires for O&G producers and county officials or local road owners. The four partnership models link the desires of the stakeholders.

PAVEMENT ASSESSMENT

Proactive and reactive performance-based approaches utilize falling weight deflectometer (FWD) test protocols to assess baseline and post-development pavement conditions. The FWD is a non-destructive test method that can be used to determine resilient modulus and remaining life values of surface and sub-surface pavement layers. During FWD operation, a falling weight impacts the pavement surface, causing it to deflect. The magnitude of this deflection is captured by several geo-phone transducers that are situated at prescribed intervals from the point of impact. Pavement deflections are used to calculate structural properties of the pavement layers and subgrade soils in a process known as back-calculation. The FWD test method is specified by American Society for Testing and Materials (ASTM) standard D4694-09 (ASTM 2009). Figure 3 and Figure 4 depict the FWD test device and portray the test configuration and response, respectively.

FIG. 3. The falling weight deflectometer (FWD) is a non-destructive test device used to assess baseline and post-development pavement strength. The trailer-mounted FWD drops a load on the pavement and measures the deflected surface profile using several geo-phone transducers.

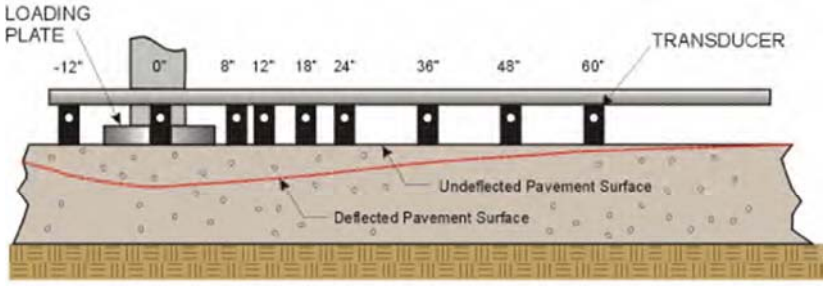

FIG. 4. The FWD loading impact generates a basin profile, which engineers analyze to determine resilient modulus and remaining pavement life values (Advanced Pavement Testing Services 2012).

The FWD has been used widely to characterize pavement structural properties. The Federal Highway Administration's (FHWA) Long-Term Pavement Performance (LTPP) program makes regular use of FWD measurements to evaluate deteriorating conditions of a variety of pavements across the country. The FWD is also used commonly in commercial projects involving ports, airports, and highway projects to evaluate resilient modulus, structural number, and remaining life. The method is particularly effective in identifying weak sections within the pavement structure. Knowledge of pavement deficiencies can inform the decision-making process regarding maintenance and rehabilitation. Assessment of deteriorated roadways can be achieved by analyzing FWD data similar to that shown in Figure 5, which illustrates how pavement structural values diminish over the course of construction and operation processes.

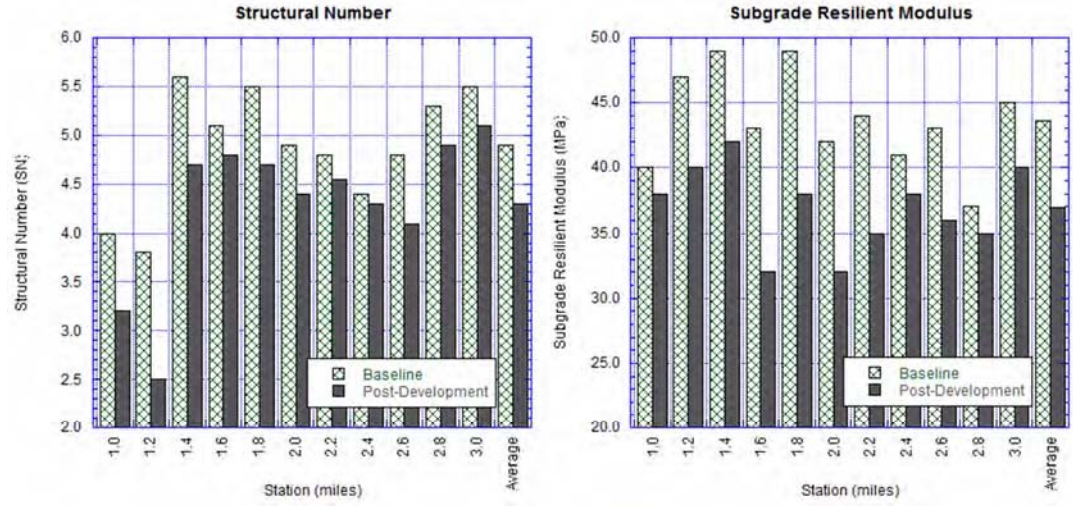

FIG. 5. Representative back-calculated FWD data showing loss of structural number (left) and subgrade resilient modulus (right) due to construction activities.

CURRENT PRACTICE IN TEXAS

Counties throughout Texas are struggling to strike a balance between the county's desire for safe, well-serviced pavement networks and the energy industry's desire for revenue and efficient delivery oil and gas products. In an effort to corral these activities and enhance collaboration amongst stakeholders, TxDOT recently formed the Energy Sector Task Force. The goal in forming the Task Force is reduce the impacts of development on transportation infrastructure by identifying common challenges and potential solutions while seeking opportunities for innovation and collaboration (Wilson 2012). The Task Force has a growing membership composed of several agencies and organizations including TxDOT, the Texas Department of Public Safety, the Texas Department of Motor Vehicles, the Texas Commission on Environmental Quality, the Railroad Commission of Texas, counties and cities, the Texas Oil and Gas Association, the Texas Farm Bureau, and the Texas Alliance of Energy Producers, among others.

While creation of the Energy Sector Task Force represents a positive initiative to enhance communication amongst stakeholders, development agreements often introduce particularly difficult negotiations. Successful negotiations between O&G producers and county governments rely on open and diplomatic relationships. One example of positive dialogue recently occurred in Johnson County, Texas. Officials in Johnson County, TX gathered major land owners and energy producers and established a friendly tone at start of discussions (Sassin 2012). Officials noted that there is a "right way" and a "wrong way" and emphasized that the wrong way means disrupting the strong working relationships with the oil and gas companies.

With new funding available at the state level, Texas legislators are considering statutes and rules regulating vehicles that are overweight or oversize (Sassin 2012). Current regulations from the Texas Department of Motor Vehicles provide vehicle length and weight limits and weight restrictions (Texas Department of Motor Vehicles 2012). Oversize permits, which allow vehicles to exceed weight restrictions, have generated more than $38 million for county roadway maintenance and nearly $19 million for the state highway fund over the past few years (Texas Department of Motor Vehicles 2012). The permits allow trucks to operate on county roads, farm-to-market (FM) and ranch-to-market (RM) roadways, state highways, and U.S. highways. Weight tolerance permits are insufficient for providing sustainable revenue streams to counties for roadway maintenance, so counties must coordinate and negotiate other partnerships to cover the costs of roadway maintenance and rehabilitation. In the 83rd Legislature, policy changes were made to the Texas Transportation Code allowing counties to designate County Energy Transportation Reinvestment Zones (CETRZ) to promote transportation infrastructure projects affected by oil and gas production activities. Funding for this approach arises from grants that are administered through a TxDOT allocation from the Rainy Day fund, which gets its revenue from the Surcharge fees paid by the oil and gas industry (Wilke and Harrell 2011).

Discussions at the county level often involve assessment of impact permit fees. Some counties utilize road-use agreements in an effort to recover costs of repairing damaged pavements, though this approach has not been widely adopted in Texas.

These agreements provide counties with approximately $8,500 to $9,000 per well (Sassin 2012). Impact permit fees are typically negotiated into the lease agreements and are dedicated specifically for road and bridge damage due to O&G equipment. Research reveals that there is little to no quantitative analysis involved in coming up with the $8,500-$9,000 fee per permit (Sassin 2012).

Other discussions often concern why O&G companies do not contribute to pavement maintenance and rehabilitation costs as wind energy companies do. Unlike the O&G industry, wind power companies typically pay for construction materials and rebuild the roads they use (Sassin 2012). The authors have found that in some cases, O&G companies are contributing explicitly to roadway maintenance and rehabilitation, but wind power companies appear to be more proactive in financing roadways upfront. One possible reason why this is happening is that O&G companies pay taxes on energy production, while wind energy producers do not.

DeWitt County stands as an example of how some Texas counties are partnering with O&G companies. Commissioners in DeWitt County have established cooperative agreements with two prolific energy developers in their county (Sassin 2012). Each of these companies has approximately 28,350 ha leased in the county. The current agreement assesses a fee of $8,000 per well, though typically multiple wells can be drilled per pad and there are no dry holes. Each well has a certain percentage of liquid and gas. County agreements with these two companies generate around $1.8 million per year, whereas overweight permits have only generated $54,000.

CONCLUSIONS AND RECOMMENDATIONS FOR FUTURE WORK

While progress is being made in establishing rapport between government officials and energy companies at the local level in counties throughout Texas and elsewhere, questions remain as to how best to address the O&G boom from a transportation infrastructure perspective. While the authors have presented four partnership models between energy companies and local governments, other effective models may exist as well. The importance of establishing strong working relationships between counties and O&G companies cannot be understated.

The authors pose several questions with the hope of spurring further discussion about relevant approaches to managing transportation assets in the wake of this energy boom. Some of these questions include:

- How can a collection of other case studies or a pooled fund study be initiated to demonstrate the utility of the four approaches presented? Such studies could provide quantitative evidence of the efficacy of each approach and compel other counties to take action.
- How can counties best initiate pavement preservation programs in conjunction with issuing permits to energy companies and land developers? Anecdotal evidence suggests that counties have found some success by tying roadway user agreements to drilling and exploration permits.
- As part of the permitting process, should roadway user agreements specify the use of non-destructive testing to evaluate baseline and post-development

structural properties of the pavement? The FWD has been widely used and appears well positioned to play a role in establishing a standard evaluation method because the technology is cost efficient and non-destructive.

- What is the appropriate decision making process, and must it be handled between county officials and O&G companies? Furthermore, what is the appropriate level of involvement from government officials? Some county governments in Texas seem to be very involved in these processes, with mixed results, while other coalitions seem less interested.

Determining who should pay for roadway use, rehabilitation, and maintenance remains a critical question as energy developments escalate in Texas and in other regions. Energy companies, counties and municipalities, state highway agencies, and engineers all have a role to play. Our research has shown that collaborative efforts hold the most promise for tackling these issues by keeping all parties engaged early in the decision-making process and reaching consensus on key issues. Proactive approaches that armor roads in preparation for energy development activities may one day be the standard approach, but as of yet reactive approaches seem to dominate in practice. By defining long-term infrastructure plans for energy development, roadways may continue to serve their purpose while enabling the exploitation of potentially vast energy resources.

REFERENCES

AASHTO. (2001). "Guidelines for Geometric Design of Very Low-Volume Local Roads (ADT < 400)." *American Association of State Highway and Transportation Officials*, Washington, D.C.

Advanced Pavement Testing Services. (2012). Falling Weight Deflectometer.

American Society for Testing and Materials. (2009). "Standard Test Method for Deflections with a Falling-Weight-Type Impulse Load Device." ASTM Standard No. D4694-09, West Conshohocken, PA.

Begley, D. (2013). "TxDOT safety plan is letting some roads kick rocks." Houston Chronicle, 25 July 2013.

DeWitt County Commissioners Court. (2012). "Road Damage Cost Allocation Study." Naismith Engineering, Inc.

Quiroga, C., Fernando, E., and Oh, J. (2012). "Energy Developments and the Transportation Infrastructure in Texas: Impacts and Strategies." Texas Transportation Institute, Report No. 0-6498-1.

Railroad Commission of Texas. (2013). Texas Monthly Oil and Gas Statistics.

Sassin, J. (2012). East and North Texas Judges Commissioners Conference. Field Tech Report, Galveston, TX.

Sassin, J. (2012). DeWitt County Approach to Handling Oil and Gas Fees and the Impact to Roads. Field Tech Report, Cuero, TX.

Sassin, J. (2012). DeWitt County Judges Office. Field Tech Report, Cuero, TX.

Sassin, J. (2012). Dimmit County Commissioners Court. Meeting Minutes, Carrizo Springs, TX.

Sassin, J. (2012). Impact Study on Bee County Roads. Field Tech Report, Beeville, TX.

Sassin, J. (2012). South Texas Judges Commissioners Conference. Field Tech Report, San Antonio, TX.

Senate Bill 1747. (2013). 83rd Legislative Regular Session, Austin, TX.

Texas Department of Motor Vehicles. (2012). "Length Limits for Vehicles & Vehicle Combinations." *Motor Carrier Division*.

Texas Department of Motor Vehicles. (2012). "Weight Tolerance Permits." *Motor Carrier Division*.

Texas Transportation Researcher. (2012). "Energy Developments and Our Roadways: Impacts and Strategies." *Texas Transportation Institute*, 48(1), 8-9.

Wilke, P. and Harrell, M. (2011). "Assessment of Impact of Energy Development Projects on Local Roads." *Transportation Association of Canada 2011 Annual Meeting*, Edmonton, Alberta.

Wilson, P. (2012). Impact of Energy Development Activities on the Texas Transportation Infrastructure. Testimony before the House Committee on Energy Resources, Texas Department of Transportation.

Zhang, Z., Wu, Z., Martinez, M., and Gaspard, K. (2008). "Pavement Structures Damage Caused by Hurricane Katrina Flooding" American Society of Civil Engineers, *J. of Geotechnical and Geoenvironmental Engineering*, 633-643.

Heavy Roadway User Permit Release Coordination

Scott K. Nale[1], P.E., P.T.O.E

[1]Staff Engineer, Pennoni Associates Inc., 680 Pittsburgh Road, Suite 2, Uniontown, PA, 15401, U.S.A., E-mail: snale@pennoni.com

ABSTRACT: As oil and gas infrastructure is developed, it has become increasingly important for the roadway users (heavy haulers) to obtain release from their PennDOT roadway bonds as quickly and efficiently as possible. Heavy roadway users are interested in being released from permits on many roads across the Commonwealth of Pennsylvania to free resources for additional infrastructure construction and reduce liability for repair of damages. This presentation would serve to discuss the release process, currently being used in PennDOT District 12-0. The process overview will include a discussion of the release requests, video review procedures, coordination within the District, and recommendations on best practices to achieve a timely release. In some cases, the roadway has been damaged by the users and repairs are required prior to release of the roadway bond. This presentation will also discuss the coordination required when road damage has been determined to be caused by single and/or multiple users. This overview will conclude with a case study of the SR 3009 (Tom's Run Road) repair and overlay in Greene County. This project provided for the repair and installation of base repair and a new overlay on five segments (4.0 km, 2.5 miles) of state maintained roadway. The project included coordination with two roadway contractors, six different roadway users and PennDOT staff both in the District Office and in the Greene County Maintenance District. Hundreds of tons of asphalt were installed to provide a safe and reliable roadway to the public. The final result was a cost controlled product that satisfied both the permit holders and PennDOT and resulted in the release of associated bonds.

INTRODUCTION

As oil and gas infrastructure is being developed, it has become increasingly important for the roadway users (heavy haulers) to obtain and release their PennDOT roadway permits as quickly and efficiently as possible to meet the demand of new well sites being added and changing pipeline construction operations. Additionally, users who do not properly manage their roadway bonds are exposing themselves to unnecessary liability in the event the roadway would be damaged by another user. The guidelines for bonding and usage of posted roads are outlined in PennDOT Publication 23, Chapter 15 and will be discussed below.

In this presentation we will discuss the requirements of PennDOT Publication 23 Chapter 15, and how the criteria are implemented in PennDOT District 12-0, including the process for add and release of road permits. We will discuss the process of the "five day letter" and practices that have been used to address those letters, keep the roadways open and accessible to the heavy hauling companies and operating safely for the traveling public.

ROADWAY PERMITTING BACKGROUND

If a company has need to haul loads that exceed a posted weight restriction on a state road, they must enter into an Excess Maintenance Agreement (EMA) with PennDOT. This agreement is typically set up by the Primary Company (operator) and will apply to all subcontractors making trips for this work. The agreement can apply to a District, County or Municipality. Upon approval of the EMA, individual permits can be issued relating to a specific road or road segment.

Following the completion of the EMA the company will need to fill out the "Application to Add or Remove a Section of Highway (M-4902APP)" PennDOT form in order to receive a permit on an individual roadway. PennDOT will determine the type (1, 2 or 3) of permit and assign the bond amount. Type 1 permits are to be carried in the vehicle on the posted road. Type 2 permits are displayed at the destination receiving the heavy loads. Type 3 permits are also to be carried in the vehicle and only issued if there is a "minimum potential" for roadway damage. In all cases the applicant must post surety bonds to protect the integrity of the roadway system, although the price varies between permit types. When the documentation and bonds are in place the permit will be issued and the company may begin to operate on the posted roads.

Adding Roadway Permits

Once the Add/Remove request form is received in the local District office the roadway(s) requested are added in the queue to be reviewed. It is important to understand that the queue of roads to review changes on a daily basis, and simply because a request is received, does not indicate that road will be bonded immediately. Queue length varies based on the requests received from road users in the District and at times the list can be lengthy.

Once the roadway is next in the queue, a representative from the Department will set a time to meet at the roadway in the field for the initial inspection. In addition to the invitation for the pending roadway user, all other Type 1 and Type 2 permit holders on that roadway also receive an invitation to the inspection. During the field view the Department representative will drive the section of road being bonded and document damage that exists on the roadway at that time. The roadway condition will be recorded via video for future reference. When completed, PennDOT will issue a heavy hauling permit to the user for that segment of roadway.

Releasing Roadway Permits

When the bondee has completed work in an area and access to the bonded road is no longer needed, the user will once again submit the Add/Remove form to PennDOT to have the heavy hauling permit removed from their EMA. Similar to the addition process, the roadway segment will be added to the queue for removal and will be addressed in the order received. In accordance with PennDOT Publication 23, Chapter 15, Section 15.11 a request to release a roadway segment shall be completed in fifteen (15) days, there is however no such requirement for the addition of a roadway segment to an EMA. Once the subject roadway has been reached in the queue, a representative from the Department will contact the user to schedule a field view for release.

During the field view, the Department representative will again drive the permitted roadway segment and complete a form to document the condition of the roadway at that time. The roadway will additionally be documented via video for reference. Once the roadway condition is documented, the Department representative will drive the roadway segment while reviewing the video obtained during the initial bonding process. Using visual comparison the initial video is reviewed versus the current condition and in cases where visible excess damage exists on the roadway that was not present in the initial video, the Department representative documents the damage which is noted in his report.

If it is determined the roadway was not damaged by the roadway user, the PennDOT representative will recommend the roadway for release from the EMA. This recommendation is reviewed by the appropriate County Maintenance Manager. If the Manager is in agreement, the roadway is released from the EMA and a letter sent to the user notifying them their permit to use the roadway is no longer in effect and they have no further liability on that roadway.

If damage is found during the review, an interim report is developed by PennDOT. The report documents the condition of the roadway and indicates locations where damage exists and needs to be repaired prior to release. Once completed the interim report is sent to the permittee seeking to have their permit released. It is then up to them to make the necessary repairs according to PennDOT specifications. Once the repairs are completed and the necessary installation documentation submitted the permittee will need to resubmit the Add/Remove form and begin the release process again.

Interim Reports and Repairs

After receiving an interim report from the Department, the bonded user is responsible to either repair the damage that is documented or contest the findings with the Department. On the issue of damage to the bonded roadways, PennDOT is not typically involved in determining which party using the roadway is responsible for the damage. If a user is bonded on the roadway and it sustains damage, the user typically will be responsible for repairing the damage no matter how many other users are bonded on the roadway, as the other companies are still using the roadway and have no interest in repairing the roadway at that point. While it is in the user's

best interest to cooperate on making the roadway repairs together, in practice this is often not the case.

As per PennDOT Publication 23, Chapter 15 "*In the event that the USERS cannot reach and understand on the assignment of responsibilities among themselves the POSTING AUTHORITY shall assess each USER in direct proportion to their percentage of the total traffic generated under agreement.*" This provision should be considered as a last step for resolution, as the Department would prefer to remain out of these discussions.

When the necessary roadway repairs have been made to PennDOT's requirements, the user will then need to resubmit the Add/Remove form and have a new final review conducted on the roadway. If repairs have been accepted by PennDOT, the user should then have their roadway bond released.

Excessive Damage and the "Five Day Letter"

PennDOT historically had no way to facilitate necessary interim repairs on a roadway that was severely damaged and presented a safety concern to the general traveling public. Therefore the roadway condition survey in conjunction with the "five day letter" has been added as a tool that PennDOT can use to get excessive roadway damage repaired. PennDOT employs staff to regularly review the posted routes in their District and develop regular reports on the roadway condition. If a roadway is found to be damaged to the point that it is not safe, the issuance of a "five day letter" is considered. The criteria that PennDOT uses to determine if a "five day letter" is applicable is when more than 152.4 m (500 ft) of damaged roadway occurs in a mile or any damage that causes a driver to leave their travel lane to avoid the damage.

If a roadway is found to be damaged to the level of one of the above criteria, each permit holder receives a letter from PennDOT informing the users the roadway damage must be repaired immediately. The users then have five days to make plans for and begin repairs and ten days to complete the repairs. If these criteria are not met, PennDOT can suspend all permits on the roadway, halting hauling operations on this route, which could cause financial ramifications. Additionally, the Department reserves the right to revoke any and all permits on the affected roadway segment if the repairs are not being made in a timely manner according to PennDOT construction methods.

As part of the repair process it will be the duty of the company completing the repairs to certify to PennDOT that the work was done according to specifications as defined in Publication 408. This includes certification of material quality from the batch plant, placement temperatures, and volumes of material and inspection of material placement. All of this information may be requested from PennDOT after the completion of work and a lack of this information can result in the repairs being rejected and the permits remaining suspended.

Summary of "Five Day Letter" Issues

As discussed above, the "five day letter" process has allowed PennDOT to effect repairs on many roads that have become a safety concern to the traveling public. There are, however, three major challenges in this process, for the bonded users.

The first issue is it leaves roadway users, who are not usually experienced in dealing with PennDOT, to coordinate with each other and reach an agreement on level of financial responsibility for making the necessary repairs, on a very short schedule. While there are provisions in place for PennDOT to assign percentages of the financial responsibility for the repair, the short timeline of the work requirements does not allow for this process to occur. In most cases, by the time a meeting could be scheduled that included the necessary parties, a significant portion of the five day lead time would have already expired. Couple that with the internal coordination of the included companies and it is most likely that the ten days completion date will also have expired before a decision to proceed has even been made.

The second issue with this approach is that the bond holders are responsible for completing roadway repairs to meet PennDOT specifications, which can be difficult if they are not familiar with the requirements. While being very knowledgeable about the work in their area, many of these firms do not have the knowledge to make effective and lasting roadway repairs in accordance with PennDOT specifications. In some cases the companies may not even know that a contractor employed to do this work must be on the PennDOT Approved Contractor List. Companies also often do not know that they are required to provide material certifications, placement inspection reports, material temperatures and other certifications to PennDOT in order to obtain approval for the work completed. This lack of knowledge can lead companies to be required to make repairs multiple times in order to meet PennDOT criteria and gain approval of the completed work.

The third issue is the absence in this process for a mechanism to encourage or coordinate permittee discussions. While each permittee will receive a copy of the letter, each one does not typically initiate a meeting to discuss repairs. The lack of clear coordination can lead to various wasteful results. Some companies could proceed to make repairs which do not meet PennDOT criteria on their own, based on criteria that company determines. Other permittees will disregard the letter in the hopes that the problem will go away. These approaches result in a waste of time and disorganization for the users involved.

However, some companies will contact roadway professionals for assistance. By including individuals who are knowledgeable of roadway conditions, materials and repair practices the work can be completed in a way that reduces the overall cost to all parties and can be accomplished within the timelines of the "five day letter" constraints. This last approach will be highlighted in the SR 3009 Case Study.

Case Study – Greene County - SR 3009

State Route 3009, Tom's Run Road, spans ten and one-half miles through southwest Greene County. The roadway, located in a rural area of the county has, for a long time, seen much use from several companies hauling loads over the posted ten

ton weight limit. Traffic on this road has been associated with coal mines, gas wells, and timbering operations, as well as some major gas transmission line activities. As a result, the roadway has been heavily damaged in many locations. This condition led PennDOT to issue a series of five "five day letters" addressing the length of the roadway. The letters were sent out over an extended time period, ranging from December 2011 to June 2012, so that the entire road didn't have to be repaired at the same time.

The initial "five day letter" was issued on December 21st 2011, addressing Segments 104 to 150, a length of 4.2 km (two and six tenths miles). At the time the letter was issued one of the companies with a permit on the roadway contacted an engineering firm with whom they have had a working relationship with to get involved on their behalf. At the request of that user, the engineering firm became involved with the repair process on this roadway. The firm, in coordination with the user, reached out to the other permit holders on the roadway to discuss the work that needed to be completed and their respective level of involvement. The engineering firm immediately took the lead on monitoring the process and coordinating these roadway repairs. A field team was sent out to evaluate the condition of the roadway and locations in need of repair and then initiate the proper approach to make those repairs. Additionally, the project was coordinated with the local PennDOT County Maintenance Manager so that all stakeholders were involved and their concerns were addressed. Working with PennDOT the firm was able to review the roadway segment that had been issued the "five day letter" and identify the locations that need corrected to satisfy PennDOT. This meeting reduced the chance for guessing which locations had to be repaired, limiting the amount of material to be required. This work allowed the team to put a repair plan together and develop quantity estimates.

With the level of work identified, paving contractors were contacted to obtain construction estimates of the field work needed. The estimates were reviewed and the engineer presented a recommendation to the various permittees of which contractor should be awarded the project, based on competitive bid and PennDOT certifications. Upon receiving authorization from the companies involved on the roadway, the engineer issued the notice to proceed to the selected paving contractor for the project. This resulted in the engineering firm acting as the prime contractor with the paving contractor reporting and billing to the engineering firm. In turn the engineering firm billed each permittee separately for their share of the roadway repairs. During construction operations, the engineer also provided construction management and inspection services for the installation of material on these roadways. Construction inspectors were on sight during all repairs to certify the work was done in accordance with PennDOT specifications and document the surface and material temperatures during material placement. This allowed staff to be present during construction should the need arise for any unforeseen circumstances to be addressed. Inspectors conducted detailed inspections and maintained installation records meeting PennDOT criteria.

Throughout the process, the engineering firm maintained the necessary State Records to certify the work as meeting PennDOT criteria. Plant certifications were collected and maintained so that it could be properly demonstrated that the material received was within PennDOT design criteria and received from a certified

production facility. Additionally, the project was only made available to contractors who were on the Approved Contractor List maintained by PennDOT. This allows the Department to maintain a level of quality control regarding the construction practices of the contractors.

Finally, during the material installation process, the engineer provided construction inspectors on hand to collect loading tickets, material temperatures and to document the installation processes for the work. Due to the time of year and requirements set forth in PennDOT Publication 408, it was complicated to complete the work according to specification. Section 305 indicated "*Do not place subbase material on soft, muddy, or frozen areas.*" which is difficult when working in late December. Additionally, it is stated that in Section 460 that asphalt material can only be placed *"when the air temperature is 40F and rising"*. With very careful coordination and a few breaks in the weather the material was able to be placed in a way that satisfied PennDOT staff and met the criteria for permanent placement. In the event these criteria were not met, PennDOT would have considered the work temporary and the patches would have been replaced in the spring when the weather improved.

After successfully addressing the first of the letters, a second "five day letter" was issued on March 14, 2012 which addressed Segments 104 to 150, a length of two and six tenths miles a second time. Due to the traffic on this roadway there was additional damage occurring at the same time the roadway was being repaired. The second letter was issued to address these additional damaged locations. As before, the engineering firm coordinated with the permittees to address the damage. Locations of damage were identified and then coordinated with the County Maintenance Manager for this area. All damaged locations were agreed upon and the project was put out to bid.

Once the permitees agreed on the contractor a notice to proceed was again issued by the engineering company for the repairs to be completed. As before staff from the engineering firm was in the field to document and certify the work in accordance with PennDOT criteria.

As the second letter was addressed and the work completed, PennDOT issued a third "five day letter" on April 4, 2012. This letter addressed Segments 10 to 30 for a distance of one and three tenths mile starting at the state line with West Virginia. The engineering firm continued to operate this work as a design build operation and worked with permitees to collect bids again. Again the engineering firm worked with PennDOT staff to satisfy the criteria and complete the necessary work.

Upon completion of the third letter a fourth letter was issued addressing Segments 30 to 80. This letter was issued on April 25, 2012. Again the engineering firm coordinated with PennDOT staff to address this letter which covered two and seven tenths miles of roadway. Work was also done to address the fifth letter, issued on June 4th, 2012 and addressing damage on Segments 80 to 140. This letter covered a length of two and four tenths miles.

Once the various roadway repairs were completed SR 3009, looked like a "patchwork" roadway with patches over much of the roadway surface. In some locations patches were placed on other patches to make the necessary repairs. This condition resulted in a very poor ride quality of the roadway and the Department

determined that the road was still damaged because of this condition. At this point a sixth, "five day letter" was considered, based on ride quality.

The potential sixth "five day letter" would have addressed the entire roadway from Segment 0104 to 0150 due to the International Ride Incentive (IRI) conditions. The roadway was considered to be a "patchwork" road. Due to all the patches on the roadway surface the ride quality of this section was very poor. After the discussion of the potential sixth "five day letter" and further talks with the permit holders for the roadway, the engineer entered into talks with another contractor.

This contractor was brought in to provide a full width overlay for the roadway section from Segment 104 to Segment 150. Once the road was fully overlaid, PennDOT had no more issues with the roadway and subsequently work continued, uninterrupted for these permit holders. Additionally, at this time several of the contributors have been released from their permits with no further repairs requested.

Throughout the course of construction the engineering firm staff worked closely with the Department, particularly the County Maintenance Manager. During each phase, PennDOT was notified on a daily basis of the day's operations. If any changes were to be made, PennDOT was called to the site to review and approve those changes. Once work was completed, the engineering firm facilitated a meeting with the Department to review all repairs and to insure they met their satisfaction.

The approximate construction related cost of this project, ten and one-half miles of roadway, was $1,335,000, a cost which could have been much higher without the coordination of work and sharing of resources among the heavy users. Once the repair work was completed, the engineer stayed involved with the project representing our initial client to PennDOT through the release of these roadway permits and permits for other roads in this area.

Conclusions

As can be seen in the illustration above, by including parties who are knowledgeable of roadway repair processes and PennDOT requirements, it was possible to complete the necessary work on a truncated time table. Additionally, it should be noted that the first letter came out in the winter and Christmas Day was one of the five days included in that time span. This additionally compressed the schedule for this letter placing even more importance on timely coordination. Due to the permitted company reaching out to a firm experienced with the criteria it was possible to meet this deadline without the permittees having any of their permits suspended.

This process was able to work because one of the permittees had a relationship with a firm that was able to complete the work needed. Had that relationship not been in place it would have been difficult to get an engineer in place in time to develop the estimates and make the repairs in time.

Recommendations to Permittees

The following recommendations to potential permit holders are based on experience and first hand observations. The first recommendation to permit holders

is to assess the project that will require permitting for Heavy Hauling. Pick the haul routes carefully following a complete review of the current condition of the roadway to be added to the EMA. Avoid, if possible, roads that are in poor, if not unsafe condition. Certain roads will be essential for the completion of the project; others may be for convenience and can be eliminated, thus reducing exposure. If the project demands the permitting of certain roads for heavy hauling (over the posted weight limit), those roads will also be used for general use by the Contractor's and other users, be prepared to upgrade some roads BEFORE using them to reduce the possibility of exasperating the poor condition and causing an unsafe condition for the public. Planning at the onset can reduce cost, maintain a good working relationship with PennDOT and keep the roadways safe for the public. When finished apply for a roadway release immediately as a roadway is done being used. By maintaining a permit on a roadway that a company is not using, the company is exposing themselves to extra financial liability. During this time, another company could be using the roadway for heavy impact types of activities and causing excessive damage to the roadway, damage that all users will have to contribute repair costs to fix. By releasing the roadway permits when hauling is completed, a company can avoid this exposure and lessen the risk of having to pay for damages done by others. The cost that a permittee has in releasing a permit and obtaining the permit at a later date is far less than the potential cost of repairing a roadway which has been badly damaged by another user.

A second recommendation would be to implement a monitoring plan for the roadways that are permitted. Such a plan, usually consisting of regular videos and reports, will allow the company to monitor the condition of the roadway during the time is permitted. The inspector who is conducting these surveys will then be able to let the company know when repairs on the roadway are necessary to maintain roadway use for the traveling public. Additionally, these videos can help to document who is using the roadway by noting the traffic during the time of the video process and by monitoring the addition and deletion of heavy users along the route. This information will allow users to provide proof to the Department of what has occurred on the roadway during the time it was permitted. The reviews of the roadway will allow a proactive permit holder to make regular minor repairs to the roadway in the event that damage should start to occur. Additionally, it will allow bond holders to know ahead of time when a roadway is in danger of receiving a "five day letter". This information can also be helpful to PennDOT when it is time to release a roadway and may greatly reduce the amount of repairs a user would be asked to make.

Another recommendation that would benefit the permit holders would be to include roadway professionals when determining types of repairs. These professionals have the knowledge and experience to address the necessary repair to a roadway and how to complete the work in a manner that will meet PennDOT criteria. In many cases the use of such professionals can reduce the need to have work done multiple times because it was not done to the proper specification. Additionally, the construction repair work should be monitored by properly certified inspectors so it is done according to PennDOT standards and specifications. It would be most useful to have

a firm that the company works with on a regular basis. That way, in the event of a "five day letter", the firm is already on hand and can begin at the outset of the letter.

A final recommendation to consider is proper maintenance, planning and potentially even advanced work on the roadway to prevent larger and more expensive issues in the future. An example of the maintenance considered would be clearing and maintaining ditches. Water around a roadway is the most likely cause of the damage types companies are being asked to fix. If water is allowed to pool around the roadbed, it can cause the pavement base to become soft, consequently allowing the road to move and break when crossed by heavy (and in some cases regular) traffic. By insuring the roadside ditches are in place and maintained, the water is allowed to flow away from the roadway, and a user can help to prevent much more expensive damage to the roadway. Additionally, by planning to avoid wet times of the year (when possible), a company can further reduce the risk of causing damage to the roadway. Finally, there are some cases where a roadway is in such poor shape, that it would be better for the roadway permit holders to be proactive and agree to take action and upgrade the roadway prior to use. Often this work can cost less than a full repair after use or in some cases may be required to keep the roadway usable by the permit holder for the loads they need to haul.

REFERENCES

Pennsylvania Department of Transportation (June 2013). "PUB 23 – Maintenance Manual Chapter 15 Weight Restrictions on Highways" Harrisburg, PA

Pennsylvania Department of Transportation (April 2014). "PUB 408/2011 – Specifications" Harrisburg, Pennsylvania, Section 300 and 400

Protecting PennDOT's Infrastructure

Melody Matter[1], P.E., PTOE and John Voda[2]

[1]Transportation Engineer, McCormick Taylor, 5 Capital Drive, Suite 400, Harrisburg, PA 17110, U.S.A, E-mail: mamatter@mtmail.biz.
[2]Field Superintendent, Chesapeake Energy Corporation, 14 Chesapeake Lane, Sayre, PA 18840, U.S.A, E-mail: john.voda@chk.com.

ABSTRACT: The Pennsylvania Department of Transportation (PennDOT) is trying to balance the economic benefit of supporting the Shale Oil and Gas Industry while protecting the public roadway infrastructure. The Shale Oil and Gas Industry utilizes a horizontal drilling process and a separate, secondary process called hydraulic fracturing (fracing). This process releases the natural gas inside the shale formations which are over a mile beneath the earth's surface. The fracing process requires approximately 19 million liters (5 million gallons) of water and other materials which can generate over 2,000 truck trips to the drilling pad. This truck traffic creates an exponential increase in truck volume and can severely reduce the life cycle of the roadway which can lead to accelerated deterioration and significant repair costs. To protect PennDOT's infrastructure, numerous roadways have been posted with weight restrictions requiring haulers to obtain a permit, post security and submit a maintenance plan to utilize the roadway. In conjunction with PennDOT's efforts to protect the roadways, the Shale Oil and Gas Industry has invested time and money to work in partnership to protect, preserve, maintain and upgrade the roadway network.

INTRODUCTION

In Pennsylvania, the Shale Oil and Gas Industry is accessing the natural gas within the Marcellus Shale formation. The Marcellus Shale formation is organic-rich black shale that was deposited in an oxygen-deficient marine environment during Middle Devonian time (approximately 390 million years ago). Due to the impermeable nature of the shale, natural gas is "trapped" within the shale formation. The supply of natural gas within the Marcellus Shale formation has been known for more than 75 years, but only until recently has the technology been available to make the otherwise difficult gas play economical (Pennsylvania Department of Conservation and Natural Resources 2013).

The Marcellus Shale formation is located throughout much of the northern and western area of Pennsylvania. The depth of the formation which has the largest potential for producing natural gas ranges between 1,500 and 2,400 meters (5,000 and

8,000 feet) below the earth's surface. To maximize access to the shale formation, the Shale Oil and Gas Industry utilizes a horizontal drilling process. This process involves drilling vertically to the target reservoir and then curving the drill bit until horizontal drilling is achieved. The well is then drilled horizontally for a distance of 1,500 to 3,000 meters (5,000 to 10,000 feet). Once the drilling process is complete and the well shaft is properly cased, the casing in the horizontal portion of the well is perforated using perforating guns containing explosive charges to create holes in the casing. These holes provide pathways for hydraulic fracturing fluids and proppants to enter the formation, prop open the shale and release the natural gas. This process, called hydraulic fracturing or fracing, has allowed for efficient extraction of natural gas from the Marcellus Shale formation.

Extracting natural gas from the Marcellus Shale formation began in 2004 with an "experimental" well drilled in Washington County, Pennsylvania (Governor's Marcellus Shale Advisory Commission 2011). Other Shale Oil and Gas Industries learned of the natural gas prospects and by 2007 there were 112 wells drilled in Pennsylvania. The number of wells has continued to grow and as of December 1, 2012 there were a total of 6,112 wells drilled (Marcellus Center for Outreach and Research 2012). Figure 1 depicts the number of wells drilled by year.

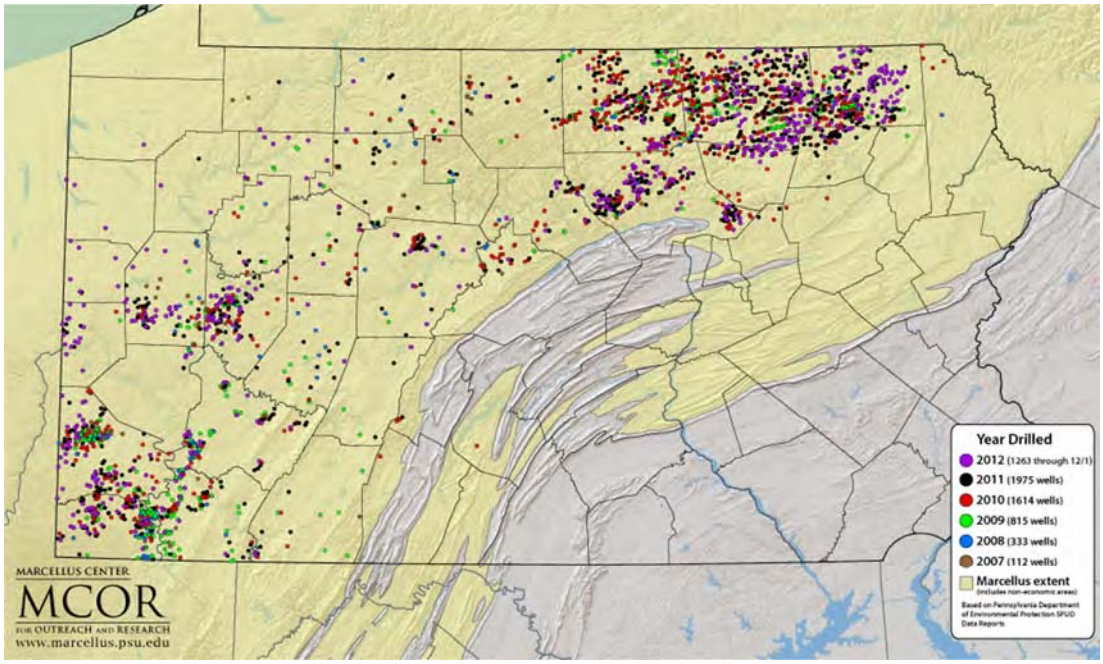

FIG. 1. Number of Marcellus Shale Wells Drilled by Year

OVERVIEW OF PENNSYLVANIA'S ROADWAYS AND PENNDOT'S POSTED AND BONDED ROADWAY PROGRAM

Pennsylvania has 195,973 kilometers (121,772 miles) of public roads (American Society of Civil Engineers 2013). The Pennsylvania Department of Transportation (PennDOT) owns and maintains approximately 64,400 kilometers (40,000 miles) of those roads; ranking Pennsylvania as the fifth largest in the nation for the number of state-owned highways (American Society of Civil Engineers 2010). Part of the reason

PennDOT has such an expansive network of roads is due to a 1930 political campaign where Gifford Pinchot promised if he was elected governor he would "get the farmers out of the mud." Pinchot won the election and the following year, the state took over 32,438 kilometers (20,156 miles) of township roads; which to this day, PennDOT still owns and maintains the majority of these roadways. The "Pinchot Roads" were paved using light construction and included little to no subbase and on average; the roads cost less than $11,300 a kilometer ($7,000 a mile) to upgrade (Beyer 1972).

Within PennDOT's organization, the Bureau of Maintenance and Operations oversees the Posted and Bonded Roadway Program. This program was established over 30 years ago to protect PennDOT's roadways which were not designed to support significant truck volumes (particularly the Pinchot Roads). At the time the program was established, significant truck volumes were being introduced by coal and forest product industries. Since then other industries have introduced significant truck volumes including oil, shallow gas wells, horizontal well (i.e. Shale Oil and Gas Industry), quarries and wind farm industries. The Posted and Bonded Roadway Program is established by law in Title 75 Vehicle Code: Chapter 49 – Size, Weight and Load. The program is part of the Commonwealth's Regulation in Title 67 Transportation: Chapter 189 – Hauling in Excess of Posted Weight Limit and is under policy in PennDOT's Maintenance Manual Publication 23: Chapter 15 – Weight Restrictions on Highways.

When PennDOT suspects a roadway may not be able to support the current or potential increase in truck volume, a Traffic and Engineering Study is completed to evaluate the pavement and geometric conditions. If the roadway is warranted to be posted with a weight restriction, the appropriate weight restriction is determined (typically 9 metric tons (10 tons)), the public and the state law enforcement agencies are notified and the signs are installed along the roadway. This is the "posted" aspect of the Posted and Bonded Roadway Program. Once a road is posted with a weight restriction, a hauler must obtain a hauling permit to operate a vehicle over the posted weight limit on that roadway. To obtain the hauling permit, the hauler must enter into an Excess Maintenance Agreement (EMA) with PennDOT. This EMA basically states the hauler is responsible for maintaining the roadway to the current conditions and is responsible for all repairs beyond normal maintenance. Requirements of the EMA include the hauler providing security ($20,100 per paved kilometer ($12,500 per paved mile)) and a Maintenance Plan which documents the hauler's approach to maintaining the roadway. The security provided is typically in the form of a bond which is the "bonded" aspect of the Posted and Bonded Roadway Program.

Once the hauler is permitted to operate on the posted roadway, PennDOT monitors the condition of the roadway to assure its condition is not deteriorating. PennDOT has developed a Roadway Condition Survey which is utilized to review the damage and assess an overall condition of the roadway. The overall roadway conditions are categorized as none/minimal, low, medium or high. If significant damage is documented during the Roadway Condition Survey (generally in the overall condition category of medium and high), the hauler will be made aware of the damage and required to repair the damage or risk suspension of their hauling permit. If critical damage is documented during the Roadway Condition Survey, where roadway

conditions are considered unsafe or unpassable, hauling operations will be suspended immediately (Pennsylvania Department of Transportation 2013).

ROAD IMPACTS GENERATED BY THE SHALE OIL AND GAS INDUSTRY

The development of a Marcellus Shale well involves three main phases:

- Well Pad Development: A typical Marcellus Shale well pad is 1.2-2.0 hectares (3-5 acres) in size and is designed to accommodate six to eight wells. To clear, level and environmentally stabilize the site (including installing protective liners and constructing containment berms) takes an average of 35 days. An average of 20 trucks per day are generated during this phase to move equipment, materials and stone.
- Drilling Operations: The drilling operations phase includes mobilizing the drill rig to/from the well pad and drilling the vertical and horizontal bores. On average it takes 25 days to drill one well with 20 trucks generated per day. The trucks generated during this phase are mainly related to hauling the rig itself and mobilizing materials to support the rig including water, fuel, and drill pipe and casing materials.
- Fracing: The final phase of the development of a Marcellus Shale well is hydraulic fracturing or fracing. The fracing process involves the delivery of approximately 2,700 metric tons (3,000 tons) of sand and approximately 19 million liters (5 million gallons) of water (Chesapeake Energy 2013). In addition to the delivery of these materials, pump trucks, blenders and storage tanks for sand and water are also mobilized to the well pad. The frac process for one well has an average duration of seven days with approximately 300 trucks per day.

The increased truck traffic introduced by the Shale Oil and Gas Industry has put additional stress on many low volume, rural roads that were not designed to carry heavy trucks. The traffic loadings are very significant considering the relationship between axle weight and inflicted pavement damage is exponential; the damage a vehicle causes is proportional to the axle load raised to the fourth power. According to the AASHO Road Test, heavily loaded trucks can do more than 10,000 times the damage done by a normal passenger car (American Association of State Highway and Transportation Officials 1962). Compounding the impacts of the vehicle loadings is the fact Pennsylvania's roadways are susceptible to weakening during the spring thaw period. During the spring thaw, the ground that was frozen in the winter thaws from the top down, so water is trapped between the pavement above and the still frozen soil underneath. This layer of saturated soil provides little support for the road above, leading to premature pavement failure and a reduced pavement life cycle. Since the Oil and Gas traffic typically continues throughout the year, their truck loading is not decreased during this vulnerable spring thaw period and the damage inflicted by each truck is much greater.

To address the impacts associated with the truck volume generated by the Shale Oil and Gas Industry, PennDOT has posted additional roadways with weight restrictions. Prior to the Shale Oil and Gas Industry's expansive presence in the Commonwealth (approximately 2006) there were 10,808 kilometers (6,716 miles) of roads posted

with a weight restriction. With the introduction of drilling, 7,200 additional kilometers (4,500 miles) have been posted with weight restrictions. Today, over 25 percent of PennDOT's roadways are posted with a weight restriction. Figure 2 summarizes the kilometers of PennDOT's roadways posted with a weight restriction.

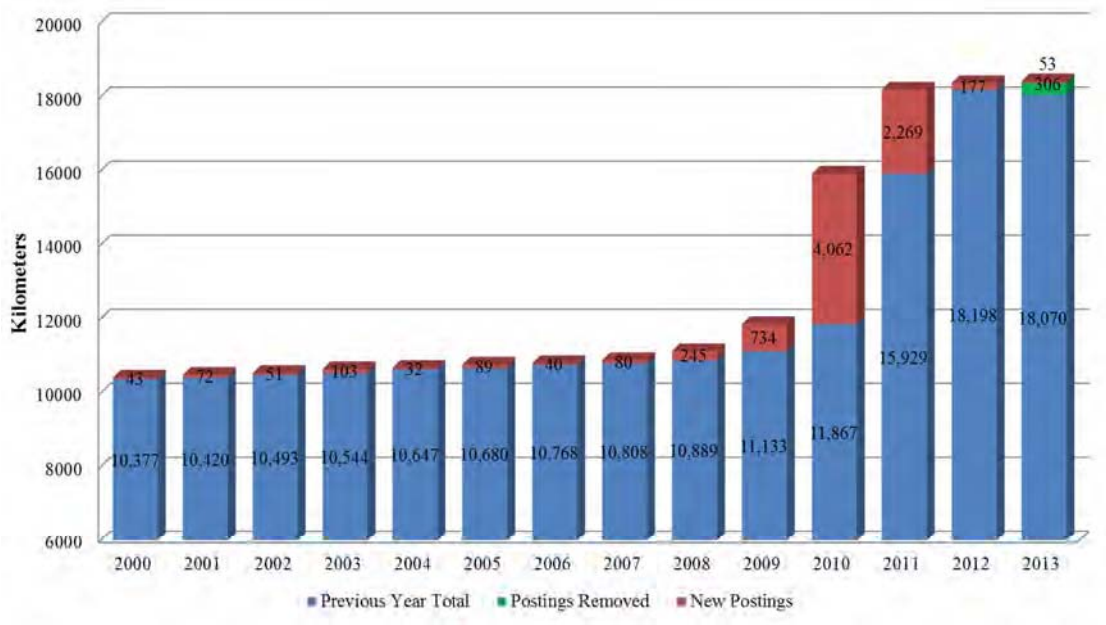

FIG. 2. Kilometers Posted with a Weight Restriction

The largest increase in roadways posted with a weight restriction was in 2010 when the number of Marcellus Shale wells drilled surpassed 2,000. With the additional road damage being introduced from the truck volume generated by the Shale Oil and Gas Industry, in June 2010 PennDOT began formally completing Roadway Condition Surveys to document and track the conditions of the posted roadways. At that time, there were 684 kilometers (425 miles) of roadway with significant damage. Examples of the roadway damage documented during this time are shown in the photos in Figure 3. The type of damage included base failure, alligator cracking, edge cracking, potholes, distortion and rutting. Through the efforts of the Shale Oil and Gas Industry the roadway damage has been addressed and the total miles of roadway with significant damage has been reduced to a minimal level; as of October 2013 there were nine kilometers (six miles) of roadways posted with a weight restriction with significant damage. Based on the data trends, there is a tendency for the miles of significant damage to increase during the spring thaw (typically in March and April) when the pavement structure is even more susceptible to damage.

SR 3001 Bradford County - 3/17/2010

SR 0664 Clinton County - 3/14/2011

SR 4008 Bradford County - 3/8/2011

SR 4016 Sullivan County - 3/19/2011

FIG. 3. Photos of Roadway Damage

ROADWAY REPAIRS AND UPGRADES

The Shale Oil and Gas Industry has made a significant effort to prevent and address roadway damage. Specifically, Chesapeake Energy Corporation (Chesapeake) has made a concerted effort to protect, maintain and upgrade roadways in northeastern Pennsylvania. Chesapeake, headquartered in Oklahoma City, Oklahoma is the second largest producer of natural gas in the United States and is currently drilling or has land leased in nine states (Chesapeake Energy 2013). In late 2008, Chesapeake drilled its first well in Pennsylvania's Marcellus Shale formation; and in 2009 bonded their first state road. With operations escalating and an intense spring thaw in 2010, roadway damage caused by the truck traffic began to occur. It quickly became evident a planned approach to assessing, repairing and in many cases significantly improving these bonded roadways was necessary. By the end of 2010, Chesapeake spent nearly $100 million to reconstruct 246 kilometers (153 miles) of roadway in four counties. By mid-2011, their total kilometers bonded grew to nearly 1,000 (620 miles) and Chesapeake continued to aggressively repair and reconstruct their bonded roadways. At the end of the 2013 season, the total of reconstructed roadways reached 624 kilometers (388 miles) with a total investment of nearly $300 million.

Route Planning and Assessment

Chesapeake's first step in protecting PennDOT's posted roadways is to identify the appropriate travel route and assess the roadway condition. When Chesapeake is ready to construct a new well pad, a specific route for traffic traveling to and from the location is established. This route is selected based on the condition of the roads, ease of travel for large loads and safety; travel distance and time are a limited component in the selection. All contractors and vendors who may travel to and from the well pad are instructed to use the identified route via an email notification prior to the start of operations on the pad. Chesapeake also maintains an ftp site which contractors and vendors can access for directions to all of their sites. Chesapeake ensures the selected route is utilized through monitoring and enforcement.

Before the selected route is utilized, the conditions of the posted roads are evaluated for existing damage and to determine whether improvements are needed before the introduction of truck traffic. The type and level of the pavement assessment is determined based on the general observation of the roadway condition and the projected traffic volumes. The assessment of the pavement condition can be accomplished in several ways ranging from field observations, referencing pavement histories, consulting with county maintenance staff, to full geotechnical testing. When full geotechnical testing is ordered, field samples are collected and tests are completed to determine the pavement and subbase strength. A geotechnical report is generated to document the findings and recommend a pavement design which if applicable could be a Full Depth Reclamation (FDR) design. If the condition of the pavement is deemed satisfactory, the roadway is scheduled for regular monitoring to assure pavement conditions do not deteriorate once hauling operations begin. If the condition of the pavement is determined to be unsatisfactory, repair and/or improvement strategies are implemented.

Repair and Upgrade Strategies

If repairs are determined to be necessary prior to operations or if repairs are needed during operations, there are several repair and upgrade strategies utilized by the Shale Oil and Gas Industry. The most commonly utilized include base repair, base repair with pavement overlay, and full reconstruction utilizing cement FDR. With any of these repair strategies, drainage improvements are often incorporated into the scope of work. In many cases the Shale Oil and Gas Industry work in partnership with PennDOT's County Maintenance forces addressing the necessary drainage improvements before roadway repairs and/or improvements begin. These drainage improvements could include replacing cross pipes, ditch and swale cleaning, and pavement base drain.

Base Repair

If the assessment reveals the pavement has a suitable subbase and existing damage is limited, base repairs are completed. Areas with alligator cracking, edge cracking, potholes, and rutting are milled 100 to 150 millimeters (4 to 6 inches) deep, patched

with 19 millimeter (0.75 inch) asphalt and the edges sealed. If the damage is severe or more widespread, base repairs along with a full pavement overlay is completed.

Full Depth Reclamation (FDR)

If the assessment of the pavement determines the conditions are such that even base repairs with a full pavement overlay will not support the potential truck traffic, cement FDR with a pavement overlay is often the method chosen to upgrade the roadway. Chesapeake has utilized cement FDR in nearly all of their reconstruction projects due to the poor subbase conditions found in northeastern Pennsylvania. The FDR process is the permanent chemical alteration of soils utilizing Portland cement (Polak & Breneman 2013). Once a determination is made that FDR is a viable option to rebuild a roadway, geotechnical testing is done to classify the soils, determine the moisture content and unconfined compressive strength. This testing, along with the projected traffic volume determines the percentage of cement to be added and the depth of the FDR. A typical design mix for Chesapeake roadways is seven percent cement at 381 millimeters (15 inches) deep for a yield of 38 kilograms per square meter (100 pounds per square yard).

The first step in the construction process is pre-pulverizing the existing road and subbase to the depth of the proposed FDR. If there is substantial asphalt present, some is milled off and utilized later for shoulder backup. Pre-pulverizing ensures uniform gradation throughout the roadway to allow even distribution of the cement. The roadway is then graded and compacted to the determined profile, including the appropriate roadway crown. The next step is applying the cement with a pneumatic spreader, utilizing skirting and water to minimize fugitive dust. Once applied, a reclaimer machine begins the mixing process (Fig. 4). Water is injected directly into the mill head to ensure proper hydration of the material though the entire depth. When the mixing is complete, the newly stabilized material is graded and compacted to proper cross slopes. Compaction and density is verified by the use of a nuclear density gauge and samples are pulled for specification compliance. Traffic can be allowed on the FDR approximately 20 to 30 minutes shortly after completion, but is allowed to cure five days before heavy truck traffic and paving begins.

Spreading Cement in the FDR Process Cement Mixing in the FDR Process

FIG. 4. Photos of the FDR Process

To improve the quality of construction, Chesapeake has included two additional components to the FDR process; these include the use of a pilot car for maintenance and protection of traffic and slot milling. The pilot car is used to lead traffic through the pattern to ensure motorists stay in the lane where cement has not been applied. In addition, the flaggers have a detour route around the pattern to advise any motorist uncomfortable with driving through the work zone. Slot milling involves removing a specified amount of material from the edges of the roadway after pre-pulverization, then grading the roadway back to the original profile. The idea behind this technique is to reduce the increase in elevation of the completed roadway due to the addition of materials in the FDR and paving processes. It is used in areas where there are overhead utilities, driveways, side roads, or anything else that may be negatively impacted by increasing the elevation of the roadway.

Pavement Overlays

For pavement overlay projects, whether it is paving over a roadway with sections of base repair or FDR, Chesapeake utilizes two different Superpave asphalt mixture designs. For roadways with a high projected truck volume (200 to 250 trucks per day for 10 years), a 90 to 140 millimeter (3.5 to 5.5 inch) thick, 25 millimeter (1 inch) asphalt base course along with a 40 millimeter (1.5 inch) thick, 9.5 millimeter (0.4 inch) asphalt wearing course is specified. For roadways with a lower projected truck volume (0 to 100 trucks per day for 10 years), a 75 millimeter (3 inch) thick asphalt binder course is specified with the idea PennDOT will sealcoat the surface as part of their normal maintenance schedule. For pavement overlays with base repair, a 9.5 millimeter (0.4 inch) asphalt scratch, or leveling course, is applied before one of the two Superpave asphalt mixture designs.

To ensure uniform mixture of the asphalt in the event segregation of material occurs during transport Chesapeake specifies a material transfer machine with an articulating boom be used on all paving projects (Fig. 5). All work is done in accordance with PennDOT's Construction Specifications found in PennDOT's Publication 408. For quality control and assurance, Chesapeake has an inspector on site at all times. The inspector will conduct sample tests to check oil content, verify temperature of the asphalt at the truck, and loose depth measurements after the paver. 150 millimeter (six inch) core samples are also taken to verify density, and nuclear gauge testing is performed to check compaction and to establish the roller pattern.

Paver and Roller in Paving Process Utilization a Material Transfer Machine

FIG. 5. Photos of the Paving Process

Shale Oil and Gas Industry Investment

The Shale Oil and Gas Industry has proven their commitment to ensuring the roads they utilize are effectively maintained and if necessary, fully upgraded. To date, the Shale Oil and Gas Industry has invested more than $750 million in roadway improvements (Spigelmyer 2013); with $500 million being on PennDOT's roadway system (Wind 2013). In the northeastern area of Pennsylvania, Chesapeake has invested nearly $350 million; with $300 million spent on state roadways. In addition to the Shale Oil and Gas Industry's direct investment in roadway and infrastructure improvements, the industry has also contributed indirect funding through impact fees. In February 2012, Pennsylvania legislators passed a bill which placed an impact fee on drilled Marcellus Shale wells. Sixty percent of the revenue generated by the impact fee stays at the local level, going to counties and municipalities hosting wells. The revenue distributed to the counties and the municipalities can be utilized to fund a number of local services including road, bridge and infrastructure projects. The remaining 40 percent is placed into the Marcellus Legacy Fund which serves as funding for statewide initiatives with local impacts (Scarnati 2013). To date, the Shale Oil and Gas Industry contributing more than $400 million in impact fees (State Impact 2013) with Chesapeake contributing $58 million.

Posting Removal

Through the Shale Oil and Gas Industry's efforts, several of PennDOT's posted roads have had their posted weight restriction removed. The Shale Oil and Gas Industry has upgraded several hundred miles of roadway and with those upgrades, PennDOT has been able to remove the weight restriction on 306 kilometers (190 miles) of roadway (see Figure 2). With Chesapeake's commitment to protect and preserve the roadways they utilize, they have upgraded 612 kilometers (380 miles) of road and account for the entire 306 kilometers (190 miles) of the posting removal. It should be noted that other Shale Oil and Gas Industry members have improved and upgraded roadways but to date have not requested the posted weight restriction be removed from the roadway.

CONCLUSION

With efforts invested by both PennDOT and the Shale Oil and Gas Industry, PennDOT's roadway network is being protected, maintained and upgraded. Pennsylvania's highway network is comprised of approximately 64,400 kilometers (40,000 miles) of state owned and maintained roadways. PennDOT utilizes their Posted and Bonded Program to protect the Commonwealth's infrastructure, particularly those roadways which were not designed to support significant truck traffic. The Shale Oil and Gas Industry has invested time and money to work with PennDOT to protect, maintain and upgrade the roadway network. Specifically, Chesapeake has made a concerted effort and has invested nearly $300 million reconstructing 612 kilometers (380 miles) of PennDOT's roadways posted with a weight restriction.

REFERENCES

American Association of State Highway and Transportation Officials. (1962). "AASHO Road Test – Report 5, Pavement Research." *National Academy of Sciences-National Research Council*. Washington D.C., 107.

American Society of Civil Engineers. (2010) "Keystone in Crisis- 2010 Report Card for Pennsylvania's Infrastructure." *American Society of Civil Engineers (ASCE)*. <http://www.pareportcard.org/PDFs/Roads%20Final-%20NATL.pdf> (Dec. 3, 2013).

American Society of Civil Engineers. (2013). "2013 Report Card for American's Infrastructure." *American Society of Civil Engineers (ASCE)*. <http://www.infrastructurereportcard.org/pennsylvania/pennsylvania-overview/> (Dec. 3, 2013).

Beyer, George R. (1972). "Pennsylvania's Roads." *Pennsylvania Historical and Museum Commission*. <http://www.portal.state.pa.us/portal/server.pt/community/things/4280/roads/478688> (Dec. 3, 2013).

Chesapeake Energy. (2014). "About Chesapeake." *Chesapeake Energy Corporation*. http://www.chk.com/About/Pages/Default.aspx (Dec. 3, 2013).

Chesapeake Energy. (2014). "Hydraulic Fracturing Fact Sheet." *Chesapeake Energy Corporation*. <http://www.chk.com/Media/Educational-Library/Fact-Sheets/Corporate/Hydraulic_Fracturing_Fact_Sheet.pdf> (Dec. 3, 2013).

Chesapeake Energy. (2014). "Operations." *Chesapeake Energy Corporation*. <http://www.chk.com/Operations/Pages/Default.aspx> (Dec. 3, 2013).

Governor's Marcellus Shale Advisory Commission (2011). "Governor's Marcellus Shale Advisory Commission Report." *PA Department of Environmental Protection*.

Marcellus Center for Outreach and Research. (2012). "Animation of Unconventional Wells." *Pennsylvania State University*. <http://www.marcellus.psu.edu/resources/maps.php> (Dec. 3, 2013).

Pennsylvania Department of Conservation and Natural Resources. (2009) "Marcellus Shale FAQ." *Pennsylvania Department of Conservation and Natural Resources*. <http://www.dcnr.state.pa.us/topogeo/econresource/oilandgas/marcellus/marcellus_faq/marcellus_shale/index.htm> (Dec. 3, 2013).

Pennsylvania Department of Transportation. (2009) "PennDOT Organizations – About PennDOT." *Pennsylvania Department of Transportation*. <http://www.dot.state.pa.us/> (Dec. 3, 2013).

Pennsylvania Department of Transportation. (2013). "Publication 23 – Maintenance Manual, Chapter 15: Weight Restrictions on Highways." *Pennsylvania Department of Transportation*.

Polak, M. L. and Breneman, E.J. (2013) "Pavement Preservation." *Asphalt Contractor.*

Scarnati, J. (2013). "2012 Marcellus Shale Impact Fee Revenue Being Distributed." *Joe Scarnati*. <http://www.senatorscarnati.com/2012-marcellus-shale-impact-fee-revenue-being-distributed/> (Dec. 3, 2013).

Spigelmyer, D. (2013). "PA's Shale Industry is Investing in Infrastructure." *The Patriot News*.

State Impact. (2014). "The Oil and Gas Law of the Land: Your Guide to Act 13." *National Public Radio (NPR)*. <http://stateimpact.npr.org/pennsylvania/tag/impact-fee/> (Dec. 3, 2013).

Wind, K. (2013). "Natural Gas Industry Fixing State Roads." *Shale Reporter.*

Blockages Detection in Pipeline Networks for Gas and Oil

Paolo Bocchini[1], Ph.D., P.E., M.ASCE, Alessandro Marzani[2], Ph.D., P.E., and Aman Karamlou[3], S.M.ASCE

[1] Assistant Professor, Department of Civil and Environmental Engineering, ATLSS Center, Lehigh University, 117 ATLSS Drive, Bethlehem, PA 18015, USA, E-mail: paolo.bocchini@lehigh.edu .
[2] Assistant Professor, DICAM Department, University of Bologna, Viale del Risorgimento 2, 40136, Bologna, Italy, E-mail: alessandro.marzani@unibo.it .
[3] Research Assistant, Department of Civil and Environmental Engineering, ATLSS Center, Lehigh University, 117 ATLSS Drive, Bethlehem, PA 18015, USA, E-mail: amk211@lehigh.edu .

ABSTRACT: This paper proposes a technique for the preliminary identification of pipes obstructed by blockages within a pipeline or a complex pipe network, relying only upon few measurements that are usually gathered to monitor the infrastructure operability. Blockages are identified as a result of an optimization procedure that minimizes the discrepancy between measured and simulated flow quantities. The framework exploits a Finite Element-like simulator of the flow problem in the system of pipes and Genetic Algorithms to perform the optimization procedure. Thermal properties of the fluid flowing inside the pipe system are considered. Results of the identification procedure are presented and advantages and disadvantages of the procedure for the on field implementation are outlined.

INTRODUCTION

The presence of a blockage or multiple blockages lowers the efficiency and reliability of the pipe network. In the long term they may even cause structural damages (Fig. 1). The early detection of blockages in pipelines and pipeline networks is thus an important issue, with a relevant economic impact on the oil and gas energy industry. Several techniques to locate and quantify the presence of blockages in a single pipe are available in the literature (see, among others, Chen 1979, Scott and Satterwhite 1998, Scott and Li 1999, Mohapatra et al. 2006). However, these techniques usually require collecting measurements of several quantities, which can be expensive and interfere with the operational conditions of the pipelines (Adewumi et al. 2003, Wang et al. 2005, Lee et al. 2008, Sattar et al. 2008, Colombo et al. 2009). Moreover, when a long pipeline or a large network of pipes is considered, it is usually impractical to apply such techniques to each individual segment of the distribution network. For these reasons, this paper addresses the problem of obtaining a preliminary identification of the pipe/pipes potentially interested by blockages at the network level, using only measurements that do not disrupt the normal

FIG. 1. Highly obstructed pipe by scale deposit (Lebedev 2010).

operational conditions of the pipe system. In this way, further analyses can be conducted only on the pipes that have already been identified as likely to have blockages.

The proposed technique is covered by an international patent (Matengazza et al. 2013) and relies on two main numerical tools. The first one is a simulator of the steady state flow within the pipe network, which uses a modelling scheme inspired by the Finite Element method. The second tool is an optimization algorithm that identifies the potential obstructions (in terms of location and severity) minimizing the discrepancy between measured and simulated data. These two numerical tools are integrated in a framework that allows a simple data input and a clear interpretation of the results.

The next section describes the proposed methodology. Then, the technique, its capability and accuracy are demonstrated by means of a numerical example. Finally, the most relevant conclusions are summarized.

PROPOSED METHODOLOGY

The general approach that is promoted by this paper consists in a two-phase identification of the blockages. The first phase is performed at the entire network level and requires a preliminary identification of pipes that have a blockage and quantify the extent of such obstruction, relying upon measurements that can be obtained with low costs and avoiding operational disruption. Then, a second technique (such as those previously cited) is used to locate the blockage within each obstructed pipe. Figure 2 provides a schematic flow-chart of the procedure proposed to accomplish the network-level identification, which is the main focus of this paper.

A network flow simulator has been developed, inspired by the Finite Element Methods (FEM). Each pipe or pipe segment is modelled as a finite element, for which the state variables (i.e. discharge Q in the pipe and piezometric head h at the nodes) are linked by well-known laws of fluid dynamics, such as:

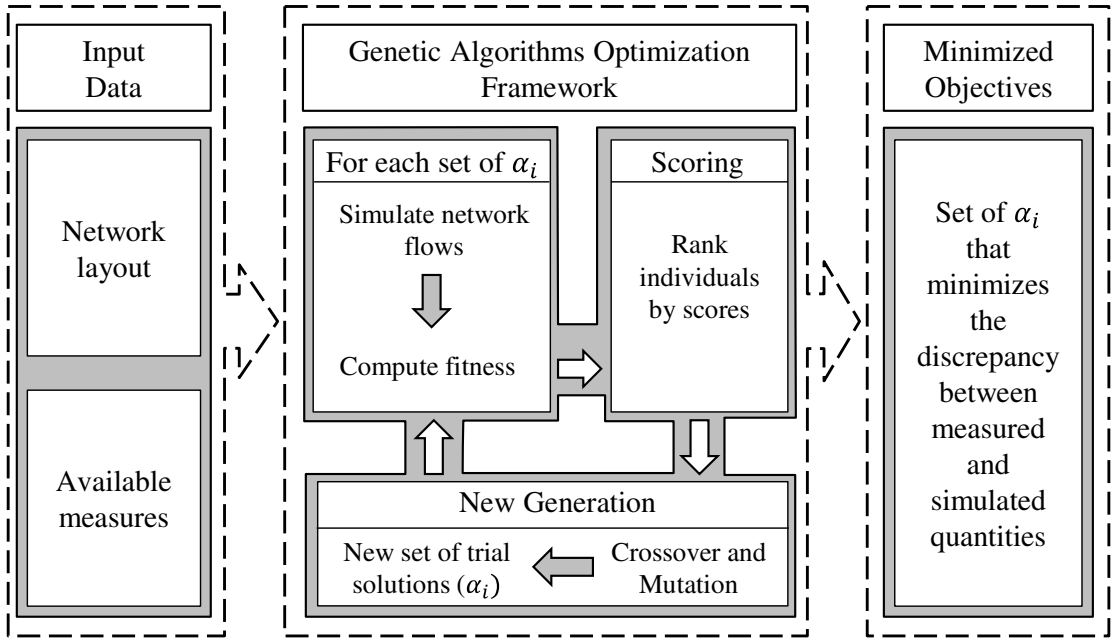

FIG. 2. Flow-chart of the proposed methodology.

$$h_L = \frac{8fL}{\pi^2 g(\alpha D)^5} Q^2 \tag{1}$$

where h_L is the head loss, f is the friction factor that depends on pipe roughness and diamater as well as on Reynold number, L is the pipe length, g is the acceleration of gravity, D is the original diameter of the pipe, Q is the pipe discharge and α is a parameter introduced here to model the occlusion as a reduction of the effective diameter. It can be proved that, for occlusions that do not affect the entire length of the pipe (as it is usually the case), the product $\alpha D = D^{eq}$ can still represent the "equivalent residual diameter" D^{eq}, which is the diameter of a pipe with a uniform occlusion that would cause the same head loss of the actual (localized) blockage. In this way, the factor α provides a quantitative assessment of the blockage in each pipe (affected length and percentage of obstructed cross-section). The flow equations associated to each finite element (i.e., pipe) are then assembled based on the network topology and form a system of equations that can be solved numerically:

$$\boldsymbol{K}(\boldsymbol{\alpha})\boldsymbol{h}(\boldsymbol{\alpha}) - \boldsymbol{z} = \boldsymbol{R}(\boldsymbol{\alpha}) \tag{2}$$

where $\boldsymbol{\alpha}$ is the vector containing the residual diameter factor for each pipe; $\boldsymbol{K}(\boldsymbol{\alpha})$ is the global governing matrix; $\boldsymbol{h}(\boldsymbol{\alpha})$ is the vector of pressure heads at all nodes; $\boldsymbol{z}$ is the vector combining nodal elevations and external nodal demands; and $\boldsymbol{R}(\boldsymbol{\alpha})$ is the global vector of residuals. For a given set of normalized residual diameters $\boldsymbol{\alpha}$, the solution of Eq. (2) yields the pressure head h at all nodes and this, in turn, allows to compute the discharge Q in all pipes.

Genetic algorithms (GAs) are a popular heuristic optimization technique that can easily avoid local minima and does not require a closed form expression of the

objective function. For these reasons, GAs have been selected as optimization engine to solve the identification problem. In particular the optimization is formulated as follows:

Find: α_p with $p = 1,2,\dots, number\ of\ pipes$
so that: $J(\boldsymbol{\alpha})$ is minimum
subjected to: $0 \le \alpha_p \le 1 \quad \forall p$

where the objective function $J(\boldsymbol{\alpha})$ measures the discrepancy between simulated and measured data. In particular, $J(\boldsymbol{\alpha})$ can be computed as:

$$J(\boldsymbol{\alpha}) = \log(\Phi_h) + \log\left(\Phi_Q\right) - \frac{\gamma}{n}\sum_{p=1}^{n}\alpha_p \tag{3}$$

where n is the number of pipes, γ is a penalty factor introduced to improve the quality of the results, Φ_h is a metric of the discrepancy between the simulated pressure heads h_i^{sim} and the n_h measured pressure heads h_i^{mea}

$$\Phi_h = \sum_{i=1}^{n_h}[(h_i^{sim} - h_i^{mea})/h_i^{mea}]^2 \tag{4}$$

and Φ_Q is a metric of the discrepancy between the simulated discharges Q_p^{sim} and the n_Q measured discharges Q_p^{mea}

$$\Phi_Q = \sum_{p=1}^{n_Q}[(Q_p^{sim} - Q_p^{mea})/Q_p^{mea}]^2 \tag{5}$$

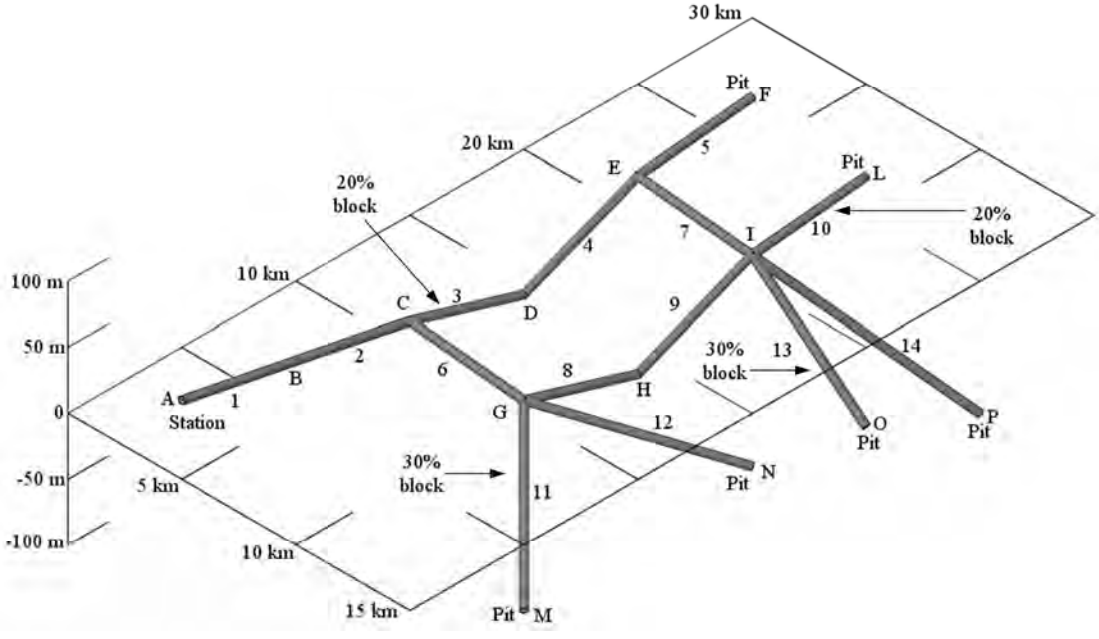

FIG. 3. Layout of the investigated network. The pipe diameter is not in scale.

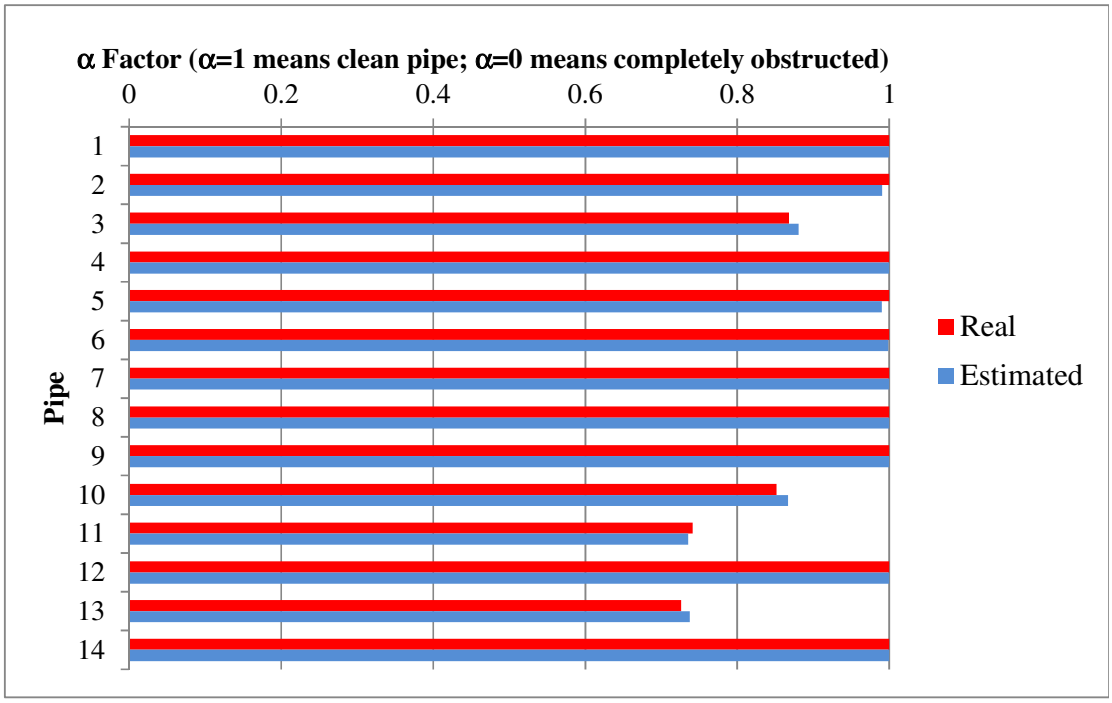

FIG. 4. Results of the blockage identification procedure.

It must be remarked that the number of measured pressure heads n_h as well as the number of measured flows n_Q can be smaller than the number of nodes and pipes in the pipe system, respectively. This, in turn, allows the proposed methodology to be used even with a limited number of measurements. The definition of the best set of measurements, considering number, position in the network, and type (flow or pressure head), involves a sensitivity study and it is the subject of an ongoing study. Similarly, a methodology that uses the same blockage identification approach, and combines it with a multi-phase flow simulator is currently in an advanced stage of development.

NUMERICAL EXAMPLE

The proposed methodology is demonstrated on the artificial network represented in Fig. 3. Node 1 is the station where the fluid is collected and nodes 6, 10-14 are pits where the fluid is introduced in the network. By design, all pipes have diameter equal to 300 mm, except for pipes 1 and 2 that have diameter 400 mm. The average temperature of pipes and fluid 1 and 2 is 28° C, whereas the rest of the network has an average temperature of 22° C. The pipe roughness is $5 \cdot 10^{-4}$. Finally, at node 1 an overpressure equivalent to a piezometric head of 10 m is imposed and all the pits have a piezometric head of 150 m over node 1. This benchmark network was selected and modeled in collaboration with the sponsoring agency (the Italian National Hydrocarbon Company ENI S.p.A.) and represents a broad pipelines system including both flow lines and transport lines. As long as the physical assumptions of the flow models are satisfied (in particular single-phase fluid and steady flow), the methodology can be applied to a network with pipes of very different dimensions.

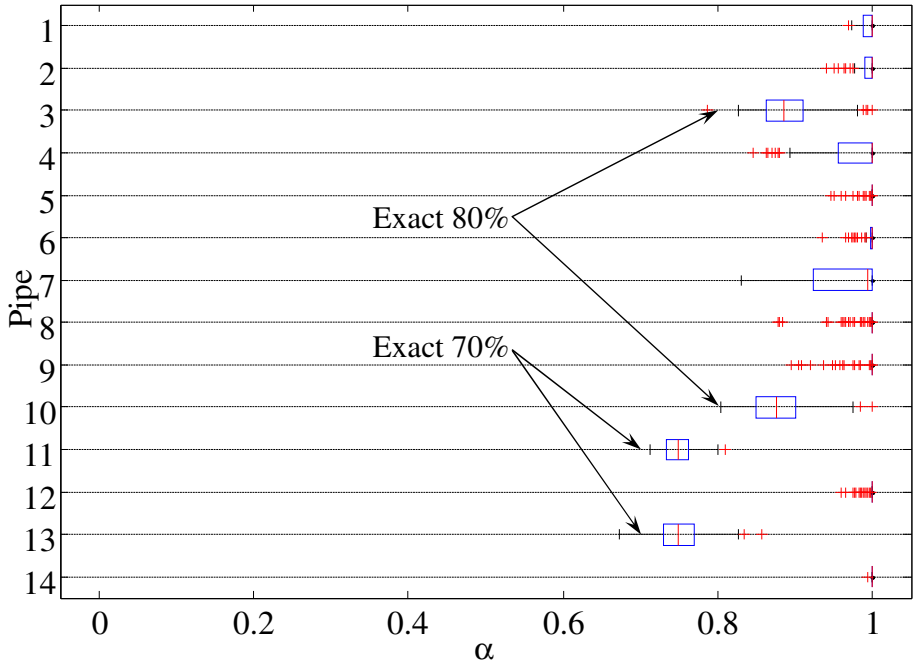

FIG. 5. Results of the statistical analysis.

The investigated scenario is characterized by the obstruction of pipes 3 (20%), 10 (20%), 11 (30%), and 13 (30%). Therefore, the methodology should identify $\alpha_3=\alpha_{10}=0.8$, $\alpha_{11}=\alpha_{12}=0.7$, and all the other $\alpha_i=1.0$. Flow data is collected at all pipes except pipes 5 and 14, whereas the piezometric head is measured at all nodes except 6 and 11. Then, to simulate measurement errors, a uniformly distributed random noise with magnitude 5% is superimposed to all input data (flow and piezometric head). This noise level can be considered a conservative value if compared to the errors expected in experimental measurements of flow and pressure heads with state-of-the-art instrumentation.

Genetic algorithms were set up to perform the optimization using 200 individuals per generation and a maximum of 200 generations. The analysis has been completed on a 12-cores workstation with two Intel Xeon E5-2620 2GHz processors and took less than a minute. The results in terms of identified residual diameters are illustrated in Fig. 4.

The results show that the technique was able to identify the 4 obstructed pipes, without false positives and with remarkable accuracy on the quantification of the residual diameters. It should be noted that this was achieved using only measurements of piezometric head and discharge that are usually easy to obtain without interfering with the operation of the pipelines. Moreover, four measurements were assumed to be unavailable and the methodology coped with this lack of information.

Then, for the above described scenario, a statistical analysis of the algorithm robustness was performed by running 100 times the proposed procedure and considering each time a new uniformly distributed random noise with magnitude 5%

superimposed to the input data. The results in terms of mean value μ and standard deviation σ of the parameter α are reported in Table 1 for the 14 pipes of the considered network. As it can be seen, even if the identified mean values for the obstructed pipes (i.e. 0.89, 0.88, 0.75, 0.75) are slightly greater than the respective target values (i.e. 0.80, .80, 0.70, 0.70), statistically the proposed procedure is capable to identify all 4 the obstructed pipes with very low dispersion.
Figure 5 shows a Box-and-Whisker plot of the results of the statistical analysis, where first, second and third quartiles of the identification results are provided for each pipe, along with the outliers. The data in this figure show that the procedure tends (on average) to slightly overestimate the residual diameter, and this is due to the use of a penalty factor in Eq. (3). On the other hand, the benefits introduced by such penalty in terms of stability and speed of convergence are substantial.

Table 1. Results of the statistical identification.

	Pipe													
	1	**2**	**3**	**4**	**5**	**6**	**7**	**8**	**9**	**10**	**11**	**12**	**13**	**14**
μ	0.99	0.99	0.89	0.97	1.00	1.00	0.96	0.99	0.99	0.88	0.75	0.99	0.75	1.00
σ %	0.82	1.33	4.21	4.11	0.96	0.97	5.15	2.30	2.20	4.11	2.03	0.85	3.16	0.06

CONCLUSIONS

A methodology for the detection of pipes affected by blockages in a large pipeline network has been presented. Moreover, the methodology provides a quantitative assessment of the blockage severity. The proposed technique formulates the identification problem as a constrained optimization that finds the set of normalized residual diameters that minimizes the discrepancy between the measured and simulated pressure heads and discharges. The technique is based on a simulator of the steady state flow in the pipeline network that was developed on the basis of a formulation inspired by the Finite Element method.

The presented numerical application demonstrates the accuracy of the technique. Other analyses with different occlusion scenarios and network layouts showed comparable accuracy and proved the robustness of the approach.

Further enhancement of the technique can consist in the development of a more sophisticate set of finite elements able to model the flow in each pipe as a multi-phase fluid.

ACKNOWLEDGMENTS

The authors appreciate the technical and financial support of ENI S.p.A. that made the presented research possible. The authors wish to thank also Lehigh University and the University of Bologna for their support.

REFERENCES

Adewumi M. A., Eltohami E. S., and Solaja A. (2003). "Possible detection of multiple blockages using transients." *Journal of Energy Resources Technology*, 125 (2), 154–159.

Chen, X. T., Butler, T., Volk, M., and Brill J. P. (1997). "Techniques for measuring wax thickness during single and multiphase flow." In *Proc. SPE Annual meeting*, San Antonio, TX.

Colombo, A. F., Lee, P., and Karney, B. W. (2009). "A selective literature review of transient-based leak detection methods." *Journal of Hydro-environment Research*, 2 (4), 212–227.

Lebedev, A. Y. (2010). "*Limescale in pipe*." Picture taken on February 27, 2010 and available at the address http://en.wikipedia.org/wiki/File:Limescale-in-pipe.jpg (visited on January 4, 2014). Available in public domain under the Wikimedia Commons License.

Lee, P. J., Vítkovský, J. P., Lambert, M. F., Simpson A.R., and Liggett J. A. (2008). "Discrete blockage detection in pipelines using the frequency response diagram: Numerical study." *Journal of Hydraulic Engineering*, 134 (5), 658–663.

Mantegazza, T, Di Lullo, A. G., Bocchini, P., and Marzani, A. (2013). "*Method for identifying obstructions in pipeline networks for transporting fluids*." International patent cooperation treaty application number WO2013171666 by ENI S.p.A.

Mohapatra, P. K., Chaudhry, M. H., Kassem A. A., and Moloo J. (2006). "Detection of partial blockages in a branched piping system by the frequency response method." *Journal of Fluids Engineering*,128 (5), 1106–1114.

Sattar, A., Chaudhry, M., and Kassem, A. (2008). "Partial blockage detection in pipelines by frequency response method." *Journal of Hydraulic Engineering*, 134 (1), 76–89.

Scott, S. L., and Satterwhite, L. A. (1998). "Evaluation of the backpressure technique for blockage detection in gas flowlines." *Journal of Energy Resources Technology*, 120 (1), 27–31.

Scott, S. L., and Yi, J. (1999). "Flow testing methods to detect and characterize partial blockages in looped subsea flowlines." *Journal of Energy Resources Technology*, 121(3), 154–160.

Wang, X. J., Lambert M. F., and Simpson A. R. (2005). "Detection and location of a partial blockage in a pipeline using damping of fluid transients." *Journal of Water Resources Planning and Management*, 131 (3), 244–249.

CSA S250-11 and CI/ASCE 38-02 – How to Effectively Utilize These Utility Standards for Shale Energy Projects.

Lawrence Arcand[1], P.Eng

[1]President, T2 Utility Engineers, 1615 Dundas St. E., Whitby, Ontario, Canada. Postal Code L1N 2L1
E-mail: Lawrence.Arcand@T2ue.com.

ABSTRACT: Published in September 2011, the CSA S250 – Mapping Underground Utility Infrastructure will play a key role in the creation of more accurate and reliable as-built utility drawings and maps. CI/ASCE 38-02 – Standard Guidelines for the Collection and Depiction of Existing Subsurface Utility Data, which was published in 2003, has already been used extensively on infrastructure projects across Canada and the US. Together these two standards form a solid foundation to both map and records utility infrastructures. The location of existing utilities can play a key role in the design and implementation of infrastructure projects associated with Shale Oil & Gas production. These impacts need to be managed properly to avoid significant cost and schedule over runs. CI/ASCE 38-02 forms the basis for engineers to create accurate drawings of existing conditions for the project. The data proved upfront is a critical, however equally important is the generation of accurate, reliable maps and drawings of new utility infrastructure placed in the ground. Creation of these new records is the primary focus of the CSA S250 Standard. The paper will review the key highlights of the new CSA S250 standard including – standard symbology, Accuracy Levels, and data records keeping - and how it will improve our future knowledge of underground infrastructure. It will highlight the government and private agencies such as the Ontario Ministry of Transportation, City of Toronto, and Fortis Gas, currently using or looking to implement the use of the standard, and identify how the knowledge learned from that exercise can assist the Shale Energy Industry. Accurate reliable drawings of our underground utility infrastructure produced in accordance with these industry standards is a benefit to all stakeholders – Project Owners, Designers, Utilities, Regulators and Contractors. Further promotion for the use of these standards is the key, if we wish to raise the bar and move forward as an industry.

INTRODUCTION

This paper outlines SUE investigations and applications in the Shale Gas industry. These investigations are typically done as part of the design phase of projects so valuable information pertaining underground utilities were provided to design team

and utility issues are managed effectively.

The primary scope of work on these projects was to establish the accurate base drawing of existing utilities. On typical projects in the past a number of common issues tended to be present regarding the underground Utilities:

- Utility records are not reliable or accurate enough for the project designers/engineers.
- Design drawings didn't accurately depict utility locations.
- Utility relocations ended up being a time consuming and costly part of the overall project.

A solution that have been proven successful on a number of major projects throughout the country is the use of Subsurface Utility Engineering (SUE) principals, in accordance with the CI/ASCE 38-02: "Standard Guidelines for the Collection and Depiction of Existing Subsurface Utility Data" as well as CSA Standard S250 – "Mapping of Underground Utility Infrastructure."

What are the benefits of following CI/ASCE 38-02 and CSA S250?

- It provides designers/engineers with valuable information during design stage of the project.
- It is a defined systematic, repeatable process with established and proven standards.
- It helps to clearly defines potential conflicts/ relocations upfront when they can be managed more effectively.
- It helps reduce number of relocations by clearly highlighting the exact location of conflicts and the relationship to the proposed project works.
- It helps reduce re-design costs by eliminating the need to redesign elements of the projects once it is determined that utilities are not where they were originally thought.
- It helps contractors reduce bid prices, by eliminating some of their risks.
- It helps reduce project delays, by reducing the probability that unexpected utilities will be encountered in the field.
- It helps improve project safety by providing that accurate reliable record that can be used as a valuable tool not only during the design but during construction (it is important to note that a SUE drawing does not replace the need for contractors to call before they dig)
- It reduces clients overall risk.
- It improves records for future projects.
- Better records improve operations and maintenance operations.

BACKGROUND INFORMATION ON ASCE 38-02 AND CSA S250 STANDARDS

There are two key standards presently used in Canada for utility mapping. ASCE 38-02 sets out guidelines for how to qualify the accuracy of mapping existing infrastructure and relay that information to a drawing. ASCE goes into the SUE process and roles and responsibilities of the SUE professional and the owner. It's more prescriptive.

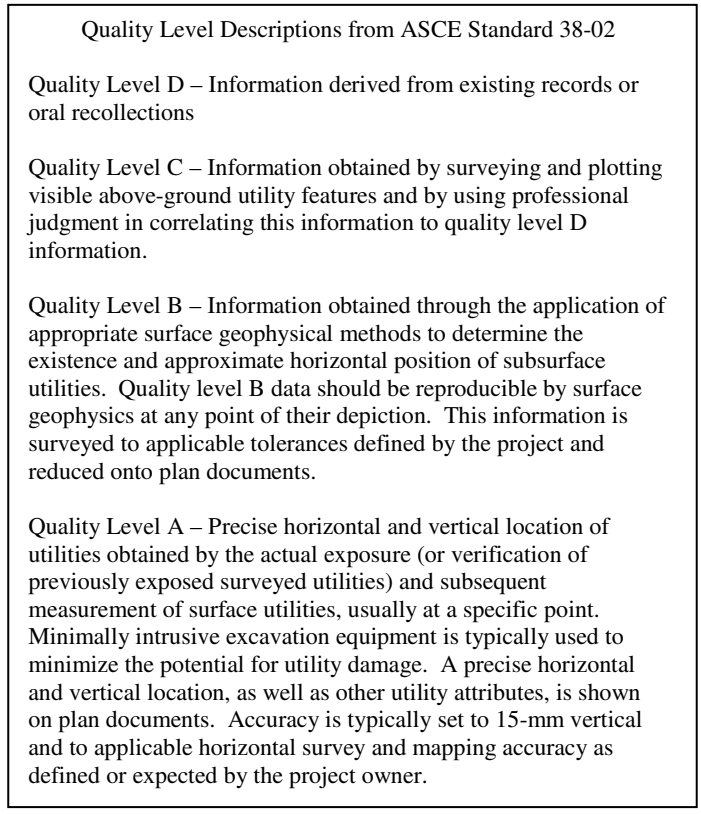

Figure #1 – Excerpt from ASCE 38-02

CSA S250 set's out requirements for classifying the accuracy of newly installed or exposed infrastructure. The CSA S250 accuracy levels provide a finer level of detail to define the positional location of the infrastructure which translates into a better defined reliability in the accuracy of the record. Both standards help to complement each other.

The American Society of Civil Engineers (ASCE) published CI/ASCE 38-02: "*Standard Guidelines for the Collection and Depiction of Existing Subsurface Utility Data"* in January of 2003. The standard is the backbone for the practice of SUE, an engineering discipline dedicated to accurately mapping and coordinating subsurface utility data. Information concerning existing underground utilities is vital during the design stage of construction projects as it provides the designers and engineers with an accurate, reliable map of the underground infrastructure. SUE allows them to determine how the existing infrastructure will be affected by the project, so they can make adjustments and plan ahead to minimize impacts.

The ASCE Standard outlines the processes that should be utilized when collecting utility data for design purposes. Early on, during the planning stages, the engineer responsible for the Utility Investigation should advise the owner of potential impacts the project could have on existing subsurface utilities and recommend a scope for the investigation. The earlier the process is started the greater the benefits that can be experience.

More recently, in September 2011, the Canadian Standard Association published CSA S250 – "*Mapping of Underground Utility Infrastructure*." This standard specifies the mapping requirements for new infrastructure being installed in the ground. It provides consistency for key items such as line color, utility description and accuracy. Accurate records will improve safety of public, environment and reduce costs.

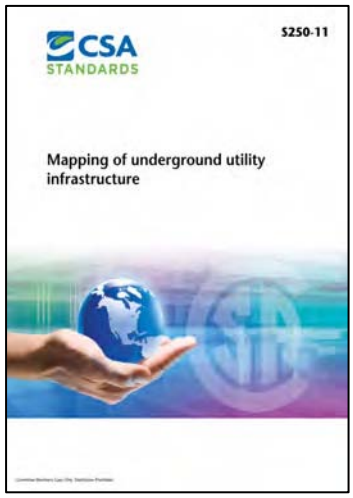

Figure # 2 – CSA S250

Colour	Colour name	Colour co-ordinates	Used to designate
	RED	RGB (205,0,50) CMYK (0,81,61,20) HTML #CD0032	Electric features, power lines, cables, conduit, and lighting cables
	YELLOW	RGB (235,210,90) CMYK (0,0,80,0) HTML #FFFF33	Gas, oil, steam, petroleum, and gaseous materials
	ORANGE	RGB (255,102,0) CMYK (0,60,100,0) HTML #FF6600	Communication, alarm, signal lines, and cable television
	BLUE	RGB (0,0,255) CMYK (100,100,0,0) HTML #0000FF	Potable water
	GREEN	RGB (50,150,50) CMYK (40,0,40,42) HTML #329632	Sewer, sanitary, storm, and combined
	PINK	RGB (255,204,204) CMYK (0,20,20,0) HTML #FFCCCC	Temporary survey markings
	PURPLE	RGB (153,51,204) CMYK (20,60,0,20) HTML #9933CC	Reclaimed and untreated water, irrigation, and slurry lines

Figure # 3 – Excerpt from CSA S250 Color Code

Accuracy level	Description	Reference
1	Accurate to within +/- 25mm in the x, y, and z coordinates, and referenced to an accepted geodetic datum with a 95% confidence level.	Absolute
2	Accurate to within +/- 100mm in the x, y, and z coordinates, and referenced to an accepted geodetic datum with a 95% confidence level.	Absolute
3	Accurate to within +/- 300mm in the x, y, and z coordinates, and referenced to an acceptable geodetic datum or topographical and cadastral features with a 95% confidence level.	Absolute or relative
4	Accurate to within +/- 1000mm in the x, y, and z coordinates, and referenced to an acceptable geodetic datum or topographical and cadastral features with a 95% confidence level.	Absolute or relative
0	No information available related to spatial accuracy.	

Figure # 4 – Excerpt from CSA S250 Mapping Record Accuracy

UTILITY INVESTIGATION METHODOLOGY AS PER ASCE 38-02

The following provides a summary of the basic step by step procedures followed by SUE consultants when following the ASCE 38-02 Standards.

Step #1:

The first step in the investigations, is to collect **Quality Level D** information by collecting all available utility records. Key sources include municipal records, as-built and utility company record drawings. Records are collected through a formal request process which outlined the general project scope, the project limits for which records information was required, and timeframes for when information is needed.

Figure # 5 – Geophysical Designating

Step #2:

The second step in the investigation is to review the topographic survey data available and upgrade any information to **Quality Level C** by surveying and plotting visible above-ground utility features and by using professional judgment in correlating this information to Quality Level D information. This process is mostly utilized for the sewer systems where crews could be sent to collect invert data at required maintenance holes, then that information used to determine alignments based on records available. Due to the linear nature of most gravity sewer systems, this is quite affective. In situations where there are complex systems or bends in the system, additional steps need to be followed.

Step # 3:

As the overall project design progresses to the stage where it can be determined which areas were most critical, the third basic step of collecting **Quality Level B** information is completed. For this step information is obtained through the application of appropriate surface geophysical methods to determine the existence and horizontal position of subsurface utilities. Electromagnetic cable locate, equipment, sondes, ground penetrating radar (GPR) and other geophysical methods are used. The designating efforts focused on the utilities located within the key impact areas of the project.

Figure # 6 – Test Holes on a Downtown Ottawa Project

Step # 4:

The fourth step is to collect **Quality Level A** information and determine the precise horizontal and vertical location of utilities obtained by the actual exposure and subsequent measurement of subsurface utilities, at key critical locations as identified via a review of the project design in consultation with all parties involved. A non-destructive air or hydro based vacuum excavation methods are used to vacuum excavates the test holes. Holes are then surveyed to provide precise x,y,z information. The test holes are backfilled and reinstated as per permit requirements.

Step # 5:

Based on all information obtained, the corresponding composite utility design drawing is completed and over laid on client's base drawings. All utility information and utility design are assigned a Quality Level and respectively color, specific line types and utility description in accordance with the Standards mentioned above. In addition to the drawing a full report is provided outlining the steps of the invsetigaiton and results obtained. Both the report and drawing are signed and sealed by the Professional Engineer responsible for the project.

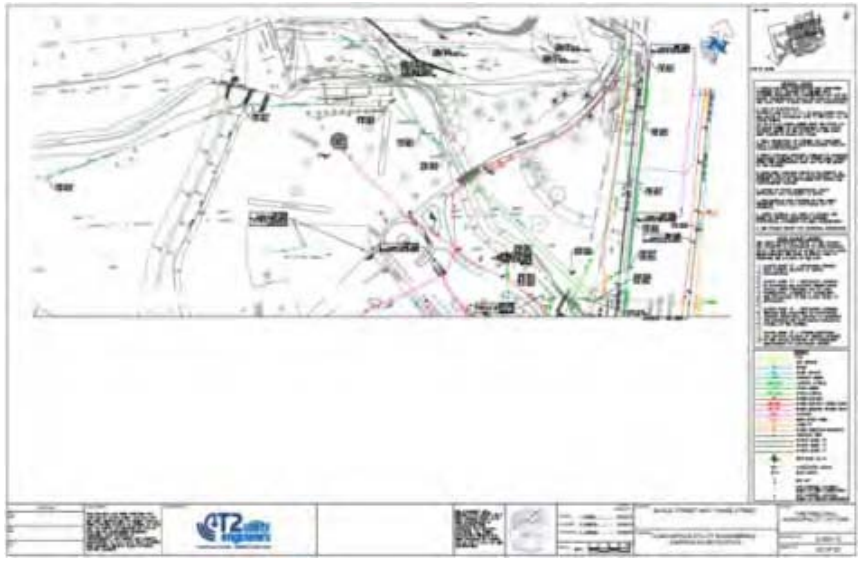

Figure # 7– Utility Drawing (sample)

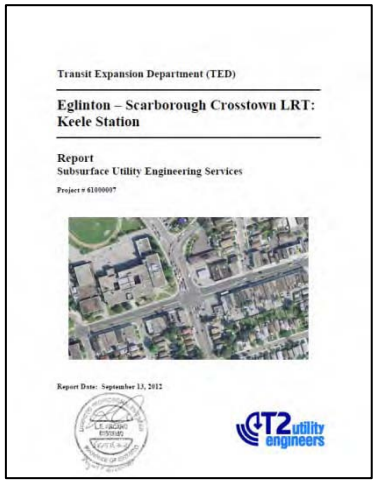

Figure # 8– SUE Report

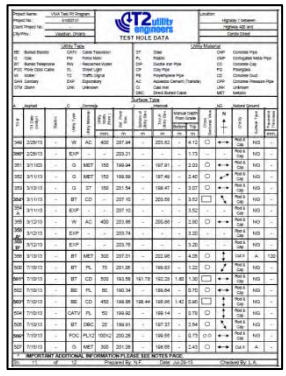

Figure # 9– Typical Test Hole Data (QL-A)

SUE COST SAVINGS

Performing a utility investigation in accordance with ASCE 38-02 leads to more accurate depiction of underground utilities which in-turn will-lead to several benefits to all project proponents, particularly coordination of utility relocations. Several studies have been completed which placed a dollar amount on the savings associated with doing a SUE mapping investigation and calculated a return on investment which was essentially Return = Savings / Cost of doing the investigation. Calculating a similar number for these projects was beyond the scope of this paper, however based on the positive results encountered and the results found by the Stevenson, Purdue and University of Toronto Studies, we can estimate that it would be between $3 and $5 dollars for every dollar spent. Collectively that would represent millions of dollars in savings to Canadian tax payers.

Based on the results of the University of Toronto Study the bulk of the cost savings are typically concentrated in two main items:

- Reduction of contractor claims, and
- Reduction in utility relocation costs

IMPLIMENTATION OF CSA S250

Several major companies and government agencies have started to review and implement the guidelines in the CSA 250 Standard as part of their record keeping practices.

Fortis Gas BC pro has undertaken a comprehensive review of their mapping and as-built practices and highlighted gap analysis of their current practices. The have identified high medium and low priority items and steps needed to ensure compliance.

Ontario Ministry of Transportation, Region of York, and City of Toronto are currently looking to prescribe Utility companies to adhere to the CSA S250 standard as part of their requirement for as-built records for their municipal consent processes.

As the CSA S250 gains more popularity across the country its use will continue to expand.

CONCLUSIONS

Both the CI/ASCE 38-02 and the CSA S250 Standards are key documents to the success of future infrastructure projects related to the Shale Gas industry. The CI/ASCE 38-02 should be followed when creating composite utility drawings of all existing utilities impacted by a new project. The CSA S250 Standard should be followed to create standardized accurate reliable as-builts and records of newly installed infrastructure.

The Shale Energy sector is emplacing thousands of miles of new pipelines every year to meet demand. Knowing where this infrastructure is located has important ramifications for safety and asset management. Adherence to both these standards will help to ensure that accurate reliable drawings of our underground utility infrastructure are produced. The benefits are numerous, but all result in an overall reduction in risk associated with the unknown. They are a benefit to all stakeholders – Project Owners, Designers, Utilities, Regulators and Contractors.

ACKNOWLEDGMENTS

The authors appreciate the time and dedication of all the volunteers who helped to write and publish boththe CI/ASCE 38-02 and the CSA S250, as well as those professionals dedicated to raising the bar on utility information.

REFERENCES

American Society of Civil Engineers. (2003) *Standard Guidelines for the Collection and Depiction of Existing Subsurface Utility Data, Standard #38-02, Reston, Virginia*.

Canadian Standard Association (2011). *Mapping of Underground Utility Infrastructure (CSA S250). Canada*

Purdue University (1999). *Cost Savings on Highway Projects Utilizing Subsurface Utility Engineering, Prepared for the Federal Highway Administration, Washington, D.C., as per FHWA contract number DTFH61-96-00090*.

Osman, Hesham & El-Diraby Tamer (2005) *Subsurface Utility Engineering in Ontario: Challenges and Opportunities. Centre for Information Systems in Infrastructure and Construction. University of Toronto*.

Underground (Well) Mapping Re-Visited

Earl F. Burkholder[1], PS, PE, F.ASCE

[1]Emeritus Faculty, New Mexico State University, Las Cruces, NM 88003, U.S.A. and
President, Global COGO, Inc., P.O. Box 3162, Las Cruces, NM 88003, U.S.A.
E-mail: eburk@globalcogo.com

ABSTRACT: Reliable underground mapping is an essential part of efficient energy production. The challenge is to determine reliable 3-D point positions in a well and/or the trajectory of a wellpath. Sensor data (e.g., measured wellbore depth (distance), wellbore inclination, and wellbore azimuth) are typically used to compute the location of discrete points in a well and a wellpath is determined using the method of minimum curvature. Part of the positioning challenge relates to specific identification of the origin, orientation of the coordinate system, knowing the quality of measurements, and knowledge of datums and map projections. Historically, survey maps showed horizontal and vertical data separately (primarily analog) but modern measurement systems produce digital 3-D spatial data. The global spatial data model (GSDM) will be described which accommodates modern measurements and 3-D digital spatial data. The GSDM uses proven rules of solid geometry to determine each 3-D position and optionally stores the standard deviation of each computed point. The subsequent relative position between any two points is easily computed and the underlying coordinate positions can be mathematically transformed to other commonly used coordinate systems. With the GSDM, all uses (site drawings, drilling, well development, production, and regulatory activities) of the position data share a common definition and the positional uncertainty of each computed quantity can be determined from stored covariance matrices.

INTRODUCTION

As a consequence of the digital revolution and development of more sophisticated measurement systems, spatial data (maps) are now characterized as being digital and three-dimensional (3-D). This paper explores methods for handling 3-D digital spatial data that exploit those characteristics rather than being encumbered by them.

Historically - and still prevalent in practice – many horizontal and vertical survey data are handled separately. That separation is driven, in part, by human experience of walking erect on a "flat-earth." More specifically, spatial data users find themselves working with horizontal datums and vertical datums. The justification for two datums is that horizontal and vertical have different origins. Horizontal is

referenced to latitude/longitude on the mathematical ellipsoid while vertical is referenced to sea level (more specifically, the geoid). Regretfully, there are no closed-form equations that relate the ellipsoid to the geoid. Those disparate origins make it difficult (awkward) to combine horizontal and vertical data into a single 3-D data base.

While the energy industry may be quite adept at determining and using "flat-earth" components to describe the relative location of surveyed points, the reality is that the earth is not flat and that location data need to be handled accordingly. The paper by Williamson and Wilson (2000) on "Directional Drilling and Earth Curvature," discusses those issues and includes the following quotes:

- "A third option, representing the well in 3D geocentric Cartesian coordinates, offers computational advantages but these are outweighed by the awkward fact that, in general, none of the axes are parallel with the vertical."
- "While use of the Flat Earth model persists, directional drilling companies planning extended-reach wells should estimate the physical error introduced by the model and compare it with target tolerances."
- "Developers of directional and survey software should consider an improved methodology, such as that described in this (Williamson/Wilson) paper, for inclusion in their products. This level of precision will be particularly desirable in software which integrates drilling and subsurface data."

The global spatial data model (GSDM) described herein accommodates each of those points. The GSDM has a single origin for 3-D geospatial data (earth's center of mass), uses time-honored rules of solid geometry to describe the unique location of points worldwide, and includes a rotation matrix to reconcile the 3-D geocentric axes with the local perspective. In addition to tracking geometrical locations with the functional model portion of the GSDM, the stochastic model portion of the GSDM provides an efficient way to compute the uncertainty (standard deviations) of surveyed locations using proven error propagation techniques. The standard deviation of derived quantities (directions/distances/etc.) can also be computed using similar error propagation techniques. But, perhaps the best feature of the GSDM is that it provides an efficient reliable connection between "flat-earth" concepts used in practice and the larger curved-earth world of modern computer data bases.

A truism is that we are where we are because of where we came from. Extensive records have been accumulated over the years that document drilling sites, the location of wells, and the trajectories of wellbores within the earth. Those records, for the most part, are based upon the best available (or other) practices at the time. Such practices include assumed coordinates, datums, map projections, zone constants, coordinate systems, and computational procedures consistent with (many analog) measurements and existing technology. The GSDM avoids many of those nuisance issues. But, while the GSDM can be beneficially used to exploit the characteristics of modern technology and 3-D digital spatial data, it is acknowledged that finding the best path forward with regard to management and use of spatial information within the constraints of historical use, productivity, and profitability remains a challenge. The caveat is that, with adoption and use of the GSDM,

incremental advancements by individuals, companies, and agencies/regulators can be aggregated for the benefit of all users.

DEFINITION AND DESCRIPTION OF THE GSDM

Burkholder (1997) provides a formal definition of the GSDM. In reality, the GSDM contains no new mathematical concepts and all equations used in the GSDM are in the public domain. But, the GSDM is a new model in that it is built on the assumption of a single origin for 3-D geospatial data. Time-honored rules of solid geometry provide the basis for coordinate computation. Features and applications of the GSDM are described more extensively in Burkholder (2008).

With reference to Fig. 1 and Fig. 2, the GSDM embodies three different coordinate systems: geodetic/geocentric/local. The geodetic coordinate system includes latitude, longitude, and ellipsoid height. The geocentric coordinate system includes earth-centered earth-fixed (ECEF) rectangular X/Y/Z coordinates and is used as a reference for global navigation satellite systems (GNSS) – including GPS. The geodetic and geocentric systems share a common origin – earth's center of mass. The origin for the local system is any point chosen by the user. Local coordinates portray a "flat-earth" view of all other points relative to the user-selected origin.

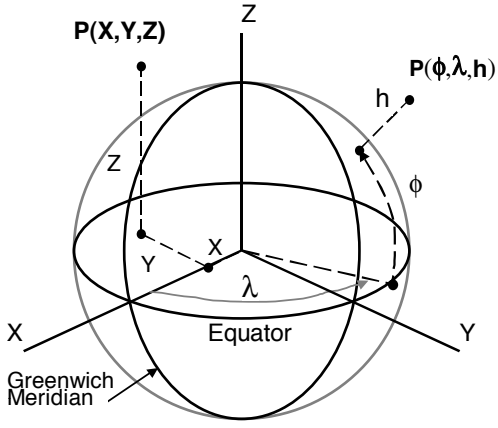

FIG. 1. Geodetic and Geocentric Coordinate Systems

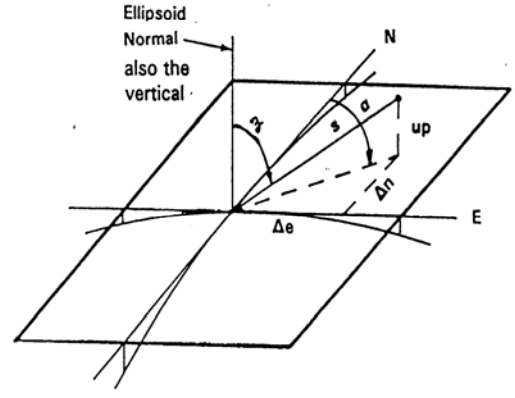

FIG. 2. Local (Flat-Earth) Coordinate System

Figure 3 provides an overview of the three coordinate systems and maps the various geometrical transformations encountered when using the GSDM.

Computation Diagram for the Global Spatial Data Model (GSDM)

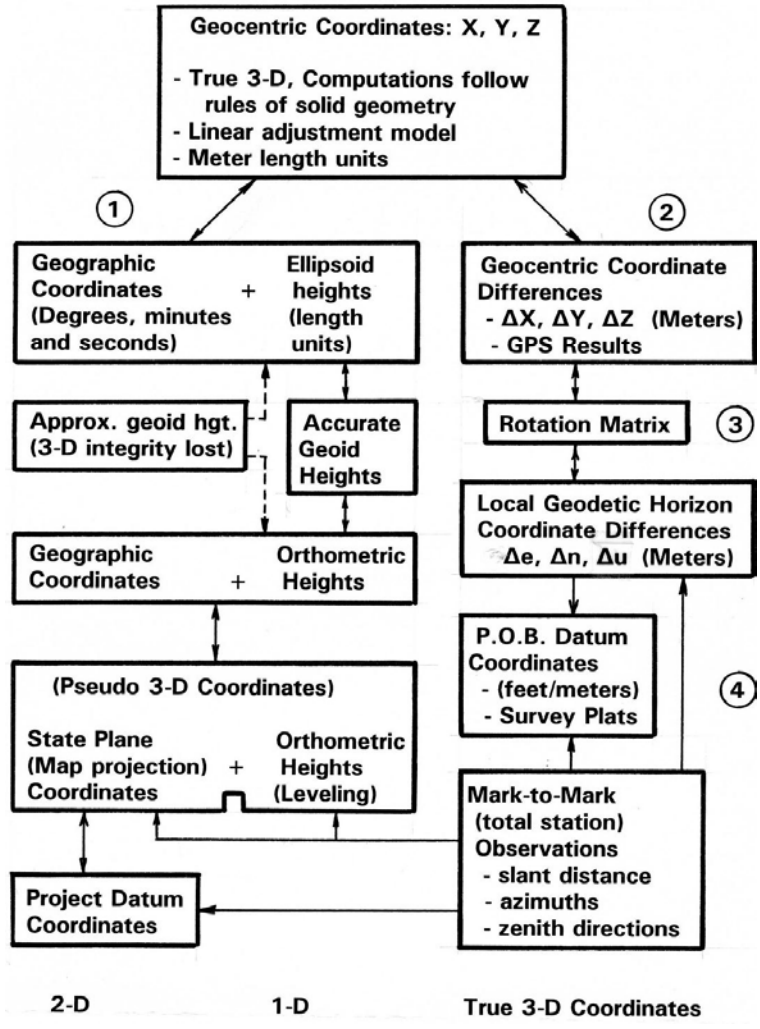

FIG. 3. Schematic Diagram of the Global Spatial Data Model (GSDM)

The top box in Fig. 3 stores the geocentric ECEF rectangular metric X/Y/X coordinates that define the location of any/all points used in the GSDM. All other expressions of coordinates and positions are derived from the ECEF values. With regard to Figures 1, 2, and 3, additional items to note are:

- The X/Y axes lie in the plane of the equator and the Z axis very nearly coincides with the earth's spin axis. The X value is zero on the prime meridian.
- A vector between any two points is easily computed as geocentric coordinate differences. $\Delta X = X_2 - X_1$, $\Delta Y = Y_2 - Y_1$, and $\Delta Z = Z_2 - Z_1$.

- A rotation matrix (Burkholder 1997 or 2008) is used to convert ECEF coordinate differences into the local perspective Δe/Δn/Δu components, thus addressing the Williamson/Wilson objection to using ECEF.
- Coordinate positions are computed in three-dimensional space, not on the ellipsoid. That avoids numerous measurement reductions to the ellipsoid.
- With a local origin selected, two operations are of interest:
  a. Geocentric coordinate differences can be rotated to local "flat-earth" components. Those local horizontal components are the same as latitudes and departures historically used in plane surveying and can be added to the horizontal northing/easting values assigned to the local origin.
  b. Local "flat-earth" components (derived from existing measurements) can be rotated to geocentric coordinate differences. Those ΔX/ΔY/ΔZ values can be added to the ECEF values of the local origin to provide defining X/Y/Z values of the new point.

  In both cases, 3-D geometrical integrity is preserved by reliance on the stored defining X/Y/Z values.

- The meter is the standard of length for all ECEF coordinates. Calculated offsets (if in non-metric units) need to be converted to meters before being rotated into the ECEF system. Conversely, after ECEF coordinate differences (meters) are rotated into the local reference frame, they can be converted to feet (or other units – see the P.O.B. Datum Box in Fig. 3).
- Compatible with existing practice, office/field users can both work with local "flat-earth" 3-D coordinate differences with no loss of geometrical integrity.
- There are no map projections, grid scale factors, or zone constants. Distance and angle measurements are not distorted to fit a map projection model.
- Azimuths are referenced to true north at a specified location. Grid north throughout a project is with respect to true north at the user-specified P.O.B.
- The GSDM is a single system equally applicable for spatial data users in all disciplines all over the world. That means distortions associated with crossing zone boundaries of traditional map projections are avoided

CONCEPTUAL CONSIDERATIONS

Functional and Stochastic Model Components

The functional model portion of the GSDM can be used without the stochastic model. If the stochastic model is not used, the positions of all control points are held fixed and all measurements are used as exact (standard deviations are all zero). Subsequently computed coordinate positions may be legitimate, but they have no standard deviation associated with them. On the other hand, the stochastic portion of the GSDM provides an opportunity for the user to assign realistic uncertainties (standard deviations) to all variables and to propagate the error. That prerogative enables the spatial data professional to make important decisions related to positional uncertainty with greater confidence. Of course, if bad information is used (or if good information is used inappropriately) unreliable answers can be obtained. The

opposite case is the important one – the GSDM supports efficient use of spatial data by all disciplines.

Absolute and Relative Issues

Another concept involves the difference between "absolute" and "relative." Absolute data are taken to be unique values expressed in a "fixed" reference system (datum) while relative is taken to be the difference of two absolute values within the same system. This is important because relative values are more closely associated with measurements and use in the field while absolute values are more closely associated with data archival and storage (data bases). Information management often focuses on absolute quantities while many practical applications work primarily with relative values. The two are inseparably related but often effort and resources are "wasted" by focusing too much attention on absolute values at the expense of relative considerations.

The value of most surveys is derived from the answer to one of two questions:

- What is the position of this point with respect to that point (and all other points in the survey)? The answer to this question is a relative quantity within the same datum. This illustrates the value of basing a survey on permanent control points.
- What is the position of this point with respect to where it was at some time (epoch) in the past? In other words, "did it move?" This too is a relative quantity within the same datum. This illustrates the importance of using permanent stable control points.

Since relative quantities are differences of absolute values in the same datum, it makes perfect sense to store absolute values and to compute relative values as needed. That practice is well established and certainly justified. But, upgrading or changing datums is a nuisance/problem faced by many spatial data users. That nuisance is exacerbated by the absence of closed-form equations for the difference between datums – old and new. Welcome to the real world of imperfect measurements and information management. As an aside, consider the consternation worldwide if, due to improved measurements/data, the scientific community decided it was necessary to update the value used for the speed-of-light every 5 years or so.

Issues of Spatial Data Accuracy

When working with spatial data accuracy, one of the most important questions is "accurate with respect to what?" Often the default answer is "accuracy with respect to the control on which the survey is based." The stochastic model portion of the GSDM accommodates mathematical definitions of both network accuracy and local accuracy. As a reminder, network accuracy applies primarily to absolute data while local accuracy is more closely related to relative data. The manner in which the GSDM handles both network and local accuracy enables the spatial data user to make

better choices as dictated by the circumstances and the available data. It puts the user in the driver's seat. For example, the network accuracy of a collection of points is often stored in the covariance matrix for each point. Data representing the correlation between points are not stored. Storing only the point covariance is better than not storing any covariance information but, if appropriate covariance data (both point and point-pair) - say from a least squares adjustment – are stored, then both the network accuracy and local accuracy between points can be readily computed. Burkholder (2013) is an example of current research that investigates network/local accuracy as applied to a ground-based GPS network. Additional research focusing on local vertical accuracy (such as that in a wellbore) is needed.

Trade-off of Costs and Benefits

The point is made that the GSDM addresses the issues raised by Williamson and Wilson (2000). But, those benefits come at a price (in some cases, one that is already being paid). Conceptually, the issue is that measurements are made in a physical environment and that computations are performed according to an adopted model. That is already being done – for example, when using "flat earth" assumptions and ignoring earth curvature. The underlying question (raised in this paper) becomes one of selecting an appropriate model. Ideally, the "best" model for any operation is one that is both simple and appropriate – Occam's Razor. It could be argued that the appropriateness of the curved-earth computations recommended by Williamson and Wilson (2000) justify the added complexity of working on the ellipsoid with geodesy equations. As a survey engineer, this author is fully sympathetic with that position. However, it is argued here, because of the features already listed, that the GSDM is even more appropriate for underground (wellbore) mapping and that the computational complexity of the GSDM is significantly less than performing computations on the ellipsoid or using a map projection model. But there are other important issues that also need to be accommodated.

For example, it is presumed that the correction between magnetic north (physical) and true north (mathematical) is already being made. The gyroscope also responds to a physical stimulus, but the gyroscope detects and references a different north than does a magnetometer. Separate models (equations) are used to relate those physical data to the adopted "north" reference. Similarly, the difference between the ellipsoid normal (mathematical) and the vertical plumb line (physical) is a correction that should be made (if the difference rises to a level of positional significance). The GSDM includes strictly mathematical components but sensor data are derived from observations of physical phenomena. Physical observations and the associated mathematical model need to be reconciled before physical measurements can be used in coordinate position computations.

At a gross level, the difference between normal and vertical (deflection of the vertical) may be inconsequential for underground mapping. But as tolerances become tighter and as computed positions are known with greater certainty (smaller standard deviations), the difference will need to be accommodated. Part of that discussion needs to recognize that relative ellipsoid height differences (in a wellbore) are not significantly different than elevation differences. The point is that knowledge

of the depth of a wellbore can be expressed in ellipsoid height (via the GSDM) more reliably than when using elevation. In short, the need for geoid modeling is largely mitigated. That point needs careful discussion and is too important to be decided here and now. Burkholder (2002) contains additional information that may be applicable to that discussion.

GSDM PROCEDURES FOR UNDERGROUND (WELL) MAPPING

For the most part, existing field procedures are valid and can continue to be used when implementing the GSDM. The differences lie primarily with the manner in which data are processed, managed, and used. First, it might be helpful to review the current map projection and "low distortion" models being used. The following are to be noted with regard to Fig. 4.

- In spite of the fact that map projections are strictly two-dimensional models, they have been used very beneficially with performing flat earth computations for many projects.
- Figure 4 illustrates how map projections have been used to minimize impact of curved-earth surveying. Low Distortion Projections have become popular with various city/county/state organizations.
- The underground mapping may begin on/near the earth's surface but the vertical portion of a wellbore quickly extends beyond the effective range of a map projection model. The reason is that a map projection is concerned primarily with horizontal relationships within a fairly narrow vertical window.
- The 3-D GSDM overcomes drawbacks of the 2-D map projection model and preserves true 3-D geometrical integrity throughout.

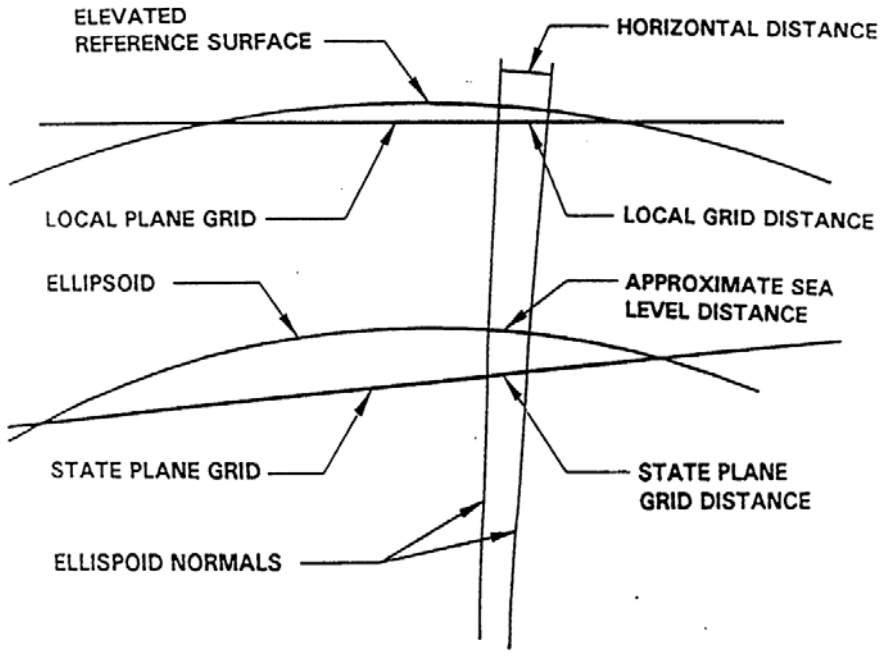

FIG. 4. Map Projections Have A Narrow Range of Vertical Validity

Implementation Procedures:

- The beginning reference point (well-head or nearby well monumented point) must have reliable 3-D ECEF coordinates (X/Y/Z) – typically determined using GPS. If it is not possible to occupy the point with GPS, those values can be determined using a total station side-shot from a known X/Y/Z reference point.
- Existing sensors and procedures are used to determine local 3-D spatial data components (calculated offsets). These local differences are converted to metric units, rotated into the ECEF environment, and added to beginning ECEF coordinate values of the known point.
- The computed ECEF coordinates are stored (top box in Fig. 3) and used as primary values. The stochastic portion of the GSDM accommodates storing the covariance values of each new point. In the case of a network adjustment, the covariance values representing point-pair correlation can also be stored.
- Using stored ECEF coordinates involves selecting a convenient point-of-beginning (P.O.B.) as a reference. The relative position from the P.O. B. to any other ECEF point is a simple subtraction to obtain geocentric coordinate differences. Those ECEF differences are transformed to the local perspective $\Delta e/\Delta n/\Delta u$ components using a rotation matrix at the P.O.B.
- Those local flat-earth components can be used to compute distances, azimuths, and other quantities in much the same manner as current practice.
- The GSDM stores ECEF values that are common to all disciplines worldwide. That means that all spatial data users are on the same page and can enjoy the

luxury of transforming those ECEF values to latitude/longitude/ellipsoid height, state plane coordinates, or UTM coordinates – see Burkholder (2008).

CONCLUSIONS

Although core 3-D coordinate computations are performed in a standard geometrical environment in which measurements are not distorted to fit the model, each user has the option of transforming those values to a user/job specific system that permits continued use of familiar practices. Additionally, the GSDM defines specific procedures for handling spatial data accuracy. But, the real take-away from this paper relates to the issues raised by Williamson and Wilson (2008):

- The disadvantage of non-parallel coordinate systems is handled by using a rotation matrix to transform the ECEF coordinate differences into local differences.
- The GSDM accommodates continued use of flat earth practices in the field while preserving geometrical integrity of the measurements and providing rigorous connection to the physical curved-earth environment.
- Using the GSDM, drilling and subsurface data can be integrated into the same data base in a manner that also supports establishing and tracking spatial data accuracy.

Additional information related to the GSDM is posted on the author's web site and gratis prototype software that validates the concepts described herein is available at http://www.globalcogo.com/WBK3D.html. Significant work remains to be done to tailor software for the energy production industry. But, it is this author's opinion that the added effort needed to relate physical sensor data measurements to mathematical geometrical components is a small price to pay for enjoying the benefits offered by using the GSDM.

ACKNOWLEGEMENTS

The following are credited with facilitating development and revisions to this paper. To each I offer my sincere thanks.

- Barbara Whitten, ASCE Manager Technical Committees (Geomatics & Energy)
- Chuck Hookham, 2012 Chair – ASCE Energy Division
- David Garber, 2013 Chair – ASCE Geomatics Division
- David M. Baker, Senior Advisor – Geoscience Technology, Chesapeake Energy Corporation
- Anonymous reviewers

REFERENCES

Burkholder, E. F., (2013). "Standard Deviation and Network/Local Accuracy of Geospatial Data." Washington, D.C., U.S. Copyright Office. http://www.globalcogo.com/StdDevLocalNetwork.pdf

Burkholder, E. F., (2008). "The 3-D Global Spatial Data Model: Foundation of the Spatial Data Infrastructure." Taylor & Francis Group – CRC Press, Boca Raton, London, New York.

Burkholder, E. F., (2002). "Elevations and the Global Spatial Data Model (GSDM)." Proceedings of the 58th Annual Meeting of The Institute of Navigation and CIGTF 21st guidance Test Symposium, Albuquerque, NM. 217-222

Burkholder, E. F., (1997). "Definition and Description of a Global Spatial Data Model." Washington, D.C., U.S. Copyright Office. http://www.globalcogo.com/gsdmdefn.pdf

Williamson, H. S., Wilson, H.F. (2000). "Directional Drilling and Earth Curvature." SPE Drill. & Completion, 15(1), 37-43.

Design of Bulk Railway Terminals for the Shale Oil and Gas Industry

C. Tyler Dick[1], P.E., M.ASCE and Lynn E. Brown[2], P.E.

[1]Senior Railway Research Engineer, Rail Transportation and Engineering Center – RailTEC, Department of Civil and Environmental Engineering, University of Illinois at Urbana-Champaign 1241 Newmark Civil Engineering Lab, MC-250, 205 N. Mathews Avenue, Urbana, IL 61801, U.S.A., E-mail: ctdick@illinois.edu.
[2]Chair, AREMA Committee 14 – Yards & Terminals, Railroad Section Leader, HDR Engineering, Inc., 8005 Hallet Street, Lenexa, KS 66215, U.S.A., E-mail: lynn.brown@hdrinc.com.

ABSTRACT: Railway transportation is playing a key role in the development of many new shale oil and gas reserves in North America. In the rush to develop new shale oil and gas plays, sites for railway transload terminals are often selected on the basis of land availability and environmental constraints before full consideration is given to rail design and operating requirements. The result can be terminals that poorly utilize the available space or operate inefficiently and face long-term capacity constraints. Additionally, preliminary concepts may omit or underestimate the need for staging tracks, switching leads and other rail infrastructure required to support train operations, potentially altering the economics of a terminal. To facilitate more informed decisions regarding railway terminal sites and better track layout concepts, this paper presents design requirements for bulk railway terminals to support shale oil and gas development. Guidelines for sizing facilities and layout of different track arrangements, including stub-end, inline and loop facilities, are presented. Considerations for mainline access and multi-train operation to ensure terminal capacity to support current and future demand are also discussed. Developers following these guidelines will likely obtain greater returns from their real estate and facility investments through faster railway approval of design concepts and more efficient rail operations.

INTRODUCTION

Large quantities of crude oil and natural gas are trapped beneath the ground surface in non-permeable shale rock in the United States. Technological advances such as directional drilling and hydraulic fracturing have combined with the recent trend of higher crude oil prices to make extraction of shale oil and gas economically feasible. The resulting increase in U.S. crude oil reserves and production is concentrated in North Dakota and Montana (and bordering Canadian provinces), and Pennsylvania and Ohio, away from traditional domestic oil production centers in Texas, Oklahoma and California. This means that these new sources of oil, or shale oil and gas "plays",

are located far from the refining and pipeline infrastructure that developed along the Gulf Coast to serve traditional production centers and in the Northeast to serve oil imported via tanker ship. Since new refining infrastructure near developing production centers will take years to permit and construct, for the oil from places such as North Dakota to reach market, it must move overland to existing pipeline and refining infrastructure. The sudden demand for transportation of large quantities of oil is being met by the rapid development of new infrastructure.

Most crude oil transportation in the United States has traditionally been via pipeline, with a dense network serving historical production centers in Oklahoma and Texas and long distance pipelines from storage hubs to refining centers in the Midwest and Northeast. Similar pipeline networks exist to move imported oil inland from Northeast and Gulf Coast ports. With a shift in production to regions where there are relatively few pipelines with limited capacity and geographic coverage, the new production centers are poorly served by this transportation mode. Like refineries, new pipelines take many years to permit and construct. Thus, it will be many years before the pipeline mode can adapt to handle all of this transportation demand. In the meantime, rail is being used as an alternative.

Due to their history of agricultural production and transportation of crops via rail, North Dakota and Montana are served by a dense network of rail lines. Thus transportation of crude oil via rail is a natural alternative to pipeline. Oil by rail can take advantage of existing transportation infrastructure to provide producers with safe, efficient and cost-effective transportation of their product until pipelines can be developed. This is evidenced by the rapid growth in oil traffic experienced by the Class 1 railroads during the past five years. In 2008, U.S. Class I railroads originated just 9,500 carloads of crude oil. In 2012, they originated nearly 234,000 carloads and, according to the Association of American Railroads (2013) are projected to originate around 400,000 carloads in 2013. Even after new pipelines are developed, rail still offers advantages such as routing flexibility to serve multiple refining centers and the ability to divert shipments to capitalize on rapid price swings and market demands. Thus, although some market share will be lost to pipeline development, oil by rail is seen as a long-term transportation option for the oil and gas industry.

The efficient and effective transportation of crude oil by rail requires the development of new transload terminals that support efficient access to railway operations. A properly planned transload terminal that can expedite the loading of railcars near a production center and unloading of railcars near a refinery or pipeline access point is key to effectively providing a continuous, uninterrupted supply of crude oil. Despite the importance of these facilities, in the rush to develop new shale oil and gas plays, sites for railway transload terminals are often selected and purchased on the basis of land availability and environmental constraints before full consideration is given to all railway design and operating requirements. The result can be track layouts that poorly utilize the available space or terminals that operate inefficiently and may face long-term capacity constraints. Additionally, preliminary concepts may omit or underestimate the need for staging tracks, switching leads and other rail infrastructure required to support train operations, potentially altering the economics of a terminal and decreasing return on investment.

To allow shale oil and gas terminal developers to make more informed decisions

regarding railway terminal sites and better plan track layout concepts, this paper presents guidelines and design requirements for bulk railway terminals to support shale oil and gas development. Guidelines for sizing facilities and layout of different track arrangements, including stub-end, inline and loop facilities, are presented. Engineering requirements for curvature, gradient and special trackwork are included in this discussion. The paper also covers considerations for mainline access and multi-train operation to ensure terminals have capacity to support efficient operations under current and future demand.

RAILCARS AND UNIT TRAINS

Two important parameters in the design of a transload terminal are the lengths of the railcars and trains to be served by the facility. To provide the most efficient transportation possible, railcars are optimally sized to carry a specific commodity. For crude oil, the optimally-sized tank car with a gross rail load of 129,727 kg is approximately 113,562 to 121,133 liters. Based on current designs, this translates into tank cars between 18 and 19 m in length over the couplers. It is this overall coupled length, and not the length of the tank itself, that is critical for terminal design.

To further increase efficiency, crude oil moves in unit trains that transport large volumes of a single product between two points. Unloaded on arrival and returned promptly for another load, unit trains cut costs by eliminating intermediate yard and switching operations. This decreases cycle time and increases equipment utilization. Crude oil tank cars are most commonly moved in unit trains ranging in length from 80 to 120 cars. The selected train length depends on several factors, including oil production rates, expected traffic volumes and any constraints on train length, such as the length of passing sidings where meets between trains traveling in opposite directions on single track occur. The overall train length (L_t) includes three components as described by Eq. 1:

$$L_t = L_l + L_b + L_r N \tag{1}$$

where L_l = length of locomotives; L_b = length of buffer cars; L_r = length of loading or unloading rack; and N = integer number of railcar "cuts" in the train, where a "cut" is a group of railcars that stay coupled together as they are moved about the facility during the transload process.

Typical loading and unloading racks are 365 to 439 m in length such that they can simultaneously handle a group of 20 to 24 railcars. Thus, a facility with a 24-car rack is likely to be served by a 96-car train that is composed of four groups of 24 tank cars. Such a train is loaded or unloaded in four stages, either by advancing the intact train in 24-car increments through an unloading rack on a continuous loop or by splitting the train in to four groups of 24 tank cars and successively moving them in and out of several storage tracks and a rack located on a stub-end track.

As noted in Eq. 1, the design train length includes the length of locomotives and buffer cars. A buffer car, minimum 13.7 m in length, must be placed between the locomotives and the tank cars to satisfy federal regulations. The typical high-horsepower mainline locomotive is 22.9 m in length and a typical unit train may

require two to five locomotives depending on the speed and grade profile of the route. All locomotives may be coupled to the front of the train or they may be split between the front and rear of the train in a radio-controlled distributed power configuration.

Based on these characteristics, an example 96-car unit train with one buffer car and three locomotives will be 1,838 m in length. Such a train can transport approximately 11,500,000 liters (72,600 barrels) of oil.

DESIGN STANDARDS AND GUIDELINES

In developing a site as a transload terminal, track curvature can be a limiting factor in the ability to efficiently use available space. In an effort to maximize the capability of a particular site, there is a tendency to squeeze in more track by using sharper curves of smaller radius and turnouts with larger diverging angles. To support unit train operations, curves should be no sharper than 7.5 degrees (233-meter radius by chord definition) and number 11 turnouts are preferred over smaller number 9 turnouts within the facility. These curves and turnouts reduce in-train forces when moving railcars about the facility, increasing efficiency, and also reduce wear and track maintenance cost. Spirals and superelevation are not used within a facility with the exception of mainline connections where trains may be entering or exiting the facility at higher speeds and larger number 15 turnouts may be required. Reverse curves may be separated by as little as one car-length of tangent but operation of unit trains is made more efficient if there is 61 m between reverse curves.

Gradient should be kept as close to level (0%) as possible where railcars are being positioned at the loading and unloading racks to reduce the in-train forces needed to precisely handle the heavy groups of tank cars. Where possible, the transload and storage tracks where railcars will be left standing should be designed with a slight 0.1% descending grade towards the middle of the track to create a depressed “bowl” shape that helps prevent railcars from rolling out of the track.

To help prevent railcars from accidentally rolling out of the facility and on to the mainline where they pose a collision hazard, the transload facility should be designed at a lower elevation than the main track. Since this is not always practical and some cars may gain enough momentum to roll up ascending grades, the lead track into the facility must be equipped with a derail. Due to the size and weight of the cuts of 20 or more railcars that are typically moved about a transload facility, it is recommended that a double-switch point derail be used.

While the preceding general guidelines are typical of the Class 1 railroads, the specific industrial track design standards of the connecting Class 1 railroad should always be referenced.

SITE AND LAYOUT CONSIDERATIONS

The guidelines in the previous section relate to the technical requirements of specific elements of rail transload facility design. They do not speak to the overall facility layout and its related operating concept. Thus it is possible to design a facility that meets all track specifications but has an overall layout that does not provide the required capacity in an efficient manner. Inefficient terminal operation

will increase railroad shipping rates, reducing the return on terminal developer investment. The terminal developer should engage the connecting Class 1 railroad early in the process to ensure the selected site and preliminary track layout provide the most effective combination of location, shipping rates and serviceability.

In evaluating potential sites along a rail line and their corresponding track layouts, a terminal developer should carefully consider the following series of questions:

- **What is the traffic density and capacity of the connecting rail line?** Class 1 railroads are taking steps to limit access to their densest and most capacity-constrained corridors. Facilities on these lines will require additional track to ensure that terminal operations have minimal impact on the fluid movement of through trains.
- **At what speed are trains expected to enter and exit the facility?** Trains that must reduce speed on the mainline to enter a transload facility consume mainline capacity. On busier mainlines where capacity is a concern, additional track will be required between the facility and mainline connection to allow acceleration to and from track speed to occur off of the mainline.
- **What signal system is in place on the connecting rail line?** Connecting to a line with wayside signals will be more expensive than in unsignaled ("dark") territory. Additional project schedule time will be required to design the signal interface prior to installation of the mainline connection. This amount of time can be reduced if the mainline turnout can be installed near an existing signal control point, passing siding or crossover.
- **What is the direction of local train service?** Stub-end facilities are most efficiently served if a train travelling in the direction of local train service can pull past the facility and then back up through the mainline turnout into the stub-end tracks of the transload terminal.
- **Can the mainline or existing siding tracks be used for terminal operations or must all operations be contained within the facility?** At facilities on low-density lines, traffic may be infrequent enough to occasionally allow transload terminal operations use of mainline and passing siding tracks for switching movements. However, where traffic density is higher, dedicated switch leads and run-arounds must be constructed, increasing the required length of track at the facility.
- **Are there any existing bridges, grade crossings or rail customers on the mainline within one train-length of the proposed site?** Existing constraints can prevent or increase the cost of establishing switching and departure tracks of length required to support efficient operations.
- **What is the anticipated frequency of train arrival/departures?** A facility that is expected to service more than one train per day will require sufficient track to stage more than one train in the facility at once, increasing space and infrastructure requirements.
- **Will mainline locomotives remain with the train or will a locomotive based at the terminal be used to reposition railcars?** At loop facilities, mainline locomotives often stay with the train but at stub-end facilities, these locomotives may be taken away and returned when a loaded crude

oil train is assembled for departure. In such cases, the track layout must include the crossovers and specific track arrangement required to remove the locomotives from the train. This can be further complicated by the presence of distributed power. Where dedicated switching locomotives will be stationed at the terminal, space must be allotted for a locomotive storage track that is convenient for refueling and servicing from trucks.

- **Will any inspection and railcar repair occur at the facility?** If routine inspection of tank cars that may result in light maintenance and running repair activities will take place at the facility, the track layout should incorporate a short set-out track with easy truck access where railcars can be repaired. A second track may be used to stage spare tank cars used to replace railcars removed from the train for repairs. Adding these cars to fill out unit trains to their desired operating length increases efficiency.

The answers to the above questions will make some potential sites more attractive than others. Sites along high-density mainlines requiring additional track to address mainline access concerns will need to be longer, favoring long rectangular parcels parallel to the mainline. Where this is impractical, it may actually be better to investigate sites that are remote from the mainline but can be accessed via a long lead track from the mainline constructed along a narrow right-of-way. Examples of these arrangements are illustrated in Figure 1. Where mainline access is less of an issue, square or rectangular parcels become more attractive as they allow for stub-end and loop layouts. Where all adjacent parcels are unavailable or there are parallel constraints, the only practical option may be to develop an inline facility on a narrow easement parallel to the railroad right-of-way. Specific layout considerations for stub-end, inline and loop facilities are presented in the following sections.

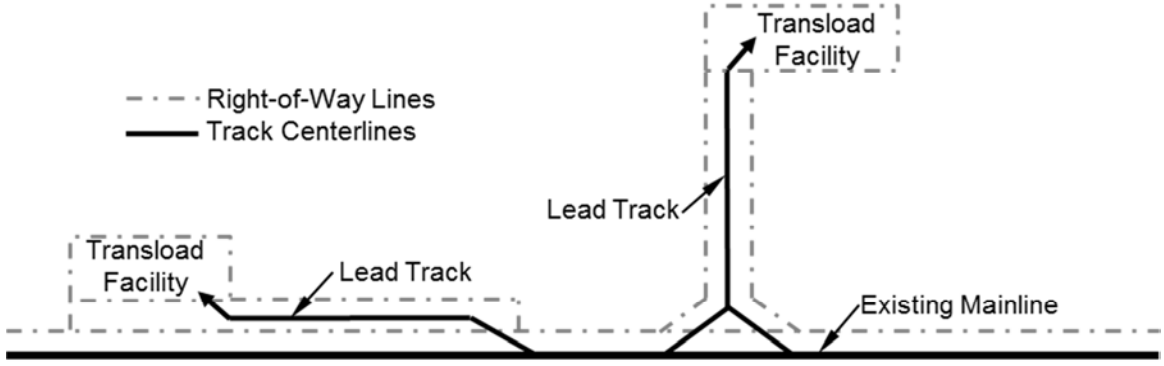

FIG. 1. Property requirements to support extended lead tracks from the crude oil transload facility to the mainline.

STUB-END FACILITIES

The most compact transload facilities consist of a series of parallel stub-end tracks. One or more of the tracks will be adjacent to the loading or unloading rack while the remaining tracks are used to temporarily store railcars before or after their turn at the

rack. The general layout of a stub-end facility is illustrated in Figure 2.

Empty trains arrive at the stub-end facility on the lead track. A terminal switching locomotive splits the unit train into groups of cars matching the length of the loading rack and moves them into the storage and loading tracks. As the groups of cars are loaded, they are moved from the loading track to a vacant storage track. Then an empty group of tank cars is moved from a storage track to the loading track. When all of the tank cars are loaded, they are reassembled into a unit train on the lead track.

Based on this operating pattern, suggested track lengths are illustrated in Figure 2. A key consideration is to have a lead track that is long enough for groups of tank cars to be moved between the loading and storage tracks without using the mainline. There must also be a single track long enough to reassemble the unit train without using the mainline track. Each storage track must be longer than the loading tracks, allowing each to hold an entire group of railcars. To reduce the number of heavy switching movements with multiple groups of railcars, it is recommended that there be one storage track for each group of railcars expected to be in the facility at a time. For a facility that will only handle one train per day, four storage tracks are required when the loading rack is one-quarter the length of a unit train. For a facility that will depart two trains per day, eight storage tracks are required.

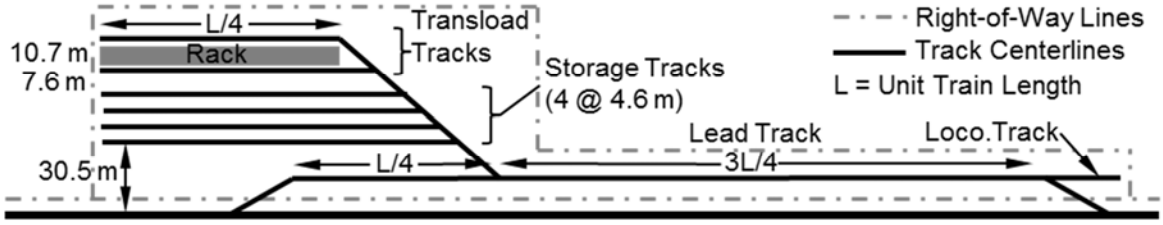

FIG. 2. General layout of parallel stub-end crude oil transload facility.

Any track used to store or transload tank cars must be located at least 30.5 m from the mainline track. Track centers can be spaced at 4.6 m but if access is required between tracks, wider track centers greater than 7.6 m are required. If a transload rack is to be located between tracks, those tracks must be spaced at 10.7 m on center.

While Figure 2 illustrates a layout with tracks parallel to the mainline, the stub tracks may also be oriented perpendicular to the mainline. This configuration can make better use of rectangular parcels with a long axis perpendicular to the mainline.

INLINE FACILITIES

Where a rectangular parcel of land is not available and a long skinny parcel parallel to the existing railroad right-of-way is the only available option, an inline design should be considered. Like a stub-end facility, the inline design requires splitting the unit train into multiple groups of tank cars that are transloaded in succession. However, instead of being sorted into a series of stub-end tracks, the groups of railcars are shuffled through the facility in a more linear manner. A general layout for an inline facility is illustrated in Figure 3.

The track lengths in Figure 3 are required to support the operating pattern

illustrated in Figure 4. Empty trains arrive at the inline facility on the long track running the length of the facility. Upon arrival, the first quarter of the train is already positioned at the rack for loading as a group. After this group is loaded, it is pushed back into the short siding track and the remainder of the train is pulled forward, positioning the second group of railcars for loading. This cycle is repeated for the third group. When the final group is pulled forward to the rack, all four groups will be positioned in line, albeit in reverse order, to be recoupled into a unit train.

Although this configuration can make very efficient use of a narrow right-of-way parallel to the existing mainline, it is difficult to stage multiple trains at the facility. Loading multiple trains per day requires offsite staging tracks where empty trains can be held until the train at the facility can complete the loading process and depart.

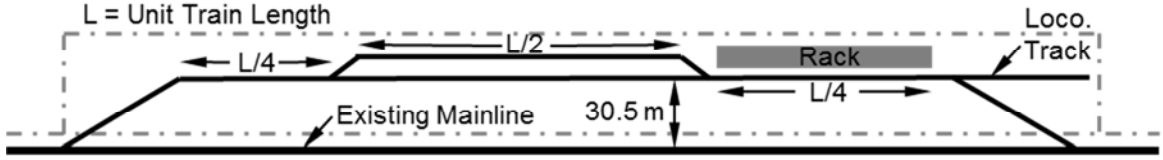

FIG. 3. General layout of an inline crude oil transload facility.

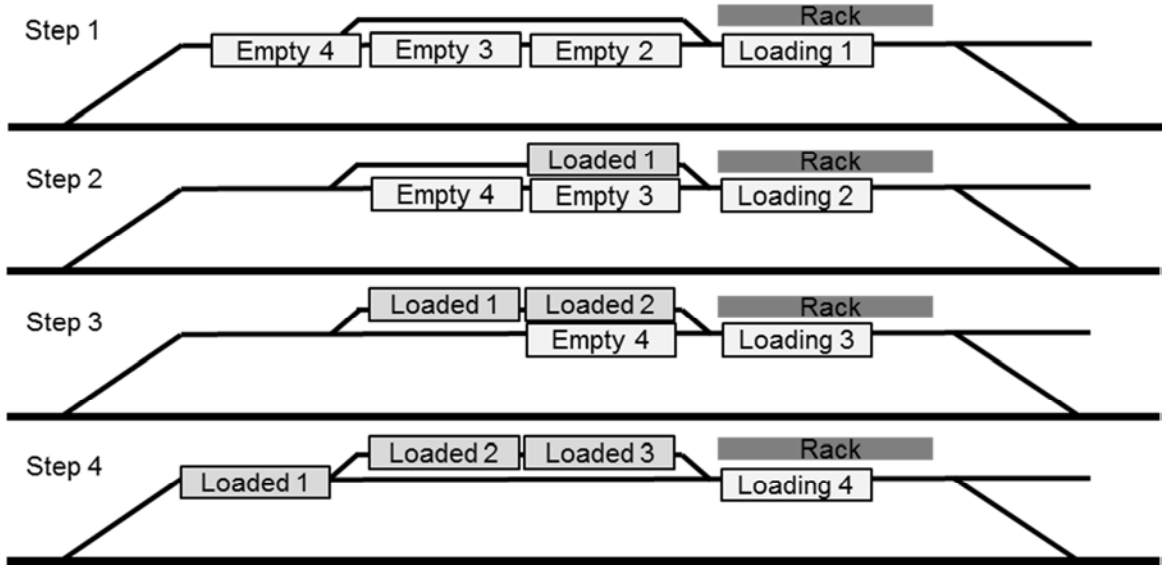

FIG. 4. Inline facility operating sequence.

LOOP FACILITIES

Unloading loops increase efficiency by allowing the crude oil unit train to transload without being split into individual cuts of railcars. As the next group of tank cars is moved forward into position at the rack, the entire train is moved around the loop together, mainline locomotives included. Loops also automatically reverse the direction of the train and eliminate movements to reposition locomotives as required

at a stub-end or inline facility. Eliminating coupling, uncoupling and switching activities reduces equipment cycle times and the cost of rail transportation.

The main disadvantage of unloading loops is the space required for a loop large enough to turn a unit train. Although tight curves decrease the overall footprint of the rail loop, they create operational and maintenance issues due to the increased friction of loaded trains on such curves. From a site selection perspective, the minimum curve radius requirement described earlier sets the minimum width required to turn a unit train on a loop at 466 m, plus allowance for roadbed and right-of-way. However, as described below, there are other considerations that can increase the required size of the loop and the least measurement of the required property.

Reverse curves on loop tracks must be separated by tangents. To avoid clearance issues, it is also desirable to have the transload racks on a tangent portion of the loop. Since crude oil transload racks can be as long as one-quarter of the unit train length, the loop cannot be round and must have one side with a considerable length of tangent, as illustrated in Figure 5a. The direction of operation around the loop should be selected to minimize in-train forces given the relative position of the loaded and unloaded railcars within the partially transloaded train.

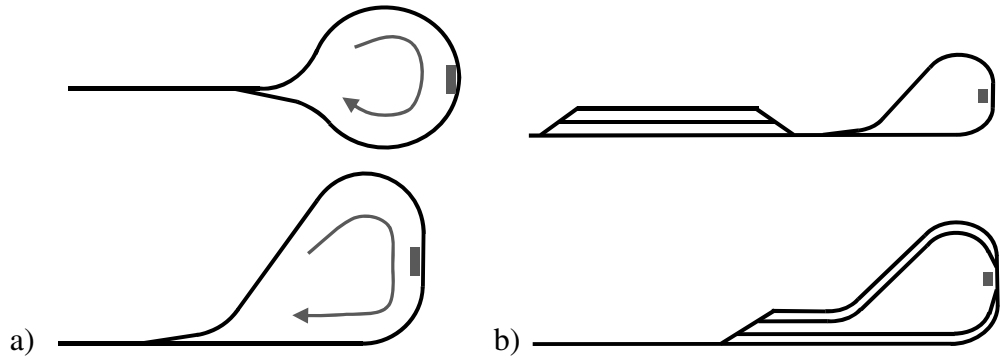

FIG. 5. a) Proper placement of tangents for loop track designs to minimize in-train forces and allow for tangent transload racks. b) Different staging track configuration to support multi-train operations at loop facilities.

On a simple loop track, the required distance around the loop is set by the length of the unit train. To obtain economies of scale and the lowest shipping rate from the railroad, this train length should be made as long as feasible. Although crude oil trains are often shorter, railroads are designing new infrastructure to accommodate 150-car trains. If space allows, designing a loop with 2,743 m of clear track length will aid the industrial shipper in future rate negotiations with the railroad.

There must be additional track between the turnout that closes the loop and the mainline connection to avoid having one end of the train on the mainline while the other end is still positioned at the transload rack. For a rack of length L/4, a minimum distance of 3L/4 is required between either end of the rack and the mainline connection. Operational considerations may dictate even longer lead track lengths.

When a terminal operator plans to have multiple trains cycling through a facility each day, it is likely that trains will be delayed, leading to bunching and multiple

trains arriving within a short time period. If the loop is configured such that only one train can be at the facility, the railroad must temporarily store the train nearby, impacting their normal operations. To avoid this possibility, railroads require a loop facility to provide staging for three trains: an empty train, a loaded train and one train being moved to/from the transload rack.

There are two different strategies for providing the required storage tracks illustrated in Figure 5b. The first is to create a parallel staging yard on the spur track leading to the transload loop facility. This has the advantage of storing trains outside the main facility where they will not interfere with site operations. However, this configuration leads to downtime at the transload rack while the first train clears the loop and returns to the staging yard and the next train moves from the yard to the rack. The second strategy maximizes rack utilization by integrating the staging tracks into the loop track. By making the loop twice as long and double track (except for the segment through the rack) three trains can be stored in serial fashion. With this configuration, the second train can start transloading immediately after the first train clears the rack. However, by providing train storage on the loop, access to the interior of the loop will almost always be blocked, reducing its utility as usable space.

OPERATIONAL CONSIDERATIONS

As described earlier, transload facilities often strive to locate on property immediately adjacent to a railroad mainline. Although this minimizes the amount of track the terminal developer must construct, the proximity of the transload tracks to the mainline can be less than ideal from the railroad perspective. On certain congested corridors, in an effort to reduce track capacity consumed by trains moving slowly on and off the mainline into terminals, the railroads require that trains enter and exit the mainline at speed via a large turnout. There must be sufficient track between the mainline turnout and facility for a train to leave the mainline at speed and then decelerate to a stop prior to commencing the transload sequence. Although braking distances vary, a good guideline is to leave a minimum of two train lengths between the mainline turnout and the entrance to the main transload facility trackage.

If typical operations require a train to pass through the diverging route of a turnout while entering or exiting the plant, turnouts located within one train length of the mainline should also be large enough so as not to restrict train speed. More expensive larger turnouts are required to support this requirement. This also suggests that from an operational perspective, on a congested corridor, it may be best to site a transload facility off the mainline at the end of a dedicated spur of approximately 4 km in length. As shown previously in Figure 1, absent engineering constraints, lengthy approach tracks could be constructed parallel to the existing mainline track to effectively create more distance between the mainline and the transload site.

CONCLUSION

Railway transportation is playing a key role in the development of many new shale oil and gas reserves in North America. To allow shale oil and gas terminal developers to make more informed decisions regarding transload sites and better plan

track layout concepts, this paper presented guidelines and design requirements for bulk railway terminals to support shale oil and gas development. Stub-end, inline and loop facilities all have their unique site space requirements. Selection of an appropriate configuration is driven by parcel shape and orientation, traffic levels, operational considerations and engineering constraints. Developers should carefully consider the exact size and shape of a potential parcel and its influence on the capacity and efficiency of possible transload facility layouts. A key consideration is sufficient lead track to avoid operational issues. Track layouts that follow the presented guidelines are more likely to fully utilize the available space, operate efficiently and provide long-term capacity for future operations. Developers of these terminals will likely obtain greater return on investment through more efficient rail operations, reduced equipment needs and potentially lower shipping rates.

ACKNOWLEDGMENTS

The authors appreciate the support of AREMA Committee 14, Yards & Terminals.

REFERENCES

Association of American Railroads. (2013). "Moving Crude Oil by Rail." *AAR Online*., <https://www.aar.org/keyissues/Documents/Background-Papers/Crude-oil-by-rail.pdf> (December 2013).

American Railcar Industries, (2013). "Tank Car Specifications." *ARI Online*, <http://americanrailcar.com/RailcarManufacturing/Car.aspx> (November 2013).

BNSF Railway. (2011). "Design Guidelines for Industrial Track Projects". < http://www.bnsf.com/customers/pdf/indytrkstds.pdf> (November 2013).

Union Pacific Railroad. (2013). "Technical Specifications for Construction of Industrial Tracks". < http://www.uprr.com/aboutup/operations/specs/ track/index.shtml> (November 2013)

CN Railway. (2011). "Engineering Specifications for Industrial Tracks". < http://www.cn.ca/-/media/Files/Customer%20Centre/Track-Specifications/Industrial_Track_Spec_12_sept_2011.pdf> (November 2013).

CSX Transportation. (2007). "Standard Specifications for the Design and Construction of Private Sidetracks". < http://www.csx.com/share/wwwcsx_mura/ assets/File/Customers/Services_and_Partners/CSX_Industrial_Sidetrack_Manual _063003.pdf> (November 2013).

Norfolk Southern. (2013). "Track Design Information". <http://www.nscorp.com/ content/nscorp/en/industrial-development/track-design-information.html> (November 2013).

American Railway Engineering and Maintenance-of-Way-Association. (2013). "Chapter 14: Yards & Terminals", *Manual for Railway Engineering*, AREMA, Lanham, MD

Management of Impoundments for Unconventional Resource Development: Application, Planning, Design, Best Practices, and Regulatory Considerations

J. Daniel Arthur[1], P.E., SPEC; Brian Bohm[2], P.G.; and Kevin Shepard[3], P.E.

[1] President/Chief Engineer, ALL Consulting, 1718 S. Cheyenne Ave., Tulsa, OK 74119, U.S.A., E-mail: darthur@all-llc.com.
[2] Professional Geologist, ALL Consulting, 1718 S. Cheyenne Ave., Tulsa, OK 74119, U.S.A., E-mail: bbohm@all-llc.com.
[3] Professional Engineer, ALL Consulting, 1718 S. Cheyenne Ave., Tulsa, OK 74119, U.S.A., E-mail: kshepard@all-llc.com.

ABSTRACT: Water management has become a critical link to shale resource development throughout the United States and elsewhere in the world (Wagner et. al. 2012, Arthur and Coughlin 2011). In order to stimulate production from deep shales, large volumes of water must be stored for rapid use during hydraulic fracturing operations. Although the majority of wells to date have been fractured using fresh water, there is increased emphasis on minimizing fresh water use, increasing the use of saline waters, and also recycling produced water for purposes of reuse in fracturing operations. This evolving water use strategy combined with a diversity of operating environments has created a number of technical and environmental challenges related to the storage of these different resources. In addition to design and water segregation considerations, there are other technical and regulatory considerations including siting, monitoring, and maintenance activities that are also a priority. Furthermore, the utilization of saline waters and recycling of produced water are causing the oil and gas regulatory environment to rapidly change, with several states updating pit and impoundment regulations to address the broader range of waters being utilized. This paper will discuss the management of impoundments used in unconventional resource development, including various applications, regulatory requirements, design, and best management practices.

INTRODUCTION

In order to maintain sufficient volumes of fluids onsite during drilling, operators typically use pits to store make-up water used as part of the drilling fluids. Also, to stimulate production from unconventional resources, large volumes of water must be stored for rapid use during hydraulic fracturing operations. With a single production well having water requirements ranging from 2 to more than 10 million gallons, and unconventional wells pads having 4 to 16 wells per pad, large volumes of water are being stored in proximity to well pads (Tang and Ringwood 2013).

Although the majority of wells to date have been fractured using fresh water, there is pressure on oil and gas operators to reduce utilization of fresh water by increasing the use of saline or brackish waters and recycling produced water (including water that flows back to the well after it has been hydraulically fractured) for reuse in fracturing operations (Mueller 2013). This evolving water use strategy, combined with diverse operating environments that range from the water-strapped Permian Basin of West Texas and southeastern New Mexico to the north slope of Alaska, has created a number of technical and environmental challenges. Information on treatment technologies and strategies to recycle produced water have greatly increased in recent years as various service companies publish case studies (Ely et. al. 2011, Horner et. al. 2011). With this knowledge, operators have to adapt water storage impoundments, resulting in the construction of larger impoundments or separate impoundments for waters of different qualities. In addition to design and water segregation considerations, issues such as siting, monitoring, and maintenance are also a priority.

Today, impoundments are used for storage of produced water and fresh water, for emergency overflow and for temporary storage of well completion and treatment fluids. Regulatory considerations are affecting the design and siting of impoundments for these and other uses related to oil and gas development. Considerations such as whether to build on-channel (fresh water only) or off-channel impact the permitting process. States may also require impoundments to be monitored, limit the duration they may be operated based on the purpose or fluids stored, and limit the types of fluids that can be contained based on the standards to which they is constructed. Further, some impoundments may be large enough that state dam permits must be acquired to address potential safety concerns.

APPLICATION AND DESIGN

Operators and regulators have come to recognize that designs for an impoundment to store fresh water are very different than those for an impoundment that is used to store saline or produced water having high concentrations of chlorides and other total dissolved solids. As with any liquid material in storage, accidental spills and mismanagement can cause releases to the environment that could contaminate nearby waters and soils. Given the volume and the frequently high concentration of dissolved solids that are in each barrel of produced water, it is important that these fluids be managed in a manner that prevents contamination of surface or ground water (Veil et. al. 2004). Lining impoundments such as that illustrated in Figure 1 prevent infiltration and limits potential impacts to groundwater.

Other considerations operators must account for are waters from different sources that may need to be segregated while they are characterized and the final use for the water is identified. For example, an operator would want to keep water that has been treated for bacteria stored separately from water that has not yet been treated. Water may also need to be segregated based on other criteria. Operators may have different water quality needs based on how the water interacts with the completion additives, further complicating the overall water management process.

FIG. 1. A lined fresh water supply pit utilized for Marcellus Shale development in Pennsylvania

REGULATORY

The use and regulation of pits have changed considerably since the early days of oil and gas development. The oil and gas industry has used pits to hold wastes from drilling and production operations from the time the first oil and gas wells were drilled to present day. In their earliest uses, oil and gas pits were simple dug holes in which fluids were stored with no care for the loss of fluids through infiltration or overflow. Early drilling wastes were disposed of via land spreading or road spreading or were simply buried onsite. The use of excavated pits is the most common manner in which drilling and workover fluids are stored today. A growing awareness of the potential impacts to the environment resulting from historic disposal practices in the 1970s led to some of the earliest regulation of oil field waste disposal. Since this time, impoundment regulations began to develop to address these concerns along with the development of some of the fundamental principles related to siting and construction requirements. The rules have become more restrictive to limit infiltration of waste fluids into the sub-surface and ensure that on-site burial of pit materials results in minimal impact.

The regulatory environment is changing rapidly. State oil and gas agencies are updating pit and impoundment regulations. Modern-day pit regulations protect groundwater and surface water resources by preventing the migration of fluids from the pits to these water resources. These regulations need to ensure the prevention of spills and overland releases, prevent direct contact by people and wildlife with pit contents, and prevent punctures and leaks in the liner during the operation and closure phases. In the post-closure phase, for those pits whose contents are buried in place, the regulations need to prevent erosion of the surface covering the pit and exposure of pit contents, and prevent the leaching of liquids from within the pit. Although oil and gas pit requirements vary from state to state, the environmental protection goals of oil and gas agencies are consistent and focused on the protection of groundwater and

surface water resources. In 19 states, use of an impoundment requires a prior authorization from the regulatory agency; in some states, separate permits are required for each functional pit use (e.g. drilling, fluid storage, emergency etc.). Sixteen states specify the duration of time for which a pit may be used (GWPC 2009).

In 2009, the Groundwater Protection Council (GWPC) published a summary of state oil and gas regulations applicable to the use of pits as part of a project funded by the U.S. Department of Energy. The GWPC report summarized the state regulations by evaluating the states' pit rules looking at six requirements. Table 1 summarizes the findings of the GWPC report relative to the number of states with oil and gas regulations that include specific rules related to each of the six requirements: permit to construct/use, liner requirements, minimum freeboard, surface water set back, water table restrictions, and duration of use. The regulatory analysis summarized in the GWPC report shows the variability in impoundment regulations among the various oil and gas producing states. One of the states with the most encompassing impoundment regulations is New Mexico, which has recently modified the impoundment rules (Rule 17) in the state (NMOCD 2013). Table 2 provides a summary of the current New Mexico impoundment regulations in addition to a comparison to the regulations of other states with similar levels of oil and gas development.

Table 1. State Regulations Related to the Use of Impoundments for Oil and Gas Development

Impoundment Requirement	Number of States
Permit Required to Construct/Use	19
Liners are Required for Some Types	23
Minimum Freeboard Requirement	16
Setback from Surface Water Bodies	10
Prohibited in Water Table Areas	12
Duration of Use Restricted/Regulated	16

Source: GWPC 2009.

The containment of fluids within a pit is critical to the prevention of shallow groundwater contamination. Depending upon the fluids being placed in the pit, the duration of the storage, and the soil conditions, pit lining may be necessary to prevent infiltration of fluids into the subsurface. In 23 states, pits of a certain type or in a particular location must have a natural or artificial liner designed to prevent the downward movement of pit fluids into the subsurface. For example, in Louisiana, liners are required for produced water and washout pits. In some states, liners are also required for emergency pits on a case-by-case basis (GWPC 2009).

Typically, pit liners are constructed of compacted clay or synthetic materials like polyethylene or treated fabric that can be joined using special equipment such as a seam welder. In addition to liners, 10 states also require pits used for long-term storage of fluids to be placed a minimum distance from surface water to prevent potential overflows that could result in an unauthorized discharges to water bodies. In California, for example, pits may not be placed in areas considered "natural drainage channels." Twelve states also explicitly either prohibit or restrict the use of pits that intersect the water table. Further, 16 states require that fluids in pits remain a

certain level below the top of the pit wall. This distance, referred to as the "freeboard," provides for a safety margin to prevent pit overflows in the event of significant rainfall (GWPC 2009).

Table 2. Comparison of New Mexico Proposed Rule 17 to other State Pit Rules for Temporary Pits

State	New Mexico	Colorado	Wyoming	Texas	Pennsylvania	Ohio	Montana
Liner Requirement	YES	YES	YES	YES	YES	YES	YES
Liner Requirement Based on Depth to Water	YES	NO	YES	YES	NO	NO	NO
Specification of Liner Material	YES	YES	YES	NO	YES	NO	NO
Minimum Liner Thickness	YES	YES	NO	NO	YES	YES	NO
Specification of Liner Seam Type	YES	YES	NO	NO	NO	NO	NO
Minimum Freeboard Rule	YES	YES	NO	NO	YES	YES	NO
Specifications for Pits Used for Disposal	YES	YES	NO	YES	YES	YES	Yes
Specified Setbacks for Pits Based on Land Use	YES	NO	NO	NO	YES	NO	NO

Source: NMOGC 2013, COGCC 2011, WOGCC 2008, TX RRC 2012, PA DEP 2012, ODNR 2012a, ODNR 2012b, and MBOGC 2012.

Best Practices and Regulation Updates

In the case of shale gas development, drilling operations have been occurring in both urban and rural locations, requiring that drilling practices and other water handling practices be adapted to facilitate development in both settings. Development of resources in urban and rural areas without historic development have also pushed the development of new regulations or updates/modifications to rules to address the changes related to water storage associated with unconventional resource development. Table 3 describes best management practices and how those practices protect select resources.

Table 3: Examples of Best Practices being Utilized for Modern Unconventional Resource Play Impoundments.

Best Management Practice	Benefit of the Practices
Steel tanks	Provides protection of water resources from berm failures or overflows, can be utilized in crowded urban environments where dug ponds would not be practical.
Geosynthetic liners	Creates barrier to infiltration preventing fluids from migrating into groundwater.
Setbacks from water resources	Creates buffer area where spilled contends of impoundments could be captured prior to impacting surface waters.
Freeboard in lined impoundments	Provides protection in the event of unexpected weather conditions that would prevent overflow of contents.
Centralized impoundments	Large central source for fluid storage that can be utilized to supply or collect resources from multiple well pad locations.
Monitoring systems	Surface or subsurface systems designed to monitor resources in the event of fluids being detected outside of the impoundments.

Storage pits are not used in every development situation as best practices and local conditions often dictate; other sources of storage such as steel tanks are cheaper or less likely to cause impacts. One best practice utilized when dug storage pits are not ideal such as the presence of shallow groundwater is steel tanks or other aboveground containment systems. In an urban setting, due to space limitations, steel storage tanks are often used. Tanks can also be used in a closed-loop drilling system. Steel tanks are usually required due to specific geologic conditions, such as the presence of highly porous bedrock at the surface or the presence of limestone (karst) environments were sinkholes or other pathways to groundwater may exist. However, excavated pits are the most common means of storing fluids during drilling and well operations in most plays.

In rural areas, storage pits may be used to hold fresh water for drilling and hydraulic fracturing. Rural storage pits for water are typically excavated containment ponds that, based on the local conditions and regulatory requirements, may be lined to minimize the loss of water from infiltration. Impoundments holding produced water are typically lined to protect against groundwater contamination.

To enhance efficiency and limit the number of impoundments, operators are can apply best practices like the use of centralized impoundments to manage produced water for recycling. Centralized impoundments are typically designed and constructed to provide improved structural integrity for the life of their operation because the large impoundments are intended for longer durations of use than temporary drilling fluid ponds or even frac water sourcing ponds. For centralized well facilities, best management practices in the design and operations phase may include an initial review of site topography, geology, and hydrogeology, especially if such impoundments are within defined distances of a water reservoir, perennial or intermittent stream, wetland, storm drain, lake or pond, or a public or private water well or domestic supply spring. While not all locations require full containment, open impoundments, also called pits, are longer term facilities designed and constructed to minimize the risk of contamination.

An example of a state responding to best management practices and changes in the industry's use of impoundments is Oklahoma. In Oklahoma, a revised set of pit rules to address the use of large flowback water recycling pits was made in 2010 that incorporate many of what were formerly Best Practices into regulations and guidance (STRONGER 2011). Now, noncommercial flowback water recycling pits with over 50,000 barrels capacity and commercial facilities are required to install monitoring wells or leachate collection systems. If a leak occurs, a remediation plan is required. In order to properly track volumes recovered or contained within a common best management practice is tracking of haul tickets and invoiced that detail fluid removals or additions at well pads.

In June 2013, the New Mexico Oil Conservation Division (NMOCD) released revised rules for pits and impoundments. The NMOCD also added a new category of pit called "Multi-Well Fluid Management Pits" that can be used for storage of produced water or a blend of water, such as fresh water mixed with produced or saline water (NMOCD 2013). The rules specify setbacks that limit how close a pit may be to a water well, surface water body, or other environmental sensitivity. The rules also specify design, construction, and monitoring requirements (such as specifications on liners), as well as how the pit must be operated and ultimately closed. Best Practices included in the Revised Multi-Well Fluid Management Pit requirements include setback and construction requirements based on the proximity to urban development and various water resources.

SUMMARY

Evolving water use strategies combined with a diversity of operating environments has created a number of technical and environmental challenges related to the storage of varying water resources. Information on treatment technologies and strategies to recycle produced water have greatly increased in recent years as various service companies publish case studies (Ely et. al. 2011, Horner et. al. 2011). The design of impoundments for water management including the storage of fresh water and produced fluids is a critical component of unconventional resource development in the United States.

This paper briefly discusses the applications, changing regulatory requirements, siting, design, and best management practices. As the number of non-fresh water resources being utilized to development unconventional resource plays increases, these considerations are likely to continue to evolve and regulatory requirements can be expected to continue to change to address the use of lower quality water to ensure continued protection of surface water and groundwater resources.

REFERENCES

Arthur, J.D., and Coughlin, B.J. (2011). "Cumulative Impacts of Shale-Gas Water Management: Considerations and Challenges." SPE Paper 142234-MS. Presented at the SPE Americas E&P Health, Safety, Security, and Environmental Conference, Houston, TX, USA, March 21-23.

Colorado Oil and Gas Conservation Commission (COGCC). (2011). 900-1. E&P Waste Management Rules. Updated May 30, 2011.

Ely, J.W., Fraim, M., Horn, A.D., and Jakhete, S.D. (2011). "Game Changing Technology for Treating and Recycling Frac Water., SPE Paper 145454-MS. Presented at SPE Annual Technical Conference and Exhibition, Denver, CO, USA, October 30-November 2.

Fontelle, L.K., Lord, P., Weston, M., and Haggstrom, J. (2013). "Recycling Water: Case Studies in Designing Fracturing Fluids Using Flowback, Produced, and Nontraditional Water Sources." SPE Paper 165641-MS. Presented at 2013 SPE Latin-America Conference on Health, Safety, Environment & Social Responsibility Conference in the Oil and Gas Industry, Lima, Peru, June 26-27.

GWPC. 2009. *State Oil and Natural Gas Regulations Designed to Protect Water Resources*. Prepared for the U.S. Department of Energy Office of Fossil Energy, Oil and Natural Gas Program and the National Energy Technology Laboratory, Washington, D.C. <http://www.gwpc.org/sites/default/files/state_oil_and_gas_regulations_designed_to_protect_water_resources_0.pdf> (February 5, 2014).

Horner, P., Halldorson, B., and Slutz, J.A. (2011). "Shale Gas Water Treatment Value Chain – A Review of Technologies, including Case Studies., SPE Paper 147264-MS. Presented at SPE Annual Technical Conference and Exhibition, Denver, CO, USA, October 30-November 2.

Montana Board of Oil and Gas Conservation (MBOGC). (2012). Administrative Rules of Montana 36.22.1005. Drilling Waste Disposal and Surface Restoration.

Mueller, D. (2013). "Identification and Evaluation of Brackish Groundwater Resources and Alternate Water Sources for Hydraulic Fracturing Operations., SPE Paper 163769-MS. Presented at 2013 SPE Americas E&P Health, Safety, & Environmental Conference, Galveston, TX, USA, March 18-20.

New Mexico Oil Conservation Division (NMOCD). (2013). Order No. R-135060D, Pits, Closed-Loop Systems, Below-Grade Tanks and Sumps, New Mexico Administrative Code Revised 19.15.17.1 published June 28, 2013.

Ohio Department of Natural Resources (ODNR). (2012a). Ohio Annotated Code 1501:9-3-08. Temporary Storage of Saltwater and Oil Field Waste.

Ohio Department of Natural Resources (ODNR). (2012b). Ohio Revised Code 1509.22. Storage or Disposal of Brine, Crude Oil, Natural Gas, or other Fluids.

Pennsylvania Department of Environmental Protection(PA DEP). (2012). Pennsylvania Code 25 § 78.56. Pits and Tanks for Temporary Containment.

State Review of Oil & Natural Gas Environemtnal Regulations (STRONGER). (2011). "Oklahoma Hydraulic Fracturing State Review." *www.strongerinc.org*. <http://www.strongerinc.org/sites/all/themes/stronger02/downloads/Final%20Report%20of%20OK%20HF%20Review%201-19-2011.pdf> (Dec. 20, 2013).

STRONGER. (2010). "Pennsylvania Hydraulic Fracturing State Review." *www.strongerinc.org*. <http://www.shalegas.energy.gov/resources/071311_stronger_pa_hf_review.pdf> (Dec. 23, 2013).

Tang, A., and Ringwood, K. (2013). "Water Sustainability Risk Assessments; Lessons from Water Sensitive Industries." SPE Paper 239013-MS. Presented at 2013 Offshore Technology Conference, Houston, TX, USA, May 6-9.

Texas Rail Road Commission (TX RRC). (2012). Texas Administrative Code 16.1.3§3.8 Water Protection.

Veil, J., Puder, M.G., Elcock, D., and Redweik, R.J., Jr. (2004). *A White Paper Describing Produced Water from Production of Crude Oil, Natural Gas, and Coal Bed Methane*. Argonne National Laboratory. Prepared for for the U.S. Department of Energy/National Energy Technology Laboratory. <http://www.circleofblue.org/waternews/wp-content/uploads/2010/08/prodwaterpaper1.pdf> (Feb. 5, 2014).

Wagner N., Florence, F., Ogg, J., Brantley, L., and Covaevich, C. (2012). "The Interaction of Social Responsibility with Water Access and Resource Utilizations in Drilling Operations., SPE Paper 158024-MS. Presented at International Conference on Health, Safety and Environment in Oil and Gas Exploration and Production, Perth, Australia, September 11-13.

Wyoming Oil and Gas Conservation Commission (WOGCC). (2008). Environmental Rules, including Underground Injection Control Program Rules for Enhanced Recovery and Disposal Projects. Chapter 4 of Wyoming Oil and Gas Rules. <http://soswy.state.wy.us/RULES/rules/6855.pdf> (Feb. 7, 2014).

Storage Tank Secondary Containment

D. S. Soemantri[1], D.E, P.E, M.ASCE

[1]Staff Facilities Engineer, Technical Services Group, Chesapeake Energy Corporation, 6100 N. Western Avenue, Oklahoma City, OK 73118; Phone (405)-849-3835; E-mail: dadi.soemantri@chk.com

ABSTRACT: This paper will compare the effectiveness of various types of secondary containment for storage tanks in onshore hydrocarbon production facilities. Secondary containment prevents liquid that might escape the tank from contacting the surrounding environment, especially any main water bodies. Secondary containment design is influenced by the 40-Code of Federal Regulation (CFR) Part 112 Oil Pollution Prevention and EPA's Spill Prevention Control and Countermeasure (SPCC) Guidance. This paper will summarize the acceptable methods of secondary containment construction utilized by Chesapeake Energy, which consist of polyethylene liner with and without aggregate cover, polyurea surface liner, concrete slab with wall, geo-synthetic clay liner, and compacted clay/silt berm construction. Seepage estimates will be calculated on secondary containments full of liquid with a 48-hour retention period based on time duration of daily field inspection and clean-up operations. The calculation methodology is based on diffusion and advective flows. The diffusion flow rate through soil, concrete or liner is calculated using Bernoulli's Equation on hydraulic head, and Darcy's Law on liquid flow through a permeable element. The advective flow rate through a possible defect on a liner is calculated using Touze-Foltz and Giroud's Equation. Finally, this paper will review the performance of the aforementioned secondary containment types and contrast estimated seepages with the SPCC requirement of a sufficiently impervious system.

INTRODUCTION

In shale energy production facilities, there are several main containments using above-ground storage tanks (AST) for liquid hydrocarbon product and produced water by-product. These tanks are equipped with a secondary containment system per the 40 CFR part 112 Spill Prevention, Control and Countermeasure (SPCC) rules. The purpose of the secondary containment is a fail-safe system to capture any liquid spilled or leaked from storage. Secondary containment should be able to temporarily retain spilled liquid until clean-up operation occurs. The recovered liquid is then returned to the storage tanks or properly disposed.

The main requirement of the 40-CFR part 112 for secondary containment construction is that dike, berm or retaining wall materials shall be sufficiently impervious to "oil" (and other liquids).

As part of company commitment to be steward of the environment and continuous improvement in reducing operational risk, in 2012, Chesapeake issued a standard to further refine the secondary containment construction (Chesapeake Energy – Corporate Responsibility Report 2012).

The first part of this paper will present various construction methods for the secondary containment. The second part of this paper will present seepage calculation methods for spillage in a secondary containment.

CONSTRUCTION METHODS OF SECONDARY CONTAINMENT

Chesapeake secondary containment standard that was recently issued specifies the following construction methods for the secondary containment:

- Rolled polyethylene liner with and without aggregate cover
- Sprayed or rolled polyurea liner
- Concrete slab floor with perimeter stub wall
- Geo-synthetic clay (bentonite) liner
- Compacted soil clay/silt berm

Current Chesapeake practices throughout field offices for the secondary containment construction utilize polyurea or polyethylene liners for production facilities, and concrete pads for salt water disposal facilities.

The following section addresses the advantages and disadvantages of the aforementioned secondary containment construction methods. The design and construction of each method will also be discussed.

POLYETHYLENE (PE) PLASTIC LINER

There are various plastic liners that could be used for containment liner, namely PVC, polypropylene and polyethylene with various densities. The liner material is selected based on its properties of UV, weathering, chemical resistance, long term life time, and ease of availability. Chesapeake uses PE (see FIG. 1) for this plastic liner. The PE liner density and thickness is selected based on its strength to withstand any normal operational loading, including clean-up operations throughout it design lifetime.

The PE liner is installed on both of the floor and wall of the secondary containment. For the floor application, the liner is installed either on top of the ground surface or below the surface with soil/gravel cover. The wall construction for this plastic liner is either corrugated metal or berm wall. The splicing (welding) joint between the rolled liners is carefully performed and inspected to avoid possible leaching. If there is any underground pipe or foundation that protrudes through the ground surface, the liner is sealed around those features.

Regular secondary containment inspection and maintenance are part of the operational tasks in the facilities. If the liner is torn or punctured, it will need to be repaired or replaced to ensure the imperviousness of the containment.

FIG. 1. Polyethylene Sub-surface Liner with Berm

POLYUREA SURFACE LINER

Polyurea surface liners (see FIG. 2) are installed in either of the following manners:

- Complete field spray-on with geo-synthetic base liner
- Field installation of rolled liner with spray-on joints and walls

This liner application typically uses corrugated metal with spray-on liner for the wall. The liner shall be able to withstand some wind up-lift, so some tie-down mechanism shall be provided if required.

Similar to the plastic liner, this polyurea liner shall be UV, chemical, and weathering resistant. Considering the possibility of combustible gas in the facilities, walking on the liner should not cause any electro static build up on the field personnel. The thickness of the liner shall be sufficiently rigid to withstand any tear or puncture of normal operation throughout the lifetime of the facilities.

Field spray-on installation requires proper quality control to make sure that the liner product achieves the required thickness, flatness and uniformity. For the safety of the operator against slip, trip and fall hazards, the liner surface shall be textured, and without excessive wave or wrinkle.

FIG. 2. Polyurea Surface Liner with Corrugated Metal Wall

CORRUGATED METAL WALL

In order to withstand the exposure of the metal against soil and possible briny liquid spill, this corrugate metal is designed and coated for the corrosive environment. The wall is structurally designed to withstand the hydrostatic load from the possible liquid spill or flood, and International Building Code (IBC) specified wind loading.

CONCRETE PAD

Concrete secondary containment pads (see FIG. 3) are used for more permanent facilities, such as salt water disposal facilities. Concrete pads are structurally more robust against the environment loading compare to liner systems. However, concrete construction is more expensive and time consuming than the liner systems. Furthermore, field reclamation of concrete pad removal will be more difficult than liner system removal.

Reinforced concrete design and construction for the wall and floor systems follow the American Concrete Institute (ACI)-318 standards. The rebar layout and concrete thickness shall be designed to withstand equipment and IBC environmental loadings.

The design of the reinforced concrete slab considers avoiding or managing any concrete crack, which is common on any large slab. Concrete design utilizes either non-shrinkage concrete mixture, or epoxy-saw-joint with water-stop system per Concrete Reinforcing Steel Institute (CRSI) to avoid any leaking cracks, which would compromise the imperviousness of the containment.

FIG. 3. Concrete Pad

SUMP SYSTEM

For some applications where it is pertinent to avoid large pooling of liquid spill in the containment, automatic sump systems are provided to recover the spilled liquid into the tank. The sump system generally consists of a small pit, diaphragm pump with float valve, and piping back to the water tank. The sump can be installed on concrete or liner containments.

GEO-SYNTHETIC CLAY LINER

Geo-synthetic clay liner (GCL) is a combination of geosysthetic with sodium bentonite clay that make it a highly impermeable barrier. The bentonite compound is the key sealing element of this liner. The sodium bentonite will become hydrated with any compatible liquid which will cause swelling and decreased hydraulic conductivity. This pre-hydration reaction shall be done during construction after the soil cover is completely laid. The bentonite swell will make the liner impervious.
This application requires some finely graded and compacted sub-grade soil which is relatively flat and smooth to avoid damage to the bottom of the liner. This GCL requires 30.5 cm (12 in) of soil or gravel cover to provide confining stress to the liner.

The design and installation of the GCL shall follow the manufacturer's procedure. Splicing between the rolled liner edges and anchorage of the rolled liner end shall be done properly to avoid possible compromise of the containment system effectiveness.

The main disadvantage of GCL is its dependency on remaining hydrated for its impermeability property. Some geographical applications might encounter severe drought during the facilities' lifetime. Such droughts can dry and crack the bentonite which reduces its imperviousness.

COMPACTED SOIL BERM

For this application, the berm material is either clay or silt with low permeability and low content of other material, such as organic peat, sand, and gravel. Compacted sand and/or gravel are pervious and would allow the spill to seep out of the secondary containment.

The clay or silt materials have large shrinkage behavior under any long term dry condition. Such shrinkage would cause surface cracking of the berm. The freeze and thaw weather cycle can also increase the permeability of the clay or silt material compacted into an embankment.

The clay material selection and layer thickness requirements are to be determined by a geotechnical engineer. The soil compaction requirement is at least 95 percent of the maximum dry density determined in accordance with standard proctor method per ASTM D-698.

Even-though this construction method is the cheapest, it is not always effective in retaining liquid spill. As part of Chesapeake's commitment to protect the environment, compacted soil berm construction is no more utilized.

SECONDARY CONTAINMENT SEEPAGE CALCULATION METHODS

In the event of an accidental fluid spill retained for a certain duration inside the secondary containment, the potential exists for some seepage to escape out of the secondary containment.

There are two mechanisms that could cause seepage on impervious secondary containment systems:

- The impervious materials are actually permeable. Therefore, prolonged liquid containment will cause some permeable seepage release.

- Cracks or accidental puncture on the liner could occur throughout the life time of the secondary containment. Seepage through the defective spot will cause a spill release.

By utilizing sufficiently impervious materials to construct the secondary containment, the seepage will be relatively insignificant. This section will address the two methods to quantify the amount of seepage.

In this paper, it will be assumed that the spill does not over flow the containment system, and there is no major structural damage to the secondary containment. The volume and dimension of the secondary containment shall follow the 40-CFR part 112 and company Best Management Practice (BMP).

PERMEABLE SEEPAGE

This calculation method is used on lined or un-lined secondary containment.
All of the impervious secondary containment materials, such as compacted clay, concrete, polyethylene and polyurea liners have some degree of permeability. In the following formulation, soil is used as the permeable material.
The permeable seepage is a function of hydrostatic pressure, soil permeability, fluid viscosity, fluid density and duration of liquid retained.

$$k_s = (\gamma_w / \eta_w) K_s \quad (1)$$

See Table 1 for definition of terms. The fluid height in the containment directly affects the hydrostatic which controls the seepage flow rate. Therefore, the seepage flow rate will be a function of time.
The permeable seepage can be calculated using combination of Darcy's law and Bernoulli's equation. Darcy's law provides a simple equation to calculate discharge flow rate of liquid through saturated permeable soil.

$$v = k_s i \quad (2)$$

The hydraulic gradient based on Bernoulli's equation is a function of head loss over the length of soil passage. Most of the fluid flow through void space of porous soil can be consider laminar, so that the hydraulic gradient has linear relation with the fluid velocity.

$$i = h_w / L_s \quad (3)$$

The fluid flow rate is a function of the permeability coefficient, cross sectional area and hydraulic gradient.

$$Q = A\ v = A\ k_s\ i \quad (4)$$
$$Q = A\ k_s\ h_w / L_s \quad (5)$$

Table 1. Definition of terms used in equations

Term	Definition (units)
A	Cross sectional area (m^2)
v	fluid velocity per Darcy's law (m/s)
k_s	permeability of soil based on specific liquid (m/s)
K_s	Absolute permeability of soil (m^2)
i	hydraulic gradient per Bernoulli's equation (-)
h_w	head loss (m)
L_s	liquid flow length for the head loss (m)
γ_w	specific weight of liquid (kg/m^3)
η_w	viscosity of liquid (Pa s)

On the berm application, the height and angles of the berm wall affect the seepage flow rate.

The permeability coefficient is determined from the spilled fluid specific weight, fluid viscosity and absolute permeability of the soil type.

This seepage evaluation is limited to the secondary containment system; native soil condition below the containment is not considered. The native soil type, condition and profile could affect the release of the spill to the environment. The native soil will vary for each location.

A spreadsheet in Appendix 1 presents a sample of this permeable seepage calculation. In this calculation, it is assumed that there is 120 barrels oil spill from a tank to its compacted clay secondary containment. It is assumed that it will take 48 hours for the operator to remove and clean-up the oil from the containment. This permeable seepage spreadsheet shows 6.2 L (1.65 gallons) of oil seeping out of the secondary containment. This is less than the 159 L (42 gallons) that the 40-CFR part 112.4 specifies for reporting to the regional administrator.

LINER DEFECT SEEPAGE

This section addresses some methods to calculate liquid seepage through any defect or damage on a geo-membrane liner above a secondary containment soil.

Touze-Foltz and Giroud (2005) proposed the following empirical equations for flow rate through several sizes of circular defects:

For defect hole diameter between 2 and 11.28 mm

$$Q = C_a\, a^{0.1}\, k_s^{0.74}\, h_w^{0.9}\, [1 + 0.1(h_w/H_s)^{0.95}] \quad (6)$$

For defect hole diameter between 100 and 600 mm

$$Q = C_A\, a^{0.18}\, k_s^{0.77}\, h_w^{0.84}\, [1 - 0.1(h_w/H_s)^{0.027}] \quad (7)$$

Where

Q	flow rate through the geomembrane defect (m^3/s)
$C_{a,A}$	contact condition factor (see Table 2)
a	area of circular defect in geomembrane (m^2)
k_s	soil hydraulic conductivity (m/s)
h_w	hydraulic head above the geomembrane (m)
H_s	thickness of soil component at secondary containment (m)

For the defect diameter in between the above range or beyond the provided range, the flow rate can be calculated by interpolation, averaging or extrapolation of the formulas (6) and (7).

Table 2. Contact condition factors

Contact Condition Factor	Contact Condition		
	Excellent	Good	Poor
C_a	0.096	0.21	1.15
C_A	0.33	0.64	2.6

Contact condition on interface flow represents the behavior of water transferring through the defective opening into the soil. Excellent contact refers to direct vertical transfers of water into the soil, and poor contact refers to liquid flow laterally in between the liner and soil surface prior to percolating through the soil.

A sample calculation using the same spill parameters (120 bbl. for 48 hours) was carried out based on this method for two liners with defect holes of 11.28 and 100 mm diameters. Both of Touze-Foltz and Giroud's formulas are utilized in this calculation for the purpose of comparison. The result total flow rates of seepage through these defect holes for 48 hours period are 4.9 L (1.3 gallons) on 11.28 mm diameter hole and 9.1 L (2.4 gallons) on 100 mm diameter hole. These seepages are lower than the 159 L (42 gallons) that the 40-CFR part 112.4 specifies for reporting to the regional administrator.

SUMMARY AND CONCLUSIONS

The presented seepage calculations using permeable soil and liner defect methods provide ways to quantify any release from various secondary containments in the event of a retained spill.

The seepage release in a case of spill incident inside a sufficiently impervious secondary containment is relatively small compared to the required reporting limit of the 40 CFR part 112.4.

REFERENCES

Code of Federal Regulation 40 Part 112 (2012) "Oil Pollution Prevention." Washington, DC

US Environmental Protection Agency 550-B-05-001(2005) "SPCC Guidance for Regional Inspectors." Washington, DC, pp. 4.1-24

"International Building Code," International Code Council, Country Club Hills, Illinois, 2003, pp. 273-297

America Concrete Institute, 318 committee (2008) "Building Code Requirements for Structural Concrete and Commentary." Farmington Hills, Michigan, pp. 115-257

Chesapeake Energy (2013). *Leading a Responsible Energy Future – 2012 Corporate Responsibility Report*, Oklahoma City, Oklahoma.

Chesapeake Energy, COI-ETG-FAC-STD-010, *Secondary Containment of Production Equipment – Standard,* Oklahoma City, Oklahoma.

Touze-Foltz, N. and Giroud, J.P. (2005a). "Empirical equations for calculating the rate of liquid flow through composite liners due to large circular defects in the geomembrane." *Geosynthetics International*, 12(4), pp. 205-207

Touze-Foltz, N. and Giroud, J.P. (2005b). "Equations for calculation the rate of liquid flow through geomembrane defects of uniform width and finite or infinite length." *Geosynthetics International*, 12(4), pp. 191-204

Secondary Containment (Un-lined) Berm Seepage Calculation

Inputs			
Soil & Liquid Parameters	Values	Units	
Permeability Coef. (k) of water in soil	1.00E-06	cm/sec	For clay
Viscosity of Liquid (water default)	6.00E-05	ft^2/s	For Oil
Unit Weight of Liquid (water default)	57	lb/ft^3	For Oil

Secondary Containment Dimensions		
Parameters	Values	Units
Length (center line)	100	ft
Width (center line)	50	ft
Thickness of Soil Fill (Tsoil)	2	ft
Height of Liquid Inside Berm (H liquid)	0.12163	ft
Berm Slope Inside (Slope in)	45	degrees
Berm Slope Outside (Slope out)	45	degrees
Width of Berm Top (top)	0.5	ft

Tanks inside the Containment (Volume reduction)		
Parameters	Values	Units
Diameter of Tank	12	ft
Height of Tank	40	ft
Number of Tank	6	

Seepage Output Summary		
Initial Spill Volume in the Containment	3,780.19	gal
Initial Seepage Rate	0.82	gal/day
Duration of Water in Berm (Time)	2	day
Total Seepage	1.65	gal

NOTES:
Fill out the green boxes
This diffusion seepage calculation is based on Bernoulli and Darcy's eq.
This calculation is not fully automated
Review the output summary using the calculation table
1 bbl = 31.5 gal
DS - CHK ETG Facility Engineering
Date - 12/11/13

Seepage Calculation Results

Conditions	Height of Liquid Inside Berm (H liquid)	Net Liquid Vol at each height section (w/o tanks)	Seepage Flow rate Through Berm Wall (Q berm)	Seepage Flow rate Through Floor (Q floor)	Total Flow rate of Env. Release (Q total)	Time Estimate To Reach This Height
Units	inch	gal	gal/day	gal/day	gal/day	day
Starting Height	1.460	380	0.004	0.819	0.824	0
Second Height	1.314	379	0.003	0.737	0.740	461
Third Height	1.168	379	0.003	0.654	0.657	1,025
Fourth Height	1.022	379	0.002	0.572	0.574	1,732
Fifth Height	0.876	378	0.002	0.490	0.491	2,641
Sixth Height	0.730	378	0.001	0.408	0.409	3,855
Seventh Height	0.584	378	0.001	0.326	0.327	5,557
Eighth Height	0.438	377	0.000	0.244	0.245	8,112
Ninth Height	0.292	377	0.000	0.163	0.163	12,372
Tenth Height	0.146	346	0.000	0.081	0.081	20,898
Final Height	0.012	31	0.000	0.007	0.007	46,103
		3,780				

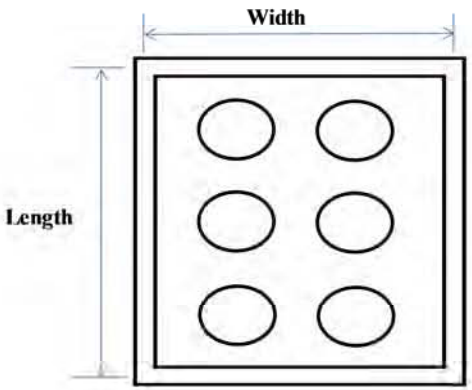

CONCEPTUAL PLAN VIEW
Not Scaled

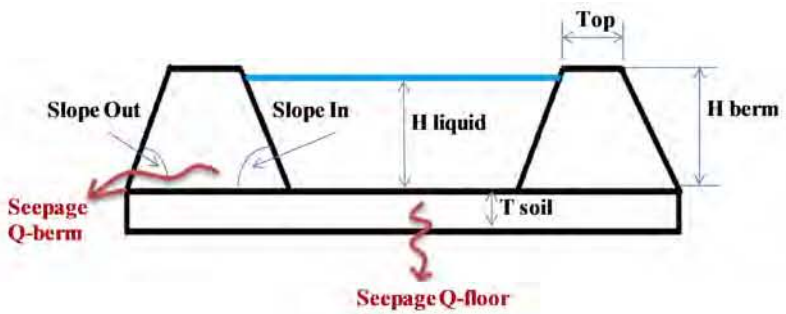

SECTIONAL ELEVATION VIEW
Not Scaled

Appendix 1. Permeability Seepage Calculation on a Berm Secondary Containment